SHOUT
SHARE
IT

MBL

Volume 188

Number 1

THE BIOLOGICAL BULLETIN

FEBRUARY/MARCH, 1995

Published by the Marine Biological Laboratory

AHK

THE
BIOLOGICAL BULLETIN

PUBLISHED BY
THE MARINE BIOLOGICAL LABORATORY

Marine Biological Laboratory
Woods Hole Oceanographic Institution
Library

FEB 15 1995

Woods Hole, [illegible]

Associate Editors

PETER A. V. ANDERSON, The Whitney Laboratory, University of Florida
WILLIAM D. COHEN, Hunter College, City University of New York
DAVID EPEL, Hopkins Marine Station, Stanford University
J. MALCOLM SHICK, University of Maine, Orono

Editorial Board

THOMAS H. DIETZ, Louisiana State University
DAPHNE GAIL FAUTIN, University of Kansas
WILLIAM F. GILLY, Hopkins Marine Station, Stanford University
ROGER T. HANLON, Marine Biomedical Institute, University of Texas Medical Branch
CHARLES B. METZ, University of Miami
K. RANGA RAO, University of West Florida
BARUCH RINKEVICH, Israel Oceanographic & Limnological Research Ltd.
RICHARD STRATHMANN, Friday Harbor Laboratories, University of Washington
STEVEN VOGEL, Duke University
J. HERBERT WAITE, University of Delaware
SARAH ANN WOODIN, University of South Carolina
RICHARD K. ZIMMER-FAUST, University of South Carolina

Editor: MICHAEL J. GREENBERG, The Whitney Laboratory, University of Florida
Managing Editor: PAMELA L. CLAPP, Marine Biological Laboratory

FEBRUARY/MARCH, 1995

Printed and Issued by
LANCASTER PRESS, Inc.
3575 HEMPLAND ROAD
LANCASTER, PA

THE BIOLOGICAL BULLETIN

THE BIOLOGICAL BULLETIN is published six times a year by the Marine Biological Laboratory, MBL Street, Woods Hole, Massachusetts 02543.

Subscriptions and similar matter should be addressed to Subscription Manager, THE BIOLOGICAL BULLETIN, Marine Biological Laboratory, Woods Hole, Massachusetts 02543. Single numbers, $37.50. Subscription per volume (three issues), $92.50 ($185.00 per year for six issues).

Communications relative to manuscripts should be sent to Michael J. Greenberg, Editor-in-Chief, or Pamela L. Clapp, Managing Editor, at the Marine Biological Laboratory, Woods Hole, Massachusetts 02543. Telephone: (508) 548-3705, ext. 428. FAX: 508-540-6902. E-mail: pclapp@hoh.mbl.edu.

THE BIOLOGICAL BULLETIN is indexed in bibliographic services including *Index Medicus* and MEDLINE, *Chemical Abstracts*, and *Current Contents*.

Printed on acid free paper,
effective with Volume 180, Issue 1, 1991.

POSTMASTER: Send address changes to THE BIOLOGICAL BULLETIN, Marine Biological Laboratory, Woods Hole, MA 02543.

Copyright © 1995, by the Marine Biological Laboratory

Second-class postage paid at Woods Hole, MA, and additional mailing offices.
ISSN 0006-3185

INSTRUCTIONS TO AUTHORS

The Biological Bulletin accepts outstanding original research reports of general interest to biologists throughout the world. Papers are usually of intermediate length (10–40 manuscript pages). A limited number of solicited review papers may be accepted after formal review. A paper will usually appear within four months after its acceptance.

Very short, especially topical papers (less than 9 manuscript pages including tables, figures, and bibliography) will be published in a separate section entitled "Research Notes." A Research Note in *The Biological Bulletin* follows the format of similar notes in *Nature*. It should open with a summary paragraph of 150 to 200 words comprising the introduction and the conclusions. The rest of the text should continue on without subheadings, and there should be no more than 30 references. References should be referred to in the text by number, and listed in the Literature Cited section in the order that they appear in the text. Unlike references in *Nature*, references in the Research Notes section should conform in punctuation and arrangement to the style of recent issues of *The Biological Bulletin*. Materials and Methods should be incorporated into appropriate figure legends. See the article by Lohmann *et al.* (October 1990, Vol. 179: 214–218) for sample style. A Research Note will usually appear within two months after its acceptance.

The Editorial Board requests that regular manuscripts conform to the requirements set below; those manuscripts that do not conform will be returned to authors for correction before review.

1. ***Manuscripts.*** Manuscripts, including figures, should be submitted in triplicate. (Xerox copies of photographs are not acceptable for review purposes.) The submission letter accompanying the manuscript should include a telephone number, a FAX number, and (if possible) an E-mail address for the corresponding author. The original manuscript must be typed in no smaller than 12 pitch or 10 point, using double spacing (*including* figure legends, footnotes, bibliography, etc.) on one side of 16- or 20-lb. bond paper, 8½ by 11 inches. Please, no right justification. Manuscripts should be proofread carefully and errors corrected legibly in black ink. Pages should be numbered consecutively. Margins on all sides should be at least 1 inch (2.5 cm). Manuscripts should conform to the *Council of Biology Editors Style Manual*, 5th Edition (Council of Biology Editors, 1983) and to American spelling. Unusual abbreviations should be kept to a minimum and should be spelled out on first reference as well as defined in a footnote on the title page. Manuscripts should be divided into the following components: Title page, Abstract (of no more than 200 words), Introduction, Materials and Methods, Results, Discussion, Acknowledgments, Literature Cited, Tables, and Figure Legends. In addition, authors should supply a list of words and phrases under which the article should be indexed.

2. ***Title page.*** The title page consists of a condensed title or running head of no more than 35 letters and spaces, the manuscript title, authors' names and appropriate addresses, and footnotes listing present addresses, acknowledgments or contribution numbers, and explanation of unusual abbreviations.

3. ***Figures.*** The dimensions of the printed page, 7 by 9 inches, should be kept in mind in preparing figures for publication. We recommend that figures be about 1½ times the linear dimensions of the final printing desired, and that the ratio of the largest to the smallest letter or number and of the thickest to the thinnest line not exceed 1:1.5. Explanatory matter generally should be included in legends, although axes should always be identified on the illustration itself. Figures should be prepared for reproduction as either line cuts or halftones. Figures to be reproduced as line cuts should be unmounted glossy photographic reproductions or drawn in black ink on white paper, good-quality tracing cloth or plastic, or blue-lined coordinate paper. Those to be reproduced as halftones should be mounted on board, with both designating numbers or letters and scale bars affixed directly to the figures. All figures should be numbered

in consecutive order, with no distinction between text and plate figures. The author's name and an arrow indicating orientation should appear on the reverse side of all figures.

4. ***Tables, footnotes, figure legends, etc.*** Authors should follow the style in a recent issue of *The Biological Bulletin* in preparing table headings, figure legends, and the like. Because of the high cost of setting tabular material in type, authors are asked to limit such material as much as possible. Tables, with their headings and footnotes, should be typed on separate sheets, numbered with consecutive Roman numerals, and placed after the Literature Cited. Figure legends should contain enough information to make the figure intelligible separate from the text. Legends should be typed double spaced, with consecutive Arabic numbers, on a separate sheet at the end of the paper. Footnotes should be limited to authors' current addresses, acknowledgments or contribution numbers, and explanation of unusual abbreviations. All such footnotes should appear on the title page. Footnotes are not normally permitted in the body of the text.

5. ***Literature cited.*** In the text, literature should be cited by the Harvard system, with papers by more than two authors cited as Jones *et al.*, 1980. Personal communications and material in preparation or in press should be cited in the text only, with author's initials and institutions, unless the material has been formally accepted and a volume number can be supplied. The list of references following the text should be headed Literature Cited, and must be typed double spaced on separate pages, conforming in punctuation and arrangement to the style of recent issues of *The Biological Bulletin*. Citations should include complete titles and inclusive pagination. Journal abbreviations should normally follow those of the U. S. A. Standards Institute (USASI), as adopted by BIOLOGICAL ABSTRACTS and CHEMICAL ABSTRACTS, with the minor differences set out below. The most generally useful list of biological journal titles is that published each year by BIOLOGICAL ABSTRACTS (BIOSIS List of Serials; the most recent issue). Foreign authors, and others who are accustomed to using THE WORLD LIST OF SCIENTIFIC PERIODICALS, may find a booklet published by the Biological Council of the U.K. (obtainable from the Institute of Biology, 41 Queen's Gate, London, S.W.7, England, U.K.) useful, since it sets out the WORLD LIST abbreviations for most biological journals with notes of the USASI abbreviations where these differ. CHEMICAL ABSTRACTS publishes quarterly supplements of additional abbreviations. The following points of reference style for THE BIOLOGICAL BULLETIN differ from USASI (or modified WORLD LIST) usage:

A. Journal abbreviations, and book titles, all underlined (for *italics*)

B. All components of abbreviations with initial capitals (not as European usage in WORLD LIST *e.g., J. Cell. Comp. Physiol.* NOT *J. cell. comp. Physiol.*)

C. *All* abbreviated components must be followed by a period, whole word components *must not* (*i.e., J. Cancer Res.*)

D. Space between all components (*e.g., J. Cell. Comp. Physiol.*, not *J.Cell.Comp.Physiol.*)

E. Unusual words in journal titles should be spelled out in full, rather than employing new abbreviations invented by the author. For example, use *Rit Vísindafjélags Islendinga* without abbreviation.

F. All single word journal titles in full (*e.g., Veliger, Ecology, Brain*).

G. The order of abbreviated components should be the same as the word order of the complete title (*i.e., Proc.* and *Trans.* placed where they appear, not transposed as in some BIOLOGICAL ABSTRACTS listings).

H. A few well-known international journals in their preferred forms rather than WORLD LIST or USASI usage (*e.g., Nature, Science, Evolution* NOT *Nature, Lond., Science, N.Y.; Evolution, Lancaster, Pa.*)

6. ***Reprints, page proofs, and charges.*** Authors receive their first 100 reprints (without covers) free of charge. Additional reprints may be ordered at time of publication and normally will be delivered about two to three months after the issue date. Authors (or delegates for foreign authors) will receive page proofs of articles shortly before publication. They will be charged the current cost of printers' time for corrections to these (other than corrections of printers' or editors' errors). Other than these charges for authors' alterations, *The Biological Bulletin* does not have page charges.

Reference: *Biol. Bull.* **188:** 1–4. (February/March, 1995)

Responses of the Medaka Fish Egg (*Oryzias latipes*) to the Photolysis of Microinjected Nitrophenyl-EGTA, a Photolabile Calcium Chelator

RICHARD A. FLUCK

Biology Department, Franklin and Marshall College, P.O. Box 3003, Lancaster, Pennsylvania 17604

Photolabile calcium chelators (calcium cages) can be used to elevate cytosolic [Ca^{2+}] at specific sites and times (1, 2, 3). They have been especially valuable in flash photolysis studies of muscle contraction (2) and secretion (4, 5). In the present report, I describe several responses of medaka eggs to the photolysis of microinjected nitrophenyl-EGTA (NP-EGTA), a new calcium cage (6). When unfertilized eggs injected with NP-EGTA were irradiated with ultraviolet irradiation in a small region of the egg, the eggs were activated and ooplasm within the irradiated region contracted and accumulated there. Eggs into which NP-EGTA was injected could also be fertilized. Subsequent irradiation of such eggs, in addition to causing the contraction and accumulation of ooplasm, also caused a global contraction of dividing blastomeres and the contraction and blebbing of embryonic cells for up to 4 days after fertilization. Injection of NP-EGTA had no apparent effect on the maturation of fertilized eggs, which developed normally and hatched.

The methods for dissection of gonads from breeding medaka, preparation of gametes, and *in vitro* fertilization of eggs have been described previously (7). Gonads, gametes, and zygotes were prepared in a balanced saline solution (BSS: 111 m*M* NaCl; 5.37 m*M* KCl; 1.0 m*M* $CaCl_2$; 0.6 m*M* $MgSO_4$; 5 m*M* HEPES, pH 7.3). A normalized time (T_n) scale in which the time between fertilization and the beginning of cytokinesis is 1 unit was used to indicate the relative temporal positions of events. A total of 80 eggs from 6 females were used in these experiments; 44 of the eggs were monitored in detail and an additional 36 were monitored intermittently. The experiments were conducted at room temperature (23°–25°C).

Methods described previously (8, 9, 10) were used to microinject 1.4–5.6 nl of an aqueous solution of NP-EGTA/Ca^{2+} (50 m*M* NP-EGTA, tetrapotassium salt; 39.6 m*M* $CaCl_2$; 10 m*M* HEPES, pH 7.3) into the thin peripheral layer of ooplasm. Assuming an accessible volume of 27.6 nl (9), injection of these volumes would give a final ooplasmic concentration of 2.5–10.0 m*M* NP-EGTA. After microinjection, the eggs were either placed in a darkened cabinet for subsequent use or fertilized within 5 min. During the experiments, the laboratory was only dimly illuminated with incandescent lamps.

For microscopic observation and irradiation, the eggs were transferred to a microscope slide on which a cover glass was supported by four pillars of petroleum jelly (7). An Osram 100 W mercury arc lamp was used to irradiate the eggs with ultraviolet light. The light from the lamp was passed through a filter cube (Omega Optical) containing a 360 DF 40 exciter filter, a DC 405 dichroic mirror, and a 486 DF32 barrier filter. An octagonal diaphragm was used to control the size of the light beam (in most experiments, it was either 200 μm or 475 μm), and neutral density filters (Omega Optical) were used to reduce the light intensity by either 34-fold or 286-fold. Ultraviolet light was projected onto the egg via one of three objective lenses (Nikon): Plan 4×, N.A. = 0.1; Fluor/Ph 2 DL 10×, N.A. = 0.5; Fluor/Ph 3 DL 20×, N.A. = 0.75. In most experiments, the equatorial region of the egg—that is, a region along a meridian and midway between the animal and vegetal poles—was illuminated *en profil* (an edge of the egg was irradiated) via the 10× objective lens. Light intensity was measured with a UVX radiometer with a long wave sensor (UVP, Inc.). Given a light intensity of 523 μW cm^{-2} (referred to as "high intensity" hereafter) and assuming that all the ultraviolet light was of wavelength 360 nm, I calculated an incident light intensity of

Received 30 August 1994; accepted 14 October 1994.

4.9×10^9 quanta second^{-1} μm^{-2} (10× objective lens, no neutral density filter). To monitor the eggs during irradiation, they were transilluminated with light from a quartz-halogen lamp, using a heat filter (KG5) and a 486 DF32 filter, and the images were recorded via a SIT camera (Dage/MTI) and a time-lapse videocassette recorder.

To monitor the development of fertilized eggs after the first cell cycle, they were transferred to embryo rearing medium (17 mM NaCl; 0.4 mM KCl; 0.3 mM $CaCl_2$; 0.67 mM $MgSO_4$; 0.001 g/l methylene blue).

When unfertilized eggs into which 1.4–5.6 nl NP-EGTA had been injected were irradiated with UV light, they activated within 16 ± 3 s ($\bar{X} \pm$ SD, $n = 5$), as evidenced by the exocytosis of cortical vesicles. Exocytosis began within the irradiated region and spread as a wave over the rest of the egg. Eggs were photoactivated even after the light intensity was reduced 34-fold with a neutral density filter; but when a second neutral density filter was added, reducing the light intensity an additional 8.5-fold, the eggs were not activated even after 3 min of continuous irradiation. Irradiation of unfertilized eggs that had not received NP-EGTA did not cause them to activate.

Continued irradiation of photoactivated eggs caused both ooplasm and oil droplets to accumulate in and next to the irradiated zone (Fig. 1A). Staining with rhodamine phalloidin showed that these accumulations of ooplasm contained filamentous actin (F-actin, Fig. 1B). Such accumulations of ooplasm and F-actin were identified in 18 eggs, 13 of which had been photoactivated and 5 of which had been fertilized. Moreover, the caps of ooplasm formed in eggs into which either 1.4 nl or 4.2 nl of NP-EGTA had been injected and in eggs that were irradiated either intermittently (5 s on/115 s off) with a high intensity of light or continuously with a 34-fold lower light intensity. However, when the light intensity was lowered 289-fold, ooplasm neither contracted nor accumulated in the irradiated zone. When UV irradiation was intermittent, the ooplasm within the irradiated zone usually contracted each time it was irradiated. For example, the region in the egg shown in Figure 1 was irradiated 29 times for 5 s and contracted 16 times, and a sibling egg contracted each of the 31 times it was irradiated for 5 s. Each contraction appeared to pull ooplasm and nearby oil droplets toward the irradiated region. Eggs that were parthenogenetically activated by the injection itself and grown in the dark segregated normally (as do eggs that have been parthenogenetically activated by pricking; Fluck, unpub. obs.), with a cap of ooplasm forming at the animal pole and the oil droplets segregating toward the vegetal pole.

Eggs into which NP-EGTA had been injected could also be fertilized. In most fertilized eggs, cortical vesicles in one small region of the egg, presumably near the in-

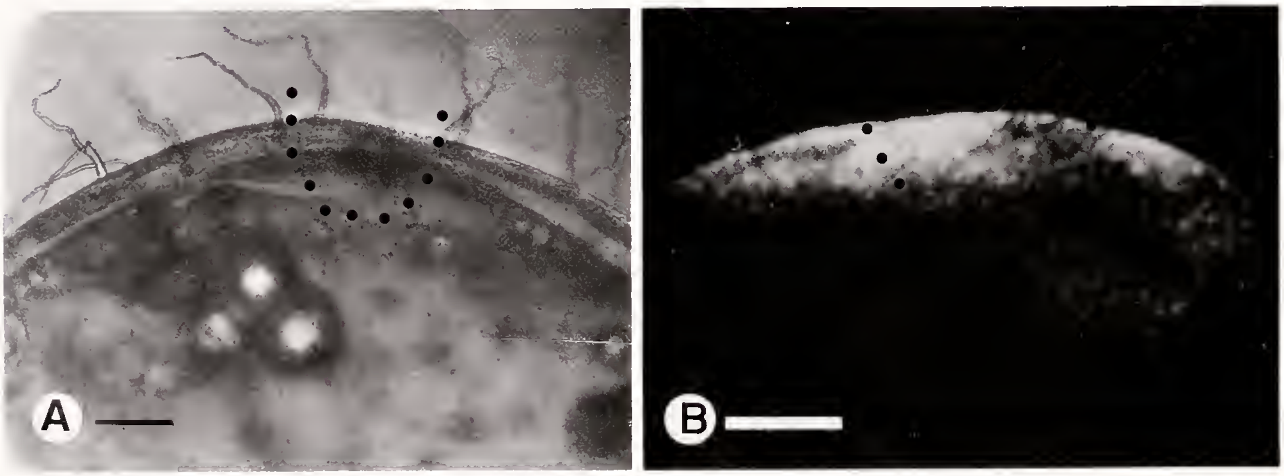

Figure 1. Accumulation of ooplasm within a UV-irradiated region of an egg. NP-EGTA/Ca^{2+} (4.2 nl) was microinjected into this egg, which was then irradiated *en profil* in a region (approximately defined by the filled circles) along a meridian and midway between its animal and vegetal poles. The UV light was projected through the 10× objective lens with no neutral density filter in the light path. Ultraviolet irradiation was intermittent, with light pulses delivered for 5 s at 2-min intervals for a total of 79 min (until $T_n = 1.0$). The egg was then fixed overnight at room temperature with formaldehyde dissolved in an actin-stabilizing buffer (24): 3.7% formaldehyde (Electron Microscopy Sciences, Fort Washington, PA), 100 mM KCl, 5 mM $MgCl_2$, 2 mM EGTA, 10 mM PIPES, pH 6.8. It was then dechorionated with fine forceps, permeabilized for 15 min with 0.3% Triton X-100 in BSS, and stained for 30 min in 0.25 μM rhodamine phalloidin (Molecular Probes, Inc., Eugene, OR) dissolved in BSS. The irradiated region of the egg was photographed with brightfield optics just before fixation (A) and with epi-illumination after staining the egg with rhodamine phalloidin (B). Note the accumulation of ooplasm, oil droplets, and F-actin in the irradiated region. Scale bars, 100 μm.

jection site, did not undergo exocytosis. Irradiation of fertilized eggs caused ooplasm to accumulate within the irradiated region, but no such accumulations were seen in fertilized eggs that were grown in the dark; in such dark-grown eggs, the ooplasm and its contents appeared to segregate normally. Moreover, irradiation of unfertilized eggs that had not received NP-EGTA caused neither contraction of the ooplasm nor accumulation of ooplasm within the irradiated region.

All eggs that received 1.4 nl of NP-EGTA underwent cytokinesis. Of eight such fertilized eggs whose subsequent development was monitored, four hatched and the other four underwent extensive morphogenesis but did not hatch. Cleavage was abnormal in eggs that received either 4.2 or 5.6 nl of NP-EGTA, and the embryos did not develop further. Irradiation of eggs (that received 1.4 nl of NP-EGTA and were subsequently fertilized) during early cleavage caused cells in the light beam to contract globally. Moreover, irradiation of early gastrulae caused blebbing and global contraction of deep blastomeres, but irradiation of the yolk sac in stage 19, 22, and 25 embryos (that is, up to 4 days after fertilization) caused contractions that appeared similar to those seen during the rhythmic contraction waves that occur in the stellate layer of the medaka embryo (11). Cells of embryos that did not receive NP-EGTA failed to contract when they were irradiated with UV light.

Taken together, these findings show NP-EGTA to be a useful new reagent for cell and developmental biologists. Several properties of this compound—its high affinity for Ca^{2+} (6), the approximately 10,000-fold decrease in its affinity for Ca^{2+} upon photolysis (6), its weak fluorescence (6), and its persistence and low toxicity in the teleost embryo (this study)—appear to make it particularly suitable for studying events that have been linked to elevations in cytosolic $[Ca^{2+}]$: egg activation (12, 13), ooplasmic segregation (9, 10), nuclear envelope breakdown (14), mitosis (15, 16, 17), cytokinesis (8, 18), and neuronal growth cone motility (19, 20).

The accumulation of ooplasm and F-actin within the UV-irradiated region of the egg is consistent with the hypothesis that cytosolic calcium gradients organize developmental localization in eggs (10, 21, 22, 23). At present, however, the evidence consistent with this hypothesis, including that presented in the present report, is indirect and must be extended by using aequorin or a fluorescent calcium indicator to measure cytosolic $[Ca^{2+}]$ in eggs during and after photolysis of NP-EGTA. Full exploitation of the apparent promise of NP-EGTA will require the development of a dextran-conjugated form of the molecule and the exploration of wider ranges of intracellular concentrations of the cage, shapes of the irradiated region (for example, a narrow rectangle that could elevate cytosolic $[Ca^{2+}]$ in a narrow band in a cell), and light intensities.

Acknowledgments

Lionel Jaffe suggested the use of calcium cages to generate zones of elevated calcium in medaka eggs. I am grateful to Jack Kaplan and Graham Ellis-Davies for providing the NP-EGTA used in these studies; to Alan Bruns for helpful discussions about units of light intensity; and to Andrew Miller for helping to improve the text of the manuscript. This work was supported by NSF DCB-9017210 and NSF MCB-9316125.

Literature Cited

1. **McCray, J. A., and D. R. Trentham. 1989.** Properties and uses of photoreactive caged compounds. *Annu Rev. Biophys. Biophys. Chem.* **18:** 239–270.
2. **Ashley, C. C., P. J. Griffiths, T. J. Lea, I. P. Mulligan, R. E. Palmer, and S. J. Simmons. 1991.** Use of fluorescent TnC derivatives and 'caged' compounds to study cellular phenomena. Pp. 177–203 in *Cellular Calcium: A Practical Approach,* J. G. McCormack and P. H. Cobbold, eds. IRL Press, Oxford.
3. **Zucker, R. 1994.** Photorelease techniques for raising or lowering intracellular Ca^{2+}. *Meth. Cell Biol.* **40:** 31–63.
4. **Zucker, R. S., and P. G. Haydon. 1988.** Membrane potential has no direct role in evoking neurotransmitter release. *Nature* **335:** 360–362.
5. **Thomas, P., A. K. Lee, J. G. Wong, and W. Almers. 1994.** A triggered mechanism retrieves membrane in seconds after Ca^{2+}-stimulated exocytosis in single pituitary cells. *J Cell Biol.* **124:** 667–675.
6. **Ellis-Davies, C. R., and J. H. Kaplan. 1994.** Nitrophenyl-EGTA, a photolabile chelator that selectively binds Ca^{2+} with high affinity and releases it rapidly upon photolysis. *Proc. Natl. Acad Sci. USA* **91:** 187–191.
7. **Abraham, V. C., S. Gupta, and R. A. Fluck. 1993.** Ooplasmic segregation in the medaka *(Oryzias latipes). Biol. Bull.* **184:** 115–124.
8. **Fluck, R. A., A. L. Miller, and L. F. Jaffe. 1991.** Slow calcium waves accompany cytokinesis in medaka fish eggs. *J Cell Biol.* **115:** 1259–1265.
9. **Fluck, R. A., A. L. Miller, and L. F. Jaffe. 1992.** High calcium zones at the poles of developing medaka eggs. *Biol Bull.* **183:** 70–77.
10. **Fluck, R. A., A. L. Miller, V. C. Abraham, and L. F. Jaffe. 1994.** Calcium buffer injections inhibit ooplasmic segregation in medaka eggs. *Biol Bull* **186:** 254–262.
11. **Cope, J., R. Fluck, L. Nicklas, L. A. Plumhoff, and S. Sincock. 1990.** The stellate layer and rhythmic contractions of the *Oryzias latipes* embryo. *J Exp Zool* **254:** 270–275.
12. **Gilkey, J. C., L. F. Jaffe, E. B. Ridgway, and G. T. Reynolds. 1978.** A free calcium wave traverses the activating egg of the medaka, *Oryzias latipes. J Cell Biol.* **76:** 448–466.
13. **Shen, S. S., and W. R. Buck. 1993.** Sources of calcium in sea urchin eggs during the fertilization response. *Dev. Biol.* **157:** 157–169.
14. **Browne, C. L., A. L. Miller, R. E. Palazzo, and L. F. Jaffe. 1992.** On the calcium pulse during nuclear envelope breakdown (NEB) in sea urchin eggs. *Biol Bull* **183:** 370–371.
15. **Hepler, P. K. 1989.** Calcium transients during mitosis: observations in flux. *J Cell Biol.* **109:** 2567–2573.

16. **Whitaker, M., and R. Patel. 1990.** Calcium and cell cycle control. *Development* **108:** 525–542.

17. **Harris, P. J. 1994.** Caffeine-induced calcium release in sea urchin eggs and the effect of continuous versus pulsed application on the mitotic apparatus. *Dev. Biol.* **161:** 370–378.

18. **Miller, A. L., R. A. Fluck, J. A. McLaughlin, and L. F. Jaffe. 1993.** Calcium buffer injections inhibit cytokinesis in *Xenopus* eggs. *J. Cell Biol.* **106:** 523–534.

19. **Eisen, J. S., P. Z. Myers, and M. Westerfield. 1986.** Pathway selection by growth cones of identified motoneurones in live zebra fish eggs. *Nature* **320:** 269–271.

20. **Lankford, K. L., and P. C. Letourneau. 1989.** Evidence that calcium may control neurite outgrowth by regulating the stability of actin filaments. *J. Cell Biol.* **109:** 1229–1243.

21. **Jeffery, W. R. 1982.** Calcium ionophore polarizes ooplasmic segregation in ascidian eggs. *Science* **216:** 545–547.

22. **Jaffe, L. F. 1986.** Calcium and morphogenetic fields. Pp. 271–288 in *Calcium and the Cell,* D. Evered and J. Whelan, eds. John Wiley and Sons, Chichester, England.

23. **Bates, W. R., and W. R. Jeffery. 1988.** Polarization of ooplasmic segregation and dorsal-ventral axis determination in ascidian embryos. *Dev. Biol.* **130:** 98–107.

24. **Yonemura, S., and S. Kinoshita. 1986.** Actin filament organization in the sand dollar egg cortex. *Dev. Biol.* **115:** 171–183.

Reference: *Biol Bull.* **188:** 5–7. (February/March, 1995)

Hemoglobin in the Symbiont-Harboring Gill of the Marine Gastropod *Alviniconcha hessleri*

JONATHAN B. WITTENBERG[1] AND JEFFREY L. STEIN[2]

[1]*Department of Physiology and Biophysics, Albert Einstein College of Medicine, Bronx, New York 10461, and* [2]*The Agouron Institute, La Jolla, California 92037*

Hydrogen sulfide of geochemical origin, mixing at oceanic hydrothermal vents with oxygen from oceanic seawater, supports dense populations of chemoautrophic, sulfur-oxidizing bacteria. Those animals, the vestimentiferan worm Riftia pachyptila, *certain bivalve molluscs, and the recently discovered Pacific gastropod* Alviniconcha hessleri, *that interiorize the bacteria as intracellular symbionts dominate the vent fauna (1, 2). The immense size of these animals, the large standing crop represented in their dense communities, and the rapid growth of individuals all attest to the effective use of an abundant food base. Dense concentrations of the mesogastropod* Alviniconcha hessleri *(2, 3) were recently discovered at deep-sea hydrothermal vents at the spreading center in the Mariana Back-Arc Basin of the Western Pacific. These animals house chemoautrophic, sulfide-oxidizing bacteria within specialized cells (bacteriocytes) of their modified gills (2). They are the only reported example of a symbiotic association between a gastropod mollusc and intracellular chemoautotrophic bacteria. We now show that the modified gill of* Alviniconcha *contains hemoglobin at a concentration of about 65 μmol/kg wet weight gill. This value falls within the range, 20–250 μmol hemoglobin per kilogram, encountered in the modified symbiont-harboring gills of many of the sulfide-dependent clams examined but is short of the very high concentrations, 550 and 1200 μmol/kg, found in* Myrtea spinifera *and* Lucina pectinata *respectively (4). Accordingly, bacteriocyte hemoglobin is a feature common to both gastropod and bivalve symbioses.*

Symbioses with intracellular carbon-fixing bacteria, believed to be dependent on bacteriocyte hemoglobin, have heretofore been described only in clams of the families Solemyidae, Lucinidae, and Vesicomyidae and in a few mussels, Mytilidae, restricted to the genus *Bathymodiolus* (4). The molluscan symbionts fix carbon from oceanic carbon dioxide into hexoses and supply almost all of the carbon nutrition of the host (5). Ribulose bisphosphate carboxylase/oxygenase (RuBisCO), the enzyme responsible for carbon dioxide fixation, has been cloned from the *Alviniconcha* symbiont and expressed in *Escherichia coli* (6). The relatively low specificity of the purified enzyme for carbon dioxide indicates that the intracellular environment of the endosymbionts may be microaerophilic for RuBisCO to maintain net carboxylation (7).

Hemoglobins, probably located in the host cytoplasm and excluded from the peribacterial space and probably coded by host genes, are a near-constant feature of symbioses between bivalve molluscs and intracellular chemoautotrophic bacteria (4, 8); such hemoglobins are also a constant feature of symbioses between plants and intracellular prokaryotic nitrogen-fixing symbionts (9). Clam gill hemoglobins have been investigated intensively (10–13), and the three-dimensional structure of one is known from x-ray diffraction analysis (14). The probable role of the hemoglobin is to bring oxygen and hydrogen sulfide to the symbiont (8, 15). In the giant tube worm *Riftia*, this function is served by blood or coelomic hemoglobin, which bathe the symbiont-harboring cells and transport oxygen at the heme and sulfide at a site remote from the heme (16). In the bacteria-housing clam gill, these functions are probably served by two separate hemoglobins of the bacteriocyte cytoplasm (17). Cytoplasmic hemoglobins are believed to supplement the diffusion of free oxygen by adding to it a contribution from oxygen combined with the protein. In those few hemoglobin-containing tissues that have been studied intensively, the hemoglobin is maintained partially desaturated with oxygen, the larger part of the oxygen flow to the intracellular organelle is carried in combination with the protein, and

Received 2 September 1994; accepted 23 November 1994.

the oxygen pressure is held low (18). This is in accord with the suggestion that low oxygen pressure is probably required to allow RuBisCO to maintain net carboxylation in the *Alviniconcha* gill (7). The concentration of hydrogen sulfide likewise is probably low, perhaps in the nanomolar range (8), and the concentration of free hydrogen sulfide may not be sufficient to support the flux of hydrogen sulfide to the symbiont.

A specimen of the Western Pacific hydrothermal vent gastropod *Alviniconcha hessleri* was collected by the submersible *Alvin* at the "Snail Pit" site (18° 10.95′ N, 144° 43.20′ E, about 3650 m depth) on Dive number 1837, 23 April 1987. The gill, 0.58 g wet weight, was stored frozen in liquid nitrogen and a clear soluble extract prepared in 1.5 ml of buffer (19). Optical direct spectra of this extract display a prominent narrow feature at 551 nm. This unchanging feature ascribed to reduced soluble symbiont bacterial cytochrome c_{552} (20), vanishes in the difference spectra. Optical difference spectra (Figs. 1 and 2)unequivocally establish the presence of hemoglobin in the extract. To confirm the identity of the spectral entities, optical difference spectra of the extract of *Alviniconcha* gill are compared to those of purified *Lucina* Hb II, isolated from the modified symbiont-harboring gill of the clam *Lucina pectinata* (10). The concentration of *Alviniconcha* hemoglobin in the solution, about 19 μM (heme), was estimated from the spectrum presented in Fig. 2A by using molar extinction coefficients appropriate for the difference: carbon monoxide *Lucina* Hb II minus ferrous *Lucina* Hb II. Optical spectra in the visible and soret regions are expected to differ only slightly (about ±10%) among similar hemoglobins. The concentration in the tissue was estimated (19) to be about 65 μmol *Alviniconcha* hemoglobin per kilogram wet weight gill.

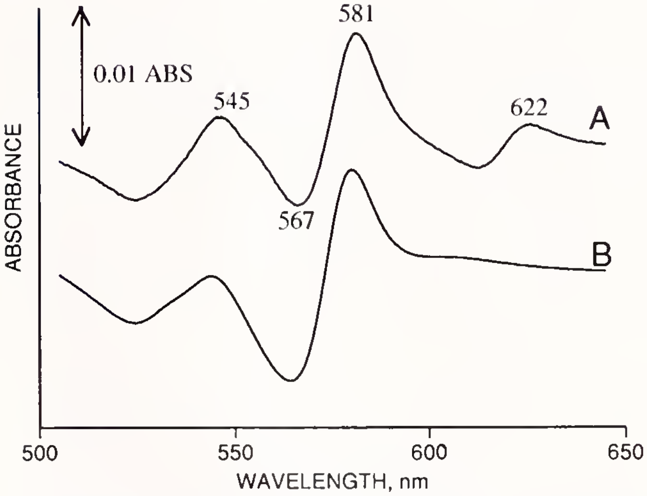

Figure 1. Optical difference spectra of the extract of *Alviniconcha* gill. Features ascribable to oxyhemoglobin were inconspicuous in the direct spectrum of the extract, suggesting that some component of the solution had consumed the dissolved oxygen. Accordingly the solution was equilibrated with oxygen gas. The difference spectrum of the oxygenated solution minus that of the initial (deoxygenated) solution (spectrum not shown) exhibits conspicuous features at 541 and 579 nm, diagnostic of oxygenated hemoglobin. A small feature near 622 nm suggested the presence of ferric hemoglobin. This feature increased in magnitude with time. The difference spectrum in the Soret region (spectrum not shown) of a portion of the sample that had been stored for 60 min at ice temperature minus that of a portion of the solution to which sodium dithionite (a reagent that removes oxygen and reduces most hemeproteins) had been added resembled the difference spectrum of ferric minus deoxy *Lucina* Hb II, and exhibited a maximum at 409 nm and a conspicuous minimum at 434 nm, diagnostic of hemoglobin. This confirms the presence of a hemoglobin in the solution. The oxygenated solution was then equilibrated with carbon monoxide. (A) Difference spectrum: Carbon-monoxide-equilibrated gill extract minus that of the oxygenated extract. Features at 545, 567, and 581 nm are diagnostic of hemoglobin. Conversion of oxy- to carbon monoxy hemoglobin shows that oxygen binding by the hemoglobin is reversible. (B) Difference spectrum: Carbon monoxide minus oxy *Lucina* Hb II.

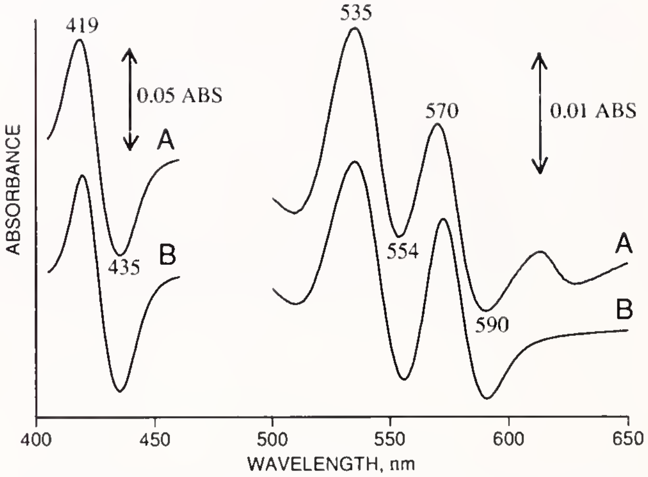

Figure 2. By adding sodium dithionite, all of the hemoglobin present in the extract of *Alviniconcha* gill is converted into single chemical species, permitting quantitative estimation of concentration. Absorbance in the visible region is amplified sixfold relative to the Soret region. (A) Difference spectrum: Carbon-monoxide-equilibrated gill extract containing sodium dithionite minus the same extract containing sodium dithionite alone. Well-defined features of 419, 435, 535, 554, 570 and 590 nm are diagnostic of hemoglobin. (B) Difference spectrum: Carbon monoxide *Lucina* Hb II minus deoxy (ferrous) *Lucina* Hb II.

Acknowledgments

We thank Dr. Robert R. Hessler for helpful discussion. This work was supported in part by Research grants DCB 90-17722 (to JBW) and OCE-93-17734 (to JLS) from The National Science Foundation. JBW was a Research Career Awardee 1-K6-733 of The U.S. Public Health Service, National Heart Lung and Blood Institute.

Literature Cited

1. **Hessler, R. R., and W. M. Smithey, Jr. 1983.** The distribution and community structure of megafauna at the Galapagos rift hy-

drothermal vents. Pp. 735–770 in *Hydrothermal Processes at Sea Floor Spreading Centers*, P. A. Rona *et al.*, eds. Plenum Press, New York.

2. **Stein, J. L., S. C. Cary, R. R. Hessler, S. Ohta, R. D. Vetter, J. J. Childress, and H. Felbeck. 1988.** Chemoautotrophic symbiosis in a hydrothermal vent gastropod. *Biol Bull.* **174:** 373–378.
3. **Okutani, T., and S. Ohta. 1988.** A new gastropod mollusk associated with hydrothermal vents in the Mariana back-arc basin, Western Pacific. *JPN J Malacol* **47:** 1–9.
4. **Wittenberg, J. B. 1985.** Oxygen supply to intracellular bacteria symbionts. In: *Hydrothermal Vents of the Eastern Pacific: An Overview*, M. L. Jones (ed.). *Bull. Biol. Soc. Washington* **6:** 301–310.
5. **Childress, J. J., and C. R. Fisher. 1992.** The biology of hydrothermal vent animals: physiology, biochemistry and autotrophic symbioses. *Oceanogr. Mar. Biol. Annu. Rev.* **30:** 337–441.
6. **Stein, J. L., M. Haygood, and H. Felbeck. 1990.** Nucleotide sequence and expression of a deep-sea ribulose-1,5-bisphosphate carboxylase gene cloned from a chemoautotrophic bacterial endosymbiont. *Proc. Natl. Acad. Sci. USA* **87:** 8850–8854.
7. **Stein, J. L., and H. Felbeck. 1993.** Kinetic and physical properties of a recombinant RuBisCO from a chemoautrophic endosymbiont. *Mol. Mar. Biol. Biotechnol.* **2:** 280–290.
8. **Wittenberg, J. B., and D. W. Kraus. 1991.** Hemoglobins of eukaryote/prokaryote symbioses. Chapter 43, pp. 323–330, in *Structure and Function of Invertebrate Oxygen Carriers*, S. N. Vinogradov and O. H. Kapp, eds. Springer-Verlag, New York.
9. **Appleby, C. 1984.** Leghemoglobin and *Rhizobium* respiration. *Ann Rev. Plant Physiol.* **35:** 443–478.
10. **Kraus, D. W., and J. B. Wittenberg. 1990.** Hemoglobins of the *Lucina pectinata*/bacteria symbiosis. I. Molecular properties, kinetics and equilibria of reactions with ligands. *J. Biol. Chem.* **265:** 16043–16053.
11. **Kraus, D. W., J. B. Wittenberg, J. F. Lu, and J. Peisach. 1990.** Hemoglobins of the *Lucina pectinata*/bacteria symbiosis. II. An electron paramagnetic resonance and optical spectral study of the ferric proteins. *J. Biol. Chem.* **265:** 16054–16059.
12. **Hockenhull-Johnson, J., M. S. Stern, P. Martin, C. Dass, D. M. Desiderio, J. B. Wittenberg, S. N. Vinogradov, and D. A. Walz. 1991.** The amino acid sequence of hemoglobin II from the symbiont-harboring clam *Lucina pectinata*. *J. Protein Chem.* **10:** 609–622.
13. **Hockenhull-Johnson, J. D., M. S. Stern, J. B. Wittenberg, S. N. Vinogradov, O. H. Kapp, and D. A. Walz. 1993.** The amino acid sequence of hemoglobin III from the symbiont-harboring clam, *Lucina pectinata*. *J. Protein Chem.* **12:** 261–277.
14. **Rizzi, M., J. B. Wittenberg, A. Coda, M. Fasano, P. Ascenzi, and M. Bolognesi. 1994.** Structure of the sulfide-reactive hemoglobin from the clam *Lucina pectinata*. Crystallographic analysis at 1.5 Å resolution. *J. Mol. Biol.* **244:** 86–89.
15. **Wittenberg, J. B. 1991.** Functions of cytoplasmic hemoglobins and myohemerythrin. Chapter 3, pp. 59–85 in *Advances in Comparative and Environmental Physiology*, Vol. 13: *Oxygen Carriers in Blood and Tissues*. C. P. Mangum, ed. Springer Verlag, Berlin, Heidelberg, New York.
16. **Arp, A. J., J. J. Childress, and R. D. Vetter. 1987.** The sulfide-binding protein in the blood of the vestimentiferan tube-worm, *Riftia pachyptila*, is the extracellular haemoglobin. *J. Exp. Biol.* **128:** 139–158.
17. **Doeller, J. E., D. W. Kraus, J. M. Colacino, and J. B. Wittenberg. 1988.** Gill hemoglobin may deliver sulfide to bacterial symbionts of *Solemya velum* (Bivalvia, Mollusca). *Biol. Bull.* **175:** 388–396.
18. **Wittenberg, J. B., and B. A. Wittenberg. 1990.** Mechanisms of cytoplasmic hemoglobin and myoglobin function. *Ann. Rev. Biophys. Biophys. Chem.* **19:** 217–241.
19. **Schuder, S., J. B. Wittenberg, B. Haseltine, and B. A. Wittenberg. 1979.** Spectrophotometric determination of myoglobin in cardiac and skeletal muscle: separation from hemoglobin by subunit-exchange chromatography. *Anal. Biochem.* **92:** 473–481.
20. **Kraus, D. W., J. E. Doeller, and J. B. Wittenberg. 1992.** Hydrogen sulfide reduction of symbiont cytochrome c_{552} in gills of *Solemya reidi* (Mollusca). *Biol. Bull.* **182:** 435–443.

Reference: *Biol. Bull.* **188:** 8–15. (February/March, 1995)

Inorganic Overgrowth of Aragonite on Molluscan Nacre Examined by Atomic Force Microscopy

R. GILES[1,*], S. MANNE[1], S. MANN[2], D. E. MORSE[3], G. D. STUCKY[4],
AND P. K. HANSMA[1,†]

[1]*Department of Physics, University of California, Santa Barbara, California 93106,*
[2]*School of Chemistry, University of Bath, Claverton Down, Bath BA2 7AY, United Kingdom,*
[3]*Marine Biotechnology Center, Marine Science Institute, University of California,*
Santa Barbara, California 93106, and [4]*Department of Chemistry,*
University of California, Santa Barbara, California 93106

Abstract. The nacre (mother-of-pearl) that forms the iridescent inner layers of mollusc shells is a highly ordered microlaminate composite of aragonite crystals and biopolymers with a strength and fracture resistance that far exceed those of the mineral crystals themselves. The processes governing the biofabrication of this material by the secretory cells of the mantle are complex and only partially understood. We have used the atomic force microscope (AFM) to investigate the aqueous solution conditions under which mineral growth can occur on the nacreous layer of the shell of the bivalve mollusc *Atrina* sp. *In situ* imaging of the mature nacre surface exposed to a pH-controlled environment of natural seawater with added carbonate ions reveals that inorganic overgrowth of aragonite can occur within the ranges of pH and inorganic ion concentrations found in the molluscan extrapallial fluid from which the mineral is produced during biological shell growth. Thus, we posit that once nucleation has occurred, nacreous tablets could grow inorganically in the extrapallial space; the role of proteins and other macromolecules may be limited to initiating growth or controlling morphology through selective adsorption and spatial constraint on the growing crystal.

Introduction

The mineral shells of a variety of molluscs are composite biomaterials consisting of crystals of calcium carbonate ($CaCO_3$) intercalated with organic materials, primarily proteins and glycoproteins (reviewed in Wilbur, 1972; Towe, 1972; Watabe, 1981; Weiner, 1986; Simkiss and Wilbur, 1989; Lowenstam and Weiner, 1989). The $CaCO_3$ occurs in two predominate crystal phases within shells: calcite and aragonite. A shell may contain one phase or the other, or both, depending on the animal species, but commonly the stronger, denser aragonite forms an inner structural layer, while calcite forms the outer layer. The inner structural layer, called nacre or mother-of-pearl, is a complex microlaminate composed of polygonal "tablets" of aragonite that measure 5 to 15 μm across, but only 0.5 to 1 μm in thickness, packed together with a thin (40 nm) "mortar" of organic macromolecules. The organic component thus amounts to a small portion of the total shell: less than 10% (Addadi and Weiner, 1992). It nevertheless is responsible for the excellent strength and resistance to crack propagation of the molluscan shell. Crystallographically, the *a* and *b* axes lie in the plane of the aragonitic tablets, with the *c* axis uniformly perpendicular to the surface.

The nacreous layer of molluscan shell has been studied extensively for several decades, principally with x-ray and electron microscopic techniques. This work has been largely successful in describing the microstructure of nacre (see Lowenstam and Weiner, 1989; Weiner, 1986; Watabe, 1981; Towe, 1972; and Wise, 1970, for reviews). Various calcium-binding, highly acidic, water-soluble proteins have been isolated from the shell in various developmental stages (Cariolou and Morse, 1988). Water-insoluble proteins from the shell have been characterized

---

Received 7 March 1994; accepted 4 November 1994.

[*] Present address: Department of Physics, Simon Fraser University, Burnaby, British Columbia, Canada V5A 1S6.

[†] Author to whom correspondence should be addressed.

with x-ray diffraction, leading to the conclusion that they resemble silk fibroin (Weiner and Traub, 1980). Both the water-soluble and the water-insoluble proteins have been proposed as multilaminar templates for the mineral tablets (Nakahara *et al.*, 1982).

The mechanism of growth of the nacreous layer is complex and not well understood. It is known that both organic and inorganic components are secreted by epithelial cells in the mantle tissue into the extrapallial space (the extracellular cavity between the mantle and the shell, which is sealed from the surrounding environment), bathing the growing shell in a mixture called the extrapallial fluid. Although the inorganic components of the extrapallial fluid are obviously necessary for mineral growth, it is not known whether they are sufficient: *i.e.*, the role of the organic components is not well known. Kitano and Hood (1962) showed that aragonite is the most favorable phase of $CaCO_3$ to nucleate in seawater supersaturated with respect to that mineral; the presence of Mg^{2+} in solution apparently acts to select aragonite over calcite. Others have measured nucleation rates of aragonite crystals in seawater and artificial extrapallial fluid (Pytkowicz, 1965; Wilbur and Bernhardt, 1984). We extended these studies by making two experimental modifications relevant to nacreous growth. First, we studied crystallization directly on a nacreous surface (rather than unseeded nucleation in solution). (Recently, Sabbides and Koutsoukos [1993] also investigated seeded growth of aragonite on a variety of substrates in seawater.) Second, we controlled both pH and total carbonate concentration simultaneously, and we compare growth conditions to those values reported for extrapallial fluid.

We have used the atomic force microscope (AFM) (Binnig *et al.*, 1986) to examine the conditions for inorganic growth of the nacre tablets. (For reviews of the AFM, see Rugar and Hansma, 1990; Sarid, 1991; Hoh and Hansma, 1992). The AFM (also known as the scanning force microscope) is a member of the family of scanning probe microscopes; these instruments form images by raster scanning a tiny probe over the surface of the sample while mapping some local interaction, such as electron tunneling or near-field optical effects, as a function of position. The AFM probe consists of a flexible cantilever, ~100 μm long, with a sharp tip attached at the end; the probe measures (through the elastic response of the cantilever) the interaction forces between the tip and the sample. The probe can thus map surface topography by scanning in gentle contact with the sample; the displacement of the cantilever (as the tip slides over surface features) is detected from the motion of a laser beam reflected from the back of the cantilever onto a position-sensing photodiode. The AFM can operate in solution and hence allows *in situ* imaging of samples from the micrometer to the nanometer scale. It recently has been applied to biomineralized composites such as diatom shells (Linder *et al.*, 1992), bone (Tao and Lindsay, 1992), teeth (Kasas *et al.*, 1993), pressed powders of clam shells and sea urchin shells (Friedbacher *et al.*, 1991), and molluscan nacre (Manne *et al.*, 1994). It has imaged *in situ* dynamic processes on relevant systems such as calcite (Gratz *et al.*, 1993; Hillner *et al.*, 1992), fluorite (Hillner *et al.*, 1993), and hydroxyapatite (Kasas *et al.*, 1993), as well as calcite growth modification in the presence of polyamino acids (Wierzbicki *et al.*, 1993) and inorganic poisons (Gratz and Hillner, 1993; Dove and Hochella, 1993). By examining the exposed aragonite surface of mature nacreous tablets for signs of growth under various solutions, we bracketed and thus defined the conditions under which aragonite growth can occur. These conditions are biologically relevant: the solutions used approximate the inorganic components of the extrapallial fluid in which new nacre is formed.

Materials and Methods

Samples of nacre from the bivalve *Atrina* sp. were kindly provided by Prof. S. Weiner at the Weizmann Institute of Science in Israel. For imaging, small pieces (approx. 1 × 0.5 × 0.1 mm) of mature nacre were prepared by mechanically cleaving a shell fragment with a razor blade and then fracturing the resulting chip down to the desired dimensions.

The solutions tested were based on natural seawater collected locally from the Pacific Ocean along the Santa Barbara coast. The water was coarsely filtered, irradiated with ultraviolet light, passed through a 0.2-μm filter, and stored at 2°–4°C in a sterilized, lightproof container until just before use. To the seawater various amounts of $NaHCO_3$ were added, and the pH was adjusted to the desired value by addition of HCl or NaOH.

Cation concentrations for the filtered seawater were measured by atomic absorption spectroscopy; total carbonate ion concentration was determined by titration with HCl. Table I lists concentrations for the measured ions (at about 20°C). These agree well with previously published concentrations for seawater (Crenshaw, 1972; Smith, 1974; Wada and Fujinuki, 1976). In addition, the cation concentrations are all within about 10% of the published values for the extrapallial fluid of bivalves. In particular, the concentration of Ca^{2+} ion we determined (Table I) is about the same as found in extrapallial fluid (Crenshaw, 1972; Wada and Fujinuki, 1976). The major difference between seawater and the inorganic composition of extrapallial fluid is the higher concentration of carbonate ion, which is approximately

Table I

Concentrations of inorganic ions in the filtered natural seawater

Ion	Concentration (m*M*) ± standard dev.
Na^+	463 ± 2
K^+	10.9 ± 0.9
Mg^{2+}	63.1 ± 1.4
Ca^{2+}	10.3 ± 0.1
Sr^+	0.085 ± 0.007
$HCO_3^- + CO_3^{2-}$ or total carbonate	2.3 ± 0.1

2-fold higher in extrapallial fluid. Therefore, only carbonate ion was added to natural seawater to create the growth solutions. A comparison of the values of ion concentrations determined for seawater and extrapallial fluid is included in Figure 5.

The samples of nacre were glued to a stainless steel disk with epikot resin and placed in the fluid cell of a commercial AFM (Nanoscope III from Digital Instruments, Santa Barbara, CA 93103). Samples were always oriented with the proximal side (the side facing the animal during life) exposed for imaging. After an appropriate area had been selected by imaging in air, growth solution was added to the fluid cell. The sample was examined for signs of growth for 15–20 min under a steady gravity flow of this solution. Typical flow rates were 5 μl/s, which corresponds to a replacement of the fluid cell volume every few seconds. The tip was then withdrawn and flow stopped for 1.5 h to allow more time for growth to occur. Only the exit line was blocked so that the cell remained in chemical contact with at least 40 ml of the solution in a reservoir above the cell. The sample was then examined again under flow for signs of growth. The procedure was repeated with an alternate growth solution; either the pH was raised while maintaining the same carbonate concentration, or *vice versa*. After growth had occurred with a given solution, only one or two more solutions could be tried with a given sample before the surface became so rough that further growth could not be analyzed. All growth experiments were conducted at about 20°C.

Results

Figure 1 shows an AFM image of the nacreous surface. Most of one polygonal tablet and portions of two others can be seen. The characteristic features of bivalve nacre (Manne *et al.*, 1994), such as concavity of the proximal tablet surfaces, a depression in the center of each of tablet, and elongate rings surrounding the depressions, are visible. Growth assessment was somewhat difficult at this scale; usually the characterization was made on the basis of images only 3-μm square, such as the area outlined in the figure.

Figure 2 illustrates the changes in surface roughness considered indicative of growth. It shows the same area (the inset in Fig. 1) before and after incubation for 1.5 h in seawater with a total carbonate concentration of 4.3 m*M*. In the sample imaged in Figure 2a, the pH was 7.9, at which point the surface had already changed somewhat from its initial appearance under plain seawater. The sample then was incubated for 1.5 h in a solution with the same total carbonate concentration, but at pH 8.1, and then shifted once more to pH 8.3. In Figure 2b the surface is shown 6 min after raising the pH to 8.3; further growth had occurred. As the images are shaded proportionally to height, the new growth can be seen by comparing the relative brightness of corresponding features in the two images; a few prominent pairs are indicated by arrows.

It is important to recognize that tip convolution (Grütter *et al.*, 1992; Allen *et al.*, 1992) dominates the growth image. This is indicated by the similarity of shape and orientation among the bumps on the surface.

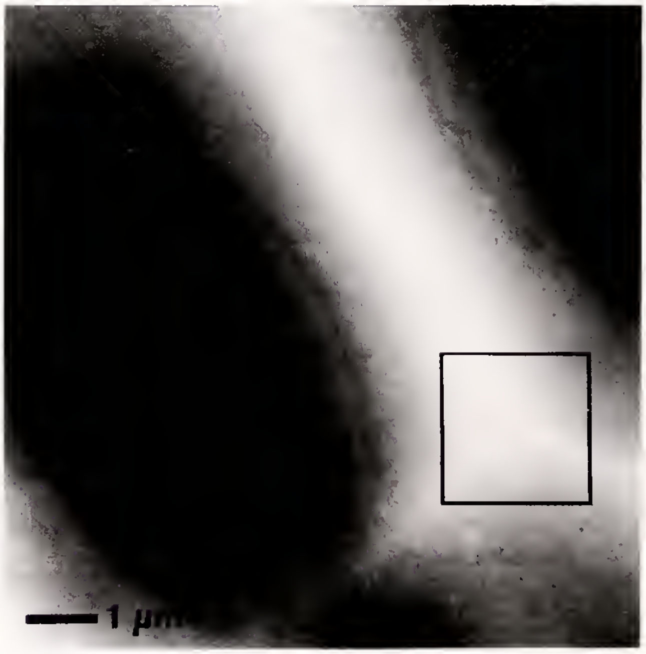

Figure 1. Atomic force microscope (AFM) image of the nacre of *Atrina* sp. The image is 11 μm². Shading is proportional to elevation, 500 nm from dark to light, with the brightest regions being the highest. The high ridge coincides with the boundary between nacreous tablets. Most of a tablet is visible in the center and left of the image, along with portions of two others. Note the general concavity, central depression and the elongate rings characteristic of bivalve nacre. The black square marks the area shown in Figure 2, centered on the intersection of the three tablet boundaries.

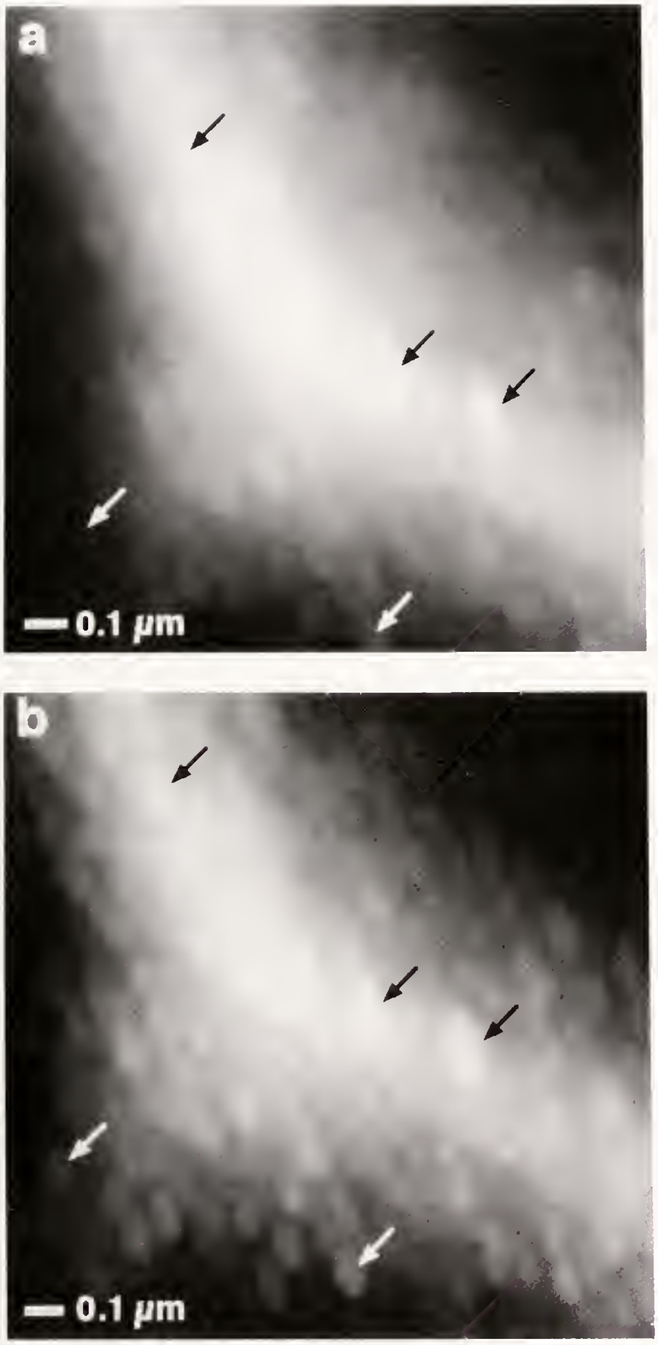

Figure 2. AFM images of the area indicated in Figure 1 before and after mineral overgrowth. Both images are 2.5 μm square; the height is 200 nm from dark to white. Comparison of corresponding features between (a) (before overgrowth) and (b) (after overgrowth) demonstrates the characteristic increase in the height of the surface asperities indicative of mineral growth on the nacreous surface. Details in text. Arrows indicate corresponding prominent asperities in the two images. These images demonstrate the topographic changes used to characterize specific solution conditions as productive of mineral overgrowth (Fig. 5).

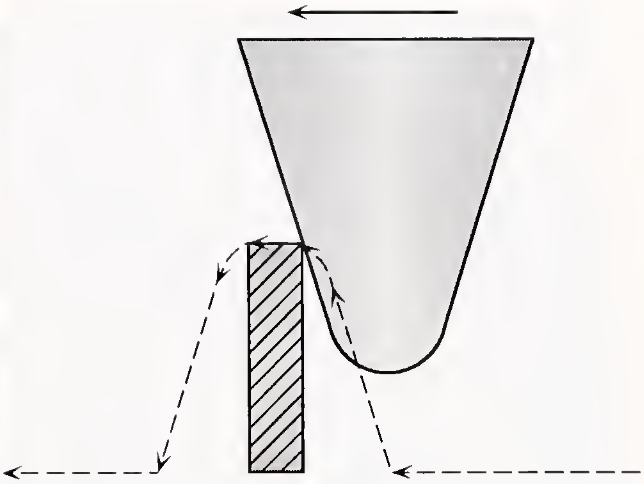

Figure 3. Illustration of the convolution between the AFM tip and a sharp asperity on the sample surface as it is scanned. The tip is shown passing from right to left over the asperity. The measured topography (dashed line) is a "convolution" of the tip shape and the asperity; it is largely an image of the tip itself, except at the very top of the asperity. Note that while the true width of the asperity is completely obscured, the height measurement is accurate.

Tip convolution is a common AFM imaging artifact; Figure 3 illustrates the mechanism responsible for this effect. The AFM measures topography by scanning a tip over the surface and measuring the vertical deflection of that tip as it slides over surface features. However, as the tip slides over an asperity with a higher aspect ratio than the tip itself, the deflection of the tip traces the tip's profile, rather than that of the asperity. In Figure 3, the dashed line indicates the path that will be traced by the tip as it passes over an asperity. Although as a consequence of tip convolution the lateral dimensions of a sharp asperity are not resolved, the overall height of that asperity is correctly measured, as is topography on the flat top (Grütter *et al.*, 1992; Allen *et al.*, 1992); thus, reliance on changes in local height detected by the AFM is justified as a measure of mineral growth. Figure 2b is consistent with the observation of surface asperities lengthening normal to the imaging plane, as expected for aragonite needles growing in their normal crystallographic habit along the *c* axis.

Although our classification of specific solution conditions into growth/no-growth categories was based on qualitative comparison of surface topography between "before" and "after" images (of which the images in Fig. 2 are an example), this method is further supported by quantitative measurements of surface roughness. Measurements of the root-mean-square deviation of height values from their collective mean was made for corresponding areas of the images in Figure 2, as well as for

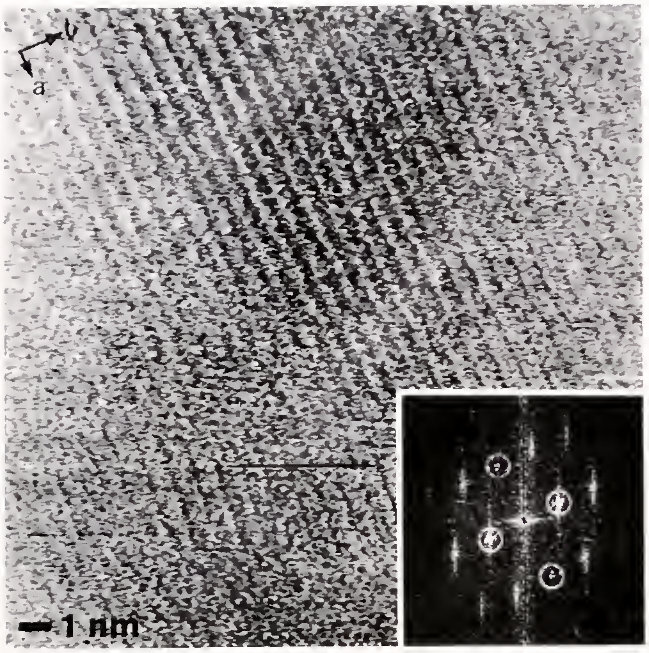

Figure 4. Unfiltered AFM image of the aragonite lattice, viewed along the *c* axis to show the (001) crystallographic plane, 30 nm square. The image was obtained on an area where overgrowth had been observed. The inset shows a Fourier transform of the image. All peaks in the transform are consistent with the expected reciprocal lattice of aragonite, and the fundamental translation vectors (circled) that define the unit cell agree with the aragonite *a* and *b* axis spacing (0.495 nm and 0.796 nm, respectively) to within 5%.

one intermediate between the two (at pH 8.1). Combining such measurements from two different areas, both away from the high tablet boundary in the center of the image, yielded a monotonically increasing surface roughness (of 2.9 nm for Fig. 2a, 3.9 nm for Fig. 2b, and 3.4 nm for the intermediate image) in agreement with the qualitative assessment of growth.

The observed changes in topography of the nacreous tablets we imaged were caused by crystal growth on the tablet surfaces, rather than by *de novo* nucleation and precipitation from the growth solution. Parallel growth experiments performed on nacreous particles embedded in epoxy showed changes in surface roughness (growth of crystal asperities) only on the nacre, and not on the surrounding epoxy. These results are described in detail elsewhere (Giles *et al.*, 1993).

Atomic lattice resolution could sometimes be obtained atop the asperities, indicating that they are terminated by small (<50 nm) flat areas. However, a wide variety of lattices were observed, perhaps indicating the presence of high-index planes on the sidewalls of the asperities. Occasionally lattices (Fig. 4) did show periodicities corresponding to the expected unit cell of the (001) plane of aragonite (*i.e.*, viewed along the *c* axis).

Figure 5 presents a summary of the growth results. The dashed lines separate the values of total carbonate concentration and pH that define the growth and no-growth conditions. The rectangular bands designate the ranges of these values previously reported for molluscan extrapallial fluid and natural seawater. Note that growth never occurs at the carbonate concentrations of seawater, but that the boundary between growth and no-growth cuts across the extrapallial fluid range, suggesting the potential for dynamic control of shell formation by changes in extrapallial fluid composition. This is consistent with previous data on seasonal variation in the acidity of the extrapallial fluid, in which high pH was correlated with a high rate of shell growth and low pH with slow growth or shell dissolution (Wada, 1961).

Supersaturation values of specific ions with respect to aragonite were estimated with the IONPRODUCT computer program (Shellis, 1988) for each of the solutions tested. Saturation fractions ranged from 0.3 to 3.6, but in general (with two exceptions) overgrowth occurred at saturation values greater than 1, and no overgrowth occurred at saturation values less than 1.

Discussion

The nacre of molluscan shell is a highly organized microlaminate composite of proteins, glycoproteins, and calcium carbonate crystals in the aragonite phase; the

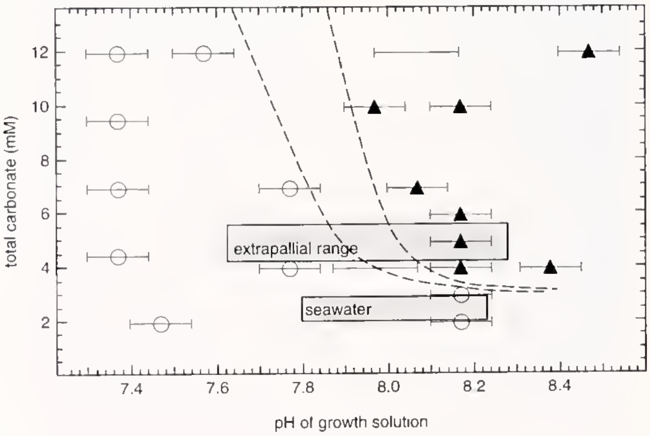

Figure 5. Aragonite growth/no-growth results as a function of pH and total carbonate concentration ($[HCO_3^-] + [CO_3^{2-}]$). Open circles indicate conditions at which no growth was observed; filled triangles indicate conditions at which growth occurred; no symbol (two horizontal lines) indicates indeterminate results. Error bars account for pH drift over the course of the 1.5 h incubation. Dashed curves approximately separate the regions of growth and no growth. The labeled bands indicate the ranges of published values for molluscan extrapallial fluid and natural seawater. Note that the range for extrapallial fluid, in which shell growth occurs biologically, spans the boundary between the growth and no-growth conditions.

biological mechanisms that control its formation are complex and only partially understood. Previous research (Wilbur, 1972; Weiner, 1986; Lowenstam and Weiner, 1989; Simkiss and Wilbur, 1989; Weiner and Addadi, 1991; Addadi and Weiner, 1992) suggests that shell mineralization commences with isolation of the site of mineralization from the external seawater environment by an insoluble matrix of macromolecules and the mantle tissue from which these molecules are secreted as an extension of the growing shell edge. The shell and the mantle epithelium enclose the extrapallial fluid, which is ionically enriched and pH-controlled by enzymatic pumping across the cell membranes of the mantle epithelium (Weiner and Traub, 1984; Weiner and Addadi, 1991). It has been suggested that insoluble matrix molecules play essential roles both in the control of crystal nucleation and by establishing compartments that limit the spaces in which the crystals grow (*e.g.*, Wilbur, 1972; Weiner, 1984; Nakahara, 1989). New aragonite crystals on the growth surface seem to be nucleated in pores of the organic matrix (Nakahara *et al.*, 1982), forming as small crystallites that grow to become the next nacreous layer (Wada, 1972). Crystal growth apparently also is controlled by several polyanionic proteins found associated with (and in some cases, occluded within) the mineral crystals; these proteins also have been suggested to act both in nucleation and in selective inhibition of crystal growth (Addadi and Weiner, 1985; Sikes and Wheeler, 1988; Addadi *et al.*, 1990; Weiner and Addadi, 1991; Morse *et al.*, 1993; Albeck *et al.*, 1993; Berman *et al.*, 1993).

The experiments reported here demonstrate that an exposed surface of mature nacre can continue to grow by purely inorganic means when the ion concentrations present in the extrapallial fluid favor the aragonite phase (primarily due to the presence of magnesium) and are supersaturated with respect to that form. This indicates that once the nucleation of the mineral phase has begun, the crystal can continue to grow without direct biological control. Therefore the requirements for nucleation, possibly including a template of acidic proteins (Aizenberg *et al.*, 1994; Morse *et al.*, 1993; Weiner *et al.*, 1983) or mineral bridges between the aragonite tablets (Manne *et al.*, 1994), can be independent of growth. Because the supersaturation levels required for overgrowth can be quite low, it is plausible that cells of the mantle could regulate growth simply by adjusting carbonate concentration and pH in the extrapallial fluid.

Although evidence for growth was decisive in most of the observed cases, quantification of the rates of mineral growth proved difficult since growth was not observed to occur uniformly over the experimental period. In some instances, growth occurred in the first few minutes of imaging after introducing a solution; in others, growth was not apparent until after the 1.5-h incubation. Unlike the case of the cleavage plane of geological calcite (Hillner *et al.*, 1993), on which growth occurs by quantifiable accretion of widely spaced steps, the aragonite tablet is much rougher and has a far greater step density. This high concentration of reactive sites may set up complex concentration gradients that affect the reaction rate in unpredictable ways.

It is interesting that the aragonitic overgrowth of nacre occurred in the form of needlelike extensions of the (001) surface, rather than as the layered growth characteristic of nacreous tablets in molluscan shells. The former is the common growth morphology of abiogenic aragonite and often results in extensive lateral intergrowth, producing fanlike aggregates of misaligned needles. Development of the highly coherent tablet morphology found in biogenic nacre, characterized by a high degree of orientation of the crystallographic *c* axes of the aragonite tablets, thus would require suppression of the tendency for disorder observed in the overgrowth process seen in our experiments. One possibility is that the highly anionic, soluble proteins (and possibly other macromolecules) found intimately associated with the aragonite crystals in molluscan nacre may prevent long-range incoherent intergrowth of the needles by specific interactions at the growing crystal surfaces (Addadi and Weiner, 1985). This would produce the coherent (001) surface and single crystal composition observed in mature nacre. In addition, the insoluble polymers of the matrix may help determine the final crystal form by creating a preformed microstructure that delimits the space in which the tablets grow (Wada, 1972; Nakahara, 1989). As neither the soluble acidic proteins nor empty sheaths of the insoluble matrix proteins were present in our experiments, growth along the *c* axis was persistently the fastest, as in abiogenic aragonite.

Acknowledgments

We thank Robert Petty (of the Marine Science Institute Analytical Laboratory, University of California, Santa Barbara) for performing the atomic absorption measurements; Monika Fritz, Angela Belcher, Charlotte Zaremba, and Deron Walters for useful discussions; and J. M. Didymus (School of Chemistry, University of Bath, UK) for kindly performing the calculations of supersaturation fractions. This work was supported by grants from the Materials Research Laboratory program of the National Science Foundation (DMR-9123048); the Molecular and Cellular Biosciences and Materials Research Divisions of the National Science Foundation (MCB-9202775 to G.D.S., D.E.M., and P.K.H.); the

Office of Naval Research (N00014-93-1-0584 to D.E.M., G.D.S., and P.K.H.); and a fellowship from AT&T (S. Manne).

Literature Cited

Addadi, L., and S. Weiner. 1985. Interactions between acidic proteins and crystals: stereochemical requirements in biomineralization. *Proc. Natl. Acad. Sci. USA* **82:** 4110–4114.

Addadi, L., and S. Weiner. 1992. Control and design principles in biological mineralization. *Angew. Chem. Int. Ed. Engl.* **31:** 153–169.

Addadi, L., A. Berman, J. Moradian-Oldak, and S. Weiner. 1990. Tuning of crystal nucleation and growth by proteins: molecular interactions at solid-liquid interfaces in biomineralization. *Croat. Chem. Acta* **63:** 539–544.

Aizenberg, J., S. Albeck, S. Weiner, and L. Addadi. 1994. Crystal-protein interactions studied by overgrowth of calcite on biogenic skeletal elements. *J. Crystal Growth* **142:** 156–164.

Albeck, S., J. Aizenberg, L. Addadi, and S. Weiner. 1993. Interactions of various skeletal intracrystalline components with calcite crystals. *J. Am. Chem. Soc.* **115:** 11691–11697.

Allen, M. J., N. V. Hud, M. Balooch, R. J. Tench, W. J. Siekhaus, and R. Balhorn. 1992. Tip-radius artifacts in AFM images of protamine-complexed DNA fibers. *Ultramicroscopy* **42–44:** 1095.

Berman, A., J. Hanson, L. Leiserowitz, T. F. Koetzle, S. Weiner, and L. Addadi. 1993. Biological control of crystal texture: a widespread strategy for adapting crystal properties to function. *Science* **259:** 776–777.

Binnig, G., C. F. Quate, and Ch. Gerber. 1986. Atomic Force Microscope. *Phys. Rev. Lett.* **56:** 930–933.

Cariolou, M. A., and D. E. Morse. 1988. Purification and characterization of calcium-binding conchiolin shell peptides from the mollusc, *Haliotis rufescens,* as a function of development. *J. Comp. Physiol. B* **157:** 717–729.

Crenshaw, M. A. 1972. The inorganic composition of molluscan extrapallial fluid. *Biol. Bull.* **143:** 506–512.

Dove, P. M., and M. F. Hochella Jr. 1993. Calcite precipitation mechanisms and inhibition by orthophosphate: *in situ* observations by scanning force microscopy. *Geochim. Cosmochim. Acta* **57:** 705–714.

Friedbacher, G., P. K. Hansma, E. Ramli, and G. D. Stucky. 1991. Imaging powders with the atomic force microscope: from biominerals to commercial materials. *Science* **253:** 1261–1263.

Giles, R., S. Manne, C. M. Zaremba, A. Belcher, S. Mann, D. E. Morse, G. D. Stucky, and P. K. Hansma. 1993. Imaging single nacreous tablets with the atomic force microscope. *Materials Res. Soc. Proc.* **332:** (Boston, Fall 1993, in press).

Gratz, A. J., and P. E. Hillner. 1993. Poisoning of calcite growth viewed in the AFM. *J. Crystal Growth* **129:** 789–793.

Gratz, A. J., P. E. Hillner, and P. K. Hansma. 1993. Step dynamics and spiral growth on calcite. *Geochim. Cosmochim. Acta* **57:** 491–495.

Grütter, P., W. Zimmermann-Edling, and D. Brodbeck. 1992. Tip artifacts of microfabricated force sensors for atomic force microscopy. *Appl. Phys. Lett.* **60:** 2741–2743.

Hillner, P. E., A. J. Gratz, S. Manne, and P. K. Hansma. 1992. Atomic scale imaging of calcite growth and dissolution in real time. *Geology* **20:** 359–362.

Hillner, P. E., S. Manne, A. J. Gratz, and P. K. Hansma. 1993. Atomic force microscope: a new tool for imaging crystal growth processes. *Faraday Discuss. Chem. Soc.* **95:** 191–197.

Hoh, J. H., and P. K. Hansma. 1992. Atomic Force Microscopy for high-resolution imaging in cell biology. *Trends Cell Biol.* **2:** 208–213.

Kasas, S., A. Berdal, and M. R. Celio. 1993. Tooth structure studied using the atomic force microscope. *Scanning Probe Microscopies II,* C. C. Williams, ed., *Proc. SPIE* **1855:** 17–25.

Kitano, Y., and D. W. Hood. 1962. Calcium carbonate crystal forms formed from seawater by inorganic processes. *J. Oceanogr. Soc. JPN* **18:** 35–39.

Linder, A., J. Colchero, H.-J. Apell, O. Marti, and J. Mlynek. 1992. Scanning force microscopy of diatom shells. *Ultramicroscopy* **42–44:** 329–332.

Lowenstam, H. A., and S. Weiner. 1989. *On Biomineralization.* Oxford University Press, New York.

Manne, S., C. M. Zaremba, R. Giles, L. Huggins, D. A. Walters, A. Belcher, D. E. Morse, G. D. Stucky, J. M. Didymus, S. Mann, and P. K. Hansma. 1994. Atomic force microscopy of the nacreous layer in mollusc shells. *Proc. R. Soc. Lond. B* **256:** 17–23.

Morse, D. E., M. A. Cariolou, G. D. Stucky, C. M. Zaremba, and P. K. Hansma. 1993. Genetic coding in biomineralization of microlaminate composites. In *Biomolecular Materials,* C. Viney, S. T. Case, and J. H. Waite, eds. *Materials Res. Soc. Proc.* **292:** 59–67.

Nakahara, H. 1989. Nacre formation in bivalve and gastropod molluscs. Pp. 343–350 in *Mechanisms and Phylogeny of Mineralization in Biological Systems,* S. Suga and H. Nakahara, eds. Springer-Verlag, New York.

Nakahara, H., G. Bevelander, and M. Kakei. 1982. Electron microscopic and amino acid studies on the outer and inner shell layers of *Haliotis rufescens. Venus* **41:** 33–46.

Pytkowicz, R. M. 1965. Rates of inorganic calcium carbonate nucleation. *J. Geol.* **73:** 196–199.

Rugar, D., and P. K. Hansma. 1990. Atomic Force Microscopy. *Physics Today* **43:** 23–30 (October).

Sabbides, T. G., and P. G. Koutsoukos. 1993. The crystallization of calcium carbonate in artificial seawater; role of the substrate. *J. Crystal Growth* **133:** 13–22.

Sarid, D. 1991. *Scanning Force Microscopy: With Applications to Electric, Magnetic, and Atomic Forces.* Oxford University Press, New York.

Sikes, C. S., and A. P. Wheeler. 1988. Regulators of biomineralization. *Chemtech* **1988:** 620–626.

Simkiss, K., and K. M. Wilbur. 1989. *Biomineralization.* Academic Press, New York.

Shellis, R. P. 1988. A microcomputer program to evaluate the saturation of complex solutions with respect to biominerals. *Cambios* **4:** 373–379.

Smith, F. G. W., ed. 1974. *CRC Handbook of Marine Science,* Vol. 1, p. 4. CRC Press, Cleveland, Ohio.

Tao, N. J., and S. M. Lindsay. 1992. Measuring the microelastic properties of biological material. *Biophys. J.* **63:** 1165–1169.

Towe, K. M. 1972. Invertebrate shell structure and the organic matrix concept. *Biomineralisation* **4:** 1–14.

Wada, K. 1961. Crystal growth of molluscan shells. *Bull. Natl. Pearl Res. Lab. JPN* **7:** 703–828.

Wada, K. 1972. Nucleation and growth of aragonite crystals in the nacre of some bivalve molluscs. *Biomineralisation* **6:** 141–159.

Wada, K., and T. Fujinuki. 1976. Biomineralization in bivalve molluscs with emphasis on the chemical composition of the extrapallial fluid. Pp. 175–190 in *The Mechanisms of Mineralization in the Invertebrates and Plants,* N. Watabe and K. M. Wilbur, eds. University of South Carolina Press, Columbia, South Carolina.

Watabe, N. 1981. Crystal growth of calcium carbonate in the invertebrates. *Prog Crystal Growth Charact.* **4:** 99–147.

Weiner, S. 1984. Organization of organic matrix components in mineralized tissues. *Am. Zool.* **24:** 945–952.

Weiner, S. 1986. Organization of extracellularly mineralized tissues: a comparative study of biological crystal growth. *CRC Crit. Rev. Biochem.* **20:** 365–408.

Weiner, S., and L. Addadi. 1991. Acidic macromolecules of mineralized tissues: the controllers of crystal formation. *Trends Biochem. Sci.* **16:** 252–256.

Weiner, S., and W. Traub. 1980. X-ray diffraction study of the insoluble organic matrix of mollusk shells. *FEBS Lett.* **111:** 311–316.

Weiner, S., and W. Traub. 1984. Macromolecules in mollusc shells and their functions in biomineralization. *Phil. Trans. R. Soc. Lond B* **304:** 425–434.

Weiner, S., Y. Talmon, and W. Traub. 1983. Electron diffraction of mollusc shell organic matrices and their relationship to the mineral phase. *Int. J Biol. Macromol.* **5:** 325–328.

Wierzbicki, A., C. S. Sikes, J. D. Madura, and B. Drake. 1993. Atomic force microscopy and molecular modeling of protein and peptide binding to calcite. *Calcif. Tiss. Int.* **54:** 133–141.

Wilbur, K. M. 1972. Shell formation in mollusks. Pp. 103–145 in *Chemical Zoology, Vol. 6: Mollusca,* M. Florkin and B. T. Scheer, eds. Academic Press, New York.

Wilbur, K. M., and A. M. Bernhardt. 1984. Effects of amino acids, magnesium, and molluscan extrapallial fluid on crystallization of calcium carbonate: *in vitro* experiments. *Biol. Bull.* **166:** 251–259.

Wise, S. W. 1970. Microarchitecture and mode of formation of nacre (mother-of-pearl) in pelecypods, gastropods, and cephalopods. *Eclogae Geol. Helv.* **63:** 775–797.

Reference: *Biol. Bull.* **188:** 16–22. (February/March, 1995)

Direct Development in the Ascidian *Molgula retortiformis* (Verrill, 1871)

WILLIAM R. BATES*

Department of Biology, Carleton University, Ottawa, Ontario, Canada K1S 5B6, and Huntsman Marine Science Centre, St. Andrews, New Brunswick, Canada E0G 2X0

Abstract. The cellular features of the ascidian *Molgula retortiformis* (Verrill, 1871), a direct developing species, were investigated with the aid of transmission electron microscopy, histochemistry, and immunocytochemistry. Developmental comparisons between direct and indirect developing ascidians will further our understanding of how developmental processes evolve. *M. retortiformis* eggs are surrounded by a follicular envelope comprising a layer of outer follicle cells attached to an acellular chorion. The cytoplasm of *M. retortiformis* eggs contains large quantities of yolk and glycogen. Immediately after hatching, at day 2.5 of development, the cells constituting a juvenile exhibited similar ultrastructural features, except that the larger, deeper cells contained more yolk and glycogen than the epidermal cells. Differentiated muscle cells were absent in newly hatched *M. retortiformis* juveniles, and acetylcholinesterase (AChE) activity was not detected. Immunocytochemistry experiments using a vertebrate intermediate filament antibody (NN18) support the idea that the failure of newly hatched *M. retortiformis* juveniles to develop muscle cells may be due to the absence of a factor localized in the egg myoplasm. This paper concludes with a discussion of the "substrate hypothesis" and the evolution of ascidian direct development.

Introduction

Most ascidians produce eggs that develop into chordate larvae that swim for a brief time and subsequently metamorphose into adults. During metamorphosis the chordate features of a larva are selectively destroyed, and the adult morphology develops (Grave, 1935; Cloney, 1978, 1982). Ascidians that produce swimming larvae are termed indirect-developing species. In striking contrast to indirect-developing species, about a dozen species produce fertilized eggs that develop directly into juveniles, bypassing the development of a swimming larva (de Lacaze-Duthiers, 1874; Berrill, 1931; Jeffery and Swalla, 1990; Bates and Mallett, 1991a). Here I report on the cellular features of a direct-developing species, *Molgula retortiformis*.

N. J. Berrill (1931) wrote that *M. retortiformis* has a direct mode of development; however, he provided only one line drawing of a juvenile. His drawing shows a *M. retortiformis* juvenile without a tail, lacking a sensory vesicle, having partially extended epidermal ampullae, and containing a cluster of large, opaque cells, which he terms "tail phagocytes," in the posterior region. Aside from these general features, no information was given on the cellular features of eggs, embryos, and juveniles in this species. Although Berrill was not concerned primarily about the cellular features of direct-developing ascidians, he was among the first to recognize that comparisons between indirect and direct modes of ascidian development can provide valuable insights about chordate evolution. In his 1931 paper, Berrill suggested that direct development in ascidians evolved by the elimination of the larval sensory vesicle and larval tail structures. He argued that the development of a swimming tadpole larva capable of selecting a habitat would be unnecessary if the adult lived in a uniform habitat. This idea, which is termed the "substrate hypothesis," is based primarily on studies of *Molgula occulta*, a direct-developing species that inhabits the sand flats of Brittany. I reexamine Berrill's substrate hypothesis in the present study of *M. retortiformis*.

Interest in ascidian direct development was renewed when Whittaker (1979) reported that *Molgula arrenata* embryos, embryos exhibiting direct development, can express acetylcholinesterase despite the lack of tail development. AChE activity in a species with direct develop-

---

Received 18 January 1994; accepted 4 November 1994.

* Present address: Bamfield Marine Station, Bamfield, British Columbia, Canada V0R 1B0

ment suggested to Whittaker that AChE activity is a vestigial trait that has not been eliminated from an ancestral program responsible for larval muscle cell development. The present study tested the possibility that newly hatched *M. retortiformis* juveniles can express AChE activity. Just-hatched tadpoles from three indirect-developing species, *Halocynthia pyriformis, Boltenia echinata,* and *Ciona intestinalis,* were also tested for AChE activity.

Since the publication of Whittaker's exciting results in 1979, a number of studies on ascidian direct development have been reported, including those by Young *et al.* (1988), Jeffery and Swalla (1990, 1991, 1992), Bates and Mallett (1991a,b), Bates (1991), and others. In 1988, Young *et al.* were the first to report that *Molgula pacifica* is a direct developer. Many of the cellular features of *M. pacifica* development have been described (Bates and Mallett, 1991a,b; Bates, 1991, 1993). The postfertilization movements of the egg cytoplasm, termed ooplasmic segregation, and early cleavage patterns in *M. pacifica* were similar to those in eggs and embryos having indirect development. Although most features of early development were similar to those in indirect developers, ampulla development in *M. pacifica* juveniles was triggered *before* hatching (Bates and Mallett, 1991a; Bates, 1993, 1994) instead of after larval settlement (Cloney, 1978; Grosberg, 1981; Grosberg and Quinn, 1986).

The elimination of larval muscle cell development in direct-developing ascidians was recently studied in *Molgula oculata* (an indirect-developer) and *Molgula occulta* (a direct-developer), the same species studied by Berrill (1931). Results of these studies suggested that the lack of larval muscle cell development in *M. occulta* may be due to the absence of a protein that is recognized by a vertebrate intermediate filament antibody (NN18) localized in the myoplasm of *M. oculata* eggs (Swalla *et al.*, 1991). In the present study, I used *M. retortiformis* and an indirect-developing species, *Boltenia villosa,* to test the correlation between the antigen recognized by NN18 and AChE activity.

In summary, the threefold aim of the present study was (1) to examine the general cellular features of *M. retortiformis* eggs, embryos, and juveniles; (2) to determine if there is a correlation between AChE activity and a factor localized in the egg myoplasm that reacts with NN18 in *M. retortiformis* juveniles and *B. villosa* tadpoles; and (3) to test Berrill's substrate hypothesis by examining the habitats of *M. retortiformis* adults.

Materials and Methods

Collection of adults, eggs and sperm, and embryo cultures

Molgula retortiformis, Halocynthia pyriformis, Boltenia echinata, and *Ciona intestinalis* adults were collected in the Bay of Fundy near Huntsman Marine Station, St. Andrews, New Brunswick, Canada. Collections were made with a dredge at depths ranging from 50 to 100 feet. *Boltenia villosa* adults were purchased from Westwind Sealab Supplies, Victoria, British Columbia. Adults were maintained in aquaria containing flowing seawater under conditions of constant light to prevent spawning. Testes and ovaries were removed from adults and placed in a Syracuse dish containing seawater; eggs and sperm were collected by using forceps to macerate the gonads. Van Name (1945) described *M. retortiformis* (Verrill, 1871). The testis on the left side of an adult was situated alongside the inner side of the lower branch of the intestinal loop and the left ovary was situated outside the intestinal loop along the upper branch of the intestinal loop. On the right side, the testis was situated ventral to the kidney and the ovary was situated along the dorsal border of the kidney. Fertilized eggs were obtained by mixing together eggs and sperm from two or more individuals in a Syracuse dish containing Millipore-filtered seawater. Eggs were inseminated for 10 min, washed with large volumes of seawater, and cultured at 11°C. Embryos were viewed at frequent intervals with an Olympus SZ stereomicroscope.

Transmission electron microscopy

Embryos and juveniles were prepared for light microscopy and transmission electron microscopy as previously described by Bates and Mallett (1991a). Specimens were fixed in 2% glutaraldehyde in 0.1 *M* sodium phosphate buffer, pH 7.4, for 30 min. After a wash in the same buffer, the specimens were immersed in 1% osmium tetroxide in the same buffer for 1 h. Specimens were dehydrated through a graded series of ethanol dilutions (10%–100%), then immersed in propylene oxide and gradually infiltrated with Spurr low-viscocity resin. Thick and thin sections were cut; the thick sections were stained with methylene blue and azure B, and the thin sections were immersed in uranyl acetate. The thin sections were viewed with a Phillips electron microscope at 80 kV. As a positive control, hatched *B. villosa* larvae were prepared for transmission electron microscopy along with hatched *M. retortiformis* juveniles. In every *B. villosa* preparation examined, sarcomeres were clearly evident within the tail muscle cells.

Acetylcholinesterase histochemistry

Day 2 *M. retortiformis* juveniles, *Boltenia echinata, Halocynthia pyriformis,* and *Ciona intestinalis* larvae were tested for acetylcholinesterase activity as previously described by Karnowski and Roots (1964), Whittaker (1973), and Bates and Jeffery (1987). Wholemount preparations were viewed with an Olympus microscope and photographed with Plus X film.

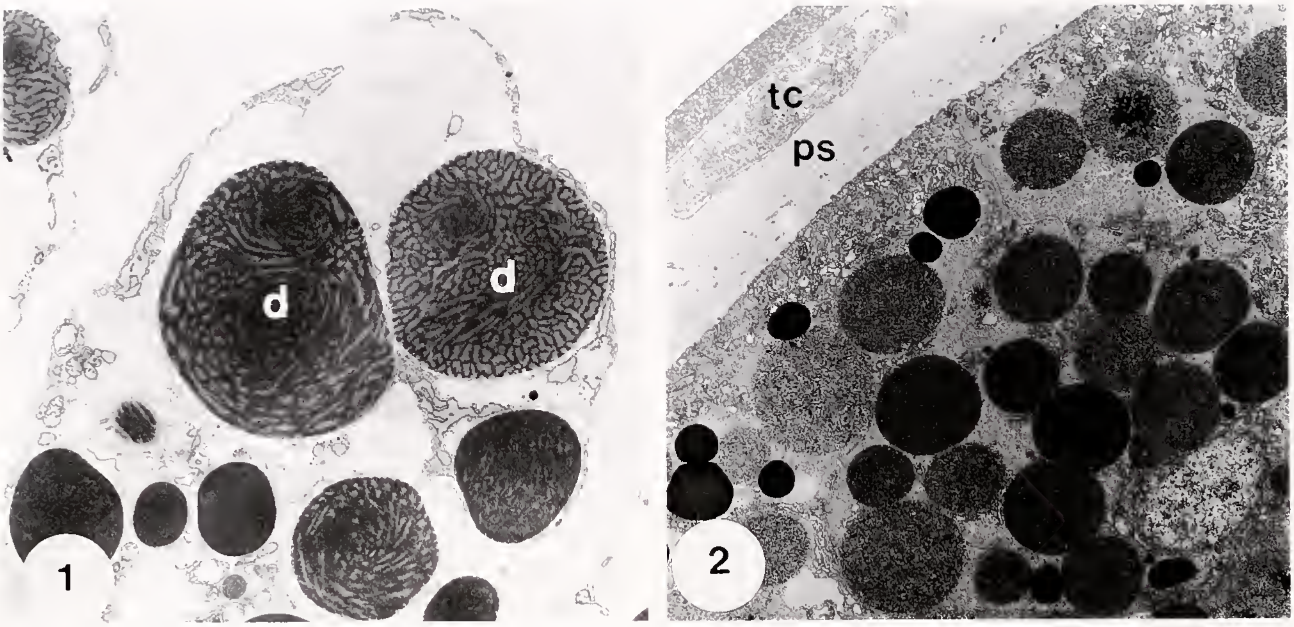

Figures 1 and 2. Transmission electron micrographs of a sectioned *Molgula retortiformis* follicle cell (1) and a sectioned *M. retortiformis* gastrula (2). The swirl patterns of follicle cell droplets (d) are evident in (1) and a test cell (tc) is seen within the perivitelline space (ps) in (2). × 3300 in (1) and in (2).

Immunocytochemistry

M. retortiformis and *B. villosa* eggs were prepared for immunocytochemistry, as previously described by Mita-Miyazawa *et al.* (1987). Eggs were immersed for 20 min in absolute methanol, and then for 20 min in cold absolute ethanol. Fixed eggs were infiltrated with 50% polyester wax (BDH Limited, Poole, England): absolute ethanol for 1 h at 40°C and then infiltrated with 100% polyester wax for 1 h at 40°C. Specimens were embedded in BEEM capsules, and 8-μm sections were cut from the blocks. Sections were mounted on gelatin-coated coverslips, de-waxed through a graded series of ethanol dilutions (100%; 90%; 80%; 70%; 50%; 30%), and rinsed in phosphate buffered saline (PBS). The specimens were incubated with a monoclonal antibody (1:25 dilution of NN18 from Sigma Chemicals) for 1 h at room temperature, washed with PBS, and incubated for 50 min in a 1:60 dilution of FITC-conjugated IgG (Sigma Chemical Company), as previously described by Swalla *et al.* (1991). The specimens were washed in PBS for 30 min, mounted in 80% glycerol dissolved in PBS, and viewed with an Olympus fluorescence microscope. Sections were photographed with Tri X film, ASA 400.

Results

A large population of *M. retortiformis* adults was discovered living on an underwater hill near Huntsman Marine Station at a depth of 50–100 feet. The animals were attached directly to rocks and lived close to several other ascidian species, *Boltenia ovifera, Molgula citrina, Ascidia callosa,* and *Halocynthia pyriformis.* The *M. retortiformis* adults collected from the underwater hill ranged from about 20 to 75 mm in diameter. Only a few specimens were collected from sand and gravel sites dredged near the underwater hill, suggesting that *M. retortiformis* adults prefer a hard substrate.

Maximum egg diameters (not including the surrounding follicular envelope) were 230–240 μm. The ultrastructural features of *M. retortiformis* follicle cells are shown in Figure 1. The cytoplasm of follicle cells contained droplets of various sizes, the contents of which display swirl patterns. Follicle cells are attached to an acellular chorion separated from the plasmalemma of the egg by a narrow perivitelline space. Cells within the perivitelline space, termed test cells, were observed in a few sections (Fig. 2).

The cytoplasm of *M. retortiformis* eggs contains large quantities of yolk and glycogen. After an egg was cross-fertilized, a thick coat of sticky adhesive material anchored it to the bottom of the glass culture dish. Fertilization triggered a rapid rearrangement of the egg cytoplasm, known as ooplasmic segregation. Opaque cytoplasm moved into one region of the egg and subsequently, just before first cleavage, formed a narrow belt of opaque cytoplasm in the equatorial region. Unlike the eggs of several other species, including *B. villosa,* the egg of *M. retortiformis* does not have colored pigment granules in its cortex. In some of the fertilized eggs, ooplasmic movements

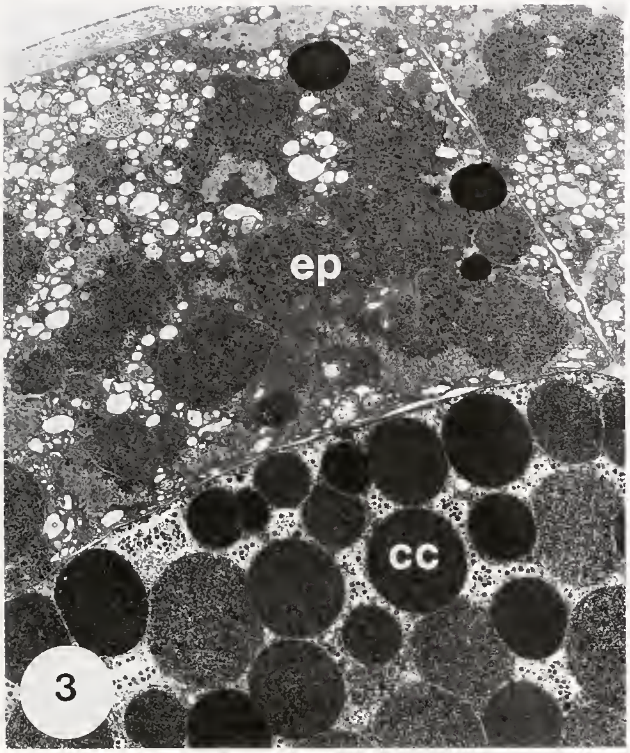

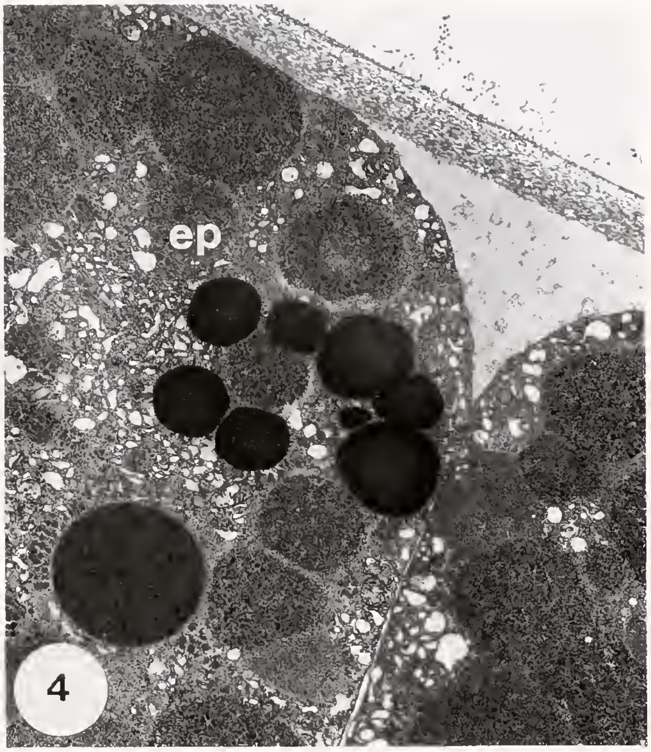

Figures 3 and 4. Transmission electron micrographs of sectioned *Molgula retortiformis* gastrulae showing the outer epidermal cells (ep) containing less yolk and glycogen than the large, centrally located cells (cc). × 3300 in Fig. 3; × 4900 in Fig. 4.

were accompanied by changes in the overall shape of the egg.

The early cleavage patterns exhibited by *M. retortiformis* embryos appeared similar to those exhibited by other ascidian embryos. The first cleavage plane bissected the narrow belt of ectoplasm into two equal regions. The two equal-sized blastomeres of a two-celled embryo continued cell division and formed a gastrula. Cells in the vegetal pole region invaginated in a manner similar to that seen in *Boltenia villosa* gastrulae. As a result of these vegetal cell movements, an archenteron resembling that of *B. villosa* formed. The ultrastructural features of the various cells that constitute a *M. retortiformis* gastrula are shown in Figures 3 and 4. The cytoplasm of the large, centrally located cells was packed with yolk and glycogen. Ectodermal cells contained less yolk and glycogen than these central cells. Other cell types, based on distinct ultrastructural features, were not evident.

Tail development was completely absent in *M. retortiformis.* No indication of a shape change of the posterior region or of notochord elongation was observed. Ampulla outgrowth was always triggered at a fixed time in development, immediately before hatching. Each juvenile developed a maximum of eight ampullae. Rhythmic contraction waves were evident in each ampulla by day 4 of development. Blood cells were evident within each ampullar lumen.

Figures 5 and 6 show the ultrastructural features of various cell types constituting day 2.5 juveniles. Yolk and glycogen stored in the egg cytoplasm persisted through day 2.5 of development and were not partitioned into any particular cell type, but were present in varying amounts in all cells. Epidermal cells contained fewer yolk granules and glycogen than the larger, central cells of a juvenile. Given that *M. retortiformis* juveniles do not start feeding until after one week of development, the energy required for all of the morphogenetic processes is likely derived from the large, yolky cells. These cells probably make up part of the adult rudiment. In striking contrast to species that produce planktonic larvae, in *M. retortiformis* juveniles have no differentiated muscle cells (compare Figs. 5 and 6 and Fig. 7). I tested the possibility that despite the absence of differentiated muscle cells, these juveniles might be able to express AChE activity. AChE histochemistry was performed on newly hatched *M. retortiformis* juveniles at day 2 of development and on day-2 larvae produced by *Halocynthia pyriformis, Boltenia echinata,* or *Ciona intestinalis.* The results of these experiments are shown in Figures 8 through 11 and Table I. Larvae from all three species that have indirect development showed AChE activity in tail muscle cells (Fig. 9), whereas *M. retortiformis* juveniles did not express AChE activity (Fig. 11). One hundred and sixty-three *M. retortiformis* juveniles from eight egg clutches collected during four sum-

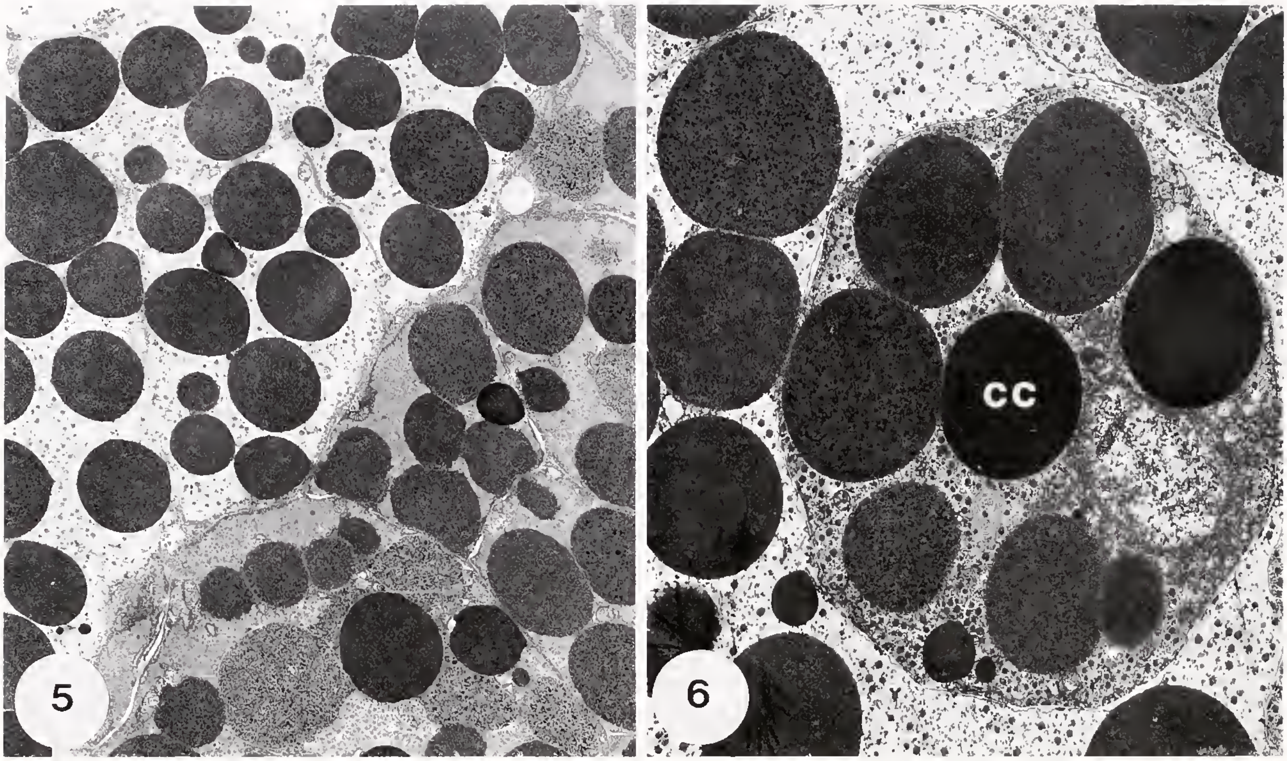

Figures 5 and 6. Transmission electron micrographs of sectioned day 2.5 *Molgula retortiformis* juveniles. Yolk and glycogen were the predominant cytoplasmic feature of juvenile cells. Centrally located cells (cc) contain large quantities of yolk and glycogen. Differentiated muscle cells were not observed in *M. retortiformis* sections. × 3300 in Fig. 5; × 4900 in Fig. 6.

mers were tested. *M. retortiformis* juveniles lack not only larval muscle cells, but also the sensory structures present in the head region of tadpole larvae. NN18, a monoclonal antibody raised to vertebrate neurofilament protein, stained the cortical region of *B. villosa* eggs (Fig. 8). In contrast, NN18 did not stain the cortical cytoplasm of *M. retortiformis* eggs (Fig. 10). More than 100 sectioned eggs from different clutches were examined together with sectioned *B. villosa* eggs.

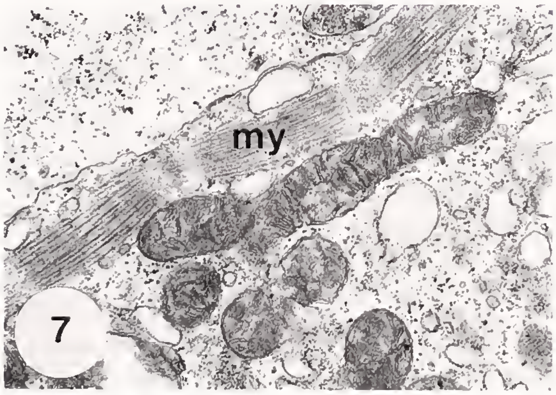

Figure 7. Transmission electron micrograph of a sectioned *Boltenia villosa* larva. Differentiated muscle cells were evident in *B. villosa* larvae, in contrast to *M. retortiformis* preparations that lacked differentiated muscle cells. my—striated myofibril. × 19,000.

Discussion

In summary, this report (1) provides new information on the ultrastructural features of *M. retortiformis* eggs, gastrulae, and day-2.5 juveniles; (2) presents ultrastructural and histochemical evidence suggesting that *M. retortiformis* embryos do not produce differentiated larval muscle cells; (3) burnishes immunocytochemical evidence that *M. retortiformis* eggs lack a cortical protein that is recognized by NN18 antibody; and (4) suggests that Berrill's substrate hypothesis is in need of revision, because *M. retortiformis* adults live on a hard, nonuniform substrate.

Large quantities of yolk and glycogen were present in the cytoplasm of eggs and most cells constituting gastrulae and day-2.5 juveniles. Two other direct-developing ascidians, *Molgula pacifica* (Bates and Mallett, 1991a,b) and *Molgula occulta* (Jeffery and Swalla, 1990), produce eggs containing large quantities of yolk and glycogen. In all three of these direct-developing molgulids, as in ascidians having indirect development (Berrill, 1975; Cloney, 1982), feeding does not begin until after the development of adult organs. Large quantities of yolk present in the cytoplasm

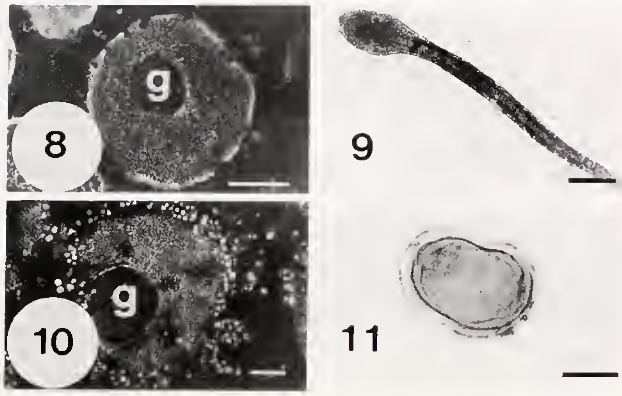

Figures 8–11. NN18 antibody staining of *Boltenia villosa* and *Molgula retortiformis* eggs and AChE expressions of *B. villosa* larvae and *M. retortiformis* juveniles. The cortical region of *B. villosa* eggs was stained with NN18 antibody (Fig. 8), whereas the cortical region of *M. retortiformis* eggs did not stain with NN18 antibody (Fig. 10). *M. retortiformis* follicle cells are autofluorescent. g—germinal vesicle. Fig. 9: Dark-stained AChE positive muscle cells in the tail of a *B. villosa* larva. Fig. 11: *M. retortiformis* juvenile exhibiting no AChE activity. Scale bars equal 50 μm in (8); 100 μm in (9); 50 μm in (10); 100 μm in (11).

of meroblastic types of eggs, such as those produced by birds and reptiles, directly affect patterns of cell division and modify cell movements associated with gastrulation. The presence of a few test cells within the perivitelline space of *M. retortiformis* eggs was surprising because such cells are thought to be involved in the development of a larval tail fin (Cloney, 1982). Despite the yolky cytoplasm of *M. retortiformis* eggs, early cell divisions were holoblastic, and gastrulation was similar to that in indirect-developing embryos containing less yolk. Vegetal pole cells invaginated to form an archenteron. In contrast, gastrulation in *M. pacifica* embryos is highly modified (Bates and Mallett, 1991a) and a typical archenteron never develops. Instead, the large, yolky endoderm cells within the central region of the embryo appear to physically impede the inward movements of vegetal pole cells.

Ooplasmic segregation movements and early cleavage patterns in *M. retortiformis* are similar to those in eggs and embryos that have indirect development (Conklin, 1905; Bates and Jeffery, 1988). Unlike the eggs produced by several species of *Styela* and by *Boltenia villosa*, the eggs of *M. retortiformis* do not contain colored pigment granules associated with the cortical region. However, the postfertilization movements of the egg cytoplasm of *M. retortiformis* could be studied in live eggs due to the presence of an opaque cytoplasm presumably derived from the contents of the germinal vesicle, as in other ascidians (Conklin, 1905). Opaque cytoplasm first accumulated in one region of the egg and was subsequently moved into the equatorial region where it spread out and formed a narrow cytoplasmic region. These cytoplasmic movements that have been described in the fertilized eggs of indirect-developing ascidians are thought to be important in the specification of cell fates and axial development (Conklin, 1905; Bates and Jeffery, 1988). It appears that in *M. pacifica* (Bates and Mallett, 1991a) and *M. retortiformis*, these precise movements of egg cytoplasm have been evolutionarily conserved.

The absence of myofilaments and AChE activity in *M. retortiformis* juveniles suggests that the developmental program responsible for the specification of larval muscle cells was eliminated. Myofilaments and AChE activity were also absent in *M. pacifica* juveniles (Bates and Mallett, 1991b). But at least two other molgulids that have direct development can express low levels of AChE activity (Whittaker, 1979; Jeffery and Swalla, 1990; Bates and Mallett, 1991b). The interpretation that AChE activity in a direct-developing ascidian is a vestige of larval muscle cell expression is based on Berrill's assumption that direct development evolved from species that have indirect development (1931). This assumption is being tested in several laboratories by comparing ascidian gene sequences. DNA sequence comparisons may suggest that *M. retortiformis* is most closely related to another molgulid that has direct development or to a molgulid with indirect development. Maybe *M. retortiformis* is closely related to *Molgula citrina*, an indirect-developing species that lives on the same underwater hill as *M. retortiformis*.

The elimination of differentiated muscle cells in *M. retortiformis* may be due to an evolutionary modification of the egg cytoskeleton, an idea first suggested by Swalla *et al.* (1991) in their study of direct-developing *M. occulta* embryos. NN18, an antibody raised to vertebrate neurofilament protein, stains the cortical myoplasmic region of *B. villosa* eggs, but did not stain *M. retortiformis* eggs. This result suggests that a cytoplasmic factor recognized by NN18 antibody, absent in *M. retortiformis* eggs, may be involved in larval muscle cell specification. The question of whether the antigens recognized by NN18 antibody are attached to the myoplasmic cytoskeletal domain, an egg cytoplasmic region thought to be involved in muscle cell specification (Jeffery and Meier, 1983), must await future studies.

Table I

The failure of newly hatched, day 2 Molgula retortiformis *juveniles to express acetylcholinesterase activity*

Species	Number tested	Number positive
Molgula retortiformis (D)	163	0
Halocynthia pyriformis (I)	65	56
Boltenia echinata (I)	78	77
Ciona intestinalis (I)	8	8

D—species with direct development; I—species with indirect development. Tested at day 2 of development.

Data collected from field sites in the Atlantic and Pacific oceans, on adults of *M. retortiformis* (present study) and *M. pacifica* (Bates and Mallett, 1991a) respectively, appear to conflict with Berrill's substrate hypothesis (1931). Berrill based his hypothesis on field and developmental studies of *Molgula occulta* (a direct developer) and *Molgula oculata* (an indirect developer), species that live on the sand-flats along the coast of Brittany. The occurrence of *M. occulta* was attributed to habitat uniformity. Berrill suggested that tadpole development was eliminated from the life cycle because tadpoles capable of selecting a habitat are unnecessary in a uniform environment. But the largest populations of *M. retortiformis* adults live in a rocky, nonuniform habitat. Seven summers of field collections along the west coast of Vancouver Island near Bamfield Marine Station indicate that *M. pacifica* adults thrive on rocky, nonuniform habitats (Young *et al.*, 1988; Bates and Mallett, 1991a; Bates, 1993). The evolution of morphogenetic processes in ascidians has been discussed at length elsewhere (Bates, 1993, 1994), with the suggestion that the evolution of a fixed timing mechanism for triggering a rapid deployment of ampullae may be important to the reproductive success of direct-developing ascidians. The finding described in the present report that ampulla morphogenesis occurs at a fixed time in *M. retortiformis* development supports this idea.

Acknowledgments

Mike Swallow is thanked for providing Figure 7. Technical help with transmission electron microscopy and darkroom assistance were provided by J. Mallett. I am grateful to Fred Purton at Huntsman Marine Science Centre, St. Andrews, New Brunswick, for making my visits productive. I am grateful for the critical reviews of a previous form of this manuscript. W.R.B. is supported by an operating grant provided by the Natural Sciences and Engineering Council of Canada.

Literature Cited

Bates, W. R. 1991. Ampulla morphogenesis in anural and urodele ascidians. *Devel. Growth Differ* **33:** 401–410.

Bates, W. R. 1993. Evolutionary modifications of morphogenetic mechanisms and alternate life history strategies in ascidians. *Microsc. Res. Tech* **26:** 285–300.

Bates, W. R. 1994. Ecological consequences of altering the timing mechanism for metamorphosis in anural ascidians. *Am. Zool* **34:** 333–342.

Bates, W. R., and W. R. Jeffery. 1987. Localization of axial determinants in the vegetal pole of ascidian eggs. *Dev. Biol* **124:** 65–76.

Bates, W. R., and W. R. Jeffery. 1988. Polarization of ooplasmic segregation and dorsal-ventral axis determination in ascidian embryos. *Dev. Biol* **130:** 98–107.

Bates, W. R., and J. E. Mallett. 1991a. Anural development of the ascidian *Molgula pacifica* (Huntsman). *Can. J. Zool* **69:** 618–627.

Bates, W. R., and J. E. Mallett. 1991b. Ultrastructural and histochemical study of anural development in the ascidian *Molgula pacifica* (Huntsman). *Roux's Arch. Dev. Biol.* **200:** 193–201.

Berrill, N. J. 1931. Studies in tunicate development. Part II. Abbreviation of development in the Molgulidae. *Phil. Trans. Soc. B* **219:** 281–346.

Berrill, N. J. 1975. Chordata: Tunicata. Pp. 241–282 in *Reproduction of Marine Invertebrates*, Vol. 2, A. C. Giese and J. S. Pearse, eds. Academic Press, New York.

Cloney, R. A. 1978. Ascidian metamorphosis: review and analysis. Pp. 255–282 in *Settlement and Metamorphosis in Marine Invertebrate Larvae*, F. S. Chia and M. Rice, eds. Elsevier, New York.

Cloney, R. A. 1982. Ascidian larvae and the events of metamorphosis. *Am. Zool* **22:** 817–826.

Conklin, E. G. 1905. The organisation and cell lineage of the ascidian egg. *J. Acad. Natl. Sci.* **13:** 1–119.

Grave, C. 1935. Metamorphosis of ascidian larvae. Papers from Tortugas Laboratory, Vol. XXIX, *Carnegie Institution of Washington Publication* **452:** 209–292.

Grosberg, R. K. 1981. Competitive ability influences habitat choice in marine invertebrates. *Nature* **290:** 700–702.

Grosberg, R. K., and J. F. Quinn. 1986. The genetic control and consequences of kin recognition by the larvae of a colonial marine invertebrate. *Nature* **322:** 456–459.

Jeffery, W. R., and S. Meier. 1983. A yellow crescent cytoskeletal domain in ascidian eggs and its role in early development. *Dev. Biol.* **96:** 125–143.

Jeffery, W. R., and B. J. Swalla. 1990. Anural development in ascidians: evolutionary modification and elimination of the tadpole larva. *Sem. Dev. Biol* **1:** 253–261.

Jeffery, W. R., and B. J. Swalla. 1991. An evolutionary change in the muscle lineage of an anural ascidian embryo is restored by interspecific hybridization with a urodele ascidian. *Dev. Biol* **145:** 328–337.

Jeffery, W. R., and B. J. Swalla. 1992. Evolution of alternate modes of development in ascidians. *BioEssays* **14:** 219–226.

Karnovsky, M. J., and L. Roots. 1964. A direct-coloring thiocholine method for cholinesterase. *J. Histochem. Cytochem.* **12:** 219–221.

de Lacaze-Duthiers, F. J. H. 1874. Histoire des ascidies simples des cotes de France. *Arch. Zool. Exp. Gen* **3:** 119–656.

Mitam-Miyazawa, I., T. Nishikata, and N. Satoh. 1987. Cell- and tissue-specific monoclonal antibodies in eggs and embryos of the ascidian *Halocynthia roretzi. Development* **99:** 155–162.

Swalla, B. J., M. R. Badgett, and W. R. Jeffery. 1991. Identification of a cytoskeletal protein localized in the myoplasm of ascidian eggs: Localization is modified during anural development. *Development* **111:** 425–436.

Van Name, W. G. 1945. The North and South American Ascidians. *Bull. Am. Mus. Nat. History* **84:** 422–424.

Whittaker, J. R. 1973. Segregation during ascidian embryogenesis of egg cytoplasmic information for tissue specific enzyme development. *Proc. Natl. Acad. Sci. USA* **70:** 2096–2100.

Whittaker, J. R. 1979. Development of vestigial tail muscle acetylcholinesterase in embryos of an anural ascidian species. *Biol. Bull* **156:** 393–407.

Young, C. M., R. F. Gowan, J. Dalby, C. A. Pennachetti, and D. Gagliardi. 1988. Distributional consequences of adhesive eggs and anural development in the ascidian *Molgula pacifica* (Huntsman 1912). *Biol. Bull* **174:** 39–46.

Reference: *Biol. Bull.* **188**: 23–31. (February/March, 1995)

Isolation of Biologically Functional RNA During Programmed Death of a Colonial Ascidian

WEN-TEH CHANG[1] AND ROBERT J. LAUZON[1,2,*]

[1]*Department of Microbiology, Immunology and Molecular Genetics, and* [2]*Department of Pediatrics, Albany Medical College, Albany, New York 12208*

Abstract. The blastogenic (asexual) cycle of the colonial ascidian *Botryllus schlosseri* (Tunicata, Ascidiaceae) concludes in a cyclical phase of programmed cell and zooid death called takeover, in which all asexually derived adults die synchronously by apoptosis. The characterization of developmentally regulated genes whose expression patterns are selectively modulated during this process could pave the way to understand how this model organism dies. However, isolation of biologically functional RNA in this and other colonial ascidians with conventional phenol/chloroform-based procedures is hampered by extensive contamination of RNA preparations by pigments. Upon cell lysis, pigments that normally reside within specialized cells in the mantle wall of the adult are released and tightly associate with nucleic acids. Here, we report on the usefulness of a single-step RNA isolation method in which acid guanidinium isothiocyanate is used as an extraction medium, followed by preparative cesium chloride ultracentrifugation. This procedure successfully isolated biologically active, high-purity total RNA ($OD_{260}/OD_{280} = 1.9–2.1$) from *Botryllus* colonies during takeover, as well as other species of colonial ascidians (*Diplosoma macdonaldii, Botrylloides diegense*) irrespective of pigmentation. Northern blot analysis performed with a ^{32}P-labeled tunicate actin probe detected two polyadenylated transcripts of 1.5 and 1.7 kilobases in length from both growth phase and takeover colonies. Two-dimensional protein gel assays from *in vitro* translated mRNA preparations further revealed that specific transcripts were up-regulated during takeover, while others were repressed or down-regulated. Growth phase and takeover-specific cDNA libraries were constructed from pooled poly(A)$^+$ RNA with a complexity of 1.0×10^7 and 1.2×10^7 recombinants respectively per 100 ng of cDNA before amplification. The procedure described herein renders feasible the cloning of developmentally regulated genes in this organism. In addition, our findings raise the possibility that zooid death in *Botryllus* involves modulated gene expression.

Introduction

Programmed cell death is a fundamental morphogenetic process within developing multicellular animals (Ellis *et al.*, 1991; Schwartz and Osborne, 1993). In adult tissues, cell death also functions as a homeostatic mechanism complementary to mitosis: changes to this balance bring about pathologic abnormalities (Ellis *et al.*, 1991). Recent studies in vertebrates (Owens *et al.*, 1991; Miura *et al.*, 1993; Woronicz *et al.*, 1994; Liu *et al.*, 1994) and invertebrates (Ellis and Horvitz, 1986; Schwartz *et al.*, 1990; White *et al.*, 1994) strongly suggest that cell death is an active process dependent on modulated gene expression. One of the most characteristic forms of cell death is a dynamic morphological process known as apoptosis, characterized by nuclear chromatin condensation and margination, cellular fragmentation into membrane-bounded bodies followed by engulfment and digestion within phagocytic cells (Kerr, 1972).

The colonial ascidian *Botryllus schlosseri* contributes a unique perspective to the study of cell death: adult colonies, derived from a chordate tadpole through palleal budding and which at peak size consist of approximately 1000 asexually derived clones (zooids), undergo weekly phases of regression (Milkman, 1967). Every 5 days at 21°C, the blastogenic (asexual) cycle concludes in a phase of programmed cell and zooid death called takeover, during which all zooids, each containing a functional heart, nervous and digestive systems simultaneously die by an

---

Received 8 July 1994; accepted 22 November 1994.

* Author to whom correspondence should be addressed.

apoptotic process over a 24-h period and are replaced by a new asexual generation of zooids (Lauzon *et al.*, 1993).

Because the temporal and morphological events of takeover can be predicted in detail in *Botryllus*, we have undertaken a multidisciplinary investigation of the molecular mechanisms underlying programmed death in this model organism. Thus far, molecular studies have been impeded by the lack of appropriate methods for isolation of biologically active mRNA. Unfortunately, *Botryllus* and other colonial ascidians harbor polyphenolic and DOPA-containing pigments that bind tightly with nucleic acids following cellular lysis with detergents and chaotropic agents, thus interfering with the isolation process as well as its subsequent analysis and cloning (Kumar *et al.*, 1988). Moreover, isolation of intact RNA molecules from regressing tissues may also prove to be difficult because, during cell death, a substantial fraction of the RNA pool is rapidly degraded through the enhanced activity of ribonucleases (Cidlowski, 1982; Owens *et al.*, 1991). Therefore, to ensure isolation of biologically active RNA from these organisms, a strategy had to be developed that would eliminate both ribonuclease activity and pigments.

Here, we report on the success of a procedure by which biologically functional RNA suitable for cDNA cloning and other molecular applications can be rapidly isolated from various colonial ascidian species, including *Botryllus*. In addition, we present evidence which indicates that changes in gene expression occur during takeover.

Materials and Methods

Animals

Ascidians (*Botryllus schlosseri, Botrylloides diegense, Diplosoma macdonaldii, Molgula manhattensis*) were collected on glass microscope slides contained within wooden enclosures submerged in the Eel Pond (Woods Hole, MA) and Monterey Bay (CA). They were subsequently maintained in a refrigerated aquarium (150-gallon capacity) containing artificial sea salts, trace and bio-elements (hw-marine mix: Hawaiian Marine Imports Inc., Houston, TX), and were continuously fed with an algal scrubber irradiated for 12 h each day with two 15-watt Aurora 50:50 bulbs (Fritz Pet Products, Dallas, TX). Individual *Botryllus* colonies were developmentally staged with the use of a stereomicroscope (Stemi SV 6, Carl Zeiss, Germany). Following removal of debris and encrusting organisms, all animals were subsequently snap-frozen in liquid nitrogen and stored at −70°C until needed.

RNA extraction

RNA was extracted using a modification of the method by Chirgwin *et al.* (1978). Individual colonies (0.5–1.0 g) were initially ground to a fine powder with liquid nitrogen in a precooled mortar and pestle, and subsequently homogenized in 2.0 ml of a lysis solution containing the following components: 4 *M* guanidium isothiocyanate (Gibco/BRL, Gaithersburg, MD) predissolved in a 0.75 *M* sodium citrate solution (pH = 7.0; 25 m*M* final concentration), 0.2 *M* sodium acetate (pH = 5.0), and 0.1 *M* β-mercaptoethanol. Following transfer of the lysate to a 50-ml polypropylene tube, the DNA was sheared with a 23-gauge needle and syringe, and sodium lauryl sarcosinate (10% stock) was added to a final concentration of 0.5%. The homogenate was incubated on ice for 15 min and centrifuged at 3500 × *g* for 5 min at 4°C. The supernatant was layered on a 1.3-ml cesium chloride (CsCl; Boehringer Mannheim, Indianapolis, IN) solution (5.7 *M* CsCl, 0.5 *M* EDTA, pH = 8.0) in a 13- × 51-mm ultracentrifuge polyallomer tube (Beckman Instruments Inc., Palo Alto, CA), and centrifuged at 40,000 rpm at 20°C for 12 h in an SW50.1 rotor (Beckman Instruments Inc.). Following centrifugation, the RNA pellet was resuspended in diethylpyrocarbonate (DEPC)-treated water (Sigma Chemical Co., St. Louis, MO), precipitated overnight at −20°C in 100% ethanol, and washed in 70% ethanol. The pellet was subsequently dried under vacuum at room temperature, resuspended in DEPC-treated water, and stored at −70°C. For phenol/chloroform-based extractions, the method described by Chomcynski and Sacchi (1987) was used.

Spectrophotometric analysis

An aliquot from each RNA preparation (1-5 μl) was diluted into 250 μl of DEPC-treated water, transferred to a quartz cuvette, and scanned between 240 and 320 nm with a Perkin-Elmer λ-2 microprocessor-controlled spectrophotometer (Perkin-Elmer Inc., Foster City, CA). A GeneQuant spectrophotometer (Pharmacia, Piscataway, NJ) was used to determine total RNA concentrations as outlined in Sambrook *et al.* (1989). During the course of our studies, we observed that OD_{260}/OD_{280} ratios were greatly affected by pH. For instance, DEPC-treated water samples that still contained residual levels of DEPC following autoclaving (pH = 5.0) gave aberrant OD_{260} absorbance readings (between 1.3 and 1.5). Consequently, we routinely autoclaved all our DEPC-treated solutions twice for 30 min each. Poly-A$^+$ RNA was isolated with the poly-A tract mRNA isolation system from Promega (Promega Corp., Madison, WI), and concentrations were determined with the Dipstick kit by Invitrogen (Invitrogen Corp., San Diego, CA). Both were used according to the manufacturer's specifications.

Northern blot hybridization

Ten micrograms of total RNA was denatured in formaldehyde, size-fractionated in 1% agarose/formaldehyde gels (4 V/cm), and transferred onto nitrocellulose membranes (Schleicher and Schuell, Keene, NH) with 20× SSC. Blots were hybridized overnight with a cytoactin cDNA probe from *Styela clava* (SpCA8; Beach and Jeffery, 1990) under high-stringency conditions (1 *M* NaCl, 10% dextran sulfate, 1% SDS, 100 μg/ml denatured salmon sperm DNA) at 65°C. The SpCA8 probe was labeled by random hexadeoxynucleotide priming to a specific activity of 10^9 cpm/μg DNA (Feinberg and Vogelstein, 1983). Blots were washed three times in 1× SSC (prepared from a 20× SSC stock solution: 3.0 *M* sodium chloride, 0.3 *M* sodium citrate, pH = 7.0) and 0.1% SDS at 65°C 5 min each, followed by two additional washes in 0.1× SSC and 0.1% SDS (65°C) 15 min each, and autoradiographed with Kodak XAR film.

Two-dimensional protein gel electrophoresis

Poly-A^+ RNA (0.2 μg/sample) was translated *in vitro* with a rabbit reticulocyte lysate from Promega using ^{35}S-methionine. Protein products were analyzed by two-dimensional polyacrylamide gel electrophoresis (O'Farrell, 1975; O'Farrell *et al.*, 1977) on a protein II xi slab cell (Bio-Rad, San Diego, CA). *In vitro*-labeled samples were focused with wide range ampholytes (pH = 3-10; Bio-Lyte 3/10, Bio-Rad) in 4 *M* urea and 10% NP-40, and size-fractionated on 10% sodium-dodecyl-sulfate polyacrylamide gels (SDS-PAGE) along with Brome Mosaic Virus (BMV) molecular weight markers (110, 97, 35 and 20 Kd) provided as a control with *in vitro* translation kits (Promega). Gels were fixed in methanol/acetic acid, enhanced with RESOLUTION (EM Corp, Chestnut Hill, MA), dried under vacuum, and autoradiographed with Kodak XAR film at −70°C. All samples were run at least twice to ensure reproducibility of translational profiles observed by autoradiography.

cDNA library construction

cDNA was synthesized from poly-A^+ RNA of pooled colonies isolated at onset and early stages of takeover (stages D-1 and D-2) or from representative growth stages (A, B-1, B-2 and C-1) with the unizap cDNA synthesis kit from Stratagene (La Jolla, CA) using ^{32}P-dATP. The cDNA products were ligated to *Eco* RI linkers, restricted with *Xho* I, and cloned unidirectionally into lambda zap vector, according to the manufacturer's specifications. Size range of first and second strand cDNA products was determined by alkaline agarose gel electrophoresis by the slide technique. Briefly, 10 ml of 1% molten alkaline agarose (containing 1 ml of 10× alkaline agarose buffer: 3 ml of 5 N NaOH, 2 ml of 0.5 M EDTA and 45 ml of sterile milli-Q water) was added near the upper center of a 5- × 7.5-cm glass slide, to which a mini-gel comb had been attached over it with high-tension clips. The gel was run in 1× alkaline buffer at 75 V for 2 h at room temperature. Following electrophoresis, the gel was blotted dry with several changes of Kimwipes EX-L (Kimberly-Clark, Roswell, GA), sealed in an air-tight hybridization bag, and autoradiographed with Kodak XAR film at room temperature. The library was packaged and titered according to Stratagene's specifications. The level of nonrecombinants was determined by plating various phage dilutions with XL1-Blue MRF′ cells along with IPTG (200 mg/ml in water) and X-gal (20 mg/ml in dimethylformamide). For either takeover or growth phase cDNA library, blue background plaques were not observed on plates containing up to 10^3 PFUs (plaque forming units), indicating that the percentage of non-recombinants was very low (less than 1 × 10^5 PFUs/μg of phage arms). Lastly, the primary library was amplified in XL1-Blue, phage suspensions were stored at −70°C, and an aliquot was prepared to assess the quality of the cDNA library. The quality of each cDNA library was assayed by probing nitrocellulose plaque lifts for representation of actin-complementary sequences using the SpCA8 cytoactin cDNA clone. Phage transfer was performed for 1 min at room temperature, and filters were sequentially placed for 3 min each onto sheets of 3MM paper saturated with the following solutions: (1) 0.5 *N* sodium hydroxide and 1.5 *M* sodium chloride, (2) 10% SDS, (3) 0.5 *M* Tris-HCl pH = 8.0 and 1.5 *M* NaCl, and (4) 2× SSC. Membranes were subsequently baked at 80°C under vacuum for 30 min, hybridized with the ^{32}P-labeled SpCA8 cDNA clone, and autoradiographed with XAR film at −70°C. Hybridization conditions and post-hybridization washes were identical to those used in the northern blot analysis.

Results

The blastogenic cycle of B. schlosseri

Developmental staging of *B. schlosseri* colonies was adapted from the nomenclature used by Mukai and Watanabe (1976), as well as Izzard (1973), and is described in Table I and depicted in Figure 1. Following metamorphosis of the free-swimming tadpole, a colony arises by weekly cycles of palleal budding, in which the bud evaginates from the wall of its parent zooid. Under optimal growth conditions, two to three primary buds are produced per zooid and can be easily observed dorsally by stage B-2 (Fig. 1, panel B). By stage C-1, organogenesis begins in the secondary bud with the formation of primary atrial folds, and at this time it exhibits an elongated appearance as primary organs (gut rudiment) begin to form (not shown). At 21°C, the cycle concludes on the fifth day with the synchronous death of all parent zooids, a process called takeover (Lauzon *et al.*, 1992). The onset of takeover is characterized by the shutdown of both oral and excurrent siphons (Fig. 1, panel C). At this stage, while buds begin to move dorsally, zooids are still re-

Table I

Developmental stages of the blastogenic cycle

Stage	Characteristic
A	Onset of new cycle; opening of oral and excurrent siphons.
B-1	Secondary bud skewing to parent zooid's anterior hemisphere. Heartbeat begins in primary bud.
B-2	Secondary bud is a closed double-layered vesicle.
C-1	Organogenesis (atrial folds) begins in secondary bud. Secondary bud elongates along its anteroposterior axis.
C-2	Primary subdivisions completed in secondary bud.
D-1	Onset of takeover: shutdown of zooid's oral and excurrent siphons. Primary buds move dorsally.
D-2	Early takeover; contraction of zooid along its anteroposterior axis.
D-3	Mid-takeover (zooid involution): visceral organs are being resorbed. Apoptotic cell death and macrophage phagocytosis are prevalent.
D-4	End of takeover: cessation of heartbeat in zooid. Siphons of new asexual generation not yet open.

sponsive to mechanical stimulus. In the early stages of takeover (3–5 h post-onset), the zooids contract along their anteroposterior axis and begin to shrink in size (Fig. 1, panel D). Pigment cells, which normally reside in the zooid's mantle wall, begin to accumulate in the vascular ampullae. In the middle stages of takeover (12–15 h post-onset), visceral organs die principally through an apoptotic process (Lauzon *et al.*, 1993), although necrotic changes can also be observed alone or in combination with an apoptotic morphology. Takeover concludes with the cessation of heartbeat in zooids, and a new cycle begins with the opening of siphons in the next asexual generation of zooids (panel A).

RNA isolated by preparative ultracentrifugation is biologically functional

As shown in Figure 2A, when RNA was extracted with the guanidine isothiocyanate/phenol/chloroform procedure (Chomcynski and Sacchi, 1987), the spectrophotometric absorbance pattern was severely disrupted, exhibiting a peak absorbance at 268 nm instead of 260 nm. All preparations extracted in this manner were significantly contaminated with blue and red pigments that could not be removed upon further phenol/chloroform extraction. In addition, the yields from these preparations were very poor (10–20 μg of total RNA/g tissue), and often displayed OD_{260}/OD_{280} ratios greater than 2.5, suggesting that pigments were contributing to the altered ratios. Furthermore, when the preparations were size-fractionated on formaldehyde/agarose gels, most of the sample remained in the loading well. We surmise that since many pigments have been reported to be polyphenolic in nature (Kumar *et al.*, 1988), RNA was most likely sequestered to the organic phase along with them. In contrast, RNA isolated by means of cesium chloride ultracentrifugation was spectrophotometrically pure (Fig. 2B), exhibited optimal OD_{260}/OD_{280} ratios between 1.9 and 2.1, and consistently produced yields ranging between 0.5 and 0.8 μg/mg of colony. When cesium-chloride-purified samples were electrophoresed, prominent 28S and 18S ribosomal RNA bands were visualized irrespective of the developmental stage of the colony (Fig. 3, lanes 2, 3, 4, 7, 8) or species (Fig. 3, lanes 5, 6). To test the integrity of the RNA, samples from various ascidians were size-fractionated by agarose/formaldehyde gel electrophoresis, transferred to a nitrocellulose membrane, and hybridized to a ^{32}P-labeled cytoactin cDNA probe from *Styela clava.* The results, which are shown in Figure 4, indicate that all colonial ascidians (*Botryllus, Botrylloides,* and *Diplosoma*) expressed two polyadenylated transcripts of 1.5 and 1.7 kb in length (panel A, lanes 1–4; panel B, lane 5). In contrast, the solitary ascidian *Molgula manhattensis* expressed only a single 1.5-kb transcript. Furthermore, both transcripts were expressed during all stages of the blastogenic cycle in *Botryllus* (Fig. 4, panel B).

We next sought to determine whether *Botryllus* RNA isolated by this method could also be *in vitro*-translated into protein. Samples (0.2 μg) of poly-A^+ RNA from various developmental stages were translated with a rabbit reticulocyte lysate with ^{35}S-methionine and analyzed by two-dimensional polyacrylamide gel electrophoresis to examine patterns of gene expression between different stages of the blastogenic cycle. The results (Fig. 5) demonstrate that RNA preparations could be successfully translated and focused into a wide spectrum of acidic- and basic-range polypeptides during both the growth phase of the cycle and takeover. Furthermore, at the onset of a new blastogenic cycle, several different spots were identified from the acidic and basic range that were absent in the early stages of takeover (panel A). Additional transcripts (for instance, arrow in panels A and B, Fig. 5) appeared to be significantly down-regulated during takeover. Conversely, other transcripts were expressed in the early stages of takeover, but absent at the beginning of a new asexual cycle (panel B) or other stages (not shown).

Lastly, in order to determine whether mRNA from takeover colonies was suitable for cDNA synthesis, poly-A^+ RNA was reverse-transcribed, and cDNA products were subsequently size-fractionated by alkaline gel electrophoresis. The results (Fig. 6) indicate that both first- and second-strand cDNA products exhibited an appropriate size range, with the bulk distributed between 300 bases and 2.5 kb. Pooled cDNA products were then used to construct a unidirectional library into lambda zap. The size of the primary nonamplified library was 1.2×10^7 PFUs/100 ng of cDNA, as determined from

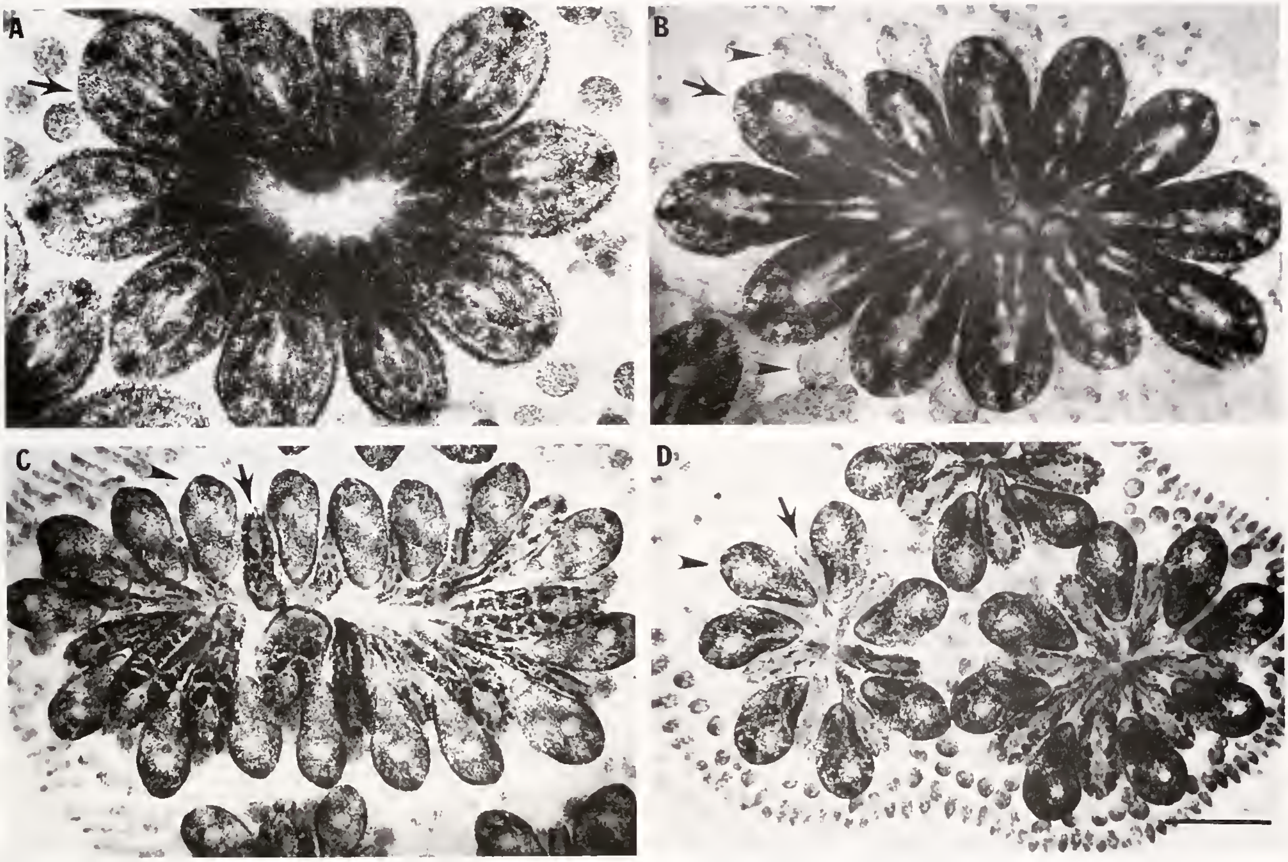

Figure 1. The blastogenic cycle of *Botryllus schlosseri* Individual colonies were developmentally staged by stereomicroscopy and are depicted dorsally in panels A through D Panel A shows a colony at the onset of a new cycle. Note that the primary buds are not visible from the dorsal plane. Panel B shows a colony during stage B-2 (see Table 1 for specific details of individual stages), in which primary buds are now visible. The onset of takeover (panel C) is characterized by the shutdown of oral and excurrent siphons in all zooids (arrow) and star-shaped systems. Buds (arrowhead) have begun their dorsal migration. In the early stages of takeover (panel D), each zooid undergoes a synchronous polarized contraction along its anteroposterior axis. Zooid regression is completed in approximately 24 h at 21°C, and a new cycle begins with the opening of siphons from the new asexual generation of zooids. Bar represents 1 mm.

plaque counts using serial dilutions of phage suspensions. A cDNA probe encoding cytoplasmic actin from *Styela clava* (as a prototype abundant sequence) was then used to screen nitrocellulose plaque lifts to ensure adequate representation of this sequence. A comparable screen was performed with a growth phase (pooled stages A, B-1 and C-1) cDNA library (1.0×10^7 PFUs nonamplified). The percentages of actin-positive clones (Fig. 7) were found to be comparable in both libraries, namely 3.0% (150 positive/5×10^3 plaques) in the takeover and 3.2% in the growth phase cDNA library (58 positive/1.8×10^3 plaques).

Discussion

The findings presented in this paper indicate that RNA isolated by cesium chloride ultracentrifugation is optimally suited for a wide range of molecular applications, including northern blot analysis, *in vitro* translation, and cDNA synthesis from dying tissues of *Botryllus schlosseri* and other colonial ascidians. Because colonial ascidians (Kumar *et al.*, 1988) and other marine invertebrates (Groppe and Morse, 1993) exhibit a spectacular range of pigmentation patterns, they have been reported to pose a distinct problem in the isolation of nucleic acids. Polyphenolic compounds and DOPA-containing proteins, which interfere with nucleic acid isolation, have been found in the adult tunic and mantle wall of both solitary and colonial ascidians (Kumar *et al.*, 1988). In *Botryllus* colonies found on the eastern coast of the United States, the problem is intensified because most colonies contain an alcohol-insoluble red pigment that cannot be removed from nucleic acids with conventional lysis buffers followed by phenol/chloroform-based extractions. The addition of

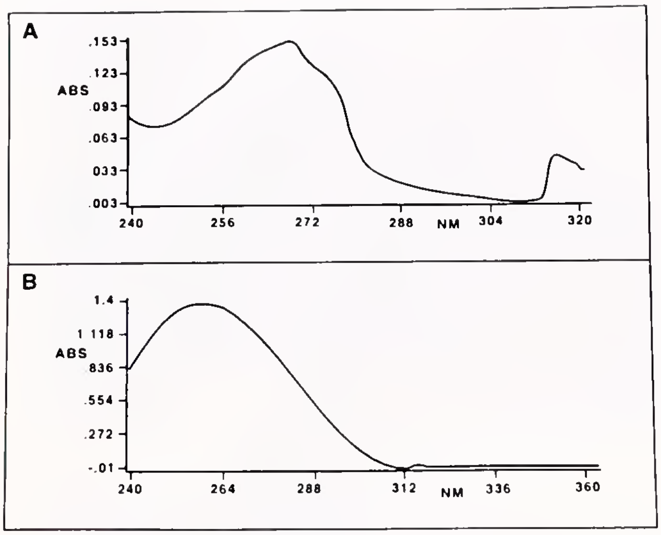

Figure 2. Spectrophotometric scanning analysis of isolated total RNA from *Botryllus schlosseri*. (A) RNA isolated from *B. schlosseri* with a conventional extraction method that utilizes phenol/chloroform/guanidine isothiocyanate (Chomcynski and Sacchi, 1987) demonstrates an altered ultraviolet absorption spectrum. In contrast (B), RNA isolated with the single-step cesium-chloride method is free of contaminants and exhibits an optimal OD_{260}/OD_{280} ratio (1.9–2.1).

a cesium chloride ultracentrifugation step permitted the recovery of high yields of spectrophotometrically and electrophoretically pure RNA preparations, irrespective of pigmentation or species. Groppe and Morse (1993) recently described a two-step cold method of isolating RNA from *Haliotis rufescens* (red abalone); the method provided high yields of pigment-free, undegraded material suitable for cDNA cloning. The first step, a phenol/chloroform extraction performed at 0°C, was crucial for the removal of ribonuclease activity, and the second step, employing ultracentrifugation through a cesium chloride gradient, removed an inhibitor of reverse transcriptase. The observations reported herein indicate that in *Botryllus* and other colonial ascidians, only a single preparative ultracentrifugation step through cesium chloride is required for isolation of biologically functional RNA.

However, our findings are in contrast with those of Kumar *et al.* (1988), who reported that they successfully isolated RNA from various ascidians by using only a phenol/chloroform-based procedure. In our hands, all preparations isolated using phenol/chloroform were significantly contaminated with pigments and gave very poor yields. Furthermore, much of the original sample was left in the loading well during formaldhyde/agarose gel electrophoresis, and the efficiencies for *in vitro* translation reactions and reverse-transcription for cDNA library construction were significantly impaired (W-T.C and R.J.L., unpub. obs.). At present, we have no explanation for the discrepancy between our results and those of Kumar *et al.* (1988).

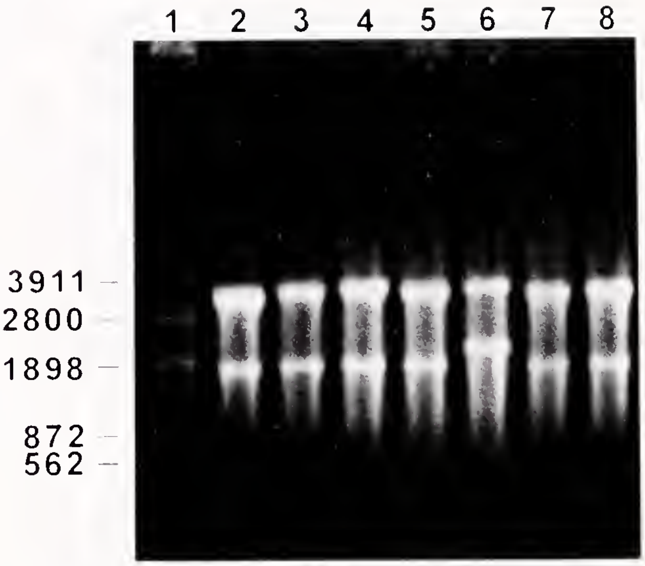

Figure 3. Ethidium bromide staining of total RNA isolated by preparative ultracentrifugation. Lane 1, RNA markers. Lanes 2, 3, 7, and 8, *Botryllus schlosseri* from Eel Pond (Woods Hole, MA): lane 2 (stage A), lane 3 (stage B-2), lane 7 (early takeover; 3 h post-onset), and lane 8 (mid-takeover, 12 h post-onset). Lane 4, *B. schlosseri* from Monterey Bay, CA (stage C-2). Lane 5, *Botrylloides diegense* (growth phase). Lane 6, *Diplosoma macdonaldii*.

One possibility is that the composition of pigments found in *Botryllus* and other botryllid ascidians may differ from those found in other solitary or colonial species reported

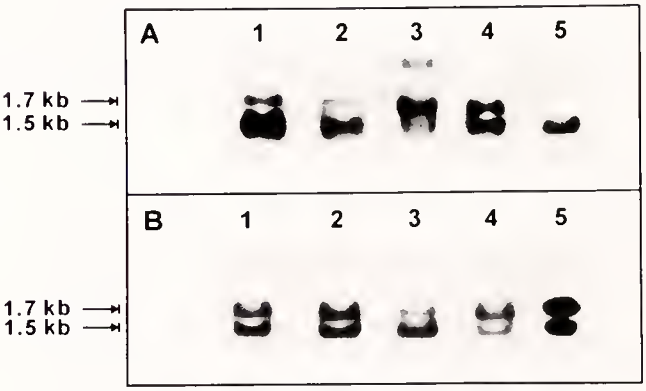

Figure 4. Northern blot analysis of RNA isolated from various species of colonial and solitary ascidians. Samples were electrophoresed on a 1% agarose/formaldehyde gel, transferred to nitrocellulose, and hybridized with a ^{32}P-labeled cytoactin probe SpCA8 from *Styela clava* (Beach and Jeffery, 1990). (A) Lane 1, *Botryllus schlosseri* (stage A) from Eel Pond (Woods Hole, MA); lane 2, *B. schlosseri* (stage C-2) from Monterey Bay (CA); lane 3, *Botrylloides diegense* (growth phase); lane 4, *Diplosoma macdonaldii*, lane 5, *Molgula manhattensis*. (B) Total RNA samples of *B. schlosseri* from Eel Pond isolated at various stages of the blastogenic cycle (lanes 1–4), and pooled poly-A$^+$ RNA from stages A–C colonies (lane 5). Lane 1, early takeover; lane 2, mid-takeover; lane 3, stage A; lane 4, stage B-1.

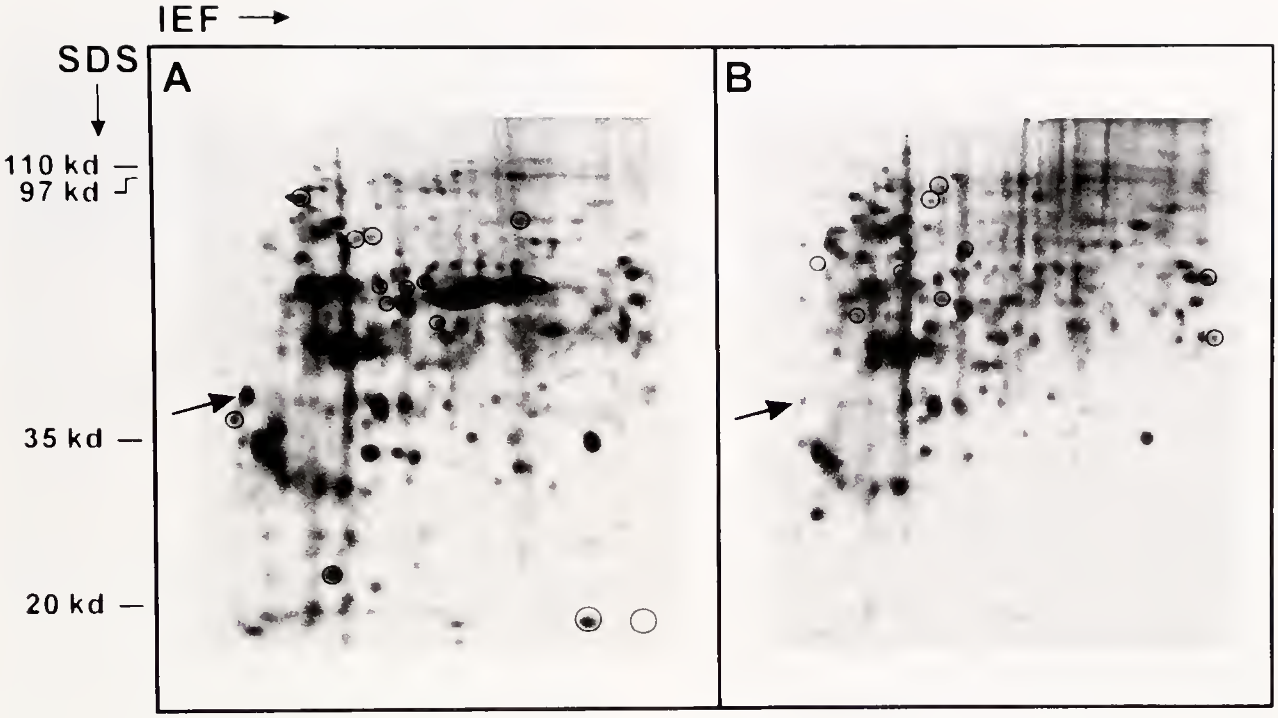

Figure 5. Two-dimensional protein gel analysis of *in vitro*-translated RNA with ^{35}S-methionine reveal changes in gene expression during takeover. Panel A depicts a colony at the onset of a new blastogenic cycle (stage A), whereas panel B is from a colony in early takeover (3 h post-onset). The circled spots in panel A represent transcripts that are repressed in the early stages of takeover. The arrows in panels A and B depict a representative polypeptide whose mRNA is down-regulated during takeover. Conversely, the circled spots in panel B are transcripts that appear to be induced *de novo* during takeover. Abbreviations: SDS, sodium dodecyl sulfate polyacrylamide gel electrophoresis (SDS-PAGE) dimension; IEF, isoelectric focusing dimension.

by Kumar *et al.* (1988). The presence of contaminating pigments markedly altered $OD_{260/280}$ ratios, presumably by absorbing in the range that is optimal for nucleic acids (*i.e.*, 260 nm). In support of this hypothesis, we have recently observed that pigment cells from live colonies are fluorescent under ultraviolet light (R.J.L., unpub. obs.).

Northern blot analysis with cesium-chloride-purified material further revealed that the RNA was not degraded by ribonuclease activity present during zooid regression. Previous studies have cautioned that isolation of intact RNA molecules from dying tissues can be significantly impeded by ribonucleases (Cidlowski, 1982; Owens *et al.*, 1991). In addition, all colonial ascidian species reported in this paper (*Botryllus schlosseri* from the East and West coasts, *Botryloides diegense*, and *Diplosoma macdonaldii*) expressed two poly-A$^+$ transcripts of 1.5 and 1.7 kb in length that hybridized to a cytoplasmic cDNA clone from *Styela clava.* This was in contrast to the single 1.5 kb-message found in the solitary ascidian *Molgula manhattensis.* The significance of two mRNAs in colonial ascidians is unclear, although another solitary tunicate, *Styela clava,* was previously reported to express a single 1.8-kb message during both embryonic and post-metamorphic development (Beach and Jeffery, 1990). The additional 1.7-kb band in colonial species may represent a cross-hybridizing muscle actin transcript. Tomlinson *et al.* (1987) showed that a probe made exclusively from the 3′ untranslated region of a *Styela* muscle actin clone detected transcripts exclusively in muscle cells, whereas one made from the coding region, such as the cytoplasmic cDNA clone used in this study (*e.g.*, SpCA8), detected both muscle and nonmuscle transcripts. However, several lines of evidence argue against this scenario. First, although both transcripts were expressed at all phases of the blastogenic cycle in *Botryllus* including takeover, the relative intensity of the bands varied at different stages of the cycle. Second, if the 1.7-kb transcript represented a cross-reactive muscle mRNA, one would expect the intensity of the hybridizing band to be less than the 1.5-kb transcript at any given time under high-stringency conditions. This condition was clearly not observed. Alternatively, both transcripts could result from alternative splicing. The expression of an additional 1.7-kb transcript could be functionally related to the colonial life style, but seems unlikely to be associated with zooid death since *Diplosoma* species do not undergo takeover. An intriguing possibility is that it may be expressed during bud development. Therefore, determination of the complete nucleotide sequences of both cDNA clones followed by *in situ* hybridization with non-cross-hybridizing probes will be required to resolve this issue.

Studies with invertebrate (Wadewitz and Lockshin, 1988) and vertebrate (Wang and Brown, 1991) developmental systems indicate that individual death programs may involve fewer than 40 up-regulated genes. For instance, thyroid-hormone-mediated changes leading to tail resorption in *Xenopus laevis* involve two periods of gene expression during which all genes belonging to a specific group are induced with identical kinetics. Conversely, about 10 additional genes are down-regulated with identical decay kinetics (Wang and Brown, 1993). These observations indicate that in amphibians the death program reflects a relatively simple pattern of gene expression. The initial findings reported here with two-dimensional protein gels from *Botryllus* suggest that modulated gene expression occurs during the takeover phase of blastogenesis. We have previously demonstrated that takeover involves the polarized breakdown of the perivisceral extracellular matrix along the zooid's anteroposterior axis, followed by apoptotic and necrotic morphological changes within dying visceral tissues (Lauzon *et al.*, 1992, 1993). Changes in gene expression may thus be associated with these morphological events. Unfortunately, the shutdown of oral siphons during takeover precluded us from analyzing ^{35}S-methionine incorporation patterns *in vivo*. Therefore, the possibility cannot be ruled out that differences in 2-D protein profiles between the onset of blastogenesis and takeover are due to inherent limitations of the *in vitro* translation kits. In addition, since clonal replicates were not used in any of these studies, the differences observed may represent intra-species polymorphisms. Lastly, since takeover involves the simultaneous regression of adult zooids along with asexual growth of the future parental generation, the possibility cannot be excluded that transcriptional changes also occur in buds or in the colonial vasculature. Therefore, assessing the specificity of transcriptional changes will require isolation of takeover-specific mRNAs and analysis of their spatial distribution pattern by *in situ* hybridization. We are currently using differential mRNA display (Liang and Pardee, 1992) as a means for ultimately characterizing full-length transcripts from the cDNA libraries. Interestingly, the percentages of actin-positive PFUs were similar in the growth phase and takeover libraries (3.2 versus 3.0). Libraries with reported actin cDNA-positive frequencies above 0.1% have yielded clones of interest for sequences of moderate to low abundance, whereas percentages below 0.05% have not (Hagen *et al.*, 1988). Collectively, our findings strongly suggest that both libraries are likely to contain cDNAs corresponding to single-copy gene transcripts. The characterization of genes involved in zooid regression could provide a fundamental understanding of molecular mechanisms of programmed cell death in *Botryllus* and other metazoans.

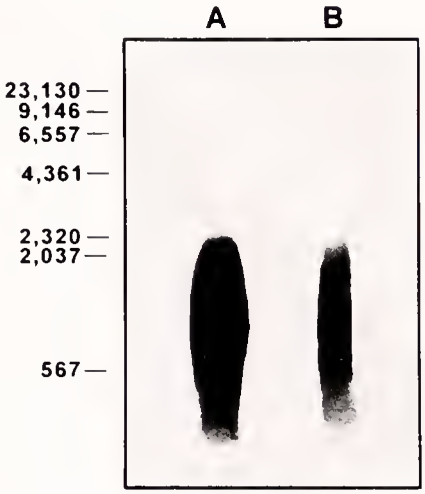

Figure 6. Alkaline agarose gel electrophoresis assay of first- and second-strand cDNA synthesis in *Botryllus schlosseri*. First- (lane A) and second-strand (lane B) cDNA products were converted using pooled poly-A$^+$ RNA isolated from colonies during takeover (onset and early takeover). Note that both lanes exhibit a broad size distribution of cDNA products, with the majority of material ranging between 1 and 2 Kb.

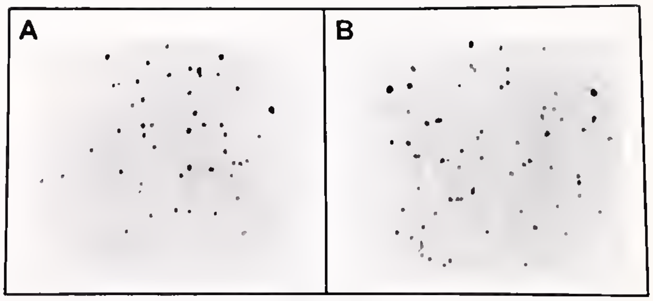

Figure 7. Nitrocellulose plaque lifts from growth stages (panel A) and takeover (panel B) cDNA libraries hybridized with an ascidian ^{32}P-labeled cytoactin probe from *Styela clava* (SpCA8). Percent positive plaque forming units in (B) was 3.0% (150 positive out of 5 × 10^3 PFUs) compared to 3.2% for the growth phase cDNA library (58 positive out of 1.8 × 10^3 PFUs), indicating that actin was adequately represented.

Acknowledgments

The authors gratefully acknowledge Dr. Craig Tomlinson for his generous gift of the SpCA8 cytoactin cDNA clone, and two anonymous reviewers for their efforts in improving the focus of this manuscript. This work was supported by a Basil O'Connor Starter Scholar Award from the March of Dimes Birth Defects Foundation #5-

FY94-0813, and from a Frederick Bang Fellowship at the Marine Biological Laboratory, Woods Hole, Massachusetts.

Literature Cited

Beach, R. L., and W. R. Jeffery. 1990. Temporal and spatial expression of a cytoskeletal actin gene in the ascidian *Styela clava. Devel. Genet.* **11**: 2–14.

Chirgwin, J. M., A. E. Przybyla, R. J. MacDonald, and W. J. Rutter. 1978. Isolation of biologically active ribonucleic acid from sources enriched by ribonuclease. *Biochemistry* **18**: 5294–5299.

Chomczynski, P., and N. Sacchi. 1987. Single-step method of RNA isolation by acid guanidinium thiocyanate-phenol-chloroform extraction. *Anal. Biochem* **162**: 156–159.

Cidlowski, J. A. 1982. Glucocorticoids stimulate ribonucleic acid degradation in isolated rat thymic lymphocytes *in vitro. Endocrinology* **111**: 184–190.

Ellis, H. M., and H. R. Horvitz. 1986. Genetic control of programmed cell death in the nematode *C. elegans. Cell* **44**: 817–829.

Ellis, R. E., J. Yuan, and H. R. Horvitz. 1991. Mechanisms and functions of cell death. *Ann. Rev. Cell Biol* **7**: 663–698.

Feinberg, A. P., and B. Vogelstein. 1983. A technique for radiolabelling DNA restriction endonuclease fragments to high specific activity. *Anal. Biochem.* **132**: 6–13.

Groppe, J. C., and D. E. Morse. 1993. Isolation of full-length RNA templates for reverse transcriptase from tissues rich in RNase and proteoglycans. *Anal. Biochem* **210**: 337–343.

Hagen, F. S., C. L. Gray, and J. L. Kuijper. 1988. Assaying the quality of cDNA libraries. *Biotechniques* **6**: 340–345.

Izzard, C. S. 1973. Development of polarity and bilateral asymmetry in the palleal bud of *Botryllus schlosseri* (Pallas). *J. Morph.* **139**: 1–26.

Kerr, J. F. R., A. H. Wyllie, and A. R. Currie. 1972. Apoptosis: a basic biological phenomenon with wide-ranging implications in tissue kinetics. *Br. J Cancer* **26**: 239–257.

Kumar S., B. M. Degnan, I. L. Ross, C. J. Hawkins, and M. F. Lavin. 1988. Isolation of DNA and RNA from ascidians. *Mar. Biol.* **98**: 95–100.

Lauzon, R. J., K. J. Ishizuka, and I. L. Weissman. 1992. A cyclical, developmentally-regulated death phenomenon in a colonial urochordate. *Dev. Dyn.* **194**: 71–83.

Lauzon, R. J., C. W. Patton, and I. L. Weissman. 1993. A morphological and immunohistochemical study of programmed cell death in *Botryllus schlosseri. Cell Tis. Res.* **272**: 115–127.

Liang, P., and A. B. Pardee. 1992. Differential display of eukaryotic messenger RNA by means of the polymerase chain reaction. *Science* **257**: 967–970.

Liu, Z-G., S. W. Smith, K. A. McLaughlin, L. M. Schwartz, and B. A. Osborne. 1994. Apoptotic signals delivered through the T-cell receptor of a T-cell hybrid require the immediate-early gene nur77. *Nature* **367**: 281–284.

Milkman, R. 1967. Genetic and developmental studies on *Botryllus schlosseri. Biol. Bull.* **132**: 229–243.

Miura, M., H. Zhu, R. Rotello, E. A. Hartwieg, and J. Yuan. 1993. Induction of apoptosis in fibroblasts by IL-1-beta-converting enzyme, a mammalian homolog of the *C. elegans* cell death gene ced-3. *Cell* **75**: 653–660.

Mukai, H., and H. Watanabe. 1976. Studies on the formation of germ cells in a compound ascidian *Botryllus primigenus* Oka. *J. Morphol.* **148**: 337–362.

O'Farrell, P. H. 1975. High resolution two-dimensional electrophoresis of proteins. *J. Biol. Chem.* **250**: 4007–4021.

O'Farrell, P. Z., H. M. Goddman, and P. H. O'Farrell. 1977. High resolution two-dimensional electrophoresis of basic as well as acidic proteins. *Cell* **12**: 1133–1142.

Owens, G. P., W. E. Hahn, and J. J. Cohen. 1991. Identification of mRNAs associated with programmed cell death in immature thymocytes. *Molec. Cell. Biol.* **11**: 4177–4188.

Sambrook, J., E. F. Fritsch, and T. Maniatis. 1989. *Molecular Cloning—A Laboratory Manual,* 2nd ed. Cold Spring Harbor Laboratory. Cold Spring Harbor Lab Press, Cold Spring Harbor, NY.

Schwartz, L. M., L. Kosz, and B. K. Kay. 1990. Gene activation is required for developmentally programmed cell death. *Proc. Natl. Acad. Sci. USA* **87**: 6594–6598.

Schwartz, L. M., and B. A. Osborne. 1993. Programmed cell death, apoptosis and killer genes. *Immunol. Today* **14**: 582–590.

Tomlinson, C. R., R. L. Beach, and W. R. Jeffery. 1987. Differential expression of a muscle actin gene in muscle cell lineages of ascidian embryos. *Development* **101**: 751–765.

Wadewitz, A. G., and R. A. Lockshin. 1988. Programmed cell death: dying cells synthesize a co-ordinated, unique set of proteins in two different episodes of cell death. *FEBS Letters* **241**: 19–23.

Wang, Z., and D. D. Brown. 1991. A gene expression screen. *Proc. Natl Acad Sci. USA* **88**: 11505–11509.

Wang, Z., and D. D. Brown. 1993. Thyroid hormone-induced gene expression program for amphibian tail resorption. *J Biol. Chem.* **268**: 16270–16278.

White, K., M. E. Grether, J. M. Abrams, L. Young, K. Farrell, and H. Steller. 1994. Genetic control of programmed cell death in *Drosophila. Science* **264**: 677–683.

Woronicz, J. D., B. Cain, V. Ngo, and A. Winoto. 1994. Requirement for the orphan steroid receptor Nur77 in apoptosis of T-cell hybridomas. *Nature* **367**: 277–281.

Reference: *Biol. Bull.* **188:** 32–45. (February/March, 1995)

Prespawning Behavior, Spawning, and Development of the Brooding Starfish *Leptasterias polaris*

JEAN-FRANÇOIS HAMEL AND ANNIE MERCIER

Département d'Océanographie, Université du Québec à Rimouski, Centre Océanographique de Rimouski, 310 allée des Ursulines, Rimouski (Québec), Canada G5L 3A1

Abstract. Our study focused on the precise reproductive behavior of the starfish *Leptasterias polaris* (Müller and Troschel) before and during spawning—a subject of much speculation and evident ecological importance. Between the third week of December 1992 and mid-January 1993, we observed spawning in the laboratory that roughly corresponded to field observations in the Lower St. Lawrence Estuary. In experimental tanks provided with natural environmental conditions, the spawning was preceded by 7 to 8 weeks of complex aggregative interactions among the starfish. The individuals, which usually avoid each other, began to make discreet arm contact, which intensified with time and eventually led to the superposition of two or more starfish, independently of sex. The interactions seem to be associated with decreasing temperature, because aggregative and spawning behaviors were not observed under stable temperature conditions. Male spawning is first initiated when the temperature falls to about 2°C during minimum daylength ($<9\ \mathrm{h \cdot d^{-1}}$). In seawater, the spermatozoa are negatively buoyant and tend to deposit as a sticky film on the substrate, where they enter a state of low activity. Stimulated by male spawning, females spawn on the layer of sperm, which is reactivated by contact with the oocytes, ensuring fertilization. In the laboratory, the fertilized eggs undergo first cleavage in 45 h, become brachiolaria in 40 days, and form fully developed young starfish within 5.5 to 6 months, synchronously with populations in the field. The embryos develop at the same rate even when not brooded, suggesting that the brooding behavior in *L. polaris* serves mainly to keep the eggs clean, healthy, and protected against predation.

Introduction

Successful fertilization constitutes a critical stage in marine invertebrate reproduction, and many organisms develop strategies to maximize this important step (Himmelman, 1981; Giese and Kanatani, 1987). Starfish show diversified reproductive behaviors. In many species, gametes are broadcasted by both sexes, with fertilization in the water being enhanced by synchronization of spawning (Hyman, 1955; Strathmann, 1987; Chia and Walker, 1991). In other starfish, males broadcast spawn in the usual fashion, and females emit fewer gametes but brood their embryos to fully developed young starfish (McClary and Mladenov, 1990; Chia and Walker, 1991). *Leptasterias polaris,* which protects its embryos for 5 to 6 months, is among the few species that brood by overlaying the eggs deposited on the substrate (Emerson, 1977; Himmelman *et al.*, 1982; Boivin *et al.*, 1986). Although brooding starfish are generally small-sized, with lecithotrophic development (Chia and Walker, 1991), *L. polaris* can reach diameters up to 50 cm (Boivin *et al.*, 1986) and are probably among the largest brooders.

Prespawning and spawning behaviors are very important to reproductive success in marine invertebrates. Breeding aggregations have been observed in a number of asteroids (Chia, 1968; Komatsu, 1983; Minchin, 1987; Young *et al.*, 1992; Slattery and Bosch, 1993). Many authors suggest that such aggregations could minimize sperm dilution and increase fertilization success (Ormond *et al.*, 1973; Levitan, 1991; Levitan *et al.*, 1992), as exemplified by the pairing strategies in *Archaster typicus* (Run *et al.*, 1988) and *Neosmilaster georgianus* (Slattery and Bosch, 1993). In those species, the male, after finding a female, mounts her before spawning (Ohshima and Ikeda, 1934; Komatsu, 1983; Run *et al.*, 1988; Slattery and Bosch, 1993). There is also evidence that the spatial distribution of broadcast spawners has a major influence on the probability of fertilization due to gamete viability (Pennington, 1985; Yund, 1990; Levitan *et al.*, 1992; Young *et al.*, 1992). Young *et al.* (1992) suggested that aggregations

Received 7 December 1993; accepted 4 November 1994.

could be useful in overcoming the absence of the usual spawning cues (*e.g.*, light, temperature) in bathyal echinoid populations. The possible role of pheromones and other possible attractants on clustering and related spawning inducement in starfish has been examined (Lewis, 1958; Miller, 1989). Komatsu (1983) suggested that initial heterosexual recognition and pairing in *A. typicus* allow male spawning to be induced by release of mature oocytes from females. However, most studies on aggregation have associated it with cooperative feeding or predation avoidance (Ormond *et al.*, 1973; Blankley and Branch, 1984; Sloan, 1984; Pearse and Cameron, 1991).

Although different kinds of aggregations during spawning have been observed, little is known about the involvement of grouping prior to spawning other than recent work on the bathyal sea urchin *Stylocidaris lineata* (Young *et al.*, 1992). Moreover, prespawning interactions have never been discussed in respect to environmental factors such as photoperiod and temperature, which are known to influence gametogenesis and spawning, respectively (Giese and Pearse, 1974; Himmelman, 1981; Pearse and Walker, 1986; Pearse *et al.*, 1986; Pearse and Cameron, 1991). As for fertilization strategies, observations on gamete interactions, other than mutual recognition and attraction, remain scarce. Sperm motility and respiration activation by egg extracts have been studied in sea urchins (Suzuki *et al.*, 1982) and in horseshoe crabs (Clapper and Epel, 1981), but only sperm chemotaxis has been described in detail for starfish (Miller, 1985).

The starfish *Leptasterias polaris* can be kept in laboratory facilities that reproduce natural conditions, and this has provided a chance to record and describe its aggregative behavior both before and during spawning. Further evidence from experiments on gamete behavior and embryonic development allowed us to better understand the evolutionary strategy that seems to link spawning, gamete fertilization, and brooding activities in this species.

Materials and Methods

Using scuba, we collected 60 specimens of *Leptasterias polaris* from a depth of about 10 m on the south shore of the Lower St. Lawrence Estuary (48° 21′ N: 68° 47′ W), eastern Canada. The animals, ranging from 150 to 200 mm in diameter, were collected in May 1992, to ensure that they were acclimatized well before the December spawning that we expected on the basis of previous observations by Boivin *et al.* (1986). The starfish were kept in tanks to which seawater from the collect site was supplied by a flow-through system and light on natural photoperiod was provided through large windows. Physical and chemical conditions were therefore similar to the natural environment. Preliminary determination of sex in *L. polaris* demonstrated a natural sex ratio close to 1:1, and this was carefully reproduced in the tanks. To establish the importance of environmental factors on prespawning aggregative behavior, spawning, and development, the temperature and the salinity of the circulating water were continuously recorded. The data for the daylength were provided by the Canadian government (Environment Canada; Atmospheric Environmental Service, Quebec airport). The starfish were given an unlimited quantity of mussels (*Mytilus edulis*, $\approx$20 mm in shell length), their favorite prey (Himmelman and Dutil, 1991). Frequently very abundant in subtidal environments (Himmelman and Dutil, 1991), *L. polaris* adapts extremely well to experimental conditions.

Prespawning behavior

Starfish behavior was recorded on a regular basis between 4 and 14 times a week depending on activities observed, from November 1992 to February 1993, with complementary observations before and after this period. The number of individuals preying on the mussels, resting on the bottom, and climbing on the sides of the tank were noted. The number of starfish in contact was recorded and categorized as light, when arms touched from the middle part to the tip; intimate, when the arms intertwined for more then half their length; or superposition, when the individuals overlaid one another (Fig. 1). Particular attention was given to reactions of the starfish after renewal of food supply, about twice a month. Data were subsequently combined for weekly comparison of contact intensities. Two control groups were also observed during all prespawning and spawning experiments. Group 1 was maintained under constant conditions in the Quebec Aquarium at a temperature of 6°C, a salinity of 28‰ and a daylength of 10 h; group 2 was kept in continuous darkness with natural conditions of salinity and temperature.

Spawning behavior

As the spawning period approached (Boivin *et al.*, 1986), observations focused on detecting gamete release in relation to the postures adopted by the starfish and to the prevailing environmental conditions. When observed, spawning events were carefully described.

To test the hypothesis that sperm induces spawning in females, a solution (1.2×10^3 spermatozoa $\cdot$ ml^{-1} determined with a hemacytometer under a light microscope) was prepared with freshly collected sperm from a single male. This sperm solution was poured into a tank (4 m^3) among mature females, and their subsequent behavior was recorded. This procedure was carried out four times at different periods under the conditions previously described for the starfish in control group 1. Male starfish were exposed to the same sperm concentrations to see if they would be induced to spawn.

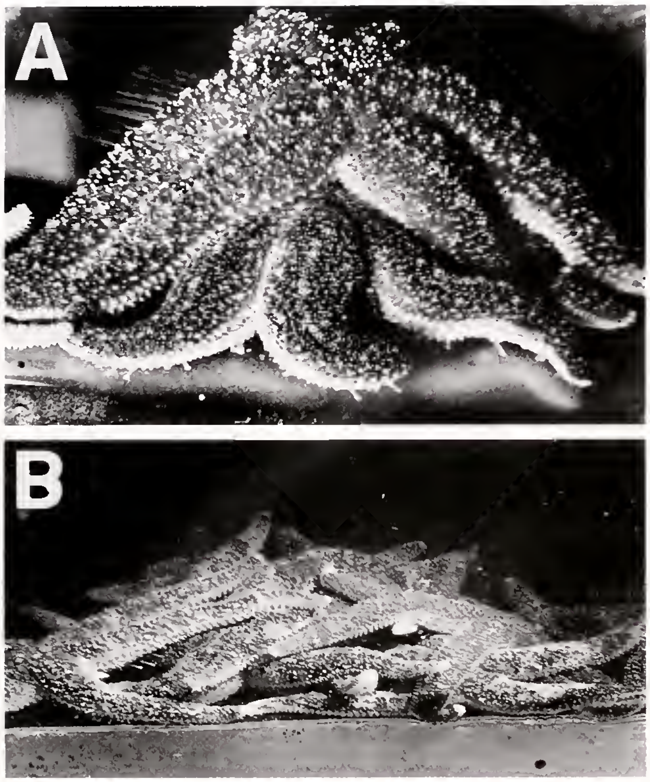

Figure 1. Photographs illustrating the prespawning aggregations of *Leptasterias polaris* in the laboratory. (A) Superposition of two individuals. (B) Massive aggregation of starfish.

Sperm behavior

The term dry sperm refers to undiluted, freshly removed sperm from the mature gonads of at least two males. Activated oocytes were obtained by spreading freshly removed female gonads (including gonoducts) in a petri dish filled with 5 ml of 1-methyladenine 10^{-5} *M*, yielding naturally spawned oocytes after about 45 min of exposure. The buoyancy, capacity for adherence to the substrate, and motility of the sperm were used to describe its behavior in seawater. All experiments on sperm behavior were conducted at a temperature close to the one recorded during the spawning period (2–4°C). All live observations of sperm samples were made under a light microscope (100–400×) and the sperm was kept cool by surrounding the slide with ice cubes. The speed of the spermatozoa was evaluated with a graduated lens, by calculating the number of bars traveled per second. Verifications were undertaken to discard any behavior induced by the light of the microscope or false sperm velocity induced by the sperm-glass interaction (thigmotaxis).

For more than 7 h we continuously recorded the speed, orientation, and flagellar activity of sperm before and after the samples were diluted in seawater (150 μl of dry sperm in 1 l). To examine the behavior of sperm in the water column and on the bottom, the protocol was carried out in both still and agitated (current of $7\ \text{cm} \cdot \text{s}^{-1}$) water. Samples were taken from the bottom of the beaker and at a middle depth every minute for 15 min, then every 15 min for 7 h, and finally at 24-h intervals until the spermatozoa were dead. This protocol, which was repeated twice using repetitive independent measurements, also allowed the estimation of the sperm concentration, with the proportion of resting and agglomerated sperm in the water and on the bottom over time. To estimate the maintenance of sperm potency, samples of sperm deposited on the bottom of the beaker were collected just after the sperm was released in the seawater and regularly over 72 h. The samples were tested on two replicates of 5–10 freshly activated oocytes. Fertilization success was determined by staining the eggs with the DNA-specific fluorescent dye Hoechst 33258. Using a Leitz Diaplan fluorescence microscope, we determined the proportion of eggs showing a male pronucleus.

After spermatozoa reached a state of low activity (>80% barely moved) in the beaker of the above experiment, we tried to stimulate the sperm by exposing it to oocytes. In separate trials, a sample of sperm collected on the bottom of the beaker was exposed to oocytes of different levels of maturity and of different origins. The conspecific previtellogenic and mature oocytes, classified according to the studies of Boivin *et al.* (1986) and Mercier *et al.* (1994), were first assayed. In the case of mature oocytes we tried both activated oocytes (showing germinal vesicle breakdown) and surgically removed unactivated ones. The activated oocytes of *Asterias vulgaris,* another species of starfish, were also tested for stimulation of *Leptasterias polaris* sperm. The oocytes of both species were routinely washed in filtered seawater and immediately used for the reactivation experiments. The speed and the flagellar activity of sperm were noted every 10 min for the first hour, then periodically until no movement was detectable, using replicates and going through the whole protocol twice. A control sample with no oocytes was tested in the same manner.

To investigate sperm sinking, dry sperm was diluted in seawater (1:60) to a concentration of 120×10^3 spermatozoa $\cdot\ \text{ml}^{-1}$. Five homogeneous replicates (10 μl) of this solution were prepared from eight males. The samples were deposited at a middle depth in a 1000-ml beaker filled with seawater, and the time needed for about 50% of the sperm (in visible filaments) to reach the bottom was recorded. These times were compared to those of sperm collected from three species in which fertilization occurs in the water column, the starfish *Asterias vulgaris,* the sea urchin *Strongylocentrotus droebachiensis,* and the sea cucumber *Cucumaria frondosa.*

To examine sperm dispersion over time, we deposited dry sperm on the bottom of a large dish filled with 1000 ml

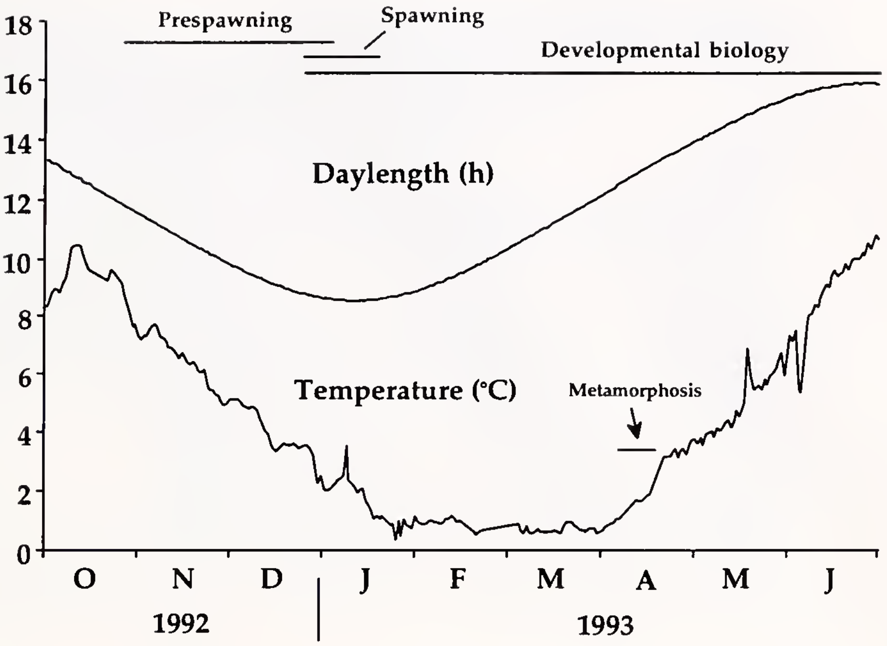

Figure 2. Variation of environmental factors during the reproductive season of *Leptasterias polaris* in the experimental tanks. The arrow points to the beginning of embryo metamorphosis.

of seawater and periodically collected water samples at the surface and on the sides of the dish. The spermatozoan concentrations of the samples were evaluated with a hemacytometer under a light microscope. This experiment was simultaneously performed on live and dead dry sperm of *Leptasterias polaris* and on dry sperm from *Asterias vulgaris, Strongylocentrotus droebachiensis,* and *Cucumaria frondosa.* Sperm longevity could thus be compared for those species under the same conditions.

Development

Whenever we discovered a naturally spawned egg mass, whether brooded or not, it was left undisturbed in the tank so that we could examine development under natural variations of environmental factors. Nonbrooded egg masses were kept clean by periodically agitating the water. Samples were regularly collected with pipettes, from fertilization to young starfish stage, and transferred to 4% formaldehyde/seawater for later examination with light microscopy. These embryos also served to determine developmental kinetics and growth. During the first hour, samples were collected every 2–5 min, then about every day until the brachiolaria stage, and finally once a week. A new stage was considered attained when 50–60% of the embryos reached it. Maximum embryo diameters were measured under a light microscope equipped with a graduated lens.

Results

Prespawning behavior

During summer and early fall, the well-fed starfish clearly avoided each other. Contacts among starfish began in mid-October, coinciding with the first significant decrease of temperature (Fig. 2). The proportion of contact-free starfish decreased, reaching a minimum plateau between 1 November and 15 December (Fig. 3) when temperatures fell to about 4°C. In that same interval, the proportion of starfish involved in intimate contacts increased progressively, with the maximum recorded in the last week of November. Superposition became more frequent in early December and was observed most often just before the main spawning period of late December (Figs. 1, 3) when the water temperature fluctuated between 3° and 4°C. When the temperature fell below 3°C (end of December), the number of superpositions and intimate contacts decreased while spawning was recorded (Fig. 3). Superposition behavior ceased after January and most individuals resumed avoiding one another (Fig. 3), with contact-free starfish accounting for more than 85% of the observed individuals. Only some light contacts and a few intimate ones were observed. No particular sex-specific patterns were noticed for the aggregations, which involved both males and females. Addition of prey to the experimental tanks always provoked a migration of the starfish toward the food source, except 1 week before spawning

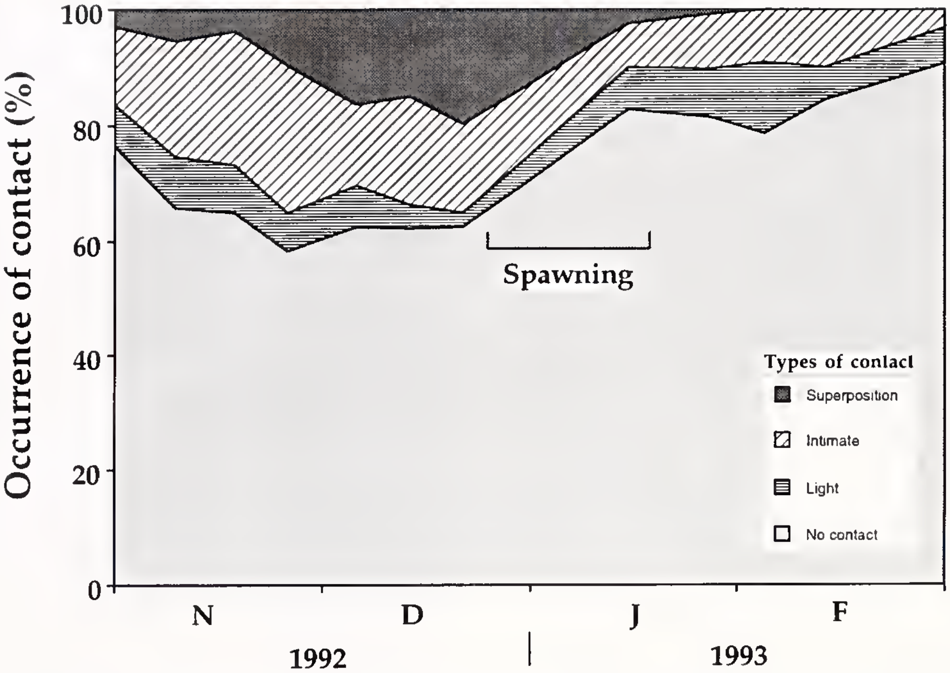

Figure 3. *Leptasterias polaris* Temporal evolution of the prespawning aggregative behavior recorded several times a week for a 3-month period. For each date, the percentage of individuals involved in a particular type of contact was recorded.

when feeding did not disturb the contact behavior between the individuals.

Environmental factors seem to be involved in the initiation and development of the prespawning aggregative behaviors. No aggregation occurred among individuals maintained at constant temperature and photoperiod, but grouping did take place among individuals kept in total darkness with natural temperature.

Spawning

Our experimental information includes actual observations of spawning events in 4 females and 3 males and additional indications from sperm agglutinates on many males and on the substrate. We also observed more than 20 brooding females, which were always discovered within 24 h of spawning. We examined the correlations of all our observations with environmental factors (Fig. 2), which were similar in the laboratory and in the field. Spawning occurred in our tanks from 19 December to 12 January, which roughly corresponded to the period when we observed spawning in the field. During spawning events, the starfish stayed close together, although there was a net decrease in frequency of contact (Fig. 3). The spawning individuals were not paired or superposed.

Spawning events. Figure 4 schematically illustrates the spawning behavior we observed in the experimental tanks. When a male spawned, it elevated the central disk, standing on the curved tip of its arms, and emitted sperm as a whitish stream from the six interradial aboral gonopores. Emission continued for more than an hour. Qualitative observations showed the sperm to be negatively buoyant, with a tendency to deposit on the substrate. The first female spawning was observed after male spawning. The female remained flat on the substrate to release eggs while its arms were extended, then progressively adopted the characteristic brooding posture in "pinwheel" shape (Figs. 4, 5a, b). The average 300–500 spawned oocytes emerged individually at a rate of about 1 oocyte every 2–5 s from each of the six aboral gonopores located between the arms. Almost all the spawning starfish observed were on a vertical substrate (aquarium wall or rock face). The eggs had a tendency to fall and were retained by the ambulacral podia and the curved arms of the female (Fig. 5c). A number of eggs (possibly 50%) were, however, lost before the end of a given spawning event. The final posture adopted by the female was not always a perfect pinwheel shape but seemed designed to cover the egg mass (around 20–25 eggs $\cdot$ cm^{-2}) in the best way possible. Consequently, some brooding individuals were seen with two or three arms extended somewhat to cover isolated groups of oocytes.

Induction of spawning. Although the first individuals to spawn were males, spawning events were subsequently recorded in both sexes alternately throughout the spawning period (Fig. 2). Nevertheless, some correlations con-

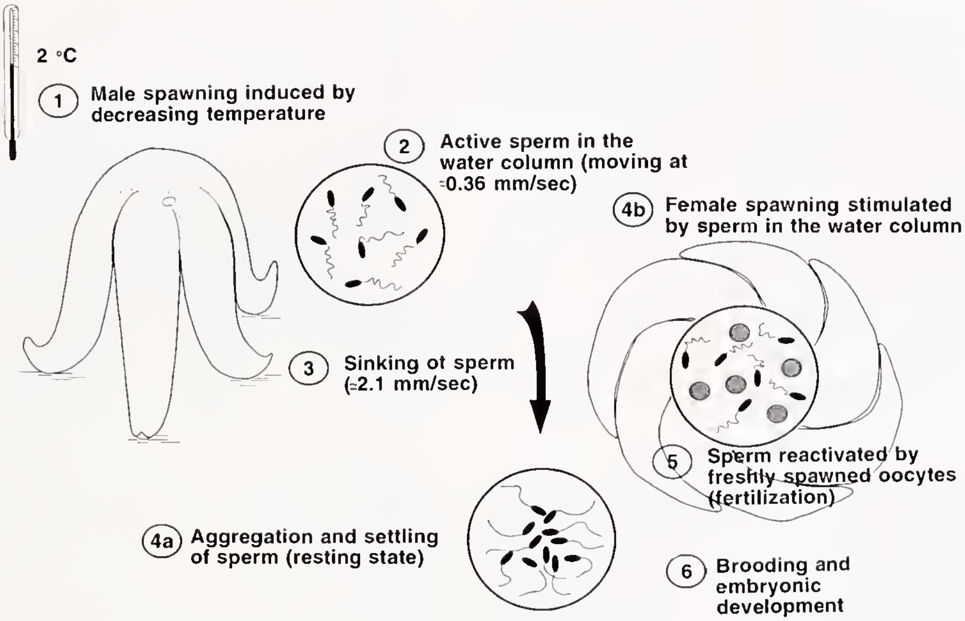
2 °C
① Male spawning induced by decreasing temperature
② Active sperm in the water column (moving at ≈0.36 mm/sec)
③ Sinking of sperm (≈2.1 mm/sec)
(4a) Aggregation and settling of sperm (resting state)
(4b) Female spawning stimulated by sperm in the water column
⑤ Sperm reactivated by freshly spawned oocytes (fertilization)
⑥ Brooding and embryonic development

Figure 4. Schematic illustration of spawning behavior for male and female *Leptasterias polaris*, showing the relation between them.

cerning the induction of spawning could be made in the course of our experiments. A few isolated male spawnings occurred during minimum daylength (≤9 h) when water temperature was around 2°–3°C (first sight of sperm filaments) in late December (Fig. 2), but most spawnings were observed in January as the temperature fell further. The temperature fluctuated between 2° and 4°C (Fig. 2) throughout the following weeks of spawning, and gamete release seemed to be closely related to these variations. The same spawning pattern was observed in control group 2, maintained in natural temperature and total darkness, whereas no spawning occurred in control group 1, kept at steady temperature and photoperiod. As a result of the seasonally low primary production, the tanks provided with seawater from the estuary, where spawnings were recorded, contained virtually no phytoplankton. Salinity continuously fluctuated between 26 and 32‰ without any consistent increasing or decreasing trends (data not presented). During qualitative observations, the presence of sperm filaments seemed to be correlated with subsequent female spawning within a few hours. Complementary experiments conducted in replicates showed that the introduction of sperm in the water induced spawning of several females in the controlled environment (control group 1), therefore minimizing the importance of temperature in female spawning. No male spawning was induced by the presence of sperm.

Sperm behavior

A microscopic examination of the sperm showed that the head (more or less spherical) measured 3.25 ± 0.25 μm and the flagellum 62 ± 3 μm. The negative buoyancy of the male spawn caused it to sink (mainly as white filaments), at a rate of about 2.1 $\text{mm} \cdot \text{s}^{-1}$. Only a small portion was resuspended after reaching the bottom. We examined the motility of sperm artificially maintained in the water column compared to the motility of sperm settled on the bottom (Fig. 6). Freshly extracted dry sperm contained nonmotile spermatozoa. Upon introduction to the seawater, the spermatozoa immediately displayed a major increase of activity, both in the water and on the bottom (Fig. 6). Within the first 30 min of water contact, 100% of the spermatozoa had reached a velocity of 250–350 $\mu\text{m} \cdot \text{s}^{-1}$ and showed intense flagellar activity, resembling a helical movement with 6–7 $\text{revolutions} \cdot \text{s}^{-1}$. The spermatozoa maintained in suspension continued to show the same high velocity and activity with no marked net decrease for the whole 425 min of observation. In contrast, after reaching a maximum velocity (after 40–50 min) in synchrony with the sperm in suspension, the sperm on the bottom showed an abrupt decrease of activity (reduced velocity and flagellar movement). The settled spermatozoa attained a low velocity ($\approx 50\ \mu\text{m} \cdot \text{s}^{-1}$) after 120 min of contact with seawater (Fig. 6a). This corresponded to an increase in the inactive population of spermatozoa, which rose from 7% to 56% in the same period (Fig. 6a). The spermatozoa seemed to gradually reach a state of almost null velocity (about 0–15 $\mu\text{m} \cdot \text{s}^{-1}$) in which they only quivered and moved by a wave along the flagellum (proximal to distal) with a 10° angle. The percentage of settled spermatozoa that attained a state of low activity was 47%

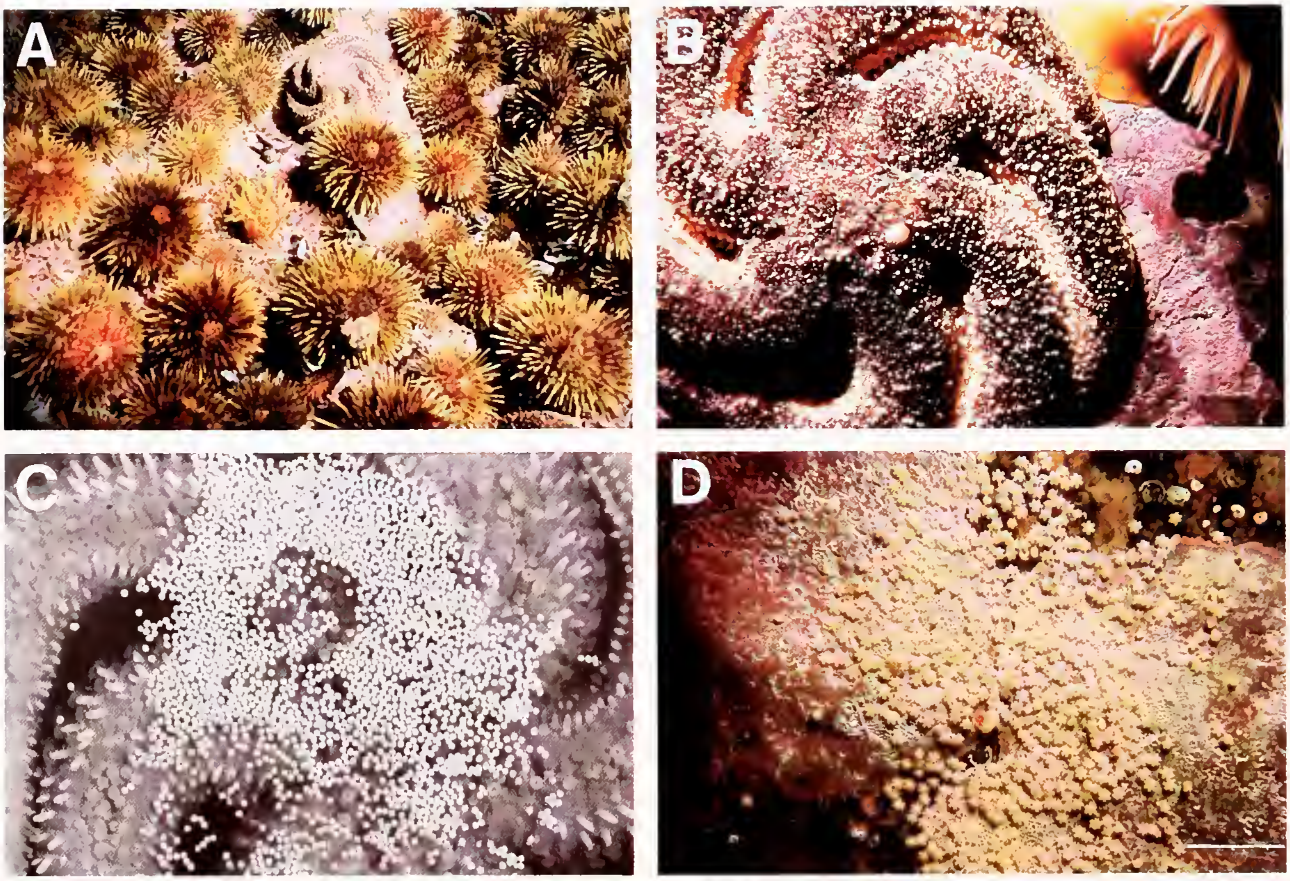

Figure 5. Underwater photographs showing (A) *Leptasterias polaris* brooding in its natural habitat surrounded by sea urchins; (B) close-up of a brooding female on the rocky bottom at 30 m depth; (C) fertilized eggs under a female; (D) young starfish after about 5.5 months of growth in their natural habitat (the female was previously removed). The scale bar represents 15 mm and applies to photographs (C) and (D).

after 120 min of contact with seawater, 62% after 250 min, and a maximum of 80% after 380 min (Fig. 6a). On the bottom and most probably on the glass walls, the increased number of nearly inactive spermatozoa was responsible for the decrease in overall velocity of the population. This correlation could also be made for the sperm in the water column, although the small apparent decrease in velocity could only be visually associated with the slight increase in inactive spermatozoa (Fig. 6b). Another progressive phenomenon was the formation of sperm conglomerates (dense aggregations), which began about 180 min after the sperm came in contact with seawater and reached a maximum (100 and more spermatozoa together) after 380 min. About 8 h after entry into still seawater, the sperm covered the bottom and glass walls of the dish. This also occurred in agitated conditions, although after a longer period, showing that the sperm of *Leptasterias polaris* is very adhesive.

The sperm behavior of *Leptasterias polaris* differed from that observed in the other species of echinoderms tested: the sperm of *Asterias vulgaris* was diluted within 2 min, before reaching bottom, and those of *Cucumaria frondosa* and *Strongylocentrotus droebachiensis* sank at 1 mm · s^{-1} and 1.5 mm · s^{-1} respectively. The sperm of these species did not adhere to the bottom, but was immediately and almost totally redispersed, becoming well dispersed in seawater within 80 min. In contrast, the majority of *L. polaris* sperm stayed on the bottom until death.

After reaching a state of almost null activity (conglomerated or not), the sperm of *Leptasterias polaris* could be reactivated by contact with conspecific activated mature oocytes (Fig. 7). Within 10 min of exposure to these oocytes, sperm motility was reinitiated. Spermatozoa velocity increased significantly, by 485% ($P < 0.01$, Student's *t* test), after 20 min of contact, and attained a peak of 230 μm · s^{-1} after 50 min. This was almost 12 times the original speed (Fig. 7). Subsequently, the sperm velocity decreased progressively and reached a minimum after 1020 min (Fig. 7). Reactivation was unsuccessful with unactivated conspecific mature and previtellogenic oo-

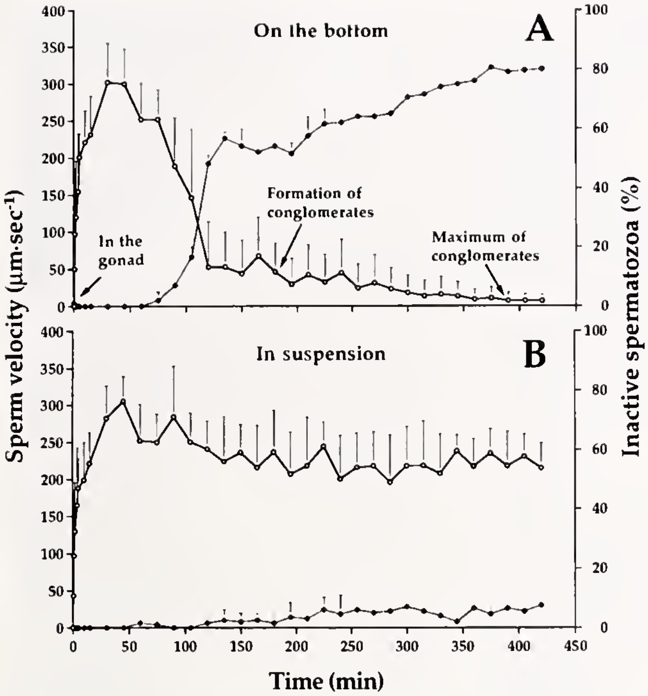

Figure 6. *Leptasterias polaris.* Temporal changes in velocity and activity of sperm settled on the bottom and kept in suspension. The sperm velocity (— O —) upon contact with seawater is given with the corresponding percentage of inactive spermatozoa (· · · ♦ · · ·). The error bars represent the confidence intervals (95%).

cytes as well as with mature activated oocytes of *Asterias vulgaris*. The spermatozoa exposed to those oocytes showed a constant low velocity, comparable to that observed in the unexposed sperm serving as control (Fig. 7).

The sperm of *Leptasterias polaris* was more resistant than that of other species. Most spermatozoa collected from other echinoderms were dead after 8–20 h, whereas those of *L. polaris* remained capable of high fertilization success (57%) for as long as 34 h in seawater (Fig. 8) and showed a high percentage of mortality only after 6–7 days.

Development

Early development. The complete chronology of embryonic development of *Leptasterias polaris* is presented in Table I and Figure 9. The large unfertilized mature oocytes (≈0.85 mm in diameter) were mainly spherical and yellowish, or occasionally light orange. They were covered with a rather thick outer membrane (average of 7.04 µm). After their fertilization, the eggs were attached to one another by the fertilization membrane, showing that the membrane was sticky, especially after reaching the 2-cell stage (Fig. 9a). All the cleavages were of the radial holoblastic type. Later in its development, from the blastula to young gastrula, the embryo decreased in size (≈6%) due to blastomere compaction (Table I). The furrows became shallower on the pole, but tended to deepen on the other pole, eventually forming the blastopore. After 711 h, the embryo's surface became uniform and ciliated. The embryo then began to spin inside the fertilization membrane and hatched 96 h later (Fig. 9e).

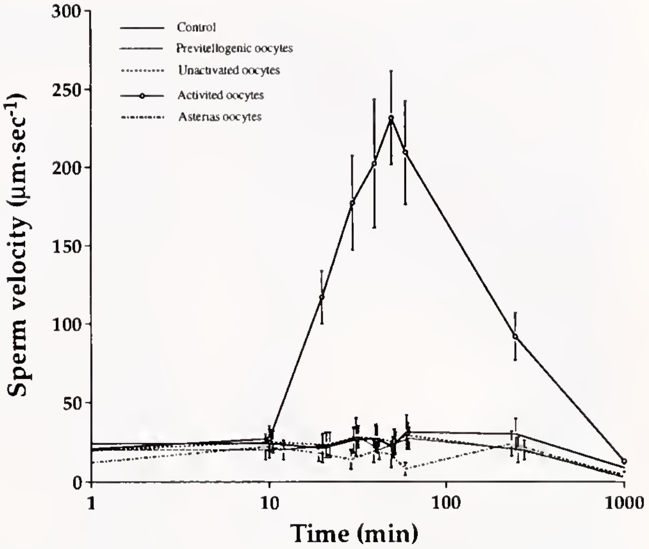

Figure 7. *Leptasterias polaris.* Influence of oocyte maturity on sperm reactivation. The horizontal axis has a log$_{10}$ scale and the error bars represent the confidence intervals (95%).

Many females moved away from their brood within a week, leaving their embryos uncared for in the experimental tank. No significant difference was observed be-

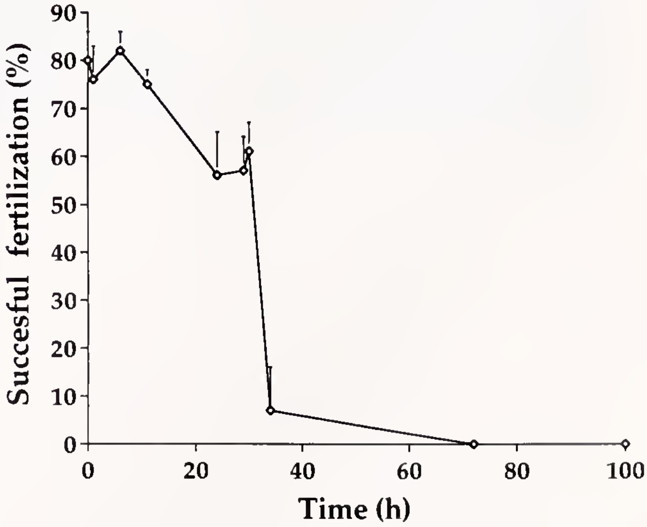

Figure 8. *Leptasterias polaris.* Sperm effectiveness to fertilize activated mature oocytes over time. The error bars represent the confidence intervals (95%).

Table I

Leptasterias polaris: *Kinetics of embryonic development in experimental tanks supplied by running seawater*

Developmental Stages	Time	Size (μm)
Spawning	0	852 ± 36
Early stage of the fertilization membrane elevation	12 min	840 ± 38
Fertilization membrane completely elevated	27 min	940 ± 48
Emission of the first polar body	45 min	939 ± 26
Second polar body	?	?
2-cell	45 h	1079 ± 15
4-cell	86 h	1032 ± 15
8-cell	92 h	1046 ± 12
16-cell	106 h (4 d)	1031 ± 18
32-cell	121 h (5 d)	1062 ± 9
64-cell	133 h (5–6 d)	1103 ± 62
128-cell	146 h (6.1 d)	1080 ± 23
256-cell	156 h (6.5 d)	1101 ± 40
Blastula (compaction)	209 h (8–9 d)	1120 ± 51
Wrinkled-blastula	260 h (10–13 d)	1144 ± 45
Young gastrula	493 h (20–21 d)	1056 ± 31
Late gastrula	666 h (27–28 d)	1288 ± 52
Spinning	711 h (29–30 d)	1375 ± 27
Hatching	807 h (33–34 d)	1121 ± 42
Brachiolaria	38–84 d	1190 ± 31
Metamorphosis	75–90 d	1207 ± 70
Young starfish (2 pairs of ambulacral podia/arm)	120–132 d	1348 ± 53
Young starfish (preoral lobe disappears and ocelli are present)	150–170 d	1534 ± 77
Free-moving starfish (visible pyloric caeca and opening of buccal cavity)	180–195 d	2102 ± 102
Small starfish (uprighting movements)	more than 200 d	over 2500

A new stage was considered attained when 50%–60% of the embryos reached it. The standard deviations about the mean size are given.

tween the developmental rate of brooded and nonbrooded embryos during early development up to hatching ($P = 0.392$, Student's t test), which is the latest brooded stage we observed in the laboratory (Table II).

Late development. After the loss of the fertilization membrane upon hatching, the unciliated portion of the late gastrula enabled it to attach to the substrate, well before the appearance of the brachiolar arms (Fig. 9f). The hatched larvae immediately settled on the bottom; however, many embryos were lost by the female at this time of development (especially for those brooding on vertical surfaces). With the growth of the embryo, the arms elongated, becoming very distinct from the dorsal ciliated bulb (larval body), and served the purpose of adhesion to the substrate. Cilia were still present, so the fixation was mainly with the sticky ramified tips that had developed at the end of each arm (Fig. 9g). A depression began to grow in the central portion delimited by the arms (fixing disk), and was used for later fixation on the substrate with the brachiolar arms. The brachiolar stage was prolonged as long as the water temperature remained around 1°C (February and March; Fig. 2), until a sudden warming coincided with metamorphosis (day 75–90). Although there was a concurrent elevated photoperiod, this factor had been increasing for months and cannot be the deciding inducer (Fig. 2). About 50% of the embryos died during the gradual metamorphosis, which was completed around mid-May following the complete disappearance of the brachiolar arms (Fig. 9h–j). At this stage the characteristic yellow color had been lost and the embryo was whitish or translucent, indicating that a large amount of vitelline reserves had been consumed. One month later (mid-June), the young starfish possessed a well-developed buccal cavity, stomach, and pyloric caeca, which were easily observed across the transparent body wall on the oral surface (Fig. 9l) with the madreporite and anus on the aboral surface. The ambulacral podia, baring suckers, became effective in helping the uprighting movement and displacement of the growing starfish, which were capable of coordinated locomotion. Having the capacity to feed and move on their own, the young were self-sufficient about 6 months after fertilization (Figs. 5d, 9k, l).

Discussion

Temporary aggregative behavior is common among marine invertebrates. It has been observed in echinoderms such as echinoids (Pearse and Cameron, 1991; Levitan *et al.*, 1992; Young *et al.*, 1992), ophiuroids (Warner, 1979) and asteroids (Ormond *et al.*, 1973; Sloan, 1980, 1984; Blankley and Branch, 1984; Run *et al.*, 1988) as well as in crustaceans (Gherardi and Vannini, 1993). Those studies have proposed many hypotheses about the meaning and usefulness of aggregation, but only a few have discussed a relationship with reproduction and spawning.

Most of the few reports of aggregation related to reproduction in echinoderms refer to aggregative spawning events in the field (Hendler and Meyer, 1982; McEuen, 1988; Pearse *et al.*, 1988). Pseudocopulation or pairing has been observed in *Archaster typicus* (Ohshima and Ikeda, 1934; Komatsu, 1983; Run *et al.*, 1988) and in *Neosmilaster georgianus* (Slattery and Bosch, 1993), but no such behavior could be detected during our study. Like Chia (1968) in observations of *Leptasterias hexactis*, we noticed that the groupings occurred only as the breeding season approached. Grouping behavior initiated well before spawning, such as observed in *L. polaris*, has not been often reported. Young *et al.* (1992) observed this behavior in the bathyal sea urchin *Stylocidaris lineata*, in which the individuals aggregate during autumn before spawning. Orton (1914) and Lewis (1958) also mentioned

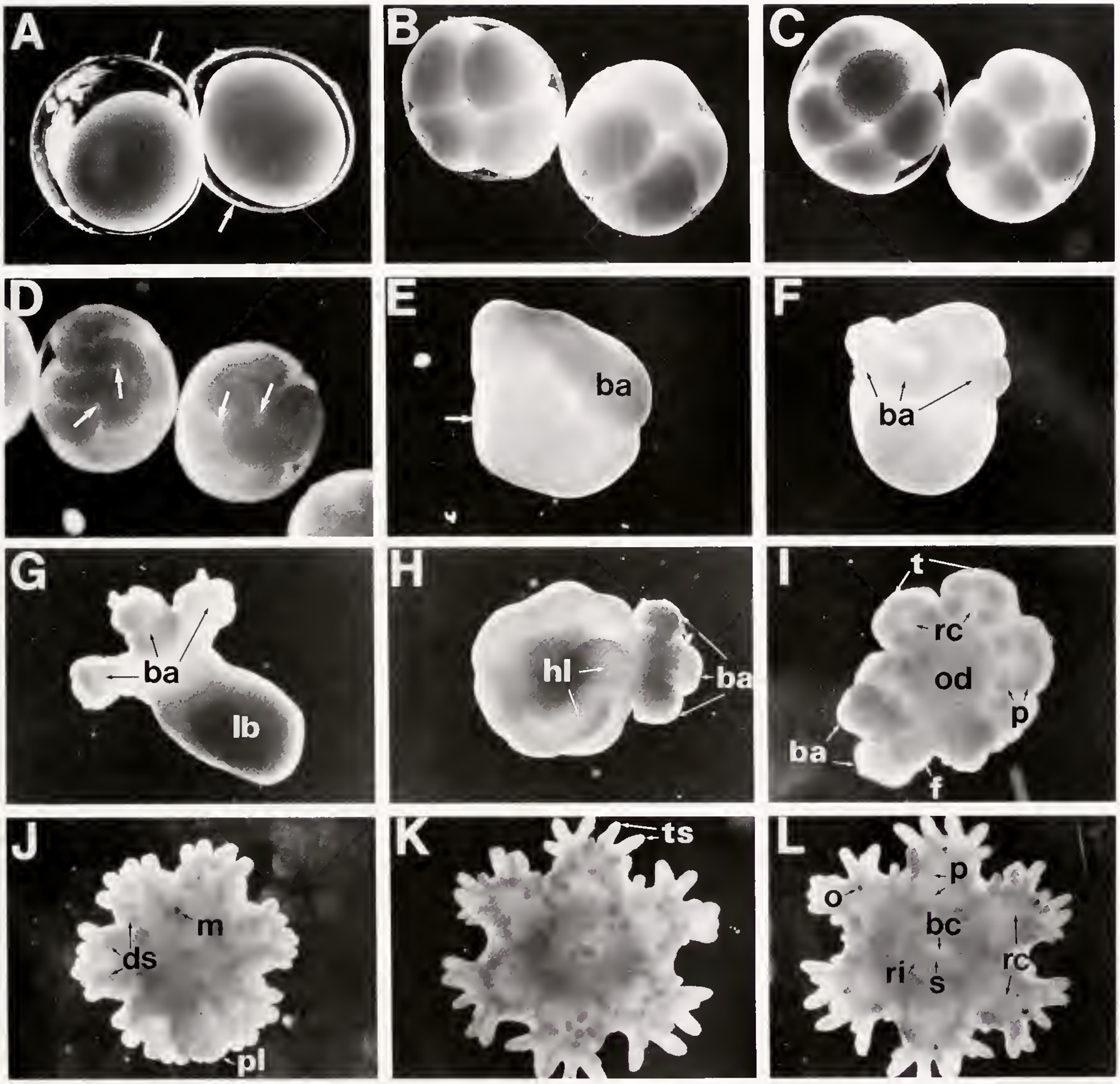

Figure 9. *Leptasterias polaris* Photographic sequence showing the principal steps of development from fertilization to young starfish (4×); see Table I for corresponding age and size of the embryos. (A) Fertilized eggs with fertilization membrane completely elevated (arrows). (B) 4-cell stage. (C) 8-cell stage. (D) Wrinkled-blastula stage on which it is possible to observe the furrows (arrows). (E) Early brachiolaria stage (newly hatched) showing early shaping of brachiolar arms (ba) and the persistent blastopore (arrow). (F) Growth of the three brachiolar arms (ba). (G) Fully developed brachiolarian embryo with the larval body (lb) and the slightly ramified brachiolar arms (ba). (H) Metamorphosing embryo with brachiolar arms (ba), showing the development of the first five hydrocoelic lobes (hl). (I) Further metamorphosed embryo with two pairs of ambulacral podia (p) and a terminal tentacle (t) on each of the five arms. The six hydrocoelic lobes are transforming into the radial canals (rc). A distinct oral disk (od) and the residual brachiolar arms (ba) with central fixing disk (f) are visible. (J) Aboral view of a free-moving, six-rayed young starfish showing clearly visible dorsal spines (ds), madreporite (m), and regressing preoral lobe (pl). (K) Aboral view of a small starfish showing the well-developed terminal spines (ts). (L) Oral view of a small starfish ready to leave the brood. The buccal cavity (bc) has opened and the stomach (s) is visible surrounded by the ring canal (ri). We can also see the ambulacral podia (p), the well-developed radial canals (rc), and the ocelli (o).

the occurrence of this prespawning aggregative behavior in echinoids.

What cues make the starfish come together and why do they display this behavior? Pheromones have often been proposed as the proximate cause (Kanatani and Shirai, 1968), principally acting to synchronize the liberation of gametes (Ormond *et al.*, 1973; Young *et al.*, 1992; Slattery and Bosch, 1993). For broadcast spawners, aggregation and synchronous gamete release appear to be important in minimizing gamete dispersion, ensuring good fertilization success (Levitan, 1988; Levitan *et al.*, 1992). For a protective brooder like *Leptasterias polaris*, synchronous spawning would not be very advantageous as the eggs laid by the female are maintained under the body at all times. Therefore, aggregation is more likely to be related to preparatory recognition. Contact chemoreception is suggested to be a strong sensory stimulus in asteroids (Sloan and Campbell, 1982), maybe to ensure adequate recognition of males and females before spawning. In *Archaster typicus* and *Neosmilaster georgianus*, this recognition is of prime importance because fertilization is ensured by the close superposition of a male and a female (Run *et al.*, 1988; Slattery and Bosch, 1993). In *L. polaris*, our results demonstrate a totally different pattern, in which the prolonged intimate contacts could be related to the chemical induction of synchronized gamete development as demonstrated in sea cucumbers *Cucumaria frondosa* (Hamel *et al.*, unpub. manuscript).

The initiation of aggregative behaviors in *Leptasterias polaris* appears to be correlated with decreasing temperature. Aggregations were observed among all starfish that were supplied with natural seawater and exposed to seasonal changes of water temperature, both when maintained in darkness and when exposed to natural photoperiod. Lower temperatures possibly trigger or enable the liberation of hormones through a pathway otherwise suppressed and may favor the formation of clumps of starfish. This would assure that a fairly good proportion of male and female individuals would be close together and ready to release their gametes during the winter spawning events. We saw no evidence of recognition between sexes but can assume that the male/female ratio close to equality ensures a 50% chance of random heterosexual encounters. Young *et al.* (1992) found that individuals of *Stylocidaris lineata* also aggregated without regard to sex. The spawning events were not synchronized—as the male began liberating sperm before any female spawning could be detected—which differs from spawning sequences mentioned for *Hymenaster membranaceus* (Pain *et al.*, 1982) and for *Archaster typicus* (Run *et al.*, 1988). Male spawning seemed to be triggered when the falling temperature reached about 2°C, an inducer previously suggested by O'Brien (1976) for *L. littoralis*.

The sperm behavior of *Leptasterias polaris* possibly further explains the need for aggregation. Upon its release, a portion of sperm can be dispersed by currents and remain active as long as it is maintained in the water column (Fig. 6), potentially limiting the genetic isolation in a population. From the spawnings successfully induced by sperm in our experimental tanks, we infer that this active fraction is the stimulus for females to spawn. Sperm as a stimulus of spawning has also been discussed by Starr *et al.* (1990) for the sea urchin *Strongylocentrotus droebachiensis*. In fact, sperm suspension in seawater is suggested to be the spawning inducer in many species of ophiuroids and echinoids (Thorson, 1950; Lewis, 1958). The lack of strong epidemic spawnings during natural breeding activities in our tanks could be explained by fluctuations of water temperature around the 2°C threshold at that time (Fig. 2). A few male spawnings could have been triggered in late December, then delayed by the rising temperature (to almost 4°C) before being induced again in the second week of January. Females followed this scattered pattern because they probably need to be close to a sperm source for spawning to be induced. The negative buoyancy and stickiness of sperm causes most spermatozoa to settle on the substrate where they gradually enter an inactive state. The settling ensures a minimal dispersion of sperm but makes fertilization dependant on the proximity of individuals, which is achieved by aggregation. Further, sperm inactivation seems an effective energy-saving behavior, extending the viability of settled sperm up to 6 or 7 days, which is much longer than the 2- to 3-day longevity of sperm maintained in the water column. The extreme endurance of *L. polaris* sperm is further emphasised upon comparison with that of the other asteroids, holothuroids, and echinoids tested, for which the spermatozoa did not survive longer than a day at the temperature normally recorded during their spawning periods. These short-lived spermatozoa display a dispersion behavior that we could probably associate with organisms having synchronously spawning males and females. The longevity of sperm from *L. polaris* is probably an advantage given the asynchronous spawning of the sexes in this species.

We could not determine whether females were attracted by deposited sperm, but the delay between male and female spawnings seems advantageous. Because the spermatozoa are present on the medium before eggs are emitted, they do not have to overcome the protective barrier maintained by the brooder. Thanks to its adhesiveness, sperm also covered the vertical substrates favored by many spawning females in our experiments. It is probable that as soon as a female spawns on the sperm-covered substrate, the oocytes can reactivate the inactive sperm (Fig. 7), and fertilization takes place. Experimentally, the best success (>75%) was achieved when the delay between the male and female spawnings was no more than 11 h; however, success was still good (>50%) after as long as 30 h (Fig. 8). A contact of 20–50 min with the oocyte seemed to be necessary for the spermatozoan to attain an optimum speed that probably maximizes its ability to fertilize. Sperm inactivity and reactivation appears to be very rare in marine habitats. Although sperm chemotaxis has been shown in echinoderms (Miller, 1985), no significant velocity increase or activation of the attracted sperm has ever been mentioned, except in cnidarians (Miller, 1979a, b) and larvaceans (Miller and King, 1983). The closest example with a similarity to *Leptasterias polaris* is the sperm of the horseshoe crab (*Limulus polyphemus*), which undergoes a brief flurry of motility and remains nonmotile until it encounters a sperm motility initiating molecule (SMI) emanating from eggs (Clapper and Epel, 1981). In contrast, both our observations and previous studies (Chia, 1968) show that the sperm of most echinoderms becomes active upon release in the water and disperses quickly. This is probably the best strategy when both male and female gametes are released in great numbers in the seawater at close intervals.

Table II

Leptasterias polaris: *Development of brooded and nonbrooded embryos*

	Brooded Embryos		Nonbrooded Embryos	
Developmental Stages	Time	Size (μm)	Time	Size (μm)
Fertilization	0	870 ± 43	0	852 ± 36
2-cell	43 h	1111 ± 22	46 h	1079 ± 15
4-cell	81 h	1092 ± 18	86 h	1032 ± 15
8-cell	93 h	1032 ± 9	92 h	1046 ± 12
16-cell	104 h	1044 ± 24	106 h	1032 ± 18
32-cell	125 h	1050 ± 33	121 h	1062 ± 9
64-cell	140 h	1082 ± 39	133 h	1103 ± 62
128-cell	152 h	1086 ± 41	146 h	1080 ± 3
256-cell	164 h	1092 ± 52	156 h	1101 ± 40
Blastula	8–9 d	1090 ± 62	8–9 d	1120 ± 51
Gastrula	20–21 d	1288 ± 52	20–21 d	1111 ± 33
Hatching	33–34 d	1121 ± 42	32–35 d	1199 ± 63

A new stage was considered attained when 50%–60% of the embryos reached it. The standard deviations about the mean size are given.

In *Leptasterias polaris*, the gamete behavior seems well adapted to the brooding mode, which in turn has a protective function. Brooded and nonbrooded embryos showed almost perfect synchrony in development through the gastrula stage (Table II). This suggests the absence of the obligatory exchange of nutrients between parent and young that is seen in *Pteraster militaris* (McClary and Mladenov, 1990), where a brood chamber is present. In *L. hexactis*, another brooding asteroid overlaying its eggs, the maternal presence is proposed to be essential to help the hatching embryo tear the fertilization membrane (Chia, 1966). Although this was thought to be the case for *L. polaris* (Himmelman *et al.*, 1982), we observed no evidence of that phenomenon. The hatching was not delayed and no loss of embryos was evident in the unbrooded group. Brooding in *L. polaris* probably serves mainly to aerate the embryos and prevent them from being covered with sediment as they lie on the substrate. Observations in the field (Himmelman *et al.*, 1982) support this hypothesis, as the substrate under a brooding starfish was always found clear of debris. Brood protection also seems to be in direct relation to adverse environmental conditions and predatory pressures. Extremely active grazers such as sea urchins, which are abundant wherever *L. polaris* is found, would rapidly decimate any unprotected starfish embryos exposed on a rock (Fig. 5a).

The embryonic development observed in *Leptasterias polaris* is similar to that described for *L. hexactis* (Chia, 1968) and *L. acceptances similispinis* (Kubo, 1951). The developmental kinetics of *L. polaris* is characteristically slower (Table I) than in all other reports for this genus, perhaps because of the lower temperatures (0°–1°C) found during the breeding and the subsequent development of this species. The major differences between our results and those of Kubo (1951) and Chia (1968) are the occurrence of a spinning stage and the much earlier hatching of *L. polaris*. Because *L. polaris* embryos hatch in late gastrula, before they develop brachiolar arms, such arms cannot contribute to the tearing of the fertilization membrane, as they are said to do in the two other species.

The freshly spawned eggs are negatively buoyant and do not adhere to one another until a few moments later, after fertilization. This stickiness was also observed by Chia (1968) for *Leptasterias hexactis*, but was correlated with a reaction to seawater rather than with fertilization. Through its growth, the embryo undergoes many changes in attachment capacity, which is first provided by the sticky fertilization membrane, then by small unciliated body areas after hatching, and later by the fixing disk and ramified tips of the brachiolar arms. The parental protection is probably useful in preventing dispersion of embryos during these changes in fixation ability, for instance during hatching, when attachment to the substrate may be ineffective for a short time. After the metamorphosis of the embryos (4–5 months), brooding individuals are still observed in the field for at least one month. The free-moving young starfish seem to remain under protection through the development of the pyloric caeca and the opening of the mouth. Environmental factors apparently play a role in the development of the embryos, especially in initiating metamorphosis by a considerable increase in temperature (Fig. 2). As previously mentioned by Boivin *et al.* (1986), this correlation seems to ensure that the young starfish are ready for release at the proper time, namely spring, when conditions are most favorable for their survival as self-sufficient individuals. This timing control, together with the possibly lower energetic cost required from the parent under cold temperatures, is probably an advantage of winter brooding.

Acknowledgments

We thank Dr. C. Bouland for her help during the experiments, A. Caron for helpful criticism and assistance with statistical analysis, and J.-L. Théberges for photoprocessing. We greatly appreciated the helpful comments of Drs. S. Demers, J. H. Himmelman, C. Bouland, M. I. El-Sabh, and two anonymous reviewers on the manuscript. We are also grateful to J. Noël for her collaboration on the sketches and to N. Piché for photographs of *Leptasterias* and field observations. This work was carried out thanks to the space and material lent to us by Drs. É. Pelletier and F. Dubé at the Station Aquicole de Pointe-au-Père and was supported by personal funds of J.-F. Hamel and A. Mercier.

Literature Cited

Blankley, W. O., and G. M. Branch. 1984. Co-operative prey capture and unusual brooding habits of *Anasterias rupicola* (Verrill) (Asteroidea) at sub-Antarctic Marion Island. *Mar. Ecol. Prog. Ser.* **20:** 171–176.

Boivin, Y., D. Larrivée, and J. H. Himmelman. 1986. Reproductive cycle of the subarctic brooding asteroid *Leptasterias polaris*. *Mar. Biol.* **92:** 329–337.

Chia, F.-S. 1966. Brooding of a six-rayed starfish, *Leptasterias hexactis*. *Biol. Bull.* **130:** 304–305.

Chia, F.-S. 1968. The embryology of a brooding starfish, *Leptasterias hexactis* (Stimpson). *Acta Zool.* Bd XLIX: 1–44.

Chia, F.-S., and C. W. Walker. 1991. Echinodermata: Asteroidae. Pp. 301–353 in *Reproduction of Marine Invertebrates.* A. C. Giese, J. S. Pearse, and V. B. Pearse, eds. Boxwood Press, Pacific Grove, California.

Clapper, D. L., and D. Epel. 1981. Isolation and utilization of a sperm motility initiating peptide in the horseshoe crab *Limulus polyphemus*: evidence for involvement of Ca^{2+} but not intracellular pH or membrane potential in motility initiation. *J. Cell Biol.* **91:** 179.

Emerson, C. J. 1977. Larval development of the sea star, *Leptasterias polaris*, with particular reference to the optic cushion and ocelli. *Scan. Elec. Micro.* **2:** 631–638.

Giese, A. C., and H. Kanatani. 1987. Maturation and spawning. Pp. 251–313 in *Reproduction of Marine Invertebrates*, Vol. 9. A. C. Giese, J. S. Pearse, and V. B. Pearse, eds. Blackwell Scientific Publications, Palo Alto, California.

Giese, A. C., and J. S. Pearse. 1974. Introduction: general principles. Pp. 1–49 in *Reproduction of Marine Invertebrates*, Vol. 1, *Acoelomate and Pseudocoelomate Metazoans.* A. C. Giese and J. S. Pearse, eds. Academic Press, New York.

Gherardi, F., and M. Vannini. 1993. Hermit crabs in a mangrove swamp: proximate and ultimate factors in the clustering of *Clibanarius laevimanus*. *J. Exp. Mar. Biol. Ecol.* **168:** 167–187.

Hendler, G., and D. L. Meyer. 1982. Ophiuroids *flagrante delicto* and notes on the spawning behavior of other echinoderms in their natural habitat. *Bull. Mar. Sci.* **32:** 600–607.

Himmelman, J. H. 1981. Synchronization of spawning in marine invertebrates by phytoplankton. Pp. 3–19 in *Advances in Invertebrate Reproduction.* W. H. Clark, Jr. and T. S. Adams, eds. Elsevier North Holland, New York.

Himmelman, J. H., and C. Dutil. 1991. Distribution, population structure and feeding of subtidal seastars in the northern Gulf of St. Lawrence. *Mar. Ecol. Prog. Ser.* **76:** 61–72.

Himmelman, J. H., Y. Lavergne, A. Cardinal, G. Martel, and P. Jalbert. 1982. Brooding behaviour of the northern sea star *Leptasterias polaris*. *Mar. Biol.* **68:** 235–240.

Hyman, L. H. 1955. *The Invertebrates: Echinodermata.* McGraw-Hill, New York, 763 pp.

Kanatani, H., and H. Shirai. 1968. Does GSS or MIS act as a pheromone? Problems concerning the participation of a pheromone in starfish spawning. *Zool. Mag.* **77:** 207–212.

Komatsu, M. 1983. Development of the sea-star, *Archaster typicus*, with a note on male-on-female superposition. *Annot. Zool. JPN* **56:** 187–195.

Kubo, K. 1951. Some observations on the development of the sea-star, *Leptasterias acceptances similispinis* (Clarck). *J. Fac. Sci. Hokkaido Univ. Ser. VI, Zool.* **10:** 97–105.

Levitan, D. R. 1988. Asynchronous spawning and aggregative behavior in the sea urchin *Diadema antillarum* (Philippi). Pp. 181–186 in *Echinoderm Biology.* R. D. Burke, P. V. Mladenov, P. Lambert, and R. L. Parsley, eds. Balkema, Rotterdam.

Levitan, D. R. 1991. Influence of body size and population density on fertilization success and reproductive output in a free-spawning invertebrate. *Biol. Bull.* **181:** 261–268.

Levitan, D. R., M. A. Sewell, and F.-S. Chia. 1992. How distribution and abundance influence fertilization success in the sea urchin *Strongylocentrotus franciscanus*. *Ecology* **73:** 248–254.

Lewis, J. B. 1958. The biology of the tropical sea urchin *Tripneustes esculentus* Leske in Barbabos, West Indies. *Can. J. Zool.* **36:** 607–621.

McClary, D. J., and P. V. Mladenov. 1990. Brooding biology of the sea star *Pteraster militaris* (O. F. Müller): energetic and histological evidence for nutrient translocation to brooded juveniles. *J. Exp. Mar. Biol. Ecol.* **142:** 183–199.

McEuen, F. S. 1988. Spawning behaviors of northeast Pacific sea cucumbers (Holothuroidea: Echinodermata). *Mar. Biol.* **98:** 565–585.

Mercier, A., É. Pelletier, and J.-F. Hamel. 1994. Metabolism and subtle toxic effects of butyltin compounds in starfish. *Aquat. Toxicol.* **28:** 259–273.

Miller, R. L. 1979a. Sperm chemotaxis in the Hydromedusae. I. Species-specificity and sperm behavior. *Mar. Biol.* **53:** 99–114.

Miller, R. L. 1979b. Sperm chemotaxis in the Hydromedusae. II. Some chemical properties of sperm attractants. *Mar. Biol.* **53:** 115–124.

Miller, R. L. 1985. Demonstration of sperm chemotaxis in Echinodermata: Asteroidea, Holothuroidea, Ophiuroidea. *J. Exp. Zool.* **234:** 383–414.

Miller, R. L. 1989. Evidence for the presence of sexual pheromones in free-spawning starfish. *J. Exp. Mar. Biol. Ecol.* **130:** 205–221.

Miller, R. L., and K. King. 1983. Sperm chemotaxis in *Oikopleura dioica* (Urochordata: Larvaceae). *Biol. Bull.* **165:** 419–428.

Minchin, D. 1987. Sea-water temperature and spawning behaviour in the seastar *Marthasterias glacialis*. *Mar. Biol.* **95:** 139–143.

O'Brien, F. X. 1976. Some adaptations of the seastar, *Leptasterias* (Stimpson) to life in the intertidal zone. *Thalassia Jugosl.* **12:** 237–243.

Ohshima, H., and H. Ikeda. 1934. Male-female superposition of the sea-star *Archaster typicus* Müller et Troschel. *Zool. Lab. Kyushu Imperial University* **54:** 125–128.

Ormond, R. F. G., A. C. Campbell, S. H. Head, R. J. Moore, P. R. Rainbow, and A. P. Saunders. 1973. Formation and breakdown of aggregations of the crown-of-thorns starfish, *Acanthaster planci* (L.). *Nature* **246:** 167–169.

Orton, J. H. 1914. On the breeding habit of *Echinus miliaris*, with note on the feeding habits of *Patella vulgata*. *J. Mar. Biol. Ass. U. K.* **10:** 254–257.

Pain, S. L., P. A. Tyler, and J. D. Gage. 1982. The reproductive biology of *Hymenaster membranaceus* from the Rockall Trough, North East Atlantic Ocean, with notes on *H. gennaeus*. *Mar. Biol.* **70:** 41–50.

Pearse, J. S., and R. A. Cameron. 1991. Echinodermata: Echinoidea. Pp. 513–662 in *Reproduction of Marine Invertebrates: Lophophorates, Echinoderms*. Vol. VI, A. C. Giese, J. S. Pearse, and V. B. Pearse, eds. Boxwood Press, Pacific Grove, California.

Pearse, J. S., and C. W. Walker. 1986. Photoperiodic regulation of gametogenesis in a North Atlantic sea star *Asterias vulgaris*. *Int. J. Invert. Reprod. Develop.* **9:** 71–77.

Pearse, J. S., D. J. Eernisse, V. B. Pearse, and K. A. Beauchamp. 1986. Photoperiodic regulation of gametogenesis in sea stars, with evidence for an annual calendar independent of fixed daylength. *Am. Zool.* **26:** 417–431.

Pearse, J. S., D. J. McClary, M. A. Sewell, W. C. Austin, A. Perez-Ruzafa, and M. Byrne. 1988. Simultaneous spawning of six species of echinoderms in Barkley Sound, British Columbia. *Int. J. Invert. Reprod. Develop.* **14:** 279–288.

Pennington, J. T. 1985. The ecology of fertilization of echinoid eggs: the consequences of sperm dilution, adult aggregation and synchronous spawning. *Biol. Bull.* **169:** 417–430.

Run, J.-Q., C.-P. Chen, K.-H. Chang, and F.-S. Chia. 1988. Mating behaviour and reproductive cycle of *Archaster typicus* (Echinodermata: Asteroidea). *Mar. Biol.* **99:** 247–253.

Slattery, M., and I. Bosch. 1993. Mating behavior of a brooding Antarctic asteroid, *Neosmilaster georgianus*. *Int. J. Invert. Reprod. Develop.* **24:** 97–102.

Sloan, N. A. 1980. Aspects of the feeding biology of asteroids. *Oceanogr. Mar. Biol. Ann. Rev.* **18:** 57–124.

Sloan, N. A. 1984. Interference and aggregation: close encounters of the starfish kind. *Ophelia* **23:** 23–31.

Sloan, N. A., and A. C. Campbell. 1982. Perception of food. Pp. 3–23 in *Echinoderm Nutrition*. M. Jangoux and J. M. Lawrence, eds. A. A. Balkema, Rotterdam.

Starr, M., J. H. Himmelman, and J.-C. Therriault. 1990. Direct coupling of marine invertebrate spawning with phytoplankton blooms. *Science* **247:** 1071–1074.

Strathmann, R. R. 1987. Evolutionary aspects of marine invertebrate reproduction. Pp. 609–665 in *Reproduction of Marine Invertebrates*. Vol. 9, A. C. Giese, J. S. Pearse, and V. B. Pearse, eds. Blackwell Scientific Publ., Palo Alto, and Boxwood Press, Pacific Grove, California.

Suzuki, N., M. Hoshi, K. Nomura, and S. Isaka. 1982. Respiratory stimulation of sea urchin spermatozoa by egg extracts, egg jelly extracts and egg jelly peptides from various species of sea urchins: taxonomical significance. *Comp. Biochem. Physiol.* **72:** 489–495.

Thorson, G. 1950. Reproductive and larval ecology of marine bottom invertebrates. *Biol. Rev.* **25:** 387–397.

Warner, G. F. 1979. Aggregation in echinoderms. Pp. 375–396 in *Biology and Systematics of Colonial Organisms*. G. Larwood and B. R. Rosen, eds. Academic Press, London.

Young, C. M., P. A. Tyler, J. L. Cameron, and S. G. Rumrill. 1992. Seasonal breeding aggregations in low-density populations of the bathyal echinoid *Stylocidaris lineata*. *Mar. Biol.* **113:** 603–612.

Yund, P. O. 1990. An *in situ* measurement of sperm dispersal in a colonial marine hydroid. *J. Exp. Zool.* **253:** 102–106.

Reference: *Biol. Bull.* **188:** 46–56. (February/March, 1995)

The Effects of Hydrodynamic Shear Stress on Fertilization and Early Development of the Purple Sea Urchin *Strongylocentrotus purpuratus*

KRISTINA S. MEAD AND MARK W. DENNY

Department of Biological Sciences, Stanford University, Hopkins Marine Station, Pacific Grove, California 93950

Abstract. Life in the highly turbulent surf zone poses a severe challenge to reproduction in free-spawning animals. Not only can breaking waves quickly dilute the gametes shed by spawning organisms, but turbulence-induced shear stresses may limit fertilization and interfere with normal development. A Couette cell was used to re-create some of the effects of turbulent water motion to study effects of environmentally relevant shear stresses on fertilization in the purple sea urchin (*Strongylocentrotus purpuratus*). Although low shear stresses improved fertilization success (presumably by increasing mixing), exposure to high shear stresses (of the magnitude found in the surf zone) substantially decreased fertilization success, probably by interfering with contact between egg and sperm. Furthermore, eggs fertilized at high shear stresses often showed abnormal development and low survival of eggs through the blastula stage.

Introduction

Like most intertidal invertebrates, *Strongylocentrotus purpuratus*, the purple sea urchin, reproduces by means of external fertilization. *S. purpuratus* is commonly found on exposed intertidal rocky shores and in nearshore benthic environments. In both of these habitats, its gametes are subject to the energetic turbulent mixing characteristic of these environments. Although a small amount of turbulence can provide beneficial mixing, bringing eggs and sperm into contact, the intense turbulence of the surf zone or the benthic boundary layer may interfere with fertilization through a variety of mechanisms. These include gamete dilution, gamete damage, decreased encounter rate between the egg and the sperm, and removal of the sperm from the egg's surface before fertilization is complete.

To date, the best studied of these mechanisms concerns the effects of gamete dilution. The percentage of eggs fertilized during spawning depends on the local concentration of viable sperm (Vogel *et al.*, 1982, Levitan *et al.*, 1991). When subjected to the type of turbulent flows found commonly in nearshore waters, sperm concentrations can decrease by several orders of magnitude within a meter of a spawning male (Denny, 1988; Denny and Shibata, 1989; Grosberg, 1991), resulting in low rates of fertilization (Pennington, 1985; Levitan *et al.*, 1992). The dilution of sperm increases with an increase in distance downstream from a spawning male and with an increase in current velocity, resulting in a decrease in fertilization (Pennington, 1985; Grosberg, 1987, 1991; Yund, 1990; Petersen, 1991; Petersen *et al.*, 1992; Levitan *et al.*, 1992; Oliver and Babcock, 1992). The detrimental effects of sperm dilution can be partially offset through an increase in the overall number, size, spatial density, synchronicity, and fecundity of spawning animals (Denny and Shibata, 1989; Levitan, 1991; Levitan *et al.*, 1992; Babcock and Mundy, 1992; Sewell and Levitan, 1992; Babcock *et al.*, 1994). Nonetheless, field studies have shown that the fraction of eggs fertilized in the water column is typically low, often less than 15% (Pennington, 1985; Levitan, 1991; Levitan *et al.*, 1992).

Under certain circumstances, however, gamete dilution may be greatly reduced. Denny and coworkers (1992) showed that the presence of surge channels can drastically reduce the rate of dilution in the surf zone of rocky shores, to the extent that gamete concentrations could locally be high enough to result in efficient fertilization. They tem-

Received 28 July 1994; accepted 28 November 1994.

pered this prediction, however, by noting that gamete dilution is only one of several factors affecting external fertilization and suggested that the effects of small-scale hydrodynamics could impose additional limits to the efficacy of this common form of reproduction.

Here we explore this possibility by recreating in the laboratory one important aspect of turbulent flow (hydrodynamic shear stress) and measuring its effect on fertilization and early development in the common purple sea urchin, *S. purpuratus*. In the next section, we describe the eddy sizes, shear stresses, and energy dissipation rates found in the surf zone. We then discuss how the average values of these parameters make it possible to mimic some aspects of turbulent flow in a rotating device called a Couette cell. Finally, by examining fertilization under a variety of conditions in the Couette cell, we show that surf zone turbulence may have important consequences for both the fertilization and the early development of sea urchin embryos.

Theoretical Background

Surf-zone turbulence

When a wave breaks on a rocky shore, its orderly motion is disrupted as the waveform degenerates into a collection of turbulent eddies (Denny, 1988). The interaction of eddies causes the water to be sheared, and the friction between layers of fluid (a result of viscosity) causes a shear stress, τ, to be exerted on the fluid and any gametes in it (Okubo, 1978; Fischer, 1979). As an additional result of friction, the wave's energy is lost to heat at a rate ϵ, called the energy dissipation rate. Shear stress has the units N/m^2, the energy dissipation rate has the units W/m^3, and for a given fluid, the two are related by viscosity:

$$\epsilon = \tau^2/\mu, \tag{1}$$

where μ is the dynamic viscosity of seawater at 12°C, here taken to be 1.24×10^{-3} Pa·s (Denny *et al.*, 1992). Shear stress and energy dissipation rate are different descriptors of the same phenomenon: the small-scale deformation of fluid by turbulence.

Rates of energy dissipation, averaged over both time and space, have been predicted for the surf zone (Thornton and Guza, 1983; Svendsen, 1987; Denny *et al.*, 1992; George *et al.*, 1994); ϵ increases with both wave height and beach slope, with expected values ranging from 10–3000 W/m^3 on wave-swept rocky shores (Fig. 1). The only direct data for energy dissipation rates in the surf zone come from hotfilm anemometer measurements of the turbulence generated by small waves breaking on the gently sloping beach at Scripps Pier (George *et al.*, 1994). For 1-m-high waves, a time-averaged value of ϵ of about 10 W/m^3 was measured, with instantaneous values ranging up to 100 W/m^3.

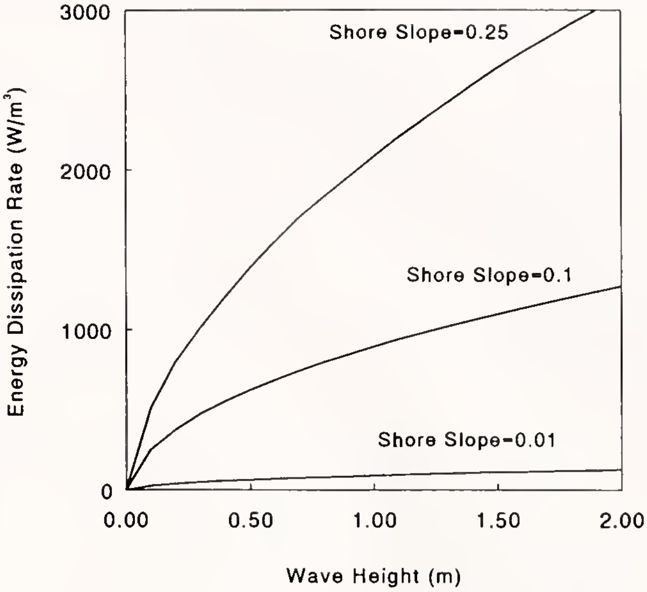

Figure 1. Energy dissipation rates in the surf zone. Predicted values given typical beach slopes and wave heights (Denny *et al.*, 1992).

The benthic boundary layer

While the intense turbulence characteristic of the surf zone is apparent to an observer, habitats occupied by *S. purpuratus* in the benthic boundary layer near shore also experience high energy dissipation rates. In this case energy is dissipated as water is sheared against the solid substratum. The shear stress exerted on the substratum by turbulent flow is ρu_*^2, where ρ is the density of the water (about 1025 kg/m^3 for seawater) and u_*, an index of turbulence intensity, is the friction velocity (Schlichting, 1979). From Equation 1, we see that this shear stress results in an energy dissipation rate of $\rho^2 u_*^4/\mu$. The friction velocity for flow over the rough substrata typical of rocky shores is typically 5% of the mainstream velocity (Middleton and Southard, 1984), which in turn depends on the height and period of the waves and the depth of the water column. Using linear wave theory to estimate mainstream water velocities near the substratum (Denny, 1988), it is thus possible to estimate energy dissipation rates in near-shore benthic boundary layers for a typical wave period of 10 s (Fig. 2). For the depths and wave heights shown, peak wave-induced velocities vary from 0.02 to 1.35 m/s, friction velocities from 0.001 to 0.067 m/s, and peak energy dissipation rates from 0.001 to 17,600 W/m^3 (resulting in average energy dissipation rates of 0.0005 to 8,800 W/m^3).

Although energy dissipation rates predicted for the benthic boundary layer can be quite high, their effect is very localized. The thickness of the benthic boundary layer under waves is approximately $0.41\ u_* T/2\pi$, where T is the wave period (Grant and Madsen, 1986). Thus, for T

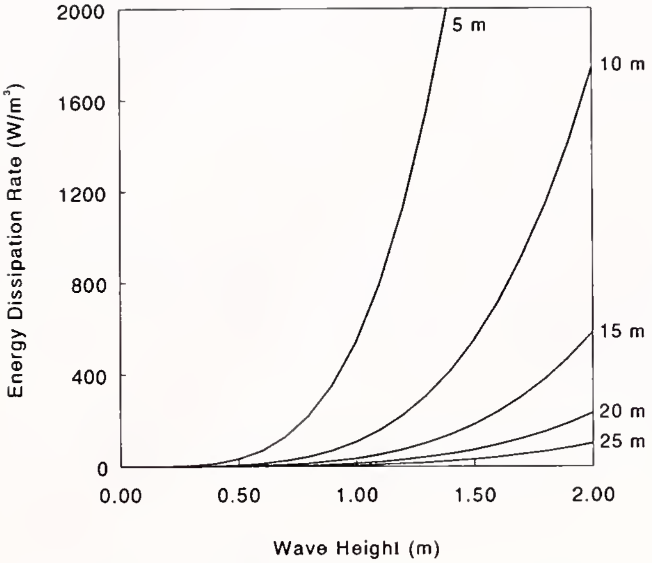

Figure 2. Energy dissipation rates in the benthic boundary layer. Predicted values given typical wave heights and water depths of habitats favored by *Strongylocentrotus purpuratus*. The wave period is assumed to be 10 s.

= 10 s and the values of u_* assumed here, the boundary layer is expected to be only 0.7 mm to 4.2 cm thick. This narrow localization of high energy dissipation rates in the benthic boundary layer is in contrast to the situation in the surf zone, where the entire volume encompassed by the breaking wave is subject to high energy dissipation rates.

In either case, once gametes or embryos leave the surf zone or the benthic boundary layer, they are no longer subject to high energy dissipation rates. Most other marine habitats have turbulent energy dissipation rates that are several orders of magnitude smaller than those found in the surf zone and in the benthic boundary layer. For example, energy dissipation rates in oceanic waters typically vary from 10^{-7} to 10^{-1} W/m^3 (Belyaev *et al.*, 1975; Dillon *et al.*, 1981; Kitaigorodskii *et al.*, 1983; Osborn and Lueck, 1985; Baker and Gibson, 1987), and energy dissipation rates in tidally mixed areas vary from 10^{-2} to 10^{-1} W/m^3 (Rothschild and Osborn, 1988).

Eddy size

To visualize how eggs and sperm respond to turbulent flow and understand how it is possible to re-create some of the effects of oceanic turbulence in the laboratory, it is useful to consider the size of the smallest vortices, or eddies, in a flow. This length, called the Kolmogorov length, is

$$L_K = \left(\frac{\upsilon^3}{\epsilon}\right)^{1/4} \tag{2}$$

(Tennekes and Lumley, 1972) where υ is the fluid's kinematic viscosity ($\upsilon = \mu/\rho$, approximately 1.2×10^{-6} m^2/s for seawater at 12°C). For example, using values for ϵ from 10 to 3000 W/m^3, the Kolmogorov length in the surf zone is predicted to be 22 to 5 μm. Note that eddy size decreases as the energy dissipation rate increases.

Few eddies have a diameter of less than 5–10 times the Kolmogorov length, and the maximum shear energy density occurs in eddies about 40 times the size of the Kolmogorov length (Lazier and Mann, 1989; Osborn *et al.*, 1990). Therefore, the most energetically significant eddies in the surf zone and benthic boundary layer are 200 to 880 μm in diameter, and are larger still in less turbulent flows. Most eddies are thus considerably bigger than a sea urchin egg (80–110 μm) and sperm (head, 3 μm; flagellum, 40–45 μm). Within an eddy, the rotational nature of the flow results in a velocity gradient (a shear) extending from the center of the eddy to its periphery (Vogel, 1981). It is reasonable to suppose, therefore, that the gametes experience turbulent eddies as a temporally variable velocity gradient with an associated shear stress and energy dissipation rate (Denny *et al.*, 1992).

Effects of shear

As yet, it has not been possible to directly observe eggs and sperm in a velocity gradient of the sort found in the surf zone. Nevertheless, general predictions about their behavior can be made. Like all spherical objects in velocity gradients, eggs are likely to tumble at many cycles per second (Happel and Brenner, 1983; Kessler, 1986; Denny *et al.*, 1992), and the axis of rotation is likely to change rapidly as different eddies shear. The rotation of the eggs induces a secondary velocity gradient (a boundary layer) around the egg. Although sperm are motile, their swimming velocity (about 150–200 μm/s; Levitan *et al.*, 1991) is substantially lower than the small-scale velocities induced by turbulence (approximately u_*; Denny, 1988). Therefore, sperm are also expected to move according to the local water motion. Due to the elongated shape and flexibility of the sperm, however, their motion is expected to differ from that of eggs, and it is possible that the effect of a velocity gradient will be to align sperm with the direction of flow. In the boundary layer surrounding the egg, this alignment would cause sperm to move tangentially to the egg's surface. It is therefore easy to imagine how the induced motion of the egg and sperm might conspire to hinder contact between the gametes.

Shear stress in the laboratory: Taylor-Couette flow

A simple way to expose eggs and sperm to shear stress (and thereby to mimic one aspect of turbulent flow) is to place them in the well-defined velocity gradient of a Couette cell (Coles, 1965; Donnelly, 1991). Couette cells and similar instruments were recently used in several biological investigations. For example, Thomas and Gibson, (1990a,b, 1992) used Couette cells to examine how turbulent motion inhibits dinoflagellate growth, cell count, and chlorophyll content, and Edwards *et al.* (1989) used a combination of Couette and cone and plate flows to observe changes in cell length, septal length, hyphal diameter, and branching frequency in two species of bacteria.

Materials and Methods

The Couette cell

The Couette cell consists of an inner stationary cylinder and a rotating coaxial outer cylinder (Fig. 3). The inner cylinder (50.5-mm outer radius) is constructed of stainless steel with an acrylic plastic base. Cold water circulates through the lumen of the inner cylinder to control the temperature of the test solution, and an air line runs to a small hole at the bottom of the inner cylinder, allowing air to be bubbled into the test solution at a controlled rate. The air bubbles keep the eggs from settling and getting caught between the bases of the two cylinders. The outer cylinder (54-mm inner radius) is made of clear acrylic plastic and has a base that fits onto a motor shaft. The distance between the two cylinders (3.5 mm) is more than 30 times larger than the diameter of the *S. purpuratus* egg. The cylinders are 20 cm long, allowing an experimental volume of more than 200 ml.

When the motor turns, the outer cylinder rotates, shearing the liquid between the two cylinders. By treating the cylinders as two wide plates a small distance apart, the shear stress τ in the test solution is calculated to be

$$\tau = \mu\left(\frac{\omega r}{h}\right) \tag{3}$$

where ω is the angular velocity (radians/s) of the outer cylinder and r is its inner radius (here 54 mm), μ is the dynamic viscosity of the test solution, and h is the radial distance between cylinders (here 3.5 mm). Equivalently, the flow inside the Couette cell can be described by the energy dissipation rate ϵ:

$$\epsilon = \mu\left(\frac{\omega r}{h}\right)^2 = \frac{\tau^2}{\mu} \tag{4}$$

Note that Equations 3 and 4 hold whether flow in the cell is laminar or turbulent (Schlichting, 1979). Both τ and ϵ will be used to describe the flow inside the Couette cell.

By varying ω (or μ) it is possible to recreate the shear stresses (and energy dissipation rates) found in the surf zone. In the experiments described here, filtered seawater was used at 12°C, and the dynamic viscosity μ was taken to be 1.24×10^{-3} Pa · s. The velocity of the outer cylinder was measured by means of a magnetic pickup system. Each time a tooth of a gear attached to the motor shaft passed by the pickup, a current pulse was induced. The pulses were amplified, counted, and converted into angular velocities. The Couette cell was run at shear stresses of 0.06 to 1.45 Pa, corresponding to energy dissipation rates of 2.8 to 1591 W/m^3. These rates cover a large portion of the range of turbulent energy dissipation rates expected on exposed rocky shores.

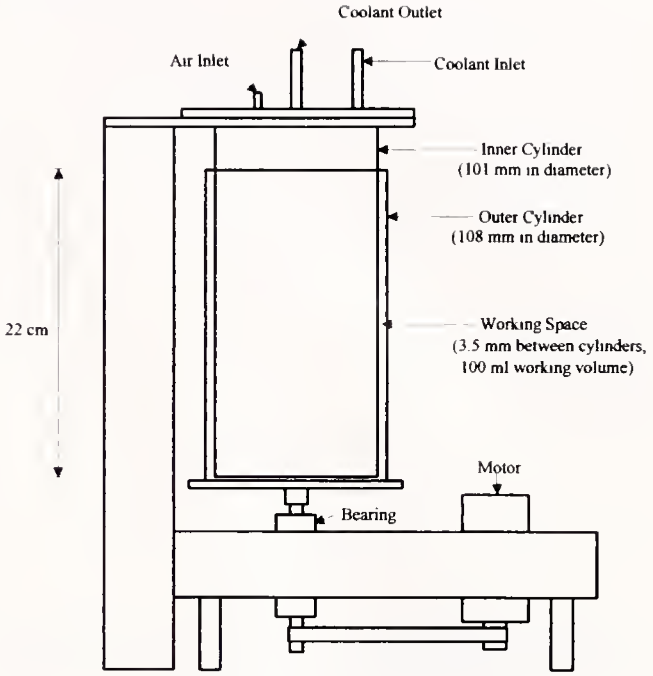
Coolant Outlet
Air Inlet
Coolant Inlet
Inner Cylinder (101 mm in diameter)
Outer Cylinder (108 mm in diameter)
22 cm
Working Space (3.5 mm between cylinders, 100 ml working volume)
Motor
Bearing

Figure 3. The Couette cell.

The Reynolds number describing the flow inside the Couette cell is $\mathrm{Re} = \rho\omega r h/\mu$. At the maximum angular velocity used in this study (75.4 rad/s), Re = 11,600. Dye studies indicated that flow became turbulent at $\mathrm{Re} \approx 4400$.

Experimental design

S. purpuratus males and females were induced to spawn by injection with 0.5 *M* KCl. Sperm were collected and stored undiluted on ice. Eggs (jelly intact) were collected in a beaker filled with filtered seawater, washed three times, and diluted to a 0.5%–1% suspension (by volume), which was stirred gently and kept at 12°C. Sperm concentrations were determined by hemacytometer counts. All experiments were performed within 8 h of gamete collection. To determine the relative concentrations of eggs and sperm to be used in each experiment, a standard fertilization curve was created for each pair of urchins (Fig. 4). Small volumes of egg suspension were exposed to so-

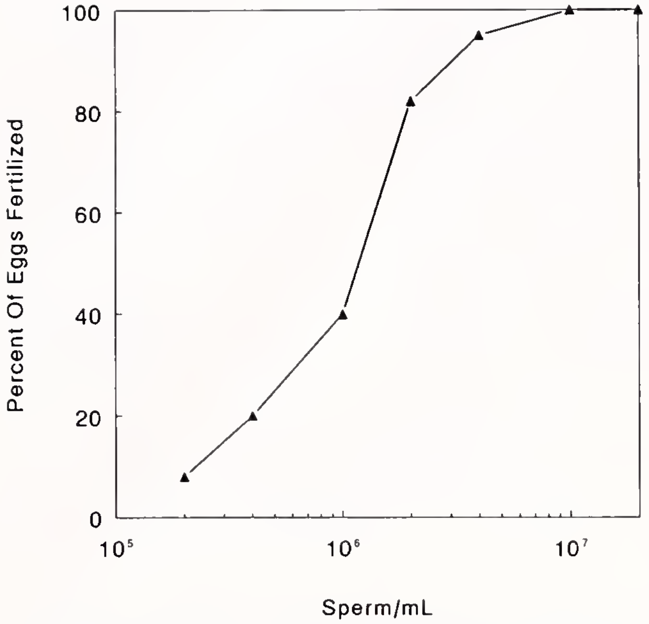

Figure 4. Representative standard fertilization curve. Concentrations and volumes of egg and sperm solutions giving 80%–90% fertilization in a test tube were used in all experiments.

lutions of sperm for 2 min in gently stirred test tubes. Fertilization was stopped by the addition of an equal volume of 0.5 *M* KCl, which renders the sperm immobile without harming the eggs (Schuel, 1984). Concentrations and relative volumes of eggs and sperm giving rise to 80%–90% fertilization in a test tube were used in the Couette cell experiments, to ensure that the decrease in fertilization success expected as a result of shear stress would not be concealed by an overabundance of sperm.

The rates of energy dissipation used in the experiments ranged from 2.8 to 1591 W/m^3. In each experiment, 45 ml of the egg suspension was put in the Couette cell. The outer cylinder was brought up to speed over about 10 s, after which 5 ml of newly diluted sperm was added to the egg suspension. Fertilization was allowed to take place at the specified energy dissipation rate for 2 min before the reaction was stopped with 50 ml 0.5 *M* KCl. Eggs were subsequently washed with filtered seawater and examined under a microscope 4 h after fertilization. Because shear stress can induce artificial activation and concomitant formation of both the fertilization envelope and the hyaline membrane (normally indicators of fertilization) in the absence of sperm, only eggs that had divided were counted as fertilized, possibly resulting in a slight underestimate of fertilization. Two hundred eggs were counted per sample.

Each experiment was repeated between 3 and 16 times at the same energy dissipation rates, using gametes from different pairs of urchins. Because the relative concentration and the "fertilizability" of the gametes varied slightly between pairs, all data were normalized to the percent fertilization obtained when the experimental concentrations of eggs and sperm were combined in a test tube in the absence of appreciable shear.

Some urchins, such as those living on exposed rocky shores, experience turbulence almost constantly. Other animals, for instance those in tide pools, may experience significant turbulence only as the waves break, or just when the largest waves break on the shore. To approximate the time-dependent nature of this kind of environmental turbulence more accurately, eggs were fertilized under intermittent shear stress. As above, 45 ml of the egg suspension was put in the Couette cell. Once the outer cylinder had been brought up to speed, 5 ml of newly diluted sperm was added to the egg suspension. Fertilization was allowed to occur for 2 min, during which time the Couette cell was alternately spun for 10 s, then allowed to stop for 10 s throughout the 2-min trial. Experiments were repeated and data were normalized as above.

To determine if exposure to shear stress decreases fertilization success by damaging gametes (as opposed to some other mechanism, such as interfering with egg-sperm binding), *S. purpuratus* eggs were sheared prior to fertilization and then combined with unsheared, newly diluted sperm in a test tube. Similarly, *S. purpuratus* sperm were sheared prior to fertilization and immediately combined with unsheared eggs in a test tube. Fertilization was stopped after 2 min by the addition of an equal volume of 0.5 *M* KCl. For comparison, eggs and sperm from the same animals were fertilized under shear in the Couette cell. All eggs were washed with filtered seawater and incubated at 12°C for 4 h before being examined. Experiments were repeated three times and data were normalized as above.

Eggs were reexamined after 24 h to determine whether exposure to shear stress (either before or during fertilization) had any effects extending past fertilization. Samples were counted, and the percentage of fertilized eggs that had developed into normal blastulae was recorded. Normal blastulae were characterized as clear, hollow balls of cells spinning rapidly about their animal-vegetal pole axes. Two hundred embryos were counted per sample.

Results

Fertilization under constant shear stress

Water motion associated with low energy dissipation rates (<70 W/m^3) enhanced fertilization success, presumably as a result of mixing. As the energy dissipation rate increased from 2.8 to 69.2 W/m^3, the mean fertilization success increased from 78% to 96%. Fertilization success decreased when fertilization occurred during exposure to moderate and high energy dissipation rates. As

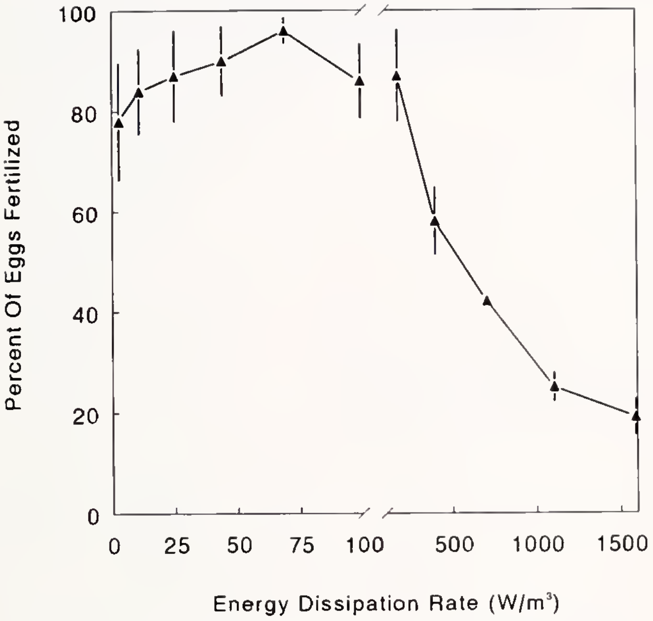

Figure 5. The effect of shear stress on fertilization. Low energy dissipation rates enhance fertilization success, whereas moderate and high energy dissipation rates decrease fertilization success. Data from 16 pairs of sea urchins. Error bars indicate the standard error.

the energy dissipation rate increased from 69.2 to 1591 W/m^3, the percentage of eggs that were fertilized decreased from 96% to 19% (Fig. 5).

Intermittent shear stress

When eggs were fertilized under conditions of intermittent shear stress, fertilization success decreased with increasing energy dissipation rate, although not as dramatically as when the shear stress was constant. As the maximum energy dissipation rate experienced during the 10-s pulses of turbulence increased from 44.1 to 1591 W/m^3, the mean fertilization success decreased from 90% to 39% (Fig. 6). In comparison, when eggs and sperm from the same pair of urchins were fertilized under constant shear, mean fertilization success decreased from 92% to 19%. At moderate energy dissipation rates (up to 397.7 W/m^3), there was no significant difference between the effects of constant and intermittent shear stress. At high energy dissipation rates (707 W/m^3 and above), eggs fertilized under intermittent shear stress had greater fertilization success than eggs fertilized under constant shear.

In this set of experiments, few measurements were made at low energy dissipation rates. Therefore, the pattern seen in constant shear stress of an increase in fertilization success at low energy dissipation rates was not observed.

Shearing gametes before fertilization

When *S. purpuratus* eggs and sperm were sheared separately before fertilization and then combined with unsheared gametes in a test tube in the absence of appreciable shear stress, fertilization success was very high. As the energy dissipation rate increased from 44.1 to 1591 W/m^3, the fertilizability of the sheared eggs decreased from 98% to 86%, and the fertilizability of the sheared sperm decreased from 100% to 92% (Fig. 7). In compar-

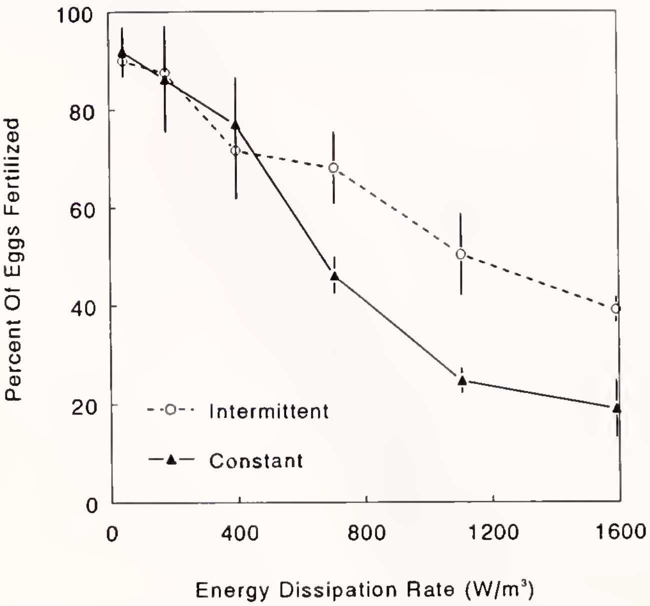

Figure 6. The effect of intermittent shear stress on fertilization. Data are from three pairs of sea urchins. Error bars indicate standard error.

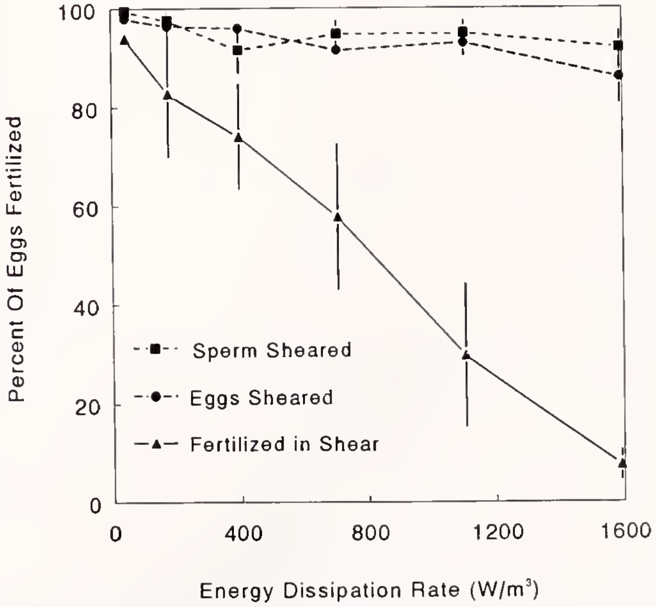

Figure 7. The fertilizability of presheared gametes. Sperm and eggs lose little fertilizability when sheared before fertilization. Data are from three pairs of sea urchins. Error bars indicate standard error.

ison, the fertilization success of eggs from the same female fertilized under shear decreased from 94% to 8%.

Effect of shear stress on early development

Although almost 100% of the *S. purpuratus* eggs fertilized in the absence of shear developed into normal blastulae, many of the eggs fertilized while exposed to shear stress showed the effects of shear-stress-induced damage; typically their development was arrested at about the 64-cell stage. As the energy dissipation rate during fertilization increased from 44.1 to 1591 W/m^3, the percentage of fertilized eggs that developed into normal blastulae decreased from 92% to 22% (Fig. 8). Given that many eggs were not fertilized, the overall fraction of eggs that developed normally was lower still. For example, as the energy dissipation rate during fertilization increased from 44.1 to 1591 W/m^3, the percentage of eggs that developed into normal blastulae decreased from 88% to 2%.

In comparison, almost all fertilized eggs developed normally when the gametes were sheared separately and then combined in a test tube (Fig. 9A). As the energy dissipation rate increased from 44.1 to 1591 W/m^3, the percentage of sheared eggs that (once fertilized) developed into normal blastulae decreased only from 99% to 89%, and the percentage of eggs fertilized by sheared sperm that developed into normal blastulae decreased only from 96% to 94%. These data can be graphed to reflect the total number of eggs that developed into normal blastulae, including the effect of reduced fertilization (Fig. 9B). As the energy dissipation rate increased from 44.1 to 1591 W/m^3, the percentage of sheared eggs that developed into normal blastulae decreased from 97% to 77%, and the percentage of eggs fertilized by sheared sperm that developed into normal blastulae decreased only from 96% to 87%.

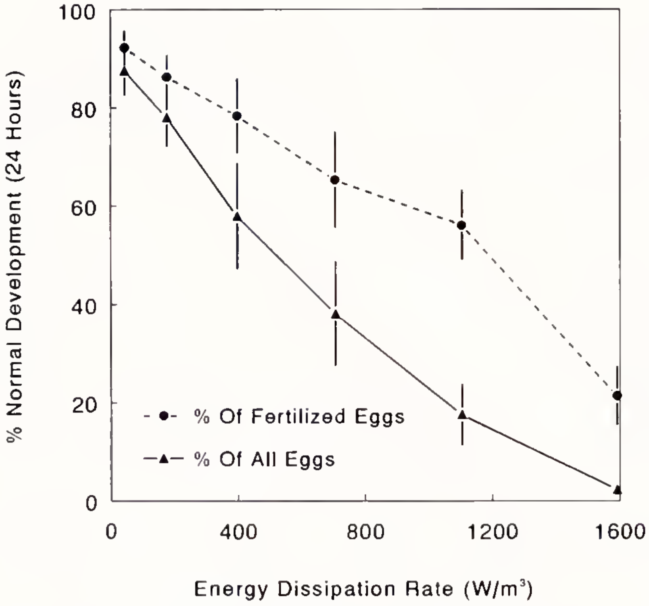

Figure 8. The effect of shear stress on development. Many eggs fertilized in shear do not develop normally. Combining fertilization and developmental data shows that the percentage of all eggs developing normally at 24 h is very low. Data are from 12 pairs of urchins. Error bars indicate standard error.

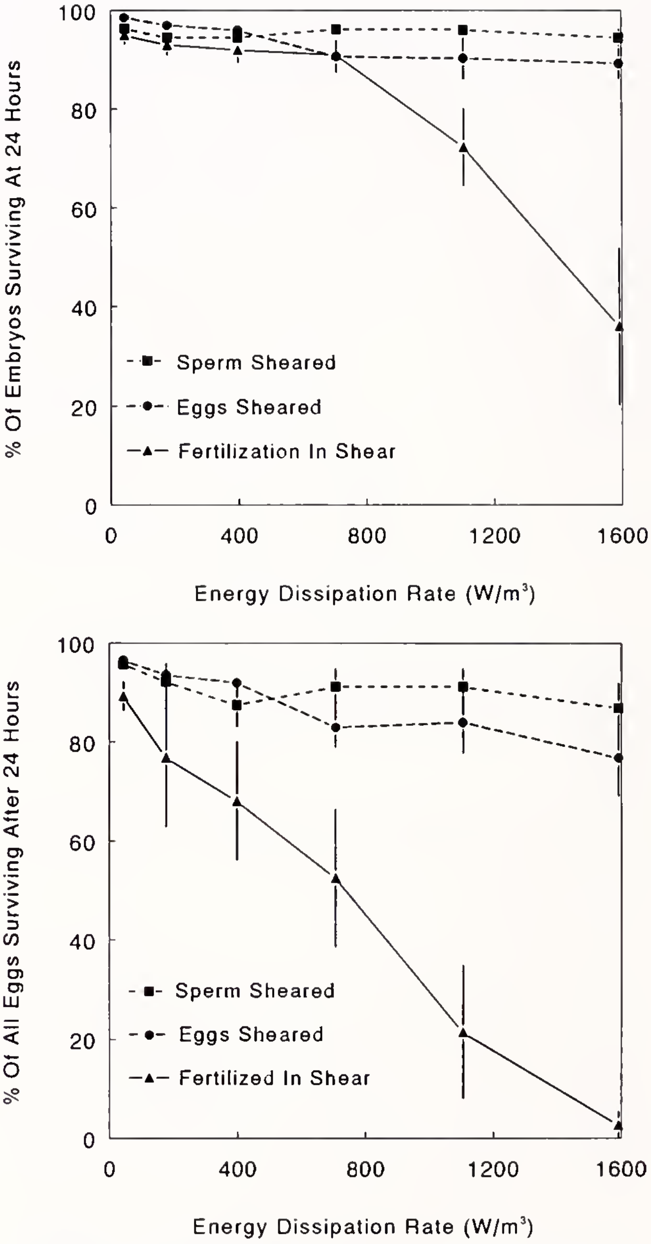

Figure 9. The effect of shearing gametes on early development. Almost all eggs fertilized in the absence of shear develop into normal blastulae, but eggs fertilized in shear do not. (A) Development of fertilized eggs. (B) Survival of all eggs to blastula, including eggs that were not successfully fertilized. Data are from three pairs of urchins. Error bars indicate standard error.

Discussion

How can low levels of turbulence increase fertilization success?

Although intense turbulence limits fertilization success, low energy dissipation rates enhance fertilization success. This is presumably because turbulent mixing increases contact rates between the egg and sperm. It is reasonable to suppose that at low turbulent intensities the tumbling of the egg in response to shifting velocity gradients may not be rapid or abrupt enough to inhibit binding of the sperm to the egg. Similarly, investigators have shown that low energy dissipation rates increase rates of contact between predator and prey in the plankton (Rothschild and Osborn, 1988; Marrasé *et al.*, 1990; Costello *et al.*, 1990; Saiz *et al.*, 1992). At high energy dissipation rates, the beneficial aspects of turbulence are outweighed by other factors.

Why does excessive turbulence decrease fertilization success?

Despite observations that turbulence decreases fertilization success by diluting gamete concentration, the data presented above indicate that environmentally relevant turbulence can dramatically decrease fertilization success even when eggs and sperm are in high concentrations. There are several possible mechanisms for this shear-induced decrease in fertilization success, including gamete damage, a decrease in the encounter rate between egg and sperm, and a removal of sperm from the egg's surface during the latent period, the period after the sperm has made initial contact with the egg, but before fertilization is complete. The fact that shearing gametes before fertilization does not dramatically reduce their fertilizability indicates that exposure to shear does not substantially damage gametes (Fig. 7). This suggests that high levels of turbulence instead may limit fertilization by reducing the effective encounter rate between gametes. If, as expected, turbulence causes the eggs to tumble rapidly and the sperm to align themselves in the direction of flow tangential to the egg surface, small-scale turbulence could hinder contact between the gametes. Alternatively (or additionally), exposure to turbulence might limit the ability of the sperm to attach to an egg once contact has been made, or it might cause attached sperm to be removed before fertilization is complete.

Our experiments provide no direct evidence that allows us to choose among these possibilities, but indirect evidence allows for reasonable speculation. We begin by asking whether it is likely that hydrodynamic shear stresses are sufficient to tear an attached sperm from an egg. Although no data are yet available for sea urchins, bond strengths between a sperm and the *zona pellucida* of an egg range in mammalian systems from 6 to 250 dyn, with 40 dyn being the most likely average value (Baltz *et al.*, 1988), and for the sake of argument we assume a similar value for urchin sperm. This force can be compared to the hydrodynamic force exerted on an urchin sperm as follows: The shear force pulling at a sperm attached to an egg is approximately equal to the hydrodynamic shear stress to which the sperm is exposed multiplied by the sperm's surface area. If a sea urchin sperm is modeled as a 41-μm-long cylinder with a radius of 0.1 μm (the flagellum) attached to a conical head with a height of 3 μm and a radius of 0.5 μm (Gray, 1955; Brokaw, 1965), its surface area is 31.4 μm^2. At a shear stress of 1.45 Pa (the maximum shear stress to which the gametes were exposed in the Couette cell, equivalent to an energy dissipation rate of 1591 W/m^3) the resulting shear force is 4.6 dyn, much less than the expected bond strength. A still smaller force would be exerted at lower shear stresses. It thus seems unlikely that sperm, once well attached, are sheared off before fertilization is complete. This suggests that the primary effect of hydrodynamic shear on fertilization is to reduce the encounter rate between gametes, to disrupt contact between sperm and egg before final sperm attachment, or both.

This proposition is supported by our experiment regarding the "dose" of turbulence to which gametes are subjected. A comparison of the effects of constant and intermittent shear stress reveals a time-dependent response. At high shear stresses, a smaller percentage of eggs is fertilized if shear is constant than if shear is applied in 10-s periods alternating with 10-s periods of quiescence (Fig. 6). In both cases gametes are exposed to the same peak shear stress. If shear stress acted primarily by tearing well-attached sperm from the egg before they could fertilize (a process that takes about 20–30 s [Epel, 1989, 1990; Ruiz-Bravo and Lennarz, 1989]), one would expect that the effects of intermittent shear would be similar to those of constant shear. If, on the other hand, the primary effect of shear stress is to prevent sperm from encountering or becoming strongly attached to eggs (processes that can occur effectively in periods less than 10 s [Epel, 1989, 1990; Ruiz-Bravo and Lennarz, 1989]), periods of quiescence would allow some sperm to encounter eggs and attach well enough to be immune from later disruption by shear stress. If this is indeed the case, fertilization rates will be higher under intermittent shear, and this is the effect that we observed. The time-dependence of the effect of shear stress is consistent with the hypothesis that shear stress limits fertilization by interfering with contact between the egg and sperm.

Further experiments will be necessary to test this speculation and to differentiate between the effects of turbulence on encounter rates and the effects on subsequent adhesion.

Why does turbulence affect development?

Only a fraction of the eggs that are fertilized under turbulent conditions develop into normal blastulae (Fig. 8), indicating that shear stress, whether constant or intermittent, affects reproductive success beyond fertilization. Somehow, exposure to shear stress curtails or irrevocably alters some process essential to normal development. Although the mechanism or mechanisms behind this effect are uncertain, reasonable speculation is again possible. Hiramoto (1974) noted a brief fivefold stiffening of the egg membrane 90 s after fertilization in the urchin *Temnopleurus toreumaticus*. If *S. purpuratus* eggs experience a similar increase in stiffness, and if the hardened membranes result in increased damage, eggs exposed to shear stress during fertilization could sustain injuries not seen when eggs were exposed to shear stress prior to fertilization. These injuries could result in leakage of some essential cytoplasmic compound or in infection, either of which could prevent the fertilized egg from completing more than a few rounds of cell division.

Not only might different types or degrees of injury arise, depending on whether the egg is exposed to turbulence before or during fertilization, but the ability of the egg to heal itself after injury might vary. Mechanically injured cells heal themselves by releasing exocytotic vesicles, which fuse to the plasma membrane (Steinhardt *et al.*, 1994). Shortly after fertilization, these vesicles are depleted (Vacquier, 1981), presumably decreasing the cell's ability to heal itself. This could help explain why a large fraction of the eggs fertilized under turbulent conditions developed abnormally.

Two further possibilities can be discounted. First, injuries resulting in parthenogenic stimulation or polyspermy cannot explain the effect of shear stress on development, because the fertilized eggs usually divide to about the 64-cell stage before degrading. In contrast, artificially activated sea urchin eggs tend not to divide, and polyspermic eggs have very characteristic disruptions in their cleavage patterns (*e.g.*, irregular or incomplete division, multiple asters, lobe formation), none of which were observed here. Second, if exposure to shear stress altered egg membranes in some way, eggs sheared prior to fertilization would show the same defects in their development, and this was not seen.

Ecological implications of the effect of turbulence on fertilization

These experiments indicate that although low levels of shear stress can aid mixing and fertilization, the intense shear stress found in the surf zone and in the benthic boundary layer can have severe mechanical effects on fertilization and early development. These effects interact with those of gamete dilution to narrow any window of opportunity open to urchins attempting to reproduce by external fertilization. For instance, although surge channels may restrict gamete dilution (Denny *et al.*, 1992), thereby promoting efficient fertilization, the deleterious effects of shear stress may still limit the fraction of eggs fertilized. Furthermore, any eggs that are fertilized are very likely to develop abnormally. Gametes shed outside of surge channels may be quickly swept out of the surf zone, thereby avoiding prolonged exposure to high shear stresses, but dilution will be rapid; consequently, the fraction of eggs fertilized will again be low. Similarly, while gametes released above the benthic boundary layer (by large or aggregated individuals) experience lower energy dissipation rates, they too are quickly diluted, and fertilization rates will still be low.

The picture is not quite as bleak as it appears. Turbulence is patchy, and even areas with high temporally averaged rates of energy dissipation may experience (short) periods of relative calm. Because of their great fecundity, urchins able to time it right may end up with abundant offspring.

There are plenty of sea urchins along our rocky shores, but the chanciness of external fertilization in a turbulent environment suggests that only a small number of them contribute to the next generation. If this is true, then the effective population is much smaller than the actual population—a situation that could have populational, conservational, and evolutionary consequences (Quinn *et al.*, 1993; Hedgecock, 1994).

Acknowledgments

We thank D. Epel for his constant moral and technical support and for his excellent advice. Both he and Friday Harbor Laboratories (University of Washington) provided generous access to laboratory facilities. H. Crenshaw made helpful suggestions, and B. Rees, P. Sund, J. Geller, and B. Podolsky made insightful comments on earlier versions of this manuscript. Two anonymous reviewers had thoughtful observations and helped clarify parts of the paper. This study was funded by grants to K. Mead from the Myers Oceanographic and Marine Biological Trust, and by NSF grants to M. Denny (OCE-9115688) and D. Epel (IBN-9205393).

Literature Cited

Babcock, R. C., and C. N. Mundy. 1992. Reproductive biology, spawning, and field fertilization rates of *Acanthaster planci*. *Aust. J. Mar. Freshwater Res.* **43:** 525–534.

Babcock, R. C., C. N. Mundy, and D. Whitehead. 1994. Sperm diffusion models and *in situ* confirmation of long-distance fertilization in the free-spawning asteroid *Acanthaster planci*. *Biol. Bull.* **186:** 17–28.

Baltz, J. M., D. F. Katz, and R. A. Cone. 1988. Mechanics of sperm-egg interaction at the *zona pellucida*. *Biophys. J.* **54:** 643–654.

Baker, M. A., and C. H. Gibson. 1987. Sampling turbulence in the stratified ocean: statistical consequences of strong intermittency. *J Phys. Ocean.* **17:** 1817–1856.

Belyaev, V. S., M. M. Lubimtzev, and R. V. Ozmidov. 1975. The rate of dissipation of turbulent energy in the upper layer of the ocean. *J. Phys. Ocean* **5:** 499–505.

Brokaw, C. J. 1965. Non-sinusoidal bending waves of sperm flagella. *J. Exp. Biol.* **43:** 155–169.

Coles, D. 1965. Transition in circular Couette flow. *J Fluid Mech* **21:** 385–425.

Costello, J. H., J. R. Strickler, C. Marrasé, G. Trager, R. Zeller, and A. J. Friese. 1990. Grazing in a turbulent environment: Behavioral response of a calanoid copepod, *Centropages hamatus. Proc. Natl. Acad. Sci.* **87:** 1648–1652.

Denny, M. W. 1988. *Biology and the Mechanics of the Wave-Swept Environment.* Princeton University Press, Princeton, NJ. 329 pp.

Denny, M., and M. Shibata. 1989. Consequences of surf-zone turbulence for settlement and external fertilization. *Am. Nat.* **134:** 859–889.

Denny, M., J. Dairiki, and S. Distefano. 1992. Biological consequences of topography on wave-swept rocky shores: I. Enhancement of external fertilization. *Biol. Bull.* **183:** 220–232.

Dillon, T. M., J. G. Richman, C. G. Hansen, and M. D. Pearson. 1981. Near-surface turbulence measurements in a lake. *Nature* **290:** 390–392.

Donnelly, R. J. 1991. Taylor-Couette flow: The early days. *Physics Today* **44:** 32–39.

Edwards, N., S. Beeton, A. T. Bull, and J. C. Merchuk. 1989. A novel device for the assessment of shear effects on suspended microbial cultures. *Appl. Microbiol. Biotechnol.* **30:** 190–195.

Epel, D. 1989. Arousal of activity in sea urchin eggs at fertilization. Chapter 15 in *The Cell Biology of Fertilization,* H. Schatten and G. Schatten, eds. Academic Press, San Diego. 404 pp.

Epel, D. 1990. The initiation of development at fertilization. *Cell Differ. Dev.* **29:** 1–12.

Fischer, H. B. 1979. *Mixing in Inland and Coastal Waterways.* Academic Press, New York. 483 pp.

George, R., R. E. Flick, and T. Guza. 1994. Observations of turbulence in the surf zone. *J. Geophys. Res.* **99:** 801–810.

Grant, W. D., and O. S. Madsen. 1986. The continental-shelf bottom boundary layer. *Ann. Rev. Fluid. Mech.* **18:** 265–305.

Gray, J. 1955. The movement of sea-urchin spermatozoa. *J. Exp. Biol.* **32:** 775–801.

Grosberg, R. K. 1987. Limited dispersal and proximity-dependent mating success in the colonial ascidian *Botryllus schlosseri. Evolution* **41:** 372–384.

Grosberg, R. K. 1991. Sperm-mediated gene flow and the genetic structure of a population of the colonial ascidian *Botryllus schlosseri. Evolution* **45:** 130–142.

Happel, J., and H. Brenner. 1983. *Low Reynolds Number Hydrodynamics.* Martinus Nijhoff Publishers, Dordrecht. 553 pp.

Hedgecock, D. 1994. Does variance in reproductive success limit effective population sizes of marine organisms? Pp. 122–143 in *Genetics and Evolution of Aquatic Organisms,* A. R. Beaumont, ed. Chapman and Hall, London.

Hiramoto, Y. 1974. Mechanical properties of the surface of the sea urchin egg at fertilization and during cleavage. *Exp. Cell Res.* **89:** 320–326.

Kessler, J. O. 1986. The external dynamics of swimming micro-organisms. Pp. 257–307 in *Progress in Phycological Research,* Vol. 4, F. E. Round and D. J. Chapman, eds. Biopress Ltd, Bristol. 481 pp.

Kitaigorodskii, S. A., M. A. Donelan, J. L. Lumley, and E. A. Terray. 1983. Wave-turbulence interactions in the upper ocean. Part II: Statistical characteristics of wave and turbulent components of the random velocity field in the marine surface layer. *J Phys. Ocean.* **13:** 1988–1999.

Lazier, J. R. N., and K. H. Mann. 1989. Turbulence and the diffusive layers around small organisms. *Deep-Sea Res.* **36:** 1721–1733.

Levitan, D. R. 1991. Influence of body size and population density on fertilization success and reproductive output in a free-spawning invertebrate. *Biol. Bull.* **181:** 261–268.

Levitan, D. R., M. A. Sewell, and F.-S. Chia. 1991. Kinetics of fertilization in the sea urchin *Strongylocentrotus franciscanus:* interaction of gamete dilution, age, and contact time. *Biol. Bull.* **181:** 371–378.

Levitan, D. R., M. A. Sewell, and F.-S. Chia. 1992. How distribution and abundance influence fertilization success in the sea urchin *Strongylocentrotus franciscanus. Ecology* **73:** 248–254.

Marrasé, C., J. H. Costello, T. Granata, and J. R. Strickler. 1990. Grazing in a turbulent environment: energy dissipation, encounter rates, and efficacy of feeding currents in *Centropages hamatus. Proc. Natl. Acad. Sci.* **87:** 1653–1657.

Middleton, G. V., and J. B. Southard. 1984. *Mechanics of Sediment Movement.* Society of Economic Paleontologists and Mineralogists, Tulsa, Oklahoma. 401 pp.

Okubo, A. 1978. Horizontal dispersion and critical scales for phytoplankton patches. Pp. 1–42 in *Spatial Pattern in Plankton Communities,* from the NATO Conference on Marine Biology, Erice, Italy, 1977. J. H. Steele, ed. Plenum Press, New York. 470 pp.

Oliver, J., and R. Babcock. 1992. Aspects of the fertilization ecology of broadcast spawning corals: sperm dilution effects and *in situ* measurements of fertilization. *Biol. Bull.* **183:** 409–417.

Osborn, T. R., and R. G. Lueck. 1985. Turbulence measurements with a submarine. *J. Phys. Ocean.* **15:** 1502–1520.

Osborn, T. R., H. Yamazaki, and K. Squires. 1990. Direct simulation of the effect of turbulence on planktonic contact rates. Pp. 99–103 in *Large Marine Ecosystems: Patterns, Processes, and Yields.* K. Sherman, L. M. Alexander, and B. D. Gold, eds. Publication 90-30S of the American Association for the Advancement of Science. Washington, DC. 242 pp.

Pennington, J. T. 1985. The ecology of fertilization of echinoid eggs: the consequences of sperm dilution, adult aggregation, and synchronous spawning. *Biol. Bull.* **169:** 417–430.

Petersen, C. W. 1991. Variation in fertilization rate in the tropical reef fish, *Halichoeres bivattatus:* correlates and implications. *Biol. Bull.* **181:** 232–237.

Petersen, C. W., R. R. Warner, S. Cohen, H. C. Hess, and A. T. Sewell. 1992. Variable pelagic fertilization success: implications for mate choice and spatial patterns of mating. *Ecology* **73:** 391–401.

Quinn, J. F., S. R. Wing, and L. W. Botsford. 1993. Harvest refugia in marine invertebrate fisheries: models and applications to the red sea urchin, *Strongylocentrotus franciscanus. Am. Zool.* **33:** 537–550.

Rothschild, B. J., and T. R. Osborn. 1988. Small-scale turbulence and plankton contact rates. *J. Plank. Res.* **10:** 465–474.

Ruiz-Bravo, N., and W. J. Lennarz. 1989. Receptors and membrane interactions during fertilization. Chapter 2 in *The Molecular Biology of Fertilization.* H. Schatten and G. Schatten, eds. Academic Press. San Diego. 384 pp.

Saiz, E., M. Alcaraz, and G.-A. Paffenhöfer. 1992. Effects of small-scale turbulence on feeding rate and gross-growth efficiency of three *Acartia* species (Copepoda: Calanoida). *J. Plank. Res.* **14:** 1085–1097.

Schlichting, H. 1987. *Boundary-Layer Theory.* 7th ed. McGraw-Hill, New York. 817 pp.

Schuel, H. 1984. The prevention of polyspermic fertilization in sea urchins. *Biol. Bull.* **167:** 271–309.

Sewell, M. A., and D. R. Levitan. 1992. Fertilization success during a natural spawning of the dendrochirote sea cucumber *Cucumaria miniata. Bull. Mar. Sci.* **51:** 161–166.

Steinhardt, R. A., B. Guoqiang, and J. M. Alderton. 1994. Cell membrane resealing by a vesicular mechanism similar to neurotransmitter release. *Science* **263:** 390–393.

Svendsen, I. A. 1987. Analysis of surf zone turbulence. *J Geophys Res.* **92:** 5115–5124.

Tennekes, H., and J. L. Lumley. 1972. *A First Course in Turbulence.* MIT Press, Cambridge. 300 pp.

Thomas, W. H., and C. H. Gibson. 1990a. Effects of small-scale turbulence on microalgae. *J Appl Phycol* **2:** 71–77.

Thomas, W. H., and C. H. Gibson. 1990b. Quantified small-scale turbulence inhibits a red tide dinoflagellate, *Gonyaulax polyedra* Stein. *Deep-Sea Res.* **37:** 1583–1593.

Thomas, W. H., and C. H. Gibson. 1992. Effects of quantified small-scale turbulence on the dinoflagellate, *Gymnodinium sanguineum (splendens)*: contrasts with *Gonyaulax (Lingulodinium) polyedra*, and the fishery implication. *Deep-Sea Res.* **39:** 1429–1437.

Thornton, E. B., and R. T. Guza. 1983. Transformation of wave height distribution. *J. Geophys. Res.* **88:** 5925–5938.

Vacquier, V. D. 1981. Dynamic changes of the egg cortex. *Dev. Biol.* **84:** 1–26.

Vogel, S. 1981. *Life in Moving Fluids.* Princeton University Press, Princeton, NJ. 352 pp.

Vogel, H., G. Chizak, P. Chang, and P. Wolf. 1982. Fertilization kinetics of sea urchin eggs. *Math. Biosci* **58:** 189–216.

Yund, P. O. 1990. An *in situ* measurement of sperm dispersal in a colonial marine hydroid. *J Exp. Zoo.* **253:** 102–106.

Reference: *Biol. Bull.* **188:** 57–67. (February/March, 1995)

Elemental Distributions in Marine Bivalve Shells as Measured by Synchrotron X-Ray Fluorescence

KURT THORN[1,*], ROBERT M. CERRATO[2], AND MARK L. RIVERS[1]

[1]*Department of Geophysical Sciences, University of Chicago, Chicago, Illinois 60637, and* [2]*Marine Sciences Research Center, State University of New York, Stony Brook, New York 11794-5000*

Abstract. The concentrations of elements from Mn to Pb in the shells of *Mercenaria mercenaria, Mya arenaria,* and *Argopecten irradians* were measured using synchrotron x-ray fluorescence. This technique provides sensitivity as low as 1 ppm and resolution of 8 μm. Elements were heterogeneously distributed, both on a large scale (several millimeters) and on a small scale (tens of micrometers). Large-scale variations were observed in the compositions of shell layers and in seasonal variations in strontium concentration. Small-scale changes in composition included elevated iron levels at the boundary between the prismatic and inner homogeneous shell of the hard clam, *Mercenaria mercenaria.* Variations in strontium concentrations were seen over time spans of several months, suggesting that this technique can be used to determine historical water temperatures. Elemental maps with a resolution of less than 10 μm were produced.

Introduction

The use of marine bivalves as environmental indicators has received considerable attention. Bivalves are believed to incorporate trace elements into their shells in proportion to the concentration of those elements in the water (Rhoads and Lutz, 1980). This incorporation is also influenced by other circumstances, including water temperature and salinity (Rosenberg, 1980). The incorporation of trace elements into marine bivalves could be used to monitor temporal changes in aspects of the marine environment, including the elemental composition and temperature of the water. Moreover, recent pollution could be studied, as well as paleoceanographic conditions. Strontium/calcium ratios have already been used as a method in paleothermometry that overcomes the limitations of the more common oxygen isotope paleothermometry (Beck *et al.*, 1992). Additionally, many bivalves produce visible growth increments in their shells, often as frequently as once per day. These growth increments provide a method of dating any observed changes in elemental composition of the shell.

When techniques like instrumental neutron activation analysis (INAA) and atomic absorption analysis are applied to whole shells of marine bivalves, heavy metal concentrations of less than 5 ppm by weight are reported (Al-Dabbas *et al.*, 1984; Koide *et al.*, 1982; Milliman, 1974). Carriker *et al.* (1982), using proton induced x-ray emission analysis (PIXE), reported concentrations of Cu and Zn in oysters (*Crassostrea virginica*) of 20 to 30 ppm weight. When such concentrations are measured by bulk analysis, fairly large amounts of shell are required for analysis, so resolution over short time scales is impossible.

All previous attempts to measure the distribution of elements within bivalve shells have been made with either PIXE microprobes or electron probe microanalysis (EPMA). Because the minimum elemental concentration measurable with EPMA is high, only those elements occurring in fairly high concentrations in the shell (Ca, Sr, Mg, S) can be observed (Wada and Suga, 1976; Rosenberg and Hughes, 1991). Three PIXE microprobe studies (Carriker *et al.*, 1982; Carell *et al.*, 1987; Swann *et al.*, 1991) report variations in heavy metal concentrations, but over fairly long (several month) time scales, although the excellent spatial resolution of the proton microprobe (3 μm) used by Carell *et al.* (1987) would have enabled

---

Received 29 October 1993; accepted 22 November 1994.

* Current Address: Whitespruce Dr., Wading River, NY 11792.

Abbreviations: SXRF, synchrotron x-ray fluorescence; PIXE, proton induced x-ray emission; EPMA, electron probe microanalysis; MDL; minimum detectable level.

them to study periods corresponding to 6–8 hours in young mussels.

In his analysis of bivalve shell chemistry, Rosenberg (1980) concludes that whole-shell analysis represents the elemental concentration incorrectly because elements are not necessarily distributed uniformly throughout the shell. Carriker *et al.* (1982) list several factors that influence the distribution of elements in shells, including structural and chemical changes that result from environmental fluctuations, fouling, adsorption, and weathering of the shell surface, elements adsorbed at shell surfaces and integrated into the shell matrix, and the heterogeneous distribution of elements within the shell.

The metal concentrations typically found in bivalve shells are considerably less than those measurable by EPMA and are near the 20 ppm detection limit of PIXE microprobes. Synchrotron x-ray fluorescence has minimum detection limits near 1 ppm, which should permit detection of these elements and resolution of variations in their concentration over short time scales.

This study attempts to evaluate the potential of synchrotron x-ray fluorescence as a technique for microanalysis of trace element distributions in bivalve shells of three species. Some samples were also analyzed with a PIXE microprobe in a pilot attempt to measure elemental distributions on scales down to 1 μm.

Materials and Methods

Preparation of shell sections

Three species were examined in this study: hard clams (*Mercenaria mercenaria*), soft-shell clams (*Mya arenaria*), and bay scallops (*Argopecten irradians*). Hard clams were obtained from a population in Moriches Bay, soft-shell clams from a population in Stony Brook Harbor, and scallops from a population in Peconic Bay. All collection locations were on Long Island, New York. Two types of sections were used in this study: thin sections (less than 250 μm thick) and thick sections (about 1 mm thick). For studies of *Mya arenaria*, sections were made of the chondrophore, an internal structure projecting from the hinge region. Sections of the chondrophore were used for analysis because the chondrophore contains better preserved growth lines than the main shell (Cerrato *et al.*, 1991). In addition, it is isolated from the environment, preventing damage and elemental contamination.

Shells were cleaned to remove adherent debris by scrubbing with a nylon brush in tap water. Thick sections were prepared by cutting a section from the shells along the axis of maximum growth. The cut surfaces were ground with successively finer silicon carbide grits and polished with aluminum oxide. The sections were then attached to cardboard mounts for synchrotron x-ray fluorescence analysis. Thin sections were prepared in the same manner as thick sections except that the shell sections, after grinding, were glued to pure SiO_2 glass slides with 5-minute epoxy. X-ray fluorescence analyses of the epoxy and slide indicated that they contained only trace amounts of zirconium and titanium. The mounted sections were resectioned to several hundred micrometers and ground to the desired thickness with successively finer silicon carbide grits. The sections were then hand polished with aluminum oxide. Previous x-ray fluorescence studies have shown that this process neither introduces significant amounts of elemental contamination nor smears the elemental distribution of the sample.

Shell microstructure

The shells of *Mercenaria mercenaria* are composed of three distinct shell layers: an outer prismatic layer and a middle and an inner homogeneous layer. The middle and inner homogeneous layers are separated by the pallial myostracum (Panella and MacClintock, 1968). All layers of the shell are aragonitic (Taylor *et al.*, 1973). During periods of stress, the organism ceases its growth and retracts its mantle, producing a translucent band, known as a growth break, in the shell. Daily growth lines are also visible in the shells of *Mercenaria mercenaria*. These consist of an aragonite-rich increment followed by a protein-rich line (Kennish, 1980).

Both the shell and the chondrophore of *Mya arenaria* contain daily growth patterns; however, the growth patterns in the chondrophore are much better preserved than those in the main shell. These growth increments are similar in form to those in *Mercenaria mercenaria*: they are composed of a thin line followed by a broad increment. It is not known whether they also exhibit the same pattern of protein-rich lines and calcium-carbonate-rich increments. The chondrophores also show strong seasonal patterns: they are opaque in spring, translucent in summer, and opaque in fall-winter. Winter and spring are separated by a prominent translucent spawning band (Cerrato *et al.*, 1991).

The shell of *Argopecten irradians* consists of an inner and an outer calcitic foliated layer separated by a middle aragonitic crossed-lamellar layer (Kennedy *et al.*, 1969). To our knowledge, these shells do not contain growth lines.

Synchrotron x-ray fluorescence analyses

Synchrotron x-ray fluorescence analyses were performed at beamline X26-A of the National Synchrotron Light Source at Brookhaven National Laboratory. Samples were mounted in a sample holder in air. X rays produced by the synchrotron travel 9 m through an evacuated pipe to the sample. The x rays produced by the synchrotron have a critical energy of 5 keV and travel through several beryllium windows (total Be thickness = 1 mm) and 35 mm of air before striking the sample. The air path of the fluorescent x rays sets the effective lower detection limit at argon (Z = 18). The x-ray beam is collimated by an 8 μm tantalum pinhole immediately before striking the sample. This produces a microbeam, allowing resolution of fine structures. Immediately upstream of the collimator, the intensity of the x-ray beam is measured by an ion chamber.

The samples were mounted on an X, Y, Z, θ stage. They could thus be rastered under the x-ray beam, allowing the measurement of elemental concentrations at different points as well as along one- and two-dimensional scans over the specimen. An optical microscope imaging the specimen permitted precise determination of the location being analyzed. The secondary x rays emitted by the sample are collected in a Si(Li) detector. The detector was filtered with 500 μm of Kapton film, to reduce the count rate from the Ca x rays. This prevents saturation of the detector. The spectra are then stored in a Micro Vax computer for further analysis. Minimum detectable levels (MDLs) were 5 ppm for Mn, 2.5 ppm for Fe and Pb, 2 ppm for Sr, and 1.5 ppm for Ni through Br, for a spectrum collected for 4 min. MDLs were calculated by measuring the background under these peaks in a typical x-ray spectrum and computing the elemental concentration of a peak with an area equal to three standard deviations of the background. The calculated concentrations from the spectra were used to standardize these measurements.

The sample is mounted with the surface oriented at 45 degrees to the incoming x-ray beam and the detector. This exploits the angular distribution of the scattered radiation to minimize background. However, it also results in the beam traveling relative to the face of the sample as it penetrates the sample. This prevents the detection of changes in elemental concentration over small areas perpendicular to the beam. This effect is more pronounced at higher x-ray energies. At Ca (3.69 keV) the horizontal travel is only 11 μm; at Sr (14.14 keV) it is 55 μm. To reduce this effect, one can make thinner samples; however, it becomes difficult to optically resolve growth lines in samples thinner than 100 μm. Thus, the samples were oriented so that the interfaces of interest were parallel to the incoming beam whenever possible.

Spectra can be recorded in one of two ways: either the entire spectrum collected by the detector is recorded, or the net areas of the peaks of interest are recorded. Generally, when analyzing individual points, the entire spectrum was saved, as this allowed a more sophisticated background and peak-fitting routine to be used. However, when scanning a region, generally only the net areas of the peaks were saved, because this greatly reduces data analysis time. The Micro Vax implements automated scanning routines that allow the collection of data over long scans with no user intervention. The setup of the x-ray microprobe is discussed more comprehensively by Gordon *et al.* (1990).

Absolute concentrations were determined from the peak areas fit to the spectra by use of a "standardless" analysis program (NRLXRF). Using fundamental parameters, this program predicts the relative intensities for the different x-ray lines in the spectrum. These predictions are based on the thickness of the sample, the filtering conditions, and the assumed concentrations. The concentration of Ca was assumed to be 40% by weight, and was used as an internal standard to calculate the composition by comparing the predicted intensities and the actual count intensities. It was checked by predicting known standards that were measured at the beginning of each measurement session. The error was typically less than 5%.

PIXE microprobe analyses

Several samples were also analyzed by proton induced x-ray emission (PIXE) at the University of Melbourne. Analyses were performed with a 3 MeV proton beam, magnetically focused to 1 and 4 μm. Samples were thick shell sections, mounted in vacuum. The secondary x rays were collected with a Si(Li) detector, which was generally filtered with 50 μm Al to reduce the Ca count rate. However, some analyses were performed without filters in an attempt to measure sulfur concentrations. Rutherford backscattering spectroscopy (RBS) analyses were also made to allow carbon and oxygen concentrations to be measured.

PIXE analyses were made by sweeping the beam over a predetermined region of interest in the shape of an unclosed lissajous figure. Every time an x-ray event is detected by the Si(Li) detector, the energy of the event and the x and y coordinates of the beam are recorded. The x-ray spectrum is generated by disregarding the x and y values and simply taking the energy spectrum. A map of the concentration of a given element can then be generated by placing a window over a given peak and plotting the intensity of events in that energy range as a function of x and y. Analyses were performed on scales from 30 by 30 μm to 100 by 100 μm and were generally collected for 30 min. The MDLs in calcium carbonate matrix were about 18 ppm for Zn and Fe. This microprobe is described in more detail in Legge *et al.* (1986).

Although the PIXE microprobe does not have elemental sensitivity as good as the synchrotron x-ray fluorescence microprobe, it does have substantially better position resolution (a beam spot of 1 μm rather than 8 μm). The mean x-ray production depth for proton excitation in calcium carbonate is also less than that of x-ray excitation. Both of these factors enabled higher resolution of trace element distributions in the shell, but increased the MDLs for many elements.

Results

Surface contamination

Both shell surfaces of all species studied were found to be extremely contaminated with many trace elements. Table I lists the concentrations of these elements on both the exterior and interior surfaces of several organisms. Transverse scans across sections of scallop and hard clam shells showed that metal concentrations were much higher on both the interior and exterior surfaces of the shell than they were within the main shell. A representative transect is shown in Figure 1. Most elements were more concentrated on the exterior surface than the interior surface. However, the ratio of surface to main shell concentrations varied widely from element to element. The Ni concentration was only 1.5 times greater on the exterior surface, but the Cu concentration was 4.5 times greater. This is not unexpected, as the processes by which the elements are deposited on these surfaces are very complex. Scans in hard clams showed similar results. Trace element contamination on the interior shell surface is present in only a very thin layer. Within 100 μm the trace element contamination drops by a factor of 20–50, typically to within a factor of 2 of its average concentration. Most elements on the exterior surface of the hard clam behave in the same way as those on the interior surface, except iron (Fig. 2). Iron concentrations peaked both near the surface (30 μm) and farther in (180 μm). This is probably due to the periostracum and adherent debris on the shell surface; but why only Fe is affected is not known. The other trace elements are present in a surface layer that contains little calcium. This effect was most pronounced on the external surface; the maximum trace metal concentrations were at 30 μm from the edge of the shell and about 240 μm from where calcium concentrations became constant.

Shell layers

Most trace and minor elements (including Sr) are preferentially incorporated into the prismatic shell of the hard clam. The ratio of concentration in the prismatic shell to concentration in the homogeneous shell varied considerably from element to element, from about 20 for Fe to 1.5 for Sr. The reason for this increased concentration is unknown. Similar differences between shell layers were observed in scallops. Sr concentration in scallops was inversely related to both Mn and Fe concentrations; and Sr concentrations were highest in the outer 500 μm of shell, while Mn concentrations were highest in the inner 400 μm of shell. Some feature of the biological precipitation process is influencing the trace element concentration, as the

Table I

Elemental concentrations (ppm) in selected marine bivalves

Location	Mn	Fe	Ni	Cu	Zn	Br	Sr	Pb
Scallops (*Argopecten irradians*)								
Exterior surface	262	1080	152	902	308	17	814	21
Interior surface	208	636	102	201	106	21	1300	21
Outer shell layer	34 ± 1.4	8.5 ± 3.5	2 ± 0	2.5 ± 2.1	3 ± 1.4	1 ± 0	1495 ± 106	2 ± 0
Inner shell layer	48.5 ± 5	8.5 ± 3.5	2 ± 0	2 ± 0	5 ± 1.4	2 ± 1.4	911.5 ± 18	5 ± 2.1
Hard-shell clams (*Mercenaria mercenaria*)								
Prismatic shell	12.4 ± 3	219 ± 59	<1.5	3.6 ± 2.2	<1.5	5.4 ± 0.8	1247 ± 448	<2.5
Prismatic (DEC)	8.3 ± 3.9	38.8 ± 35	2.8 ± 1.5	1.5 ± 0.6	1.5 ± 0.6	3 ± 0	1139 ± 211	1 ± 0
Prismatic (PIXE)	9.8 ± 15	349 ± 518	<18	<18	13 ± 6.8	12.8 ± 8.3	3832 ± 961	
Prism./homog. boundary	3.5 ± 2.1	1085 ± 302	<1.5	3.3 ± 0.4	<1.5	5.5 ± 1.1	1115 ± 345	<2.5
Middle homog. shell	7.2 ± 2.2	11.6 ± 7.3	<1.5	3 ± 0.9	<1.5	5.4 ± 0.5	984 ± 353	<2.5
Middle homog. (DEC)	6.8 ± 8.2	4 ± 4.1	1 ± 0.8	1.8 ± 0.5	1.3 ± 0.5	2 ± 0	1007 ± 336	2.3 ± 2.5
Middle homog. (Thick)	1.25 ± 0.5	<2.5	1 ± 0	1 ± 0	1.5 ± 0.6	2.5 ± 1.3	725 ± 132	1 ± 0
Inner homog. (DEC)	1.8 ± 1.3	2.8 ± 2.5	1 ± 0	3 ± 2.6	1.4 ± 0.6	1.4 ± 0.6	1673 ± 180	1.7 ± 0.6
Soft-shell clams (*Mya arenaria*)								
Chondrophore	10 ± 4.4	<2.5	<1.5	<1.5	2 ± 0.6	<1.5	1383 ± 133	<2.5

All concentrations are in parts per million. Errors are given as the standard deviation of multiple measurements within the same shell layer; they do not reflect measurement error. Numbers without listed errors are based on single measurements. DEC: Shells came from collections in waters closed by the Department of Environmental Conservation. Thick: Data were taken on shell thick sections.

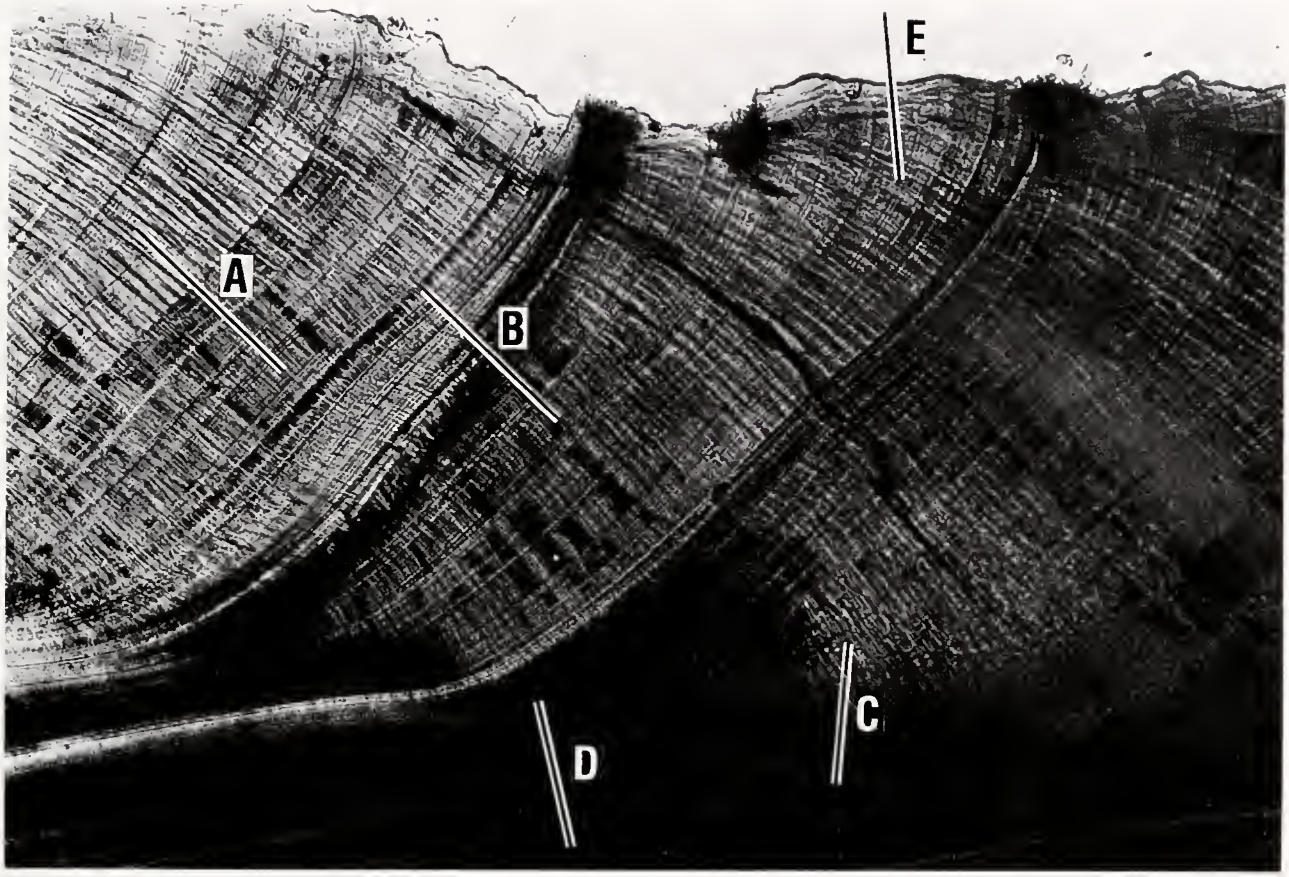

Figure 1. Representative transects along which scans were taken in *Mercenaria mercenaria* (A) Transect across daily growth increments in prismatic shell. (B) Transect across growth break. (C) Transect across prismatic-homogeneous boundary. (D) Transect across daily growth increments in homogeneous shell. (E) Transect across exterior shell surface.

chemistry of the scallop shell does not behave like geological carbonates. However, differences in chemical composition between biologically precipitated carbonates and geologically precipitated carbonates are not unknown; Buchardt and Fritz (1978) described aragonitic shell precipitated by a freshwater gastropod in which the strontium concentration of the shell is 5 times less than that of geologically precipitated aragonite under the same conditions. In addition, White *et al.* (1977) showed that Mn can replace Ca in aragonite formed by *Mya arenaria*, whereas this is not possible in geologically precipitated aragonite.

At the boundary between the prismatic shell and the middle homogeneous shell in the hard clam, very pronounced changes in elemental composition were observed (Figs. 3, 1). At this boundary, iron concentrations are typically 4.5 times greater than in the prismatic shell and 100 times greater than in the homogeneous shell. This iron peak is very narrow, about 40 μm wide, and was present in every measurement made across this boundary. The peak was always within 50 μm of where the boundary was located optically. Strontium concentrations declined between the prismatic and the homogeneous boundary, but this occurred more gradually, over about 100 μm, and appears to be associated only with the difference in Sr concentration in the two shell layers. Sr concentration reaches its nominal concentration in homogeneous shell at the same location as the peak in iron concentration. Manganese concentrations are lower at this boundary than in either the prismatic shell or the homogeneous shell, perhaps because the much greater concentration of iron is occupying the sites in the crystal lattice that are normally occupied by manganese. No feature similar to this has been observed in other organisms to our knowledge.

Sr concentration maps

Both the x-ray microprobe and the proton microprobe can be used to make high-resolution elemental maps, so changes in elemental concentration can be explored over very small areas. And with bivalve shells, fine variations

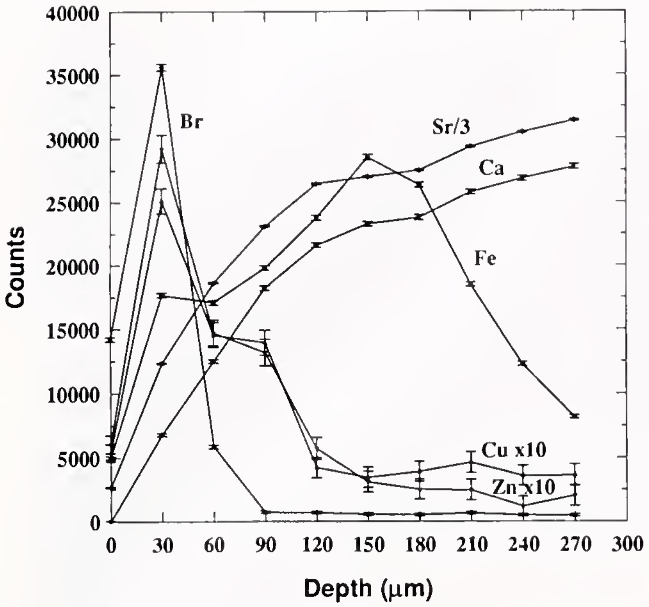

Figure 2. Scan across the outer surface of a *Mercenaria mercenaria* thick section. Data were recorded as individual spectra at each point. The spectra were then fitted to a sum of gaussian peaks and a background. The counts reported are the net areas of the peaks, less the background. Data was recorded for 40 s per point (detector live time).

with ontogeny can also be studied. We have used this scanning ability to elucidate changes within the shell structure, as with the prismatic-homogeneous boundary described above; but we have also measured the variations of trace element concentrations with time. The measurements of strontium were most successful. Because of its high concentration in the shell, strontium can be measured very accurately with counting times of only 5 s at each point in the shell. One-dimensional scans can therefore be made very quickly: a millimeter can be scanned at 10-μm resolution in less than 10 min. We could easily map a 2-year area of shell deposition at a resolution of a few days (Fig. 4) and produce very high-resolution two-dimensional elemental maps. A map of the hinge region of *M. mercenaria* is shown in Figure 5. Note the very good correlation between the strontium concentration and the banding in the thin section. Such scans are also possible for other elements, though reduced concentrations require proportionally longer counting times. Scans to measure Fe concentration were typically recorded at 30 s per point. For elements at levels of a few parts per million, counting times of several minutes are necessary.

High-resolution maps of Sr concentration made with the PIXE microprobe have shown variations in Sr concentration over scales as small as 10 μm. These variations appear to be correlated with the presence of growth breaks. However, because only a few PIXE measurements were made, this is not conclusive.

Growth lines

A comprehensive attempt was made to find trace element correlations with the daily microgrowth lines in the prismatic shell of *M. mercenaria.* The results strongly suggest that, although there is variation in trace element concentration in the prismatic shell of *M. mercenaria,* it is not necessarily correlated with the presence of microgrowth lines. All scans showed that iron concentration in the prismatic shell was nonuniform, but in most cases, no correlation with the microgrowth lines could be made. However, one scan (nsls106.10) showed very high correlation between the microgrowth lines and fluctuations in the iron content. In that scan, every microgrowth line was accompanied by a drop in iron concentration. Other scans showed some correlation between the presence of microgrowth lines and iron concentration, but none was as pronounced as this one. In an effort to improve the detectability of any iron fluctuations, we oriented samples so that the microgrowth lines were parallel to the incident beam. Thus, as the beam penetrated, it would stay within the microgrowth lines rather than transversing them. In addition, images were captured digitally after the beam position had been determined, enabling precise comparison between the image and the elemental concentration. Neither of these improvements showed further correlations between iron concentration and the presence of microgrowth lines. PIXE microprobe analyses were not sensitive enough to detect variations in the iron concentration of less than 40 ppm, and no structures were seen in the PIXE measurements of iron concentration. A correlation between microgrowth lines and iron concentration in the shell seems unlikely, but this is an area deserving further study.

Discussion

Synchrotron x-ray fluorescence (SXRF) microprobes provide lower minimum detectable levels than PIXE and EPMA microprobes. The experimentally determined MDL for Fe in thick clamshell sections was 3 ppm for SXRF and 18 ppm for PIXE. Our experience is that PIXE microprobes can make much larger and higher resolution maps than SXRF microprobes, although at lower sensitivity. PIXE measurements are generally made for long times (30 min) over large areas (1000 μm^2), whereas SXRF measurements are made for short times (1 min) over small areas (64 μm^2). Electron microprobes have MDLs of several hundred parts per million, worse than either PIXE or SXRF. But electron microprobes are typically more sensitive to low-Z elements than SXRF and PIXE microprobes (Janssens *et al.*, 1992). The minimum spot size of the NSLS microprobe is 8 μm; for EPMA and PIXE mi-

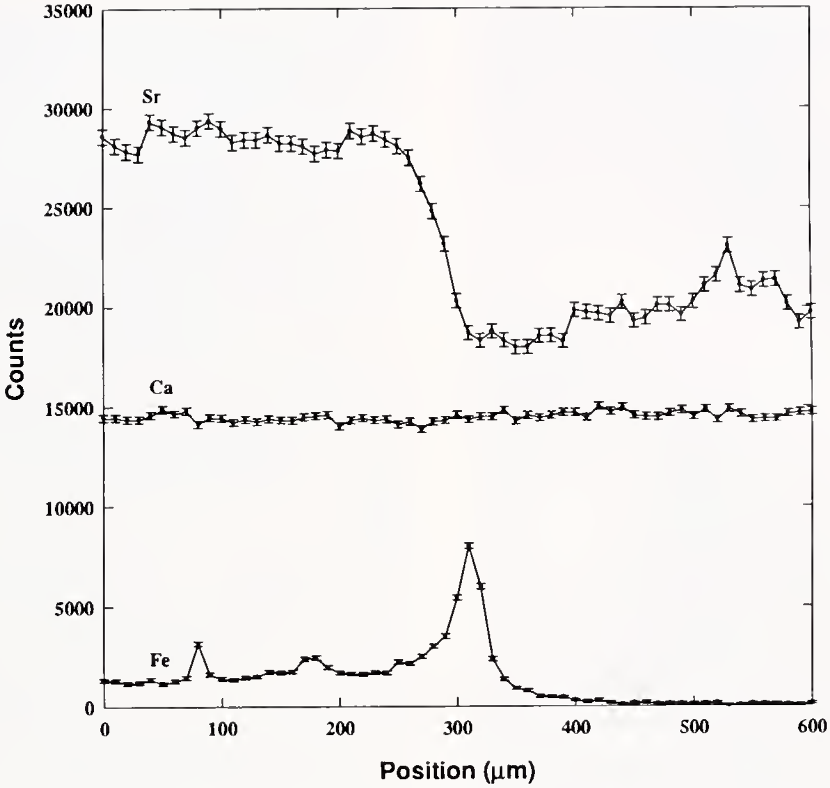

Figure 3. Scan across the prismatic/homogeneous boundary in a *Mercenaria mercenaria* thin section. Data were recorded as the area under user-defined regions of interest, with the background subtracted. Data was recorded for 15 s per point (detector live time). Initial Fe concentration is 211 ppm, initial Sr concentration is 1550 ppm. The Fe peak concentration is 1420 ppm.

croprobes it is 1 μm. New PIXE microprobes claim spot sizes of 300 nm.

For low-Z elements ($Z < 18$) EPMA has the greatest sensitivity as well as small spot size. Because of the ready availability of electron microprobes, EPMA is also suited to measurements of higher-Z elements present in quantities of several hundred parts per million or more. For measurements of elements present in concentrations of a few parts per million, SXRF is the method of choice. This is the only technique that combines MDLs of a few parts per million with spot sizes of a few micrometers. However, for some measurements, the spot size of the NSLS microprobe (8 μm) is too large. In these cases, PIXE microprobes can be used, if the elements are present in large enough concentrations. The greater accessibility of PIXE microprobes also makes them attractive for studies of elements present in concentrations of several tens of parts per million.

Bulk analysis techniques cannot provide the same spatial resolution as microprobes. The neutron activation studies of Carell *et al.* (1987) were performed on shell samples of 10–50 mg. This corresponds to a shell section 0.5 mm thick by 6 mm long by 3 mm deep. If this section is cut with the thin direction normal to the ventral margin, it represents approximately 1 month of growth. Atomic absorption analysis can detect much smaller amounts of trace elements, hence the limiting factor is the size of the shell section that can be obtained. This probably limits bulk analysis techniques to time resolutions of a few weeks. In addition, many clamshell sections must be prepared to make a study at this resolution over a significant period. In contrast, microprobe techniques require only one section per shell. Consequently, bulk analysis techniques are suitable for situations where resolution of small time scales is not necessary and integration of elemental concentrations over all dimensions of the shell is not a problem. In practice, microprobe techniques are probably more suitable for time-resolved studies of trace elements in bivalve shells. Bulk analysis methods can, however, detect elemental concentrations a factor of a thousand smaller than microprobes can.

Wavelength-dispersive detectors should improve the usefulness of SXRF microprobes for analyzing trace elements in bivalve shells. Because wavelength-dispersive

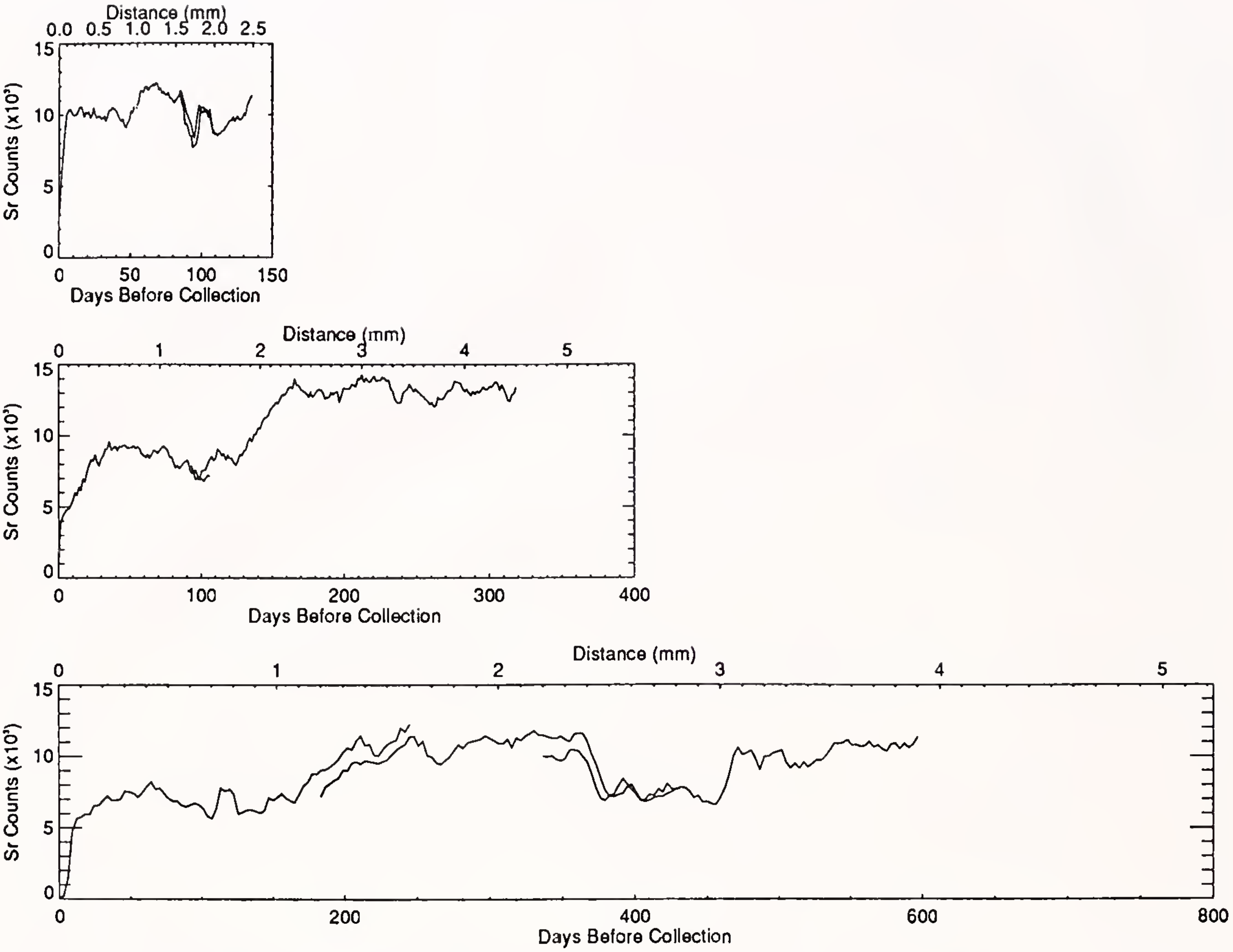

Figure 4. Variation in Sr concentration across growth increments in the chondrophore of *Mya arenaria*. Each of the three scans was taken on a different shell; all shells were harvested at the same time. Distance is measured in millimeters from the ventral margin of the chondrophore. Time before harvesting was calculated by dividing the distance from the margin by the average growth rate per day, which was determined by measuring the distance from the margin to the spawning break which occurred approximately 90 days before harvest. Each plot consists of three separate scans separated by up to 150 μm parallel to the growth increments. Notice the strong correlation of variations in each of the separate scans. Note also the correlations between the shells. We believe that these variations represent changes in the water temperature over time.

spectrometers detect only a single x-ray wavelength, they eliminate the filtering necessary to prevent saturation of an energy-dispersive detector by Ca x rays. This filtering also attenuates other low-energy x rays, preventing the detection of low-Z elements and resulting in high (200 ppm) MDLs for Ti. Use of a wavelength-dispersive detector would allow the detection of much smaller quantities of low-Z elements, and possibly improve MDLs for higher-Z elements as well. Such a device is now in use at the National Synchrotron Light Source at Brookhaven National Laboratory (Rivers *et al.*, 1992). Future SXRF microprobes will become even more useful as they are developed at third-generation synchrotrons, such as the Advanced Photon Source (APS) at Argonne National Laboratory. A planned SXRF microprobe at the APS will have 10^4 times more photons in a given energy range. This will allow the use of extremely small spot sizes (0.1 μm) at current detection limits, or lower detection limits at small spot sizes (1 μm).

SXRF microprobes are not limited merely to the applications discussed here. It is also possible to use SXRF to study other calcified samples, such as corals or fish otoliths. Studies of fish otoliths with EPMA (Gunn *et al.*, 1992) and PIXE (Gauldie *et al.*, 1992) suggest that the

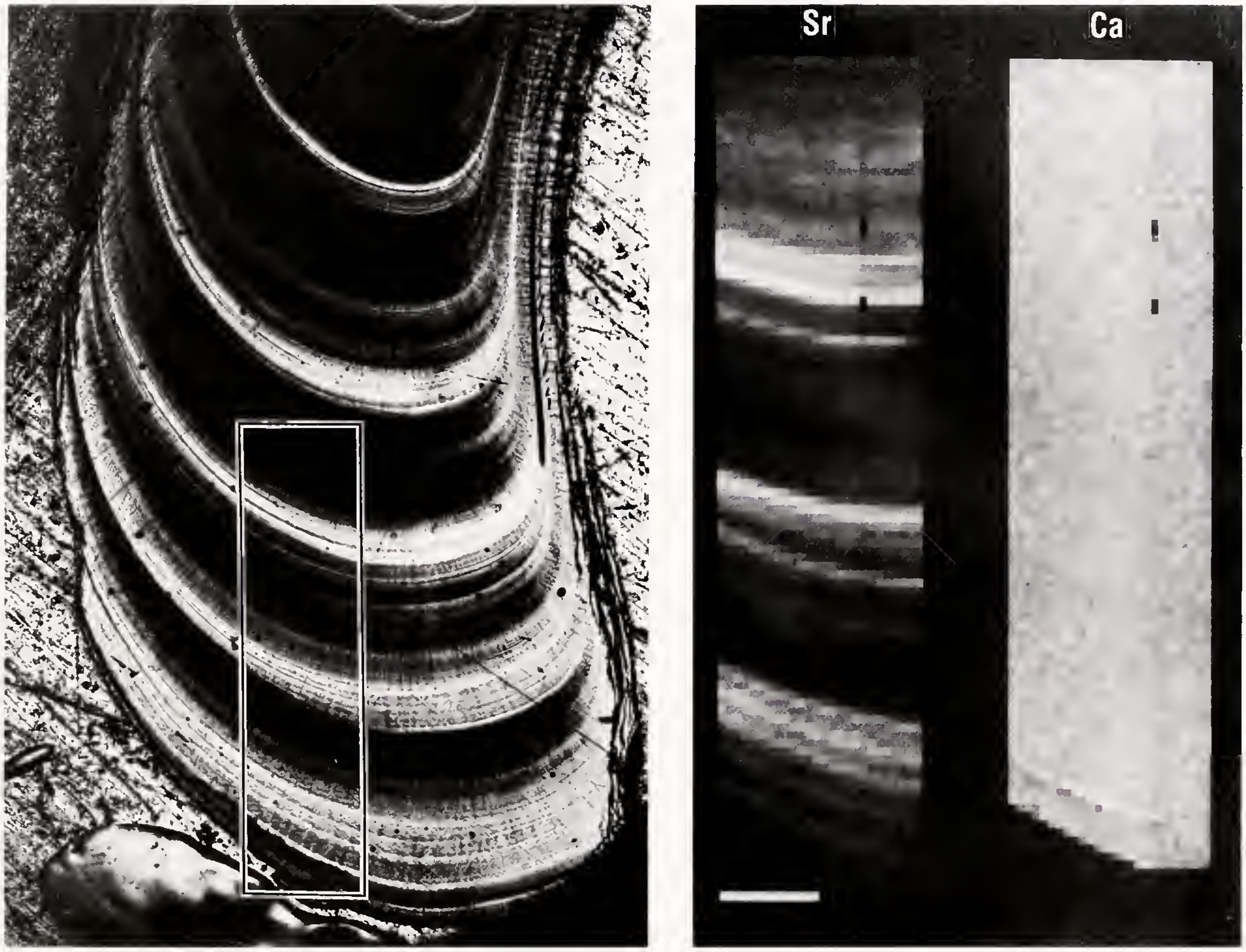

Figure 5. Two-dimensional scan (map) of Sr and Ca concentration in the hinge region of *Mercenaria mercenaria.* Each pixel measures 20 μm on a side, and was collected for 20 s. The data were recorded as background-subtracted regions of interest and have been normalized to beam intensity and detector live time. The box on the photomicrograph approximately corresponds to the region scanned. Note the correlation of the variations in strontium concentration with the seasonal banding in the chondrophore.

SXRF microprobe would be a valuable tool for such studies. Spatial resolution and elemental sensitivity similar to that obtained here should be achievable in studies of other calcified samples. Furthermore, it is not necessary to sacrifice the molluscs and section their shells to use the SXRF microprobe. Because the beam deposits relatively little energy in the shell and stops within the first few hundred micrometers of the shell, live molluscs can be studied, though this raises the problems of removing surface contamination and dating the sampled positions accurately. SXRF can also be used to detect organometallic compounds, provided the metals are of sufficiently high Z. Techniques such as extended x-ray absorption fine structure (EXAFS) also promise the ability to determine the oxidation state of metals detected by SXRF.

The measurements made on bivalve shells have revealed several interesting features. The contamination of the exterior surface is most likely due to the adsorption of elements onto the calcium carbonate from seawater. However, the contamination could also be due to adherent debris on the surface of the shell. The contamination of the interior surface is probably not due to elements adsorbed onto the calcium carbonate during active growth, because they would then have to be removed before additional shell was deposited. Although there is some evidence that the shell undergoes structural changes after deposition (Gordon and Carriker, 1978), it seems more likely that the elemental contamination arose after the shells were collected, either from adsorption of metals from the pallial fluid or from contamination after collection.

Seasonal variations in strontium concentration were observed in the shells of both hard- and soft-shell clams (Fig. 4). Differences in strontium concentration of 30% to 40% were typical between winter and summer. Each of the high and low Sr regions was about 180 days long. We believe these variations are a result of the seasonal temperature change of the seawater. In addition, shorter-term variations (100 μm long) were observed; these probably correspond to shorter-term temperature variations. As with paleothermometry done with Sr/Ca ratios in corals (Beck *et al.*, 1992), our results show that increases in Sr concentration correspond to decreases in temperature. Assuming that the change in Sr concentration is linearly related to the change in water temperature, the change in the observed Sr count rate is 18 counts/s/C°. In a 10-s per point scan, changes of 6 counts/s are observable. This corresponds to a temperature change of 0.33°C. The use of x-ray fluorescence to measure small (0.3°C) temperature variations over short (3-day) time scales seems quite simple. In practice, the resolution is probably limited by the rate at which shell strontium concentrations equilibrate to the ambient water temperature. Our scans show good correlation between different transects on an individual shell and between different shells harvested from the same location at the same time. This strongly suggests that we are observing environmental effects upon the shell. Figure 5 also shows very good correlation between Sr concentration and seasonal banding in the shell.

One problem complicating the use of x-ray fluorescence as a means of paleothermometry using Sr/Ca ratios is that for samples thinner than 200 μm, sample thickness influences the Sr count rate. This is especially a problem near the edges of shells, which were often inadvertently ground thinner during preparation than other parts of the shell. Such "thickness effects" show up as a gradual increase in the Sr (and in extreme cases Ca) count rate as the sample is scanned. In practice, the best way to avoid such effects is to use samples thicker than the mean fluorescence depth for Sr K x rays, because preparing samples uniform in thickness to within a few percent is difficult to do. In that case, the Sr count rate is unaffected by small variations in sample thickness.

The synchrotron x-ray fluorescence microprobe has significant advantages for trace element analyses in calcified structures. It combines very low detection limits with very small spot sizes. This allows the measurement of elemental concentrations as low as 1 ppm over scales as small as 10 μm. Synchrotron x-ray fluorescence microprobes have significantly better detection limits than EPMA and PIXE microprobes, and are probably the best instrument for most studies of trace element distributions in calcified structures. When structures smaller than 10 μm are to be resolved, the extremely small spot size of PIXE microprobes makes them the analytical technique of choice.

Acknowledgments

We are grateful to David Jamieson for performing the PIXE and RBS analyses at the University of Melbourne.

Literature Cited

Al-Dabbas, M. A. M., F. H. Hubbard, and J. McManus. 1984. The shell of *Mytilus* as an indicator of zonal variations of water quality within an estuary. *Estuarine Coastal Shelf Sci.* **18:** 263–270.

Beck, J. W., L. R. Edwards, E. Ito, F. W. Taylor, J. Recy, F. Rougerie, P. Joannot, and C. Henin. 1992. Sea-surface temperature from coral skeletal strontium/calcium ratios. *Science* **257:** 644–647.

Buchardt, B., and P. Fritz. 1978. Strontium uptake in shell aragonite of the freshwater gastropod *Limnaea stagnalis. Science* **199:** 291–292.

Carell, B., S. Forberg, E. Grundelius, L. Henrikson, A. Johnels, U. Lindh, H. Mutvei, M. Olsson, K. Svaerdstroem, and T. Westermark. 1987. Can mussel shells reveal environmental history? *Ambio* **16:** 2–10.

Carriker, M. R., C. P. Swann, and J. W. Ewart. 1982. An exploratory study with the proton microprobe of the ontogenetic distribution of 16 elements in the shell of living oysters. *Mar. Biol.* **69:** 235–246.

Cerrato, R. M., H. V. E. Wallace, and K. G. Lightfoot. 1991. Tidal and seasonal patterns in the chondrophore of the soft-shell clam *Mya arenaria. Biol. Bull.* **181:** 307–311.

Gauldie, R. W., G. C. Coote, K. P. Mulligan, and I. F. West. 1992. A chemical probe of the microstructural organization of fish otoliths. *Comp. Biochem. Physiol.* **102A:** 533–545.

Gunn, J. S., I. R. Harrowfield, C. H. Proctor, and R. E. Thresher. 1992. Electron probe microanalysis of fish otoliths—evaluation of techniques for studying age and stock discrimination. *J. Exp. Mar. Biol. Ecol.* **158:** 1–36.

Gordon, J., and M. R. Carriker. 1978. Growth lines in a bivalve mollusk: subdaily patterns and dissolution of the shell. *Science* **202:** 519–521.

Gordon, B., A. L. Hanson, K. W. Jones, J. G. Pounds, M. L. Rivers, G. Schidlovsky, P. Spanne, and S. R. Sutton. 1990. The application of synchrotron radiation to microprobe trace element analysis of biological samples. *Nucl. Inst. Meth.* **B45:** 527–531.

Janssens, K. H., F. van Langevelde, F. C. Adams, R. D. Vis, S. R. Sutton, M. L. Rivers, K. W. Jones, and D. K. Bowen. 1992. Comparison of synchrotron X-ray microanalysis with electron and proton microscopy for individual particle analysis. *Adv. X-Ray Anal.* **35B:** 1265–1275.

Kennedy, W. J., J. D. Taylor, and A. Hall. 1969. Environmental and biological controls on bivalve shell mineralogy. *Biol. Rev.* **44:** 499–530.

Kennish, M. J. 1980. Shell microgrowth analysis: *Mercenaria mercenaria* as a type example for research in population dynamics. Pp. 255–294 in *Skeletal Growth of Aquatic Organisms.* D. C. Rhoads and R. A. Lutz, eds. Plenum, New York.

Koide, M., D. S. Lee, and E. D. Goldberg. 1982. Metal and transuranic records in mussel shells, byssal threads and tissues. *Estuarine Coastal Shelf Sci.* **15:** 679–695.

Legge, G. J. F., C. D. MacKenzie, A. P. Mazzolini, R. M. Sealock, D. N. Jamieson, P. M. O'Brien, J. C. McCallum, G. L. Allan, R. A. Brown, R. A. Colman, B. J. Kirby, M. A. Lucas, J. Zhu, and J. Cerini. 1986. Microbeam imaging at micron and submicron resolution. *Nucl. Inst. Meth.* **B15:** 669–674.

Milliman, J. D. 1974. Marine Carbonates, Part I of *Recent Sedimentary Carbonates.* Springer-Verlag, New York. 375 pp.

Panella, G., and C. MacClintock. 1968. Biological and environmental rhythms reflected in molluscan shell growth. *J Paleontol.* **42:** 64–80.

Rivers, M. L., K. Thorn, S. R. Sutton, and K. W. Jones. 1992. Wavelength dispersive detectors in synchrotron x-ray fluorescence microprobe analysis. *EOS, Trans. Am. Geophys. Union.* 73(43): 620.

Rhoads, D. C., and R. A. Lutz. 1980. Skeletal records of environmental change. Pp. 1–19 in *Skeletal Growth of Aquatic Organisms.* D. C. Rhoads and R. A. Lutz, eds. Plenum, New York.

Rosenberg, G. D. 1980. An ontogenetic approach to the environmental significance of bivalve shell chemistry. Pp. 133–168 in *Skeletal Growth of Aquatic Organisms.* D. C. Rhoads and R. A. Lutz, eds. Plenum, New York.

Rosenberg, G. D., and W. W. Hughes. 1991. A metabolic model for the determination of shell composition in the bivalve mollusc, *Mytilus edulis. Lethaia* **24:** 83–96.

Swann, C. P., K. M. Hansen, K. Price, and R. Lutz. 1991. Application of PIXE in the study of shellfish. *Nucl. Inst. Meth.* **B56/57:** 683–686.

Wada, K., and S. Suga. 1976. The distribution of some elements in the shell of freshwater and marine bivalves by electron microprobe analysis. *Bull. Natl. Pearl Res. Lab* **20:** 2219–2240.

White, L. K., A. Szabo, P. Carkner, and N. D. Chasteen. 1977. An electron paramagnetic resonance study of manganese(II) in the aragonite lattice of a clam shell, *Mya arenaria. J. Phys. Chem.* **81(14):** 1420–1424.

Reference: *Biol Bull* **188**: 68–77. (February/March, 1995)

Life History Patterns of *Discorsopagurus schmitti*, a Hermit Crab Inhabiting Polychaete Tubes

FRANCESCA GHERARDI[1] AND PAUL M. CASSIDY[2]

[1]*Dipartimento di Biologia Animale e Genetica "Leo Pardi," Università di Firenze, Via Romana 17, 50125 Firenze, Italy; and* [2]*Shannon Point Marine Center, Western Washington University, 1900 Shannon Point Rd., Anacortes, Washington 98221*

Abstract. *Discorsopagurus schmitti* is a hermit crab that inhabits empty polychaete tubes in the North Pacific. Here we describe some aspects of its life history (relative growth, population structure, reproductive biology, and incidence of parasitism) and discuss the relationships among them. Unlike most hermits, the two sexes of this species have similar size distributions. In both sexes, larger body size is accompanied by a higher reproductive output (larger clutch size in females and more intrasex competitive potential in males). The energy the females expend in egg production might be equaled in this species by the energy the males expend in supporting parasites. In fact, the extent of infestation by two rhizocephalans [*Peltogaster boschmae* and *Thilacoplethus* (=*Thompsonia*) *reinhardi*] is more pronounced in males, especially those in the larger size classes. However, rhizocephalans have little effect on their hosts; growth and secondary sexual characters are not influenced. The only morphological modification is the more frequent loss of the second pleopod. Infected hermits also showed a mock parental behavior, fanning the externae with the pleopods as ovigerous females fan their eggs. Larvae are released in sequential bursts, and hatching occurs exclusively at night, possibly to minimize predation by diurnal fishes. Hatching is also synchronized with neap tides, which might keep the larvae from being flushed out into open waters. In a species whose habitat (sabellarian bioherms) is rare and quite unpredictable, it is beneficial to retain larvae near the parental population.

Introduction

Discorsopagurus schmitti (Stevens, 1925) is an anomuran crab that occurs widely along the North Pacific coasts from Japan to Puget Sound (McLaughlin, 1974). In both its geographical distribution and its ecological role, this species is strictly dependent on the polychaete *Sabellaria cementarium* Moore, 1906. The hermit uses attached worm tubes as housing and occupies a niche within the community associated with sabellarian bioherms (Gherardi and Cassidy, 1994a). A bioherm is a rock formed by accretions from sedentary organisms and surrounded by other kinds of rocks. Within the habitat, *D schmitti* has a contagious distribution, the crabs occurring with a density averaging 6 specimens per dm^2 (Gherardi and Cassidy, 1994b).

Despite its peculiar habits and widespread distribution, the main life history traits of the species are still unknown. Previous papers were concerned only with its adaptations to the sessile worm tubes (Caine, 1980) and its ecology (Gherardi and Cassidy, 1994b). Our study investigates the relative growth, population structure, reproductive biology, and incidence of parasitism by rhizocephalans in *D. schmitti*.

Materials and Methods

D. schmitti was collected from a wide sabellarian bioherm in Burrows Channel, Fidalgo Island (northern Puget Sound, Washington). A total of 440 specimens were collected: 329 from June to August 1992, and 111 from January to April 1993. See Gherardi and Cassidy (1994a, b) for details on habitat and sampling procedure.

Sixty-four animals were individually weighed to the nearest 0.01 g. Chelipeds were excluded from the weight because they are variable and sometimes absent. For each specimen, we recorded sex, size (shield length, SL, to the nearest 0.1 mm), missing chelipeds (*i.e.*, the number of "injured" specimens), and the number and maximum

Received 10 December 1993; accepted 18 November 1994.

diameter of any egg present. When possible, the maximum axis of the occupied polychaete tube was measured with a caliper. The number and position of externae of the parasitic rhizocephalans *Peltogaster boschmae* Reinhard and *Thilacoplethus* (=*Thompsonia*) *reinhardi* Lützen were also noted. Because we did not assess the presence of rootlets penetrating major organs (stage of interna), which precedes the parasite's sexual development, we may have underestimated the extent of infestation within the sample.

To describe the format of relative growth (*i.e.*, the change in shape with growth; Hartnoll, 1982), we measured the length of the dactyl (DL) and palm (PA) of both chelae, and their depth (DE) in 130 hermits. To represent the patterns of the relative growth of these measures (y) with respect to the SL as an independent variable (x), the natural logarithmic transformation ($\ln y = \ln a + b \ln x$) of the exponential function $y = a\, x^b$ was used. This relationship fits nearly all the instances of allometric growth in crustaceans (Hartnoll, 1982). The values of b define the type of allometry ($b = 1$: isometry; $b < 1$: negative allometry; $b > 1$: positive allometry). This and the other parameters of $\ln y$ on $\ln x$, calculated using the Least-Squares Method, allowed us to use standard tests for significance and to compare slopes and intercepts between groups.

Within winter samples, pleopods were examined and their configuration related to the occurrence of parasites. The configuration of pleopods in *D. schmitti* was first described by McLaughlin (1974); the species shows pleopods 2–5, with the exception of some males, in which the second pleopod is absent.

The behavior of animals occupying pieces of transparent glass tubing was recorded with a Panasonic color camera and played back on a Mitsubishi recorder.

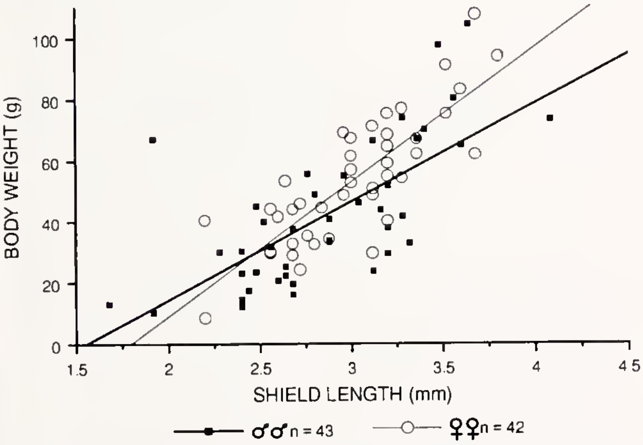

Figure 1. Relationship between size (shield length) and body (without chelipeds) weight, compared between sexes. A positive correlation was found in both males (r = 0.692, df = 41, P < 0.01), and females (r = 0.809, df = 40, P < 0.01).

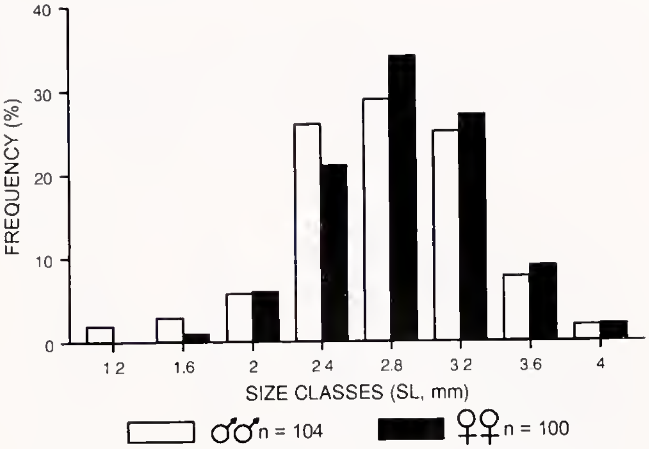

Figure 2. Size class distributions compared between sexes from summer collections.

Data on egg incubation and hatching were obtained from 19 ovigerous females, collected on January 18 (5), February 8 (5), and April 27 (9) 1993. In the laboratory, the females were placed in individual glass bowls 20 cm in diameter, in filtered seawater with a salinity of 28–31‰. The bowls were kept in a constant temperature unit at 10°C under a light:dark regime of 14:10. Until they released larvae, ovigerous females were checked twice a day for hatching, placed in bowls of clean seawater, and fed *Artemia*. The number of larvae released daily was recorded for ten of the females.

For statistical analysis, we followed the methods and recommendations of Siegel (1956) and Zar (1984). The level of significance under which the null hypothesis was rejected is $\alpha = 0.05$.

Results

Population structure

Figure 1 shows the relationship between SL and body weight (excluding chelipeds) compared between sexes. No between-sex difference was found in either the slope (32.12 *vs.* 43.96, t = 1.549, df = 81, ns) or the intercept (−49.90 *vs.* −78.98, t = 1.781, df = 82, ns) of the regression line.

The sizes of crabs (SL) during summer were analyzed (Fig. 2). No significant difference in size distributions was found between the two sexes (G = 4.442, df = 7, ns). The smallest specimens measured 1.1 (prepubertal, showing no gonopores), 1.4 (male), and 1.9 mm SL (female), and the maximum size attained 3.9 mm SL in the two sexes.

The sex ratio was 50.98% (104 males to 100 females), which did not differ from 1:1 (χ^2 = 0.044, df = 1, ns). Similarly, the sexes remained balanced when three size classes were distinguished (<2.6 mm SL: χ^2 = 0.5, df = 1, ns; 2.6–3.4 mm SL: χ^2 = 0, df = 1, ns; >3.4 mm SL: χ^2 = 0, df = 1, ns).

Table I

Isometric or allometric growth with size of Discorsopagurus schmitti *(shield length) of three measures of both the major (right) and the minor (left) chela, compared between sexes*

ln shield length *vs.*:	♂♂				♀♀			
	r	*b*	*t* $b \neq 1$	*a*	*r*	*b*	*t* $b \neq 1$	*a*
ln DC (major chela)	0.721	0.79	2.173	0.13	0.337	0.40	4.367*	0.65
ln PA (major chela)	0.878	0.66	7.450*	0.12	0.624	0.47	7.435*	0.36
ln DE (major chela)	0.900	0.84	3.010*	−0.04	0.740	0.57	6.727*	0.33
ln DC (minor chela)	0.831	0.70	4.928*	−0.07	0.484	0.41	6.590*	0.31
ln PA (minor chela)	0.811	0.60	7.238*	−0.04	0.682	0.51	7.371*	0.07
ln DE (minor chela)	0.634	0.48	6.831*	0.19	0.752	0.56	7.445*	0.11

DC = dactyl length; PA = palm length; DE = chela depth.

a = intercept of the regression line.

* $P < 0.01$.

All the correlation coefficients (r) are significant ($P < 0.01$). Isometry is satisfied when the regression coefficient (b) equals 1 after Student's t-test (t), otherwise an allometric growth (here only negative) occurs. The numbers of males and females are 63 and 69, respectively.

The size and sex of specimens in three individually collected clumps were separately analyzed; the comparison did not show any difference in either size distribution ($G = 6.08$, df = 4, ns) or sex ratio ($\chi^2 = 1.458$, df = 2, ns).

Chelipeds

The growth of both chelae relative to hermit size (SL) was always negatively allometric for DC, PA, and DE, with the exception of the DC of the major chela in the males, where it was isometric (Table I). Table II gives the between-sex differences in the parameters of the regression lines; the males had a more voluminous major chela than similarly sized females, as well as a longer dactyl in the minor chela. However, the male and female regression lines crossed at a large crab size (major chela: 3.8, 3.4, 4.1 mm SL for DC, PA, and DE, respectively; minor chela DC: 3.7 mm SL).

In all the examined specimens, the right chela was the major one. This had constantly higher values than the left one with SL increment (equal slope, but a higher intercept), with the exception of the major chela DE, where the growth increased with size (Table III).

Injured specimens represented 24.11% of the sample, without any significant difference between sexes (25% in males, 24.26% in females: $\chi^2 = 1.762$, df = 1, ns). Right

Table II

Between-sex comparison of chelar growth in Discorsopagurus schmitti

	b		*a*	
	t	♂ *vs.* ♀	*t*	♂ *vs.* ♀
DC (major chela)	2.298*	>	—	—
PA (major chela)	2.265*	>	—	—
DE (major chela)	3.190**	>	—	—
DC (minor chela)	2.734**	>	—	—
PA (minor chela)	1.003	=	0.301	=
DE (minor chela)	0.713	=	1.428	=

— test not applicable.

DC = dactyl length; PA = palm length; DE = chela depth.

* $P < 0.05$; ** $P < 0.01$.

Comparisons after Student's t-test (t) between sexes in both the slope (b) and the intercept (a) of the regression lines (after a ln-ln transformation) describing the relationships between hermit size (shield length) and three chelar measures. The degrees of freedom are 127 and 128.

Table III

Between-side comparison of chelar growth in Discorsopagurus schmitti

♂♂:	*b*		*a*	
	t	*r vs. l*	*t*	*r vs. l*
DC	0.755	=	16.342**	>
PA	0.847	=	20.505**	>
DE	3.935**	>	—	—
♀♀:	*b*		*a*	
	t	*r vs. l*	*t*	*r vs. l*
DC	0.037	=	17.964**	>
PA	0.418	=	21.289**	>
DE	1.636	=	24.428**	>

— test not applicable.

DC = dactyl length; PA = palm length; DE = chela depth.

** $P < 0.01$.

Comparison after Student's t-test (t) between the right (r) and the left (l) chela in both the slope (b) and the intercept (a) of the regression lines (after a ln-ln transformation) describing the relationships between hermit size (shield length) and three chelar measures. The degrees of freedom are 121, 122 in males, and 134, 135 in females.

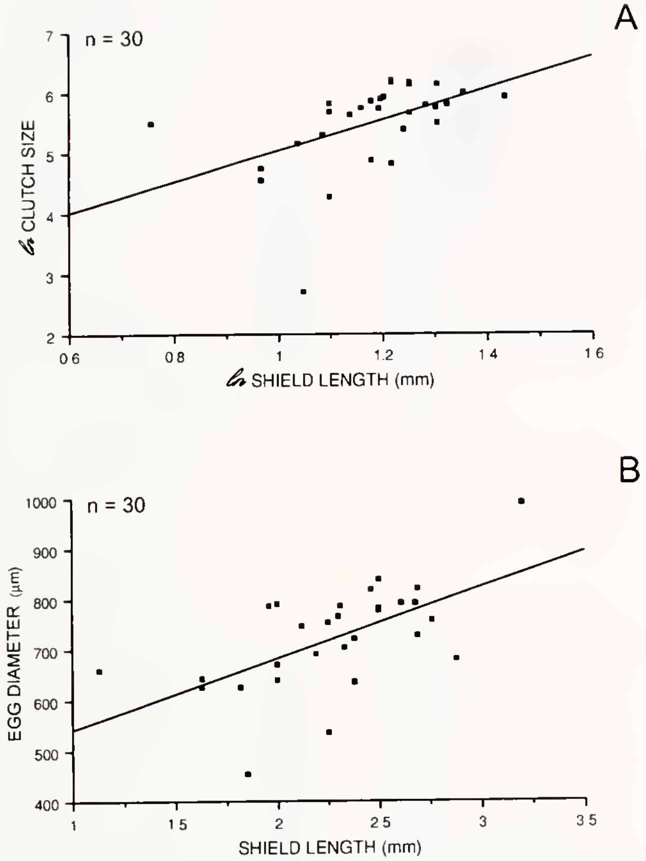

Figure 3. Relationships between the size of ovigerous females (shield length) and both the number (after a ln-ln transformation, A) and the diameter (maximum axis, B) of the spawned eggs.

chelipeds were missing more often than left ones (65.96% *vs.* 34.04%, $\chi^2 = 4.17$, df = 1, $P < 0.05$).

Eggs

Egg-bearing females occurred in winter samples only. They were first found in January and were still present at the end of April, though their percentage was low (20%, 9 out of 45). Their numbers did not differ from those of nonovigerous females (January 18: 19 *vs.* 10, $\chi^2 = 2.207$, df = 1, ns; February 1: 15 *vs.* 21, $\chi^2 = 0.694$, df = 1, ns), and specimens in the two reproductive states shared the same size distribution ($G = 2.906$, df = 5, ns) and frequency per size class (<2.6 mm SL 45.10%, *vs.* a uniform distribution: $G = 0.486$, df = 1, ns; ≥2.6 mm SL 70%, $G = 1.567$, df = 1, ns). The smallest and largest females found bearing eggs measured, respectively, 1.1 and 3.2 mm SL.

Egg number per clutch ranged from 14 to 496, averaging 287. Female size (SL) was positively correlated with the number of eggs (after a ln-ln transformation: $r = 0.478$, df = 28, $P < 0.01$, $b = 2.56$, $a = 2.48$) (Fig. 3A). The value of the correlation coefficient did not significantly differ from 3 ($t = 0.495$, df = 28, ns): that is, clutch size is proportional to the cube of the SL (roughly equaling the body mass).

The mean egg diameter was 722 µm (SE = 19, $n = 30$), ranging from 455 to 990 µm. A positive correlation was also found between the SL of the female and the average diameter of her eggs ($r = 0.586$, df = 28, $P < 0.01$, $b = 0.14$, $a = 0.40$) (Fig. 3B), showing that bigger females produce larger (and more numerous) eggs.

Eggs are attached to the second through the fourth pleopods, about 100 per pleopod, in bunches of 7 to 15. They are slightly ovate and attached by a funiculus, measuring around 1.2 mm. Ovigerous females kept inside transparent tubing were seen fanning the eggs with a reversing current created by the second and third pleopods.

Hatching

Hatching occurred between 1 and 75 days ($n = 17$) after collection. Because all the analyzed females bore eggs when collected, this is only a minimum estimate of the actual length of egg incubation.

The number of larvae per individual ranged from 80 to 541 (average = 226, SE = 46) in the 10 females analyzed, and did not differ significantly from the number of eggs per batch ($t = 1.31$, df = 38, ns), being on average 98.74% of the eggs spawned. Larvae were released in 3–6 days (average = 5.1 day, SE = 0.3), with a maximum of 209 larvae in the fourth day. No correlation was found between the length of the hatching period and the female size ($r = 0.074$, df = 8, ns), but the former was positively related to the overall number of larvae (Spearman rank correlation test: $r_s = 0.742$, $t = 3.134$, df = 8, $P < 0.02$). Larvae were not released at a constant rate; the percentage released (Fig. 4) differed significantly throughout the hatching period (Kruskal-Wallis one-way analysis of vari-

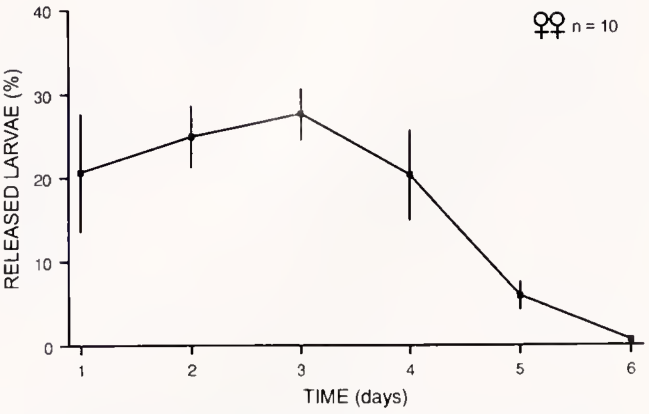

Figure 4. Percentage (average ± SE) of the larvae released by 10 females plotted against the length of hatching (in days).

ance: $H = 29.975$, df = 5, $P < 0.001$), peaking in the third day and then falling off abruptly after the fifth day.

Hatching occurred exclusively at night, and mostly during the neap phase of the tide (Mann-Whitney test: $U = 0$, $n = 7$ and 7, $P < 0.01$), when the mean tidal current is consistently slower (Fig. 5). For our comparison, we defined neap (or spring) phase as the day of the minimum (or maximum) tidal excursion for a lunar tidal cycle plus the 3 days preceding and following that date.

Parasite distribution

Peltogaster boschmae was the most common rhizocephalan parasite in our samples, affecting 18.5% of the specimens; *Thilacoplethus* (=*Thompsonia*) *reinhardi* infected 6.8%; and the two rhizocephalans co-occurred in 2.5%. These figures are similar to the percentages reported by Lützen (1992) for a previous study in the same area.

A sexual difference in the degree of infestation was seen in both the number of externae per individual (males: average = 2.9, SE = 0.6; females: average = 2.3, SE = 0.9; $\chi^2 = 9.312$, df = 2, $P < 0.01$) (Fig. 6) and the prevalence of parasitism (*i.e.*, the percentage of the parasitized hermits; Margolis *et al.*, 1982) (males *vs.* females: 28.17% *vs.* 14.39%, $\chi^2 = 7.144$, df = 1, $P < 0.01$). Similar results were obtained from the winter samples, where parasitized males and females scored 28.26% and 9.37% respectively ($\chi^2 = 5.424$, df = 1, $P < 0.02$). The number of parasitized specimens did not differ between sampling periods (summer: 60 out of 281, winter: 19 out of 110; $\chi^2 = 0.01$, df = 1, ns).

The maximum number of externae from the summer samples was 15 in males and 18 in females. We counted 23 externae in one female collected in winter. None of the ovigerous females in our sample had parasites (0 *vs.* 20% in nonovigerous ones: $\chi^2 = 5.334$, df = 1, $P < 0.05$). Only one female has been collected bearing both eggs and three externae (P. M. Cassidy, pers. obs.), but it is plausible that infestation occurred after spawning. The number of externae was significantly correlated with the host size if the host was male (Spearman rank correlation test: $r_s = 0.413$, $t = 2.759$, df = 37, $P < 0.01$), but not if it was female ($r_s = 0.299$, $t = 1.331$, df = 18, ns).

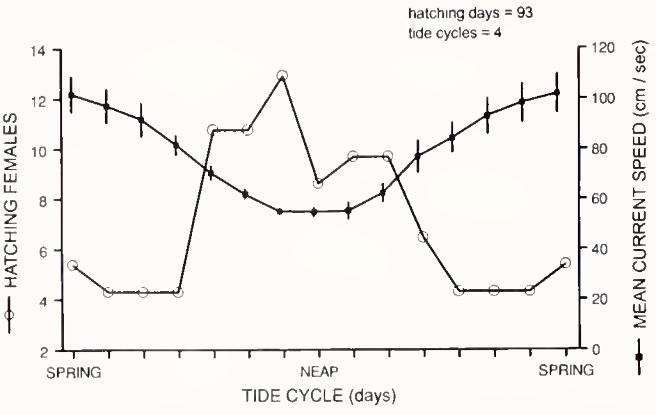

Figure 5. Occurrence of hatching within a lunar tidal cycle, compared with the mean tidal current speed per day (average ± SE).

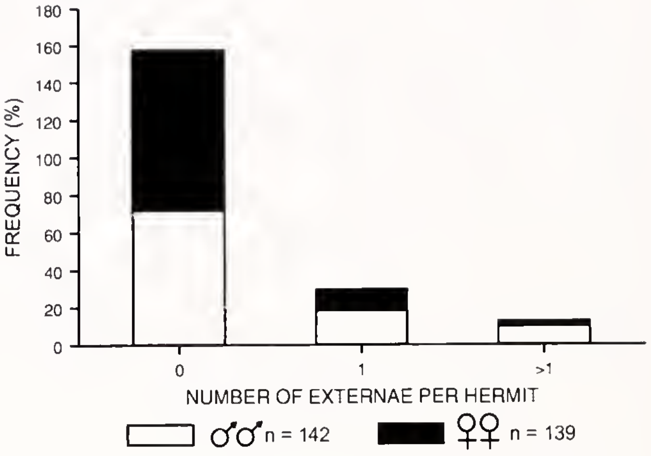

Figure 6. Number of the externae of rhizocephalan parasites per hermit host, compared between sexes.

The frequency distribution per size class of the infested specimens compared with respect to the healthy ones did not show any difference in the males ($G = 4.816$, df = 3, ns) (Fig. 7A); a difference (though slight) was found in the females, where parasites occurred more often within smaller size classes ($G = 6.913$, df = 3, P *ca.* 0.05) (Fig. 7B). When three size classes were distinguished, no between-sex difference was found in small specimens ($G = 0.004$, df = 1, ns), but the difference was significant in larger classes (intermediate: $G = 10.643$, df = 1, $P < 0.01$; biggest: $G = 2.744$, df = 1, P *ca.* 0.05). The minimum size of parasitized specimens was 1.8 in females and 1.4 mm SL in males.

Peltogaster boshmae externae never exceeded two per individual. They were more frequently found on the left side of the hermit abdomen (left, center, and right *vs.* a uniform distribution: $\chi^2 = 76.513$, df = 2, $P < 0.001$), and at the proximal end, close to the carapace (proximal, middle, distal *vs.* a uniform distribution: $\chi^2 = 34.241$, df = 1, $P < 0.001$), without any difference between sexes (side: $G = 1.118$, df = 2, ns; extremity: $\chi^2 = 0.029$, df = 1, ns). Their first point of eruption corresponded to the position of the second pleopod. In contrast, the externae of *Thilacoplethus* (=*Thompsonia*) *reinhardi*, ranging from 1 to 23, were more clumped on the host, equally distributed on the right and left halves of the hermit body, and more diffused, involving the dorsal side of the abdomen, the cephalothorax, and even the pereiopods and chelipeds.

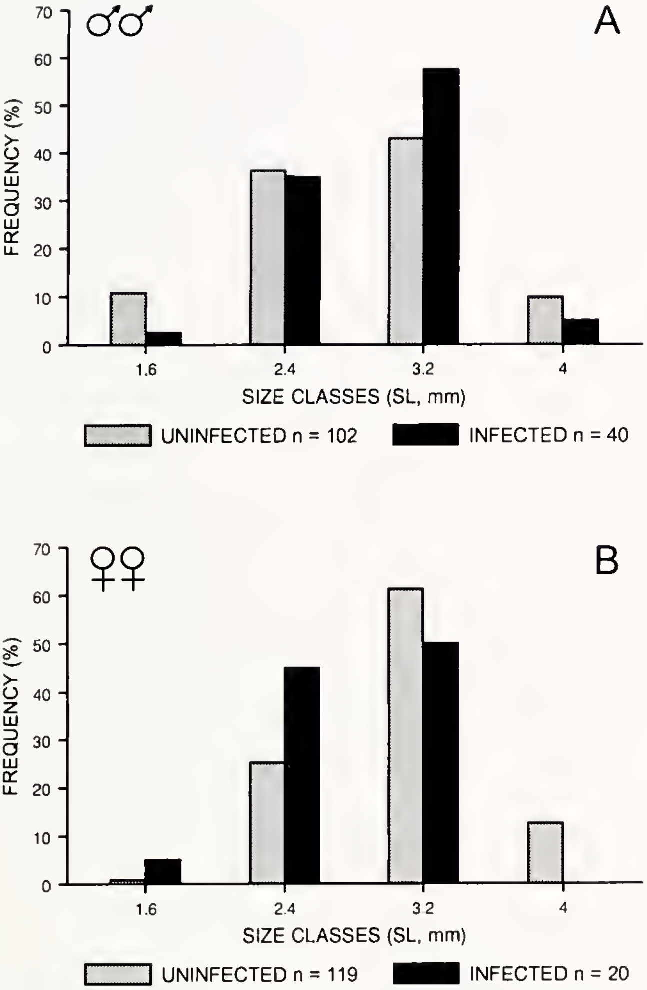

Figure 7. Size frequency distributions compared between hermits that were either uninfected or infected by rhizocephalan parasites in males (A) and females (B).

Parasites' effects on the host external morphology and behavior

To evaluate the effect of parasites on their hosts, we examined various aspects of the hermit external morphology. The pleopod number did not show any significant difference between infested and noninfested specimens in either sex (distinguishing animals with 4, 3, and less than 3 pleopods, males: $G = 1.645$, df = 2, ns; females: $G = 0.31$, df = 2, ns). However, the second pleopod was absent more often in parasitized specimens (7 out of 16 *vs.* 5 out of 54: $G = 8.333$, df = 1, $P < 0.01$). The difference was more pronounced in the males (6 out of 12 *vs.* 5 out of 31: $G = 4.576$, df = 1, $P < 0.05$) than in females (1 out of 5 *vs.* 0 out of 23: $G = 1.839$, df = 1, ns).

The relative growth of the DE of the major chela, one "maleness" character, was analyzed. No difference was found between parasitized and unparasitized specimens, either in males (after a ln-ln transformation: b, 0.63 *vs.* 0.93, $t = 1.772$, df = 56, ns; a, 0.21 *vs.* −0.15, $t = 1.847$, df = 57, ns) or in females (b, 0.52 *vs.* 0.57, $t = 0.237$, df = 63, ns; a, 0.40 *vs.* 0.33, $t = 0.011$, df = 64, ns). Analogously, parasites seemed not to affect hermit relative body weight in either sex (after ln-ln transformation, SL *vs.* weight without chelae, males: b, 3.45 *vs.* 5.08, $t = 1.539$, df = 39, ns; a, −1.13 *vs.* −3.31, $t = 0.043$, df = 40, ns; females: b, 1.70 *vs.* 3.59, $t = 0.778$, df = 38, ns; a, 1.32 *vs.* −1.04, $t = 1.216$, df = 39, ns). The same was also true when cheliped weight was examined (males: b, 8.80 *vs.* 7.26, $t = 0.537$, df = 24, ns; a, −15.41 *vs.* −11.97, $t = 0.858$, df = 25, ns; females: b, −2.19 *vs.* 6.41, $t = 1.664$, df = 22, ns, a, 13.89 *vs.* −9.34, $t = 1.043$, df = 23, ns).

Several parasitized hermits were seen molting and preserved their externae after the ecdysis, even when externae belonged to the latest stages, already containing oocytes and embryos (Lützen, 1992).

One possible behavioral effect of parasites is lethargy, which might reduce the ability of naked hermits to find empty tubes. However, in pilot experiments in the laboratory, parasitized and unparasitized *D. schmitti* individuals were about equally matched when competing for a single empty tube. In the field, no difference was seen in the relative opening diameter of the occupied tubes between hermits belonging to the two conditions (males: b, $t = 0.025$, df = 64, ns, a, $t = 0.169$, df = 65, ns; females: b, $t = 0.86$, df = 68, ns, a, $t = 1.913$, df = 69, ns).

Parasitized specimens of both sexes placed inside transparent tubing were seen fanning the externae of *Peltogaster boschmae.* The behavior was the same as that already described for ovigerous females fanning their eggs.

Discussion

The structure of the D. schmitti *population*

In the species of hermit crabs studied to date (Table IV), sex ratio in relation to size mostly follows the "anomalous" pattern described by Wenner (1972). This implies that sexes in small size classes are approximately balanced, a large excess of females is found in intermediate size classes, and an excess of males is found in the largest ones. Exceptions are reported by Wenner (1972) in *Clibanarius zebra* and *Calcinus latens,* by Abrams (1988) in *Pagurus ochotensis* and *P. aleuticus,* and by Gherardi and McLaughlin (1994) in *Calcinus laevimanus* from the Mascarenes. A further exception is *D. schmitti,* in which an equal number of males and females are represented in each size class.

One obvious bias in the size distribution analysis is the large- or small-scale habitat segregation between sexes. Species have been reported to show between-sex differences in habitat utilization (*e.g.,* males of *Pagurus hirsutiusculus* occupy high tidepools, but females are dom-

Table IV

Species of hermit crabs reported from the literature following the "anomalous" pattern (Wenner, 1972) in the sex-ratio-to-size relation

Genus	Species	Reference
Coenobita	*compressus*	Wenner, 1972
Calcinus	*laevimanus*	Wenner, 1972
	latens	Gherardi and McLaughlin, 1994
Clibanarius	*digueti*	Harvey, 1988
	erythropus	Gherardi, 1991
	laevimanus	Gherardi *et al.*, 1994
	humilis	Gherardi and McLaughlin, 1994
Diogenes	*brevirostris*	Walters and Griffiths, 1987
Elassochirus	*tenuimanus*	Abrams, 1988
Paguristes	*turgidus*	Abrams, 1988
Pagurus	*granosimanus*	Abrams, 1988
	hirsutiusculus	Abrams, 1988
	samuelis	Abrams, 1988
	kennerly	Abrams, 1988
	beringanus	Abrams, 1988
	dalli	Abrams, 1988

inant in microhabitats without standing water at low tide; Abrams, 1988). The size of clustering species is also segregated within clumps (in *Clibanarius laevimanus*, Gherardi *et al.*, 1994). However, both sexes of *D. schmitti* are restricted within sabellarian bioherms (Gherardi and Cassidy, 1994b), starting from the late megalopa stage, and although the species has a contagious distribution (Gherardi and Cassidy, 1994b), clumps do not significantly differ in either sex ratio or size.

The sexual selection hypothesis

Under the rationale of the sexual selection hypothesis (Bertness, 1981a), the between-sex balance in the size distribution of *D. schmitti* implies that the two sexes get the same benefits (or handicaps) from larger dimension.

Reproductive potential might be enhanced with size. From the perspective of *D. schmitti* females, clutch size significantly increases with the body mass, and larger females also bear more voluminous eggs.

Larger size might also provide a higher reproductive potential to males. A sexual dimorphism was evident in the major chela dimensions (dactyl length, and palm length and width): the chela (especially the biggest) was more massive in the male than in the female. The functional significance of this sexual difference has been widely discussed for Brachyura (Hartnoll, 1974), where it was related to the use of chelipeds in territorial defense, combat, display, and courtship. In several hermit crabs, males showed complex precopulatory behaviors, involving the chelae, for example, either rotating and shaking the female (Diogenidae) or jerking her toward himself (Paguridae) (Hazlett, 1966, 1968). Sexual behavior has not yet been observed in *D. schmitti*, but the importance for males of having larger chelipeds might be associated with the intrasexual competition to mate. Chelipeds are widely used in aggressive interactions, both in displays (cheliped extension, waving, and wig-wag display; F. Gherardi, in prep.), and in fights (hits and grasps), where the bigger and stronger the chelipeds are, the more likely the hermit is to win.

In hermit crabs, factors that could reduce the tendency to grow are the interspecific competition for shells and the scarcity of large housings within the habitat. By its ability to occupy empty polychaete tubes as a new housing, *D. schmitti* has freed itself from the harsh war for shells that occurs within the subtidal hermit crab assemblage in northern Puget Sound (Abrams *et al.*, 1986). Its small relative size must have preadapted this species to this narrow microhabitat, but its body mass is certainly constrained by the size distribution of the available empty tubes. In his ecological notes on the endemic Bermuda hermit *Calcinus verrilli*, Markham (1977) observed that the mean size of the crabs occupying attached vermetid shells was far smaller than that of crabs in mobile *Cerithium* shells. Members of the *D. schmitti* population analyzed here occupy the largest tubes at their disposal in the bioherm, and size in both sexes was positively correlated with tube opening, suggesting that crabs must change their housing with growth (Gherardi and Cassidy, 1994b).

The growth hypothesis

The growth hypothesis (Abrams, 1988) refers to the between-sex difference in the available energy for growth; the male-biased sex ratio in larger size classes in most hermit species is attributed to the additional energy that males can allocate to growth because they do not have to produce eggs (Bertness, 1981b). Data are still missing for the extent of growth through molts in *D. schmitti* and its energy-time budget is unknown, but a number of clues suggest that the distribution of the rhizocephalan parasites might affect growth in this species.

In the population we examined, the extent of infestation and parasite prevalence varied significantly between sexes, reaching in the males an average of 2.9 externae per individual and a percentage of 28 infested specimens. Prevalence is unaffected by the male host size, but the frequency of infested females decreases in the intermediate and larger size classes, where the infestation is significantly less diffused than in similar sized males.

Within the framework of the growth hypothesis, one likely conclusion drawn from these data is that if (1) the males are more frequently infected than the females, and if (2) parasites cause a reduction in the growth rate of the host, then the two sexes grow to the same extent because the energy the females expend in producing eggs equals that which the males consume to support parasites. However, the two assumptions require further clarification and open new questions.

First, we do not know why the parasites are unequally distributed between the sexes. The observed pattern could not be explained by either an increased mortality rate of infested females or the occurrence of sex reversal, because the sex ratio was 50% in all the size classes. The attachment of the parasite larvae may be impeded by the efficiency of cleaning and grooming (Bauer, 1981), but the two sexes did not differ in either the extent or the modes of cleaning behavior (Gherardi, 1994). As a third explanation, immunological responses by the hosts might vary between sexes. Parasitized, but not normal, *Carcinus mediterraneus* have a substance in their blood that fixes complement in the presence of extracts of *Sacculina* (reviewed in Bang, 1983). However, in that parasitic relationship, electrophoregrams did not show any marked difference between the parasitized males and females (Herberts, 1978). *D. schmitti* females differ in their susceptibility to infection according to their reproductive states. No parasitized females have been found in ovigerous condition (other examples in Hoggarth, 1990, and Lützen and Jespersen, 1992; exceptions in Høeg and Lützen, 1985); one explanation is that parasitized females lose their eggs after a few days (Lützen and Jespersen, 1992), but the reasons remain unknown.

The second assumption, that growth rate of the host is affected by the parasite, is supported by the previous literature on rhizocephalan infestation (O'Brien and Van Wyk, 1984; Hawkes *et al.*, 1986; Hoggarth, 1990; Abelló and Macpherson, 1992; Bang, 1983; Overstreet, 1983). Nevertheless, a direct investigation of molt frequency is lacking and figures on the relative increase at ecdysis compared between infected and uninfected individuals are provided only by Lützen and Jespersen (1992). Our findings that parasites do not inhibit molting in *D. schmitti* or influence either body or cheliped weight in either sex make the growth hypothesis questionable, at least in this species.

Other effects of parasites

A variety of morphological and behavioral alterations exhibited by rhizocephalan-infected decapods and the hormonal involvement in those phenomena are extensively described by Hartnoll (1967), Nielsen (1970), and Phillips and Cannon (1978) among others (see, *e.g.*, bibliography by Overstreet, 1983). *D. schmitti* males do not undergo the process of feminization observed in other species (Hartnoll, 1982; O'Brien and Van Wyk, 1984), as evidenced by the preservation of some "maleness" characters (*e.g.*, the high relative depth of the major chela). The only alteration is the frequent absence of the second pleopod, which cannot result from an attempt by the parasite to provide a safe accommodation for the externae, but seems instead to be a consequence of the eruption of *Peltogaster boschmae* externae within the soft tissue lining the host abdomen, which corresponds to the attachment point of the second pleopod.

Neither do infected hermits exhibit behavioral alterations, such as lethargy, that could decrease their ability in direct or exploitative competition: in the laboratory, parasitized and healthy *D. schmitti* had the same probability of getting an empty polychaete tube, and in the field, they occupied equally sized housings. Besides, relative weight, and thus possibly feeding efficiency, was unaffected by the presence of rhizocephalans. The only behavioral result of parasite manipulation is the initiation of mock parental care, in which infected hermits of both sexes ventilate *Peltogaster boschmae* externae in the same way that gravid females ventilate their eggs.

Reproductive patterns

D. schmitti females attain maturity at a relatively small size: the smallest egg-bearing specimen measured 1.1 mm SL. On the other hand, the allometry of chela growth should indicate that maturity (at least, functional maturity; Hartnoll, 1969) occurs in males at larger size (over 3.4 mm SL).

A precocious onset of sexual behavior in females has been reported in the decapod literature and associated with a reduced possibility of encountering males; in the parasitic females of the Pinnotheridae (Christensen and McDermott, 1958) and in the freshwater crab *Potamon fluviatile* (Micheli *et al.*, 1990) copulation can occur even in prepubertal females, and sperm are kept in the seminal receptacles until ovulation.

A second remarkable feature of reproduction is the low frequency (50%) of gravid females in all the size classes. This is particularly evident when we consider that *D. schmitti* breeds only once per year (Nyblade, 1974), and that the breeding period (January–April) is short, but the time necessary for eggs to mature is relatively long (exceeding, on average, 1 month).

One explanation is that due to the shortage of food, females may have limited energy for producing clutches, causing them to skip the reproductive season. If this were the case here, we should expect a gradient in the clutch size depending on the available energy. Nonetheless, egg number is a function of female size, and the latter is not related to feeding efficiency (Gherardi, 1994). In addition, the annual egg production (52.8 mg of eggs per 100 mg female weight per year; Nyblade 1974) is high compared with that of the other hermit crabs in northern Puget Sound.

Another hypothesis refers again to the difficulty that this sedentary species encounters in finding a mate. *D. schmitti* is gonochoristic and mating in hermit crabs requires copulation (Hazlett, 1966), but it is still unclear how this is effected in this species. Males, females, or both are assumed to leave the attached tube and roam about with their abdomens naked (or at best in broken pieces of tubes; Nyblade as reported by Caine, 1980) to seek receptive mates. Despite the clumped distribution of the population, this is a risky behavior; in the laboratory, wandering hermits inhabiting loose tubes are easy prey for the crabs and fishes (F. Gherardi, in prep.), that frequent sabellarian bioherms (Gherardi and Cassidy, 1994a).

Hatching lasts from 1 to 6 nights, the length of time being related to the overall number of larvae. This suggests either that development of embryos belonging to the same batch is out of phase or that hatching is controlled by the embryos themselves, by the females, or by both (Saigusa, 1992). Such an extension of hatching in sequential bursts might be a mechanism to allow survival of at least a number of larvae in a difficult, predator-filled, and unpredictable environment, such as the current-swept channels of Puget Sound.

In *D. schmitti*, hatching occurs exclusively at night, possibly to minimize predation on the newly released larvae by diurnal fishes. In contrast to the other decapods inhabiting enclosed habitats (estuaries and mangrove swamps; Forward, 1987; Hartnoll, 1988), in this species larval release is synchronized with neap tides, when the tidal current is consistently lower than in the spring phase. This timing seems to be controlled by an endogenous clock (De Vries and Forward, 1989), persisting under laboratory conditions in which the tidal cycle corresponding to the rhythm is absent. This pattern of larval release seems unrelated to salinity tolerance (Forward *et al.*, 1982), because salinity is nearly constant in the examined area (SPMC, 1992). Its adaptive meaning is suggested by *D. schmitti's* behavioral ecology. For this species—so dependent upon a habitat (sabellarian bioherms) that is rare and quite unpredictable (Gherardi and Cassidy, 1994a)—it is more beneficial if larvae are retained within the basin near the parental population than if they are flushed out to open waters for planktonic development (see McConaugha, 1992, for a discussion of larval retention *vs.* dispersal in decapods).

Acknowledgments

We thank Dr. Jorgen Lützen (University of Copenhagen) who kindly identified parasites of *D. schmitti*. The study was encouraged by Dr. Patsy A. McLaughlin (Shannon Point Marine Center, WWU), to whom we are greatly indebted. Part of the work was conducted at the Shannon Point Marine Center, Anacortes, Washington. Partial funding was provided by M.U.R.S.T. to the first author.

Literature Cited

Abelló, P., and E. Macpherson. 1992. Epibiosis and rhizocephalan infestation patterns in relation to the reproductive biology of *Lithodes ferox* (Filhol, 1885) (Anomura: Lithodidae). *J. Crustacean Biol.* **12:** 561–570.

Abrams, P. A. 1988. Sexual difference in resource use in hermit crabs; consequences and causes. Pp. 283–296 in *Behavioural adaptation to the Intertidal Life*. G. Chelazzi and M. Vannini, eds. Plenum Press, New York.

Abrams, P., C. Nyblade, and S. Sheldon. 1986. Resource partitioning and competition for shells in a subtidal hermit crab species assemblage. *Oecologia* **69:** 429–445.

Bang, F. B. 1983. Crustacean disease responses. Pp. 113–153 in *The Biology of Crustacea*, Vol. 6, *Pathobiology*, A. J. Provenzano, Jr., ed. Academic Press, New York.

Bauer, R. T. 1981. Grooming behavior and morphology in the decapod Crustacea. *J. Crustacean Biol.* **1:** 153–173.

Bertness, M. D. 1981a. Interference, exploitation, and sexual components of competition in a tropical hermit crab assemblage. *J. Exp. Mar. Biol. Ecol.* **49:** 189–202.

Bertness, M. D. 1981b. Competitive dynamics of a tropical hermit crab assemblage. *Ecology* **62:** 751–761.

Caine, E. A. 1980. Adaptations of a species of hermit crab (Decapoda, Paguridea) inhabiting sessile worm tubes. *Crustaceana* **38:** 306–310.

Christensen, A. M., and J. J. McDermott. 1958. Life-history and biology of the oyster crab, *Pinnotheres ostreum* Say. *Biol. Bull.* **114:** 146–179.

De Vries, M. C., and R. B. Forward, Jr. 1989. Rhythms in larval release of the sublittoral crab *Neopanope sayi* and the supralittoral crab *Sesarma cinereum* (Decapoda: Brachyura). *Mar. Biol.* **100:** 241–248.

Forward, R. B., Jr. 1987. Larval release rhythms of decapod crustaceans: an overview. *Bull. Mar. Sci.* **41:** 165–176.

Forward, R. B., Jr., K. Lohmann, and T. W. Cronin. 1982. Rhythms in larval release by an estuarine crab (*Rhithropanopeus harrisii*). *Biol. Bull.* **163:** 287–300.

Gherardi, F. 1991. Relative growth, population structure, and shell-utilization of the hermit crab *Clibanarius erythropus* in the Mediterranean. *Oebalia* **17:** 181–196.

Gherardi, F. 1994. Multiple feeding techniques in the sessile hermit crab *Discorsopagurus schmitti*, inhabiting polychate tubes. *Oecologia* **98:** 139–146.

Gherardi, F., and P. M. Cassidy. 1994a. Macrobenthic associates to the polychaete *Sabellaria cementarium* bioherm from northern Puget Sound, Washington. *Can. J. Zool.* **72:** 516–525.

Gherardi, F., and P. M. Cassidy. 1994b. Sabellarian tubes as the housing of *Discorsopagurus schmitti*. *Canad. J. Zool.* **72:** 526–532.

Gherardi, F., and P. A. McLaughlin. 1994. Shallow-water hermit crabs from Mauritius and Rodrigues Islands, with the description of a new species of *Calcinus*. *Raffles Bull. Zool.* **42:** 613–636.

Gherardi, F., F. Zatteri, and M. Vannini. 1994. Hermit crabs in a mangrove swamp: the structure of *Clibanarius laevimanus* clusters. *Mar. Biol.* **121:** 41–52.

Hartnoll, R. G. 1967. The effects of sacculinid parasites on two Jamaican crabs. *J. Linn. Soc. London Zool.* **46:** 275–295.

Hartnoll, R. G. 1969. Mating in the Brachyura. *Crustaceana* **16:** 11–181.

Hartnoll, R. G. 1974. Variation in growth pattern between some secondary sexual characters in crabs (Decapoda Brachyura). *Crustaceana* **27:** 131–136.

Hartnoll, R. G. 1982. Growth. Pp. 111–196 in *The Biology of Crustacea*, Vol. 2, *Embryology, Morphology and Genetics*, L. G. Abele, ed. Academic Press, New York.

Hartnoll, R. G. 1988. Eco-ethology of mangroves. Pp. 477–489 in *Behavioural Adaptation to the Intertidal Life*, G. Chelazzi and M. Vannini, eds. Plenum Press, New York.

Harvey, A. W. 1988. Size- and sex-related aspects of ecology of the hermit crab *Clibanarius digueti* Bouvier (Decapoda: Anomura: Diogenidae). Ph.D. dissertation. University of Arizona, Tucson, AZ.

Hawkes, C. R., T. R. Meyers, T. C. Shirley, and T. M. Koeneman. 1986. Prevalence of the parasitic barnacle *Briarosaccus callosus* on king crabs of southeastern Alaska. *Trans. Am. Fish. Soc.* **115:** 252–257.

Hazlett, B. A. 1966. Social behaviour of the Paguridae and Diogenidae of Curaçao. *Stud. Fauna Curaçao Other Caribb. Isl.* **23:** 1–143.

Hazlett, B. A. 1968. The sexual behavior of some European hermit crabs (Anomura: Paguridae). *Pubbl. Stn. Zool. Napoli* **36:** 238–252.

Herberts, C. 1978. Relation hôte-parasite entre *Carcinus mediterraneus* and *Sacculina carcini;* analyse immunochimique et mise en évidence d'une précipitine antisacculine. *C. R. Acad. Sci.* **286:** 725–728.

Hoeg, J. T., and J. Lützen. 1985. Crustacea Rhizocephala. Pp. 1–92 in *Marine Invertebrates of Scandinavia*, Vol. 6. Norwegian University Press, Oslo.

Hoggarth, D. D. 1990. The effects of parasitism by the rhizocephalan, *Briarosaccus callosus* Boschma on the lithodid crab, *Paralomis granulosa* (Jacquinot) in the Falkland Islands. *Crustaceana* **59:** 156–170.

Lützen, J. 1992. Morphology of *Thompsonia reinhardi*, new species (Cirripedia: Rhizocephala), parasitic on the northeast Pacific hermit crab *Discorsopagurus schmitti* (Stevens). *J. Crustacean Biol.* **12:** 83–93.

Lützen, J., and A. Jespersen. 1992. A study of the morphology and biology of *Thompsonia littoralis* (Crustacea: Cirripedia: Rhizocephala). *Acta Zool.* **73:** 1–23.

Margolis, L., G. W. Esch, J. C. Homes, A. M. Kuris, and G. A. Schad. 1982. The use of ecological terms in parasitology. *J. Parasitol.* **68:** 131–133.

Markham, J. C. 1977. Preliminary note on the ecology of *Calcinus verrilli*, an endemic Bermuda hermit crab occupying attached vermetid shells. *J. Zool. (Lond.)* **181:** 131–136.

McConaugha, J. R. 1992. Decapod larvae: dispersal, mortality, and ecology. A working hypothesis. *Am. Zool.* **32:** 512–523.

McLaughlin, P. A. 1974. The hermit crabs (Crustacea Decapoda, Paguridea) of Northwestern North America. *Zool. Verhand.* **130:** 1–396.

Micheli, F., F. Gherardi, and M. Vannini. 1990. Growth and reproduction in the freshwater crab, *Potamon fluviatile* (Decapoda, Brachyura). *Freshwater Biol.* **23:** 491–503.

Nielsen, S. O. 1970. The effects of the rhizocephalan parasites *Peltogaster paguri* Rathke and *Gemmosaccus sulcatus* (Lilljeborg) on five species of paguridan hosts (Crustacea Decapoda). *Sarsia* **42:** 17–32.

Nyblade, C. F. 1974. *Coexistence in Sympatric Hermit Crabs.* Ph.D. dissertation. University of Washington, Seattle, WA.

O'Brien, J., and P. Van Wyk. 1984. Effect of crustacean parasitic castrators (Epicaridean isopods and Rhyzocephalan barnacles) on growth of crustacean hosts. *Crustacean Issues* **3:** 191–218.

Overstreet, R. M. 1983. Metazoan symbionts of crustaceans. Pp. 155–250 in *The Biology of Crustacea*, Vol. 6, *Pathobiology*, A. J. Provenzano, Jr., ed. Academic Press, New York.

Phillips, W. J., and L. R. G. Cannon. 1978. Ecological observations on the commercial sand crab, *Portunus pelagicus* (L.), and its parasite, *Sacculina granifera* Boschma, 1973 (Cirripedia: Rhizocephala). *J. Fish Dis.* **1:** 137–149.

Saigusa, M. 1992. Control of hatching in an estuarine terrestrial crab. 1. Hatching of embryos detached from the female and emergence of mature larvae. *Biol. Bull.* **183:** 401–408.

Siegel, S. 1956. *Nonparametric Statistics for the Behavioral Sciences.* McGraw-Hill, New York.

SPMC. 1992. *Water Quality Record.* Annual Report from Shannon Point Marine Center, Anacortes, WA.

Walters, W. L., and C. L. Griffiths. 1987. Patterns of distribution, abundance and shell utilization amongst hermit crabs, *Diogenes brevirostris. S. Afr. J. Zool.* **22:** 269–277.

Wenner, A. M. 1972. Sex ratio as a function of size in marine Crustacea. *Am. Natur.* **106:** 321–350.

Zar, J. H. 1984. *Biostatistical Analysis.* Prentice-Hall, Englewood Cliffs, NJ.

Reference: *Biol. Bull.* **188**: 78–82. (February/March, 1995)

Taurine-like Immunoreactivity in the Motor Nerve Net of the Jellyfish *Cyanea capillata*

MATS CARLBERG[1], KARIN ALFREDSSON[1], SVEN-OLLE NIELSEN[1],
AND PETER A. V. ANDERSON[2]

[1]*Department of Zoology, University of Lund, Helgonavägen 3, S-223 62 Lund, Sweden, and*
[2]*Whitney Laboratory and Departments of Physiology and Neuroscience,*
University of Florida, St. Augustine, Florida 32086

Abstract. Two antisera against the sulfonated amino acid taurine were applied to subumbrella tissue of the jellyfish *Cyanea capillata.* Taurine-immunoreactive nerve nets were found in both the ectoderm and endoderm. The ectoderm had two morphologically and immunocytochemically distinct populations of neurons, the motor nerve net (MNN), which was immunoreactive to the taurine-like molecule, and the diffuse nerve net (DNN), which was immunoreactive to the neuropeptide Phe-Met-Arg-Phe-NH_2 (FMRFamide). In the endoderm, immunoreactivity was found in the endodermal DNN. This localization was confirmed by double-labeling experiments, which also revealed that the endodermal DNN neurons may contain both taurine and FMRFamide-related peptide. The presence of a taurine immunoreactivity in the MNN supports the hypothesis that taurine or some chemically related compound is the neurotransmitter at synapses within the MNN of *Cyanea.*

Introduction

Cnidarians are the earliest extant animals to have a nervous system and, as such, they may provide useful information about the evolution of the nervous system and its components. Furthermore, their structural simplicity affords opportunities for studying functional aspects of these nervous systems, including the cellular mechanisms underlying chemical synaptic transmission (Anderson, 1985; Spencer *et al.*, 1989; Anderson and Spencer, 1989). A focus of considerable interest in recent years has been the identity of neurotransmitters in the Cnidaria. Neuropeptides are known to be common within the phylum (Grimmelikhuijzen *et al.*, 1989a, b; 1992), and evidence for a role of small molecules and amino acids as neurotransmitters is growing (Anctil, 1989; Scemes, 1989; Chung *et al.*, 1989; Chung and Spencer, 1990; Umbriaco *et al.*, 1990), but remains limited.

The sulfonated amino acid taurine, which is ubiquitous in animals and prokaryotes and has been implicated as an inhibitory neurotransmitter in both vertebrates (Huxtable, 1989) and invertebrates (Nistri and Constanti, 1976; Hue *et al.*, 1979; Giles and Usherwood, 1985), has recently been shown to depolarize neurons in the motor nerve net (MNN) of the scyphozoan jellyfish *Cyanea capillata* (Anderson and Trapido-Rosenthal, 1990). The mode of action of taurine on these neurons is very similar to that of the endogenous neurotransmitter, raising the possibility that taurine may serve as an excitatory neurotransmitter at these synapses. To determine whether taurine is present in the tissues of *Cyanea* and if so, to delineate its distribution, we used antisera raised against a taurine-bovine serum albumin complex (Campistron *et al.*, 1986; Madsen *et al.*, 1985). The results indicate that taurine, or a taurine-like molecule, is indeed present in the MNN and that its distribution is consistent with a role as a neurotransmitter in the *Cyanea* MNN.

Materials and Methods

Specimens of *Cyanea* were collected at the Tjärnö Marine Biological Laboratory on the west coast of Sweden. Pieces of perirhopalial tissue (Anderson and Schwab, 1981) were removed from the animal and pinned out to prevent curling. In some preparations the myoepithelium that envelops the MNN neurons was removed to expose the nerve net (Anderson and Schwab, 1984). Tissues were

Received 24 May 1994; accepted 27 October 1994.

fixed for 3 h in freshly prepared 5% glutaraldehyde in 0.05 *M* Na-cacodylate buffer containing 1% sodium metabisulphite and 2.4% sodium chloride (pH 7.5). After fixation, the tissues were given three 15-min washes in Tris-buffered saline (TBS; 0.05 *M* TRIS-HCl buffer, pH 7.5, 1% sodium metabisulphite and 2.4% sodium chloride), followed by 30 min in 0.1 *M* sodium borohydride in TBS, then a further three 15-min rinses in TBS. Twelve specimens from 5 to 20 cm in diameter were used for immunocytochemical investigations.

Samples were incubated for 4–6 days in rabbit anti-taurine antisera diluted 1:200 (Chemicon) or 1:1000 (Immunotech S.A.) in TBS with 0.2% Triton X-100 (TBS/TX) and 1% bovine serum albumin (BSA). After three 15-min rinses in TBS/TX, the samples were incubated for 3 h with fluorescine isothiocyanate- (FITC)-conjugated swine anti-rabbit IgG (Dakopatts, Denmark) diluted 1:10 in TBS. The samples were then given three 15-min rinses in TBS, stained in a 1% solution of Evans blue (Merck) in phosphate-buffered saline (PBS), pH 7.4, rinsed for 2 h in PBS, and mounted in phosphate-buffered glycerol. Specificity was tested by preabsorbtion of antiserum with 1 *μM* taurine-glutaraldehyde-BSA conjugate.

Double labeling with rabbit antisera raised against taurine and the neuropeptide FMRFamide was carried out in the manner developed by Würden and Homberg (1993). Specifically, tissues were first stained with antibodies to taurine, and the location of the primary antibody was visualized by a 3-h incubation with Texas-red-conjugated donkey anti-rabbit IgG (Jackson Immuno Research) diluted 1:40. After a 3-h incubation in rabbit IgG (Dakopatts) diluted at 1:25, the tissues were then incubated for 24 h with biotinylated (Bayer and Wilcheck, 1980) anti-FMRFamide antibodies (Incstar), diluted 1:800. The FMRFamide immunostaining was then visualized by treatment with streptavidin-FITC (Dakopatts) at 1:20 for 3 h. All light microscopical observations were made with a Leitz Aristoplan microscope.

The specificity of taurine antiserum from Chemicon has been characterized by the company. Cross-reactivity with glutaraldehyde-conjugated hypotaurine was 0.067 (1:15) and was less than 0.002 for other glutaraldehyde-conjugated amino acids including GABA, beta-alanine, aspartate, glycine, cysteine, and glutamate.

Results

Light microscopy

Taurine-like immunoreactivity (Tau-IR) was found in both the ectoderm and endoderm of the perirhopalial tissue of *Cyanea*.

Ectodermal-specific Tau-IR was found in neurons and, to a lesser extent, in myoepithelial cells. Ectodermal myoepithelial cells in this species contain a large central vacuole (Anderson and Schwab, 1981). Immunoreactivity was restricted to the narrow layer of cytoplasm that surrounds each vacuole; vacuolar contents were not immunoreactive. The Tau-IR neurons were large, bipolar cells with lengths up to 2 mm, cell-body diameters of 15 to 20 μm, and axonal diameters from 1 to 5 μm (Fig. 1A). These were clearly motor nerve net (MNN) neurons (Anderson and Schwab, 1981) and were easily distinguished from the FMRFamide-immunoreactive (FMRF-IR) cells that form the diffuse nerve net (DNN) (Fig. 1C), the other nerve net present in the perirhopalial tissue ectoderm. In the MNN, synapses occur wherever two neurons are in physical contact with one another (Anderson, 1985), and, as can be seen in these micrographs (Fig. 1B), such contacts are abundant. The Tau-IR within the MNN was restricted to the perirhopalial tissue; although MNN neurons are known to extend into the radial and circular muscle bands that surround the perirhopalial tissue (Anderson and Schwab, 1981), no Tau-IR neurons were found in the radial or circular muscle bands.

In the endoderm, at least two cells types were immunoreactive. One was a population of bipolar neurons. These cells, which had cell-body diameters of 10 to 15 μm and axon diameters of 0.5 to 2 μm, were at least 0.6 mm long and formed a loose nerve net (Fig. 1D). Their overall appearance is consistent with that of the diffuse nerve net (DNN) known to be present in this tissue. The other obviously immunoreactive endodermal cell type was more difficult to characterize. The cells in question occurred relatively densely, and their immunoreactivity appeared as a rather amorphous, frequently circular mass. Whether this mass represents an intracellular compartment of the cell or the true dimensions of the cell was not clear. Both of these cell types were surrounded by a low level of background immunoreactivity interspersed with occasional nonfluorescent areas that are presumably spaces in the endodermal epithelium.

Preabsorbtion of antiserum with taurine-GA-BSA conjugate completely abolished all immunostaining.

Double labeling

Double labeling revealed two distinct nerve nets in the ectoderm. Again, Tau-IR was restricted to MNN neurons, whereas FMRF-IR was localized to a separate population of smaller, multipolar cells (Fig. 2A). FMRF-IR was also evident in the marginal rhopalia and in regions covered by the circular and radial muscle bands. At no time were the two signals co-localized in the ectoderm.

In the endoderm, both antibodies stained what appeared to be the DNN. In smaller animals, the neurons were FMRF-IR, but in larger animals they were apparently Tau-IR. In one specimen, both FMRF-IR and Tau-IR were evident in the same cells, indicating co-localization (Fig. 2B).

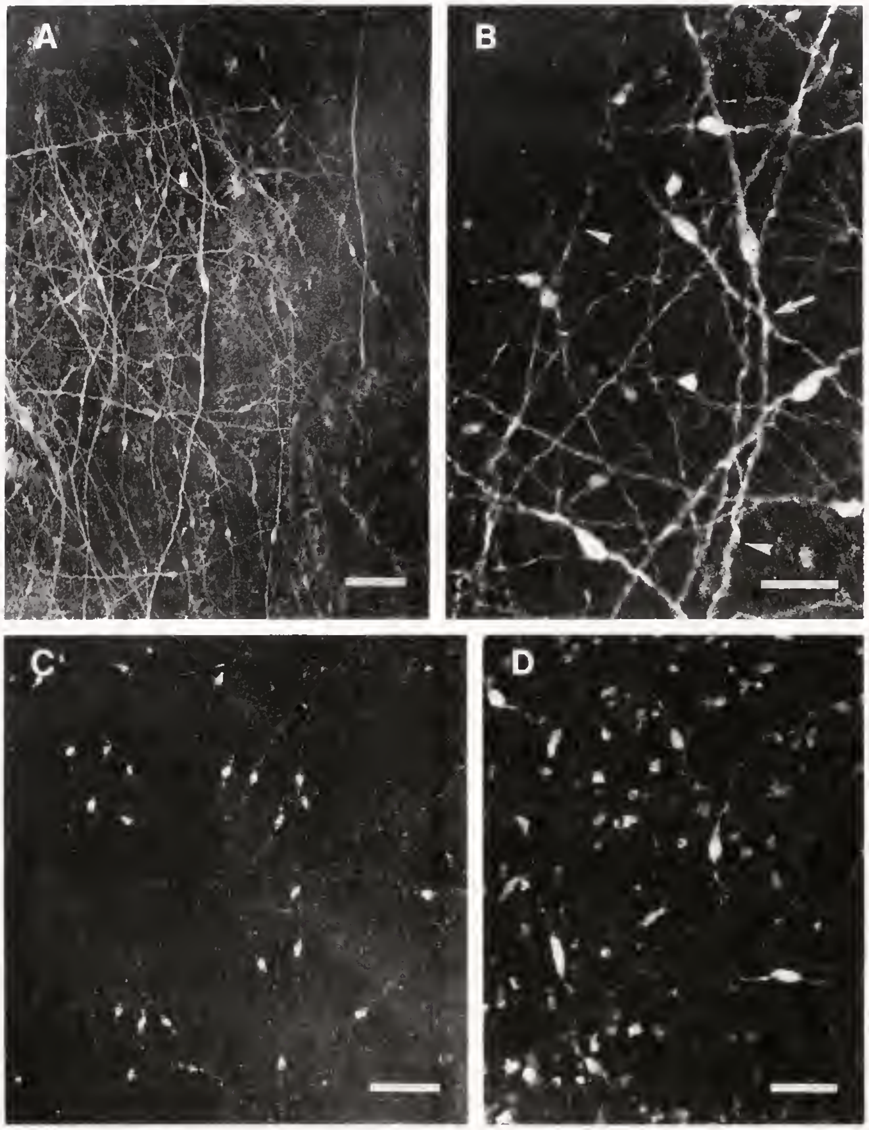

Figure 1. Whole-mount immunostaining of perirhopalial tissue of *Cyanea capillata.* (A) Low power micrograph of Tau-IR in the ectoderm. Neurons in the MNN stain readily. Scale bar = 0.1 mm. (B) Micrograph of the Tau-IR MNN in the ectoderm. Several apparent contact sites between the axons (arrows) and thinner elements twined together (arrowheads) can be seen. Scale bar = 50 μm. (C) Low-power micrograph of FMRFamide-immunoreactive diffuse nerve net (DNN) in the ectoderm. Scale bar = 0.1 mm. (D) Tau-IR in the endoderm of the perirhopalial tissue. Immunoreactivity was present in bipolar neurons and in undifferentiated endodermal cells. Scale bar = 50 μm.

Discussion

In cnidarians, nerve nets are located under an overlying epithelium that forms a permeability barrier for pharmacological agents and microelectrodes. The ectodermal MNN in the perirhopalial tissue of *Cyanea* is one of the very few instances in which a coelenterate nerve net can be exposed, permitting access for electrophysiological and pharmacological studies (Anderson and Schwab, 1984; Anderson, 1985). The size of the neurons makes them suitable for electrophysiological recordings. The accessibility of this nerve net and, in particular, its synapses provides a useful preparation for studying the pharmacology of chemical neurotransmission in a cnidarian.

The MNN is a plexus of large bipolar neurons that innervates the swimming muscle bands and serves as the pathway to coordinate swimming motor activity. Synapses between the MNN neurons are fast, chemical synapses that are bidirectional (Anderson, 1985). Previous work (Anderson and Trapido-Rosenthal, 1990) has implicated taurine or a closely related molecule as a potential neuro-

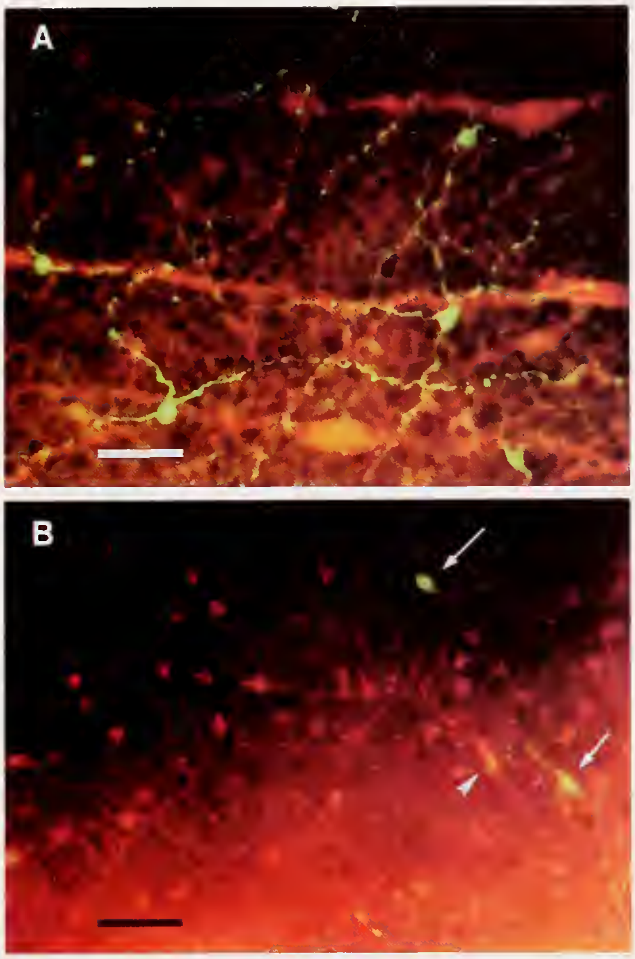

Figure 2. Double labeling. (A) Whole mount of perirhopalial tissue ectoderm, stained with antibodies against taurine (red) and FMRFamide (green). The clear anatomical separation between the Tau-IR MNN neurons and FMRFamide DNN neurons is evident. (B) Endodermal tissues stained in the same manner. The majority of cells in this preparation are Tau-IR. Two neurons (arrows) were more (yellow) or less (green) intensely immunoreactive to FMRFamide, but at least one (arrowhead) was reactive to both antibodies. Scale bars = 50 μm.

transmitter at these synapses. The current investigation provides immunocytochemical evidence that a taurine-like molecule is indeed present in MNN neurons and in an endodermal nerve net, but is not present, at least in detectable quantities, in neurons of another ectodermal nerve net, the diffuse nerve net (DNN). This was particularly obvious in the double-labeling experiments, in which the ectodermal FMRFamide-IR was clearly restricted to the DNN (Anderson *et al.*, 1992). Although Tau-IR was also present in the ectodermal myoepithelial cells, its absence in the DNN indicates that taurine is not a constituent component of all nerve nets in this animal. This distinction is important because taurine acts as an osmoregulator in many marine organisms (Thurston *et al.*, 1980). If it were serving the same function in *Cyanea*, one might expect it to be widespread in different cell types and present in all nerve nets.

The presence of Tau-IR in the endodermal DNN in *Cyanea* was unexpected considering that immunoreactivity to antibodies raised against the sea anemone neuropeptide AnthoRFamide was found in these neurons (Anderson *et al.*, 1992). In the present study, endodermal Tau-IR neurons also were found to be immunoreactive to antibodies to FMRFamide. In addition, however, morphologically similar neurons in larger animals were found to have Tau-IR, and one specimen showed apparent co-localization of the two transmitter candidates. It may be worth further investigations to find out if there is a progression from an FMRFamide or AnthoRFamide-like peptide to taurine (or a related compound) as the animal grows. To meet the requirement for faster transmission in a large medusa, a switch from peptidergic metabotrophic receptors to fast excitatory ionotrophic receptors would be functional. In either case, it is clear from this work that cnidarian synapses may have a hitherto unappreciated complexity in the number of neurotransmitters present in single neurons.

Tau-IR was also found in a very abundant, non-neuronal cell type in the endoderm (Fig. 1D). The identity of this cell is unclear. The presence of Tau-IR in these cells, and perhaps all endodermal cells if the light background fluorescence is indeed indicative of low levels of taurine, may imply that it has an alternative function such as osmoregulation. It is also possible, however, that some of the small circular profiles represent interstitial cells differentiating into DNN neurons.

The antibody used in the light microscopical component of this study is known to have low cross reactivity to the most abundant metabolites of taurine including hypotaurine and cysteine. However, one cannot as yet exclude the possibility that the antigen is a closely related compound or a small taurine-containing oligopeptide (Marnela *et al.*, 1985). Free taurine is, however, an abundant constituent of MNN neurons (Anderson and Trapido-Rosenthal, unpub.).

The MNN extends over the entire subumbrella surface, forming a network that connects all eight marginal ganglia, or rhopalia, with the circular and radial swimming muscle bands. To do this, the nerve net must transit the muscle bands, and individual, Lucifer-yellow-filled neurons have been seen to extend from the perirhopalial tissue into radial muscle bands (Anderson and Schwab, 1981). However, Tau-IR neurons were never observed in either the radial or circular muscle bands. Although the MNN neurons located within the confines of these muscle bands may employ a different neurotransmitter in this region, it is also possible that failure to observe Tau-IR in these areas is due to a technical problem. To get adequate staining of neurons in these preparations, they had to be incubated with the antibodies for as long as 6 days. In contrast, anti-FMRFamide antibodies usually penetrate the tissues easily, typically requiring 24 h (Anderson *et al.*, 1992). The staining difficulty may reflect either a low antibody titer or poor penetration by anti-Tau antibody. In either case, the thick layer of muscle that overlies the MNN in the radial and circular muscle bands may have compromised the ability of the anti-Tau antibodies to reach their targets in this region.

The major conclusion of this study is that MNN neurons are Tau-IR. This, together with electrophysiological evidence that taurine depolarizes the MNN neurons in a manner consistent with that of the endogenous neurotransmitter, provides compelling evidence that taurine, or a taurine-like molecule, is the neurotransmitter in *Cyanea*. This possibility has evolutionary implications. Taurine is one of the most abundant amino acids in the animal cell, and it is conceivable that carnivores and scavengers developed olfactory receptors for taurine very early in evolution. Receptors for taurine are, indeed, known to be present on the olfactory antennae of lobsters (Derby and Atema, 1982), and one could envisage how neurotransmitter receptors might have developed from external chemoreceptors (Carr, 1989).

Acknowledgments

We are very grateful to the Director, Dr. Larz Afzelius, and to Drs. Lars Hagström and Benno Magnusson for providing us with facilities at the Tjarnö Marine Station. This work was supported by grant B-BU 1781-303 from the Swedish Natural Research Council to Mats Carlberg and by NSF grant BNS 9109155 to Peter Anderson.

References

Anctil, M. 1989. The antiquity of monoaminergic neurotransmitters: evidence from Cnidaria. Pp 141–155 in *Evolution of the First Nervous Systems*, P. A. V. Anderson, ed. Plenum Press, New York.

Anderson, P. A. V. 1985. The physiology of a bidirectional, excitatory, chemical synapse. *J Neurophysiol* **53:** 821–835.

Anderson, P. A. V., and W. E. Schwab. 1981. The organization and structure of nerve and muscle in the jellyfish *Cyanea capillata* (Coelenterata; Scyphozoa). *J Morphol.* **170:** 383–399.

Anderson, P. A. V., and W. E. Schwab. 1984. An epithelial cell-free preparation of the motor nerve net of *Cyanea* (Coelenterata; Scyphozoa). *Biol. Bull* **166:** 396–408.

Anderson, P. A. V., and A. N. Spencer. 1989. The importance of cnidarian synapses for neurobiology. *J. Neurobiol.* **20:** 435–457.

Anderson, P. A. V., and H. G. Trapido-Rosenthal. 1990. Electrophysiological evidence that a taurine-like amino acid is the neurotransmitter at a fast excitatory synapse. *Soc. Neurosci. Abstr* **16:** 1185.

Anderson, P. A. V., A. Moosler, and C. J. P. Grimmelikhuijzen. 1992. The presence and distribution of Antho-RFamide-like material in scyphomedusae. *Cell Tissue Res* **267:** 67–74.

Bayer, E. A., and M. Wilchek. 1980. The use of avidin-biotin complex as a tool in molecular biology. *Meth. Biochem. Anal* **26:** 1–45.

Campistron, G., M. Geffard, and R. M. Buijs. 1986. Immunological approach to the detection of taurine and immunocytochemical results. *J Neurochem.* **46:** 862–868.

Carr, W. E. S. 1989. Chemical signalling systems in lower organisms: a prelude to the evolution of chemical communication in the nervous system. Pp. 81–94 in *Evolution of the First Nervous Systems*, P. A. V. Anderson, ed. Plenum Press, New York.

Chung, J. M., and A. N. Spencer. 1990. On the potassium conductance increase activated by dopamine in the jellyfish *Polyorchis penicillatus. Soc. Neurosci. Abstr* **16:** 1020.

Chung, J. M., A. N. Spencer, and K. H. Gahm. 1989. Dopamine in tissues of the hydrozoan jellyfish *Polyorchis penicillatus* as revealed by HPLC and GC/MS. *J Comp. Physiol. B.* **159:** 173–181.

Derby, C. D., and J. Atema. 1982. Narrow-spectrum chemoreceptor cells in walking legs of the lobster *Homarus americanus:* Taste specialists. *J. Comp. Physiol. A* **146:** 181–189.

Giles, D. P., and P. N. R. Usherwood. 1985. The effects of putative neurotransmitters on somata isolated from neurons of the locust central nervous system. *Comp. Biochem. Physiol.* **80C:** 231–236.

Grimmelikhuijzen, C. J. P., D. Graff, O. Kiozumi, J. A. Westfall, and I. D. McFarlane. 1989a. Neurones and their peptide neurotransmitters in coelenterates. Pp. 95–109 in *Evolution of the First Nervous Systems*, P. A. V. Anderson, ed. Plenum Press, New York.

Grimmelikhuijzen, C. J. P., D. Graff, and I. D. McFarlane. 1989b. Neurones and neuropeptides in coelenterates. *Arch. Histol. Cytol.* **52:** 265–276.

Grimmelikhuijzen, C. J. P., K. Cartensen, D. Darmer, A. Moosler, H-P. Nothacker, R. K. Reinscheid, C. Schmutzler, and H. Vollert. 1992. Coelenterate neuropeptides: structure, action and biosynthesis. *Am. Zool.* **32:** 1–12.

Hue, B., M. Pelhate, and J. Chanelet. 1979. Pre- and postsynaptic effects of taurine and GABA in the cockroach central nervous system. *Can. J. Neurol. Sci.* **6:** 243–250.

Huxtable, R. J. 1989. Taurine in the central nervous system and the mammalian actions of taurine. *Prog. Neurobiol.* **32:** 471–533.

Madsen, S., O. P. Ottersen, and J. Storm-Mathisen. 1985. Immunocytochemical visualization of taurine: neuronal localization in the rat cerebellum. *Neurosci Lett.* **60:** 255–260.

Marnela, K-M., H. R. Morris, M. Panico, M. Timonen, and P. Lähdesmärki. 1985. Glutamyl-taurine is the predominant synaptic taurine peptide. *J. Neurochem.* **44:** 752–754.

Nistri, A., and A. Constanti. 1976. The action of taurine on the lobster muscle fibre and the frog spinal cord. *Neuropharmacology* **15:** 635–641.

Scemes, E. 1989. Rethinking the role of cholinergic neurotransmission in the Cnidaria. Pp. 157–166 in *Evolution of the First Nervous Systems* P. A. V. Anderson, ed. Plenum Press, New York.

Spencer, A. N., J. Przysiezniak, J. Acosta-Urquidi, and T. A. Basarsky. 1989. Presynaptic spike broadening reduces junctional potential amplitude. *Nature* **340:** 636–638.

Thurston, J. H., R. E. Hauhart, and J. A. Dirgo. 1980. Taurine: a role in osmotic regulation of mammalian brain and possible clinical significance. *Life Sci.* **26:** 1561–1568.

Umbriaco, D., M. Anctil, and L. Descarres. 1990. Serotonin-immunoreactive neurons in the cnidarian *Renilla koellikeri. J. Comp. Neurol.* **291:** 167–178.

Würden, S., and U. Homberg. 1993. A simple method for immunofluorescent double staining with primary antisera from the same species. *J. Histochem. Cytochem.* **41:** 627–630.

Reference: *Biol. Bull.* **188:** 83–88. (February/March, 1995)

The Influence of Opponent-Related and Outcome-Related Memory on Repeated Aggressive Encounters in the Paradise Fish (*Macropodus opercularis*)

ÁDÁM MIKLÓSI*, JÓZSEF HALLER**, AND VILMOS CSÁNYI*

**Department of Ethology, Eötvös Loránd University and **Institute of Experimental Medicine, Hungarian Academy of Sciences*

Abstract. The aggressive behavior of male paradise fish (*Macropodus opercularis*) was studied. Fish were subjected to three aggressive encounters on consecutive days. If submissive males encountered the same opponent three times, the last aggressive encounter was very different than the first one. When the animals faced a new opponent each day, the changes were much less pronounced. We conclude that (1) fish are able to recognize their opponents at least one day after the encounter ("social recognition"), and (2) social recognition modifies the effect of prior defeat ("status-related memory") in subsequent encounters.

Introduction

An overwhelming amount of evidence indicates that prior agonistic experience influences the outcome of future aggressive encounters (Beacham and Newman, 1987; Frank and Ribowsi, 1987). One can hypothesize that prior aggressive experience may influence subsequent aggressive encounters by two kinds of processes: one related to the outcome of the encounter ("winner" or "loser" effect) and the other specifically related to the opponent. The significance of the former process was recently examined in detail (Bevan *et al.*, 1960; Poll *et al.*, 1982; Francis, 1983; Beaugrand and Zayan, 1985; Beacham and Newman, 1987; Bakker *et al.*, 1989). Most studies demonstrate an asymmetrical effect of prior winning or losing on subsequent winning probability. For example, in paradise fish (*Macropodus opercularis;* Francis, 1983) and in sticklebacks (*Gasterosteus aculeatus;* Bakker and Sevenster, 1983) losing greatly enhances the probability of also losing the subsequent contest. Winning usually has no strong effect, but under some experimental conditions it might increase the probability of winning again (Bakker and Sevenster, 1983; Bakker *et al.*, 1989).

The possibility of the involvement of the second process—individual recognition—in agonistic encounters has been also demonstrated. Fricke (1973) showed that *Amphiprion bicinctus* males more frequently attacked unknown individuals than known ones in a two-choice experiment. The importance of individual recognition in the stickleback was demonstrated by Peeke and Veno (1973), who observed that a resident male that had been habituated to an intruder presented in a glass cylinder would resume aggressive behavior if the individual in the cylinder was changed. Thresher (1979) used a similar method to study rival recognition in the threespot damselfish (*Eupomaceus planifrons*), and those field observations further confirm that some fish species might be able to recognize individuals. Myrberg and Riggio (1985) showed that coral reef fish (*Pomacentrus partitus*) recognize territorial neighbors acoustically. Recently Waas and Colgan (1994) provided experimental evidence that male sticklebacks can distinguish between familiar rivals on the basis of visual cues alone.

Assuming that the effects of previous encounters are mediated by memory—and that the behavioral differences are not due to energetic consequences of aggression (Haller and Wittenberger, 1988; Haller, 1991)—the problem of interference between social recognition and status-related memory arises.

As a continuation of a recent study (Miklósi *et al.*, 1992) on aggressive behavior in the paradise fish, we experimentally examined these processes in the aggressive behavior of the paradise fish. To clarify the relationship be-

Received 15 April 1993; accepted 18 November 1994.

Address for correspondence: Ádám Miklósi, Eötvös Loránd University, Department of Ethology, Göd, Jávorka S. u 14, H-2131, Hungary.

tween social recognition and status-related memory, two questions have been posed: (1) Does the behavior of the fish change if it encounters the same or different opponents for two subsequent encounters? (2) Are there differences between these experimental manipulations?

Materials and Methods

Experiments were conducted with 6-month-old, 8-cm to 10-cm-long *Macropodus opercularis* males, which were raised and kept in our laboratory. Three days before the start of the experiment, pairs of size-matched fish were placed in 40 × 20 × 20 cm glass tanks provided with filtration and aeration. Each tank was separated into two equal parts by a green opaque screen, and a single fish was kept in each part of the tank. The animals were visually isolated from each other: all sides but the front side of the tanks were covered with green plastic sheets. This isolation lasted 3 days prior to the experiment. Water temperature was kept at 28°C, and a 14:10 h light:dark cycle was maintained. The fish were fed daily on *Tubifex* worms.

Animals were exposed to three aggressive encounters on successive days. Encounters were begun by removing the plastic partition. All encounters were videotaped until dominance relationships were established. We defined this as the point at which one of the fighting males no longer participated in simultaneous or reciprocal threatening and fighting but instead became the "subordinate," showed fleeing and escaping behavior when approached by the "dominant," which in turn chased and bit its opponent. A submissive fish remains motionless for a long time in "oblique position" near to the water surface and does not retaliate against the winner (Miklósi *et al.*, unpub. obs.; Forselius, 1957). Both fish were observed for an additional hour to monitor the stability of the dominant-subordinate relationship. One hour after the end of fighting, the contact between the fish was interrupted by lowering the plastic door, and the animals were kept in isolation for the next 24 h.

Two groups were tested: the fish in group A (n = 10) faced the same opponent throughout the experiment; in group B (n = 10) the dominant animals were randomly changed between the tanks after each fight. Thus, in group B, the submissive fish remained in the tank and faced a new, previously dominant opponent each day. The dominant fish was changed immediately after the end of the encounter and remained isolated in its new tank until the following day when the partition was removed again. The time between two consecutive encounters was long enough for the dominant to acclimate to the new place (Csányi *et al.*, 1985), thus the advantage of prior residency of the submissive fish was minimized.

Videotapes were later analyzed by recording behavioral units with an event recorder (Nagy *et al.*, 1985). On the basis of earlier findings, each aggressive encounter was divided into three main phases: latency, threatening, and fighting. After the latency for initiation of the first display, a second phase was defined, which lasted until the first appearance of contact behavior (biting or mouthlocking). This was called threatening, which in turn was followed by the escalation of the fighting—fighting phase—until one of the males showed submissive behavior. The behavior units we identified are as follows:

Display at distance (DIS): The fish stay in head-tail position with erected tailfin, but the distance between them is larger then one body length.

Head-head display (HHD): The fish are oriented parallel to one other and face in the same direction, with one fish slightly behind the other.

Parallel swimming (PAS): The fish swim very close to each other in the same direction.

Head-tail display (HTD): The fish in parallel orientation are facing opposite directions. Sometimes this behavior is associated with circling.

Shaking (SHA): This behavior is similar to the head-tail display, but it is associated with fast circling, vigorous body-shaking, and a downward movement of the pair; the pattern stops when the animals reach the bottom.

Bite (BIT): One fish makes a swift dart and slashes at the other fish.

Mouthlock (MOU): The fish reciprocally bite and hold one another's mouths for up to 2 min.

Air gulping (AG): A fish takes an air bubble in its mouth by breaking the surface of the water.

Each of these behavioral units was recorded in all of the pairs investigated. Two samples of behavior were registered. The first sample, which characterized behavior during the threatening phase, lasted for 10 min from the raising of the door or until the first instance of contact behavior (biting or mouthlocking). The second sample, which characterized the fighting phase, was a 20-min observation following the first observed bite.

To permit comparison between pairs, the values of observed behavior units were divided by the sampling time. This adjustment was necessary because in many contests fish finished the threatening or fighting phase before our predetermined interval (10 or 20 min) of observations ended, resulting in shorter time samples. Thus the relative duration (minutes per hour) or frequency (number per minute) of behavior units was used for statistical analysis.

Because the measured variables were not normally distributed (according to the Kolgomorov-Smirnov test), nonparametric statistical methods were used. Kruskal-Wallis's one-way ANOVA was used separately for groups A and B to examine the change in the general pattern of aggressive behavior.

Results

The difference between the two groups—that is, the different effects of the "treatments"—can be seen in Table I.

Repeated encounters with the same opponent, group A, caused marked change in aggressive behavior. Although the duration of the threatening phase did not change significantly in the course of the three encounters, shaking and air-gulping were significantly reduced. All measured variables (with the exception of head-head display) of fighting, including its duration, decreased significantly when submissive fish faced the same opponent three times.

Interestingly, the changes in the other group (B) were much less pronounced. When the submissive fish repeatedly faced new opponents, only minor changes could be observed in their aggressive behavior. The threatening phase did not change significantly; only the relative duration of shaking and the frequency of biting showed a marked decrease.

A comparison with current literature showed that some behavioral elements and parameters are of special importance. Thus head-tail display (*e.g.*, Baerends and Baerends-Van Roon, 1950; Barlow, 1962; Enquist and Jakobsson, 1986), biting (*e.g.*, Peeke and Veno, 1973; Frank *et al.*, 1985; Enquist and Jakobsson, 1986; Halperin and Dunham, 1994), mouthlocking (*e.g.*, Baerends and Baerends-Van Roon, 1950; Enquist and Jakobsson, 1986), duration of threatening (*e.g.*, Frank *et al.*, 1985), and duration of fighting (*e.g.*, Enquist *et al.*, 1990; Haller, 1992) were examined further when we used the nonparametric Mann-Whitney test to compare the behavior of the two groups in the first, second, and third encounters (Fig. 1).

The two groups did not differ in the first and second encounter; however, with the exception of head-tail display, they differed markedly in the third encounter. The time spent with mouthlocking ($z = -2.4$, $P < 0.02$), the number of bites ($z = -2.3$, $P < 0.02$), and the duration of threatening ($z = -2.6$, $P < 0.01$) and fighting ($z = -1.9$, $P < 0.05$) were lower in the group (A) with the same opponent than in the group (B) with different opponents.

The same variables were compared by the nonparametric Wilcoxon test to show within-group differences during the three encounters. In group A—same opponent in each encounter—we found a significant change from the first to the second encounter only in fighting duration ($z = -2.8$, $P < 0.01$). However, significant changes occurred between the second and the third encounters in all of the selected variables (head-tail display: $z = -2.8$, $P < 0.01$; mouthlocking: $z = -2.6$, $P < 0.01$; biting: $z = -2.8$, $P < 0.01$; threatening: $z = -2.5$, $P < 0.02$; fighting: $z = -2.1$, $P < 0.04$). In contrast, no significant differences could be found in the group (B) with unknown opponents.

Discussion

The results clearly show that the type of opponent (familiar *versus* nonfamiliar) has a major effect on the aggressive behavior of male paradise fish. In the case of familiar opponents (group A), three consecutive encounters

Table I

Analysis of elements of aggressive behavior shown by fighting paradise fish pairs during three consecutive contests in both groups

	Group A: familiar opponent					Group B: unfamiliar opponent				
	encounter 1 Mean (SE)	encounter 2 Mean (SE)	encounter 3 Mean (SE)	Chi	Signif.	encounter 1 Mean (SE)	encounter 2 Mean (SE)	encounter 3 Mean (SE)	Chi	Signif.
Dur. of threatening	12.6 (2.1)	13.4 (2.9)	5.5 (1.8)	4.7	ns	12.3 (1.9)	12.1 (2.2)	11 (2.2)	1.7	ns
Head-head display	2.3 (0.9)	2.5 (0.7)	3.7 (1.4)	0.02	ns	4.4 (0.8)	6.2 (1.6)	3.6 (0.8)	0.7	ns
Shaking	2.3 (0.6)	1.7 (0.4)	0.4 (0.2)	7.3	$P < 0.03$	2.1 (0.7)	1.4 (0.3)	1.1 (0.3)	0.8	ns
Air-gulping	1.7 (0.4)	1.9 (0.7)	0.3 (0.1)	10.5	$P < 0.01$	3.2 (1.4)	1.9 (0.8)	2.5 (0.6)	2.5	ns
Parallel swimming	1.4 (0.7)	3.5 (1.3)	0.7 (0.3)	2.5	ns	2.1 (0.6)	4.4 (1.6)	1.6 (0.6)	2.1	ns
Head-tail display	32.2 (4.5)	36.1 (6.6)	19 (4.7)	4.7	ns	28.7 (4.4)	25.5 (5.1)	26.5 (4.3)	0.4	ns
Display at distance	4.1 (1.3)	3.1 (0.7)	5.1 (1.9)	0.2	ns	5.5 (1.8)	6.9 (3.5)	6.3 (2.1)	0.2	ns
Dur. of fighting	142.6 (40.1)	59.8 (22.8)	7.3 (3.5)	18.1	$P < 0.01$	115 (42.4)	50.1 (16.5)	54.8 (32.7)	4.9	ns
Head-head display	1.9 (0.8)	1.8 (0.8)	2.1 (1.4)	4.7	ns	4.4 (0.8)	6.2 (1.7)	3.6 (0.8)	0.1	ns
Shaking	1.3 (0.5)	1.2 (0.5)	0.5 (0.4)	5.9	$P < 0.01$	1.3 (0.2)	0.5 (0.2)	0.5 (0.2)	9.2	$P < 0.01$
Air-gulping	3.4 (0.9)	1.7 (0.5)	0.4 (0.3)	15.1	$P < 0.01$	3.1 (0.6)	2.6 (0.9)	1.6 (0.6)	4.0	ns
Parallel swimming	22.4 (6.2)	16.2 (5.7)	12.3 (2.8)	8.8	$P < 0.01$	20.4 (7.9)	3.1 (1.4)	2.5 (0.4)	0.9	ns
Head-tail display	39.6 (2.6)	31.4 (3.2)	10 (5.2)	8.8	$P < 0.02$	32.8 (2.2)	22 (5.5)	17 (5.4)	0.2	ns
Biting	1 (0.2)	1.1 (0.2)	0.1 (0.1)	15.3	$P < 0.01$	1.6 (0.3)	0.9 (0.3)	0.9 (0.3)	16.9	$P < 0.01$
Mouthlocking	13.8 (2.5)	9.2 (3.4)	0.8 (0.8)	17.3	$P < 0.01$	9.1 (1.8)	6.1 (2.4)	5.9 (2.2)	3.3	ns

Note: As a summary of the results, the mean (standard error) and the result of the one-way Kruskal-Wallis ANOVAs are given. The level of significance was greater than 0.05.

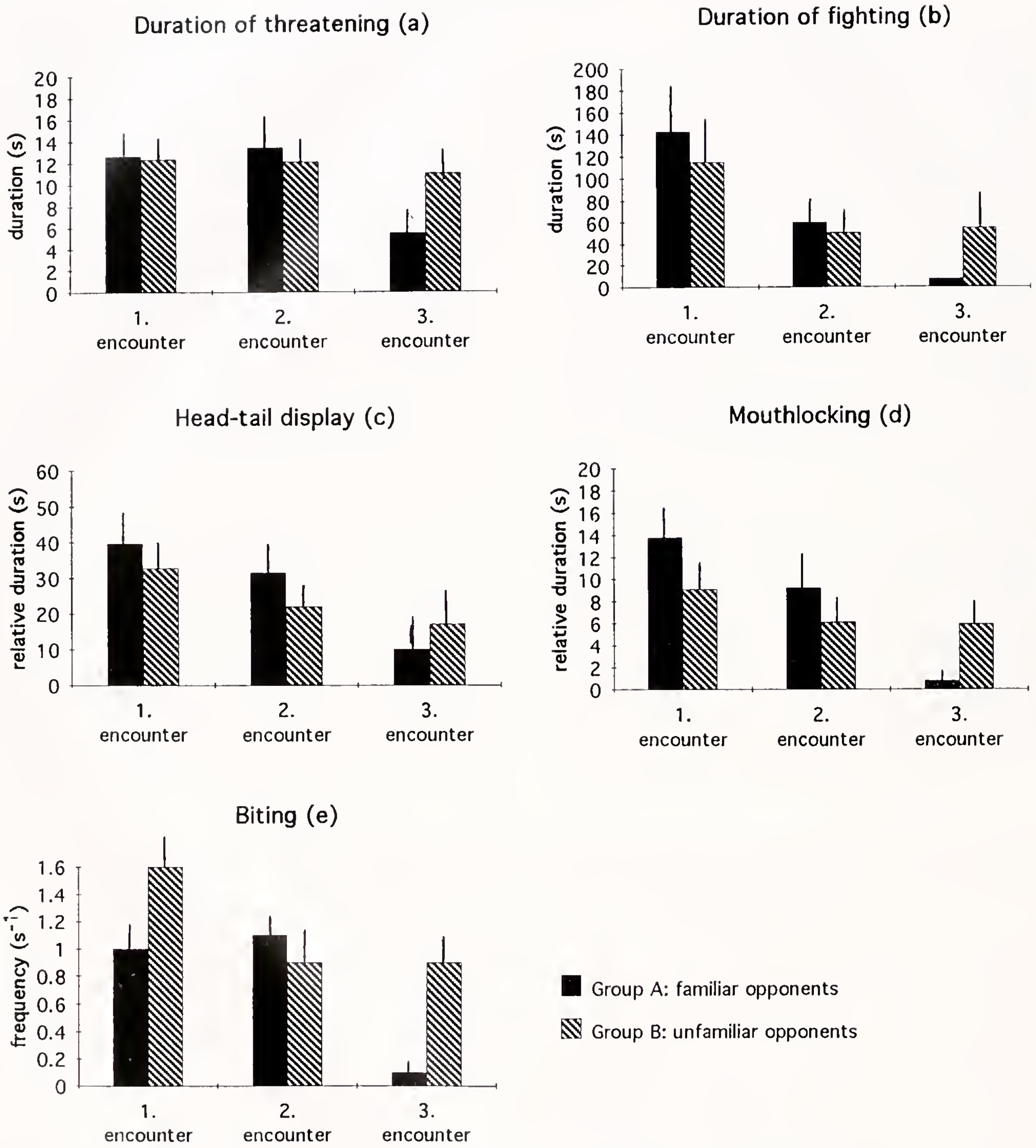

Figure 1. The mean duration of threatening (a) and fighting (b), and the mean relative duration of head-tail display (c) and mouthlocking (d) and biting (e) in the three consecutive encounters of the experimental groups. In group A the opponents were the same for each contest; in group B the former dominant was replaced by a new dominant male for each fight.

were needed to induce significant changes in aggression. On the other hand, repeated encounters with unfamiliar individuals (group B) caused significant changes in only some parameters of fighting. However, the changes that occurred in group B are much less dramatic than those in group A.

The behavior of the contestants was markedly similar during the first two encounters in both groups. This means that (1) there was no significant change within a group from the first to the second encounter, and (2) behavior did not seem to depend on the familiarity of the opponent during the second encounter. The significant decrease in the duration of fighting can be explained by noting that the first encounter occurred after 3 days of isolation, during which fish could build up energy reserves depleted during the rather long fight (about 2 h on average) at the first encounter (Haller and Wittenberger, 1988; Haller, 1991). Without these energy reserves the second encounter became shorter. However, it is also possible that isolation increased aggression levels.

The defeated fish in group A (same opponents) fought very similarly during the first and second encounters. Although all defeated fish lost the fight again, they gave up fighting only after a considerable time and engaged in both signaling behavior (*e.g.*, head-tail display) and strength-testing behavior (*e.g.*, mouthlocking). The same happened in the group with unfamiliar opponents (B): although defeated fish lost against the formerly dominant opponents, the previous defeat did not seem to change their behavior significantly.

Thus comparing the first two encounters in both groups we find the effect of previous experience on behavior—"status-related memory"—but no direct evidence of social recognition. Since the initial work of Ginsburg and Allee (1942), many studies have documented the effects of prior experience (*e.g.*, Bakker and Sevenster, 1983, Beacham and Newman, 1987). In the case of the paradise fish, defeat decreases the probability of subsequent winning in an aggressive encounter, but prior winning has no influence (Francis, 1983). However, three other factors might decrease the difference between a first and second encounter. (1) Following longer isolation before the first contest (3 days) and between contests (about 22 h), fish fight longer in both the first and second encounters (Miklósi *et al.*, unpub. obs.). (2) The encounter was terminated 1 h after fighting had finished, and fish were fed only following separation, thus opportunities for expressing dominance or submission were limited. (3) The weight symmetry between contestants rendered mutual assessment more difficult, according to the resource holding power (RHP) hypothesis (Parker, 1974). Usually larger animals initiate aggressive encounters and are more likely to win in a shorter fight. Thus similarity in size will increase both the latency of initiation and the duration of a contest.

The third encounter separates the two groups clearly. For fish facing familiar opponents (group A), the duration of the threatening phase decreased by half, and previously submissive fish gave up fighting soon after they began. In contrast, no significant change was observed in the behavior of fish facing unfamiliar opponents (group B). There was about a sixfold difference in biting, mouthlocking, and duration of fighting between the two groups, which rules out the role of exhaustion. In both groups, submissive fish lost two fights before engaging in the third contest: thus experience in submission or dominance cannot explain the observed difference. As a result, the involvement of some form of social recognition should also be taken into account for the third encounter.

Nevertheless, this experiment does not directly prove that individual recognition takes place. As Waas and Colgan (1994) recently noted, "Individual recognition implies that subjects can distinguish between animals that belong to the same social and physical class." But it is very difficult to tell the exact basis of this form of recognition because individuals can be categorized into several subcategories, and the same animal can use different arrays of variables to categorize its opponents. Because opponents were always of the same social class in both groups (submissive or dominant), the recognition might have occurred on a different level, which suggests that paradise fish are capable of categorization within dominants or submissives. Whether this can be described as individual recognition remains to be seen, and Waas and Colgan (1994) show a good way to examine this subject.

On the other hand, we already have some evidence that individual recognition exists in fish (Gandolfi *et al.*, 1973; Zayan, 1975; Myrberg and Riggio, 1985). For example, as shown by Zayan (1975), individual recognition of formerly dominant fish can reverse the effect of prior residence. Thus, the process of individual recognition interacts with the effects of both prior experience and prior residence in a way similar to that in our present experiment.

It is usually assumed that the end of the fight depends on the decision of the future submissive fish. This idea stems from the classical conditioning view of aggression, in which contact behaviors (biting, mouthlocking) are seen as punishment for the opponent, which learns during the aggressive encounter to avoid these aversive effects (McDonald *et al.*, 1968; Bakker *et al.*, 1989). In this context an individual opponent becomes a conditioned signal for future punishment, but a new opponent acts as a discriminative signal, which does not predict aversive stimulation.

Another theory interprets aggressive encounters in terms of an associative habituation process (Peeke, 1969; Lorenz, 1981). New opponents (or territorial neighbors) disrupt habituation and release an aggressive response. For example, Peeke and Veno (1973) found that resident male sticklebacks attacked unknown territorial neighboring sticklebacks more often than they attacked familiar ones.

The problem of small changes in a complex stimulus, like an opponent, raises a major problem to the incorporation of individual recognition into the learning models presented above. Either dishabituation or discrimination suppose some form of recognition of the opponent, but we do not know whether this categorization process is similar in the two models or not. As is the case with other processes described mainly on a behavioral level (*e.g.*, imprinting), it is very difficult to explain them in the framework of classical learning models.

At least in paradise fish, it seems that submissive fish try to use every occasion that offers the possibility of winning. Winning a contest presumably has many advantages.

Paradise fish males defend territories and build bubblenests in shallow waters of rice-fields, where several males breed at the same time near each other (Forselius, 1957). Recognizing neighbors could be advantageous because males spend less time in aggression, leaving time for courtship and later caring for the fry.

Our results support the hypothesis that aggressive experience in the paradise fish influences subsequent aggressive encounters by means of two kinds of memory: one related to the outcome of the encounter ("status-related memory") and the other related to the opponent ("social recognition").

Acknowledgments

This study was supported by the Hungarian Academy of Sciences by an OTKA grant (No. 368-0813\1991). Three anonymous reviewers gave helpful comments on the earlier version of this paper.

Literature Cited

Baerends, G. P., and J. M. Baerends-Van Roon. 1950. An introduction to the study of the ethology of cichlid fishes. *Behaviour* **1** (suppl.): 1–243.

Bakker, Th. C. M., and P. Sevenster. 1983. Determinants of dominance in male sticklebacks (*Gasterosteus aculeatus* L.) *Behaviour* **86:** 55–71.

Bakker, Th. C. M., E. Feuth-De Bruijn, and P. Sevenster. 1989. Asymmetrical effects of prior winning and losing on dominance in sticklebacks *(Gasterosteus aculeatus). Ethology* **82:** 224–229.

Barlow, G. W. 1962. Ethology of the Asian teleost *Badis badis* III. Aggressive behaviour. *Z. Tierpsychol.* **19:** 29–55.

Beacham, J. L., and J. A. Newman. 1987. Social experience and the formation of dominance relationships in the pumkinseed sunfish, *Lepomis gibbosus. Anim. Behav.* **35:** 1560–1563.

Beaugrand, J. P., and R. Zayan. 1985. An experimental model of aggressive dominance in *Xiphophorus helleri* (Pisces, Poeciliidae). *Behav. Proc.* **10:** 1–52.

Bevan, W., W. F. Daves, and G. W. Levy. 1960. The relation of castration, androgen therapy and pre-test fighting experience to competitive aggression in male C57 B1/10 mice. *Anim. Behav.* **8:** 6–12.

Csányi, V., P. Tóth, V. Altbäcker, A. Dóka, and J. Gervai. 1985. Behavioural elements of the paradise fish (*Macropodus opercularis*) I. Regularities of defensive behaviour. *Acta Biol. Hung.* **36:** 115–130.

Enquist, M., and S. Jakobsson. 1986. Decision making and assessment in the fighting behaviour of *Nannacara anomala* (Cichlidae, Pisces). *Ethology* **72:** 143–153.

Enquist, M., O. Leimar, T. Ljungberg, Y. Mallner, and N. Segerdahl. 1990. A test of the sequential assessment game: fighting in the cichlid fish *Nannacara anomala. Anim. Behav.* **40:** 1–14.

Forselius, S. 1957. Studies of anabantoid fishes. I. A quantitative description of the reproductive behaviour. *Zoologiska Bidrag fran Uppsala* **32:** 93–302.

Frank, D., R.-P. Hannes, H. Lanffermann, and A. Ribowski. 1985. Effects of social isolation on aggressiveness in fish with special reference to the swordtail *(Xiphophorus helleri). Behav. Proc.* **10:** 415–427.

Frank, D., and A. Ribowski. 1987. Influences of prior agonistic experiences on aggression measures in the male swordtail *(Xiphophorus helleri). Behaviour* **91:** 218–239.

Francis, R. C. 1983. Experiential effects on agonistic behavior in the paradise fish, *Macropodus opercularis. Behaviour* **85:** 292–313.

Fricke, H. W. 1973. Individual partner recognition in fish: field studies on *Amphiprion bicinctus. Naturwissenschaften* **60:** 204–205.

Gandolfi, G., R. Gandolfi, and F. Le Moli. 1973. Short-term individual recognition in *Padogobius martensi. Lincei Rend. Sc. Fis. Mat. e Nat.* **54:** 281–285.

Ginsburg, B., and W. C. Allee. 1942. Some effects of conditioning on social dominance and subordination in inbred strains of mice. *Physiol. Zool.* **15:** 485–506.

Haller, J., and C. Wittenberger. 1988. Biochemical energetics of hierarchy formation in *Betta splendens. Physiol. Behav.* **43:** 447–450.

Haller, J. 1991. Muscle metabolic changes during the first six hours of cohabitation in pairs of male *Betta splendens. Physiol. Behav.* **49:** 1301–1305.

Haller, J. 1992. Group size modifies the patterns and carbohydrate effects of aggression in *Betta splendens. Physiol. Behav.* **52:** 278–290.

Halperin, J. R. P., and D. W. Dunham. 1994. Social overstimulation reduces subsequent aggression in *Betta splendens. Aggressive Behav.* **20:** 135–142.

Lorenz, K. 1981. *Foundations of Ethology.* Springer-Verlag, Wien.

McDonald, A. L., N. W. Heimstra, and D. K. Damkot. 1968. Social modification of agonistic behaviour in fish. *Anim. Behav.* **16:** 437–441.

Miklósi, A., J. Haller, and V. Csányi. 1992. Different duration of memory for conspecific and heterospecific fish in the paradise fish *(Macropodus opercularis). Ethology* **90:** 29–36.

Myrberg, A. A., and R. J. Riggio. 1985. Acoustically mediated individual recognition by a coral reef fish *(Pomacentrus partitus). Anim. Behav.* **33:** 411–416.

Nagy, A., A. Dóka, and V. Csányi. 1985. A microcomputer method for recording and analysing behavioural elements. *Acta Biol. Hung.* **36:** 239–244.

Parker, G. A. 1974. Assessment strategy and the evolution of fighting behaviour. *J. Theor. Biol.* **47:** 223–43.

Peeke, H. V. S. 1969. Habituation of aggression in the three-spined stickleback *(Gasterosteus aculeatus* L.). *Behaviour* **35:** 137–156.

Peeke, H. V. S., and A. Veno. 1973. Stimulus specificity of habituated aggression in the stickleback *(Gasterosteus aculeatus). Behav. Biol.* **8:** 427–432.

Poll, van de, L., F. Jonge, H. G. van Oyen, and J. van Pelt. 1982. Aggressive behaviour in rats. Effects of winning or losing on subsequent aggressive interactions. *Behav. Proc.* **7:** 143–155.

Thresher, R. E. 1979. The role of individual recognition in the territorial behaviour of the threespot damselfish *(Eupomacentrus planifrons). Mar. Behav. Physiol.* **6:** 83–93.

Waas, J. R., and P. W. Colgan. 1994. Male sticklebacks can distinguish between familiar rivals on the basis of visual cues alone. *Anim. Behav.* **47:** 7–13.

Zayan, R. C. 1975. Defense du territorielle et reconnaissance individuelle chez *Xiphophorus* (Pisces, Pecillidae). *Behaviour* **52:** 266–313.

Reference: *Biol. Bull.* **188**: 89–97. (February/March, 1995)

Rapid Arm Movements in Stalked Crinoids

CRAIG M. YOUNG[1] AND ROLAND H. EMSON[2]

[1]*Department of Larval Ecology, Harbor Branch Oceanographic Institution, 5600 U.S. Hwy 1 N.,*
Ft. Pierce, Florida 34946, and [2]*Division of Life Sciences, King's College, London,*
Campden Hill Road, London, W8 7AH, United Kingdom

Abstract. Stalked crinoids in the family Isocrinidae have been observed to wave individual arms actively. Using video cameras mounted on a manned submersible, we studied these movements and investigated the factors that elicit them. Crinoids wave their arms in response to sand or detritus dropped on their crowns, to entanglement in tentacles of adjacent sea anemones, and to contact by small crustaceans that might steal from the food grooves. There was no evidence that arm waving functions in food collection. In most cases, the movements could be attributed directly to mechanical stimulation by some natural stimulus. The rapid effective stroke of an arm flexure is caused by contraction of dorsal longitudinal arm muscles. The slower return stroke results from the elastic recoil of large ligaments near the aboral sides of the arms.

Introduction

Stalked crinoids are passive suspension feeders with limited mobility but are nevertheless capable of several kinds of movements. The most characteristic behaviors are slow movements used to orient with respect to currents and to hold the arms and pinnules in a parabolic feeding-fan posture (Macurda and Meyer, 1974, 1976; Conan *et al.*, 1981). The mechanisms by which these postures are maintained and controlled are poorly understood. Orientation of the stalk, which contains no muscles, is dependent on mutable collagenous tissues (Wilkie *et al.*, 1993). The tonic posture of the parabolic feeding fan is probably maintained by a similar mechanism, but there is as yet no morphological or physiological evidence for mutable arm ligaments (I. Wilkie, pers. comm.).

Stalked crinoids occasionally demonstrate fast muscular movements. Several species are thought to be capable of moving between attachment sites (Carpenter, 1884; Conan *et al.*, 1981; Roux, 1976), and stalked crinoids have recently been observed crawling across the bottom (Messing, 1985; Messing *et al.*, 1988). When stimulated by the manipulator arm of a submersible or by very bright lights, this same species, *Endoxocrinus parrae,* rapidly flexes some or all of its arms in an adoral direction (Messing *et al.*, 1988; Young and Emson, unpub.). Except for an unpublished anecdotal observation suggesting that crinoids may respond to suspended sediment (W. I. Ausich, pers. comm.), all reports of rapid active arm movements have involved strong artificial stimuli. The natural roles of rapid arm movements remain undocumented. Here, we describe in detail rapid arm flexures of some bathyal isocrinids and present evidence that this behavior defends crinoids against various biotic and abiotic threats.

Materials and Methods

Several species of stalked crinoid were observed from Johnson-Sea-Link (JSL) submersibles at depths ranging from 400 to 900 m in the northern Bahamas (see map in Young, 1992). Still photographs were taken with a Benthos 35-mm camera equipped with an 80-mm lens, mounted on the front of the submersible and focused with twin laser beams that converged on a fixed focal plane. Video footage was obtained with a Photosea Camera on a pan-and-tilt mechanism and was recorded on ½″ or hi-8 videotape. Video still sequences were taken from the tape with a Seikosha VP-1500 video printer.

We obtained numerical data on arm-waving frequency and crustacean abundance directly from the videotape. We stopped the tape every 30 s and counted the number of arm movements, the number of crinoids involved in arm-waving behavior, and the total number of crinoids visible in the frame. We ran the tape forwards and backwards a few frames at each census point to be certain that arms counted as waving were really in motion and not

Received 16 March 1993; accepted 2 December 1994.

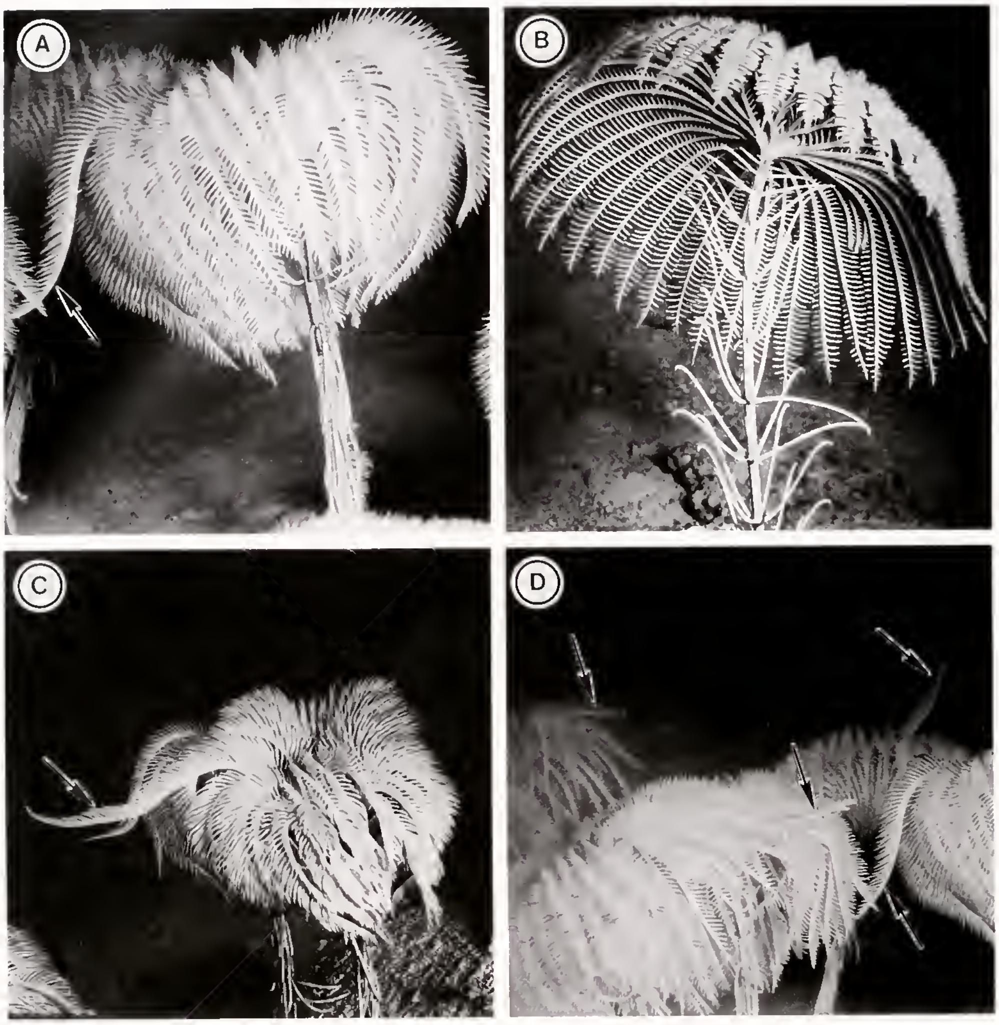

Figure 1. (A) *Endoxocrinus parrae* with arms drooping in slack current. Note the single arm waving in the water column (arrow). (B) *Cenocrinus asterius* in current, showing parabolic feeding fan characteristic of all Bahamian isocrinids. (C) *E. parrae* engaged in arm-waving behavior (arrow indicates moving arm). (D) A dense population of *E. parrae* with numerous individuals waving arms (indicated by arrow).

being held in a static posture. The number of small crustaceans in a frame was estimated by repeatedly passing the video forward and back, frame by frame, while scanning each part of the frame in succession for moving organisms.

The velocity of arm movement during effective and recovery strokes was documented by laying down a time code on the videotape with a hi-8 video editing machine (Sony EVO-9700), then, during frame-by-frame analysis, recording the time that movements were initiated and completed (resolution: 0.067 s).

To investigate the possibility that sediment particles might elicit arm waving, we used a suction tube on the manipulator arm of the submersible to pick up a small amount of sediment and release it about 1 m above an aggregation of crinoids. This experiment was repeated on six different occasions, while recording the responses of crinoids on videotape. On some occasions, the sediment consisted of fine silt; at other times, it was dominated either by coarse sand or coarse, flocculent organic particles.

Crinoid arm pieces were fixed in 4% neutral buffered formalin, decalcified in 70% acid alcohol, then embedded in paraffin by standard histological procedures. Sections were cut at a thickness of 8 μm and stained with Milligan's trichrome (Humason, 1972).

Results

Description and mechanics of arm waving

At times of slack current, three Bahamian isocrinids, *Endoxocrinus parrae, Cenocrinus asterius,* and *Diplocri-*

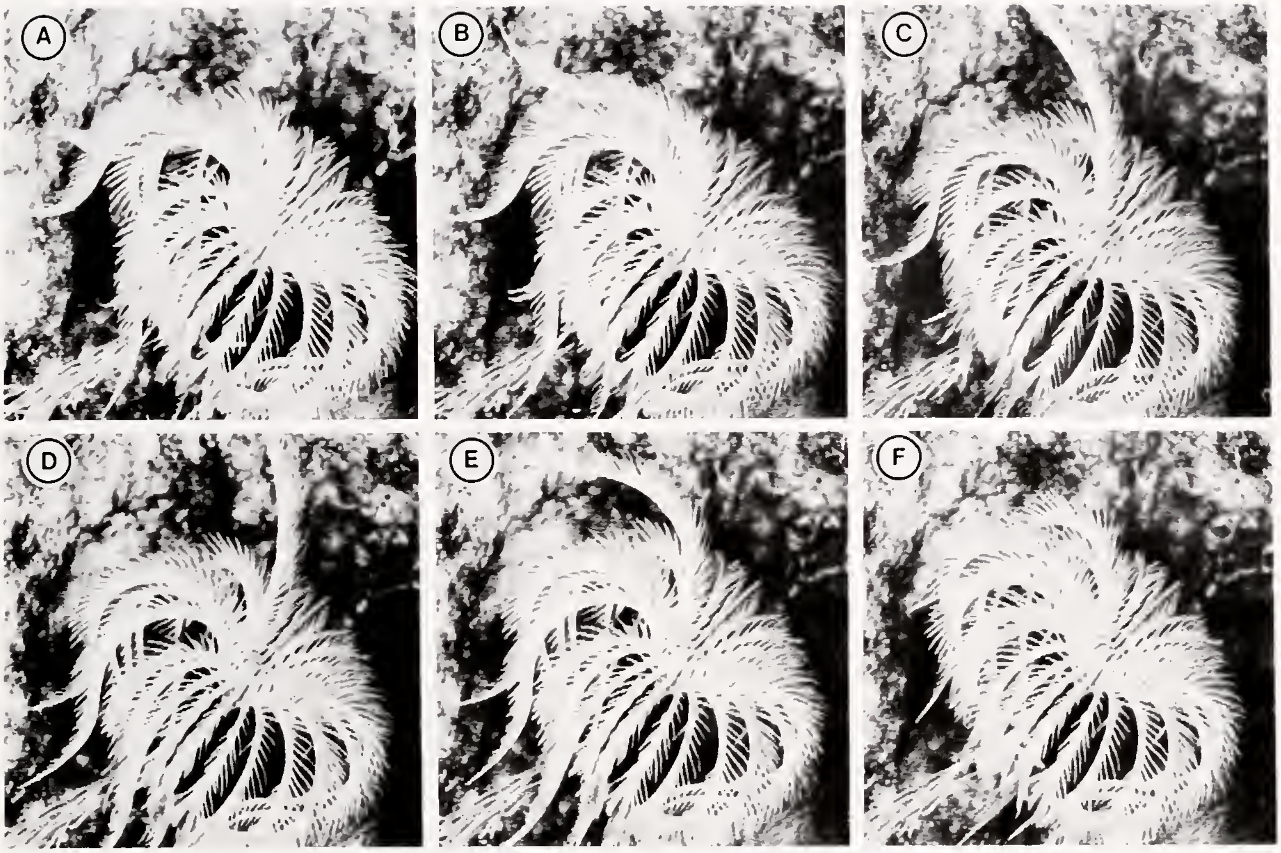

Figure 2. Video sequence of characteristic arm waving behavior in *Endoxocrinus parrae.* (A–C) Sequential steps of the effective stroke. (D) Maximum arm extension. (E–F) Recovery stroke.

nus maclearanus, stand erect with arms drooping down near the stalk (Fig. 1A). In a current, these same species form their arms into a parabolic fan for feeding (Fig. 1B; see also Macurda and Meyer, 1974, 1976), though the uppermost few arms of the fan may sometimes be extended straight up into the water column. All three species have been observed with individual arms waving up and down rapidly (Fig. 1A, 1C). In dense populations, large numbers of individuals have been observed to engage in arm-waving behavior simultaneously (Fig. 1D), particularly after several minutes of illumination by the submersible.

Although we have occasionally observed arm flicking or waving in animals with their arms extended in the feeding posture, arm-waving behavior has been observed more commonly in animals with drooping arms. The arm is moved rapidly away from the stalk, sweeping outward and upward until it is fully extended above or to the side of the calyx (Fig. 2). The arm pauses only briefly at the end of the stroke before reflexing downward more slowly to its initial position. This entire movement may take as little as 2 s or as much as 21 s. Frequency histograms of the durations of effective and recovery strokes (Fig. 3) show that the recovery strokes were more variable and often longer than the effective strokes, but the two distributions overlapped substantially. For individual strokes, the ratio of the effective component to the recovery was nearly always greater than 1 (Fig. 4), and the difference between the durations of paired effective and recovery strokes was highly significant (paired Student's t test, 54 d.f., $t = 5.75$, $P < 0.0000$). The arms were flexed through arcs ranging from a few degrees to more than 180 degrees. Most arms were flexed only once before another arm was brought into play. Often, one arm was flexed while another on the same animal was in its recovery stroke.

Examination of histological sections of the arm of *E. parrae* revealed the presence of large dorsal (oral) longitudinal muscles linking the arm segments (Fig. 5). These muscles, which are described elsewhere (Hyman, 1955) as flexor muscles, are clearly responsible for the flexure of the arms. There are no opposing longitudinal muscles, but large ligaments are found ventral (aboral) to the flexor muscles (Fig. 5). The recovery phase of arm waving must

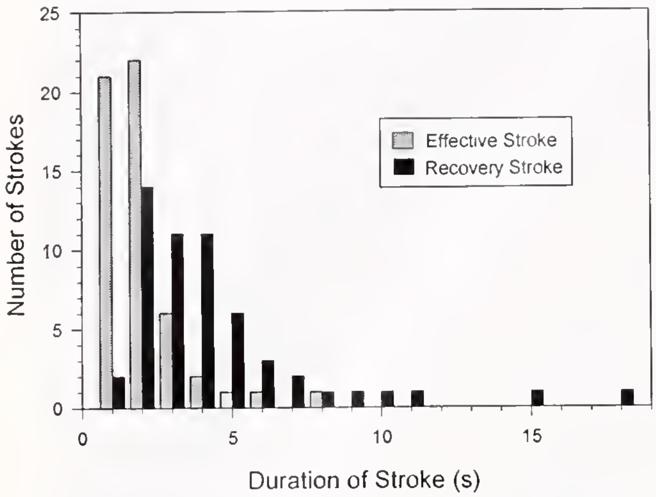

Figure 3. Frequency histogram comparing the durations of the effective strokes (hatched) and recovery strokes (solid black) during arm flexure of *Endoxocrinus parrae.*

therefore be achieved by elastic recoil. Small dark-staining cell bodies at the insertions of the ligaments (Fig. 5B) appear to be juxtaligamental cells (Wilkie, 1984), which are known to regulate collagen viscosity in other echinoderms. The largest axons in arm cross sections measured 3.75 μm in diameter, and most were between 2.5 and 3.5 μm in diameter.

Functions of arm waving

With the use of a close-up video camera, we determined that flexures often occurred in response to mechanical stimuli caused by various organisms and particles. For example, when the arms of stalked crinoids become entrapped in the tentacles of adjacent sea anemones, arm flexures allow them to escape. Arms are also flexed in response to contacts by small crustaceans. Such crustaceans are always attracted to the lights of the submersible in large numbers, affording us increased opportunities for observing encounters between crinoids and crustaceans. On 17 February 1980, we came upon a rocky ridge supporting more than 200 *E. parrae* and *C. asterius* at a depth between 409 and 500 m off Booby Rocks, New Providence Channel, Bahamas. As we passed up the ridge without stopping, we filmed 49 crinoids in two aggregations, observing all the while only two instances of arm-waving behavior. We then rested the submersible near a third large aggregation and filmed it from a distance of 3 m for 7 min. The percentage of animals participating in arm waving and the number of arm waves per individual increased linearly with the number of crustaceans visible (Fig. 6). Although these regressions are consistent with the idea that crustaceans stimulate arm waving, we could not dismiss the possibility that density of crustaceans covaried with some other factor (*e.g.,* illumination time) until video cameras with higher resolution were installed in 1991.

On 24 October 1991 at a depth of 642 m off Egg Island, we located a large aggregation of *E. parrae.* By focusing on inactive individuals, we recorded 10 instances of arm waving that were clearly stimulated by a single crustacean. A representative encounter is shown in Figure 7. The time required for initiation of a visible response to the impact of this crustacean was 0.47 s. In every case, the crustacean contacted the crinoid on the oral side of the arm between the pinnules and in the region of the food groove. In one observed encounter, the crustacean remained attached during three sequential flexures before becoming dislodged; in all other instances, the crustacean was dislodged by the initial arm movement and swam away. On subsequent dives, crustacean-induced arm movements were also recorded for *C. asterius,* one of which is shown in Figure 8. Here, the crustacean was swimming upstream in the turbulent downstream wake of a crinoid feeding passively in the current. When the crustacean contacted the oral side of the arm, a small flexure was elicited immediately (Fig. 8), and the crustacean moved downstream.

We dropped sediment from the manipulator on six separate occasions with two to four attempts on each experiment. Sediment containing a mixture of particles ranging in size from 1 to several millimeters elicited discrete flexures of individual arms when individual particles struck (Fig. 9). Small amounts of very fine silt did not

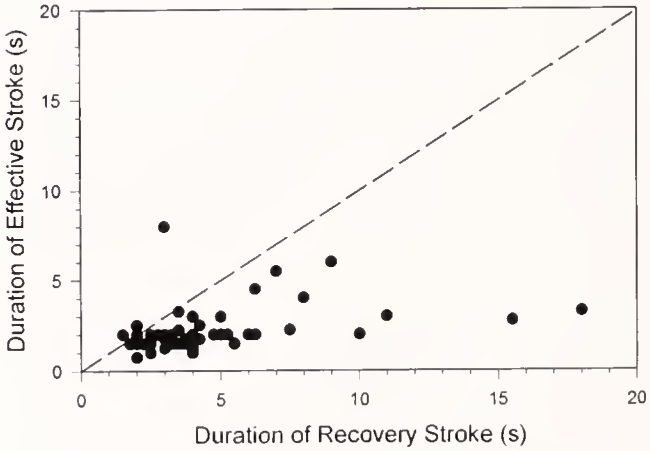

Figure 4. Durations of individual effective strokes plotted against durations of corresponding individual recovery strokes for individual arm flexures of *Endoxocrinus parrae.* If flexure and recovery were of the same duration, all points would fall on the dashed line. Most points lie below the line, indicating that recovery strokes are generally, but not always, longer than effective strokes.

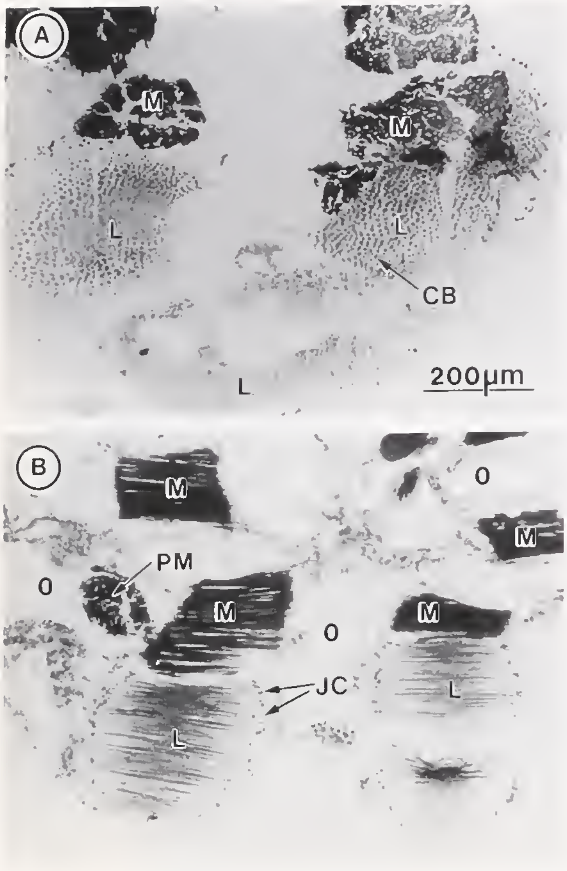

Figure 5. Cross section (A) and longitudinal section (B) of an arm of *Endoxocrinus parrae* showing longitudinal flexor muscles (M), and extensor ligaments (L) connecting portions of ossicles (O). Individual bundles of collagen (CB) are visible in the ligaments. Cell bodies of juxtaligamental cells (JC) are visible at the points where collagen fiber bundles insert into the brachial ossicles. PM: longitudinal muscle of a pinnule cut in cross section.

stimulate waving, but fine sediment in large quantities sometimes elicited a dramatic arm-waving response involving numerous arms. Figure 10 shows the response of one *E. parrae* individual to a large piece of flocculent organic matter that lodged firmly on an arm. The crinoid moved the affected arm as well as adjacent arms several times until the material was dislodged.

Various kinds of crabs and ophiuroids (*e.g.*, euryalids) commonly perch on sessile organisms, including large sponges, gorgonians, and antipatharians, on the Bahamian slope. These same organisms live on the stalks of crinoids, but we have never seen a single individual occupying the crown region. We suppose that arm waving might deter occupation of the crown by ophiuroids and crabs, but cannot prove this with observations.

Discussion

Virtually all sessile animals have neuromuscular mechanisms for ridding themselves of impinging organisms or objects that threaten them or that interfere with the feeding process. It is not surprising, therefore, that stalked crinoids would have an active mechanism of protection appropriate to their form and life style. In echinoderms, some protective mechanisms involve the use of giant nerve fibers and very rapid (0.25 s) reaction times (Cobb, 1985; Cobb and Ghyoot, 1993). The nerve fibers of *E. parrae* measured between 2.5 and 3.75 μm in diameter, only about 30% as large as the giant fibers in *Ophiura ophiura* (Cobb, 1985). However, these are larger than the 1 μm diameter neurons found in most echinoderms (Cobb, 1985). Reaction times of stalked crinoids (about 0.5 s) were about twice as long as those reported for ophiuroids (Moore and Cobb, 1985).

On the basis of behavioral and histological observations, it appears that arm flexure results from the contraction of large flexor muscles, and that recovery results from the elastic recoil of ligaments. This interpretation is consistent

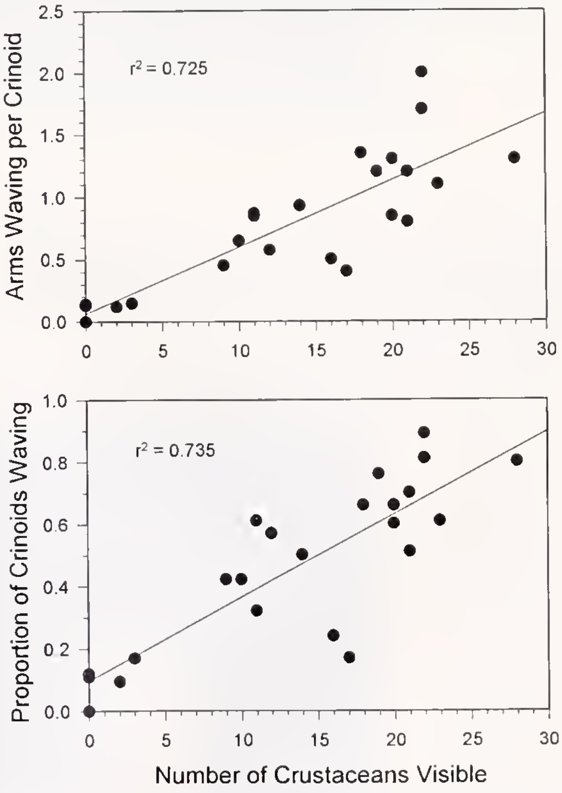

Figure 6. The relationships between crustacean density and the number of arms waving per crinoid (top panel) and proportion of crinoids waving arms (bottom panel) during a single 7-min taping session in a dense bed of *Endoxocrinus parrae* at 409 m depth at Booby Rocks, Bahamas.

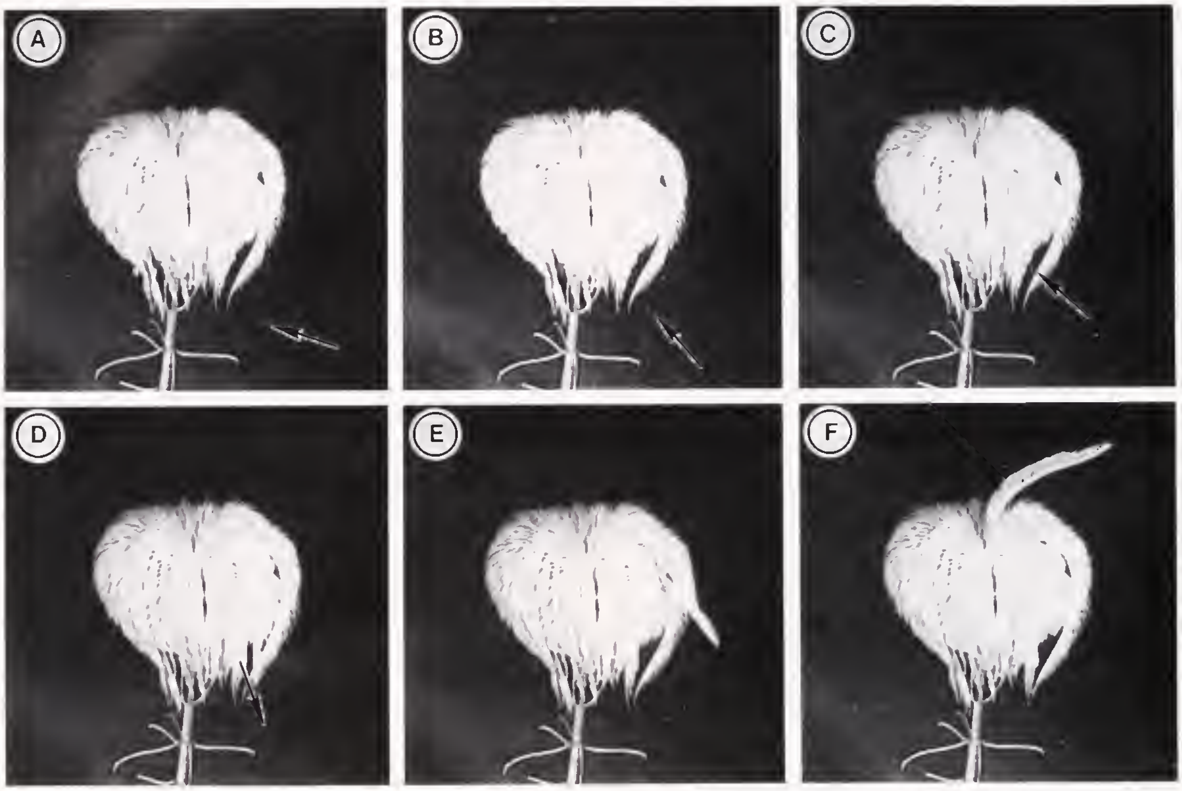

Figure 7. Response of *Endoxocrinus parrae* to an individual crustacean contacting the arm. (A–C) Crustacean (position and direction of swimming indicated by arrows) enters rapidly from the right side of the field and moves into crown region of crinoid. (D) Arm begins to flex immediately after crustacean contacts it, and crustacean responds by swimming rapidly away (arrow). (E–F) Arm contacted by crustacean continues to flex until it is maximally extended.

with the views of most previous workers (*e.g.*, Muller, 1843; Breimer, 1978; Grimmer and Holland, 1987). An alternative hypothesis, invoking hydraulic pressure in the coelomic canals of the arms as a mechanism of arm extension, has been put forward by Candia Carnevali and Saita (1985). Grimmer and Holland (1987), however, showed experimentally that destruction of these coelomic canals did not affect recovery from flexure in the coma-

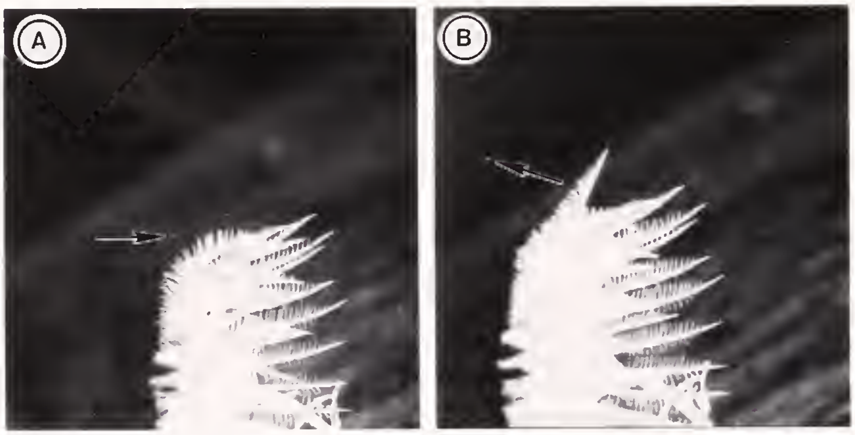

Figure 8. (A) Small crustacean swimming upstream (in direction of arrow) within the turbulent wake of a feeding *Cenocrinus asterius.* (B) Small arm flexure following contact by crustacean (arrow), which is thrown downstream.

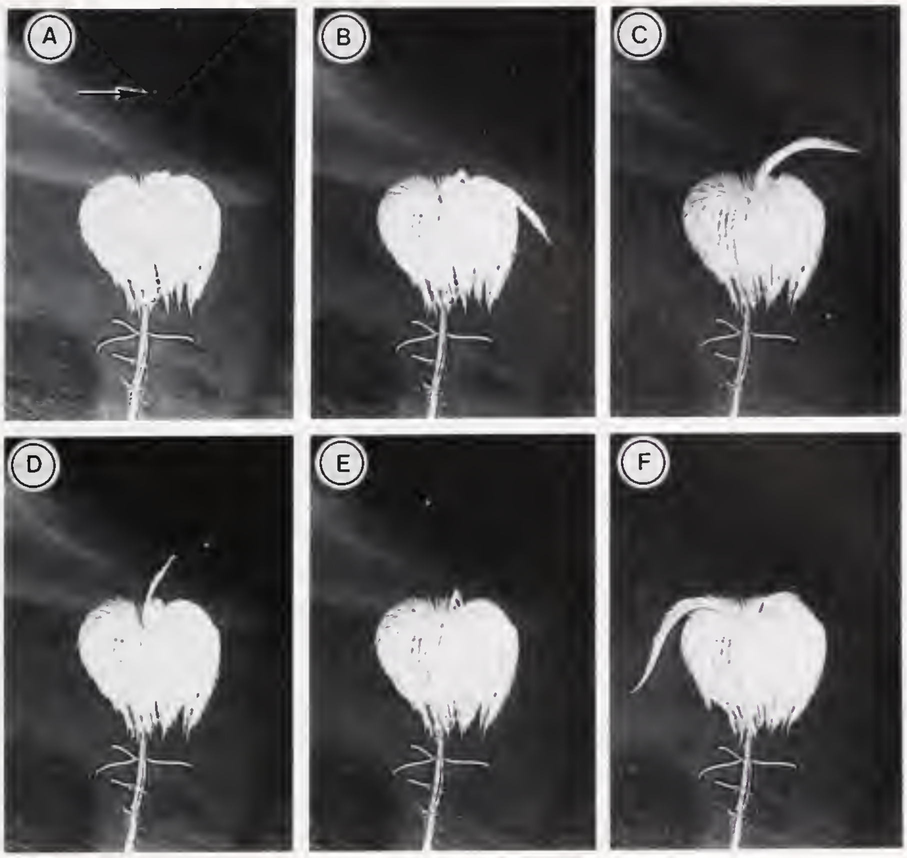

Figure 9. Arm flexures of *Cenocrinus asterius* in response to sand particles dropped on the crown. Sand particles (one is indicated by arrow in A) were falling throughout this sequence, which involved movements by arms on all sides of the crown.

tulid *Florometra serratissima*. In fact, their experimental results demonstrate that elastic forces in the aboral soft tissues of the arm of a comatulid were alone sufficient to drive a power stroke in active swimming. We suggest that a similar mechanism is involved in the recovery stroke of stalked crinoids such as *E. parrae*.

Existing evidence does not support the idea that arm waving is involved in food collection. Unlike some other sedentary filter-feeding echinoderms at bathyal depths (*e.g.*, brisingid asteroids: Emson and Young, 1994), stalked crinoids are not known to capture large particles (Meyer, 1982; Lawrence, 1987). Indeed, our observations indicate that large particles contacting the crown are thrown away from the crown, not toward the mouth. Arm waving could enhance encounters with small particles, particularly in still water. However, such a feeding strategy would seem inefficient in the oligotrophic habitats where these animals live, since arm flexure requires considerable muscular involvement and might result in a net energy loss. By contrast, the maintenance of posture for passive feeding may involve catch connective tissues (Wilkie and Emson, 1988) which require little energy expenditure. Our observation of apparent juxtaligamental cells (Fig. 5B) is equivocal evidence for mutable collagenous tissues in stalked crinoid arms. The use of arm flexing for filter feeding seems unlikely, but cannot be discounted completely.

Arm-waving behavior appears on present evidence to be principally a mechanism to eliminate inorganic particles from the crown and to deter small organisms from settling on the arms of the crinoid. Specifically, we have demonstrated that the behavior has a deterrent effect on small crustaceans, preventing them from acting as predators, food thiefs, or opportunistic commensals. Arm movements may prevent colonization of the crown by crabs, ophiuroids, and other epifauna, and they permit escape from the feeding structures of adjacent sessile organisms such as sea anemones. Inorganic and organic particles that fall on the arms also elicit arm waving, so the behavior may have evolved as a general mechanism for ridding the crown of unwanted particles. As all stalked crinoids that have been examined histolog-

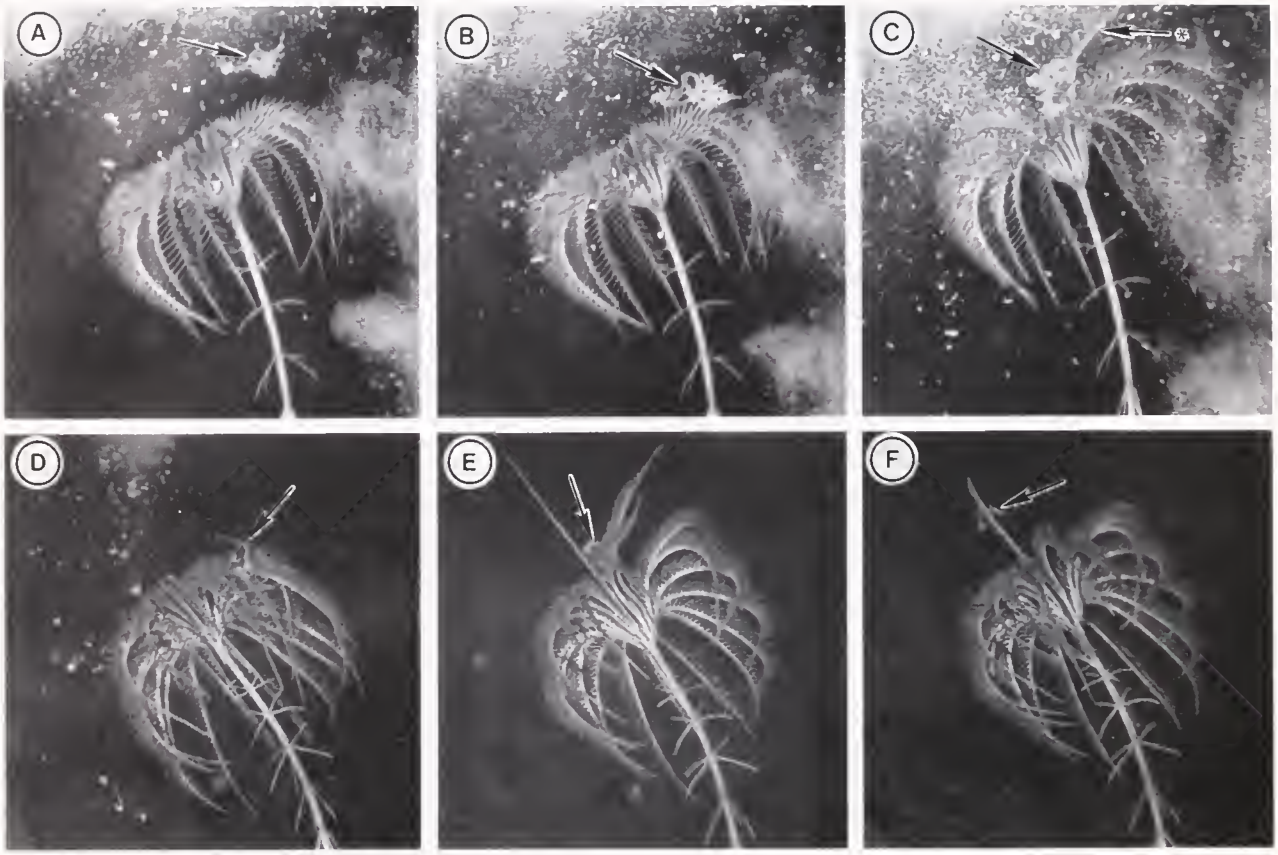

Figure 10. Response of *Cenocrinus asterius* to fine sediment and a large flocculent mass of detritus dropped on the crown. (A) Sediment contacts the crown, and a large particle of detritus (arrow) falls toward one arm. (B) Detrital mass lands on the arm. Note that the fine silt elicits no dramatic responses from the arms. (C) Arm (asterisk) with large detrital particle flexes, dislodging a portion of the mass. (D) Remainder of detrital mass (arrow) remains on the arm. (E, F) Various arms in the region of the detrital mass flex repeatedly, apparently attempting to dislodge the attached detritus.

ically have similar flexor muscles, we suspect that arm waving may be a behavior of great antiquity and common to many living and extinct crinoids.

Acknowledgments

We thank the skilled pilots of the JSL submersibles for assistance with close-up video. This work was funded by the National Science Foundation (OCE-8916264 and OCE-9116560) and by a NATO Collaborative Research Grant (CRG-900628). Harbor Branch Contribution No. 1064.

Literature Cited

Breimer, A. 1978. Recent crinoids. Pp. 9–58 in *Treatise on Invertebrate Paleontology, Part T. Echinodermata,* I. R. C. Moore and C. Teichert, eds. University of Kansas Press, Lawrence, and the Geological Society of America, Inc., Boulder, CO.

Candia Carnevali, M. D., and A. Saita. 1985. Muscle system organization in the echinoderms: II. Microscopic anatomy and functional significance of the muscle-ligament-skeleton system in the arm of the comatulids (*Antedon mediterranea*). *J Morph.* **185:** 59–74.

Carpenter, P. H. 1884. Report on the Crinoidea collected during the voyage of HMS 'Challenger' during the years 1874–1876. The stalked crinoids. *Challenger Rep. Zool.* **11,** 442 pp.

Cobb, J. L. S. 1985. The neurobiology of the ectoneural/hyponeural synaptic connection in an echinoderm. *Biol. Bull.* **168:** 432–446.

Cobb, J. L. S., and M. Ghyoot. 1993. The giant through conducting neuron of the brittlestar *Ophiura ophiura*—a key neuron? *Comp. Biochem. Physiol.* **105A:** 697–703.

Conan, G., M. Roux, and M. Sibuet. 1981. A photographic survey of a population of the stalked crinoid *Diplocrinus (Annacrinus) wyvillethomsoni* (Echinodermata) from the bathyal slope of the Bay of Biscay. *Deep-Sea Res.* **28A(5):** 441–453.

Emson, R. H., and C. M. Young. 1994. The feeding mechanism of a deep-water brisingid asteroid, *Novodinea antillensis. Mar. Biol.* **118:** 433–442.

Grimmer, J. C., and N. D. Holland. 1987. The role of ligaments in arm extension in feather stars (Echinodermata: Crinoidea). *Acta Zool.* **68:** 79–82.

Humason, G. L. 1972. *Animal Tissue Techniques.* W. H. Freeman, San Francisco. 641 pp.

Hyman, L. H. 1955. *The Invertebrates. IV. Echinodermata.* McGraw-Hill, New York. 763 pp.

Lawrence, J. 1987. *A Functional Biology of Echinoderms.* Johns Hopkins University Press, Baltimore. 340 pp.

Macurda, D. B., and D. L. Meyer. 1974. Feeding posture of modern stalked crinoids. *Nature* **247:** 394–396.

Macurda, D. B., and D. L. Meyer. 1976. The identification and interpretation of stalked crinoids from deep-water photographs. *Bull. Mar. Sci.* **26:** 205–215.

Meyer, D. L. 1982. Food and feeding mechanisms: Crinozoa. Pp. 25–42 in *Echinoderm Nutrition,* M. Jangoux and J. M. Lawrence, eds. A. A. Balkema, Rotterdam.

Messing, C. 1985. Submersible observation of deep-water crinoid assemblages in the tropical western Atlantic Ocean. Pp. 185–193 in *Echinodermata,* B. F. Keegan and B. D. S. O'Connor, eds. A. A. Balkema, Rotterdam.

Messing, C. G., M. C. RoseSmyth, S. R. Mailer, and J. E. Miller. 1988. Relocation movement in a stalked crinoid (Echinodermata). *Bull. Mar. Sci.* **42:** 480–487.

Moore, A., and J. L. S. Cobb. 1985. Neurophysiological studies on photic responses in *Ophiura ophiura. Comp. Biochem. Physiol.* **80A:** 11–16.

Müller, J. 1843. Über den Bau des *Pentacrinus caput medusae. Abd. Kgl. Akad. Wiss. Berlin* **1841** (Part 1): 177–248.

Roux, M. 1976. Aspects de la varibilitè et de la croissance au sein d'une population de la Pentacrine actuelle: *Annacrinus wyvillethomsoni* Jeffreys (Crinoidea). *Thalassia Jugosl.* **12:** 307–320.

Wilkie, I. C. 1984. Variable tensility in echinoderm collagenous tissues: a review. *Mar. Behav. Physiol.* **11:** 1–34.

Wilkie, I. C., and R. H. Emson. 1988. Mutable collagenous tissues and their significance for echinoderm paleobiology and phylogeny. Pp. 311–330 in *Echinoderm Phylogeny and Evolutionary Biology,* C. R. C. Paul and A. B. Smith, eds. Clarendon Press, Oxford.

Wilkie, I. C., R. H. Emson, and C. M. Young. 1993. Smart collagen in sea lilies. *Nature* **366:** 519–520.

Young, C. M. 1992. Episodic recruitment and cohort dominance in echinoid populations at bathyal depths. Pp. 239–246 in *Marine Eutrophication and Population Dynamics,* G. Colombo, I. Ferrari, V. U. Ceccherelli, and R. Rossi, eds. Olsen and Olsen, Fredensborg.

Reference: *Biol. Bull.* **188:** 98–110. (February/March, 1995)

The Structure and Mode of Function of the Water Vascular System of a Brittlestar, *Ophioderma appressum*

JOHN C. FERGUSON

Galbraith Marine Science Laboratories, Eckerd College, P.O. Box 12560, St. Petersburg, Florida 33733

Abstract. Unlike the asteroids, which have large madreporite structures, the ophiuroid *Ophioderma appressum* possesses only two small hidden madreporite pores. Experiments with labeled amino acids, fluorescent microbeads, and surgical obstruction show that small amounts of seawater do routinely enter these pores and become distributed throughout the water vascular system; but this uptake does not seem essential. The flagellated stone canal draws its fluid from the axial sinus, to which the pores connect through a tortuous ampulla. Thus, the stone canal mainly recirculates fluid from hyponeural (perihemal) passages. That perihemal fluid is augmented by seawater from the pores. As perihemal fluid moves towards the stone canal, it passes by or through the axial organ, where nutritive materials may be removed and passed into the hemal channels. Pressure generated by the stone canal forces flow out to the oral tube feet, polian vesicles, and, through valves, eventually to the arm tube feet. Inflation of the tube feet also might occur through osmotic mechanisms, but their activity was not impeded by raising the external osmotic level with dextran. Observations indicate that negative coelomic pressures must be generated during respiratory movements, and these could lead to sufficient body fluid production (by filtration) that the need for substantive madreporitic inflows would be alleviated.

Introduction

One of the most distinctive characteristics of echinoderms is their water vascular system—a unique arrangement of fluid-filled coelomic passages and associated parts. The general form of these structures in the different echinoderm classes has been summarized by Hyman (1955) and Nichols (1966) from the works of pioneer microscopists. In most types, the water vascular passages open to the exterior through a hydropore or compound madreporite, and fluid within the system is used hydraulically to extend agile appendages, the tube feet. With their variety of functional adaptations, the tube feet are probably responsible for much of the evolutionary success of this major animal group. The water vascular system, however, is much more complex in both structure and function than is generally realized, and it presents many attributes that are puzzling and, as yet, little studied.

It is generally assumed, for example, that the madreporite admits seawater into the system, and that ciliary pumping by the stone canal connected to it forces the seawater taken in to flow out to the tube feet where it replenishes fluid losses due to their activity. That view, however, was challenged by Binyon (1964, 1966, 1976a, b, 1980, 1984), who observed that starfish tube feet remain active for long periods without access to the madreporite. He noted that ionic elevation of the water vascular fluid, particularly of potassium ion, could produce an osmotic entry of water into the structures, making madreporitic inflow unnecessary. Binyon opined that the madreporite might be a relief valve, a supplemental mechanism, or have some other unknown functions.

More recently, my own work with fluorescent molecular tracers and microbeads, and other methods, has shown that seawater does routinely enter the madreporite of all starfishes tested; but this uptake is not specifically directed at tube foot inflation. Rather, the uptake plays a more important role in keeping the spacious asteroid body filled with fluid (Ferguson, 1988, 1989, 1990a, 1992, 1994). Further, the stone canal, through connections with

Received 25 July 1994; accepted 4 November 1994.

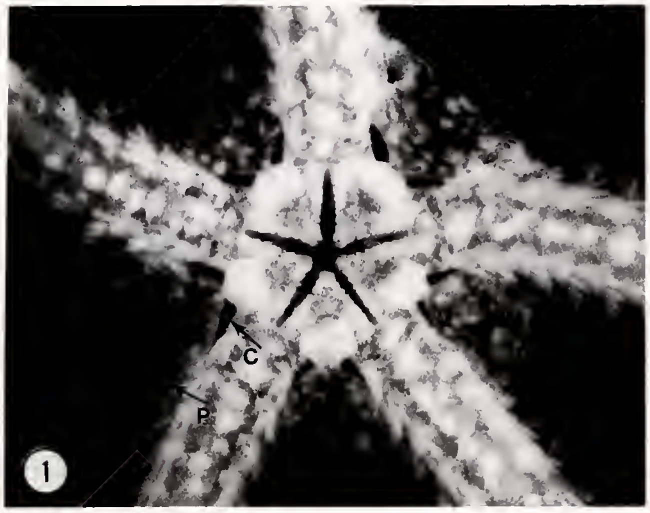

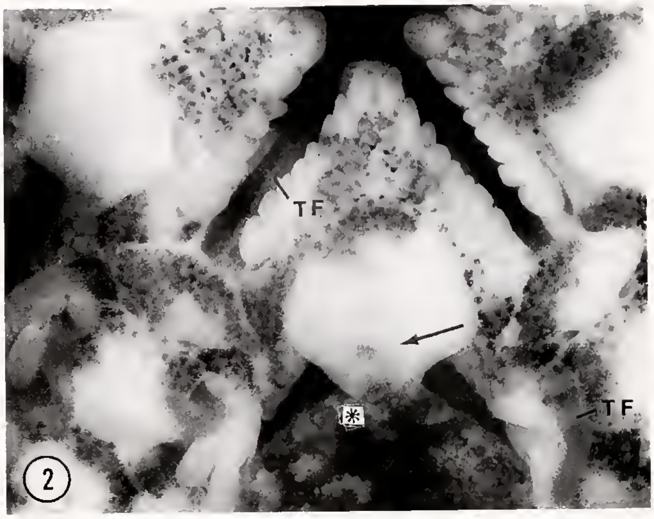

Figure 1. Oral disk of *Ophioderma appressum.* The arrows mark a pair of central (C) and peripheral (P) slits that open into one of the 10 genital bursae. Seawater is drawn from the side of the disk through the peripheral genital bursal slits and is vented by the central ones.

Figure 2. Magnified view of the oral shield overlaying the axial complex, visible as a slightly darkish area (arrow). The madreporite pores are out of sight in the crevice near the asterisk. Extended tube feet (TF) can be seen in the mouth and on the arms.

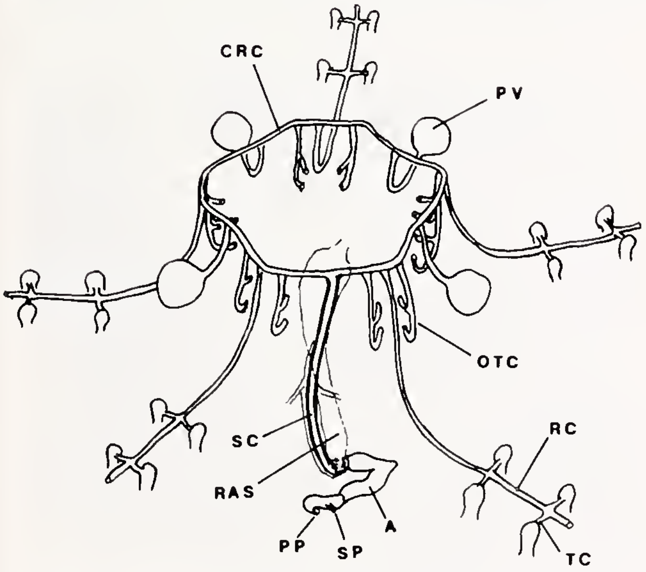

Figure 3. Organization of the water vascular system. The oral tube feet have been omitted and the arm tube feet and axial complex are only partially shown. A, ampulla; CRC, circumoral ring canal; OTC, oral tube feet canal; PP, primary madreporite pore; PV, polian vesicle; RAS, right axial sinus; RC, radial canal; SC, stone canal; SP, secondary madreporite pore; TC, transverse canal.

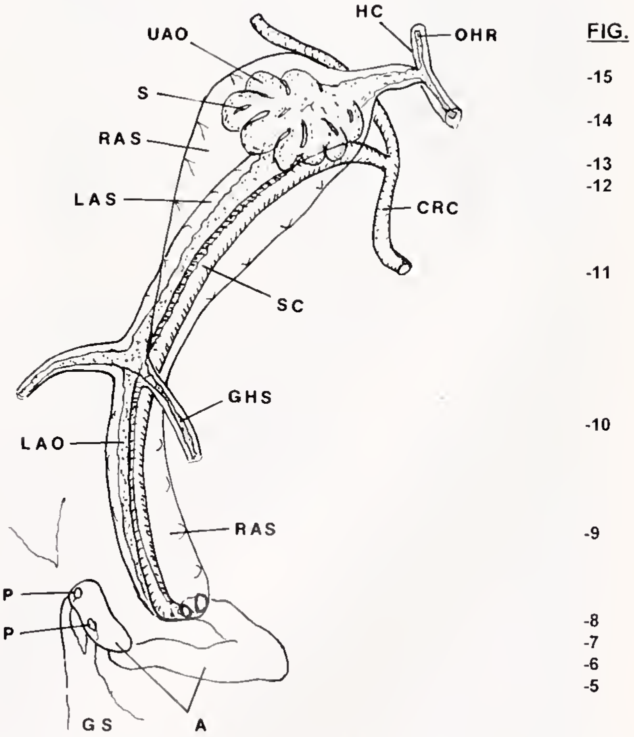

Figure 4. Detailed diagram of the madreporite-axial complex, with a scale showing the approximate level of serial sections (Figs. 5–15). A, ampulla; CRC, circumoral ring canal; GHS, genital hemal strand; GS, genital bursal slit; HC, hyponeural coelom; LAO, lower axial organ; LAS, left axial sinus; OHR, oral hemal ring; PP, primary madreporite pore; UAO, upper axial organ; RAS, right axial sinus; S, slit in axial organ connecting left and right axial sinus; SC, stone canal; SP, secondary madreporite pore.

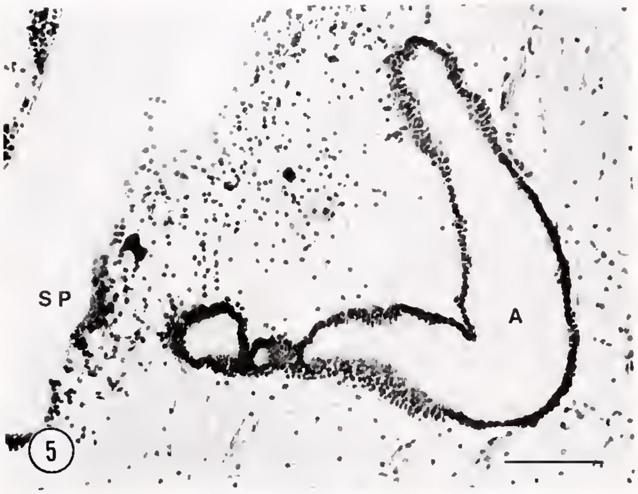

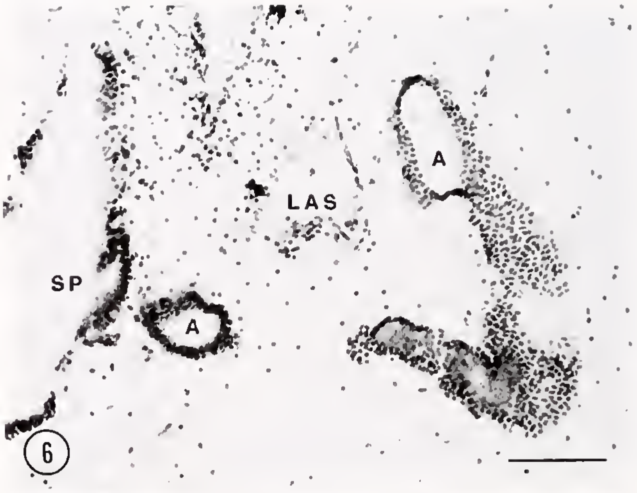

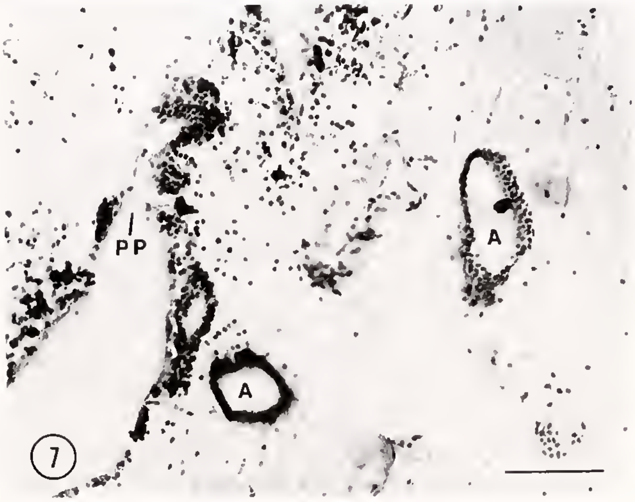

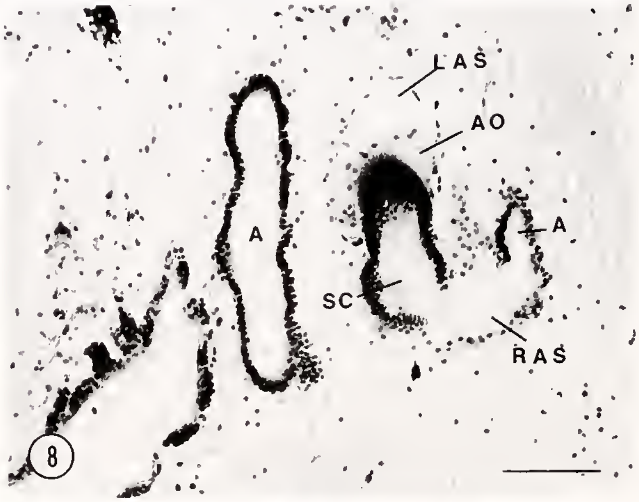
LAS
AO
A
A
SC
RAS
8

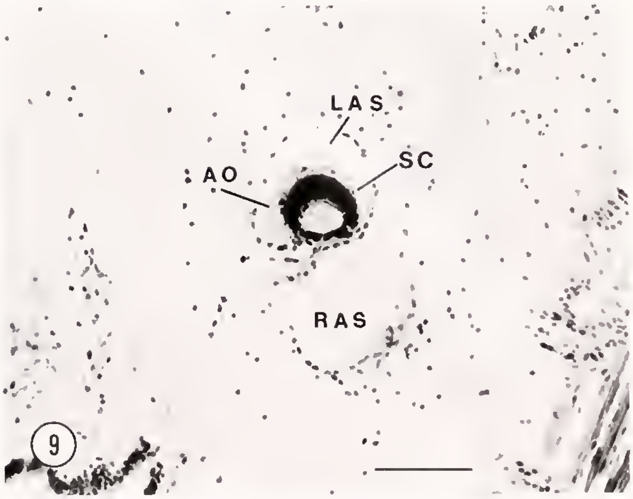
LAS
AO
SC
RAS
9

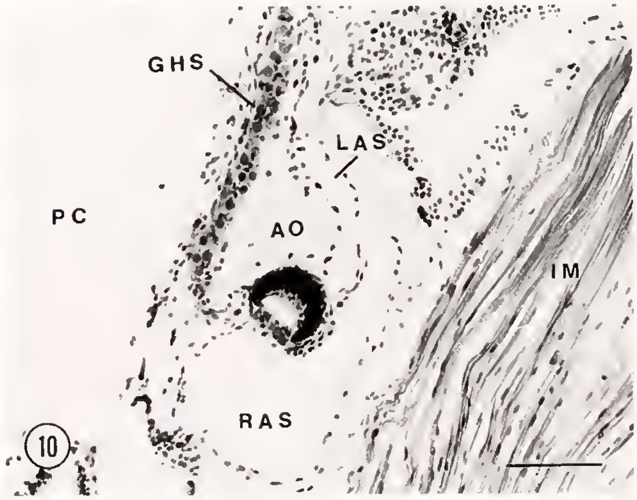
GHS
LAS
PC
AO
IM
RAS
10

Figure 5. First of a set of serial frontal sections from the madreporite oral shield upwards. It shows part of the large, angular ampulla (A) that lies within the oral shield. The edge of the secondary madreporite pore (SP) can be seen on left, facing the cleft formed by the edge of the genital bursal slit. (All scale bars = 50 μm).

Figure 6. Section located 20 μm higher than Figure 5, showing the secondary pore opening (SP) and the lowest portion of the left axial sinus (LAS). The pore canal leads towards the site of the primary pore, away from the direction of inflow through the tortuous ampulla (A).

other parts, must maintain an internal system of circulation and filtration of the body fluids. Some starfish, such as the intertidal *Pisaster ochraceus*, cannot adequately maintain their body fluid volume without access to the madreporite, while others, such as *Pycnopodia helianthoides*, rely more heavily on osmotic uptake (Ferguson, PN100,,,L,I01992, 1994). Physical differences between species largely reflect their individual adaptations to fluid volume maintenance. *Pisaster* has a heavy, stiff, and impermeable integument, while that of *Pycnopodia* is light, flexible, and much more permeable.

Because the function of madreporite mechanism in different asteroids varies considerably, similar diversity should be expected in the other classes; indeed, differences in body form between the classes might relate to their individual approaches to solving the problems of body fluid maintenance. Although ophiuroids share many characteristics with the asteroids, they are also quite different. Here I begin a detailed examination of the structure and function of an ophiuroid water vascular system—that of *Ophioderma appressum*. Comparison of its properties with those of other echinoderms should broaden our understanding of the adaptations of these diverse organisms.

Materials and Methods

Specimens of *Ophioderma appressum* were collected from tidal grass flats in Tampa Bay and maintained in running, fresh seawater until used for experiments. This species is very similar to *Ophioderma brevispinum* (referred to in earlier work), but grows larger and possesses more equal-dimensioned oral shields (five large plates surrounding the mouth). As in other ophiodermids, the openings into its genital bursae (pairs of pouches invaginated into the disk on either side of the arm bases) are each separated into two slits—a "central" one near the mouth and a "peripheral" one on the edge of the disk. Its madreporite cannot be seen externally, and the structure of its water vascular system must be inferred from old descriptions of other ophiuroid species (*cf.* Hyman, 1955; Nichols, 1966).

Because the internal parts of the water vascular system are all small and embedded in ossicle and fibrous connective tissue, they are best studied with histological methods. To locate the site of the madreporite and examine the organization of the entire system, two small specimens (6–7 mm disk diameter) were fixed in Helly's fixative and decalcified for one week in changes of cold (4°C) 5% disodium EDTA. After paraffin embedding, serial frontal sections (from the mouth through the top of the disk) were cut at 10 μm thickness and stained in Delafield's hematoxylin, with eosin and orange G as counter stains.

The extent of seawater entry through the madreporite was evaluated in two sets of experiments. The first of these was actually an unpublished part of a former study dealing with ingestion and hemal transport by *Ophioderma* (Ferguson, 1985). A pair of brittlestars was placed for 8 h in seawater containing 100 μCi^{14}C synthetic algal protein hydrolysate, 375 mg glycine, 990 mg glucose, and 10 mg chloramphenicol per liter. They were then fixed and decalcified in Bouin's solution, embedded in paraffin, sectioned (8 μm), and exposed for up to 6 months to Kodak AR-10 autoradiographic film. In the second set of experiments, fluorescent microbeads were employed. These had been used to study madreporite function of the starfish *Leptasterias hexactis* (see Ferguson, 1990a). Two brittlestars were placed in a dish containing about 100 ml of seawater along with about 0.5 ml of 0.2-μm YG "Fluoresbrite" carboxylate beads (Polysciences, Inc.). After 48 h they were removed, rinsed in seawater, fixed for 24 h in 10% formalin, decalcified for 7 days in cold 5% disodium EDTA, embedded in gelatin, and cut as 20-μm frozen sections. The distribution of the beads was then observed by epifluorescent UV microscopy.

Further tests were conducted to see if madreporite oblation would lead to diminished functions. Specimens (groups of 6) were anesthetized by a brief immersion in 8% MgCl in tap water. The region of the madreporite and stone canal (identified by the pigmentation pattern) was then surgically destroyed and sealed with a small

Figure 7. Section just above Figure 6, showing the primary madreporite pore (PP) in the crevice of the genital bursal slit. A, ampulla.

Figure 8. Section located 40 μm higher than Figure 7. The ampulla (A) is opening into the bottom of the right axial sinus (RAS), opposite to the opening of the stone canal (SC), which contains long flagella. The lower axial organ (AO) can now be seen in the left axial sinus (LAS).

Figure 9. Section located 60 μm above Figure 8, showing typical form of the axial complex in this region. nThe axial organ (AO) here is thin and contains only a few cell nuclei. It is applied closely to the flagellated columnar cells of the stone canal (SC). LAS, left axial sinus; RAS, right axial sinus.

Figure 10. Section about 100 μm higher than Figure 9. At this level the axial complex lies between the perivisceral coelom (PC) and the interradial muscle (IM). The axial organ (AO) gives off a pair of genital hemal strands (GHS), surrounded by extensions of the left axial sinus (LAS). The right axial sinus (RAS) is beginning to expand.

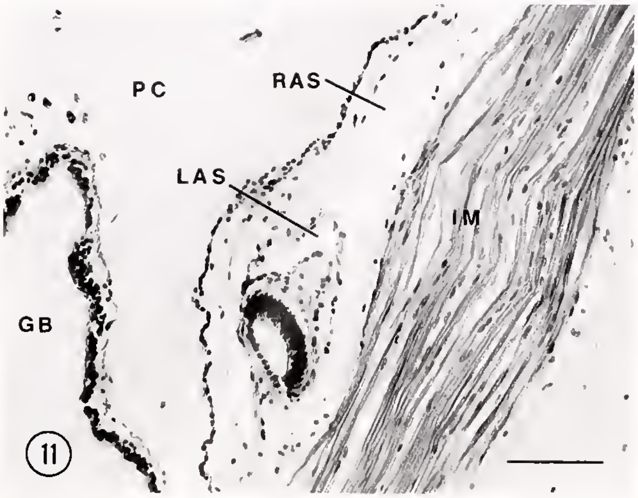
PC
RAS
LAS
IM
GB
⑪

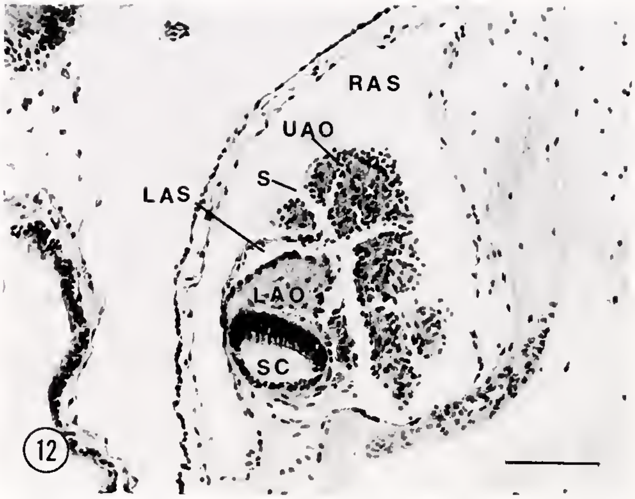
RAS
UAO
S
LAS
LAO
SC
⑫

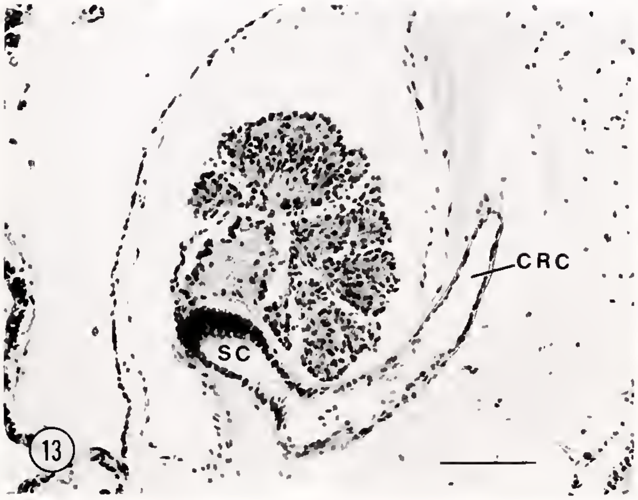

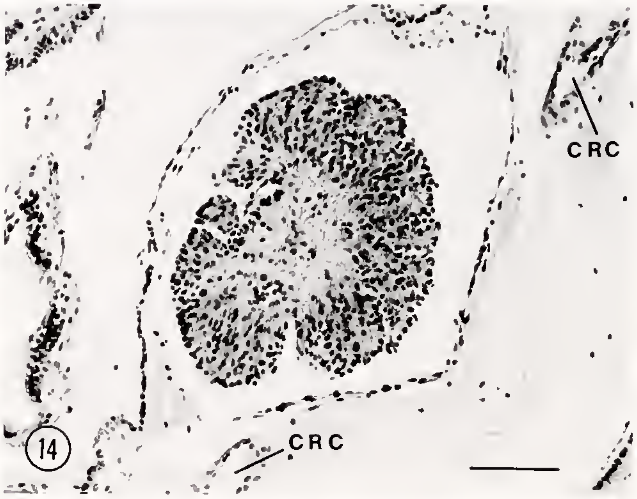

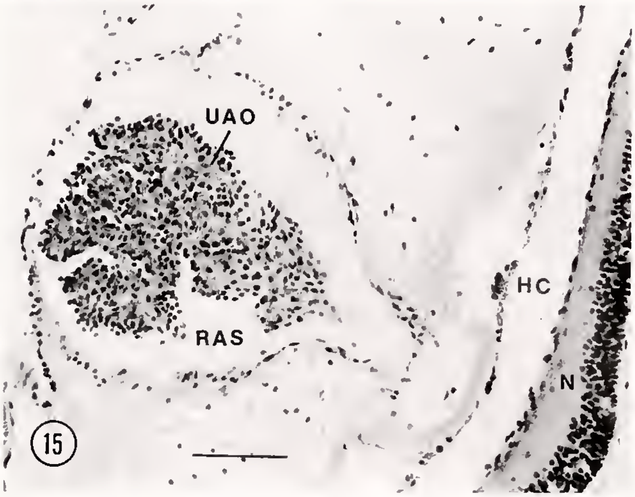
UAO
HC
RAS
N
⑮

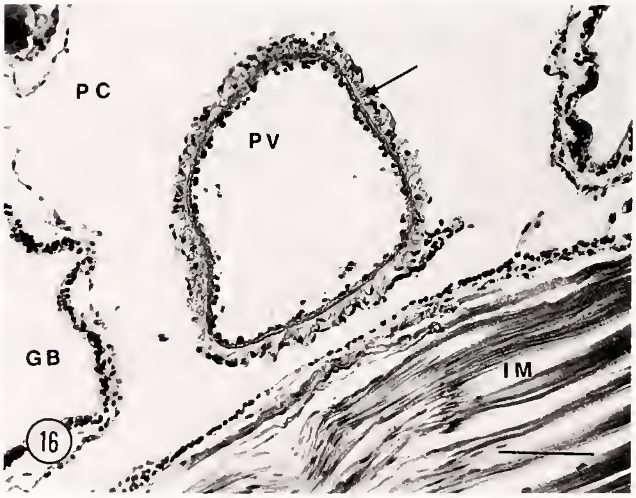

Figure 11. Section about 170 μm higher than Figure 10. In this region the right axial sinus (RAS) has expanded laterally and nearly surrounds the rest of the axial complex. It is separated by only a very thin double peritoneal membrane from the extension of the perivisceral coelom (PC) that accompanies the large interradial muscle (IM). GB, genital bursa; LAS, left axial sinus.

cement plug. Control animals were treated similarly, but a comparable wound was made through an oral shield on the opposite side of the body from the madreporite. All of the animals recovered from the immediate effects of the anesthetic in about an hour. They were then observed for 7 days to see if their tube feet would extend and make normal stepping motions, and if the specimens would right themselves when overturned. The animals also were periodically blotted and weighed to see if weight variations could demonstrate any changes in body fluid content. The cement plugs were usually lost after about the second day as growing tissue sealed the wound. Otherwise, all animals except one, which fractured in two, appeared healthy throughout the study period.

In a final set of observations, groups of three specimens (tests and controls) previously operated on in the above manner were placed in seawater to which sufficient dextran (M.W. 5300) had been added to raise the osmotic concentration 20 mosmoles/kg. The purpose of this approach was to try to counter any osmotic inflow by using an osmolyte that should be neither permeable nor chemically harmful to the integument. The animals were observed and weighed as before until, on the third day, the experiment was terminated.

Results

As previously noted madreporitic pores cannot be seen in intact specimens of *Ophioderma appressum*. Examination of the serial sections revealed that they are small and hidden by the outer edge of one of the oral shields. It was found, however, that their position on the body could usually be determined by the slightly greater amount of pigmentation on that oral shield compared to the others, or if the pigmentation were absent, by the dark shadow of the ampullary complex showing through the translucent oral shield (Figs. 1, 2). From the oral perspective, the pores lie just within the crevice of the central genital bursal slit on the distal left side of the oral shield. Normally, water currents could be seen passing into the peripheral slits of the genital bursae and exiting through the central ones. Thus, while the animals lie on the silty bay bottom, the madreporitic pores are mainly bathed by seawater that has passed through the genital bursae from the presumably cleaner source at the edge of the disk. The water currents within the genital bursae are maintained by cilia as well as by rhythmical expansions and contractions of the whole upper part of the disk.

Structure

The organization of the entire water vascular system is shown in Figure 3, and a more detailed representation of the complex madreporite-axial structure in Figure 4. Figures 5–18 show views of some of the serial sections from which these two diagrams were developed (differences between the two specimens studied were negligible). To avoid confusion in the following descriptions, the photomicrographs have been reversed in printing to compensate for the normal optical inversion of the compound microscope.

The primary opening into the system from the exterior is a 10–15 μm diameter pore located in the folded edge of the central genital bursal slit, just under the lip of the oral shield (Fig. 7). Several undulations occur in the layer of cuboidal cells that line the pore passage; raising the possibility that more pores might develop in specimens more fully grown then the two studied. A second pore of nearly the same diameter is located about 150 μm lateral and slightly lower than the first (Fig. 6). Its duct points towards the first and away from the stone canal. This orientation suggests that the secondary pore may be a rejection pathway, but there is no way of verifying that.

Both pores lead to a discrete lobe of the madreporite "ampulla." This spacious chamber lies just under the surface of the oral shield. It is lined with a distinctive cuboidal epithelium, and it has several regions separated by sharp angles (Figs. 5–8). After making tortuous turns, it opens broadly into the lower end of the "right" axial sinus (Fig.

Figure 12. Section 70 μm above Figure 11. The upper axial organ (UAO) has formed large cellular lobes that hang down into the right axial sinus (RAS). The left axial sinus (LAS) penetrates the axial organ with slit-like spaces (S) that continue through to the surrounding right axial sinus. The lower axial organ (LAO), containing only scattered cell nuclei, still lies close to the stone canal (SC).

Figure 13. Next section above Figure 12. The stone canal (SC) here connects to the circumoral ring canal (CRC). The cellular lobes of the axial organ and the slits between them connecting the two parts of the axial sinus are quite evident.

Figure 14. Section 40 μm above Figure 13, showing the top of the axial organ forming its cellular lobes. Parts of the undulating circumoral ring canal (CRC) are visible on either side of it.

Figure 15. Section 60 μm above Figure 14, showing extensions from the upper axial organ (UAO) and the right axial sinus (RAS) toward the circumoral hyponeural coelom (HC) and the oral hemal ring (not visible). N, nerve ring.

Figure 16. A polian vesicle (PV) lying in the perivisceral coelom (PC) next to an interradial muscle (IM). Note the heavy wall of the vesicle and its elastic membrane (arrow). GB, genital bursa.

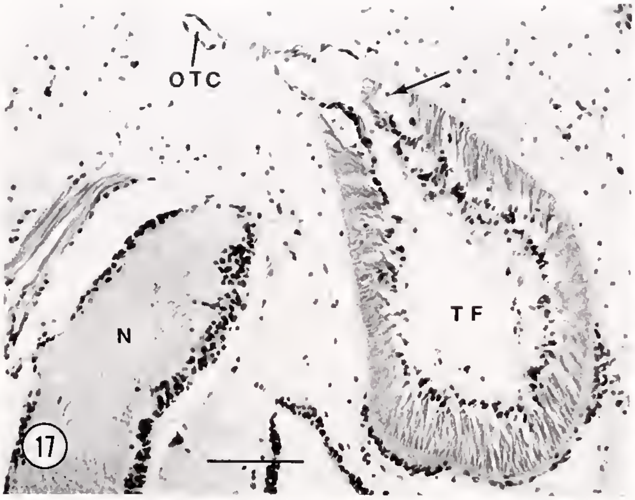

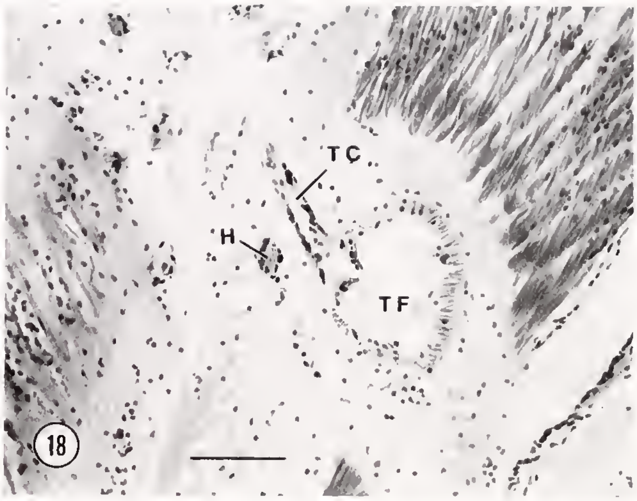

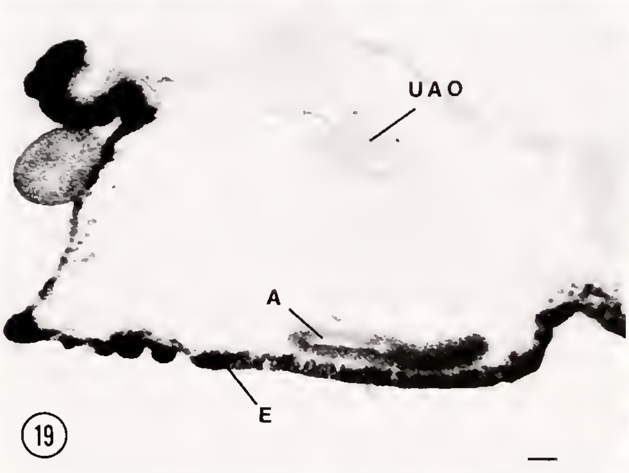

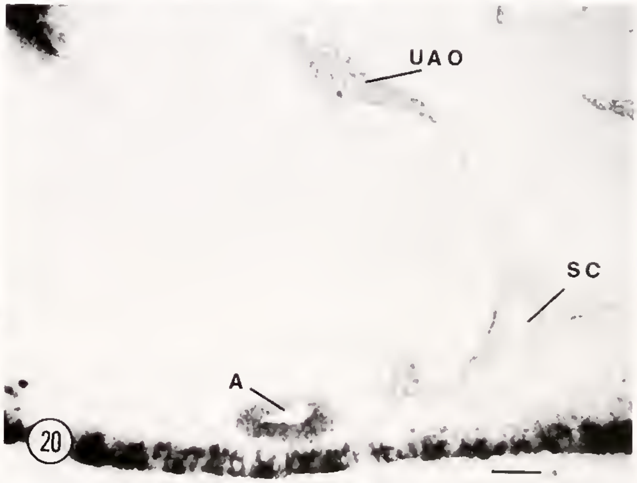

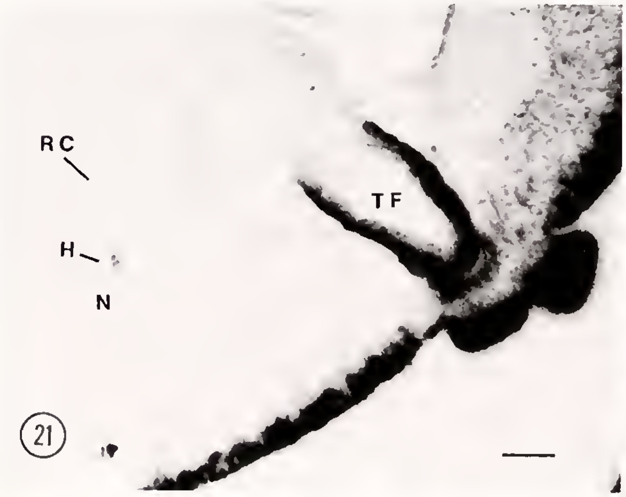

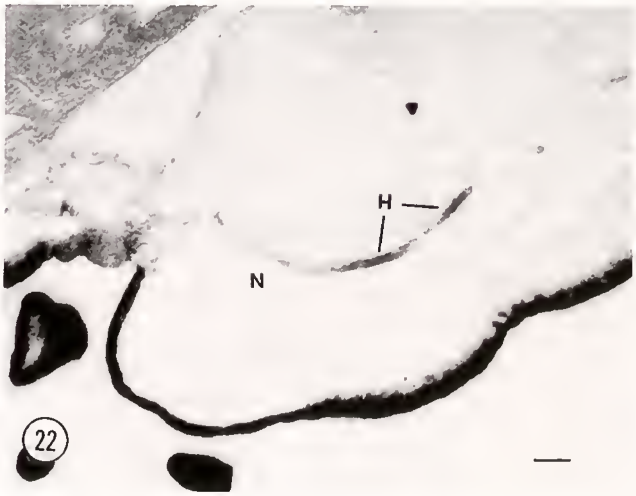

Figure 17. The connection of an oral tube foot (TF) with its canal (OTC) from the circumoral ring canal. There is a muscular restriction at the neck (arrow), but no valve. N, nerve ring.

Figure 18. A transverse canal (TC) in an arm connecting to a tube foot (TF). It has a well-developed valve. A strand of hemal tissue (H) connecting the tube foot to the radial hemal vessel lies nearby.

8). Opposite this opening is the entrance to the lower end of the stone canal (Fig. 8), which thus does not directly connect with the ampulla, but rather with the right axial sinus. On the far side of the stone canal (and attached separately to it) is the "left" axial sinus, a somewhat smaller chamber. It has no opening at the lower end, but contains the axial organ (part of the hemal system), broadly attached to the wall of the stone canal. Both parts of the axial sinus are lined with a thin, simple squamous peritoneum. The cells forming the stone canal stain densely. They are cuboidal adjacent to the right axial sinus, and columnar next to the axial organ. Long flagella extend from the columnar cells and reach nearly across the 15–20 μm width of the somewhat flattened lumen (Figs. 9–12). The close proximity of the hemal tissue to the position of the flagellated cells suggests that hemal fluid might supply the high levels of energy nutrients that must be needed by these cells to produce a current within the stone canal.

The four structures (the two separate parts of the axial sinus, the stone canal, and the axial organ) all rise in a long arch towards the ring complex located high up in the mouth frame. As they rise, they sweep over the large interradial muscles (Figs. 10, 11). About one third of the way up, the axial organ gives off the genital hemal strands surrounded by extensions of the left axial sinus (Fig. 10). These are thought to supply nutritive materials to the gonads (Walker, 1982; Byrne, 1988, 1989). Above that point, the right axial sinus begins to expand and stretch out laterally (Fig. 11). It comes to surround, almost completely, the other three structures, and medially it forms a long thin boundary with the perivisceral coelomic extension that partially encases the interradial muscle. On the distal side, it is separated from the perivisceral coelom by a thin layer of connective tissue (Figs. 11–15).

After the right axial sinus begins its expansion, the left axial sinus splits into a series of slit-like passages that enter the axial organ, which now becomes highly cellular and bulges out like a cauliflower (Figs. 12, 13). These passages then open extensively into the right axial sinus, completing the connection between the two portions of that cavity. At its upper end, the axial organ becomes more solid again (Fig. 14) and gives off an extension to the oral hemal ring (Fig. 15). This extension is surrounded by a portion of the right axial sinus, which appears to connect with the hyponeural (perihemal) compartment that lies adjacent to the nerve ring. This connection is not a spacious opening, but a complex grouping of peritoneal cells and hemal tissues that were difficult to resolve in the preparations studied.

At the same level in which the two parts of the axial sinus join, the top of the stone canal bends over and joins the ring canal that encircles the mouth (Fig. 13). The ring canal, like the other canals of the water vascular system, is lined with squamous cells surrounded by an elastic membrane, fibrous connective tissue, and a few muscle cells (Figs. 13, 14). In the other four interradii, the ring canal gives off canals that open into bulbous polian vesicles. These lie in the perivisceral coelom next to the interradial muscles. Their walls possess a conspicuous elastic membrane like that of the water canals (Fig. 16). In each radius, the ring canal gives off three branches—a radial canal that descends and runs out the arm, and, well to either side of it, canals that connect to upper and lower oral tube feet that lie horizontally between the jaws, within the mouth frame. There are no valves between the oral tube feet and their connecting passages, although sphincter muscles may be able to restrict the openings (Fig. 17).

Along the arms, transverse canals extend in pairs from the radial canal. At the opening of each canal into a tube foot, there is a well-developed valve that holds fluid within the appendage (Fig. 18). Accessory elastic vesicles, such as Woodley (1967) described as extending from the radial canals of *Amphiura filiformis*, were not seen. When the tube foot retracts, it pulls up into a surrounding sheath that is then closed over by two or three flattened spines. When it extends, it slides out of this sheath as a unit and then stretches out as a dexterous tentacle. Reiger and Lombardi (1987) have reported on the ultrastructure of the wall of the tube feet of *Ophioderma brevispinum* and other species.

The radial canals lie in loose connective tissue in the lower portion of the arm. Below them (above the nerve cord) are extensions of the hemal tissues and hyponeural

Figure 19. An autoradiograph of an unstained radial section of the disk of an animal exposed to ^{14}C-amino acids in seawater for 8 h. Note the considerable darkening (radioactivity) in the ampulla (A). A small amount of label, perhaps from ingestion, is in the upper axial organ (UAO). The exposed epidermis (E) is intensely labeled.

Figure 20. Autoradiograph of a section near that of Figure 18. Label is seen in the ampulla (A), lightly in the stone canal (SC), and a bit more intensely in the upper axial organ (UAO).

Figure 21. Autoradiograph of a transverse section of an arm of the same specimen as Figures 19, 20. No radioactivity is seen in the radial canal (RC), but it is found clearly in the radial hemal vessel (H). Some label may be in the lining of the tube foot (TF), but there is strong background from the heavily labeled epidermis. N, radial nerve cord.

Figure 22. Autoradiograph of a radial section of arm base of the same specimen as others. Note the high level of uptake in the radial hemal vessel (H). N, radial nerve cord.

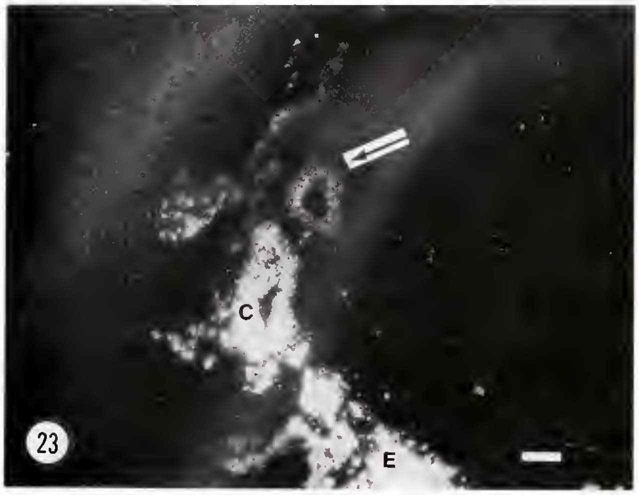

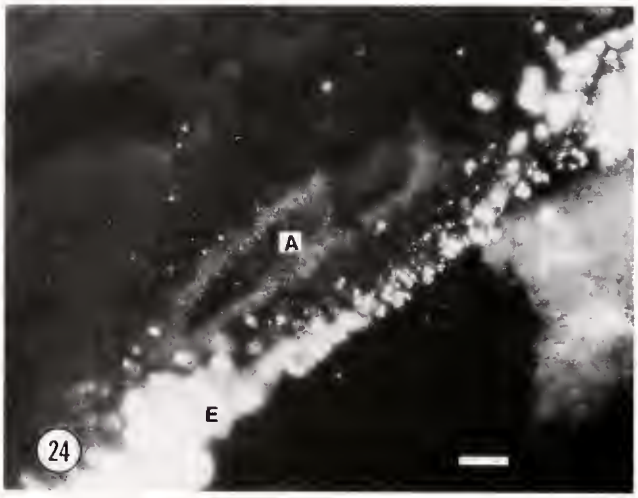

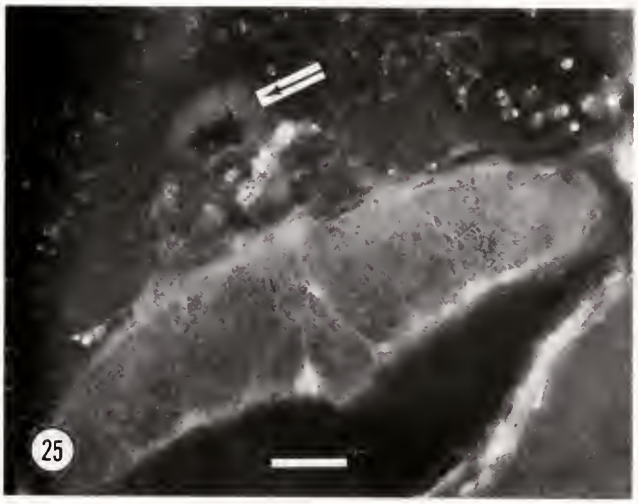

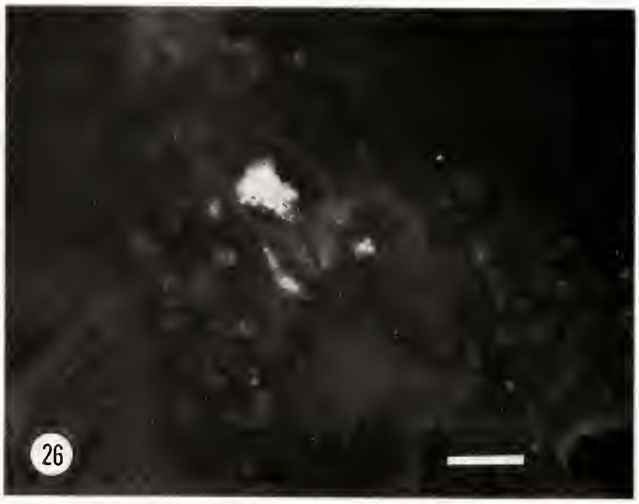

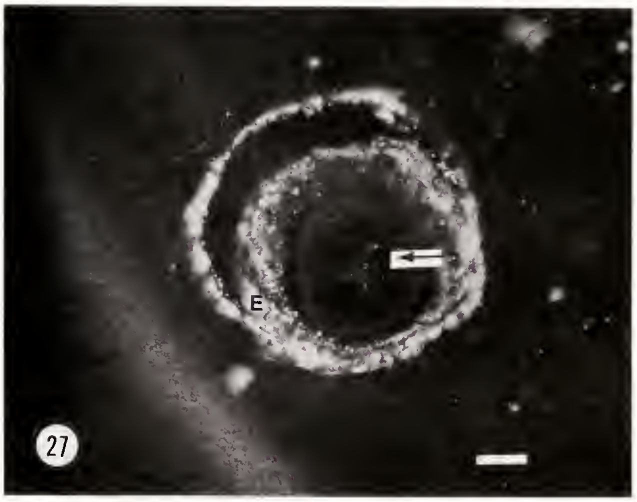

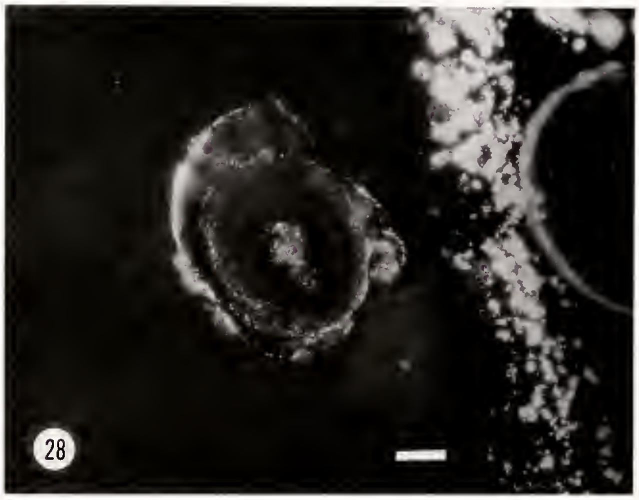

Figure 23. This and the next five figures show epifluorescent views of specimens exposed for 48 h to fluorescent microbeads in seawater. Here a pore canal (C) extends towards the ampulla (arrow). Numerous beads are in the pore canal and epidermis (E); smaller numbers are in the cellular lining of the ampulla.

Figure 24. A view of the ampulla (A) just above the epidermis (E) of the oral shield. A few beads are found in the ampullary chamber and some in its cellular lining.

Table I

Weight variations (g) of Ophioderma appressum *following destruction of the madreporite area, and control animals with a comparable injury to another site*

Specimen	Start	1 day	2 days	3 days	4 days	7 days
Madreporite destroyed						
1	1.14	1.12	1.11	1.07	1.07	1.09
2	1.01	1.01	1.02	1.02	1.07	1.04
3	1.29	1.28	1.29	1.26	1.32	1.28
4	1.49	1.50	1.57	1.50	1.57	1.55
5	0.61	0.61	0.60	0.62	0.66	0.63
6	1.10	1.09	(fragmented)			
Controls						
1	0.98	0.98	0.97	0.97	0.98	0.94
2	1.97	1.96	1.98	1.97	1.99	1.96
3	0.83	0.83	0.87	0.85	0.83	0.83
4	0.58	0.50	0.48	0.50	0.50	0.50
5	0.59	0.56	0.57	0.58	0.58	0.59
6	0.64	0.59	0.58	0.59	0.58	0.59

coelomic spaces. Hemal tissue extends laterally to each tube foot (Fig. 18) where it appears to join, near the valve, with the middle connective tissue layer of the appendage.

Tracer studies

Autoradiographs of animals placed for 8 h in ^{14}C-amino acid mixture showed intense incorporation of the tracer within all exposed epidermal cells including those of the tube feet and their sheaths. This result was expected from earlier studies (Ferguson, 1967; Fontaine and Chia, 1968). The concern here was whether the tracer could demonstrate seawater entry into the water vascular system. That was the case, as notable radioactivity was found in the lining cells of the madreporite ampulla (Figs. 19, 20). This labeling diminished rapidly up the stone canal (Fig. 20). [In animals fed labeled surf clams, radioactivity was found abundantly in the hemal tissues, but not extensively in the water vascular passages (Ferguson, 1985)]. No label was visible within the radial canals, and amounts in the lumen of tube feet were low and not readily distinguished from background (Fig. 21). The radial hemal vessels accumulated considerable amounts of label (Figs. 21, 22), and a small amount was seen in the upper, cellular portion of the axial organ (Fig. 19). These accumulations could have come from an oral route (*cf.* Ferguson, 1985).

Fluorescent microbeads were employed as a means of more directly following the flow of seawater into the water vascular passages. Unlike the labeled amino acids, these beads should not easily penetrate membranes or become rapidly depleted by cells as they take up nutrients from the fluid flowing by them. However, the entry of beads into the body must overcome the animal's natural defenses against foreign particles. A very large number of beads was used in the medium with the expectation that a proportion of them would get through if bulk fluids were indeed entering the body through the pores. After 48 h of exposure, fluorescent beads were found in many water vascular passages, but not in great abundance (Figs. 23–28). Beads were seen moderately distributed within the lining of the ampulla (Figs. 23, 24). Some were found free in the radial canals (Fig. 25) and in the tube feet (Fig. 27). More commonly, beads were found engorged in clumps of coelomocytes. These often accumulated in the lateral canals just before the valves (Fig. 26), or within the lumen of tube feet (Fig. 28). Many tube feet, however, could be seen without any beads within them. Coelomocytes bearing many beads collected in the hemal tissues of the arms, especially between the radial hemal vessels and the tube feet, and beneath the radial canals (Fig. 25). A few clumps of coelomocytes containing beads were found in the perivisceral coelomic spaces of the arms. All exposed epidermal areas were filled with beads, including the areas just outside the madreporitic pores (Fig. 23) and the sheaths of the tube feet (Figs. 27, 28).

Experiments

Because the tracer studies showed that seawater must enter the madreporitic pores, at least in small quantities, a study was made to see whether that uptake was essential to the animals. It was found that surgical obliteration of the madreporite, ampulla, and lower stone

Figure 25. Transverse section through the ambulacrum of an arm. Several discrete microbeads lie in the radial canal (arrow). Below the arrow is part of a hemal strand extending towards a tube foot. It contains many coelomocytes engorged with the beads. Most of the other fluorescence is natural.

Figure 26. A clump of coelomocytes engorged with beads lying in a transverse canal just before the valve. Two or three coelomocytes containing beads are nearby, within the tube foot.

Figure 27. Transverse section through a tube foot lying in its sheath. A number of the fluorescent beads are seen in the lumen (arrow). The epidermal tissue (E) of the tube foot and its sheath contains many beads that were taken up directly from the seawater.

Figure 28. Transverse section through another tube foot. This one contains, in its lumen, many free beads as well as coelomocytes engorged with beads.

Table II

Weight variations (g) of Ophioderma appressum *in seawater raised 20 mosmoles/kg with dextran (5300 M.W.); specimens with madreporites destroyed and control animals with a comparable injury to another site*

Specimen	Start	4 hours	1 day	2 days	3 days
Madreporite destroyed					
1	1.09	1.04	1.05	1.06	1.12*
2	1.28	1.24	1.23	1.23	1.28*
3	0.65	0.61	0.60	0.60	0.69*
Controls					
1	0.69	0.66	0.64	0.64	0.65*
2	0.45	0.43	0.41	0.40	0.42*
3	1.09	1.05	1.01	1.02	1.04*

* Animals abnormal—arched up and rigid.

canal had very little effect on tube foot function for at least a week. For the first two or three days, tube foot activity declined somewhat, especially in the oral tube feet, but there was no consistent difference in observed behavior when compared to controls. All tube feet could extend and bend, and when animals were overturned, righting movements involving the arms were unaffected. The number of tube feet active at any one moment may have diminished, but with the diversity of individual behavioral responses demonstrated by the specimens, that could not be quantified. Nor were there any consistent variations in body weights that would reflect fluid volume changes (Table I). Both test animals and controls varied a few percent from day to day, but not significantly.

If tube foot inflation and body fluid content are maintained by osmotic elevation, as by a potassium ion pump in the tube feet (*cf.* Prusch, 1977), the mechanism could be sensitive to elevated colloidal osmotic pressure in the medium. To test this possibility, animals with obliterated madreporites, and controls, were placed in dishes of seawater in which the osmotic levels had been elevated a modest amount (20 mosmoles/kg) with dextran (5300 M.W.). In both groups the immediate effect was a small loss in weight (2 to 4%) over the first few hours and then stability within a normal range (Table II). For the next two days there was no diminishment of tube foot function or other observable effects. On the third day, animals in both groups showed some arching rigidity of their arms, rather similar to that seen previously in animals placed in ionically altered seawaters. At that point the experiment was terminated.

Discussion

This study has shown that *Ophioderma* has a complex water vascular system, but one in which the passages from the exterior (the madreporite pores) appear to be of minor importance compared to provisions for internal recirculation of fluid *via* the axial sinus and its extensions. Although it was shown that seawater routinely enters the pores, it must do so only in small quantities. Under the laboratory conditions employed, this uptake seemed to provide little advantage. Perhaps under the stresses of the natural environment uptake may be important in some circumstances, but such conditions have yet to be discovered. Fluid might also exit the pores when pressures in the system become too great.

In contrast to the minimal madreporite of *Ophioderma*, the madreporites of asteroids have many pores and complex arrangements of ciliated gutters to keep them free of suspended foreign particles (Ferguson and Walker, 1991). In one study on *Echinaster graminicola*, seawater uptake through the madreporite was equal to about 5.5% of the animal's body weight per day; and more than half of it went into replacing the general body fluid (Ferguson, 1989). The two small pores of *Ophioderma*, located very inconspicuously at the edge of a genital bursal slit, clearly cannot allow much seawater into the system. Reduced inflow would alleviate contamination from the silty environment in which the animals normally live. Further, the genital bursa might protect the pores from silt, as the asteroid gutters do. Likewise, the complex form of the ampulla probably plays a sanitary role, because many beads were seen taken up by its cells.

The stone canal itself is fairly well developed. It is smaller in diameter than those of asteroids, and it does not have the internal ridges that make a larger diameter tube more efficient as a ciliary pump. It also does not have as much bony ossicle material, needed by a larger structure for strength. However, for the much smaller body size of *Ophioderma*, the stone canal seems proportionately scaled. Its lumen is somewhat flattened, which allows the flagellated cells to be very efficient in sweeping fluid through the canal.

As noted, the stone canal does not connect directly with the ampulla, but rather with the right axial sinus. If fluid flows down this sinus into the stone canal, as it appears to, it would be drawn from three sources: (1) the left axial sinus (and the genital perihemal vessels), through the slits of the axial organ; (2) the circumoral hyponeural (perihemal) coelom (and its connections with the radial hyponeural coelomic spaces of the arms), over the surface of the axial organ; and (3) through the delicate peritoneal membranes separating much of the axial sinus from the perivisceral coelom. I conclude, then, that most of the fluid pumped by the stone canal is coelomic—not seawater flowing in through the two madreporitic pores. As the fluid flows over the axial organ it is probably purified, and it probably gives up nutritive materials to form hemal fluid. [The transport of nutritive material by hemal systems was previously described (Ferguson, 1984, 1985)].

The fluid pumped by the stone canal then passes through the water vascular canals, and most of it eventually travels out the arms. Some is diverted to the oral tube feet and the polian vesicles, which among other functions, probably collectively serve as a general reservoir and pressure stabilizer for the system. In the arms, the fluid passes through the valves into the tube feet only when the hydrostatic pressure of the system surpasses that maintained in the appendages. The tube feet also might be kept inflated by osmotic inflow. Based on the observations on other animals by Robertson (1949), Binyon (1976b), Prusch (1977), and Ferguson (1990b), the tube feet likely contain a higher osmotic pressure than the surrounding seawater. In the present experiments, however, the tube feet failed to collapse when the external osmotic pressure was increased with dextran, though by the third day the treatment appeared to produce pervasive detrimental effects on the bodies of the animals. Although the water vascular vessels can deliver fluid to the tube feet, they may be equally valuable in providing a more general circulatory flow by permeation to all the tissues of the lower arms, and return *via* the hyponeural spaces. Additional circulation is achieved by the perivisceral coelomic passages.

When compared with the body cavities of asteroids, the perivisceral coelom of *Ophioderma* is not large. Within the arms it consists mostly of canals that expand into larger spaces between the vertebral-like ossicles. Asteroid perivisceral fluid is kept under low, but positive, hydrostatic pressure (Ferguson, 1988). That cannot be the case in *Ophioderma*. Distinct "breathing" motions of the aboral disk alternately stretch and compress the coelomic space, and that movement pumps seawater in and out of the genital bursae. The ventilation must produce negative coelomic pressures that should lead to the accumulation of fluid in the coelomic space by filtration. Pressure from pumping by cilia in the genital bursae would have the same effect. [Net negative coelomic pressures have recently been described in sea urchins by Ellers and Telford (1992), but these are produced by a different mechanism.] It appears, then, that *Ophioderma* has little need to take up seawater through its madreporite either to support its tube feet or to maintain its perivisceral coelomic fluid, and it has a limited ability to do so. Asteroids, on the other hand, often do tend to lose large amounts of fluid from their bodies and must replace it. For them, the madreporite system (together with the Tiedemann's bodies) is a much more important and well-developed mechanism.

Literature Cited

Binyon, J. 1964. On the mode of functioning of the water vascular system of *Asterias rubens* L. *J. Mar. Biol. Assoc. U. K.* **44:** 577–588.

Binyon, J. 1966. Salinity tolerance and ionic regulation. Pp. 359–378 in *Physiology of Echinodermata*, R. A. Boolootian, ed. Wiley-Interscience, New York.

Binyon, J. 1976a. The permeability of the podial wall to water and potassium ions. *J. Mar. Biol. Assoc. U. K.* **56:** 639–647.

Binyon, J. 1976b. The effects of reduced salinity upon the starfish *Asterias rubens* L. together with a special consideration of the integument and its permeability to water. *Thalassia Jugoslav.* **12:** 15–20.

Binyon, J. 1980. Osmotic and hydrostatic permeability of the integument of the starfish *Asterias rubens*. *J. Mar. Biol. Assoc. U. K.* **60:** 627–630.

Binyon, J. 1984. A re-appraisal of the fluid loss resulting from the operation of the water vascular system of the starfish, *Asterias rubens*. *J. Mar. Biol. Assoc. U. K.* **64:** 726.

Byrne, M. 1988. Evidence for endocytotic incorporation of nutrients from the hemal sinus by the oocytes of the brittlestar *Ophiolepis paucispina*. Pp. 557–563 in *Echinoderm Biology: Proceedings of the Sixth International Echinoderm Conference, Victoria/23–28 August 1987*, R. D. Burke, P. Mladenov, P. Lambert and R. L. Parsley, eds. Balkema, Rotterdam.

Byrne, M. 1989. Ultrastructure of the ovary and oogenesis in the ovoviparous ophiuroid *Ophiolepis paucispina* (Echinodermata). *Biol. Bull.* **176:** 79–95.

Ellers, O., and M. Telford 1992. Causes and consequences of fluctuating coelomic pressure in sea urchins. *Biol. Bull.* **182:** 424–434.

Ferguson, J. C. 1967. An autoradiographic study of the utilization of free exogenous amino acids by starfishes. *Biol. Bull.* **133:** 317–329.

Ferguson, J. C. 1984. Translocative functions of the enigmatic organs of starfish—the axial organ, hemal vessels, Tiedemann's bodies, and rectal caeca: an autoradiographic study. *Biol. Bull.* **166:** 140–155.

Ferguson, J. C. 1985. Hemal transport of ingested nutrients by the ophiuroid, *Ophioderma brevispinum*. Pp. 663–626 in *Proceedings of the Fifth International Echinoderm Conference Galway/24–29 September 1984*, D. F. Keegan and B. D. S. O'Connor, eds. Balkema, Rotterdam.

Ferguson, J. C. 1988. Madreporite and anus function in fluid volume regulation of a starfish (*Echinaster graminicola*). Pp. 603–609 in *Echinoderm Biology: Proceedings of the Sixth International Echinoderm Conference, Victoria/23–28 August 1987*, R. D. Burke, P. Mladenov, P. Lambert and R. L. Parsley, eds. Balkema, Rotterdam.

Ferguson, J. C. 1989. Rate of water admission through the madreporite of a starfish. *J. Exp. Biol.* **145:** 147–156.

Ferguson, J. C. 1990a. Hyperosmotic properties of the fluids of the perivisceral coelom and watervascular system of starfish kept under stable conditions. *Comp. Physiol. Biochem.* **95A:** 245–248.

Ferguson, J. C. 1990b. Sea water inflow through the madreporite and internal body regions of a starfish (*Leptasterias hexactis*) as demonstrated with fluorescent microbeads. *J. Exp. Zool.* **255:** 262–271.

Ferguson, J. C. 1992. The function of the madreporite system in body fluid volume maintenance by an intertidal starfish, *Pisaster ochraceus*. *Biol. Bull.* **183:** 482–489.

Ferguson, J. C. 1994. Madreporite inflow of seawater to maintain body fluids in five species of starfish. *Proceedings of the 8th International Echinoderms Conference, Dijon, France*. D. Bruno and A. Guille, eds. Balkema, Rotterdam (*in press*).

Ferguson, J. C., and C. W. Walker. 1991. Cytology and function of the madreporite systems of the starfish *Henricia sanguinolenta* and *Asterias vulgaris. J. Morphol.* **210:** 1–11.

Fontaine, A. R., and F. S. Chia. 1968. Echinoderms: an autoradiographic study of the assimilation of dissolved organic molecules. *Science* **161:** 1153–1155.

Hyman, L. 1955. *The Invertebrates. IV. Echinodermata.* McGraw-Hill, New York.

Nichols, D. 1966. Functional morphology of the water-vascular system. Pp. 219–244 in *Physiology of Echinodermata,* R. A. Boolootian, ed. Wiley-Interscience, New York.

Prusch, R. D. 1977. Solute secretion by the tube foot epithelium in the starfish *Asterias forbesi. J. Exp. Biol.* **68:** 35–43.

Reiger, R. M., and J. Lombardi. 1987. Ultrastructure of coelomic lining in echinoderm podia: significance for concepts in evolution of muscle and peritoneal cells. *Zoomorphology* **107:** 191–208.

Robertson, J. D. 1949. Ionic regulation in some marine invertebrates. *J. Exp. Biol.* **26:** 182–200.

Walker, C. W. 1982. Nutrition of gametes. Pp. 449–468 in *Echinoderm Nutrition.* M. Jangoux and J. M. Lawrence, eds. Balkema, Rotterdam.

Woodley, J. D. 1967. Problems in the ophiuroid water-vascular system. *Symp. Zool. Soc. Lond.* **20:** 75–104.

CONTENTS

No. 1, February/March 1995

RESEARCH NOTES

Fluck, Richard A.
Responses of the medaka fish egg (*Oryzias latipes*) to the photolysis of microinjected nitrophenyl-EGTA, a photolabile calcium chelator 1

Wittenberg, Jonathan B., and Jeffrey L. Stein
Hemoglobin in the symbiont-harboring gill of the marine gastropod *Alvinichoncha hessleri* 5

BIOMINERALIZATION

Giles, R., S. Manne, S. Mann, D. E. Morse, G. D. Stucky, and P. K. Hansma
Inorganic overgrowth of aragonite on molluscan nacre examined by atomic force microscopy . . . 8

DEVELOPMENT AND REPRODUCTION

Bates, William R.
Direct development in the ascidian *Molgula retortiformis* (Verrill, 1871) 16

Chang, Wen-Teh, and Robert J. Lauzon
Isolation of biologically functional RNA during programmed death of a colonial ascidian 23

Hamel, Jean-François, and Annie Mercier
Prespawning behavior, spawning, and development of the brooding starfish *Leptasterias polaris* 32

ECOLOGY AND EVOLUTION

Mead, Kristina S., and Mark W. Denny
The effects of hydrodynamic shear stress on fertilization and early development of the purple sea urchin *Strongylocentrotus purpuratus* 46

Thorn, Kurt, Robert M. Cerrato, and Mark L. Rivers
Elemental distributions in marine bivalve shells as measured by synchrotron x-ray fluorescence . . . 57

Gherardi, Francesca, and Paul M. Cassidy
Life history patterns of *Discorsopagurus schmitti*, a hermit crab inhabiting polychaete tubes 68

NEUROBIOLOGY AND BEHAVIOR

Carlberg, Mats, Karin Alfredsson, Sven-Olle Nielsen, and Peter A. V. Anderson
Taurine-like immunoreactivity in the motor nerve net of the jellyfish *Cyanea capillata* 78

Miklósi, Ádám, József Haller, and Vilmos Csányi
The influence of opponent-related and outcome-related memory on repeated aggressive encounters in the paradise fish (*Macropodus opercularis*) 83

Young, Craig M., and Roland H. Emson
Rapid arm movements in stalked crinoids 89

PHYSIOLOGY

Ferguson, John C.
The structure and mode of function of the water vascular system of a brittlestar, *Ophioderma apressum* 98

Volume 188 Number 2

THE BIOLOGICAL BULLETIN

[illegible] Institution
APR [illegible] 4 1995
[illegible]

APRIL, 1995

Published by the Marine Biological Laboratory

THE
BIOLOGICAL BULLETIN

PUBLISHED BY
THE MARINE BIOLOGICAL LABORATORY

Associate Editors

PETER A. V. ANDERSON, The Whitney Laboratory, University of Florida
WILLIAM D. COHEN, Hunter College, City University of New York
DAVID EPEL, Hopkins Marine Station, Stanford University
J. MALCOLM SHICK, University of Maine, Orono

Editorial Board

PETER B. ARMSTRONG, University of California, Davis
THOMAS H. DIETZ, Louisiana State University
DAPHNE GAIL FAUTIN, University of Kansas
WILLIAM F. GILLY, Hopkins Marine Station, Stanford University
ROGER T. HANLON, Marine Biomedical Institute, University of Texas Medical Branch
MICHAEL LABARBERA, University of Chicago
CHARLES B. METZ, University of Miami
K. RANGA RAO, University of West Florida
BARUCH RINKEVICH, Israel Oceanographic & Limnological Research Ltd.
RICHARD STRATHMANN, Friday Harbor Laboratories, University of Washington
STEVEN VOGEL, Duke University
J. HERBERT WAITE, University of Delaware
SARAH ANN WOODIN, University of South Carolina
RICHARD K. ZIMMER-FAUST, University of South Carolina

Editor: MICHAEL J. GREENBERG, The Whitney Laboratory, University of Florida
Managing Editor: PAMELA L. CLAPP, Marine Biological Laboratory

APRIL, 1995

Printed and Issued by
LANCASTER PRESS, Inc.
3575 HEMPLAND ROAD
LANCASTER, PA

THE BIOLOGICAL BULLETIN

THE BIOLOGICAL BULLETIN is published six times a year by the Marine Biological Laboratory, MBL Street, Woods Hole, Massachusetts 02543.

Subscriptions and similar matter should be addressed to Subscription Manager, THE BIOLOGICAL BULLETIN, Marine Biological Laboratory, Woods Hole, Massachusetts 02543. Single numbers, $37.50. Subscription per volume (three issues), $92.50 ($185.00 per year for six issues).

Communications relative to manuscripts should be sent to Michael J. Greenberg, Editor-in-Chief, or Pamela L. Clapp, Managing Editor, at the Marine Biological Laboratory, Woods Hole, Massachusetts 02543. Telephone: (508) 548-3705, ext. 428. FAX: 508-540-6902. E-mail: pclapp@hoh.mbl.edu.

THE BIOLOGICAL BULLETIN is indexed in bibliographic services including *Index Medicus* and MEDLINE, *Chemical Abstracts*, and *Current Contents*.

Printed on acid free paper,
effective with Volume 180, Issue 1, 1991.

POSTMASTER: Send address changes to THE BIOLOGICAL BULLETIN, Marine Biological Laboratory,
Woods Hole, MA 02543.

Copyright © 1995, by the Marine Biological Laboratory

Second-class postage paid at Woods Hole, MA, and additional mailing offices.
ISSN 0006-3185

INSTRUCTIONS TO AUTHORS

The Biological Bulletin accepts outstanding original research reports of general interest to biologists throughout the world. Papers are usually of intermediate length (10–40 manuscript pages). A limited number of solicited review papers may be accepted after formal review. A paper will usually appear within four months after its acceptance.

Very short, especially topical papers (less than 9 manuscript pages including tables, figures, and bibliography) will be published in a separate section entitled "Research Notes." A Research Note in *The Biological Bulletin* follows the format of similar notes in *Nature*. It should open with a summary paragraph of 150 to 200 words comprising the introduction and the conclusions. The rest of the text should continue on without subheadings, and there should be no more than 30 references. References should be referred to in the text by number, and listed in the Literature Cited section in the order that they appear in the text. Unlike references in *Nature*, references in the Research Notes section should conform in punctuation and arrangement to the style of recent issues of *The Biological Bulletin*. Materials and Methods should be incorporated into appropriate figure legends. See the article by Lohmann *et al.* (October 1990, Vol. **179:** 214–218) for sample style. A Research Note will usually appear within two months after its acceptance.

The Editorial Board requests that regular manuscripts conform to the requirements set below; those manuscripts that do not conform will be returned to authors for correction before review.

1. ***Manuscripts.*** Manuscripts, including figures, should be submitted in triplicate. (Xerox copies of photographs are not acceptable for review purposes.) The submission letter accompanying the manuscript should include a telephone number, a FAX number, and (if possible) an E-mail address for the corresponding author. The original manuscript must be typed in no smaller than 12 pitch or 10 point, using double spacing (*including* figure legends, footnotes, bibliography, etc.) on one side of 16- or 20-lb. bond paper, 8½ by 11 inches. Please, no right justification. Manuscripts should be proofread carefully and errors corrected legibly in black ink. Pages should be numbered consecutively. Margins on all sides should be at least 1 inch (2.5 cm). Manuscripts should conform to the *Council of Biology Editors Style Manual*, 5th Edition (Council of Biology Editors, 1983) and to American spelling. Unusual abbreviations should be kept to a minimum and should be spelled out on first reference as well as defined in a footnote on the title page. Manuscripts should be divided into the following components: Title page, Abstract (of no more than 200 words), Introduction, Materials and Methods, Results, Discussion, Acknowledgments, Literature Cited, Tables, and Figure Legends. In addition, authors should supply a list of words and phrases under which the article should be indexed.

2. ***Title page.*** The title page consists of a condensed title or running head of no more than 35 letters and spaces, the manuscript title, authors' names and appropriate addresses, and footnotes listing present addresses, acknowledgments or contribution numbers, and explanation of unusual abbreviations.

3. ***Figures.*** The dimensions of the printed page, 7 by 9 inches, should be kept in mind in preparing figures for publication. We recommend that figures be about 1½ times the linear dimensions of the final printing desired, and that the ratio of the largest to the smallest letter or number and of the thickest to the thinnest line not exceed 1:1.5. Explanatory matter generally should be included in legends, although axes should always be identified on the illustration itself. Figures should be prepared for reproduction as either line cuts or halftones. Figures to be reproduced as line cuts should be unmounted glossy photographic reproductions or drawn in black ink on white paper, good-quality tracing cloth or plastic, or blue-lined coordinate paper. Those to be reproduced as halftones should be mounted on board, with both designating numbers or letters and scale bars affixed directly to the figures. All figures should be numbered

in consecutive order, with no distinction between text and plate figures. The author's name and an arrow indicating orientation should appear on the reverse side of all figures.

4. ***Tables, footnotes, figure legends, etc.*** Authors should follow the style in a recent issue of *The Biological Bulletin* in preparing table headings, figure legends, and the like. Because of the high cost of setting tabular material in type, authors are asked to limit such material as much as possible. Tables, with their headings and footnotes, should be typed on separate sheets, numbered with consecutive Roman numerals, and placed after the Literature Cited. Figure legends should contain enough information to make the figure intelligible separate from the text. Legends should be typed double spaced, with consecutive Arabic numbers, on a separate sheet at the end of the paper. Footnotes should be limited to authors' current addresses, acknowledgments or contribution numbers, and explanation of unusual abbreviations. All such footnotes should appear on the title page. Footnotes are not normally permitted in the body of the text.

5. ***Literature cited.*** In the text, literature should be cited by the Harvard system, with papers by more than two authors cited as Jones *et al.*, 1980. Personal communications and material in preparation or in press should be cited in the text only, with author's initials and institutions, unless the material has been formally accepted and a volume number can be supplied. The list of references following the text should be headed Literature Cited, and must be typed double spaced on separate pages, conforming in punctuation and arrangement to the style of recent issues of *The Biological Bulletin.* Citations should include complete titles and inclusive pagination. Journal abbreviations should normally follow those of the U. S. A. Standards Institute (USASI), as adopted by BIOLOGICAL ABSTRACTS and CHEMICAL ABSTRACTS, with the minor differences set out below. The most generally useful list of biological journal titles is that published each year by BIOLOGICAL ABSTRACTS (BIOSIS List of Serials; the most recent issue). Foreign authors, and others who are accustomed to using THE WORLD LIST OF SCIENTIFIC PERIODICALS, may find a booklet published by the Biological Council of the U.K. (obtainable from the Institute of Biology, 41 Queen's Gate, London, S.W.7, England, U.K.) useful, since it sets out the WORLD LIST abbreviations for most biological journals with notes of the USASI abbreviations where these differ. CHEMICAL ABSTRACTS publishes quarterly supplements of additional abbreviations. The following points of reference style for THE BIOLOGICAL BULLETIN differ from USASI (or modified WORLD LIST) usage:

A. Journal abbreviations, and book titles, all underlined (for *italics*)

B. All components of abbreviations with initial capitals (not as European usage in WORLD LIST *e.g., J Cell Comp. Physiol.* NOT *J. cell. comp. Physiol.*)

C. *All* abbreviated components must be followed by a period, whole word components *must not* (*i.e., J. Cancer Res.*)

D. Space between all components (*e.g., J. Cell. Comp. Physiol.*, not *J Cell.Comp.Physiol.*)

E. Unusual words in journal titles should be spelled out in full, rather than employing new abbreviations invented by the author. For example, use *Rit Vísindafjélags Islendinga* without abbreviation.

F. All single word journal titles in full (*e.g., Veliger, Ecology, Brain*).

G. The order of abbreviated components should be the same as the word order of the complete title (*i.e., Proc.* and *Trans.* placed where they appear, not transposed as in some BIOLOGICAL ABSTRACTS listings).

H. A few well-known international journals in their preferred forms rather than WORLD LIST or USASI usage (*e.g., Nature, Science, Evolution* NOT *Nature, Lond., Science, N.Y.; Evolution, Lancaster, Pa.*)

6. ***Reprints, page proofs, and charges.*** Authors receive their first 100 reprints (without covers) free of charge. Additional reprints may be ordered at time of publication and normally will be delivered about two to three months after the issue date. Authors (or delegates for foreign authors) will receive page proofs of articles shortly before publication. They will be charged the current cost of printers' time for corrections to these (other than corrections of printers' or editors' errors). Other than these charges for authors' alterations, *The Biological Bulletin* does not have page charges.

Reference: *Biol. Bull.* **188:** 111–116. (April, 1995)

Odor Plumes and Animal Navigation in Turbulent Water Flow: A Field Study

RICHARD K. ZIMMER-FAUST[1,2,3], CHRISTOPHER M. FINELLI[2,3],
N. DEAN PENTCHEFF[1,3], AND DAVID S. WETHEY[1,2,3]

[1]*Department of Biological Sciences,* [2]*Marine Science Program, and* [3]*Belle W. Baruch Institute for Marine Biology and Coastal Research, University of South Carolina,*
Columbia, South Carolina 29208

Turbulence causes chemical stimuli to be highly variable in time and space; hence the study of animal orientation in odor plumes presents a formidable challenge. Through combined chemical and physical measurements, we characterized the transport of attractant released by clam prey in a turbulent aquatic environment. Concurrently, we quantified the locomotory responses of predatory crabs successfully searching for sources of clam attractant. Our results demonstrate that both rheotaxis and chemotaxis are necessary for successful orientation. Perception of chemical cues causes crabs to move in the upstream direction, but feedback from attractant distributions directly regulates movement across-stream in the plume. Orientation mechanisms used by crabs differ from those employed by flying insects, the only other system in which navigation relative to odor plumes has been coupled with fluid dynamics. Insects respond to odors by moving upstream, but they do not use chemical distributions to determine across-stream direction, whereas crabs do. Turbulent eddy diffusivities in crab habitats are 100 to 1000 times lower than those of terrestrial grasslands and forests occupied by insects. Insects must respond to plumes consisting of highly dispersed, tiny filaments or parcels of odor. Crabs rely more heavily on spatial aspects of chemical stimulus distributions because their fluid dynamic environment creates a more stable plume structure, thus permitting chemotaxis.

The ability to detect chemical stimuli is nearly universal among animals. Chemical signals are generated by liberating stimulus molecules into a fluid, where they are transported by advection and diffusion (eddy and molecular) until detected and acted upon by a biological sensor. Thus the physical process governing chemical transport has a profound impact on the nature and success of chemosensory-mediated behavior (1, 2, 3, 4, 5, 6). Except at microscopic scales, turbulence causes a stimulus pattern whose concentration is highly variable in time and space (3, 4, 5, 6, 7). As a result, the study of chemoreceptive behavior presents a formidable challenge. It demands simultaneous measurements of stimulus release, fluid dynamics, and animal responses to perceived chemical cues. Until now, however, these determinations have not been combined in a single field study.

Received 8 December 1994; accepted 25 January 1995.

We experimentally establish a direct link between the transport of chemical stimuli and animal navigation in a natural, turbulent flow environment. Attraction of predatory blue crabs (*Callinectes sapidus*) to odor released by clam prey (*Mercenaria mercenaria*) was investigated. The mechanisms directing predator to prey were identified for crabs foraging naturally in estuarine tidal creeks, where water flows unidirectionally for hours at a time. These creeks were shallow enough to permit direct, noninvasive observations of crab locomotory behavior.

Experiments were conducted in the North Inlet Estuary, near Georgetown, South Carolina, USA (32° 20′ N, 79° 15′ W). Flow records were obtained with an electromagnetic flow meter (Marsh-McBirney 523) equipped with a two-dimensional sensor (1 cm diam), mounted on a flat base, and submerged in the tidal creek. The base was positioned flush with the sandy bottom, and the sensor was placed 5 cm above the substrate. Sensor height was chosen to match the elevation of a typical, adult crab body. A data logger (Campbell CR10) was used to record both horizontal and vertical flow velocities continuously measured by the sensor at 1 Hz, between 26 June and 8

August 1993. Horizontal flow (downstream advection) typically ranged from 0 cm/s at slack tides, to 30 cm/s during peak ebb and flood tides. We applied the eddy correlation method to calculate shear velocities, at 1-min intervals, using the correlation between the horizontal and vertical flow velocities (8, 9). Shear velocity (u_*) is a measure of the strength and correlation of turbulent fluctuations in flow speed near the substratum. Finally, we determined the coefficients of turbulent mixing as the products of shear velocity, sensor height above the substratum, and Von Karman's constant (9). These mixing coefficients were remarkably low, ranging from 0.5 to 1.5 cm^2/s. They indicated that across-stream mixing occurred very slowly in the tidal creek even though water flow was turbulent.

The dynamics of odor plumes were characterized by measuring the transport of fluorescent dye (sodium fluorescein) and an electrochemical (dopamine) following their combined release from a point source. Input concentrations of fluorescein and dopamine were 1.0 g/liter and 2 mmol/l, respectively, with ascorbic acid added to the mixture at 20 mmol/l as an antioxidant. The mixture was introduced through polyethylene tubing (0.5 mm ID) at 6 ml/min.

Fluorescein provided a visual marker, and fluorometric determinations were used to establish the time-averaged distributions of dye at downstream and at across-stream sites, relative to the release point. Water samples were collected (at 1 ml/s) simultaneously over 1-min intervals by syringes placed at each of 18 to 30 sites per trial. These sites were distributed in a grid, with six sites placed across-stream (0, 2, 4, 6, 8, 10 cm distant from the plume midline) at three to five locations downstream of the release point (5, 25, 50, and in some trials, 100 and 275 cm distant from the source). The bell-shaped distribution of fluorescein concentration with gradual decay downstream (Fig. 1) is what a Gaussian plume model would predict (Pearson's product-moment correlation: $r^2 \geq 0.95$; $P < 0.001$; all replicate plume measurements). Concentration dropped sharply at the plume's visible lateral edges (Fig. 1).

Fluorometric measurements also provided an alternative method of calculating the mixing coefficient for comparison with determinations made using the electromagnetic flow meter. Temporal changes in the across-stream variance in fluorescein concentration were used to estimate the mixing coefficient (9). Results from the two methods matched well. For example, estimates based on fluorometric determinations ranged from 0.5 to 1.2 cm^2/s during a time when estimates of 0.5 to 0.8 cm^2/s were made from electromagnetic flow meter records.

When measured at fast temporal scales, chemical stimuli in odor plumes are patchily distributed due to turbulence. Mean concentrations and time-averaged distributions of fluorescein dye, therefore, may not be indicative of the information available for crabs attempting to orient towards an odor source (3, 4, 5, 6, 7). Because arthropod chemoreceptors detect intermittent (or pulsed) chemical stimuli applied at a maximum frequency of 4–10 Hz (10, 11), we employed carbon fiber microelectrodes (150 μm diam) and a computer recording system (MedSystems Corp. IVEC-10) to sample dopamine at 10 Hz (12). Electrode recordings were made at the fluorescein sampling sites (see above). Turbulent mixing caused the concentration of dopamine sampled downstream of the source to fluctuate strongly in time and space. Bursts of highly concentrated chemical passed over the sensor, alternating with periods of low or zero concentration (Fig. 1). The plume's lateral edge, as defined by our high-speed dopamine measurements, was positioned identically relative to the edge detected both by our time-averaged fluorescein measurements and by our visual observations. This lateral edge, separating clean from chemical-laden water, was very narrow (2–4 cm wide) compared to the body size of an adult crab (10–15 cm carapace width). Thus a steep concentration gradient was found across-stream, but not downstream of chemical release.

We previously demonstrated that some crabs search for and find intact live clams, and that these crabs are responding to odor plumes created by the excurrent release of attractant metabolites at low concentration (13). Once a clam is found, however, it is chipped open by a crab and attractants are released to form a plume of high concentration. High-concentration plumes then immediately attract other crabs to the predation site. Hence, depending on the situation, crabs may be exposed either to low or high attractant concentrations, and crabs respond effectively in each case.

Concurrently with hydrodynamic and chemical measurements, we assessed crab orientation in odor plumes. Our field studies focused on plumes characteristic of chipped clams. We chose to work with chipped clams because high attractant concentrations would better ensure an effective stimulus through the broad range of hydrodynamic conditions encountered by crabs in the field. Stimulus plumes (dyed with fluorescein for visibility) were created, either presenting a chipped clam or introducing clam mantle fluid (membrane filtered to 0.22 μm) at a rate mimicking its release from a chipped clam. Each stimulus plume was always paired with a control plume that delivered fluorescein in filtered seawater. Both stimulus and control solutions were introduced at 6 ml/min, with inputs separated by 60 cm across-stream.

Free amino acid compositions of effluent leaking from chipped clams (n = 8 clams assayed), mantle fluid of intact live clams (n = 8 clams), and homogenized clam flesh (n = 7 clams) were all determined using a Beckman 6300 System Gold high-performance liquid chromato-

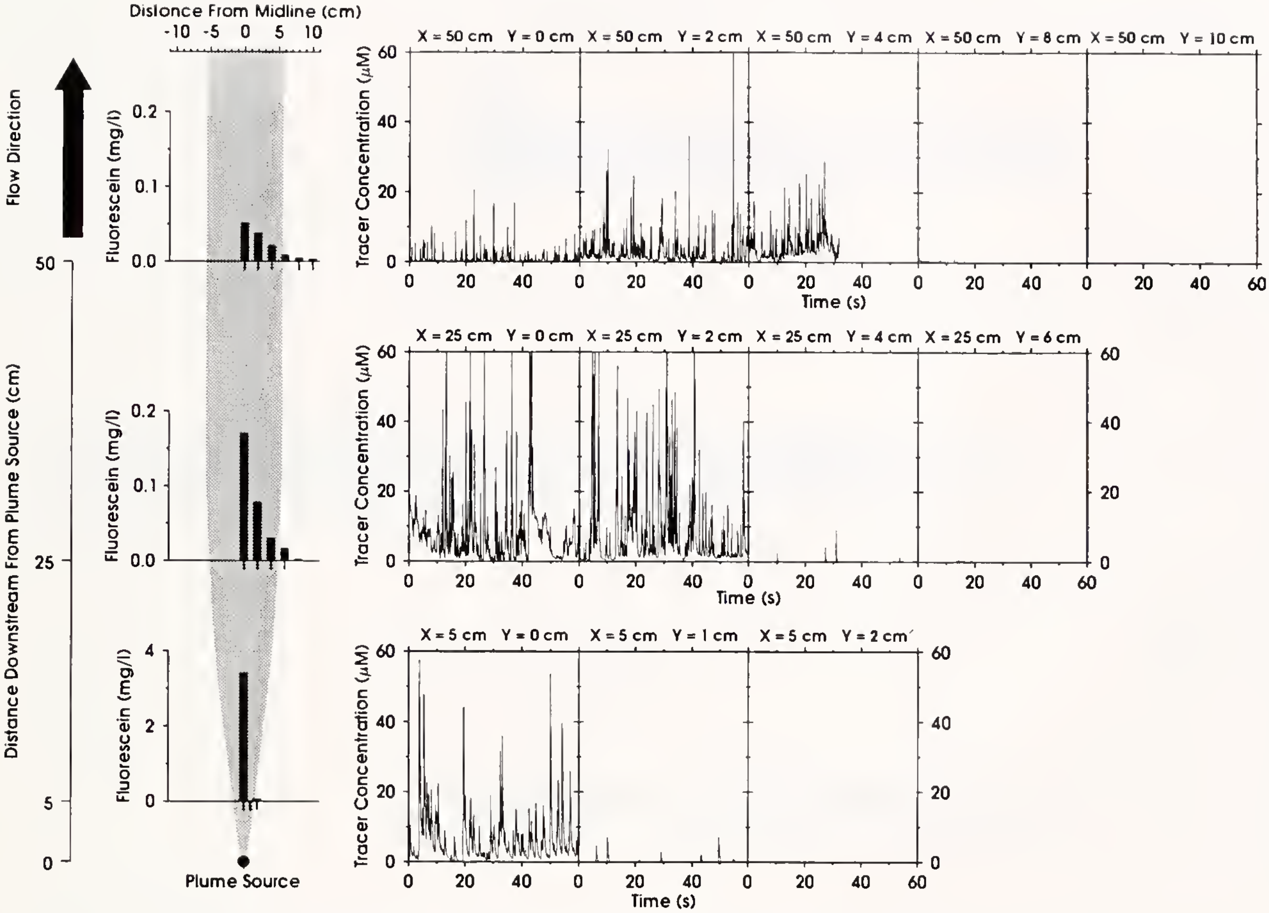

Figure 1. Representative concentration distributions downstream from a point source in a tidal creek. Histograms represent fluorescein concentrations (mg/l) in samples collected at 5 cm (bottom row), 25 cm (middle row), and 50 cm (top row) downstream from the source and at 0, 2, 4, 6, 8, and 10 cm from the midline of the plume. Note the scale difference between fluorescein concentrations at downstream locations. The visible region of the fluorescein plume at each position is denoted by the shading. Panels to the right of the histograms represent 60-s records of instantaneous fluctuations in dopamine (tracer) concentration, measured at 10 Hz with a carbon fiber electrode, at locations where the fluorescein was sampled. The left-most panel in each row is the sample from the midline of the plume, and successive panels are samples from 2, 4, 8, and 10 cm from the midline (see tick marks on histogram axes for sampling sites). Highly concentrated bursts of dopamine were common in all samples taken within the visible portion of the plume.

graph with a sodium ion-exchange column (4-mm ID × 120 mm; Beckman) for separation. In this system, amino acids were monitored spectrophotometrically after post-column reaction with ninhydrin. Compositions of clam effluent and mantle fluid were almost identical (Pearson's product-moment correlation: $r^2 = 0.998$; $P < 0.001$; $n = 18$ amino acids chromatographed), indicating that mantle fluid was the source of effluent material. Because taurine was by far the most abundant amino acid in both clam effluent and mantle fluid (accounting for >50% of the total amino acid composition), we used it as a marker to measure the rates of fluid release from chipped clams. In the laboratory, clams ($n = 12$) of various sizes were chipped by using a metal rod to deliver a single firm blow to the lateral shell margin. The resulting chip was similar in size and shape to one produced by a blue crab as it begins to feed. Each chipped clam was then placed individually into a separate beaker of artificial seawater. The beakers were stirred, and they were maintained at the same temperature and salinity as seawater in the tidal creek from which clams were collected. Artificial seawater was sampled from each beaker before placement of the clam, and again at 30- to 60-s intervals for 15 min after placement; HPLC analysis of this seawater indicated that taurine (and mantle fluid) release was constant throughout the trial period. The relation between taurine release rate and clam size was then used to scale our delivery of mantle fluid in field experiments, simulating the

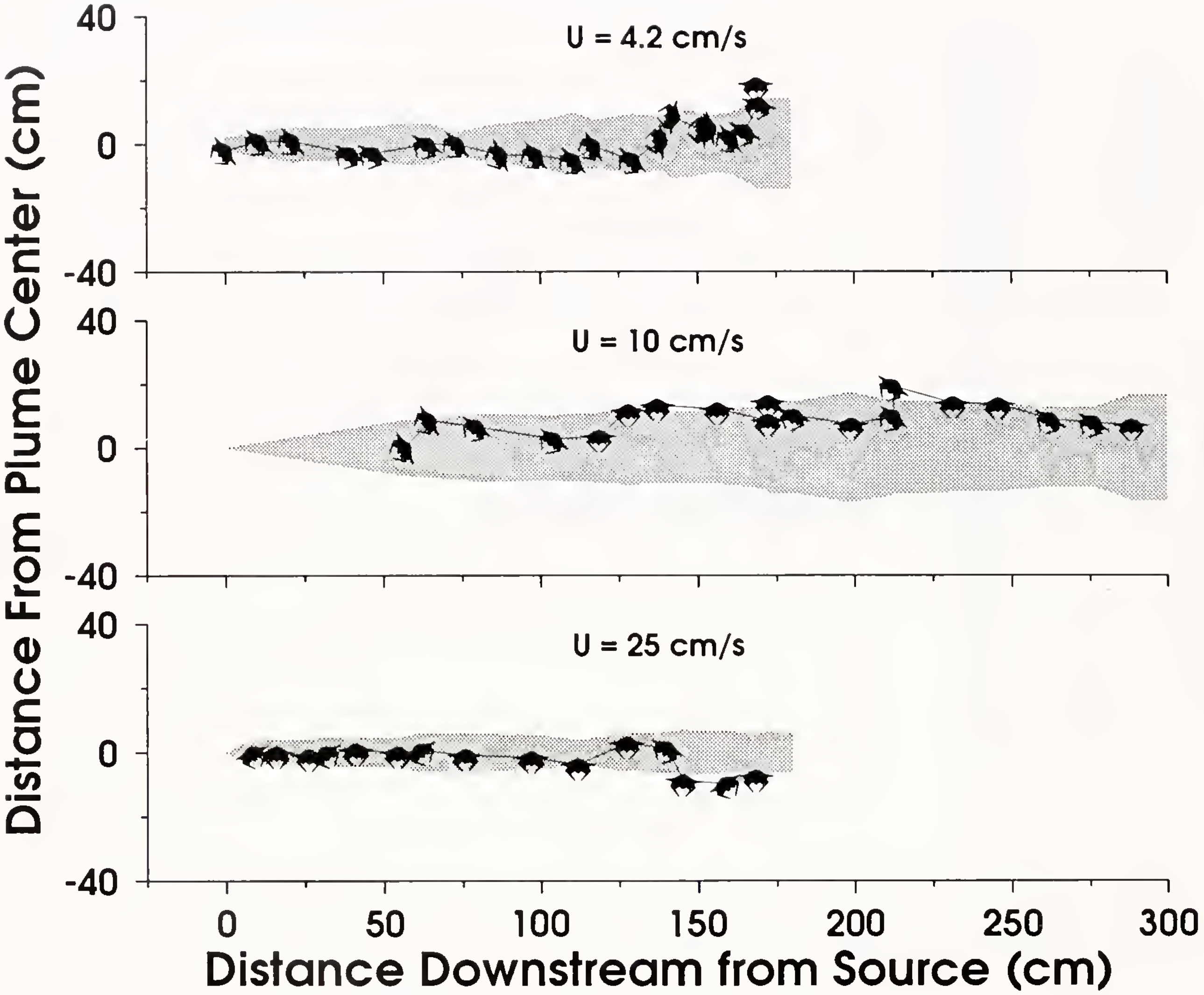

Figure 2. Representative tracks of crabs following odor plumes. The crab symbols represent the positions and orientations of individuals at 1-s intervals as they moved upstream toward the odor source. Naturally foraging crabs normally walk sideways as well as forward. The visible region of the fluorescein/odor plume is noted by the shading. The water velocity (*U*) at 5 cm above the bottom was 4.2 cm/s (top panel), 10 cm/s (center panel), and 25 cm/s (bottom panel). Distances downstream and across stream are in centimeters.

fluid input from an intermediate-sized chipped clam (6 cm total shell length).

Quantitative observations of foraging crabs were made noninvasively with a video camera (Sony TR81) mounted 4 m above the tidal creek. Video records of crabs responding to plumes were made during ebbing tides. A 3-m field of view was dictated by the resolution of the video camera and the size of the crabs (10–15 cm carapace width), whose positions could not be reliably quantified in wider field images. A scale bar in the field of view was employed to measure distance and to correct for distortion due to perspective. In the laboratory, plume edges and crab positions at 1-s intervals were traced onto acetate sheets from video playbacks to a monitor. Both crab location, in relation to the plume edge, and crab locomotory kinematics were measured (Fig. 2).

Crab responses to the plumes were dramatic and unambiguous: 29 crabs contacted the control plumes, but only 4 of these crabs walked upstream towards the input source. The near absence of positive responses to control plumes demonstrated a lack of attractant effect by fluorescein dye. In comparison, after contacting stimulus plumes, 68 of 80 crabs walked upstream to the input source. Crabs turned upstream within 1.5 s (±0.3 SD) of contacting an odor plume. Percentages of crabs responding positively to plumes from either chipped clams or mantle fluid were nearly identical, being 86% (n = 52 crabs) or 82% (n = 28 crabs), respectively (G-test for homogeneity: $G^2 = 0.270$; df = 1; $P > 0.50$). Our results demonstrate an odor-conditioned rheotaxis that orients crabs upstream. Previously, we reached an identical conclusion for blue crabs foraging in a laboratory flume. Crabs walked upstream to find intact live clams in flowing water, but they oriented indiscriminately and searched unsuccessfully for clams in still water (13).

Oriented movements by crabs lateral to water flow are controlled by chemotaxis. As crabs walked upstream towards an attractant source, they frequently approached the lateral edges of the plume. When crabs did reach the edge, they nearly always turned directly back to the plume (50 of 61 turns; *G*-test for goodness-of-fit, 1:1 hypothesized ratio, $G^2 = 14.97$; df = 1; $P < 0.001$), without exhibiting either casting or zigzagging (Fig. 2). Lateral movements were initiated as crabs began to exit a plume and partially contacted clean water. Fluorescein did not act as a visual cue, because crabs displayed identical oriented responses when tests were conducted in the dark (under infrared illumination) and without fluorescein (13, and in prep.). It took, on average, less than 1 s (0.8 ± 0.2 s SD) for crabs to renew upstream walking after they had begun moving laterally towards the plume midline. Remarkably, we did not observe walking speeds to change significantly as crabs moved closer to attractant sources (analysis of covariance: $F = 0.60$; df = 4,237; $P = 0.66$; walking speed: 12.8 ± 0.4 cm/s SD), and we found no significant correlation between walking speed and water flow velocity (Pearson's product-moment correlation: $r^2 = 0.037$; df = 1,64; $P = 0.12$). We hypothesize that crabs perceive clam attractant as a binary cue (present/absent), both in their upstream movement and in their across-stream walking. Because the plume edges were very sharp, when crabs partially exited the plume, some pereiopods (legs or claws) were outside the plume while others remained inside. A comparison of simultaneous chemosensory inputs from the appendages inside and outside the plume would presumably allow the crabs to determine the correct direction and return to the plume. This binary response would lead crabs to locations of higher concentration of clam attractant.

Orientation mechanisms used by crabs in upstream movement are similar to those of flying insects. However, crabs differ from insects in their across-stream response. Insects provide the only other system in which navigation relative to odor plumes has been coupled with fluid dynamics. Flying insects locate a source of chemical attractant by moving upwind upon contacting a filamentous trace of attractant odor (14, 15). After several seconds of flying in clean air, insects shift to casting (regular reversals of flight directed across-stream) until contact with another odor trace causes a return to upwind flight (16). Flying insects, therefore, do not use chemical concentration gradients to determine either their upwind or across-wind directions (16, 17, 18). The use of chemotaxis may be impractical in their environment, where complex fluid dynamics do not permit stable zones of high attractant concentrations to exist. Crabs in contrast, consistently turn back into the attractant plume rather than zigzagging after losing the plume signal.

The difference between estuarine tidal creek flow and atmospheric winds may explain why blue crabs and insects use contrasting mechanisms for successful navigation towards an odor source. The crop fields and forests used as experimental models for insect flight are hydraulically rough, with high advection. Eddy diffusivities in insect habitats are 100 to 1000 times greater than those we recorded in estuarine tidal creeks (19, 20). Higher diffusivities yield plumes consisting of tiny, highly dispersed filaments or parcels of odor. Wind direction changes frequently, causing plumes to meander (3, 6). The dispersal pattern of odor, coupled with the relatively fast flight speed of insects, means that a flying insect has little chance to detect more than the occasional pulse of passing odor. Casting, zigzagging, and rapid behavioral modulation in response to fine-scale changes in odor concentration may be strategies appropriate for situations in which the entire plume meanders away from the animal.

In contrast, the flow environment of estuarine tidal creeks is markedly less turbulent, yielding relatively stable, straight, and sharply delineated odor plumes. Plumes cannot meander substantially, because flow is constrained by water depth and by the sides of the creeks. A stable plume structure permits direct binary comparisons of chemical concentration inside and outside the plume, to guide movement lateral to flow. The more direct plume-following behavior and across-stream chemotactic responses shown by crabs reflect a strategy appropriate to the plume structure characteristic of their environment. Mechanisms of plume-following behavior, therefore, arise in response to chemical stimulus distributions, as determined by the specific fluid dynamic environments in which animals must naturally navigate.

Acknowledgments

We thank Dr. D. M. Allen, Director of the USC Baruch Field Laboratory, for providing laboratory space and logistical support for field work. Dr. Y. Ishikawa, USC Institute for Biological Research and Technology, performed amino acid composition analyses. We also thank Dr. S. A. Woodin, whose comments on earlier drafts greatly improved this manuscript. This research was sponsored by the National Science Foundation (IBN 92-22225) and the University of South Carolina Research and Productive Scholarship Fund.

Literature Cited

1. **Wright, R. H. 1958.** The olfactory guidance of flying insects. *Can. Entomol* **90:** 81–89.

2. **Bossert, W. H., and E. O. Wilson. 1963.** The analysis of olfactory communication among animals. *J. Theor. Biol.* **5:** 443–469.
3. **Murlis, J., and C. D. Jones. 1981.** Fine-scale structure of odour plumes in relation to insect orientation to distant pheromone and other attractant sources. *Physiol. Entomol.* **6:** 71–86.
4. **Elkinton, J. S., R. T. Cardé, and C. J. Mason. 1984.** Evaluation of time-average dispersion models for estimating pheromone concentration in a deciduous forest. *J. Chem. Ecol.* **10:** 1081–1108.
5. **Zimmer-Faust, R. K., J. M. Stanfill, and S. B. Collard, III. 1988.** A fast, multi-channel fluorometer for investigating aquatic chemoreception and odor trails. *Limnol. Oceanogr.* **33:** 1586–1595.
6. **Murlis, J., J. S. Elkinton, and R. T. Cardé. 1992.** Odor plumes and how insects use them. *Annu. Rev. Entomol.* **37:** 505–532.
7. **Moore, P. A., and J. Atema. 1991.** Spatial information in the three-dimensional fine structure of an aquatic odor plume. *Biol. Bull.* **181:** 408–418.
8. **Schlichting, H. 1979.** *Boundary Layer Theory.* McGraw-Hill, New York. 486 pp.
9. **Denny, M. W. 1988.** *Biology and Mechanics of the Wave-Swept Environment.* Princeton University Press, Princeton, NJ. 329 pp.
10. **Kaissling, K. E., C. Z. Straussfeld, and E. Rumbo. 1987.** Adaptation processes in insect olfactory receptors: mechanisms and behavioral significance. *Annals N. Y. Acad. Sci.* **510:** 104–112.
11. **Gomez, G., R. Voigt, and J. Atema. 1994.** Frequency filter properties of lobster chemoreceptor cells determined with high-resolution stimulus measurement. *J. Comp. Physiol. A* **174:** 803–811.
12. **Moore, P. A., G. A. Gerhardt, and J. Atema. 1989.** High resolution spatio-temporal analysis of aquatic chemical signals using microelectrochemical electrodes. *Chem. Senses* **14:** 829–840.
13. **Weissburg, M. J., and R. K. Zimmer-Faust. 1993.** Life and death in moving fluids: hydrodynamic effects on chemosensory-mediated predation. *Ecology* **74:** 1428–1443.
14. **Mafra-Neto, A., and R. T. Cardé. 1994.** Fine-scale structure of pheromone plumes modulates upwind orientation of flying moths. *Nature* **369:** 142–144.
15. **Vickers, N. J., and T. C. Baker. 1992.** Male *Heliothis virescens* maintain upwind flight in response to experimentally pulsed filaments of their sex pheromone (Lepidoptera: Nocturidae). *J. Insect Behav.* **5:** 669–687.
16. **Baker, T. C. 1986.** Pheromone-modulated movements of flying moths. Pp. 39–48, in *Mechanisms of Insect Olfaction*, T. L. Payne, M. C. Birch, and C. E. Kennedy, eds. Clarendon Press, Oxford.
17. **David, C. T., J. S. Kennedy, and A. R. Ludlow. 1983.** Finding of a sex pheromone source by gypsy moths released in the field. *Nature* **303:** 804–806.
18. **Arbas, E. A., M. A. Willis, and R. Kanazaki. 1993.** Organization of goal-oriented locomotion: pheromone-modulated flight behavior of moths. Pp. 159–198, in *Biological Neural Networks in Invertebrate Neuroethology and Robotics*, R. D. Beer, R. E. Ritzmann, and T. McKenna, eds. Academic Press, New York.
19. **Shaw, R. H., J. Tavangar, and D. P. Ward. 1983.** Structure of the Reynolds stress in a canopy layer. *J. Climate Appl. Meteorol.* **22:** 1922–1931.
20. **Arya, S. P. 1988.** *Introduction to Micrometeorology.* Academic Press, San Diego. 303 pp.

Reference: *Biol. Bull.* **188:** 117–119. (April, 1995)

Evidence for Selection Against Heterozygotes: Post-Settlement Excess of Allozyme Homozygosity in a Cohort of the Chilean Oyster, *Ostrea chilensis* Philippi, 1845

J. E. TORO AND A. M. VERGARA

Instituto de Biología Marina, Universidad Austral de Chile, Casilla 567, Valdivia, Chile

Reports of heterozygote deficiencies in electrophoretic surveys carried out in marine bivalves abound in the literature (1–6), but the mechanism or mechanisms producing this phenomenon have not been well defined. We report that, in the Chilean oyster (Ostrea chilensis), *heterozygote deficiencies in a cohort obtained by mass spawning in the laboratory are not randomly distributed in time among genotypes. The eggs of the Chilean oyster are internally fertilized, and the larvae, which are brooded within the mantle cavity, have limited dispersal capabilities because of their extremely short pelagic stage (7). These features could allow mechanisms such as inbreeding or Wahlund effect to produce heterozygote deficiencies. However, we observed no significant heterozygote deficiencies in juveniles at 6 months of age; instead allozyme heterozygosity decreased over time. Inbreeding, Wahlund effect, aneuploidy, and null alleles are unlikely to be main causes of the heterozygosity deficiency in this cohort; if they were, the deficiency should be evident from the juvenile stage and would not necessarily increase over time (2, 5, 8, 9, 10). We suggest that selection against heterozygotes is the most probable cause of the increasing degree of heterozygote deficiency with age in this cohort of* O. chilensis, *a proposition that accords with data for other marine bivalve species (2, 4, 11).*

Populations of marine bivalves exhibit deficiency of allozyme heterozygotes. This deficiency has been demonstrated in laboratory studies of mussels and clams (2, 3), in studies using wild populations (8, 12) of *Mytilus edulis*, and in several studies of oysters *(Crassostrea virginica)* (13–15). In the Chilean oyster *(Ostrea chilensis)* a heterozygote deficiency was found in the carbonic anhydrase (CA) locus from a southern population (Melinka, 43°53′S) (1). The time at which heterozygote deficiency first appears in the population can help distinguish causative mechanisms (16). In laboratory studies with mussels, an overall significant deficiency of heterozygotes was found at the juvenile stage but not at the spat stage (4).

In the present study, we used a cohort of *O. chilensis* settled on artificial collectors in the Quempillén hatchery, Ancud, Chiloé (45°52′S, 73°46′W). The parental stock was a cohort of *O. chilensis* collected during December 1987 from a natural spatfall in the wild population at Quempillén estuary. The Chilean oyster becomes sexually mature at the beginning of the second year of life with a shell length of about 27 mm (7). After three years of growth under uniform conditions, 800 randomly chosen oysters were mass spawned in the laboratory. The temperature and salinity used in the experiment were within the range of those in the natural environment (10–18°C and 27–32 ppt). Although the use of mass spawning prevents one from knowing how many individuals contribute genes to the offspring obtained, the female contribution can be estimated by keeping track of the number in each brood of eyed larvae. Fecundity in *O. chilensis* ranges between 10,000 and 115,000, with an average of 60,000 (7). The number of larvae released, more than 8.2×10^6, indicates that at least 130 females contributed larvae. This number of females may be an underestimation because some of the eyed larvae released set within 5 min (7); thus this cohort cannot be treated as a product of restricted matings.

From an initial population size of 4050 randomly tagged juveniles grown at the Hueihue location (41°58′S,

Received 10 May 1994; accepted 26 January 1995.

Table I

Heterozygote frequency and D *values for four loci at three stages of the life cycle of* Ostrea chilensis *(6, 18, and 30 months of age)*

Age (months)	Locus	O.H.	E.H.	*D*	(*P*)
6	LAP	0.419	0.398	0.053	NS
	GPI	0.581	0.458	0.283	*
	CA	0.645	0.617	0.046	NS
	PGM	0.155	0.167	−0.072	NS
18	LAP	0.338	0.457	−0.260	*
	GPI	0.373	0.389	−0.041	NS
	CA	0.514	0.607	−0.153	*
	PGM	0.247	0.383	−0.355	*
30	LAP	0.447	0.591	−0.243	*
	GPI	0.268	0.292	−0.082	NS
	CA	0.408	0.631	−0.353	*
	PGM	0.231	0.374	−0.382	*

Genotype frequencies were investigated using random samples of 150 oysters taken from each class interval. Each locus was tested individually, using the χ^2 goodness of fit test with *D* as an index of heterozygote deviation. Starch gel electrophoresis was used (18, 19) to score the loci leucine aminopeptidase (LAP, EC 3.4.1.1), glucose phosphate isomerase (GPI, EC 5.3.1.9), carbonic anhydrase (AC, EC 4.2.1.1), and phosphoglucomutase (PGM, EC 2.5.7.1).

O.H. = proportion of observed heterozygotes; E.H. = proportion of expected heterozygotes; *D* = heterozygote deviation index defined as (O.H. − E.H.)/E.H.; (*P*) = probability of the χ^2 goodness of fit to the Hardy Weinberg model (NS = nonsignificant; * = significant at alpha = 0.05).

73°30′W), the percentages of mortality at ages from 6 to 18 and 18 to 30 months were 25% and 17% respectively. At each class interval, 150 oysters were sampled without replacement. Neither significant deficiencies nor an excess of heterozygotes was found in three of four loci in the 6-month-old oysters; the exception was glucose phosphate isomerase (GPI), which showed an excess of heterozygotes (Table I). At 18 months, significant deficiencies of heterozygotes were found at LAP ($D = -0.260$), CA ($D = -0.150$), and PGM ($D = -0.355$) (Table I). In adult oysters (30 months), negative values of *D* were present at three of four analyzed loci, presenting significant values at LAP ($D = -0.243$), AC ($D = -0.353$), and PGM ($D = -0.382$) (Table I). The data showed that between the age of 6 and 18 months, three out of four loci studied showed a genotype-dependent mortality. This differential mortality produces a significant overall deficiency of heterozygosity in the cohort. One of the loci studied (GPI) showed an excess of heterozygotes at 6 months and neither an excess nor a deficiency of heterozygotes at 18 and 30 months; this result agrees with other studies carried out on this locus in natural populations of bivalve molluscs (1, 17, 18). High fecundity, external fertilization, and extensive larval dispersal—characteristics common to most of the bivalves molluscs—make it unlikely that inbreeding or the Wahlund effect could be the main cause of heterozygote deficiencies. The reproductive features of *O. chilensis* favor mechanisms such as inbreeding or Wahlund effect to act and produce heterozygote deficiencies. However, in accord with data for other marine bivalve species, we suggest that selection against heterozygotes is the most probable cause of the heterozygote deficiencies (2, 4, 11), because the deficiency is not evident at the juvenile stage but increases over time. We discarded inbreeding (which would affect the whole genome), Wahlund effect, aneuploidy, and null alleles as possible causes for the heterozygosity deficiency in this cohort because a deficiency produced by these factors should be evident from the juvenile stage and not necessarily increase over time (2, 5, 8, 9, 10).

Acknowledgments

We thank Dr. J. B. Mitton and two anonymous reviewers for their valuable suggestions and advice for improving our manuscript. This work was supported by the Fondo Nacional de Desarrollo Científico y Tecnológico (Fondecyt 91/0897) and by the Dirección de Investigación y Desarrollo, U.A.Ch. (S-94-18).

Literature Cited

1. **Guiñez, R., and R. Gallegillos. 1985.** Clinal variation in morphological distance between genotypes at the carbonic anhydrase locus in the Chilean oyster, *Tiostrea chilensis* (Philippi, 1845) Chanley and Dinamani, 1980. *Braz. J. Genet.* **8:** 609–616.
2. **Mallet, A. L., E. Zouros, K. E. Gartner-Kepkay, K. R. Freeman, and L. M. Dickie. 1985.** Larval viability and heterozygote deficiency in populations of marine bivalves: evidence from pair matings of mussels. *Mar. Biol.* **87:** 165–172.
3. **Gaffney, P. M., T. M. Scott, R. K. Koehn, and W. J. Diehl. 1990.** Interrelationships of heterozygosity, growth rate and heterozygote deficiencies in the Coot Clam, *Mulinia lateralis. Genetics* **124:** 687–699.
4. **Beaumont, A. R. 1991.** Genetics studies of laboratory reared mussels, *Mytilus edulis:* heterozygote deficiencies, heterozygosity and growth. *Biol. J. Linn. Soc.* **44:** 273–285.
5. **Borsa, P., M. Zainuri, and B. Delay. 1991.** Heterozygote deficiency and population structure in the bivalve *Ruditapes decussatus. Heredity* **66:** 1–8.
6. **Pogson, G. H., and E. Zouros. 1994.** Allozyme and RFLP heterozygosities as correlates of growth rate in the scallop *Placopecten magellanicus:* a test of the associative overdominance hypothesis. *Genetics* **137:** 221–231.
7. **Toro, J. E., and O. R. Chaparro. 1990.** Conocimiento biológico de *Ostrea chilensis* (Philippi, 1845): Impacto y Perspectivas en el Desarrollo de la ostricultura en Chile. Pp. 231–264 in *Cultivo de Moluscos en América Latina,* A. Hernadez, ed. Memorias segunda reunión grupo trabajo técnico, Ancud, Chile. Nov. 1989.
8. **Gosling, E. M., and N. P. Wilkins. 1985.** Genetics of settling cohorts of *Mytilus edulis* (L.): preliminary observations. *Aquaculture* **44:** 115–123.
9. **Gaffney, P. M. 1993.** Heterosis and heterozygote deficiencies in marine bivalves: more light? In *Genetics and Evolution of Aquatic Organisms,* A. R. Beaumont, ed. Chapman & Hall, London.

10. **Thiriot-Quievreux, C., T. Noel, S. Bougrier, and S. Dallot. 1988.** Relationship between aneuploidy and growth rate in pair matings of the oyster *Crassostrea gigas*. *Aquaculture* **75:** 89–91.
11. **Alvarez, G., C. Zapata, R. Amaro, and A. Guerra. 1989.** Multilocus heterozygosity at protein loci and fitness in the European oyster, *Ostrea edulis* L. *Heredity* **63:** 359–372.
12. **Gosling, E. M., and D. McGrath. 1990.** Genetic variability in exposed-shore mussels, *Mytilus* spp. along an environmental gradient. *Mar Biol* **104:** 413–418.
13. **Singh, S. M., and E. Zouros. 1978.** Genetic variation associated with growth rate in the American oyster *(Crassostrea virginica). Evolution* **32:** 342–353.
14. **Zouros, E., S. M. Singh, D. W. Foltz, and A. L. Mallet. 1983.** Post-settlement viability in the American oyster *(Crassostrea virginica):* an overdominant phenotype. *Genet. Res.* **41:** 259–270.
15. **Zouros, E., S. M. Singh, and H. E. Miles. 1980.** An overdominant phenotype and its possible explanations. *Evolution* **34:** 856–867.
16. **Zouros, E., and D. W. Foltz. 1984.** Minimal selection requirements for the correlation between heterozygosity and growth, and for the deficiency of heterozygotes, in oyster populations. *Dev. Genet.* **4:** 393–405.
17. **Koehn, R. W., R. Milkman, and J. B. Mitton. 1976.** Population genetics of marine pelecypods. IV. Selection, migration and genetic differentiation in the blue mussel *Mytilus edulis*. *Evolution* **30:** 2–32.
18. **Shaw, C. H., and R. Prasad. 1970.** Starch gel electrophoresis of enzymes: a compilation of recipies. *Biochem. Genet.* **4:** 297–320.
19. **Selander, R. K., M. H. Smith, S. Y. Yang, W. E. Johnson, and J. B. Gentry. 1971.** Biochemical polymorphism and systematics in the genus *Peromyscus*. I. Variation in the oldfield mouse *(Peromyscus polionotus). Stud Genet* **6:** 49–90.

Reference: *Biol. Bull.* **188:** 120–127. (April, 1995)

Catch in the Primary Spines of the Sea Urchin *Eucidaris tribuloides:* A Brief Review and a New Interpretation

JOSÉ DEL CASTILLO*, DAVID S. SMITH**, ADA M. VIDAL*, AND CÉSAR SIERRA*

**Institute of Neurobiology, University of Puerto Rico M.S.C., Blvd. del Valle 201, San Juan, Puerto Rico 00901; and **Department of Zoology, University of Oxford, South Parks Road, Oxford, OX1 3PS, United Kingdom*

Abstract. Previous models of reversible catch in echinoid spines, as a property of muscle or of collagen, are briefly reviewed and discussed. This brief review offers a new interpretation of catch in primary spines of *Eucidaris tribuloides,* viewing the collagen and small muscles of the catch ligament working together as a variable-length tendon. In the model presented, changes in ligament length when out of catch are accommodated by sliding of discontinuous, interdigitating and cross-link-stabilized columns of collagen fibrils, the muscle layer external to the ligament effecting spine movement. Catch is viewed as a consequence of contraction of small muscles inserted on the collagen columns within the ligament. Ligament shortening tightens the profuse (*ca.* 30,000/mm^2) and highly ordered collagen insertion loops within the stereoms of the spine base and test, and catch results from the multiplicative effect of these friction sites in series. New data are presented on novel structural cross-links between collagen fibrils. The cross-links stabilize the ligament columns. The central ligament in *Eucidaris* plays a purely passive mechanical role in maintaining the alignment of the spine-test articulation. It contains no muscle and neither contracts nor undergoes catch; its insertions are simple, unlike the complex stereom insertions of the main ligament.

Introduction

From the time that it was first recognized, the phenomenon of catch in sea urchin spines has attracted the interest of investigators, but its basis has remained unclear. Two seemingly contradictory theories have been proposed to explain catch; but recent experimental observations allow a new interpretation that reconciles the two discrepant hypotheses.

Catch is an operational concept that can be defined in this instance as a reversible, neurally controlled enhancement of the passive mechanical resistance offered by the spine test articulation (Fig. 1) to forces tending to change the position of the spine. The sudden inducement of catch freezes the primary spines in their respective positions, whether normal to the test surface or angled from this axis, thereby allowing the animal to maintain a fixed posture for long periods.

von Uexküll's catch muscle

At the turn of the last century, Count Jakob von Uexküll, a self-supporting German biologist noted for his strong vitalist convictions, published a paper (1900) titled "The Physiology of the Sea-urchin Spine" in which he reported that the voluntary and reflex movements of the spine are powered by a thin layer of muscle fibers that surrounds the thick articular capsule. In addition, he found that the integrity of this capsule, which is also known as the spine ligament or catch apparatus, is essential for the development of catch.

Von Uexküll described the breakage of the capsule by forcible displacement of the spine while in catch: spines treated in this manner failed to show catch, but they retained the ability to perform voluntary and reflex movements because the thin muscle layer was not disrupted. Accordingly, von Uexküll called this muscle layer *Bewegungsmuskulatur* (motion-supporting muscle) as opposed to the articular capsule, which he believed also to be a muscle, the *Sperrmuskulatur* (catch or holding muscle). As we shall see below, this was an inspired guess that

Received 5 January 1995; accepted 7 February 1995.

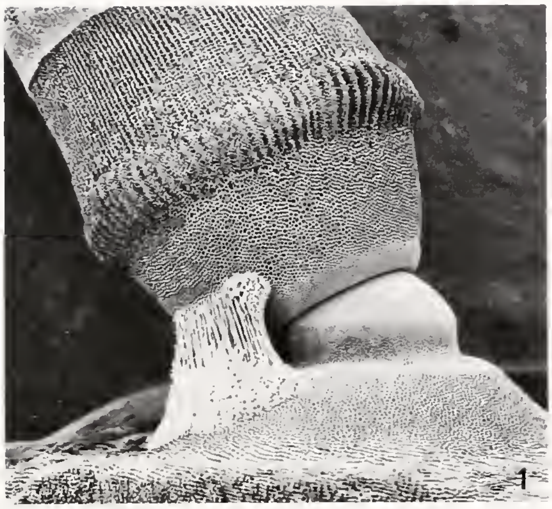

Figure 1. The spine-test articulation of *Eucidaris*. In this Chlorox-digested preparation a small area of ligament remains, maintaining the ball-and-socket arrangement. × 18

defied contemporary evidence, because the latter tissue had been studied by 19th century microscopists (Prouho, 1887; Hamann, 1887) and was recognized by them as being primarily a connective tissue.

Takahashi's mutable connective tissue

The problem of catch in echinoderm spines was studied again in the 1960s by Takahashi (1966, 1967a, b, c), who confirmed von Uexküll's results while disagreeing with him on the nature of the ligament. In the discussion of his landmark paper (1967b) on "Responses to stimuli," Takahashi gave an account of the experimental results that led him to propose a new hypothesis to explain catch.

Because at that time the ligament was still regarded as a muscle, Takahashi first attempted to record its contraction following the application of chemical or electrical stimuli. He was not successful. Yet Takahashi was greatly impressed by the effects of the same chemical stimuli on the rate of elongation of ligaments subjected to a constant load (isotonic recording; creep test). In his words "the effects were clear, sometimes even dramatic, and they varied according to the kind of drug applied." Lengthening was retarded by acetylcholine, while adrenaline exerted an accelerating effect.

These observations led Takahashi to seek the identity of the structural element responsible for the ligament extension under constant load, and he saw a plausible candidate in the collagen. He accounted for his results on the premise that the mechanical consistency of collagen can switch reversibly between two extreme conditions or states: one pliant and extensible and the other stiff and inextensible. This hypothesis was attractive because it explained a variety of experimental observations and was accepted by most workers including ourselves (Morales *et al.*, 1989, 1993). This view gave rise, more or less directly, to the concepts of "connective tissue catch" (Rüegg, 1971), "mutable connective tissue" (Eylers, 1982) and "variable tensility" (Wilkie, 1984).

Takahashi's observations had a great impact on the study of echinoderm connective tissue, and it is now accepted that the members of each of the five extant classes of the phylum possess some connective tissue with properties that differ significantly from those of vertebrate collagen (Motokawa, 1984, 1985). In this context, we stress that the present account deals only with the primary spine ligament of *Eucidaris tribuloides*, and while we do not extrapolate our conclusions to other echinoderms, neither do we suggest that our model of catch is restricted to this echinoid.

The Ligament as a Myotendinous Organ

Muscle fibers

The fine structure of the ligament was first studied by Smith *et al.* (1981) and Hidaka and Takahashi (1983), who noted the presence of muscle fibers in the spaces between the cylinders or columns of collagen fibrils that occupy most of the volume. As described by the above authors, the muscle cells are slender (only about 0.1–1 μm in diameter) and unstriated, and they include large paramyosin filaments in their contractile array. They make only a small contribution to the volume of the ligament: about 1.5% of the cross-sectional area in our micrographs of *Eucidaris*. We have determined that they insert directly onto the collagen columns. Although we lack information about their length and arrangement, the almost exact alignment of the muscle fibers and the collagen columns in transverse sections suggests that the two are virtually parallel, and we view the muscle as probably extending between adjacent collagen columns.

In addition, Hidaka and Takahashi suggested that changes in length of the ligament might reflect sliding within the array of collagen fibrils, and that catch could be accounted for by the formation of cross-links between the sliding elements. This suggestion stimulated work and speculation on the nature of the proposed cross-links, which were pictured variously as simple divalent cations, notably calcium (Hidaka, 1983; Diab and Gilly, 1984), and proteoglycans binding together the collagen fibrils (Trotter and Koob, 1989).

Insertion of the muscle fibers

Working on *Anthocidaris*, Hidaka and Takahashi (1983) noted that the muscle fiber surfaces were very closely apposed to the peripheral fibrils of the collagen columns and, while favoring the view that the muscles are long, running from insertions on collagen near the spine base and test, they suggested that the muscle cells might be relatively short and serve as cross-links between the collagen columns. They further described the fine structure of the ligament stretched to three times its resting length, noting "empty spaces" in the collagen array. They attributed this pattern to the slippage of collagen fibrils relative to one another. Thus they regard the individual collagen fibrils as the units responsible for sliding during forced ligament elongation. In contrast, we view the columns, rather than individual fibrils, as the functional units of the ligament length change accomplished by sliding. Each column is separated from its neighbors by 'matrix spaces,' but there is no fine structural evidence of cross-links between columns; *i.e.*, between the peripheral fibrils of adjacent columns. We suggest that the linkage between columns is effected by the muscle fibers.

We offer a rather different interpretation of Hidaka and Takahashi's micrographs: namely, that during irreversible, non-physiological stretching, peripheral portions of discontinuous collagen columns are torn away at the region where the muscle fibers are firmly inserted onto the columns. Before describing our reinterpretation of Hidaka and Takahashi's experimental findings, however, we should introduce a further piece of evidence concerning the collagen columns in *Eucidaris.*

Structure of the collagen columns

Other than the presence of transient links invoked in previous models of catch, the columns have been regarded as groups of mechanically independent fibrils. Indeed Hidaka and Takahashi's model is based on this assumption. But, in *Eucidaris* (Figs. 2, 3) we have observed a novel feature in conventionally prepared material[1], the fibrils of each column are profusely cross-linked by asymmetrical junctions and by apparently different, simpler, and symmetrical bridges; a single large-diameter fibril profile often shows multiple links with its neighbors. The apparent stability of the collagen columns seen in the transverse plane is also suggested by the regularity of organization of the columns seen in longitudinal sections (Fig. 6). Not only are individual fibrils precisely parallel, but some degree of register is often seen in the striation pattern of adjacent fibrils. As previously noted by Scott (1988) in the holothurian body wall and in vertebrate tendons, and by Trotter and Koob (1989) in *Eucidaris,* proteoglycan strands form a regular meshwork between the fibrils. In *Eucidaris* the regularity of their placing with respect to the fibril striations is noteworthy (Fig. 6), although their function remains undetermined. Proteoglycans are visualized only after special tissue preparation (Scott, 1980, 1988), and it is unlikely that the cross-bridges seen in conventionally prepared material, mentioned above, are related to the proteoglycan moieties of the columns. Although the nature of these bridges remains unknown—and neither type matches the fine proteoglycan strands described by Scott in tendon, by Trotter and Koob in *Eucidaris* ligament, and shown here in Figure 6—we regard this elaborate system as likely to give added mechanical stability to each column as a structural unit.

Trotter and Koob's model

Trotter and Koob (1989) reported a model of the ligament in which the collagen fibrils are the discontinuous fiber phase of a fiber-reinforced composite material. Their measurements of single isolated collagen fibrils revealed that, although varying in length and radius by more than an order of magnitude, they have a high and constant length/radius ratio, which was interpreted as indicating that the non-fibrillar material must act to transfer stress between fibrils. Trotter and Koob suggested that proteoglycan "may be an important component of the stress-transfer matrix," and illustrated the regular disposition of this material with respect to the collagen band pattern. We repeated this, with similar results (Fig. 6). But such proteoglycan components seem to be commonly associated with collagen, including that of vertebrate tendon (Scott 1980, 1988).

Nature of the sliding elements in the collagen array

We envisage ligament length change as being accomplished by a sliding movement between stabilized, discontinuous, and interdigitating columns. Adopting this view, we see Hidaka and Takahashi's observations in a different light. First, we noted, in *Eucidaris,* a very close apposition of muscle cell surface to column periphery, as Hidaka and Takahashi reported in *Anthocidaris: i.e.*, a gap of only about 10 nm separates the muscle plasma membrane from the outermost collagen fibrils, and this membrane is often contoured to match the fibrillar surfaces (Figs. 4, 5). Whereas Hidaka and Takahashi favored the view that the muscle fibers run from insertions near the spine base and the test, the high frequency with which

Figure 2. Transverse section of collagen fibrils. Note the frequent inter-fibrillar cross-links, shown further in the next figure. ×60,000

Figure 3. The collagen filaments of the ligament are linked by frequent asymmetrical (arrows) and symmetrical (arrowheads) cross-bridges. ×110,000

---

[1] Material illustrated in Figures 2–5 and 10 was conventionally fixed (2.5% glutaraldehyde, 0.05 *M* cacodylate buffer pH 7.4 with 14% sucrose), treated with 1% OsO_4 and embedded in Araldite. Contrast was enhanced on the grid by treatment with lead citrate followed by unbuffered 1% $KMnO_4$. Proteoglycans (Fig. 6) were visualized by the method of Scott (1980, 1988); low contrast enhancement of the collagen was obtained by treating sections with lead citrate alone. Material for SEM examination was fixed as for thin sectioning, but without OsO_4 treatment, and critical point dried. Details of preparation of frozen-fractured material (Fig. 9) are given in Smith *et al* (1990).

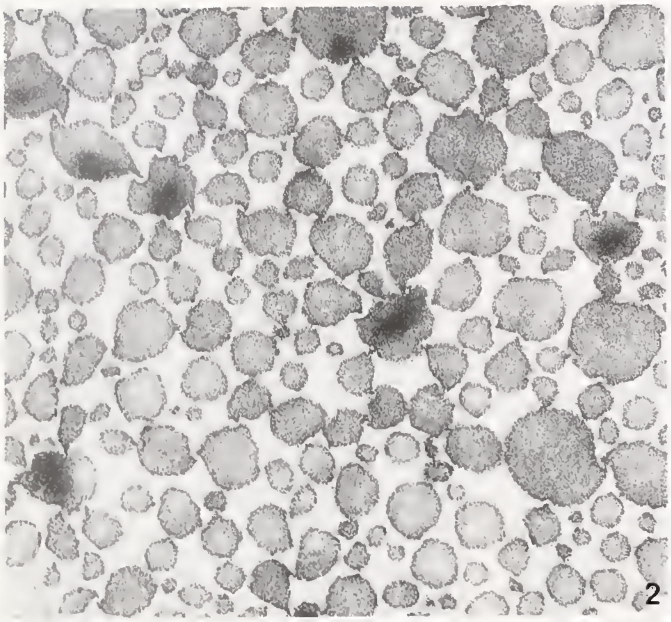

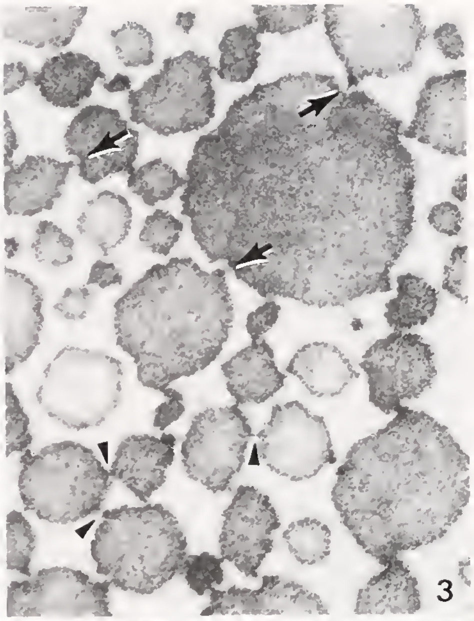

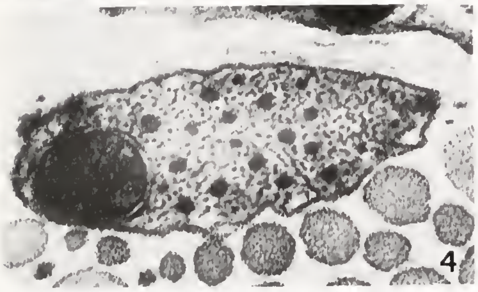

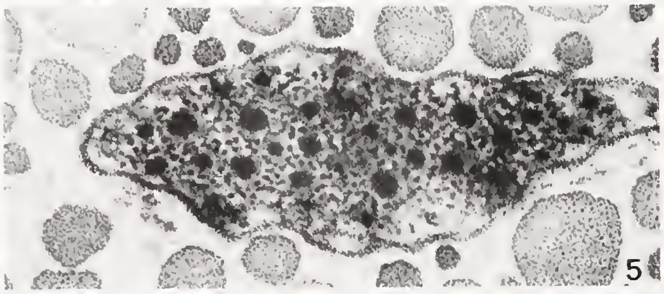

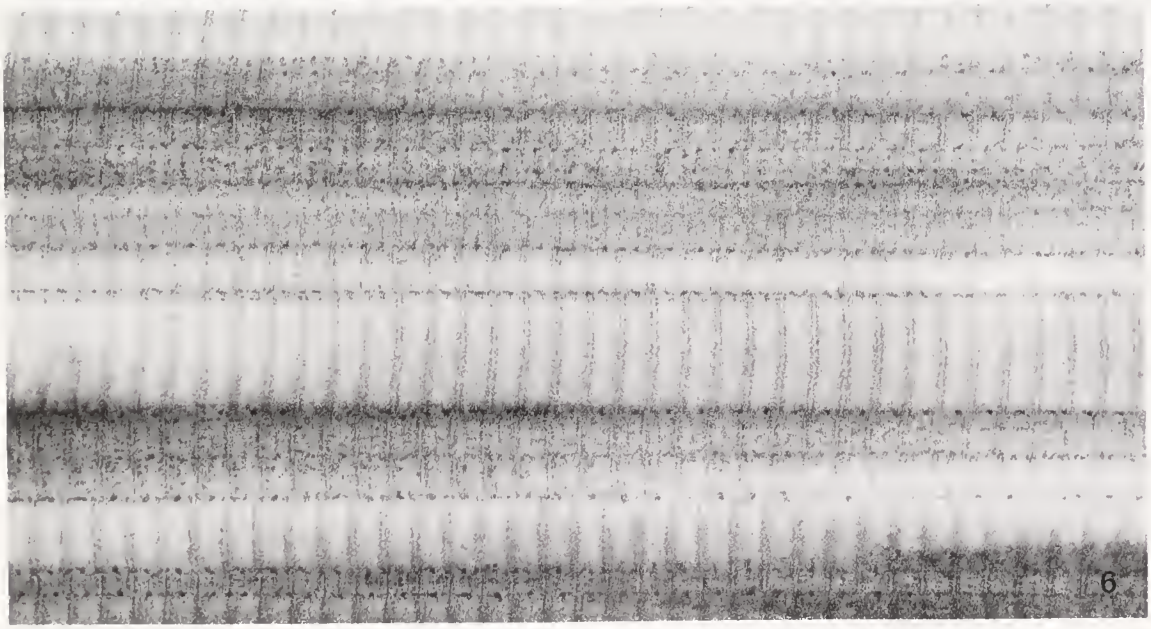

Figures 4, 5. Illustration of the close apposition of muscle fibers and collagen fibrils in the main ligament of *Eucidaris.* A gap of about 10 nm separates the fiber plasma membrane from the collagen surface, and the membrane is often indented around the fibrilar contours. Figure 4, ×90,000; Figure 5, ×120,000

Figure 6. Longitudinal section of the main ligament in *Eucidaris.* Proteoglycan is visualized by staining with cuprolinic blue. Note the precisely parallel disposition of the fibrils and areas of alignment of collagen banding. ×72,000

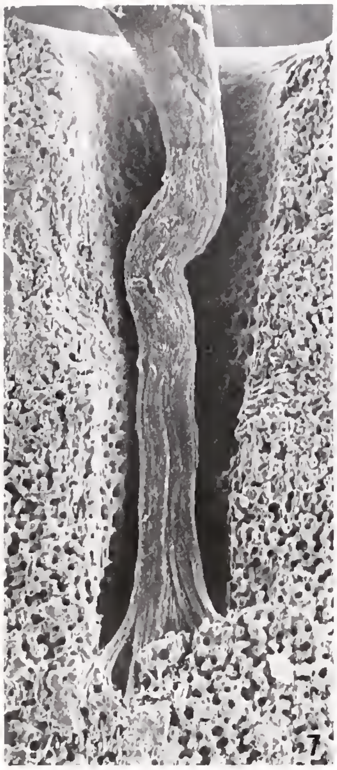

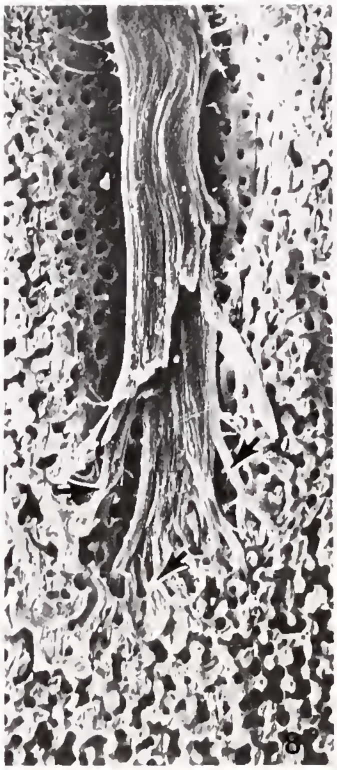

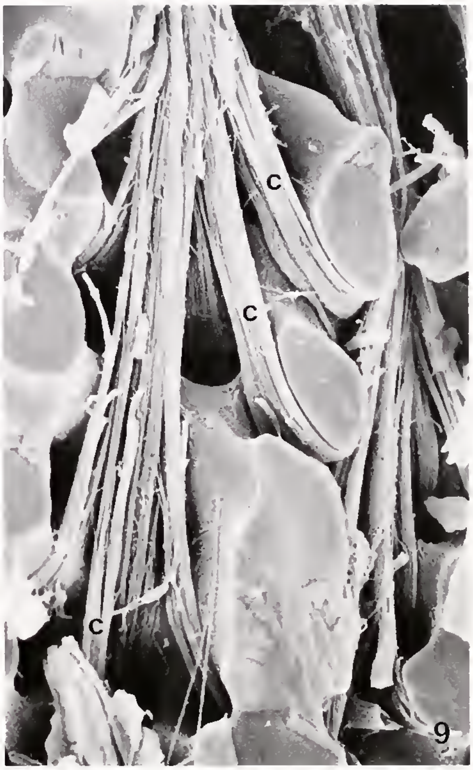

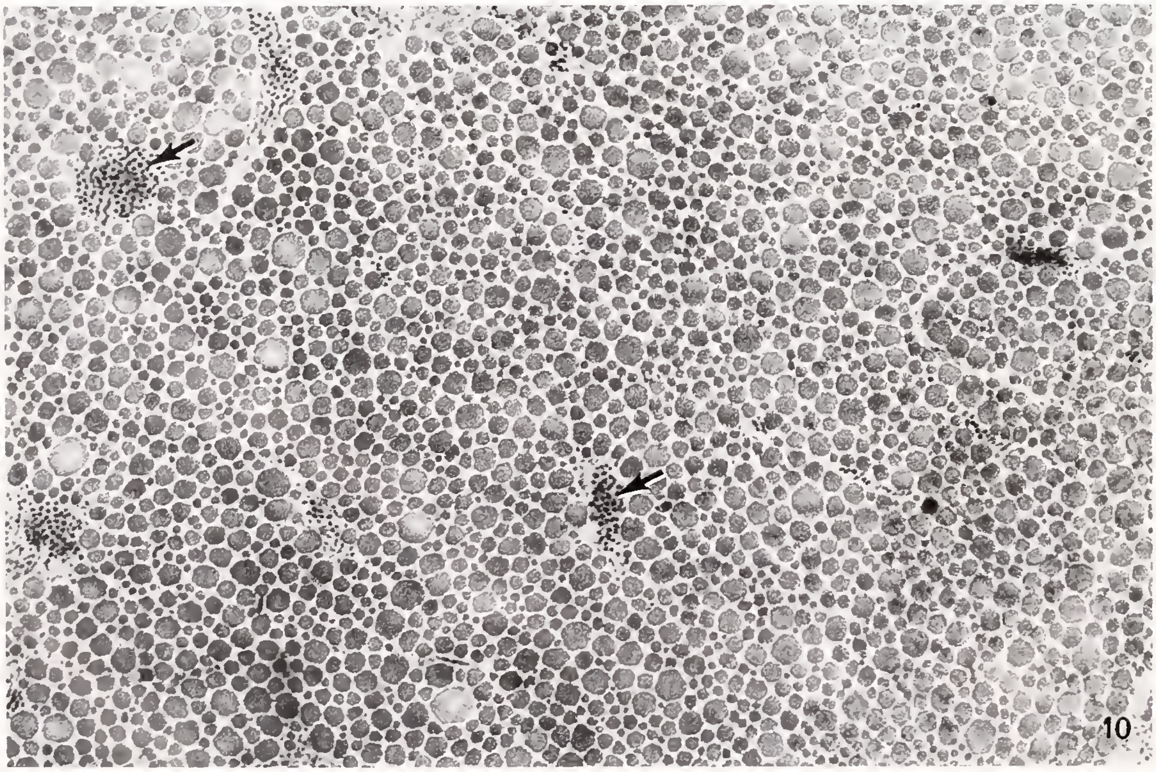

Figure 7. SEM of the insertion cavity and the central ligament on the test of *Eucidaris*. ×90

Figure 8. As in Figure 7, but with insertion of the central ligament exposed. The ligament ramifies into slender processes (arrows), which loop through stereom trabeculae. ×130

Figure 9. SEM of frozen-fractured main ligament insertion on the *Eucidaris* test. Note collagen straps (c) looping through stereom trabeculae and tightly appressed to the stereom struts. (From Smith *et al.*, 1990). ×1,500

we have observed muscle insertions on thin sections of the ligament led us to the alternative view that the muscle fibers are very numerous and relatively short, linking adjacent collagen columns throughout the ligament. A reexamination of their figures (*i.e.*, Hidaka and Takahashi, 1983, Figs. 8, 9) suggests that stretching somewhat distorts but does not obscure the arrangement of collagen columns and that the 'holes' appearing in the transversely sectioned array are not random but represent lenticular gaps where bundles of fibrils have been torn apart. In addition we regard the muscle fibers as very strong, as shown, for example, by the presence of highly stretched but essentially intact muscle fibers in pictures published by Hidaka and Takahashi (1983). The linkage between muscle fibers and columns must be strong if our model is correct.

Although there is no fine structural evidence of discontinuity, it seems likely that the columns taper at their ends. Profiles of 'tiny' columns are dispersed in transverse sections, probably columns near their ends (see Fig. 3).

The Ligament Contracts

In view of the presence of contractile cells, one should expect that cholinergic agonists would induce some mechanical effect on the ligament. The very modest contribution of muscle to the volume of the ligament seemed to rule out a leading role for them in ligament mechanics analogous to that of muscle in the molluscan catch mechanism. Indeed, the only functional alternative that Smith *et al.* (1981) suggested was the relatively minor task of returning an extended sector of the ligament to its 'normal' position.

To obtain further information on the physiological properties of the ligament, we reinvestigated its responses to electrical and chemical stimuli. We found that the ligament behaves as an excitable motile tissue, shortening and developing a mechanical force following the application of either type of stimulus (Vidal *et al.*, 1983). The most probable explanation of the discrepancy, in identical experiments, between our positive results and the negative ones of Takahashi is that prior to stimulating the ligament, we treated it briefly with tyramine (1 m*M*, 2–5 min). This compound, like its close analog octopamine, exerts a lytic effect on catch and a relaxing effect on contraction (Morales *et al.*, 1989). The use of tyramine allowed us to work with a fully relaxed preparation in every experiment. In addition, we applied a force of 2 to 3 g, which tends to separate the two calcareous moieties of the spine-test joint. By comparing the kinetics of the catch with the contracture induced by cholinergic agonists on the same preparation, we concluded that these phenomena are two sides of the same coin. In other words, we believe that catch is simply the expression of the shortening of the ligament.

Mechanism of Catch

We must now consider how the contraction of the ligament opposes, or counteracts altogether, the passive movements of the spine. An answer to this question must explain how the force generated by the scant and slender muscle fibers can overpower the stresses generated, often with considerable mechanical advantage, by the external forces acting on the shaft of the spine. The fine structure of the essentially simple but highly ordered insertions of the ligament onto the stereom in *Eucidaris* was described by Smith *et al.* (1990) and revealed an order first hinted at in the light micrographs of Takahashi (1966). Within the stereom, the collagen columns divide into a series of successive, parallel slender straps, passing reflexively across struts or microbeams that border spaces considerably wider than the straps they accommodate. In most micrographs obtained by Smith and co-workers, the straps appear to be tightly cinched to the struts (see Fig. 9), but they are sometimes seen lying free within the lacunae, suggesting that they are not 'glued' immovably to the stereom microbeams. The lacunae are sufficiently wide to permit some movement of the straps when disengaged.

An answer to the main question posed above may be found in the frictional resistance generated at the ligament insertions by minute but crucial movement of the straps over the struts. As the friction between two sliding surfaces is proportional to the force that keeps them together, the resistance between straps and struts will be modulated by the muscle fibers in parallel with the collagen columns. In this model, shortening of the ligament that initiates catch will increase the force that presses the straps upon the struts, thereby increasing the friction between these two structures.

Our model of catch is shown in Figure 11. In the absence of cholinergic stimulation, the muscle fibers will be relaxed and, therefore, the ligament will be slack. The straps will rest loosely on the struts, and the spine-test joint can be moved passively without offering significant resistance. As muscle contraction starts to tighten the ligament, a very small change in the position of the straps is envisaged as introducing frictional resistance at the sites where they appressed the struts within the stereom. The friction between the surfaces of both structures, according to this model, will absorb the energy applied by external forces. The model further emphasizes that, rather than

Figure 10. Transverse section of *Eucidaris* central ligament. Note that the collagen forms a continuous array largely filling the field. Groups of microfilaments are present (arrows) but nerve processes and muscle cells are absent. ×30,000

acting as a work-generating device, the function of the muscle fibers of the ligament seems to be (like the braking pedal of a car) that of controlling an energy-absorbing or energy-dissipating system, similar in design to an automotive friction brake, engineered to take advantage of the roughly 30,000 bands or straps underlying each square millimeter of the insertion surfaces both at the spine base and test. The resistance generated at single strap-strut contacts will be greatly amplified by the multiplicative effect of friction sites in series.

The Central Ligament

A final piece of evidence in support of the above model is provided by comparing the structure and function of the main ligament and a supplementary structure, the central ligament, that is present in many echinoid spines including those of *Eucidaris.* The central ligament extends across the midpoint of, and inserts into cylindrical cavities in, each surface of the spine-test articulation (Cuénot, 1948; Hyman, 1955). Motokawa (1983) described this structure in *Diadema setosum:* it is relatively robust, about 0.5 mm in diameter, and responsible for maintaining the attachment between spine and test, even when the joint is dislocated by extreme spine declination (Takahashi, 1967c). In our observations on *Eucidaris* (Fig. 7), the corresponding structure is <0.1 mm in diameter, considerably smaller in relation to the articulation than in *Diadema.* The central ligament in *Eucidaris* differs strikingly in both fine structure and stereom insertion from the main ligament. First, the collagen fibrils form a continuous and compact block that is not divided into discrete columns (Fig. 10). Second, it contains neither muscle cells nor granule-containing neurites. In common with the main ligament, collagen straps do enter the stereom, but they loop irregularly through cavities of the unmodified, tetragonal, stereom fabric (Fig. 8), and the elaborate system of struts and straps of the main ligament is absent. Furthermore, we were unable to detect any mechanical response to acetylcholine in the central ligament in contrast to the contracture and catch elicited in the main ligament. We view the central ligament in *Eucidaris* as a physiologically inactive link, presumably safeguarding the alignment of the articulation during spine movement.

The structural peculiarities of the central ligament are consistent with our view of the way in which the main ligament achieves the catch state. Without muscle fibers, the central ligament cannot shorten. Because the central ligament does not undergo length change and is not involved in catch, the collagen is arranged for maximal tensile strength, not to accommodate an intra-ligament sliding movement. Rather than being arranged in interdigitating columns, as in the main ligament, the collagen fibrils are disposed as a continuous block virtually filling the structure. In the main ligament, columns of collagen fibrils are stabilized by cross-links; we suggest that similar links present in the central ligament stabilize it for its purely passive, mechanical role. Furthermore, the central ligament, stressed only by spine movement, is well-served by an unspecialized anchorage, contrasting with the precise arrays of collagen straps and stereom struts of the main ligament, discussed above.

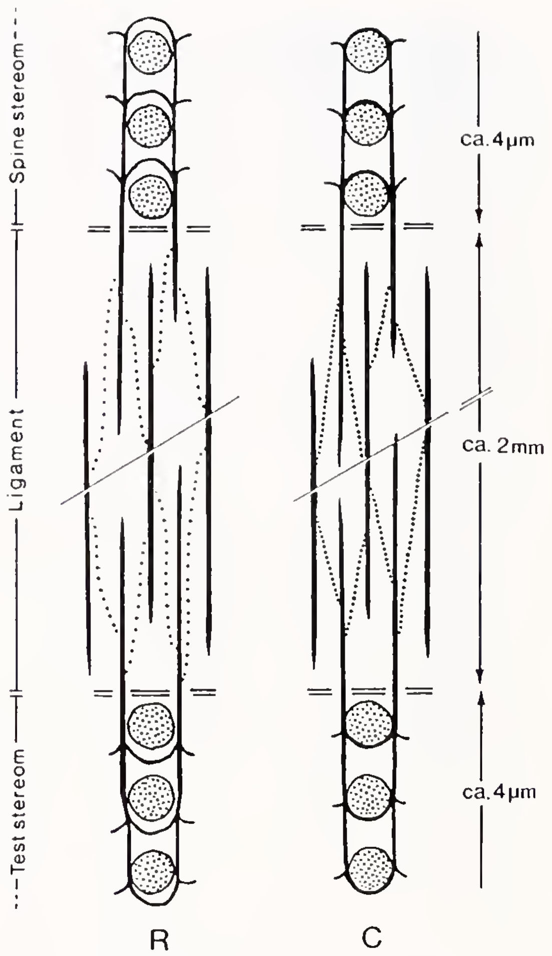

Figure 11. Schematic diagram of model discussed in the text. *R* relaxed ligament; *C* contracted ligament. Approximate dimensions of the spine and test stereom, and the ligament, included in the diagram are indicated; note the great difference in scale. *Stippled circles* represent transverse profiles of stereom struts: only three struts are shown in each stereom (of the five or six actually present in each row). In *R* the collagen straps are represented as looping loosely between the struts; in *C* they are tightly applied to the struts. In *R* relaxed muscle fibers inserting on collagen cylinders of the main ligament are represented by wide-spaced dotted lines (. . . .); in *C* contracted fibers are represented by close-spaced dotted lines (. . . . . .).

Our findings in *Eucidaris* differ in important respects from those of Motokawa (1983) in *Diadema.* He found the central ligament physiologically similar to the main ligament, its viscosity was increased by acetylcholine and decreased by epinephrine. He suggested that the central ligament is mechanically and structurally similar to the main ligament, except for the apparent absence of muscle fibers in the former. Moreover, in *Diadema* the collagen fibrils are grouped in columns in both main and central ligaments. Other than noting the very different functions of spines in *Eucidaris* and *Diadema*, we can at present only draw attention to these discrepancies, not account for them.

Conclusions

In the model of catch we have proposed, we view evolutionary experimentation as providing a solution to the problem of minimizing muscle tissue mass, while achieving maximal efficiency. Indeed, a catch apparatus that would meet the mechanical needs of the spine, but made up of conventionally arranged muscle fibers, might be too 'expensive' for the very limited energetic resources of the sea urchin (Bianconcini *et al.*, 1985). The layer of conventional muscles external to the ligament is responsible for moving the spine, whereas the muscle of the catch system was diverted from power generation to the regulation of the energy-absorbing function of the ligament. In a sense, von Uexküll and Takahashi were both correct in seeing catch as a property, respectively, of muscle and collagen. The spine ligament, with its catch capacity, may be regarded as a myotendinous organ that combines in a uniquely efficient manner the contractile properties of muscle with the tensile strength of collagen fibrils, to produce a variable-length tendon.

Acknowledgments

We are grateful to Dr. Mark Miller and Dr. Richard Orkand for their critical reading of the manuscript, and to Mr. Faustino McKenzie for collecting and maintaining the sea urchins. TEM and SEM preparations were made with the assistance of Mrs. Barbara Luke. Supported by NIH Grants Nos. NS-07464 and NS-14938, and HRD 9353130 (NSF-RIMI).

Literature Cited

Bianconcini, M. S., E. G. Mendes, and D. Valente. 1985. The respiratory metabolism of the lantern muscle of the sea urchin *Echinometra lucunter* L.-I. The respiratory intensity. *Comp. Biochem. Physiol.* **80A:** 1–4.

Cuénot, L. 1948. *Anatomie, éthologie et systématique des echinodermes.* In *Traité de Zoologie: Anatomie, Systématique, Biologie* Vol. 11, Echinodermes, Stomocordes, Procordes, P. P. Grasse, Pp. 128–131. Masson, Paris.

Diab, M., and W. F. Gilly. 1984. Mechanical properties and control of non-muscular catch in spine ligaments of the sea-urchin, *Strongylocentrotus franciscanus J. Exp. Biol.* **111:** 155–170.

Eylers, J. P. 1982. Ion-dependent viscosity of holothurian body wall and its implications for the functional morphology of echinoderms. *J. Exp. Biol.* **9:** 1–8.

Hamann, O. 1887. Beiträge zur Histologie der Echinodermen. *Jenaische Zeit. Naturwiss* **21:** 87–266.

Hidaka, M. 1983. Effects of certain physico-chemical agents on the mechanical properties of the catch apparatus of the sea-urchin spine. *J Exp. Biol* **103:** 15–29.

Hidaka, M., and K. Takahashi. 1983. Fine structure and mechanical properties of the catch apparatus of the sea-urchin spine, a collagenous connective tissue with muscle-like holding capacity. *J Exp Biol.* **103:** 1–14.

Hyman, L. 1955. *The Invertebrates. Echinodermata,* Vol. 4, Ch. 9, Class Echinoidea. McGraw-Hill, New York. Pp. 413–589.

Morales, M., J. del Castillo, and D. S. Smith. 1989. Acetylcholine sensitivity of the spine-test articular capsule of the sea-urchin *Eucidaris tribuloides Comp. Biochem Physiol* **94C:** 547–554.

Morales, M., C. Sierra, A. Vidal, J. del Castillo, and D. S. Smith. 1993. Pharmacological sensitivity of the articular capsule of the primary spines of *Eucidaris tribuloides Comp. Biochem Physiol.* **105:** 25–30.

Motokawa, T. 1983. Mechanical properties and structure of the spine-joint central ligament of the sea-urchin, *Diadema setosum* (Echinodermata, Echinoidea). *J Biol. Lond* **201:** 223–235.

Motokawa, T. 1984. Connective tissue catch in echinoderms. *Biol. Rev.* **59:** 255–270.

Motokawa, T. 1985. Catch connective tissue: the connective tissue with adjustable mechanical properties. Pp. 69–73 in *Echinodermata,* B. F. Keegan and B. D. S. O'Connor, eds. Balkema, Rotterdam.

Prouho, H. 1887. Recherches sur le *Dorocidaris papillata* et quelques autres échinids de la Méditerranée. *Arch Zool. Exp. Gen.* **5:** 213–380.

Rüegg, J. C. 1971. Smooth muscle tone. *Physiol. Rev.* **51:** 201–248.

Scott, J. E. 1980. Collagen-proteoglycan interactions. Localization of proteoglycans in tendon by electron microscopy. *Biochem. J.* **187:** 887–891.

Scott, J. E. 1988. Proteoglycan-fibrillar collagen interactions. *Biochem. J* **252:** 3313–3323.

Smith, D. S., S. A. Wainwright, J. Baker, and M. L. Cayer. 1981. Structural features associated with the movement and 'catch' of the sea-urchin spines. *Tissue & Cell* **13:** 299–320.

Smith, D. S., J. del Castillo, M. Morales, and B. Luke, 1990. The attachment of collagenous ligament to stereom in primary spines of the sea-urchin. *Eucidaris tribuloides. Tissue & Cell* **22:** 157–176.

Takahashi, K. 1966. Muscle physiology. Pp. 513–527 in *Physiology of Echinodermata,* R. A. Boolootian, ed. Interscience, New York.

Takahashi, K. 1967a. The catch apparatus of the sea-urchin spine. I. Gross histology. *J Fac. Sci. Univ Tokyo, Sec IV* **11:** 109–120.

Takahashi, K. 1967b. The catch apparatus of the sea-urchin spine. II. Response to stimuli. *J Fac. Sci. Univ Tokyo, Sec IV* **11:** 121–130.

Takahashi, K. 1967c. The ball-and-socket joint of the sea-urchin spine: geometry and its functional implications. *J. Fac. Sci. Univ. Tokyo. Sec IV* **11:** 131–135.

Trotter, J. A., and T. J. Koob. 1989. Collagen and proteoglycan in a sea urchin ligament with mutable mechanical properties. *Cell Tissue Res.* **258:** 527–539.

von Uexkull, J. 1900. Die Physiologie des Seeingelstachels. *Zeit Biol.* **37:** 334–403.

Vidal, A., J. del Castillo, and D. S. Smith, 1983. Contractile properties of the articular capsule or ligament, in the primary spines of the sea-urchin *Eucidaris tribuloides Comp. Biochem. Physiol.* **106C:** 643–647.

Wilkie, I. C. 1984. Variable tensility in echinoderm collagenous tissues: a review. *Mar. Behav. Physiol* **11:** 1–34.

Reference: *Biol Bull* **188**: 128–135. (April, 1995)

Protein-Membrane Interaction Is Essential to Normal Assembly of the Microsporidian Spore Invasion Tube

EARL WEIDNER[1,2], S. B. MANALE[1,2], S. K. HALONEN[1,3], AND J. W. LYNN[1]

[1]*Department of Zoology and Physiology, Louisiana State University, Baton Rouge, Louisiana 70803;*
[2]*Marine Biological Laboratory, Woods Hole, Massachusetts 02543; and* [3]*Department of Neurology, Albert Einstein College of Medicine, Bronx, New York 10461*

Abstract. Changes in the protein-membrane interaction during assembly of the microsporidian spore invasion tubes were followed by electron microscopy, by video imaging with differential interference contrast (DIC), and by the fluorescent probes 4′,6-diamidino-2-phenylindole (DAPI) and 9-diethylamino-5H-benzo[α]phenoxazine-5-one (Nile red). Microsporidian spore invasion tubes form by the eversion of polar filament protein (PFP) and presumptive extrusion apparatus (EAP) membrane. Both of these components are essential for formation of the invasion tube. The results indicate that the behavior of the EAP membrane is greatly affected by the position and chemical state of the PFP at the eversion area that constitutes the advancing tube terminal assembly site (TAS). Visual evidence indicates that the EAP membrane is the vehicle for PFP and that this membrane also provides the envelope that surrounds the sporoplasm after its passage through the invasion tube.

Introduction

Microsporidians are a large group of intracellular parasites widely distributed within many animal groups (Canning and Lom, 1986). Some species, as opportunistic parasites, have developed a significant presence in AIDS patients (Ornstein *et al.*, 1990; Canning and Hollister, 1991; Cali *et al.*, 1993). The spore stage is characterized by an extrusion apparatus (EAP) with two principal assemblages, a polar filament protein (PFP) coil, and an envelope consisting of an extensive pleated system of membranes (Cali, 1991). The infective microsporidian spore is remarkable because it discharges its entire contents (excluding the plasma membrane) through a 100-nm-wide tube and into a target cell with the time frame of 100–150 ms (Lom and Vavra, 1963; Undeen, 1990; Frixione *et al.*, 1992). During spore discharge, the invasion tube cinematographically resembles an extruding cnidarian nematocyst (Blanquet, 1983), a discharging capsule from a myxosporean spore (Lom and Noble, 1984; El-Matbouli *et al.*, 1992), or a discharging toxicyst from the ciliate *Loxophyllum* (Hausmann, 1978). In all of these extreme forms of exocytosis, the extrusion apparatus is confined to an organelle with an outer wall; but, with microsporidians, the EAP is segregated from the spore cytoplasm by a membrane, rather than a walled structure (Weidner *et al.*, 1984).

The primary components of the microsporidian extrusion apparatus, the PFP and the EAP membrane, display a significant interactive change during invasion tube discharge. In the presence of PFP, the EAP membrane initially develops into a tubular shape; but with removal of the PFP, the membrane develops a saccular shape. The PFP is a low molecular weight peptide (recently, resolved to two elements) that assembles into stable polymers. Polymeric PFP is stable in sodium dodecyl sulfate but dissociates in dithiothreitol after urea pretreatment (Weidner, 1976). The fluidity of polymerized PFP is modulated by Ca^{2+} and by pH yielding unstable monolayers (Weidner, 1976, 1982).

Here, we report that the EAP membrane is essential for the formation of the invasion tube because it affects the assembly of PFP. Major modulations in the interactions between the PFP and the EAP membrane occur at the advancing tube tip terminal assembly site (TAS). Video imaging with differential interference contrast

Received 24 October 1994; accepted 18 January 1995.

Abbreviations: Nile red, 9-diethylamino-5H-benzo[α]phenoxazine-5-one; DAPI, 4′,6-diamidino-2-phenylindole; DIC, differential interference contrast; EAP, extrusion apparatus; PFP, polar filament protein; TAS, terminal assembly site.

(DIC) and fluorescent probes were used in this study. 4′,6-diamidino-2-phenylindole (DAPI), a binder of certain polyanionic substrates and double-stranded DNA (Bonne *et al.*, 1985; Meszaros *et al.*, 1987), was used to identify the nuclear and cytosol positions during invasion tube discharge. A lipophilic generalized membrane probe, 9-diethylamino-5H-benzo[α]phenoxazine-5-one (Nile red) (Greenspan *et al.*, 1985; Greenspan and Fowler, 1985), was used to monitor the membrane because it provides an intense fluorescence and did not affect spore discharge. A preliminary study using fluorescent probes to monitor spore discharge has been previously published (Weidner *et al.*, 1994).

Materials and Methods

Microsporidian spores

Spraguea lophii spores were recovered from the central nervous system of the monkfish, *Lophius americanus*. Monkfish were provided by the Marine Resources department of the Marine Biological Laboratory in Woods Hole, Massachusetts. Spores were purified by a wash cycle described elsewhere (Weidner, 1976).

Spore activation

Isolated spores previously maintained in 0.05 *M* Hepes were placed in medium adjusted to pH 7 with 10^{-5} *M* Ca^{2+} for 30 min and then transferred into activation medium consisting of 2.0% mucin (human or porcine type 1 from Sigma) and Hepes buffer adjusted to pH 9.5.

Fluorescence

S. lophii spores were placed in incubation medium containing 0.1 μg/ml 4′,6-diamidino-2-phenylindole (DAPI) or 0.1 μg/ml 9-diethylamino-5H-benzo[α]phenoxazine-5-one (Nile red) in 0.05 *M* Hepes buffer for 30–45 min. Spores were then transferred to activation medium and examined with a Nikon Microphot FXA or Zeiss Axiophot optical system. The DAPI imaging was carried out with a 365-nm excitation frequency and with a 400-nm highpass barrier filter. Nile red imaging was carried out using an FITC Filter set (Nikon) with a 480-nm excitation frequency and a 510-nm highpass barrier filter. Images were examined with 60× or 100× Fluor or Planapochromatic oil immersion lenses.

Video

Images of microsporidian spore discharge were recorded using a customized Nikon Optiphot-2 adapted to an Odyssey X11 laser confocal unit (Noran Instruments, Inc.). Video recordings were recovered with a Nikon 60× oil immersion lens (Nikon Inc., Melville, NY). Confocal fluorescence measurements were recorded using a 488-nm excitation wavelength and a 515-nm highpass barrier filter. Image recordings were saved on an optical memory disk (Panasonic 2028F), digitalized, and analyzed with Intervision (Noran Instruments, Inc.). Photographs were taken using a 35-mm camera to capture images from a 23-in silicon graphics monitor.

Electron microscopy

Negative-stained material was prepared by applying discharged spores onto Formvar-coated grids. Grids were stained with 2% phosphotungstic acid adjusted to pH 6.9. For topographical images of discharged spores, platinum-carbon replicas were prepared as described earlier (Koo *et al.*, 1973). Material prepared for sectioning was fixed in 1% glutaraldehyde in 0.1 *M* cacodylate buffer, post-fixed in osmium, and processed by standard procedures (Weidner, 1976).

Results

Transmission electron microscopy of microsporidian spore invasion tubes

Polar filament protein (PFP) and membrane assembly were the main part of the extrusion apparatus of *S. lophii* spores. Before filament extrusion and tube formation, paracrystalline-like proteins organized as a coil at the polar end and extended to a subsurface spore aperture (Fig. 1A). In unfired spores, a single membrane surrounded the filament coil and extended as a system of pleats along with the ascending filament near the polar aperture. However, with spore discharge, PFP emerged from the aperture and became positionally reversed in reference to the filament membrane (Fig. 1A, B, and C). The discharged membrane was a double cylinder at the distal region of the emerging tube with PFP apparent within the membrane cylinders (Fig. 1B and C). However, the extruded tubes showed significant amounts of PFP on the membrane exterior assembled as a stable outer envelope (Fig. 1C). Platinum-carbon replicas of discharged tubes show a distinction between empty, incompletely extruded, and fully extruded invasion tubes. The incompletely extruded tubes (50 μm or less) had internal cylinders of material (Fig. 1D), whereas the fully extruded invasion tubes (measuring 65–70 μm) were devoid of internal cylinders (Fig. 1D).

DAPI and DIC imaging of discharging S. lophii *spores*

The DNA fluorophore, DAPI, labeled *S. lophii* nuclei without significantly affecting spore activation and tube discharge when incubations were for less than 1 h with

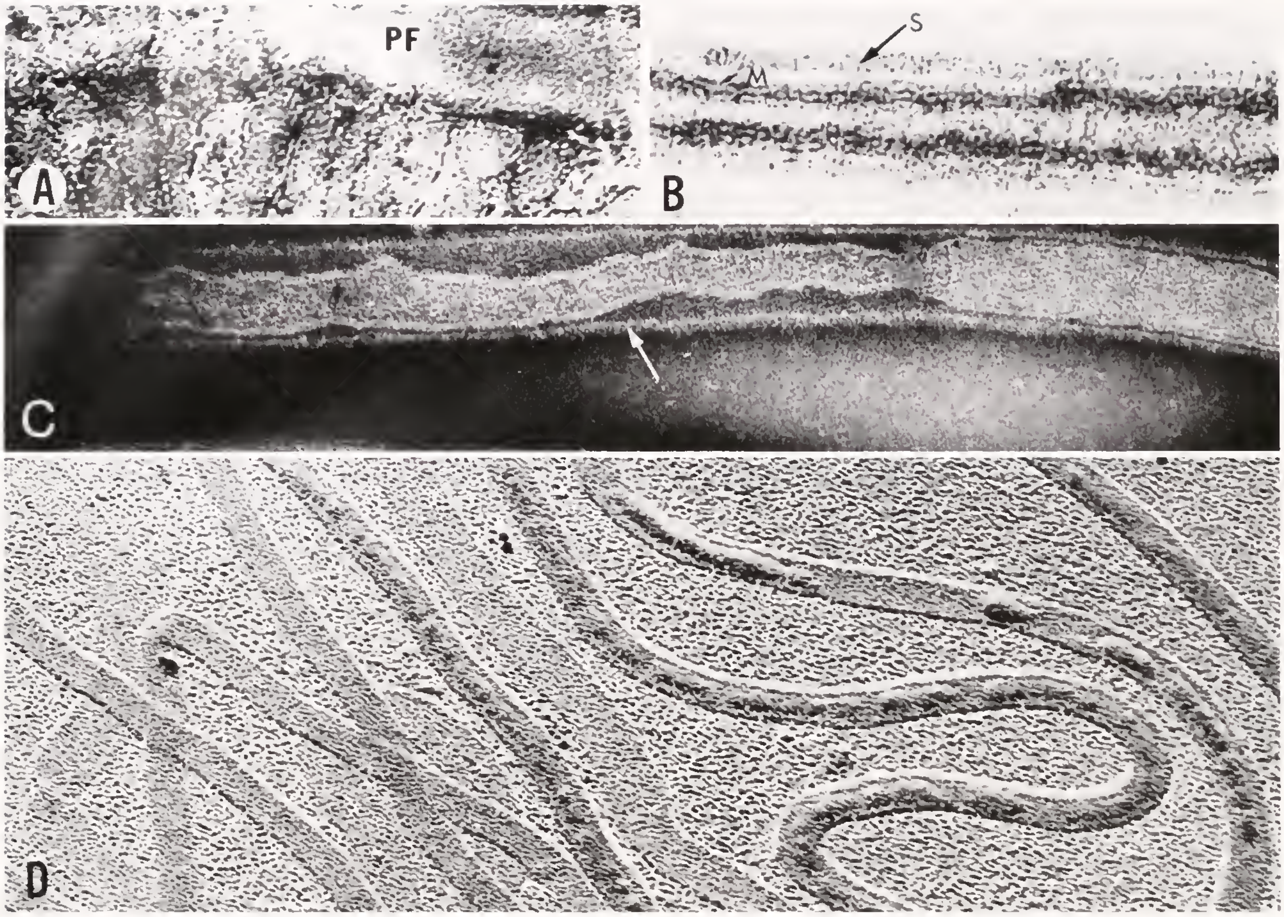

Figure 1. Electron micrographs of microsporidian extrusion apparatus. (A) Unfired spore of *Spraguea lophii* with ascending part of polar filament protein (PFP) surrounded by membrane pleats. (B) Partially discharged spore is shown in section: the double cylinders of membrane are apparent (M), as is the exteriorized PFP (S). (C) Negative-stained invasion tube shows outer protein envelope (arrow) and an inner membrane cylinder bearing what appears to be PFP material. (D) The platinum-carbon replica distinguishes between extruded invasion tubes with inner cylinders of membrane (incomplete), and completely extruded tubes that appear empty.

5 μM of label. However, extended (overnight) incubations with 50 μM DAPI affected tube extrusion and sporoplasmic sac emergence at the end of the tube. When DIC was coupled with DAPI fluorescence, nuclear movement was observed in association with invasion tube formation and sporoplasmic sac emergence (Fig. 2A–F). Sporoplasmic sacs did not appear at the tube ends until the tubes had reached a maximum length of 70 μm. The spore nucleus did not begin to traverse the tube until 90–95% of the discharged tube had emerged from the spore. However, in 1–2% of the discharged spores with extruded sporoplasmic sacs, the nuclei were still within the invasion tube (Fig. 2D). The failure rate of sporoplasmic sac emergence or of sporoplasm extrusion was increased with extended spore incubations (6–12 h) in higher concentrations of DAPI (50 μM).

Video imaging of microsporidian spore invasion tube discharge with Nile red

Intense Nile red fluorescence was apparent during membrane discharge through invasion tubes, but the intensity diminished rapidly after the sporoplasmic sacs had emerged (Fig. 3A and B). Similarly, discharged tubes prewashed in SDS detergent showed little fluorescence. Because of the intensity of Nile red fluorescence for membrane, this dye was used to monitor the movement of membrane down the invasion tube during spore extrusion (Fig. 4A–F). Video analyses showed that at the onset of spore discharge, the Nile red fluorescence was highest at the distal end of the emerging tube (Fig. 5A–F). Although the fluorescence was strongest along the distal 15 μm of invasion tubes 50–55 μm in length, fully extruded invasion tubes (70 μm) exhibited an even fluorescence

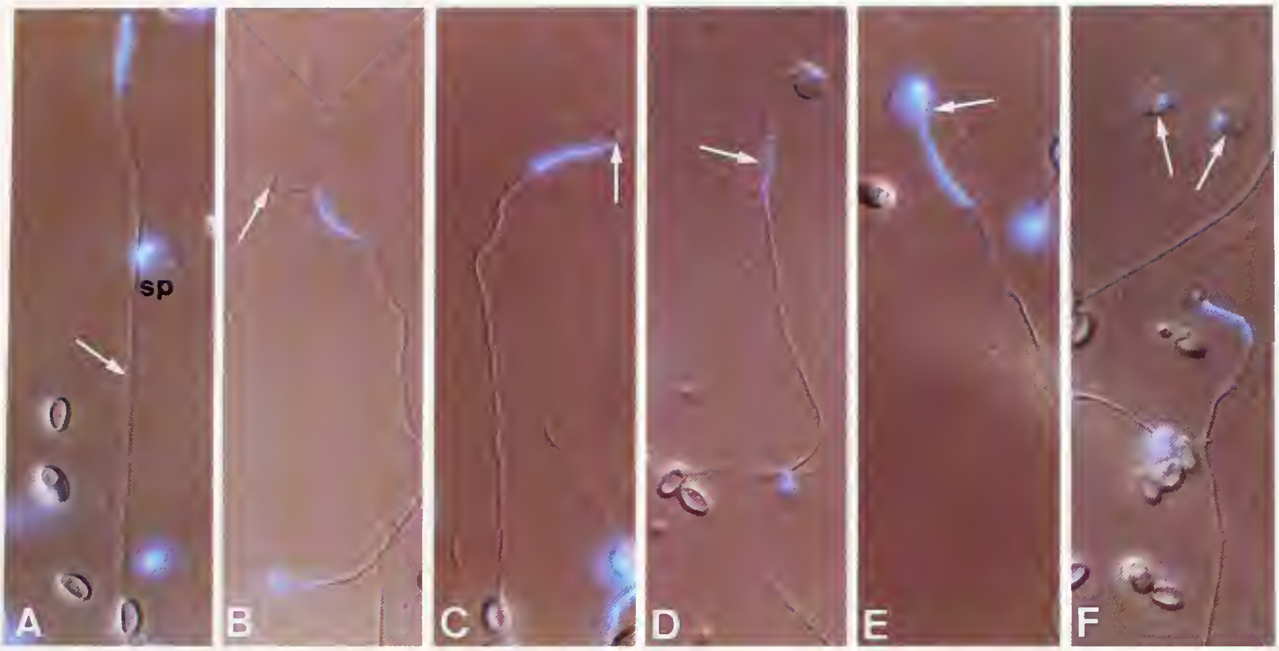

Figure 2. Light optics showing discharging *Spraguea lophii* spores prelabeled with DAPI and examined with DIC imaging. (A) The discharged spore invasion tube has emerged (arrow) with the nucleus (DAPI-blue stain) at the tube tip. Note the fully emerged sporoplasm (sp) from another spore. (B and C) Sporoplasmic sac emerging at the invasion tube tip (arrows). (D) The sporoplasmic sac has fully emerged, but the nucleus (arrow) is still within the invasion tube. (E) Nucleus is emerging into the sporoplasmic sac at the invasion tube tip. (F) Fully emerged sporoplasm with nuclear components (arrows).

throughout the tube (Fig. 5G). Ultrastructural observations indicate that discharged tubes 40–50 μm in length had double membrane cylinders at the distal ends; however, fully extruded invasion tubes did not exhibit double membranes. Tube fluorescence was reduced significantly with the emergence of the sporoplasmic sac membrane at the tube ends (Figs. 4F, 5G and H). Ultrastructural observations of discharged spores with extruded sporoplasmic sacs revealed discharged tubes without membranes.

DIC imaging of microsporidian invasion tubes immediately prior to sporoplasmic sac emergence

Ultrastructural studies indicate that the invasion tube tips had double membrane cylinders at the emerging tube

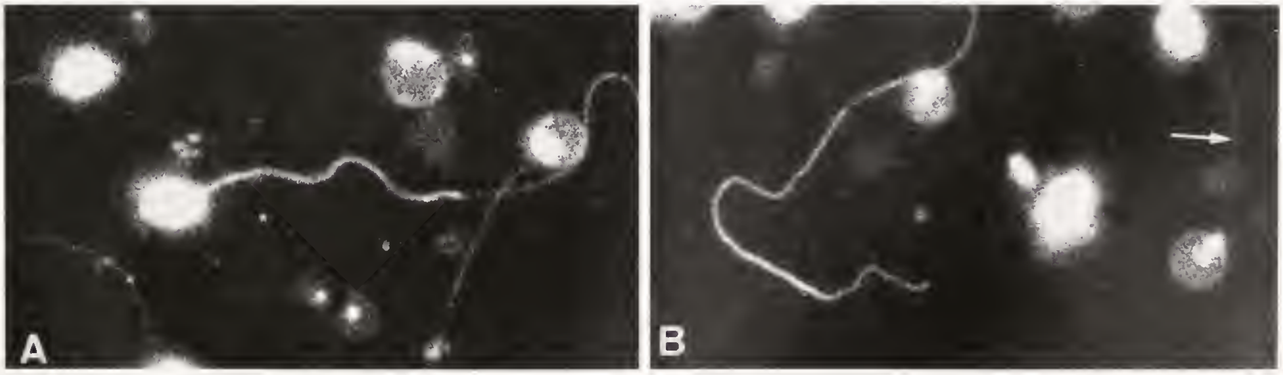

Figure 3. Light optics showing discharging *Spraguea lophii* prelabeled with Nile red. Note the intensity of the fluorescence in the incompletely discharged tubes, indicating the presence of the membrane cylinders extruding from the discharge apparatus (A and B). Arrow shows a completely discharged invasion tube that has been cleared of the membrane cylinders; fluorescence is nearly absent. The spherical body at the tip of this invasion tube is the sporoplasmic sac (arrowhead).

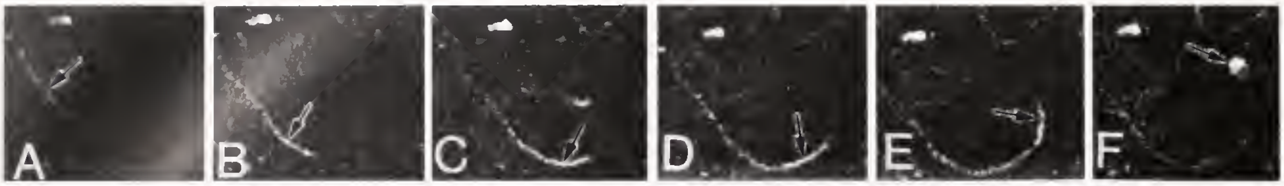

Figure 4. Video sequence showing Nile-red–labeled *Spraguea lophii* spore undergoing tube discharge. (A–E) The fluorescence is higher at the tube tip; ultrastructural images show this area to have two membrane cylinders. (F) Tube is completely assembled and the membrane has emerged into a sporoplasmic sac. Arrows show the end of the extruding tube (A–E) and sporoplasm (F).

ends. With the completion of tube assembly (65–70 μm), membrane sacs emerged followed by a flow of sporoplasm into the sacs. We used DIC imaging to investigate the nature of the tube tip immediately before sporoplasmic sac emergence. Assuming that the inner membrane cylinder moved by an everting motion over the surface of the external cylinder of membrane at the tube tip, a predictable funnel-shaped bladder would be expected before full sporoplasmic emergence. Such a funnel-shaped emergence was observed milliseconds before the appearance of the full sporoplasmic sac (Fig. 6A–C). The timing for this event was significantly increased by preincubating spores in 50 *μM* DAPI overnight. This did not affect spore activation, but produced either a block or a delay in sporoplasmic sac emergence at the tube end.

Discussion

Interactions of invasion tube protein and membrane during assembly

Nile red video data indicate a strong fluorescence for membrane along the length of the invasion tube throughout tube assembly; however, this fluorescence moves to the assembled tube end with the emergence of the sporoplasmic sac. Ultrastructural observations indicate that tube fluorescence is due to the double membrane cylinders that extend the length of forming tubes. Before the PFP begins the eversion process with membrane at the advancing tube terminal assembly site (TAS), the protein is believed to be monomeric and confined to the inside of the tube membrane. However, when the PFP begins eversion with membrane at the TAS, evidence indicates that the protein transforms into a stable polymer (Weidner, 1976). Ultrastructural observations of the TAS indicate that the PFP polymer and adjoining membrane are continuous with the inner tube monomeric PFP and inner membrane at the TAS. At the opposite end of the invasion tube from the TAS, the polymerized PFP and the external cylinder of membrane are attached to the polar aperture of the spore. This membrane has a short-term attachment restricted to the period of tube assembly as indicated by ultrastructural and fluorescent probe studies showing that this membrane is liberated and discharged during sporoplasmic sac formation at the end of the invasion tube.

Video analysis of discharging spores shows invasion tubes growing exclusively at the TAS. This is most obvious in discharging tubes that follow a tortuous path, since all points on the formed tube remain fixed in position while the TAS movement continues by eversion (Weidner, 1982). Furthermore, when video recording data of tube discharge were analyzed with digital sequential frame subtractions (30-ms intervals), the only apparent change was at the discharging tube tip, indicating membrane movement exclusively at the TAS. Finally, DIC imaging clearly indicates tube growth at the TAS by eversion, especially after completion of tube assembly when the membrane at the TAS begins eversion by forming a funnel-shaped bladder (as modeled in Fig. 8).

Membrane behavior in the microsporidian invasion tube is affected by PFP

When membrane assemblages move on or within a cell, the shape the membrane assumes depends on the interactions between the membrane and the associated proteins (Cunningham and Edelman, 1990). The question of whether this general rule applies to specialized organelles that explosively discharge membrane by eversion has arisen because a tubular shape was thought to be an inherent property of this membrane configuration. However, specific examples indicate that this is not the case. Certain kinds of nematocysts (rhopalonemes of siphonophores and spirocysts of anemones) evert a saccular membrane rather than a slender tubular one (Hyman, 1940). Although the end result of microsporidian spore discharge is membrane that is saccular in shape, the initial process begins with the eversion of membrane in a slender tube. Assembly of the microsporidian spore invasion tube continues until all the PFP has emerged to complete tube assembly. After all the PFP has emerged at the TAS, membrane continues to exit the tube. Since this membrane is without associated PFP, it shows an altered behavior by forming a saccular shape at the TAS.

Evidence indicates that the PFP effect on membrane depends on its position and chemical state within the ex-

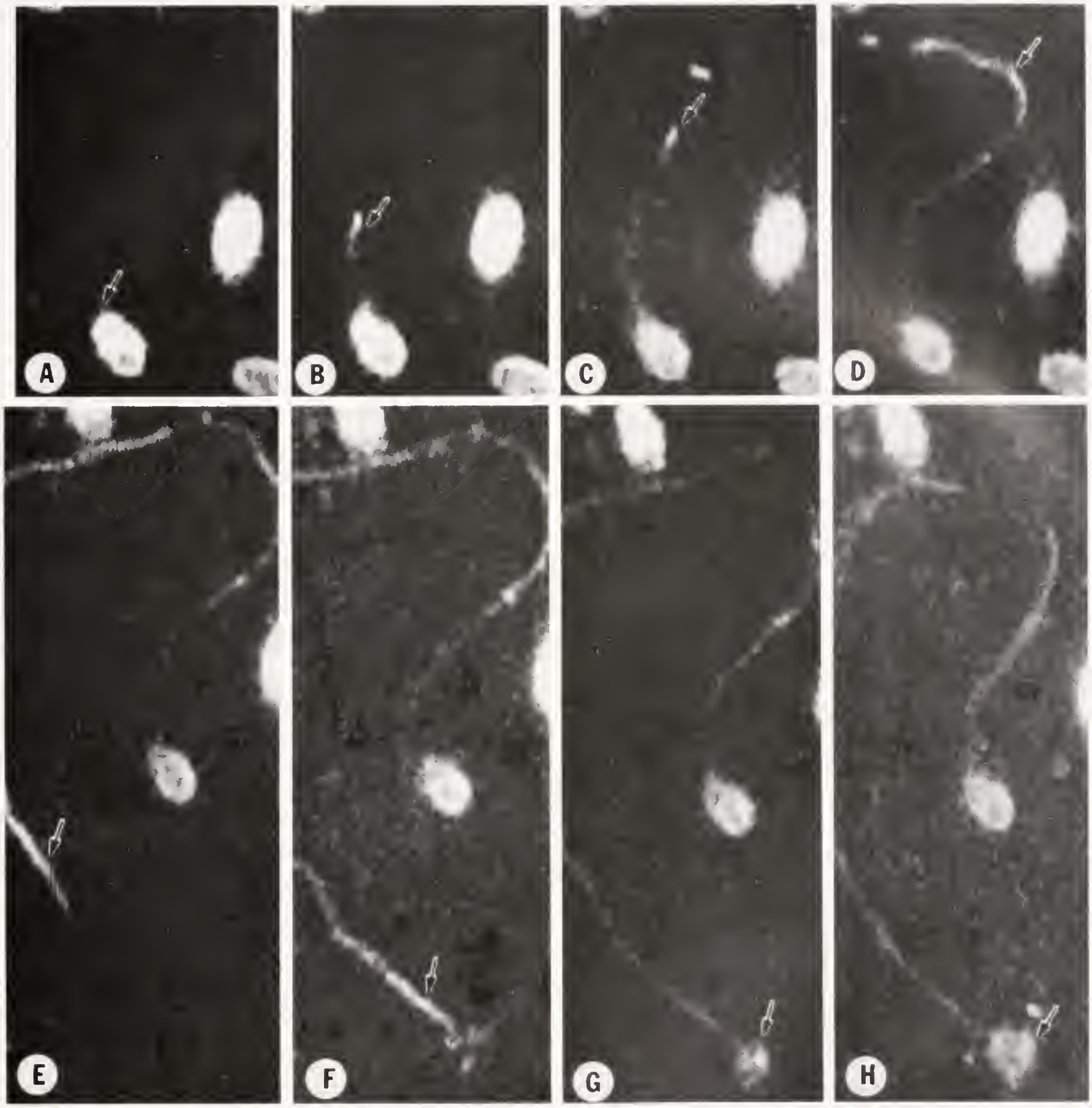

Figure 5. Digital sequential frame subtractions showing Nile-red–labeled *Spraguea lophii* spore undergoing tube discharge and sporoplasmic sac emergence. Each image represents a 30-ms shift in the video. (A–F) The invasion tube is emerging, with the highest level of membrane fluorescence at the tube tip (arrows). (G and H) Fluorescence is greatest in the extruded sporoplasmic sac (arrows), while the remaining tube has lost much of the fluorescence.

trusion tube. During tube assembly, the PFP first appears fluid and has an apparent adhesive affinity for membrane, as indicated by the sharpness by which the PFP everts with its adjoining membrane at the TAS. The sharpness of eversion at the TAS is believed to give the tube some capacity to pierce through substrate (Lom and Vavra, 1963), an ability that would be essential to penetration of host-cell membrane. Although the fluidity of the PFP within the invasion tubes is not clear, isolated PFP polymer displays increased fluidity when subjected to 10^{-4} *M* Ca^{2+}; moreover, discharged PFP tubes show some tendency to fuse or branch when exposed to medium with

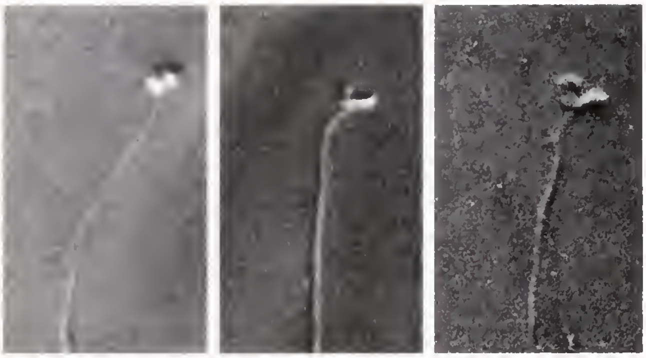

Figure 6. DIC imaging of microsporidian spore invasion tubes immediately before sporoplasmic sac emergence. These three images show a characteristic funnel-shaped bladder emerging from the tube tip milliseconds before the full sporoplasmic sac emerges. Such a shape is predicted when an inner cylinder of membrane is everting and sliding over an outer envelope. Tube thickness is 0.1–0.13 μm

calcium (Weidner, 1982). Also, isolated PFP displays significant fluidity under *in vitro* conditions, although it will not form discrete tubular profiles (Weidner, 1976). When the PFP emerges from discharging tubes at the TAS, the PFP is clearly a polymer, and its stability is obvious because it resists shape change across the pH range and because it resists dissociation in 1% SDS. On the other hand, internal tube PFP that has yet to reach the TAS appears to dissociate in SDS (Weidner, 1976), indicating that it is not a polymer, but monomeric. When monomeric PFP approaches the TAS, it apparently retains an adherence for membrane since these two elements always exteriorize together at the TAS regardless of the physical conditions of the external medium. Several observations indicate that polymerized PFP has little or no membrane adhesiveness. Ultrastructural observations indicate that a substantial space is present between exteriorized PFP polymer and the adjoining membrane within the invasion tube. Also, after all the internal PFP has exited the tube, the remaining membrane of the tube is liberated from the attachment point at the polar aperture and passes to the sac at the end of the tube. Therefore, it appears that monomeric PFP has a strong affinity for membrane until it is exteriorized from the invasion tube, where it becomes a polymer and loses some of its membrane affinity. In a sense, PFP is a morphoregulatory molecule with the membrane behavior being regulated by its association with protein (see Cunningham and Edelman, 1990).

Plasma membrane origins during microsporidian spore discharge

One remarkable feature of microsporidian spore discharge is the discard of the plasma membrane with the spore ghost while all of the sporoplasm (nucleus and cytoplasm) exits through a tube and into a new membrane sac. This discharged sac is thought to develop by the eversion of the extrusion apparatus (EAP) membrane. The EAP membrane is the only probable source for the sporoplasmic sac membrane (Weidner *et al.*, 1984). The model proposed here illustrates how the sporoplasm nucleus and cytoplasm are transferred out of the spore by membrane eversion of the EAP (Figs. 7 and 8). The movement of sporoplasm into the sporoplasmic sac generally appears to occur concurrently. Whether any spo-

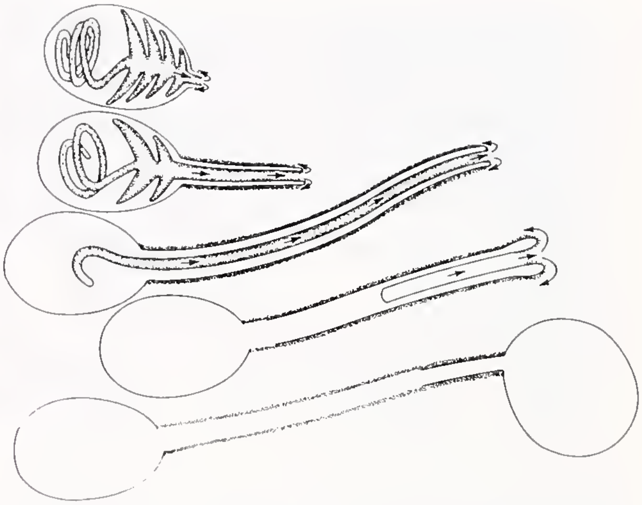

Figure 7. Model illustrating the emergence of the extrusion apparatus (EAP) from the spore. The membrane-bound polar filament everts, with membrane sliding on the membrane, as the inner cylinder delivers the polar filament protein (PFP) (dots within the apparatus) to the tube tip, and the protein stabilizes into outside polymer. Ultimately, when all the protein has been assembled, the remaining membrane continues to slide out and contributes to the sporoplasmic sac at the end of the tube. The last diagram in the sequence shows the empty tube, now represented only by the PFP polymer, and the emerging sporoplasmic sac. The sporoplasm characteristically enters the sporoplasmic sac milliseconds after its emergence.

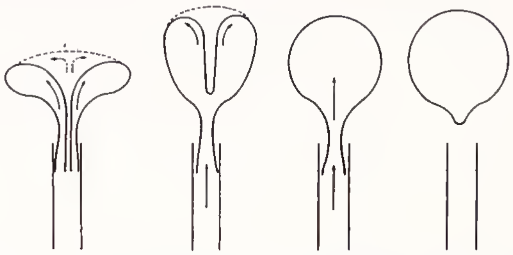

Figure 8. Scheme illustrating how the inner cylinder of membrane slides over the outer cylinder during the emergence of the sporoplasmic sac at the end of the discharged invasion tube. Such an event happens only when the discharged tube is fully assembled. This scheme is primarily based on the DIC images of the tube tip (see Fig. 6) in addition to the ultrastructural observations.

roplasm moves into the sporoplasmic sac without membrane is not clear at this time. The following observations with DAPI and DIC imaging indicate that the EAP membrane system is exterior to the nuclear and cytosolic components of the spore. First, the nucleus and cytosol do not enter the invasion tube until it is fully assembled. Because the invasion tube forms by everting membrane from the EAP, its membrane system segregates it from the sporoplasm within the spore. Thus, the EAP membrane probably has to turn itself inside out before the sporoplasm can move into the EAP compartment. Second, discharged, empty EAP membranous sacs are occasionally observed attached to the ends of invasion tubes while the DAPI stained nucleus remains within the tube. This condition would be impossible unless the EAP and sporoplasm were initially segregated within the spore. The most logical explanation is that the EAP membrane provides the new plasma membrane for the discharged sporoplasm through an everting process.

Figure 8 illustrates our model for EAP eversion into the plasma membrane sac. It is based on DIC images of the TAS immediately preceding full emergence of the membrane sac. The funnel-shaped bladder that commonly appears at the end of the tube is believed to be derived from the inner cylinder of the EAP membrane moving in relation to the outer envelope. Prolonged incubations of activated spores with DAPI slowed the rate of membrane emergence at the ends of assembled tubes and made it easier to observe sac formation. Extended DAPI incubations are thought to affect the membrane movement by perturbing the Ca^{2+} levels within the tube. PFP assembly and disassembly are affected by Ca^{2+} (Weidner, 1982) and, because DAPI can affect the kinetics of Ca^{2+} uptake or release in molecular systems (Meszaros *et al.*, 1987), the changes in membrane behavior caused by prolonged incubations in DAPI may be due either to direct interference with the PFP or to alterations in Ca^{2+} uptake that change the PFP polymerization.

Literature Cited

Banquet, R. S. 1983. Dissolving the nematocyst capsule wall and identifying its protein components. Pp. 335–339 in *Hydra: Research Methods.* H. M. Lenhoff, ed. Plenum Press, New York.

Bonne, D., C. Heusele, C. Simon, and D. Pantaloni. 1985. 4′6-diamidino-2-phenyl-indole, a fluorescent probe for tubulin and microtubules. *J. Biol. Chem* **260:** 2819–2825.

Cali, A. 1991. General microsporidian features and recent findings on AIDS isolates. *J Protozool.* **38:** 625–630.

Cali, A., D. P. Kotler, and J. M. Orenstein. 1993. *Septata intestinalis* N. G., N. sp., an intestinal microsporidian associated with chronic diarrhea and dissemination in AIDS patients. *J Euk Microbiol* **40:** 101–112.

Canning, E. U., and W. S. Hollister. 1991. *In vitro* and *in vivo* investigations of human microsporiosis. *J Protozool* **38:** 631–635.

Canning, E. U., and J. Lom. 1986. *The Microsporidia of Vertebrates* Academic Press, New York.

Cunningham, B. A., and G. M. Edelman. 1990. Structure, expression, and cell surface modulation of cell adhesion molecules. Pp. 9–40 in *Morphoregulatory Molecules* G. M Edelman, B. A. Cunningham, and J. P. Thiery, eds. John Wiley and Sons, New York.

El-Matbouli, M., T. Fischer-Scheri, and R. W. Hoffmann. 1992. Present knowledge on the life cycle, taxonomy, pathology and therapy of some myxosporea spp. important for freshwater fish. *Annu Rev Fish Diseases* 367–402.

Frixione, E., L. Ruitz, M. Santillan, L. V. deVargas, J. M. Tejero, and A. H. Undeen. 1992. Dynamics of polar filament discharge and sporoplasm expulsion by microsporidian spores. *Cell Motil Cytoskel.* **22:** 781–789.

Greenspan, P., and S. D. Fowler. 1985. Spectrofluorometric studies of the lipid probe, Nile red. *J Lipid Res* **26:** 781–789.

Greenspan, P., E. P. Mayer, and S. D. Fowler. 1985. Nile red: a selective fluorescent stain for intracellular lipid droplets. *J Cell Biol* **100:** 965–973.

Hausmann, K. 1978. Extrusive organelles in protists. Pp. 197–276 in *Internatl Rev Cytol* Vol. 52, G. H. Bourne and J. F. Danielli, eds. Academic Press, New York.

Hyman, L. H. 1940. *The Invertebrates Protozoa through Ctenophora,* pp. 382–392. McGraw-Hill, New York.

Koo, G. C., C. W. Stackpole, E. A. Boyse, U. Hammerling, and M. P. Lardis. 1973. Topographical location of H-Y antigen on mouse spermatozoa by immuno-electron microscopy. *Proc. Natl Acad Sci. USA* **70:** 1502–1505.

Lom, J., and E. R. Noble. 1984. Revised classification of the class Myxosporea Butschli, 1881. *Folia Parasitol.* **31:** 193–205.

Lom, J., and J. Vavra. 1963. The mode of sporoplasmic extrusion in microsporidian spores. *Acta Protozool.* **1:** 81–89.

Meszaros, L. G., K. L. Brown, and N. Ikemoto. 1987. 4′6-diamidino-2-phenylindole, a novel conformational probe of the sarcoplasmic reticulum Ca^{2+} pump, and its effect on Ca^{2+} pump, and its effect on Ca^{2+} release. *J Biol Chem* **262:** 11553–11558.

Orenstein, J. M., J. Chiang, W. Steinberg, P. D. Smith, H. Rotterdam, and D. P. Kotler. 1990. Intestinal microsporidiosis as a cause of diarrhea in human immunodeficiency virus-infected patients: a report of 20 cases. *Hum Pathol.* **21:** 475–481.

Undeen, A. H. 1990. A proposed mechanism for the germination of microsporidian (Protozoa: Microspora) spores. *J Theor Biol* **142:** 233–235.

Weidner, E. 1976. The microsporidian spore invasion tube. The ultrastructure, isolation and characterization of the protein comprising the tube. *J Cell Biol.* **71:** 23–34.

Weidner, E. 1982. The microsporidian spore invasion tube. III. Tube extrusion and assembly. *J Cell Biol.* **93:** 976–979.

Weidner, E., W. Byrd, A. Scarborough, J. Pleshinger, and D. Sibley. 1984. Microsporidian spore discharge and the transfer of polaroplast organelle membrane into plasma membrane. *J Protozool* **31:** 208–213.

Weidner, E., S. B. Manale, S. K. Halonen, and J. W. Lynn. 1994. Microsporidian spore invasion tubes as revealed by fluorescent probes. *Biol. Bull.* **187:** 255–256.

Reference: *Biol. Bull.* **188**: 136–145. (April, 1995)

Microtubule Arrays During Ooplasmic Segregation in the Medaka Fish Egg (*Oryzias latipes*)

V. C. ABRAHAM[1], A. L. MILLER[2], AND R. A. FLUCK[1],*

[1]*Biology Department, Franklin and Marshall College, Lancaster, Pennsylvania 17604-3003; and*
[2]*Marine Biological Laboratory, Woods Hole, Massachusetts 02543*

Abstract. We used indirect immunofluorescence to study microtubule arrays in the medaka egg between fertilization (normalized time, T_n, = 0) and the first cleavage (T_n = 1.0). Eggs were fixed at various times after fertilization and examined with conventional fluorescence microscopy, laser scanning confocal microscopy, and three-dimensional fluorescence microscopy. Soon after the eggs were fertilized ($T_n = 0.02$), we saw microtubules oriented perpendicular to the plane of the plasma membrane but none parallel to the plasma membrane. Later ($T_n = 0.08$), we saw an array of microtubules oriented more or less parallel to the plasma membrane but having no apparent preferred orientation with respect to the animal-vegetal axis of the egg. In the interpolar regions of the egg, this network increased in density by $T_n = 0.24$ and remained a constant feature of the ooplasm until the first cleavage. From $T_n = 0.30$ to 0.76 the polar regions of the egg contained dense arrays of organized microtubules. At the animal pole, microtubules radiated from a site near the pronuclei; while at the vegetal pole, an array of parallel microtubules was present. Injection of the weak (K_D = 1.5 μM) calcium buffer 5,5′-dibromo-BAPTA disrupted the radial pattern of microtubules near the animal pole but had no apparent effect on the parallel array of microtubules near the vegetal pole. Because this buffer has previously been shown to suppress a zone of elevated cytosolic calcium at the animal pole and to disrupt ooplasmic segregation in this egg, the results of the present study (1) are consistent with a model in which microtubules are required for ooplasmic segregation in the medaka egg, and (2) suggest that the normal function of a microtubule-organizing center at the animal pole of the egg requires a zone of elevated calcium.

Introduction

Ooplasmic segregation in the medaka egg consists of the approximately simultaneous streaming of ooplasm toward the animal pole, the saltatory movement of parcels toward the animal pole and vegetal pole, and the movement of oil droplets toward the vegetal pole (Abraham *et al.*, 1993a; Webb and Fluck, 1993). These movements are roughly simultaneous and are essentially completed during the first cell cycle. Streaming of ooplasm toward the animal pole is inhibited by cytochalasin D and thus presumably requires microfilaments (Webb and Fluck, 1993), whereas saltatory movements and the movement of oil droplets toward the vegetal pole are both inhibited by microtubule poisons and thus presumably require microtubules (Abraham *et al.*, 1993a). All of these movements can be easily observed in the optically clear medaka egg, in which a thin (≈15 μm thick) peripheral layer of ooplasm surrounds a large, central yolk vacuole.

In a number of diverse animals, including annelids (Astrow *et al.*, 1989), ctenophores (Houliston *et al.*, 1993), echinoderms (Harris *et al.*, 1980), ascidians (Sawada and Schatten, 1988), and amphibians (Elinson and Rowning, 1988; Houliston and Elinson, 1991; Schroeder and Gard, 1992; Elinson and Palaček, 1993), a network of microtubules that forms during the first cell cycle is required for the movement of specific components of the ooplasm, including the pronuclei. In the present study, we describe the development of such an array of microtubules during the first cell cycle of the medaka egg. Previous studies of microtubules in teleost embryos either have provided very little information (Beams *et al.*, 1985) or have been done on later stages of development (Strähle and Jesuthasan, 1993; Solnica-Krezel and Driever, 1994).

We also pursued the hypothesis that gradients of cytosolic free Ca^{2+} organize the multimolecular assemblies

Received 20 June 1994; accepted 11 January 1995.

* To whom correspondence should be addressed.

involved in ooplasmic segregation in the medaka egg. Zones of elevated calcium are present at the animal and vegetal poles of the medaka egg during segregation (Fluck *et al.*, 1992). Moreover, injection of 5,5′-dibromo-BAPTA (hereafter referred to as dibromo-BAPTA), a weak calcium buffer that dissipates cytosolic calcium gradients (Pethig *et al.*, 1989; Speksnijder *et al.*, 1989; Fluck *et al.*, 1992), inhibits ooplasmic segregation in this egg (Fluck *et al.*, 1994). In the present study we monitored the effects of this buffer on the spatiotemporal pattern of microtubules and on pronuclear movements. A preliminary account of these findings has been published (Abraham *et al.*, 1993b).

Materials and Methods

Procedures

Methods for removing gonads from breeding medaka and for the *in vitro* fertilization of eggs have been described previously (Abraham *et al.*, 1993a). Some eggs were incubated in 100 μ*M* colchicine (dissolved in buffered saline solution: 111 m*M* NaCl; 5.37 m*M* KCl; 1.0 m*M* $CaCl_2$; 0.6 m*M* $MgSO_4$; 5 m*M* HEPES, pH 7.3) for 1 h at room temperature (20°–25°C) before they were fertilized.

Using a high-pressure microinjection system, we injected enough 50 m*M* dibromo-BAPTA (tetrapotassium salt; containing 5 m*M* HEPES, pH 7.2, and sufficient $CaCl_2$ to set $[Ca^{2+}]_{free}$ at 100 n*M*) to raise the cytosolic concentration to 2.7 m*M* (Fluck *et al.*, 1992). Injections were made within 10° arc toward the vegetal pole from the equator within 6 min after fertilization. Control eggs received a comparable volume (*ca.* 1.5 nl) of 150 m*M* KCl, 5 m*M* HEPES, pH 7.2.

The procedures for indirect immunofluorescence were those developed by Gard (1991) for the study of microtubules in *Xenopus laevis* eggs. At regular intervals after fertilization, eggs were transferred to fixative solution at room temperature (3.7% formaldehyde, 0.25% glutaraldehyde, 0.2% Triton X-100, 5 m*M* EGTA, 1 m*M* $MgCl_2$, 80 m*M* potassium PIPES, pH 6.8). After 4 h, the eggs were dechorionated with fine forceps and post-fixed in absolute methanol (−20°C) overnight. The eggs were then washed with phosphate-buffered saline (PBS: 128 m*M* NaCl; 2 m*M* KCl; 8 m*M* NaH_2PO_4; 2 m*M* KH_2PO_4, pH 7.2) and incubated in 100 m*M* sodium borohydride (in PBS) for 6 h. The eggs were then washed with cold Tris-buffered saline (TBS: 155 m*M* NaCl; 10 m*M* Tris-Cl, pH 7.4; 0.1% Nonidet P-40); transferred to Lab-Tek chamber slides (Thomas Scientific, Swedesboro, New Jersey); incubated with a monoclonal mouse anti-α-tubulin antibody (ICN, DM1A; diluted 1:250 with TBS containing 2% bovine serum albumin); washed with TBS for 24 h; incubated with the secondary antibody (rhodamine-conjugated goat anti-mouse IgG, diluted 1:25 with TBS containing 2% bovine serum albumin); and washed for 24 h with TBS. We performed two kinds of antibody controls: omission of the primary antibody and omission of both the primary and the secondary antibodies. To stain the nuclei, we incubated the eggs for 30 min in a solution of Hoechst 33258 (10 μg ml^{-1}) in TBS.

The eggs were mounted between a coverglass and a microscope slide as described previously (Abraham *et al.*, 1993a) and examined by one of three methods. Conventional epifluorescence microscopy was performed with a Nikon Optiphot microscope coupled to a Dage-MTI SIT camera and video monitor; in later replicates, the SIT camera was coupled to a Dage-MTI DSP-2000 image processor. In either case, the image on the monitor was photographed through a Ronchi grating (Rolyn Optics Co., Covina, California; Inoué, 1981). Some eggs were examined with a laser scanning confocal microscope (Zeiss LSCM 410) at the Marine Biological Laboratory.

We also acquired and processed images at the Science and Technology Center at Carnegie-Mellon University. Images at each focal plane were acquired on a multimode microscope (Biological Detection Systems, Inc., Pittsburgh, Pennsylvania) equipped with a 576 × 384 Thompson chip, cooled CCD camera (Photometrics Ltd., Tucson, Arizona). Three-dimensional fluorescence microscopy used the nearest neighbor algorithm to correct for out-of-focus fluorescence (Biological Detection Systems, Inc.) The final three-dimensional representation was generated with the program ANALYZE (Biomedical Imaging Resource, Mayo Foundation, Rochester, Minnesota) on the SGI, Inc., ONYX workstation.

The results summarized herein represent 11 replicate experiments in which we fixed eggs at various intervals after fertilization and three replicate experiments in which we examined the effects of dibromo-BAPTA on microtubules. In all, we have examined a total of 117 eggs from 17 females, including 20 eggs into which we injected dibromo-BAPTA and 8 eggs into which we injected KCl.

Chemicals

Formaldehyde and glutaraldehyde were obtained from Electron Microscopy Sciences (Fort Washington, Pennsylvania); Triton X-100, Nonidet P-40, sodium borohydride, bovine serum albumin, Hoechst 33258, and colchicine from Sigma (St. Louis, Missouri); 5,5′-dibromo-BAPTA from Molecular Probes (Eugene, Oregon); anti-α-tubulin antibody from ICN (Costa Mesa, California); and rhodamine-conjugated goat anti-mouse IgG from Organon Teknika (Malvern, Pennsylvania).

Results

The various events that constitute ooplasmic segregation in the fertilized medaka egg have already been described in detail (Abraham *et al.*, 1993a) and are only summarized below. To indicate the relative temporal position of these events, we have used a normalized time (T_n) scale in which the time between fertilization and the beginning of cytokinesis is 1 unit. In the range of room temperatures in which the experiments were done (20°–25°C), 1 unit of normalized time corresponds to 75–110 min. Fertilization in the medaka egg is followed by a cortical granule reaction and a contraction, during which the ooplasm and its contents appear to be pulled toward the animal pole. The second meiotic division is completed by $T_n \approx 0.12$ and is followed closely by a second animal-pole-directed contraction at $T_n \approx 0.15$. This second contraction heralds the beginning of ooplasmic segregation in the form of streaming of ooplasm toward the animal pole, saltatory movements of parcels toward both polar regions, and movement of oil droplets (a class of ooplasmic inclusions) of various sizes toward the vegetal pole. At $T_n = 1.0$, the blastodisc divides into two blastomeres. By this time the oil droplets have formed a crude ring around the vegetal pole.

Microtubule network dynamics during ooplasmic segregation

We identified three regions of the medaka egg on the basis of the spatiotemporal pattern of microtubules in them (Figs. 1–3): (1) a region within 30° (≈300 μm) arc of the animal pole; (2) a region within 60° (≈600 μm) arc on both sides of the equator; and (3) a region within 30° (≈300 μm) arc of the vegetal pole. In all regions of the egg except the animal pole, all the microtubules were within 2–3 μm of the surface of the egg and were visible in a single optical section.

$T_n \approx$ *0.02, 0.08, and 0.16.* The earliest time at which we fixed eggs was $T_n = 0.02$; that is, immediately after the contraction that follows the cortical granule reaction. Though we searched the ooplasm everywhere on these eggs (and all of the ooplasm is peripheral, see Introduction), we saw no microtubules parallel to the surface of the egg but saw instead a punctate pattern of fluorescence (Fig. 1A). Analysis of these eggs by three-dimensional fluorescence microscopy suggests that the sources of fluorescence were microtubules oriented perpendicular to the surface of the egg (Fig. 1B). This punctate pattern was a prominent feature of eggs fixed at $T_n = 0.02$ and 0.08 and was less prominent at later stages.

In eggs fixed at $T_n \approx 0.08$, we saw a very sparse network of microtubules oriented parallel to the surface of the egg but having no apparent preferred orientation with respect to the animal-vegetal axis of the egg. This network was roughly confined to the animal hemisphere, and we saw no microtubules in most of the vegetal hemisphere (Fig. 1C, D).

In eggs fixed at $T_n \approx 0.16$—by which time ooplasmic segregation has begun in the form of streaming, saltatory movements, and oil droplet movement—a network of microtubules was present throughout the ooplasm, and the network in the equatorial region was denser than at $T_n \approx 0.08$ (Fig. 1E). The network did not yet appear to have a preferred orientation.

To test for autofluorescence, we examined fixed eggs that were incubated with no antibodies and that were processed for viewing up to the first wash with TBS. We saw no fluorescence at all in these eggs (data not shown). We also examined eggs that were incubated with the secondary antibody but not with the primary antibody. In these eggs, we saw diffuse fluorescence but no linear elements or punctate sources of fluorescence (Fig. 1F). In eggs incubated with 100 μM colchicine before fixation and incubated with both the primary and secondary antibodies, we saw diffuse fluorescence but no microtubules or any punctate sources of fluorescence (data not shown).

The pattern of microtubules in eggs fixed at $T_n \approx 0.16$ is summarized in Fig. 3A.

$T_n =$ *0.24, 0.3, 0.4, 0.76.* In ooplasm near the equator, the network of microtubules was denser than at $T_n = 0.16$ (Fig. 2A; compare with Fig. 1E) but still showed no preferred orientation with respect to the animal-vegetal axis. In contrast, oriented microtubule networks were present near the vegetal pole and animal pole by $T_n = 0.24$ and $T_n = 0.3$, respectively. Near the vegetal pole, an array of (mostly) parallel microtubules was present (Fig. 2B). This "vegetal mat" extended about 30° arc (300 μm) in all directions from the vegetal pole and covered at least 30% of the area of the vegetal hemisphere. The orientation of microtubules was uniform throughout the vegetal mat. Beyond the edges of the mat, the network of microtubules abruptly lost its orientation and became the network characteristic of interpolar ooplasm. Using the z-sectioning function of the LSCM 410, we determined that the thickness of the microtubule network in the vegetal mat (≈2.7 μm) was the same as the thickness of the unoriented microtubule network just outside the mat. The two networks appeared to be continuous with each other and were in the same optical section, suggesting that the two networks are located at the same depth in the ooplasm.

Near the animal pole, microtubules were oriented more or less along meridian lines and appeared to radiate from a microtubule-organizing center near the male and female pronuclei, which were 38.6 ± 6.7 μm ($\bar{X} \pm$ SD, $n = 5$) below the surface of the blastodisc at $T_n \approx 0.76$ (Fig. 2D–I). This network of oriented microtubules extended approximately 30° arc (300 μm) in all directions from the animal pole.

The pattern of microtubule distribution in eggs fixed at $T_n = 0.30$–0.76 is summarized in Fig. 3B.

$T_n =$ *1.0.* In these eggs, the blastodisc has begun to divide into two blastomeres, and essentially all oil droplets have aggregated in a crude ring near the vegetal pole. Each

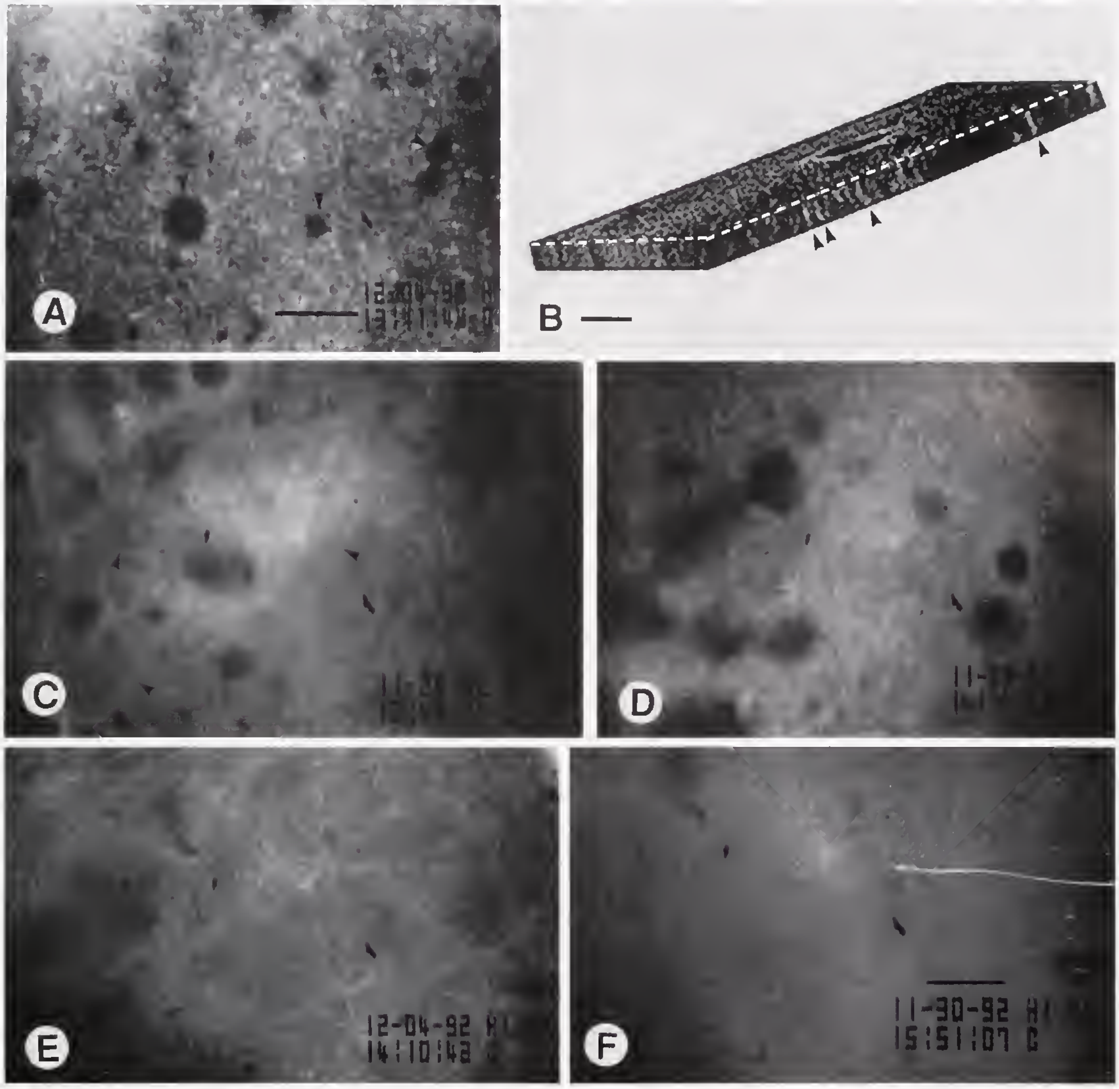

Figure 1. Formation of a network of microtubules in the fertilized egg. A, C, D, E, and F were obtained by conventional epifluorescence microscopy and B by three-dimensional fluorescence microscopy. Scale bars, 10 μm. A, C, D, and E are printed at the same magnification, B at another, and F at another. (A) Ooplasm near the equator of an egg fixed at $T_n = 0.02$. Characteristic of this stage of development are a punctate pattern of fluorescence throughout the ooplasm and the absence of unambiguous microtubular elements oriented parallel to the plasma membrane. The dark structures (arrowheads) are ooplasmic inclusions. (B) Three-dimensional rendering of optical sections of ooplasm near the equator at $T_n = 0.024$. Using a 100× objective lens, we made 33 optical sections at steps of 0.158 μm, beginning at the surface of the egg. Visible in this reconstruction are both the punctate pattern at the surface of the egg (the top of the image) and linear elements that are oriented perpendicular to the surface of the egg (arrowheads). Two edges of the reconstruction are marked by a white dashed line. (C) Ooplasm near the animal pole of an egg fixed at $T_n = 0.08$. Note the presence of unambiguous microtubules in the field (arrowheads). (D) Ooplasm near the vegetal pole of an egg fixed at $T_n = 0.08$. This image was obtained from the same egg as Fig. 2C. No unambiguous microtubules oriented parallel to the plasma membrane can be seen. (E) Ooplasm near the equator of an egg fixed at $T_n = 0.16$. The animal-vegetal axis runs from lower left to upper right. This unoriented network is denser than that found at the equator of an egg fixed at $T_n = 0.08$ (not shown). (F) In eggs not incubated with the primary antibody after fixation ($T_n = 0.4$), we saw only weak and diffuse fluorescence but saw neither any filamentous structures nor a punctate pattern of fluorescence. These images were obtained by standard epifluorescence microscopy.

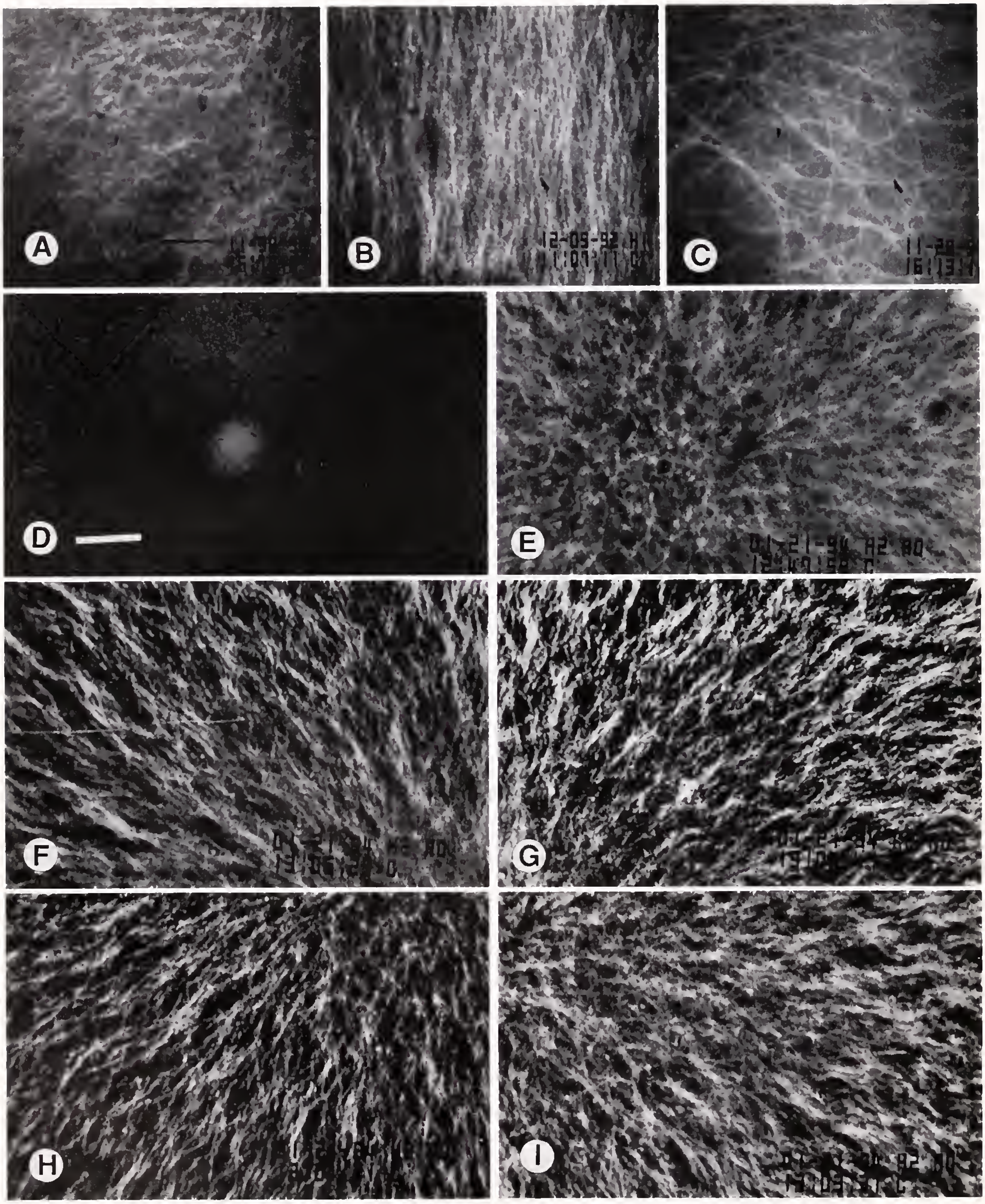

Figure 2. Microtubule arrays in eggs fixed at $T_n = 0.4$–1.0. All images were obtained by conventional epifluorescence microscopy. Scale bars: A, 10 μm; D, 25 μm. A–C were printed at one magnification, D–I at another. (A) Equatorial ooplasm of an egg fixed at $T_n = 0.4$. The animal-vegetal axis runs from lower left to upper right. The microtubule network here is denser than in eggs fixed at $T_n = 0.16$ (compare with Fig. 1C) and still has no apparent preferred orientation. (B) The vegetal mat of parallel microtubules in an egg fixed at $T_n = 0.4$. Practically all the microtubules share a single orientation in this mat, which we saw at $T_n = 0.24$–0.76. (C) Ooplasm at the vegetal pole of an egg fixed at $T_n = 1.0$. The parallel organization of microtubules near the vegetal pole is gone. (D and E) The same microscopic field of a double-stained egg

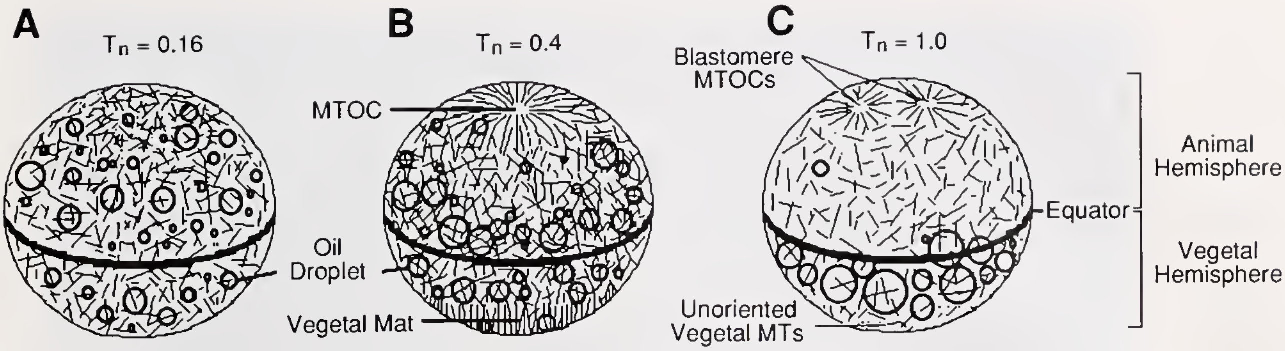

Figure 3. Summary of the spatial distribution of microtubules in medaka during the first cell cycle. The diagrams were drawn approximately to scale with respect to the size of the microtubule-organizing center, the vegetal mat, and oil droplets; but the thickness of individual microtubules has been greatly exaggerated to demonstrate the arrays clearly. The diameter of the egg is about 1140 μm. (A) Microtubules in an egg fixed at $T_n = 0.16$. An unoriented network of microtubules, denser near the animal pole, is present throughout the egg. (B) Microtubules in an egg fixed at $T_n = 0.4$. An array of microtubules that radiate from a zone in the blastodisc near the pronuclei forms by $T_n = 0.3$ and persists until at least $T_n = 0.76$, while at the vegetal pole, a mat of parallel microtubules forms by $T_n = 0.24$ and persists until at least $T_n = 0.76$. Microtubules in interpolar ooplasm have no preferred orientation at any time. Note that most of the oil droplets from the animal hemisphere have moved into the equatorial region by this time. (C) Microtubules in an egg fixed at $T_n = 1.0$. Two microtubule-organizing centers, one at each pole of the dividing blastodisc, are present. The density of microtubules in interpolar ooplasm has decreased, and the parallel organization of microtubules at the vegetal pole has been lost.

of these blastomeres had a microtubule-organizing center (data not shown) similar to the one present in the blastodisc from $T_n = 0.30$ to at least $T_n = 0.76$. The parallel organization of the microtubule network near the vegetal pole was lost by this stage (Fig. 2C). The pattern of microtubules in eggs fixed at $T_n \approx 1.0$ is summarized in Fig. 3C.

Microtubule networks in eggs injected with 5,5'-dibromo-BAPTA

The effects of injected KCl and dibromo-BAPTA on microtubule networks are summarized in Figures 4 and 5. The microtubule networks in eggs into which we injected KCl were indistinguishable from those found in uninjected eggs fixed at the same time ($T_n = 0.76$ [from 57 min to 84 min after fertilization, depending on the temperature]; Fig. 4A [compare with Fig. 2B], 5A [compare with Fig. 2A]). The parallel organization of microtubules in the vegetal mat was not disrupted by dibromo-BAPTA (Fig. 4B). However, the injection of dibromo-BAPTA had profound effects on the microtubule networks near the animal pole, where the radiating pattern of microtubules near the animal pole was disrupted (Fig. 4C, D). The only apparent effect of dibromo-BAPTA on the microtubule arrays in the equatorial region was a decrease in the density of microtubules near the injection site (Fig. 5B, C).

Dibromo-BAPTA also inhibited the movement of the pronuclei. At $T_n \approx 0.5$, the distance between the male and female pronuclei was as follows: uninjected control eggs, 1.8 ± 3.0 μm ($\bar{X} \pm SD$, $n = 10$ eggs); eggs into which we injected KCl, 1.7 ± 3.4 μm ($n = 4$ eggs); eggs into which we injected dibromo-BAPTA, 40.4 ± 28.6 μm ($n = 5$ eggs). A one-way analysis of variance and *post-hoc* Student's *t*-tests revealed that the BAPTA-treated eggs differed significantly ($P = 0.038$) from the other two treatments.

Discussion

The pattern of microtubules in the fertilized medaka egg varied both temporally and spatially during the first cell cycle. Temporal changes included an increase in the density of microtubules throughout the ooplasm and changes in the degree of orientation of microtubules in

---

($T_n = 0.4$) is shown, using either a filter to show the fusing Hoechst-stained pronuclei (D) or one to show rhodamine-stained microtubules (E). Microtubules radiate from a region near the pronuclei, roughly following meridian lines. (F–I) These are photographs of four quadrants around, and just outside, the region containing the pronuclei. Note the strong orientation of microtubules along meridian lines. The pronuclei are to lower right in F, lower left in G, upper right in H, upper left in I.

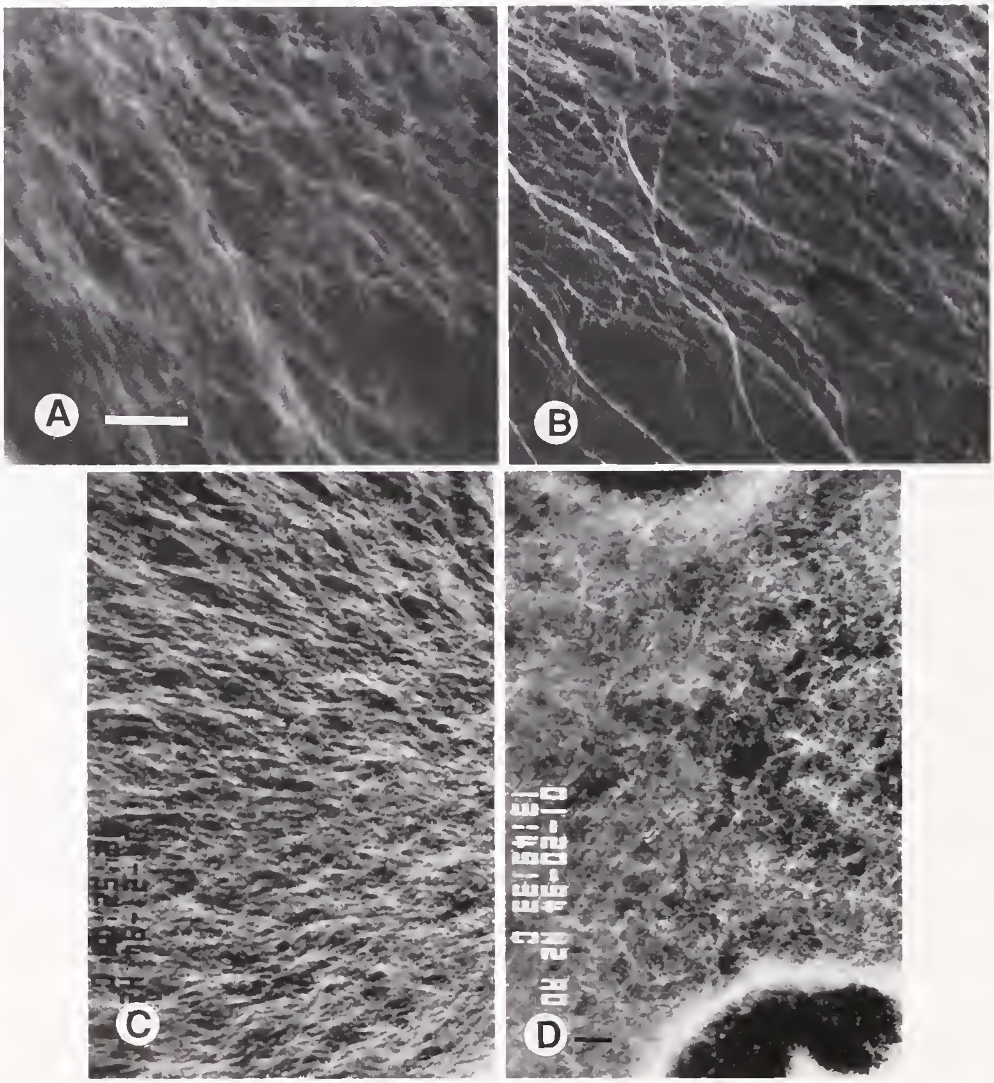

Figure 4. The effect of dibromo-BAPTA on microtubule arrays in polar ooplasm. All eggs were fixed at $T_n = 0.50$. A and B are confocal images obtained using the Zeiss laser scanning confocal microscope; C and D were obtained by standard epifluorescence microscopy. Scale bar = 10 μm; A and B are at the same magnification, C and D at another. (A and B) Injection of neither KCl (A) nor dibromo-BAPTA (B; fixed 32 min after fertilization and about 26 min after injection of dibromo-BAPTA) had any apparent effect on the parallel array of microtubules in the vegetal mat. (C) Microtubules are oriented along meridian lines near the animal pole of this control (uninjected) egg. The pronuclei are to the right of the region shown in this photograph. (D) Injection of dibromo-BAPTA disrupted the radial pattern of microtubules in the blastodisc. This egg was fixed about 52 min after fertilization and about 46 min after the injection of dibromo-BAPTA. Note the absence of radially oriented microtubules in this photograph, which is of the same region of the egg as the one shown in Fig. 4C.

the polar regions of the egg. The striking feature of the region near the animal pole was the development of an array of microtubules that radiated from near the pronuclei to approximately 30° arc from the animal pole. Though microtubules were initially ($T_n = 0.08$) present near the animal pole as a sparse unoriented network, a dense network of radially oriented microtubules had formed by $T_n = 0.3$. Such radial arrays of microtubules are present in fertilized eggs of a number of animals, including annelids (Astrow *et al.*, 1989), ctenophores (Houliston *et al.*, 1993), echinoderms (Harris *et al.*, 1980), ascidians (Sawada and Schatten, 1988), and amphibians (Houliston and Elinson, 1991; Schroeder and Gard, 1992; Elinson and Palaček, 1993), and are associated with the sperm aster and sometimes with the female pronucleus as well.

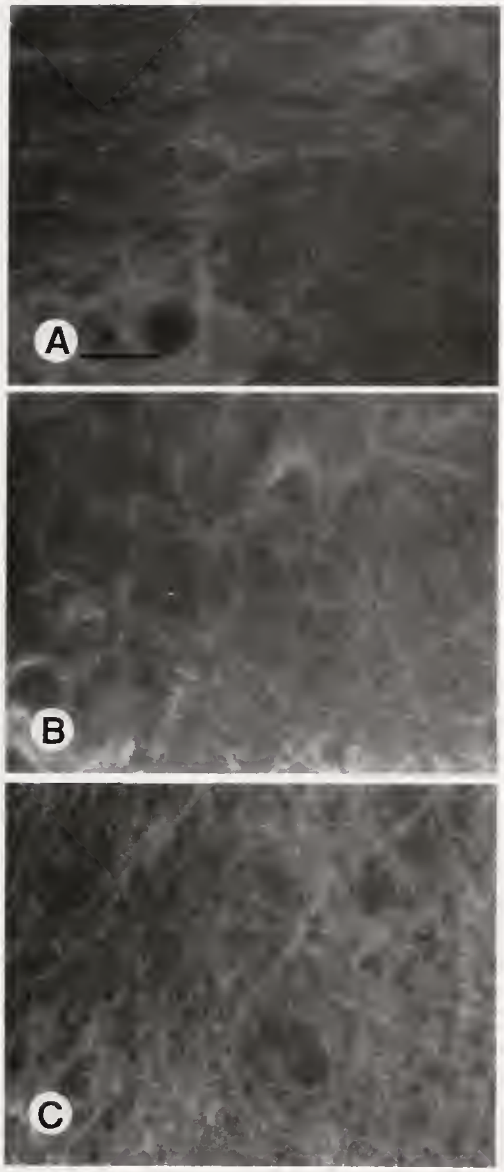

Figure 5. The effects of KCl and dibromo-BAPTA on microtubule arrays in equatorial ooplasm. All eggs were fixed at $T_n = 0.76$ (about 60 min after fertilization and about 54 min after injection of dibromo-BAPTA), and all images were obtained using the Zeiss laser scanning confocal microscope. Scale bar, 10 μm. (A) In eggs into which we injected KCl, the array of microtubules was similar to uninjected controls (not shown). The animal-vegetal axis runs from left to right. (B and C) Injection of dibromo-BAPTA appeared to decrease the density of microtubules near the injection site (B: the animal-vegetal axis runs from right to left) relative to the density observed at the antipode of the injection site (C: the animal-vegetal axis runs from bottom to top).

The mat of parallel microtubules at the vegetal pole of the medaka egg is reminiscent of the one found at the vegetal pole of amphibian eggs, where it is involved in the cortical rotation that forms the gray crescent and thus determines the dorsal-ventral axis of the embryo (Manes *et al.*, 1978; Scharf and Gerhart, 1983; Vincent *et al.*, 1987; Gerhart *et al.*, 1989; Elinson and Rowning, 1988; Elinson and Palaček, 1993). A similar array of parallel microtubules is also present at the vegetal pole of the zebrafish (*Danio rerio*) egg (see Fig. 9C in Strähle and Jesuthasan, 1993). Although there is no evidence for the occurrence of a cortical rotation in the medaka egg, embryos of some primitive fishes that undergo holoblastic cleavage (species in the Superorder Chondrostei within the Actinopterygii, for example the sturgeon, *Acipenser güldenstädti*) do form a gray crescent and thus perhaps do undergo a cortical rotation (reviewed by Bolker, 1993; see also Clavert, 1962; Ginsburg and Dettlaff, 1991). In amphibian eggs, the plane of the first cleavage is parallel to the microtubules near the vegetal pole; and in both amphibians and primitive fishes, the plane of the first cleavage bisects the gray crescent along a meridian (Bolker, 1993). We are currently pursuing the question of the relationship between the orientation of microtubules in the vegetal mat and that of the embryonic axes in the medaka egg. In both *Xenopus laevis* and the medaka, the parallel orientation of the microtubules in the vegetal pole region is transient. In *X. laevis*, this mat begins to form at $T_n \approx 0.55$ and disappears after $T_n \approx 0.8$ (Elinson and Palacek, 1993). In medaka eggs, it is present by $T_n \approx 0.24$ and is still present at $T_n \approx 0.76$; but by the beginning of the first cleavage, the network has lost its parallel organization.

In sharp contrast to the strongly oriented networks of microtubules in polar ooplasm, interpolar ooplasm contained a network of crisscrossed microtubules having no apparent preferred orientation. Microtubules were present here by $T_n = 0.08$ and subsequently increased in density through $T_n = 0.24$. The lack of orientation of microtubules in this region of the medaka eggs contrasts with the situation in the zebrafish egg, in which microtubules are oriented along the animal-vegetal axis during both the first cell cycle and epiboly (Strähle and Jesuthasan, 1993; Solnica-Krezel and Driever, 1994).

Because microtubule poisons inhibit the movement of oil droplets toward the vegetal pole of the medaka egg, it has been suggested that these droplets are transported along microtubules by microtubule-based motors (Abraham *et al.*, 1993a). Further, because oil droplets move toward the vegetal pole roughly along meridians, we predicted that a network of microtubules, also oriented more or less along meridians, would extend from the animal pole to near the vegetal pole. Although such a pattern did develop near the animal pole by $T_n = 0.3$, a time when oil droplets have begun to move toward the vegetal pole, we saw no such preferred orientation of microtubules in most of the interpolar ooplasm, suggesting that oil droplets move toward the vegetal pole along a biochemically distinct (Gard, 1991; Wolff *et al.*, 1992) subset of interpolar microtubules that are oriented along meridian lines.

The movement of most oil droplets toward the vegetal pole of the medaka egg begins at $T_n \approx 0.15$–0.30 (Catalone and Fluck, 1994). The results of the present study, which show that microtubules are present before oil droplets begin to move toward the vegetal pole, suggest that this movement is triggered by some factor other than the appearance of microtubules. We have also shown that even though the movement of oil droplets is "frozen" at the antipode of the site at which dibromo-BAPTA is injected into the egg (Fluck *et al.*, 1994), many microtubules are present in this region of the ooplasm. Factors that could initiate the movement of oil droplets toward the vegetal pole include the formation of an appropriate subtype of microtubules, the activation of a microtubule-based motor such as kinesin (Brady *et al.*, 1990; Schnapp *et al.*, 1992), fulfillment of a requirement that a minimum number of microtubules be associated with an oil droplet before it begins to move, or a gel-sol transition of the ooplasm (Janson and Taylor, 1993) that frees the droplets and enables them to move toward the vegetal pole.

We have also demonstrated in the present study that injection of dibromo-BAPTA into medaka eggs affects the pattern of microtubules in the egg. This relatively weak calcium buffer ($K_D = 1.5\ \mu M$; Pethig *et al.*, 1989) is believed to act as a shuttle buffer, one that binds Ca^{2+} at the high end of a [Ca^{2+}] gradient and releases it at the low end; in other words, the buffer facilitates the diffusion of Ca^{2+} within the cell (Speksnijder *et al.*, 1989). The time between injection of dibromo-BAPTA and fixation of the eggs in the present study was sufficient for the buffer to diffuse to both the animal pole and vegetal pole, to dissipate cytosolic Ca^{2+} gradients near the poles, and to inhibit the formation of the blastodisc and the movement of oil droplets toward the vegetal pole (Fluck *et al.*, 1992, 1994).

Our results suggest that at least some of the effects of dibromo-BAPTA on ooplasmic segregation in the medaka egg are caused by its disruption of microtubule formation and organization, which are controlled by a number of calcium-binding regulatory proteins (Weisenberg, 1972; Schliwa *et al.*, 1981; Keith *et al.*, 1983; Lieuvin *et al.*, 1994). Facilitated diffusion theory predicts that calcium buffer concentrations similar to those found effective in the present study act by dissipating zones of cytosolic $[Ca^{2+}]_{free}$ in the micromolar range (Speksnijder *et al.*, 1989). An example of a protein that is responsive to changes in $[Ca^{2+}]_{free}$ in this range is calmodulin (Cheung, 1980), which regulates the activity of proteins that interact with microtubules (Ishikawa *et al.*, 1992).

The inhibition of pronuclear movements by dibromo-BAPTA is consistent with the explanation that the buffer disrupts the organization of microtubules near the animal pole. In a number of species, including the medaka, the movement of the pronuclei is inhibited by microtubule poisons (Hiramoto *et al.*, 1984; Sawada and Schatten, 1989; Abraham *et al.*, 1993a), suggesting that microtubules are necessary for these movements.

The parallel array of microtubules near the vegetal pole was apparently resistant to the effects of the buffer, suggesting that microtubules in this region of the egg differ in some way from those in other regions of the egg. This possible difference could be probed by microinjecting a microtubule poison, for example demecolcine, directly into the vegetal ooplasm.

The suggestion that the medaka egg has two independent microtubule networks is consistent with the situation in *X. laevis*, in which two independent networks of microtubules are present during the first cell cycle: one is near the animal pole and is associated with the pronuclei, while the other is the parallel array of microtubules near the vegetal pole (Elinson and Rowning, 1988; Houliston and Elinson, 1991; Elinson and Palaček, 1993; Sardet *et al.*, 1994). Moreover, in both amphibian eggs (Houliston and Elinson, 1991; Elinson and Palaček, 1993) and medaka eggs (Webb and Fluck, unpub. obs.), vegetal cortical arrays of microtubules form in parthenogenetically activated eggs. Using the "Colcemid-UV" method (Hiramoto *et al.*, 1984; Webb and Fluck, 1993), we are currently pursuing the question of the existence of independent arrays of microtubules in the animal pole region, vegetal pole region, and interpolar ooplasm. Our data at this time do not permit us to say whether microtubules are continuous from one region of the egg to another.

Acknowledgments

Supported by NSF DCB-9017210 and NSF MCB-9316125 to RAF, NSF BIR 9211855 to Lionel F. Jaffe and ALM, and grants from Franklin & Marshall College's Hackman Scholar Program and Harry W. and Mary B. Huffnagle Fund to VCA. Louis Kerr provided technical assistance in the use of the laser scanning confocal microscope in the Central Microscope Facility at the Marine Biological Laboratory, Tamika Webb assisted in the preparation and examination of one batch of eggs, and Bob Golder assisted in the preparation of Figure 3. The research at Carnegie-Mellon University was supported by National Science Foundation and Technology Center grant DIR-8920118. We thank Robbin L. DeBiasio for image acquisition, data processing, and 3-D representation; and Gregory M. LaRocca for technical assistance and image acquisition.

Literature Cited

Abraham, V. C., S. Gupta, and R. A. Fluck. 1993a. Ooplasmic segregation in the medaka (*Oryzias latipes*) egg. *Biol. Bull.* **184:** 115–124.

Abraham, V. C., A. L. Miller, L. F. Jaffe, and R. A. Fluck. 1993b. Cytoplasmic microtubule arrays in *Oryzias latipes* (medaka) eggs during ooplasmic segregation. *Biol Bull.* **185:** 305–306.

Astrow, S. H., B. Holton, and D. A. Donovan. 1989. Teloplasm formation in a leech, *Helobdella triserialis*, is a microtubule-dependent process. *Dev. Biol.* **135:** 306–319.

Beams, H. W., R. G. Kessel, C. Y. Shih, and H. N. Tung. 1985. Scanning electron microscopy studies on blastodisc formation in the zebrafish, *Brachydanio rerio*. *J Morphol.* **184:** 41–49.

Bolker, J. A. 1993. Gastrulation and mesoderm morphogenesis in the white sturgeon. *J Exp Zool* **266:** 116–131.

Brady, S. T., K. K. Pfister, and G. S. Bloom. 1990. A monoclonal antibody against kinesin inhibits both anterograde and retrograde fast axonal transport in squid axoplasm. *Proc. Natl. Acad. Sci. USA* **87:** 1061–1065.

Catalone, B. J., and R. A. Fluck. 1994. Oil droplet movement during ooplasmic segregation in the medaka fish egg (*Oryzias latipes*). *J PA Acad Sci* **67:** 173.

Cheung, W. Y. 1980. Calmodulin—an introduction. Pp. 1–12 in *Calmodulin and Cell Function*, Vol. 1, W. Y. Cheung, ed. Academic Press, Orlando, FL.

Clavert, J. 1962. Symmetrization of the egg of vertebrates. Pp. 27–60 in *Advances in Morphogenesis*, Vol. 2, M. Abercrombie and J. Brachet, eds. Academic Press, New York.

Elinson, R. P., and J. Palaček. 1993. Independence of two microtubular systems in fertilized frog eggs: the sperm aster and the vegetal array. *Roux's Arch. Dev. Biol.* **202:** 224–232.

Elinson, R. P., and B. Rowning. 1988. A transient array of parallel microtubules in frog eggs: potential tracks for a cytoplasmic rotation that specifies the dorso-ventral axis. *Dev. Biol.* **128:** 185–197.

Fluck, R. A., A. L. Miller, and L. F. Jaffe. 1992. High calcium zones at the poles of developing medaka eggs. *Biol. Bull.* **183:** 70–77.

Fluck, R. A., A. L. Miller, V. C. Abraham, and L. F. Jaffe. 1994. Calcium buffer injections inhibit ooplasmic segregation in medaka eggs. *Biol Bull.* **186:** 254–262.

Gard, D. L. 1991. Organization, nucleation, and acetylation of microtubules in *Xenopus laevis* oocytes: a study by confocal immunofluorescence microscopy. *Dev Biol.* **143:** 346–362.

Gerhart, J., M. Danilchik, T. Doniach, S. Roberts, B. Rowning, and R. Stewart. 1989. Cortical rotation of the *Xenopus* egg: consequences for the anteroposterior pattern of embryonic dorsal development. *Development* **1989 Supplement:** 37–51.

Ginsburg, A. S., and T. A. Dettlaff. 1991. The Russian sturgeon *Acipenser güldenstädti*. Part 1. Gametes and early development up to time of hatching. Pp. 15–65 in *Animal Species for Developmental Studies*, Vol. 2, *Vertebrates*. T. A. Dettlaff and S. G. Vassetsky, eds. Consultants Bureau, New York.

Harris, P., M. Osborn, and K. Weber. 1980. Distribution of tubulin-containing structures in the egg of the sea urchin *Strongylocentrotus purpuratus* from fertilization through first cleavage. *J Cell Biol.* **84:** 668–679.

Hiramoto, Y., M. S. Hamaguchi, Y. Nakano, and Y. Shoji. 1984. Colcemid uv-microirradiation method for analyzing the role of microtubules in pronuclear migration and chromosome movement in sand-dollar eggs. *Zool. Sci.* **1:** 29–34.

Houliston, E., D. Carré, J. A. Johnston, and C. Sardet. 1993. Axis establishment and microtubule-mediated waves prior to first cleavage in *Beroe ovata*. *Development* **117:** 75–87.

Houliston, E., and R. P. Elinson. 1991. Patterns of microtubule polymerization relating to cortical rotation in *Xenopus laevis* eggs. *Development* **112:** 107–117.

Inoué, S. 1981. Video image processing greatly enhances contrast, quality, and speed in polarization-based microscopy. *J Cell Biol.* **89:** 346–356.

Ishikawa, R., O. Kagami, C. Hayashi, and K. Kohama. 1992. Characterization of smooth muscle caldesmon as a microtubule-associated protein. *Cell Motil. Cytoskel.* **23:** 244–251.

Janson, L. W., and D. L. Taylor. 1993. *In vitro* models of tail contraction and cytoplasmic streaming in amoeboid cells. *J Cell Biol* **123:** 345–356.

Keith, C., M. DiPaola, F. R. Maxfield, and M. L. Shelanski. 1983. Microinjection of Ca^{++}-calmodulin causes a localized depolymerization of microtubules. *J Cell Biol.* **97:** 1918–1924.

Lieuvin, A., J.-C. Labbé, M. Dorée, and D. Job. 1994. Intrinsic microtubule stability in interphase cells. *J Cell Biol.* **124:** 985–996.

Manes, M. E., R. P. Elinson, and F. D. Barbieri. 1978. Formation of the amphibian grey crescent: effects of colchicine and cytochalasin B. *Roux's Arch Dev. Biol.* **185:** 99–104.

Pethig, R., M. Kuhn, R. Payne, E. Adler, T.-H. Chen, and L. F. Jaffe. 1989. On the dissociation constants of BAPTA-type calcium buffers. *Cell Calcium* **10:** 491–498.

Sardet, C., A. McDougall, and E. Houliston. 1994. Cytoplasmic domains in eggs. *Trends Cell Biol.* **4:** 166–172.

Sawada, T., and G. Schatten. 1988. Microtubules in ascidian eggs during meiosis, fertilization, and mitosis. *Cell Motil. Cytoskel.* **9:** 219–230.

Sawada, T., and G. Schatten. 1989. Effects of cytoskeletal inhibitors on ooplasmic segregation and microtubule organization during fertilization and early development in the ascidian *Molgula occidentalis*. *Dev. Biol.* **132:** 331–342.

Scharf, S. R., and J. C. Gerhart. 1983. Axis determination in eggs of *Xenopus laevis*: a critical period before first cleavage, identified by the common effects of cold, pressure, and ultraviolet irradiation. *Dev. Biol.* **99:** 75–87.

Schliwa, M., U. Euteneuer, J. C. Bulinski, and J. G. Izant. 1981. Calcium lability of cytoplasmic microtubules and its modulation by microtubule-associated proteins. *Proc. Natl Acad Sci. USA* **78:** 1037–1041.

Schroeder, M. M., and D. L. Gard. 1992. Organization and regulation of cortical microtubules during the first cell cycle of *Xenopus* eggs. *Development* **114:** 699–709.

Schnapp, B. J., T. S. Reese, and R. Bechtold. 1992. Kinesin is bound with high affinity to squid axon organelles that move to the plus-end of microtubules. *J Cell Biol* **119:** 389–399.

Solnica-Krezel, L., and W. Driever. 1994. Microtubule arrays of the zebrafish yolk cell: organization and function during epiboly. *Development* **120:** 2443–2455.

Speksnijder, J. E., A. L. Miller, M. H. Weisenseel, T.-H. Chen, and L. F. Jaffe. 1989. Calcium buffer injections block fucoid egg development by facilitating calcium diffusion. *Proc. Natl. Acad Sci USA* **86:** 6607–6611.

Strähle, U., and S. Jesuthasan. 1993. Ultraviolet irradiation impairs epiboly in zebrafish embryos: evidence for a microtubule-dependent mechanism of epiboly. *Development* **119:** 909–919.

Vincent, J.-P., S. R. Scharf, and J. C. Gerhart. 1987. Subcortical rotation in *Xenopus* eggs: a preliminary study of its mechanochemical basis. *Cell Motil. Cytoskel.* **8:** 143–154.

Webb, T. A., and R. A. Fluck. 1993. Microfilament- and microtubule-based movements during ooplasmic segregation in the medaka fish egg (*Oryzias latipes*). *Mol. Biol. Cell* **4:** 274a.

Weisenberg, R. C. 1972. Microtubule formation *in vitro* in solutions containing low calcium concentrations. *Science* **177:** 1104–1105.

Wolff, A., B. Néchaud, D. Chillet, H. Mazarguil, E. Desbruyères, S. Audebert, B. Eddé, F. Gros, and P. Denoulet. 1992. Distribution of glutamylated α and β-tubulin in mouse tissues using a specific monoclonal antibody, GT335. *Eur. J Cell Biol.* **59:** 425–432.

Reference: *Biol Bull* **188**: 146–156. (April, 1995)

Microtubule-Based Movements During Ooplasmic Segregation in the Medaka Fish Egg (*Oryzias latipes*)

TAMIKA A. WEBB, WENDY J. KOWALSKI, AND RICHARD A. FLUCK*

Franklin and Marshall College, Department of Biology, Lancaster, Pennsylvania 17604

Abstract. We used time-lapse video microscopy to monitor the effects of cytochalasin D (CCD) and demecolcine on cytoplasmic streaming toward the animal pole of the medaka egg, the formation of the blastodisc at the animal pole, the movement of oil droplets in the cytoplasm toward the vegetal pole, and the saltatory movement of small cytoplasmic parcels toward the animal pole and vegetal pole. Cytochalasin D inhibited both cytoplasmic streaming toward the animal pole and the formation of the blastodisc, suggesting a role for microfilaments in these processes. However, CCD had no apparent effect on saltatory movement or on the movement of oil droplets toward the vegetal pole. Thus, the segregation of oil droplets toward the vegetal pole is not the result of the bulk movement of ooplasm toward the animal pole.

In eggs treated with demecolcine, oil droplets did not move toward the vegetal pole but instead floated to the uppermost portion of the egg, and saltatory movement was absent, suggesting that microtubules are required for these movements. The effects of demecolcine on oil droplet movement and saltatory movement could be reversed by irradiating the eggs with UV light (360 nm). Using indirect immunofluorescence, we showed that irradiation of demecolcine-treated eggs with UV light regenerated microtubules within the irradiated region.

The specificity of the mechanism responsible for the vegetal poleward movement of oil droplets was assessed by microinjecting droplets of five other fluids—mineral oil, silicone oil, vegetable oil, and two fluorinated aliphatic compounds—into the ooplasm. None of these fluids segregated with the endogenous oil droplets. These results suggest that a specific mechanism, probably involving microtubules, is responsible for the segregation of oil droplets to the vegetal pole.

Introduction

The optical clarity, size (diameter = 1.2 mm), and year-round availability of the medaka fish egg make it a favorable system in which to study ooplasmic segregation. Ooplasmic segregation in this egg consists of the bulk flow of ooplasm toward the animal pole of the egg, the movement of oil droplets toward the vegetal pole, and the saltatory movement of small ooplasmic inclusions toward the animal and vegetal poles of the egg (Iwamatsu, 1973; Abraham *et al.*, 1993a), all of which take place more or less simultaneously. Formation of the blastodisc at the animal pole of zebrafish (*Danio rerio*) and loach (*Misgurnus fossilis*) eggs is inhibited by cytochalasin—cytochalasin B (CCB) in zebrafish (Katow, 1983) and cytochalasin D (CCD) in loach (Ivanenkov *et al.*, 1987). This inhibition suggests that microfilaments are involved in the movement of ooplasm toward the animal pole of these eggs. However, there are no reports of the effects of CCD on streaming or on formation of the blastodisc in the medaka egg. Thus, one objective of the present study was to monitor the effects of CCD on these phenomena in the medaka egg.

The possible involvement of microtubules in segregation in the medaka egg has been explored more fully (Abraham *et al.*, 1993a, 1993b). A network of microtubules is organized during the period of ooplasmic segregation in the medaka (Abraham *et al.*, 1993b), and this network is absent from eggs incubated with a microtubule poison (Abraham *et al.*, 1993b). Moreover, three microtubule poisons—colchicine, demecolcine, and nocodazole—inhibit the normal movement of oil droplets toward the vegetal pole, eliminate the saltatory motion of small inclusions, and slow the growth of the blastodisc; eggs treated with β-lumicolchicine, an inactive derivative of colchicine, segregated normally (Abraham *et al.*, 1993a). The second objective of the present study was to determine

Received 19 July 1994; accepted 11 January 1995.

* To whom correspondence should be addressed.

whether the inhibitory effects of one of these poisons (demecolcine) on microtubules and ooplasmic segregation could be reversed by illuminating the eggs with ultraviolet light (360 nm), which photolyzes demecolcine, converting it to lumidemecolcine, a molecule that is not a microtubule poison (Aronson and Inoué, 1970). This "Colcemid-UV method" (Colcemid is a trade name for demecolcine) has been used by a number of investigators to study microtubule-mediated movements (Sluder, 1976; Hiramoto *et al.*, 1984; Hamaguchi and Hiramoto, 1986; Ladrach and La Fountain, 1986).

The suggestion that microtubules are involved in the segregation of oil droplets toward the vegetal pole is inconsistent with the hypothesis that this segregation is caused simply by the bulk flow of ooplasm in the opposite direction, that is, toward the animal pole (Sakai, 1965). This hypothesis can be tested directly by determining whether oil droplets segregate toward the vegetal pole when there is no bulk flow of ooplasm toward the animal pole. Thus, another objective of the present study was to monitor the effects of CCD on the segregation of oil droplets toward the vegetal pole.

Sakai's hypothesis was based in part on the observation that when droplets of three oils—vegetable oil, liver oil, and mineral oil—were injected into the ooplasm of medaka eggs, they segregated toward the vegetal pole along with endogenous droplets (Sakai, 1965). However, it is possible that the injected droplets simply *floated* toward the vegetal pole, because the eggs in the experiments were all oriented with their vegetal pole uppermost. Thus, another objective of the present study was to monitor the movement of injected droplets of five fluids that differ widely in their chemical and physical properties; the eggs in the present study were oriented with either their animal pole or their vegetal pole uppermost.

A preliminary account of these findings has been published (Webb and Fluck, 1993).

Materials and Methods

Biological material

The dissection of gonads from breeding medaka, the preparation of gametes, and the *in vitro* fertilization of eggs have been previously described (Yamamoto, 1967; Abraham *et al.*, 1993a). To indicate the relative temporal position of these events, we used a normalized time (T_n) scale in which the time between fertilization and the beginning of cytokinesis is 1 unit.

Effects of cytochalasin D on segregation

Stock solutions of CCD (Sigma) in dimethylsulfoxide (DMSO, Fisher) were diluted 100-fold to make working solutions. Four eggs were placed in a small Syracuse watch glass containing 500 μl of either 1% DMSO in buffered saline solution (BSS: 111 mM NaCl; 5.37 mM KCl; 1.0 mM $CaCl_2$; 0.6 mM $MgSO_4$; 5 mM HEPES, pH 7.3) or 10 μg ml^{-1} CCD/1% DMSO in BSS and incubated for 1 h at room temperature (24–25°C). The eggs were fertilized by pipetting 50 μl of a fresh sperm suspension, prepared by mincing testis in BSS, onto the eggs and stirring quickly. Fertilized eggs were transferred to a microscope slide on which a cover glass was supported by four pillars of petroleum jelly (Abraham *et al.*, 1993a). The volume of the blastodisc was measured with an image analysis program (Microcomp Planar Morphometry, Southern Micro Instruments; Abraham *et al.*, 1993a). To monitor cytoplasmic streaming, we oriented the eggs with their animal pole–vegetal pole axis parallel to the surface of the slide, placed the slide on the stage of a compound microscope (Nikon Optiphot), and used time-lapse video microscopy via a 40× phase-contrast objective and a Dage/MTI Newvicon camera to record ooplasmic movements. On playback, the positions of five particles in each egg at $T_n \approx 0.35$ were mapped onto acetate sheets (Abraham *et al.*, 1993a). At the end of recording, the eggs were washed twice with embryo reading medium (17 mM NaCl; 0.4 mM KCl; 0.3 mM $CaCl_2$; 0.67 mM $MgSO_4$; 0.001 g/l methylene blue) and transferred to a petri dish containing 3 ml of embryo rearing medium. Subsequent development of the eggs was monitored for several days. A total of 111 eggs from six females were used in these experiments; we monitored ooplasmic segregation closely in 30 eggs.

Effects of demecolcine on segregation

Working solutions of demecolcine (N-deacetyl-N-methyl-colchicine; Sigma) were prepared by diluting (at least 100×) an aqueous stock solution of 0.35 mM demecolcine. Eggs were placed in BSS containing the appropriate concentration of demecolcine and incubated for 1 h at room temperature in dim light. Typically three eggs were incubated in 375 μl or four eggs in 500 μl of medium. To fertilize the eggs, we minced a portion of testis in 200 μl of BSS and pipetted 50 μl of sperm suspension onto the eggs in the appropriate (drug-containing) medium. Eggs were then transferred to a coverglass-slide assembly for microscopy. To monitor ooplasmic segregation in these eggs, we transilluminated the egg with light from a quartz-halogen lamp, using a heat filter (KG5) and a 486 DF32 filter (Omega Optical). Movements were recorded by time-lapse video microscopy with a Dage/MTI SIT camera.

In some experiments, we treated eggs with both CCD (10 μg ml^{-1}) and demecolcine (0.35 μM).

Irradiating eggs with ultraviolet light

To irradiate eggs with UV light, we used an Osram 100 W mercury arc lamp. The light from the lamp was passed through a custom filter cube (Omega Optical) containing a 360 DF 40 filter and a DC 405 dichroic mirror. An octagonal diaphragm was used to control the size of the light beam. To reduce the light intensity in some experiments, we used either an ND16 filter (Nikon, which reduced the intensity ≈ 94%) or an ND 1.5 filter (Omega Optical, which reduced the intensity ≈ 97%). The light was projected onto the egg via one of three objective lenses (all from Nikon): Plan 4×, N.A. = 0.1; Fluor/Ph 2 DL 10×; N.A. = 0.5; Fluor/Ph 3 DL 20×, N.A. = 0.75. Specific regions of the egg—animal pole, vegetal pole, equatorial region—were illuminated either *en face* or *en profil*. In most of the experiments described herein, we used the 10× objective lens and irradiated an octagonal region having a diameter of 475 μm and an area of 1.9×10^5 μm^2. Light intensity was measured with a UVX radiometer with a long wave sensor (UVP, Inc.). Given a light intensity of 523 $\mu W\ cm^{-2}$ and assuming that all the UV light was of wavelength 360 nm, we calculated an incident light intensity of 4.9×10^9 quanta s^{-1} μm^{-2} (10× objective lens; no neutral density filter). To monitor the subsequent development of eggs, we washed them twice with embryo rearing medium and transferred them to a petri dish containing 3 ml of embryo rearing medium. A total of 292 eggs from 18 females were used in these experiments; we monitored ooplasmic segregation closely in 96 eggs.

Indirect immunofluorescence

The methods for fixing eggs and performing indirect immunofluorescence assays for alpha-tubulin have been described previously (Gard, 1991; Abraham *et al.*, 1993b). Briefly, the eggs were fixed for 4 h in a mixture of formaldehyde (Electron Microscopy Sciences) and glutaraldehyde (Electron Microscopy Sciences) at room temperature and then in cold (−20°C) methanol; treated with sodium borohydride; incubated with a monoclonal mouse anti-alpha-tubulin antibody (ICN, DM1A; diluted 1:250 with TBS (155 m*M* NaCl; 10 m*M* Tris-Cl, pH 7.4; 0.1% Nonidet P-40) containing 2% bovine serum albumin; and incubated with a secondary antibody (Organon Teknika, rhodamine-conjugated goat anti-mouse IgG, diluted 1:25 with TBS containing 2% bovine serum albumin). Control eggs were not incubated with the primary antibody. Eggs that were in a solution of demecolcine and being irradiated with UV light were fixed on the stage of the microscope for 5 min before being transferred to a vial of fixative. To stain nuclei, we incubated the eggs for 30 min in a solution of Hoechst 33258 (Sigma, 10 $\mu g\ ml^{-1}$) in TBS. A total of 68 eggs from 11 females were used in these experiments.

Microinjecting fluids into medaka eggs

Using methods described previously (Fluck *et al.*, 1991, 1992, 1994), droplets of fluid were microinjected into the ooplasm between 35° and 90° arc from the animal pole. Of the 25 eggs used in these experiments, 21 were parthenogenetically activated by the injection needle, and four others were fertilized after injection. Similar results were obtained with parthenogenetically activated and fertilized eggs. Droplets of five fluids were injected: mineral oil, density = 0.84 $g\ ml^{-1}$; vegetable oil, density = 0.9 $g\ ml^{-1}$; silicone fluid (Sigma), density = 1.05 $g\ ml^{-1}$; and two fluorinated aliphatic compounds, FC-77 and FC-3275 (3M), density = 1.78 $g\ ml^{-1}$. Although droplets of silicone fluid and the fluorinated compounds could be distinguished visually from endogenous oil droplets, we stained the vegetable oil and mineral oil with either Sudan black B or Sudan III to identify them.

To monitor the movement of the injected droplets, we used one of two techniques. In the first, we placed an egg on a small mound of Dow Corning high vacuum grease in the bottom of a rectangular plastic spectrophotometer cuvette and used two video cameras and two time-lapse videocassette recorders to record the movement of the droplets simultaneously from two perspectives: a polar view and a side view. In the second technique, we glued the egg to the bottom of a petri dish (diam., 35 mm) with Cel-Tak (Bio-Polymers, Inc.) and placed a right-angle prism (Melles-Griot) next to the egg. The petri dish was then placed on the stage of an inverted microscope (Nikon Diaphot) and viewed either directly (polar view) or indirectly via the prism (side view). To view the egg indirectly, we illuminated it from the side, using a fiber optic cable.

Results

Effects of cytochalasin D and demecolcine on ooplasmic segregation and development

Eggs treated with 1% DMSO formed a blastodisc (volume at $T_n \approx 0.85–1.0 = 15.4 \pm 2.0$ nl, $\bar{X} \pm$ SD, $N = 7$ eggs; Fig. 1A), displayed cytoplasmic streaming (speed of parcels toward the animal pole = 9.00 ± 5.52 $\mu m\ min^{-1}$, $\bar{X} \pm$ SEM, $N = 7$ eggs), and developed normally. In contrast, eggs treated with CCD (10 $\mu g\ ml^{-1}$) had essentially no cytoplasmic streaming (velocity = -0.66 ± 0.84 $\mu m\ min^{-1}$, $\bar{X} \pm$ SEM, $N = 5$ eggs), did not form a blastodisc (Fig. 1B), and did not undergo cell division. CCD had no apparent effect on the segregation of oil droplets toward the vegetal pole (Fig. 1B) or on the saltatory movement of particles toward either the animal or vegetal pole.

The effects of demecolcine on the eggs were those previously described by Abraham *et al.* (1993a): (1) oil droplets did not segregate to the vegetal pole but instead floated to the portion of the egg that was uppermost during the experiment—equator (Fig. 1C), animal pole (Fig. 2C and D), or vegetal pole (not shown); (2) a smaller-than-normal blastodisc formed (Fig. 1C); (3) saltatory motion was absent; and (4) the eggs did not cleave.

In eggs treated with both CCD and demecolcine, we saw no saltatory movement, no cytoplasmic streaming, and no movement of oil droplets toward the vegetal pole (Fig. 1D). These eggs also did not cleave (Table I).

Reversal of the inhibitory effects of demecolcine on ooplasmic segregation and embryonic development

When demecolcine-treated eggs were irradiated with UV light, the inhibitory effects of demecolcine were reversed: oil droplet movement and saltatory movement were restored; and the eggs subsequently cleaved, formed an embryonic axis, and hatched. The effects of UV irradiation were less pronounced at higher concentrations of demecolcine. For example, of 11 eggs treated with 0.35 μM demecolcine and irradiated *en face* at the animal pole (2.8×10^8 quanta s^{-1} μm^{-2}), vegetal pole, or equator, all 11 cleaved and developed an embryonic axis; while of three eggs treated with 3.5 μM demecolcine and irradiated under similar conditions, all three cleaved but none developed an embryonic axis. The effects of UV irradiation were also less pronounced when we irradiated the eggs *en profil* instead of *en face*. For example, of five eggs treated with 0.35 μM or 1.0 μM demecolcine and irradiated *en face* near the equator (2.8×10^8 quanta s^{-1} μm^{-2}), all five cleaved and developed an embryonic axis. However, of three eggs treated similarly but irradiated *en profil* at the equator, none cleaved.

Apparently normal oil droplet movement was restored when we irradiated the animal pole or equatorial region *en face*, with oil droplets near the animal pole or equator moving away from the animal pole and toward the vegetal pole more or less along meridian lines (Fig. 2A–F). Under appropriate experimental conditions (1.0 μM demecolcine; irradiation with low intensities of UV light), this reversal of the effects of demecolcine on oil droplet movement was restricted to the portion of the egg that was irradiated. In such eggs, oil droplets outside the irradiated region floated to the top of the egg and accumulated at the edge of the irradiated region, while droplets within the irradiated region moved out of the irradiated region and toward the vegetal pole (Fig. 2G and H).

When we irradiated an equatorial region *en profil*, oil droplets in the irradiated region moved toward the vegetal pole, while oil droplets in the rest of the egg either floated

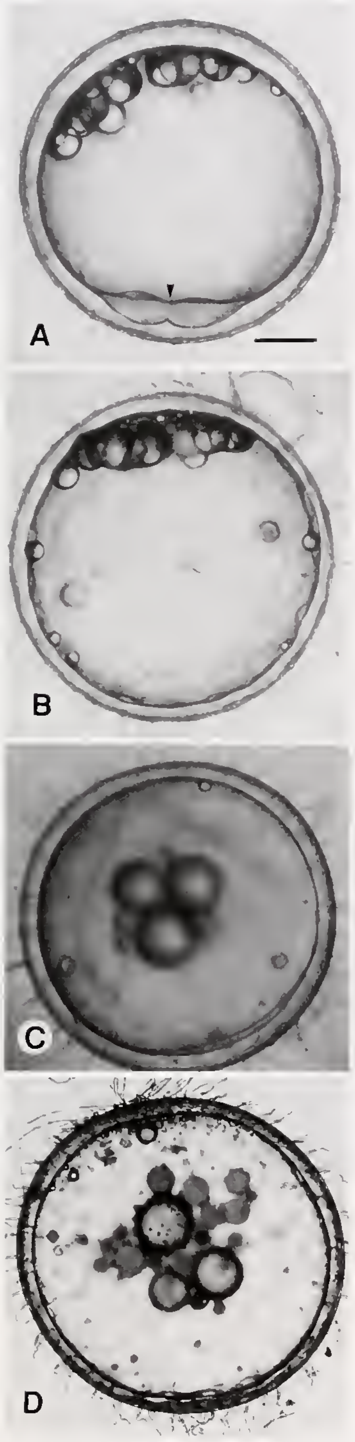

Figure 1. The effects of CCD and demecolcine on formation of the blastodisc and movement of oil droplets. The animal pole is near the bottom and the vegetal pole near the top of each figure. (A) $T_n = 1.24$. DMSO (1% in BSS) had no apparent effect on the formation of the blastodisc at the animal pole of the egg, the movement of oil droplets toward the vegetal pole, or cell division (note the cleavage furrow, arrowhead). (B) $T_n = 1.34$. CCD (10 μg ml^{-1}) inhibited formation of the blastodisc but had no apparent effect on the segregation of oil droplets toward the vegetal pole. (C) $T_n = 1.0$. This egg was treated with 1.0 μM demecolcine. Note the small blastodisc at the animal pole (compare with Figure 1A) and that most oil droplets did not move toward the vegetal pole but floated to the top of the egg. (D) $T_n = 0.73$. This egg was treated with both CCD and demecolcine (0.35 μM). Note the absence of a blastodisc at the animal pole and that the oil droplets have floated to the top of the egg. Scale bar, 250 μm.

to the top of the egg or did not move at all (Fig. 2I and J). In eggs irradiated *en profil* at the equator, we also saw a small accumulation of ooplasm at the animal-pole side of the irradiated region (Fig. 2I and J).

The effects of UV irradiation on oil droplet movement and other phenomena clearly extended beyond the irradiated region when we used a lower concentration of demecolcine or a higher intensity of UV light. For example, eggs irradiated *en face* with a high intensity of UV light near their equator often underwent cleavage and formed an embryonic axis. In addition, oil droplets in such eggs moved beyond the edge of the irradiated region (Fig. 2K).

The movements of droplets within the irradiated regions were very similar to those in control (not treated with demecolcine) eggs; that, is roughly along meridian lines and away from the animal pole (Fig. 3).

Segregation appeared normal in medaka eggs that were irradiated with UV light intensities $\leq$ about 530 μW cm^{-2} (4.9×10^9 quanta s^{-1} μm^{-2}) but not treated with demecolcine (not shown). However, in preliminary experiments, we found that higher light intensities ($\geq$1100 μW cm^{-2}, 1.0×10^{10} quanta s^{-1} μm^{-2}) inhibited both the growth of the blastodisc and the movements of oil droplets.

Microtubule regeneration by ultraviolet irradiation

We saw no microtubules in eggs that were treated with demecolcine but not irradiated with UV light before fixation (Fig. 4A). Moreover, we saw no or very few microtubules outside the irradiated region of eggs that were irradiated with UV light (Fig. 4B and C). However, the UV-irradiated regions contained microtubules that in number and orientation were very similar to those in control eggs that had not been treated with demecolcine (Fig. 5).

The movement of droplets of injected fluids

Droplets of mineral oil were injected into five eggs, which were oriented with their animal pole uppermost. In two of them, the injected droplets fused with native droplets, and the hybrid droplets moved toward the vegetal pole. In two eggs in which the injected droplets were not observed to fuse with native droplets, the injected droplets moved up, toward the animal pole (Fig. 6A); and in another egg, the droplet of mineral oil did not move at all, even though nearby native droplets did move toward the vegetal pole. The eggs into which we injected FC-77 (four eggs), FC-3275 (one egg), and silicone oil (four eggs), were oriented with their vegetal pole uppermost. In all these eggs, the droplets of injected fluids moved toward the animal pole and came to rest in the blastodisc (Fig. 6B–D).

We injected vegetable oil into 11 eggs and oriented them with their animal pole uppermost. In eight of these eggs, the injected droplet fused with endogenous oil droplets, and these hybrid droplets segregated toward the vegetal pole. However, in one egg in which the injected droplet was not observed to fuse with endogenous droplets, the injected droplet moved up, toward the animal pole, and came to rest near the blastodisc, while nearby endogenous droplets moved by it in the opposite direction on their way to the vegetal pole. In two cases in which we injected vegetable oil, the injected droplets appeared to follow larger endogenous droplets that they were touching.

In the case of every fluid—vegetable oil, mineral oil, FC77, FC3275, and silicone oil—the movements of nearby or immediately adjacent endogenous oil droplets appeared to be unaffected by the presence of the injected fluid. In other words, endogenous droplets, moving toward the vegetal pole, passed by the droplets of injected fluid, which were either stationary or moving toward the animal pole.

Discussion

The inhibition of cytoplasmic streaming and formation of the blastodisc by CCD in medaka eggs is consistent with data obtained from other teleost eggs (Katow, 1983; Ivanenkov *et al.*, 1987) and from eggs of other organisms, including ascidians (Sawada and Osanai, 1981; Jeffery,

Table I

Cytoplasmic streaming, saltatory movement, oil droplet movement, and cleavage in the presence of CCD (10 μg ml^{-1}), demecolcine (0.35 μM), and CCD/demecolcine

Treatment	Cytoplasmic streaming	Oil droplet movement toward vegetal pole	Saltatory movement	Cleavage
Cytochalasin D	No	Yes	Yes[a]	No
Demecolcine	Yes	No[b]	No	No
Cytochalasin D and demecolcine	No	No	No	No

[a] Saltatory movement toward both the animal and vegetal poles of the egg.

[b] Oil droplets floated to the top of the egg.

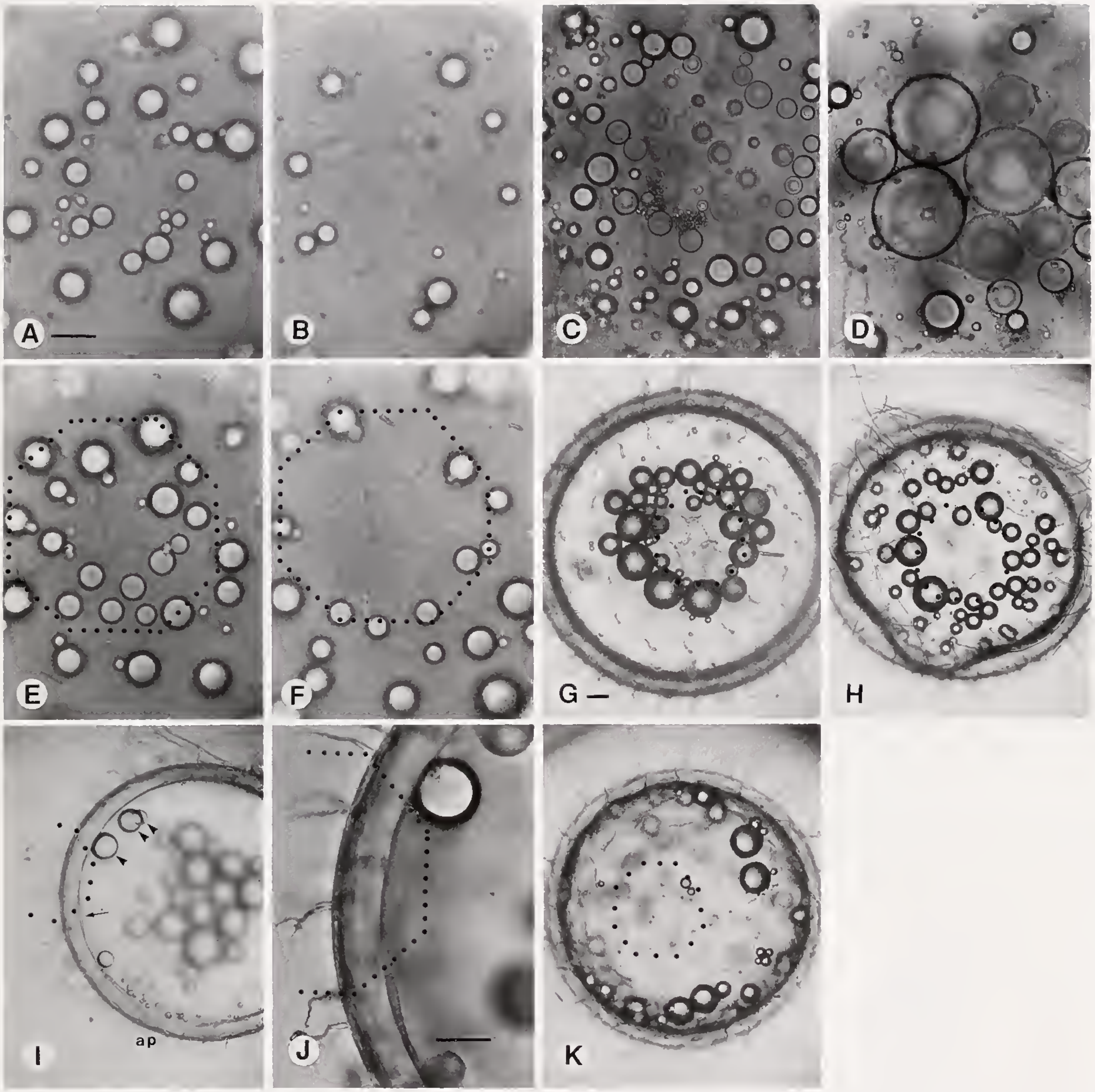

Figure 2. Ultraviolet light reverses the effect of demecolcine on oil droplet movement. (A) and (B) show oil droplets near the animal pole of a control egg (not treated with demecolcine) at $T_n = 0.3$ and 0.5, respectively. Note that many oil droplets have left this region of the egg by $T_n = 0.5$. In (C), where $T_n = 0.14$, and (D), where $T_n = 0.65$, oil droplets have floated to the top and accumulated at the animal pole of an egg treated with 0.35 μM demecolcine and oriented with animal pole uppermost. An egg that was treated with 1.0 μM demecolcine and irradiated with UV light (7.6×10^8 quanta s^{-1} μm^{-2}) *en face* at the animal pole is shown at $T_n = 0.3$ in (E) and $T_n = 0.5$ in (F). The edges of the diaphragm are shown (●●●). Note that the oil droplets have moved away from the animal pole. The egg shown in (G) at $T_n = 0.75$ was incubated in 1.0 μM demecolcine and irradiated *en face* at its animal pole (2.8×10^8 quanta s^{-1} μm^{-2}). The ring of oil droplets is the result of (1) oil droplets outside the irradiated region floating to the top of the egg (toward the viewer) and accumulating at the edge of the irradiated region, and (2) oil droplets within the irradiated region moving to the edge of the irradiated region. This embryo developed normally and hatched. The egg shown in (H) at $T_n = 0.67$, was incubated in 1.0 μM demecolcine and illuminated *en face* at its equator (2.8×10^8 quanta s^{-1} μm^{-2}). As in Figure 2G, note the absence of oil droplets from the irradiated region and the presence of a ring of oil droplets at the edge of the irradiated region. This egg cleaved and formed an embryonic axis, but morphogenesis was very abnormal and the embryo did not hatch. (I) at $T_n = 1.1$, shows an egg that was treated with 1.0 μM demecolcine and irradiated *en profil* near its equator (2.8×10^8 quanta s^{-1} μm^{-2}). Note the accumulation of most oil droplets at the top of the egg (toward the viewer and out of focus) and the formation of a smaller than normal blastodisc at the animal pole. Three oil droplets

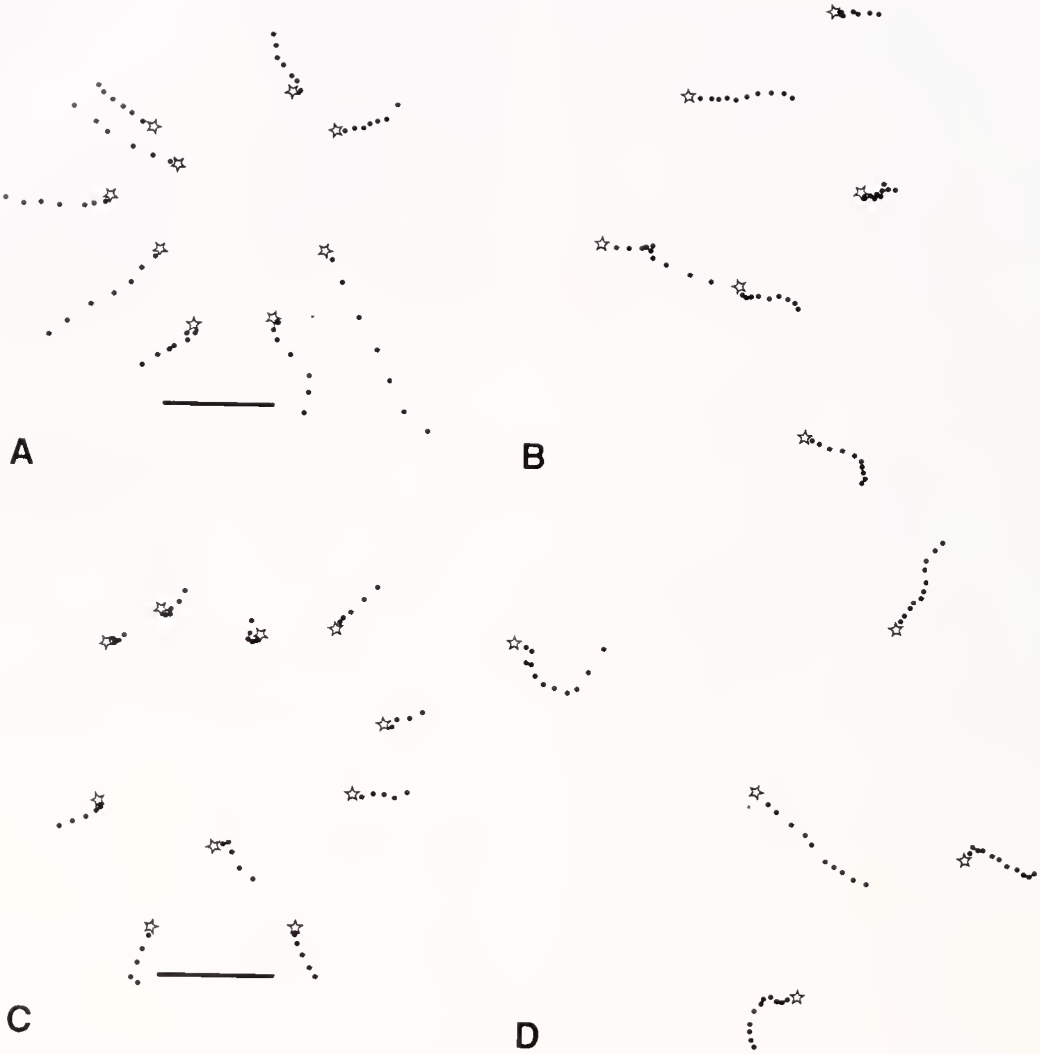

Figure 3. Oil droplets within UV-irradiated regions move toward the vegetal pole. A star marks the starting position of each droplet, and black circles mark the positions at 2-min intervals. The eggs in (A) and (B) were untreated controls shown from either the animal pole (A) or the equator (B); the eggs shown in (C) and (D) were treated with 1.0 μM demecolcine and irradiated *en face* (3.3×10^8 quanta s^{-1} μm^{-2}) at either the animal pole (C) or equator (D). Oil droplets near the animal pole (near the center of the figure) in (A) and (C) moved away from that pole more or less along meridian lines; droplets near the equator in (B) and (D) moved toward the vegetal pole (to the right). Scale bars: (A) and (B), 200 μm; (C) and (D), 100 μm. (A) and (B) were printed at one magnification and (C) and (D) at another.

1984) and an oligochaete (Shimizu, 1982). The inhibition suggests that the formation of the blastodisc in the medaka egg is the result of the streaming of ooplasm to the animal pole and that microfilaments are involved in this streaming. This suggestion should be pursued by staining eggs with fluorescently labeled phalloidin during segregation.

The solation-contraction coupling hypothesis (Janson and Taylor, 1993) provides a model for how this stream-

Figure 2. (*Continued*) (arrowheads) were observed to move through the irradiated region toward the vegetal pole. The small accumulation of ooplasm at the animal pole side of the irradiated region (arrow) is shown at higher magnification in (J). The egg in (K), where $T_n = 0.60$, was treated with 1.0 μM demecolcine and irradiated at the animal pole *en face* with a high intensity of UV light (5.0×10^9 quanta s^{-1} μm^{-2}). Note that oil droplets have moved beyond the edges of the irradiated region. Scale bar, 100 μm. (A–F) are printed at the same magnification, (G–I) at another, and (J) at another.

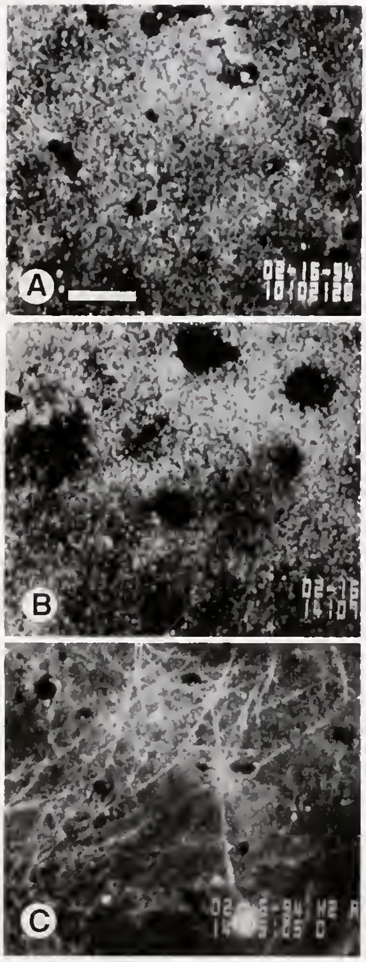

Figure 4. Microtubules in eggs treated with demecolcine. All three photographs were taken near the equator of the egg. The egg shown in (A) was treated with 3.5 μM demecolcine but was not irradiated with UV light. Note the absence of microtubules. Of 17 such eggs we observed, we found no microtubules in 15 and a few scattered ones in 2. (B) and (C) show ooplasm near the equator in eggs that were treated with 3.5 μM demecolcine and irradiated with UV light (5.2×10^8 quanta s^{-1} μm^{-2}) *en face* at the animal pole (B) or *en profil* at the vegetal pole (C). Note the apparent absence of microtubules in (B), a typical field, and the relatively few even in (C), which had the most microtubules that we observed outside an irradiated region (compare with Fig. 5). Scale bar, 10 μm.

ing, which is likely driven by the interaction of actin and myosin, could be organized and driven by the zone of elevated cytosolic Ca^{2+} present at the animal pole throughout the period of segregation (Fluck *et al.*, 1992). Dissipation of this zone of elevated Ca^{2+} inhibits formation of the blastodisc (Fluck *et al.*, 1992, 1994).

The experiments with CCD directly test the hypothesis that the movement of oil droplets toward the vegetal pole is caused by the movement of ooplasm in the opposite direction—toward the animal pole. The results are not consistent with this hypothesis, because oil droplets moved toward the vegetal pole even when we did not observe any cytoplasm streaming to the animal pole. Other data from the present study also conflict with the hypothesis. Specifically, in demecolcine-treated eggs oriented with their animal pole uppermost, oil droplets collected at the animal pole even as ooplasm was also streaming in that direction.

Moreover, the failure of injected droplets of several other fluids—fluorinated aliphatic compounds, silicone fluid, mineral oil, and vegetable oil—consistently to move away from the animal pole and toward the vegetal pole during segregation is inconsistent with the hypothesis. This failure was probably not due to a toxic effect of the fluids on nearby cell components, because the movements of adjacent endogenous droplets appeared to be unaffected by proximity to a droplet of injected fluid. The behavior of the injected droplets also suggests a specificity of the mechanism responsible for the movement of endogenous oil droplets.

We have previously suggested that microtubules are required for the segregation of oil droplets to the vegetal pole of the medaka egg (Abraham *et al.*, 1993a). In the present study, we explored the connection between microtubules and oil droplet movement further by using the "Colcemid-UV" method to photolyze demecolcine in specific regions of the egg and thus presumably create conditions that might support microtubule polymerization (Dustin, 1984, ch. 5; Bray, 1992, p. 207). We found that irradiation of the egg with UV light regenerated both microtubules and apparently normal oil droplet movement within the irradiated region of the egg. These results are consistent with a role for microtubules in the movement of oil droplets. To determine whether the microtubule-based motor protein, kinesin, has any role in oil droplet movement, we are planning experiments in which we will microinject anti-kinesin antibodies (Ingold *et al.*, 1988) into medaka eggs.

Microtubule poisons also disrupt intermediate filaments in a number of cells (Knapp *et al.*, 1983; Hunt and Davis, 1990; Pasdar *et al.*, 1992), so it is possible that some of the effects we observed were caused by such disruption in the medaka egg. We are investigating whether intermediate filaments are present in the medaka egg and can be disrupted by microtubule poisons.

Although the effects of UV irradiation on oil droplet movement could be localized under appropriate experimental conditions, the effects of irradiation sometimes clearly extended beyond the irradiated region. For example, eggs that were irradiated *en face* at their equator usually cleaved and formed an embryonic axis. These results suggest that UV irradiation at the equator lowered the concentration of demecolcine in the animal pole region (where cell division occurs) enough to permit the polymerization of tubulin. Moreover, oil droplets often

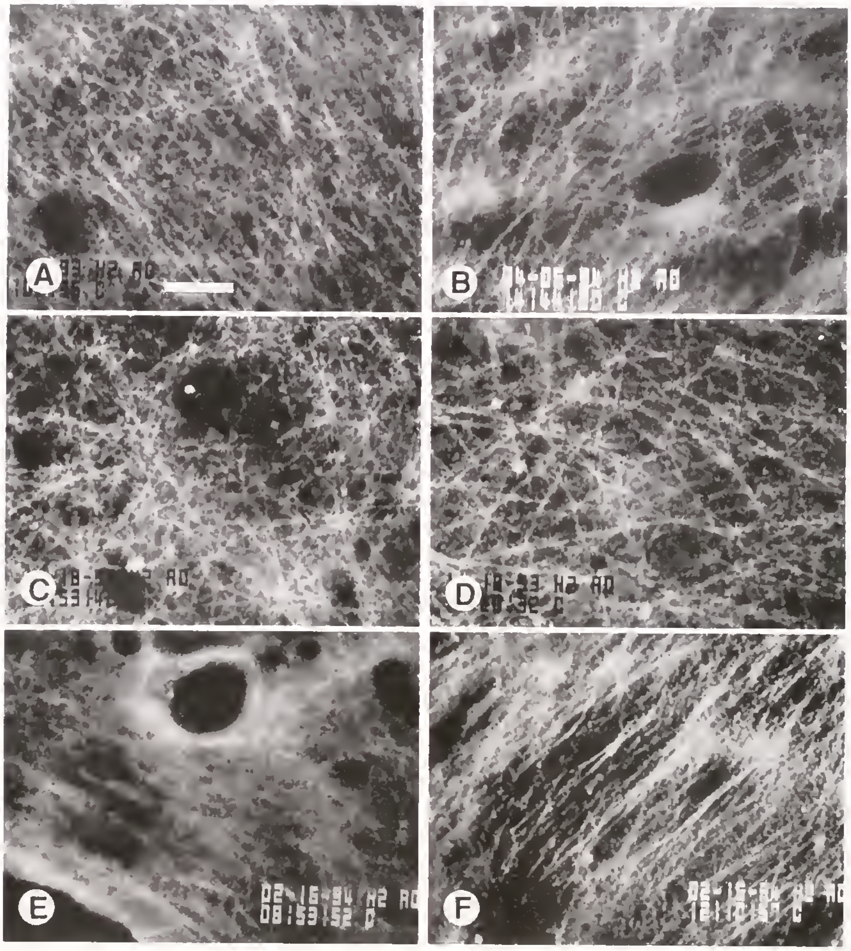

Figure 5. UV light reverses the effect of demecolcine on tubulin polymerization. The eggs shown in (A), (C), and (E) were neither treated with demecolcine nor irradiated with UV light; those shown in (B), (D), and (F) were treated with 3.5 μM demecolcine and irradiated with UV light (5.2×10^8 quanta s^{-1} μm^{-2}) either *en face* at the animal pole (B) or equator (D) or *en profil* at the vegetal pole (F). All eggs were fixed at $T_n = 0.3$. Near the animal pole, in (A) and (B), and the equator, in (C) and (D), a dense network of microtubules having no apparent preferred orientation is present, but near the vegetal pole, in (E) and (F), most of the microtubules are parallel to each other. *En profil* and *en face* irradiation gave identical results in all three regions of the egg. Scale bar, 10 μm.

moved beyond the edge of the UV-irradiated region, suggesting that microtubules that formed in the irradiated region subsequently extended beyond this region. Irradiation of the egg *en face* likely photolyzed demecolcine in the ooplasm on both the near side of the egg and its antipode as well as in the portion of the yolk vacuole that is in the light path. As molecules of demecolcine were inactivated within the irradiated region and the product diffused away from it, molecules of demecolcine in adjacent, unirradiated regions diffused into the irradiated region. In other words, the irradiated region acted as a demecolcine sink, and eventually the concentration of demecolcine decreased throughout the egg. The spatiotemporal pattern of the change in demecolcine concentration in an irradiated egg presumably depends on at least three variables: (a) the initial concentration of demecolcine in the egg, (b) the intensity of the UV light, and (c) the volume of the irradiated region. Our results demonstrate that all three variables affected the extent to which UV irradiation reversed the effects of demecolcine on oil droplet movement, cleavage, and subsequent development.

Irradiation of control medaka eggs with UV light (360 nm) at intensities adequate to regenerate microtubules and normal movement of oil droplets in poisoned eggs had no apparent effect on ooplasmic segregation. These results are consistent with those of other studies in which UV light has been used to modify amphibian development (Grant and Wacaster, 1972; Scharf and Gerhart, 1980; Holwill *et al.*, 1987). In all these studies, the predominant wavelength emitted by the lamps was about 254 nm. Moreover, an action spectrum of the effects of UV irradiation on the inactivation of components required for neural induction in the amphibian egg showed a peak at 280 nm and a decline toward both 250 and 320 nm (Youn and Malacinski, 1980). However, irradiation of cells with high-intensity near-UV light (360 nm, 2.5 mW cm^{-2}, about 5-fold higher than that used in the present study) disrupts f-actin in epithelial cells (Rafferty *et al.*, 1993). Although we saw an inhibition of segregation at such a high UV light intensity in preliminary experiments, UV light intensities sufficient to regenerate microtubules and normal oil droplet movement had no apparent effect on ooplasmic segregation in the medaka egg.

That we could regenerate microtubules and oil droplet movement near the animal pole by irradiating this region *en face* is not surprising, given the apparent presence of a microtubule-organizing center there (Abraham *et al.*, 1993b). More interesting is the observation that we could regenerate microtubules and oil droplet movement near the equator region and could regenerate microtubules at the vegetal pole. This result is consistent with Sakai's observation (1964) that oil droplets will segregate toward the vegetal pole in vegetal halves of eggs that have been surgically separated from their animal halves. This result suggests the presence of microtubule-organizing centers outside the animal pole region of the medaka egg. In *Xenopus laevis* eggs, the biochemical basis for such an ability may be the presence of γ-tubulin in cortical cytoplasm in the vegetal hemisphere of the egg (Gard, 1994). We are currently pursuing this question.

Finally, we note that when we irradiated an equatorial region of an egg *en profil*, ooplasm accumulated at the animal pole side of the irradiated region, suggesting that microtubules are involved not only in the movement of oil droplets toward the vegetal pole but also in the movement of components of the ooplasm toward the animal pole. Though the growth of the medaka blastodisc is slowed by microtubule poisons (Abraham *et al.*, 1993a), no specific effect of these poisons on the movement of the ooplasm or its constituents toward the animal pole has been reported. However, here we have described the saltatory movement of subcellular parcels toward the animal pole and its inhibition by demecolcine. This movement was especially apparent in eggs treated with CCD, which displayed no cytoplasmic streaming; this streaming obscures the component of saltatory movement directed toward the animal pole. Ooplasm in and near these irradiated interpolar regions appeared to segregate along the same axis as that of the entire egg: oil droplets moved toward the vegetal pole and certain other components of the ooplasm toward the animal pole. These results suggest that a local mechanism, operating with a predetermined polarity, is responsible for the segregation of ooplasm in

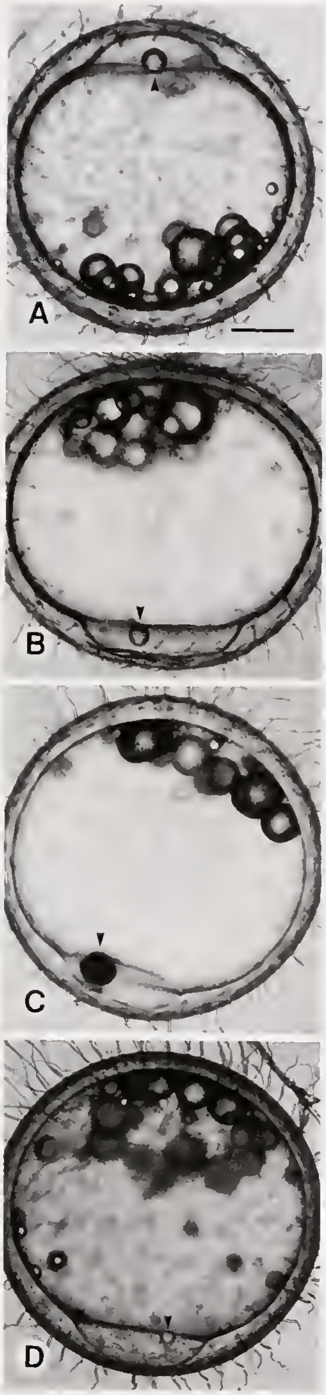

Figure 6. Behavior of injected droplets of fluids. Droplets of fluids were injected into unfertilized eggs, which were parthenogenetically activated by the injection. The egg in (A) was oriented with its animal pole uppermost; all others had vegetal pole uppermost. In all four eggs, the droplets of injected fluid (arrowheads) moved toward the animal pole of the egg and came to rest in the blastodisc at the boundary between the blastodisc and the yolk vacuole. (A) Mineral oil stained with Sudan black B, (B) FC-77, (C) FC-3275, (D) silicone fluid. Scale bar, 250 μm.

the medaka egg. This suggestion is consistent with results obtained by Gilkey (1983), who achieved local activation of medaka eggs by injecting them with Ca/EGTA mixtures. He reported that oil droplets in such eggs moved to the vegetal-pole side of the activated region and a small amount of ooplasm accumulated at the animal pole side. We are seeking to determine whether these localized regions of segregation in the medaka egg are accompanied by polar zones of elevated cytosolic [Ca^{2+}] like those present at the poles of the egg during segregation (Fluck *et al.*, 1992).

Acknowledgments

Supported by NSF DCB-9017210 and NSF MCB-9316125 to RAF, Franklin and Marshall College's Hackman Scholar Program, and a grant from GTE to Franklin and Marshall College. We thank Shinya Inoué for suggesting the use of the Colcemid-UV method and for his advice in the selection of fluids for microinjection into the eggs, Vivek Abraham for helpful discussions, Richard Elinson for telling us about the paper by Youn and Malacinski, and Valerie Stone for improving the text of the manuscript.

Literature Cited

Abraham, V. C., S. Gupta, and R. A. Fluck. 1993a. Ooplasmic segregation in the medaka *(Oryzias latipes)* egg. *Biol Bull* **184:** 115–124.

Abraham, V. C., A. L. Miller, L. F. Jaffe, and R. A. Fluck. 1993b. Cytoplasmic microtubule arrays in *Oryzias latipes* (medaka) eggs during ooplasmic segregation. *Biol Bull.* **185:** 305–306.

Aronson, J., and S. Inoué. 1970. Reversal by light of the action of *N*-methyl, *N*-desacetyl colchicine on mitosis. *J Cell Biol* **45:** 470–477.

Bray, D. 1992. *Cell Movements.* Garland Publishing, Inc., New York.

Dustin, P. 1984. *Microtubules*, 2nd ed. Springer-Verlag, Berlin.

Fluck, R. A., A. L. Miller, and L. F. Jaffe. 1991. Slow calcium waves accompany cytokinesis in medaka fish eggs. *J Cell Biol.* **115:** 1259–1265.

Fluck, R. A., A. L. Miller, and L. F. Jaffe. 1992. High calcium zones at the poles of developing medaka eggs. *Biol Bull* **183:** 70–77.

Fluck, R. A., A. L. Miller, V. C. Abraham, and L. F. Jaffe. 1994. Calcium buffer injections inhibit ooplasmic segregation in medaka eggs. *Biol. Bull.* **186:** 254–262.

Gard, D. L. 1991. Organization, nucleation, and acetylation of microtubules in *Xenopus laevis* oocytes: a study by confocal immunofluorescence microscopy. *Dev. Biol* **143:** 346–362.

Gard, D. L. 1994. γ-tubulin is distributed asymmetrically in the cortex of *Xenopus* oocytes. *Dev. Biol* **161:** 131–140.

Gilkey, J. C. 1983. Roles of calcium and pH in activation of eggs of the medaka fish, *Oryzias latipes. J Cell Biol.* **97:** 669–678.

Grant, P., and J. F. Wacaster. 1972. The amphibian gray crescent region—a site of developmental information? *Dev Biol* **28:** 454–471.

Hamaguchi, M. S., and Y. Hiramoto. 1986. Analysis of the role of astral rays in pronuclear migration in sand dollar eggs by the Colcemid-UV method. *Dev Growth & Differ* **28:** 143–156.

Hiramoto, Y., M. S. Hamaguchi, Y. Nakano, and Y. Shoji. 1984. Colcemid uv-irradiation method for analyzing the role of microtubules in pronuclear migration and chromosome movement in sand-dollar eggs. *Zool Sci.* **1:** 29–34.

Holwill, S., J. Heasman, C. R. Crawley, and C. C. Wylie. 1987. Axis and germ line deficiencies caused by u.v. irradiation of *Xenopus* oocytes cultured *in vitro Development* **100:** 735–743.

Hunt, R. C., and A. A. Davis. 1990. Altered expression of keratin and vimentin in human retinal pigment epithelial cells *in vivo* and *in vitro J Cell. Physiol.* **145:** 187–199.

Ingold, A. L., S. A. Cohn, and J. M. Scholey. 1988. Inhibition of kinesin-driven microtubule motility by monoclonal antibodies to kinesin heavy chains. *J Cell Biol.* **107:** 2657–2667.

Ivanenkov, V. V., A. A. Minin, V. N. Meshcheryakov, and L. E. Martynova. 1987. The effect of local microfilament disorganization on ooplasmic segregation in the loach *(Misgurnus fossilis)* egg. *Cell Differ.* **22:** 19–28.

Iwamatsu, T. 1973. On the mechanism of ooplasmic segregation upon fertilization in *Oryzias latipes. Jpn. J. Ichthyol.* **20:** 273–278.

Janson, L. W., and D. L. Taylor. 1993. *In vitro* models of tail contraction and cytoplasmic streaming in amoeboid cells. *J Cell Biol.* **123:** 345–356.

Jeffery, W. R. 1984. Pattern formation by ooplasmic segregation in ascidian eggs. *Biol Bull.* **166:** 277–298.

Katow, H. 1983. Obstruction of blastodisc formation by cytochalasin B in the zebrafish, *Brachydanio rerio. Dev. Growth & Differ* **25:** 477–484.

Knapp, L. W., W. M. O'Guin, and R. H. Sawyer. 1983. Drug-induced alterations of cytokeratin organization in cultured epithelial cells. *Science* **219:** 501–503.

Ladrach, K. S., and J. R. LaFountain, Jr. 1986. Malorientation and abnormal segregation of chromosomes during recovery from Colcemid and Nocodazole. *Cell Motil. Cytoskel.* **6:** 419–427.

Pasdar, M., Z. Li, and K. A. Krzeminski. 1992. Desmosome assembly in MDCK epithelial cells does not require the presence of functional microtubules. *Cell Motil. Cytoskel* **23:** 201–212.

Rafferty, N. S., S. Zigman, T. McDaniel, and D. L. Scholtz. 1993. Near-uv radiation disrupts filamentous actin in lens epithelial cells. *Cell Motil Cytoskel* **26:** 40–48.

Sakai, Y. T. 1964. Studies on the ooplasmic segregation in the egg of the fish *Oryzias latipes* I. Ooplasmic segregation in egg fragments. *Embryologia* **8:** 129–134.

Sakai, Y. T. 1965. Studies on the ooplasmic segregation in the egg of the fish *Oryzias latipes*. III. Analysis of the movement of oil droplets during the process of ooplasmic segregation. *Biol. Bull.* **129:** 189–198.

Sawada, T., and K. Osanai. 1981. The cortical contraction related to the ooplasmic segregation in *Ciona intestinalis* eggs. *Wilhelm Roux's Arch. Dev Biol.* **190:** 208–214.

Scharf, S. R., and J. C. Gerhart. 1980. Determination of the dorsal-ventral axis in eggs of *Xenopus laevis:* complete rescue of UV-impaired eggs by oblique orientation before first cleavage. *Dev. Biol* **79:** 181–198.

Shimizu, T. 1982. Ooplasmic segregation in the *Tubifex* egg: mode of pole plasm accumulation and possible involvement of microfilaments. *Wilhelm Roux's Arch. Dev. Biol.* **191:** 246–256.

Sluder, G. 1976. Experimental manipulation of the amount of tubulin available for assembly into the spindle of dividing sea urchin eggs. *J Cell Biol* **70:** 75–85.

Webb, T. A., and R. A. Fluck. 1993. Microfilament- and microtubule-based movements during ooplasmic segregation in the medaka fish egg *(Oryzias latipes). Mol. Biol. Cell* **4:** 274a.

Yamamoto, T. 1967. Medaka. Pp. 101–111 in *Methods in Developmental Biology* F. M. Wilt and N. K. Wessells, eds. Thomas Y. Crowell Company, New York.

Youn, B. W., and G. M. Malacinski. 1980. Action spectrum for ultraviolet irradiation inactivation of a cytoplasmic component(s) required for neural induction in the amphibian egg. *J Exp. Zool* **211:** 369–377.

Reference: *Biol. Bull.* **188:** 157–165. (April, 1995)

Expression of the *Engrailed* Gene Reveals Nine Putative Segment-Anlagen in the Embryonic Pleon of the Freshwater Crayfish *Cherax destructor* (Crustacea, Malacostraca, Decapoda)

GERHARD SCHOLTZ*

*School of Biological Science, The University of New South Wales,
P.O. Box 1, Kensington, NSW 2033, Australia*

Abstract. Segment formation in the embryonic pleon of the freshwater crayfish *Cherax destructor* was analyzed by using the monoclonal antibody mAb 4D9 against the product of the segment-polarity gene *engrailed*. As in other body regions, *engrailed* is expressed in transverse stripes in the posterior portion of segments in the pleon. Nine *engrailed* stripes are formed in the pleon. The anterior six stripes correspond to the six pleon segments of adult eumalacostracan crustaceans. The uropods are clearly the appendages of the sixth pleon segment. The seventh *engrailed* stripe marks the anlage of a seventh ganglion. Stripes eight and nine are transient and disappear before morphogenesis begins. The *engrailed* stripes seven to nine are interpreted as vestiges of ancestral segments. The seventh segment anlage is thus a recapitulation of the seventh pleonic segment, which is retained in recent adult leptostracans and is considered to be part of the malacostracan ground plan. The stripes eight and nine might point still further back into the phylogeny of crustaceans or even mandibulates. The use of rhodamine-labeled phalloidin reveals that the terminal ganglion of adult crayfish is the fusion product of the anlagen of the sixth and seventh pleonic ganglia and an eighth hemiganglion that is devoid of *engrailed* expression.

Introduction

The Malacostraca constitutes a monophyletic taxon well defined by several apomorphic characters such as a characteristic tagmosis, the position of the gonopores, the subdivision of the stomach into specific functional units, and a ring of 19 embryonic ectoteloblasts (for review and discussion of different views see Dahl, 1992; Wägele, 1992). Within the Malacostraca, the Leptostraca possess a pleon (abdomen) consisting of seven segments and a telson. In contrast to all anterior segments, the seventh pleonic segment is limbless. The other malacostracan groups, unified as the Eumalacostraca (*sensu* Grobben, 1892), have only six pleomeres, all equipped with limbs. The posteriormost limbs are the uropods which, together with the flattened telson, form the tail fan. The general view is that the pleon of the Leptostraca represents the plesiomorphic condition, and the loss of a pleon segment and the evolution of the tail fan are considered to be derived characters of the Eumalacostraca (*e.g.*, Lauterbach, 1975; Hessler, 1983). However, there has been some controversy over which pleomere has been lost in the course of evolution and to which segment the uropods belong. On the basis of anatomical and paleontological data, Siewing (1956, 1963) argued that the uropods might be the appendages of the seventh pleomere and that the sixth (penultimate) pleomere has been lost in most eumalacostracans. Based on her embryological studies in mysidaceans, Manton (1928a, b), in contrast, suggested that the uropods belong to the sixth pleomere and that the original seventh is fused to the sixth pleomere. Although it was shown in the meantime that paleontological data do not support Siewing's suggestions (Dahl, 1983)—and although Manton's view has been adopted by many carcinologists such as Lauterbach (1975), Hessler (1983), and Dahl (1992)—the problem is still far from being settled

---

Received 15 November 1994; accepted 18 January 1995.

* Present address: Institut für Zoologie, Freie Universität Berlin, Königin-Luise-Str. 1-3, D-14195 Berlin, Germany.

(see, for instance, the discussion after the 1983 paper by Hessler) and a different approach seemed to be required to clarify this issue.

Within the arthropods, insects and crustaceans have the segment-polarity gene *engrailed* already expressed in transverse stripes at the posterior margin of embryonic segments before morphogenesis takes place (*e.g.*, Patel *et al.*, 1989; Manzanares *et al.*, 1993; Scholtz *et al.*, 1993, 1994; Patel, 1994). Therefore, it is a suitable marker for the analysis of the terminal regions of arthropods where segmentation is obscured by morphological rearrangements and the loss of segmental structures in the adult. Several studies have used *engrailed* to analyze the segmentation of the head in insects and crustaceans (*e.g.*, Fleig, 1994; Schmidt-Ott *et al.*, 1994; Scholtz, 1995), but the caudal segments have been analyzed only in insects (*e.g.*, Kuhn *et al.*, 1992; Schmidt-Ott *et al.*, 1994).

In the present investigation, I used the anti-*engrailed* antibody mAb 4D9 (Patel *et al.*, 1989) to analyze the segmentation of the embryonic pleon of a eumalacostracan, the Australian freshwater crayfish *Cherax destructor.* I found that, posterior to the six pleomeres typical for adult eumalacostracans, three additional vestigial segment anlagen occur in front of the telson. Furthermore, a true seventh pleonic ganglion and an eighth partial ganglion are formed embryologically. These fuse with the sixth pleonic ganglion anlage to form the terminal ganglion of the adult animal. I interpret these findings as recapitulations of ancestral characters, and they shed new light on the evolutionary transformation of crustacean segmentation patterns.

Material and Methods

The rearing and maintenance of embryos of the Australian freshwater crayfish *Cherax destructor* were described by Sandeman and Sandeman (1991). Their paper also defines the embryonic stages in percent of development and the postembryonic stages (*e.g.*, PO 1) that are used in the present investigation. Immunocytochemistry and fluorescent staining were described in detail in Scholtz *et al.* (1994) and Scholtz (1995).

Results

A short summary of previous investigations

The cell lineage in the ectoderm of the germ band of *Cherax* was described in a previous study (Scholtz, 1992). As in most other malacostracans, the largest part of the germ band is formed by stem cells in the posterior growth zone, the ectoteloblasts. The ectoteloblasts produce transverse cell rows in an anterior direction by highly unequal divisions. Thirteen of these rows are formed (eI to eXIV) before the ectoteloblasts divide equally into the fourteenth and fifteenth rows (eXIV and eXV). Each row (eI to eXIV) cleaves twice, forming four regularly arranged descendant rows. The intersegmental furrow, separating two adjacent segments, is formed within the descendants of one original ectoderm row. In contrast to all other rows, row fifteen cleaves rapidly several times, forming a field of cells in a grid-like arrangement.

In *Drosophila*, the segment-polarity gene *engrailed* plays a crucial role in specifying the fate of the cells in the posterior part (compartment) of segments and in establishing the segmental boundaries (Lawrence, 1992). The expression pattern of *engrailed* is very similar in different insect and crustacean species. Therefore, a conserved function of the *engrailed* gene throughout the arthropods has been suggested (Patel, 1994). The basic modes of pleonic *engrailed* stripe formation described in the following correspond to those reported for other body regions of *Cherax* (Scholtz *et al.*, 1993; Scholtz, 1995) and for other crustacean species (Patel *et al.*, 1989; Scholtz *et al.*, 1993, 1994). In the post-naupliar germ band of *Cherax* and other malacostracans, *engrailed* is expressed in the anterior descendants of each ectoderm row, and the intersegmental furrow is formed posterior to the *engrailed* stripes.

The formation of engrailed *stripes*

Nine *engrailed* stripes are formed in the embryonic pleon of *C. destructor* (Fig. 1). The first pleonic stripe appears in ectoderm row eIX and the sixth stripe in row eXIV. Stripes seven to nine are formed within the derivatives of row eXV.

The stripes appear in a strictly anteroposterior sequence (Fig. 1). At about 40% to 42% development the first *engrailed* stripe is formed and indicates the posterior margin of the prospective first pleomere (Fig. 1A). The ninth pleonic *engrailed* stripe appears at about 65% development (Fig. 1D, E). The formation of each individual stripe starts close to the midline and proceeds laterally (Fig. 1D). The initial distance between the last two *engrailed* stripes of any stage is one row of *engrailed* negative cells. This is also true for stripes seven to nine (Fig. 1E). Stripes one to seven are associated with the complex metamerically repeated cleavage pattern in the post-naupliar germ bands of *Cherax*. The cell division pattern in the area of stripes eight and nine, although not analyzed in detail, is somewhat different (Scholtz, 1992).

Initially, all stripes are one cell wide (Fig. 1). Also, at least pleonic stripes one to eight (not confirmed for pleonic stripe nine) pass through a transient widening phase caused by divisions of the *engrailed*-positive cells (Fig. 1B, C). The widening phase is followed by narrowing to a one-cell width again due to the loss of *engrailed* expression in posterior cells in the stripe (Fig. 1B, C). After nar-

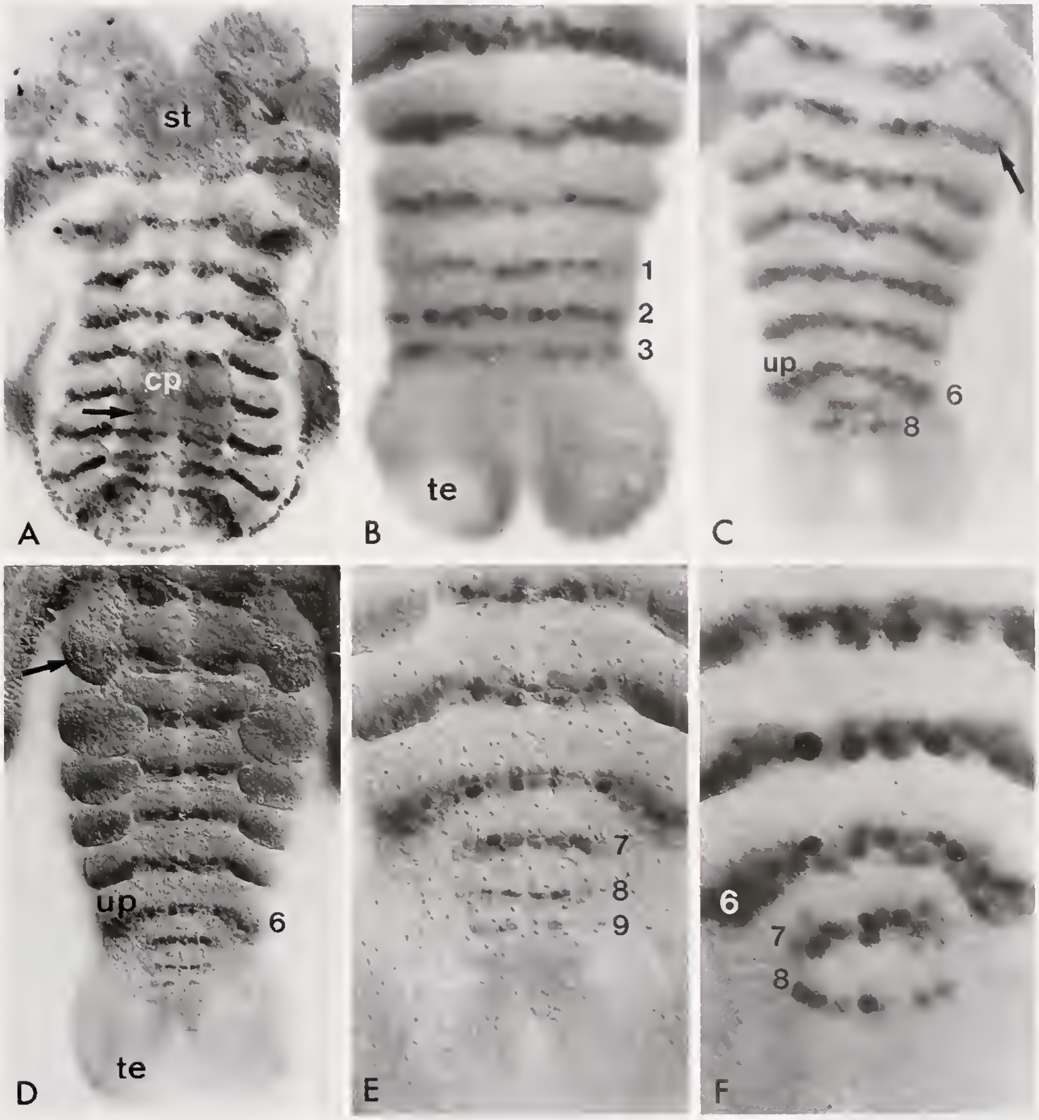

Figure 1. Formation of *engrailed* stripes: st, stomodeum; cp, caudal papilla; te, telson anlage; up, uropods. (A) Germ band at 40% to 42% development. All *engrailed* stripes of head and thorax are formed. The *engrailed* stripe marking the first pleonic segment appears (arrow) on the ventral side of the ventrally flexed caudal papilla. (B) Posterior part of the caudal papilla of an embryo at 45% development (ventral view). The *engrailed* stripes up to the third pleonic segment (1, 2, 3) are formed. The posteriormost stripe (3) is one cell wide. The next anterior stripe (2) is in the narrowing phase after the initial widening. The stripe of the first pleonic segment (1) is in the phase of secondary widening in correlation with the formation of the intersegmental furrow and the limb buds (for details see Scholtz *et al.*, 1993). (C) Posterior part of the caudal papilla of an embryo at about 60% development (ventral view); *engrailed* stripes seven and eight are formed. Stripe eight is in the first widening phase; stripe seven has already narrowed to one cell width. The uropods begin to appear in the area of the sixth *engrailed* stripe (sixth pleonic segment). Note the buds of the first pleopods (arrow), which are lacking in the adults of *Cherax* (comp. Fig. 1D). (D) Posterior part of the caudal papilla of an embryo at about 65% development (ventral view). The ninth *engrailed* stripe appears following a mediolateral sequence of *engrailed* expression. The ninth stripe is the posteriormost area of *engrailed* expression, the posterior margin of the telson anlage does not express *engrailed*. The arrow points to the buds of the first pleopods. (E) Closeup of the same preparation as in (D); 7 to 9 seventh to ninth pleonic *engrailed* stripes. (F) Posterior part of the caudal papilla of an embryo at 70% development (ventral view). Neuronal *engrailed* expression begins in the area of the seventh pleonic stripe (7). The cells of *engrailed* stripe eight begin to cease *engrailed* expression; stripe nine has disappeared.

rowing, stripes one to seven widen during the morphogenesis of segmental structures such as intersegmental furrows, ganglia, and limb buds (Fig. 1). Stripes eight and nine disappear before widening takes place (Fig. 1F).

Stripes one to six surround the caudal papilla and form complete circles of about 40 *engrailed*-positive cells (Fig. 1, 2A). Thus, *engrailed* is expressed in the midventral neurogenic region, in the lateral limb budding area, and in the dorsal portion of the forming segments one to six. Stripes seven to nine are restricted to the medioventral part, which includes the neurogenic region (Fig. 1D, E). They consist of seven to nine *engrailed* expressing cells.

Stripes one to seven show a twofold *engrailed* expression in the embryonic epidermis and in the forming ganglia (Figs. 1, 2). In the stages examined, the superficial epidermal *engrailed* expression continues in the forming limbs and the dorsal portions of the segments (Fig. 2). In the neurogenic area of advanced stages, *engrailed* expression is restricted to individual neuronal precursors and neurons, whereas the superficial *engrailed* expression has disappeared (Figs. 1, 2). In contrast to this, stripes eight and nine appear only transiently in the embryonic epidermis (Figs. 1, 2).

Morphogenesis

In all other body regions, the intersegmental furrows are formed immediately posterior to the *engrailed* stripes (Fig. 1). This is also true for pleonic stripes one to six, but stripes seven to nine are not related to the formation of intersegmental furrows (Figs. 1D, E, 2). In segments one to six, limb buds are formed whose posterior portions are also *engrailed* positive (Figs. 1, 2). No limb buds occur in segments seven to nine, and in the corresponding regions the cells do not show *engrailed* expression (Figs. 1, 2). Interestingly enough, embryonic limb buds are formed in the first pleonic segment (Fig. 1C, D) where the adult *C. destructor*, like all parastacid crayfish species, is devoid of appendages in both sexes (Hobbs, 1988). The limbs associated with the sixth pleonic *engrailed* stripe are clearly the posteriormost appendages on the germ band (Figs. 1C, D, E, 2). On the basis of their shape in advanced developmental stages, they can be identified to be the uropods (Figs. 1, 2).

Neurogenesis

In the pleonic segments one to seven, *engrailed* is expressed in cells of the forming ganglia (Figs. 1, 2). Thereby, the arrangement of *engrailed*-positive cells (neurons ?) is very similar between the seventh and more anterior segments (Fig. 2). The *engrailed* expression in stripes eight and nine disappears at about 70% to 75% development and is not correlated with neurogenesis. The staining of the embryonic central nervous system with rhodamine-

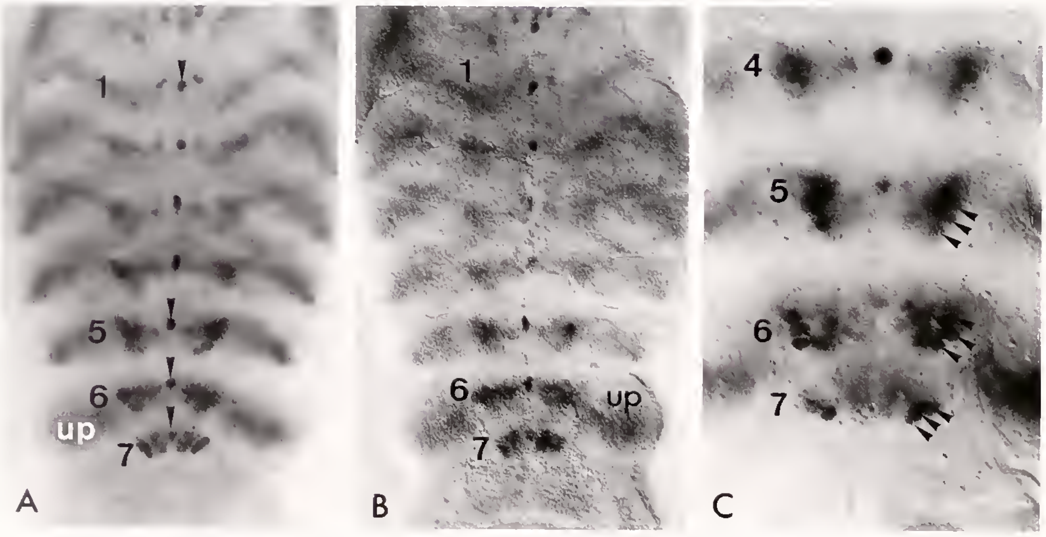

Figure 2. Early neuronal *engrailed* expression in the pleon: up, uropods. (A) Posterior part of the caudal papilla of an embryo at about 75% development (ventral view; brightfield micrograph). The pattern of *engrailed* expression in neuronal precursors and early neurons in the seventh pleonic ganglion anlage is very similar to that of more anterior pleonic ganglion anlagen, indicating a serial homology between all seven pleonic ganglia. The resemblance concerns, in particular, a median *engrailed*-positive cell (arrowheads) and a set of three intensely stained cells at the posterior margin of the *engrailed*-positive area (compare Fig. 2C). Note the dorsal *engrailed* expression in pleomeres one to six. (B) Same preparation as in (A), with Nomarski optics. This technique shows the buds of the pleonic limbs. The uropods are beginning to get their characteristic shape and are clearly connected with the sixth pleomere. (C) Closeup of another preparation (Nomarski optics). The serially homologous group of three intensely stained cells in ganglion anlage seven and more anterior ganglion anlagen is marked by arrowheads.

labeled phalloidin reveals that a true seventh embryonic ganglion is formed in addition to the anterior six pleonic ganglion anlagen (Fig. 3). All pleonic ganglion anlagen one to seven share the occurrence of two main commissures and a characteristic median Y-shaped neuron that might correspond to the neuron S described by Whitington *et al.* (1993) (Fig. 3A, B). Posterior to the seventh, an eighth ganglion anlage is formed. It possesses only one commissure, and the characteristic median cell is lacking (Fig. 3B). Furthermore, no neuronal *engrailed* expression occurs. From this eighth hemiganglion, two nerves run posteriorly towards the embryonic telson region (Fig. 3B). During further ontogenesis the anlagen of ganglia six, seven, and eight fuse and become a morphological unit that forms the terminal ganglion of the adult animals (Fig. 3C). Thereby the commissures remain separated. The coalescence of these ganglion anlagen is clearly visible from about 80% development. However, *engrailed* expression still indicates the composed origin of the terminal ganglion in postembryonic stages (*e.g.*, PO 1) (Fig. 4).

Discussion

Development of the terminal ganglion

The present investigation shows that the terminal ganglion of the adult parastacoid crayfish *Cherax destructor* is the fusion product of three embryonic ganglion anlagen—the sixth and seventh pleonic ganglia and a partial eighth ganglion. This developmental pattern corresponds to that described for the astacoid crayfish *Procambarus clarkii* (Dumont and Wine, 1987). Furthermore, these embryological data are consistent with results from neuroanatomical and immunohistochemical studies analyzing the terminal ganglia of the adults of several freshwater crayfish species (Stoll, 1925; Kondoh and Hisada, 1986; Audehn *et al.*, 1993) and of the lobster *Homarus gammarus* (Winlow and Laverack, 1972). The embryonic morphology and the pattern of *engrailed* expression of the seventh pleonic ganglion resemble to a high degree those of the anterior pleonic ganglia. This suggests that it represents a true segmental ganglion homologous with the anterior segmental ganglia. The eighth pleonic ganglion anlage shows only one commissure. Furthermore, this ganglion lacks any *engrailed* expression which characterizes the posterior part of forming ganglia, although an epidermal eighth pleonic *engrailed* stripe is formed. Taken together, this suggests that the eighth pleonic ganglion of the embryo might be the anterior part of a true segmental ganglion anlage. On the basis of the occurrence of specifically arranged identified neurons, Audehn *et al.* (1993) came to similar conclusions.

The formation of an embryonic anlage of a seventh pleonic ganglion that later fuses with the sixth ganglion has been reported from representatives of most higher malacostracan taxa including Leptostraca (Claus, 1888; Manton, 1928b, 1934), Hoplocarida (Shiino, 1942), Syncarida (Hickman, 1937), Mysidacea (Manton, 1928a, b), Tanaidacea (Scholl, 1963), and Isopoda (Strömberg, 1967). No seventh pleonic ganglion occurs in the embryo of the amphipod *Gammarus pulex*; however, for a short time during development, the anlage of the sixth pleonic ganglion is subdivided into two distinct adjacent areas—a phenomenon interpreted as a vestigial formation of a seventh pleonic ganglion (Weygoldt, 1958). None of these authors has mentioned the partial eighth pleonic ganglion, but this might be due to the techniques used (no wholemounts or horizontal sections). Adult eumalacostracans possess only six pleonic ganglia (see Hanström, 1928), and this is also true for leptostracans with a seventh pleomere (Claus, 1888; Manton, 1928a). Against this background, I conclude that the composite nature of the terminal (sixth) ganglion and the pattern of its formation by fusion during embryogenesis is part of the malacostracan ground plan. Thus, the fusion of the terminal ganglion is apparently not correlated with the evolution of the uropods and their complex function in eumalacostracans.

Origination of the uropods from the sixth pleomere

The anterior six *engrailed* stripes in the embryonic pleon of *Cherax* mark the posterior border of the six pleomeres that persist in the adult. *Engrailed* is expressed in the ventral region comprising the ganglion primordia and the limb buds as well as the lateral and dorsal sides of each segment. The seventh to ninth pleonic *engrailed* stripes are restricted to the ventral side of the embryo. However, from the mode of formation and the distance between them, they correspond to the anterior stripes. Thus I conclude that all pleonic *engrailed* stripes are serial homologues and that stripes seven to nine also indicate segment anlagen.

The pattern of the sixth *engrailed* stripe clearly reveals that the uropods of *Cherax* are the limbs of the sixth pleomere, which is also true for the mysid *Neomysis integer* (unpub. obs.). This result confirms some of the suggestions of Manton (1928a, b), and since there is good evidence that the tail fans of all eumalacostracean groups are homologous (Hessler, 1983; Wägele, 1994), the findings presented here might also be valid for eumalacostracans in general. Therefore, Siewing's (1956, 1963) hypothesis that the uropods originate from the seventh pleon segment cannot be maintained. The present results also contradict the assumption that the caudal rami of the telson of leptostracans are homologous with the eumalacostracan uropods (Bowman, 1971; for further arguments against this view see Schminke, 1976). Furthermore, the telson of decapods does not correspond to the ancestral seventh pleomere, as was suggested by Kondoh and Hisada (1986).

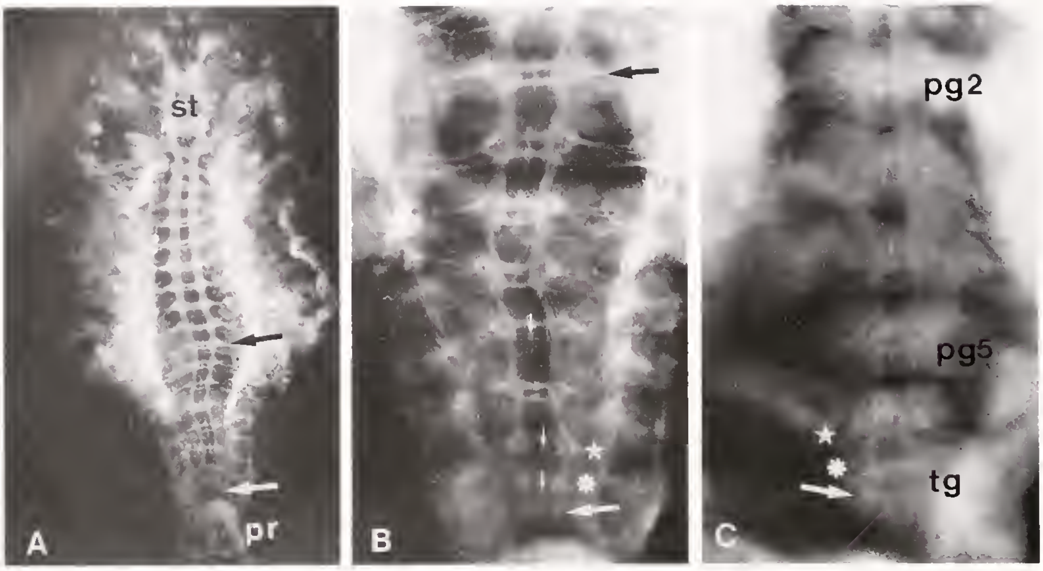

Figure 3. Gangliogenesis as seen with rhodamine-labeled phalloidin: st, stomatodeum; pr, proctodeum; pg2, second pleonic ganglion; pg5, fifth pleonic ganglion; tg, terminal ganglion. (A) The nerve cord of an embryo at 75% to 80% development. The black arrow points to the eighth thoracic ganglion anlage; the white arrow indicates the eighth pleonic (hemi)ganglion anlage. (B) Closeup of posterior ganglion anlagen. The seventh ganglion anlage (asterisk) shows the same pattern as those of more anterior segments (*e.g.*, the sixth ganglion anlage; star). The eighth ganglion anlage (large white arrow) consists of only one commissure. The black arrow shows the eighth thoracic ganglion anlage; the small white arrows point to the median Y-shaped neurons. (C) Advanced stage (85% to 90% development) showing that the sixth (star), seventh (asterisk), and eighth (white arrow) ganglion anlagen are embedded in a morphological unit, forming one large terminal ganglion.

The additional *engrailed* stripes seven to nine lie clearly in front of the telson anlage, which is characterized by the proctodeum and which lacks *engrailed* expression. Against this background, the seemingly "seven-segmented" pleon with uropods originating from the "seventh" pleomere of some lophogastrids is not plesiomorphic, as considered by Manton (1928b), Siewing (1956), and Lauterbach (1975), but is a derived feature. There is ontogenetic and phylogenetic evidence for this suggestion. Manton's (1928b) hypothesis that the uropods migrate posteriorly before the border between the last two segments is formed is not consistent with the finding that the intersegmental furrows are formed before limb buds appear (Scholtz, 1990; present investigation). We know from *Drosophila* genetics that the establishment of the segmental border is the prerequisite for the subsequent differentiation of segments (Lawrence, 1992). Therefore, the "seventh pleonic segment" of lophogastrids is apparently the result of a secondary nonsegmental(?) subdivision of the terminal eumalacostraean segment, as was suggested earlier by Claus (1888). With respect to the position of lophogastrids in the eumalacostracan phylogenetic tree (*e.g.*, Siewing, 1956; Richter, 1993), it is more likely that a subdivision of the terminal segment occurred only once in the lophogastrid line than that the seventh pleomere has been lost independently in several eumalacostracan lines.

The seventh pleonic *engrailed* stripe in the embryo of *Cherax* is an obvious example of the recapitulation of ancestral conditions (see Sudhaus and Rehfeld, 1992). It demarcates the posterior border of an additional (seventh) pleonic segment that is missing in adult crayfish and other eumalacostraeans but is present in adult Leptostraca, the sister-group of the Eumalacostraea. There is no reason to assume that pedomorphosis led to the occurrence of the seventh segment in adult leptostracans and to the loss of the highly complex eumalacostracan tail-fan (Hessler, 1983; Paul *et al.*, 1985) in this group.

Interestingly, in the crayfish as in other eumalacostracans, the corresponding seventh pleonic ganglion persists and is fused with the sixth to form a morphological and functional unit (see above). In addition, some authors report that the embryos of several malacostracan species contain terminal mesodermal somites that might be related to a vestigial seventh pleonic segment and that also fuse with the sixth pleonic somites (*e.g.*, Manton, 1928a; Shiino, 1942). Those processes can be characterized as fusions, but fusion does not seem to be the appropriate description for events in the superficial segmental parts. The pleonic *engrailed* stripe seven (like stripes eight and nine) is more like a transient segment anlage that is not involved in morphogenesis

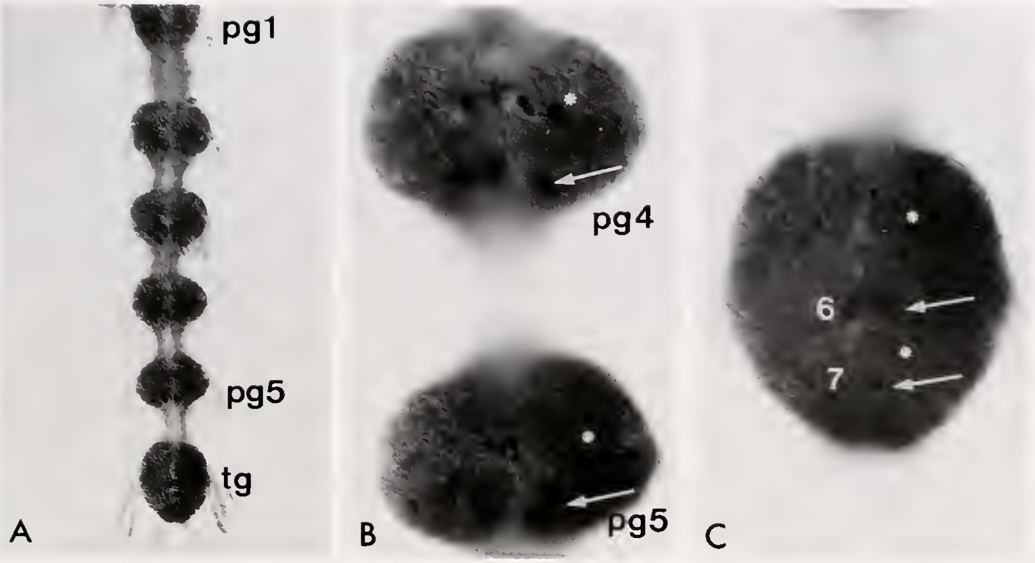

Figure 4. Expression of *engrailed* in the pleonic nerve cord of the first postembryonic stage (PO 1): pg1, first pleonic ganglion; pg4, fourth pleonic ganglion; pg5, fifth pleonic ganglion; tg, terminal ganglion. (A) The six ganglia of the pleon of the first stage after hatching (PO 1) (ventral aspect). (B) Higher magnification of the same preparation, showing the ganglia of the fourth and fifth pleomeres. They exhibit a serially repeated pattern of two areas of *engrailed* expression. An anterior region of cells (neurons, glia, or their precursors) with relatively small nuclei (asterisks) and a posterior region with large *engrailed*-positive cells (arrows). (C) The terminal ganglion (same preparation as in (A)). The pattern of *engrailed* expression reveals the composed nature of this ganglion. The asterisks indicate the anterior segmental *engrailed* area and the arrows point to the posterior segmental *engrailed* area (compare Fig. 4B). The pattern of *engrailed* expression in the seventh ganglion anlage (7) is somewhat reduced when compared with that of the sixth ganglion anlage (6).

and that disappears during further development. From the outset, the morphological border between the terminal segment and the telson lies behind the sixth pleonic *engrailed* stripe.

Phylogenetic significance of pleonic engrailed *stripes eight and nine*

The eighth and ninth pleonic *engrailed* stripes are also considered to indicate vestigial segments that recapitulate ancestral conditions. This suggestion is based on the similar appearance of stripes seven to nine and on the fact that many non-malacostracan crustaceans possess more segments than malacostracans. However, it is difficult to say how far back stripes eight and nine point in phylogeny and in which ancestral lineage these segments have been lost in the adults. The question of whether segmentation and tagmatization of the Malacostraca are primitive or are derived within the Crustacea has been debated, and the many attempts to reconstruct the crustacean stem species have yielded very different results concerning tagmosis and segment number. The proposals reach from short animals with only a few segments (Müller, 1864) to forms with many segments (Hessler and Newman, 1975; Lauterbach, 1986), and from forms with a more or less homonomously segmented trunk (Hessler and Newman, 1975; Schram, 1982; Walossek, 1993) to animals with a distinct subdivision of the trunk into thorax and a limbless abdomen (Lauterbach, 1986; Fryer, 1992). But until the phylogenetic relationships between the higher crustacean taxa are resolved—see Siewing (1963), Schram (1986), and Wilson (1992) for various proposals—the reconstruction of a crustacean ground plan (*sensu* Hennig, 1966) will be pure speculation.

Nevertheless, the present findings permit some tentative conclusions. The occurrence of additional segment remnants in the embryonic pleon of *Cherax* argues against an original number of 15 trunk segments in crustaceans or even mandibulates as suggested by Walossek (1993); the number of trunk segments in the crustacean stem species must have been higher. Therefore, the additional *engrailed* stripes in the pleon of *Cherax* rather argue in favor of Lauterbach's (1975) hypothesis of a loss of posterior segments in the ancestral lineage of malacostracans. The restriction of these additional stripes to the neural region and the entire lack of limb anlagen furthermore support the suggestion that these segments are vestiges of the limbless abdomen postulated by Lauterbach (1986) and Fryer (1992) for the crustacean stem species.

Acknowledgments

I thank David Sandeman and Renate Sandeman for their helpful advice as well as for the opportunity to use their crayfish culture and to work in their laboratory. The anti-*engrailed* antibody was a generous gift from Nipam Patel. I am grateful to Stefan Richter, Wolfgang Dohle, and David Sandeman for critically reading the manuscript. This work was supported by grants from the University of New South Wales (Visiting Fellowship) and from the Deutsche Forschungsgemeinschaft (Scho 443/3-1).

Literature Cited

Audehm, U., A. Trube, and H. Dircksen. 1993. Patterns and projections of crustacean cardioactive-peptide-immunoreactive neurones of the terminal ganglion of crayfish. *Cell Tissue Res.* **272:** 473–485.

Bowman, T. E. 1971. The case of the non-ubiquitous telson and the fraudulent furca. *Crustaceana* **21:** 165–175.

Claus, C. 1888. Über den Organismus der Nebaliden und die systematische Stellung der Leptostraken. *Arb. Zool. Inst. Wien* **8:** 1–148, 15 plates.

Dahl, E. 1983. Malacostracan phylogeny and evolution. Pp. 189–212 in *Crustacean Phylogeny.* F. R. Schram, ed. Balkema, Rotterdam.

Dahl, E. 1992. Aspects of malacostracan evolution. *Acta Zool.* **73:** 339–346.

Dumont, J. P. C., and J. J. Wine. 1987. The telson flexor neuromuscular system of the crayfish. I. Homology with the fast flexor system. *J. Exp. Biol.* **127:** 249–277.

Fleig, R. 1994. Head segmentation in the embryo of the Colorado beetle *Leptinotarsa decemlineata* as seen with anti-*en* immunostaining. *Roux's Arch. Dev. Biol.* **203:** 227–229.

Fryer, G. 1992. The origin of the Crustacea. *Acta Zool.* **73:** 273–286.

Grobben, K. 1892. Zur Kenntnis des Stammbaums und des Systems der Crustaceen. *Sitzber. Akad. Wiss. Wien* **101:** 237–274.

Hanström, B. 1928. *Vergleichende Anatomie des Nervensystems der wirbellosen Tiere.* Springer, Berlin.

Hennig, W. 1966. *Phylogenetic Systematics.* University of Illinois Press, Urbana. 263 pp.

Hessler, R. R. 1983. A defense of the caridoid facies: wherein the early evolution of the Eumalacostraca is discussed. Pp. 145–164 in *Crustacean Phylogeny.* F. R. Schram, ed. Balkema, Rotterdam.

Hessler, R. R., and W. A. Newman. 1975. A trilobitomorph origin for the Crustacea. *Fossils Strata* **4:** 437–459.

Hickman, V. V. 1937. The embryology of the syncarid crustacean *Anaspides tasmaniae. Pap. R. Soc. Tasm.* :1–36.

Hobbs, H. H. 1988. Crayfish distribution, adaptive radiation and evolution. Pp. 365–400 in *Freshwater Crayfish. Biology, Management and Exploitation.* D. M. Holdich and R. S. Lowery, eds. Croom Helm, London.

Kondoh, Y., and M. Hisada. 1986. Neuroanatomy of the terminal (sixth abdominal) ganglion of the crayfish, *Procambarus clarkii* (Girard). *Cell Tissue Res.* **243:** 273–288.

Kuhn, D. T., M. Sawyer, G. Packert, G. Turenchalk, J. A. Mack, Th. E. Sprey, E. Gustavson, and T. B. Kornberg. 1992. Development of the *D. melanogaster* caudal segments involves suppression of the ventral regions of A8, A9 and A10. *Development* **116:** 11–20.

Lauterbach, K.-E. 1975. Über die Herkunft der Malacostraca (Crustacea). *Zool. Anz.* **194:** 165–179.

Lauterbach, K.-E. 1986. Zum Grundplan der Crustacea. *Verh. naturwiss. Ver. Hamburg (NF)* **28:** 27–63.

Lawrence, P. A. 1992. The making of a fly: the genetics of animal design. Blackwell Scientific Publications, Oxford. 228 pp.

Manton, S. M. 1928a. On the embryology of a mysid crustacean, *Hemimysis lamornae. Phil. Trans. R. Soc. Lond. (B)* **216:** 363–463.

Manton, S. M. 1928b. On some points in the anatomy and habits of the lophogastrid Crustacea. *Trans. R. Soc. Edin.* **56:** 103–119, 3 Plates.

Manton, S. M. 1934. On the embryology of the Crustacean *Nebalia bipes. Phil. Trans. R. Soc. Lond. (B)* **223:** 163–238.

Manzanares, M., R. Marco, and R. Garesse. 1993. Genomic organization and developmental pattern of expression of the *engrailed* gene from the brine shrimp *Artemia. Development* **118:** 1209–1219.

Müller, F. 1864. Für Darwin. Pp. 200–263 reprint (1915) in *Fritz Müller. Werke, Briefe und Leben.* A. Möller, ed. Gustav Fischer, Jena.

Patel, N. H. 1994. Developmental evolution: insights from studies of insect segmentation. *Science* **266:** 581–590.

Patel, N. H., T. B. Kornberg, and C. S. Goodman. 1989. Expression of *engrailed* during segmentation in grasshopper and crayfish. *Development* **107:** 201–212.

Paul, D. H., A. M. Then, and D. S. Magnuson. 1985. Evolution of the telson neuromusculature in decapod Crustacea. *Biol. Bull.* **168:** 106–124.

Richter, S. 1993. Die Eucarida sind nicht monophyletisch—Ommatidienstruktur deutet auf nähere Verwandtschaft von Euphausiacea, Syncarida und Peracarida (Crustacea). *Verh. Deutsch. Zool. Ges.* **86.1:** 144.

Sandeman, R., and D. Sandeman. 1991. Stages in the development of the embryo of the fresh-water crayfish *Cherax destructor. Roux's Arch. Dev. Biol.* **200:** 27–37.

Schmidt-Ott, U., K. Sander, G. M. Technau. 1994. Expression of *engrailed* in embryos of a beetle and five dipteran species with special reference to the terminal regions. *Roux's Arch. Dev. Biol.* **203:** 298–303.

Schminke, H. K. 1976. The ubiquitous telson and the deceptive furca. *Crustaceana* **30:** 292–300.

Scholl, G. 1963. Embryologische Untersuchungen an Tanaidaceen (*Heterotanais oerstedi* KRÖYER). *Zool. Jb. Anat.* **80:** 500–554.

Scholtz, G. 1990. The formation, differentiation and segmentation of the post-naupliar germ band of the amphipod *Gammarus pulex* L. (Crustacea, Malacostraca, Peracarida). *Proc. R. Soc. Lond. (B)* **239:** 163–211.

Scholtz, G. 1992. Cell lineage studies in the crayfish *Cherax destructor* (Crustacea, Decapoda): Germ band formation, segmentation, and early neurogenesis. *Roux's Arch. Dev. Biol.* **202:** 36–48.

Scholtz, G. 1995. Head segmentation in Crustacea—an immunocytochemical study. *Zoology* **98:** 104–114.

Scholtz, G., W. Dohle, R. E. Sandeman, and S. Richter. 1993. Expression of *engrailed* can be lost and regained in cells of one clone in crustacean embryos. *Int. J. Dev. Biol.* **37:** 299–304.

Scholtz, G., N. H. Patel, and W. Dohle. 1994. Serially homologous *engrailed* stripes are generated via different cell lineages in the germ band of amphipod crustaceans (Malacostraca, Peracarida). *Int. J. Dev. Biol.* **38:** 471–478.

Schram, F. R. 1982. The fossil record and evolution of Crustacea. Pp. 93–147 in *The Biology of Crustacea, Vol. 1.* L. G. Abele, ed. Academic Press, New York.

Schram, F. R. 1986. *Crustacea.* Oxford University Press, New York. 606 pp.

Shiino, S. M. 1942. Studies on the embryology of *Squilla oratoria* de Haan. *Mem. Coll. Sci. Kyoto Imp. Univ. B* **17:** 77–174, 10 plates.

Siewing, R. 1956. Untersuchungen zur Morphologie der Malacostraca (Crustacea) *Zool. Jb. Anat.* **75:** 39–176.

Siewing, R. 1963. Studies in malacostracan morphology: results and problems. Pp. 85–103 in *Phylogeny and Evolution of Crustacea.* H. B. Whittington and W. D. I. Rolfe, eds. Mus. Comp. Zool., Cambridge, MA.

Stoll, E. 1925. Über den Bau des Zentralnervensystems von *Astacus fluviatilis* (*Potamobius astacus* L.). *Z. wiss. Zool.* **126:** 145–179.

Strömberg, J. O. 1967. Segmentation and organogenesis in *Limnoria lignorum* (RATHKE) (Isopoda). *Ark. Zool.* **20:** 91–139.

Sudhaus, W., and K. Rehfeld. 1992. *Einführung in die Phylogenetik und Systematik.* Gustav Fischer, Stuttgart. 241 pp.

Wägele, J. W. 1992. Synopsis of discussion on 'relationships between malacostracan groups and reconstruction of the ur-malacostracan.' Chairman: Les Watling. *Acta Zool.* **73:** 347–348.

Wägele, J. W. 1994. Review of the methodological problems of 'Computer cladistics' exemplified with a case study on isopod phylogeny (Crustacea: Isopoda). *Z. zool. Syst. Evolut.-forsch.* **32:** 81–107.

Walossek, D. 1993. The Upper Cambrian *Rehbachiella* and the phylogeny of Branchiopoda and Crustacea. *Fossils Strata* **32:** 1–202.

Weygoldt, P. 1958. Die Embryonalentwicklung des Amphipoden *Gammarus pulex pulex* (L.). *Zool. Jb. Anat.* **77:** 51–110.

Whitington, P. M., D. Leach, and R. Sandeman. 1993. Evolutionary change in neural development within the arthropods: axonogenesis in the embryos of two crustaceans. *Development* **118:** 449–461.

Wilson, G. D. F. 1992. Computerized analysis of crustacean relationships. *Acta Zool.* **73:** 383–389.

Winlow, W., and M. S. Laverack. 1972. The control of hindgut motility in the lobster *Homarus gammarus* (L.), 3. Structure of the sixth abdominal ganglion (6 A.G.) and associated ablation and microelectrode studies. *Mar. Behav. Physiol.* **1:** 93–121.

Reference: *Biol. Bull.* **188:** 166–178. (April, 1995)

The Tidal Rhythm of Emergence, and the Seasonal Variation of This Synchrony, in an Intertidal Midge

MASAYUKI SAIGUSA[1] AND TADASHI AKIYAMA[2]

[1]*Department of Biology, Faculty of Science, Okayama University, Tsushima 2-1-1, Okayama 700, Japan; and* [2]*Ushimado Marine Laboratory, Okayama University, Oku-Ushimado, Okayama 701-43, Japan*

Abstract. The emergence of an intertial midge was investigated at a site on the coast of the Inland Sea of Japan. The population emerging at this site was drawn from a single species of the genus *Clunio*, probably *C. tsushimensis*. Emergence was not synchronized with the day-night cycle, but with the tidal cycle. Moreover, the pattern of synchrony changed with season. A bimodal phase appeared in midwinter; but the pattern of synchrony shifted gradually, during January and February, from morning low tides to afternoon low tides, and a unimodal phase appeared in March. This pattern—*i.e.*, synchrony with afternoon low tides—lasted until early October. In mid-October, the synchrony shifted to the morning low tides. Only a brief bimodal phase appeared in autumn. The phase modality was clearly correlated with the height of tides; *i.e.*, when the low waters in a day were very different in height, emergence was synchronized only with the lower one (April to December). During January and February, the higher low tide, as well as the lower low tide, recedes considerably. The exposure of the larval habitat at the higher low tide may stimulate emergence, resulting in bimodal phases in midwinter. But the unimodal pattern in March cannot be accounted for by a simple synchrony with lower low tide, or with exposure of the larval habitat to the air; the day-night cycle not only would be one of the *zeitgebers* of the tidal rhythm in every season, but also must participate in the expression of the unimodal phase in spring. Furthermore, the number of midges that emerged each day fluctuated with a semilunar cycle with the season. The phase of this rhythm would be shifted by water temperature.

Introduction

Tidal and semilunar rhythms of reproductive activity have been reported in many intertidal and estuarine organisms (*e.g.*, see Korringa, 1947; Hauenschild, 1960; DeCoursey, 1983; Pearse, 1990). Marine midges of the genus *Clunio* are among such animals. The imagines emerge around the full and new moons, and the time of daily emergence corresponds to that of low tides at the habitat (Caspers, 1951; Koskinen, 1968; Hashimoto, 1976; Neumann, 1966; 1976; 1987). But in most of the species observed, eclosion occurs in a very short period, *i.e.*, at most the 4–5 days bracketing the full and new moons. In these cases, therefore, the rhythm underlying the observed events in the field—*i.e.*, daily or tidal—was not clear.

The circadian rhythm of terrestrial animals exhibits at least two essential and distinctive characteristics: (1) a free-running period approximating the 24-h day-night cycle; and (2) synchrony with the local light-dark cycle (and sometimes with 24-h temperature cycles, too). But in marine organisms, such characteristics are not sufficient evidence of a circadian rhythm. For example, the circatidal rhythm of larval release in a few semiterrestrial crabs is surely entrained by 24-h, light-dark cycles (Saigusa, 1986; 1992). We supposed that the emergence rhythm of *Clunio* might be similarly timed. As the first step in testing this hypothesis, the rhythm was examined in the field.

A further problem in tidal rhythm research is the relationship between the modulation of the tidal amplitude and the modality of the phase. In some of the oceans in the world, there are two high (or low) tides, of approximately equal height, per day, at intervals of about 12.4 h. But in the Pacific Ocean, the two high and low tides on a given day often show very different heights, and they recur at asymmetrical intervals (see Saigusa, 1985). Enright (1963) reported a circatidal rhythm of swimming in freshly collected specimens of the sand-beach amphipod *Synchelidium* sp. A feature of this rhythm was that the relative amplitudes of activity peaks seemed to reflect contemporary tidal amplitudes. An isopod, *Excirolana*

Received 11 June 1993; accepted 1 February 1995.

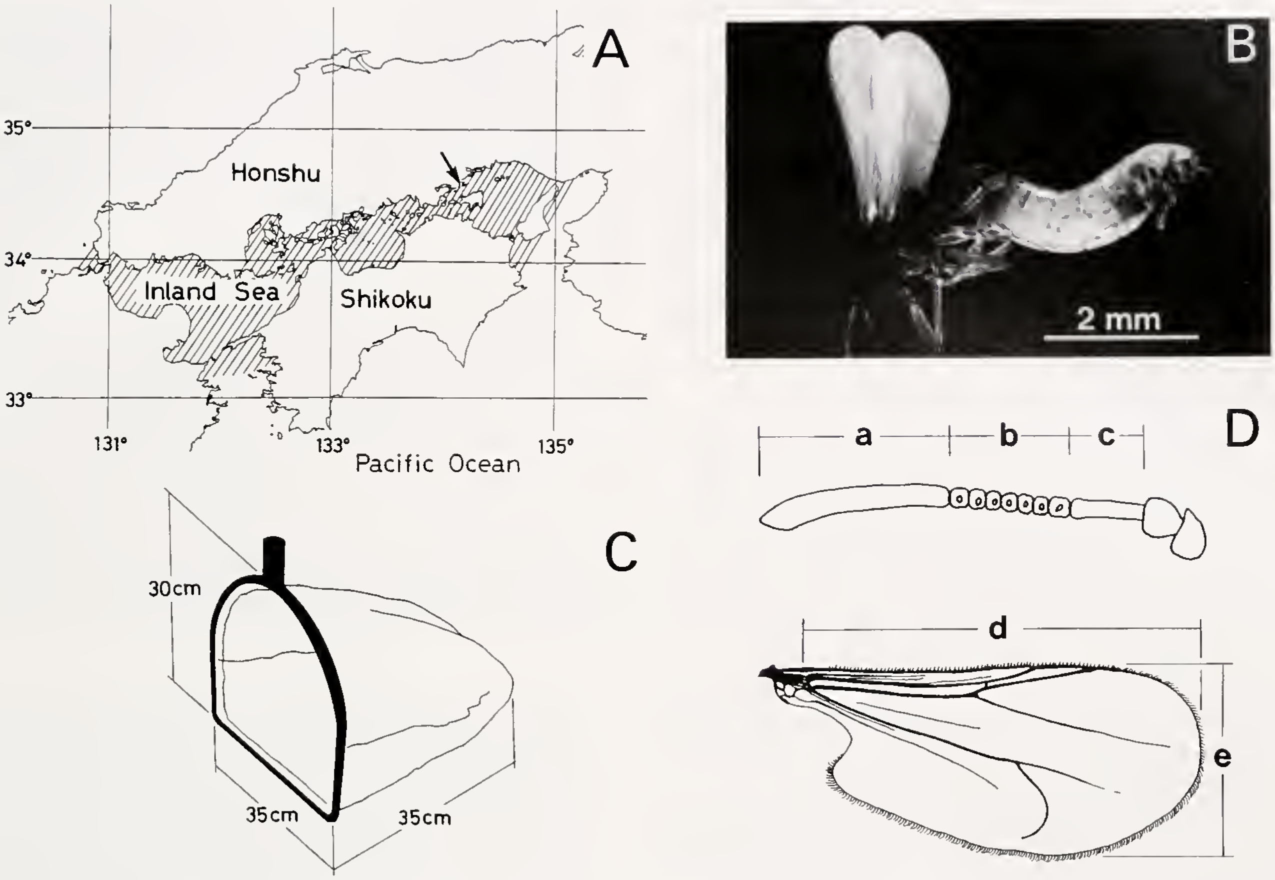

Figure 1. (*A*) The site of emergence of the *Clunio* population studied (arrow). The Inland Sea is situated between Honshu and Shikoku (shown by the diagonal lines). As its east and west sides are open to the Pacific Ocean through the straits, the salinity is not greatly reduced, averaging 28–29 ppt through the year. (*B*) Recently emerged male and female imagines shown mating. The pupal eclosion of the female is completed with the assistance of the male. As soon as he has stripped off the female's pupal skin, the male runs or flies carrying the female in the mating position shown in this figure. (*C*) The nylon net used to catch flying midges. Since many midges fly on the water film, the sampling was carried out with the net touching the water. (*D*) Antenna and wing venation of a male *Clunio* studied: *a*, the third segment; *b*, adjoining seven small segments; *c*, the ultimate segment; *d*, length of the wing; *e*, width of the length. See the text for the antennal and wing indices.

chiltoni, inhabiting a similar environment exhibited a similar activity rhythm (Enright, 1972).

Tidal amplitudes vary with the season. Thus, if the activity of an organism is correlated with tidal amplitude, then the pattern of the rhythm must also vary with the season. We have already reported on the swimming activity rhythm of the sublittoral crustacean *Dimorphostylis asiatica*, whose pattern was modified seasonally (Akiyama and Yoshida, 1990). The midge *Clunio* is also an appropriate animal with which to investigate this problem, because emergence occurs in every season. Oka and Hashimoto (1959) reported a seasonal change in daily emergence in *Clunio tsushimensis*. But their data were only qualitative (see also Hashimoto, 1976) so it was not clear whether the daily timing of emergence is correlated with modulations of tidal amplitude or with other seasonal factors, such as the ratio of day-night length or the fluctuation of water temperature.

An additional problem is the uncertain classification of the genus of midges and the distribution of species along Japanese seacoasts. Hashimoto (1969, 1976) reported a sympatric species, *C. aquilonius*, whose morphology is quite similar to that of *C. tsushimensis*. So we had to identify the species whose imagines were emerging in our study area along the shoreline of the Inland Sea.

Materials and Methods

Collections of flying midges

Field investigations were carried out on the coast of the Inland Sea of Japan, Okayama Prefecture (Fig. 1A);

the exact site was the rocky seashore in front of the Ushimado Marine Laboratory. The Inland Sea is bounded to the south by Shikoku and is connected to the Pacific Ocean through straits at both sides of Shikoku. Thus, heavy waves do not roll ashore except when there are strong winds. The tidal amplitude varies between −15 cm (minimum level of low waters in the tide table published by the Japan Meteorological Agency) and 260 cm (maximum in high waters) during the year. The tidal pattern is semidiurnal, but morning low waters recede much further than afternoon low waters in winter, and the pattern is reversed in summer.

Male imagines fly or swarm immediately after eclosion. They are most abundant within a narrow area—a strip about 3–4 m wide along the water line of the rocky shore. Outside this narrow strip, the number of flies rapidly decreases. The emerged males scurry about on the rocks or stones while vigorously vibrating their wings or they skim rapidly over the water. When the male finds a female pupa, he strips off her pupal cuticle and copulates with her. The female (Fig. 1B) soon lays eggs on the rocky substrate. The females are always much less numerous than the males—less than 10% of the males emerging at the same time. In any event, when the tide starts to rise, the emerged adult midges all die.

We collected the adult males by sweeping the surface of the water with a nylon net (Fig. 1C). At the beginning of the emergence, the midges were seen only on the surface of the water, but around the time of low tide, large numbers of males were seen on the rocks as well as on the water surface. But it was hard to collect them on the rocks without some type of suction device, so the surface water was scooped up to capture the midges skimming over the water.

The sweeping was carried out on the rocks for 5 min every 30 min: the sampling range was 1–1.5 m along the water's edge (220–240 strokes per 5-min sampling period). Most emergence occurred within the 4–5 h surrounding the time of low water, and the water receded, at most, 50 cm during the period, *i.e.*, the time between the start and end of emergence. Therefore, we were not required to move the collection site frequently as the tide declined; we always swept only two rocks that differed by about 50 cm in height. The samples were quickly brought to the laboratory and transferred to a pail containing warm water (20–30°C). The midges rose to the surface of this water and were picked up with a forceps and counted.

We needed to determine whether the midges emerge and fly at the time of high tides as well as low. In the daytime, flying midges can be seen from the shore, but if only a few specimens were flying on the water surface, we might overlook them, especially at night. To eliminate this possibility, we used a light for some collections. Like other insects, marine midges are attracted to light at night. The light (180 W) was placed at the edge of a floating pier (5–6 m long), and the midges that swarmed around this spot were collected by sweeping only two strokes with the net. This method—collection under the light—was used only for the initial and preliminary observations, and the resulting data about emergence at high tide are only in Figure 4A. All other data were obtained by sweeping without lighting.

Investigations of the larval habitat

The habitat of the larvae with respect to the level of tides was examined. While the tide was ebbing, the algae growing on the rock were taken along with their associated sand or mud. These substrata (36 cm^2) were removed from various heights within the intertidal zone and transferred, in the laboratory, to a vessel containing seawater. When the vessel was shaken by hand, most larvae escaped from the nest tubes buried in the sand or mud. Each larva was picked up by forceps and counted. These samples were taken on 21 and 31 March 1991.

Identification of the species emerging

The taxonomic classification of the genus *Clunio* is not easy because definitive morphological differences are lacking. Hashimoto (1969) reported a sympatric species, *C. aquilonius*, that is extremely similar to *C. tsushimensis* and also occurs along the coasts of Japan. The two species can be distinguished on the basis of three morphological properties: antennal index, wing index, and body length. The antennal index is determined on the 11-segmented antennae of the male: *i.e.*, the ratio of the length of the ultimate segment (c) to the length of the 3rd to 10th segments (a + b) (Fig. 1D). The wing index is the ratio of the width (e) to the length (d) of the wing (Fig. 1D, and Hashimoto, 1968, 1969).

It was critical for us to determine whether both species are sympatric along the coasts of the Inland Sea, because different species might emerge during the day and night. Therefore, specimens were compared under a stereomicroscope, not only for the characters described by Hashimoto (1968, 1969), but also for their emergence during morning and afternoon low tides.

Results

Morphology of the Inland Sea population and larval habitat

To determine whether a single species of *Clunio* emerges during both the morning and evening low tides, we compared the antennal and wing indexes and the body length of specimens collected at those times. As shown in Figure 2A, the distribution of the antennal index (AI) was almost the same whether the specimens were collected at morning

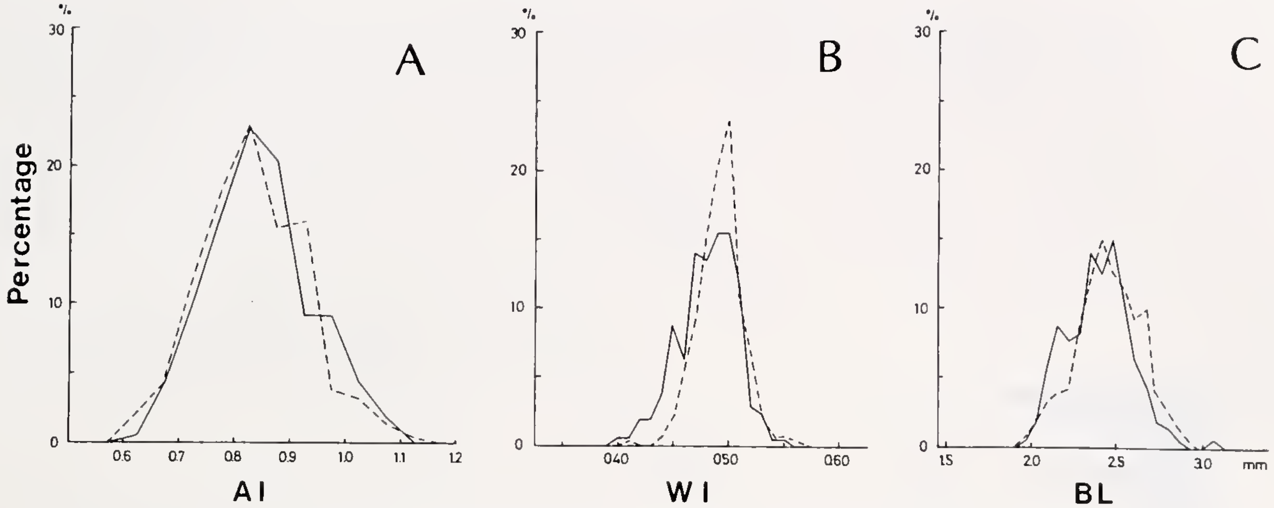

Figure 2. Comparison of the distribution of antennal index (AI), wing index (WI), and body length (BL) among the male *Clunio* population. Date of collection: 30 March 1991. Solid lines: specimens collected at the afternoon low water. Broken lines: those collected at the morning low water. Total number of the specimens measured: about 250 individuals at each tide.

low tides (mean 0.83) or afternoon low tides (mean 0.85). The wing index (WI) was also much the same (mean 0.49 and 0.48, respectively) among the two groups (Fig. 2B). Furthermore, as shown in Figure 2C, the mean body length (BL) was also much the same for specimens emerging in morning and afternoon (2.43 mm and 2.37 mm, respectively). The lack of a clear difference between the specimens collected at the morning and afternoon low waters suggests that the population of *Clunio* emerging in this location is a single species.

Figure 3 summarizes the distribution of the larvae with respect to the tidal height. The larvae of *Clunio* preferred the thin, feltlike substratum found in shallow hollows on the rocks; this substratum consisted of filiform green algae and sandy mud. The highest larval densities were recorded at 70–110 cm, and the fewest larvae were at the sites lower than 50 cm.

On this rocky shore (Fig. 1A), *Spaniotoma nemalione* (Subfamily Orthocladinae) was also abundant in March. Imagines of this species were easily distinguished from those of *Clunio:* their bodies were much slimmer, they had a different swarming site (*i.e.*, above oysters exposed to the air), and their way of flying was different. Although we could not specifically identify the larvae of this species, the difference in the swarming site would suggest that *Spaniotoma* larvae were not mixed in the substrata samples.

Tidal rhythm of emergence and its pattern in winter

To determine the relationship between the timing of emergence and the tidal cycles, collections were made through the night. As shown in Figure 4A, emergence did not occur at the time of high tide. Emergence and swarming started a few hours before the time of low tide and had ceased by 3–5 hours after. The pattern of emergence was clearly that of a tidal rhythm, and not that of a daily rhythm. Another feature of this emergence rhythm is the semilunar timing; *i.e.*, the fluctuation in the number of midges emerging every day is correlated with the lunar cycle. But the peaks of the semilunar rhythm did not accurately coincide with the days of full and new moons; in the data of Figure 4A, they occurred a few days before the full and new moons, respectively (see also Fig. 7b).

Figure 4B indicates the time of emergence from January to February. Emergence is clearly synchronized with the low tides. Moreover, the phase of the tidal rhythm is bimodal; i.e., the timing is clearly synchronized with *both* of the low tides that occur each day. A further aspect of this rhythm is a modulation of the tidal synchrony. As noticed from the data of the first 17 days (*i.e.*, 9–25 January), the midges emerging during the afternoon low tides are outnumbered by those emerging during the morning low tides. During the next 14 days (26 January–8 February), the number of midges emerging in synchrony with the morning low tides is about equivalent to the number emerging during the evening low tides. During the following 20 days in February (Figs. 4B and 5A), the midges emerging at the morning low tides are outnumbered by those emerging at the afternoon low tides.

The pattern of emergence in spring and summer

In March, the synchrony with the afternoon low waters is remarkable. As shown in Figure 5A, very few midges

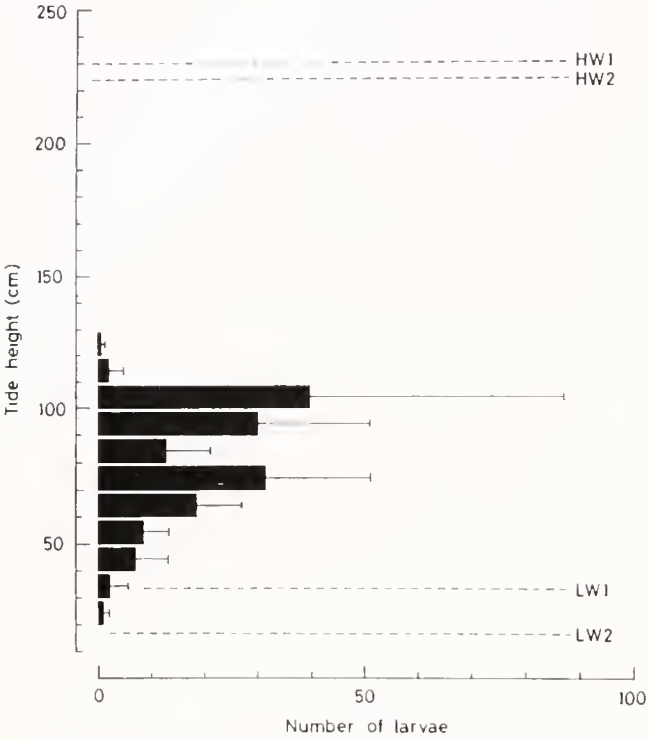

Figure 3. Relationship between the tidal height and the density of the larvae. Thick horizontal bars indicate the mean of the number of the larvae at each height; the error bars show the standard deviations; 74 samples were collected. *HW1, HW2* and *LW1, LW2* show the two high and low tides about the time of sampling, respectively. The height is based on the data in the tide table published by the Japan Meterological Agency.

emerged in synchrony with the morning low tides (see the morning on 13, 14, 16, 17, and 27–30 March); a great majority of the animals were collected during the afternoon low tides. Another feature is that the number of midges emerging in March and April increased drastically with respect to the population observed in January and February (compare the data of Fig. 7b and 7c).

After April, the timing in synchrony with the early morning low tides completely disappeared. Therefore, the tidal rhythm clearly shows a unimodal phase (Fig. 5A and 5B). Although field observations were not made frequently during the early morning low tides from May to September, it is clear that no midges emerged at these times; rather all midges emerged during the midday and afternoon low tides (Fig. 5B, 5C, and unpub. data). Comparison of the rhythmic patterns shown in Figure 5, A–D demonstrates that the time of emergence advances from spring to summer, with respect to the 24-h day-night cycle. In Figure 5A, emergence was observed around sunset; *i.e.*, 1600–2100 in early March, 1400–2000 around the new moon on 16 March, and 1300–1800 around the full moon on 30 March. In April and May (Fig. 5B), emergence occurs between noon and sunset. It advances a few hours further in June and July, when most midges appeared between 1000 and 1600 (Fig. 5C). In August and September, emergence occurs at midday (Fig. 5D). In every case, the daily timing of emergence is clearly synchronized with the times of low tides. If we were to assume a circadian rhythm underlying the *Clunio* emergence rhythm, then we would have to consider a drastic phase-advance of the rhythm from March to September. Such an assumption is not reasonable; these results must be interpreted in terms of an expression of the tidal rhythm corresponding to a phase-advance of the peak of the semilunar rhythm (see Fig. 7c–7f).

Alteration of synchrony in autumn

The unimodal tidal pattern was synchronized with the daytime low tides until September (Fig. 5, A–D). But in the latter half of October (Fig. 6A), the synchrony of timing was altered from daytime low tides to nighttime low tides. Most midges emerge in synchrony with the low tides at night in November (Fig. 6A) and December (Fig. 6B). Unlike the winter population (Fig. 4B), the autumnal emergence shows no clear bimodal phase (see also Fig. 9). A feature of the autumnal tidal rhythm is that the daytime emergence occurs only for the first several days of the fortnightly peak of emergence (*i.e.*, 17–22 October, 30 October–2 November, and 16–17 November in Fig. 6A; and 30 November–1 December, and 14–16 December in Fig. 6B).

Seasonal fluctuations in the number of midges emerging, semilunar timing, and a seasonal shift of the peak

Figure 7 summarizes the fluctuations in the number of flies emerging every day in relation to the lunar cycle. The number of collected midges is extremely small in January and February (Fig. 7b); but it suddenly increases thereafter. A large number of the midges were collected in March and early April (Fig. 7c). In late April and May (Fig. 7d), the number of emerging midges decreases. Not many midges emerge in June and July (Fig. 7e), and the number of midges is very small in August, September (Fig. 7f), and early October (Fig. 7g), reaching a maximum in November (Fig. 7h). The number of midges emerging every day thus fluctuates seasonally with two peaks: one in March–April, and another in November. Moreover, very few midges emerge in January–February and August–September.

Another feature of seasonal fluctuation is the semilunar periodicity. But the peak of this rhythmicity shifts several days in relation to the lunar cycle. In February and March (Fig. 7b, 7c), it occurs 2–4 days after the full and new moon; it just coincides with the days of full moon in April

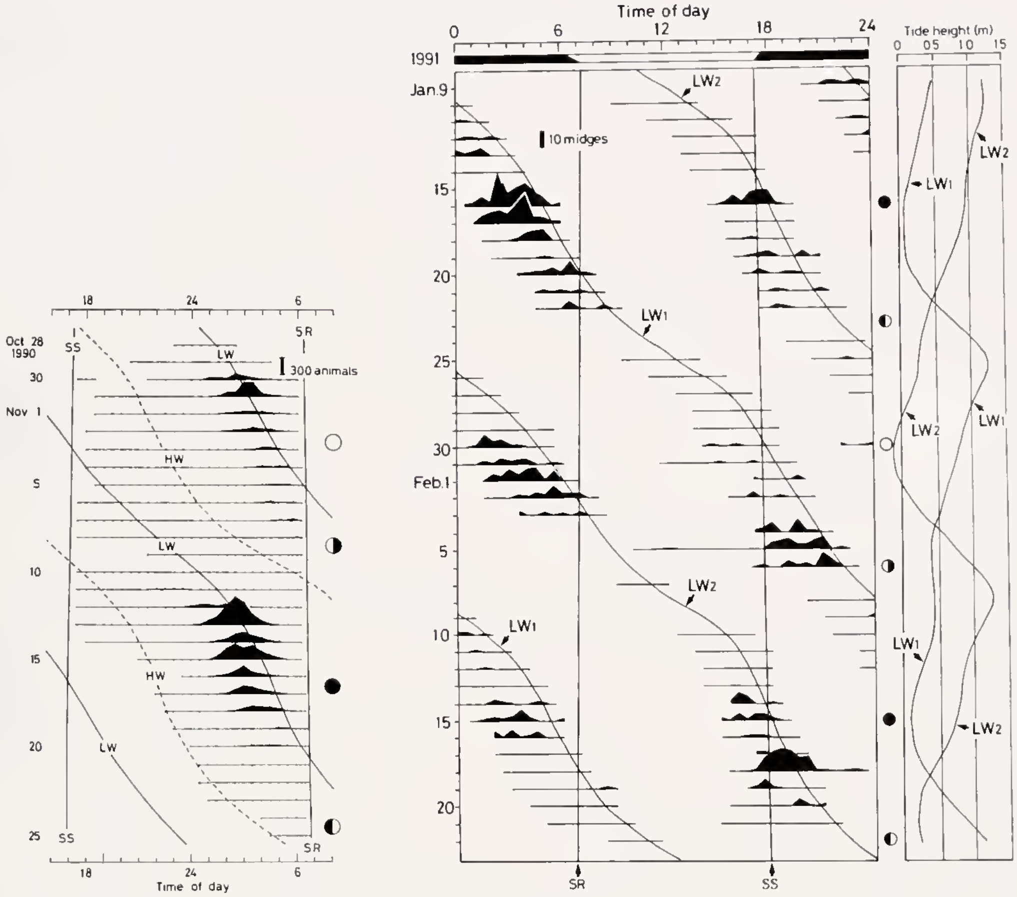

Figure 4. Daily timing of emergence of *Clunio tsushimensis* males in relation to day-night, tidal, and lunar cycles. (Left) The record from 28 October to 25 November 1990. Midges were collected using a light trap method. The number of midges is plotted vertically on the horizontal lines, which also show the 5-min period every 30 min (dot) during which sampling was done. Absence of the horizontal bars indicates no sampling. *SS* and *SR* represent the times of sunset and sunrise, respectively. *HW* and *LW* connect the respective times of high tides and low tides at the habitat. Open circle: full moon; black circle: new moon; semicircles: the first and last quarters of the moon. The vertical scale indicates 300 midges. (Right) Wide left panel: the pattern of emergence in midwinter (the record from 9 January to 22 February 1991). Midges were collected by sweeping for 5 min every 30 min. The number of midges is plotted vertically on the horizontal line during which the sampling was made. The vertical scale shows 10 midges. *LW1* and *LW2* connect the times of low tides at the habitat. Other symbols are as in Figure 4A. Narrow right panel: fluctuations in the height of the two low tides, *LW1* and *LW2*.

(Fig. 7c, 7d). The peak then advances from the days of full and new moon: in June and July (Fig. 7e), it appears 4 days before the syzygy, and from August to October (Fig. 7f, 7g), it advances near the half moon. The peak is again close to the full and new moon from November to December (Fig. 7h).

To examine the relationship between the shift of the semilunar peak and the temperature of the habitat, each peak of the semilunar rhythm was plotted in relation to the seasonal fluctuation of water temperature. As shown in Figure 8, the peak (*i.e.*, the mean of the distribution of emerging midges in each semilunar cycle) is represented by the days shifted from each full and new moon. The water temperature is expressed by the average values of 15 days at each month. The shift of the peak from the days of full and new moon clearly coincides with the fluctuations of water temperature in the habitat, suggesting that the phase of the semilunar rhythm is influenced by the temperature.

Discussion

The emergence of *Clunio tsushimensis* imagines has a clear tidal rhythm. Moreover, the pattern of synchrony changed with season. A bimodal phase appeared in midwinter; but the synchrony shifted gradually, during Jan-

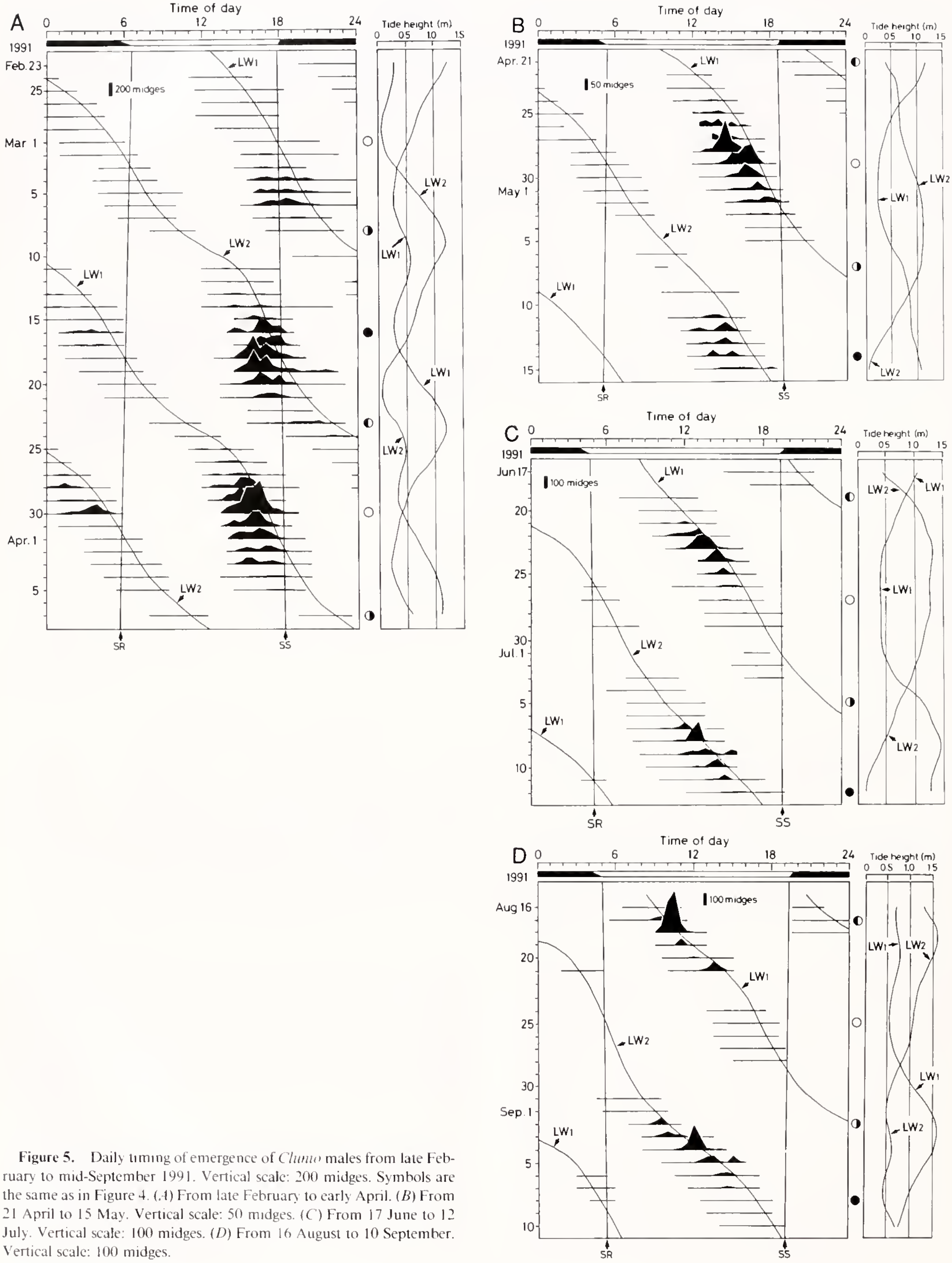

Figure 5. Daily timing of emergence of *Clunio* males from late February to mid-September 1991. Vertical scale: 200 midges. Symbols are the same as in Figure 4. (*A*) From late February to early April. (*B*) From 21 April to 15 May. Vertical scale: 50 midges. (*C*) From 17 June to 12 July. Vertical scale: 100 midges. (*D*) From 16 August to 10 September. Vertical scale: 100 midges.

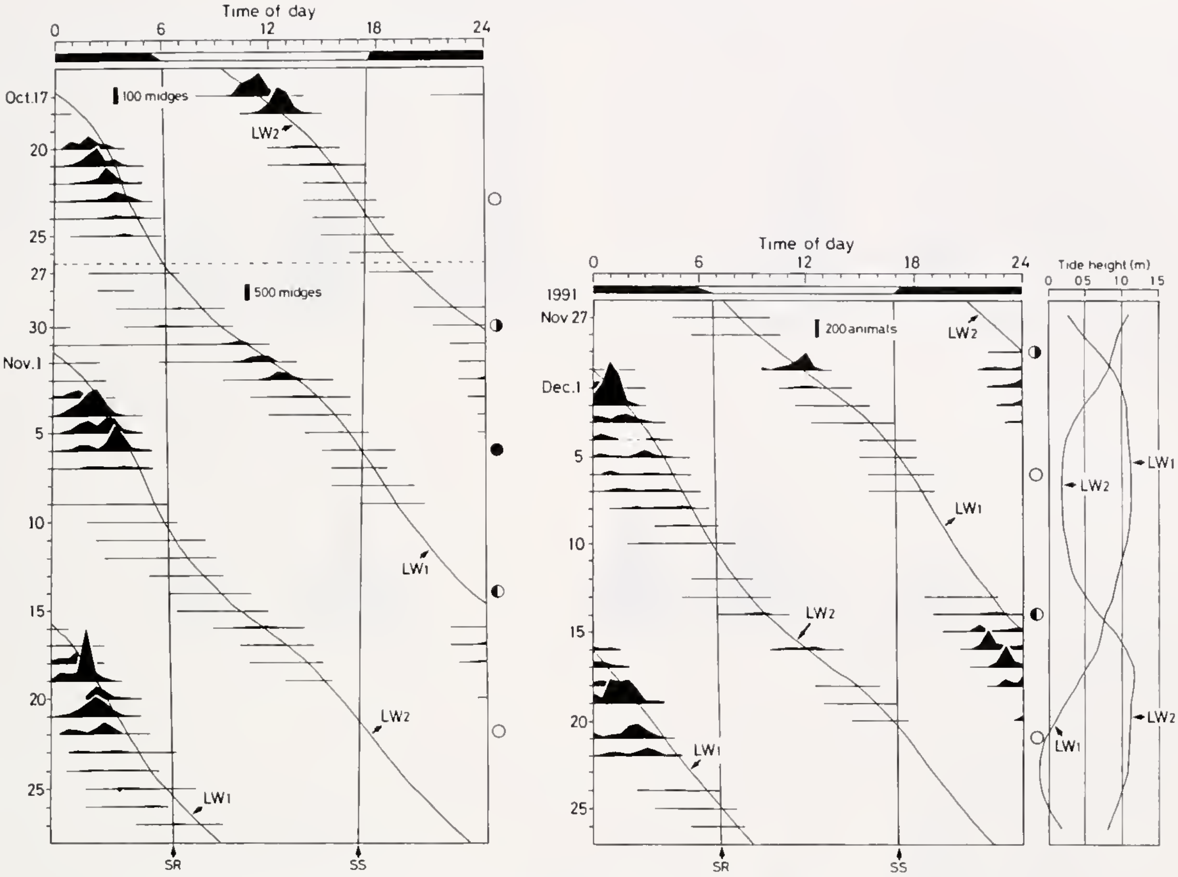

Figure 6. Daily timing of emergence of *Clunio* males from mid-October to the end of December 1991. Symbols are the same as in Figure 4. (Left) In autumn (17 October–27 November). The number of emerged midges drastically increased from October to November (compare Fig. 7g and 7h), so the figure was separated into two panels (horizontal dashed lines) with different vertical scales. The data on emergence in this period are shown in duplicate in Figure 9, with the fluctuations of the two low tides (*LW1* and *LW2*). (Right) From 27 November to 26 December. Vertical scale: 200 midges.

uary and February, from morning low tides to afternoon low tides, and a unimodal tidal rhythm in synchrony with afternoon low tides appeared in March. This pattern lasted until early October. In mid-October, the synchrony shifted to the morning low tides. As a result, emergence was observed during the day from spring to autumn, at night in early winter, and in both daytime and nighttime in midwinter. Therefore, we must ask a question about the modulation of the expression of that rhythm: What are the factors that induce the expression of the bimodal pattern and that cause one of the two low tides to synchronize the timing?

Relations between the tidal patterns and the phase expression of the tidal rhythm

On most Japanese seacoasts fronting the Pacific Ocean, there are two high and two low tides per day, at mean intervals of 12.4 h; the amplitude of these tides changes with a fortnightly periodicity, resulting in spring and neap tides. But the amplitude of these tides on a given day varies with season. For example, on 16 January (new moon; see Fig. 4B), a *low* low tide (+0.09 m) occurs at 0500. A *high* high tide (+2.3 m) is followed after 7 h by this low tide, which is then followed after 6 h by a *high* low tide (+0.9 m), and further followed after 5 h by a *low* high tide (+1.9 m). The height of the two low tides becomes similar 6 days after the new moon. Thus, from late autumn to winter, a *low* low tide always occurs in the morning, and a *high* low tide always occurs in the afternoon (Figs. 4B, 6B, and 9). In contrast, as shown in Figure 5, B–D, a *low* low tide always occurs in the afternoon, and a *high* low tide occurs in the morning during spring and summer.

A similar complex tidal regime is seen on the Pacific coast of North America. Enright (1963, 1972) recorded the swimming activity of several kinds of crustaceans that were freshly collected from the sandy beach of Cali-

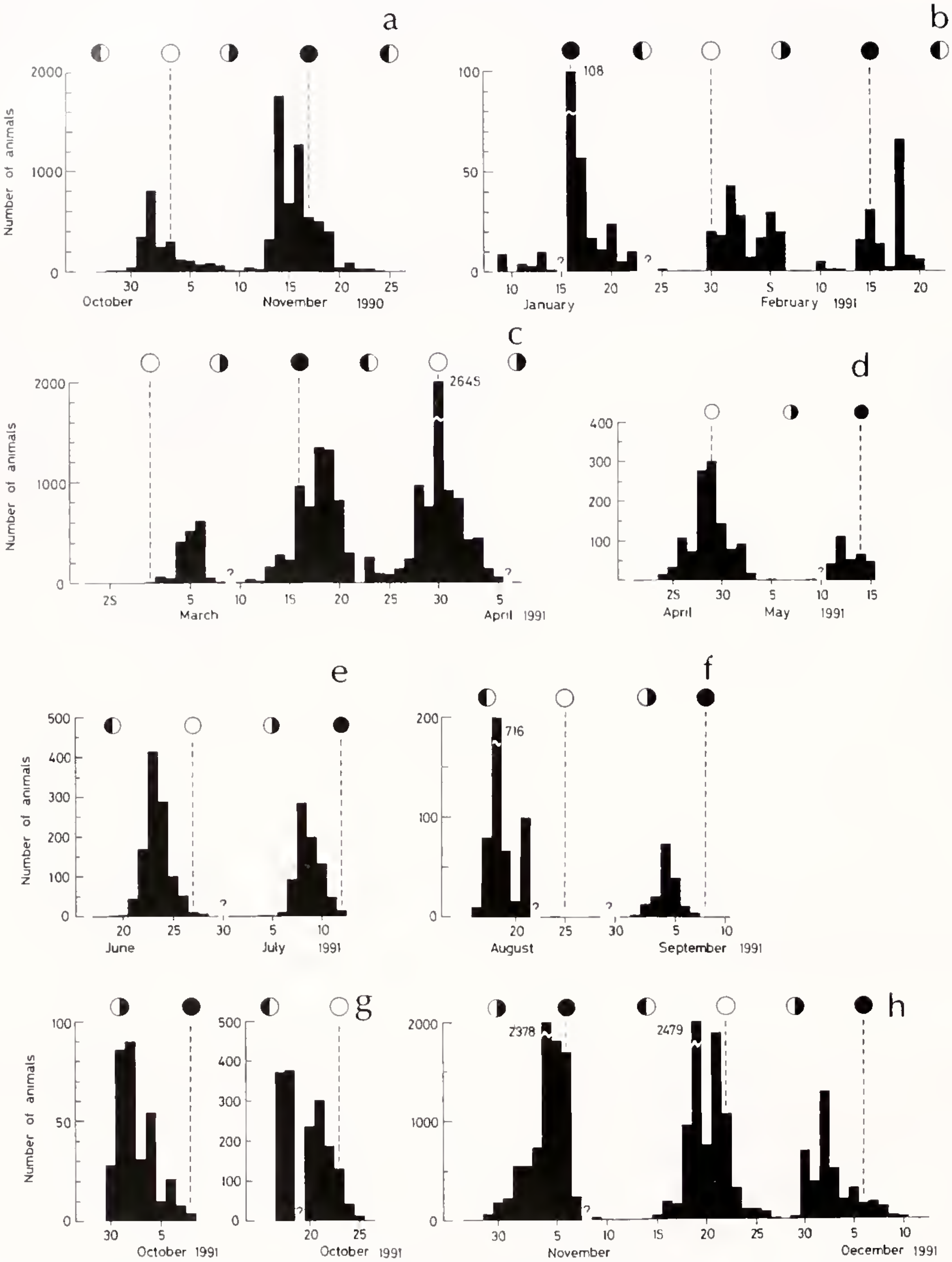

Figure 7. Semilunar rhythm of emergence of *Clunio tsushimensis* males, and the seasonal fluctuation of the number emerging every day. The vertical black bars indicate the number collected per day in relation to lunar cycles. Open circles: full moon; dark circles: new moon; semicircles: the first and last quarters of the moon. Question marks on the horizontal axis indicate days when the sampling was not made.

fornia. The activity rhythm of the amphipod *Synchelidium* sp. was progressively damped as the animal's time in the laboratory was prolonged, but it was well defined for the first few days after collection. Another feature of the activity pattern is that the relative amplitude of its peaks reflects the amplitude of the tides occurring at the nearby seacoast (Enright, 1963). Similar activity rhythms were also recorded from the isopod *Excirolana chiltoni* (Enright, 1972). This animal showed a persistent tidal rhythm for 2 months under the constant conditions in the laboratory. The temporal variation in activity seems to parallel predicted changes in the height of high tide.

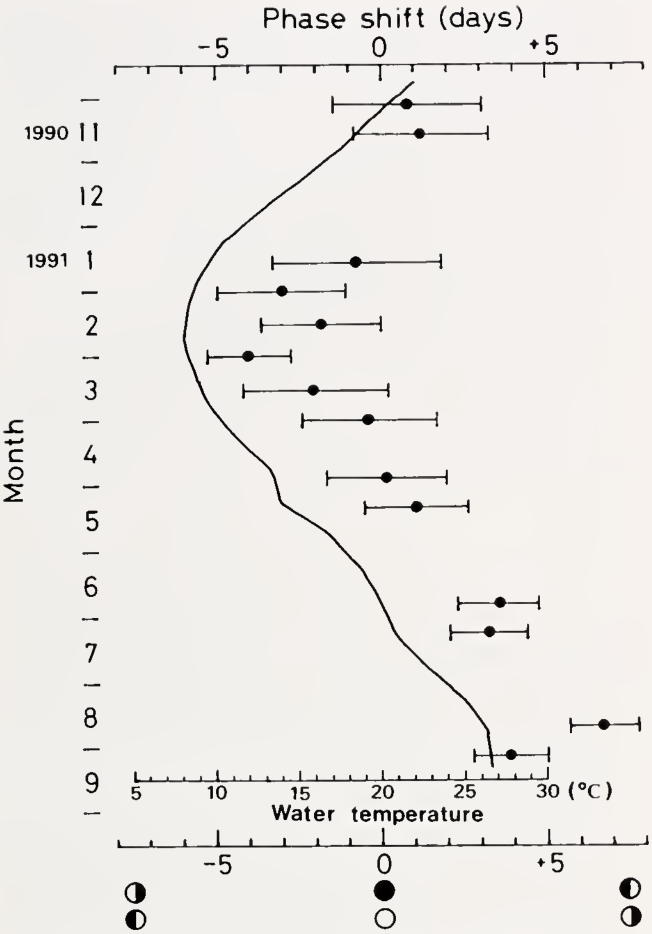

Figure 8. The relationship between the phase of the semilunar rhythm and the seasonal change of the mean water temperature at the habitat (solid curve). Each peak (black circles) of the semilunar rhythm is indicated as the days of shift from full or new moon (*i.e.*, 'zero' on the horizontal axis). The error bars indicate a standard deviation within each peak of the semilunar rhythm. The peaks on the right of 'zero' show a phase-advance of the semilunar rhythm with respect to the syzygy, and those on the left of 'zero' show a phase-delay from the syzygy.

To examine whether the tidal synchrony of the rhythm of emergence of *C. tsushimensis* could be altered by irregularities in the amplitude of the semidiurnal tides in the habitat, the water level of low tides was plotted against the time of emergence. Through the autumn, as shown in Figure 9, the relative heights of the two low tides—*i.e.*, the *low* low tide and *high* low tide—vary continuously, but cyclically, with an interval of 2 weeks. When the two tides were different in amplitude, emergence clearly coincided with *low* low tides alone, which produced the unimodal phase of the tidal rhythm. A bimodal phase appeared for only a few days every fortnight when the heights of the low tides were close to equal.

Similar relations are also seen in December, when emergence occurred in synchrony with the *low* low tides (*i.e.*, the nighttime low tides), causing a unimodal phase except a few days around the half moon (Fig. 6B). The tidal pattern in January (Fig. 4B) somewhat changes from that of October–December (Figs. 6B and 9): while the height of the *high* low tide exceeds 1 m on many days in December (Fig. 6B), it is less than 1 m on most days in January (Fig. 4B). Therefore, in January, the main part of the larval habitat (see Fig. 3) is exposed to the air two times per day, except a few days after the half moon. The decrease in height of the *high* low tide might influence the larval habitat, which might have evoked an emergence, resulting in bimodal phases during a relatively long period in January and February.

The correlation between the relative difference in the tidal heights and phase modality was noticed no later than the first 10 days of March; thereafter it was lost. In March, for example, the height of both low tides is close to equal around the full and new moons, yet far more midges emerged in the afternoon than in the morning (Fig. 5A). This result cannot be accounted for by a simple synchrony with *low* low tide, or by the exposure of the larval habitat to the air at low tides. Day-night cycles must participate in the selection of the afternoon low tides. Thus, the synchrony of emergence with the two low tides per day is correlated, not only with the relative difference in the heights of the tides, but possibly also with the day-night cycle.

In May, the timing of emergence is again synchronized with the lowest of two different low tides, and a unimodal phase appears in the daytime (Fig. 5B). During June and September (Fig. 5C and 5D), neither of the two low tides ebbs less than those of spring. In each case the timing of emergence is synchronized with the *low* low tides, and a unimodal tidal rhythm appears. Since the *low* low tides occur in the daytime from the end of April to September, the unimodal phase also appears in the daytime.

The relationship between the *low* low tides and the 24-h day-night cycle is reversed in autumn. As shown in Figure 9, the *low* low tides appear in the morning. Emergence is synchronized with the *low* low water, and shows a unimodal tidal rhythm. As a result, the phase of this tidal rhythm appears in the morning. Moreover, the *high* low tides occur in the afternoon, and do not ebb lower than 0.8–0.9 m. If the larval habitat is not moved in height from that of March (Fig. 3), there are only a few days every 2 weeks when the habitat is exposed to the air at each low tide (*i.e.*, twice a day). This might have resulted in a brief bimodal phase in autumn and early winter (Fig. 6A and 6B).

Zeitgeber *of* Clunio *tidal and semilunar rhythm*

Few cyclical environmental factors are known to be *zeitgebers* of tidal rhythms. One such is the cycle of water

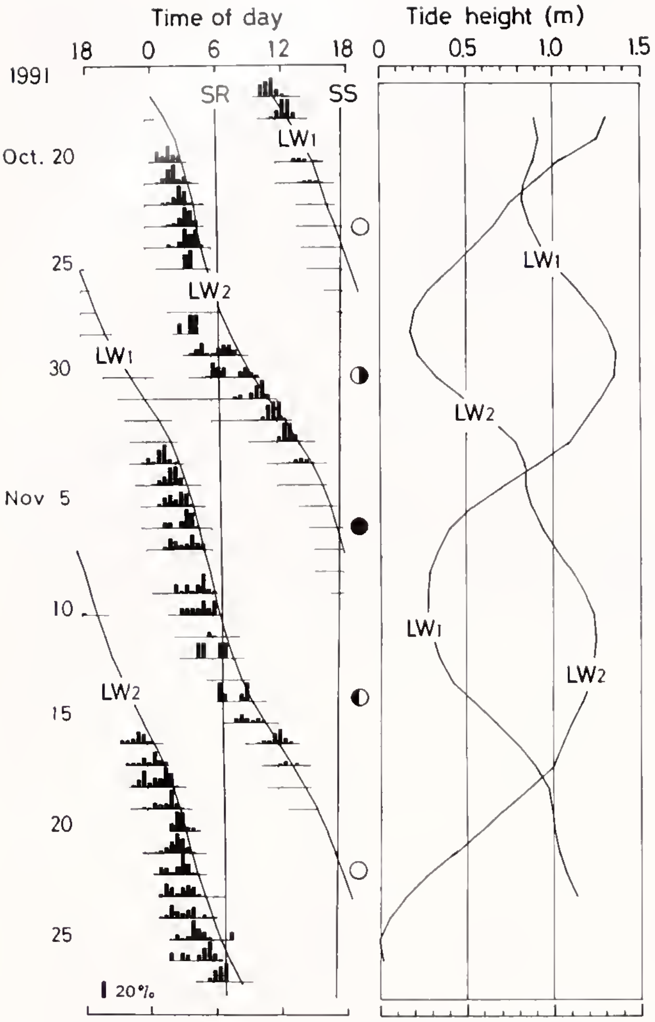

Figure 9. The relationship between the daily timing of emergence and the heights, on the same day, of two low tides (*LW1* and *LW2*). The data on emergence are the same as in Figure 6A. To make that relationship much clearer than in Figure 6A, the numbers of emerged midges are shown as a percentage of the total number collected per day. The vertical bar shows the scale of 20%. The right panel shows the fluctuation of the heights of the two low tides (*LW1* and *LW2*).

turbulence (Enright, 1965). Cyclical or noncyclical changes in hydrostatic pressure also cause behavioral responses in amphipods (Enright, 1962; Morgan, 1965). Hydrostatic pressure fluctuations do not entrain an 'endogenous' rhythm, but since they coincide with the tidal cycles in the field, they could be the *zeitgeber* of the tidal rhythm. But, at least for the swimming activity of intertidal isopods, the 24-h day-night cycle does not seem to be a *zeitgeber* of tidal rhythms (Enright, 1963).

In *Clunio* emergence rhythm, Neumann (1966, 1976) showed that the semilunar timing is entrained by the artificial moonlight given in the laboratory for 3-4 nights every 30 days. According to Neumann's hypothesis (Neumann, 1976, 1985, 1987), daily timing of emergence is controlled by a circadian clock that is entrained by a 24-h day-night cycle only. But the phase of the tidal cycle differs according to the habitat of animals (*e.g.*, see Fig. 9 in Saigusa, 1988). Neumann's hypothesis cannot explain why the phase of the daily emergence rhythm coincides with the time of low tide in each larval habitat. Moreover, as indicated by this study, the phase of the daily emergence cycle was largely shifted through the year, with respect to the 24-h day-night cycle. Such a large phase-shift could be explained in terms of the tidal rhythm.

In crab larval release activity (Saigusa, 1986), the 24-h day-night cycle causes the phase shift of the tidal rhythm with a unimodal phase. Similarly, as shown in other species (Saigusa, 1992), this factor also causes the phase shift of the bimodal tidal rhythm. Thus, it is clear that the 24-h day-night cycle can be one of the *zeitgebers* of circatidal rhythms.

But it would be impossible that the tidal rhythms are entrained by the 24-h day-night cycle alone; other factors correlated with the tidal cycle, such as water turbulence, must be considered. Moreover, moonlight cycles in parallel with the tidal cycle could be the candidate, although the phase angles of these two environmental cycles differ according to geographical conditions. Cycles of artificial moonlight do entrain the tidal rhythm of larval release in an estuarine terrestrial crab; and the phase relations between the evoked tidal rhythm and the artificial moonlight cycle correspond to the phase relations between the time of high tide and the moonlight cycle in the habitat of a local population (Saigusa, 1988).

As this study indicates, the timing of emergence is synchronized with the time of low tides and shows a tidal rhythm through the year. So we can speculate that among the possible *zeitgebers* of the *Clunio* tidal rhythm is the ebb-flow cycle of the tides, the moonlight cycle, or both. In addition, as suggested from the experiments with *Clunio* (Neumann, 1966, 1976) and crabs (Saigusa, 1986, 1992), the 24-h day-night cycle could also be the *zeitgeber* of the *Clunio tsushimensis* tidal rhythm. Furthermore, while the day-night cycle entrains the tidal rhythm in every season, it would be involved in the expression of a unimodal phase (see Fig. 5A).

A problem in understanding tidal rhythms having a semilunar component

Enright (1972) reported endogenous swimming activity rhythm of *Excirolana chiltoni* inhabiting the sandy beaches of the Pacific coast of North America. The tidal regime in this habitat includes semidiurnal inequality in amplitude. The tidal scheme recurs at double-tidal intervals (*i.e.*, 24.8 h), which further changes at intervals of 2 weeks. *E. chiltoni* shows a persistent circatidal rhythm with a lunar component under constant conditions in the laboratory; even under such conditions, activity reflects different heights of the tides (see Fig. 1 in Enright, 1972). Nevertheless, if the activity were plotted on a 24-h time scale, the rhythm would appear to be circadian.

Similar phenomena occur in *Clunio tsushimensis*, as we have reported here. The tidal rhythm of this animal showed a unimodal phase except in January and February. Furthermore, this tidal rhythm features a semilunar timing, with emergence occurring for several days near the times of the full and new moon (Fig. 7). From March to September, emergence is synchronized with the afternoon low tides (Fig. 5A–5D). If the data for these periods are plotted against the time of emergence, a daily rhythm with a peak at the afternoon appears (*e.g.*, Fig. 10A). On the other hand, from November to December, emergence occurs at the time of morning low tides (Fig. 6A and 6B). Now if the timing is plotted, a daily rhythm appears with a peak in the morning (Fig. 10B).

The emergence of *Clunio* is concentrated around the times of the full and new moon. So, if the data were arranged as shown in Figure 10, we could not readily determine whether the rhythm that underlies the daily and semilunar cycle of emergence is tidally correlated or day-night correlated. Yet, as stated repeatedly, the daily timing of emergence is not explicable in terms of a circadian rhythm or a modified circadian rhythm. It would be a tidally correlated rhythm that underlies the expression of a semilunar rhythm. Moreover, this rhythm is surely entrained by a 24-h, day-night cycle. Nevertheless, there is no evidence that the two internal rhythmic systems—circadian and circatidal rhythms—couple or interact together, resulting in a semilunar rhythm (Saigusa, 1986, 1988, 1992). These problems bear on the timing mechanism of tidal and semilunar rhythms and require further consideration.

A local population of Clunio tsushimensis

The systematics of the genus *Clunio* is not yet settled because distinctive morphological features characteristic of the various geographical strains are lacking. Within *C. marinus*, which is widely distributed on the European coast of the Atlantic Ocean, five races were distinguished on the basis of the larval habitat and the timing of emergence (Neumann, 1976). Among these local races, the Baltic Sea population was somewhat different from other Atlantic populations: it inhabits the sublittoral zone and tolerates salinities as low as 4–6 ppt in some areas (Palmén and Lindeberg, 1959; Olander and Palmén, 1968). The differences in larval habitat and time of emergence tend to isolate these populations, even at the site where both are simultaneously distributed, so they might be divisible into two species (*e.g.*, see Heimbach, 1978).

Distributions of the antennal index, wing index, and body length (Fig. 2) all showed a single peak, and there was no difference between the population collected at the morning low tides and that collected at the afternoon low tides. This suggests that the midge *Clunio* inhabiting the seacoast of the Inland Sea is a single species. But which species? To determine whether the collected specimens are *C. tsushimensis* or *C. aquilonius*, the data in Figure 2 were compared with those obtained by Hashimoto (1968, 1969) in the Izu Peninsula, Shizuoka Prefecture. The antennal index (AI) of the individuals collected in March (Fig. 2A) was between 0.60 and 1.12, and the mean

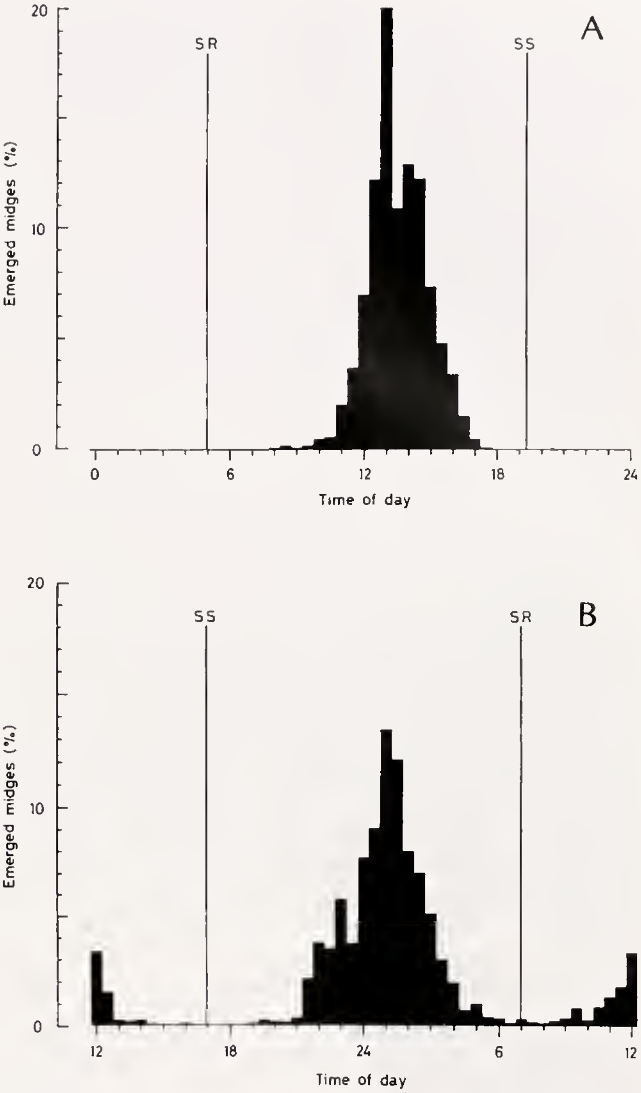

Figure 10. A pseudo-daily rhythm. (*A*) The time of emergence recorded from 17 June to 2 July 1991. (*B*) The time of emergence recorded from 28 November to 26 December 1991. The vertical axis shows the percentage of the midges collected. *SR* and *SS* indicate the times of sunrise and sunset, respectively. These times shift only a few minutes in June, and at most 15 min in December. In this figure, *SR* and *SS* show the times of sunrise and sunset on 17 June (A) and 28 November (B), respectively. See text for details.

was 0.84, intermediate between the Izu populations of *C. tsushimensis* (mean 1.12) and *C. aquilonius* (mean 0.62) collected in the same month. Moreover, the wing index (WI) of the Inland Sea species (Fig. 2B) ranged from 0.40 to 0.56, about the same as the mean for both *C. tsushimensis* and *C. aquilonius* at the Izu Peninsula. The body length (Fig. 2C) was between 2.00 and 3.10 mm (mean 2.40 mm), much larger than for *C. tsushimensis* from Izu collected during the same month (1.4–2.4 mm; mean about 1.8 mm). In summary, none of these indices could provide a positive identification of either *C. tsushimensis* or *C. aquilonius* at our observation site.

In the marine midges studied by Hashimoto (1969, 1976), the AI fluctuates with the season, with a minimum in early spring, a maximum in late summer, and no overlap between *C. tsushimensis* and *C. aquilonius* in any season; that is, whereas the AI (mean) of *C. aquilonius* varied from 0.6 in winter to 0.75 in summer, that (mean) of *C. tsushimensis* varied from 1.05 in winter to 1.4 in summer (see Fig. 7 in Hashimoto, 1969). The body length was also closely correlated with the annual change of water temperature (Hashimoto, 1976). Now, the atmospheric and water temperatures on the coast of the Inland Sea are 5–6°C lower in winter and spring than those on the Izu Peninsula. We therefore speculate that the decreased AI and increased body length are due to the temperature differential between the two larval habitats. Hence, we conclude that the species reported here is a local population of *C. tsushimensis*, and not a new species.

Acknowledgments

We thank Prof. Masamichi Yamamoto, Director of Ushimado Marine Laboratory, who gave us every facility for the present work.

Literature Cited

Akiyama, T., and M. Yoshida. 1990. The nocturnal emergence activity rhythm in the cumacean *Dimorphostylis asiatica* (Crustacea). *Biol. Bull.* **179:** 178–182.

Caspers, H. 1951. Rhythmische Erscheinungen in der Fortpflanzung von *Clunio marinus* (Dipt. Chiron.) und das Problem der lunaren Periodizität bei Organismen. *Archiv. Hydrobiol. Suppl.* **18:** 415–594 (plus 4 photograph pages).

DeCoursey, P. J. 1983. Biological timing. Pp. 107–162 in *The Biology of Crustacea VII. Behavior and Ecology*, F. J. Vernberg and W. B. Vernberg, eds. Academic Press, Washington.

Enright, J. T. 1962. Pressure sensitivity of an amphipod. *Science* **133:** 758–760.

Enright, J. T. 1963. The tidal rhythm of activity of a sand-beach amphipod. *Zeit. Vergl. Physiol.* **46:** 276–313.

Enright, J. T. 1965. Entrainment of a tidal rhythm. *Science* **147:** 864–867.

Enright, J. T. 1972. A virtuoso isopod: circa-lunar rhythms and their tidal fine structure. *J. Comp. Physiol.* **77:** 141–162.

Hashimoto, H. 1968. Seasonal variation in the marine chironomid, *Clunio tsushimensis* Tokunaga (Diptera). *Ann. Zool. Fenn.* **5:** 41–48.

Hashimoto, H. 1969. Affinity and differentiation of species in the marine chironomids, *Clunio aquilonius* and *C. tsushimensis* (Diptera). *Jpn. J. Zool.* **16:** 19–45.

Hashimoto, H. 1976. Non-biting midges of marine habitats (Diptera: Chironomidae). Pp. 377–414 in *Marine Insects*, L. Cheng, ed. North-Holland Publishing Company, Amsterdam.

Hauenschild, C. 1960. Lunar periodicity. Pp. 491–497 in *Biological Clocks. Cold Spring Harbor Symposia on Quantitative Biology*, Vol. 25.

Heimbach, F. 1978. Sympatric species, *Clunio marinus* Hal. and *C. balticus* n. sp. (Dipt., Chironomidae), isolated by differences in diel emergence time. *Oecologia* **32:** 195–202.

Korringa, P. 1947. Relations between the moon and periodicity in the breeding of marine animals. *Ecol. Monogr.* **17:** 349–381.

Koskinen, R. 1968. Seasonal emergence of *Clunio marinus* Haliday (Dipt., Chironomidae) in western Norway. *Ann. Zool. Fenn.* **5:** 71–75.

Morgan, E. 1965. The activity rhythm of the amphipod *Corophium volutator* (Pallas) and its possible relationship to changes in hydrostatic pressure associated with the tides. *J. Anim. Ecol.* **34:** 731–746.

Neumann, D. 1966. Die lunare und tägliche Schlüpfperiodik der Mücke *Clunio*. Steuerung und Abstimmung auf de Gezeitenperiodik. *Zeit. Vergl. Physiol.* **53:** 1–61.

Neumann, D. 1976. Adaptation of chironomids to intertidal environments. *Annu. Rev. Entomol.* **21:** 387–414.

Neumann, D. 1985. Circadian range of entrainment in the semilunar eclosion rhythm of the marine insect *Clunio marinus*. *J. Insect Physiol.* **31:** 549–557.

Neumann, D. 1987. Tidal and lunar rhythmic adaptations of reproductive activities in invertebrate species. Pp. 152–170 in *Comparative Physiology of Environmental Adaptation: Tide, Moon, Magnetic Field and Rhythmic Functions, Vol. 3*, P. Pevet, ed., S. Karger, Basel.

Oka, H., and H. Hashimoto. 1959. Lunare Periodizität in der Fortpflanzung einer pazifischen Art von *Clunio* (Diptera, Chironomidae). *Biol. Zentralblatt* **78:** 545–559.

Olander, R., and E. Palmén. 1968. Taxonomy, ecology and behaviour of the northern Baltic *Clunio marinus* Halid. (Dipt., Chironomidae). *Ann. Zool. Fenn.* **5:** 97–110.

Palmén, E., and B. Lindeberg. 1959. The marine midge, *Clunio marinus* Hal. (Dipt., Chironomidae), found in brackish water in the northern Baltic. *Int. Rev. Gesam. Hydrobiol. Hydrogr.* **44:** 384–394.

Pearse, J. S. 1990. Lunar reproductive rhythms in marine invertebrates: maximizing fertilization? Pp. 311–316 in *Advances in Invertebrate Reproduction 5*, M. Hoshi and O. Yamashita, eds. Elsevier Science Publishers B.V., London.

Saigusa, M. 1985. Tidal timing of larval release activity in non-tidal environment. *Jpn. J. Ecol.* **35:** 243–251.

Saigusa, M. 1986. The circa-tidal rhythm of larval release in the incubating crab *Sesarma*. *J. Comp. Physiol. A* **159:** 21–31.

Saigusa, M. 1988. Entrainment of tidal and semilunar rhythms by artificial moonlight cycles. *Biol. Bull.* **174:** 126–138.

Saigusa, M. 1992. Phase shift of a tidal rhythm by light-dark cycles in the semi-terrestrial crab *Sesarma pictum*. *Biol. Bull.* **182:** 257–264.

Reference: *Biol. Bull.* **188:** 179–185. (April, 1995)

The Role of the Cardioregulatory Nerves in Mediating Heart Rate Responses to Locomotion, Reduced Stroke Volume, and Neurohormones in *Homarus americanus*

M. S. GUIRGUIS AND J. L. WILKENS*

Department of Biological Sciences, University of Calgary, Calgary, Alberta, Canada T2N 1N4

Abstract. Control of decapod crustacean heart activity is believed to be dependent on the regulation of the cardiac ganglion by external input from the central nervous system as well as by circulating neurohormones. This study investigated the roles of these inputs on the heart rates of lobsters exercising on a treadmill. Heart rate increased rapidly at the onset of walking in control animals. This rapid phase was lost after the regulatory nerves were cut, but small increases still occurred. When stroke volume was reduced by cutting alary ligaments, the animals compensated by increasing heart rate; this compensation was lost when the regulatory nerves were cut. In resting animals, injection of serotonin, octopamine, and dopamine induced increases in heart rate. After the regulatory nerves were cut, only dopamine and serotonin injections caused increases in heart rate, suggesting that these amines act on the cardiac ganglion as independent effectors.

Introduction

The neurogenic decapod crustacean heart consists of a single ventricle suspended in the pericardial sinus by an array of alary ligaments. The energy stored as these ligaments are stretched during systole is recovered to re-expand the heart during diastole. The heart fills by means of valved ostia and supplies hemolymph to seven arteries. There is no direct venous supply to the heart.

The basic contraction rhythm of the heart arises from the bursting discharges of the nine-cell cardiac ganglion located on the inner dorsal wall of the heart (Alexandrowicz, 1932). The cardiac ganglion receives extrinsic nerve fibers *via* the paired dorsal nerves that arise from the central nervous system (Alexandrowicz, 1932). Each dorsal nerve contains two accelerator axons and one inhibitory axon. In isolated hearts, stimulation of the accelerator nerves speeds the contraction rate, and stimulation of the inhibitory nerves slows or stops the heart (Maynard, 1953; Florey, 1960; Wilkens and Walker, 1992). *En passant* recordings from the dorsal nerves in semi-intact animals reveal periodic increases in inhibitory nerve firing rates; these increases cause bradycardia (Field and Larimer, 1975; Young, 1978). The role of this autonomic-like control system in regulating heart rate responses in intact animals has not been studied.

Heart rate (f_H) is also modified by all of the neurohormones that have been identified in the pericardial organs (see reviews by Wilkens, 1987; Wilkens and McMahon, 1992). Each of the aminergic neurohormones, dopamine (DA), octopamine (OA) and serotonin (5-HT), trigger tachycardia in isolated hearts (Cooke, 1966; Florey and Rathmayer, 1978; Grega and Sherman, 1975) and in intact animals (Wilkens *et al.*, 1985). In intact animals the possibility cannot be discounted that the neurohormones act indirectly *via* the nervous system as well as directly (Berlind *et al.*, 1970). The experiments reported here were designed to test the hypothesis that f_H in intact lobsters is under continuous modulatory control by cardioregulatory nerves and pericardial aminergic neurohormones.

Materials and Methods

Source and holding condition of lobsters

Homarus americanus of 490–670 g mass were obtained from a commercial supplier and maintained in flowing artificial seawater at 12°C. No differences in performance were observed between males and females.

Received 2 September 1994; accepted 8 December 1994.

* To whom correspondence should be addressed.

Abbreviations: f_H, heart rate; DA, dopamine; OA, octopamine; 5-HT, 5-hydroxytryptamine.

f_H measurement and surgical procedures

Heart beat was measured by electrodes implanted next to the heart in the pericardial sinus. Wires were inserted through holes drilled in the carapace and cemented in place. Signals were amplified (Grass P15 amplifier) and digitized by a Mac Lab/8 and visualized on the Macintosh SE/30 computer running CHART/8 software. In some cases data were also displayed on a Gould RS200 chart recorder.

For surgical interventions, animals were first packed in crushed ice for about 30 min to effect cold "anesthesia." Next, the carapace and hypodermis over the heart were removed. A dam molded from dental impression wax was placed around the opening to prevent hemolymph from spilling over into the bath. The wax was secured to the carapace with cyanoacrylate adhesive. With the heart so exposed, the two dorsal anterior alary ligaments, the dorsal nerves, or both could be cut. The dorsal nerves approach the heart along the dorsal surface of the posterior dorsal alary ligaments and traverse the posterior half of the ventricle in the connective tissue covering the heart before penetrating to the cardiac ganglion. Superficial cuts through the connective tissue over the heart severed these nerves without impairing the alary ligaments. After surgery, the square of carapace was replaced and sealed with melted dental wax and cyanoacrylate adhesive. Sham operations consisted of removing the square of carapace and opening the hypodermis only. Following the return of animals to seawater, f_H usually returned to preoperation rest levels in 2 h; however, tests were not run until the next day.

Induced locomotion

To measure cardiac responses to exercise, lobsters were trained to walk on an underwater treadmill. The treadmill consisted of a cloth-backed sanding belt passed around a motor driven and a tensioning drum. The treadmill chamber was submerged in aerated seawater siphoned from the holding tank and was maintained at 13°–14°C. Some lobsters walked readily from the outset, but others required several training runs before they would exhibit continuous walking. Touching the telson and uropods with a test tube brush was usually an adequate stimulus to induce walking. The treadmill belt traveled at 1.7 $\text{m} \cdot \text{min}^{-1}$. All observations in this study were carried out in the treadmill chamber. The walls of the chamber were covered with black plastic to isolate the animal from visual stimuli.

Administration of neurohormones

Saline or neurohormones—dopamine (DA), octopamine (OA), and serotonin (5-HT) (Sigma Chemical Co.)—dissolved in lobster saline (Cole, 1941) were injected into the lateral pericardial sinus of resting animals. A syringe pump was used to deliver the injection over a period of 1 min. An Intermedic polyethylene tube (P.E. 160) ran from the syringe to a needle that was inserted into the sinus through a hole that had been drilled into the carapace and covered with dental dam. The injection volume was adjusted to the weight of the animal so that no more than 240 μl would produce a circulating concentration of 1 μM, assuming a 30% hemolymph volume (Gleeson and Zubkoff, 1977). Animals were not handled during the injection and did not appear to be disturbed by the saline injections. They often became agitated, however, during hormone injections. When more than one test was conducted during a day, an average of 4–5 h was allowed for recovery between injections.

Statistical tests

Significance was evaluated with a two-tailed paired Student's t test. A P value < 0.05 was considered significant. Paired t tests were used to compare the heart rates during the last 6 min of the rest period to the first 6 min after the onset of walking or following injections. Examination of the significance of denervation was carried out with an analysis of covariance. In this case the slope of heart rate change, during exercise, in denervated animals was compared to the change seen in intact animals.

Results

Role of dorsal nerves in heart response to startle and exercise

In settled animals, novel stimuli such as shadows, movements in the visual field, and touches to the carapace always triggered periods of bradycardia known as startle responses. These responses diminished when the stimuli were repeated (Fig. 1). Successful cutting of the dorsal nerves was confirmed by the loss of the startle response.

Settled lobsters resting in the treadmill chamber exhibited regular heart rates of 54 ± 13 min^{-1}. At the onset of walking, f_H rapidly increased to 87 ± 5 min^{-1} over the first 2–3 min and then more slowly to 90 ± 5 min^{-1} by the end of the 30-min walk (Fig. 2). While an animal was walking, the swimmerets beat and the abdomen and chelipeds were held slightly elevated and extended. During the 30-min exercise period, animals often stopped and then, when they had drifted back to the bottle brush, accelerated and then resumed a steady pace. The frequency and length of pauses tended to increase with time during the exercise period. At the point of exhaustion, animals would not respond to tactile stimulation. Heart rate and walking behavior were not different between sham-operated and unoperated control animals.

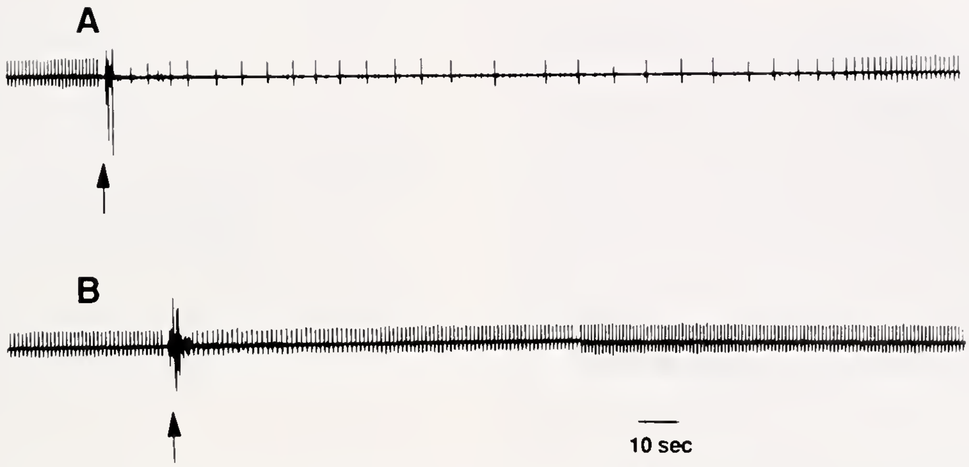

Figure 1. The startle response, a period of bradycardia, seen after passing a shadow (A) across the visual field of a settled lobster. The startle response is usually diminished if the same or a different stimulus is repeated within a few minutes of a first stimulus, in this case tapping the carapace (B). Parts A and B are continuous records.

Following denervation surgery, heart rate returned to previous resting rates in 2–3 h, but it gradually increased over several days thereafter. The data shown in Figure 2 were collected over several days following surgery, and the slightly elevated settled rates reflect this gradual increase. Walking behavior was unchanged from that of controls; however, the rapid phase of tachycardia did not occur. Heart rates did increase slowly from 62 min^{-1} at rest to a maximum of 72 min^{-1}, an increase significantly below that observed in controls. Rates during the last 6 min of walking did not differ significantly from those recorded during the 6-min period prior to walking.

Role of dorsal nerves in response to cardiac impairment

In *Carcinus maenas,* cutting the two dorsal anterior alary ligaments reduced cardiac output of semi-isolated hearts by 25% (Wilkens and McMahon, 1992). One day after these same two ligaments were cut in lobsters, the resting f_H was elevated by 20.6% above controls (Fig. 3).

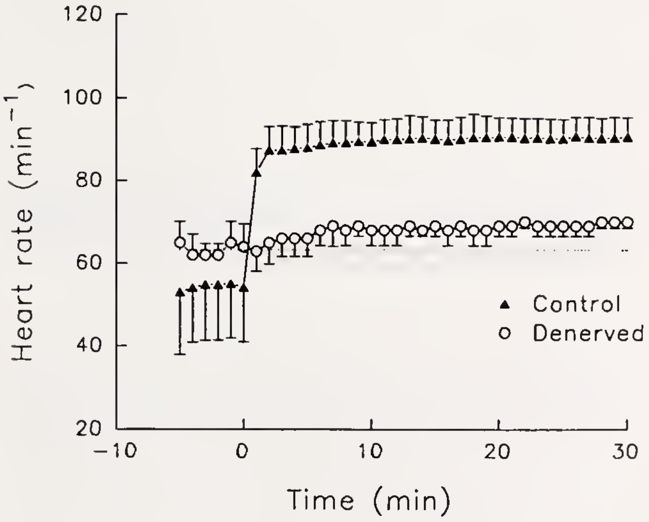

Figure 2. The effects of exercise on the heart rate of intact lobsters (n = 11) and following sectioning of both dorsal cardioregulatory nerves (n = 3). The dotted line is drawn at the mean heart rate of denervated animals for the 6-min period before the start of walking. The treadmill was started at time zero and traveled at 1.7 m · min^{-1}. Mean ± SD.

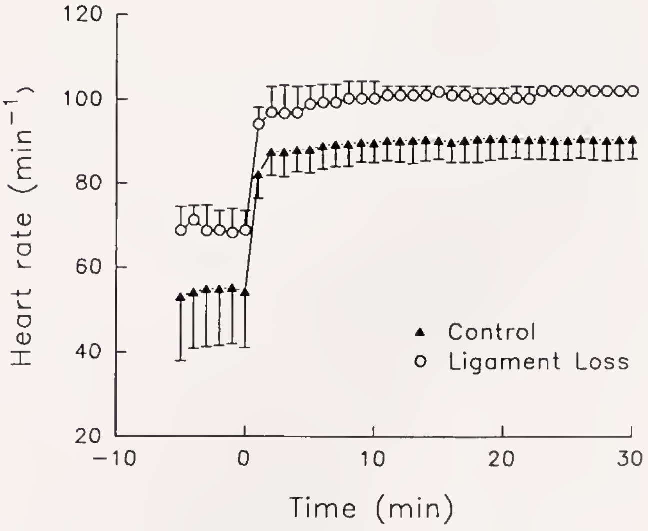

Figure 3. The effect of severing the two dorsal-anterior alary ligaments on heart rate in resting and exercising lobsters (n = 11 for control, n = 5 for operated). The control data are reproduced from Figure 2. The five operated lobsters were taken from that group. The treadmill was started at time zero. Mean ± SD.

During walking, f_H increased on average 11.7% above controls (102 ± 2 min^{-1}). These animals showed no impairment in walking behavior.

On the second or third day after the ligaments were cut, the heart chamber was reopened and the dorsal nerves were sectioned. After this procedure the compensatory increases seen in resting f_H after ligament loss were reversed (Fig. 4). During locomotion, f_H increased slowly and steadily. The final rates after 25 min were significantly lower than those of control or ligament-loss animals. The rates were not significantly different from those observed during the same period in animals with only dorsal nerve loss (Fig. 2). These animals were reluctant to walk and continued to do so only if continuously prodded. Three of the animals refused to walk longer than 21 min. The chelae often dragged along the belt, and after about 10 min of walking the animals seemed to be trying to recruit the chelae to aid walking. The abdomen also dragged.

Responses of heart to aminergic neurohormones

When settled lobsters were injected with enough of each of the aminergic neurohormones to produce a circulating concentration of 1 μM (assuming complete mixing), the result was significant and prolonged tachycardia (Fig. 5), whereas injection of the same volume of saline had no effect. DA caused the largest increase (83 ± 2 min^{-1}), followed by 5-HT (79 ± 2 min^{-1}) and OA (71 ± 3 min^{-1}). Heart rate remained elevated for more than an hour in almost all cases.

The maximum f_H values following injection of DA and 5-HT in denervated settled animals were similar to those in the control animals (Fig. 6), but they were not maintained at the maximum levels as they were in the controls. All of these animals showed elevated rates at rest compared to controls. OA injections had no effect on f_H; however, the preinjection f_H values were at the same level as in control animals following OA.

Injection of the same amounts of 5-HT into control lobsters just before the treadmill was turned on caused similar increases in f_H, but prevented walking for as long as 15 min. The animals appeared to be stiff and did not

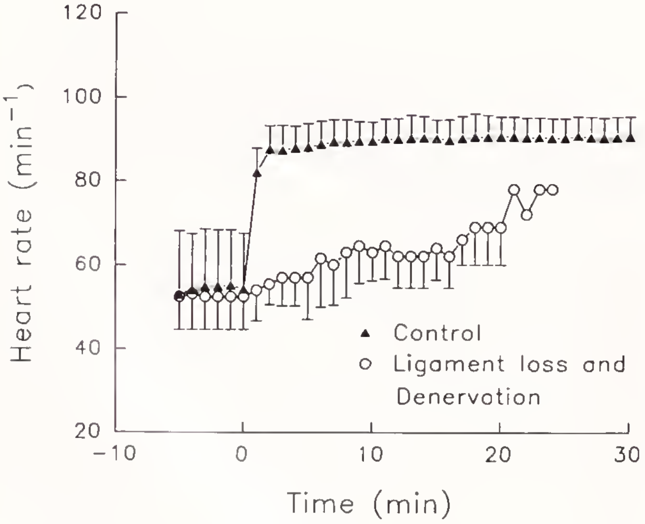

Figure 4. The compounded effects of alary ligament loss and denervation on the heart rate of exercising lobsters (n = 11 for control, same animals illustrated in Figs. 2 and 3; n = 5 for operated, the same denervated animals illustrated in Fig. 3). The treadmill was started at time zero. Mean ± SD.

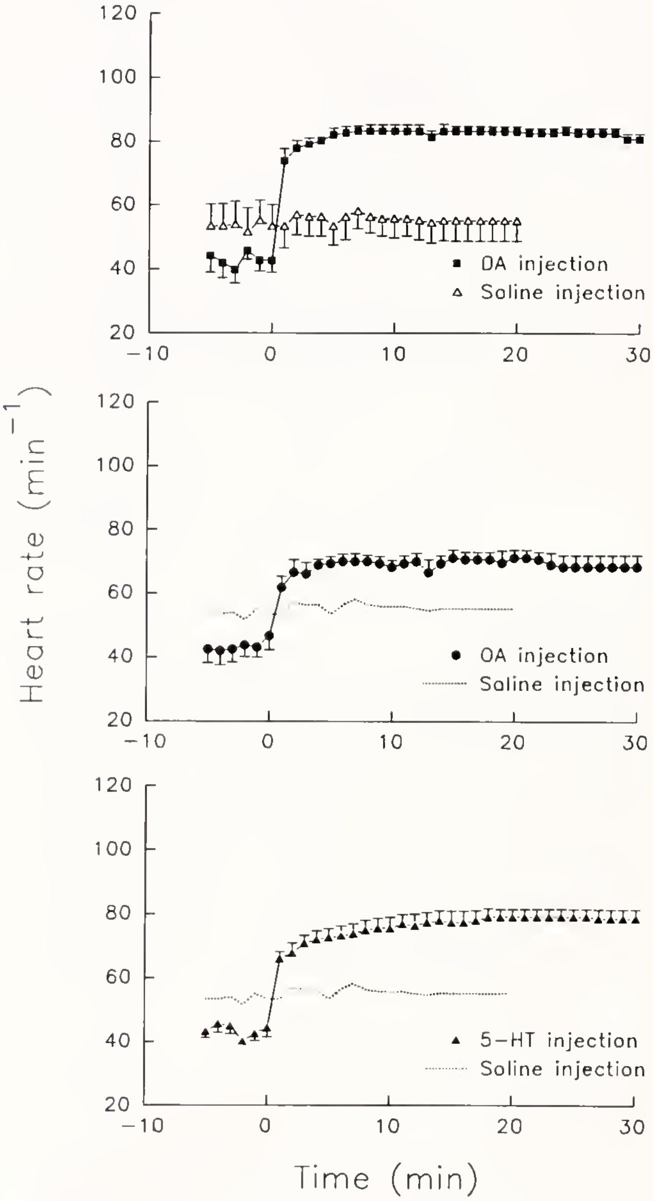

Figure 5. The effects of saline, OA, DA, and 5-HT injections on heart rate of settled lobsters (n = 5). The responses to saline injections are copied in each panel as a reference trace. The amines were presented in random order from animal to animal. Mean ± SEM.

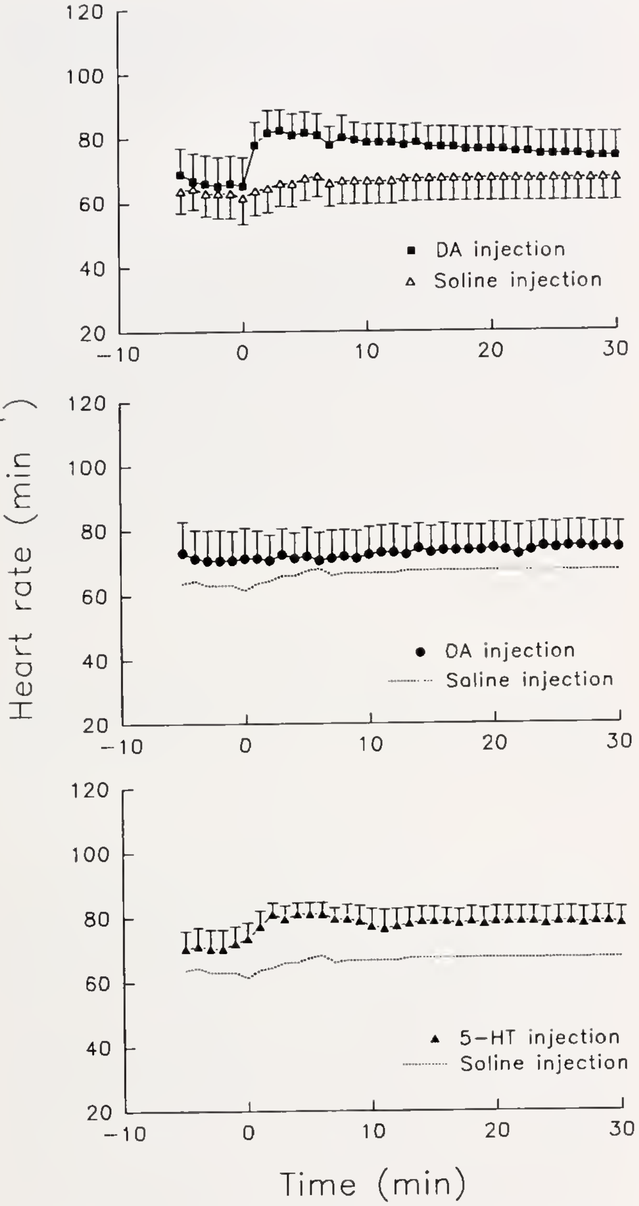

Figure 6. The effects of saline, OA, DA, and 5-HT injections on heart rate in denervated lobsters ($n = 5$). The responses to saline injections are copied in each panel as a reference trace. The amines were presented in random order from animal to animal. Mean ± SEM.

walk even when prodded. Over the next 30 min the willingness to walk gradually increased. DA and OA did not impair walking.

Discussion

Role of dorsal nerves in heart response to exercise

The loss of startle-induced bradycardia after dorsal nerve cutting indicates that the cardioinhibitor nerves are the causative inputs for this behavior. The heart rate response to exercise involves two phases. Phase I is rapid-onset tachycardia, which occurs within the first 2 to 3 min of exercise (Fig. 2). The control system is rather like an on-off switch and does not seem to be graded with duration of exercise. Phase II is a sustained and gradually increasing f_H throughout the period of exercise. The role of the cardioregulatory innervation in these two phases was evaluated following nerve sectioning. In the absence of the dorsal excitatory and inhibitory nerves, the regulation of the heart activity can occur only *via* hemolymph-borne factors. Such factors could include neurohormonal secretions from the pericardial organs lining the pericardial cavity and metabolite end products produced during walking. The absence of Phase I in denervated animals demonstrates the ineffectiveness of these secondary processes in compensating for cardiovascular stress. Therefore, the cardioaccelerator nerves must be responsible for this response, whereas the pericardial neurohormone secretions are not. This finding is consistent with prior *in vitro* investigations, which demonstrated that stimulation of accelerator nerves causes a quick increase in f_H (within 30 s of stimulation; Maynard, 1953; Florey, 1960; Hagiwara, 1961). The small increases in f_H during Phase II of exercising in control, denervated, and dual-operated (ligament loss and denervation) animals may arise from neurohormonal inputs even though the rates never reached control levels. Apparently pericardial secretions alone do not contribute to Phase I, but they may play a role in Phase II. Therefore, Phase II is most likely due to dual action of nervous input and pericardial secretions.

Role of dorsal nerves in response to cardiac impairment

The effects of reduced stroke volume, resulting from ligament loss, were compensated for by an increase in f_H both at rest and while walking. This supports the finding of McGaw *et al.* (1994) that the primary mechanism used to offset the effects of cardiovascular stress is an increase in f_H. The subsequent denervation of these hearts eliminated the elevated resting rates, although the very slow increases in f_H still occurred during exercise. Following the dual insults on cardiac output of ligament loss and denervation, lobsters were reluctant to walk for more than short periods and appeared to fatigue rapidly. These results demonstrate that cardioregulatory innervation plays an important role in primary compensatory cardiovascular responses to exercise.

An examination by McGaw *et al.* (1994) of hemolymph flow patterns during short periods of spontaneous walking showed preferential hemolymph flow to the sternal artery that supplies the periopods and scaphognathites (ventilatory pumps). This redistribution of hemolymph flow is thus another compensatory measure used by animals in the face of cardiovascular stress. Those authors also found that short-term cardiovascular stress was accompanied by an increase in f_H and stroke volume.

Role of extrinsic nerves in mediating neurohormone action

Injection of any one of the three aminergic neurohormones (OA, DA, and 5-HT) into resting animals brought about a significant increase in the f_H that was maintained for more than 30 min. The circulating half life of these three animals in crayfish and crabs varies from 2 to 13 min (Hoeger and Florey, 1989; Hoeger, 1990; Bininda *et al.*, 1992). These clearance studies were performed at temperatures similar to those used during the present study. Clearance rates in lobsters have not been determined, but if we can assume that they are similar to those in crayfish and crabs, then the duration of the elevation in f_H is greater than the expected residence time of the hormones. In denervated animals, only DA and 5-HT produced short-term increases in resting f_H; OA injection produced no change. The initial increase in f_H brought about by DA and 5-HT injection lasted for only about 10 min and gradually declined thereafter. The initial responses may have arisen from the period when circulating amines were highest, while the decline thereafter may indicate that the dorsal nerves play a role in maintaining neurohormone action beyond the expected amine residence time. In other words, the prolonged elevation of f_H in intact animals may arise from long-term increases in cardioaccelerator or decreases in cardioinhibitor tonic firing rates. The exogenously applied DA may be mimicking the action of the cardioaccelerator nerves, because recent evidence suggests that DA may be the neurotransmitter released by the cardioaccelerator nerves (Yazawa and Kuwasawa, 1992, 1994).

Effect of neurohormones on posture and walking

The injection of 5-HT and octopamine into lobsters induces stereotypical postures thought to resemble those seen in dominant (5-HT) and subordinate (OA) animals (Livingstone *et al.*, 1980; Kravitz, 1990). 5-HT caused animals to stand tall on the tips of their walking legs with their chelae extended and open and their abdomens flexed. OA injections caused the animals to stand low to the substrate with their claws and walking legs extended and pointing forward and with their abdomens hyperextended upward. In our experiments, lobsters injected with similar doses of 5-HT also assumed the expected stance, but were quite stiff and unable to walk for up to 15 min. They slowly regained ability to walk over the following 30 min. In *Carcinus*, 5-HT triggers a rigid posture and reduces an animal's ability to right itself when placed on its back (McPhee and Wilkens, 1989). Perhaps it is inappropriate to suggest that the 5-HT-induced posture mimics the dominant stance displayed by untreated lobsters in natural settings, because these animals are unable to move. On the other hand, the ability of lobsters to walk was unaffected by OA injections.

Conclusions

The focus of this investigation was to determine the role of cardioregulatory nerves in regulating the f_H of *H. americanus*. Our data support the conclusions that the cardioinhibitor nerves are responsible for startle-induced bradycardia and that the cardioaccelerator nerves cause the rapid-onset tachycardia associated with walking. The continued gradually increasing heart rate during long walks may be partially accounted for by hemolymph-borne factors including neurohormones. The cardioaccelerator nerves are also responsible for the compensatory increases in f_H in animals whose stroke volume was artificially reduced.

Acknowledgments

This study was supported by a grant from the Natural Science and Engineering Research Council of Canada to JLW.

Literature Cited

Alexandrowicz, J. S. 1932. The innervation of the heart of the Crustacea. I. Decapoda. *Quart. J. Microscop. Sci.* **75:** 181–249.

Berlind, A., I. M. Cooke, and M. W. Goldstone. 1970. Do the monoamines in crab pericardial organs play a role in peptide neurosecretion? *J. Exp. Biol.* **53:** 669–677.

Bininda, D. H., B. R. McMahon, and J. L. Wilkens. 1992. Circulating levels and clearance rates of dopamine, octopamine and serotonin in hemolymph of the crab *Cancer magister. Am. Zool.* **32:** 47A.

Cole, W. 1941. A perfusing solution for the lobster (*Homarus*) heart and the effects of its constituent ions on the heart. *J. Gen. Physiol.* **25:** 1–6.

Cooke, I. M. 1966. The sites of action of pericardial organ extract and 5-hydroxytryptamine in the decapod crustacean heart. *Am. Zool.* **6:** 107–121.

Field, L. H., and J. L. Larimer. 1975. The cardioregulatory system of crayfish: neuroanatomy and physiology. *J. Exp. Biol.* **62:** 519–539.

Florey, E. 1960. Studies on the nervous regulation of the heart beat in decapod Crustacea. *J. Gen. Physiol.* **3:** 1061–1081.

Florey, E., and M. Rathmayer. 1978. The effects of octopamine and other amines on the heart and on neuromuscular transmission in decapod crustaceans: further evidence for a role as neurohormone. *Comp. Biochem. Physiol.* **61C:** 229–237.

Gleeson, R. A., and P. L. Zubkoff. 1977. The determination of hemolymph volume in the blue crab *Callinectes sapidus*, utilizing ^{14}C-thiocyanate. *Comp. Biochem. J. Neurosci.* **6:** 1560–1569.

Grega, D. S., and R. G. Shermann. 1975. Responsiveness of neurogenic hearts to octopamine. *Comp. Biochem. Physiol.* **52C:** 5–8.

Hagiwara, S. 1961. Nervous activities of the heart in Crustacea. *Ergeb. Biol.* **24:** 287–311.

Hoeger, U. 1990. Fate of circulating serotonin in the hemolymph of the crayfish, *Orconectes limosus. Z. Naturforsch.* **45c:** 1053–1059.

Hoeger, U., and E. Florey. 1989. Catecholamine degradation in the hemolymph of the Chinese crab, *Eriocheir sinensis. Comp Biochem. Physiol.* **92C:** 323–327.

Kravitz, E. A. 1990. Hormonal control of behavior: Amines as gain-setting elements that bias behavioral output in lobsters. *Am Zool.* **30:** 595–608.

Livingstone, M. S., R. M. Harris-Warrick, and E. A. Kravitz. 1980. Serotonin and octopamine produce opposite postures in lobsters. *Science* **208:** 76–79.

Maynard, D. M. 1953. Activity in a crustacean ganglion. I. Cardio-inhibition and acceleration in *Panulirus argus. Biol. Bull.* **109:** 420–436.

McGaw, I. J., C. N. Airriess, and B. R. McMahon. 1994. Patterns of haemolymph flow variation in decapod crustaceans. *Mar. Biol.* **131:** 53–60.

McPhee, M. J., and J. L. Wilkens. 1989. Serotonin, but not dopamine or octopamine, modifies locomotor and phototaxic behavior of the crab, *Carcinus maenas. Can. J. Zool.* **67:** 391–393.

Wilkens, J. L. 1987. Cardiac and circulatory control in decapod Crustacea with comparisons to molluscs. *Experientia* **43:** 990–994.

Wilkens, J. L., and B. R. McMahon. 1992. Intrinsic properties and extrinsic neurohormonal control of crab cardiac hemodynamics. *Experientia* **48:** 827–834.

Wilkens, J. L., and R. L. Walker. 1992. Nervous control of crayfish cardiac hemodynamics. *Comp Physiol.* **11:** 115–122.

Wilkens, J. L., A. J. Mercier, and J. Evans. 1985. Cardiac and ventilatory responses to stress and to neurohormonal modulations by shore crab *Carcinus maenas. Comp. Biochem. Physiol.* **82C:** 337–343.

Yazawa, T., and K. Kuwasawa. 1992. Intrinsic and extrinsic neural and neurohormonal control of the decapod heart. *Experientia* **48:** 834–840.

Yazawa, T., and K. Kuwasawa. 1994. Dopaminergic acceleration and GABAergic inhibition in extrinsic neural control of the hermit crab heart. *J Comp Physiol. A.* **174:** 65–75.

Young, R. E. 1978. Correlated activities in the cardioregulator nerves and ventilatory system in the Norwegian lobster, *Nephrops norvegicus* (L.). *Comp. Biochem. Physiol.* **61A:** 387–390.

Reference: *Biol. Bull.* **188:** 186–196. (April, 1995)

The FMRFamide-Related Peptides F1 and F2 Alter Hemolymph Distribution and Cardiac Output in the Crab *Cancer magister*

I. J. McGAW* AND B. R. McMAHON

Department of Biological Science, University of Calgary, Calgary, Alberta, T2N 1N4, and Bamfield Marine Station, Bamfield, British Columbia, V0R 1B0 Canada

Abstract. The FMRFamide-related peptides F1 and F2, originally isolated from lobster pericardial organs, have been shown to exert cardioexcitatory effects on isolated or semi-isolated crustacean hearts. The present study sought to determine the *in vivo* effects of F1 and F2 on cardiac and circulatory performance of *Cancer magister* using a pulsed-Doppler technique. In general the effects of F1 and F2 were similar; however, F1 was more potent and its effects were of longer duration than those exerted by F2. Infusion of either F1 or F2 caused a decrease in heart rate and subsequent periods of acardia. These decreases in rate occurred concurrently with a short-term increase in stroke volume of the heart, followed by a longer-term decrease in stroke volume. Hemolymph flow rates through the anterior aorta, anterolateral arteries, sternal artery, and posterior aorta also showed the same trend, with an initial short-term increase in flow rate followed by a longer-term decrease with periods of ischemia. Hemolymph flow through the paired hepatic arteries simply decreased, but recovery to pretreatment levels was faster than in the other arterial systems. Threshold for these responses occurred at circulating concentrations between 10^{-9} mol · l^{-1} and 10^{-8} mol · l^{-1} for F1 and somewhat higher, between 10^{-8} mol · l^{-1} and 10^{-7} mol · l^{-1}, for F2.

Introduction

The neuropeptide FMRFamide (Phe-Met-Arg-Phe-NH_2) was first isolated and sequenced from the clam *Macrocallista nimbosa* (Price and Greenberg, 1977). FMRFamide is now known to belong a large family of neuropeptides, collectively called the FMRFamide-related peptides (FaRPs), that share the sequence Arg-Phe-NH_2 and exist throughout the invertebrate and vertebrate kingdom (for reviews see Greenberg and Price, 1983; Raffa, 1988; Price and Greenberg, 1989). FaRPs generally function as neurohormones or neurotransmitters; their action on the cardiovascular system is predominantly excitatory, but inhibitory or biphasic effects occur in some species (*e.g.*, Painter and Greenberg, 1982; Cuthbert and Evans, 1989; Price *et al.*, 1990; Duve *et al.*, 1993; Lesser and Greenberg, 1993).

In crustaceans, FMRFamide-like immunoreactivity has been found throughout the nervous system, the highest amounts being concentrated in the pericardial organs (Kobierski *et al.*, 1987; Marder *et al.*, 1987; Trimmer *et al.*, 1987; Krajniak, 1991; Mercier *et al.*, 1991). Two of these peptides have been isolated and sequenced from the pericardial organs of the lobster *Homarus americanus* (Trimmer *et al.*, 1987) and have been identified as having the sequences TNRNFLFRamide (F1) and SDRNFLFRamide (F2). Both have since been reported in the stomatogastric system of the rock crab *Cancer borealis* (Weimann *et al.*, 1993). The high concentration of these peptides in the pericardial organs suggests that they may be released into the circulatory system to directly affect the heart or cardioarterial valves. Both F1 and F2 excite isolated lobster (*H. americanus;* Kravitz *et al.*, 1987) and blue crab (*Callinectes sapidus;* Krajniak, 1991) hearts, and increase amplitude and frequency of hearts isolated from crayfish (*Procambarus clarkii;* Mercier and Russenes, 1992) and shore crab (*Carcinus maenas;* Wilkens and McMahon, 1992). In the lobster and crayfish, these pep-

---

Received 13 June 1994; accepted 25 January 1995.

* Present address: Department of Biology, College of Charleston, Charleston, SC 29424.

Abbreviations. FaRPs, FMRFamide-related peptides; F1, TNRNFLRFamide; F2, SDRNFLFRamide; CNS, central nervous system.

tides restrict hemolymph flow by their actions on the cardioarterial valves (J. L. Wilkens, pers. comm.).

In addition to their action on the heart, F1 and F2 also activate the pyloric and gastric rhythms in *Cancer borealis* (Weimann *et al.*, 1993), and F1 has powerful effects on the phasic extensor muscle of the lobster (Pasztor and Golas, 1993). There are very few reports of the effects of neurohormones on the cardiovascular dynamics of whole-animal preparations. We recently developed a pulsed-Doppler technique for measuring blood flow and cardiac output in *Cancer magister in vivo* (Airriess *et al.*, 1994). This technique is minimally invasive and allows simultaneous measurement of blood flow in all arteries leaving the heart. This permits calculation of cardiac output which, when divided by heart rate, yields stroke volume.

A number of amine and peptide neurohormones have been shown to have distinctive effects on cardiac and circulatory function in crustaceans *in vivo* compared with isolated or semi-isolated preparations (McMahon and Reiber, 1991; Airriess and McMahon, 1992; McGaw *et al.*, 1994a). Thus the aim of the present study was to determine the effects of the FMRFamide-related peptides F1 and F2 on hemolymph flow and cardiac output *in vivo* in the Dungeness crab *C. magister.*

Materials and Methods

Adult male intermolt *Cancer magister* weighing 600–850 g were purchased from local fishermen and held at Bamfield Marine Station, British Columbia, Canada, in filtered running seawater at a temperature of 12 ± 1°C and a salinity of 33 ± 1% for at least 1 week prior to experimentation. Crabs were usually fed chopped fish twice a week but were isolated from food supplies for 2 days prior to experimentation.

A 545C-4 directional pulsed-Doppler flowmeter (Bioengineering, University of Iowa) was used to measure hemolymph velocity in each of the major arteries. This technique of minimally invasive flow measurement and probe calibration is described in detail in Airriess and McMahon (1994) and Airriess *et al.* (1994). Briefly, piezoelectric crystal probes (Iowa Doppler Products, Crystal Biotech) were implanted in grooves abraded to the dermis of the carapace directly above each artery except the sternal and hepatic arteries, which were monitored by means of internal catheter mounted probes. Hemolymph loss during the latter procedure was minimal. Probe performance was first optimized manually, then fine focused electronically to obtain maximum signal amplitude and fixed in place using cyanoacrylate glue and dental wax. Output from the flowmeter was recorded on a Gould 6-channel oscillograph.

Heart rate was determined by counting the peaks on the arterial flow traces. This method, evaluated by Airriess and McMahon (1994), gives values analogous to those produced by the more familiar impedance conversion technique as long as there is measurable hemolymph flow through at least one arterial system. Cardiac output was calculated by summation of the mean flow through each artery (values for paired arteries were doubled), and this value was divided by mean heart rate to obtain a mean value for cardiac stroke volume. Scaphognathite beat frequency was recorded with a hydrostatic pressure transducer (Statham/Gould) connected *via* a saline-filled catheter to the right branchial chamber.

During experiments, crabs were held in a covered acrylic plastic box, dimensions 28 × 20 × 10 cm, that was supplied with a constant flow of aerated seawater. The size of the box allowed the crabs minimum movement and thus restricted damage to the probe implants. After electrodes were implanted, animals were allowed to settle for at least 24 h before experimentation. Experiments were carried out in constant darkness at a temperature of 12 ± 1°C.

F1 was obtained from Bachem Bioscience, Inc., and F2 was a gift from Dr. Joffre Mercier. The peptides were dissolved in *Cancer* saline (Morris and McMahon, 1989) and diluted to achieve final calculated circulating concentrations of 10^{-6} to 10^{-12} mol · l^{-1}. Test solutions were infused directly into the lateral pericardial sinus by means of a chronically implanted polyethylene catheter (PE20). A syringe pump (Sage Instruments) was used to infuse 350 μl of the test solution followed by 150 μl of saline for catheter washout over a 3-min period. This interval was long enough to ensure that the hormone did not reach the pericardial sinus as a concentrated bolus of injectate but was distributed slowly and homogeneously (Airriess and McMahon, 1992). Control infusions were carried out with *Cancer* saline. Each experimental animal received the entire concentration range of either F1 or F2.

Heart rate, hemolymph flow rates, and scaphognathite beat frequency were determined for 11 animals tested with F1 and for 10 animals tested with F2. Recordings were carried out at 10-min intervals during a 30-min control period, during and immediately after infusion of either saline or peptide solution, and at regular intervals after infusion up to a total time of 120 min for each hormone concentration.

One-way analysis of variance with repeated measures design (Potvin *et al.*, 1990) was carried out on the data to test for significant differences between pre- and post-treatment levels; any missing values were statistically estimated (Zar, 1984).

Results

The heart rate, scaphognathite rate, and hemolymph flow through each of the arterial systems leaving the heart were determined for 11 crabs tested with F1 and 10 crabs tested with F2 (Figs. 1–3 and 8). The figures show mean responses (with SE) to a control infusion of *Cancer* saline and a circulating concentration of F1 and F2 (10^{-7} mol · l^{-1}) that had distinct effects.

Saline infusion of 350 μl caused no significant change (ANOVA $P > 0.05$) in any of the measured cardiovascular parameters (Figs. 1–3 and 8, dashed line). In general, the effects of F1 and F2 were similar, but F1 was more potent and its mediated effects tended to be of longer duration than those elicited by F2.

Infusion of either F1 or F2 caused a decrease in heart rate (Fig. 1a and c) ($F = 6.18$ and 4.47, $P < 0.01$) for up to 60 min after peptide treatment, often with periods of acardia. Both the magnitude and duration of these effects were greater with F1. This response was observed between circulating concentrations of 10^{-9} and 10^{-8} mol · l^{-1} for F1, while the threshold for F2 was somewhat higher, between 10^{-8} and 10^{-7} mol · l^{-1}. This long-term decrease in heart rate was initially accompanied by a short-term increase (5 min) in the stroke volume of the heart. Mean stroke volume increased from about 0.15 ml/beat to 0.28 ml/beat with F1 (Fig. 1b) and from about 0.22 ml/beat to 0.31 ml/beat upon administration of 10^{-7} mol · l^{-1} F2 (Fig. 1d). Thereafter, stroke volume decreased in both cases and pretreatment values were not regained until after the end of the 2-h measurement period.

F1 and F2 also elicited similar responses in patterns of hemolymph flow through each of the five major arterial systems. Hemolymph flow through the anterior aorta (Fig. 2a, d), the left anterolateral artery (Fig. 2b, e), the posterior aorta (Fig. 3a, c), and the sternal artery (Fig. 3b, d) showed a short-term increase (<5 min). These changes proved to be statistically significant in all cases (ANOVA, $P < 0.05$) except for the anterior aorta treated with F2 ($F = 1.40$, $P > 0.05$). Thereafter hemolymph flow in each arterial system decreased significantly and often could not be detected for extended periods. In most animals pretreatment flow levels were not regained within the experimental time period (120 min), and often took 3–4 h to recover fully. This long-term decline in hemolymph flow was most apparent in the anterolateral arteries, which also showed evidence

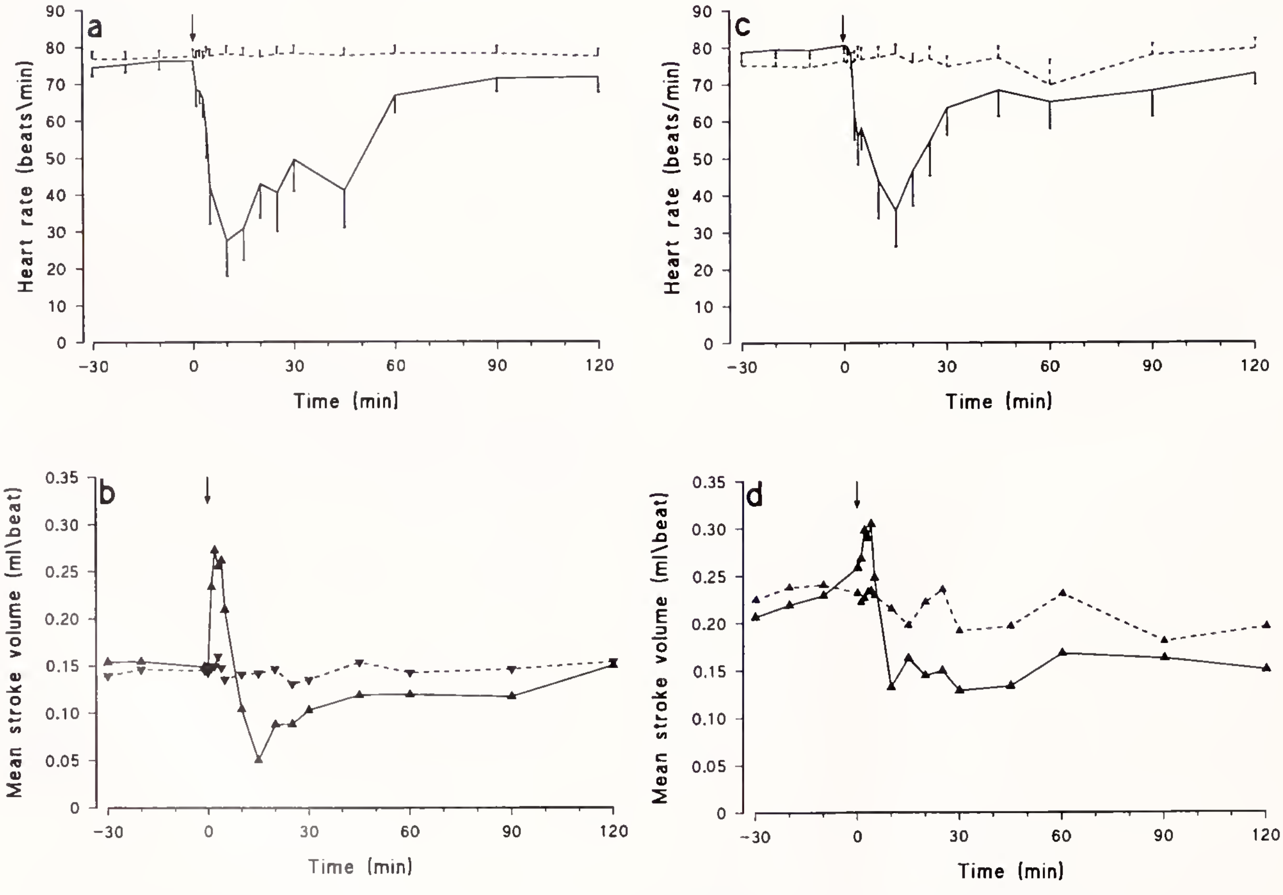

Figure 1. Changes in (a, c) mean heart rate (±SE) and (b, d) mean stroke volume of the heart of *Cancer magister* after infusion of 350 μl of saline (dashed line) and 350 μl of 10^{-7} mol · l^{-1} F1 (a, b) and F2 (c, d) (solid line) at time 0 min (arrow).

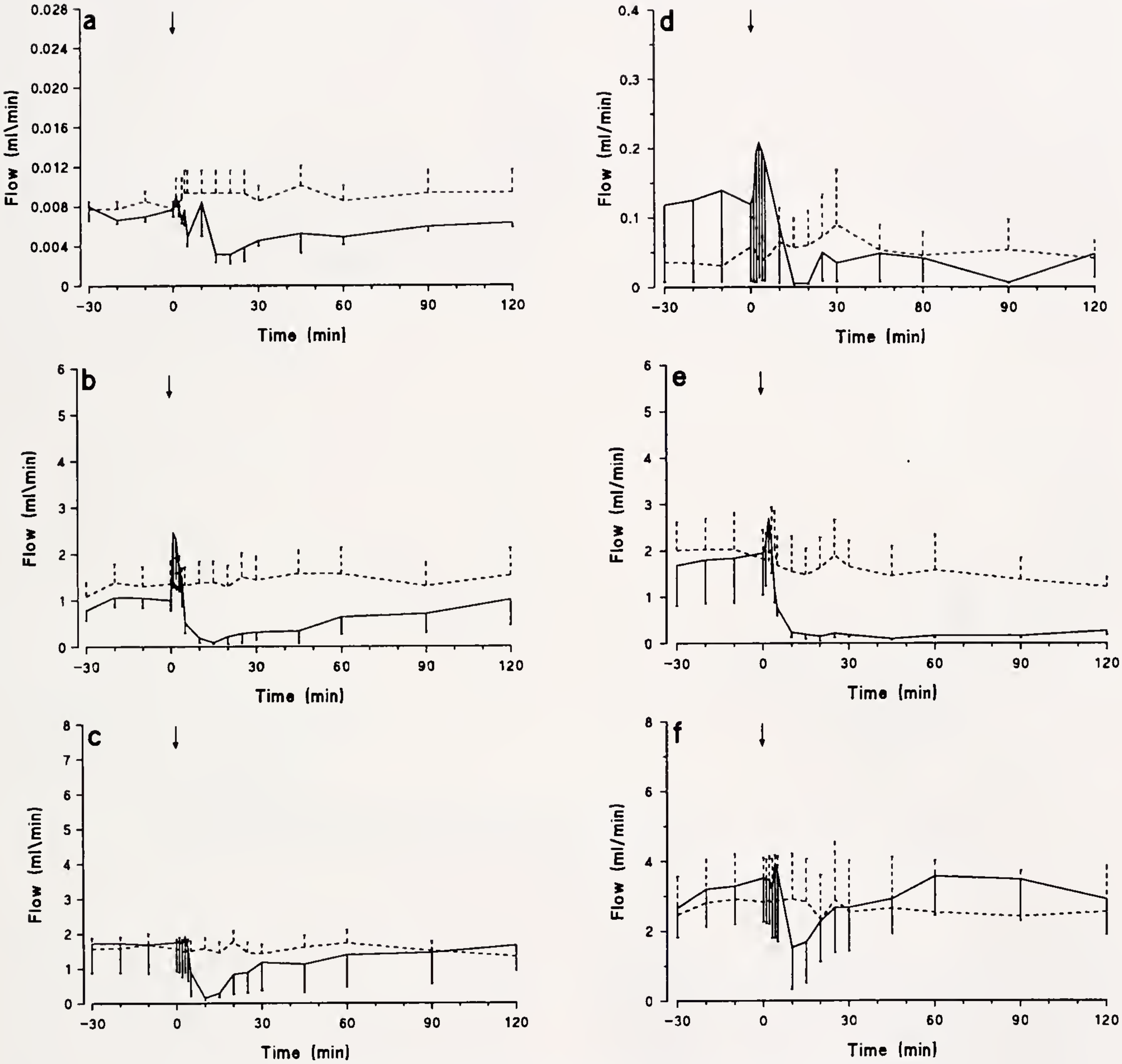

Figure 2. Changes in hemolymph flow (mean ± SE) through the anteriorly directed arteries of *Cancer magister* in response to a 350 μl saline injection (dashed line) or a 350 μl treatment of 10^{-7} mol · l^{-1} F1 or F2 (solid line) at 0 min (arrow). (a, d) Anterior aorta, (b, e) left anterolateral arteries, and (c, f) right hepatic arteries after F1 and F2 infusion respectively.

of a slight reduction in flow at the lower concentrations of F1 and F2 tested (10^{-12} mol · l^{-1} to 10^{-10} mol · l^{-1}).

Hemolymph flow through the right hepatic artery (Fig. 2c, f) did not show the initial short-term increase in response to F1 or F2. Flow through this artery decreased after treatment with F1, although owing to the large variance there was no significant decrease for F2 ($F = 1.49$, $P > 0.05$). The effect of F1 and F2 on hemolymph flow through the hepatic arteries was of shorter duration than in the other arterial systems, and pretreatment levels were usually regained within 30–45 min after hormone infusion.

There was large inter-individual variability in both the duration and the magnitude of hormone-induced changes in hemolymph flow through each arterial system (duration varied from 20 s to 10 min). Because such changes tended to be obscured when shown only as mean responses (Figs. 1–3), representative examples are given in Figures 4 and 5. Increases in flow through each arterial system were not simultaneous. In the majority of animals tested there was

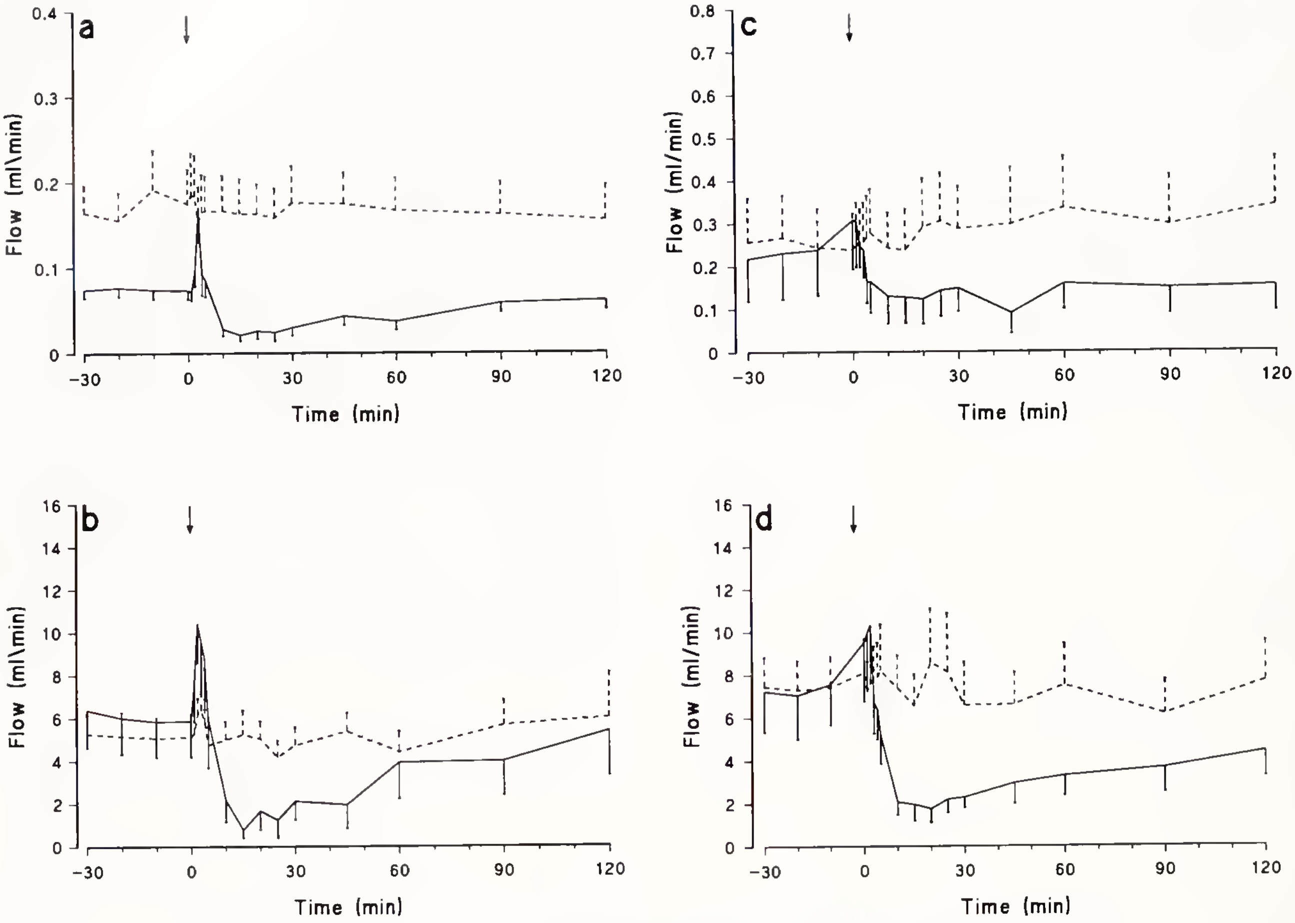

Figure 3. Changes in hemolymph flow (mean ± SE) through the ventrally directed arteries of *Cancer magister* after infusion at 0 min (arrow) of 350 μl of saline (dashed line) or 10^{-7} mol · l^{-1} F1 and F2 respectively (solid line). (a,c) Posterior aorta, and (b, d) sternal artery.

a tendency for the anteriorly directed arteries to be affected first and for the ventrally and posteriorly directed systems to respond slightly later (Fig. 4). After the initial short-term increase in hemolymph flows there was a decrease followed by periods of ischemia (Figs. 4 and 5), and evidence suggested that this interval of both decreased flow and ischemia was dose dependent.

Dose response curves (heart rate, $n = 11$) for F1 and F2 are presented in Figure 6. Heart rate decreased in a simple dose-dependent manner. F1 significantly decreased heart rate at concentrations between 10^{-9} mol · l^{-1} and 10^{-8} mol · l^{-1}, whereas the threshold for F2 was somewhat higher, between 10^{-8} mol · l^{-1} and 10^{-7} mol · l^{-1}.

Total mean cardiac output was calculated by summation of mean flows in all arteries (values for paired arteries were doubled) and expressed as a percentage of flow through each artery (Figs. 7a, b, and c). Saline infusion did not alter the percentage of hemolymph delivered through each system (Fig. 7a). The sternal artery received about 45% of the total cardiac output, about 25% was channeled into each of the hepatic and anterolateral artery systems, and less than 5% was delivered to the smaller-diameter posterior and anterior aortae.

F1 not only produced an overall long-term reduction in cardiac output infusion of 350 μl of 10^{-7} mol · l^{-1}, it also radically altered the distribution of cardiac output (Fig. 7b). The anteriorly directed arteries were affected first: within a minute of hormone infusion a short-term increase in percentage output delivered to the anterolateral arteries and a decrease to the hepatic arteries occurred, while flow through the anterior aorta was routinely low. After about 3 min the percentage of output delivered to the sternal artery and posterior aorta increased for up to 10 min. The longer-term decrease in all arteries except for the hepatic arteries (which recovered to pretreatment flows before the rest of the systems) meant that after 15 min most of the cardiac output was delivered through the hepatic arteries. Similar changes in the distribution of cardiac output resulted from infusion of F2 (Fig. 7c), but the longer duration of flow inhibition in most arteries

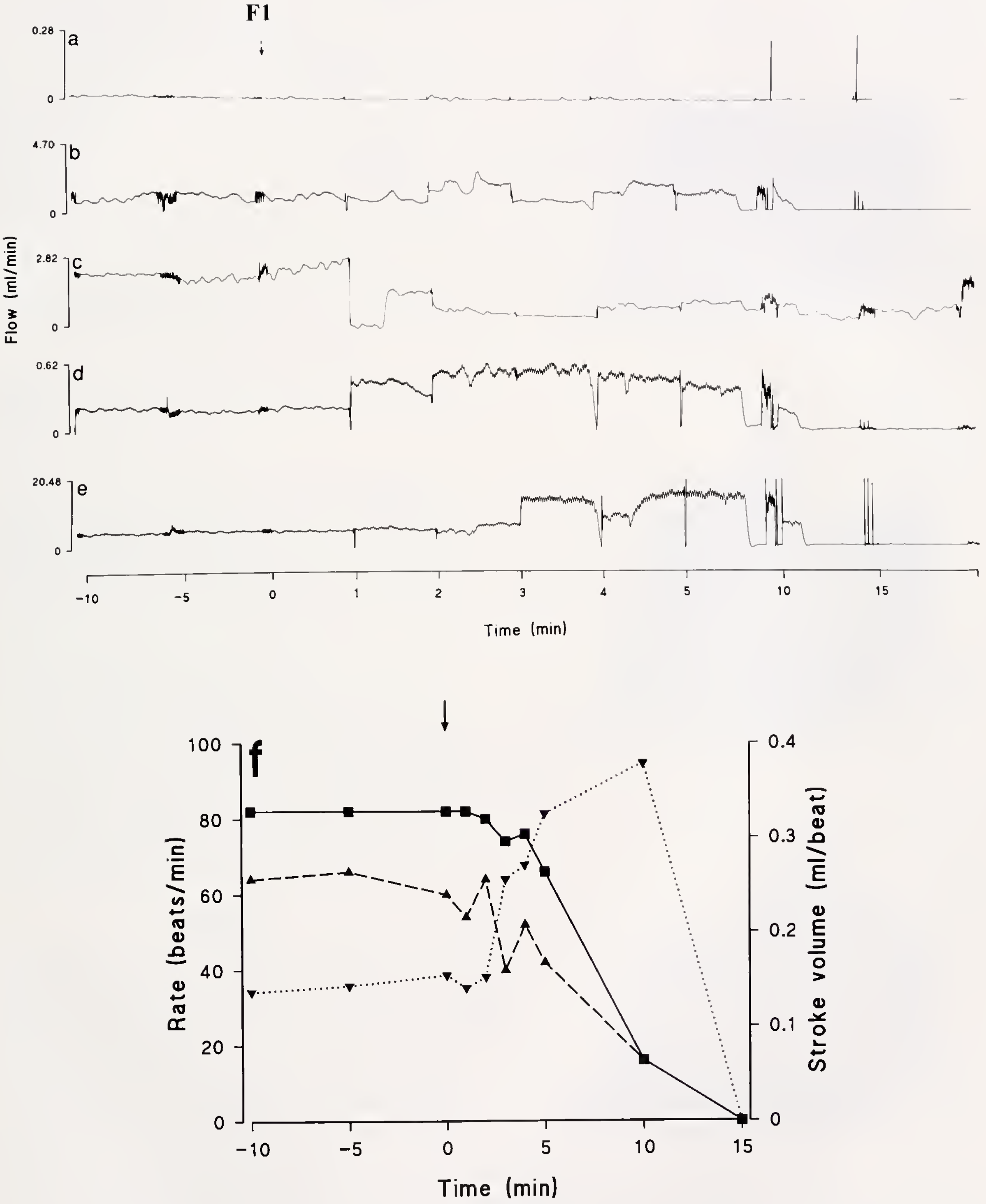

Figure 4. Changes in hemolymph flow (ml/min) and cardiac function in a single specimen of *Cancer magister* after administration of 350 μl of 10^{-7} mol · 1^{-1} F1 at 0 min. (a) Anterior aorta, (b) left anterolateral artery, (c) right hepatic artery, (d) posterior aorta, and (e) sternal artery. (f) Represents changes in heart rate (solid), cardiac stroke volume (dotted), and scaphognathite beat frequency (dashed).

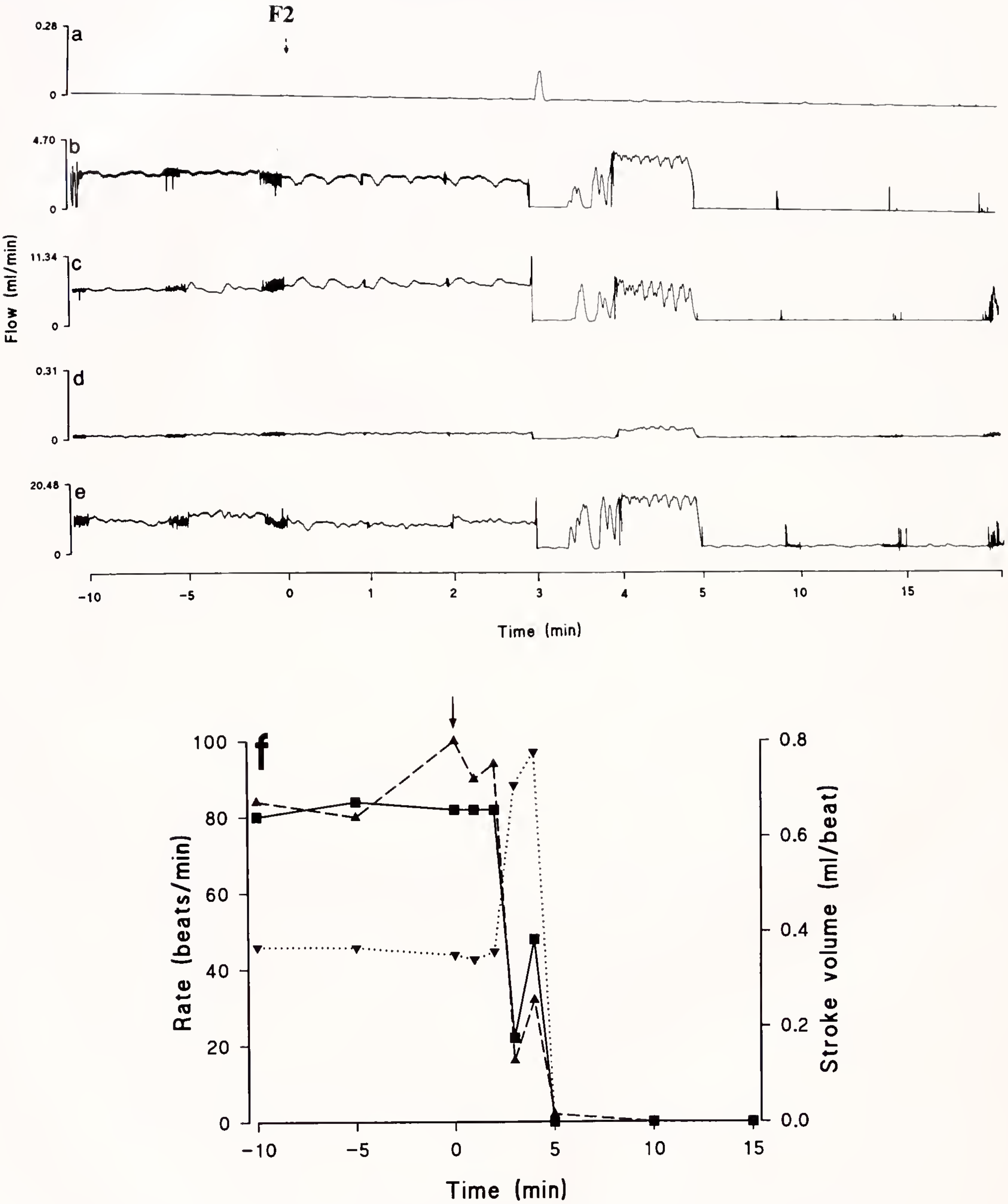

Figure 5. Changes in hemolymph flow (ml/min) and cardiac function in a single specimen of *Cancer magister* after administration of 350 μl of 10^{-7} mol · l^{-1} F2 at 0 min. (a) Anterior aorta, (b) left anterolateral artery, (c) right hepatic artery, (d) posterior aorta, and (e) sternal artery. (f) Represents changes in heart rate (solid), cardiac stroke volume (dotted), and scaphognathite beat frequency (dashed).

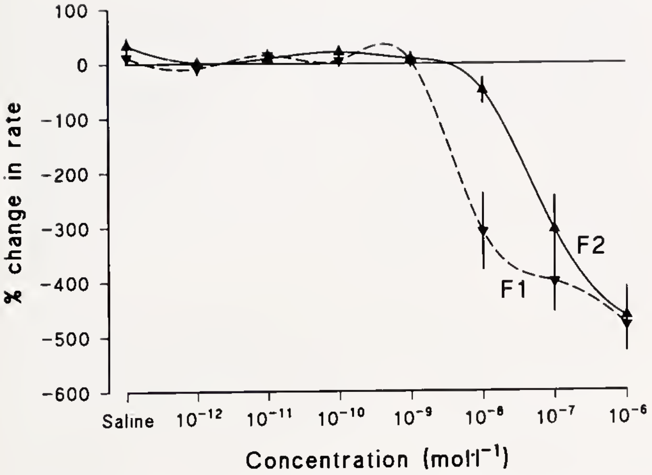

Figure 6. Dose response curves for F1 and F2, depicting cumulative percentage decrease in heart rate (mean ± SE) over a 60-min period after hormone infusion.

extended the period during which most of the flow passed through the hepatic arteries. Note that the hepatic artery flow is not potentiated concurrently. Diversion of a greater percentage of flow into the hepatic arteries at this time is a function of an overall reduction in cardiac output, coupled with a much faster restoration of flow in this arterial system.

The fastest and most dramatic effects of F1 and F2 infusion were on the scaphognathite beat frequency ($F = 11.91$ and 4.52, $P < 0.01$), and they occurred at lower concentrations (10^{-9} mol · l^{-1} and 10^{-8} mol · l^{-1} respectively) than observed for the cardiac or circulatory indicators. Within 1 min of the start of infusion, beating was disrupted, and subsequently ceased (Fig. 8a, b). As with changes in heart rate, reductions by F1 were of greater magnitude and longer duration than those of F2.

Discussion

Investigation of neuropeptidergic modulation of cardiovascular dynamics in decapod crustaceans has focused largely on the effects on isolated or semi-isolated preparations. The present study provides evidence of the actions of the FaRPs F1 and F2 on heart and circulatory function in whole-animal preparations.

In isolated heart preparations of *Callinectes sapidus* (Krajniak, 1991), *Procambarus clarkii* (Mercier and Russenes, 1992; J. L. Wilkens, pers. comm.), and *Carcinus maenas* (Wilkens and McMahon, 1992), F1 and F2 are positively chronotropic and the thresholds for responses tend to be lower than those reported in the present study. Interestingly, F1 and F2 also excite the isolated heart of *Cancer magister* (McGaw, Wilkens, McMahon, and Airriess, in prep.), elevating frequency for up to 30 min

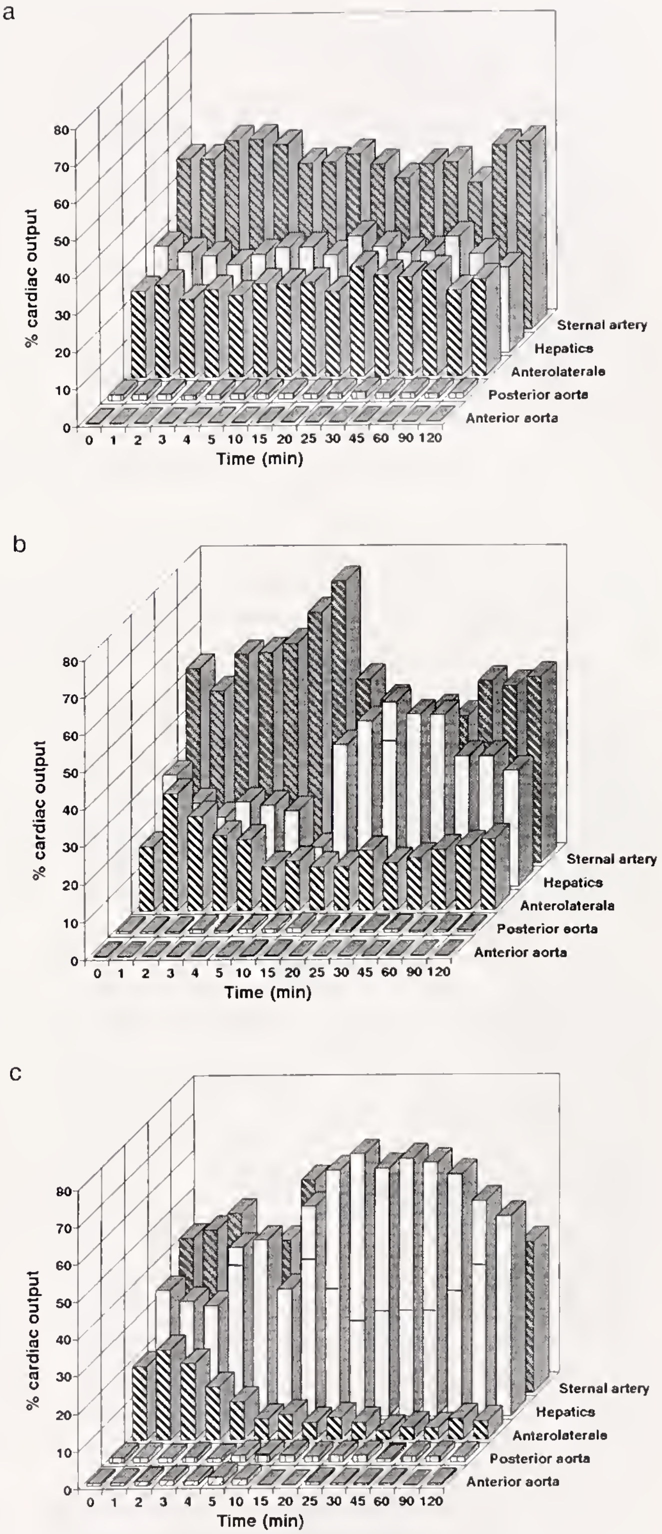

Figure 7. (a) Percentage of total cardiac output delivered through each arterial system after infusion of 350 μl of saline, (b) infusion of 350 μl of 10^{-7} mol · l^{-1} F1, and (c) infusion of 350 μl of 10^{-7} mol · l^{-1} F2. Where values for percentage cardiac output delivered through the sternal artery are obscured, they are shown as horizontal lines on the bars for the hepatic artery.

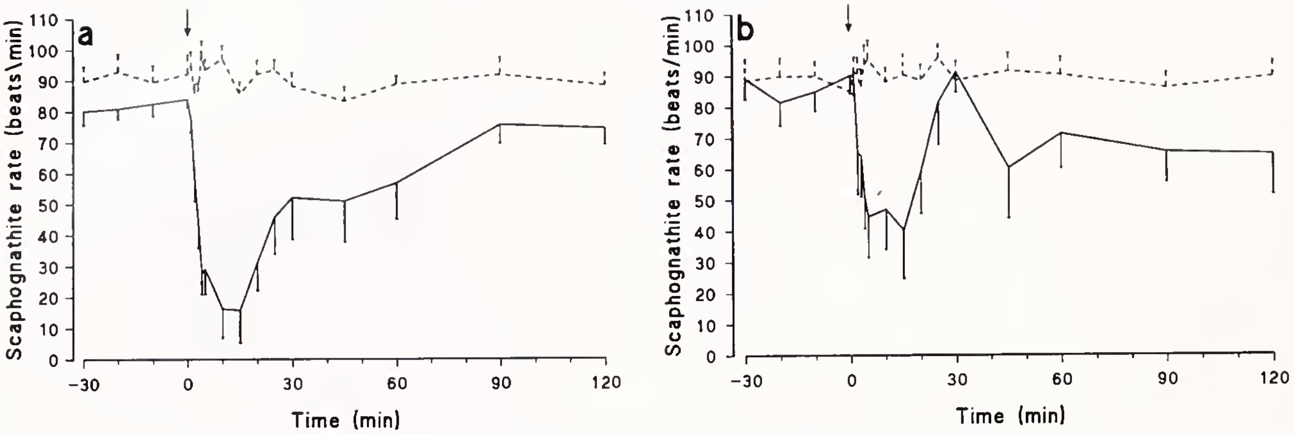

Figure 8. Changes in mean scaphognathite beat frequency after administration of 350 μl of saline (dashed line) or 10^{-7} mol · l^{-1} F1 (a) and F2 (b) (solid line) at time 0 min (arrow).

after hormone application. The threshold for response of the isolated heart is between 10^{-10} mol · l^{-1} and 10^{-9} mol · l^{-1}, which is higher than for intact *C. magister* hearts (Fig. 6). Despite their published reputation as cardioexcitatory peptides, both F1 and F2 induced a rapid bradycardia in intact *C. magister*, followed by periods of acardia (Figs. 1a and c, 4f, and 5f). Similar responses to F1 occur in the lobster *Homarus americanus* (McMahon and Reiber, 1991), although the threshold for inhibition is some 100,000-fold lower, occurring at 10^{-13} mol · l^{-1} instead of at 10^{-8} mol · l^{-1} as in *C. magister*.

F1 and F2 also increase the amplitude of contraction of the isolated heart of *P. clarkii* (Mercier and Russenes, 1992; J. L. Wilkens, pers. comm.). However, this increase in contractility is persistent and, in contrast to the present study, F2 was more potent; similar increases in cardiac stroke volume occur in isolated *C. magister* preparations (McGaw *et al.*, in prep.). In contrast, F1 and F2 have negative inotropic effects on isolated *C. maenas* hearts (Wilkens and McMahon, 1992), whereas no clear pattern is observed in *C. sapidus* (Krajniak, 1991). The action of these hormones on cardiac stroke volume of intact *C. magister* was more complex. Both F1 and F2 caused an initial increase in stroke volume that lasted between 30 s and 10 min. This increase was followed by a longer-term depression; in many cases pretreatment levels of mean stroke volume were not regained within the 120-min test period (Fig. 1b and d).

The discrepancy in cardiac function between isolated and whole-animal preparations suggests that in intact *C. magister* F1 and F2 either exert their effects on the heart by means of inhibitory innervation from the central nervous system (CNS) or cause secondary release of other cardioregulatory hormones (Groome and Watson, 1989). The rapid action of these peptides in disruption and subsequent cessation of scaphognathite beating (Fig. 8) also suggests inhibitory nervous input directly from the CNS.

Modulation of hemolymph flow by F1 and F2 in each of the arterial systems was also complex, and changes were not as uniform as those reported for the heart (Figs. 2 and 3). Duration and magnitude of responses in arterial flow varied quite considerably, not only between animals (Figs. 4 and 5) but even within single animals. Such variability in circulatory function may be associated with the many (but invisible) changes in physiological state that may occur in quiescent animals held under similar conditions (McGaw *et al.*, 1994b). Hemolymph flow increased briefly through all vessels except the paired hepatic arteries and decreased thereafter (Figs. 2 and 3). The initial increase in flow in all arteries except the hepatics must have been brought about by increases in the stroke volume of the heart, since heart rate fell (Fig. 1), and might also involve differential contraction of the cardioarterial valves at the base of each arterial tree. The subsequent decreases in flow resulted from decreases in both heart rate and stroke volume (Fig. 1) and might be associated with simultaneous contraction of all the cardioarterial valves. F2 has not been tested on flow in other crustaceans, but F1 causes similar biphasic effects on hemolymph flow through arteries of the lobster. A short-term increase followed by longer-term decreases and pauses in hemolymph flow occurs in the anterior aorta and the lateral and sternal arteries. A simple decrease occurs in the posterior aorta at higher concentrations (10^{-11} mol · l^{-1} and above). At lower concentrations (10^{-13} mol · l^{-1}) F1 has purely inhibitory effects on lobster hemodynamics (McMahon and Reiber, 1991).

In the present study, the effects of F1 and F2 on the anterolateral arteries were not wholly consistent. In about 75% of the animals tested, flow initially increased; in the remainder, it just decreased. Similar responses are also reported for the lobster (McMahon and Reiber, 1991). The anterolateral arteries are often subject to periodic cycles of hemolymph flow without any apparent *zeitgeber* in *C. magister* (McGaw *et al.*, 1994b) and, therefore, responses may depend on the underlying cycle and the time of hormone infusion. Certainly modification of the pyloric and gastric rhythms of *C. borealis* by F1 or F2 depends on the original state of each of these rhythms (Weimann *et al.*, 1993). At F1 or F2 concentrations of 10^{-7} mol · l^{-1} and above, hemolymph flow through the anterolateral arteries of *C. magister* often did not regain pretreatment capacity until 3–6 h after hormone infusion (unpubl. obs.). The cardioarterial valves of the anterolateral vessels in *P. clarkii* show a persistent increase in resistance to F1 (J. L. Wilkens, pers. comm.). Thus it is possible that long-term contraction of the valves in *C. magister* also decreased blood flow through these arteries.

The paired hepatic arteries, which perfuse the hepatopancreas (Pearson, 1908; McLaughlin, 1983), were the only vessels that did not show an initial increase in flow. However, these arteries recovered pretreatment levels of flow before the other systems, and therefore most of the cardiac output was diverted to the digestive gland (Fig. 7a and b). The FaRPs are thought to be implicated in digestive processes in crustaceans (Mercier *et al.*, 1991; J. L. Wilkens, pers. comm.). They initiate pyloric and gastric rhythms in *C. borealis* (Weimann *et al.*, 1993) and act on the cardioarterial valves of the lobster to increase cardiac output to vessels supplying the gut; they also increase hindgut motility in *P. clarkii* (J. L. Wilkens, pers. comm.). This explanation does not, however, account for the long-term decrease in perfusion of the anterolateral arteries that supply the foregut of *C. magister* (Pearson, 1908; McLaughlin, 1983). A further anomaly is echoed in work on the isolated heart of the crayfish *P. clarkii*, in which the hepatic artery valves contract in response to F1 administration and thus decrease perfusion of the hepatopancreas (J. L. Wilkens, pers. comm.).

The overall effect, therefore, of F1 and F2 in *C. magister* is to induce a temporary increase in perfusion of the locomotory structures, mouthparts, CNS, brain, and telson *via* the sternal, anterolateral, anterior, and posterior arterial systems (Fig. 7a, b, c). These structures are thus perfused either periodically (Figs. 4 and 5) or at a lower rate, and the largest part of a reduced cardiac output is delivered to the hepatopancreas *via* the hepatic arteries (Fig. 7b, c). The functional significance of this is unclear; however, the overall pattern is not dissimilar to that characteristic of burrowing, when hemolymph is diverted to the locomotory structures and mouthparts. Once submerged in the mud, crabs become quiescent and perfuse the system only periodically (McGaw and McMahon, unpubl. obs.). While an animal is burrowed, channeling cardiac output to the hepatopancreas may aid digestion, which implicates FaRPs in a postprandial role in crustaceans.

In the present study, F1 was about 10 times more potent than F2 (Fig. 6), although the activity of these two peptides differs amongst the decapod crustaceans and appears to depend upon the species under investigation (Krajniak, 1991; Mercier and Russenes, 1992; Wilkens and McMahon, 1992; J. L. Wilkens, pers. comm.).

The function of the FaRPs is still not fully understood—in other invertebrate phyla their action on the cardiovascular system is variable, and excitatory, inhibitory, or biphasic responses vary with the concentration of the hormone or the species of organism (*e.g.*, Painter and Greenberg, 1982; Cuthbert and Evans, 1989; Price *et al.*, 1990; Duve *et al.*, 1993; Lesser and Greenberg, 1993). Future work will focus on the sites of action of these peptides to ascertain their role in cardioregulation, and measurement of circulating levels will determine whether they are released from the pericardial organs in amounts sufficient to effect the reported changes.

Acknowledgments

This work was supported by NSERC grant #A5762 to BRM and a grant from WCUMBS (Bamfield Marine Station) to IJM. We are grateful to Dr. Joffre Mercier for donation of F2 and to Dr. Kevin Krajniak for helpful discussion.

Literature Cited

Airriess, C. N., and B. R. McMahon. 1992. Aminergic modulation of circulatory performance in the crab, *Cancer magister*. Pp. 123–131 in *Comparative Physiology*, Vol 11, R. B. Hill, K. Kuwasawa, B. R. McMahon, and T. Kuramoto, eds. Karger, Basel.

Airriess, C. N., and B. R. McMahon. 1994. Cardiovascular adaptations enhance tolerance of hypoxia exposure in the crab *Cancer magister*. *J. Exp. Biol.* **190:** 23–41.

Airriess, C. N., B. R. McMahon, I. J. McGaw, and G. B. Bourne. 1994. Application and *in situ* calibration of a pulsed-Doppler flowmeter for blood flow measurements in crustaceans. *J. Mar. Biol. Ass. U.K.* **74:** 455–458.

Cuthbert, B. A., and P. D. Evans. 1989. A comparison of the effects of FMRFamide-like peptides on locust heart and skeletal muscle. *J. Exp. Biol.* **144:** 395–415.

Duve, H., A. J. Elia, I. Orchard, A. H. Johnsen, and A. Thorpe. 1993. The effects of CalliFMRFamides and other FMRFamide-related neuropeptides on the activity of the heart of the blowfly *Calliphora vomitoria*. *J. Insect Physiol.* **39:** 31–40.

Greenberg, M. J., and D. A. Price. 1983. Invertebrate neuropeptides: native and naturalized. *Ann. Rev. Physiol.* **45:** 271–288.

Groome, J. R., and W. H. Watson III. 1989. Second messenger systems underlying amine and peptide actions on cardiac muscle in the horseshoe crab *Limulus polyphemus*. *J. Exp. Biol.* **145:** 419–438.

Kobierski, L. A., B. S. Beltz, B. A. Trimmer, and E. A. Kravitz. 1987. FMRFamide-like peptides of *Homarus americanus*: distribution, immunocytochemical mapping, and ultrastructural localization in the terminal varicosities. *J. Comp. Neurol.* **266:** 1–15.

Krajniak, K. G. 1991. The identification and structure-activity relations of a cardioactive FMRFamide-related peptide from the blue crab *Callinectes sapidus*. *Peptides* **12:** 1295–1302.

Kravitz, E. A., L. Kobierski, B. A. Trimmer, and M. F. Goy. 1987. Peptide F1: a myoactive lobster peptide related to FMRFamide. *Soc. Neurosci. Abstr.* **13:** 1257.

Lesser, W., and M. J. Greenberg. 1993. Cardiac regulation by endogenous small cardioactive peptides and FMRFamide-related peptides in the snail *Helix aspersa*. *J. Exp. Biol* **178:** 205–230.

Marder, E., R. L. Calabrese, M. P. Nusbaum, and B. Trimmer. 1987. Distribution and partial characterization of FMRFamide-like peptides in the stomatogastric nervous systems of the rock crab *Cancer borealis*, and the spiny lobster *Panulirus interruptus*. *J Comp. Neurol* **259:** 150–163.

McGaw, I. J., C. N. Airriess, and B. R. McMahon. 1994a. Peptidergic modulation of cardiovascular dynamics in the Dungeness crab *Cancer magister*. *J. Comp Physiol B.* **164:** 103–111.

McGaw, I. J., C. N. Airriess, and B. R. McMahon. 1994b. Patterns of hemolymph flow variation in decapod crustaceans. *Mar Biol* **121:** 53–60.

McLaughlin, P. A. 1983. Internal anatomy. Pp. 1–41 in *The Biology of Crustacea*, Vol 5, L. H. Mantel, ed. Academic Press, New York.

McMahon, B. R., and C. L. Reiber. 1991. Peptidergic modulation of hemolymph flow in the lobster *Homarus americanus*. *FASEB J* **5(6):** 3390A.

Mercier, A. J., and R. T. Russenes. 1992. Modulation of crayfish hearts by FMRFamide-related peptides. *Biol. Bull.* **182:** 333–340.

Mercier, A. J., I. Orchard, and V. TeBrugge. 1991. FMRFamide-like immunoreactivity in the crayfish nervous system. *J Exp. Biol* **156:** 519–538.

Morris, S., and B. R. McMahon. 1989. Neurohumor effects on crustacean haemocyanin oxygen affinity. *J Exp. Zool.* **249:** 334–337.

Painter, S. D., and M. J. Greenberg. 1982. A survey of responses of bivalve hearts to the molluscan neuropeptide FMRFamide and to 5-hydroxytryptamine. *Biol. Bull.* **162:** 311–332.

Pasztor, V. M., and L. B. Golas. 1993. The modulatory effects of serotonin, neuropeptide F1 and proctolin on the receptor muscles of the lobster abdominal stretch receptor and their exoskeletal muscle homologues. *J Exp. Biol* **174:** 363–374.

Pearson, J. 1908. Cancer. *Liverpool Mar. Biol. Comm. Mem.* **16:** 1–209.

Potvin, C., M. J. Lechowicz, and S. Tardif. 1990. The statistical analysis of ecophysiological responses curves obtained from experiments involving related measures. *Ecology* **71:** 1389–1400.

Price, D. A., and M. J. Greenberg. 1977. Purification and characterization of a cardioexcitatory neuropeptide from the central ganglia of a bivalve mollusc. *Prep Biochem.* **7:** 261–281.

Price, D. A., and M. J. Greenberg. 1989. The hunting of the FaRPs: the distribution of FMRFamide-related peptides. *Biol. Bull.* **177:** 198–205.

Price, D. A., W. Lesser, T. D. Lee, K. E. Doble, and M. J. Greenberg. 1990. Seven FMRFamide-related and two SCP-related cardioactive peptides from Helix. *J. Exp. Biol.* **154:** 421–437.

Raffa, R. B. 1988. The action of FMRFamide (Phe-Met-Arg-Phe-NH_2) and related peptides on mammals. *Peptides* **9:** 915–922.

Trimmer, B. A., L. A. Kobierski, and E. A. Kravitz. 1987. Purification and characterization of FMRFamide-like immunoreactive substances from the lobster nervous system: isolation and sequence analysis of two closely related peptides. *J Comp. Neurol.* **266:** 16–26.

Weimann, J. M., E. Marder, B. Evans, and R. L. Calabrese. 1993. The effects of SDRNFLFRamide and TNRNFLFRamide on the motor patterns of the stomatogastric ganglion of the crab *Cancer borealis*. *J Exp. Biol* **181:** 1–26.

Wilkens, J. L., and B. R. McMahon. 1992. Intrinsic properties and extrinsic neurohormonal control of crab cardiac hemodynamics. *Experientia* **48:** 827–833.

Zar, J. H. 1984. *Biostatistical Analysis* Prentice-Hall, Englewood Cliffs, NJ.

Reference: *Biol. Bull.* **188:** 197–209. (April, 1995)

The Functional Morphology of Starfish Tube Feet: The Role of a Crossed-Fiber Helical Array in Movement

R. SKYLER McCURLEY AND WILLIAM M. KIER[1]

Department of Biology, CB#3280 Coker Hall, University of North Carolina, Chapel Hill, North Carolina 27599-3280

Abstract. The morphology and mechanics of the tube feet, ampullae, and lateral and radial canals of the water vascular systems of *Luidia clathrata* and *Astropecten articulatus* (Echinodermata, Asteroidea) were analyzed. Histological methods, based on embedding in both paraffin and glycol methacrylate, were used to document the arrangement of muscle and connective tissue. The tube foot wall includes longitudinal muscles and connective tissue fibers, the latter arranged in a crossed-fiber helical array, with a fiber angle of about 67° in elongated tube feet. No evidence was found for the circular rings of connective tissue reported in earlier studies; the appearance of rings is probably an artifact of folding. The ampullae are bilobed and include circumferentially arranged muscle fibers and connective tissue fibers aligned 90° to the muscle. The lateral canals are short and equipped with one-way flap valves similar to those described for other echinoderms. The radial canal is thin-walled, nonmuscular, and enclosed in the connective tissue and ossicles of the ambulacrum. Frame-by-frame video analysis of both intact animals and animals with "windows" cut in the arm wall was used to document the movements of the tube feet and ampullae. No evidence was found for the previously suggested role of the radial canal in protracting the tube feet. The ampullae protract the tube feet and antagonize the tube foot musculature. The fiber angle of the connective tissue allows protraction and prevents dilation of the tube feet, and limits elongation of the ampullae.

Introduction

The water vascular system of asteroids serves crucial roles in locomotion, food handling, respiration and, in many species, burrowing. The major components of the system are the circumoral ring canal, the radial canals extending from the ring canal down each arm, and the tube feet with their associated ampullae that are connected to the radial canal by the lateral canals. Studies of the tube feet and associated ampullae in asteroids have included analyses of general morphology and function (Mangold, 1908; Hamilton, 1921; Paine, 1926, 1929; Smith, 1937, 1946, 1947; Kerkut, 1953; Heddle, 1967; Nichols, 1966, 1969, 1972), of innervation and neuromuscular control (Smith, 1945, 1950a, b; Bargmann *et al.*, 1962; Cobb, 1967, 1970, 1987; Cobb and Laverack, 1967; Cavey and Wood, 1981), of ultrastructure (Souza Santos and Silva Sasso, 1968, 1970; Dolder, 1972; Engster and Brown, 1972; Wood and Cavey, 1981), and of permeability and maintenance of fluid volume (Binyon, 1962, 1964; Prusch and Whoriskey, 1976; Prusch, 1977; Ferguson, 1990a, b). Although the tube foot–ampulla complex of asteroids has been well studied, two crucial aspects of its function have not been completely resolved. The first concerns connective tissue fiber reinforcement of the walls of the complex, and the second concerns the role of the radial canal in tube foot movements.

The production of force and movement in these appendages depends on a hydraulic mechanism in which contraction of muscle displaces water vascular fluid from one portion of the system to another. In most hydrostatic skeletal support systems that rely on such a mechanism, the walls of the hydraulic appendage or body are reinforced with connective tissue fibers arranged in a specific pattern, referred to as a 'crossed-fiber helical array' (for reviews, see Chapman, 1958; Clark, 1967; Trueman, 1975; Wainwright *et al.*, 1976; Alexander, 1983). In such a system, sheets of connective tissue fibers wrap the structure in regular arrays of right- and left-hand helices. The reinforcement provided by the fibers allows shape change

---

Received 13 May 1994; accepted 10 January 1995.

[1] To whom correspondence should be sent.

and bending and prevents torsion. Although crossed-fiber helical arrays of connective tissue fibers in the walls of the tube feet of ophiuroids have been described and analyzed (Woodley, 1967, 1980), previous studies of the tube feet of asteroids do not describe crossed-fiber helical reinforcement of the tube foot walls. Instead, the connective tissue reinforcement has been reported as consisting of circular rings (Smith, 1946, 1947). The present study was therefore undertaken to reexamine the connective tissue and muscle in the tube feet of two asteroid species, *Luidea clathrata* and *Astropecten articulatus*. Our analysis has revealed crossed-fiber helical connective tissue reinforcement of the tube foot wall, as in other hydraulic systems.

Many of the previous studies cited above have emphasized the interdependence of the tube foot and ampulla in movement; *i.e.*, extension of the tube foot results from contraction of the ampulla, and distension of the ampulla results from contraction of the tube foot. However, recent reviews (Nichols, 1969, 1972) of tube foot functional morphology describe the radial canal in asteroids (species not specified) as being directly involved in extending the tube feet and being capable of accommodating water vascular fluid from contracted tube feet. Indeed, Lawrence (1987, citing Nichols, 1972) describes the radial canal as being responsible for most of the elongation of the tube feet in asteroids. But in the species analyzed in the present study, the radial canal is unlikely to serve in these roles.

Materials and Methods

Experimental animals

Specimens of the grey sea star, *Luidia clathrata*, and the margined sea star, *Astropecten articulatus*, were supplied by Gulf Specimen Supply, Inc., Panacea, Florida. They were maintained in a recirculating artificial seawater system in the Department of Biology, University of North Carolina, Chapel Hill.

Histology

Segments of the arms of *L. clathrata* and *A. articulatus* were removed from specimens that had been anesthetized with a 1:1 mixture of 7.5% $MgCl_2 \cdot 6H_2O$ and seawater (Messenger *et al.*, 1985). The tissue was fixed in 10% formalin in seawater for 24 h. The tissue was then decalcified in a solution of 0.7 g/l ethylenediaminetetraacetic acid, tetrasodium; 8 mg/l sodium potassium tartrate; 99.2 ml/l hydrochloric acid; 0.14 g/l sodium tartrate (S/P Decalcifying Solution, Baxter Scientific Products, McGaw Park, IL) and then washed in water for 2 h. The fixed and decalcified arm tissue was cut into segments that included three to four pairs of tube feet, and these tissue blocks were embedded in paraffin (*L. clathrata* and *A. articulatus*) or glycol methacrylate plastic (*L. clathrata*).

For paraffin embedding, the fixed, decalcified tissues were dehydrated in ethanol, cleared in Histo-Clear (National Diagnostics, Manville, NJ), and embedded in Paraplast Plus (MP 56°C) (Monoject Scientific, St. Louis, MO). The blocks were then serially sectioned on a rotary microtome at 10 μm in three mutually perpendicular planes. The sections were stained with picro-ponceau with Weigert iron hematoxylin (see Kier, 1992). For glycol methacrylate embedding, the fixed and decalcified tissues were partially dehydrated in an ethanol series to 95% ethanol and then infiltrated with unpolymerized glycol methacrylate plastic (Reichert-Jung Historesin, Leica Instruments GmbH, Heidelberg, Germany). Following polymerization, the blocks were sectioned at 0.5–3.0 μm with glass knives. The sections were stained with Lee's methylene blue–basic fuchsin stain (Bennett *et al.*, 1976) and were examined with brightfield, phase contrast, and polarized light microscopy.

In addition to the sectioned material, whole mounts were also examined with brightfield, phase contrast, and polarized light microscopy. Tube feet and ampullae were dissected from fixed and decalcified arm tissue and were partially macerated in 1.0 *M* potassium hydroxide and 50% glycerine for 2–3 days (Woodley, 1967). The epidermis was removed from the tube feet, and whole mounts of the tube feet and ampullae were prepared.

Computer-assisted three-dimensional reconstruction

The morphology of the valve located between the tube foot–ampulla complex and the radial canal was examined with the aid of a computer program for three-dimensional reconstruction (PC3D, Jandel Scientific, Corte Madera, CA). Parasagittal sections (defined here as vertical planes parallel to the long axis of the arm) and frontal sections (defined here as horizontal planes) were used for the reconstructions of *L. clathrata* tissues. A microscope equipped with a camera lucida was used to trace, from sections, the outline of the internal and external surface of the tube foot, the profile of the valve tissue, and the position of the valve muscle fibers. The tracings were aligned according to the visual best-fit method (Gaunt and Gaunt, 1978; Young *et al.*, 1985) and digitized with a Numonics 2210 digitizing tablet. The PC3D software stacked the tracings of the internal structures to produce a three-dimensional image that could be viewed in any orientation with a Gateway 2000 4DX2-66V microcomputer. The reconstructions were plotted with a Hewlett-Packard HP 7475A plotter.

Video recordings

Locomotion and feeding movements of *L. clathrata* in a glass-bottom aquarium were videotaped from the side and from below with a Panasonic AG-450 S-VHS camera–

recorder. In addition, movements of the tube feet during burrowing were recorded by placing the animals in the aquarium, but with a thin layer of sand on the bottom, and filming from below. The movements were analyzed frame by frame with a Panasonic AG-1960 videocassette recorder.

Direct observations of ampullae

Under anesthesia, the distal portion of an arm and a portion of the dorsal body wall of *L. clathrata* were removed. After such an operation, the animals appear to behave normally. Movements of the ampullae and their associated tube feet were observed directly, both during normal movement of the animal and in response to manual mechanical stimulation of individual tube feet with a dissecting probe.

Results

Morphology of the tube foot–ampulla complex

This study focuses on the components of the water vascular system associated with the radial canal: the tube feet, ampullae, and lateral canals (see Fig. 1). The following morphological description is based on *L. clathrata*. Any observed differences between *Luidia* and *Astropecten* are noted below.

Tube feet. The tube feet project from the ambulacral groove on the ventral surface of the arm; they are cylindrical and have conical ends. Each arm has more than 100 tube feet arranged in pairs along the length of the arm, thus constituting two parallel rows, one on either side of the ambulacral groove. Most of the tube foot is external to the body wall (Fig. 2).

The tube foot epithelium is covered by a thin cuticle continuous with that covering adjacent areas of the ambulacrum (See Engster and Brown, 1972, for details). The appearance of the epithelium in sectioned histological material depends on the state of elongation or contraction of the tube foot. In retracted tube feet, the epithelium is thick and the epithelial surface is highly folded into annular rings (Fig. 3). In protracted tube feet, the epithelium appears thinner and the folding is reduced. The epithelium of the distal conical end appears to be secretory; it consists of tall columnar epithelial cells with intensely staining cell inclusions (Fig. 3).

Underlying the epithelium is a layer of nervous tissue, similar in disposition to the basiepithelial (ectoneural) plexus described previously in other echinoderms (see Smith, 1937; Coleman, 1969; Raymond, 1979). Underlying the nervous tissue layer is a dense layer of fibrous connective tissue. Fibers in this layer show staining reactions typical of collagen and are highly birefringent when viewed with polarized light microscopy. Grazing sections through the connective tissue layer show that it is composed of connective tissue fibers arranged as a crossed-fiber helical array (Fig. 4). Such an array consists of connective tissue fibers that wrap the tube foot in both left- and right-hand helices. The fiber angle, defined as the angle that the connective tissue fibers make with the long axis of the tube foot, was measured in whole mounts and in grazing sections of protracted tube feet; the angle is about 67° and is relatively constant along the length of the tube foot. In retracted tube feet, the crossed-fiber helical connective tissue layer becomes somewhat folded, and grazing sections may then sometimes give the misleading impression that this layer consists of circumferential rings of connective tissue. Because the fibers are highly birefringent, their arrangement as a crossed-fiber helical array is more easily observed with polarized light microscopy (Fig. 4). The whole-mount preparations were also useful in visualizing the disposition of the connective tissue fibers.

Internal to the crossed-fiber helical connective tissue layer is a robust layer of muscle fibers (see Dolder, 1972, for details) (Figs. 2, 3, 4). The fibers are arranged longitudinally, parallel to the long axis of the tube foot. No striations were observed in the muscle cells. The internal lumen of the tube foot is lined with epithelium (see Wood and Cavey, 1981, for details).

1

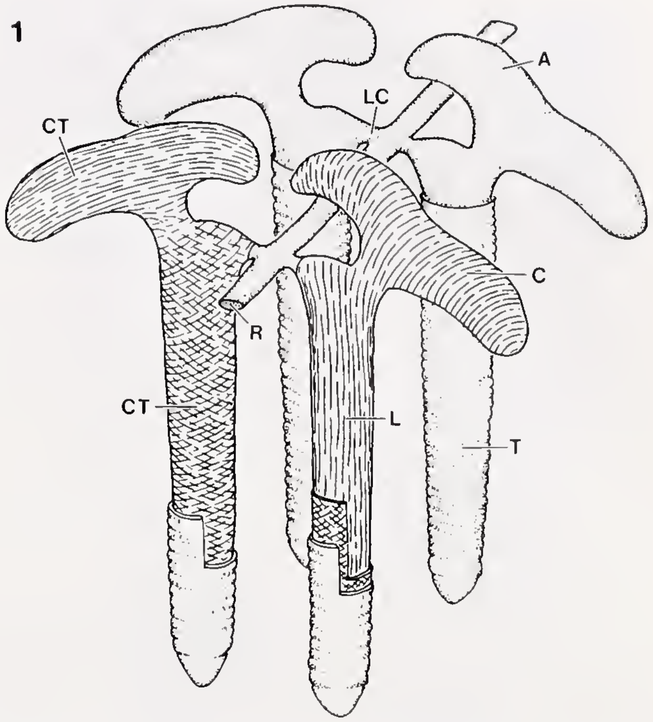

Figure 1. Schematic cutaway drawing of the arrangement of the tube feet (T), ampullae (A), and the lateral (LC) and radial canals (R), showing the trajectories of the connective tissue fibers (CT), longitudinal muscle (L) of the tube feet, and circular muscle (C) of the ampullae.

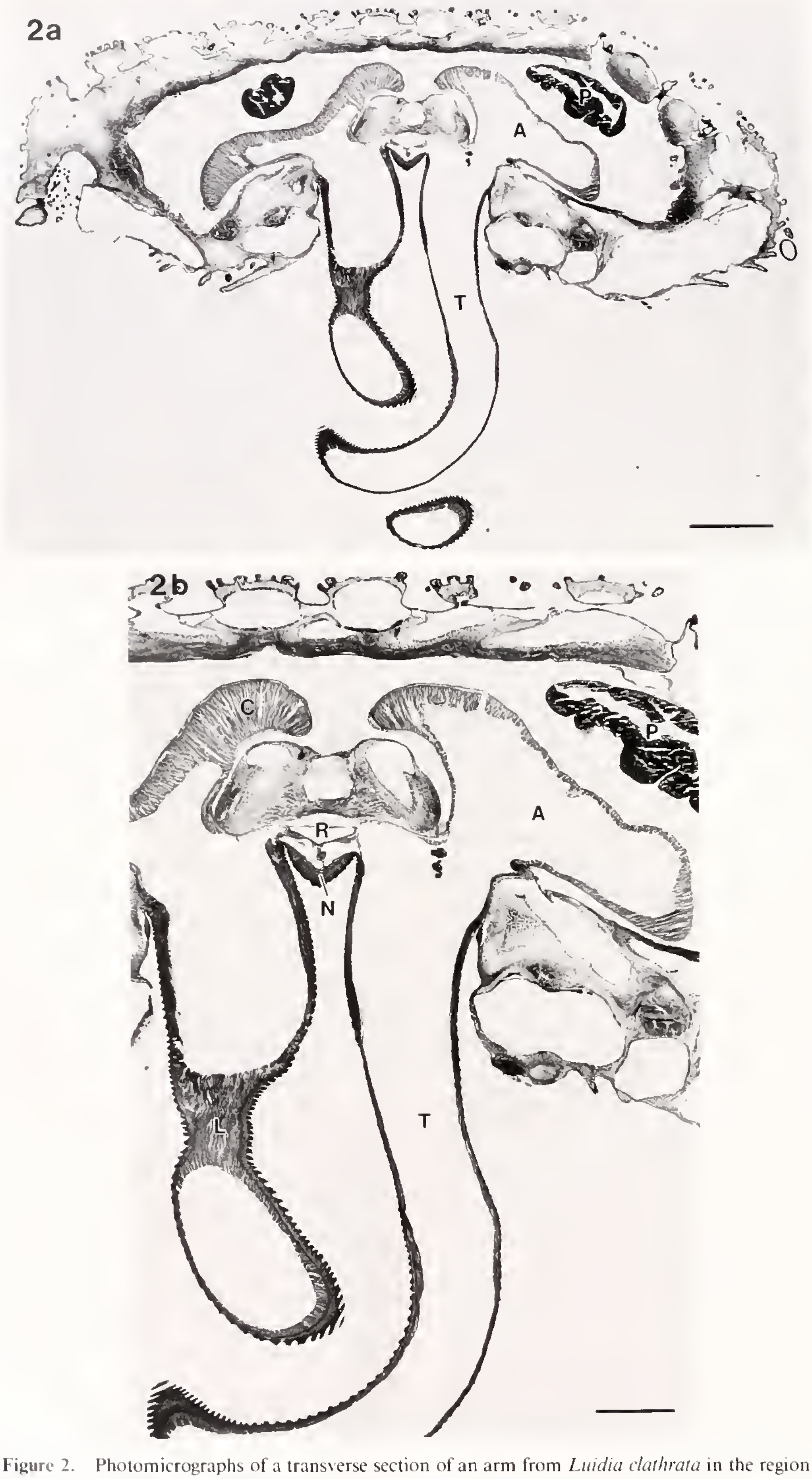

Figure 2. Photomicrographs of a transverse section of an arm from *Luidia clathrata* in the region of a pair of tube feet (T) and their associated bilobed ampullae (A). A 10-μm-thick paraffin section stained with picro-ponceau and iron hematoxylin was photographed with brightfield illumination. (a) Low power view showing relative proportions of the arm and tube foot–ampulla complex. The section includes a portion of the pyloric cecum (P) on each side of the arm. Scale bar, 1 mm. (b) Higher power view showing the radial canal (R) located dorsal to the radial nerve cord (N). The epithelium on the roof of the radial canal has

Ampullae. Located within the coelomic cavity of the arm are the bulbous ampullae. In both *L. clathrata* and *A. articulatus* the ampullae are bilobed, one lobe extending laterally from the union with the tube foot and the other extending medially (Figs. 2, 5). Each lobe is elongate, cylindrical, and curved toward the oral surface. In *L. clathrata*, the lateral lobe is longer than the medial lobe, whereas in *A. articulatus* the medial lobe is the longer. The long axes of the two lobes are roughly parallel and in the same plane, and so form what is essentially a single cylindrical tube more or less perpendicular to the long axes of both the tube foot and the arm. The connection between the tube feet and the ampullae is made by a slightly narrowed neck that is displaced laterally relative to the axis of the tube foot (Figs. 2, 5). Two bands of tissue, which Smith (1950b) named 'seams' (see also Cobb, 1967; Cobb and Laverack, 1967), run dorsoventrally in the ampullar neck: one seam occupies a medial position on the portion of the neck closest to the central axis of the arm, and the other is located laterally on the opposite side of the ampullar neck (Fig. 5). The tube foot and ampullar wall are continuous through the neck region.

A layer of epithelium covers the outer surface of the ampulla (*i.e.*, the surface exposed to the coelomic cavity of the arm). Beneath the epithelium is the ectoneural nervous tissue layer. Beneath the nervous tissue layer is a thin layer of dense, fibrous, birefringent connective tissue that shows staining reactions typical of collagen. The connective tissue fibers of this layer are closely packed and aligned in parallel. Grazing sections show the fibers to be oriented parallel to the long axis of the ampulla (Fig. 6). Underneath the dense connective tissue sheet is a robust layer of muscle fibers. The muscle fibers are arranged in circumferential bands around the lumen of the ampullae in planes perpendicular to the long axis of the ampulla. Thus, the muscle cells are arranged at right angles to the connective tissue fibers of the dense connective tissue layer. No striations were observed in the muscle cells. The lumen of the ampulla is lined with a simple epithelium.

Lateral canal and valve. Short lateral canals extend from each side of the radial canal to connect to each tube foot along the length of the arm (Fig. 7). The internal lumen of the lateral canals is lined with a simple squamous epithelium that appears to be continuous with that of the tube foot and the radial canal. The canals are wrapped by fibrous birefringent connective tissue continuous with the connective tissue that surrounds the arm ossicles and forms the structure of the arm.

3

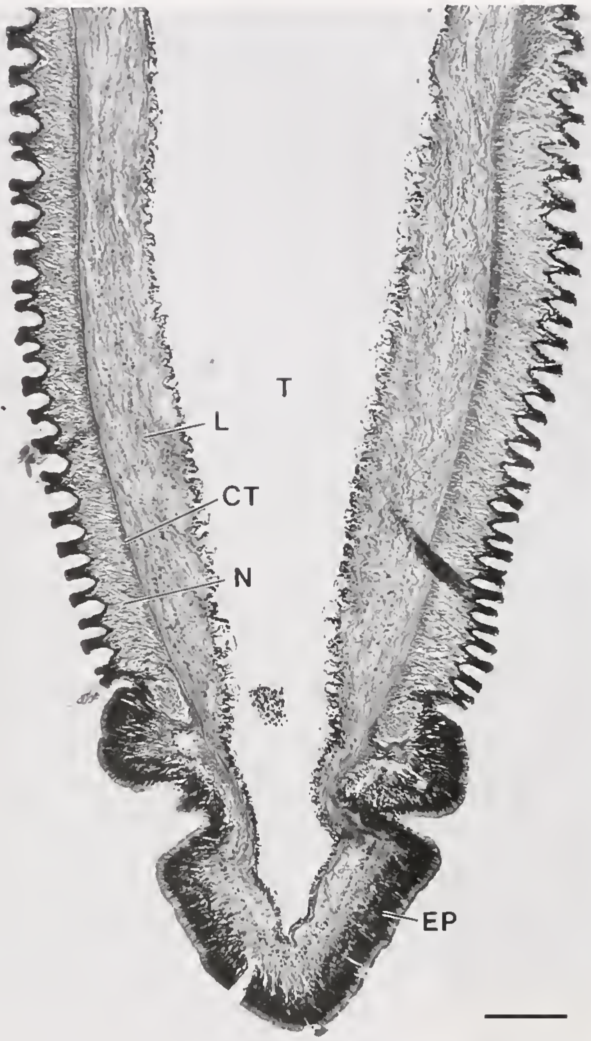

Figure 3. Photomicrograph of a longitudinal section of an individual tube foot (T) from *Luidia clathrata*. The epithelium (EP) of the tip includes tall columnar cells. Folding of the epithelium on the sides of the foot is visible. Underlying the epithelium is a layer of nervous tissue (N), and underneath this is the crossed-fiber helical connective tissue layer (CT). Longitudinal muscle (L) is visible under the connective tissue layer and is separated from the tube foot lumen (T) by a thin epithelium. Scale bar, 100 μm. A 10-μm-thick paraffin section stained with picroponceau and iron hematoxylin was photographed under brightfield illumination.

The lateral canal joins the tube foot wall at the top of the tube foot. A pair of flaps are present on either side of the opening of the lateral canal into the tube foot, forming a valve (Figs. 7, 8). The flaps are parallel to one another

---

pulled away from the ambulacral connective tissue; glycol methacrylate sections (see Fig. 9) show the epithelium to be attached to the ambulacral connective tissue. The longitudinal muscle (L) of the tube foot (T) and the circumferential muscle (C) of the ampulla (A) are also visible. A portion of a pyloric cecum (P) is visible. Scale bar, 0.5 mm.

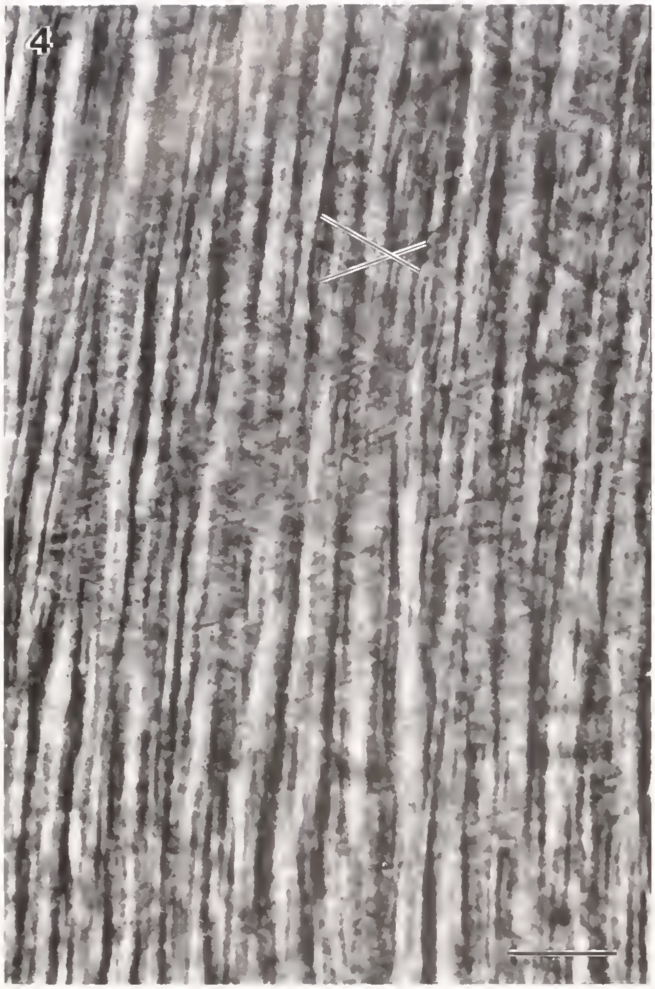

Figure 4. Photomicrograph, taken under polarized light, of a partially macerated portion of a tube foot wall from *Luidia clathrata*. The long axis of the tube foot is oriented vertically. The crossed lines indicate the approximate trajectories of the crossed-fiber helical connective tissue array. The longitudinal muscles of the tube foot wall are oriented vertically in the photomicrograph and can be seen behind the crossed fibers. Scale bar, 25 μm.

and extend down from the roof of the tube foot and laterally from the medial wall of the tube foot on either side of the opening of the lateral canal into the tube foot. Muscle fibers originate on the tube foot roof and wall and insert on the side of the flap opposite to that facing the opening of the lateral canal (Figs. 7, 8). The trajectory of these muscle fibers is such that their contraction pulls the two flaps away from one another, opening the connection between the lateral canal and the tube foot. The flaps consist of a thin sheet of connective tissue covered by a simple squamous epithelium that appears to be continuous with the epithelium of the tube foot and lateral canal. On either side of the valve, the roof of the tube foot is slightly domed.

Radial canal. The radial canal is adjacent to the ventral surface of the arm and extends from the ring canal to the tips of the arms. It is encased in the connective tissue and calcite ossicles of the ambulacrum and is dorsoventrally flattened in cross section (Fig. 9). The radial canal is lined with a simple squamous epithelium, lacks musculature, and is surrounded by connective tissue. The connective tissue is continuous with that surrounding the calcite ossicles of the ambulacrum. No valves or sphincter muscles were observed along its length. The floor of the radial canal is raised as a transverse ridge midway between each pair of tube feet along the length of the arm. The ridges are formed by a bundle of connective tissue and muscle fibers, called 'transverse ambulacral muscles' (Hyman, 1955), that connect ambulacral ossicles on opposite sides of the arm.

Tube feet and ampullae kinematics

Two general categories of movement were observed in the tube feet: length change and bending. As for length change, the tube feet of a large *L. clathrata* (arm length = 9 cm) are about 12 mm long when fully protracted and 2 mm when retracted. During such a retraction, the diameter of the tube foot, measured midway between the base and tip, increases from 0.9 to 1.3 mm. The tube foot wall is opaque, white, and thrown into a series of closely spaced annular folds when retracted. When protracted, the folding is reduced, and the tube foot wall becomes translucent.

The tube feet may bend either in combination with change in length or at constant length, and in virtually any direction relative to the axis of the arm. Both localized and general bending movements were observed. Localized bending typically occurs at the base, while the remainder of the tube foot remains essentially straight and thus pivots about the base. General bending occurs along the entire length of a tube foot, sometimes causing the tip of the tube foot to be oriented at 90° to the base.

During locomotion, the tube feet undergo repeated, stereotyped stepping cycles. An individual tube foot first elongates and bends at the base so that the tip of the foot points in the direction of motion. Once the tube foot is fully protracted, it bends downward until the tip contacts and attaches to the substratum. The tube foot then bends at its base and moves the animal over the point of attachment. In the final phase of the cycle, the tube foot releases its attachment and retracts. The cycle is then repeated. The tube feet do not move synchronously but are coordinated so that those on different arms create movement in a single direction. *L. clathrata* may reach speeds of 2 cm/s when moving across the surface of a crushed oyster shell substratum.

Tube foot movements during burrowing involve bending away from the ambulacrum toward the sides of the

5

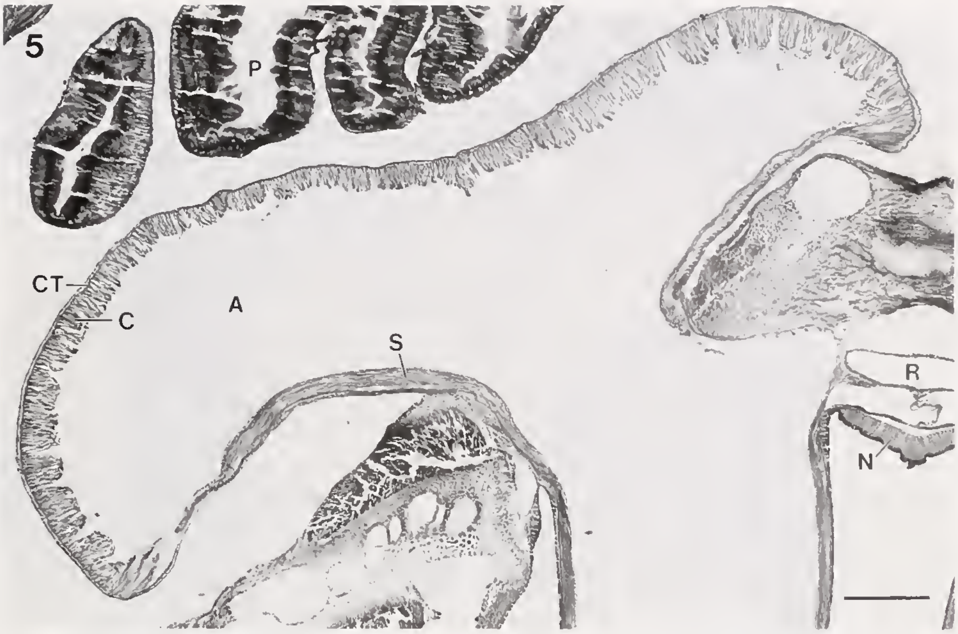

Figure 5. Photomicrograph of a transverse section of an arm from *Luidia clathrata* showing the bilobed ampulla. A thin connective tissue layer (CT) surrounds the circumferential muscles (C) of the ampulla (A). The ampullar seam (S) is visible. Also included are the radial canal (R), radial nerve (N), and a portion of a pyloric cecum (P). Scale bar, 0.25 mm. A 10-μm-thick paraffin section stained with picro-ponceau and iron hematoxylin was photographed under brightfield illumination.

6

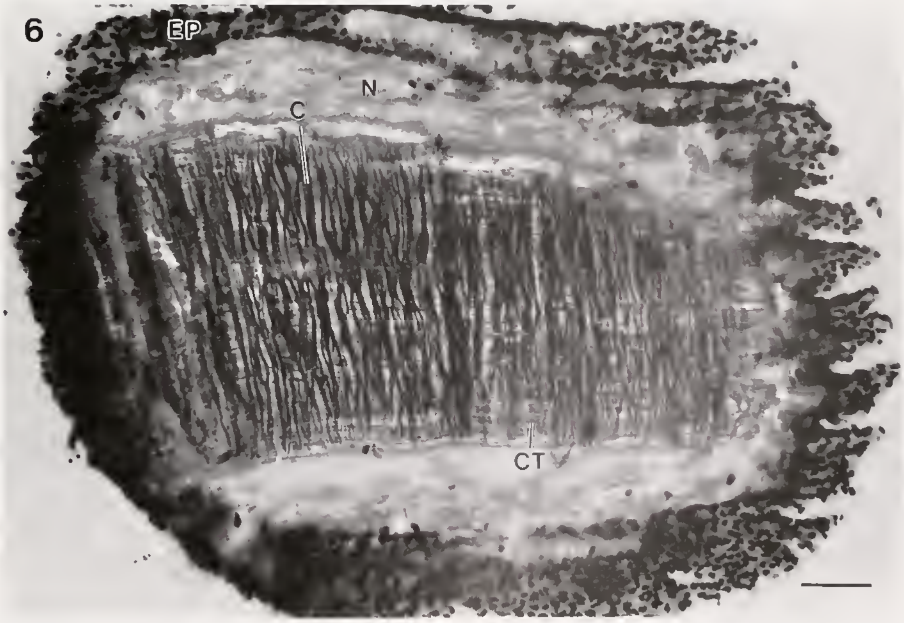

Figure 6. Photomicrograph, taken under polarized light, of a grazing section of an ampulla from *Luidia clathrata*. The long axis of the ampulla is oriented horizontally. The tenuous fibers in the connective tissue layer (CT) are also horizontally disposed, *i.e.*, parallel to the long axis of the ampulla. The robust, vertically oriented circumferential muscle fibers (C) lie underneath the connective tissue layer. The epithelium (EP) and ectoneural nervous tissue layer (N) are also visible. Scale bar, 25 μm. A 10-μm-thick paraffin section stained with picro-ponceau and iron hematoxylin was photographed under polarized light.

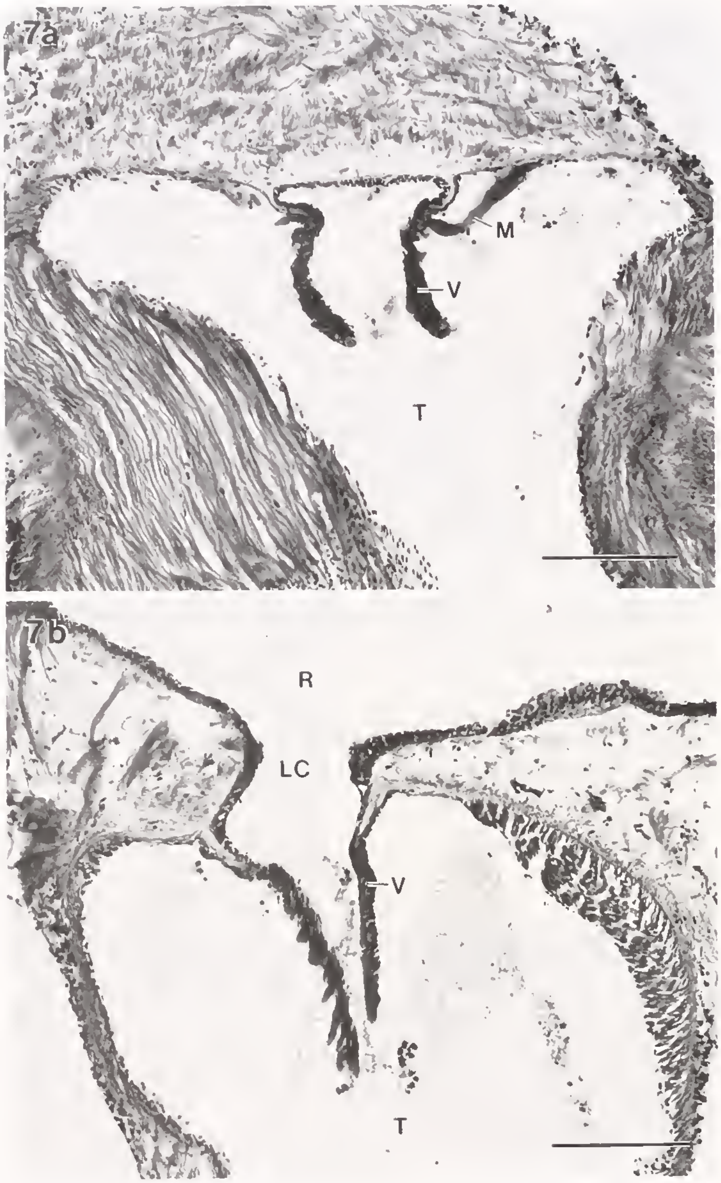

Figure 7. (Top) Photomicrograph of a parasagittal section (vertical section parallel to long axis of the arm) of the arm of *Luidia clathrata* showing the valve at the entrance to the lateral canal. The valve flaps (V) project down from the roof of the tube foot into the tube foot lumen (T). Muscle fibers (M) originate on the roof of the tube foot and insert on the valve flaps. Scale bar, 100 μm. A 10-μm-thick paraffin section stained with picro-ponceau and iron hematoxylin was photographed under brightfield illumination. (Bottom) Photomicrograph of a frontal section of the arm of *Luidia clathrata* showing details of the valve structure. The lateral canal (LC) extends from the radial canal (R) which is oriented horizontally in the figure. The valve flaps (V) project into the tube foot lumen (T) on either side of the entrance of the lateral canal. Scale bar, 100 μm. A 10-μm-thick paraffin section stained with picro-ponceau and iron hematoxylin was photographed under brightfield illumination.

arm. As in locomotion, the burrowing movements of the tube feet are stereotyped and cyclical. An individual tube foot is first protracted downward from the ambulacrum into the sediment. Next, the tube foot bends laterally, sweeping sediment from under the arm. The bending during this phase occurs both at the base of the tube foot and along its entire length. The tube foot then retracts and bends back toward the ambulacrum to repeat the cycle.

The tube feet are also involved in conveying food down the length of the ambulacral groove to the mouth. As a particle of food approaches a given tube foot, it bends

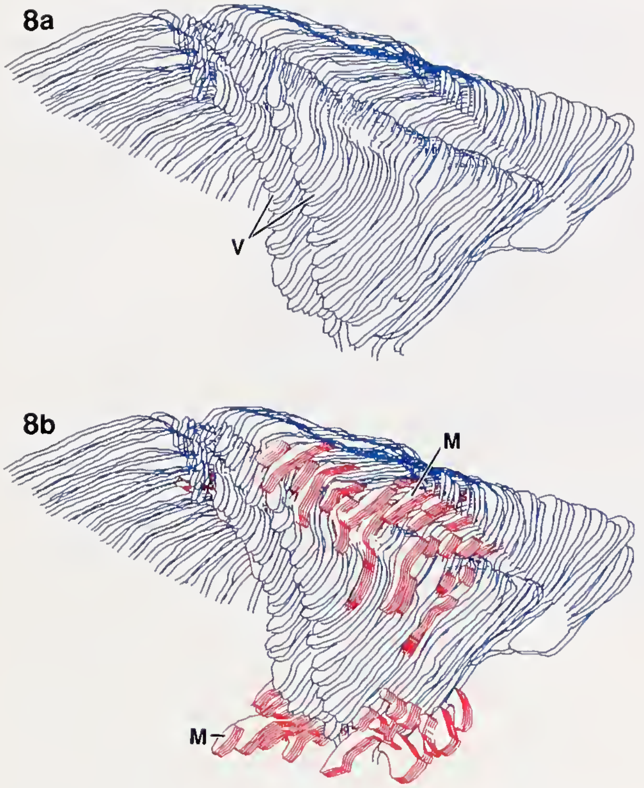

Figure 8. Computer-assisted three-dimensional reconstructions showing the morphology of the valve and valve muscles at the entrance to the lateral canal. Scale bar, 100 μm. (a) Reconstruction showing valve flaps (V) projecting down into the tube foot lumen from the tube foot roof. The flaps are longer adjacent to the wall of the tube foot (not shown, right side of figure) and become shorter as they extend away from the wall along the roof. The opening to the lateral canal is located between the flaps and is thus hidden from view. (b) Reconstruction showing locations of valve muscles (M). Muscles originate on the tube foot roof and insert on the sides of the valve flaps. Additional muscles originate on the tube foot wall and insert near the free edges of the valve flaps.

toward the particle and protracts until the tip adheres to the food. Once attached, the tube foot retracts, pulling the food toward the mouth. At the same time, neighboring tube feet bend toward the food, adhere, and contract. The particle may move beyond the location of a given tube foot while it is still attached, and thus the tube foot elongates further. Whether this elongation involves active protraction by the individual tube foot or passive elongation due to the contraction of neighboring tube feet attached to the same particle remains unclear. The final steps in the cycle are release of the attachment of the tube foot to the particle, and retraction.

The experiments in which the distal portion of the arm and part of the dorsal body wall of *L. clathrata* were removed show that contraction of an ampulla occurs during protraction of its associated tube foot and *vice versa.* Elongation of the tube foot appears to occur only when its associated ampulla decreases in volume, and expansion of an ampulla occurs only when its associated tube foot contracts. There was no evidence of elongation of the tube feet without contraction of their associated ampullae.

Discussion

Basic tube foot mechanics

The functioning of the tube foot–ampulla complex of *L. clathrata* and *A. articulatus* relies on a hydraulic mechanism similar to that proposed originally by Smith (1945, 1946, 1950a). As described by Kier (1988), in hydraulic systems, force transmission for movement and muscular antagonism results from localized muscle contraction that displaces fluid from one portion of the system to another. The functioning of this system relies on the incompressibility of the hydraulic fluid—in this case the water vascular fluid. Because the fluid is an aqueous liquid and no gas-filled spaces are present, a decrease in volume in one portion of the system results in an increase in volume in another rather than in compression of the fluid.

Tube foot elongation. Elongation of a tube foot is caused by a decrease in volume of its associated ampulla. The musculature of the bilobed ampulla is arranged circumferentially in the ampulla wall. Upon contraction, the muscle decreases the volume of the lumen, displacing water vascular fluid from the lumen into the tube foot. The connective tissue of the ampullar wall plays a crucial role in controlling the shape change of the ampulla (see below). Contraction of the ampullar musculature creates a pressure difference between the lumen of the tube foot and the lumen of the lateral canal. Because the flaps of the valve at the entrance of the lateral canal protrude into the tube foot, the difference in pressure closes the valve, preventing water vascular fluid in the tube foot from backing into the lateral and radial canals. The tube foot is therefore inflated by the fluid displaced from the ampulla, and this increase in volume causes elongation of the tube foot. As in the ampulla, the connective tissue fibers of the tube foot wall play a crucial role in controlling shape change during tube foot elongation (see below). When the tube foot elongates, its longitudinal muscle is extended.

Tube foot shortening. This is caused by contraction of the longitudinal muscle of the tube foot wall. When the tube foot shortens, its volume decreases, and water vascular fluid moves into the ampulla, which expands. Again, the valve at the entrance to the lateral canal closes, preventing fluid from leaking into the water vascular canals, as described above. The increase in fluid volume that expands the ampulla also reextends the circumferential muscle of the ampulla. Thus the circumferential muscle of the ampulla and the longitudinal muscle of the tube foot function as antagonists during length change in the tube foot.

9

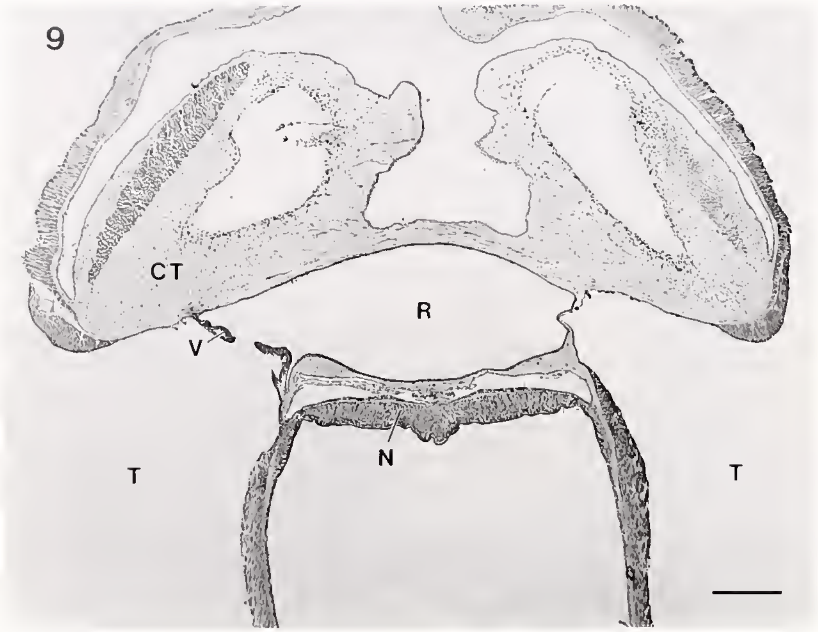

Figure 9. Photomicrograph of a transverse section of the radial canal (R) of *Luidia clathrata*. The connective tissue (CT) of the ambulacrum surrounds the radial canal. No muscle fibers encircle the radial canal. The section is slightly oblique and includes a portion of the valve (V) on the left side of the figure. The radial nerve (N) is located in the center, between the two tube feet (T). Scale bar, 100 μm. A 1-μm-thick glycol methacrylate section stained with Lee's methylene blue–basic fuchsin and photographed under brightfield illumination.

Tube foot bending. Bending of the tube foot involves the same musculature as that used for elongation and shortening. During bending, however, the longitudinal muscles of the tube feet and the circumferential muscles of the ampullae operate synergistically rather than antagonistically. Bending of a hydrostatic structure requires unilateral longitudinal muscle contraction on the inside radius of the bend. The force of this contraction not only bends the structure, but also tends to decrease its length. For bending without shortening, the longitudinal compressional force must be opposed by a resistance to expansion of the ampulla, which prevents displacement of the fluid from the tube foot. Expansion of the ampulla is resisted by contractile activity of the circumferential muscles. Thus, bending requires simultaneous unilateral longitudinal muscle contraction of the tube foot and circumferential muscle contraction of the ampulla. Generation of a localized rather than a more generalized bend is dependent on the degree to which the pattern of activity of the longitudinal musculature of the tube foot is localized. No morphological subdivision of the longitudinal musculature at the base of the tube foot was observed in the species examined in this study.

The role of the radial canal. There is no evidence in the species studied here that the radial canal plays a role in protraction, as has been suggested previously (*e.g.*, Nichols, 1969, 1972). Nichols (1972) described the radial canal as being highly muscular in modern starfish (species not identified) and capable of receiving fluid from retracted tube feet, and then contracting to distribute the fluid. In the species analyzed in the present study, the radial canal completely lacks musculature. There is no evidence for sphincter muscles or other structures that might allow the radial canal to be partitioned along its length. Further, it is wrapped by the connective tissue and calcite ossicles of the ambulacrum and is thus prevented from expanding. Our results are in agreement with those of Smith (1946) who suggested, on the basis of both direct observation of the tube feet and ampullae and calculations of volume accommodated by the ampullae during tube foot retraction (*Astropecten irregularis, Asterias rubens*), that "little, if any fluid enters or leaves the tube foot ampulla system during these movements" (p. 280). The species examined by Nichols (1972) were not identified, so we can say only that participation by the radial canal in tube foot elongation is not a universal feature of the water vascular system of asteroids.

The role of the connective tissue. The connective tissue fibers observed in both the tube foot and the ampullar wall play a crucial role in the mechanics of the tube foot and the ampulla. Consider first the requirement that an increase in pressure (due to contraction of the ampulla) causes elongation of a tube foot. The stress distribution in a pressurized cylinder is such that the hoop stress (which tends to increase diameter) is twice as large as the longitudinal stress (which tends to increase length) (see Wainwright *et al.*, 1976; Wainwright, 1982; for details). Thus, in a pressurized cylinder lacking fiber reinforcement, the result of increasing pressure is swelling of the diameter of the cylinder, rather than elongation. The crossed-fiber helical array of connective tissue fibers described here reinforces the wall so that an increase in pressure causes an increase in length, rather than diameter. Previous reports (Smith, 1946, 1947) of circular "rings" of connective tissue fibers in the tube foot wall (*Astropecten irregularis, Asterias rubens*) are probably the result of misinterpretations of folding of the connective tissue in the wall of retracted tube feet. No circular rings of connective tissue were seen in any of the material from the species examined in this study.

To understand how fiber reinforcement can control shape change, consider a simple geometrical model derived from those described by Chapman (1958), Clark and Cowey (1958), Cowey (1952), and Woodley (1980). The tube foot can be modeled as a right circular cylinder wrapped by a single turn of an inextensible helical fiber. Because the tube foot is essentially cylindrical and the connective tissue fibers are likely to be collagenous and thus quite stiff in tension, the assumptions of this simple model are reasonable. For a helical fiber of given length, the volume of such a cylinder is a function of the length of the cylinder and the fiber angle (the angle that the fiber makes with the long axis of the cylinder) (Fig. 10). The fiber angle of the helical fiber ranges from 90° (when the cylinder length is at a minimum) to 0° (when the cylinder length is at a maximum). The maximum volume occurs at an intermediate length, when the fiber angle is 54°44′. If the fiber angle of the cylinder is greater than 54°44′, an increase in its volume causes an elongation and a decrease in the fiber angle (see Fig. 10). If the fiber angle is initially less than 54°44′, an increase in volume causes the cylinder to shorten. At an angle of 54°44′, the stiffness in the hoop direction is double the stiffness in the longitudinal direction, and the fibers therefore resist both an increase in length *and* an increase in diameter. The fiber angle of the crossed-fiber helical array thus determines the shape change that results from an increase in volume of the tube foot.

This model predicts that the fiber angle of the connective tissue fibers in the wall of the tube foot must be greater than 54°44′ if the increase in volume due to contraction of the ampulla is to cause elongation. Indeed, a fiber angle of about 67° was measured in the connective tissue fibers of elongated tube feet of *L. clathrata*. Although the fiber angle in retracted tube feet could not be measured or calculated due to the folding of the wall, shortening of the tube foot from the elongated state must increase the fiber angle to greater than 67°.

10

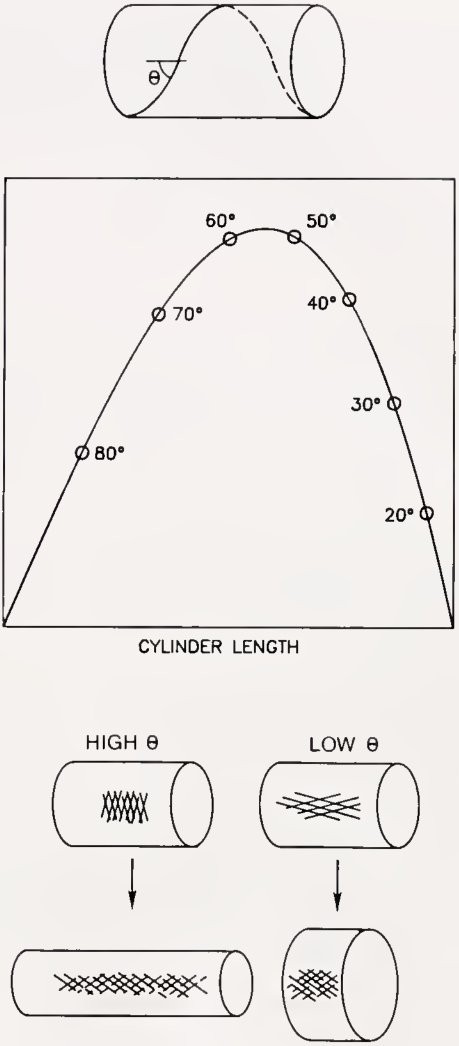

Figure 10. Plot of the length versus volume of a cylinder wrapped by a single inextensible helical fiber. The fiber angle Θ, defined as the angle that the helical fiber makes with the long axis of the cylinder, is diagrammed above the plot and is included parametrically on the plot. The volume is maximal when the fiber angle is 54°44′. Note that increasing the volume of such a cylinder causes an increase in length only when the initial fiber angle is greater than 54°44′ (high Θ in diagram below the plot). If the initial fiber angle is less than 54°44′, increasing the volume decreases the cylinder length (low Θ in diagram below the plot).

The connective tissue fiber reinforcement of the ampullar wall is also functionally important. Contraction of the circumferential musculature of an ampulla increases the pressure of the fluid in the ampulla, generating a stress that tends to elongate the ampulla. Lacking longitudinal muscle fibers (*i.e.*, fibers aligned parallel to the long axis of the ampulla), some other component of the structure must resist this longitudinal stress. The connective tissue fibers of the ampulla are ideally oriented—*i.e.*, parallel to the long axis—and they therefore will resist the longitudinal stress directly. This is a novel example of fiber reinforcement of hydrostatic skeletons; in all other cases, the fibers are in a crossed-fiber helical array (Wainwright *et al.*, 1976; Wainwright, 1982), which allows length change, smooth bending without kinking, and resistance to torsion about the long axis. These are important characteristics of tube feet, but not ampullae, where the most important role of the connective tissue is to resist elongation.

The role of the valve. The valves located at the opening of the lateral canals into the tube feet also have an important function in the water vascular system of asteroids. As described above, the valve flaps are arranged so that an increase in pressure in the tube foot–ampulla complex tends to close the valve, preventing loss of fluid from the tube foot (Märkel and Röser, 1992). Since forceful movement of the tube feet requires significant pressure, fluid is probably lost from the system due to ultrafiltration through the tube foot and ampulla wall (Binyon, 1964, 1984; Prusch and Whorisky, 1976). As a result of active pumping of K^+, the fluid in the water vascular system is hyperosmotic to the surrounding seawater and to the perivisceral (coelomic) fluid (Binyon, 1962, 1964; Prusch and Whorisky, 1976; Prusch, 1977; Ferguson, 1990a). Because the hydrostatic pressure in temporarily inactive tube feet is low, uptake of water probably occurs across the tube foot wall and ampullar wall. Perhaps uptake in one portion of the water vascular system can replenish the fluid lost in others; the valves could open, allowing fluid to flow via the radial canals. Active opening of the valves is likely because, as described above, the flaps are equipped with muscle fibers with appropriate trajectories. In addition, the madreporite may contribute water to the water vascular system and perivisceral coelom (Ferguson, 1989, 1990b). This mechanism would also require that the valves open to allow fluid to flow from the radial canals into the tube foot–ampulla complex. Active opening of the valves by contraction of the valve musculature, allowing water vascular fluid to flow from contracting tube feet into the radial canal, has been described for ophiuroids (Buchanan and Woodley, 1963; Woodley, 1980), asteroids (Nichols, 1972), and for echinoids under extreme conditions (Märkel and Röser, 1992). For the species studied here, our observations (described earlier) suggest that the tube foot–ampulla complex functions as an autonomous unit during normal activity. Significant flow of water vascular fluid in and out of the radial canal during normal movement appears unlikely.

Implications for neural control. The anatomy, function, and coordination of the nervous system of the tube foot–ampulla complex of asteroids has received considerable attention previously (Smith, 1945, 1946, 1950a, 1950b; Cobb, 1967, 1970, 1987; Cavey and Wood, 1981). Several points arising from the analysis of the present study have not been previously considered in discussions of the neural control of the tube foot–ampulla complex. Although bending of the tube foot in any direction was known to require localized control of the musculature of the tube foot, the role of synergistic ampulla muscle contraction in providing the support required for bending was not recognized. These two muscle groups operate sequentially during elongation and retraction, and simultaneously during bending movements, so their neural control is complex.

In addition, complexity of nervous control is also implied by the ability of the tube feet either to bend locally and pivot around the base or to form a more generalized bend along the length of the tube foot. In a study of the innervation of the tube feet and ampullae of *Astropecten irregularis*, Smith (1950b) observed a separate innervation restricted to the muscle at the base of the tube foot (which he referred to as postural muscles), as well as a distinct innervation of the musculature of the tube foot wall (which he called retractor muscles). This pattern of innervation is to be expected if the musculature at the base of the tube foot acts alone to create a localized bending while that of the tube foot wall is responsible for more generalized bending.

Acknowledgments

The authors are grateful to S. Johnsen and K. K. Smith for comments on the manuscript. This research was supported by a National Science Foundation Presidential Young Investigator Award (DCB-8658069) and NSF Research Experiences for Undergraduates Supplement.

Literature Cited

Alexander, R. McN. 1983. *Animal Mechanics.* 2nd ed., Blackwell, Oxford.

Bargmann, W., M. von Harnack, and K. Jacob. 1962. Über den Feinbau des Nervensystems des Seesternes (Asterias rubens L.). I. Mitteilung. Ein Beitrag zur vergleichenden Morphologie der Glia. *Z. Zellforsch. Mikrosk. Anat* **56:** 573–594.

Bennett, H. S., A. D. Wyrick, S. W. Lee, and J. H. McNeil. 1976. Science and art in preparing tissues embedded in plastic for light microscopy, with special reference to glycol methacrylate, glass knives and simple stains. *Stain Technol.* **51:** 71–97.

Binyon, J. 1962. Ionic regulation and mode of adjustment to reduced salinity in the starfish *Asterias rubens* L. *J. Mar. Biol. Assoc. U.K.* **42:** 49–64.

Binyon, J. 1964. On the mode of functioning of the water vascular system of *Asterias rubens* L. *J. Mar. Biol. Assoc. U.K.* **44:** 577–588.

Binyon, J. 1984. A re-appraisal of the fluid loss resulting from the operation of the water vascular system of the starfish, *Asterias rubens*. *J. Mar. Biol. Assoc. U.K.* **64:** 726.

Buchanan, J. B., and J. D. Woodley. 1963. Extension and retraction of the tube feet of ophiuroids. *Nature* **197:** 616–617.

Cavey, M. J., and R. L. Wood. 1981. Specializations for excitation-contraction coupling in the podial retractor cells of the starfish *Stylasterias forreri*. *Cell Tissue Res.* **218:** 475–485.

Chapman, G. 1958. The hydrostatic skeleton in the invertebrates. *Biol. Rev. Camb. Philos. Soc.* **33:** 338–371.

Clark, R. B. 1967. *Dynamics in Metazoan Evolution. The Origin of the Coelom and Segments.* Clarendon Press, Oxford.

Clark, R. B., and J. B. Cowey. 1958. Factors controlling the change of shape of certain nemertean and turbellarian worms. *J. Exp. Biol.* **35:** 731–748.

Cobb, J. L. S. 1967. The innervation of the ampulla of the tube foot in the starfish *Astropecten irregularis. Proc. R. Soc. Lond. B. Biol.* **168:** 91–99.

Cobb, J. L. S. 1970. The significance of the radial nerve cords in asteroids and echinoids. *Z. Zellforsch.* **108:** 457–474.

Cobb, J. L. S. 1987. Neurobiology of the Echinodermata. Pp. 483–525 in *Nervous Systems in Invertebrates,* M. A. Ali, ed. Plenum Press, New York.

Cobb, J. L. S., and M. S. Laverack. 1967. Neuromuscular systems in echinoderms. *Symp. Zool. Soc. Lond.* **20:** 25–51.

Coleman, R. 1969. Ultrastructure of the tube foot wall of a regular echinoid, *Diadema antillarum* Phillipi. *Z. Zellforsch.* **96:** 162–172.

Cowey, J. B. 1952. The structure and function of the basement membrane muscle system in *Amphiporus lactifloreus* (Nemertea). *Q J Microsc. Sci.* **93:** 1–15.

Dolder, H. 1972. Ultrastructural study of the smooth muscle in the tubefeet of the echinoderms, *Asterina stellifera* and *Pentacta petersem. J Submicr. Cytol.* **4:** 221–232.

Engster, M. S., and S. C. Brown. 1972. Histology and ultrastructure of the tube foot epithelium in the phanerozoan starfish *Astropecten. Tissue and Cell* **4:** 503–518.

Ferguson, J. C. 1989. Rate of water admission through the madreporite of a starfish. *J Exp. Biol.* **145:** 147–156.

Ferguson, J. C. 1990a. Hyperosmotic properties of the fluids of the perivisceral coelom and water vascular system of starfish kept under stable conditions. *Comp. Biochem. Physiol.* **95A(2):** 245–248.

Ferguson, J. C. 1990b. Seawater inflow through the madreporite and internal body regions of a starfish (*Leptasterias hexactis*) as demonstrated by fluorescent microbeads. *J. Exp. Zool.* **255:** 262–271.

Gaunt, P. N., and W. A. Gaunt. 1978. *Three Dimensional Reconstruction in Biology.* University Park Press, Baltimore. 174 pp.

Hamilton, W. F. 1921. Coördination of the starfish. I. Behavior of the individual tube feet. *J. Comp. Psychol.* **1:** 473–488.

Heddle, D. 1967. Versatility of movement and the origin of the asteroids. *Symp. Zool. Soc. Lond.* **20:** 125–141.

Hyman, L. H. 1955. *The Invertebrates: Echinodermata. The Coelomate Bilateria.* **4,** McGraw-Hill, New York. 763 pp.

Kerkut, G. A. 1953. The forces exerted by the tube feet of the starfish during locomotion. *J. Exp. Biol.* **30:** 575–583.

Kier, W. M. 1988. The arrangement and function of molluscan muscle. Pp. 211–252 in *The Mollusca, Form and Function,* Vol. 11, E. R. Trueman and M. R. Clarke, eds., Academic Press, New York.

Kier, W. M. 1992. Hydrostatic skeletons and muscular hydrostats. Pp. 205–231 in *Biomechanics (Structures and Systems): A Practical Approach,* A. A. Biewener, ed. IRL Press at Oxford University Press, Oxford.

Lawrence, J. 1987. *A Functional Biology of Echinoderms.* Johns Hopkins University Press, Baltimore. 340 pp.

Mangold, E. 1908. Studien zur Physiologie des Nervensystems der Echinodermen. *Arch. Gesamte Physiol. Mens. Tiere (Pfluegers)* **122:** 315–360.

Märkel, K., and U. Röser. 1992. Functional anatomy of the valves in the ambulacral system of sea urchins. *Zoomorphology* **111:** 179–192.

Messenger, J. B., M. Nixon, and K. P. Ryan. 1985. Magnesium chloride as an anaesthetic for cephalopods. *Comp. Biochem. Physiol.* **82C:** 203–205.

Nichols, D. 1966. Functional morphology of the water-vascular system. Pp. 219–244 in *Physiology of the Echinodermata,* R. A. Boolootian ed. John Wiley and Sons, New York.

Nichols, D. 1969. *Echinoderms. 4th ed.* Hutchinson University Library, London.

Nichols, D. 1972. The water vascular system in living and fossil echinoderms. *Palaeontology (Lond.)* **15:** 519–538.

Paine, V. L. 1926. Adhesion in the tube feet in starfishes. *J Exp. Zool* **45:** 361–366.

Paine, V. L. 1929. The tube feet of starfishes as autonomous organs. *Am. Nat.* **63:** 517–529.

Prusch, R. D. 1977. Solute secretion by the tube foot epithelium in the starfish *Asterias forbesi. J Exp. Biol.* **68:** 35–43.

Prusch, R. D., and F. Whoriskey. 1976. Maintenance of fluid volume in the starfish water vascular system. *Nature (Lond.)* **262:** 577–578.

Raymond, A. M. 1979. Innervation of echinoid tube feet. Pp. 277–283 in *Echinoderms. Present and Past: Proceedings of the European Colloquium on Echinoderms. Brussels, 3–8 September 1979* M. Jangoux, ed. Balkema, Rotterdam.

Smith, J. E. 1937. The structure and function of the tube feet in certain echinoderms. *J Mar. Biol. Assoc. U K* **22:** 345–357.

Smith, J. E. 1945. The role of the nervous system in some activities of starfishes. *Biol. Rev. Camb. Philos. Soc.* **20:** 29–43.

Smith, J. E. 1946. The mechanics and innervation of the starfish tube foot-ampulla system. *Philos. Trans. R. Soc. Lond. B Biol. Sci.* **232:** 279–310.

Smith, J. E. 1947. The activities of the tube feet of *Asterias rubens* L. I. The mechanics of movement and of posture. *Q. J. Microsc. Sci.* **88:** 1–14.

Smith, J. E. 1950a. Some observations on the nervous mechanisms underlying the behaviour of starfishes. *Symp. Soc. Exp Biol.* **4:** 196–220.

Smith, J. E. 1950b. The motor nervous system of the starfish, *Astropecten irregularis* (Pennant), with special reference to the innervation of the tube feet and ampullae. *Philos. Trans. R. Soc. Lond B Biol. Sci.* **234:** 521–558.

Souza Santos, H., and W. Silva Sasso. 1968. Morphological and histochemical studies on the secretory glands of starfish tube feet. *Acta Anat.* **69:** 41–51.

Souza Santos, H., and W. Silva Sasso. 1970. Ultrastructural and histochemical studies on the epithelium revestment layer in the tube feet of the starfish *Asterina stellifera. J. Morph.* **130:** 287–296.

Trueman, E. R. 1975. *The Locomotion of Soft-Bodied Animals.* Edward Arnold, London.

Wainwright, S. A. 1982. Structural systems: hydrostats and frameworks. Pp. 325–338 in *A Companion to Animal Physiology,* C. R. Taylor, K. Johansen, and L. Bolis, eds. Cambridge University Press, New York.

Wainwright, S. A., W. D. Biggs, J. D. Currey, and J. M. Gosline. 1976. *Mechanical Design in Organisms.* John Wiley and Sons, New York. 423 pp.

Wood, R. L., and M. J. Cavey. 1981. Ultrastructure of the coelomic lining in the podium of the starfish *Stylasterias forreri. Cell Tissue Res.* **218:** 449–473.

Woodley, J. D. 1967. Problems in the ophiuroid water-vascular system. *Symp. Zool. Soc. Lond.* **20:** 75–104.

Woodley, J. D. 1980. The biomechanics of ophiuroid tube-feet. Pp. 293–299 in *Echinoderms: Present and Past: Proceedings of the European Colloquium on Echinoderms. Brussels, 3–8 September 1979.* M. Jangoux, ed. Balkema, Rotterdam.

Young, S. L., E. K. Fram, and B. L. Craig. 1985. Three-dimensional reconstruction and quantitative analysis of rat lung type II cells: a computer-based study. *Am. J. Anat.* **174:** 1–14.

Reference: *Biol Bull* **188**: 210–218. (April, 1995)

Ammonium Metabolism in the Green Hydra Symbiosis

P. J. McAULEY

School of Biological and Medical Sciences, Sir Harold Mitchell Building, University of St. Andrews,
St. Andrews, Fife, KY16 9TH, United Kingdom

Abstract. Inhibitors of enzymes of ammonium assimilation were used to test if assimilation of ammonium in the green hydra–*Chlorella* symbiosis was due to host or symbionts. Both methionine sulphoximine (MSX, an inhibitor of glutamine synthetase, found in both host and symbionts) and azaserine (AZS, an inhibitor of 2-oxoglutarate amido transferase, not found in the host) inhibited ammonium uptake by the intact symbiosis. MSX was taken up and caused predictable changes in pools of glutamate and glutamine in both freshly isolated symbionts and cultured ex-symbiotic *Chlorella*. However, after treatment of the intact symbiosis with MSX, no MSX was found in the symbiotic *Chlorella*, and glutamine and glutamate pools of both host and symbionts were unaffected. Although both MSX and AZS inhibited ammonium uptake by *Chlorella*, MSX caused seven times as much ammonium release from the intact symbiosis as did AZS. AZS treatment of the intact symbiosis caused an increase in glutamine pools in both host and symbionts, and AZS also competitively inhibited glutamine uptake by *Chlorella*. Further, ammonium treatment of intact hydra did not affect the nitrogen status of the algal symbionts, although it did cause a small increase in the number of algae in each digestive cell of the host. It is suggested that primary ammonium assimilation in the green hydra symbiosis occurs by means of animal glutamine synthetase, and that the resulting glutamine may be taken up and further processed by the symbiotic algae. Freshly isolated symbionts were able to process glutamine into glutamate even when incubated at low pH, which causes them to release a substantial proportion of fixed carbon as maltose.

Introduction

Invertebrate-microalgal symbioses are able not only to reassimilate catabolically produced ammonium but also to take up and assimilate ammonium from the environment (Kawaguti, 1953; Cates and McLaughlin, 1976; Szmant-Froelich and Pilson, 1977; Muscatine and D'Elia, 1978; Muscatine *et al.*, 1979; Wilkerson and Muscatine, 1984; Wilkerson and Trench, 1986; Rees, 1986; McAuley, 1990). However, there is some controversy over whether ammonium assimilation is due to the symbiotic algae, or to the animal host, or to the combined activities of both (Miller and Yellowlees, 1989). The possibility that animal rather than algal enzymes may be responsible, in part or in whole, for assimilation of ammonium has important implications for the mechanisms by which animal hosts regulate cell division in populations of symbiotic algae, since a number of workers have suggested that the growth of populations of symbiotic algae may be nitrogen-limited (Rees, 1986; Cook and D'Elia, 1987; McAuley, 1987a).

Miller and Yellowlees (1989) pointed out that in corals symbiotic with dinoflagellates (zooxanthellae), levels of the ammonium assimilatory enzyme NADPH-glutamate dehydrogenase (NADPH-GDH) are higher in host tissue than in symbionts, although the catabolic production of ammonium probably exceeds the capacity of host NADPH-GDH (Rahav *et al.*, 1989; Falkowski *et al.*, 1993; Spencer-Davies, 1992), which has a low specificity for ammonium (Catmull *et al.*, 1987). More recently, glutamine synthetase (GS) activity was reported in giant clam (*Tridacna gigas*) and coral (*Pocillopora damicornis*) host tissues (Fitt *et al.*, 1993; Yellowlees *et al.*, 1994). Because there are relatively high levels of ammonium-assimilating enzyme in host tissues, it is possible that much of the ammonium present in natural seawater concentrations is assimilated before it reaches the symbiotic zooxanthellae (Yellowlees *et al.*, 1994).

However, several lines of evidence suggest that some if not all ammonium assimilation is due to the zooxanthellae. Assimilation is light dependent and does not occur in aposymbiotic animals (for review, see Rees, 1986).

Received 10 March 1994; accepted 12 January 1995.

Rates of uptake by intact associations are similar to those of freshly isolated symbionts (D'Elia *et al.*, 1983; Wilkerson and Trench, 1986), and intact associations exhibit uptake kinetics which suggest that symbionts assimilate ammonium from seawater by depleting ammonium in host tissue and causing a diffusion gradient to form (D'Elia and Cook, 1988). Finally, addition of ammonium to seawater causes increases in zooxanthellar mitosis, biomass, and amino acid levels (Cook *et al.*, 1988; Muscatine *et al.*, 1989; Hoegh-Guldberg and Smith, 1989; Dubinsky *et al.*, 1990; Fitt and Cook, 1990; Stambler *et al.*, 1991; McAuley, 1994; Muller-Parker *et al.*, 1994; McAuley and Cook, 1994), and reduces ammonium uptake rates (Yellowlees *et al.*, 1994). Ammonium assimilation is assumed to involve the coupled glutamine synthetase/2-oxoglutarate amido transferase (GS/GOGAT) pathway. At present, GS but not GOGAT has been detected in zooxathellae (Summons and Osmond, 1981; Wilkerson and Muscatine, 1984), although azaserine, a potent inhibitor of GOGAT, prevents ammonium uptake in intact corals (Rahav *et al.*, 1989), and the presence of GS/GOGAT activity is supported by the data of Summons *et al.* (1986).

In contrast to marine symbioses, in the symbiosis between the freshwater cnidarian *Hydra viridissima* (green hydra) and *Chlorella* algae, the host rather than the algal symbionts may be responsible for assimilation of ammonium. Ammonium assimilation by maltose-releasing *Chlorella* is inhibited at the low pH that stimulates maltose release (Rees, 1989). Recent evidence suggests that in symbiosis the algae are carbon- rather than nitrogen-limited, in that *in vivo* release of maltose consumes considerable amounts of photosynthetically fixed carbon that would otherwise be used to assimilate ammonium into amino acids (McAuley, 1992). Treatment of the intact symbiosis with the photosynthetic inhibitor DCMU does not cause ammonium excretion into the medium, and rates of ammonium uptake by freshly isolated symbionts are only 40% of those of the intact symbiosis (Rees, 1986; McAuley, 1990). Finally, the hosts possess GS, and levels of GS activity are higher in symbiotic than aposymbiotic animals (Rees, 1986).

Although green hydra do not normally excrete ammonium into the medium, release can be induced by treatment with methionine sulphoximine (MSX), which inhibits GS in intact hydra (Rees, 1986). However, the effect of MSX on algal GS has not been tested, because of the difficulty in isolating sufficient numbers of symbionts uncontaminated by host material. This paper describes the effects of inhibitors of enzymes of ammonium assimilation on perturbation of animal and algal internal pools of glutamate and glutamine, amino acids closely associated with ammonium assimilation (Miflin and Lea, 1976). Recovery of symbiotic algae after SDS washing, which is necessary to remove host contamination, is low (McAuley, 1986a), but unlike assays for enzyme activity, measurement of free amino acid pools by HPLC requires only small numbers of algae (the equivalent of 10^4 cells or fewer per sample injection). Uptake of MSX by algae *in vitro* and in the intact symbiosis was also measured using HPLC.

Materials and Methods

Maintenance of organisms

Green hydra of the European strain (EE hydra) were grown in unbuffered 'M' solution (Muscatine and Lenhoff, 1965) at 15°C in constant light (60 μmol photons m^{-2} s^{-1} PAR). Cultures were fed each Monday, Wednesday, and Friday with freshly hatched brine shrimp. All hydra used in experiments had not been fed for the previous 3 days to allow complete digestion of food. Cultures of the 3N813A strain of maltose-releasing *Chlorella*, grown in Kessler's medium (Kessler *et al.*, 1963), pH 6.3, were maintained in a shaking, illuminated incubator in growth conditions similar to those of hydra cultures.

Isolation of symbiotic algae from hydra

The SDS-washing technique (McAuley, 1986a) was used to isolate symbiotic *Chlorella* algae from hydra.

Determination of numbers of algae per digestive cell

Five gastric regions of hydra were isolated in a drop of macerating fluid (David, 1973). After 10 min, pieces of hydra were teased apart into individual cells and examined using phase contrast microscopy. Numbers of algae were determined in 100 randomly selected digestive cells in each preparation.

Measurement of ammonium uptake

Ammonium uptake was measured as depletion from the medium of either hydra or algae. Duplicate samples (200 μl) were taken at the beginning and end of experiments, and amounts of ammonium were determined with a scaled-down hypochlorite-nitroprusside colometric assay (Rees, 1986). After reagents were added, samples were incubated for 20 min in darkness, then absorbence was read at 630 nm and compared to that of ammonium sulphate standards (reagents and standards from Sigma Chemical Company).

Inhibitors

Methionine sulphoximine (MSX), an inhibitor of GS (Ranzio *et al.*, 1969; Meister, 1974), and azaserine (AZS), an inhibitor of 2-oxoglutarate amido transferase (GOGAT) (Wallsgrove *et al.*, 1977; Elrifi and Turpin, 1986), were purchased from the Sigma Chemical Company.

Stock solutions were stored at 4°C and routinely tested by measuring their effectiveness in inhibiting ammonium uptake by cultured 3N813A cells. In all experiments, MSX was used at a final concentration of 200 μM and AZS at 1 mM.

Extraction and measurement of free amino acid pools

Samples of algae, or of animal homogenates centrifuged at 1000 × g for 5 min to remove algae, were added to absolute ethanol to give 80% ethanol (v:v) and extracted for 24 h at 4°C. Protein contents of homogenates were determined using the Bradford method (Bradford, 1976). In some cases, algal samples were filtered at low vacuum through Whatman GF/C filters, which were then extracted twice in 80% ethanol. Extracts were dried *in vacuo* and resuspended in an appropriate volume of 12.5 μM α-amino-butyric acid (AABA), which acted as an internal standard. Amino acid contents of aliquots of extracts were determined by *o*-phthaldialdehyde pretreatment and reverse-phase HPLC as previously described (McAuley, 1992). MSX but not AZS was detectable using this system; the MSX peak occurred 0.8 min after that of serine.

Glutamine and methylamine uptake

Glutamine uptake was determined from cultured 3N813A cells resuspended in 10 mM MES buffer pH 7 at a density of 5×10^7 cells ml^{-1}. After 30 min of preincubation, the assay was started by adding 2–20 μM glutamine containing 3.7 μBq [U-^{14}C]-glutamine (Amersham International; specific activity 9.25 GBq mmol^{-1}) with or without additional 20 μM AZS. At intervals of 1, 2, and 3 min after addition of radioactivity, 200-μl samples were filtered onto Whatman GF/C filters at low vacuum and washed with 20 ml distilled water. Filters were dried in scintillation vials, 10 ml of scintillation fluid was added (McAuley, 1988), and samples were counted on an LKB 1214 Rackbeta scintillation counter. V_{max} and K_M were determined from Lineweaver Burke double reciprocal plots of uptake rates against substrate concentration.

Uptake of [^{14}C]-methylamine was determined by the same method as glutamine uptake, except that [^{14}C]-methylamine (Amersham International; specific activity 2.22 GBq mmol^{-1}) was added to give a final concentration of 5 μM. At intervals, 100-μl samples were filtered onto Whatman GF/C filters and radioactivity was determined as described above.

Enzyme assay

About 100 hydra, previously starved for 3 days, were homogenized in extraction buffer as described by Rees (1986). The homogenate was centrifuged at 13000 × g for 5 min at 4°C, and the supernatant was assayed for GOGAT activity by determining the rate of oxidation of NAD(P)H at 340 nm by the method of Bhandari and Nicholas (1981). Blanks were run without addition of α-ketoglutarate.

Results

Effect of ammonium on symbionts in intact hydra

Incubation of EE hydra for 7 days in M solution supplemented with 50 μM ammonium chloride had no effect on the size of the glutamate and glutamine pools of their algal symbionts (Table I). However, significantly more algae (one-way ANOVA, $P < 0.05$, $n = 6$ independent experiments) were present in digestive cells of hydra maintained in ammonium-supplemented medium (24.94 ± 1.71 SD) than in controls (22.58 ± 1.48).

Effect of MSX and AZS on ammonium uptake

As previously observed (Rees, 1986; McAuley, 1990), MSX not only inhibited ammonium assimilation but also caused release of ammonium from both intact hydra and cultured 3N813A algae (Table II). AZS inhibited ammonium assimilation but did not cause release in 3N813A algae; ammonium release by green hydra treated with AZS was seven times lower than that observed with MSX treatment.

Effect of MSX and AZS on internal pools of glutamate and glutamine in 3N813A

3N813A algae were incubated with either MSX or AZS in the absence or presence of a nitrogen source (either glutamine or ammonium), and amino acid pools were compared to those of untreated controls (Table III). MSX and AZS had distinct effects on internal glutamine and glutamate pools irrespective of the nitrogen supply, and

Table I

Effect of incubation of intact hydra in ammonium on glutamate and glutamine pools of algal symbionts

	Controls	Ammonium treated
Glu	574.1 ± 38.0	578.9 ± 56.7
Gln	150.3 ± 18.5	146.7 ± 29.3
Gln:Glu	0.26 ± 0.03	0.26 ± 0.06

EE Hydra were starved for 7 days in M solution ±50 μM ammonium chloride; incubation solutions were changed every day. After 7 days, hydra were washed five times in large volumes of M solution and homogenized, and amino acid pools in SDS-washed freshly isolated symbionts were determined as described in Materials and Methods. Values are the means ± SD of amino acid content (amol cell^{-1}) of glutamate and glutamine pools determined from three independent experiments.

Table II

Effect of MSX and AZS on uptake (+) or release (−) of ammonium by intact green hydra and 3N813A algae

	Hydra (nmol hydra^{-1} h^{-1})	3N813A (fmol cell^{-1} h^{-1})
Control	+0.192 ± 0.045	+1.51 ± 0.35
MSX	−0.220 ± 0.036	−0.86 ± 0.25
AZS	−0.031 ± 0.006	+0.05 ± 0.03

Hydra were preincubated in MSX or AZS for 24 h and washed twice in large volumes of growth medium before being placed in new medium; 3N813A algae (5×10^7 cells ml^{-1}) were preincubated for 30 min in 10 n*M* MES pH 7. Uptake of ammonium was measured by the difference in ammonium content of aliquots taken immediately after addition of ammonium chloride to give a concentration of 50 μ*M* (hydra) or 100 μ*M* (algae) and of aliquots taken after 1 h. Figures are the means ± SD of three (hydra) or four (algae) independent experiments. All treatment values are significantly different from controls (one-way ANOVA, $P < 0.001$).

Table III

Effect of MSX and AZS on free glutamate and glutamine pools of 3N813A algae

	Control	MSX	AZS
−N			
Glu	379.9 ± 24.2	295.9 ± 40.3*	68.4 ± 20.2*
Gln	77.3 ± 10.3	11.4 ± 2.3*	437.7 ± 72.8*
+NH4			
Glu	335.0 ± 14.2	300.4 ± 22.1	50.5 ± 13.1*
Gln	166.1 ± 47.2	11.5 ± 5.5*	438.4 ± 51.0*
+Gln			
Glu	625.4 ± 99.0	407.1 ± 62.7*	56.8 ± 6.3*
Gln	330.1 ± 62.3	49.7 ± 16.4*	495.9 ± 91.6

Algae were incubated with MSX or AZS or in 10 m*M* MES buffer pH 7 for 30 min before addition of 100 μ*M* ammonium chloride, glutamine, or an equivalent volume of distilled water (−N). After 1 h, aliquots were filtered at low vacuum onto Whatman GF/C filters, washed, and extracted for amino acid analysis. Figures are the means ± SD of amino acid content (amol cell^{-1}) of glutamate and glutamine pools determined from three independent experiments.

* Significantly different from control, one-way ANOVA, $P < 0.05$.

these effects were consistent with inhibition of GS or GOGAT respectively. MSX significantly decreased glutamine and AZS significantly decreased glutamate in all treatments. In algae without a nitrogen source or supplied with glutamine, MSX also significantly decreased glutamate pools; in algae without a nitrogen source or supplied with ammonium, AZS significantly increased glutamine pools.

Supply of nitrogen also affected glutamine and glutamate pools. Glutamine increased in algae supplied with ammonium and glutamine, and glutamate increased in algae supplied with glutamine (one-way ANOVA, $P < 0.05$). Tukey post-hoc tests showed that the size of the glutamine pools was similar in all MSX and all AZS treatments ($P > 0.05$). The size of the glutamate pools was also similar in all AZS treatments ($P > 0.05$), but glutamate levels were higher in algae treated with MSX in the presence of glutamine than in the presence of ammonium or the absence of a nitrogen source.

Effect of MSX and AZS on internal pools of glutamate and glutamine in freshly isolated symbionts and in the intact symbiosis

The effect of maltose release on the changes the two inhibitors produce in glutamate and glutamine pools was tested on freshly isolated symbionts treated at pH 5 and at pH 7. Maltose release is pH dependent (Cernichiari *et al.*, 1969) and occurs at the former but not the latter pH.

When freshly isolated symbionts were treated with MSX and AZS at pH 7, the effects were similar to those seen when 3N813A algae were treated without a nitrogen source: MSX caused a significant decrease in glutamine and glutamate; AZS caused a significant decrease in glutamate and an increase in glutamine (Table IV). At pH 5, AZS treatment also caused a significant decrease in glutamate and an increase in glutamine, but whereas MSX treatment decreased glutamate, glutamine levels tended to increase, although this trend was not significant. Uptake of MSX at pH 5 was considerable (over 3000 amol cell^{-1}), and the large MSX peak, adjacent to that of glutamine, may have interfered with detection of glutamine. When an amount of MSX equivalent to that found in the algae was added to a sample containing 10 pmol glutamine, the apparent amount of glutamine detected by HPLC increased 30%. The smaller MSX peak at pH 7 did not interfere with glutamine detection.

Table IV

Effect of MSX or AZS on free glutamate and glutamine pools of freshly isolated symbiotic algae

	Control	MSX	AZS
pH 7.0			
Glu	334.1 ± 62.3	182.2 ± 29.1*	63.6 ± 13.1*
Gln	120.1 ± 27.2	50.9 ± 12.7*	297.1 ± 102.3*
pH 5.0			
Glu	156.0 ± 4.5	84.0 ± 22.1*	62.1 ± 14.7*
Gln	60.6 ± 6.5	95.4 ± 23.1	89.2 ± 11.4*

Algae were incubated with MSX or AZS or in 10 m*M* MES buffer only (controls) for 90 min, and then aliquots were filtered at low vacuum onto Whatman GF/C filters, washed, and extracted for amino acid analysis. Figures are the means ± SD of amino acid content (amol cell^{-1}) of glutamate and glutamine pools determined from three independent experiments.

* Significantly different from control value, one-way ANOVA, $P < 0.05$.

Treatment of freshly isolated symbionts at pH 5 caused a significant reduction in both glutamate and glutamine pools compared to those at pH 7 (one-way ANOVA, $P < 0.05$).

Incubation of intact green hydra in MSX caused no significant change in the glutamate or glutamine pools of either the symbiotic algae or the host (Table V). Only 16.2 ± 30.2 SD amol cell^{-1} MSX was detected in algal pools after 24-h treatment of intact hydra, compared to high levels in freshly isolated symbionts after only 90 min of treatment (3126.0 ± 227.6 amol cell^{-1} in freshly isolated symbionts treated at pH 5; 495.3 ± 175.7 amol cell^{-1} in freshly isolated symbionts treated at pH 7). Treatment of intact hydra with AZS increased glutamine pools in both hydra and algae, although the increase was significant only in hydra. AZS treatment did not cause a reduction in either host or algal glutamate pools, in contrast to the consistent effect of AZS on glutamate pools measured in both freshly isolated symbionts and 3N813A irrespective of pH or nitrogen supply.

Effect of MSX and AZS on glutamine and methylamine uptake by 3N813A algae

[^{14}C]-glutamine uptake by 3N813A algae was competitively inhibited by a low concentration of AZS (Fig. 1). K_M was 17.3 μM in the absence of AZS and 28.6 μM in the presence of AZS. In both cases, V_{max} was 250 amol glutamine cell^{-1} h^{-1}.

There was linear uptake of the ammonium analog [^{14}C]-methylamine in the presence of both MSX and AZS, although uptake rates were reduced by 25.1% and 33.4% respectively, in comparison to controls (Fig. 2). In contrast, ammonium chloride inhibited methylamine uptake by 98% for the first 4 min, although the uptake increased gradually thereafter. Calculations based on ammonium uptake rates in Table I indicated that the algae would have greatly depleted ammonium concentration at the time that uptake of methylamine began to increase.

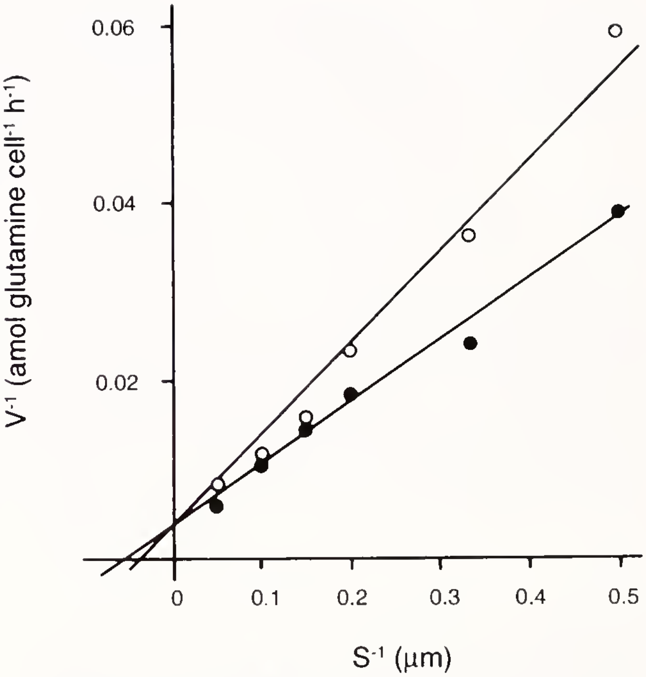

Figure 1. Effect of the absence (● —— ●) and presence (○ —— ○) of AZS on the apparent K_M value of the glutamine transport system of 3N813A algae. Algae were preincubated in 10 mM MES buffer pH 7 for 30 min before addition of 2–20 μM [^{14}C]-glutamine with or without 20 μM AZS. Uptake of glutamine and K_M and V_{max} was determined as described in Materials and Methods.

Table V

Effect of incubating hydra in MSX or AZS on free glutamate and glutamine pools of hydra (pmol μg protein^{-1}) and symbiotic algae (amol cell^{-1})

	Control	MSX	AZS
Hydra			
Glu	24.3 ± 10.4	24.3 ± 12.8	25.1 ± 12.0
Gln	1.3 ± 0.4	1.8 ± 0.9	5.9 ± 3.0*
Algae			
Glu	551.3 ± 82.7	571.5 ± 143.6	554.8 ± 94.6
Gln	146.2 ± 54.3	156.6 ± 65.8	224.1 ± 128.1

One hundred and twenty hydra were incubated in MSX or AZS for 24 h, washed five times in large volumes of M solution and homogenized, and amino acid pools in homogenized hydra and in SDS-washed freshly isolated symbionts were determined as described in Materials and Methods. Figures are the means ± SD of six independent experiments.

* Significantly different from control value, one-way ANOVA, $P < 0.05$.

Uptake of glutamine by freshly isolated symbionts

Short-term experiments showed that incubation of freshly isolated symbionts in 100 μM glutamine caused an increase in internal glutamine and glutamate pools at both pH 5 and pH 7 (Fig. 3).

GOGAT activity

Neither NADH- or NADPH-specific GOGAT activity was detectable in hydra tissue.

Discussion

Several lines of evidence suggest that assimilation of ammonium in the green hydra–*Chlorella* symbiosis is due to GS in the animal host rather than in the algal symbiont. Incubation of green hydra in medium supplemented with ammonium chloride caused a small, significant increase in numbers of algae per host digestive cell, but there was

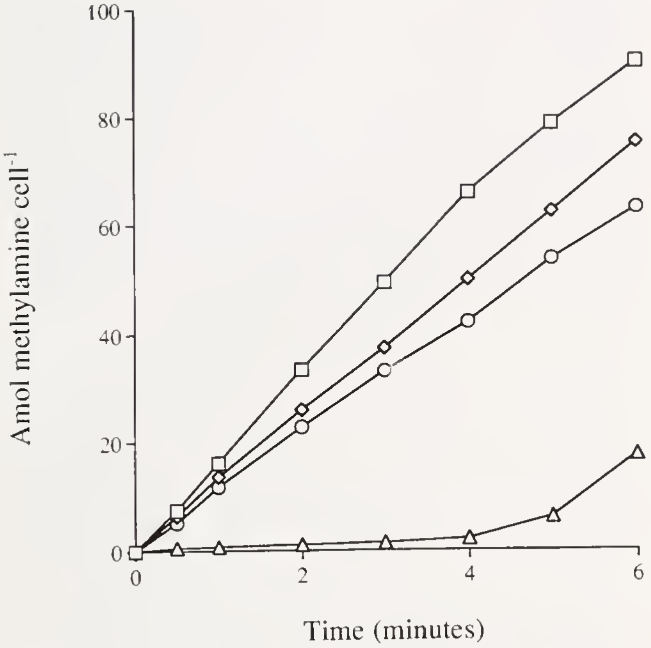

Figure 2. Effect of MSX, AZS, and ammonium on uptake of [^{14}C]-methylamine by 3N813A algae. Algae were preincubated in 10 m*M* MES buffer pH 7 for 30 min before addition of 5 μ*M* [^{14}C]-methylamine together with either 10 μ*M* MSX (——), 10 μ*M* AZS (○ —— ○), 10 μ*M* ammonium chloride (△ —— △), or an equivalent volume of buffer only as control (□ —— □) to give a final density of 5 × 10^7 cells ml^{-1}. At intervals, 100-μl samples were filtered and radioactivity was determined.

no effect on glutamine and glutamate pools or on the Gln:Glu ratio of the algae (Table I), the latter being an indicator of nitrogen sufficiency in microalgae (Flynn *et al.*, 1989). In marine symbioses, in which it is believed that symbionts are able to assimilate ammonium from seawater, ammonium supplementation not only causes large increases in the population density of symbionts (Muscatine *et al.*, 1989; Hoegh-Guldberg and Smith, 1989; Dubinsky *et al.*, 1990; Fitt and Cook, 1990; Stambler *et al.*, 1991; Muller-Parker *et al.*, 1994), but, in a coral and a hydroid, also increases the size of internal glutamine pools of symbionts and hence their Gln:Glu ratio (McAuley, 1994; McAuley and Cook, 1994).

Further, although MSX inhibits ammonium uptake by intact hydra (Rees, 1986; McAuley, 1990; Table II, this paper), almost no MSX was detected in symbiotic algae isolated from hydra that had been incubated in MSX for 24 h, and there was no change in algal internal pools of glutamate and glutamine. In contrast, freshly isolated symbionts treated with MSX rapidly accumulated large amounts of the inhibitor, and MSX treatment caused predictable changes in glutamate and glutamine pools of freshly isolated symbionts and cultured 3N813A algae in a variety of conditions (Tables III and IV).

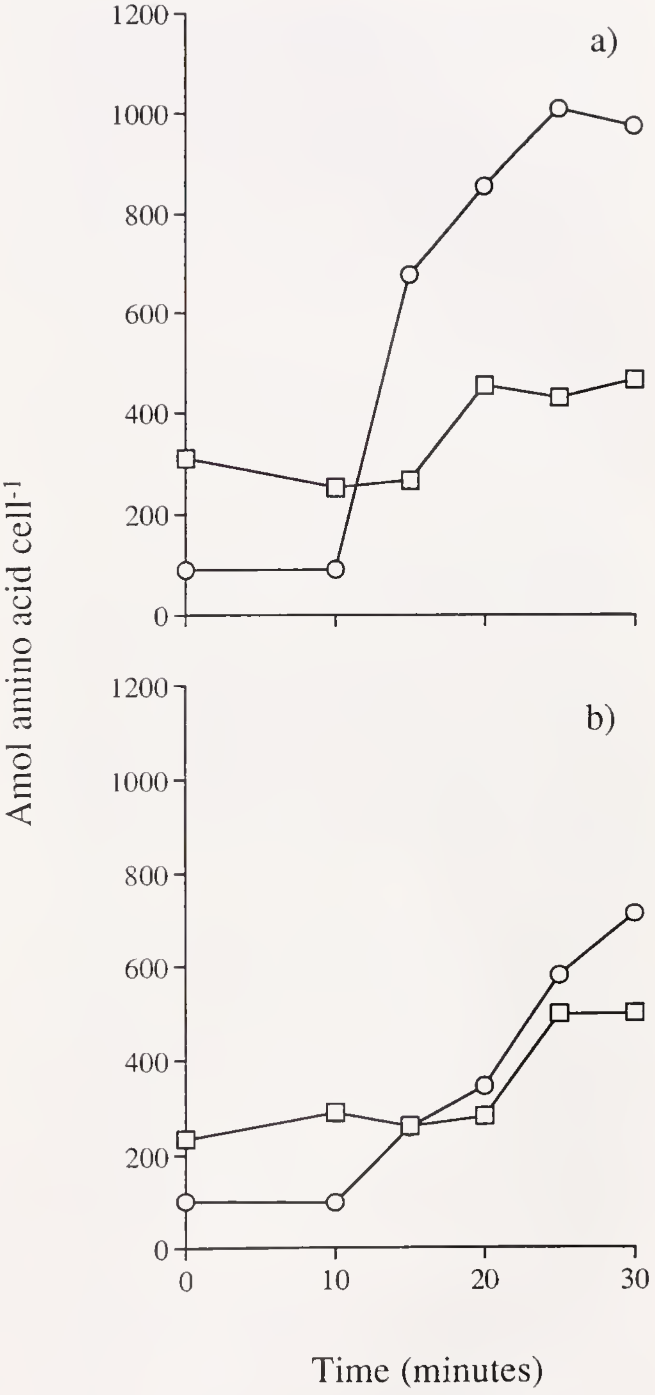

Figure 3. Effect of glutamine uptake on internal pools of glutamine (○ —— ○) and glutamate (□ —— □) in freshly isolated symbionts. Freshly isolated symbionts (10^7 cells ml^{-1}) were preincubated for 30 min in 10 m*M* McIlvaine's buffer at either pH 5 (a) or pH 7 (b). Ten minutes after the start of the experiment, glutamine was added to give a concentration of 100 μ*M* Samples (200 μ*M*) taken at each time point were filtered onto GF/C disks under low vacuum, washed with 20 ml ice-cold distilled water, and extracted for amino acid analysis.

In addition to inhibiting GS, MSX has been shown to be a noncompetitive inhibitor of active ammonium transport in *Anabaena flos-aquae* (Turpin *et al.*, 1984). In 3N813A, both MSX and AZS caused a degree of inhibition of uptake of methylamine (Fig. 2), a structural analog of ammonium that is taken up by the same transport system (Hackette *et al.*, 1970; Pelley and Bannister, 1979; Smith, 1982; Wright and Syrett, 1983). However, if both MSX and AZS caused noncompetitive inhibition of entry of ammonium into symbionts, release of ammonium from the intact symbiosis would presumably be the same in both treatments. Instead, release was seven times higher in hydra treated with MSX than in hydra treated with AZS (Table II). As shown in 3N813A cells, MSX blocks assimilation of ammonium into glutamine *via* GS (Ranzio *et al.*, 1969; Meister, 1974), leading to low glutamine pools and release of ammonium. AZS blocks subsequent metabolism of glutamine to glutamate *via* GOGAT (Wallsgrove *et al.*, 1977; Elrifi and Turpin, 1986), leading to accumulation of glutamine, low glutamate pools, and no ammonium release. That hydra release more ammonium when treated with MSX than with AZS is consistent with inhibition of GS activity pathways rather than with noncompetitive inhibition of ammonium transport into the algae. Because very little MSX was detected in symbionts after treatment of intact hydra, the ammonium release observed during MSX treatment of the intact symbiosis must have been due to inhibition of host GS.

No GOGAT was detected in crude, alga-free extracts of homogenized green hydra. However, treatment of intact hydra with AZS, an inhibitor of GOGAT, prevented uptake of ammonium from the medium by the intact symbiosis and caused a significant increase in host glutamine pools (Tables II and V). This may be explained if glutamine resulting from activity of host GS was taken up by the algae and converted into glutamate *via* GOGAT. Uptake of glutamine by algae would also explain why MSX treatment did not cause an increase in host glutamine pools.

AZS treatment may have affected this coupling in two ways. First, AZS may have specifically inhibited algal GOGAT, although AZS treatment of the intact symbiosis did not cause the reduction in glutamate and increase in glutamine consistently observed in 3N813A or in freshly isolated symbionts. Second, AZS, which competitively inhibited uptake of glutamine in 3N813A algae (Fig. 1), prevented entry of glutamine into either the perialgal vacuole or the symbiotic algae themselves. In either case, the glutamine transport system must be specific for glutamine and AZS but not MSX. Given that symbionts accumulated MSX *in vitro* but not *in hospice*, it is possible that transport systems in the host perialgal vacuolar membrane differentially control entry of substances into the perialgal vacuole.

Supply of nitrogen to algal symbionts as glutamine or other amino acids rather than as ammonium may be important because a supply of carbon is required for assimilation of ammonium into amino acids (Turpin, 1991), and symbionts release a high proportion of fixed carbon to their host in the form of maltose (Mews, 1980). In cultured 3N813A, maltose synthesis and release inhibits ammonium uptake because it diverts photosynthetically fixed carbon from assimilation of ammonium into amino acids (McAuley, 1992). Maltose release is stimulated by low pH, and ammonium uptake by freshly isolated symbionts and cultured maltose-releasing algae falls as pH is reduced and maltose release increases (Rees, 1989). Below a critical pH value, the algae actually begin to release ammonium, not only because fixed carbon is diverted from the TCA cycle to maltose release, but also because amino acids may be deaminated to provide carbon skeletons for maltose synthesis (Rees, 1990).

Given that high rates of maltose release and ammonium assimilation are incompatible, amino acids may provide an alternative source of nitrogen for algae in symbiosis with green hydra. Freshly isolated symbionts have active amino acid transport systems (McAuley, 1986b), and algae in the intact symbiosis can assimilate a variety of amino acids supplied by host feeding (McAuley, 1987b, 1988, 1991). Further, the rate of glutamine uptake by freshly isolated symbionts peaks between pH 4 and 5, the same range over which release of maltose is maximum (McAuley, 1991). Maltose-releasing symbionts using glutamine as a nitrogen source would require carbon skeletons in the form of 2-oxoglutarate to produce two molecules of glutamate from each molecule of glutamine. But even if one molecule of glutamate was deaminated, the carbon recycled to 2-oxoglutarate, and the ammonium released to be reassimilated by the host, the algae would still gain a new molecule of glutamate for each molecule of glutamine taken up. Short-term experiments showed that uptake of glutamine by freshly isolated symbionts at both pH 5 (with maltose release) and pH 7 (without maltose release) caused an increase in the size of internal glutamate pools (Fig. 3). Although the increase in glutamate pools was similar, it should be noted that the rate of glutamine uptake by freshly isolated symbionts is more than 5 times higher at pH 5 than at pH 7 (McAuley, 1991).

This scheme is qualitatively but not quantitatively different from that in marine algal–invertebrate symbioses, in which symbiotic zooxanthellae appear to assimilate ammonium *via* coupled GS/GOGAT (for review, see Spencer-Davies, 1992). In green hydra, although both GS and GOGAT are involved in ammonium assimilation, they may be located in different compartments, and the necessity for glutamine to traverse the perialgal vacuole would produce a point at which nitrogen supply to the algae could be regulated.

Acknowledgments

This work was supported by grants from the Royal Society and the Natural Environmental Research Council. My thanks to Mr. Harry Hodge for his help in HPLC analysis of amino acids, and to an anonymous referee for helpful comments on a draft of this paper.

Literature Cited

Bhandari, B., and D. J. D. Nicholas. 1981. Some properties of glutamine synthetase from the nitrifying bacterium. *Nitrosomonas europaea. Aust. J. Biol. Sci.* **34:** 527–539.

Bradford, M. M. 1976. A rapid sensitive method for the quantitation of microgram quantities of protein utilizing the principle of protein dye binding. *Analyt. Biochem.* **72:** 248–254.

Cates, N., and J. J. A. McLaughlin. 1976. Differences in ammonia metabolism in symbiotic and aposymbiotic *Condylactus* and *Cassiopea* spp. *J. Exp. Mar. Biol. Ecol.* **21:** 1–5.

Catmull, J., D. Yellowlees, and D. J. Miller. 1987. NADP-dependent glutamate dehydrogenase from *Acropora formosa:* purification and properties. *Mar. Biol.* **95:** 559–563.

Cernichiari, E., L. Muscatine, and D. C. Smith. 1969. Maltose excretion by the symbiotic algae of *Hydra viridis. Proc. R. Soc. Lond. B* **173:** 557–576.

Cook, C. B., and C. F. D'Elia. 1987. Are natural populations of zooxanthellae ever nutrient-limited? *Symbiosis* **4:** 199–212.

Cook, C. B., C. F. D'Elia, and G. Muller-Parker. 1988. Host feeding and nutrient sufficiency for zooxanthellae in the sea anemone *Aiptasia pallida. Mar. Biol.* **98:** 253–262.

David, C. N. 1973. A quantitative method for maceration of hydra tissue. *Wilhelm Roux Arch. EntwMech. Org.* **171:** 259–268.

D'Elia, C. F., and C. B. Cook. 1988. Methylamine uptake by zooxanthellae-invertebrate symbioses: insights into host ammonium environment and nutrition. *Limnol. Oceanogr.* **35:** 1153–1165.

D'Elia, C. F., S. L. Domotor, and K. L. Webb. 1983. Nutrient uptake kinetics of freshly isolated zooxanthellae. *Mar. Biol* **75:** 157–169.

Dubinsky, Z., N. Stambler, M. Ben-Zion, L. R. McCloskey, L. Muscatine, and P. G. Falkowski. 1990. The effect of external nutrient resources on the optical properties and photosynthetic efficiency of *Stylophora pistillata. Proc. R. Soc. Lond. B* **239:** 231–246.

Elrifi, I. R., and D. H. Turpin. 1986. Nitrate and ammonium induced photosynthetic suppression in N-limited *Selenastrum minutum. Plant Physiol.* **81:** 273–279.

Falkowski, P. G., Z. Dubinsky, L. Muscatine, and L. McCloskey. 1993. Population control in symbiotic corals. *BioScience* **43:** 606–611.

Fitt, W. K., and C. B. Cook. 1990. Some effects of host feeding on growth of zooxanthellae in the marine hydroid *Myrionema ambionese* in the laboratory and in nature. Pp. 281–284 in *Endocytobiology IV*, P. Nardon, V. Gianinazzi-Pearson, A. M. Grenier, L. Margulis, and D. C. Smith, eds. INRA, Paris.

Fitt, W. K., T. A. V. Rees, R. D. Braley, J. S. Lucas, and D. Yellowlees. 1993. Nitrogen flux in giant clams: size-dependency and relationship to zooxanthellae density and clam biomass in the uptake of dissolved nitrogen. *Mar. Biol.* **117:** 381–386.

Flynn, K. J., D. M. J. Dickson, and O. A. Al-Amoudi. 1989. The ratio of glutamine:glutamate in microalgae: a biomarker for N-status suitable for use at natural cell densities. *J. Plankton Res.* **11:** 165–170.

Hackette, S. L., G. E. Skye, C. Burton, and I. H. Segel. 1970. Characterisation of an ammonium transport system in filamentous fungi with methylammonium-^{14}C as the substrate. *J. Biol. Chem.* **245:** 4241–4250.

Hoegh-Guldberg, O., and G. J. Smith. 1989. Influence of the population density of zooxanthellae and supply of ammonium on the biomass and metabolic characteristics of the reef corals *Seriatopora hystrix* and *Stylophora pistillata. Mar. Ecol. Prog. Ser.* **57:** 173–186.

Kawaguti, S. 1953. Ammonium metabolism of the reef corals. *Biol. J. Okayama Univ.* **1:** 171–176.

Kessler, E., W. Langer, I. Ludwig, and H. Wiechmann. 1963. Bildung von Sekundaer-Carotinoiden bei Stickstoffmangel und Hydrogenase-Activataet als taxonomische Merkmale in der Gattung *Chlorella.* Pp. 7–20 in *Studies on Microalgae and Photosynthetic Bacteria.* Jpn. Soc. Plant Physiol., University of Tokyo Press, Tokyo.

McAuley, P. J. 1986a. Isolation of viable uncontaminated *Chlorella* from green hydra. *Limnol. Oceanogr.* **31:** 222–224.

McAuley, P. J. 1986b. Uptake of amino acids by cultured and freshly isolated symbiotic *Chlorella. New Phytol.* **104:** 415–427.

McAuley, P. J. 1987a. Nitrogen limitation and amino-acid metabolism of *Chlorella* symbiotic with green hydra. *Planta* **171:** 532–538.

McAuley, P. J. 1987b. Quantitative estimation of movement of an amino acid from host to *Chlorella* symbionts in green hydra. *Biol. Bull.* **173:** 504–512.

McAuley, P. J. 1988. Uptake of leucine by *Chlorella* symbionts of green hydra. *Proc. R. Soc. Lond. B* **234:** 319–332.

McAuley, P. J. 1990. Uptake of ammonium by green hydra. *Proc. R. Soc. Lond. B* **242:** 45–50.

McAuley, P. J. 1991. Amino acids as a nitrogen source for *Chlorella* symbiotic with green hydra. *Hydrobiologica* **216/217:** 369–376.

McAuley, P. J. 1992. The effect of maltose release on growth and nitrogen metabolism of symbiotic *Chlorella. Br. Phycol. J.* **27:** 417–422.

McAuley, P. J. 1994. Amino acid content of zooxanthellae freshly isolated from *Pocillopora damicornis. Pac. Sci.* **48:** 247–253.

McAuley, P. J., and C. B. Cook. 1994. Effects of host feeding and dissolved ammonium on cell division and nitrogen status of zooxanthellae in the hydroid *Myrionema amboinense. Mar. Biol.* **121:** 343–348.

Meister, A. 1974. Glutamine synthetase in mammals. Pp. 699–754 in *The Enzymes,* Vol. 10, 3rd ed., P. P. Boyer, ed. Academic Press, New York.

Mews, L. 1980. The green hydra symbiosis. III. The biotrophic transport of carbohydrate from alga to animal. *Proc. R. Soc. Lond. B* **209:** 377–401.

Miflin, B. J., and P. J. Lea. 1976. Review: the pathway of nitrogen assimilation in plants. *Phytochemistry* **15:** 873–885.

Miller, D. J., and D. Yellowlees. 1989. Inorganic nitrogen uptake by symbiotic marine cnidarians: a critical review. *Proc. R. Soc. Lond B* **237:** 109–125.

Muscatine, L., and H. M. Lenhoff. 1965. Symbiosis of hydra and algae. I. Effects of some environmental cations on the growth of symbiotic and aposymbiotic hydra. *Biol. Bull.* **128:** 415–424.

Muscatine, L., and C. F. D'Elia. 1978. The uptake, retention, and release of ammonium by reef corals. *Limnol. Oceanogr.* **23:** 725–734.

Muscatine, L., H. Masuda, and R. Burnap. 1979. Ammonium uptake by symbiotic and aposymbiotic reef corals. *Bull. Mar. Sci.* **29:** 572–575.

Muscatine, L., P. G. Falkowski, Z. Dubinsky, P. A. Cook, and L. R. McCloskey. 1989. The effect of external nutrient resources on the population dynamics of zooxanthellae in a reef coral. *Proc. R Soc. Lond B* **236:** 311–324.

Muller-Parker, G., L. R. McCloskey, O. Hoegh-Guldberg, and P. J. McAuley. 1994. Response of animal-algal biomass of the coral *Pocillopora damicornis* to seawater ammonium enrichment. *Pac. Sci* **48:** 273–283.

Pelley, J. L., and T. T. Bannister. 1979. Methylamine uptake in the green alga *Chlorella pyrenoidosa. J Phycol* **15:** 110–112.

Rahav, O., Z. Dubinsky, Y. Achituv, and P. G. Falkowski. 1989. Ammonium metabolism in the zooxanthellate coral, *Stylophora pistillata Proc R. Soc. Lond. B* **236:** 325–337.

Ranzio, A. A., W. B. Rowe, and A. Meister. 1969. Studies on the mechanism of inhibition of glutamine synthetase by methionine sulfoximine. *Biochemistry* **8:** 1066–1075.

Rees, T. A. V. 1986. The green hydra symbiosis and ammonium. I. The role of the host in ammonium assimilation and its possible regulatory significance. *Proc. R Soc. Lond B* **229:** 299–314.

Rees, T. A. V. 1989. The green hydra symbiosis and ammonium. II. Ammonium assimilation and release by freshly isolated symbionts and cultured algae. *Proc. R Soc. Lond B* **235:** 365–382.

Rees, T. A. V. 1990. The green hydra symbiosis and ammonium. III. Characteristics of ammonium release by a high maltose-releasing symbiotic strain of *Chlorella Proc R Soc. Lond B* **242:** 249–253.

Smith, F. A. 1982. Transport of methylammonium and ammonium ions by *Elodea densa J Exp Bot.* **33:** 221–232.

Spencer-Davies, P. 1992. Endosymbiosis in marine cnidarians. Pp. 511–540 in *Plant-Animal Interactions in the Marine Benthos*, D. M. John, S. J. Hawkins, and J. H. Price, eds. Systematics Association Special Volume No. 46. Clarendon Press, Oxford.

Stambler, N., N. Popper, Z. Dubinsky, and J. Stimson. 1991. Effects of nutrient enrichment and water motion on the coral *Pocillopora damicornis Pac Sci.* **45:** 299–307.

Summons, R. E., and C. B. Osmond. 1981. Nitrogen assimilation in the symbiotic marine alga *Gymnodinium microadriaticum*: direct analysis of ^{15}N incorporation by GC-MS methods. *Phytochemistry* **20:** 575–578.

Summons, R. E., T. S. Boag, and F. R. S. Osmond. 1986. The effect of ammonium on photosynthesis and the pathway of ammonium assimilation in *Gymnodinium microadriaticum in vitro* and in symbiosis with tridacnid clams and corals. *Proc. R. Soc. Lond. Ser. B* **227:** 147–159.

Szmant-Froelich, A., and M. E. Q. Pilson. 1977. Nitrogen excretion by colonies of the temperate coral *Astrangia danae* with and without zooxanthellae. *Proc. 3rd Int. Coral Reef Symp* **1:** 417–423.

Turpin, D. 1991. Effects of inorganic N availability on algal photosynthesis and carbon metabolism. *J Phycol.* **27:** 14–20.

Turpin, D. H., S. A. Edie, and D. T. Canvin. 1984. *In vivo* nitrogenase regulation by ammonium and methylamine and the effect of MSX on ammonium transport in *Anabaena flos-aquae. Plant Physiol.* **74:** 701–704.

Wallsgrove, R. M., H. Harel, P. J. Lea, and B. J. Miflin. 1977. Studies on glutamate synthase from leaves of higher plants. *J Exp. Bot.* **28:** 588–596.

Wilkerson, F. P., and L. Muscatine. 1984. Uptake and assimilation of dissolved inorganic nitrogen by a symbiotic sea anemone. *Proc. R. Soc Lond. B* **221:** 71–86.

Wilkerson, F. P., and R. K. Trench. 1986. Uptake of dissolved inorganic nitrogen by the symbiotic clam *Tridacna gigas* and the coral *Acropora* sp. *Mar Biol* **93:** 237–246.

Wright, S. A., and P. J. Syrett. 1983. The uptake of methylammonium and dimethylammonium by the diatom, *Phaeodactylum tricornutum. New Phytol.* **95:** 189–202.

Yellowlees, D., T. A. V. Rees, and W. K. Fitt. 1994. Effect of ammonium-supplemented seawater on glutamine synthetase and glutamate dehydrogenase activities in host tissue and zooxanthellae of *Pocillopora damicornis* and on ammonium uptake rates of the zooxanthellae. *Pac. Sci* **48:** 291–295.

Reference: *Biol. Bull.* **188:** 219–230. (April, 1995)

On the Giant Octopus (*Octopus giganteus*) and the Bermuda Blob: Homage to A. E. Verrill

SIDNEY K. PIERCE[1], GERALD N. SMITH, JR.[2], TIMOTHY K. MAUGEL[1], AND EUGENIE CLARK[1]

[1]*Department of Zoology, University of Maryland, College Park, Maryland 20742; and*
[2]*Department of Medicine, Division of Rheumatology, Indiana University School of Medicine, Indianapolis, Indiana 46202*

> *"The substance looks like blubber, and smells like blubber and it is blubber, nothing more or less."*
> —*F. A. Lucas, 1897*

Abstract. We have obtained samples of two large carcasses. One washed up on a beach in St. Augustine, Florida, in 1896 and has been occasionally attributed to a species of gigantic octopus (*Octopus giganteus*). The other carcass washed up on Bermuda in 1988 and has remained unidentified, although its gross morphology, except for a much smaller total mass, was remarkably similar to the Florida carcass. We have subjected both samples to electron microscopic and biochemical analyses. Our results show that both carcasses are masses of virtually pure collagen. Furthermore, neither sample has the biochemical characteristics of invertebrate collagen, nor the collagen fiber arrangement of octopus mantle. Instead, they are large pieces of vertebrate skin, the Bermuda sample from a poikilotherm and the Florida sample from a huge homiotherm. We conclude that there is no evidence to support the existence of *Octopus giganteus.*

Introduction

The first evidence that seemed to document the existence of a species of gigantic octopus washed ashore on an oceanic beach at St. Augustine, Florida, late in the year of 1896. The so-called carcass was taken in charge by a local physician, Dr. DeWitt Webb, who was also president of the St. Augustine Scientific Society (Wood, 1971). Webb set about to photograph the body, dig it out of the sand, haul it up above the high tides (a task that required the efforts of several horses and men), and to inform the scientific community of its existence. Because Webb believed the carcass to be the remains of a huge octopus, one of the scientists he contacted was the preeminent invertebrate naturalist, Professor A. E. Verrill at Yale (Fig. 1). Based at first only upon a letter from Webb, Verrill reported the finding, speculating that it might be a specimen of *Architeuthis* (Verrill, 1897a). Shortly thereafter, having received additional correspondence and photographs from Webb, Verrill concluded that it was a "true *Octopus*, of colossal size . . . one of those upon which the sperm whale feeds regularly." On the basis of the descriptive and photographic evidence, Verrill proposed to name the species *Octopus giganteus* (Verrill, 1897b). However, almost immediately, Verrill changed his mind. Based upon more photographs, measurements, and descriptions of the carcass after it had been entirely unearthed from the beach sand, along with several formalin-preserved pieces of the tissue, Verrill retracted his rapidly drawn, initial conclusions, writing that "the creature could not have been an *Octopus*" (Verrill, 1897c, d). Instead, Verrill, together with some other biologists of the time, came to the conclusion that the carcass was from a large vertebrate, most likely a whale (Lucas, 1897; Verrill, 1897d, e). However, other biologists, notably Dr. William H. Dall, then the Curator of Mollusks at the National Museum of Natural History, still favored Verrill's original species diagnosis according to correspondence between him, Webb, and Verrill (archived at the Smithsonian Institution, Washington, DC).

Although Verrill disavowed his species description of *Octopus giganteus* several times, the carcass was never properly identified. The matter rested quietly for 70 years,

Received 31 October 1994; accepted 25 January 1995.

Figure 1. A. E. Verrill. Courtesy of the Marine Biological Laboratory Archives.

and then a report appeared stating "it can be safely said that the gigantic mass of tissue that washed up on the beach at St. Augustine in 1896 was the remains of an octopus . . . 200 feet . . ." between tentacle tips (Wood, 1971). That report continued to detail the chronology of the events summarized above and also indicated that sizable pieces of the carcass had been preserved and were held at the Smithsonian Institution. A cursory histological comparison of the tissue from the Smithsonian with that of "contemporary" squid and octopus was carried out. Although the specific squid and octopus tissues that were compared to the Florida carcass were not reported, no cellular structure was found in any of the tissues. Instead, a connective tissue fiber network in all three tissues was revealed with polarized light. The conclusions reached were that none of the samples looked mammalian, that the St. Augustine tissue looked much more like the octopus fiber network than that of the squid, and therefore, "the St. Augustine sea monster was in fact an octopus" (Gennaro, 1971). Because the report of these histological studies was written for a general, rather than scientific audience, it lacked a rigorous description of protocol and observations.

The matter rested again, this time for another decade and a half, until the appearance of a report about the amino acid composition of an acid hydrolysate of the St. Augustine tissue, by now almost 100 years old. Although neither hydroxylysine nor hydroxyproline concentrations were determined, the amino acid composition suggested that the St. Augustine tissue was likely to have been a huge mass of collagen (Mackal, 1986), explaining the lack of cellular structure found in it by Gennaro (1971) (but not the lack of such structure in the "contemporary" tissues) and the persistence of the carcass as it lay on the beach. (According to the correspondence between Webb and Dall, the carcass was still on the beach on March 17, 1897, almost 4 months after the initial discovery.) Mackal (1986) concluded that the amino acid data together with some inconclusive Cu and Fe measurements "support the original identification of the tissue and carcass by A. E. Verrill as an exceptionally large cephalopod, probably octopus, not referable to any known species," in spite of both Verrill's change of mind and the complete lack of a suitable test of taxonomic relationships in Mackal's data. In the end, while the existence of the St. Augustine carcass is well documented and the discovery often cited [most recently in the popular press (Ellis, 1994) and in a biological science text book (Milne, 1995)], there is no unequivocal evidence at all that it belonged to a giant octopus or, indeed, to any particular species.

During the summer of 1988 another carcass washed into a lagoon on the island of Bermuda. This unrecognizable carcass (~2.50 × 1.25 × 0.30 m), immediately labeled the "Bermuda Blob" by the popular press, was photographed and sampled by Teddy Tucker, a renowned local diver and fisherman who often works with scientists on Bermuda. While considerably smaller than the St. Augustine discovery, the Bermuda carcass fit Verrill's description exactly, on a gross level. "No bones or hard parts. . . . Instead of being muscular . . . [the tissues] are firm, tough and elastic, and composed mainly of much interlaced fibers and large bundles of tough fibrous, white connective tissue. [The tissue is] difficult to cut or tear apart . . . . Some large irregular canals permeate the [tissue]. These may have contained blood vessels originally. From the inner surface of some of the pieces large cords of elastic fibers proceeded inward" (Verrill, 1897c). Gennaro's additional description of the St. Augustine tissue also fit the Bermuda carcass exactly. "White as soap . . . the connective tissue was so tough that it dulled four blades . . . the same homogenous, tough, white, fibrous texture [throughout]" (Gennaro, 1971).

We have been able to obtain small pieces of both the St. Augustine and Bermuda carcasses. We have subjected both to electron microscopic examination as well as biochemical analyses to test the similarity between the two tissue masses and to determine their taxonomic origin. In addition, we have carried out light and electron microscopic examinations of octopus (*Bathypolypus arcticus*) mantle tissue and humpback whale (*Megaptera novaeangelae*) blubber.

Materials and Methods

Electron microscopy

Bermuda and St. Augustine Carcasses. Specimens from both the Bermuda and St. Augustine tissue masses were

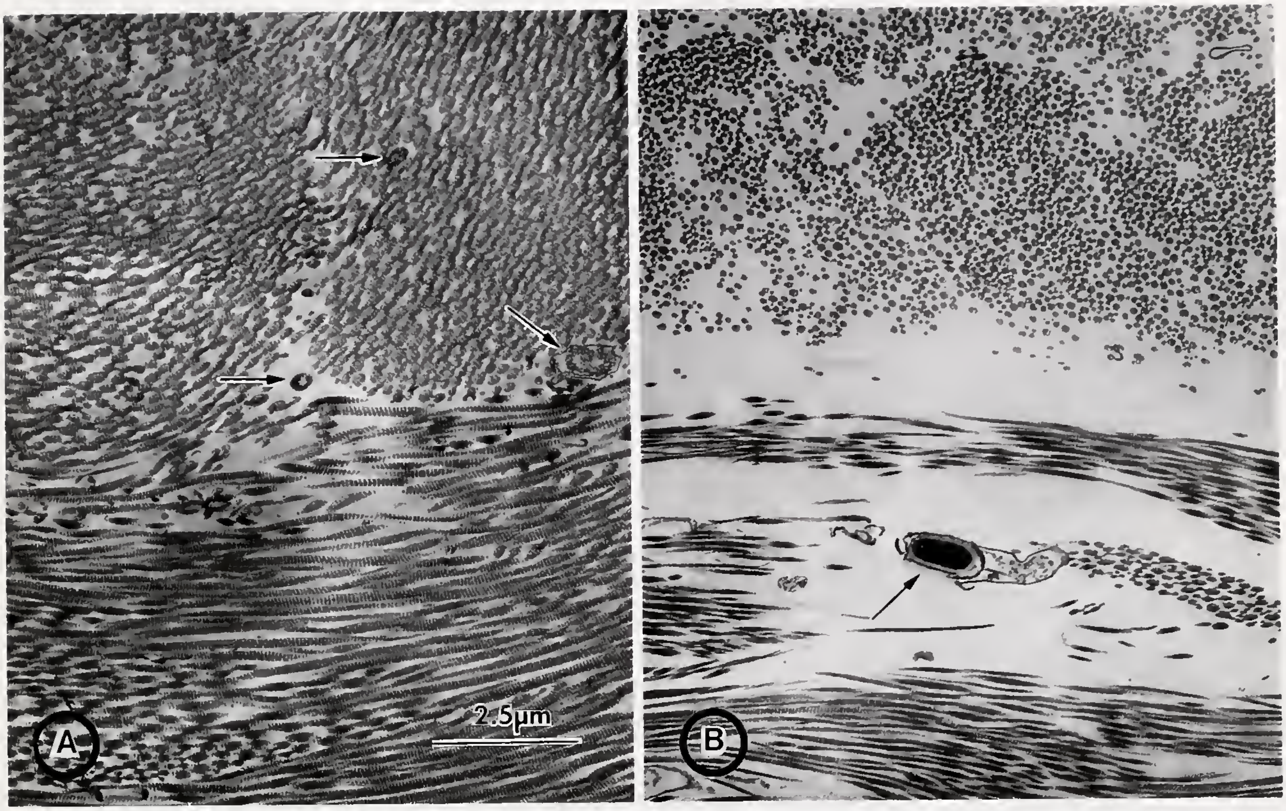

Figure 2. Low magnification transmission electron micrographs of sections of the Bermuda (A) and St. Augustine (B) carcasses. The collagen fibers of both tissues run in layers that are perpendicular to each other. Within each layer the fibers appear to be organized in bundles (see the upper half of A). This type of fiber organization is typical of skin collagen (see Discussion). Other than the fibers, no other cellular elements were found. Bacteria and bacterial spores (arrows) were scattered throughout the fiber layers in both samples.

prepared for electron microscopic examination. Although the exact composition of the original preservation medium was unknown for either tissue, the distinct odor of formalin was obvious in both. Indeed, Webb, in his correspondence with Dall, indicated that he had put several pieces of the body in formalin before sending them off to both Dall and Verrill (cited in Wood, 1971). We cut several pieces (1 mm^3) from each of the original tissue samples and placed them directly into 2.5% glutaraldehyde/2% paraformaldehyde in 0.1 M cacodylate buffer containing 0.3 M sucrose (~1100 mosm) (Bermuda sample) or 2% glutaraldehyde in 0.15 M cacodylate buffer containing 0.58 M sucrose (~1100 mosm) (Florida sample). The tissue samples remained in the fixative for several days. After fixation, the tissue pieces were post-fixed in 2% OsO_4 in the cacodylate-sucrose buffer, treated *en bloc* with 2% aqueous uranyl acetate, dehydrated in an ethanol series (35–100%), and embedded in epoxy resin (Spurr's medium). Thin sections showing a silver interference color were cut with a diamond knife on an ultramicrotome (Reichert, Ultracut E). The sections were mounted on copper grids and stained with 2% uranyl acetate for 5 min, followed by 0.2% lead citrate for 1.5 min (Venable and Coggeshall, 1965). The stained sections were examined with a transmission electron microscope (Zeiss EM 10 CA) at 80 kV.

Octopus mantle. The specimen of *B. arcticus* (USNM catalogue #884184) that provided a mantle tissue sample had been collected by trawl off the New Jersey coast during a 1981 cruise of the R/V *Delaware II* and had been placed immediately into formalin upon its capture. At some point, the octopus was transferred into isopropyl alcohol and had been stored in that solution until we were given access to it. We cut a section of the mantle off the octopus, rehydrated it and placed it into 2% glutaraldehyde. The tissue was then prepared for electron microscopy, as described above for the Florida sample. For light microscopy, thick sections were cut from the same specimen, stained with Richardson's stain (a mixture of methylene blue and Azure II), and viewed with bright-field optics (Zeiss, Photomicroscope II).

Whale blubber. We cut a small sample of blubber from a much larger piece that came from a male humpback whale that had died at sea and washed onto a beach in

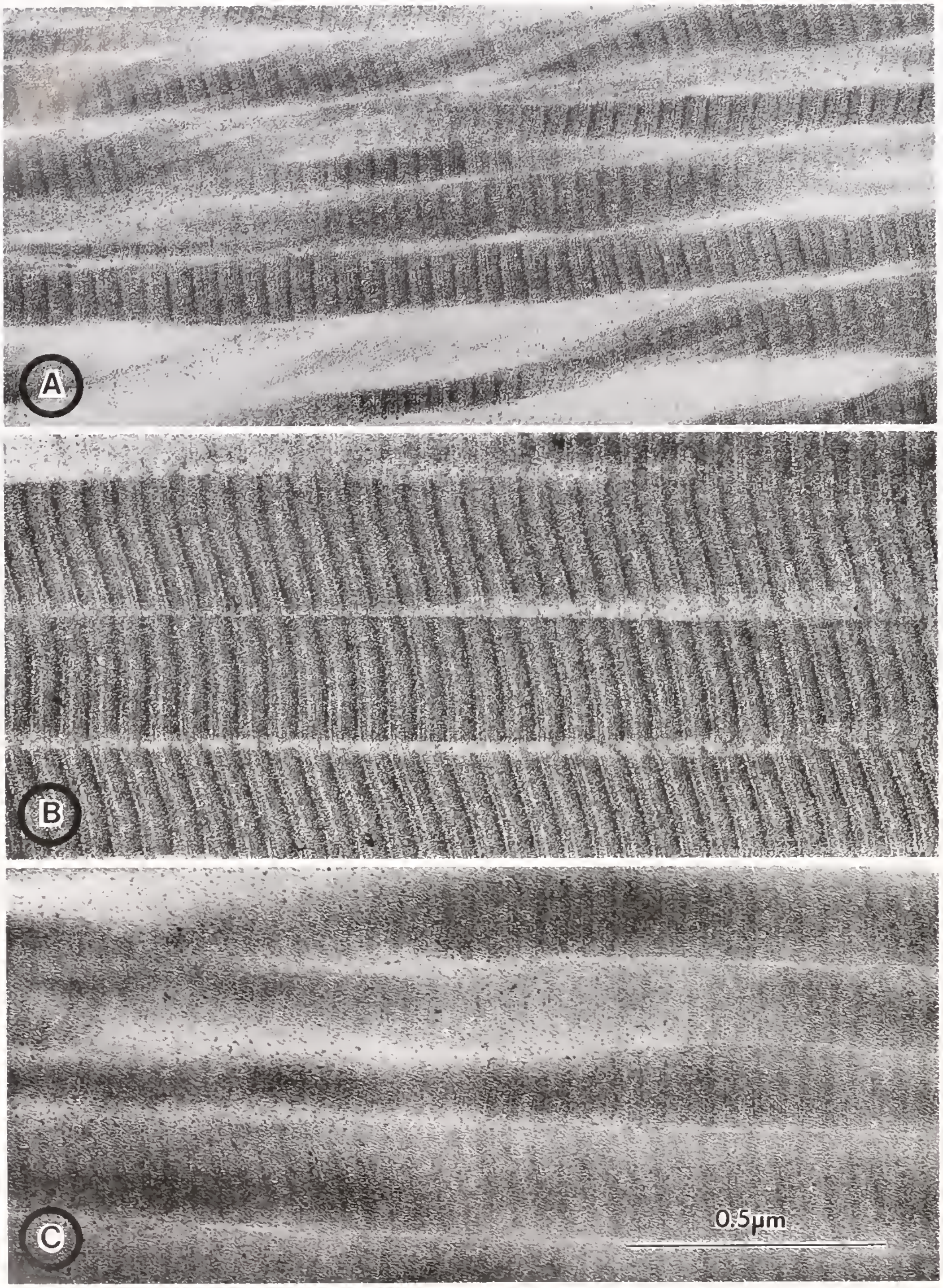

Figure 3. Higher magnification transmission electron micrographs showing the periodicity along the fibers of the St. Augustine collagen (A), rat tail tendon collagen (B), and the Bermuda collagen (C), all at the same magnification. The fibers of the St. Augustine and Bermuda samples are thinner than those in the rat tail tendon—a characteristic of skin collagen. The somewhat indistinct banding pattern of the Bermuda fibers is likely due to the poor original fixation. The dense deposits in this sample also derive from the original fixative solution.

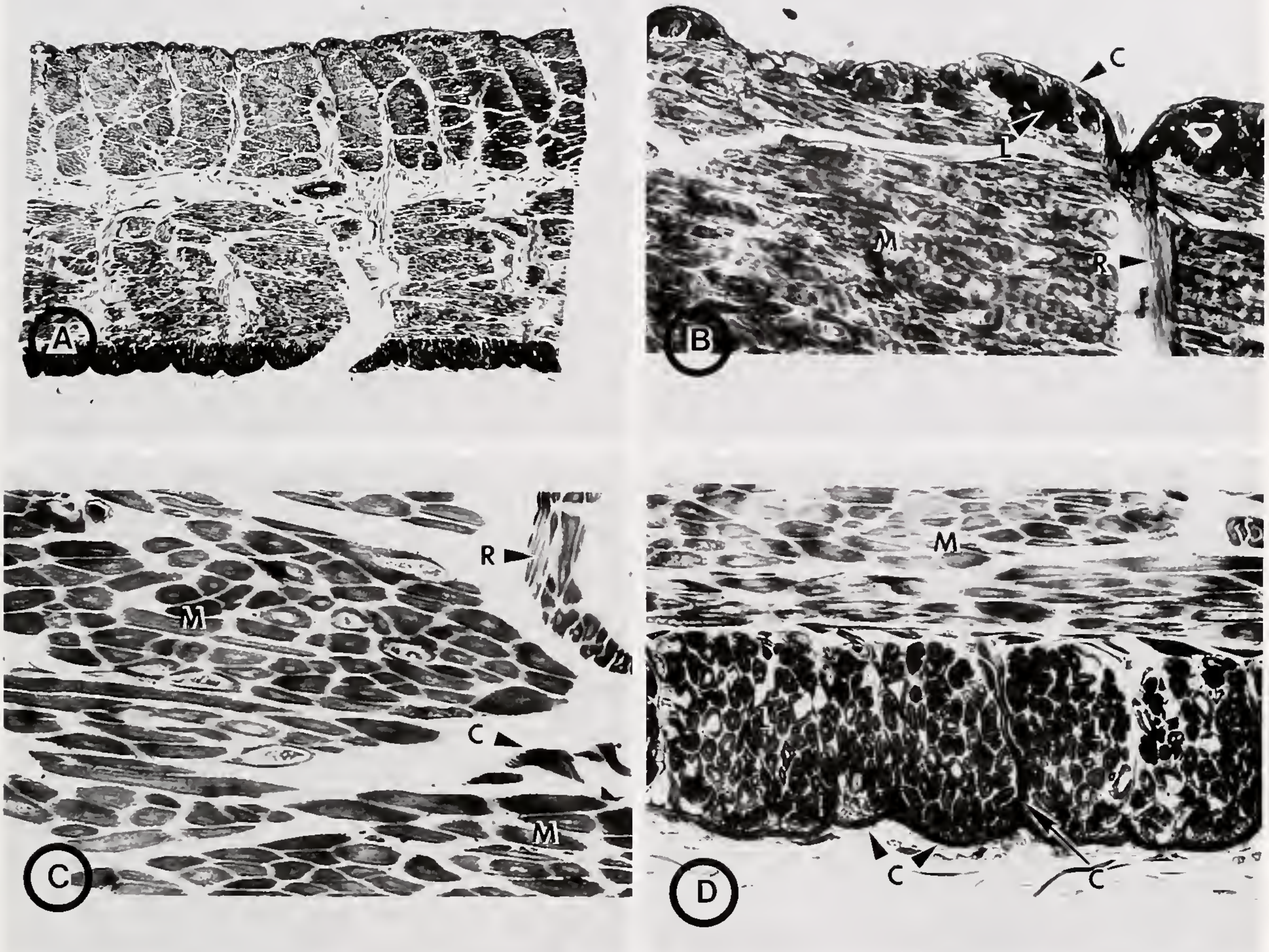

Figure 4. Light micrographs of cross sections taken through the width of the mantle of *Bathypolypus arcticus*. The epidermis, which consists of an epithelium underlain with a thin layer of dispersed collagen fibers, has been removed. (Micrograph A) The mantle consists of two primary layers of muscle bundles of about equal width. These layers are separated by a space that contains blood vessels (oval structure in the center) (magnification = 62×). (Micrograph B) The outer surface of the mantle consists of small bundles of longitudinal muscles (L) covered by a very thin layer of collagen (arrowhead C). Underlying the longitudinal muscles are muscle bundles that also run longitudinally, but containing individual fibers within each bundle that are not parallel to each other (M). Interspersed between these deeper bundles run thin radial muscles (R) which span the width of the mantle (see micrograph A, also) (magnification = 390×). (Micrograph C) Below the blood vessel layer run additional muscle bundles containing fibers with a wide array of orientations (M). Small bundles of collagen (arrowheads C) containing fibers that run parallel to each other occur occasionally between the muscle bundles. The hollow, tubular structure of the muscle cells is evident in this section (magnification = 390×). (Micrograph D) The inner surface of the mantle is also covered by a thin layer of collagen (arrowhead C) that extends upward between (arrow C) adjacent bundles of the longitudinal muscles (L). Although not shown in this section, the radial muscles insert between the longitudinal muscle bundles (see micrograph A). The longitudinal muscle bundles are much larger on this aspect of the mantle than those on the outer surface (compare with micrograph B). Immediately above the longitudinal muscles runs a thin bundle of circularly oriented muscle fibers (magnification = 390×).

Virginia Beach County, Virginia, in October 1992. According to the Virginia Museum of Science collection record, this carcass was 906 cm long (about 200 cm longer than the St. Augustine carcass) and only moderately decayed. The original piece of the blubber, still attached to the epidermis, had been preserved in formalin and deposited at the Smithsonian (catalogue #VMSM 921025). Our sample was transferred into 2% glutaraldehyde, small

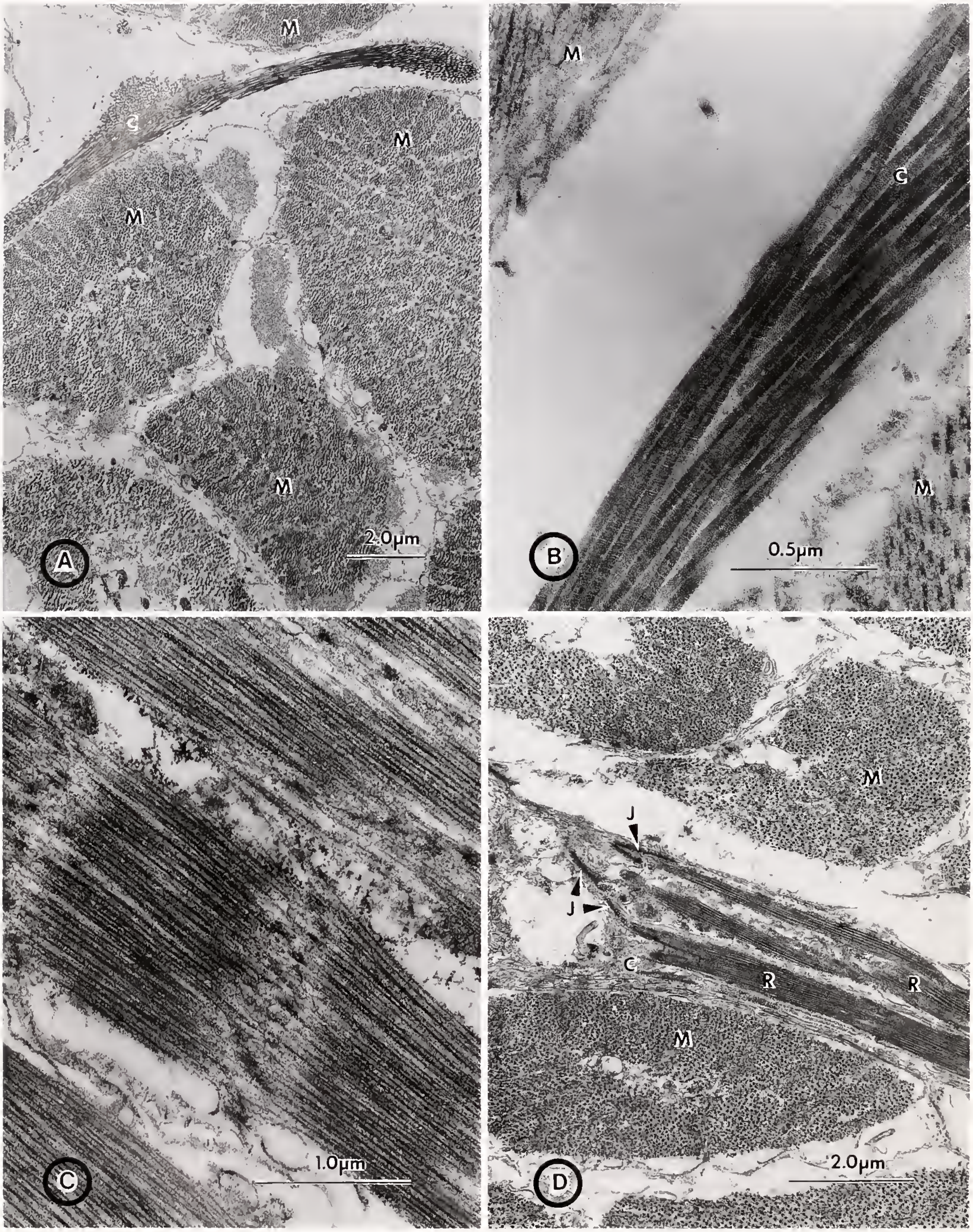

Figure 5. Electron micrographs of *Bathypolypus arcticus* mantle. (Micrograph A) This cross section shows the arrangement of the contractile proteins in bundles that radiate from the hollow center of each tubular muscle cell (M). Adjacent muscle fibers are separated by occasional bundles of collagen fibers (C). (Micrograph B) The fibers within the collagen bundles (C) always run parallel to each other. Adjacent layers of perpendicularly running collagen fibers were never seen. (Micrograph C) The contractile proteins within

pieces were cut from immediately under the epidermis, the middle, and the inner regions of the blubber, and all were prepared for electron microscopy as described above for the Florida sample.

Rat tail tendon and skin. Because our initial microscopic examination of sections from the carcasses found fibers that resembled collagen, we proceeded to measure the periodicity of the banding pattern of the fibers to confirm that identification. We used collagen fibers from rat tail tendon as an internal standard for these measurements. A piece of tail was obtained from a white rat that had been decapitated and immediately frozen for other experimental purposes. The tail was thawed, skinned, and the tail tendon removed. Pieces (1 mm^3) were cut from both the skin and tendon and fixed in 2% glutaraldehyde in 0.12 M phosphate buffer (pH 7.4). Following initial fixation, the tissue pieces were washed in the above buffer and then postfixed in 2% OsO_4 in the phosphate buffer. Subsequent preparative steps were the same as described above for the Florida sample.

Amino acid analysis

In the case of both samples, the small piece of tissue that remained following the microscopy (256 mg, Bermuda, 216 mg, St. Augustine) was soaked in several changes of artificial seawater (940 mosm) overnight at 4°C to wash out the preservative solution. The tissue was then cut into pieces (2 mm^3) and hydrolyzed for 24 h in 6 N HCl at 100°C. Both samples dissolved within 15 min of being placed into the acid. The hydrolysate was neutralized with NaOH and the amino acids extracted with an equal volume of 95% ethanol. The extract was centrifuged at 20,000 × g (4°C), and the supernatant was freeze-dried overnight. The residue was dissolved in 0.2 N lithium citrate buffer (pH 2.2), and the amino acid composition of this last solution determined with an automatic amino acid analyzer with ninhydrin detection (Beckman, System Gold). Amino acid concentrations were calculated by the System Gold software with norleucine as an internal standard, and then converted to residues/1000 residues for each individual amino acid. These data were graphically compared to the amino acid compositions of the collagens of 97 species from diverse phyla, according to the protocol described by Matsumura (1972).

Briefly, the Matsumura protocol consists of calculating the sum of each of the hydrophobic (valine, methionine, leucine, isoleucine, tyrosine, and phenylalanine), hydroxylated (hydroxyproline, threonine, serine, tyrosine, and hydroxylysine), and polar (aspartate, glutamate, hydroxylysine, lysine, histidine, ornithine, and arginine) amino acid residues per 1000 in the collagen hydrolysate. Each sum was divided by the grand sum of the three amino acid groups and then multiplied by 1000 to yield a set of three of Matsumura's R values. A vector **R** is then plotted on a triangular coordinate graph using the R values ($R_{\text{hydrophobic}}$, $R_{\text{hydroxylated}}$, and R_{polar}) as coordinates (Matsumura, 1972).

Results

The electron microscopy and the amino acid analysis indicate that both the Bermuda and St. Augustine carcasses are made up almost exclusively of collagen fibers.

The pieces of tissue from the Bermuda and St. Augustine carcasses contain layers of fibers showing banding patterns that are characteristic of collagen, a few scattered bacteria and bacterial spores, and no other cellular structures (Fig. 2). In both specimens, adjacent layers of the collagen fibers run perpendicular to each other. Although the fixation of the Bermuda sample is not very good, longitudinal sections of the two specimens appear very similar at low, and even at high, magnifications. Certainly, the banding periodicity along the fibers is similar both to each other and to rat tail tendon collagen (Fig. 3). We measured the distance between the major periods along several fibers in several sections at both low and high magnification. The averages were 54.3 nm (±2.72 SD, n = 150 measurements) for the St. Augustine collagen and 57.9 nm (±5.37 SD, n = 154 measurements) for the Bermuda fibers. Although these values are slightly less than the usually published periodicity for collagen banding (60 nm), control samples of both rat tail tendon (Fig. 3B) and rat skin collagen yielded a banding periodicity of 55.7 nm (±5.6 SD) with our protocol. The diameter of the individual fibers was also determined from micrographs of both cross sections and longitudinal sections. The average for the St. Augustine collagen was 109 nm (±25.2 SD, n = 68), 156 nm (±34.7 SD, n = 106) for the Bermuda collagen, and 173 nm (±82.0 SD, n = 31) for rat tail tendon collagen.

Microscopic examination of *Bathypolypus arcticus* mantle revealed a structure that is dramatically different from that of the two carcasses. In particular, the massive, perpendicular collagen fiber arrangement characteristic of the two carcasses is completely absent in the octopus

---

the sarcomeres of the mantle muscle cells are not in register. (Micrograph D). The radial muscles (R) that span the width of the mantle between the rest of the mantle musculature (M) are attached to the inner and outer layer of collagen (C) by junctional complexes (J). The dorsal surface of the mantle lies to the left of this micrograph.

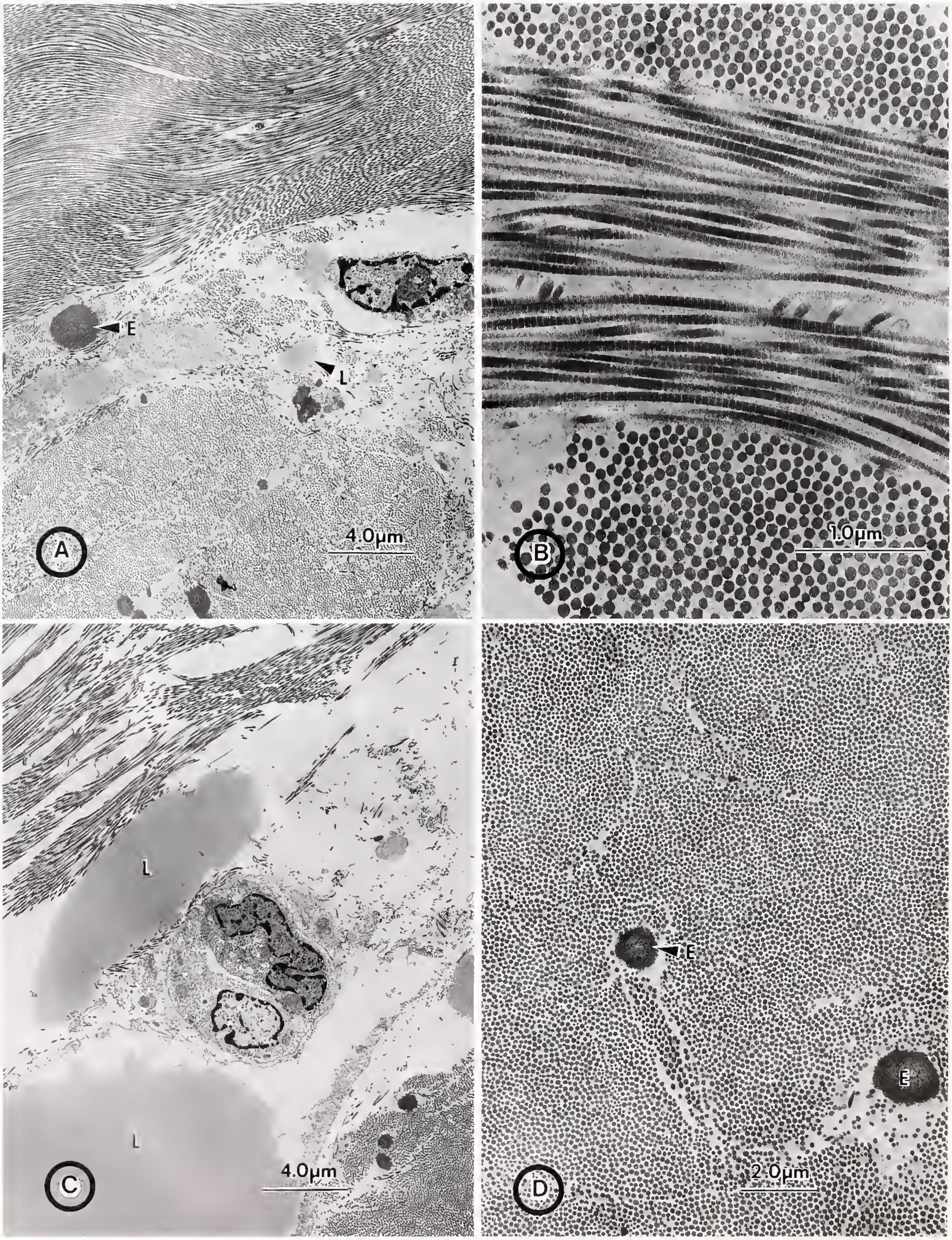

Figure 6. Electron micrographs of blubber from *Megaptera novaeangelae* (Micrograph A—taken near the epidermis) Large bundles of perpendicularly oriented collagen fibers are interspersed with cells (most of which appear to be fibroblasts), lipid deposits (L), and occasional elastin fibers (E). (Micrograph B) Collagen

mantle. Instead, the bulk of the mantle is composed of muscle. Small amounts of collagen are located in thin sheets, one between the epithelial cell layer of the epidermis and the outer surface of the mantle, the other covering the inner surface of the mantle. In addition, collagen also occurs in an internal network of small bundles of parallel fibers running between the muscle bundles (Fig. 4). The banding periodicity along the octopus collagen fibers was 46.6 nm (±8.6 SD, $n = 90$), 15% smaller than the periodicity of the St. Augustine collagen.

The muscle fibers that make up the bulk of the mantle are arranged in several layers (Fig. 4). Immediately under a thin external collagen layer is a layer of parallel muscle fibers that runs longitudinally from the mantle edge. These fibers are separated laterally from each other by thin downward extensions of the covering collagen sheet (Fig. 4B). A similar muscle layer, although consisting of larger diameter fibers, is located immediately inside the collagen layer that forms the inner surface of the mantle (Fig. 4D). The center of the mantle is occupied by a space that contains blood vessels (Fig. 4A). Ventrally—between the blood vessel space and the inner, longitudinal muscle layer—lie several layers of muscle fibers that run at a variety of angles oblique to the cross-section (Fig. 4C). Dorsally, between the blood vessel space and the outer longitudinal muscle layer, the muscle fibers generally run in the same direction as the fibers of the outer muscle bundles (Fig. 4B). Lastly, the outer and inner collagen sheets are occasionally connected to each other by thin, radial muscle bundles that traverse the width of the mantle, perpendicular to the rest of the musculature and attached to the collagen sheets by a junctional complex (Figs. 4A, B, C; 5D). All of this structure is supported by occasional thin bundles of parallel-running collagen fibers (Fig. 5A, B). Altogether, there is nothing in the octopus mantle morphology that resembles anything in the two relics.

The mantle muscle cells are basically hollow tubes, tapered at each end. The contractile proteins are arranged in bundles that are rectangular in cross-section and radiate out from the hollow center of the cell like tightly packed spokes (Fig. 5A). The nucleus and mitochondria are located in the center of the cell. The arrangement of sarcomeres in the octopus mantle muscle gives the appearance of oblique striations in occasional sections, but the contractile filaments within each sarcomere are not striated (Fig. 5C). Thick filaments, reminiscent of paramyosin, surrounded by thin filaments are evident in cross sections of the muscle cells. Squid mantle muscle cells have a similar fine structure (Ward and Wainwright, 1972).

Microscopic examination of the blubber from the humpback whale revealed a massive matrix of collagen fibers present throughout the entire thickness of the tissue (Fig. 6). Fat deposits and poorly fixed cellular structure were evident between layers of collagen fibers in the sections of the blubber taken both close to the epidermis and from the medial region (Fig. 6A, C). Neither fat nor any remnant of cellular structure was found in either the Florida or Bermuda carcass. The sections taken from the inner aspect of the blubber layer contained only collagen fibers in very large bundles, interspersed with occasional larger fibers that appeared to be elastin (Fig. 6D). At all levels of section, the collagen fiber arrangement of the blubber was exactly that of the Florida and Bermuda carcasses, namely, bundles arranged in layers running perpendicular to adjacent layers (Fig. 6A, B, C). The banding periodicity along the whale collagen fibers was 54.6 nm (±5.1 SD, $n = 83$), essentially identical to the banding of the St. Augustine collagen.

The amino acid analyses of the tissues from the two carcasses were also suggestive of collagen. Glycine accounts for about one third of the amino acid residues in both tissues, and both hydroxylysine and hydroxyproline were present as well; these features are virtually diagnostic of collagen (Table I). However, the amino acid compositions of the hydrolysates of the two carcasses are quite different from each other. In particular, the St. Augustine carcass is very rich in proline (169 residues/1000) and quite low in lysine (0.4 residues/1000), in comparison to both the Bermuda collagen (88 residues/1000 and 10 residues/1000, respectively) and skin collagens from several other species (Table I). Of course, the unusually low lysine values in the St. Augustine sample may be an artifact of a century in formalin. Only whale skin collagen (species not reported in Eastoe, 1955) has proline residues/1000 that are anywhere near those from the St. Augustine collagen (Table I). In addition, the amino acid composition of the St. Augustine collagen is very different from that

fibers arranged in bundles running perpendicular to each other are everywhere throughout the entire thickness of the blubber. The size of the bundles varies, depending upon location within the width of the blubber. (Micrograph C—from the middle of the blubber layer). The lipid deposits (L) in this region of the blubber were larger and more frequent than the other areas examined. The perpendicular arrangement of the collagen bundles surrounding the fat deposits was still evident (lower right hand corner and upper left hand corner). (Micrograph D—taken from the inner aspect of the blubber layer) The collagen bundles were very large in this region. The expanse of collagen fibers shown here are all in cross section, and were bounded by equally large expanses of perpendicularly running collagen fibers. Very few cells or lipid deposits were encountered in this region of the blubber, although elastin fibers (E) were quite common.

Table I

Comparative amino acid compositions of skin collagens of several species and the Bermuda and St. Augustine carcasses (values are amino acid residues/1000 residues)

Amino acid	Bermuda carcass	St. Augustine carcass	Octopus mantle[1]	Squid mantle[2]	Carp[3]	Whale skin[4]	Shark skin[5]
Asp	52	50	53	58	48	46	43
Thr	27	28	28	26	25	24	23
Ser	47	45	52	47	43	41	61
OH-Pro	79	54	95	89	82	89	60
Pro	88	169	101	96	117	128	106
Glu	83	82	64	86	69	70	68
Gly	339	330	324	308	326	326	338
Ala	113	106	100	89	119	111	106
Val	25	18	19	21	18	21	25
Cys	0	0	8	4	0	0	0
Met	0	0	6	8	14	5	18
Ileu	14	11	22	21	11	11	15
Leu	32	28	30	32	22	25	25
Tyr	0	0	5	5	3	4	3
Phe	16	14	8	12	14	13	13
OH-Lys	13.1	15.3	15.7	16.1	7.1	6	5.5
Lys	10	0.4	11	15	25	26	27
His	6	4	3	7	5	6	13
Arg	55	48	58	59	52	50	51

[1] Pepsin-extracted collagen from *Octopus vulgaris* body wall (Kimura *et al.*, 1969).

[2] Pepsin-extracted collagen from *Todarodes pacificus* body wall (Kimura *et al.*, 1969).

[3] Gelatin from skin (Piez and Gross, 1960).

[4] Whale skin gelatin, species not reported (Eastoe, 1955).

[5] 0.5 *M* acetic-acid-extracted skin collagen from *Squalus acanthus* (Piez *et al.*, 1963).

of both squid (*Todarodes pacificus*) and octopus (*Octopus vulgaris*) mantle (Kimura *et al.*, 1969), especially with respect to the proline, hydroxyproline and lysine residues (Table I).

Finally, the ratios of hydrophobic, hydroxylated, and polar amino acids, calculated according to the procedures described by Matsumura (1972), were 183, 353, and 464 for the Bermuda sample and 172, 345, and 483 for the St. Augustine sample. These values mapped both collagens into Matsumura's "S range" along with most striated, structural collagens from both invertebrate and vertebrate species. Interestingly, within the S range, the values for the St. Augustine sample were quite close to those for a frog (*Rana temporaria*) skin, while the Bermuda sample mapped near a number of bovine collagens, as well as chick bone, carp skin, and wallaby tail tendon collagens. The results of this comparison must be viewed with some caution, because the lengthy formaldehyde fixation of the Bermuda and St. Augustine fibers may have caused some changes in the amino acid composition of the protein. In addition, the small amount of tissue we had to work with limited the number of analyses we could do for statistical purposes. Nevertheless, neither of the relic specimens mapped close to invertebrate collagens within the S range, including those of octopus and squid (Matsumura, 1972).

Discussion

The microscopy and amino acid analyses clearly demonstrate that both the St. Augustine and Bermuda carcasses were large pieces (extremely large, in the case of the former) of almost pure collagen. Apparently, both pieces of tissue had been in the ocean long enough, *post mortem*, that bacterial action had recycled all but the most resistant of the proteins. Neither carcass is from a giant octopus nor any other invertebrate, but they are also not from the same species.

The electron micrographs of both the St. Augustine and Bermuda samples show fibers with the characteristic banding pattern of collagen. The width of the repeating unit along the fibers is essentially identical to that of rat tail tendon collagen, and the intraperiod banding, although somewhat indistinct, is typical of collagen. In addition, the whale blubber collagen banding periodicity was the same as that of the St. Augustine collagen, while that of the octopus mantle collagen was much less than any of the other samples. This comparison must be viewed cautiously, however, since the differences in the original fixations may have produced artifacts in the banding patterns.

The organization of the collagen fiber bundles in the two relic samples is typical of dermis from a number of vertebrate groups, including fish, amphibians, and reptiles, where the bundles are distinctly layered (Moss, 1972). A similar layering pattern of the collagen fibers was nowhere to be found in the octopus mantle tissue we examined here. Instead, the octopus mantle is composed mainly of a complex network of muscle fibers containing only small amounts of widely dispersed collagen fibers, as might be expected of an animal so capable of shape-changing. We found absolutely nothing in the octopus mantle morphology that was comparable to the collagen fiber arrangement in the two carcasses, nor has anything similar been reported in squid or cuttlefish mantle (reviewed by Packard, 1988). In contrast, the similarity between the layering pattern of the collagen fiber support matrix of the humpback whale blubber and the fiber pattern in the carcasses is quite obvious. In addition, unlike the octopus mantle, but very much like the Florida and Bermuda tissues, collagen fibers are the main component of the blubber. The whale tissue we examined here also contained fat deposits and cellular structures that were not present in either the Florida or the Bermuda carcass. However, the humpback whale that provided our blubber sample had only recently expired and did not approach the advanced state of decay of the tissues of the two relics. Thus, the fine structure indicates that both carcasses were actually only the collagenous remains of skin, rather than an entire animal, and the organization of the skins is reminiscent of both lower vertebrates and whale blubber. In addition, the thickness of the St. Augustine carcass [3.5 inches (Webb's letter to Verrill dated Jan. 14, 1897) to 10.5 inches (Webb's letter to Dall dated Feb. 12, 1897)] is consistent with whale blubber.

Collagen fiber diameters within an organism range widely from the very thin fibers typical of cartilage and cornea to the comparatively thick fibers of dermis and tendon. The thickness of the fibers within both our samples is also consistent with the diagnosis of their origin in skin. Furthermore, while the diameter of skin collagen fibers can vary both with the age of the organism and the distance from the epithelium (Flint *et al.*, 1984), the unimodal distribution of fiber diameter and the tight packaging of the fibers within both our specimens are typical of a "non-active skin" characteristic of mammals (including pygmy sperm whale blubber, Craig *et al.*, 1987) and birds. In contrast, collagen fiber diameters from the "active" skins of fish, sharks, and reptiles usually have either a bimodal distribution or a distribution skewed towards larger diameters (Craig *et al.*, 1987).

The amino acid compositions of the hydrolysates of the St. Augustine and Bermuda specimens confirm the collagen identification indicated by our microscopy. In addition, they provide some indication of the phyletic source of the two carcasses. One third of the amino acid residues in both samples are glycine. That large an amount of glycine, taken together with the presence of hydroxyproline and hydroxylysine, is diagnostic of collagen. The absence of methionine from both samples and the extremely low lysine values in the St. Augustine sample are unusual and are, perhaps, the result of exposure to whatever preservation chemicals were actually used. The number of proline residues in the St. Augustine collagen is surprisingly high, and the level of that imino acid may be the most important clue to its specific origin. The denaturation temperature of collagen is directly proportional to its total imino acid content. In particular, the imino acids provide the collagen molecule with a degree of thermal stability required at the elevated body temperatures of the homiothermic species (Rigby, 1968; Hochachka and Somero, 1984). Thus, the collagens from invertebrates and poikilothermic vertebrates are relatively low in total imino acid residues (generally less than 200 residues/1000), while homiothermic vertebrate collagens have a combined imino acid total that is usually higher (210 residues/1000 or greater; for examples see the data tabulated in Kimura *et al.*, 1969; Eastoe, 1955). Thus, the total imino acid content of the Bermuda sample (167 residues/1000), together with the rest of the amino acid composition and morphological data presented above, suggests that the source of that collagen was the skin of a poikilothermic vertebrate. Indeed, the relatively small mass of the carcass is easily within the size range of either a large teleost or an elasmobranch. On the other hand, the elevated imino acid content of the St. Augustine collagen (223 residues/1000) together with its amino acid composition, fine structure, and size of the carcass all indicate that it was the remains of the skin of an enormous warm-blooded vertebrate.

Altogether, and with profound sadness at ruining a favorite legend, we find no basis for the existence of *Octopus giganteus*. We concur with Verrill's (1897e) and Lucas' (1897) final words on the matter, that the St. Augustine sea monster was "the remains of a whale, likely the entire skin [blubber layer] . . . nothing more or less."

Acknowledgments

Samples of the St. Augustine and Bermuda carcasses were kindly provided by Professor Joseph Gennaro of the University of Florida and Teddy Tucker of Bermuda, respectively. Samples of *Bathypolypus arcticus* mantle were kindly provided by both Dr. Clyde Roper of the Smithsonian Museum of Natural History and Dr. Don Flecher of the NOAA Laboratory in Woods Hole, Massachusetts. The sample of humpback whale blubber was kindly provided by Dr. Charles Potter, also of the Smithsonian Museum of Natural History. The sample of rat tail was kindly provided by Dr. Tom Castonguay of the Department of Nutrition and Food Science at the University of Maryland.

This work was supported with funds provided by the University of Maryland Agricultural Experiment Station and the National Science Foundation (IBN-9117248). It is contribution #71 from the Laboratory for Biological Ultrastructure at the University of Maryland and contribution #313 from the Tallahassee, Sopchoppy & Gulf Coast Marine Biological Association.

Literature Cited

Craig, A. S., E. F. Eikenberry and D. A. D. Parry. 1987. Ultrastructural organization of skin: classification on the basis of mechanical role. *Connective Tissue Res.* **16:** 212–223.

Eastoe, J. E. 1955. The amino acid composition of mammalian collagen and gelatin. *Biochem. J.* **61:** 589–600.

Ellis, R. 1994. *Monsters of the Sea.* A. A. Knopf, New York. Pp 301–322.

Flint, M. H., A. S. Craig, H. C. Reilly, G. C. Gillard, and D. A. D. Parry. 1984. Collagen fibril diameters and glycosaminoglycan content of skins—Indices of tissue maturity and function. *Connective Tissue Res.* **13:** 69–81.

Gennaro, J. F., Jr. 1971. An octopus trilogy. Part 2. The creature revealed. *Nat. History* **80:** 24.

Hochachka, P. W., and G. N. Somero. 1984. *Biochemical Adaptation.* Princeton University Press, New Jersey. Pp. 415–416.

Lucas, F. A. 1897. The Florida monster. *Science* **5(116):** 476.

Kimura, S., Y. Nagoka, and M. Kubota. 1969. Studies on marine invertebrate collagens—I. Some collagens from crustaceans and molluscs. *Bull. Jpn. Soc. Sci. Fish.* **35:** 743–748.

Mackal, R. P. 1986. Biochemical analyses of preserved *Octopus giganteus* tissue. *Cryptozoology* **5:** 55–62.

Matsumura, T. 1972. Relationship between amino acid composition and differentiation of collagen. *Int. J. Biochem.* **3:** 265–274.

Milne, D. H. 1995. *Marine Life and the Sea.* Wadsworth, New York. p. 171.

Moss, M. L. 1972. The vertebrate dermis and the integumental skeleton. *Am. Zool.* **12:** 27–34.

Packard, A. 1988. The skin of cephalopods (coleoids): general and special adaptations. Pp. 37–67 in *The Mollusca Volume 11–Form and Function,* E. R. Trueman and M. R. Clarke, eds. Academic Press, New York.

Piez, K. A., E. A. Eigner, and M. Lewis. 1963. The chromatographic separation and amino acid composition of several collagens. *Biochemistry* **2:** 58–66.

Piez, K. A., and J. Gross. 1960. The amino acid composition of some fish collagens: the relationship between composition and structure. *J. Biol. Chem.* **235:** 995–998.

Rigby, B. J. 1968. Temperature relationships of poikilotherms and the melting temperature of molecular collagen. *Biol. Bull.* **135:** 223–229.

Venable, J. H., and R. Coggeshall. 1965. A simplified lead citrate stain for use in electron microscopy. *J. Cell Biol.* **25:** 407–408.

Verrill, A. E. 1897a. A gigantic cephalopod on the Florida Coast. *Am. J. Sci.* 4th series, **3:** 79.

Verrill, A. E. 1897b. Additional information concerning the giant cephalopod of Florida. *Am. J. Sci.* 4th series, **3:** 162.

Verrill, A. E. 1897c. The supposed great Octopus of Florida; certainly not a cephalopod. *Am. J. Sci.* 4th series, **3:** 355.

Verrill, A. E. 1897d. The Florida monster. *Science* **5(114):** 392.

Verrill, A. E. 1897e. The Florida sea monster. *Science* **5(116):** 476.

Ward, D. V., and S. A. Wainwright. 1972. Locomotory aspects of squid mantle structure. *J. Zool.* **167:** 437–449.

Wood, F. G. 1971. An octopus trilogy. Part 1. Stupefying colossus of the deep. *Nat. History* **80:** 15–24.

CONTENTS

RESEARCH NOTES

Zimmer-Faust, Richard K., Christopher M. Finelli, N. Dean Pentcheff, and David S. Wethey
Odor plumes and animal navigation in turbulent water flow: a field study 111

Toro, J. E., and A. M. Vergara
Evidence for selection against heterozygotes: post-settlement excess of allozyme homozygosity in a cohort of the Chilean oyster, *Ostrea chilensis* Philippi, 1845 117

REVIEWS

del Castillo, José, David S. Smith, Ada M. Vidal, and César Sierra
Catch in the primary spines of the sea urchin *Eucidaris tribuloides:* a brief review and a new interpretation 120

CELL BIOLOGY

Weidner, Earl, S. B. Manale, S. K. Halonen, and J. W. Lynn
Protein-membrane interaction is essential to normal assembly of the microsporidian spore invasion tube 128

DEVELOPMENT AND REPRODUCTION

Abraham, V. C., A. L. Miller, and R. A. Fluck
Microtubule arrays during ooplasmic segregation in the medaka fish egg (*Oryzias latipes*) 136

Webb, Tamika A., Wendy J. Kowalski, and Richard A. Fluck
Microtubule-based movements during ooplasmic segregation in the medaka fish egg (*Oryzias latipes*) 146

Scholtz, Gerhard
Expression of the *engrailed* gene reveals nine putative segment-anlagen in the embryonic pleon of the freshwater crayfish *Cherax destructor* (Crustacea, Malacostraca, Decapoda) 157

ECOLOGY

Saigusa, Masayuki, and Tadashi Akiyama
The tidal rhythm of emergence, and the seasonal variation of this synchrony, in an intertidal midge 166

NEUROBIOLOGY AND BEHAVIOR

Guirguis, M. S., and J. L. Wilkens
The role of the cardioregulatory nerves in mediating heart rate responses to locomotion, reduced stroke volume, and neurohormones in *Homarus americanus* 179

PHYSIOLOGY

McGaw, I. J., and B. R. McMahon
The FMRFamide-related peptides F1 and F2 alter hemolymph distribution and cardiac output in the crab *Cancer magister* 186

McCurley, R. Skyler, and William M. Kier
The functional morphology of starfish tube feet: the role of a crossed-fiber helical array in movement 197

McAuley, P. J.
Ammonium metabolism in the green hydra symbiosis 210

SEA MONSTERS

Pierce, Sidney K., Gerald N. Smith, Jr., Timothy K. Maugel, and Eugenie Clark
On the giant octopus (*Octopus giganteus*) and the Bermuda Blob: homage to A. E. Verrill 219

Volume 188 Number 3

THE BIOLOGICAL BULLETIN

Marine Biological Laboratory/
Woods Hole Oceanographic Institution
Library

JUN 26 1995

Woods Hole MA 02543

JUNE, 1995

Published by the Marine Biological Laboratory

THE
BIOLOGICAL BULLETIN

PUBLISHED BY
THE MARINE BIOLOGICAL LABORATORY

Associate Editors

Peter A. V. Anderson, The Whitney Laboratory, University of Florida
William D. Cohen, Hunter College, City University of New York
David Epel, Hopkins Marine Station, Stanford University
J. Malcolm Shick, University of Maine, Orono

Editorial Board

Peter B. Armstrong, University of California, Davis
Thomas H. Dietz, Louisiana State University
Daphne Gail Fautin, University of Kansas
William F. Gilly, Hopkins Marine Station, Stanford University
Roger T. Hanlon, Marine Biomedical Institute, University of Texas Medical Branch
Michael LaBarbera, University of Chicago
Charles B. Metz, University of Miami
K. Ranga Rao, University of West Florida
Baruch Rinkevich, Israel Oceanographic & Limnological Research Ltd.
Richard Strathmann, Friday Harbor Laboratories, University of Washington
Steven Vogel, Duke University
J. Herbert Waite, University of Delaware
Sarah Ann Woodin, University of South Carolina
Richard K. Zimmer-Faust, University of South Carolina

Editor: MICHAEL J. GREENBERG, The Whitney Laboratory, University of Florida
Managing Editor: PAMELA L. CLAPP, Marine Biological Laboratory

JUNE, 1995

Printed and Issued by
LANCASTER PRESS, Inc.
3575 HEMPLAND ROAD
LANCASTER, PA

THE BIOLOGICAL BULLETIN

THE BIOLOGICAL BULLETIN is published six times a year by the Marine Biological Laboratory, MBL Street, Woods Hole, Massachusetts 02543.

Subscriptions and similar matter should be addressed to Subscription Manager, THE BIOLOGICAL BULLETIN, Marine Biological Laboratory, Woods Hole, Massachusetts 02543. Single numbers, $37.50. Subscription per volume (three issues), $92.50 ($185.00 per year for six issues).

Communications relative to manuscripts should be sent to Michael J. Greenberg, Editor-in-Chief, or Pamela L. Clapp, Managing Editor, at the Marine Biological Laboratory, Woods Hole, Massachusetts 02543. Telephone: (508) 548-3705, ext. 428. FAX: 508-540-6902. E-mail: pclapp@hoh.mbl.edu.

THE BIOLOGICAL BULLETIN is indexed in bibliographic services including *Index Medicus* and MEDLINE, *Chemical Abstracts*, and *Current Contents*.

Printed on acid free paper,
effective with Volume 180, Issue 1, 1991.

POSTMASTER: Send address changes to THE BIOLOGICAL BULLETIN, Marine Biological Laboratory,
Woods Hole, MA 02543.

Copyright © 1995, by the Marine Biological Laboratory

Second-class postage paid at Woods Hole, MA, and additional mailing offices.
ISSN 0006-3185

INSTRUCTIONS TO AUTHORS

The Biological Bulletin accepts outstanding original research reports of general interest to biologists throughout the world. Papers are usually of intermediate length (10–40 manuscript pages). A limited number of solicited review papers may be accepted after formal review. A paper will usually appear within four months after its acceptance.

Very short, especially topical papers (less than 9 manuscript pages including tables, figures, and bibliography) will be published in a separate section entitled "Research Notes." A Research Note in *The Biological Bulletin* follows the format of similar notes in *Nature*. It should open with a summary paragraph of 150 to 200 words comprising the introduction and the conclusions. The rest of the text should continue on without subheadings, and there should be no more than 30 references. References should be referred to in the text by number, and listed in the Literature Cited section in the order that they appear in the text. Unlike references in *Nature*, references in the Research Notes section should conform in punctuation and arrangement to the style of recent issues of *The Biological Bulletin*. Materials and Methods should be incorporated into appropriate figure legends. See the article by Lohmann *et al.* (October 1990, Vol. 179: 214–218) for sample style. A Research Note will usually appear within two months after its acceptance.

The Editorial Board requests that regular manuscripts conform to the requirements set below; those manuscripts that do not conform will be returned to authors for correction before review.

1. ***Manuscripts.*** Manuscripts, including figures, should be submitted in triplicate. (Xerox copies of photographs are not acceptable for review purposes.) The submission letter accompanying the manuscript should include a telephone number, a FAX number, and (if possible) an E-mail address for the corresponding author. The original manuscript must be typed in no smaller than 12 pitch or 10 point, using double spacing (*including* figure legends, footnotes, bibliography, etc.) on one side of 16- or 20-lb. bond paper, 8½ by 11 inches. Please, no right justification. Manuscripts should be proofread carefully and errors corrected legibly in black ink. Pages should be numbered consecutively. Margins on all sides should be at least 1 inch (2.5 cm). Manuscripts should conform to the *Council of Biology Editors Style Manual*, 5th Edition (Council of Biology Editors, 1983) and to American spelling. Unusual abbreviations should be kept to a minimum and should be spelled out on first reference as well as defined in a footnote on the title page. Manuscripts should be divided into the following components: Title page, Abstract (of no more than 200 words), Introduction, Materials and Methods, Results, Discussion, Acknowledgments, Literature Cited, Tables, and Figure Legends. In addition, authors should supply a list of words and phrases under which the article should be indexed.

2. ***Title page.*** The title page consists of a condensed title or running head of no more than 35 letters and spaces, the manuscript title, authors' names and appropriate addresses, and footnotes listing present addresses, acknowledgments or contribution numbers, and explanation of unusual abbreviations.

3. ***Figures.*** The dimensions of the printed page, 7 by 9 inches, should be kept in mind in preparing figures for publication. We recommend that figures be about 1½ times the linear dimensions of the final printing desired, and that the ratio of the largest to the smallest letter or number and of the thickest to the thinnest line not exceed 1:1.5. Explanatory matter generally should be included in legends, although axes should always be identified on the illustration itself. Figures should be prepared for reproduction as either line cuts or halftones. Figures to be reproduced as line cuts should be unmounted glossy photographic reproductions or drawn in black ink on white paper, good-quality tracing cloth or plastic, or blue-lined coordinate paper. Those to be reproduced as halftones should be mounted on board, with both designating numbers or letters and scale bars affixed directly to the figures. All figures should be numbered

in consecutive order, with no distinction between text and plate figures. The author's name and an arrow indicating orientation should appear on the reverse side of all figures.

4. ***Tables, footnotes, figure legends, etc.*** Authors should follow the style in a recent issue of *The Biological Bulletin* in preparing table headings, figure legends, and the like. Because of the high cost of setting tabular material in type, authors are asked to limit such material as much as possible. Tables, with their headings and footnotes, should be typed on separate sheets, numbered with consecutive Roman numerals, and placed after the Literature Cited. Figure legends should contain enough information to make the figure intelligible separate from the text. Legends should be typed double spaced, with consecutive Arabic numbers, on a separate sheet at the end of the paper. Footnotes should be limited to authors' current addresses, acknowledgments or contribution numbers, and explanation of unusual abbreviations. All such footnotes should appear on the title page. Footnotes are not normally permitted in the body of the text.

5. ***Literature cited.*** In the text, literature should be cited by the Harvard system, with papers by more than two authors cited as Jones *et al.*, 1980. Personal communications and material in preparation or in press should be cited in the text only, with author's initials and institutions, unless the material has been formally accepted and a volume number can be supplied. The list of references following the text should be headed Literature Cited, and must be typed double spaced on separate pages, conforming in punctuation and arrangement to the style of recent issues of *The Biological Bulletin.* Citations should include complete titles and inclusive pagination. Journal abbreviations should normally follow those of the U. S. A. Standards Institute (USASI), as adopted by BIOLOGICAL ABSTRACTS and CHEMICAL ABSTRACTS, with the minor differences set out below. The most generally useful list of biological journal titles is that published each year by BIOLOGICAL ABSTRACTS (BIOSIS List of Serials; the most recent issue). Foreign authors, and others who are accustomed to using THE WORLD LIST OF SCIENTIFIC PERIODICALS, may find a booklet published by the Biological Council of the U.K. (obtainable from the Institute of Biology, 41 Queen's Gate, London, S.W.7, England, U.K.) useful, since it sets out the WORLD LIST abbreviations for most biological journals with notes of the USASI abbreviations where these differ. CHEMICAL ABSTRACTS publishes quarterly supplements of additional abbreviations. The following points of reference style for THE BIOLOGICAL BULLETIN differ from USASI (or modified WORLD LIST) usage:

A. Journal abbreviations, and book titles, all underlined (for *italics*)

B. All components of abbreviations with initial capitals (not as European usage in WORLD LIST *e.g., J. Cell. Comp. Physiol.* NOT *J. cell. comp. Physiol.*)

C. *All* abbreviated components must be followed by a period, whole word components *must not* (*i.e., J. Cancer Res.*)

D. Space between all components (*e.g., J. Cell. Comp. Physiol.*, not *J.Cell.Comp.Physiol.*)

E. Unusual words in journal titles should be spelled out in full, rather than employing new abbreviations invented by the author. For example, use *Rit Vísindafjélags Islendinga* without abbreviation.

F. All single word journal titles in full (*e.g., Veliger, Ecology, Brain*).

G. The order of abbreviated components should be the same as the word order of the complete title (*i.e., Proc.* and *Trans.* placed where they appear, not transposed as in some BIOLOGICAL ABSTRACTS listings).

H. A few well-known international journals in their preferred forms rather than WORLD LIST or USASI usage (*e.g., Nature, Science, Evolution* NOT *Nature, Lond., Science, N.Y.; Evolution, Lancaster, Pa.*)

6. ***Reprints, page proofs, and charges.*** Authors receive their first 100 reprints (without covers) free of charge. Additional reprints may be ordered at time of publication and normally will be delivered about two to three months after the issue date. Authors (or delegates for foreign authors) will receive page proofs of articles shortly before publication. They will be charged the current cost of printers' time for corrections to these (other than corrections of printers' or editors' errors). Other than these charges for authors' alterations, *The Biological Bulletin* does not have page charges.

CONTENTS

No. 1, February 1995

RESEARCH NOTES

Fluck, Richard A.
Responses of the medaka fish egg (*Oryzias latipes*) to the photolysis of microinjected nitrophenyl-EGTA, a photolabile calcium chelator 1

Wittenberg, Jonathan B., and Jeffrey L. Stein
Hemoglobin in the symbiont-harboring gill of the marine gastropod *Alviniconcha hessleri* 5

BIOMINERALIZATION

Giles, R., S. Manne, S. Mann, D. E. Morse, G. D. Stucky, and P. K. Hansma
Inorganic overgrowth of aragonite on molluscan nacre examined by atomic force microscopy . . . 8

DEVELOPMENT AND REPRODUCTION

Bates, William R.
Direct development in the ascidian *Molgula retortiformis* (Verrill, 1871) 16

Chang, Wen-Teh, and Robert J. Lauzon
Isolation of biologically functional RNA during programmed death of a colonial ascidian 23

Hamel, Jean-François, and Annie Mercier
Prespawning behavior, spawning, and development of the brooding starfish *Leptasterias polaris* 32

ECOLOGY AND EVOLUTION

Mead, Kristina S., and Mark W. Denny
The effects of hydrodynamic shear stress on fertilization and early development of the purple sea urchin *Strongylocentrotus purpuratus* 46

Thorn, Kurt, Robert M. Cerrato, and Mark L. Rivers
Elemental distributions in marine bivalve shells as measured by synchrotron x-ray fluorescence . . . 57

Gherardi, Francesca, and Paul M. Cassidy
Life history patterns of *Discorsopagurus schmitti*, a hermit crab inhabiting polychaete tubes 68

NEUROBIOLOGY AND BEHAVIOR

Carlberg, Mats, Karin Alfredsson, Sven-Olle Nielsen, and Peter A. V. Anderson
Taurine-like immunoreactivity in the motor nerve net of the jellyfish *Cyanea capillata* 78

Miklósi, Ádám, József Haller, and Vilmos Csányi
The influence of opponent-related and outcome-related memory on repeated aggressive encounters in the paradise fish (*Macropodus opercularis*) 83

Young, Craig M., and Roland H. Emson
Rapid arm movements in stalked crinoids 89

PHYSIOLOGY

Ferguson, John C.
The structure and mode of function of the water vascular system of a brittlestar, *Ophioderma apressum* 98

No. 2, April 1995

RESEARCH NOTES

Zimmer-Faust, Richard K., Christopher M. Finelli, N. Dean Pentcheff, and David S. Wethey
Odor plumes and animal navigation in turbulent water flow: a field study 111

Toro, J. E., and A. M. Vergara
Evidence for selection against heterozygotes: post-settlement excess of allozyme homozygosity in a cohort of the Chilean oyster, *Ostrea chilensis* Philippi, 1845 117

REVIEWS

del Castillo, José, David S. Smith, Ada M. Vidal, and César Sierra
Catch in the primary spines of the sea urchin *Eucidaris tribuloides*: a brief review and a new interpretation 120

CELL BIOLOGY

Weidner, Earl, S. B. Manale, S. K. Halonen, and J. W. Lynn
Protein-membrane interaction is essential to normal assembly of the microsporidian spore invasion tube 128

DEVELOPMENT AND REPRODUCTION

Abraham, V. C., A. L. Miller, and R. A. Fluck
Microtubule arrays during ooplasmic segregation in the medaka fish egg (*Oryzias latipes*) 136

Webb, Tamika A., Wendy J. Kowalski, and Richard A. Fluck
Microtubule-based movements during ooplasmic segregation in the medaka fish egg (*Oryzias latipes*) 146

Scholtz, Gerhard
Expression of the *engrailed* gene reveals nine putative segment-anlagen in the embryonic pleon of the freshwater crayfish *Cherax destructor* (Crustacea, Malacostraca, Decapoda) 157

ECOLOGY

Saigusa, Masayuki, and Tadashi Akiyama
The tidal rhythm of emergence, and the seasonal variation of this synchrony, in an intertidal midge 166

NEUROBIOLOGY AND BEHAVIOR

Guirguis, M. S., and J. L. Wilkens
The role of the cardioregulatory nerves in mediating heart rate responses to locomotion, reduced stroke volume, and neurohormones in *Homarus americanus* 179

PHYSIOLOGY

McGaw, I. J., and B. R. McMahon
The FMRFamide-related peptides F1 and F2 alter hemolymph distribution and cardiac output in the crab *Cancer magister* 186

McCurley, R. Skyler, and William M. Kier
The functional morphology of starfish tube feet: the role of a crossed-fiber helical array in movement 197

McAuley, P. J.
Ammonium metabolism in the green hydra symbiosis 210

SEA MONSTERS

Pierce, Sidney K., Gerald N. Smith, Jr., Timothy K. Maugel, and Eugenie Clark
On the giant octopus (*Octopus giganteus*) and the Bermuda Blob: homage to A. E. Verrill 219

No. 3, June 1995

RESEARCH NOTE

Stokes, M. D., and N. D. Holland
Ciliary hovering in larval lancelets (=amphioxus) 231

PHYSIOLOGY

Black, Nancy A., Richard Voellmy, and Alina M. Szmant
Heat shock protein induction in *Montastraea faveolata* and *Aiptasia pallida* exposed to elevated temperatures 234

CELL BIOLOGY

Leys, Sally P.
Cytoskeletal architecture and organelle transport in giant syncytia formed by fusion of hexactinellid sponge tissues 241

Chen, Jiun-Hong, and Christopher J. Bayne
Bivalve mollusc hemocyte behaviors: characterization of hemocyte aggregation and adhesion and their inhibition in the California mussel (*Mytilus californianus*) 255

Nicosia, Santo V., and Janice M. Sowinski
Cytological analysis of the urn cell complex of *Sipunculus nudus* before and after serum-induced secretion 267

ECOLOGY AND EVOLUTION

Weedon, Michael J., and Paul D. Taylor
Calcitic nacreous ultrastructures in bryozoans: implications for comparative biomineralization of lophophorates and molluscs 281

Byrne, M.
Changes in larval morphology in the evolution of benthic development by *Patiriella exigua* (Asteroidea: Asterinidae), a comparison with the larvae of *Patiriella* species with planktonic development 293

Ilan, Micha
Reproductive biology, taxonomy, and aspects of chemical ecology of Latrunculiidae (Porifera) . . . 306

Wikfors, Gary H., and Roxanna M. Smolowitz
Experimental and histological studies of four life-history stages of the eastern oyster, *Crassostrea virginica*, exposed to a cultured strain of the dinoflagellate *Prorocentrum minimum* 313

Carlon, David B., and John P. Ebersole
Life-history variation among three temperate hermit crabs: the importance of size in reproductive strategies 329

Index to Volume 188 338

Reference: *Biol. Bull.* **188:** 231–233. (June, 1995)

Ciliary Hovering in Larval Lancelets (=Amphioxus)

M. D. STOKES AND N. D. HOLLAND

Marine Biology Research Division, Scripps Institution of Oceanography,
La Jolla, California 92093-0202

Larvae of lancelets (=amphioxus) are of special interest because they figure prominently in debates about vertebrate origins (1), can sometimes grow into a giant "amphioxides" form (2, 3), have a puzzling right-left asymmetry (4), and constitute a major zooplankton resource in parts of the Atlantic (5). By using improved methods (6, 7) to culture and observe healthy pre-metamorphic larvae in relatively deep containers, we demonstrated a prominent hovering behavior. The larvae spend most of their time suspended in midwater by metachronal beating of epidermal cilia. The body is usually tilted at an angle such that the anterior end and ventral side are oriented towards the water surface. This posture is maintained in the dark and in the light, although there is directional photosensitivity. Hovering may help account for the giant "amphioxides" and may be related to the curious asymmetry of the larval body.

We raised developing lancelets (*Branchiostoma floridae*) in the laboratory (6, 7) in 8-cm diameter containers filled to a depth of 6 cm with seawater, and we used a television camera fitted with a macro lens (8) to record behavior at room temperature (23°C). Locomotion of the embryos (hatching to 2 days after fertilization) was by the spiral, ciliary swimming that has been described previously (9). In contrast, during the month-long stage of the pre-metamorphic larva, the behavior differs markedly from most previously published accounts, which were often based on gradually starving animals maintained in very shallow dishes. We found that the larvae cultured in deeper water spent most of their time hovering almost motionlessly in midwater at various depths in the culture vessel. The body of each hovering larva was oriented at an angle of about 60° from horizontal, with the anterior end and ventral side oriented toward the water surface (Fig. 1).

The motive force for larval hovering was the beating of epidermal cilia in metachronal waves that pass down the body from anterior to posterior at about 0.3 mm/s (Fig. 2). Brief exposure to 0.1% glutaraldehyde in seawater arrested ciliary beating, and the larvae sank, usually anterior first, at about 0.25 mm/s, close to values previously found for larvae of another lancelet species (10). This sinking indicates that the larvae do not use gas bubbles or a high lipid content to remain suspended. Drag was calculated by the formula for the low Reynolds number drag of a cylinder moving parallel to its long axis (11). By equating this drag to the forces (buoyant and gravitational) acting on the larvae, we estimated that approximately 1.4×10^{-9} Newtons were required for ciliary hovering.

The hovering larvae maintain their characteristic slanted posture in the dark and in moderate light. They do, however, show some directional photosensitivity: as seen from above, they will slowly orient themselves with their heads away from an eccentrically placed light source (Fig. 3). Because complete orientation requires about 20 min, it is difficult to understand what, if any, function this could have in the natural environment. Significantly, however, the phenomenon indicates that lancelet larvae have directional photoreceptors. As recently proposed (12), such receptors could well be the neurons associated with the pigment spot at the anterior end of the cerebral vesicle. When the head of a hovering larva is oriented directly away from an eccentric light source, the pigment spot would provide maximal shading to the putative photoreceptive cilia of the anterior neurons.

Our results vindicate Willey (13), who clearly described larval hovering in *Branchiostoma lanceolatum*, but whose observations were never repeated and were strongly doubted by some (10, 14). In our cultures, the few larvae that were not hovering swam for a few seconds at infrequent intervals by muscular undulation or occasionally crawled on the bottom of the container by means of their

Received 9 December 1994; accepted 28 March 1995.

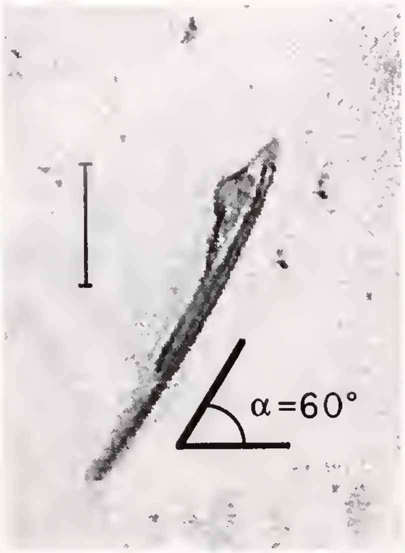

Figure 1. Lateral view (from video) of a hovering, 4-day-old lancelet larva, illuminated by white light. The body axis is oriented 60° from the horizontal and the anterior end and ventral surface is uppermost, directed towards the surface. The long axis of the body is at an angle (α) of about 60° from horizontal; for a random sample of 4-day-old larvae (n = 115) the mean angle was 61° (±1 SD = 6.7). Scale bar, 0.5 mm.

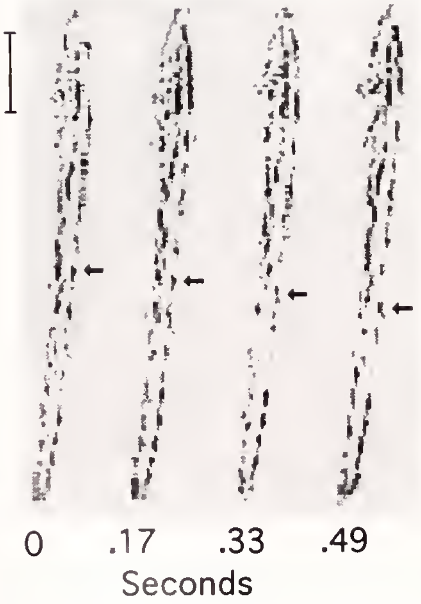

Figure 2. Lateral views of a hovering 4-day-old larva from video (30 frames/s) taken at 5-frame intervals. Animals were observed under darkfield laser Schlieren illumination (25) to visualize the beating of the epidermal cilia. The arrowheads follow the movement of one of a series of metachronal waves moving down the body from the anterior (top) to the posterior (bottom) at approximately 0.3 mm/s. Scale bar, 0.25 mm.

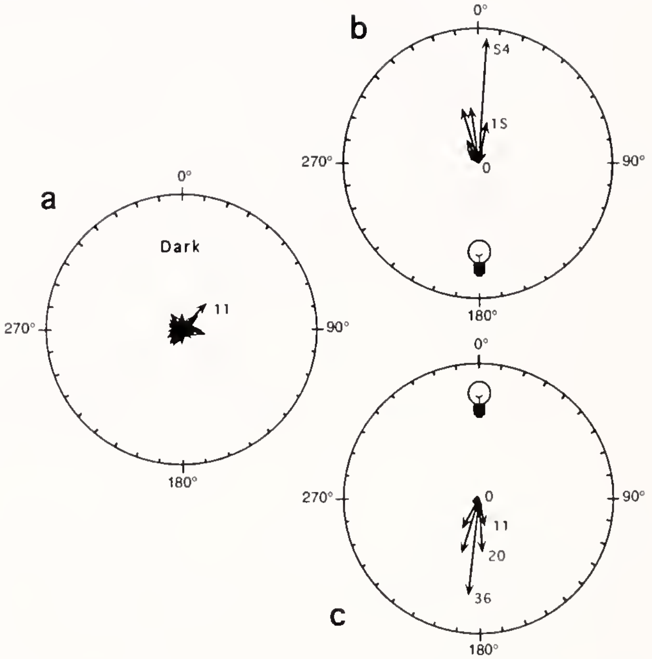

Figure 3. Orientation of 4-day-old hovering larvae, as viewed from above, in the presence and absence of an incandescent light source (intensity approximately 2.6 log Lum/m^2, positioned 50 cm from the observation vessel). The anterior ends of the larvae point in the direction of the arrowheads, while the length of the arrow shaft shows the number of larvae in each 10° sector. The number of larvae in some sectors is indicated. Orientations of a group of larvae (n = 125): (a) after 3 h of darkness; (b) after 20-min exposure to a light source originating from one side; (c) 20 min after moving the light to the opposite side of the observation vessel.

epidermal cilia. Most previous studies of larval lancelets were under conditions (very shallow culture containers and insufficient food) that did not permit hovering, but mainly favored ciliary crawling interspersed with brief episodes of undulatory swimming. Some studies (14, 15) even used such unsanitary culture conditions that the larvae became heavily infected with bacteria, moribund, and attached artifactually to the substratum.

Pre-metamorphic larval lancelets are not infrequently captured in the plankton (5, 10, 16), sometimes even far above the ocean bottom, although it has never been determined how they remain in midwater. Plankton ecologists usually imply that such larvae use muscular undulation continuously or sporadically to remain in the water column (10, 14, 17); however, we prefer the minority view (9, 13) that lancelet larvae under field conditions remain suspended chiefly by the beating of their epidermal cilia. In comparison to undulatory swimming, ciliary hovering probably conserves energy, favors continuous filter feeding, is less attractive to predators, and permits the larvae to attain a relatively large planktonic size.

Lancelet larvae lose most of their cilia at metamorphosis (7). However, the "amphioxides" larvae (2, 3, 18, 19) delay metamorphosis and evidently the loss of cilia. Such larvae could use energy-efficient ciliary hovering to remain continuously in the plankton where they can then attain lengths up to 13.8 mm. In contrast, the post-metamorphic lancelets that are occasionally (and temporarily) present in the plankton (20) must remain in the water column entirely by muscular undulation, which is probably less efficient than ciliary hovering.

The ciliary hovering of lancelet larvae could well be related to their curious asymmetry, which has been explained by some as inherited from an ancestor (21, 22), but by others as a larval adaptation (23, 24). We favor the latter view and suggest that larval hovering co-evolved with a laterally compressed body that, by optimizing the surface-to-volume ratio, increased the effectiveness of the ciliary propulsion. Such lateral compression may in turn be related to the asymmetric displacement of the larval mouth to one of the broad body surfaces [as previously suggested by Bone (2)] simply to ensure an opening large enough to permit effective filter feeding.

Acknowledgments

We thank J. Lawrence and D. Mahoney for providing facilities and assistance in Tampa, Florida, and P. K. Dayton and L. Z. Holland for providing critical comments on this manuscript.

Literature Cited

1. **Gans, C. 1989.** Stages in the origin of vertebrates: analysis by means of scenarios. *Biol. Rev.* **64:** 221–268.
2. **Bone, Q. 1957.** The problem of the 'amphioxides' larva. *Nature* **180:** 1462–1464.
3. **Wickstead, J. H. J. 1964.** The status of the 'amphioxides' larvae. *J. Linn. Soc. (Zool.)* **45:** 201–207.
4. **Jefferies, R. P. S. 1986.** *The Ancestry of the Vertebrates.* British Museum of Natural History, London.
5. **Flood, P. R., F. Gosselk, and J. G. Braunn. 1982.** Larvas de "Branchiostoma" en el area de "upwelling" del NW de Africa. *Boll. Inst. Espan. Oceanogr.* **7:** 73–86.
6. **Holland, N. D., and L. Z. Holland. 1994.** Embryos and larvae of invertebrate deuterostomes. Pp. 21–32 in *Essential Developmental Biology: a Practical Approach.* C. Stern and P. W. H. Holland, eds. IRL Press, Oxford.
7. **Stokes, M. D., and N. D. Holland. 1995.** Embryos and larvae of a lancelet, *Branchiostoma floridae,* from hatching to metamorphosis: growth in the laboratory and external morphology. *Acta Zool. Stockh.* **76:** 105–120.
8. **Holland, N. D., J. R. Strickler, and A. B. Leonard. 1986.** Particle interception, transport and rejection by the feather star *Oligometra serripinna* (Echinodermata: Crinoidea), studied by frame analysis of videotapes. *Mar. Biol.* **93:** 111–126.
9. **Bone, Q. 1958.** Observations upon the living larva of amphioxus. *Pubbl. Staz. Zool. Napoli* **30:** 458–471.
10. **Webb, J. E. 1969.** On the feeding and behaviour of the larva of *Branchiostoma lanceolatum. Mar. Biol.* **3:** 58–72.
11. **Cox, R. G. 1970.** The motion of long, slender bodies in viscous fluids. Part 1. General theory. *J. Fluid Mech.* **44:** 791–810.
12. **Lacalli, T. C., N. D. Holland, and J. E. West. 1994.** Landmarks in the anterior central nervous system of amphioxus larvae. *Phil. Trans. Roy. Soc. B* **344:** 165–185.
13. **Willey, A. 1891.** The later larval development of amphioxus. *Q. J Microsc. Sci.* **32:** 183–234.
14. **van Wijhe, J. W. 1927.** Observations on the adhesive apparatus and the function of the ilio-colon ring in the living larva of amphioxus in the growth period. *Proc. Konin. Akad. Wet.* **30:** 991–1003.
15. **Orton, J. H. 1914.** On a hermaphrodite specimen of amphioxus with notes on experiments in rearing amphioxus. *Mar. Biol. Assoc. U. K.* **10:** 506–512.
16. **Wickstead, J. H., and Q. Bone. 1959.** Ecology of acraniate larvae. *Nature* **184:** 1849–1851.
17. **Wickstead, J. H. 1975.** Chordata: Acrania (Cephalochordata). Pp. 308–314 in *Reproduction of Marine Invertebrates.* A. C. Giese and J. S. Pearse, eds. Academic Press, New York.
18. **Goldschmidt, R. 1906.** Amphioxides und Amphioxus. *Zool. Anz.* **30:** 443–448.
19. **Gibson, H. O. S. 1910.** The Cephalochorda: "Amphioxides." *Trans. Linn. Soc. Lond. Zool.* **13:** 213–256.
20. **Boschung, H. T., and R. F. Shaw. 1988.** Occurrence of planktonic lancelets from Louisiana's continental shelf, with a review of pelagic Branchiostoma (order Amphioxi). *Bull. Mar. Sci.* **43:** 229–240.
21. **Klaatsch, H. 1898.** Uber den Bau und die Entwickelung des Tentakelapparates des Amphioxus. *Verh. Anat. Ges. Jena* **12:** 184–195.
22. **MacBride, E. W. 1909.** The formation of the layers in amphioxus and its bearing on the interpretation of the early ontogenetic processes in other vertebrates. *Q. J. Microsc. Sci* **54:** 279–345.
23. **van Wijhe, J. W. 1913.** On the metamorphosis of amphioxus lanceolatus. *Proc. Konin. Akad. Weten. Sci. Sect.* **16:** 574–583.
24. **Garstang, W. 1928.** The morphology of the Tunicata, and its bearings on the phylogeny of the Chordata. *Q. J. Microsc. Sci.* **72:** 51–187.
25. **Strickler, J. R. 1985.** Feeding currents in calanoid copepods: two new hypotheses. Pp. 459–485 in *Physiological Adaptations for Marine Animals.* M. S. Laverack, ed. Soc. Exp. Biol., New York.

Reference: *Biol. Bull.* **188:** 234–240. (June, 1995)

Heat Shock Protein Induction in *Montastraea faveolata* and *Aiptasia pallida* Exposed to Elevated Temperatures

NANCY A. BLACK[1], RICHARD VOELLMY[2], AND ALINA M. SZMANT[1,*]

[1]*Division of Marine Biology and Fisheries, Rosenstiel School of Marine and Atmospheric Science, University of Miami, Miami, Florida 33149; and* [2]*Department of Biochemistry and Molecular Biology, School of Medicine, University of Miami, Miami, Florida 33136*

Abstract. Frequent widespread episodes of coral bleaching have made researchers aware of the sensitivity of reef corals to moderately elevated temperatures and led us to investigate mechanisms of temperature stress tolerance in this group. One such mechanism may be the induced synthesis of heat shock proteins (hsps), which have been shown to play a role in thermotolerance in other organisms. However, induced synthesis of hsps in scleractinian corals was not reported until recently.

Experiments were conducted in which *Montastraea faveolata* was exposed to high temperatures (up to 35°C) for short periods (2 h). Under the conditions tested, the corals produced seven different hsps with approximate molecular weights of 95, 90, 78, 74, 33, 28, and 27 kDa. Another zooxanthellate species, the sea anemone *Aiptasia pallida*, also synthesized hsps during temperature stress, but fewer and with different molecular weights (82, 72, 68, and 48 kDa) than those produced by *Montastraea*. It now remains to be determined whether hsps are involved in differences in thermotolerance and susceptibility to bleaching within and between the various species of *Montastraea*, and between species of reef cnidarians.

Introduction

Heat shock proteins (hsps) are also referred to as "stress proteins" because their expression can be induced by a number of stressful conditions, only one of which is heat shock (reviewed in Craig, 1985). These proteins are highly conserved evolutionarily: they have been found in all phyla examined thus far, from bacteria and yeast to humans.

Several functions have been proposed for hsps, including the transport of newly transcribed proteins to the endoplasmic reticulum and mitochondria and involvement in the insertion of these proteins into these organelles (reviewed in Gething and Sambrook, 1992; Parsell and Lindquist, 1993). Hsps may also play a role in translation and, during stress, may interact with unfolding (denaturing) proteins to either keep them in a refoldable conformation or target them for degradation (Welch, 1992). The production of hsps has also been correlated with the acquisition of enhanced thermotolerance (Parsell and Lindquist, 1993). Because of their important functions in normal metabolic and repair processes, moderate amounts of many hsps are present in unstressed cells at all times, but synthesis increases after a stress. In some cases, this increase in hsp synthesis is accompanied by a decrease in the production of other non-hsp proteins (Parsell and Lindquist, 1993).

Interest in the effects of elevated temperature on scleractinian reef-building corals and their ability to produce heat shock proteins has increased with recent frequent, widespread episodes of coral bleaching (Glynn, 1991; Williams and Bunkley-Williams, 1990). Corals have a complex symbiotic relationship with photosynthesizing dinoflagellates, called zooxanthellae, that are contained within the gastrodermal cells of corals. Bleaching results from the loss of the zooxanthellae, the degradation of chlorophyll pigments within zooxanthellae, or a combination of both. Many conditions have been shown to induce bleaching or are implicated in its production (reviewed in Williams and Bunkley-Williams, 1990), but the

Received 8 June 1994; accepted 17 March 1995.

[*] Author to whom correspondence and reprint requests should be sent.

condition most often correlated with recent bleaching events is prolonged exposure to moderately elevated temperatures.

Hsp induction has been reported in a number of cnidarians. Two thermotolerant species of the hydrozoan *Hydra* were found to increase the synthesis of hsp60 when exposed to elevated temperature or to the chemical inducers sodium azide and cadmium chloride; six more thermosensitive species failed to produce this hsp (Bosch *et al.*, 1988). In the scyphozoan jellyfish *Aurelia aurita*, six hsps were identified when various developmental stages were exposed to elevated temperatures for a few hours (Black and Bloom, 1984). An anemone, *Anemonia viridis*, produced six different hsps in response to elevated temperatures or copper chloride (Miller *et al.*, 1992). Hsp70 was found in the coral *Goniopora djiboutiensis* (Sharp *et al.*, 1994), and other reports of hsp production in zooxanthellate cnidarians have been presented at recent scientific meetings.

The objective of this research was to determine whether the Caribbean reef coral *Montastraea faveolata* (Ellis and Solander)—formerly *Montastraea annularis* (Knowlton *et al.*, 1992; Weil and Knowlton, 1994)—produces hsps; and if so, which ones. Individual colonies and sibling species of this coral have various degrees of susceptibility to temperature-induced bleaching (Gates, 1990; Szmant and Gassman, 1990; Black, 1993). Samples of this coral were subjected to acute exposure to higher temperature followed by variable recovery periods at control temperature and then tested for elevation of hsp synthesis. Sea anemones, *Aiptasia pallida* (Verrill), were also used to work out techniques and to illustrate hsp production by another zooxanthellate cnidarian species. The exposure conditions tested for each species are summarized in Table I.

Methods and Materials

Collection and maintenance of the animals

Multiple cores from large colonies of *Montastraea faveolata* were collected from a depth of 5–7 m on a reef near Joulters Cay (25° 19′ N, 78° 05′ W), north of Andros Island, Bahamas, in 1988 and 1989. A pneumatic drill fitted with a hole-saw and powered by compressed air from a scuba tank was used to obtain short cores, 5 cm in diameter, with live tissue only on the top. The corals were used in nondestructive and nonstressful laboratory experiments involving temperature and light exposure and then returned to uncontrolled ambient laboratory conditions for several months before the start of these experiments.

Sea anemones of the species *Aiptasia pallida* were obtained from holding tanks at the Florida Keys Marine Laboratory on Long Key in February 1993. They were allowed one week to acclimate to laboratory conditions before experiments were started.

Specimens were maintained in flowing, sand-filtered seawater at ambient seawater temperature (*ca.* 28°C for the corals used in experiment 1, 20°–24°C for the corals and anemones used in experiments 2–4, Table I) under cool-white fluorescent or metal halide lights (*ca.* 200 μEin m^{-2} s^{-1} of light) on a 14:10 hour light:dark schedule. Thawed frozen brine shrimp were provided as food once a week.

Incubation procedures

For all experiments, the organisms were incubated in filtered (Whatman GF/A) seawater with 5 μCi/ml of either ^{3}H-leucine (156.0 or 179.6 Ci/mmol specific activity) or ^{35}S-methionine/cysteine (1141.0 Ci/mmol specific activity) purchased from New England Nuclear.

Incubation was either in glass dishes with gentle aeration in a dark incubator or in covered beakers in a shallow water bath. The specimens were placed in the containers with the radiolabeled amino acid at the beginning of the temperature exposure, left there for the duration of the recovery periods of each experiment, then rinsed three times with filtered seawater (to remove excess radiolabel before processing). Each treatment group contained two or three corals or four anemones, but anemones were pooled for processing.

Table I

Summary of the animals, conditions, and isotopes used in the heat shock experiments

Exp. no.	Species	Control temp. (°C)	Treatment conditions	Recovery conditions	N per treatment*	Isotope
1	*Montastraea faveolata*	28	31°C: 1 week, 34°C: 2 h	none	2	^{3}H
2	*M. faveolata*	22	27, 29, 31, 33, 35°C: 2 h	22°C: 2 h	3	^{35}S
3	*M. faveolata* *Aiptasia pallida*	22	33°C: 2 h	22°C: 4 h	2 corals 4 anemones	^{35}S
4	*A. pallida*	22	27, 29, 31, 33, 35°C: 2 h	22°C: 2 h	4	^{35}S
5	*A. pallida*	22	33°C: 2 h	22°C: 0, 1, 2, 4, 24, 48 h	4	^{35}S

* Because of their small size, tissues of sea anemones were pooled for analysis.

Tissue preparation

Coral tissues were removed from the skeletons with a jet of 0.1 *M* Tris (pH 6.8) sprayed through an airbrush; resulting tissue slurry volumes ranged from 3 to 13 ml. Preparations were kept on ice throughout processing. The tissue slurry was homogenized and centrifuged (850 × *g*, 15 min, 4°C) to separate the coral animal fraction (supernatant) from the zooxanthellae (pellet). Anemones were ground in 2 ml of cold Tris buffer (0.1 *M*, pH 6.8) in a glass tissue grinder with a Teflon-tipped pestle. Zooxanthellae and unbroken cells were removed by centrifugation (6600 × *g*, 20 min, 4°C).

In the first experiment, the supernatants were centrifuged again at 12,000 × *g* (15 min, 4°C) to remove cellular debris and larger organelles (Ford and Graham, 1991). To 100 μl of the latter supernatants was added 50 μl of 2X protein loading buffer [PLB; 0.125 *M* Tris, 20% glycerol, 2% 2-mercaptoethanol, and 4% SDS (Gallagher and Smith, 1991)]. The amount of radioactivity in a subsample of each supernatant was measured with a Beckman model LS180 scintillation counter. The remainder of each sample was boiled for 1 min and frozen at −80°C.

In the later experiments, proteins were precipitated from the supernatants with 8% trichloroacetic acid (TCA). Proteins were pelleted by centrifugation (12,000 × *g*, 20 min, 4°C). The pellets were rinsed three times with 8% TCA and three times with acetone to remove TCA-soluble and acetone-soluble contaminants, and then redissolved in 1 ml of PLB. A subsample was removed for scintillation counting and the rest was boiled and frozen at −80°C.

Gel electrophoresis and autoradiography

Proteins were separated by one-dimensional SDS-polyacrylamide gel electrophoresis (SDS-PAGE) (10% running gel; 3% stacking gel). Equal amounts of radioactivity per sample (approx. 400,000 dpm) were loaded in each lane, and protein molecular weight standards were run in parallel. The electrophoresis buffer consisted of 0.025 *M* Tris, 0.192 *M* glycine, and 0.1% SDS (Laemmli, 1970). After electrophoresis, gels were fixed (50% methanol, 5% glacial acetic acid, 30 min), rinsed in water (three times, 10 min each), incubated in a solution of 10% salicylic acid and 3% glycerol (20 min), and vacuum dried at 80°C (2 h.). Autoradiograms were produced by exposing Kodak X-Omat AR film to the dried gels for several days at −80°C. The approximate molecular weights (M_r) of protein bands on the autoradiograms were estimated by comparison with the positions of molecular standards on the gels.

Because the gels were loaded with equal amounts of radiolabel rather than equal amounts of protein, the results provide us with a relative comparison of how radiolabel was incorporated within each treatment, but do not allow us to compare rates of synthesis of the various hsps between treatments.

Densitometry

The autoradiogram from experiment 4 (Fig. 2A), in which specimens of *Aiptasia pallida* were incubated in a temperature series from 22° to 35°C (Table I), was analyzed with densitometry to compare quantitatively the densities of the hsp68 and hsp72 bands from animals exposed to the various temperatures. The densitometry image analysis system consisted of a NEC single-chip color video camera to produce the image, a Targa + 64 frame-grabber board to capture the image, and the MOCHA software package (Jandel Scientific) to do the density scan of the image. Equal areas of each temperature lane were scanned, and the density values associated with each band summed. Figure 3 includes the density scans for each lane (A), and histograms that present the density and the percentage of total density of each hsp in each lane (B, C).

Results

Exposure to elevated temperature increased the synthesis of several discrete proteins (hsps) in both corals and sea anemones. Each species produced its own characteristic set of hsps. The results of each experiment are summarized separately for each species.

Montastraea faveolata (Fig. 1)

31° & 34°C vs. 28°C. Corals exposed to 34°C expressed several hsps with M_r of 33, 74, 78, 90, and 95 kDa. In this experiment, but not subsequent ones, there was reduced synthesis of other proteins such as a 40 kDa protein presumed to be actin and an unknown 99 kDa protein (Fig. 1a). The patterns of proteins synthesized at 28° and 31°C were similar and did not include any discernible hsp bands.

27°–35°C vs. 22°C. Hsp synthesis was tested at five temperatures from 27° to 35°C. No hsps were synthesized at 27°, 29°, or 31°C (not shown). The only hsps that were distinguishable in this experiment were hsp74 in the 33°C (faint) and 35°C (darker) treatments as well as two bands of *ca.* 27 and 28 kDa at 35°C (Fig. 1b). A repeat of the 33°C exposure experiment produced a pattern of hsps at 90, 78, and 74 kDa (Fig. 1c) similar to that seen before at 34°C.

Aiptasia pallida (Figs. 2, 3)

27°–35°C vs. 22°C. In this experiment, anemones were exposed to five different 2-h heat treatments (Fig. 2a). At 22° (control), 27°, and 29°C, the anemones did not appear stressed. At 31°C, however, the anemones were partially

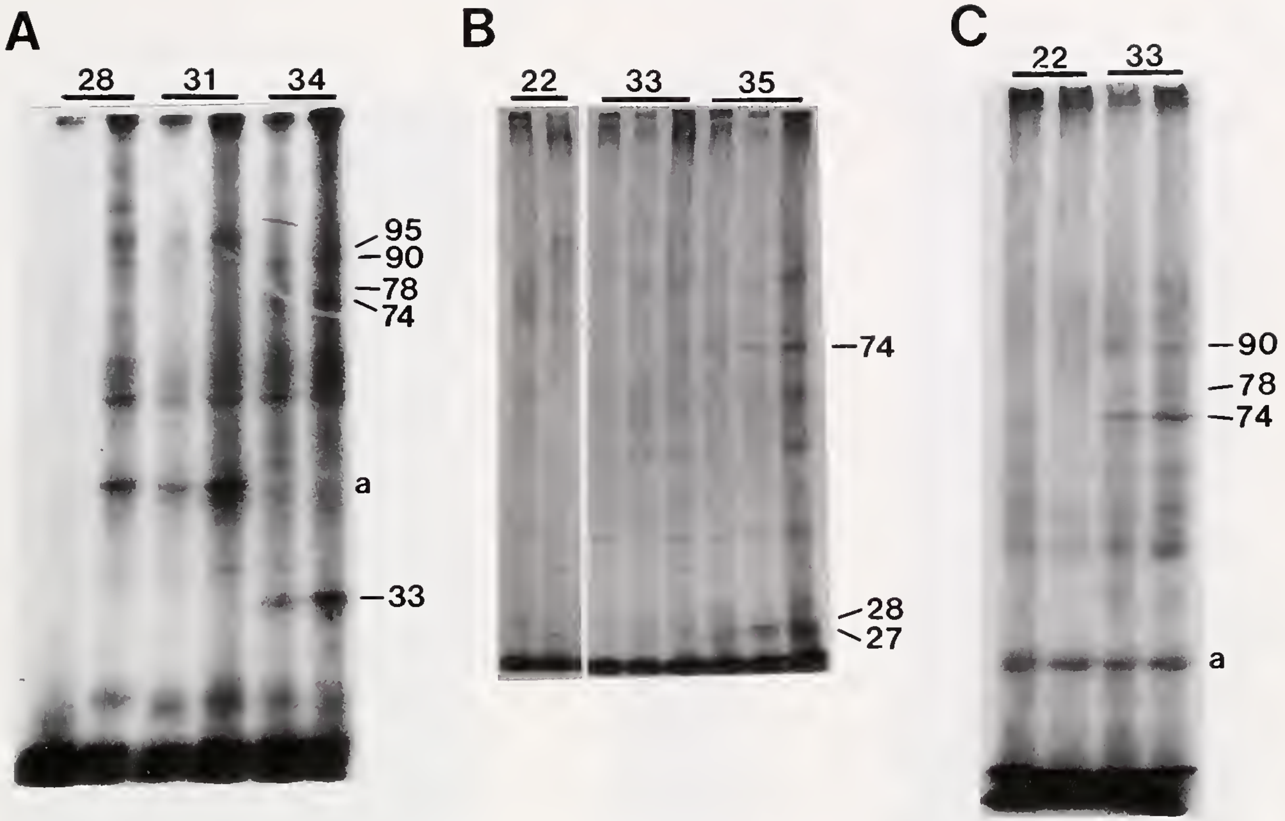

Figure 1. Autoradiograms showing proteins synthesized by *Montastraea faveolata* after exposure to various temperatures. (A) Synthesis after 1 week at 31°C or 2 h at 34°C compared to controls (28°C). The positions of hsps produced at approximately 95, 90, 78, 74, and 33 kDa are indicated. (B & C) Synthesis after 2 h at 33° or 35°C compared to controls (22°C). The positions of hsps produced at approximately 74, 28, and 27 kDa (B) and 90, 78, and 74 kDa (C) are indicated. Each lane represents the proteins of an individual coral, with two or three replicate corals per temperature treatment. a = protein presumed to be actin.

contracted during heat exposure, but recovered to normal appearance during the 2-h recovery period at 22°C. At 33° and 35°C, the anemones were severely stressed: all were totally contracted and some were lying on their sides. The 33°C anemones returned to normal appearance during the recovery period, but the 35°C anemones did not.

Only two hsps (68 and 72 kDa) could be distinguished visually in this experiment (Fig. 2A). The densitometry was used to quantify the amounts of radiolabel incorporated into each band with respect to the total amount of radiolabel in protein in each sample (Fig. 3). The density scans for each lane are presented in Figure 3A and the relative densities within the hsp68 and hsp72 bands in Figures 3B and 3C, respectively. The 72 kDa hsp was present as a faint band in the control (22°C) and 27°C anemones (2.8% of total density for each), with up to a 32% increase in the 29°, 31°, and 33°C animals (3.7%, 3.2%, and 3.3% of total, respectively), and then declined at 35°C (to 2.3% of total). Hsp68 was present at very low levels (1.9% of total) at the lowest two temperatures, increased by 30% to 50% at the intermediate temperatures, (29°, 31°, and 33°C: 2.6%, 2.4%, and 3.0% of total, respectively), and then increased dramatically by 280% at the highest temperature (35°C: 7.25% of total). In some experiments additional hsps were detected at 82 and 48 kDa (Fig. 2B), that were apparently induced to a lower extent than the hsps 68 and 72.

33°C vs. 22°C, variable recovery period. This experiment examined the turnover of hsps synthesized during the temperature stress and post-stress recovery periods. Increased amounts of hsps 68 and 72 (and 48 and 82, to a minor extent) were synthesized after a 2-h heat treatment at 33°C (comparison of lanes C and 0 in Fig. 2C; especially notice the increased density of the hsp68 and hsp82 bands in lane 0). Both of these hsps remained elevated for up to 24 h at 22°C (Fig. 2C), but were less evident in the 4-h and 48-h samples. Because of the experimental design (specimens were incubated with the radiolabel during both the stress and recovery periods), we cannot distinguish between radiolabeled hsps produced during the stress itself

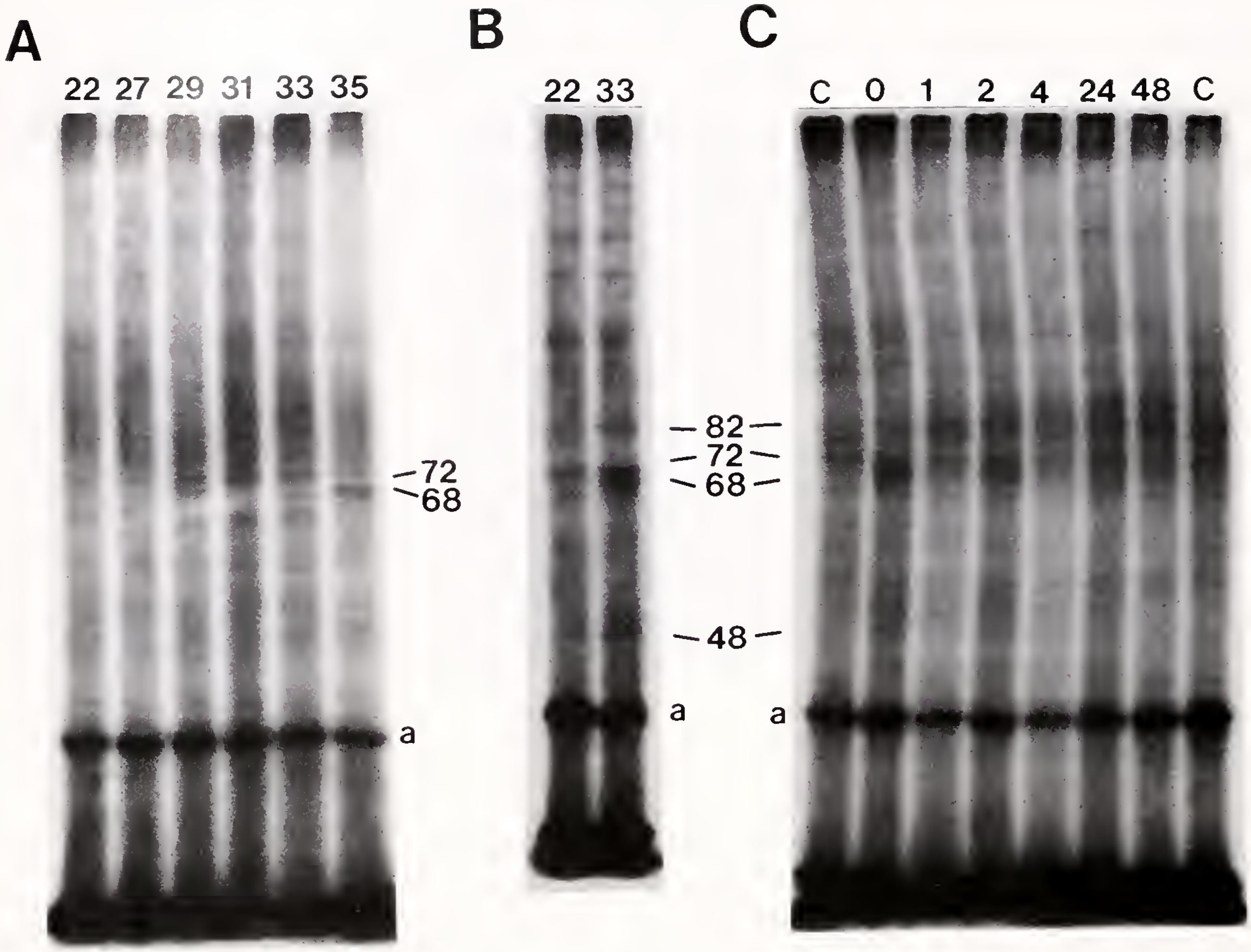

Figure 2. Autoradiogram showing proteins synthesized by *Aiptasia pallida* after exposure to various temperatures. (A) Synthesis after 2 h at 27°, 29°, 31°, or 35°C compared to controls (22°C). (B) Synthesis after 2 h at 33°C compared to controls (22°C). (C) Synthesis after 2 h at 33°C with variable recovery times (for 0, 1, 2, 4, 24, or 48 h) at 22°C compared to controls (22°C). Each lane contains a sample consisting of pooled tissues from four sea anemones. a = protein presumed to be actin. The positions of hsps produced at approximately 72 and 68 kDa (A) and 82, 72, 68, and 48 kDa (B, C) are indicated.

and subsequently during recovery. However, in other studies in which we have incubated reef corals with radiolabeled amino acids, the medium was depleted of more than 80% of the radiolabel within the first 3 h (FitzGerald and Szmant, 1988, in prep.). Thus, it is likely that most of the radiolabeled hsps (and other proteins) in the samples were synthesized during the stress period and the early hours of the recovery period.

Discussion

Several hsps were found in both *Montastraea faveolata* and *Aiptasia pallida* after brief exposures to elevated temperature. Overall, hsp74 for *Montastraea*, and hsps 68 and 72 for *Aiptasia* were the dominant hsps produced in response to heat stress. In the latter species, hsp72 appears to be constitutive, with moderately increased synthesis after moderate temperature shock, and down-regulation at the highest temperature tested (35°C). In *Aiptasia*, hsp68 appears to be the major one produced with more extreme temperature stress. Given the near-background levels of this hsp in the control and 27°C samples, hsp68 may be inducible rather than constitutive.

Comparison of our results with those reported for other cnidarian species reveals a few common hsps and hsp families (Table II). According to Craig (1985), nearly all species produce hsps in the same three size classes: hsp90 (80 to 90 kDa), hsp70 (68 to 74 kDa), and small hsps (18 to 30 kDa). Variability regarding the number and size of hsps is generally greater for small hsps. Five of the cnidarian species studied produced one hsp in the 80 to 90

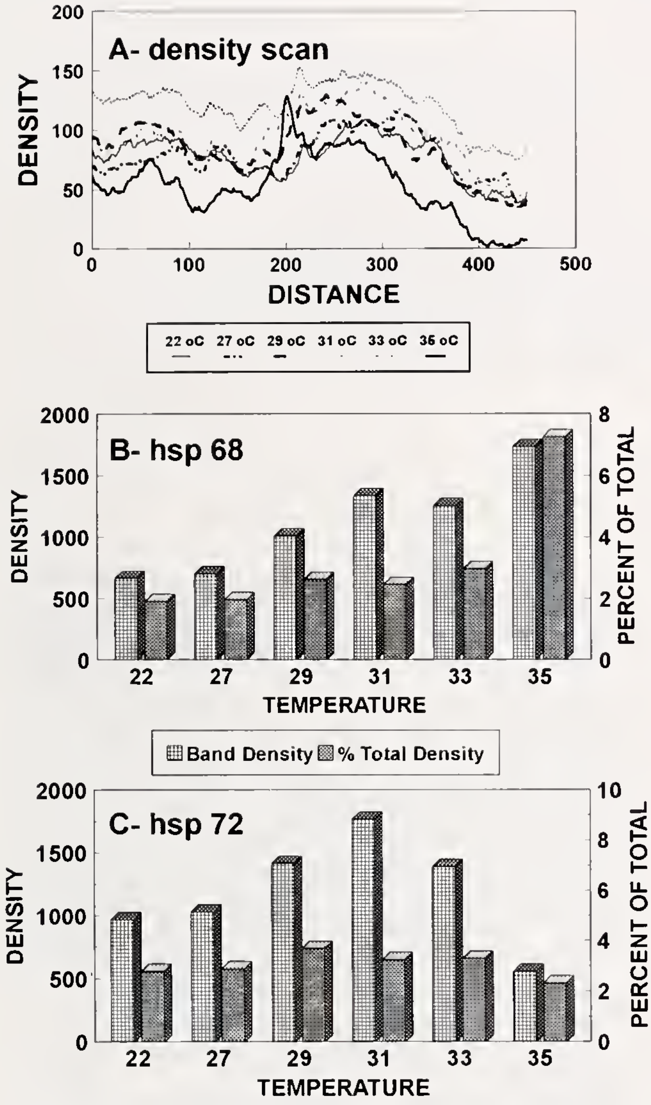

Figure 3. (A) Density profile along the central portion of each lane shown in Figure 2A, extending lengthwise about the mid-third of each lane. The scan width was about two-thirds the width of each lane. See text for further details. (B) The total density assigned to the hsp68 band of each sample, and as a percentage of total lane density. (C) Same as (B) but for the hsp72 band.

range, and all but *Hydra* produced one or more hsps in the 68 to 74 range.

As has been observed for other species, the number and relative quantities of hsps synthesized in our experiments increased with increasing severity of heat treatment. There was, however, variability between experiments in the amount and type of hsps produced, especially in *Montastraea*. Some of this variation may be due to individual differences in thermotolerance or ability to turn on hsp synthesis. This possibility should be addressed by repeating these experiments with greater replication. In addition, immunochemical techniques (*i.e.*, Western blots) should be applied to determine whether the hsps detected are members of the known hsp families. This approach has been used recently by Sharp *et al.* (1994) to identify members of the hsp70 family in a coral and a sea anemone (Table II).

Hsps in *Aiptasia* appear to have a moderate turnover rate. Radiolabeled hsps synthesized during and after the 2-h heat shock were still present 24 h after temperature exposure, but had apparently been degraded by 48 h after treatment. Experiments should be conducted to determine the duration of heat stress during which these animals can continue to synthesize hsps.

An attempt to determine whether zooxanthellae in *Montastraea* produce hsps failed because tissue homogenates of the zooxanthellae preparations contained too little radiolabel (4% or less) to allow detection of hsps. Although hsps have not yet been reported in zooxanthellae, the degradation and loss of pigments from the chloroplasts of zooxanthellae in bleached corals (Gladfelter, 1988; Kleppel *et al.*, 1989; Porter *et al.*, 1989; Glynn and D'Croz, 1990; Szmant and Gassman, 1990; Black, 1993) would indicate that the zooxanthellae are heat stressed and could also benefit from hsps.

In this study, we have shown that *Montastraea faveolata* can produce hsps in response to short exposures (several hours) to relatively highly elevated temperatures (≥33°C). Our experimental conditions differ from those associated with natural bleaching, which is thought to be caused by exposure to more moderately elevated temperatures (29°–30°C) for longer periods (several weeks to months) (Glynn and D'Croz, 1990; Black, 1993; Black and Szmant, in prep.). No hsp production was observed in corals exposed to moderately elevated temperatures (27°–31°C) for 2 hours to one week. In addition, the duration of our experiments was too short to expect any visible bleaching. Susceptibility of corals to bleaching varies between different species (Williams and Bunkley-Williams, 1990). The present results suggest that further work is warranted to determine whether hsps are involved in differences in thermotolerance and susceptibility to bleaching within and between reef cnidarian species.

Conclusions

(1) Both *Montastraea faveolata* and *Aiptasia pallida* produce heat shock proteins in response to short periods of extreme but sublethal thermal stress. Most of the hsps produced appear to fall into a molecular weight range similar to those found in other cnidarian species. Western blots are needed to learn whether the hsps produced by *Montastraea* and *Aiptasia* belong to the same families as the hsps found in other groups. (2) The involvement of heat shock proteins in coral bleaching remains to be determined.

Table II

Comparison of the heat shock proteins observed in six different cnidarian species

Species	Class	Molecular weight (kilodaltons)									
Hydra attenuata[a]	Hydrozoa		28				60			80	
Aurelia aurelia[b]	Scyphozoa				39	45	68	70		83	93
Anemonia viridis[c]	Anthozoa	30	31	35	39		69			82	
Anemonia viridis[d]	Anthozoa	28	29								
Goniopora djiboutiensis[d]	Anthozoa							70			
Aiptasia pallida[e]	Anthozoa					48	68	72		82	
Montastraea faveolata[e]	Anthozoa	27	28	33				74	78	90	95

[a] Bosch *et al.* (1988).

[b] Black and Bloom (1984).

[c] Miller *et al* (1992).

[d] Sharp *et al.* (1994).

[e] This study.

Acknowledgments

We thank Ruben Baler for his advice and assistance and the Florida Keys Marine Laboratory for providing the anemones. The manuscript was greatly improved by helpful comments from two anonymous reviewers. This research was supported by NSF grant OCE-9114424 to A.M.S.

Literature Cited

Black, N. A. 1993. Bleaching and Physiological Changes in the Scleractinian Coral *Montastrea annularis in Response to Heat Stress.* M. S. Thesis, Univ. Miami, 76 pp.

Black, R. E., and L. Bloom. 1984. Heat shock proteins in *Aurelia* (Cnidaria, Scyphozoa). *J. Exp. Zool.* **230:** 303–307.

Bosch, T. C. G., S. M. Krylow, H. R. Bode, and R. E. Steele. 1988. Thermotolerance and synthesis of heat shock proteins: These responses are present in *Hydra attenuata* but absent in *Hydra oligactis. Proc. Natl. Acad. Sci. USA* **85:** 7927–7931.

Craig, E. A. 1985. The heat shock response. *CRC Crit. Rev. Biochem.* **18:** 239–280.

FitzGerald, L. M., and A. M. Szmant. 1988. Amino acid metabolism: adaptations to low nutrient conditions. *Proc. 6th Internat. Coral Reef Symp.* (Townsville, Australia) **3:** 5–9.

Ford, T. C., and J. M. Graham. 1991. *An Introduction to Centrifugation.* Bios Scientific, Oxford. 118 pp.

Gallagher, S. R., and J. A. Smith. 1991. Electrophoretic separation of proteins. Pp 11.2.1–21 in *Current Protocols in Molecular Biology, vol. 2.* John Wiley & Sons, New York.

Gates, R. D. 1990. Seawater temperature and sublethal coral bleaching in Jamaica. *Coral Reefs* **8:** 193–197.

Gething, M. J., and J. Sambrook. 1992. Protein folding in the cell. *Nature* **355:** 33–45.

Gladfelter, E. H. 1988. The physiological basis of coral bleaching. Pp. 15–18 in *Mass Bleaching of Coral Reefs in the Caribbean: A Research Strategy.* J. Ogden and R. Wicklund, eds., NOAA, Nat'l. Undersea Research Prog. Report 88-2. Rockville, MD.

Glynn, P. W. 1991. Coral reef bleaching in the 1980's and possible connections with global warming. *Trends Ecol. Evol.* **6:** 175–179.

Glynn, P. W., and L. D'Croz. 1990. Experimental evidence for high temperature stress as the cause of El Niño-coincident coral mortality. *Coral Reefs* **8:** 181–191.

Kleppel, G. S., R. E. Dodge, and C. J. Reese. 1989. Changes in pigmentation associated with the bleaching of stony corals. *Limnol Oceanogr.* **34:** 1331–1335.

Knowlton, N., E. Weil, L. A. Weigt, and H. M. Guzman. 1992. Sibling species in *Montastraea annularis*, coral bleaching, and the coral climate record. *Science* **255:** 330–333.

Laemmli, U. K. 1970. Cleavage of structural proteins during the assembly of the head of bacteriophage T4. *Nature* **227:** 680–685.

Miller, D., B. E. Brown, V. A. Sharp, and N. Nganro. 1992. Changes in the expression of soluble proteins extracted from the symbiotic anemone *Anemonia viridis* accompany bleaching induced by hyperthermia and metal stressors. *J. Therm. Biol.* **17:** 217–223.

Parsell, D. A., and S. Lindquist. 1993. The function of heat-shock proteins in stress tolerance: degradation and reactivation of damaged proteins. *Ann. Rev. Genet.* **27:** 437–496.

Porter, J. W., W. K. Fitt, H. J. Spero, C. S. Rogers, and M. W. White. 1989. Bleaching in reef corals: physiological and stable isotopic responses. *Proc. Natl. Acad. Sci. USA* **86:** 9342–9346.

Sharp, V. A., D. Miller, J. C. Bythell, and B. E. Brown. 1994. Expression of low molecular weight HSP 70 related polypeptides from the symbiotic sea anemone *Anemonia viridis* Forskall in response to heat shock. *J. Exp. Mar. Biol. Ecol.* **179:** 179–193.

Szmant, A. M., and N. J. Gassman. 1990. The effects of prolonged bleaching of the reef coral *Montastrea annularis* on the tissue biomass and reproduction. *Coral Reefs* **8:** 217–224.

Weil, E., and N. Knowlton. 1994. A multi-character analysis of the Caribbean coral *Montastraea annularis* (Ellis and Solander, 1786) and its two sibling species, *M. faveolata* (Ellis and Solander, 1786) and *M. franksi* (Gregory, 1895). *Bull. Mar. Sci.* **55:** 151–175.

Welch, W. J. 1992. Mammalian stress response: cell physiology, structure/function of stress proteins, and implications for medicine and disease. *Physiol. Rev.* **72:** 1063–1081.

Williams, E. H., and L. Bunkley-Williams. 1990. The world-wide coral reef bleaching cycle and related sources of coral mortality. *Atoll Res. Bull.* **335:** 1–71.

Reference: *Biol. Bull.* **188**: 241–254. (June, 1995)

Cytoskeletal Architecture and Organelle Transport in Giant Syncytia Formed by Fusion of Hexactinellid Sponge Tissues

SALLY P. LEYS

Department of Biology, University of Victoria, Victoria, British Columbia V8W 2Y2, Canada

Abstract. Dissociated tissue from the hexactinellid sponge *Rhabdocalyptus dawsoni* adheres to coated substrates and aggregates by the fusion of tissue pieces to form a giant syncytium. Video microscopy shows that the pieces contact each other by way of lamellipodia or filopodia. Fusion, corroborated by evidence of dye spread, occurs about 1 hour after plating and is characterized by two-way transport of individual organelles, including nuclei, at an average rate of 2.15 $\mu m \cdot s^{-1}$, and bulk streaming of cytoplasm at an average velocity of 1.72 $\mu m \cdot s^{-1}$. In the cellular sponge *Haliclona*, by contrast, dye does not spread through aggregates and no streaming can be seen. That transport in *Rhabdocalyptus* is microtubule-based is indicated by the reversible inhibition of streaming caused by colcemid and nocodazole. Immunofluorescence and electron microscopy reveal an extensive network of microtubule bundles within the aggregates. The cytoskeleton also includes microfilament bundles that traverse aggregates and run around the periphery and giant, actin-dense rods that extend from the edges. Cytochalasin B reversibly disrupts the microfilamentous framework without blocking streaming.

In contrast to demosponges where the cytoskeleton is organized on the basis of individual cells, in hexactinellids it provides a supporting framework and transport pathways within vast, multinucleate tissue masses. If we take this preparation as a model for tissue organization in the intact sponge, these findings support the view that hexactinellids are syncytial organisms, probably the largest in the animal kingdom, and suggest that food products may be distributed through the sponge intracellularly rather than by wandering amoebocytes. The findings strengthen the case for establishing the Hexactinellida as a subphylum within the Porifera.

Introduction

The syncytial organization of hexactinellid sponge tissue has been in question since the histology of dredged specimens was first examined. These animals, commonly known as glass sponges because of their siliceous skeleton, inhabit deep waters throughout the world's oceans, making their retrieval in good condition difficult. Early sponge researchers reported that there were no discernible membrane boundaries between nuclei (Schulze, 1887; Ijima, 1901). Although two cell types, archaeocytes and thesocytes, could be distinguished, most of the sponge was thought to be syncytial. At the time, however, many animal tissues were considered to be syncytial, including the pinacoderm of demosponges (Hyman, 1940), but phase contrast and electron microscopy have since revealed their cellular nature. Thus, the idea that hexactinellids were syncytial animals received little serious attention from modern sponge workers until recently.

Reiswig (1979) investigated hexactinellid histology using several populations accessible by scuba on the coast of British Columbia, Canada. Although his first attempts at electron microscopy with *Aphrocallistes vastus* and *Chonelasma calyx* were thwarted by difficulties with ultrastructural preservation, Reiswig nonetheless found no evidence to contradict Schulze's and Ijima's conclusions. Perseverance with electron microscopy with *Rhabdocalyptus dawsoni* (Fig. 1a) resulted in an improved fixation technique that provided ultrastructural evidence for two kinds of reticular, multinucleate tissues, the trabecular syncytium and the choanosyncytium, and for several types of cells (Mackie and Singla, 1983) (Fig. 1b). Most inter-

Received 14 December 1994; accepted 28 March 1995.

A video of cytoplasmic streaming and fusion in *Rhabdocalyptus dawsoni* is available from the author at cost.

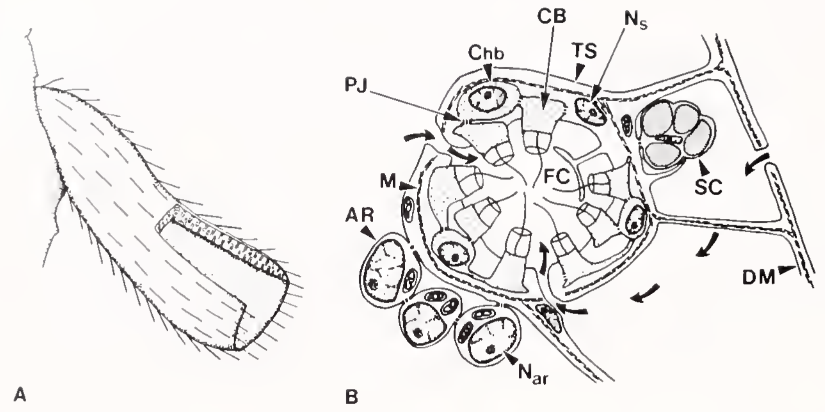

Figure 1. (A) Drawing of the hexactinellid sponge *Rhabdocalyptus dawsoni* with its osculum partially cut open. (B) Diagram illustrating the tissues of whole sponges. Water flows into choanoflagellate chambers (FC) as shown by the curved arrows, and is pumped out directly up from the center of the chamber. Trabecular syncytium (TS), collar body (CB), choanoblast (Chb), plugged junction (PJ), mesohyl (M), dermal membrane (DM), nucleus in the syncytium (N_s), nucleus of an archaeocyte (N_{ar}), spherulous cell (SC), archaeocyte (AR).

estingly, the syncytial cytoplasm was found to be connected to cellular components either by open cytoplasmic bridges or by a unique osmiophilic perforated plugged junction (Mackie, 1981). Sclerocytes were the only cell type not connected by plugs to the syncytium.

Concurrent electrophysiological studies with *Rhabdocalyptus* showed that following mechanical or electrical stimulation this sponge was capable of propagating signals at a rate of $0.26\ \text{cm} \cdot \text{s}^{-1}$ that stopped the flow of feeding currents throughout the whole animal, presumably by causing flagellar arrest (Lawn *et al.*, 1981; Mackie *et al.*, 1983). Because no nerves could be found, the syncytial tissues were proposed as the pathways for conduction, though no recordings of propagated electrical signals could be obtained.

Plugged junctions have since been reported in five of the six hexactinellids examined by electron microscopy, the exception being *Dactylocalyx pumiceus* (Reiswig, 1991). In this animal, no such junctions were found, but their presence could not be completely ruled out. Because of the remarkable differences in cellular organization between hexactinellids and other sponges and the physiological evidence of signal conduction, it was proposed that this group be separated from cellular sponges at the subphylum level (Reiswig and Mackie, 1983). Nonetheless, conclusive proof of syncytial organization from dye exchange experiments or from observations of cytoplasmic movements in living tissues has not been obtained, and recent investigations have raised doubts about the syncytial nature of hexactinellid larvae (Boury-Esnault and Vacelet, 1994).

When demosponges are dissociated by squeezing them through a fine mesh, the cells have the ability to reaggregate, forming a new individual (Wilson, 1907). The mechanisms underlying reaggregation have been extensively studied. The process is homeotypic and therefore of interest in relation to self and non-self discrimination in the earliest metazoa (Curtis, 1962; Moscona, 1968; McClay, 1971; Müller, 1982). Studies of newly dissociated demosponge cells shows that they exhibit rapid nondirectional crawling along the substrate (Noble and Peterson, 1972; Gaino *et al.*, 1985). Initial contacts between cells may be made by membrane bridges (Evans and Bergquist, 1974), whereas the formation of secondary aggregates is by species-specific cell adhesion molecules (Müller, 1982). Whether aggregation is brought about by cell migration or artificially, for example, by the rotary technique of Humphreys (1963), aggregates rapidly grow in size, becoming opaque under the light microscope.

In earlier work (Pavans de Ceccatty, 1982), aggregates in hexactinellids, like those in demosponges, were found to form large spherical masses, and their contents could not be observed with light microscopy. In the present study, however, substrates containing sponge tissue extract or concanavalin A were used (Leys, 1995). The tissues adhere and spread out on these substrates, permitting observation of the cytoskeleton *in vitro*. The findings reported here show that, in such preparations of *Rhabdocalyptus*, tissue aggregation leads to the formation of giant syncytia in which multidirectional streaming occurs over great distances in a manner unique among the Porifera.

Materials and Methods

Specimens of *Rhabdocalyptus dawsoni* were collected by scuba from a depth of 30 m in Barkley Sound and

Saanich Inlet, British Columbia, and kept in flow-through seawater tanks at the Bamfield Marine Station and at the University of Victoria. Specimens of *Haliclona* sp. were collected intertidally at Clover Point, Victoria, British Columbia, for use in dye exchange experiments only.

Preparation of substrate

The preparation of tissue extract dried onto coverslips or plastic petri dishes, to which dissociated tissue of *R. dawsoni* adheres, is described elsewhere (Leys, 1995). Alternatively, 50 μl (100 $\mu g \cdot ml^{-1}$) Concanavalin A (Con A) was pipetted onto coverslips and allowed to air dry before being used as an adhesion substrate for dissociated tissue.

Preparation of aggregates

Pieces (1 cm^3) of cleaned whole sponge tissue were squeezed through 100 μm Nitex mesh into a beaker to make 3.0–5.0 ml of dissociated tissue, then diluted to 200 ml with seawater. About 2 ml of the suspension was poured into 1.8 cm diameter plastic petri dishes containing coated coverslips and held at 11°C either by floating dishes on seawater or by placing them in an incubator. Alternatively, for video microscopy, the dissociated tissue was briefly pelleted at $1000 \times g$ for 15 s to remove spicule debris, and the top of the pellet was pipetted onto a coated coverslip in a dish of seawater.

Computer-assisted light microscopy

Preparations were viewed with a compound microscope equipped with phase contrast and differential interference contrast (DIC) optics and with a cooling stage. Images were captured with a Panasonic digital color CCTV video camera and OMNEX digital image processor (Imagen Inc.). Photographs were taken from the screen of a Technitron television monitor.

Immunolabeling and vital staining

To prevent depolymerization of the cytoskeleton due to excess calcium, aggregates were transferred to calcium-free seawater (CFSW) for 30 min prior to fixation. For microfilament labeling, preparations were lysed at 2, 6, 12, and 24 h after plating the tissue, in a PEM buffer consisting of 50 mM piperazine-N,N'-bis[2-ethane sulfonic acid], 1 mM ethyleneglycol-bis-(β-aminoethyl ether)N,N'-tetraacetic acid, 0.5 mM $MgCl_2$ at pH 6.9 with 10% dimethylsulfoxide and 0.1% Triton X-100 for 2 min and fixed in 2% paraformaldehyde in CFSW with 10 μM EGTA and 0.04% tannic acid for 10 min. For microtubule labeling, preparations were fixed without lysing, in 2% paraformaldehyde in PEM buffer, at 30 min, 1, 6, and 12 h after plating. After one 30-min wash in 0.05 M Tris buffer pH 7.0 with 0.1% TX-100, coverslips were incubated overnight in tubulin antibodies or rhodamine-phalloidin (Molecular Probes, Inc.) to visualize actin microfilaments. The tubulin antibodies used included a polyclonal anti-tubulin antibody (Chemicon); a monoclonal antibody against flagellar axonemes or isolated basal apparatus of *Polytomella* (Protista, Chlorophyceae), designated 5A6 (kindly provided by Dr. David Brown, University of Ottawa); a monoclonal antibody against yeast tubulin clone YOL1/34 (Sera Labs); a monoclonal antibody against native chick brain alpha tubulin (Amersham); and a monoclonal antibody against *Drosophila* (insect) beta tubulin, designated E7, which was developed by M. Klymkowski and obtained from the Developmental Studies Hybridoma Bank maintained by the Department of Pharmacology and Molecular Science, Johns Hopkins University School of Medicine, Baltimore, Maryland, and the Department of Biological Sciences, University of Iowa, Iowa City, Iowa. After a 30-min rinse, preparations were incubated in their respective secondary antibody for 5 h, rinsed thoroughly in phosphate buffered saline (PBS) pH 7.2, and mounted in PBS-glycerol with *n*-propyl gallate. To stain the nuclei, coverslips were incubated in 100 $\mu g \cdot ml^{-1}$ Hoechst #33342 (Sigma) for 5 min at 11°C, and immediately observed with a 40× water immersion lens. To examine the microtubule network in severed streams, a stream was cut with a scalpel while the preparation was still in a dish of seawater on an inverted microscope. After the material downstream of the wound had completely drained away, the preparation was fixed and labeled for anti-tubulin immunofluorescence as above.

Electron microscopy

For scanning electron microscopy (SEM), dissociated tissue from *Rhabdocalyptus* adhered to coverslips was transferred to CFSW for 30 min prior to fixation. Preparations were briefly lysed for 5–15 s, or fixed directly, in a fixative containing 2% glutaraldehyde, 1% OsO_4, 0.45 M sodium acetate buffer at pH 6.4 (Harris and Shaw, 1984), 10% sucrose and 5 μM EGTA final concentration, for 2 h on ice. Coverslips were dehydrated through a graded ethanol series, critical-point dried in CO_2, mounted on stubs with silver conducting paint, coated with gold in an Edwards S150B sputter coater, and examined in a JEOL JSM-35 scanning electron microscope.

For transmission electron microscopy (TEM), whole mounts were prepared on extract-coated, Formvar-coated gold grids, lysed for 2 min, and fixed as above. Whole preparations, adhered to 5 cm diameter plastic petri dishes, were acclimated to CFSW for 30 min and fixed as above. Grids were critical-point dried and viewed in a Hitachi H-7000 electron microscope. Whole preparations, fixed in plastic petri dishes, were treated with 4% hydrofluoric acid overnight to remove silica, dehydrated in ethanol, and embedded in Epon. For cross sections, the embedded material was taken out of the petri dish and reembedded in Epon. Thin sections were cut on a Reichert UM2 ultramicrotome and stained with uranyl acetate and lead citrate.

Pharmacological manipulations

To demonstrate the effect of various cytoskeletal disruptors on streaming, drugs (cytochalasin B, colcemid, nocodazole, Taxol, EGTA) were added to 2 ml seawater in a Falcon petri dish containing one preparation. To demonstrate reversibility of the effects, preparations were incubated in these drugs for 5 min and 2 min respectively, and transferred immediately to clean seawater every 15 min thereafter for 4.5 h. Preparations were kept at 11°C for the duration of the experiment.

Dye exchange experiments

To confirm that fusion of tissues and exchange of cytoplasm occurred during aggregation in syncytial sponges but not in cellular sponges, dissociated tissues of both sponges were loaded with fluorescent, membrane-impermeable dyes and allowed to aggregate. Dissociated tissue from both *Rhabdocalyptus* (R) and *Haliclona* (H) was briefly centrifuged at 1000 × *g* for 15–30 s to remove spicule and other debris. Calcein acytoxymethyl ester (CAM) and Calcein blue acytoxymethyl ester (CBAM) (Molecular Probes, Inc., Eugene, OR) were made up in DMSO to stock concentrations of 1 and 2 m*M* respectively. The dyes were added to the sponge tissue at a final concentration of 10 μM in microfuge tubes that were left at 10°C for 15 min. The tissue was then rinsed three times by pelleting the tissue, drawing off the remaining seawater by pipette and resuspending the pellet in fresh seawater. After the final rinse, equal volumes were plated in a 1.8-cm, extract-coated plastic petri dish as follows: (R)-CAM with (R)-CBAM; (R)-CAM with (H)-CBAM; (H)-CAM with (H)-CBAM.

Results

Fusion

Immediately after being plated, the dissociated tissues consisted of unattached rounded masses of various sizes, some of which could be identified by their collars and flagella as parts of choanoflagellate chambers. All pieces adhered to the coverslip within seconds of plating and flattened and spread out between 5 s and 10 min after plating (Fig. 2). The larger (10 μm diameter) pieces developed a broad, skirt-like lamellipodium or extended long filopodia into which the cytoplasm streamed. These adhered tissue pieces incorporated other smaller, rounded

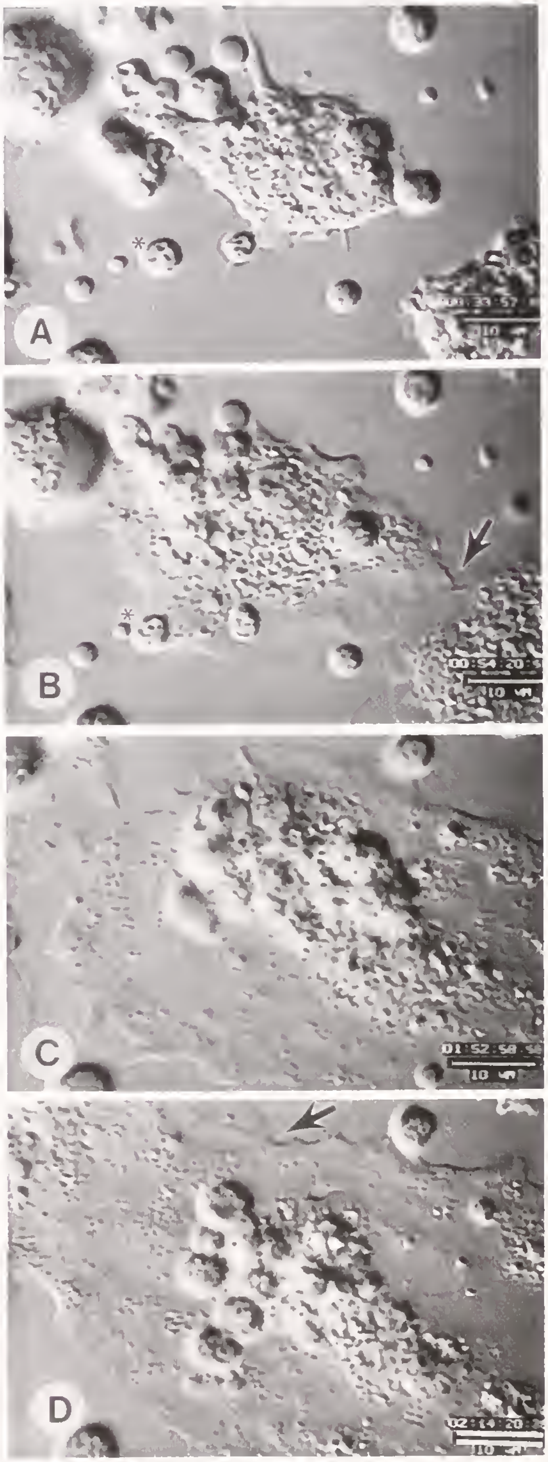

Figure 2. Fusion in adhered aggregates of *Rhabdocalyptus* taken from a video recording of tissue aggregation. Upon plating, pieces of tissue adhere and spread a skirt-like lamellipodium or long filopodia. After about 1 h of spreading, such pieces encounter each other, as shown by the overlapping lamellipodia (B, arrow). Tissues fuse and exchange cytoplasm between 5 and 30 min after first contact (C). Fused tissue pieces continue to grow in diameter, incorporating some tissue pieces (* in A and B) and fusing with others (D, arrow). Minutes after plating dissociated tissue: A, 33 min; B, 54 min; C, 102 min; D, 134 min. Bar: 10 μm. (Video available; see footnote on title page.)

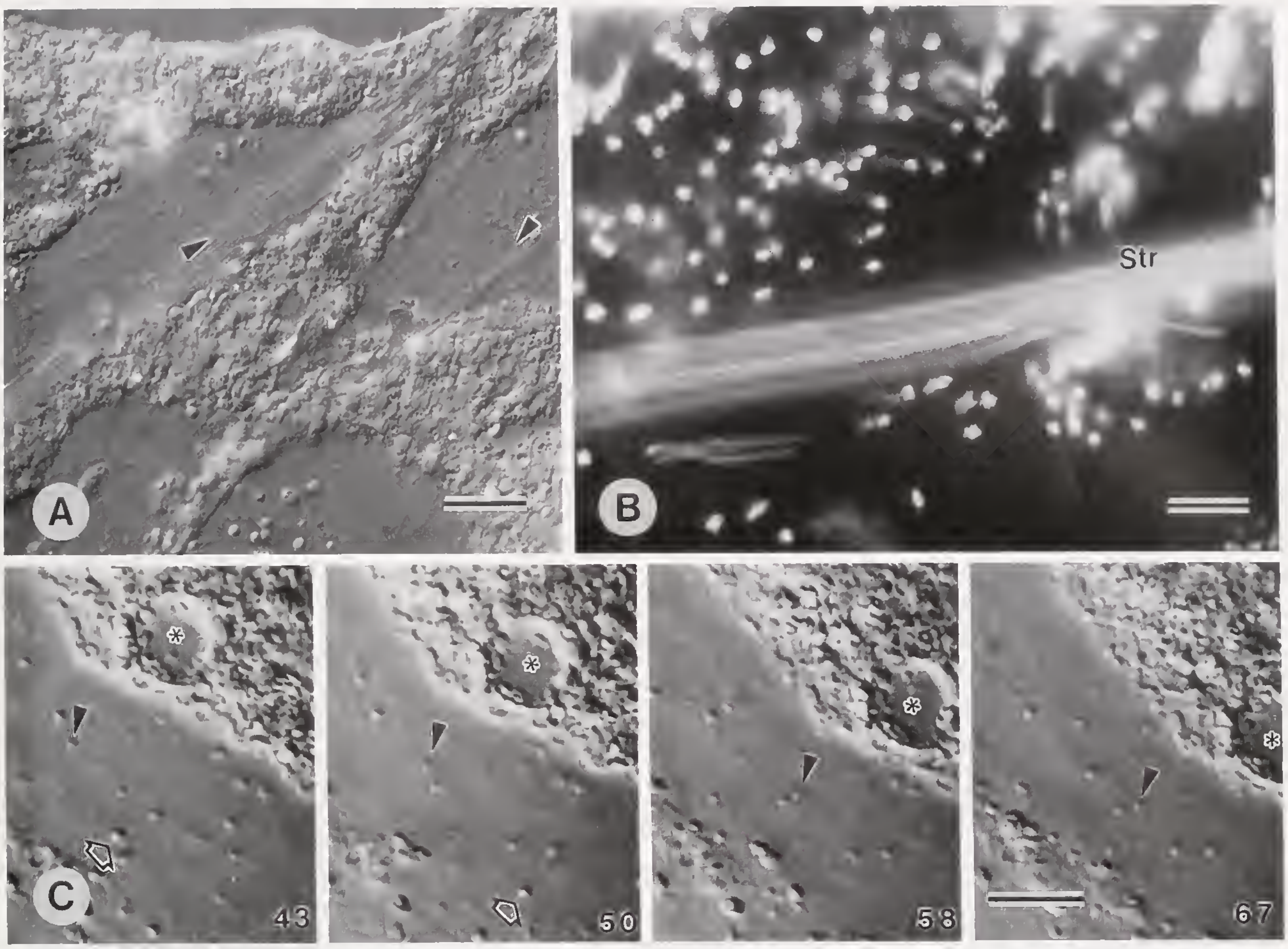

Figure 3. Twenty-four hours after plating sponge tissue, a single tissue mass covers an entire petri dish. (A) Streams (arrowheads) are abundant and run in opposite directions, winding throughout the entire coverslip. A 5-s shutter exposure allowed moving objects to leave trails. Bar: 20 μm. (B) Hoechst-labeled nuclei are visible in both streaming (STR) and stationary cytoplasm. Nuclei move in streams at just over 2 μms^{-1}. A 30-s shutter exposure causes all moving nuclei to leave a trail of light marking their path. Bar: 20 μm. (C) Images from a video monitor showing bulk transport of material in streams (*) beside organelles that are being transported individually (arrow and arrowhead). Streams move continuously but at a slower rate than individual organelles. The organelle marked by an open arrow moves steadily, leaving the field of view in the third frame, while the organelle marked by an arrowhead moves haltingly and eventually stops. Frames shown are at 8-s intervals. Bar: 10 μm. (Video available; see footnote on title page.)

pieces of tissue by drawing them in to a central location within the aggregate. Independent adhered pieces encountered each other by way of the lamellipodia or filopodia. Fusion did not always occur immediately upon contact of lamellipodia. Lamellipodia even overlapped one another for 10–30 min before the exchange of organelles could be clearly detected (Fig. 2b, 54 min). A clear sign of fusion, however, was a shared lamellipodium at the point of touching, followed by exchange of organelles. Within minutes of fusion there was no evidence that the single piece of tissue had been otherwise. Lamellipodial extension continued in all directions, and streams of cytoplasm started to become clearly visible circumnavigating the aggregate in both directions. Fusion continued with other tissue pieces that were encountered.

Cytoplasmic streaming

As aggregates increased in size by incorporating neighboring tissue masses, organelle movement became organized into wider and straighter streams, until eventually the entire coverslip was covered in tissue that consisted of dramatic rivers of flowing cytoplasm traversing the coverslip, sometimes running parallel in opposite directions (Fig. 3a) and even crossing each other without apparent interruption in volume or velocity of flow. Streams of cytoplasm flowed uninterrupted for distances up to several centimeters, limited only by the area of coated substrate available. Large streams continually changed direction and both gained and lost volume. Under DIC microscopy, bulk cytoplasm in streams could be seen to contain spicule debris and vesicles of various sizes. With electron microscopy, cytoplasm fixed while it was streaming showed similar objects along with numerous mitochondria, nuclei, Golgi bodies, and some archaeocytes. Fluorescent staining with Hoechst #33342 showed nuclei in both the flowing and stationary cytoplasm (Fig. 3b). Individual nuclei could be followed in streams for distances up to several millimeters.

Organelles resolvable by video-enhanced contrast microscopy in thin areas of tissue moved at an average rate of $2.15 \pm 0.33\ \mu m \cdot s^{-1}$ ($n = 100$), while bulk streams moved at an average rate of $1.72 \pm 0.30\ \mu m \cdot s^{-1}$ ($n = 100$) (Fig. 3c). However, some organelles moved haltingly, sometimes reversing direction or apparently bumping into each other; these organelles seemed to buckle or bend as they reversed. Organelles moving in broad lamellipodia followed no one direction, and occasionally paused for some seconds. In some streams the bulk cytoplasm that had been flowing diminished in volume to isolated organelles, to be followed once again by bulk cytoplasm.

Cutting a stream with a scalpel caused cytoplasm to build up on the upstream side of the wound. Downstream of the wound, cytoplasm continued to flow away until no movements of organelles could be detected, but birefringent tracks could still be seen by phase contrast and DIC microscopy (Fig. 4a). Immunofluorescence of tubulin on the depleted side showed that microtubule bundles remained, even though all streaming along them had ceased (Fig. 4b). Eventually the cytoplasm upstream of the wound began to turn back upon itself, initiating a new stream parallel to the original one but in the reverse direction. At the same time, lamellipodial and filopodial processes were extended toward the downstream side until, after several minutes, contact was once again made, followed by fusion; a few organelles, soon followed by the full stream, then began to flow along the original track. These stages are summed up diagrammatically in Figure 4c.

With time, the tissue amassed in central locations and gradually withdrew from the substrate until an opaque

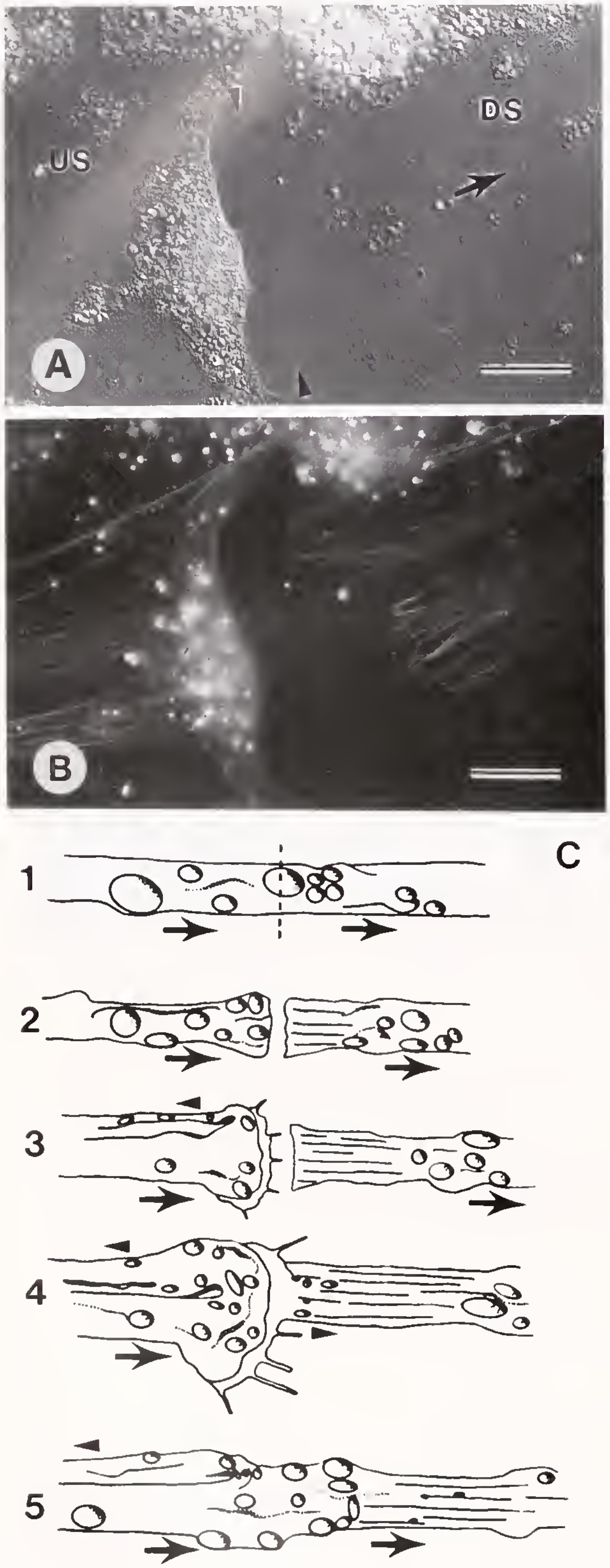

Figure 4. The effect of severing streams of cytoplasm. (A) When cut, the cytoplasm downstream (DS) of the wound (arrowhead) continues to drain in the direction of the arrow, while that upstream (US), builds up. Bar: 30 μm. (B) Anti-tubulin labeling of microtubules in the wounded stream. Microtubules remain, even though all visible organelle movement has ceased downstream of the wound. Bar: 30 μm. (C) Diagram illustrating the sequence of events after wounding a stream. The cut cytoplasm, represented by the dashed line in (1), builds up on the upstream side (2), eventually forging a new path in the reverse direction (3), as indicated by arrowheads. Filopodial and lamellipodial projections extend across the wound, making contact with the original tracks (4). Single organelles, rapidly followed by the bulk cytoplasm, begin to stream along the former path (4). Arrows indicate direction of flow.

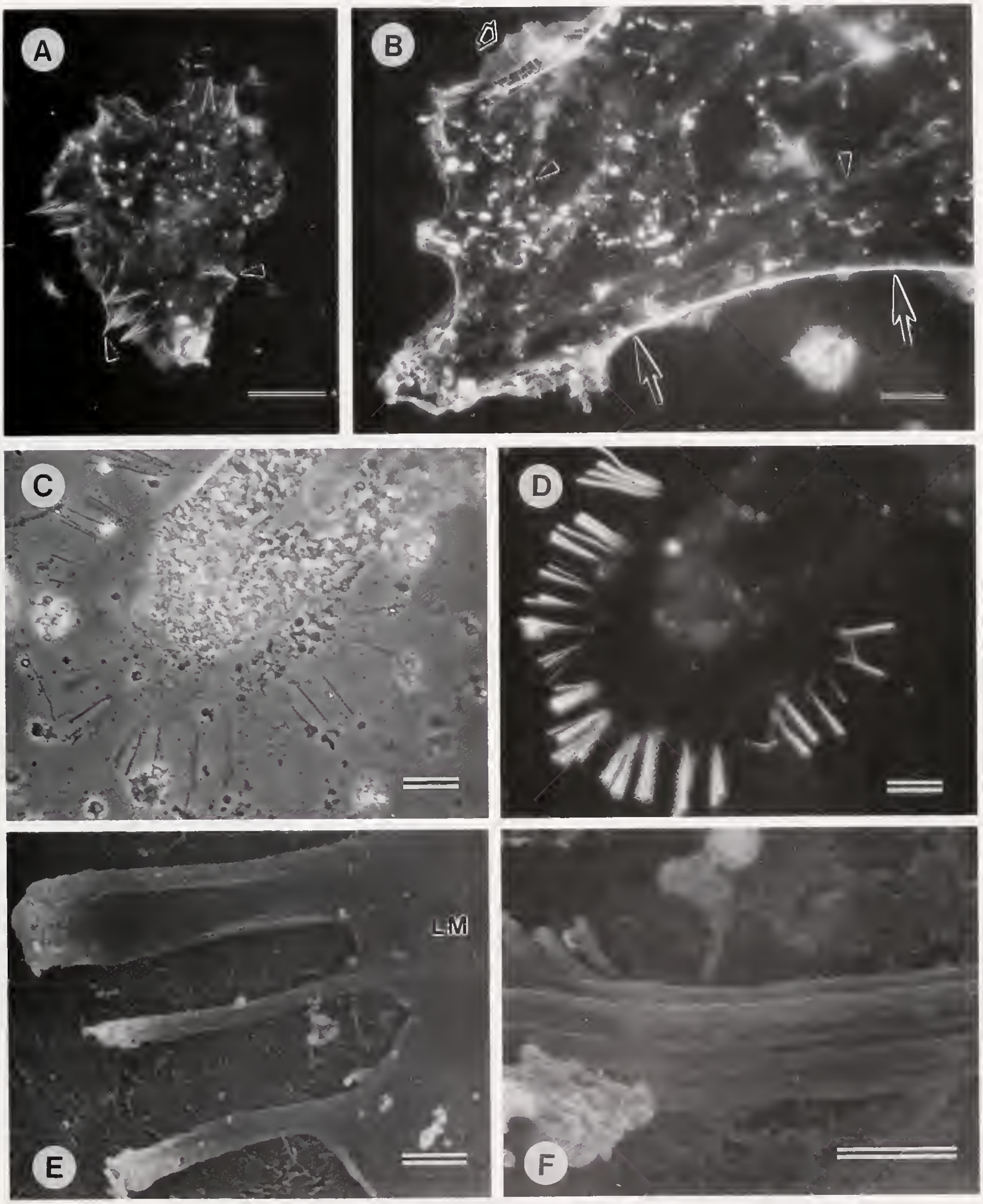

Figure 5. The actin cytoskeleton in adhered aggregates after lysing. (A) Rhodamine-phalloidin labeling of aggregates 2 h after plating reveals tissue masses 30–100 μm in diameter that possess well-defined rods projecting from their periphery (arrowheads). Bar: 20 μm. (B) Six hours after plating dissociated tissue, aggregates are already 0.5 mm in length and can be much larger. A portion of a fused aggregate shows giant

sphere was formed. Such spheres could temporarily adhere once again if new substrate was offered.

The actin cytoskeleton

Only by briefly lysing preparations before fixation was it possible to obtain a clear picture of actin distribution in adhered tissue preparations. Attempts to label microfilaments with a polyclonal antibody to actin and with rhodamine-phalloidin in whole preparations gave, at best, weak labeling of microfilament bundles whose precise location could not be determined. However, lysing the tissue for 5 s–2 min resulted in detachment of the superficial part of the tissue mass, exposing the layer adjacent to the substrate in which actin labeling produced clearer results.

Two hours after plating, aggregates were 30–100 μm in diameter and possessed blunt rods containing thick actin bundles that projected from the periphery (Fig. 5a). The edges of large lamellipodia labeled strongly with rhodamine-phalloidin and stress fibers some 20 μm in length transected the tissue. After 6 h, these masses had joined, and no membranes demarcating cell boundaries could be seen within the tissue mass by phase-contrast microscopy. Rhodamine-phalloidin–labeled microfilament bundles up to several hundred micrometers long were observed to run around the edges of adhered aggregates (Fig. 5b). A network of fine filaments was apparent beneath the stress fibers throughout the syncytium. One-day-old adhered aggregates showed no change in general morphology or in actin distribution, although the distances over which bundles of microfilaments could be followed now exceeded 500 μm. After 24 h, much of the tissue had been drawn into central, opaque areas. The edges of such dense tissue masses possessed blunt rod-like extensions reaching some 18.0 ± 4.5 μm ($n = 20$) out from the edge of the lamellipodium, forming a "hairbrush effect" (Fig. 5c). These extensions labeled very strongly for actin (Fig. 5d). The organization of actin in aggregates older than 48 h did not change significantly, because most tissue was centralized at that time, anchored firmly by massive projections from the edges. Scanning electron microscopy of the giant rods in intact and lysed preparations revealed thick actin bundles forming their core (Fig. 5e, f).

The microtubule cytoskeleton

Preservation of microtubules required the use of a special fixation method (see *Immunolabeling and vital staining* in the Materials and Methods), after which it was possible to visualize microtubule bundles by phase contrast and immunofluorescence microscopy. These bundles were still visible after cytochalasin B treatment, but not after treatment with nocodazole or colcemid. Of five anti-tubulin antibodies, only two monoclonal antibodies—one prepared against beta tubulin in *Drosophila* and the other against chick brain alpha tubulin—gave good immunofluorescence in whole mounts. Control experiments showed that all antibodies labeled microtubules in neurons and cilia of tunicate branchial basket and veliger larvae.

Immunofluorescence microscopy revealed a remarkable change in the microtubule network over the course of aggregation. At 30 min, microtubules formed a fine meshwork in tissue pieces up to 80 μm in diameter; microtubules appeared delicate, some directly crossing and others winding around the tissue mass. Nuclei appeared randomly scattered among the microtubules. After 6 h, the microtubules were already well organized into striking bundles, many of which traversed an entire coverslip (Fig. 6a). Where many bundles of microtubules converged into one path they became rigidly straight (Fig. 6b). At the edge of preparations, the entire bundle gave way to a reticular network of lines (Fig. 6c). These often wound through giant lamellipodia before joining the main stream and traversing the coverslip again.

Double labeling of actin and tubulin proved unsatisfactory because the lysing procedure required for clear visualization of the microfilament network usually destroyed the continuity of microtubules. However, double labeling of nuclei and microtubules clearly demonstrated that nuclei were randomly distributed among microtubules (Fig. 8f).

The microtubules were difficult to fix for electron microscopy. The fixative used by Mackie and Singla (1983) does not stabilize microtubules except in flagella. The fixative of Harris and Shaw (1984) gave excellent results for both general ultrastructure and microtubule preservation. In cross sections of the adhered tissue, microtubules were seen both in bundles and lying individually (Fig. 7a and inset). In thicker areas of the tissue, large bundles were seen at the surface of the preparation as well as through the depth of the tissue. Rarely in these areas did they occur singly, and rarely were they on the bottom of thick tissue masses. In horizontal section, microtubule bundles could be traced for many hundreds of micrometers (Fig.

bundles of microfilaments delineating the border (filled arrows). A network of microfilament bundles traverses the basal layer adjacent to the substrate (arrowheads) and small, actin-dense rods lie within lamellipodia (open arrow). Bar: 20 μm. (C, D) Adhered aggregates older than 12 h possess giant rods projecting from the periphery as a "hairbrush" (C: phase contrast; D: rhodamine-phalloidin labeling of unlysed tissue.) Bar: 10 μm. (E) SEM shows several giant rods extending from the lamellipodium (LM). (F) High magnification SEM of a lysed actin-dense rod. E, F, bar: 0.5 μm.

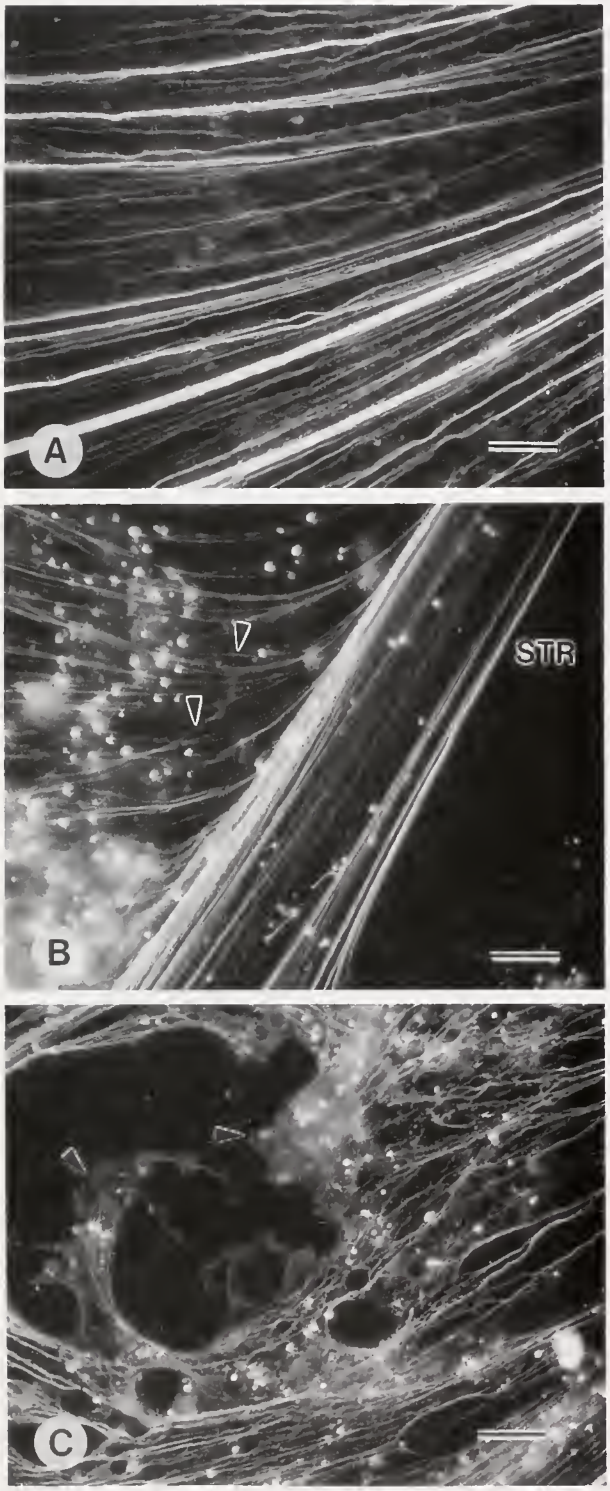

Figure 6. Immunofluorescence of the microtubule cytoskeleton in adhered aggregates. (A) Six hours after plating, microtubule bundles already stretch up to a centimeter across an entire coverslip. A–C, bar: 20 μm. (B) Microtubule bundles are rigidly straight (STR) in streams, while those leaving or converging on a stream (arrowheads) are often curved. (C) At the edges of preparations, bundles give way to a fine meshwork of microtubules that reach into lamellipodia (arrowheads).

7b). Nuclei, mitochondria, coated vesicles, and tubulovesicular organelles were all found adjacent to microtubule bundles as well as lying free in the cytosol. Tracts of microtubules ran beside, but not through, clusters of archaeocytes and spherulous cells. In whole mounts of aggregates adhered to tissue extract on Formvar-coated gold EM grids, organelles of various sizes were also seen associated with linear structures with diameters of approximately 22 nm, presumably microtubules (Fig. 7c).

Inhibition experiments

Organelle movement was reversibly inhibited by both nocodazole and colcemid but was unaffected by cytochalasin B (Table I), although the latter caused the tissue to detach from the substrate. Neither Taxol nor 10 μM EGTA had any effect on rate of organelle transport.

Dye exchange

Attempts to inject the fluorescent dyes carboxyfluorescein or lucifer yellow through glass capillary microelectrodes were not successful because of difficulty in obtaining stable penetrations. The surface membrane of adhered aggregates either blocked the electrode or did not reseal around the electrode after penetration. However, fluorescent dyes coupled to acytoxymethyl esters such as Calcein AM (CAM) and Calcein blue AM (CBAM) could be readily loaded into dissociated tissue. Tissue loaded with CAM plated in the same culture dish with tissue loaded with CBAM produced fused aggregates in which streaming occurred. After 6–12 hours, these aggregates were uniformly blue-green (Fig. 8a, b, c). In control experiments in which dissociated tissue from the cellular sponge *Haliclona permolis* loaded with CAM was plated with tissue from *Rhabdocalyptus* loaded with CBAM, *Haliclona* cells rapidly formed large round aggregates, did not mix with *Rhabdocalyptus* tissue, and did not take up the blue dye (Fig. 8d). *Haliclona* tissue, even if adhered, showed no sign of cytoplasmic streaming. When two samples of *Haliclona* tissue were loaded with CAM and CBAM respectively and plated together, there was no exchange of dye, although after 12 h aggregates were mosaics of both colors (Fig. 8e).

Discussion

This remarkable preparation provides the first evidence of fusion during aggregation of dissociated hexactinellid sponge tissues and reveals an entirely novel form of cytoplasmic streaming. It further reveals a cytoskeletal framework that is unique in the histology of sponges and, perhaps, the entire metazoa, for sheer size. Given the evidence of syncytialization in other hexactinellids, streaming may be widespread within the group. The syncytial

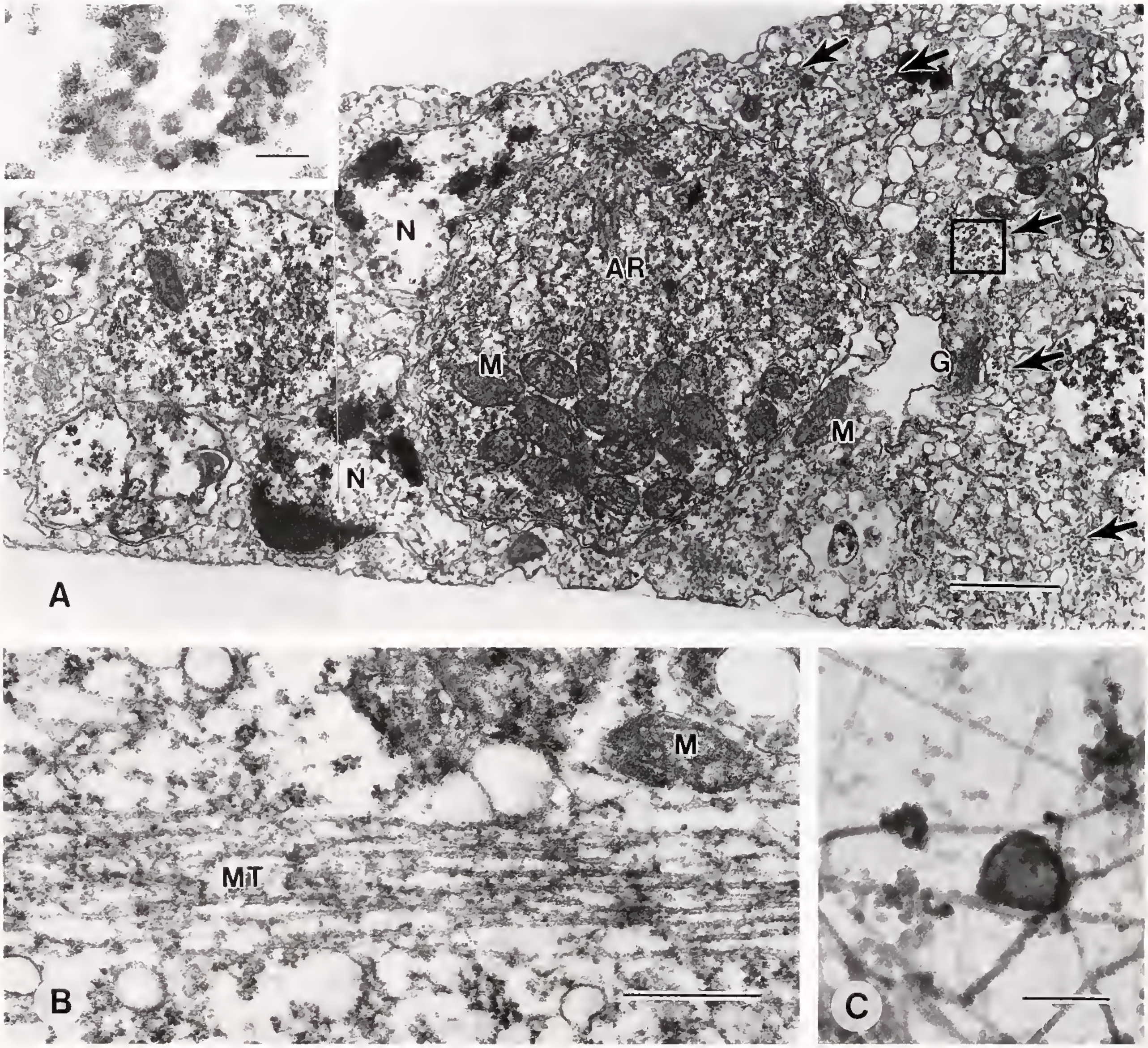

Figure 7. Electron microscopy of adhered aggregates. (A) In cross section, cellular components (such as archaeocytes) lie within the multinucleated cytoplasm, which is surrounded above and below by a continuous membrane. Microtubule bundles lie at the surface of streams and throughout the tissue (arrows). Bar: 1 μm. Inset shows an enlargement of microtubules from within the box. Bar: 0.1 μm. Nuclei, N; archaeocyte, AR; Golgi, G; mitochondria, M. (B) Horizontal section through a stream showing a bundle of microtubules (MT) with associated organelles. Bar: 0.5 μm. (C) A whole-mount preparation showing an organelle associated with linear structures. Bar: 0.2 μm.

condition of hexactinellid sponges appears to be significant in two ways. First, syncytialization would allow the transport of nutrients throughout the animal in the absence of mobile archaeocytes (Mackie and Singla, 1983). The present findings suggest that cytoplasmic streams may be the transport routes. Second, the lack of membrane barriers within the syncytium presumably makes possible the propagation of impulses coordinating flagellar arrests (Lawn *et al.*, 1981; Mackie *et al.*, 1983). Cellular sponges, lacking nerves and gap junctions, have no such capability.

Formation of a syncytium

Membrane fusion is the means by which *Rhabdocalyptus* forms a syncytium during aggregation. Nonetheless, not all tissue components fuse. Small rounded pieces of tissue, which do not form lamellipodia, are drawn into

Table I

The effect of cytoskeletal disruptors and stabilizers on transport in Rhabdocalyptus dawsoni

Drug	Action	Effect on streaming
Colcemid (10 μg/ml)	Depolymerizes	Stops streaming
Nocodazole (1 μg/ml)	Depolymerizes	Stops streaming
Taxol (10 μg/ml)	Stabilizes MTs	No effect
EGTA (10 μM)	Chelates calcium	No effect

MTs, microtubules; MFs, microfilaments.

the center of larger aggregates that are fusion products. Whether syncytia can be formed by fusion of tissues from two species of hexactinellids has not yet been tested. The observation of dye spread following fusion in *Rhabdocalyptus* confirms the syncytial state of the tissues of this sponge, in contrast to *Haliclona*, where no dye spread was observed during aggregation. Failure of dye to spread within *Haliclona* might be due to inability of Calcein to pass through gap junctions or to the absence of gap junctions or other aqueous intercellular pathways (see Mackie, 1984).

Streaming

Before the first fusion event, organelles appear to move in adhered tissue pieces in the way described for other cells, including basal epithelial cells of freshwater sponges (Wachtmann and Stockem, 1992). After fusion, however, streaming in *Rhabdocalyptus* aggregates takes on characteristics unlike any transport mechanism previously described. For example, streams maintain neither a constant volume nor a single direction. Flow may reverse direction, albeit with a slight decrease in rate at the point of turning. And there is no limit to the length of streams. The closest parallel to this system is the streaming of bulk cytoplasm and individual organelles in reticulopodia of the protists *Allogromia* and *Reticulomyxa* (Travis and Allen, 1981; Koonce *et al.*, 1986), and there may be parallels with bulk cytoplasmic flow in characean algae, where a mechanism for coupling of bulk cytoplasm to microfilament bundles by means of the endoplasmic reticulum has been described (Kachar and Reese, 1988).

Rates of organelle transport in *Rhabdocalyptus* are within the range reported for fast axoplasmic transport (Allen *et al.*, 1982) and other systems involving microtubule-associated motors. The prominence of the network of microtubule bundles and the inhibition of streaming by colcemid and nocodazole, drugs that depolymerize microtubules, strongly implicate the microtubules as the transport pathway, making it likely that microtubule-associated motor proteins are involved. A recent account of cell shape changes in newly hatched freshwater sponges and sandwich cultures of marine sponges showed that these sponge cells are capable of movement at rates of up to 15 $\mu m \cdot min^{-1}$ (Bond, 1992). Lamellipodial movements in *Rhabdocalyptus* aggregates appear to occur at about the same rate. However, the transport of nuclei and other organelles in streaming cytoplasm at seven to ten times that rate suggests that the two mechanisms of movement are different.

The effects of cutting cytoplasmic streams in *Rhabdocalyptus* are reminiscent of the effects of ligaturing axons (Weiss and Hiscoe, 1948). Streams, when cut, build up on the upstream side and drain on the downstream side. Furthermore, the lamellipodium that extends in search of the lost distal stump greatly resembles a nerve growth cone. Nonetheless, although streams may run in opposite directions beside or above one another, there is no evidence of the bidirectional flow within the same stream or along the same microtubule that may occur in axons. Further work with a perfused, reactivated sponge preparation will help to determine the precise mechanism of transport.

Cytoskeletal architecture

One of the most exciting findings of this study is the vast cytoskeletal framework of the adhered aggregates. The lengths of both microfilament and microtubule bundles are of proportions unheard of in any other tissue. Figure 9 presents a three-dimensional summary diagram of the cytoskeletal architecture in a stream at the edge of an adhered preparation, showing the relationship between cytoplasmic organelles and microtubules.

It is tempting to infer from the difficulty of fixing and labeling microtubules that, as in *Reticulomyxa* (Koonce *et al.*, 1986), tubulin in lower eukaryotes differs significantly from mammalian tubulin, or that bundling somehow interferes with antibody recognition. The composition of microtubules, sites of microtubule nucleation, and microtubule polarity are topics that merit further study in this sponge.

Filopodia containing dense actin cores have been reported in aggregating cells from cellular sponges (Burlando *et al.*, 1984; Gaino and Burlando, 1985), suggesting functional similarities. However, the stiff, actin-filled extensions that form a "hairbrush" effect in older adhered aggregates are unique. These enormous processes are implicated in the adhesion of aggregates because some areas could be found where the tissue had detached, leaving the "hairbrush" attached.

Adhered aggregates as a model of whole sponges

The difficulty of visualizing cytoplasmic movements in intact sponges makes it hard to say if processes similar to those seen in cultured aggregates are going on. Neverthe-

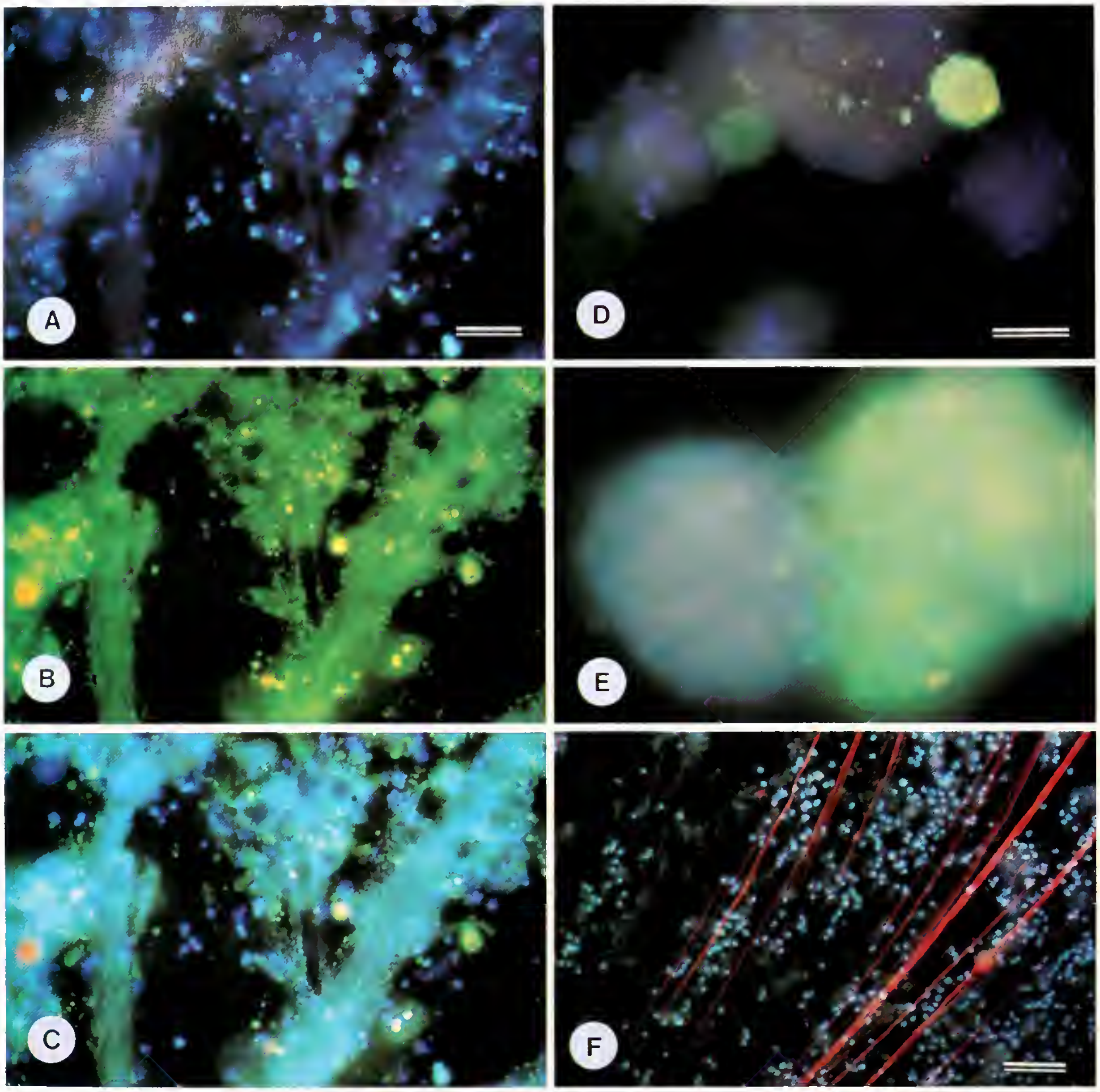

Figure 8. Demonstration of syncytial tissues in *Rhabdocalyptus* (A–C) Spread of dye in aggregates. *Rhabdocalyptus* tissue loaded separately with Calcein AM and Calcein blue AM and plated together fuses to allow blue dye throughout (a) and green dye throughout (b); thus a double exposure shows a blend of the two colors (C). A–C, bar: 25 μm. (D) *Rhabdocalyptus* tissue loaded with Calcein AM (green) and plated with tissue from the cellular sponge *Haliclona* loaded with Calcein blue AM (blue) shows that neither dye was membrane permeable once loaded, because neither sponge incorporated the other dye. Although both small and large round aggregates of *Rhabdocalyptus* have adhered to the larger *Haliclona* aggregate, no exchange of dye occurs. D, E, bar: 50 μm. (E) Tissue from *Haliclona* loaded separately with Calcein AM and Calcein blue AM and plated together did not exchange dye after 12 h, although aggregates often consisted of mosaics of both colors, as shown by a double exposure. (F) Double labeling of microtubules (red) and nuclei (blue) in day-old adhered aggregates of *Rhabdocalyptus dawsoni* demonstrates that the tissue is multinucleate. Bar: 25 μm.

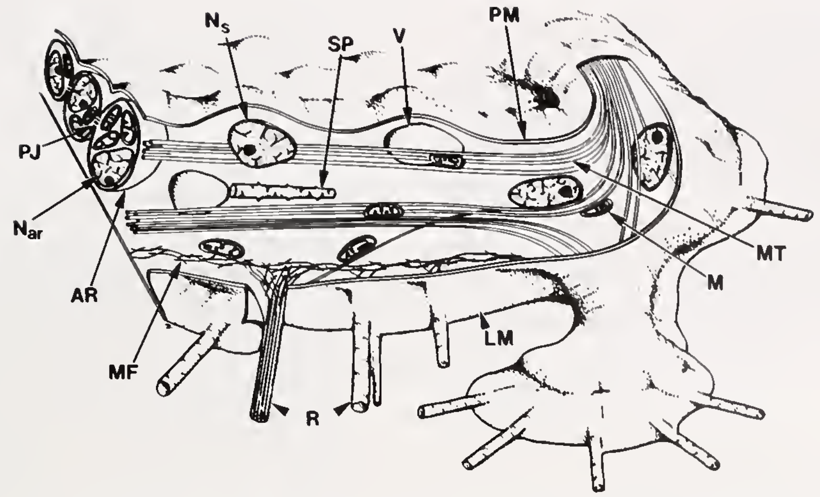

Figure 9. An illustration summarizing the cytoskeletal architecture in a 24-h adhered aggregate of *Rhabdocalyptus*. Microfilament bundles (MF) traverse the basal layer of aggregates. At the periphery, microfilament bundles give rise to giant actin-dense rods (R), which extend through lamellipodia (LM) to anchor the preparation to the substrate. Inside a cutaway of the plasma membrane (PM), a stream is exposed showing bundles of microtubules (MT) with associated nuclei (N$_s$), mitochondria (M), and vesicles (V). Also adjacent to the microtubules are groups of archaeocytes (AR), with their own nuclei (N$_{ar}$), connected to each other and the rest of the cytoplasm by perforate plugged junctions (PJ).

less, the likelihood that streaming occurs in the intact sponge is borne out by observations of streaming in regenerating fragments of the whole animal (Leys and Mackie, 1994). Video microscopy of aggregates suggests that streaming, or the microtubule network involved in streaming, may play a role in organizing the tissues of intact sponges, for instance by influencing the distribution and clustering of archaeocytes, spherulous cells, choanoblasts, and collar bodies. Archaeocytes do not appear to play the central role during aggregation in *Rhabdocalyptus* that they do in cellular sponges (Buscema *et al.*, 1980). Because adults of this species can be up to 2 m in length, and assuming that the trabecular tissues are continuous throughout the animal, *Rhabdocalyptus* must represent one of the largest syncytial organisms within the metazoa.

The evidence presented in this paper shows that adhered aggregates of *Rhabdocalyptus* possess a unique cellular motile system and a giant cytoskeleton. The observations strongly support the view that most of the cytoplasm in hexactinellids constitutes a multinucleate syncytium. It now seems clear that hexactinellids differ substantially from cellular sponges and should be differentiated from them at a high taxonomic level (Bergquist, 1978), as reflected in the subphyla Symplasma and Cellularia proposed by Reiswig and Mackie (1983).

Acknowledgments

I am indebted to G. O. Mackie for the enthusiasm he has shared with me throughout this project, and in particular for advice in preparing this manuscript. I thank L. R. Page for suggestions about Figures 1 and 9, N. Lauzon for invaluable help in collecting the animals, and an anonymous reviewer for helpful comments. This research was supported by Natural Sciences and Engineering Research Council grant no. OGPOO1427 to G.O.M., NSERC equipment grant no. EQM105188 for the purchase of a Hitachi EM7000, and a NSERC postgraduate scholarship to S.P.L. Portions of this work were conducted at the Bamfield Marine Station.

Literature Cited

Allen, R. D., J. Metuzals, I. Tasaki, S. T. Brady, and S. P. Gilbert. 1982. Fast axonal transport in squid giant axon. *Science* **218:** 1127–1128.

Bergquist, P. R. 1978. *Sponges.* Hutchinson and Co., London.

Bond, C. 1992. Continuous cell movements rearrange anatomical structures in intact sponges. *J. Exp. Zool.* **263:** 284–302.

Boury-Esnault, N., and J. Vacelet. 1994. Preliminary studies on the organization and development of a hexactinellid sponge from a Mediterranean cave, *Oopsacas minuta.* Pp. 407–416 in *Sponges in Time and Space. Proc. 4th Int. Porifera Congress,* R. W. M. van Soest, T. M. G. van Kempen, and J. Braekman, eds. A. A. Balkema, Rotterdam.

Burlando, B., E. Gaino, and P. C. Marchisio. 1984. Actin and tubulin in dissociated sponge cells. Evidence for peculiar actin containing microextensions. *E. J. Cell Biol.* **35:** 317–321.

Buscema, M., D. De Sutter, and G. Van de Vyver. 1980. Ultrastructural study of differentiation processes during aggregation of purified sponge archaeocytes. *Wilhelm Roux's Archives* **188:** 45–53.

Curtis, A. S. G. 1962. Pattern and mechanism in the reaggregation of sponges. *Nature* **196:** 245–248.

Evans, C. W., and P. R. Bergquist. 1974. Initial cell contact in sponge aggregates. *J. Microsc* **21:** 185–188.

Gaino, E., and B. Burlando. 1985. Cytoskeleton and morphology of dissociated sponge cells. A whole mount and scanning electron microscopic study. *Eur. J Cell Biol.* **39:** 328–332.

Gaino, E., L. Zunino, B. Burlando, and M. Sara. 1985. The locomotion of dissociated sponge cells: a cell-by-cell, time-lapse film analysis. *Cell Motil.* **5:** 463–474.

Harris, P., and G. Shaw. 1984. Intermediate filaments, microtubules and microfilaments in epidermis of sea urchin tube feet. *Cell Tissue Res.* **236:** 27–33.

Humphreys, T. 1963. Chemical dissolution and *in vitro* reconstruction of sponge cell adhesions. I. Isolation and functional demonstration of the components involved. *Dev. Biol.* **8:** 27–47.

Hyman, L. H. 1940. *The Invertebrates.* Vol. 1, McGraw-Hill, New York.

Ijima, I. 1901. Studies on the Hexactinellida. Contribution I (Euplectellidae). *J. Coll. Sci. imp. Univ Tokyo* **15:** 1–299.

Kachar, B., and T. S. Reese. 1988. The mechanism of cytoplasmic streaming in characean algal cells: sliding of endoplasmic reticulum along actin filaments. *J. Cell Biol.* **106:** 1545–1552.

Koonce, M. P., U. Euteneuer, K. L. McDonald, D. Menzel, and M. Schliwa. 1986. Cytoskeletal architecture and motility in a giant freshwater amoeba. *Cell Motil. Cytoskeleton* **6:** 521–533.

Lawn, I. D., G. O. Mackie, and C. L. Singla. 1981. Conduction system in a sponge. *Science* **211:** 1169–1171.

Leys, S. P. 1995. Sponge cell culture: use of a native tissue extract as a culture substrate. *In Vitro Cell. Dev. Biol. Animal.* (in press).

Leys, S. P., and G. O. Mackie. 1994. Cytoplasmic streaming in the hexactinellid sponge *Rhabdocalyptus dawsoni* (Lambe 1873). Pp. 417–423 in *Sponges in Time and Space. Proc. 4th Int. Porifera Congress.* R. W. M. van Soest, T. M. G. van Kempen, and J. Braekman, eds. A. A. Balkema, Rotterdam.

Mackie, G. O. 1981. Plugged syncytial interconnections in hexactinellid sponges. *J Cell Biol.* **91:** 103a.

Mackie, G. O. 1984. Introduction to the diploplastic level. Pp. 43–46 in *Biology of the Integument,* Vol. 1: Invertebrates, J. Bereiter-Hahn, A. G. Matoltsy, and K. S. Richards, eds. Springer-Verlag, Berlin.

Mackie, G. O., and C. L. Singla. 1983. Studies on hexactinellid sponges. I. Histology of *R. dawsoni* (Lambe 1873). *Phil. Trans. Royal Soc. Lond. B* **301:** 365–400.

Mackie, G. O., I. D. Lawn, and M. Pavans de Ceccatty. 1983. Studies on hexactinellid sponges. II. Excitability, conduction and coordination of responses in *Rhabdocalyptus dawsoni* (Lambe, 1873). *Phil. Trans. R. Soc. Lond B* **301:** 401–418.

McClay, D. R. 1971. An autoradiographic analysis of the species specificity during sponge cell reaggregation. *Biol. Bull.* **141:** 319–330.

Moscona, A. A. 1968. Cell aggregation: properties of specific cell-ligands and their role in the formation of multicellular systems. *Dev. Biol.* **18:** 250–277.

Muller, W. E. G. 1982. Cell membranes in sponges. *Int. Rev. Cytol.* **77:** 129–181.

Noble, P. B., and S. C. Peterson. 1972. A two-dimensional random-walk analysis of aggregating sponge cells prior to cell contact. *Exp. Cell Res.* **75:** 288–290.

Pavans de Ceccatty, M. 1982. *In vitro* aggregation of syncytia and cells of a Hexactinellida sponge. *Dev. Comp. Immunol.* **6:** 15–22.

Reiswig, H. M. 1979. Histology of Hexactinellida (Porifera). *Colloq. Int. Cent Natn. Res. Scient.* **291:** 173–180.

Reiswig, H. M. 1991. New perspectives on the hexactinellid genus *Dactylocalyx* Stutchbury. Pp. 7–20 in *Fossil and Recent Sponges,* J. Reitner and H. Keupp, eds. Springer, Berlin.

Reiswig, H. M., and G. O. Mackie. 1983. Studies on hexactinellid sponges. III. The taxonomic status of Hexactinellida within the Porifera. *Phil. Trans. R. Soc. Lond. B* **301:** 419–428.

Schultz, F. E. 1887. Report on the hexactinellida collected by H.M.S. *Challenger* during the years 1873–1876. *Rep. Sci. Res. Challenger Zool.* **21:** 1–513.

Travis, J. L., and R. D. Allen. 1981. Studies on the motility of the foraminifera. I Ultrastructure of the reticulopodial network of *Allogromia laticollaris* (Arnold). *J. Cell Biol.* **90:** 211–221.

Wachtmann, D., and W. Stockem. 1992. Microtubule- and microfilament-based dynamic activities of the endoplasmic reticulum and the cell surface in epithelial cells of *Spongilla lacustris* (Porifera, Spongillidae). *Zoomorphology* **112:** 117–124.

Weiss, P., and H. B. Hiscoe. 1948. Experiments on the mechanism of nerve growth. *J Exp. Zool.* **107:** 315–396.

Wilson, H. V. 1907. On some phenomena of coalescence and regeneration in sponges. *J Exp. Zool.* **5:** 245–258.

Reference: *Biol. Bull.* **188:** 255–266. (June, 1995)

Bivalve Mollusc Hemocyte Behaviors: Characterization of Hemocyte Aggregation and Adhesion and Their Inhibition in the California Mussel (*Mytilus californianus*)

JIUN-HONG CHEN* AND CHRISTOPHER J. BAYNE

Department of Zoology, Oregon State University, Oregon 97331-2914

Abstract. Within minutes of removal from the California mussel, *Mytilus californianus*, hemocytes become sticky for one another and for foreign surfaces. We sought to understand the cell surface changes responsible for this altered state. Hemocyte aggregation and adhesion assays were used in experiments in which a variety of reagents potentially capable of interfering with aggregation were screened. Caffeine, nor-ethylmaleimide, cytochalasin B, and EDTA were completely or partially inhibitory towards aggregation and adhesion. However, RGD-containing peptides, glycosaminoglycans, protease inhibitors, heparin, or poly-L-lysine were without effect. Low temperature (4°C) slowed hemocyte adhesion and hemocyte cohesion. Based on the findings, it appears that (1) *Mytilus* hemocyte aggregation, *in vitro*, is a two-step process that requires metabolic energy and divalent cations (calcium and magnesium), and is temperature-sensitive; and (2) *Mytilus* hemocyte adhesion and hemocyte aggregation are two associated but different cell behaviors.

Introduction

Cell aggregation (cell clumping) in bivalves was first reported by Geddes (1880, cited by Narain, 1973). In molluscs, it has been presumed that clump formation is involved in hemostasis and wound healing (Bang, 1961; Sparks, 1972; Sminia, 1981). However, hemocyte aggregation in bivalves differs from blood clotting in vertebrates in that no extracellular fibers are formed. The aggregation of hemocytes in bivalves is reversible, and most aggregated cells later disperse, re-entering the circulatory system as wound repair progresses (Feng and Feng, 1974). Mussel hemocytes will spontaneously aggregate *in vitro*. When hemolymph is removed from a mussel, the free hemocytes form aggregates during the bleeding or immediately thereafter. When the aggregates and the free cells settle down on a foreign surface, they adhere (cell-substratum adhesion) and usually spread, and later migrate away. Although the phenomena of clump formation and hemocyte adhesion and spreading have been described both *in vivo* and *in vitro* in bivalves (Drew, 1910, cited by Narain, 1973; Dundee, 1953; Bang, 1961; Sparks, 1972; Cheng, 1981), few attempts have been made to unravel the operative mechanisms (Seifert, 1983). To study this rapid, spontaneous cell adhesion, it was first necessary to find effective inhibitors that could reversibly block the reaction. In this study, we used hemocytes of the California mussel, *Mytilus californianus*, to (1) identify inhibitors of hemocyte aggregation or adhesion *in vitro*, and then (2) investigate differences between hemocyte clump formation (cell-cell interaction) and hemocyte adhesion (cell-substratum interaction) *in vitro*.

Materials and Methods

Chemicals

The following chemicals, tested at the indicated concentrations for their abilities to inhibit aggregation and adhesion of mussel hemocytes, were obtained from Sigma

---

Received 26 August 1993; accepted 9 February 1995.

* Present address: Department of Zoology, National Taiwan University, Taipei, Taiwan, R.O.C.

Abbreviations: NEM = *N*-ethyl maleimide; EDTA = ethylenediaminetetraacetic acid; RGD = arginine-glycine-aspartic acid; GAG = glycosaminoglycan; CMTBS = calcium- and magnesium-containing Tris-buffered saline; CMFTBS = calcium- and magnesium-free Tris-buffered saline; DMSO = dimethyl sulfoxide.

Co. *Protease inhibitors:* phenylmethylsulfonylfluoride (PMSF, 20 μg/ml), soybean trypsin inhibitor (20 μg/ml), aprotinin (10 μg/ml), leupeptin (10 μg/ml), bovine α_2-macroglobulin (1 mg/ml); *glycosaminoglycans* (each at 1 mg/ml): hyaluronic acid, chondroitin sulfate (types A and C). *Others:* heparin (10 units/ml), protamine (1 mg/ml), poly-L-lysine (1 mg/ml), poly-L-glutamic acid (1 mg/ml). Ethylenediaminetetraacetic acid (EDTA), caffeine, cytochalasin B and nor-ethyl-maleimide (NEM) were tested at several concentrations stated in the results. Most of the suspected inhibitors were dissolved in CMTBS (Ca^{++}, Mg^{++} Tris-buffered saline: 10 m*M* $CaCl_2$, 60 m*M* $MgCl_2$, 50 m*M* Tris HCl, NaCl to 960 mOsm), but PMSF, pepstatin, aprotinin, leupeptin, and cytochalasin B were first dissolved in DMSO, then mixed with CMTBS. The final concentration of DMSO in the medium was <0.5%. Peptides containing the Arg-Gly-Asp (RGD) amino acid sequence were kindly provided by Dr. D. W. Barnes, Biochemistry, Oregon State University. BCA protein assay reagents were purchased from Pierce. All other chemicals were purchased from Sigma Co. The suspected inhibitors were dissolved in CMTBS (Ca^{++}, Mg^{++} Tris-buffered saline: 10 m*M* $CaCl_2$, 60 m*M* $MgCl_2$, 50 m*M* Tris HCl, NaCl to 960 mOsm). The EDTA was dissolved in calcium- and magnesium-free Tris-buffered saline (CMFTBS). Hydrophobic chemicals were first dissolved in DMSO, and then mixed with CMTBS. The final concentration of DMSO in treated hemolymph was lower than 0.5%. The pH value of solutions was adjusted to 7.4 with NaOH, and osmolarities were checked by freezing-point osmometer before they were mixed with hemolymph.

Animals

Individual *Mytilus californianus* larger than 8 cm in length were collected monthly from the rocky intertidal zone at Seal Rock State Park (15 miles south of Newport, Oregon). On the same day, these mussels were transferred to a filtered, recirculating, continuously aerated seawater system that was maintained at pH 7.6, nitrate < 10 ppm, nitrite < 0.2 ppm, 15°C, and close to normal salinity. Mussels were held in this system for at least three days before being used as a source of hemolymph.

Hemolymph collection

A plastic rod (3 mm diameter) was inserted between the two shells to prevent them closing, and seawater was drained from the mantle cavity. Animals were then transferred to a cold room (4°C). Hemolymph was collected from the posterior adductor muscle using a cooled sterile syringe with 18G 1½″ needle. With the needle removed, the colorless (slightly opalescent) hemolymph was immediately transferred to cooled sterile tissue culture tubes (Falcon) for further treatment. Hemolymph was collected from each animal only once.

Coating of surfaces for cell adhesion assay

Except for agarose, the coating process was as follows: the solution of coating material (see Table I) was loaded on the clean surface for 30 min at room temperature. Then the excess was washed and replaced by CMTBS. For agarose coating, melted agarose was added to washed eight-well slides (5 μl/well; Cel-Line, New Jersey), and then mounted by a cover slip which was held off the slide by two small pieces of coverslip. The coverslips were removed after keeping the slide at 4°C for a few minutes. The thin layer of agarose allowed satisfactory microscopic observation.

Inhibitor screening assay

The solutions of suspected inhibitors (see Results) were aliquoted into siliconized microtubes (PGC Scientifics, Maryland), and kept at 4°C. Slides with eight wells, cleaned by immersion in acid alcohol overnight, were dried and placed in a humidity chamber that was also kept at 4°C before use. As soon as the hemolymph had been transferred to a cooled sterile tissue culture tube, it was aliquoted and mixed (1:1) with test solutions by vortexing for about 3 s. The treated hemolymph was then loaded onto the undersurface of an inverted, cooled eight-well slide (50 μl/well). Each sample was loaded in duplicate onto the same position on a different slide. These were maintained as hanging-drops during gyration at 100 rpm performed by Gyrotory® Shaker-Model G2 (New Brunswick Scientific Co., Inc., New Jersey) at room temperature (22 ± 1°C). The purpose of using hanging-drops was to avoid cell adhesion to glass during gyration. Following 15 min gyration, the slide was carefully turned over. Two 1-mm-thick spacers were placed on the slide, followed by a coverslip (24 × 50 mm). Cell aggregation, cell adhesion, and cell spreading were observed under phase contrast microscopy.

Those inhibitors that interfered with cell aggregation or cell adhesion were selected for further studies. Due to occasional individual differences between mussels, each reagent was tested on at least three hemolymph samples taken from separate mussels at different times.

Assay for inhibition of cell aggregation

This assay followed the same protocol used in the screening test. After the slide was turned so the hemolymph was on the upper side, 100% formalin was added (1 μl/well) to fix the cells. The final concentration of formalin in hemolymph was 2%. Cells at the center of each preparation were then immediately dispersed *in situ* by gentle pipetting five times. Samples were then mounted by a coverslip (24 × 50 mm) held on two 1-mm-thick spacers. The extent of cell aggregation was assessed by counting the total free cell numbers in five different areas in each well. To obtain values for "no aggregation," we proceeded as follows: fresh hemolymph was mixed with 20% formalin (1:1) to immediately block cell aggregation. The total (control) free cell number was counted in hemolymph fixed this way in 10% formalin as soon as it was taken from the mussel.

$$\text{The percentage of cells remaining free} = \frac{\text{Total free cell numbers in test treatment}}{\text{Total free cell numbers in fixed fresh hemolymph}} \times 100$$

Assay for inhibition of cell adhesion

After hemolymph had been mixed with test solutions, it was then loaded (50 μl/well) into wells of a pre-cooled (4°C), flat-bottom 96-well tissue culture plate (Corning, New York). Each treatment was loaded in triplicate. After 15 min at room temperature for cell adhesion to occur, the plasma and unattached cells were removed and each well was washed three times with CMTBS (100 μl/well). As a measure of the number of remaining (adherent) cells, protein concentrations were measured by means of the BCA protein assay (Pierce). The adherent cells were first lysed in 20 μl cell lysis solution (2% Na_2CO_3, 0.1 *M* NaOH) for at least 30 min at RT with occasional shaking by vortex, and then the fresh Pierce BCA protein assay reagent was added (100 μl/well). After 30 min incubation at 60°C, the plate was cooled to RT, and the absorbance of each well was read at 550 nm using a microtiter plate reader (Titertek Multiskan MCC/340).

The percentage of cell adhesion was calculated using the following equation:

$$[(A_i - A_b)/(A_c - A_b)] \times 100$$

A_i: Absorbance of inhibitor-treated well
A_b: Absorbance of background well (lysis solution and BCA reagent only)
A_c: Absorbance of CMTBS-treated well

According to this equation, the absorbance in background wells indicates 0% adhesion, and the absorbance in CMTBS-treated wells indicates 100% adhesion.

To correlate cell number with protein values, serial two-fold dilutions of hemolymph in CMTBS (50 μl each) were loaded in quintuplicate into wells of 96-well plates. After 15 min for adherence, all wells were washed three times with CMTBS. Then three were used for protein determinations as described above, and Hoechst 33342 (50 μl, 20 μg/mL CMTBS) was added to the other two. Using an inverted fluorescence microscope, nuclei were counted in the Hoechst-stained wells corresponding to those for which protein values were also obtained.

Data analysis

Each experiment was repeated at least three times, using fresh hemolymph samples from different animals. Data are presented as mean ± S.D. Statistical analysis of data was performed using paired or unpaired Student's *t*-test as appropriate. Differences were considered significant when $P < 0.05$.

Cell viability

Following the adhesion/spreading and aggregation assays, hemocyte viability was determined by visual observation of hemocyte spreading, and by cell exclusion of propidium iodide. This test was performed only on the samples in which cell aggregation or adhesion was interrupted. Treated hemolymph (40 μl) was gently removed from well slides or culture plates, and replaced by 40 μl CMTBS. If the remaining cells had not aggregated or spread in 10 min, two possibilities were considered; either the treated cells had been killed by the chemical or the inhibitory effect of the chemical was irreversible. To determine whether the treated cells were alive or not, the propidium iodide staining protocol was followed: 1 μl propidium iodide solution (500 μg/ml in CMTBS) was added to each sample (50 μl). In cells which are dead, the dye enters and binds to nuclear DNA with high affinity. Stained nuclei generate bright red fluorescence under epifluorescence using a Zeiss microscope with appropriate filter set.

Results

Normal hemocyte aggregation, adhesion, and spreading in vitro

Mytilus hemolymph contains three types of hemocyte (Moore and Lowe, 1977). Preliminary studies showed that hemocytes of distinct densities, separated on 60% Percoll, were all competent in adhesion and aggregation assays. All the following experiments were conducted with freshly taken, unseparated hemocyte populations.

When hemocytes were first removed from the mussels, they remained dispersed and were round (Fig. 1a). However, they changed from round to elongated in one minute or less (Fig. 1b). Sometimes aggregation occurred extremely rapidly during the bleeding, or while the hemolymph was being dispensed into the test tube. After initial cellular contact, cells were seen to pull together before the cells or aggregates began to spread. Aggregates formed this way without shaking were small (Fig. 1c), and the cell-cell binding strength was weak. The individual cells

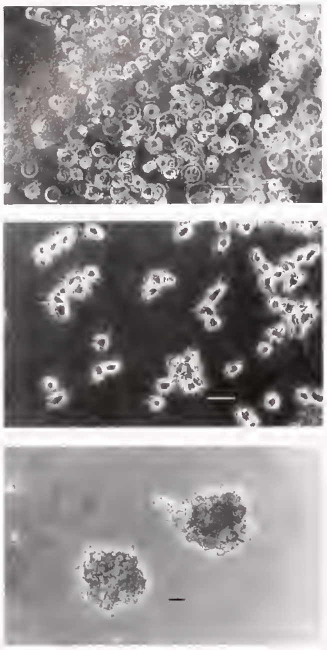

Figure 1. The sequential processes of *Mytilus californianus* hemocyte aggregation *in vitro* (a) The naive free cell stage: these fresh hemocytes are approximately spherical in outline. (b) The initial stage of cell aggregation and adhesion: Within one minute, all of the cells form spikes, and some cells form small aggregates (cell number < 10). (c) Medium sized clumps: when these small aggregates collide, they can form bigger clumps. Each medium sized clump may be composed of about one hundred cells. Bars = 30 μm.

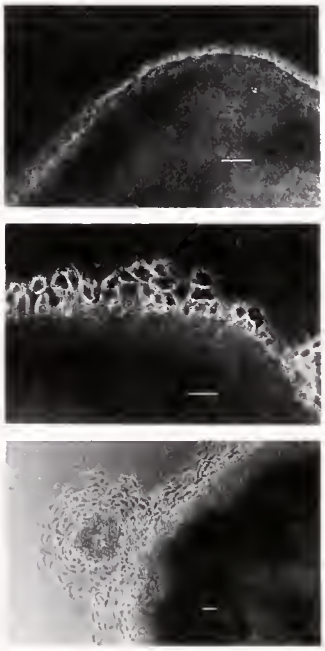

Figure 2. *Mytilus californianus* hemocyte spreading and migration *in vitro*. (a) Part of a large clump: each large aggregate like this may contain more than ten thousand cells. These cohere tightly together, and the individual cells are difficult to distinguish. Bar = 30 μm. (b) Early stage of hemocyte migration: cells at the edge begin to move out of the aggregate about 3 minutes after the aggregate settles down. Bar = 30 μm. (c) Late stage of hemocyte migration: cells have radially migrated from the aggregate after 10 min *in vitro* Bar = 50 μm.

were distinguishable and could be easily dispersed from the aggregates by pipetting.

In contrast, clumps that formed during 10 or more minutes of shaking often contained more than ten thousand cells (Fig. 2a). This kind of clump was resistant to mechanical dispersion by pipetting or vortexing. When cells or aggregates were allowed to settle down onto glass or plastic, they attached, flattened, and developed pseudopodia. During subsequent incubation, cells located at the surface of the clump and in contact with the substratum adhered to the substratum and migrated radially out of the clump (Fig. 2b, c). The attached and spread cells moved by amoeboid locomotion. The cells possess a strong ability to adhere, spread, and migrate on foreign surfaces. Only on agarose substrata were such kinds of cell behaviors inhibited (Table I).

Assay of cell adhesion

The numbers of cells in individual wells and protein quantified in these wells were dependably correlated. When 50 μl of hemolymph (serially diluted twofold in CMTBS to $^1/_{16}$) was held in wells of flat-bottomed 96-well plates for 15 min at 22 ± 1°C, nuclear counts and protein values indicated 1215 cells yielding 69.5 pg protein in $^1/_{16}$ strength hemolymph, 1597 cells yielding 134 pg protein in $^1/_8$ strength hemolymph, and 6636 cells yielding 478.5 pg protein in $^1/_4$ strength hemolymph. These values, from one experiment representative of two runs, indicate a protein value of approximately 71 pg protein per 1000 cells.

Table I

Mytilus californianus *hemocyte behavior on various surfaces*

Surface	Adhesion	Spreading	Migration
Glass (well slide)	+++	+++	+++
Polystyrene (PS) (culture plate)	+++	+++	+++
Sigmacoted® glass	+++	+++	+++
Siliconized PS	+++	+++	+++
Poly-L-lysine (1 mg/ml) coated glass	+++	+++	+++
Poly-glutamate (1 mg/ml) coated glass	+++	+++	+++
BSA (1%) coated glass	+++	+++	+++
Fibronectin (1%) coated glass	+++	+++	+++
1% agarose coated glass	−	−	−

BSA: Bovine serum albumin.

+++: strong; ++: medium; +: weak; −: inhibition.

Fresh hemolymph was loaded onto different surfaces. After 15 min incubation at room temperature, the non-adherent cells were removed, and then cell adhesion, spreading, and migration were observed under a phase contrast microscope.

Table II

Chemicals tested for inhibition of aggregation and adhesion of Mytilus californianus *hemocytes*

	Chemicals (final concentration)
Protease inhibitors*	phenylmethylsulfonylfluoride (PMSF) (20 μg/ml), soybean trypsin inhibitor (20 μg/ml), pepstatin A (10 μg/ml), aprotinin (10 μg/ml), leupeptin (10 μg/ml), α_2-macroglobulin (1 mg/ml).
RGD peptides	RGDS, GRGDSP, GDSP, TGRG (2.5 mg/ml).
Glucosamino-glycans (1 mg/ml)	hyaluronic acid, chondroitin sulfate (type A, type C).
Others	heparin (10 unit/ml), protamine (1 mg/ml), poly-L-lysine (1 mg/ml), poly-L-glutamic acid (1 mg/ml).

* PMSF, pepstatin A, aprotinin, and leupeptin were dissolved in DMSO. The final concentration of DMSO was less than 0.5%.

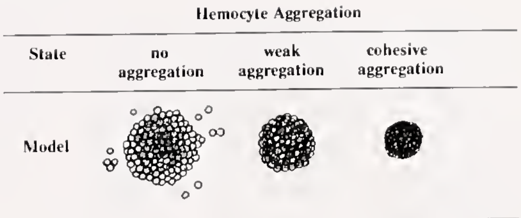

Figure 3. The appearances of *Mytilus californianus* hemocytes at three states of aggregation *in vitro.* The aggregation of California mussel hemocytes *in vitro* can be categorized into three levels, namely no aggregation, weak aggregation, and cohesive aggregation. No aggregation: cells accumulate at the central area of the well as a result of the gyratory force. A few small aggregates are sometimes seen, while in most cases the centralized cells just pile up, and no binding occurs between them. Such cells can be freely dispersed by gentle pipetting. Weak aggregation: individual cells are distinguishable, especially those located at the edge of the aggregate. Large clumps like this can be separated by pipetting to yield several small aggregates. Possibly due to the presence of mucous material (which is induced by certain inhibitors such as EDTA, $NaIO_4$), hemocyte contacts are sometimes restricted, and the morphology of weak aggregation varies. Cohesive aggregation: the compact nature of such aggregates prevents dispersion by pipetting or vortexing. The aggregated cells cannot be seen individually.

Influences of suspected inhibitors on hemocyte aggregation, adhesion, and spreading

From data obtained in screening assays, the tested reagents could be allocated into four categories. The first includes caffeine (25 m*M*) and *N*-ethyl maleimide (0.1 m*M*), which strongly inhibited both hemocyte aggregation and adhesion. The second category of chemicals poorly blocked hemocyte aggregation but significantly inhibited hemocyte adhesion. They include EDTA (60 m*M*), and poly-L-glutamic acid (MW 50,000–100,000; 1 mg/ml). Cytochalasin B (5 μg/ml) is the only chemical in the third category: it effectively inhibited hemocyte aggregation, but poorly blocked hemocyte adhesion. The fourth group of chemicals had no detectable inhibitory effect on either hemocyte aggregation or adhesion. They included RGD- (Arg-Gly-Asp-) containing peptides, glycosaminoglycans (GAGs), poly-L-lysine, heparin, protamine, protease inhibitors, and colchicine (Table II). Because inhibited hemocytes recovered their aggregation and adhesion competence after caffeine, EDTA, poly-L-glutamic acid, or cytochalasin B was replaced by CMTBS, the inhibitory effects of such chemicals, unlike NEM, were reversible (data not shown). The extent of hemocyte aggregation can be easily distinguished at three different states, namely no aggregation, weak aggregation, and cohesive aggregation (Fig. 3). Five different stages of hemocyte adhesion/spreading were scored (Fig. 4).

Hemocytes aggregated and adhered in 10 m*M* sodium azide (NaN_3). However, when the cells were co-incubated in 10 m*M* NaN_3 with 25 m*M* caffeine for 30 min, cell aggregation and adhesion were still affected after the caffeine/azide was replaced by azide solution. Such azide-poisoned cells aggregated weakly after the NaN_3 + caffeine solution was replaced by NaN_3. When the NaN_3 + caffeine was replaced by CMTBS, the cells recovered eventually and formed cohesive aggregates.

Low temperature (4°C) delayed cell adhesion for the first few minutes, but after 15 min no differences from controls could be seen (Fig. 5). In cell aggregation assays, cells still aggregated weakly at 4°C. With an increase in temperature, the aggregates contracted and cohered to form tight masses as if no interruption had occurred (Fig. 6).

Osmolarity seems not to be critical for *M. californianus* hemocyte aggregation and adhesion *in vitro.* There were

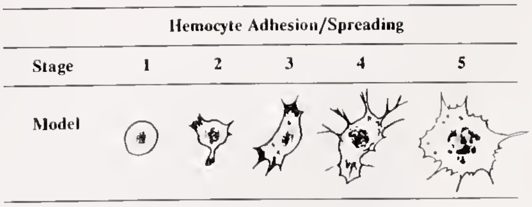

Figure 4. Illustration of the stages of *Mytilus californianus* hemocyte adhesion, and spreading *in vitro* Hemocyte adhesion and spreading are continuous processes which can be divided into five stages from 1° to 5°. Normally, hemocytes *in vitro* can adhere and spread well (4°) in 5–10 minutes. 1° illustrates naive hemocytes in suspension; these resemble cells in which adhesion and spreading are inhibited. 2°: cell adhesion and spreading are blocked, but spike formation is not. 3°: cells adhere and flatten, but without extension of pseudopodia. 4°: cells extend small pseudopodia as the cells spread (5).

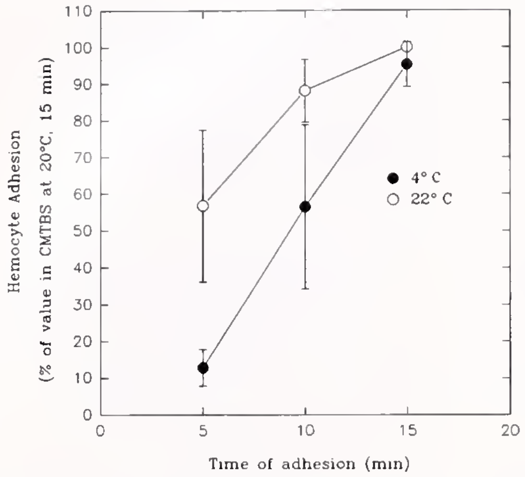

Figure 5. The influence of temperature on the adhesion of *Mytilus californianus* hemocytes *in vitro*. Hemolymph was loaded into 96-well culture plates (50 μl/well). These were then incubated at 4°C or 22 ± 1°C. At 5, 10, and 15 min, the non-adherent cells and plasma were removed. The wells were washed three times with CMTBS, and then the adherent cells were lysed for BCA protein assay. The protein values obtained for wells in which hemolymph was held at 22 ± 1°C for 15 min were used as 100% hemocyte adhesion. There is a significant difference ($P < 0.05$) at 5 min incubation at 4°C, and at 22°C.

no significant differences in hemocyte adhesion and aggregation when hemolymph was mixed (1:1) with CMTBS in the range of 800–1100 mOsm.

The inhibitory effects of caffeine, NEM, EDTA, and cytochalasin B on cell aggregation

Hemocytes exposed to 25 m*M* caffeine, 5 μg/ml cytochalasin B, or 0.1 m*M* NEM were strongly inhibited from aggregating (95%, 71%, and 72%, respectively, remained free). When hemocytes were treated with EDTA, the morphology of aggregates varied. Under the microscope, some colorless material was seen among the aggregates. Its presence seemed to restrict hemocyte contact. Though caffeine inhibition at 25 m*M* or 50 m*M* was reversible and rapid, it did not kill the cells. At a caffeine concentration of 15 m*M*, cells formed weak aggregates. The difference between the percent free cells in 25 m*M* and 15 m*M* caffeine (means of 61.5% and 7.1%) was statistically significant ($P < 0.05$) (Fig. 7a). Cytochalasin B (5 μg/ml) in 0.5% DMSO resulted in 70% of the hemocytes remaining free. DMSO (0.5%) did not influence hemocyte aggregation and adhesion (Fig. 7b). At 0.1 m*M*, NEM significantly inhibited hemocyte aggregation ($P < 0.05$) (Fig. 7c). EDTA at concentrations 15–60 m*M* significantly inhibited hemocyte aggregation (Fig. 7d). However, most cells were observed forming weak aggregates; in three experiments, values for percent free cells were 9.5, 18.2, and 21.8 at 60 m*M*; 8.0, 19.7, and 23.1 at 30 m*M*; and 8.4, 20.4, and 13.4 at 15 m*M*.

The inhibitory effects of caffeine, NEM, EDTA, and cytochalasin B on hemocyte adhesion and spreading

When hemolymph was treated with 5 μg/ml cytochalasin B or 0.1 m*M* NEM, the hemocytes remained round, thus resembling naive cells. Cytochalasin B (1 μg/ml) could retard hemocyte spreading, affect the morphology of spread hemocytes, and inhibit hemocyte migration. Cells exposed to 25 m*M* caffeine were irregular in outline (Fig. 8a). EDTA in the range 0.6–60 m*M* inhibited cell adhesion (Fig. 8b).

The concentration of caffeine necessary to inhibit cell adhesion was similar to that needed to inhibit aggregation. At 15 m*M* caffeine, cell adhesion was significantly greater relative to that in 25 m*M* caffeine (Fig. 9a). Cytochalasin B significantly inhibited cell adhesion at concentrations between 1 and 5 μg/ml ($P < 0.05$), though 60% of the

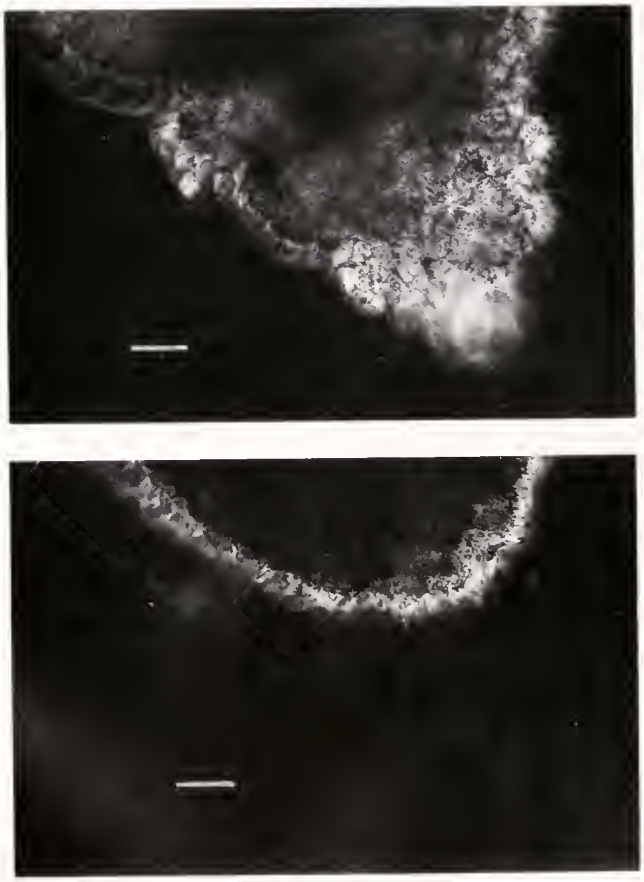

Figure 6. The effect of temperature on *Mytilus californianus* hemocyte aggregation *in vitro*. Weak aggregates like this one formed during 15 min gyration at 4°C. This photo (a) was taken immediately after the aggregate was removed from 4°C. Cohesive aggregates (b) formed after the incubation temperature was warmed up to 22 ± 1°C. The whole cell mass gradually shrunk when the incubation temperature increased. This contraction led to the formation of a tighter clump. Photograph (a) and (b) were taken from the same microscopic field at 1 and 15 min, respectively. Bars = 30 μm.

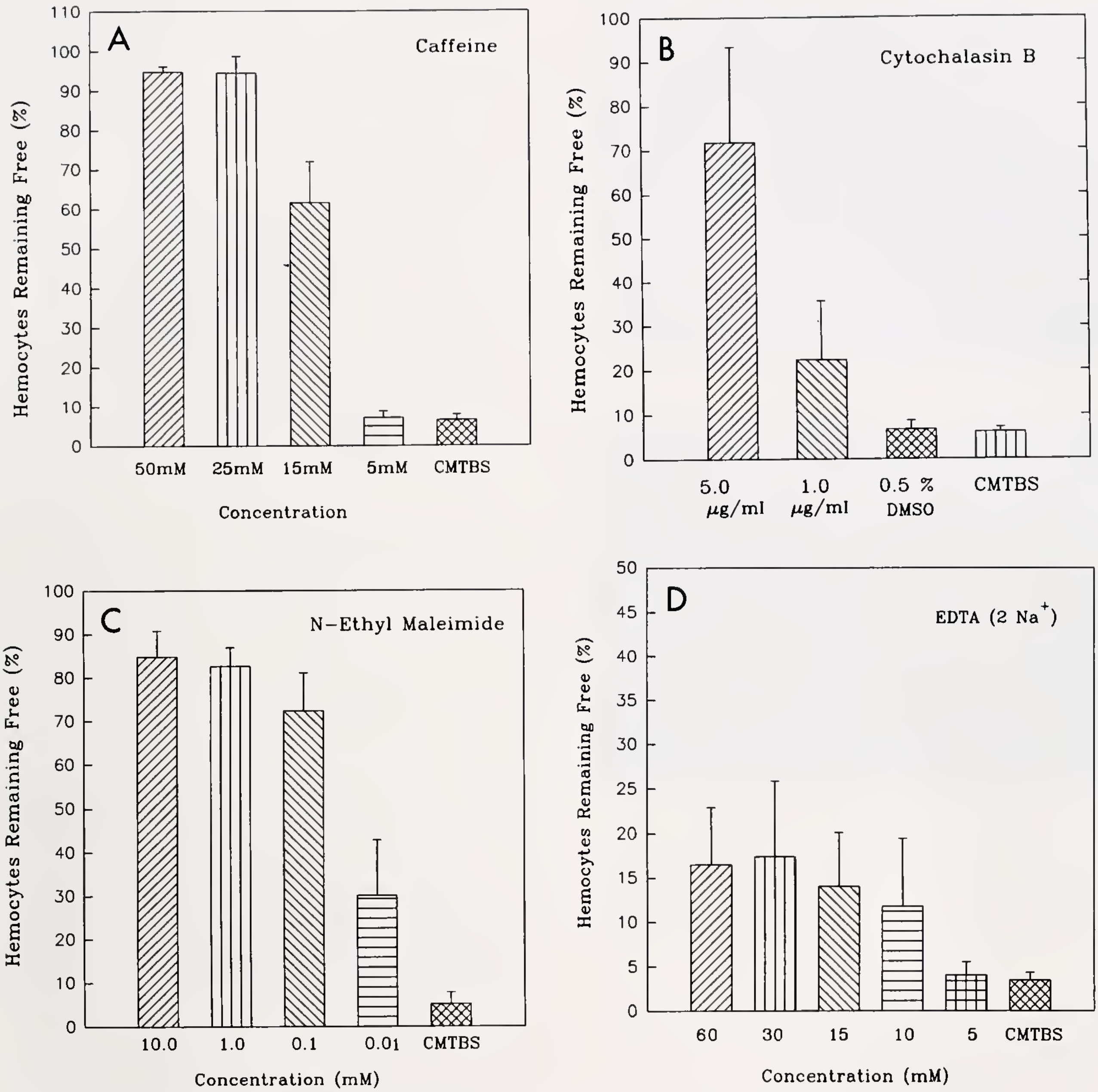

Figure 7. The influences of caffeine, cytochalasin B, NEM, and EDTA on *Mytilus californianus* hemocyte aggregation *in vitro*. Data are pooled from three separate experiments. In these figures, each value (%) is the mean number of free cells in inhibitor solution as a percent of free cells in 10% formalin. The counts in 10% formalin differed between individual bleeds; for the three caffein bleeds, for example, these were 1,480, 1,610 and 1,779. The highest count was 3,602 (2nd experiment with cyt B) and the lowest was 1,028 (3rd experiment with NEM). (a) At 25 m*M* or 50 m*M*, caffeine completely blocked hemocyte aggregation, thus most cells remained free. At 15 m*M*, caffeine still significantly inhibited hemocyte aggregation ($P < 0.05$). Like saline (CMTBS), 5 m*M* caffeine had no inhibitory effect. (b) Cytochalasin B (5 μg/ml in 0.5% DMSO) significantly inhibited hemocyte aggregation ($P < 0.05\%$). The vehicle, DMSO, did not have any inhibitory effect. (c) Hemocyte aggregation was strongly inhibited by 0.1 m*M* or higher concentrations of NEM ($P < 0.05$). (d) EDTA within the range of concentrations from 15 m*M* to 60 m*M* has significant influence on hemocyte aggregation ($P < 0.05$).

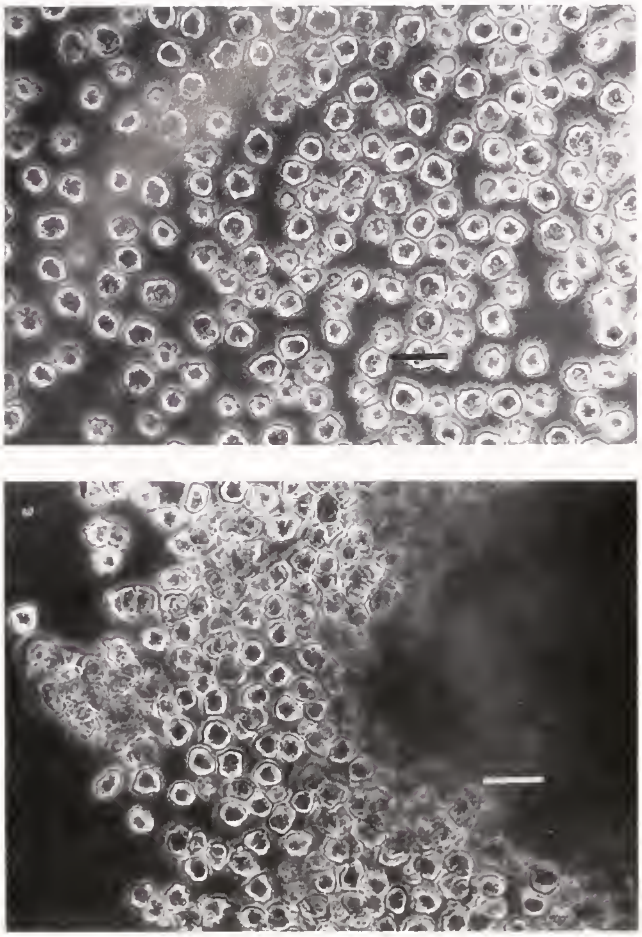

Figure 8. The morphology of inhibitor-treated *Mytilus californianus* hemocytes *in vitro*. (a) The irregular shape is the main characteristic of hemocytes which were treated with caffeine (25 m*M*). Such cells gradually become spherical over 30 min. (b) Part of a cell clump in 60 m*M* EDTA (pH 7.4). These cells could not further spread when the EDTA concentration was above 0.6 m*M* Bars = 30 μm.

cells were still adherent in 5 μg/ml cytochalasin B treatment (Fig. 9b). The inhibitory activity of NEM (0.01 mM to 10 mM) was significant (Fig. 9c). Concentrations in this range inhibited 90% of cell adhesion on culture plates (polystyrene). EDTA ($\geq$0.6 m*M*) influenced cell adhesion on culture plates also (Fig. 9d). When EDTA-treated hemolymph was replaced by 20 m*M* or a higher concentration of buffered isotonic Ca^{++} or Mg^{++} solution, 80% of hemocytes recovered their adhesion competence (Fig. 10). Therefore, *Mytilus* hemocyte adhesion is Ca^{++} or Mg^{++}-dependent.

Discussion

A variety of buffers have been used in mussel hemocyte studies (Moore and Lowe, 1977; Renwrantz *et al.*, 1985; Dageförde *et al.*, 1986). Although the buffer osmolarity can affect phagocytic activity in *M. edulis* (Renwrantz, pers. comm., 1989), pH in the range of 7.4 to 8.4 or osmolarity in the range of 800 to 1050 mOsm did not interfere with hemocyte aggregation in studies reported here (data not shown). To resemble the seawater in which the mussels were held, a pH of 7.4 and salt content of 960 mOsm were selected for the CMTBS.

The fact that naive hemocytes circulating *in vivo* remain free in suspension is taken to imply an absence of mutual adhesiveness. This could be due to the effects of surface charge. Most cells are negatively charged on their surfaces (often by sialic acids), and the resulting repulsive forces between blood cells have been postulated to separate cells in their naive state (Bell, 1983). Cell activation may reduce the negative surface charge by loss of sialic acids (Rutishauser *et al.*, 1988). To evaluate possible charge effects on cell aggregation and adhesion, heparin and protamine were added to cell suspensions. These reagents failed to influence cell behaviors (data not shown). Heparin is widely used to inhibit platelet clotting, however, it did not affect hemocyte aggregation in this study, in accordance with results in insects (Ratner and Vinson, 1983) and *Limulus* (Bryan *et al.*, 1964). In this study, hemocytes adhered to glass coated with a variety of compounds, and only 1% agarose was inhibitory. Agarose has been used to inhibit cell adhesion of various cell types; the inhibitory mechanism is unknown.

In both platelet clotting (Guyton, 1986) and the prophenoxidase (proPO) system of arthropods (Lackie, 1988; Johansson and Söderhäll, 1989), serine-protease cascade reactions have been implicated. These reactions are controlled by various protease inhibitors (Hergenhahn *et al.*, 1987). Protease inhibitors can affect hemocyte phagocytosis also (Fryer *et al.*, 1991). However, protease inhibitors tested here failed to block mussel hemocyte aggregation or adhesion, leading us to conclude that these behaviors are probably not dependent on proteases in the hemolymph.

Both GAGs and RGD-containing peptides are involved in cell-substratum and cell-cell interactions (Underhill, 1982; Roseman, 1985). Furthermore, a sponge aggregation factor has been revealed that is a sulfated polysaccharide (Coombe and Parish, 1988). In our hemocyte aggregation and adhesion tests, none of the GAGs or RGD peptides had significantly inhibitory effects, though they did retard hemocyte spreading.

N-Ethyl-maleimide has been reported to irreversibly inhibit the aggregation of horseshoe crab hemocytes (Bryan *et al.*, 1964). Similarly, NEM interfered with *Mytilus* hemocyte aggregation and adhesion. Thus, it can be inferred that, in both these species, normal hemocyte behaviors require intact disulfide bond structures in cell proteins.

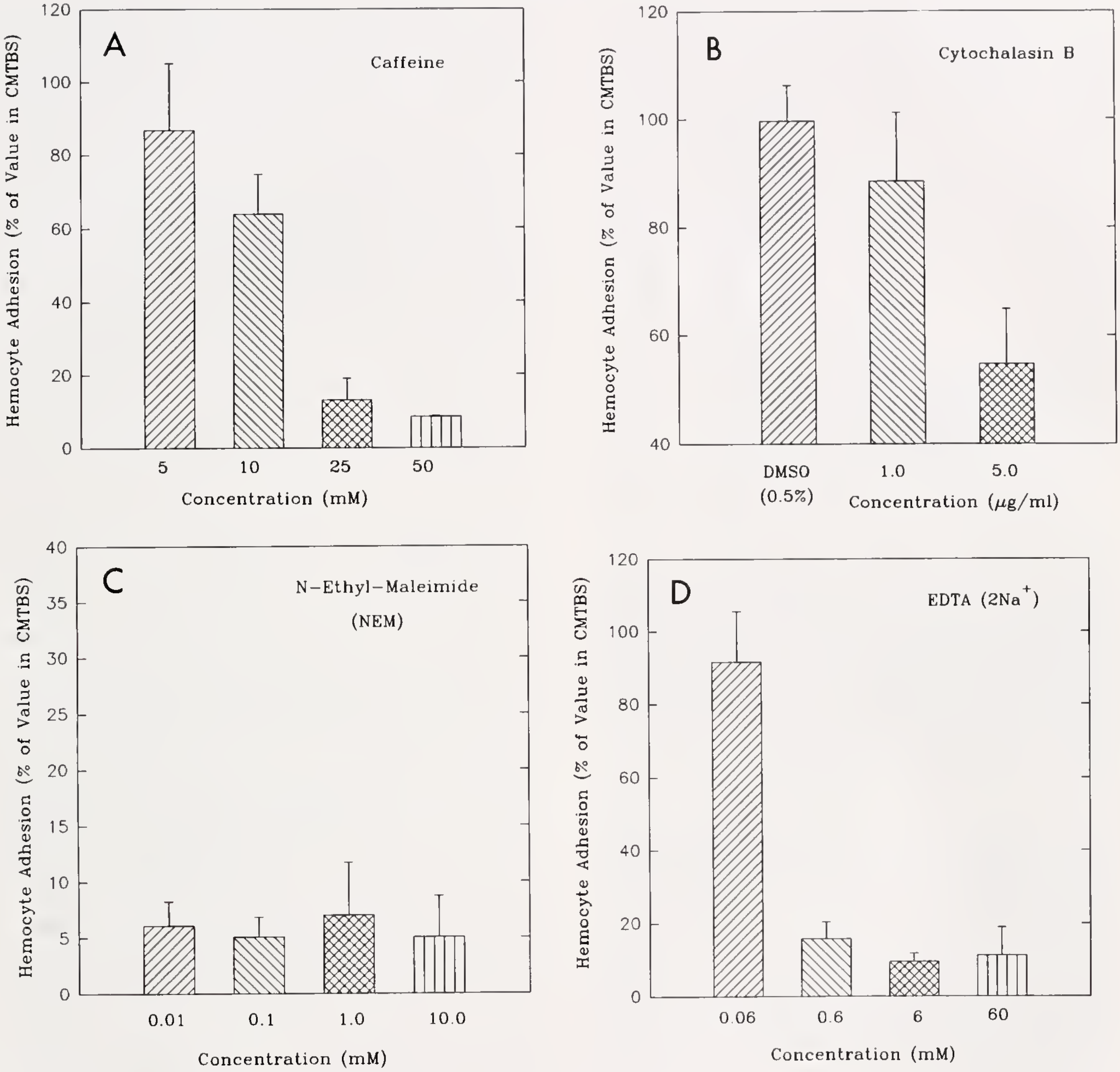

Figure 9. The influences of caffeine, cytochalasin B, NEM, and EDTA on *M californianus* hemocyte adhesion *in vitro*. In these figures, each bar represents (%) the ratio of the protein value of adherent cells in inhibitor solution to the equivalent value in CMTBS. That is, CMTBS-mixed hemocyte adherence is taken as 100% adhesion competence. (a) At 25 m*M* or higher, caffeine significantly blocked hemocyte adhesion ($P < 0.05$). At 10 m*M*, caffeine was still partially inhibitory. (b) Cytochalasin B (5 μg/ml in 0.5% DMSO) significantly inhibited hemocyte adhesion ($P < 0.05$), but about 55% of hemocytes remained adherent. The vehicle, DMSO, did not have any inhibitory effect. (c) NEM strongly inhibited hemocyte adhesion. Less than 10% hemocyte adherence could be detected in 0.01 m*M* or higher concentrations of NEM ($P < 0.05$). (d) At 0.6 m*M*, EDTA significantly inhibited hemocyte adhesion ($P < 0.05$), but this agent was without effect at 0.06 m*M*

Inhibition of cytoskeleton assembly has been reported to disrupt insect plasmatocyte encapsulation (Davies and Preston, 1987), and mollusc hemocyte chemotaxis and cell migration (Cheng and Howland, 1982), as well as cell surface receptor redistribution (Cheng and Howland, 1982; Dageförde *et al.*, 1986). Because bivalve hemocytes alter their shapes in both cell aggregation and cell adhesion (Jones and Gillett, 1976; Feng, 1988), it is inferred that

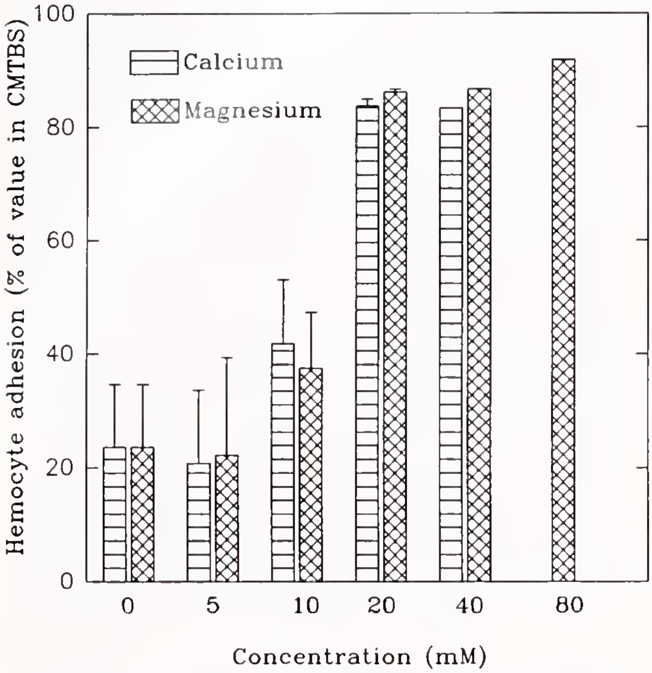

Figure 10. The effects of calcium and magnesium on *Mytilus californianus* hemocyte adhesion. After three washes in 30 m*M* EDTA, hemocytes were suspended in buffered isotonic calcium or magnesium solutions. The cells were loaded into culture plates, then cell adhesion was assayed after 15 min incubation at 22 ± 1°C. Cells without EDTA treatment were taken as 100% adherent. More than 80% of EDTA-treated hemocytes recovered their adhesion competence at 20 m*M* or higher concentrations of calcium or magnesium in isotonic buffer.

the cytoskeleton plays an important role in these two processes. Cytochalasin B and colchicine have been widely used to reduce the rate of actin polymerization into microfilaments and the assembly of microtubules from monomeric tubulins, respectively. In this study, cytochalasin B was more inhibitory towards hemocyte aggregation than towards hemocyte adhesion. It also retarded hemocyte spreading, and restricted hemocyte migration. These data imply that actin microfilaments are involved in shape change during cohesion. Hemocyte spreading and migration are actin-dependent, but hemocyte adhesion may not be associated with actin.

Caffeine has been used as an anticoagulant in slime molds (Brenner and Thoms, 1984) and in several invertebrates (Bertheussen and Seljelid, 1978; Ratner and Vinson, 1983), but its inhibitory mechanism is not clear. The pharmacological effect of caffeine is due to phosphodiesterase inhibition and the consequent increase in intracellular cAMP (Brenner and Thoms, 1984; Snyder, 1984). In *M. californianus*, inhibition by caffeine is a dose-dependent, reversible reaction that does not affect cell viability. We suspect that the inhibitory effect of caffeine on cell aggregation and adhesion is receptor-associated. Hemocytes treated with caffeine for 30 min were able to recover their aggregation and adhesion competences immediately when caffeine was replaced by CMTBS. And previously spread hemocytes rounded up immediately when they were exposed to caffeine. If the inhibitory targets of caffeine were inside the cells, the cell behaviors would not be affected by caffeine so quickly.

Cell spike formation is involved in both platelet aggregation (Born, 1962) and slime mold aggregation (Garrod and Born, 1971). In this study, some EDTA-treated hemocytes formed spikes, but still remained free. Similar results were reported with the eastern oyster (Fisher, 1986) and limpet hemocytes (Davies and Partridge, 1972). Therefore, spike formation seems not to be sufficient to cause aggregation in these molluscan hemocytes.

Ca^{++} and Mg^{++} are important in many ligand-receptor binding mechanisms, and in maintaining normal functions of various cell adhesion molecules (Müller, 1980; Springer, 1990). In hemocyte aggregation studies, Ca^{++} and Mg^{++} are essential for normal cell behaviors (Davies and Partridge, 1972; Kenney *et al.*, 1972; Jumblatt *et al.*, 1980; Kanungo, 1982; Shozawa and Suto, 1990). For *M. californianus* hemocytes, 0.6 m*M* EDTA could completely block hemocyte adhesion. Normally, mussel hemolymph contains 10 m*M* calcium, 60 m*M* magnesium, and trace amounts of other divalent cations (Bayne *et al.*, 1976). Apparently, 0.6 m*M* EDTA chelating capacity did not remove all divalent cations from mussel hemolymph. However, its inhibitory effect was significant. It has been suggested that EDTA may not only serve as chelator, but also influence membrane permeability to divalent cations (Kenney *et al.*, 1972; Kanungo, 1982). In the present studies, EDTA-treated hemocytes aggregated weakly, and the inhibitory effect of EDTA on cohesive aggregation could be overcome by Ca^{++} or Mg^{++} supplements. Therefore, *Mytilus* hemocyte aggregation may proceed through two sequential stages. Weak aggregation is the early stage, and is Ca^{++}/Mg^{++}-independent. Cohesive aggregation is the late stage, and is Ca^{++}/Mg^{++}-dependent. Similar results were described for hemocyte aggregation in limpets (Davies and Partridge, 1972), and in *Limulus* (Kenney *et al.*, 1972), as well as for coelomocyte aggregation in holothurians (Fontaine and Lambert, 1977), and in sea stars (Kanungo, 1982). All of these hemocyte or coelomocyte aggregations are two-stage reactions. One is Ca^{++}/Mg^{++}-independent, and the other is Ca^{++}/Mg^{++}-dependent.

Retardation of hemocyte aggregation has been observed at reduced temperature (4°C) in *Mytilus* (this study), *Limulus* (Kenney *et al.*, 1972), and limpets (Davies and Partridge, 1972). It remains to be determined if this is due to altered fluidity of cell membranes, altered kinetics of metabolic reactions, or alternative mechanisms.

In summary, *Mytilus* hemocyte aggregation is a two-step process that is retarded at low temperature, and requires endogenous metabolic energy and divalent cations.

Based on these results and on aggregation studies in several other cell models (Davies and Partridge, 1972; Jumblatt *et al.*, 1980; Kanungo, 1982; Gibralter and Turner, 1985; Pizzey *et al.*, 1988), two-step cell aggregation mediated by divalent cations and temperature appears to have been well conserved during evolution.

A major goal of this study was to characterize distinctive features of self recognition (hemocyte-hemocyte binding) and non-self recognition (hemocyte-matrix binding). Because no aggregation-specific inhibitor was found, these results do not constitute strong evidence that cell aggregation and adhesion are two independent cell activities. However, some observations imply that this is likely. First, higher concentrations of inhibitor are necessary to block hemocyte aggregation than to affect hemocyte adhesion. Second, when reversible inhibitors such as caffeine and EDTA were removed or diluted, hemocyte aggregation occurred earlier than hemocyte adhesion.

Literature Cited

Anderson, R. S., and R. A. Good. 1976. Opsonic involvement in phagocytosis by mollusk hemocytes. *J. Invertebr. Pathol.* **27:** 57–64.

Bang, F. B. 1961. Reaction to injury in the oyster (*Crassostrea virginica*). *Biol. Bull.* **161:** 57–68.

Bayne, B. L., J. Widdow, and R. J. Thompson. 1976. Physiology: II. Pp. 207–260 in *Marine Mussels Their Ecology and Physiology*, B. L. Bayne ed. Cambridge Univ. Press, Cambridge.

Bell, G. I. 1983. Cell-cell adhesion in the immune system. *Immunol. Today* **4:** 237–240.

Born, G. V. R. 1962. Aggregation of blood platelets by adenosine diphosphate and its reversal. *Nature* **194:** 927–929.

Bertheussen, K., and R. Seljelid. 1978. Echinoid phagocytes *in vitro*. *Exp. Cell Res.* **111:** 401–412.

Brenner, M., and S. D. Thoms. 1984. Caffeine blocks activation of cyclic AMP synthesis in *Dictyostelium discoideum*. *Dev. Biol.* **101:** 136–146.

Bryan, F. T., C. W. Robinson, G. F. Gilbert, and R. D. Langdell. 1964. N-ethylmaleimide inhibition of horseshoe crab hemocyte aggregation. *Science* **144:** 1147–1148.

Cheng, T. C. 1981. Bivalves. Pp. 233–300 in *Invertebrate Blood Cells*, N. A. Ratcliffe and A. F. Bowley, eds. Academic Press, New York.

Cheng, T. C., and K. H. Howland. 1982. Effects of colchicine and cytochalasin B on chemotaxis of oyster (*Crassostrea virginica*) hemocytes. *J. Invertebr. Pathol.* **40:** 150–152.

Coombe, D. R., and C. R. Parish. 1988. Sulfated polysaccharide-mediated sponge cell aggregation: the clue to invertebrate self/nonself-recognition? Pp. 31–54 in *Invertebrate Historecognition*, R. K. Grosberg, D. Hedgecock, and K. Nelson, eds. Plenum Publishing Co., New York.

Dageförde, S., A. Schmücker, and L. Renwrantz. 1986. Capping of cell surface receptors on blood cells from the molluscs *Helix pomatia* (Gastropoda) and *Mytilus edulis* (Lamellibranchiata). *Eur. J. Cell Biol.* **41:** 113–120.

Davies, D. H., and T. M. Preston. 1987. Effect of disruption of plasmatocyte microfilaments on encapsulation *in vitro*. *Dev. Comp. Immunol.* **11:** 353–362.

Davies, P. S., and T. Partridge. 1972. Limpet haemocytes I. Studies on aggregation and spike formation. *J. Cell Sci.* **11:** 757–769.

Dundee, D. S. 1953. Formed elements of the blood of certain freshwater mussels. *Trans. Am. Microsc. Soc.* **72:** 254–264.

Feng, S. Y. 1988. Cellular defence mechanisms of oysters and mussels. Pp. 153–168 in *Disease Processes in Marine Bivalve Molluscs*, W. S. Fisher, ed. Am. Fish. Soc. Special Publication 18. Bethesda, Maryland.

Feng, S. Y., and J. S. Feng. 1974. The effect of temperature on cellular reactions of *Crassostrea virginica* to the injection of avian erythrocytes. *J. Invertebr. Pathol.* **23:** 22–37.

Fisher, W. S. 1986. Structure and functions of oyster hemocytes. Pp. 25–35 in *Immunity in Invertebrates*, Chap. 3, M. Brehélin, ed. Springer-Verlag, Berlin, West Germany.

Fontaine, A. R., and P. Lambert. 1977. The fine structure of the leucocytes of the holothurian, *Cucumaria miniata*. *Can. J. Zool.* **55:** 1530–1544.

Fryer, S. E., R. C. Bender, and C. J. Bayne. 1991. Proteinase inhibitory activity in the plasma of the gastropod mollusc, *Biomphalaria glabrata*. *Dev. Comp. Immunol.* **15**(supplement 1): S45.

Garrod, D. R., and G. V. R. Born. 1971. Effect of temperature on the mutual adhesion of pre-aggregation cells of the slime mold, *Dictyostelium discoideum*. *J. Cell Sci.* **8:** 751–765.

Gibralter, D., and D. C. Turner. 1985. Dual adhesion systems of chick myoblasts. *Dev. Biol.* **112:** 292–307.

Guyton, A. C. 1986. Hemostasis and blood coagulation. Pp. 76–86 in *Textbook of Medical Physiology*, chap. 8, A. C. Guyton, ed. W. B. Saunders Co., Philadelphia.

Hergenhahn, H.-G., A. Aspan, and K. Söderhäll. 1987. Purification and characterization of a high-M_r proteinase inhibitor of pro-phenol oxidase activation from crayfish plasma. *Biochem. J.* **248:** 223–228.

Johansson, M. W., and K. Söderhäll. 1989. Cellular immunity in crustaceans and the proPO system. *Parasitol. Today* **5:** 171–176.

Jones, G. E., and R. Gillett. 1976. Rapid modification of the morphology of cell contact sites during the aggregation of limpet haemocytes. *J. Cell Sci.* **22:** 21–33.

Jumblatt, J. E., V. Schlup, and M. M. Burger. 1980. Cell-cell recognition: specific binding of *Microciona* sponge aggregation factor to homotypic cells and the role of calcium ions. *Biochemistry* **19:** 1038–1042.

Kanungo, K. 1982. *In vitro* studies on the effects of cell-free coelomic fluid, calcium, and/or magnesium on clumping of coelomocytes of the sea star, *Asterias forbesi* (Echinodermata: Asteroidea). *Biol. Bull.* **163:** 438–452.

Kenney, D. M., F. A. Belamarich, and D. Shepro. 1972. Aggregation of horseshoe crab (*Limulus polyphemus*) amoebocytes and reversible inhibition of aggregation by EDTA. *Biol. Bull.* **143:** 548–567.

Lackie, A. M. 1988. Immune mechanisms in insects. *Parasitol. Today* **4:** 98–105.

Moore, M. N., and D. M. Lowe. 1977. The cytology and cytochemistry of the hemocytes of *Mytilus edulis* and their responses to experimentally injected carbon particles. *J. Invertebrt. Pathol.* **29:** 18–30.

Müller, W. E. G. 1980. Cell membranes in sponges. *Int. Rev. Cytol.* **77:** 129–181.

Narain, A. S. 1973. The amoebocytes of lamellibranch molluscs, with special reference to the circulating amoebocytes. *Malacol. Rev.* **6:** 1–12.

Pizzey, J. A., G. E. Jones, and F. S. Walsh. 1988. Requirements for the Ca^{2+}-independent component in the initial intercellular adhesion of C2 myoblasts. *J. Cell Biol.* **107:** 2307–2317.

Ratner, S., and S. B. Vinson. 1983. Encapsulation reactions *in vitro* by haemocytes of *Heliothis virescens*. *J. Insect Physiol.* **29:** 855–863.

Renwrantz, L., J. Daniels, and P.-D. Hansen. 1985. Lectin-binding to hemocytes of *Mytilus edulis*. *Dev. Comp. Immunol.* **9:** 203–210.

Roseman, S. 1985. Studies on specific intercellular adhesion. *J. Biochem.* **97:** 709–718.

Rutishauser, U., A. Acheson, A. K. Hall, D. M. Mann, and J. Sunshine. 1988. The neural cell adhesion molecule (NCAM) as a regulator of cell-cell interaction. *Science* **40:** 53–57.

Seifert, R. A. 1983. On the mechanism of oyster amoebocyte aggregation. Ph.D. thesis. University of Washington.

Shozawa, A., and C. Suto. 1990. Hemocytes of *Pomacea canaliculata:* I. Reversible aggregation induced by Ca^{2+}. *Dev. Comp. Immunol* **14:** 175–184.

Sminia, T. 1981. Gastropods. Pp. 191–232 in *Invertebrate Blood Cells,* N. A. Ratcliffe and A. F. Rowley, eds. Academic Press, New York.

Snyder, S. H. 1984. Adenosine as a mediator of the behavioral effects of xanthines. Pp. 129–141 in *Caffeine: Perspectives From Recent Research*, P. B. Dews, ed. Spring-Verlag.

Springer, T. A. 1990. Adhesion receptors of the immune system. *Nature* **346:** 425–434.

Sparks, A. K. 1972. Reaction to injury and wound repair in invertebrates. Pp. 22–133 in *Invertebrate Pathology: Noncommunicable Diseases,* Academic Press, New York.

Underhill, C. B. 1982. Interaction of hyaluronate with the surface of simian virus 40-transformed 3T3 cells: Aggregation and binding studies. *J Cell Sci* **56:** 177–189.

Reference: *Biol. Bull.* **188:** 267–280. (June, 1995)

Cytological Analysis of the Urn Cell Complex of *Sipunculus nudus* Before and After Serum-Induced Secretion

SANTO V. NICOSIA[1] AND JANICE M. SOWINSKI[2]

[1]*University of South Florida College of Medicine, Department of Pathology and H. Lee Moffitt Cancer Center, Tampa, Florida 33612; and* [2]*Department of Pathology and Toxicology, SmithKline and French Laboratories, Philadelphia, Pennsylvania 19101*

Abstract. This study analyzes the cytology of the urn cell complex (UCC) of *Sipunculus nudus*, an invertebrate cell model for humorally regulated mucus secretion. An unstimulated UCC is composed of a vesicle cell and a ciliated cell joined together by desmosomes. Another cell population (third-type cells) is frequently associated with ciliated cells. Vesicle cells are thin, have few mitochondria or lipid droplets, and enclose a bubble-like cavity containing microfibrillar material. Ciliated cells contain several rows of cilia that are anchored by prominent rootlets and propel UCCs forward. Five to six concentric bundles of microfilaments are distributed along the outer convexity of ciliated cells and may have a role in the plasticity of the UCC. Many fibrillar deposits that lack a demonstrable limiting membrane are distributed around intracytoplasmic vacuoles facing the mouth-like opening of the UCC. These deposits are reactive to periodic acid-Schiff and resistant to diastase. After stimulation with serum, they appear to migrate through the ciliated cell's plasma membrane, contributing to the formation of a secretory tail. Discharge of secretory material is not observed in third-type cells, which instead contain lysosome-like granules and autophagic-like vacuoles and become displaced distalward by the emerging tail of the UCC. This study indicates that formation and elongation of the UCC secretory tail are functions of ciliated cells.

Introduction

Mucous secretions regulate bacteria and sperm migration and protect against foreign irritants. The control of mucus secretion in non-innervated cells, such as those lining the respiratory and reproductive tracts, is poorly understood (Chantler and Debruyne, 1977; Richardson and Phipps, 1978; Nicosia, 1986). Using an invertebrate mucociliary cell model, Bang and Bang (1962, 1979) reported that one or more mucus-releasing macromolecule is present in body fluids under physiologic and pathologic conditions. A similar factor or factors may also be present in vertebrate external secretions and sera (Bang and Bang, 1974, 1979; Mastroianni *et al.*, 1979; Nicosia, 1979; Kurlandsky *et al.*, 1980; Nicosia *et al.*, 1982). This possibility has indeed been verified with cat tracheal cells (Hall *et al.*, 1978) and rabbit endocervical mucous cells (Nicosia *et al.*, 1982; Nicosia, 1986).

The cell model used by Bang and Bang (1962, 1972) is derived from the benthic coelomate *Sipunculus nudus* (Linnaeus). This marine invertebrate belongs to a phylum of sipunculids (peanut worms) with an unsegmented, cylindrical body and a retractile anterior introvert (Hyman, 1959). A characteristic of this sipunculid is the presence of a large number of circulating mucociliary cells, or urn cell complexes (UCCs), within its coelomic cavity (Catacuzéne, 1928). Swimming freely within such a cavity, UCCs play an important role in the sipunculid immune defense by releasing sticky, mucoid tails that promptly trap invading bacteria, thereby curtailing infection (Bang and Bang, 1974, 1975).

Morphological data on the UCCs of *S. nudus* derive mostly from the elegant light microscopic observations of Bang and Bang (1962, 1964, 1976, 1980). These studies indicate that the UCC is composed of two cells, a vesicle cell and a saucer-shaped ciliated cell, fitted together like an acorn into its cap. A third type of cell is often contig-

Received 10 May 1994; accepted 24 March 1995.

uous with the former two cells and may contribute to or regulate mucus secretion. Only two brief reports on the ultrastructure of the UCC of *S. nudus* have been published (Nicosia and Sowinski, 1979; Reissig *et al.*, 1979). A more detailed study of UCCs and of other coelomic cells has been carried out in *Phascolosoma agassizii*, but significant differences appear to exist between the cell complexes of that worm and those of *S. nudus* (Dybas, 1976, 1981a).

The present study was carried out to verify the multicellular nature and cell relationships of UCCs in *S. nudus* and to analyze the cytology of these cells before and after serum-induced mucus release.

Materials and Methods

Animals

Adult specimens of *Sipunculus nudus* were obtained from two sources. Some worms were dug from the sand at low tide in their natural habitat in Salerno, Italy. Worms that were traumatized were discarded. Several dozen worms were placed in oxygenated, airtight containers partially filled with seawater and fresh sand and flown to our laboratory. Healthy worms were immediately transferred to an aerated aquarium (Instant Ocean Inc., Wickliffe, OH) with a good cover of sand and recirculating, filtered seawater (FSW). Other worms were originally collected at Loquemeau (Finistére, France) and then maintained at the Marine Biology Laboratory, Woods Hole, Massachusetts, in large tanks with circulating seawater.

Harvesting of urn cell complexes

Suspensions of UCCs were obtained by withdrawing 2–3 ml of coelomic fluid with a 25-g needle through an opening at the posterior end of each female worm. Fluid aliquots (1.0 ml) were stored in capped, 6.0-ml plastic tubes (Falcon-Bioquest, Cockersville, MD) held in an upright position at 4°C.

In vitro *bioassay for serum-induced secretion*

Five microliter samples of coelomic fluid supernatant, each containing 50–100 UCCs, were incubated in a Clay-Adams microculture slide dish (Thomas Co., Philadelphia, PA) with 20 μl of FSW, pH 7.9, or with 20 μl of rabbit serum previously diluted 1:10 with FSW. Following the protocol outlined by Bang and Bang (1979), diluted serum was heated at 85°C for 5 min, then stored at 4°C in a sterile container. Seawater was boiled for 5 min, filtered through a 0.22-μm Millipore filter (Millipore Co., Bedford, ME) and also stored at 4°C. UCCs in FSW alone or with 1:10 treated serum were incubated from 0–30 min at room temperature inside a humidified dish. After 0, 2, 5, 10, 20, and 30 min, each UCC preparation was observed under a Wild M20 phase-contrast microscope. Secretory tails released by UCCs were measured with a calibrated cross-line ocular disk at a final magnification of 125× (Fig. 1A). Ten incubations were carried out for each investigated time period, with an average of 50 UCCs evaluated to calculate secretory tail length. The secretory response of each cell preparation was expressed as mean tail length in micrometers.

Cytochemical studies

After each incubation, UCCs were resuspended in FSW and pelleted (1400 rpm for 10 min) onto a microscope slide in a Shandon cytocentrifuge (Shandon Southern Instruments, Sewickley, PA). After air-drying, cells were processed for cytochemical evaluation of metachromatic material, lipid, glycogen, glycoproteins, and sugars. For observations of general morphology (with a light microscope) and for studies of metachromasia, cells were fixed in 10% formalin in FSW and stained with 1:5000 methylene blue. For demonstration of lipids, cells were fixed in Baker's fixative and stained with Sudan black B (Lillie, 1965). As controls, some cells were stained after incubation in ether: ethanol (1:1) to extract lipids. For demonstration of glycogen and glycoproteins, cells were fixed in formalin–acetic-acid–alcohol and stained with periodic acid-Schiff (PAS) reagents (Luna, 1968) before and 30 min after digestion with diastase (0.1% in 0.16 M phosphate buffer, pH 6.0) at room temperature to remove glycogen. For demonstration of sugar residues in secretory tails of stimulated UCCs, these cells were fixed in 10% formalin for 5 min, rinsed three times in FSW, and incubated for 10 min with fluorescein isothiocyanate-conjugated (FITC) *Ricinus communis* agglutinin (RCA_1) or *Lotus tetragonolobulus* agglutinin (LTA). Both lectins were purchased from Sigma (St. Louis, MO) and used at a concentration of 200 μg/ml in FSW adjusted to pH 7.9. Controls for specific lectin binding contained 10^{-1} M L-fucose or D-galactose in staining and washing solutions. After washing, cells were covered with a coverslip, using nonfluorescent mounting medium, and viewed under a Leitz Ortholux microscope using excitation and barrier filters for fluorescein fluorescence. Photomicrographs were taken using Kodak Tri-X film.

Electron microscopy

For transmission electron microscopy, UCCs before and after 2, 10, and 20 min of exposure to serum were fixed for 60 min at 4°C in 3% glutaraldehyde buffered with 0.1 M sodium cacodylate in FSW. Cells were post-fixed with 1% osmium tetroxide, dehydrated in graded ethanols, and embedded in Epon 812 (Luft, 1961). Specimens were step-sectioned with a diamond knife, and 600–800 Å thin sections were stained with uranyl acetate and lead citrate (Reynolds, 1963) and viewed in a Hitachi 12A

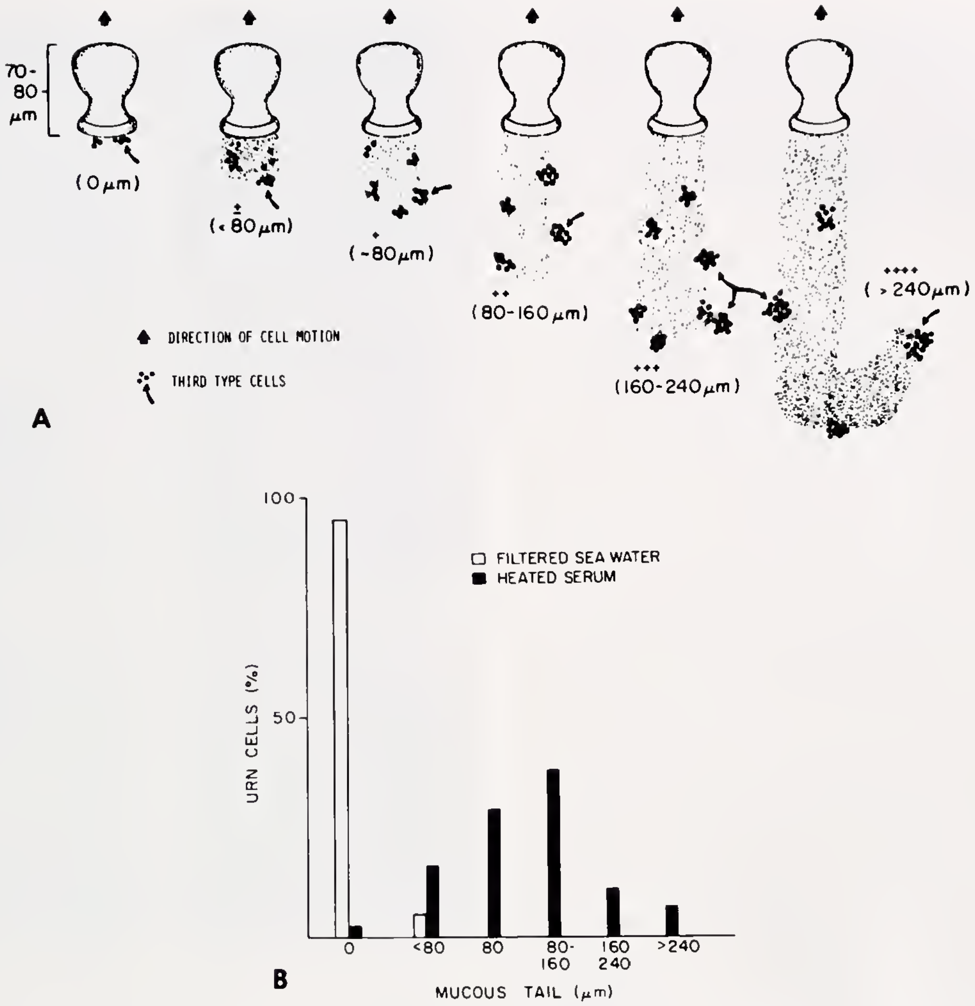

Figure 1. Secretory response of the urn cell complex (UCC) to serum. (A) Schematic diagram. Tails released by UCCs after exposure to heated serum have various lengths (from 0 to > 240 µm) and are easily quantifiable with the aid of an ocular micrometer under phase-contrast microscopy. Large arrows indicate direction of UCC swimming motion. Smaller arrows point to third-type cells, which are progressively displaced distalward by the emerging tails. (B) Typical distribution of secretory responses (expressed as percentage of UCCs with various tail lengths) 20 min after exposure to heated serum (full bars) or filtered seawater (empty bars).

electron microscope at an initial accelerating voltage of 75 kV.

For scanning electron microscopy, UCCs were pipetted onto round coverslips (20 mm diameter, Carolina Biological Supplies, Burlington, NC) previously coated with 0.1% poly-D-lysine (Sigma Chemical Co., St. Louis, MO). Cells were then fixed *in situ* for 60 min at 4°C with a 3% glutaraldehyde buffered with 0.1 *M* sodium cacodylate buffer in FSW. After they were rinsed in the same buffer, cells were dehydrated in graded acetones and critical-point dried in a Tousimis device (Tousimis Inc., Rockville, MD) using liquid Freon as transitional fluid. Coverslips were then mounted onto stubs with a thin layer of conductive silver point (Fullam, Schenectady, NY) and sputter-coated with a layer (~15 nm) of gold-palladium in a Balzer device (Balzer Union, Nashua, NH). Specimens were viewed in a Jeolco SM-35 scanning electron microscope operated at 10 kV with a 0–60°C stage tilt. Photographs were taken using Polaroid 55 P/N film.

Results

Effect of serum

UCCs exposed to 1:10 heated serum extruded distinct secretory tails as early as 2 min after stimulation (Fig. 1A). The length of these tails increased after the ensuing 10 min, reaching a peak after 20 min. The average tail length during the observed intervals was 10 µm at 2 min, 30 μm at 5 min, 55 μm at 10 min, 100 μm at 20 min, and 110 μm at 30 min. After 20 min, a wide distribution of secretory response was observed, with more than 50% of UCCs exhibiting tails 80 μm or longer (Fig. 1B). About 5% of UCCs exposed to serum showed no visible tails. Tails were absent or shorter than 80 μm in UCCs incubated with FSW alone (Fig. 1B).

Light microscopy

Living or fixed UCCs measured from 70 to 80 μm in their longest dimension. The apical, or vesicle, cell contained a single nucleus and was translucent (Fig. 2A). The basal, or ciliated, cell was saucer-shaped, also contained a single nucleus, and was recognized by the active and rapid beating of cilia (Fig. 2A). The site where the neck of the vesicle cell fitted into the ciliated cell was marked in its outer profile by five to six parallel arrays of refractile and wavy "lines" (Fig. 2B). Below this area, the outer aspect of the ciliated cell contained several rows of circumferentially arranged cilia, 5–10 μm long. In oblique and "tail-on" views, the cytoplasmic insertion shafts of these cilia were observed as refractile "ribs" (Fig. 2B–C). In live UCCs, cilia swept very rapidly to ensure forward motility and also to sweep surrounding particles. The concave or inner aspect of the ciliated cell was devoid of cilia, smooth, and formed a mouth-like opening at the junction with the lower region of the vesicle cell (Fig. 2D). A cluster of round cells was frequently found at or near the lower aspect of UCC. These third-type cells measured 7–9 μm in diameter and were best observed in lateral views of UCCs (Fig. 2B and E). These views revealed 5–10 or more cells often surrounded by the scanty secretory material present on the underside of unstimulated UCCs (Fig. 2E) or more distally within the secretory tails of stimulated UCCs (Fig. 2F).

Cytochemistry

Ciliated cells of unstimulated UCCs contained glycogen as indicated by a light PAS staining abolishable by diastase digestion. These cells also contained granular, PAS-positive, and diastase-resistant deposits that measured 0.3–0.5 μm in diameter and were confined to the concave side of the ciliated cell (Fig. 3A). Both intracellular glycogen and granules decreased markedly after exposure of the UCC to serum (Fig. 2D). Numerous granules that also stained with PAS after diastase were demonstrated in third-type cells. These granules measured 0.4–0.6 μm in diameter and were still present in various amounts in stimulated UCCs. Both ciliated and vesicle cells contained variable amounts of lipid droplets (Fig. 3B). These droplets were more frequent in vesicle cells, and their staining reaction was abolished by pretreatment with lipid solvents (Fig. 3C).

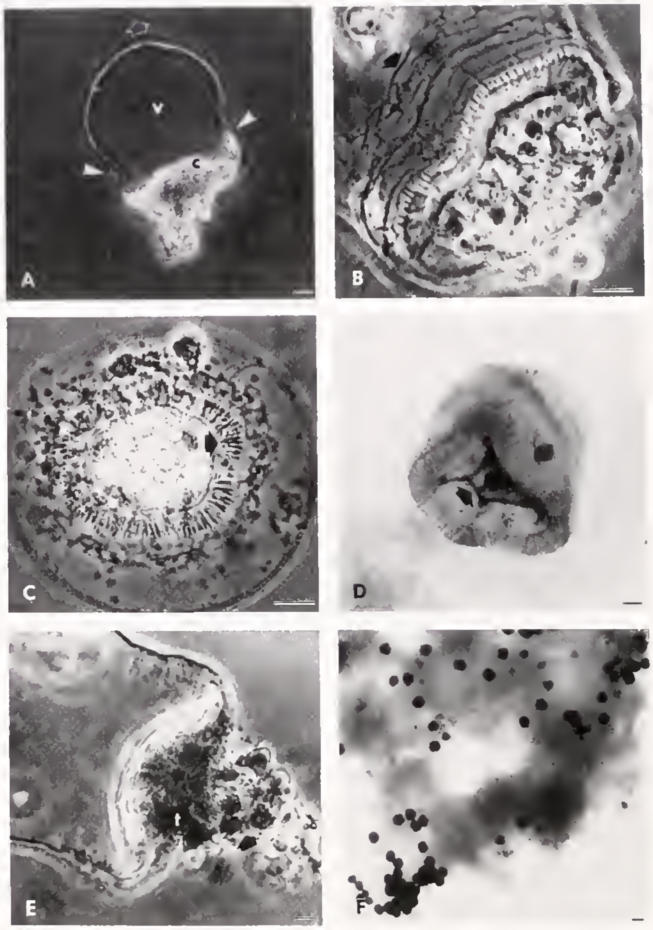

Figure 2. Light microscopy of the urn cell complex (UCC) before (A–C) and after (D–F) exposure to serum. (A) Living UCCs showing the apical vesicle cell (v) which fits into the basal ciliated cell (c), much like an acorn into its cap (arrows). Direction of UCC swimming motion is indicated by empty arrow. (Phase-contrast.) (B) Parallel and refractile rows of filaments (arrow) on the outer aspect of the ciliated cell in a living UCC. (Phase-contrast.) (C) Tail-on view of a living UCC. Note rib-like cytoplasmic insertions of cilia (arrow). (Phase-contrast.) (D) Oblique view of a serum-treated UCC after periodic acid-Schiff (PAS) staining and diastase digestion. Note PAS-positive, putative glycoproteinaceous material (arrow), delimiting a mouth-like opening at the inner periphery of the ciliated cell. A faintly stained secretory tail can also be seen. (E) Lateral view of a UCC fixed 5 min after exposure to serum and stained with methylene blue. The emerging tail (t) stains metachromatically and is pushing distalward a group of third-type cells (arrow). (F) Leading front of a UCC secretory tail 20 min after serum stimulation. Note numerous third-type cells. (PAS.) All scale bars: 10 μm.

The tails of stimulated UCCs stained metachromatically with methylene blue (Fig. 2E) and with PAS after diastase digestion (Fig. 3D). The intensity of the PAS staining varied from mild to marked in different UCCs. In stimulated UCCs, the innermost lining of ciliated cells appeared as a thick and somewhat fuzzy outline that was not abolished by diastase after PAS staining (Fig. 2D). Released tails fluoresced brightly after incubation with FITC-RCA1 and

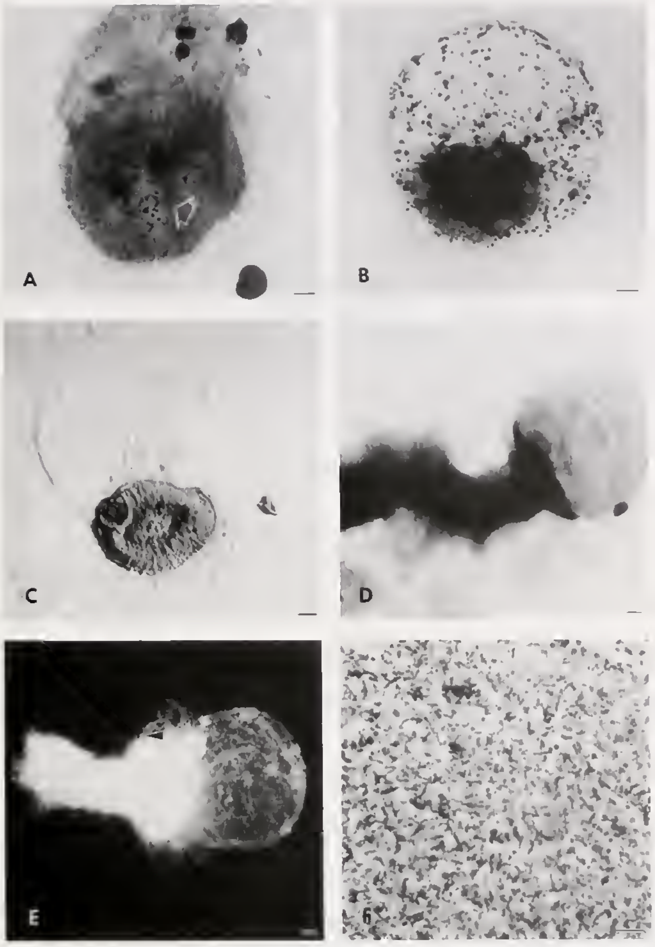

Figure 3. Cytochemistry of the urn cell complex (UCC). (A) PAS-positive, putative glycoproteinaceous material in the ciliated cell component of an unstimulated UCC (arrow). Note that this material is distributed predominantly toward the inner aspect of the UCC. (PAS after diastase digestion.) (B) Unstimulated UCC showing abundant lipid deposits (black) both in the vesicle and ciliated cells. (Sudan black B.). (C) Unstimulated UCC stained with Sudan black B after lipid extraction. Note absence of lipid deposits. (D) UCC 20 min after exposure to serum. The long secretory tail contains PAS-positive material. (PAS after diastase digestion.) (E) Secretory tail 20 min after serum treatment and after incubation with FITC-LTA. Bright fluorescence indicates the presence of fucose-rich moieties. (F) Fibrillary structure of secretory tail. (Methylene blue.) All scale bars: 10 μm.

LTA lectins (Fig. 3E). This fluorescence was specific since it was markedly reduced by D-galactose or L-fucose. Tails stained with methylene blue revealed a fibrillar or fibrillar-granular structure (Fig. 3F).

Ultrastructure

The structural relationship between the vesicle and ciliated cell of the UCC was best appreciated in longitudinal sections (Fig. 4A–B). Both cells were marginally joined by desmosomes (Fig. 4B, inset). The vesicle cell was characterized by a thin cytoplasm containing vacuoles, lipid droplets, and mitochondria (Fig. 5A–B). A single and elongated nucleus was present, usually in the midportion of the cell. As a result of processing for electron microscopy, the vesicle cell frequently appeared collapsed. The bubble-like space enclosed by this cell contained a diffuse electron-dense, fibrillar material (Fig. 5B). No periodicity was observed in individual fibrils. The electron density and fibrillar composition of this material resembled the matrix of the material seen near the mouth-like underside of UCCs (Figs. 4B and 10A–B).

The ciliated cell spanned the entire lower aspect of the UCC. The outer lining of this cell contained numerous prominent microvilli measuring from 0.2–0.4 μm in width and from 1–3 μm in length (Figs. 4A and 6A–B). Straight filaments were seen to run longitudinally inside each microvillus and extend downward into the adjacent ectoplasm (Fig. 6B). Rows of cilia were present between the microvilli. These cilia, 5–10 μm long, with a characteristic 9 + 2 microtubule arrangement (Fig. 6A–B), were anchored onto the underlying cytoplasm by basal bodies and by long (3–5 μm), curving rootlets with a periodicity of 65 nm (Fig. 6C). Away from the ciliary attachment, the cytoplasm contained prominent bundles of 14- to 17-mm-wide microfilaments (Fig. 6D). These appeared to correspond to the filamentous "lines" observed in the neck region of living UCCs (Fig. 2B). In addition to these circular bundles, other smaller bundles of microfilaments and individual microfilaments were seen to traverse the cytoplasm of ciliated cells (Fig. 6C–D). The remainder of the cytoplasm not occupied by cytoskeletal elements contained diffuse glycogen particles, alone (Fig. 7A) or in aggregates (Fig. 7B); mitochondria (Figs. 7C and F); lysosome-like bodies with electron-dense cores (Fig. 6C); and lipid droplets (Figs. 7F–G). Profiles of granular endoplasmic reticulum and Golgi complex were not prominent.

Some of the most prominent structures seen in ciliated cells were irregular vacuoles of various size (Fig. 4A–B). These vacuoles contained no demonstrable products and were surrounded by deposits of electron-dense material that did not appear membrane-bound (Fig. 7C–D and G). A material of similar structure and density was present in the ectoplasmic regions of the ciliated cells that faced the inner neck cavity of the UCC (Fig. 7D–G). This material appeared to cross the cell membrane and merge with fibrillar material that was present in the extracellular space (Fig. 7E–G).

Third-type cells were present below the ciliated cell of the UCC (Figs. 4B and 8C). The former cells were closely juxtaposed to the ciliated cell (Fig. 8A), although no obvious junctional devices were observed between these cells (Fig. 8B). Third-type cells also appeared partly surrounded by small amounts of fibrillar material (Fig. 4B) and cell

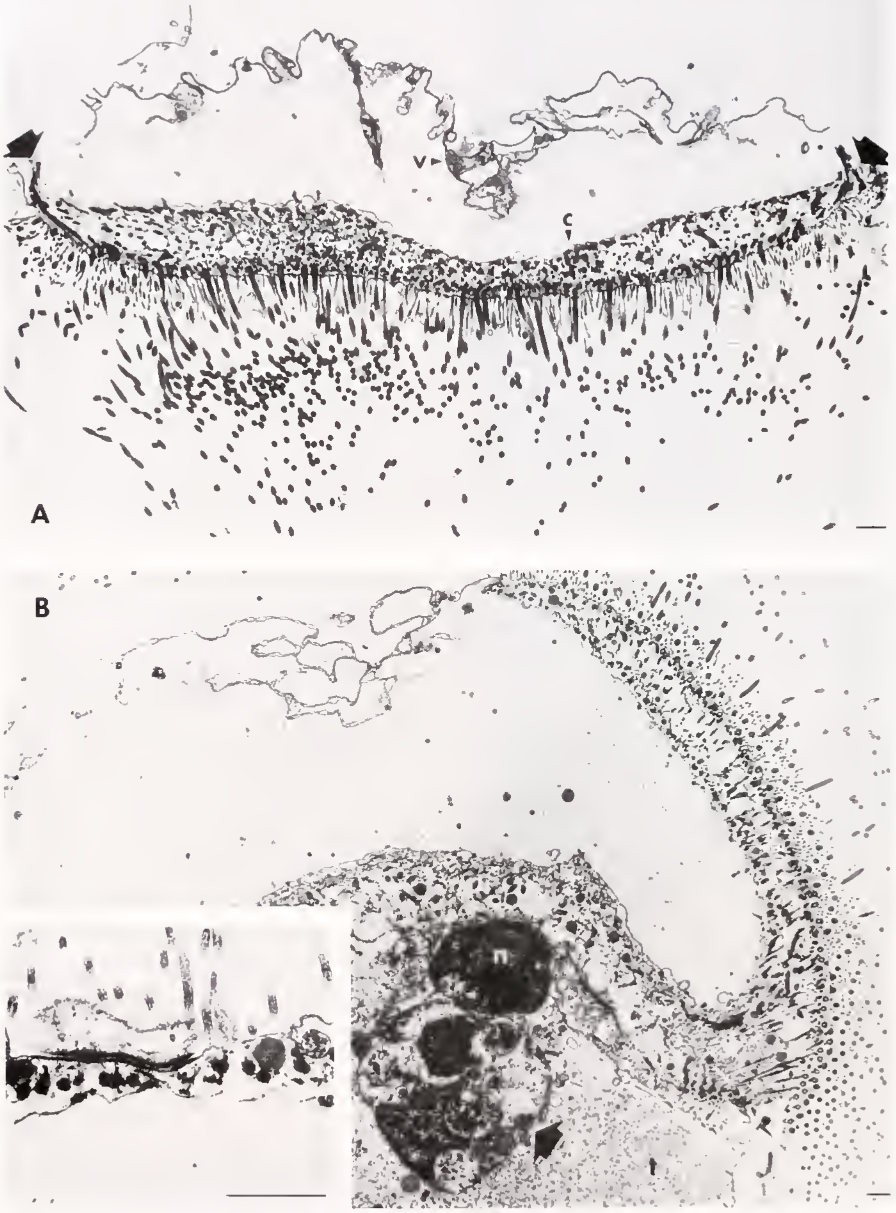

Figure 4. Longitudinal (A) and oblique (B) views of the urn cell complex (UCC). (A) Note partially collapsed vesicle cell (v), ciliated cell (c), and curving bundles of filaments at the junction between these two cells (arrows) before exposure to serum. The ciliated cell contains vacuoles and abundant granular material. (B) Stimulated UCC. The cytoplasm of the ciliated cell contains mostly vacuoles and lipid droplets. Note also ciliated cell nucleus (n), adjacent third-type cells (arrow), and secretory tail (t). Ciliated and vesicle cells are complexed by desmosomes (inset). All scale bars: 1 μm.

debris (Fig. 8C). These cells had an irregular nucleus, and their cytoplasm contained few phagocytic vacuoles and many granules, 0.4–0.6 μm in diameter, with electron-dense cores (Fig. 8C).

To analyze the cytology of stimulated UCCs, these cells were studied after 2, 10, and 20 min of exposure to 1:10 heated serum. The initial formation of a secretory tail was heralded by numerous round elevations of the cell membrane in the underside of the ciliated cell (Fig. 9A). These bleb-like structures had a width of 0.3–0.4 μm and appeared to correspond to underlying ectoplasmic vacuoles (Fig. 9B–C). Ten minutes after stimulation, UCCs exhib-

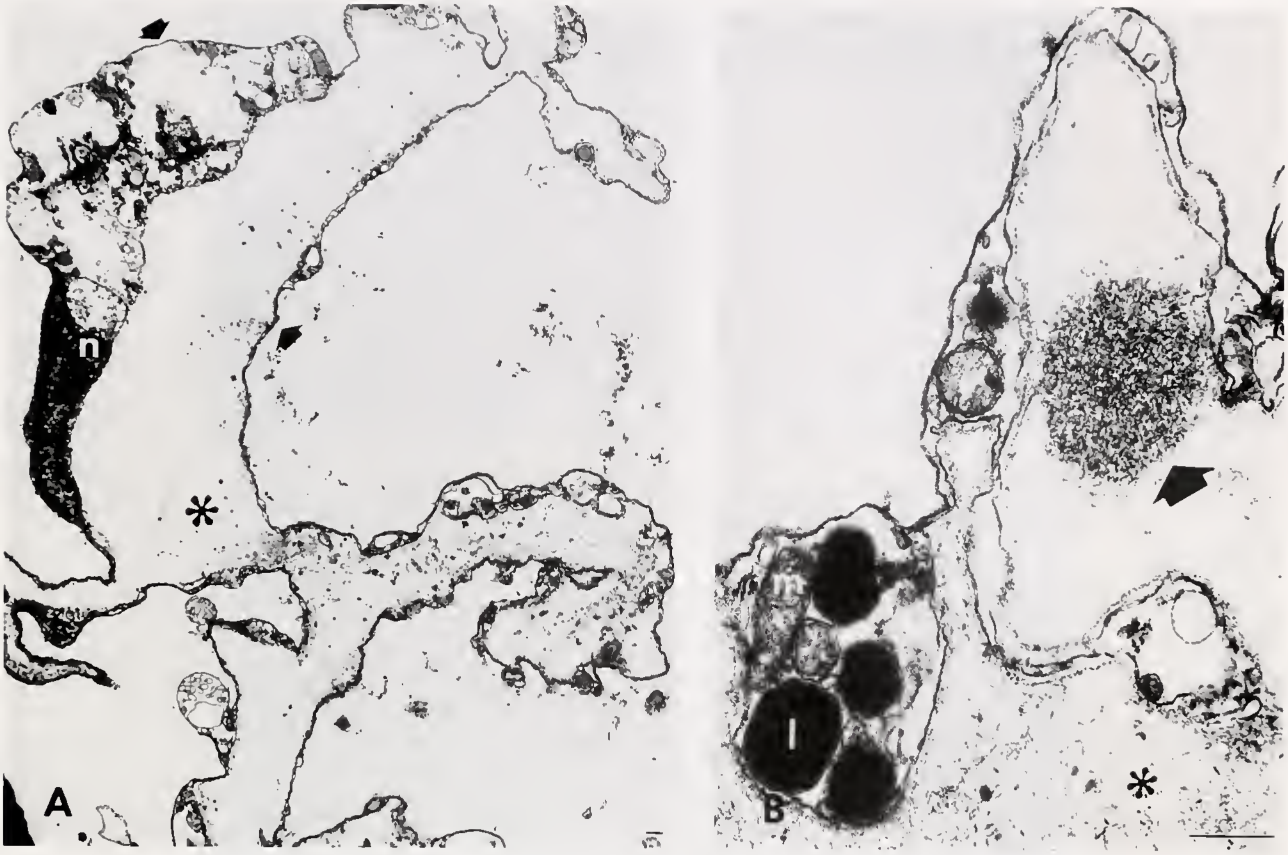

Figure 5. Vesicle cell of the urn cell complex (UCC). (A) Note external surface (arrows) and central space (asterisk). Partial collapse of cell is due to fixation. n, nucleus. (B) Filamentous material in dispersed units (asterisk) or in aggregates (arrow) is present within the UCC central space. Note also lipid droplets (l) and mitochondria (m) within the vesicle cell. Both scale bars: 0.5 μm.

ited abundant extracellular material in this region. The material had a fibrillar-granular structure and was continuous with fibrillar strands originating from ectoplasmic areas of the inner aspect of ciliated cells (Fig. 9D) and from distended bleb-like structures (Fig. 9E). Electron-dense granules were also observed among extracellular fibrils and immediately above the cell membrane (Fig. 9D). Tail-on views of UCCs in transmission and scanning electron micrographs showed that the fibrillar material encircled the inner circumference of the ciliated cell (Fig. 9F–G). This cell contained many empty vacuoles and lipid droplets, little glycogen, and few of the electron-dense aggregates observed in UCCs at rest around intracellular vacuoles and below the cell's plasma membrane. Prominence of intracytoplasmic vacuoles was also obvious in UCCs examined 20 min after exposure to serum (Fig. 10A). When seen in appropriate longitudinal sections, the released tail contained a fibrillar material and occasional third-type cells (Fig. 10B). The electron density and structure of the tail were similar to those of the fibrillar material present within the bubble-like cavity of the UCC (Fig. 10A).

Discussion

The present study analyzed the cytology of free-swimming urn cell complexes of the benthic coelomate *Sipunculus nudus*. The two large cells, ciliated and vesicle, of the UCC are complexed by marginal desmosomes. A smaller and variable population of cells (third-type cells) is frequently, but not invariably, found in close juxtaposition to the ciliated cell. Exposure of a UCC to serum causes a prompt and massive release of a fibrillar-granular material that appears first in the concave side of the ciliated cell and elongates rapidly to form a characteristic tail. During and after release of this tail, increasing cytoplasmic vacuolization occurs in the ciliated cell, together with an apparent transmembranous discharge of fibrillar material and some loss of glycogen. When observed, third-type cells exhibit phagocytic vacuoles and are displaced distalward by the elongating fibrillary tail. Exocytosis cannot be demonstrated in either ciliated or third-type cells.

To this date, the cytology of the UCC of *S. nudus* has been investigated almost exclusively by light microscopy.

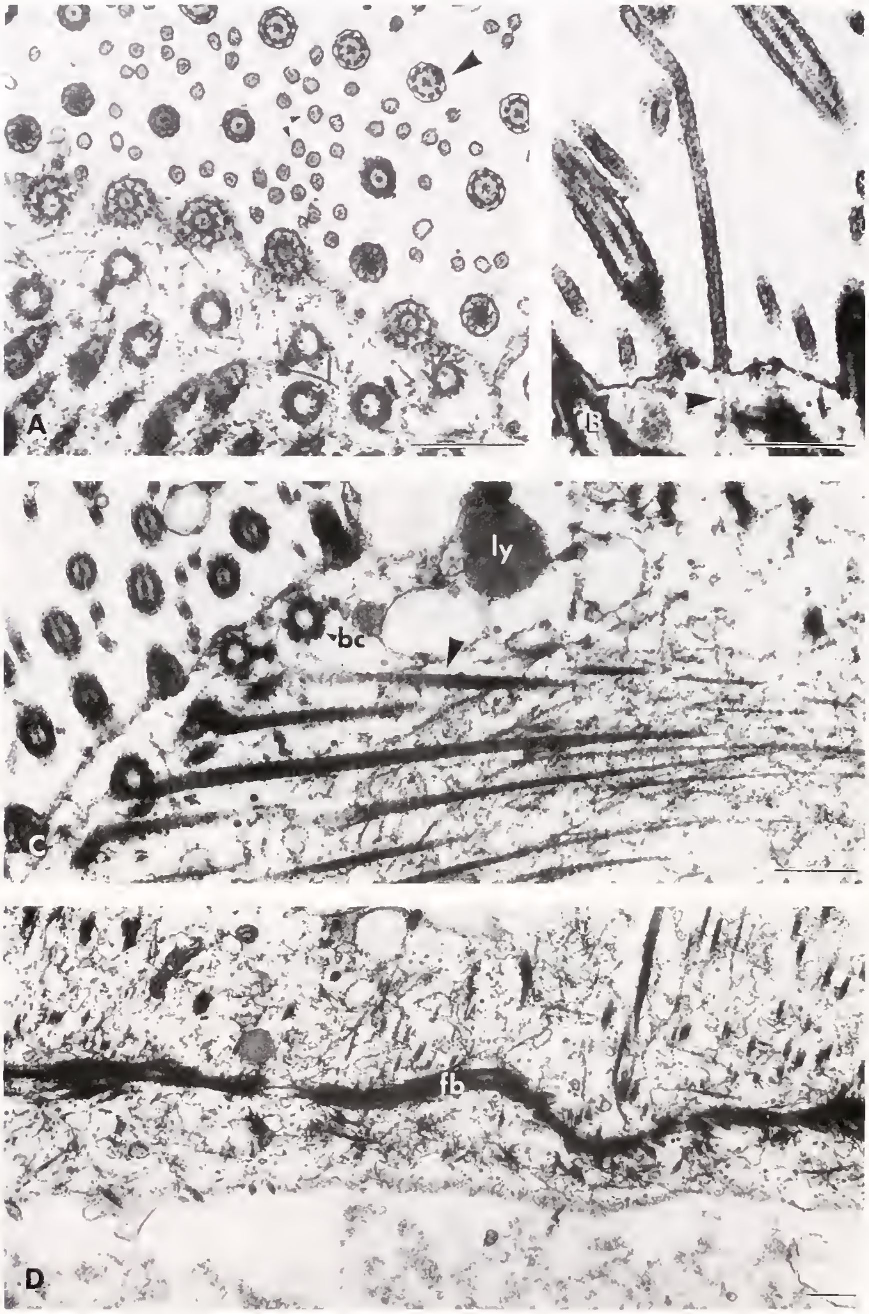

Figure 6. Ciliated cell of the urn cell complex (UCC). (A) Cross-section view of cilia revealing typical spoke-wheel morphology (large arrow) and microvilli (small arrow). (B) Longitudinal view of cilia and microvilli. Note filamentous extension from the core of a microvillus into ectoplasmic area (arrow). (C) Basal corpuscles (bc) and prominent rootlets (arrow) of cilia. Note also individual filaments crossing the cytoplasm in various directions. ly, lysosome-like body. (D) Filamentous bundles (fb) at the outer periphery of the ciliated cell. These prominent bundles run parallel to the cell membrane and correspond to the refractile concentric rows observed in the living UCC (see Fig. 2B). All scale bars: 0.5 μm.

These studies have indicated that not only ciliated and vesicle cells but also a third cell population, so-called R cells, are integral components of the UCC (Reissig *et al.*, 1979; Bang and Bang, 1976, 1980). It has been suggested that R cells may slowly secrete a type of mucus that is selectively sticky for cell debris and foreign particulates (Bang and Bang, 1980). During exposure of a UCC to bacteria or to other foreign substances, R cells become

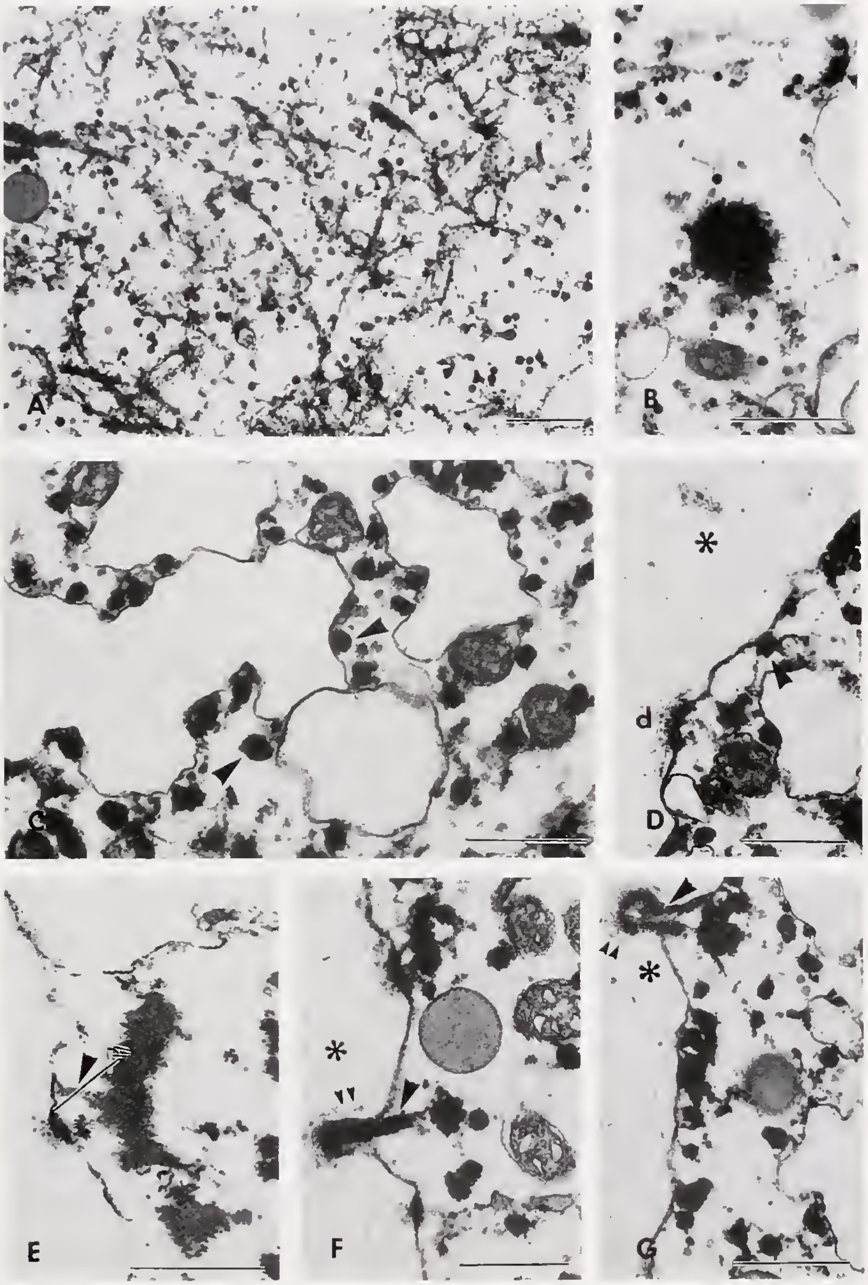

Figure 7. Ciliated cell of the unstimulated urn cell complex UCC. (A–B) Glycogen as individual particles (A) or in aggregate form (B). (C) Electron-dense granular material (arrows) around vacuolar spaces. (D) Similar material (arrow) in close proximity with the ciliated cell membrane facing the UCC central space (asterisk). d, hemidesmosome. (E–G) This material makes frequent contact with the ciliated cell's plasma membrane (arrow) and appears continuous (double arrows) with extracellular fibrillar material of similar electron density (asterisk). All scale bars: 0.5 μm.

detached from the UCC while large streams of mucus are released by the ciliated cell. The loss of R cells is thus accompanied by an apparent progressive increase in the synthesis and release of mucus by the ciliated cell. These observations have suggested that a dual secretory system may exist in the UCC (Bang and Bang, 1980). The first system provided by R cells would be operational at rest. The second system, represented by the ciliated cell, would normally be regulated or held in check by R cells and would become operational during conditions causing hypersecretion and loss of R cells. The present morphological study did not find clear evidence of a dual secretory system

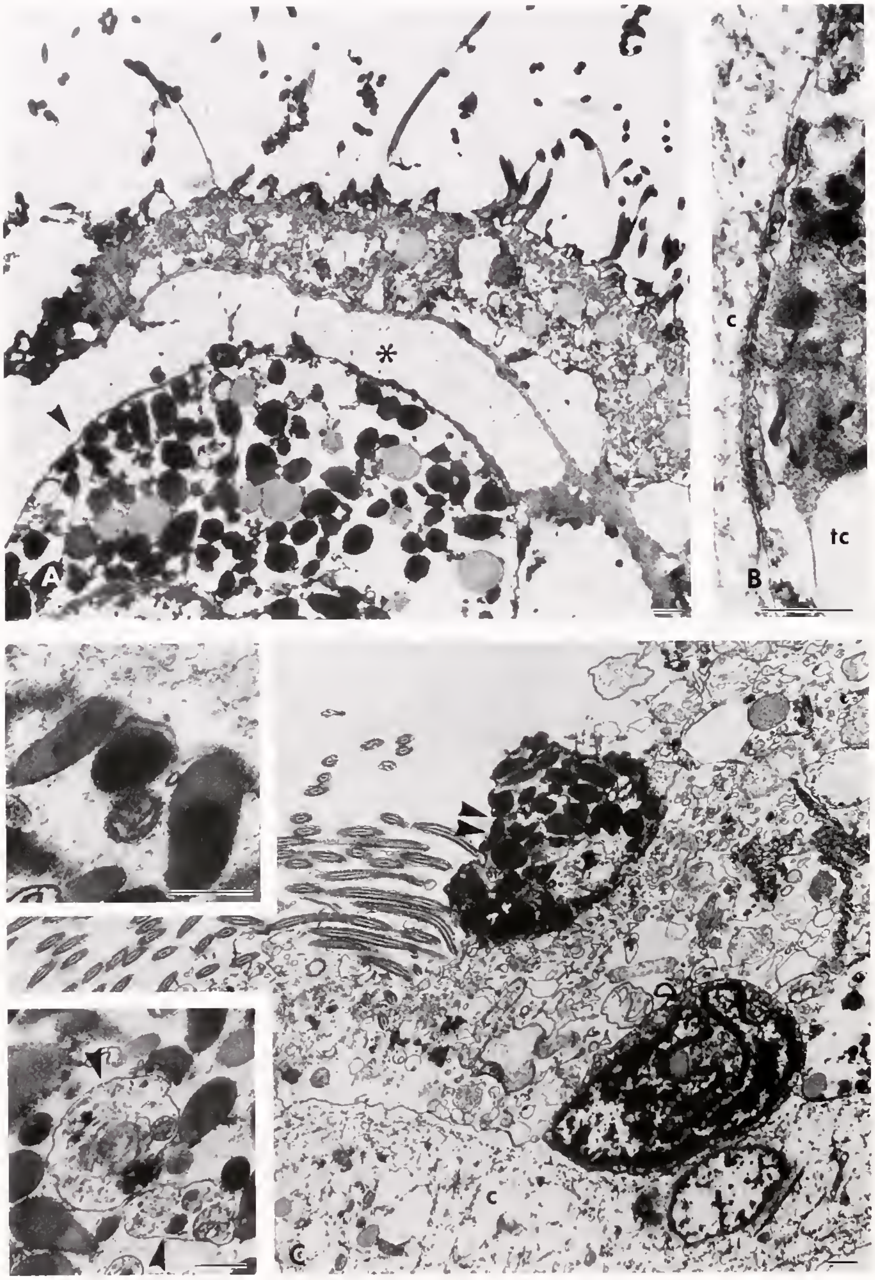

Figure 8. Third-type cell of the urn cell complex (UCC). (A) These cells (arrow) can also be found inside the UCC central space (asterisk). (B) Juxtaposition between ciliated (c) and third-type cell (tc). (C) Two third-type cells 20 min after serum stimulation. The more distal cell (double arrow) contains abundant, lysosome-like granules (upper inset) exhibiting electron-dense cores. Phagocytic vacuoles are also present (lower inset, arrows). c: ciliated cell. All scale bars: 0.5 μm.

in the UCC since release of secretory material from third-type cells could not be documented ultrastructurally at rest or during serum stimulation. Most of the granules of third-type cells had a heterogeneous content and resembled those described in coelomic granulocytes of *Sipunculus nudus* by Valembois and Boiledieu (1980). As in granulocytes, granules of third-type cells often coalesced and became associated with degenerated organelles or engulfed material, indicating phagocytosis. Similar granules, containing enzymes implicated in bacterial killing or in intracellular digestion, have also been described in the coelomic granulocytes of a different sipunculid worm (Dybas, 1981a, b) and in tunicate hemocytes (Sawada *et al.*, 1993).

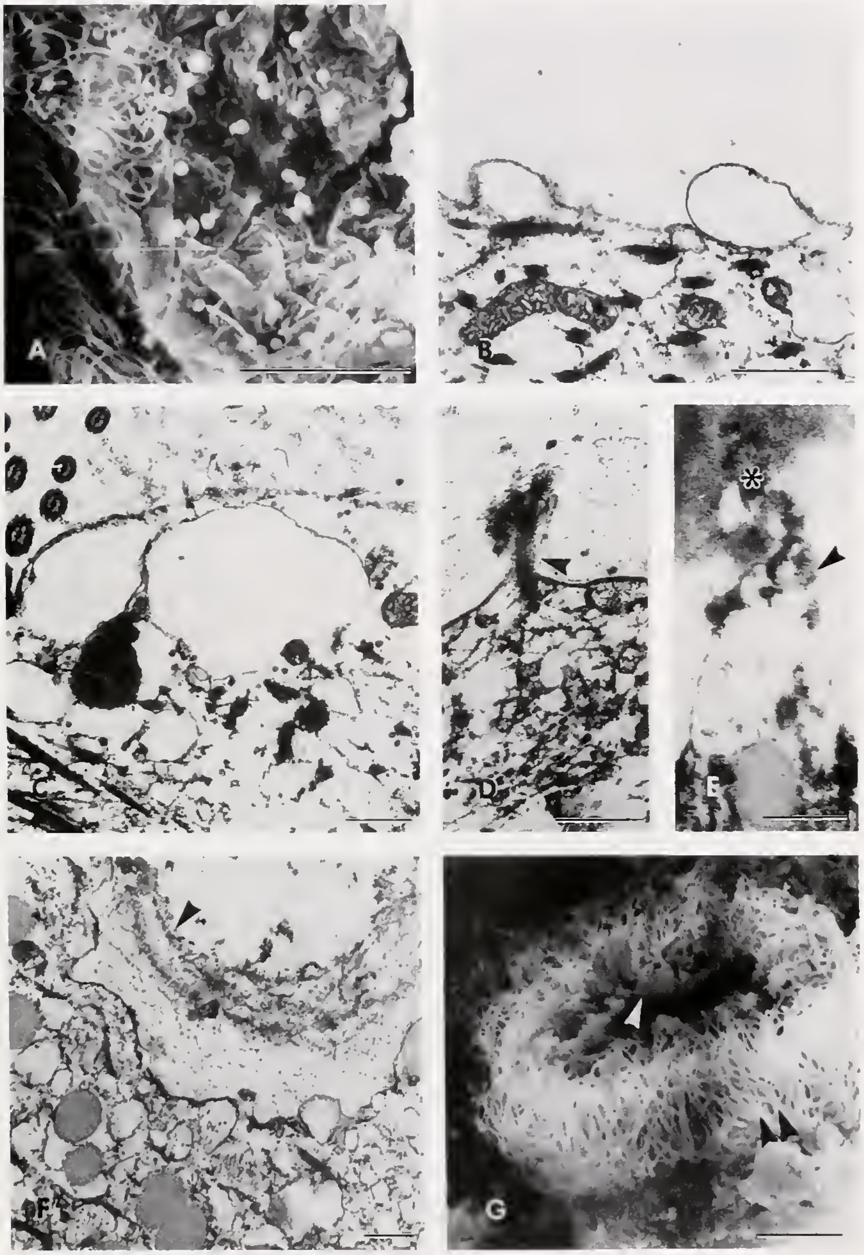

Figure 9. Stimulated urn cell complex (UCC). (A–B) (2 min after exposure to serum). Note bleb-like elevations of cell membrane at the inner side of the ciliated cell. (C) Vacuoles in ciliated cell. (D–E) Tail-on views of UCCs 10 min after exposure to serum. Note electron-dense, fibrillar and granular material seemingly crossing the ciliated cell membrane (D, arrow) or extruding from a distended bleb-like structure (E, arrow) to merge with similar material in a forming tail (E, asterisk). (F–G) Fibrillar material (arrows) surrounding the inner aspect of the mouth-like opening of a UCC 20 min after exposure to serum. Most of the UCC tail has been mechanically removed prior to fixation to better reveal the inner side of the cell. Note also, peripheral and concentric rows of cilia (double arrow). Scale bars: A and G, 10 μm; B–F, 0.5 μm.

Although the present study did not exhaustively characterize either the ultrastructure or the cytochemistry of third-type cells, we suggest that these cells may be macrophages. Clearly, this possibility must be confirmed by functional analysis of living cells and by cytochemical evaluation of third-type cells. We believe that the juxtaposition of third-type cells with the ciliated cell of the UCC does not contradict the phagic nature of third-type cells, since a similar relationship occurs in other mucociliary systems (Jeffery and Reid, 1975; Odor, 1974). The

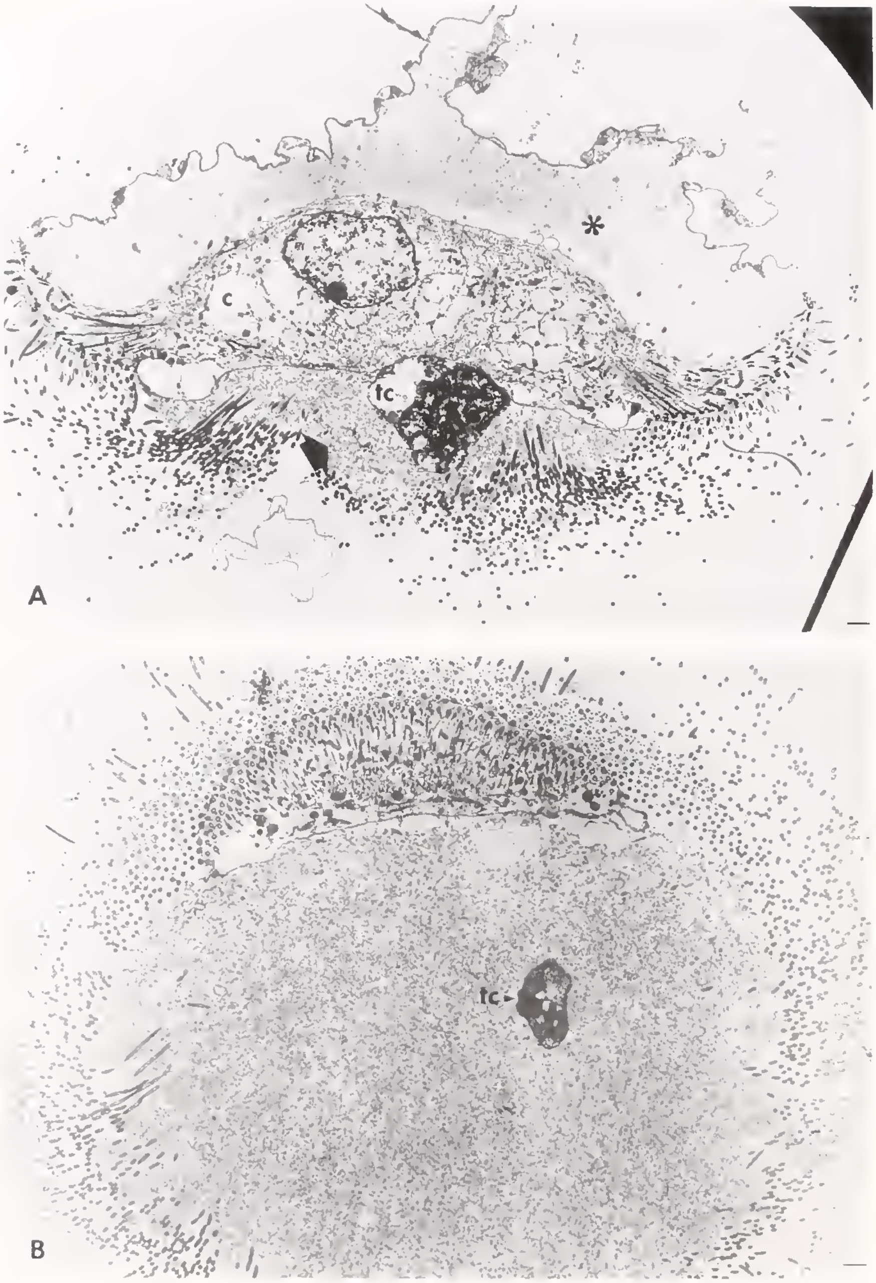

Figure 10. Longitudinal sections of the urn cell complex (UCC) 20 min after exposure to serum. (A) Note moderately electron-dense material within the UCC central space (asterisk) and tail (arrow). c, ciliated cell; tc, third-type cell. (B) Abundant, electron-dense material in released tail of a UCC. tc, third-type cell. Both scale bars: 1 μm.

diversity of cell types in the UCC also suggests some degree of specialization. It is reasonable to assign secretory and locomotory functions to the ciliated component of the UCC. Cilia may also assist the UCC to trap foreign matter and organisms. Third-type cells may phagocytize trapped matter and secrete antibacterial lysins (Bang and Bang, 1962; Dybas, 1981a). These cells may also regulate local secretion (Bang and Bang, 1980). Because the incubation medium we used contained 2% of sipunculid coelomic fluid, the possible contribution of third-type cells and other circulating cellular constituents to tail formation must be investigated further. It is of interest that a lymphoblastoid cell line produces trypsin-sensitive substances that stimulate mucus release in the UCC (Kuleman-Kloene *et al.*, 1982). The role of the vesicle-cell component of the UCC is unclear. This cell encloses a bubble-like space containing diffuse fibrillar material. In UCCs of *Phascolosoma agassizii*, this space contains connecting fibers that may act as a cementing unit to which the various components of the UCC are attached by hemidesmosomes (Dybas, 1976).

The exact composition and precise mode of origin of the tail released by a UCC after serum stimulation have not yet been determined. Until now, it has been maintained that UCC tails have the physicochemical properties of mucus, including viscoelasticity, structure, and mucoprotein content (Bang and Bang, 1978). However, mucolytic agents that reduce disulfide bonds do not consistently solubilize tails of UCCs (Bang and Bang, 1980). Typical mucous secretory granules have not been detected in the ciliated UCC component of two different sipunculid species: *Sipunculus nudus* (this report) and *Phascolosoma agassizii* (Dybas, 1976). Instead, we have observed in this cell numerous deposits of PAS-positive and diastase-resistant fibrillar material. This material was often seen distending the ciliated cell membrane and migrating across it to merge with similar material present within the UCC cavity. A possibility worth investigating is that this filamentous material is related to fibrin and that released tails are not mucous but fibrinous. Certainly, a fibrinous clot may act as well as mucus in trapping foreign matter, and the coelomic fluid of sipunculids has remarkable clotting properties (Dybas, 1981b). The mechanisms regulating the release of UCC tails also remain to be clarified. The marked depletion of glycogen stores in the ciliated cell suggests a requirement for energy supply. It is not clear if synthesis and secretion of tails are coupled or uncoupled processes, although the sustained production of long tails under certain stimuli supports the former possibility (Bang and Bang, 1972).

The urn cell complex of *Sipunculus nudus* is an interesting model for studying invertebrate and vertebrate mucosal defense mechanisms. Work in our laboratory indicates that rabbit endocervical cells respond in similar fashion *in vivo* and *in vitro* to serum and antigenic challenges, suggesting that the defense systems of invertebrates and vertebrates are phylogenetically convergent (Nicosia, 1986; Nicosia *et al.*, 1982).

Acknowledgments

This investigation was partly supported by USPHS Grant HD-06274 Sub-4 during the senior author's (S.V.N.) stay at the University of Pennsylvania. Live specimens of *Sipunculus nudus* or urn cell complexes were obtained through the courtesy of the late Dr. Frederick B. Bang (School of Hygiene and Public Health, Johns Hopkins University, Baltimore, MD) and Dr. Alberto F. Monroy (Zoological Station of the University of Naples, Italy) to both of whom this article is dedicated. The invaluable assistance of Ms. Young Hae Hyun and Mr. Edward Haller with preparation of the microphotographs and Ms. Neisha P. Sun and Mrs. Lydia Hagenkotter with preparation of the manuscript are also gratefully acknowledged.

Literature Cited

Bang, F. B., and B. G. Bang. 1962. Studies on *Sipunculus* blood: Immunologic properties of coelomic fluid and morphology of "urn cells." *Cah. Biol. Mar.* **3:** 363–374.

Bang, B. G., and F. B. Bang. 1964. Mucus hypersecretion in a normally isolated non-innervated cell. *Cah. Biol. Mar.* **6:** 257–264.

Bang, B. G., and F. B. Bang. 1972. Mucus hypersection induced in isolated mucociliated epithelial cells by a factor in heated serum. *Am. J. Pathol.* **68:** 407–422.

Bang, B. G., and F. B. Bang. 1974. Invertebrate model for study of macromolecular regulators of mucus secretion. *Lancet* **ii:** 1292–1297.

Bang, B. G., and F. B. Bang. 1975. Cell recognition by mucus secreted by urn cells of *Sipunculus nudus*. *Nature* **253:** 634–635.

Bang, B. G., and F. B. Bang. 1976. The mucous secretory apparatus of the free urn cell of *Sipunculus nudus*. *Cah. Biol. Mar.* **17:** 423–432.

Bang, B. G., and F. B. Bang. 1978. Successive histochemical changes in mucus secreted by individual cells. *Fed. Proc.* **37:** 266a.

Bang, B. G., and F. B. Bang. 1979. Mucus-stimulating substances in human body fluid assayed in an invertebrate mucous cell system. *Johns Hopkins Med. J.* **145:** 209–216.

Bang, B. G., and F. B. Bang. 1980. The urn cell complex of *Sipunculus nudus*: a model for study of mucus-stimulating substances. *Biol. Bull.* **159:** 571–581.

Catacuzène, J. 1928. Réchérches sur les réactions de immunité chéz les invertebres. Réactions de immunité chéz *Sipunculus nudus*. *Archiv. Roum. Pathol Exp Microbiol.* **1:** 7–80.

Chantler, E., and E. Debruyne. 1977. Factors regulating the changes in cervical mucus in different hormonal states. Pp. 131–141 in *Mucus in Health and Disease*, M. Elstein and D. V. Parke, eds. Plenum Press, New York.

Dybas, L. 1976. A light and electron microscopic study of ciliated urn of *Phascolosoma agassizii* (sipunculid). *Cell Tissue Res.* **169:** 67–75.

Dybas, L. 1981a. Sipunculids and echiuroids. Pp. 161–188 in *Invertebrate Blood Cells*. Vol 1. N. A. Ratchliffe and A. F. Rowley, eds. Academic Press, New York.

Dybas, L. 1981b. Cellular defense reactions of *Phascolosoma agassizii*, a sipunculan worm: phagocytosis by granulocytes. *Biol. Bull.* **161:** 104–114.

Hall, R. L., A. C. Peatfield, and P. S. Richardson. 1978. The effect of serum on mucus secretion in the trachea of the cat. *J. Physiol. (Lond.)* **282:** 477–478.

Hyman, L. H. 1959. *The Invertebrates: Smaller Coelomate Groups.* Vol. 5, pp. 611–695, McGraw-Hill, New York.

Jeffery, P. K., and L. Reid. 1975. New observations of rat airway epithelium: a quantitative and electron microscopic study. *J. Anat.* **120:** 295–320.

Kuleman-Kloene, H., S. S. Krag, and F. B. Bang. 1982. Mucus secretion stimulating activity in human lymphoblastoid cells. *Science* **217:** 736–737.

Kurlandsky, L. E., R. W. Berninger, and R. C. Talamo. 1980. Mucus-stimulating activity in the sera of patients with cystic fibrosis: demonstration and preliminary fractionation. *Pediatr. Res.* **14:** 1267–1268.

Lillie, R. D. 1965. *Histologic Technic and Practical Histochemistry,* p. 38. McGraw-Hill, New York.

Luna, L. G. 1968. *Manual of Histologic Staining Methods of the Armed Forces Institute of Pathology,* 3rd ed. McGraw-Hill, New York.

Luft, J. M. 1961. Improvements in epoxy resin embedding methods. *J. Biophys. Biochem. Cytol.* **9:** 409–414.

Mastroianni, L., Jr., S. V. Nicosia, and E. Streibel. 1979. Studies on urn cell complexes of *Sipunculus nudus* (Linnaeus): influence of physiologic and pathologic mammalian sera on mucus secretion. *Biol. Bull.* **157:** 381a.

Nicosia, S. V. 1979. Lectin-induced mucus release in the urn cell complex of the marine invertebrate *Sipunculus nudus* (Linnaeus). *Science* **206:** 698–700.

Nicosia, S. V. 1986. Physiology of cervical mucus production. *Sem. Reprod. Endocrinol.* **4:** 313–321.

Nicosia, S. V., and J. Sowinski. 1979. Ultrastructure of urn cell complexes of *Sipunculus nudus* (Linnaeus) before and after serum-induced mucus release. *Biol. Bull.* **157:** 385a.

Nicosia, S. V., J. H. Johnson, E. J. Streibel, and L. Mogul. 1982. Serum-induced hypersecretion in isolated and native rabbit endocervical mucous cells. *EMSA* **40:** 244–245.

Odor, L. 1974. The question of "basal" cells in oviductal and endocervical epithelium. *Fertil. Steril.* **25:** 1047.

Reissig, M., B. G. Bang, and F. B. Bang. 1979. Mucus secretion in the urn cell complex of *Sipunculus nudus. J. Cell Biol.* **83:** 433a.

Reynolds, E. S. 1963. The use of lead citrate at high pH as an electron opaque stain in electron microscopy. *J. Cell Biol.* **17:** 208–212.

Richardson, P. S., and R. J. Phipps. 1978. The anatomy, physiology, pharmacology and pathology of tracheobronchial mucus secretion and the use of expectorant drugs in human disease. *Pharmacol. Ther.* **3:** 441–479.

Sawada, T., J. Zhang, and E. L. Cooper. 1993. Classification and characterization of hemocytes in *Styela clara. Biol. Bull.* **184:** 87–96.

Valembois, P., and D. Boiledieu. 1980. Fine structure and functions of haemerythrocytes and leucocytes of *Sipunculus nudus. J. Morphol.* **163:** 69–77.

Reference: *Biol. Bull.* **188:** 281–292. (June, 1995)

Calcitic Nacreous Ultrastructures in Bryozoans: Implications for Comparative Biomineralization of Lophophorates and Molluscs

MICHAEL J. WEEDON AND PAUL D. TAYLOR

Department of Palaeontology, The Natural History Museum, London SW7 5BD, U.K.

Abstract. The occurrence of nacreous-type fabrics in bryozoans has broad implications for our understanding of similarities between lophophorate and molluscan biomineralization. Calcitic semi-nacreous ultrastructures in the skeletons of several species of cyclostome bryozoans belonging to the suborders Tubuliporina and Articulata are described. In these taxa semi-nacre is the dominant ultrastructure of the walls, and often succeeds a precursory fabric of tiny wedge-shaped crystallites. The semi-nacre comprises laminar sheets of irregularly stacked, typically six-sided tablets with frequent screw dislocations. Tablets usually have inclined edges and an upper surface with a central depression. The surfaces of etched six-sided tablets have six subtriangular sectors: three soluble sectors alternating with three less-soluble sectors. The less-soluble sectors have outward-sloping edges and sometimes have slightly longer sides than the more soluble sectors, which have inward-sloping edges. Newly seeded crystallites comprise only the three less-soluble sectors separated by a 'trilete' suture. They are not nucleated on a particular sector type. Similar fabrics have previously been recorded in the cyclostome suborder Cancellata. The substructure of the calcitic semi-nacreous tablets of cyclostomes resembles molluscan aragonitic nacre, particularly that of bivalves, but differs in the precise arrangement of the sectors. Morphologically, the bryozoan semi-nacre is at least as similar to bivalve nacre as bivalve nacre is to gastropod and cephalopod nacre. The existence of a distinct substructure in the component tablets of molluscan nacre has been used as evidence that a greater evolutionary potential characterizes molluscan rather than lophophorate (bryozoans and brachiopods) biomineralization. This claim is contradicted by the recognition of substructured semi-nacre in cyclostome bryozoans.

Introduction

Processes involved in the secretion of mineralized hard parts in the shells and skeletons of invertebrates are poorly understood. This is true even in phyla such as molluscs for which there is a large literature on biomineralization. We are still documenting basic ultrastructural patterns for bryozoans and some other groups. Bryozoans are a diverse biomineralizing phylum. The great majority of the estimated 5,000–10,000 species of living bryozoans (Horowitz and Pachut, 1992) secrete calcareous skeletons. The ability to do so probably evolved at least twice from soft-bodied ancestors (Taylor and Larwood, 1990), first in the Ordovician (c. 500 million years ago) and subsequently in the Jurassic (c. 150 million years ago). The earlier of these events marked the origin of the class Stenolaemata, of which the Cyclostomata are the only extant order; the later event marked the origin of the order Cheilostomata (of the class Gymnolaemata).

Recent research on the skeletal ultrastructure of cyclostome bryozoans has revealed an unanticipated diversity of calcitic fabrics (*e.g.*, Boardman *et al.*, 1992; Taylor and Jones, 1993; Taylor *et al.*, 1995). Earlier studies of cyclostomes largely employed fractured and polished or etched sections and provided only limited information. However, by examining the surfaces of skeletal walls upon which crystallites are directly secreted and grow, the range of fabrics, as well as the pattern of their growth, can be appreciated more fully. The emergence of a new database of bryozoan skeletal ultrastructures enables broader questions of biomineralization to be addressed. In particular, comparisons of the patterns and processes of biomineralization of bryozoans and molluscs can be reassessed.

Received 5 October 1994; accepted 20 March 1995.

Models of skeletal growth developed from brachiopods (the other lophophorate phylum with biomineralized skeletons) are commonly applied to bryozoans (*e.g.*, see Williams, 1990a, b). However, the intricate nature of the bryozoan skeleton entails a more complex pattern of skeletal development than the essentially linear, two-dimensional growth of brachiopod shells. A diversity of fabrics distinct from those of brachiopods is beginning to be recognized in bryozoans. The combination of brachiopods and bryozoans within a single unified secretory model and the relative dearth (in comparison with molluscs) of studies of bryozoan ultrastructures have contributed to the theory that lophophorates are incapable of producing the range and diversity of skeletal ultrastructures found in molluscs (Carter, 1979; Carter and Clark, 1985).

Indeed it has been argued that all skeletal ultrastructural types that occur in lophophorates are also present in molluscs, whereas molluscs have evolved a number of ultrastructures that do not occur in lophophorates (Carter, 1979; Carter and Clark, 1985). This phenomenon has been termed the "L-M discontinuity" (*i.e.*, lophophorate-molluscan discontinuity; Carter and Clark, 1985). It has been particularly stressed that, unlike molluscs, lophophorates generally lack the capacity to form organizationally complex ultrastructural units oriented in all three dimensions of the shell layer (Carter, 1979; Carter and Clark, 1985).

One ultrastructure commonly regarded as being unique to molluscs is nacre, or "mother-of-pearl." Nacre is the best known and most thoroughly studied calcareous fabric in mollusc shells (Taylor *et al.*, 1969; Wise, 1970a). True nacre is, by definition, always an aragonitic structure consisting of thin, flat-lying, platey laminae built up from polygonal to rounded tabular crystals. The tablets and laminae are separated from each other by thin layers of organic matrix. Different structural patterns of this organic matrix are found in nacres from the molluscan classes Bivalvia, Gastropoda, and Cephalopoda (*e.g.*, Grégoire *et al.*, 1949, 1950, 1955; Grégoire, 1957, 1959), and the arrangement of the aragonitic tablets also varies considerably between and within these classes (Wise, 1970a, b; Carter, 1990). Columnar nacre, where the tablets are arranged in vertical stacks, is the most common nacreous fabric among gastropods and cephalopods. Sheet nacre, with tablets in vertical sections in a stair-step or brick-wall pattern, is the common fabric of bivalves and monoplacophorans and occurs less commonly in cephalopods and only rarely in gastropods (Wise, 1970a, b; Carter and Clark, 1985). Hybrid structures—row stack nacre—may also occur in some bivalves, as may columnar nacre (Carter and Clark, 1985; Carter, 1990).

Differences can also be found between the molluscan classes in the internal substructure of the nacreous tablets. These are revealed by differential chemical etching of the tablet surfaces (Mutvei, 1977, 1978, 1980, 1983a, b). Mutvei suggested that rather than being single crystals of aragonite, the tablets are compound structures composed of "crystal individuals" of different orientation, possibly twinned. The arrangement of the crystal individuals is related to the distribution of new seeds and therefore to the structure of the underlying layer of nacre. Aragonitic nacre is apparently restricted to the Mollusca. However, semi-nacre, which may be calcitic or aragonitic, is found in some other taxonomic groups. Semi-nacre is characterized by sheets of horizontal tablets with higher frequencies of screw dislocations and perhaps less structural continuity of the laminae than in nacre *sensu stricto*. The structure has been recorded in the calcitic craniacean brachiopods (Williams, 1970; Williams and Wright, 1970, pl. 6, figs. 3, 4) and in the Carboniferous archaeogastropods *Platyceras* (*Orthonychia*) *spinigerum* and *Cyclonema* (Batten, 1984; Carter and Hall, 1990). Many laminar fabrics described in bryozoans (*e.g.*, Sandberg, 1971, 1977, 1983; Tavener-Smith and Williams, 1972; Ristedt, 1977; Ross, 1977) were reinterpreted as semi-nacre by Carter and Clark (1985), but none have been fully described nor properly compared with molluscan nacres.

New investigations of cyclostome bryozoans have shown that calcitic semi-nacre is widespread, particularly in the fixed-walled suborders Tubuliporina and Articulata. These fabrics are described here for the first time. The organization of cyclostome semi-nacres shows considerable similarity to irregularly stacked aragonitic nacres in some molluscs. Importantly, the tablets are subdivided into sectors or crystal individuals in a very similar way to those of molluscan nacre. The resemblance between the semi-nacre of cyclostome bryozoans and the nacre of molluscs has important implications for the comparative organizational control of skeletal ultrastructures in the two groups. Discovery in bryozoans of more diverse and complex ultrastructures may be indicative of a "greater evolutionary potential" for biomineralization (in the sense of Carter and Clark, 1985) than has been previously acknowledged.

Previous work on bryozoans

Semi-nacreous structures are characterized by growth surfaces with irregularly arranged platey tablets. The tablets are roughly hexagonal, rhombic, or sub-rounded in outline. Screw dislocations are much more frequent than in nacre *sensu stricto*. Using these criteria, Carter and Clark (1985) categorized structures illustrated in various studies of bryozoan ultrastructures as semi-nacreous. These included the cheilostomes *Membranipora* [*Biflustra*] *savartii* (Ristedt, 1977, p. 88; pl. 4, figs. 3, 4, 6; pl. 5, figs. 1–8), *Labioporella calypsonis* (Sandberg, 1977), *Cupuladria biporosa* (Tavener-Smith and Williams, 1972, pl. 13, fig. 45), and *Thalamoporella californica* (Sandberg, 1971, p. 136, pl. 2, fig. 12). In addition, similar fabrics have also been described by Sandberg (1983) in the cheilostomes *Metrarabdotos tenue* (fig. 102, 1, 2), *Tremogasterina robusta* (fig. 102, 3, 4), and *Arachnopusia unicornis* (fig. 102, 5).

Despite Carter and Clark's assignment of the fabrics described in cyclostomes by Ross (1977) to semi-nacre, the first well-supported claim of semi-nacre in cyclostomes was made by Taylor and Jones (1993) for *Hornera robusta* and *H. squamosa* (suborder Cancellata). These free-walled cyclostomes have laminated walls comprising sub-hexagonal tablets, often with characteristic triple spikes located at their centers. The tablets are initially about 0.5 μm in diameter and are best seen near distal wall margins where seeding is concentrated. Small seeds in *H. squamosa* show radial sectoring with three roughly surfaced sectors alternating with three smooth sectors. Only the three rough sectors reach the centers of the tablets where their junction forms a "trilete" structure. Screw dislocations are also common near the distal edges of walls. With increasing maturity the crystallites broaden and may coalesce. A pattern of predominantly proximally imbricated crystallites characterizes older, more proximal walls. Taylor and Jones (1993) suggested that this mature fabric was regularly foliated in the sense of Carter *et al.* (1990).

Other investigations of cyclostome skeletons have failed to reveal unequivocal semi-nacre. In his study of the articulate *Crisia eburnea*, Söderqvist (1968) described an inner fabric of polygonal, tabular crystals, stacked like roofing tiles, and found a similar fabric in the skeletons of *Stomatopora* sp., *Diplosolen intricarius* (Smitt), *Idmonea* [*Idmidronea*] *atlantica* Forbes in Johnston, and *Heteropora pelliculata* Waters. Brood (1976) also described the skeleton of *C. eburnea* as having a laminar secondary (inner) layer, illustrating (figs. 5–6) overlapping, imbricated tablets.

Material and Methods

Eight species of the suborder Tubuliporina were studied for this paper. The following six species were collected from the Marseille region of southern France by J-G Harmelin: *Plagioecia patina* (Lamarck) from Rech Lacaze-Duthiers at a depth of 300 m; *P. dorsalis* (Waters) from Morgiou at a depth of 40 m; *Desmeplagioecia amphorae* Harmelin from Moyadon Island at a depth of 27 m; *"Cardioecia" watersi* (O'Donoghue and de Watteville) from Jarre Island, cave II, at a depth of 15 m; *Entalophoroecia deflexa* (Couch) from Riou Island at a depth of 30 m; *Platonea stoechas* Harmelin from Canyon Cassidaigne at a depth of 140–170 m. In addition, colonies of *Diplosolen* cf. *obelium* (Johnston) were collected by P. J. Hayward from Emborios Cave on the Greek (Aegean) island of Chios, and *Stomatopora* sp. by PDT from the Otago Shelf (80–100 m), New Zealand.

Four species from the suborder Articulata were also used in the study, three of them collected by J.-G. Harmelin from Riou Island, near Marseille, at a depth of 30 m: *Crisia fistulosa* Heller, *C. sigmoidea* Waters, and *C. oranensis* Waters. Additionally, *Bicrisia* cf. *edwardsiana* MacGillivray was collected by PDT from shoreline drift on the Otago Peninsula, New Zealand.

Colonies were air dried after collection and subsequently soaked in a 20% volume/volume solution of commercial bleach for 48–72 h depending on the thickness of enveloping organic cuticle. The combination of bleaching and periodic ultrasonic cleaning and rinsing in distilled water facilitated the removal of organic material from the calcite skeleton. Air-dried, bleached colonies and broken or sawn parts of colonies were mounted on stubs and sputter-coated with gold-palladium. Stubs were examined with a Hitachi S-800 field emission scanning electron microscope at an accelerating voltage of 8 kV and imaged using secondary electrons. Most detail was derived from observing growth surfaces preserving original crystallite fronts.

Results

All of the species studied have complex skeletons comprising more than one ultrastructural fabric, but semi-nacre dominates, occurring as the inner fabric of frontal exterior walls (Fig. 1) and peristomes (walls initially secreted directly onto the cuticle). Full details of the ultrastructural compositions of the skeleton in the various species will be given in future papers. This paper focuses on the semi-nacre. However, it is necessary to describe first the precursory fabric of the interior walls laid down prior to the semi-nacre.

Precursory fabric

Interzooidal walls originate as ridges (septa) on the upper surface of the basal or frontal exterior walls. In the tubuliporines studied, the ridges comprise densely packed, tiny, wedge-shaped crystallites (0.1–0.3 μm in width and up to 0.6 μm in length) with no preferred orientation or alignment (Figs. 2, 4). The wedges are highly variable in size, with the smallest wedges at the distalmost edge of the ridges being secreted on top of progressively larger wedges, suggesting continued growth after initial seeding. Identical crystallites occur along the apertural margins of newly formed zooids, and at the distal edge of the median budding wall in those taxa (*Plagioecia dorsalis* and *"Cardioecia" watersi*) where this structure is present. Precursory fabric is absent in newly formed septa of articulates, the leading edges of the walls being formed of semi-nacre.

Semi-nacreous fabric

The bulk of the walls comprise laminar sheets of semi-nacre (Fig. 5). The structure of this semi-nacre is described

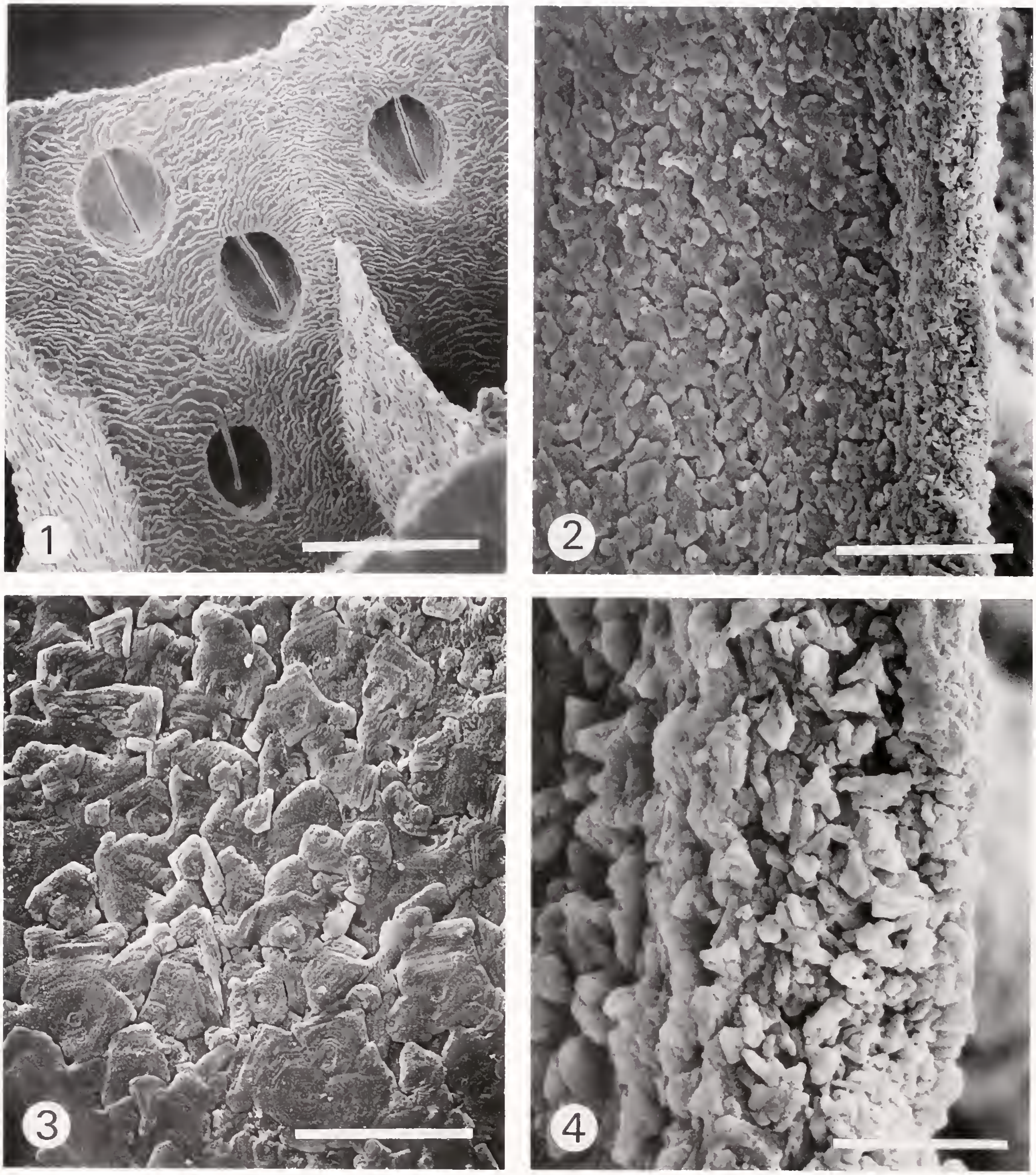

Figures 1–4. Scanning electron micrographs of precursory and semi-nacreous fabrics in the articulate *Crisia* cf. *sigmoidea* (Fig. 1) and the tubuliporine *Platonea stoechas*. (Fig. 2–4).

Figure 1. Inside surface of frontal exterior wall with large pseudopores. Note the distally imbricated, "pseudofoliated" semi-nacreous fabric. Tablets curve around and are smoothly continuous between the frontal wall and vertical interior walls. Distal is towards the top. Scale bar = 25 μm.

Figure 2. Distal growing edge of interior wall, showing the precursory fabric of tiny wedge-shaped crystallites, succeeded by a highly irregular semi-nacreous fabric largely comprising more or less anhedral tablets, which increase in size proximally. Distal is to the right. Scale bar = 7.5 μm.

Figure 3. Irregular semi-nacreous fabric. Despite their anhedral outlines, the tablets have internal growth lines delineating euhedral hexagons. Note central depressions in a number of the tablets. Distal is towards the top. Scale bar = 6 μm.

Figure 4. Detail of wedge-shaped crystallites of precursory fabric shown in Figure 2. Scale bar = 2 μm.

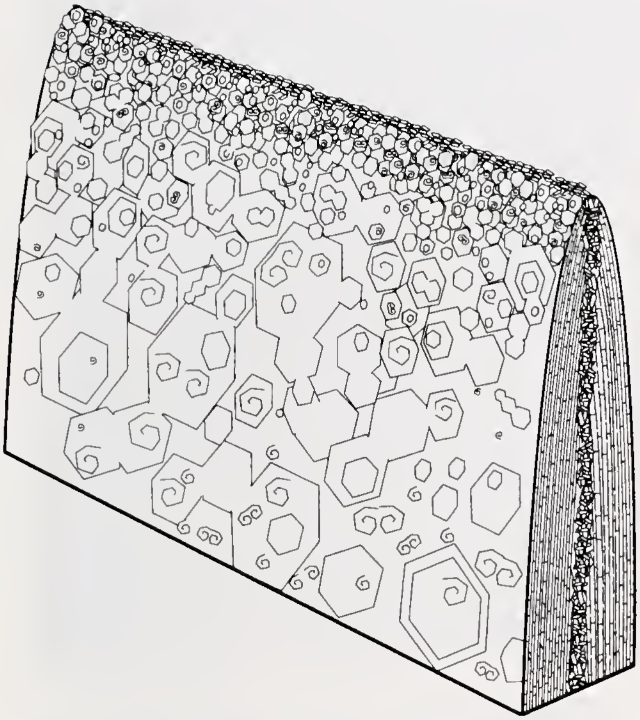

Figure 5. Stylized diagram of the growing edge of an interior wall in a semi-nacre dominated cyclostome. Tiny wedge-shaped crystallites lacking a preferred orientation are seeded at the distalmost edge of the wall. Further seeding of flat hexagonal tablets follows and continues throughout the growth of the wall. Tablets grow by accretion on all sides. Screw dislocations are common and are the dominant mechanism for wall thickening in the older parts of the skeleton.

along a transect running proximally from the distalmost edge of the growing wall.

Immediately proximal to the wedge-shaped crystallites, and overlying them, is a transitional zone of tiny crystallites (up to 2 μm diameter). These flat-lying crystallites are about 0.2 μm thick, have no preferred growth direction, and appear to be randomly distributed (Fig. 2). The boundaries between crystallites are not well-defined: there is considerable overlap or lateral fusion with neighboring crystallites on all sides.

Tablets become better defined further proximally, where they are generally six- or four-sided. On some wall surfaces the tablets are euhedral (Fig. 6, 8): edges are straight and have angular intersections with adjacent edges. On other wall surfaces, however, tablets are anhedral and have subcircular outlines (Fig. 7). The angles between the edges of euhedral hexagonal tablets consistently approximate 120°. In *Platonea stoechas* the mean value was 121.3° (SD = 7.57°; range = 108–137°; n = 56). Tablet surfaces often have very fine, concentric growth lines, showing that radial growth rates were equal in all directions (Fig. 3). Surfaces may also have fine striations perpendicular to these growth lines (Fig. 9). Tablets usually have a gently concave upper surface, with a slight depression at the center. This is particularly apparent on larger crystallites where the central depression may be up to 1 μm in diameter. Newly seeded tablets (less than 0.5 μm in diameter) are distributed without apparent pattern over the surfaces of larger, older tablets. The size of the tablets on any given surface varies considerably. Tablets fuse laterally with neighbors on the same level to form sheets or laminae. The contact suture between fused tablets is visible as a very thin furrow, or as a disruption in the growth lines.

Further proximally still, on more mature wall surfaces, screw dislocations (Fig. 10–13) become very common and are responsible for wall thickening. Seeding is less frequent than in younger walls. The screw dislocations can be either dextral or sinistral spirals. Angles of approximately 120° usually occur between adjacent edges of euhedral spiralled crystallites. Anhedral spirals may also be found. Screw dislocations often occur in congruent groups in which different screws have parallel edges and the same direction of spiralling. Frequently two screw dislocations with opposite coiling directions are linked together to form a double scroll-shape (Fig. 10).

In older walls, well proximal of growing edges, large areas of the wall surface may be covered by crystallites that have undergone multiple divisions by screw dislocation, or by step-like splitting. These surfaces may show regular imbrication in a predominantly distal direction (Fig. 1). Few centers of screw dislocation are evident and the wall surface resembles a foliated fabric ("pseudofoliated"). The semi-nacre may conform to strongly curved surfaces; for example, laminae wrap around the inner surface of pseudopores in exterior walls.

Tablet surfaces are sometimes partially etched (Fig. 14–17), possibly as a result of deterioration after collection or through bleaching during sample preparation. Six-sided tablets are differentially etched in six alternating triangular sectors. In the three more soluble sectors the tablet surface has a pimpled surface, whereas the surface of the less-soluble sectors remains smooth with well-defined growth lines. Persistent bleaching for long periods causes complete removal of the more soluble sectors, leaving the three less-soluble sectors relatively intact. On unetched wall surfaces sectoring may still be detected because the more soluble sectors have a darker shade under SEM, and the less soluble sectors usually appear to be raised and have better defined growth lines and striations.

In many six-sided tablets three of the growing edges are slightly longer than the other three, giving three alternately narrow and broad sectors. The more soluble sectors in these cases are the narrow sectors; the less soluble are the broad sectors. Only the three less-soluble sectors reach the very center of the tablets. Here the three sectors are separated by "sutures" forming a "trilete" pattern.

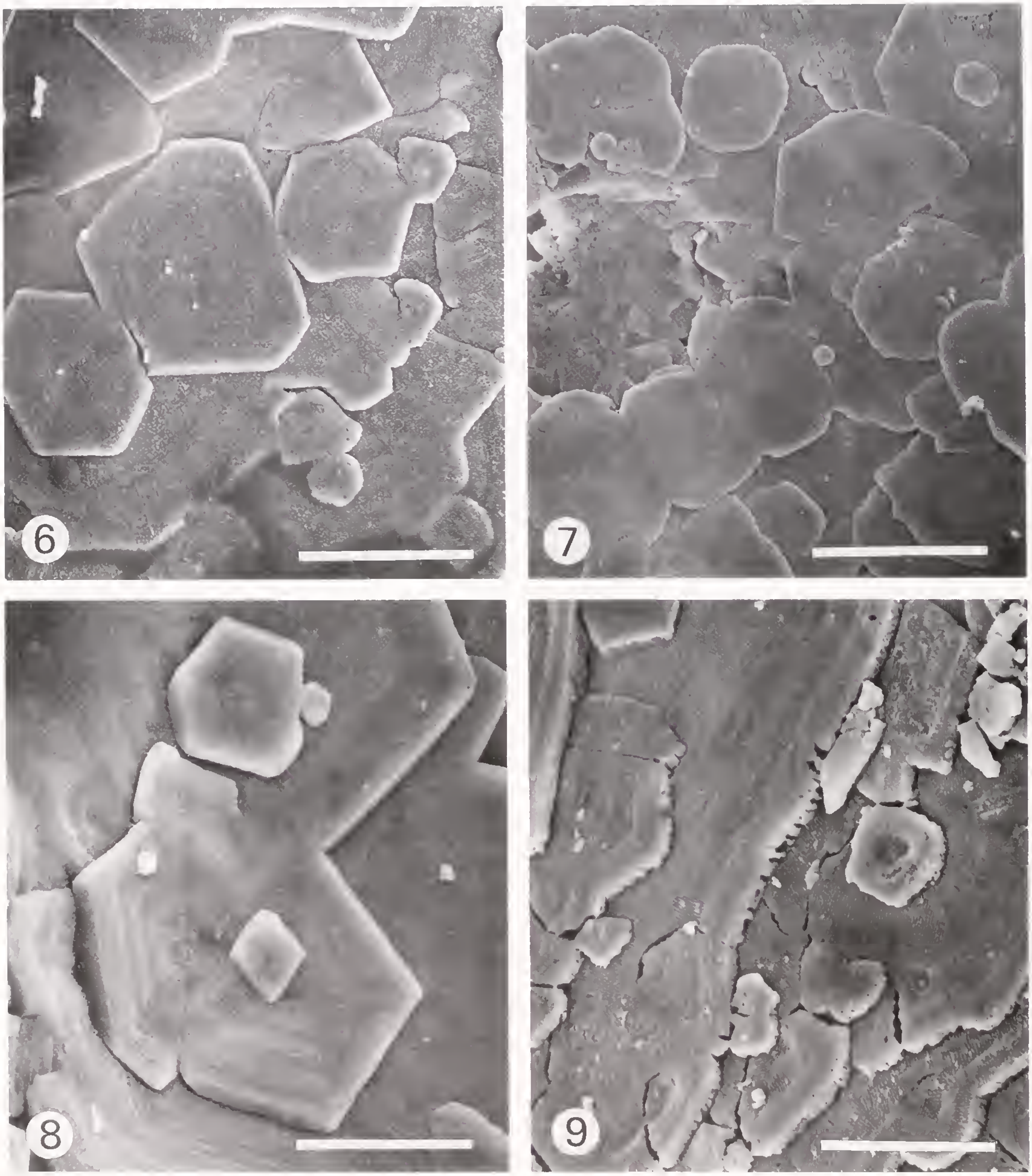

Figures 6–9. Scanning electron micrographs of semi-nacre in the articulates *Bicrisia* cf. *edwardsiana* (Fig. 6, 8) and *Crisia* cf. *sigmoidea* (Fig. 7, 9).

Figure 6. Euhedral hexagonal and sub-hexagonal tablets of semi-nacre. Note differences in the slopes of sector edges and fusion of adjacent tablets to form horizontal sheets. Scale bar = 6 μm.

Figure 7. Laterally fused, anhedral tablets without visible sectoring. Scale bar = 7.5 μm.

Figure 8. Tablets of different ages with sizes ranging from tiny new seeds to broader fused tablets. Note the rhombic form of the central tablet, differences in slope of sector edges and growth lines. Scale bar = 3 μm.

Figure 9. Lightly etched semi-nacre showing well-defined striations perpendicular to tablet edges. Note depressed tablet centers. Scale bar = 3 μm.

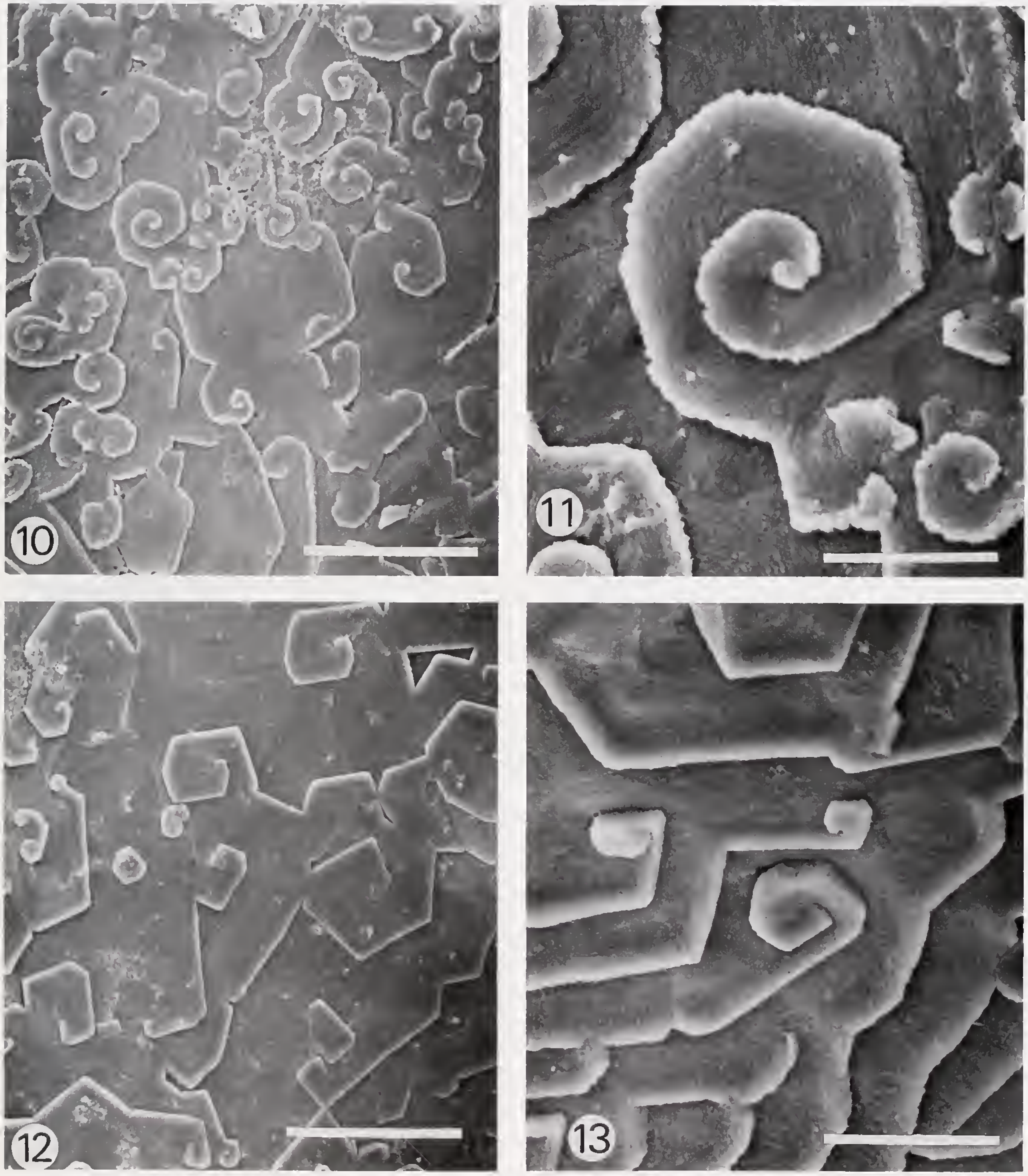

Figures 10–13. Scanning electron micrographs of semi-nacre in *Plagioecia dorsalis.*

Figure 10. Anhedral tablets with abundant screw dislocations, some occurring as pairs with opposite spiral directions. Scale bar = 10 μm.

Figure 11. Detail of screw dislocation from Figure 10. Note the different surface textures of the more-soluble and less-soluble sectors, the former having slightly rougher surfaces with less well-defined growth lines. Scale bar = 2.5 μm.

Figure 12. Euhedral tablets with screw dislocations. Scale bar = 10 μm.

Figure 13. Screw dislocations in imbricated semi-nacre. Scale bar = 4 μm.

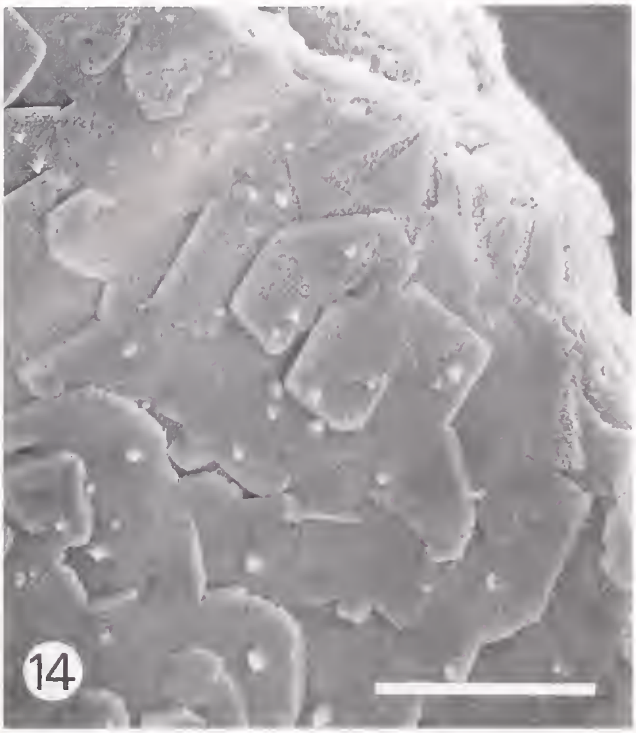

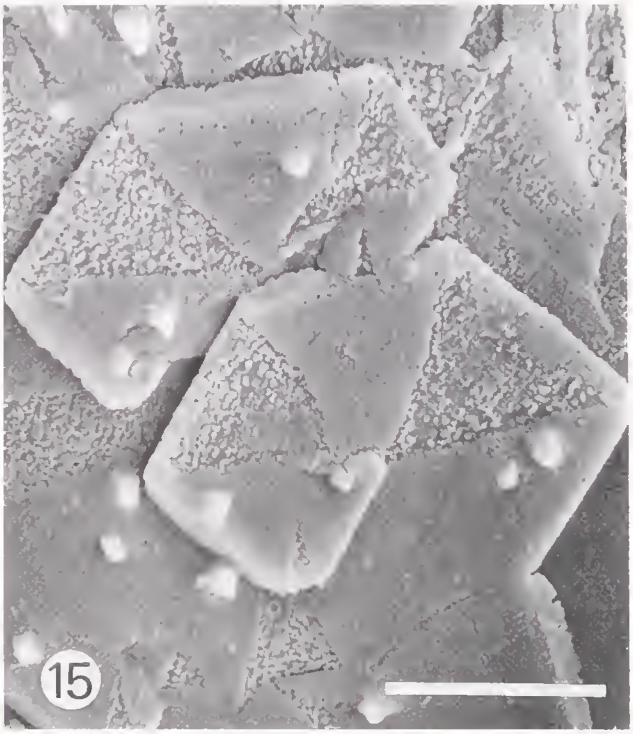

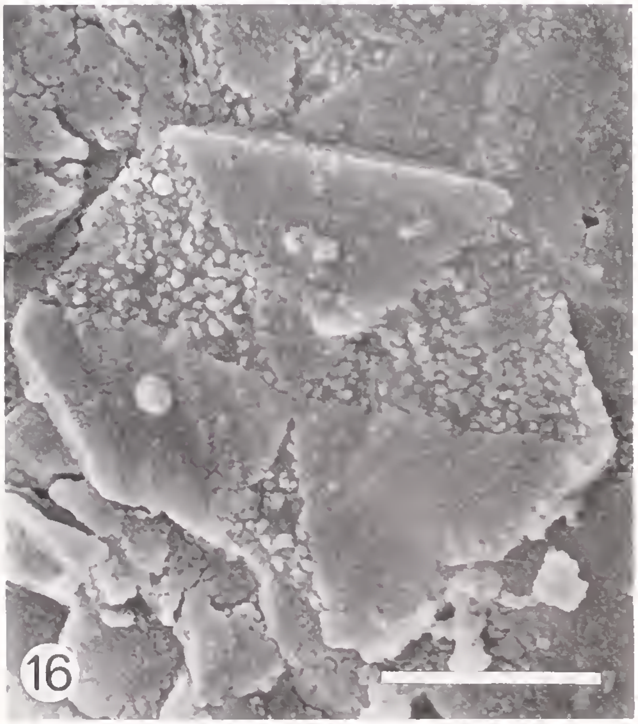

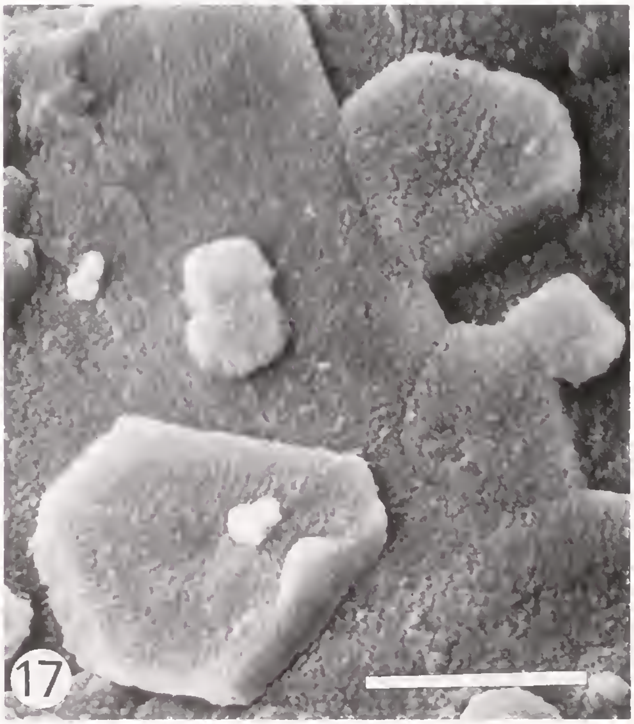

Figures 14–17. Scanning electron micrographs of semi-nacre in the tubuliporine *Platonea stoechas*.

Figure 14. Semi-nacreous fabric near a broken edge of an interior wall. Note screw dislocations, differential etching of tablets, revealing their sectored substructure and spikes predominantly associated with the less-soluble sectors. Scale bar = 6 μm.

Figure 15. Detail of etched tablets that have undergone screw dislocation. Note the parallel alignment of sectors in different layers of the screw dislocations as well as between adjacent screws, perhaps indicating crystallographic continuity. The more-soluble sectors are narrower than their less-soluble neighbors and have edges with different slope angles. Scale bar = 2.5 μm.

Figure 16. Heavily etched tablet showing differentiation of less-soluble and more-soluble sectors. The broader, less-soluble sectors meet at the center of the tablet with a trilete suture. Growth lines and perpendicular striations are most clearly seen on the less-soluble sectors. Scale bar is 2 μm.

The three more soluble sectors first appear about 0.1–0.3 μm outward from the centers of the tablets.

The bounding edges of the tablets are not perpendicular to the upper surface but are inclined at an angle, producing a "bevelled edge." The angle of inclination differs in the three less-soluble and the three more-soluble sectors. The edges of the more-soluble sectors slope inwards to form an overhang, whereas those of the less-soluble sectors slope outwards.

In some species (*Platonea stoechas*, *Crisia* spp.), tiny spikes occur on the surfaces of tablets (Fig. 14–16). The spikes are up to 1 μm long (usually <0.5 μm). They occur in highest concentrations inside interzooidal pores and around pustules (short mural spines). The great majority of spikes arise from the less-soluble sectors, and sometimes can be observed to originate along the growing edges of the tablets.

Discussion

Comparison with other cyclostome bryozoan ultrastructures

The wall structure described here comprises thin hexagonal or sub-hexagonal tablets arranged in horizontal sheets, or laminae. The platey tablets are arranged in well-defined laminar sheets but do not form regular columnar stacks, brick-wall, or row stack patterns. The abundance of screw dislocations and steps, the disordered distribution of newly seeded crystallites, the arrangement of the tablets, and the calcitic mineralogy permit the fabric to be characterized as semi-nacre (*sensu* Carter and Clark, 1985; Carter *et al.*, 1990).

The interior walls of tubuliporines with predominantly semi-nacreous skeletons comprise two types of ultrastructural fabric: an initial precursory fabric of wedge-shaped crystallites, which is succeeded by a fabric of flat-lying, hexagonal semi-nacreous tablets. A fabric of wedge-shaped crystallites also occurs as the initial layer in the interior walls of lichenoporids (Taylor *et al.*, 1995). In these free-walled cyclostomes (suborder Rectangulata) there is a gradation between the granular fabric and a succeeding foliated fabric of elongate crystallites that are distally oriented and imbricated. A very similar gradation has been found in the basal wall of tubuliporines (Weedon and Taylor, unpubl.). Crystallite seeding in lichenoporids is almost totally restricted to the initial layer of wedges, with the succeeding platey laminae developing by accretion of the wedges. In the interior walls of the tubuliporines described here, however, the platey crystallites succeeding the wedges are discrete tablets that accrete radially and initially lack a parallel growth orientation or imbrication. Seeding is of two types: as wedge-like laths in the initial layers of the walls, and as the hexagonal tablets in the succeeding platey layer. Thickening of the walls occurs by continued seeding of new tablets as well as by screw dislocations and divisions of the tabular crystallites. Parallel growth of imbricated crystallites can develop in older walls where screw dislocations are few and a pseudofoliated fabric appears.

The semi-nacreous structure is very similar to that described in *Hornera* (Taylor and Jones, 1993), a free-walled cyclostome belonging to the suborder Cancellata. In *H. robusta* MacGillivray the tablets are characterized by distinctive spikes, usually arranged as triplets at the center of the tablets, and always arising from the less-soluble sectors. These spikes are similar in size and shape to the single spikes found in some tubuliporines and articulates but differ in their location in the middle of the tablets as well as their increased abundance in areas of new seeding. Spikes are largely absent in older, more mature walls.

Seeding of new crystallites in hornerid semi-nacre is concentrated at the distal edges of walls. Subsequently, a pseudofoliated fabric quickly develops, with the imbricated crystallites growing predominantly proximally (Taylor and Jones, 1993). In the tubuliporines and articulates described here, most seeding similarly occurs near the distal edges of walls, but seeding can also be found in more mature areas where screw dislocations provide the dominant means of wall thickening.

Like tubuliporines and articulates, the semi-nacreous tablets of hornerids are subdivided into alternating triangular sectors that are susceptible to different degrees of surface etching. [Note that the more-soluble sectors described in tubuliporines and articulates are the equivalent of the "smooth-surfaced sectors" of hornerids described by Taylor and Jones (1993; p. 136); the relative smoothness of the more-soluble sectors in hornerids is probably a consequence of greater etching of these sectors.] On very small, relatively young tablets, the three less-soluble sectors reach the center of the crystallite where their contact forms a trilete "suture." The more heavily etched sectors do not reach the center of the tablets but appear slightly later in crystal growth (Taylor and Jones, 1993). Screw dislocations are quite frequent in hornerid semi-nacre. Hence

Figure 17. Lightly etched sub-hexagonal tablets newly seeded upon a sheet of fused tablets. The edges of the less-soluble sectors slope outwards and downwards. The more-soluble sectors are narrower and their edges form overhangs. Note the striations perpendicular to the edges, the development of a spike on the lower right hand edge of tablet at bottom left, and the slight depression in the center of the tablets. Scale bar is 1.5 μm.

the semi-nacre of tubuliporines and articulates is a very similar fabric to that of hornerids. However, tubuliporine and articulate semi-nacre differs in the absence of triple spikes, the more widespread occurrence of seeding and screw dislocation, and in the predominantly distally imbricated pseudofoliated fabric of the mature skeleton.

The close similarity of the semi-nacres of tubuliporines and articulates has potential as a synapomorphic character shared by the two suborders. With further investigation of fossil and Recent cyclostomes it should be possible to evaluate this and other skeletal ultrastructures as phylogenetic characters.

Comparison with molluscan nacres

The subdivision of the cyclostome bryozoan tablets into alternating soluble and less-soluble sectors has important bearing on the relationship between cyclostome calcitic semi-nacre and molluscan aragonitic nacres. Mutvei (1977, 1978, 1980, 1983a, b) has described a range of internal sectoring and substructures in molluscan aragonitic nacre, using gluteraldehyde etching to enhance the differences in the radial sectors. Importantly, different tablet substructures occur in different molluscan classes (Fig. 18B, C). In bivalves (specifically *Mytilus, Nucula,* and *Unio*), the etched hexagonal tablets are subdivided into four "crystal individuals" or sectors, which Mutvei suggested were probably cyclically twinned (Fig. 18B). The crystals represent two structurally distinct pairs, with the individuals of each pair arranged opposite each other. One of the pairs comprises relatively insoluble triangular sectors with a central angle of about 64°. These crystal individuals are more or less fused at the center of the tablet. The other pair of crystal individuals are rhombic in outline with a central angle of about 116°. They lack the lamellar substructure and are much more soluble. It is possible that the rhombic crystal individuals are really two adjacent triangular sectors (H. Mutvei, *pers. comm.,* 1994). Etching enhances concentric "lamellae" on the tablet surface, just as in bryozoan semi-nacre. Nucleation, or seeding, of new tablets occurs invariably on the relatively insoluble sectors. Hence a more or less regular brick-wall or staircase pattern of arrangement of the tablets is generated. The tablets have inclined edges so that in side view incipient tablets have a sub-pyramidal shape with a broader diameter at the base than at the top. The inclination of the edges may be as great as 40°. In some tablets the direction of inclination is reversed, with the broader diameter being on the top surface. The tablets have a concave upper surface with a central depression.

In gastropods (specifically *Gibbula, Calliostoma, Trochus,* and *Haliotus*) the tablets comprise radial sectors of polysynthetically twinned individuals (usually 1 to 6 pairs but exceptionally up to 25 pairs), separated by thin vertical organic partitions (Mutvei, 1978; Fig. 18C). The center of the tablets has a partially calcified organic accumulation that serves as a nucleation site for successive layers of newly seeded tablets. Hence vertical columns develop; the greatest concentration of growth occurs at the shell margin. A similar pattern of development occurs in the nautiloids (Cephalopoda; Mutvei, 1980).

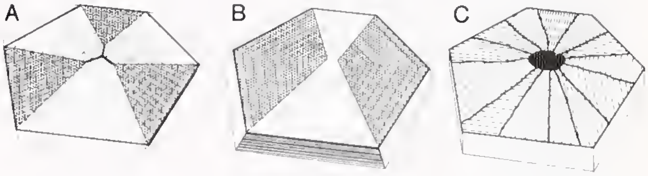

Figure 18. Schematic diagrams of typical nacreous and semi-nacreous tablets in cyclostome bryozoans and molluscs. (A) Cyclostome semi-nacreous tablet. The tablet is divided into six roughly equal sectors or crystal individuals. The more-soluble sectors (shaded darker) do not occur at the center of the tablet where there is a "trilete" suture. Note the sloping outer edges of the less-soluble sectors. (B) A typical bivalve nacreous tablet divided into a pair of sub-triangular, less-soluble sectors that meet at the center and two rhombic (or paired triangular), more-soluble sectors. Note that the less-soluble sectors have a finely laminated appearance and all the outer edges have regularly sloping surfaces (after Mutvei, 1977). (C) A typical gastropod or cephalopod nacreous tablet divided into polysynthetically twinned sectors (crystal individuals). The central hollow represents the site of the central organic accumulation. Note the vertical side faces (after Mutvei, 1978).

The form and complexity of the organization of the calcitic semi-nacre of cyclostome bryozoans resembles that of the aragonitic nacreous tablets in molluscs. The cyclostome fabric is especially similar to bivalve sheet nacre, which also has a regular arrangement of sectors (or crystal individuals) of different solubilities. Both types of tablet also have gently concave surfaces with a slight central depression as well as inclined (not vertical) side faces. The bryozoan semi-nacre differs structurally from the molluscan nacre only in the particular pattern of sectoring and in the more irregular stacking of the tablets. Indeed the structural differences between cyclostome semi-nacres and molluscan nacres are no greater than the differences between the nacres of different classes of molluscs.

Carter and Clark (1985) and Carter *et al.* (1990) devised classifications of invertebrate microstructures that stressed structural and morphological arrangements rather than mineralogy, and could be applied across the different biomineralizing groups. Paradoxically, however, they incorporated into the definition of nacreous fabrics that true nacres must be aragonitic; cf. semi-nacre that could be calcitic or aragonitic. In view of the considerable morphological similarity demonstrated here between the calcitic semi-nacres of bryozoans and the aragonitic nacres of molluscs, it seems reasonable to group these structures together regardless of their different mineralogy.

It has been proposed that the perceived greater diversity of ultrastructural fabrics in molluscs compared to lophophorates is a consequence of the greater evolutionary potential of molluscan biomineralization (Carter, 1979; Carter and Clark, 1985). Comparison of lophophorate and molluscan skeletal fabrics revealed a pattern that Carter and Clark (1985) termed the "lophophorate-molluscan discontinuity" (L-M discontinuity). They claimed that lophophorates are incapable of developing the range of aragonitic and calcitic structures found in molluscs, whereas all of the fabrics found in brachiopods and bryozoans have also evolved in molluscs.

Carter and Clark (1985) used two main arguments to support their hypothesis for greater evolutionary potential of molluscs with respect to lophophorates. Their first argument was that all organizationally complex molluscan fabrics that are uniformly oriented in the plane of shell deposition as well as with repect to the shell margins are absent in lophophorates. They cited as examples of such fabrics radial and concentric crossed lamellar and crossed foliated structures, row stack nacreous structure, and crossed composite prismatic structure.

The second argument cited by Carter and Clark (1985) in support of the L-M discontinuity is the complex substructure of nacreous fabrics in molluscs. They suggested that tablet substructures, which could have a direct bearing on tablet stacking patterns, may be unique to the Mollusca and absent in the semi-nacre of lophophorates. The tablet substructures described here in bryozoan semi-nacre indicate that conclusions about evolutionary potential of biomineralization should not be drawn until the balance of research on molluscs and lophophorates is equalized. The bulk of research on calcareous skeletal biomineralization in invertebrates has been dedicated to molluscs, but current studies of bryozoans are revealing an increasing range and complexity of fabrics.

Convergence of microstructures is common within the Mollusca. It has been argued that, of the common molluscan shell microstructures, only nacre evolved just once within the phylum (see Carter and Clark, 1985). Regular aragonitic nacres occur in the gastropods, cephalopods, and bivalves, all of which may have evolved from nacreous monoplacophoran ancestors. The differences in the substructures of the nacreous tablets in the different classes may, however, indicate convergent evolution of nacreous fabrics. The Ordovician bivalve *Palaeoconcha* has a tablet substructure resembling more closely that of modern and fossil gastropods and cephalopods than modern bivalves (Carter and Clark, 1985). Therefore, the modern four (six?) sectored bivalve nacre must have evolved separately (Carter and Clark, 1985). The separate evolution in bryozoans of semi-nacre, which is very similar morphologically (if not mineralogically) to molluscan nacre, lends credence to the possibility that nacre evolved more than once within the Mollusca.

Acknowledgments

This work was supported by NERC Grant GR3/9138. We thank Drs. J.-G. Harmelin and P. J. Hayward for donating study material.

Literature Cited

Batten, R. L. 1984. The calcitic wall in the Paleozoic families Euomphalidae and Platyceratidae (Archaeogastropoda). *J. Paleont.* **58:** 1186–1192.

Boardman, R. S., F. K. McKinney, and P. D. Taylor. 1992. Morphology, anatomy, and systematics of the Cinctiporidae, new family (Bryozoa: Stenolaemata). *Smithson. Contr. Paleobiol.* **70:** 1–81.

Brood, K. 1976. Wall structure and evolution in cyclostomate Bryozoa. *Lethaia* **9:** 377–389.

Carter, J. G. 1979. Comparative shell microstructure of the Mollusca, Brachiopoda and Bryozoa. *Scanning Electron Microsc.* **1979:** 439–446.

Carter, J. G. 1990. Evolutionary significance of shell microstructure in the Palaeotaxodonta, Pteriomorphia and Isofilibranchia (Bivalvia: Mollusca). Pp. 135–411 in *Skeletal Biomineralization: Patterns, Processes and Evolutionary Trends. Volume 1.* J. G. Carter, ed. Van Nostrand Reinhold, New York.

Carter, J. G., and G. R. Clark II. 1985. Classification and phylogenetic significance of molluscan shell microstructure. In *Mollusks, notes for a short course,* T. W. Broadhead, ed. *Univ. Tenn. Dept. Geol. Sci. Stud. Geol.* **13:** 50–71.

Carter, J. G., and R. M. Hall. 1990. Polyplacophora, Scaphopoda, Archaeogastropoda and Paragastropoda (Mollusca). Pp. 29–51, Pls. 122–134 in *Skeletal Biomineralization. Patterns, Processes and Evolutionary Trends. Volume 2,* J. G. Carter, ed. Van Nostrand Reinhold, New York.

Carter, J. G., K. Bandel, V. de Buffrénil, S. J. Carlson, J. Castanet, M. A. Crenshaw, J. E. Dallingwater, H. Francillon-Vieillot, J. Géraudie, F. J. Meunier, H. Mutvei, A. de Ricqlés, J. Y. Sire, A. B. Smith, J. Wendt, A. Williams, and L. Zylberberg. 1990. Glossary of skeletal biomineralization. Pp. 609–627 in *Skeletal Biomineralization: Patterns, Processes and Evolutionary Trends. Volume I,* J. G. Carter, ed. Van Nostrand Reinhold, New York.

Grégoire, C. 1957. Topography of the organic components in mother-of-pearl. *J Biophys. Biochem. Cytol.* **3:** 797–808.

Grégoire, C. 1959. A study of the remains of organic components in fossil mother-of-pearl. *Bull. Inst. R Sci. Nat. Belg.* **35:** 1–14.

Grégoire, C., G. Duchâteau, and M. Florkin. 1949. Examen au microscope electronique de la pellicule prenacrée et de la nacre decalcifiée de l'anodonte. *Arch. Int. Physiol. Biochimie* **57:** 121–124.

Grégoire, C., G. Duchâteau, and M. Florkin. 1950. Structure, étudé au microscope électronique de nacre décalcifiées de Mollusques (Gastéropodes, Lamellibranches et Céphalopodes). *Arch. Int. Physiol. Biochimie* **58:** 117–120.

Grégoire, C., G. Duchâteau, and M. Florkin. 1955. La trame protidique des nacres et des perles. *Annls. Inst. Océanogr., Paris, Nouvelle Série* **31:** 1–36.

Horowitz, A. S., and J. F. Pachut. 1992. Estimates of nomenclatorial and taxonomic diversity among Recent Entoprocta and Ectoprocta. *Abstracts of the 9th International Conference on Bryozoa, Swansea* **1992:** 25.

Mutvei, H. 1977. The nacreous layer in *Mytilus, Nucula,* and *Unio* (Bivalvia). Crystalline composition and nucleation of nacreous tablets. *Calc. Tiss. Res.* **24:** 11–24.

Mutvei, H. 1978. Ultrastructural characteristics of nacre in some gastropods. *Zoologica Scr.* **7:** 287–296.

Mutvei, H. 1980. The nacreous layer in molluscan shells. Pp. 49–56 in *The Mechanisms of Biomineralization in Animals and Plants,* *Proceedings of the Third International Biomineralization Symposium,* M. Omori and N. Watabe, eds. Tokai University Press.

Mutvei, H. 1983a. Ultrastructural evolution of molluscan nacre. Pp. 267–271 in *Biomineralization and Biological Metal Accumulation,* P. Westbroek and E. W. de Jong, eds. D. Riedel Co., Boston.

Mutvei, H. 1983b. Flexible nacre in *Isorthoceras* (Cephalopoda: Nautiloidea), with remarks on the evolution of cephalopod nacre. *Lethaia* **16**: 233–240.

Ristedt, H. 1977. On the ultrastructure of the zooecia of living *Membranipora* species. *Biomineralization Res. Reports* **9**: 86–98.

Ross, J. R. P. 1977. Microarchitecture of body wall of extant cyclostome ectoprocts. *Am. Zool.* **17**: 83–105.

Sandberg, P. A. 1971. Scanning electron microscopy of cheilostome bryozoan skeletons; techniques and preliminary observations. *Micropaleontology* **17**: 129–151.

Sandberg, P. A. 1977. Ultrastructure, mineralogy and development of bryozoan skeletons. Pp. 143–181 in *Biology of Bryozoans,* R. M. Woollacott and R. L. Zimmer, eds. Academic Press, New York.

Sandberg, P. A. 1983. Ultrastructure and skeletal development in cheilostomate Bryozoa. Pp. 238–286 in *Treatise on Invertebrate Paleontology. Part G. Bryozoa. Revised Volume 1,* R. S. Boardman *et al.,* eds. Geological Society of America and University of Kansas, Boulder and Lawrence.

Söderqvist, T. 1968. Observations on extracellular body wall structure in *Crisia eburnea. Atti. Soc. Ital. Sci. Nat.* **108**: 115–118.

Tavener-Smith, R., and A. Williams. 1972. The secretion and structure of the skeleton of living and fossil Bryozoa. *Phil. Trans. R. Soc., Series B* **264**: 97–159.

Taylor, J. D., W. J. Kennedy, and A. Hall. 1969. The shell structure and mineralogy of the Bivalvia. Introduction. Nuculacea-Trigonacea. *Bull. Br. Mus. Nat. Hist., Zool.* Supplement **3**: 125 pp.

Taylor, P. D., and C. G. Jones. 1993. Skeletal ultrastructure in the cyclostome bryozoan *Hornera. Acta Zool. Stockh.* **74**: 135–143.

Taylor, P. D., and G. P. Larwood. 1990. Major evolutionary radiations in the Bryozoa. Pp. 209–233 in *Major Evolutionary Radiations,* P. D. Taylor and G. P. Larwood, eds. *Systematics Association Special Volume* **42**. Clarendon Press, Oxford.

Taylor, P. D., M. J. Weedon, and C. G. Jones. 1995. Skeletal ultrastructure in the cyclostome bryozoan family Lichenoporidae. *Acta Zool. Stockh.* **76**. (in press).

Williams, A. 1970. Origin of the laminar shell of the brachiopod *Crania. Calc. Tiss. Res.* **6**: 329–342.

Williams, A., and A. D. Wright. 1970. Shell structure of the Craniacea and other calcareous inarticulate brachiopods. *Spec. Pap. Palaeont.* **1**: 1–51.

Williams, A. 1990a. Biomineralization in the Lophophorates. Pp. 67–82 in *Skeletal Biomineralization: Patterns, Processes and Evolutionary Trends. Volume 1,* J. G. Carter, ed. Van Nostrand Reinhold, New York.

Williams, A. 1990b. Brachiopoda and Bryozoa. Pp. 57–61, Pls. 141–156 in *Skeletal Biomineralization: Patterns, Processes and Evolutionary Trends Volume 2,* J. G. Carter, ed. Van Nostrand Reinhold, New York.

Wise, S. W., Jr. 1970a. Microarchitecture and mode of formation of nacre (mother-of-pearl) in pelecypods, gastropods and cephalopods. *Ecolog. Geol. Helv.* **63**: 775–797.

Wise, S. W., Jr. 1970b. Microarchitecture and deposition of gastropod nacre. *Science* **167**: 1486–1488.

Reference: *Biol. Bull.* **188:** 293–305. (June, 1995)

Changes in Larval Morphology in the Evolution of Benthic Development by *Patiriella exigua* (Asteroidea: Asterinidae), a Comparison with the Larvae of *Patiriella* Species with Planktonic Development

M. BYRNE

Department of Anatomy and Histology, F-13, University of Sydney,
New South Wales 2006, Australia

Abstract. *Patiriella exigua* (Lamarck) is a small asterinid sea star that deposits large eggs onto the substratum. Development is lecithotrophic and entirely benthic, proceeding without parental care. The embryos develop to the brachiolaria stage before hatching and there is no trace of a bipinnaria larva. In its early stage the larva of *P. exigua* resembles a planktonic brachiolaria in having one long central brachium and two short lateral brachia. By hatching, the brachia are equal in length, giving the larva a tripod-like appearance. Comparison of the larva of *P. exigua* with the brachiolaria of *Patiriella* species with planktonic development supports the hypothesis that the tripod larval form results from differential growth of the lateral brachia. At hatching, the *P. exigua* larva has a well-developed attachment complex composed of a large adhesive disk and three muscular brachia; the latter bear a striking resemblance to adult tube feet. This hypertrophic elaboration of the brachiolar complex is an adaptation for permanent benthic attachment. Internally, one large enterocoel forms at the anterior end of the archenteron. The archenteron then closes to form the rudiment for the adult gut. Metamorphosis involves gradual resorption of the brachiolar complex concomitant with formation of the first tube feet. The adhesive disk plays a major role in attachment during late metamorphosis but is gradually reduced to a plug of tissue as the tube feet become functional. Juvenile *P. exigua* are negatively geotactic and float on the water surface, behavior that may act as a mechanism for dispersal. The similarity of the early larva of *P. exigua* to planktonic brachiolariae suggests that the evolution of benthic lecithotrophy by this species involved modification of a planktonic larval form. These modifications include elimination and reduction of larval feeding structures, formation of one rather than three enterocoels, and hypertrophy of the brachiolar complex to form a tripod larva. Heterochronies in the ontogeny of *P. exigua* include the delay in hatching to the brachiolaria stage and the accelerated development of the juvenile form and adult skeleton.

Received 17 June 1994; accepted 27 March 1995.

Introduction

The sea star *Patiriella exigua* (Lamarck) is a conspicuous component of the intertidal echinoderm fauna of southeastern Australia and is a member of a sympatric group of *Patiriella* species distributed around the south coast from Western Australia to north Queensland (Dartnall, 1971; Keough and Dartnall, 1978; Lawson-Kerr and Anderson, 1978; Byrne, 1991, 1992; Byrne and Barker, 1991). This genus of sea stars exhibits a striking diversity of life histories that span the range of developmental patterns seen in the Asteroidea. *P. regularis* shows what is considered to be the ancestral pattern for asteroids (Strathmann, 1978), developing through planktotrophic bipinnaria and brachiolaria larvae (Byrne and Barker, 1991). In contrast, the other *Patiriella* species have modified ontogenies. *P. gunnii, P. calcar, P. brevispina,* and *P. pseudoexigua* develop through lecithotrophic planktonic brachiolariae, whereas *P. exigua* develops through a lecithotrophic benthic brachiolaria (Lawson-Kerr and Anderson, 1978; Byrne, 1991, 1992; Chen and Chen, 1992). *P. vivipara* and *P. parvivipara* show the most modified development, having reduced intragonadal larvae and giving birth to juveniles (Dartnall, 1971; Keough and Dartnall, 1978; Byrne, 1991; Chia and Walker, 1991). These congeneric species, which occupy similar habitats and latitude and which have such developmental diversity, are a model system with which to examine the evolutionary modification of larval form because of the ease with which homologous structures can be identified and compared (Byrne, 1991; Byrne and Barker, 1991). The planktotrophic development of *P. regularis* (Byrne and Barker, 1991) provides the basis against which the ontogeny of the lecithotrophic developers, including *P. exigua*, can be compared (Lawson-Kerr and Anderson, 1978; Byrne, 1991).

P. exigua is a small cushion-shaped asterinid sea star (maximum R = 15 mm) that releases large eggs (390 μm diameter) through orally directed gonopores (Lawson-Kerr and Anderson, 1978; Byrne, 1991, 1992). The eggs adhere to the substratum with their sticky jelly coat, and development proceeds without parental care. *P. exigua* is a hermaphrodite and occasionally lays what appear to be self-fertilized eggs (Byrne, 1991; Byrne and Anderson, 1994). Reproduction and aspects of the development of this species are described in several studies (Lawson-Kerr and Anderson, 1978; Byrne, 1991, 1992; Cerra and Byrne, 1995a, b).

External and internal morphogenesis in the larvae of *P. exigua* is documented in detail here through the use of light, confocal, and scanning electron microscopy. Unlike *Patiriella* species with planktonic larvae, *P. exigua* lacks a discrete settlement stage and the larvae do not exhibit rapid metamorphosis. The juvenile form in *P. exigua* is attained through a gradual transformation in morphology. Particular attention is paid to the larval specializations involved with benthic attachment and to the gradual resorption of these structures during metamorphosis. Initial examination of the brachiolaria of *P. exigua* suggested that benthic development in this species is associated with hypertrophic elaboration of the larval attachment complex (Byrne, 1991). The hypothesis that the robust brachia of *P. exigua* are the result of differential growth is examined here through comparison with the brachia of *Patiriella* species with planktonic development. The ontogeny of *P. exigua* is compared with that of *P. regularis, P. calcar*, and *P. gunnii* to determine the morphological and heterochronic changes associated with the evolution of benthic lecithotrophy. As applied here to *Patiriella*, the term benthic development refers strictly to the situation in which the developmental stages either adhere to the substratum or are brooded by the parent; it does not include unattached demersal larvae (see Janies and McEdward, 1993).

Materials and Methods

Patiriella exigua is distributed from northern New South Wales (28°39′S; 153°37′E) to the Eyre Peninsula in South Australia (34°44′S; 135°52′E). Adult specimens and egg masses attached to the undersurface of small boulders were collected at low tide from an intertidal rock platform at Clovelly, Sydney (33°54′S; 151°17′E), between August and October 1990 and 1991. The boulders and attached egg masses were transferred to laboratory aquaria to document the development and behavior of the larvae. Development was also examined in fertilizations carried out in the laboratory. Mature ovaries were dissected from *P. exigua* and placed in dishes containing 10^{-5} *M* 1-methyladenine (1-MA) in filtered seawater to induce maturation and release of eggs (Kanatani, 1969). Upon release, the eggs adhered to the bottom of the dishes with their jelly coats. The ovarian tissue was removed and the eggs were rinsed by decanting the 1-MA solution followed by a wash in fresh seawater. Sperm obtained from mature males through dissection of the testes were stored at 4°C until used for fertilization. For fertilization, a few drops of diluted sperm were added to the culture chambers. After 5–10 min, the eggs were washed in fresh seawater to remove excess sperm and the embryos were cultured at 19–21°C.

Development of *P. exigua* was documented by light microscopy (LM), confocal microscopy, and scanning electron microscopy (SEM). Live specimens were photographed with a photomicroscope. For LM and SEM, the embryos and larvae were fixed in 2.5% glutaraldehyde in filtered seawater for 1 h at room temperature. The larvae were relaxed in 6.8% $MgCl_2$ in distilled water before being placed in the primary fixative. Following primary fixation, the specimens were washed in 2.5% $NaHCO_3$ (pH 7.2) and post-fixed in 2% OsO_4 in 1.25% $NaHCO_3$ for 1 h at room temperature. The specimens were then washed in distilled water and dehydrated in a graded series of ethanols. For LM sections, the larvae were embedded in Spurr's resin. Serial sections (0.5 μm) were stained with 1% toluidine blue in 0.5% ethanolamine. For SEM, the specimens were critical-point dried, sputter coated, and viewed with a JOEL JSM-35C scanning electron microscope.

For confocal microscopy, relaxed larvae were fixed in 2% paraformaldehyde in seawater. The larvae were then dehydrated in graded ethanols, cleared in Histo-Clear (National Diagnostics; Atlanta, Georgia), and mounted on slides. Optical sections of the specimens were made with a BIO-RAD MRC600 confocal microscope.

Development of the skeleton was documented by utilizing the birefringent properties of the calcite ossicles. The larvae are opaque, and whole mounts of early larvae fixed in glutaraldehyde, dehydrated in alcohol, and cleared in Histo-Clear were observed with polarized light. To examine development of the skeleton during metamorphosis, advanced larvae were fixed in glutaraldehyde and during dehydration were stained with 70% alcoholic eosin for 1 h. Whole-mounts of these specimens were examined with bright-field illumination.

The arms and body lengths of the brachiolaria of *P. exigua* and several *Patiriella* species with planktonic development were measured to compare the development of the brachia. For *P. exigua,* live larvae were measured with an ocular micrometer. The arms and body lengths of the brachiolariae of *P. regularis, P. calcar,* and *P. gunnii* were measured from photographs of live larvae. These measurements were used to calculate the ratio of body to arm length for each species.

Results

External morphogenesis

The chronology of development of *Patiriella exigua* is outlined in Table I. By 24 h the embryos are gastrulae with a large blastopore (Fig. 1a). The embryos rotate inside their fertilization envelopes due to the action of the cilia that cover their surface. They are negatively buoyant, and after dissection from their envelopes, the embryos swim across the substratum or in the overlying water, propelled by their cilia. Subsequently the gastrulae elongate and a blunt projection forms at the anterior region, marking the formation of the preoral lobe and the future position of the central brachium (Figs. 1b, 2a). The blastopore narrows to a slit and closes about 2 days after fertilization. As the blastopore closes, two lateral folds appear in the preoral lobe 3 days after fertilization (Fig. 1c). These folds are pressed against the internal surface of the fertilization envelope and mark the formation of the two lateral brachia. The embryos are now early brachiolariae with three recognizable arms, or brachia (Figs. 1d, 2b). The central adhesive disk also begins to form (Fig. 2c). The larvae occupy all the space within the envelope and their cilia propel the surrounding fluid across their epithelium. Removal of 3-day-old larvae ($\bar{X} = 500$ μm, length; SE = 4.9; $n = 6$) from the fertilization envelope reveals the presence of the large central brachium ($\bar{X} = 174$ μm, length; SE = 7.1, $n = 6$) flanked by two small lateral brachia ($\bar{X} = 124$ μm, length; SE = 4.6, $n = 6$). The body-to-arm-length ratio of the central arm is 2.9:1; that of the lateral arms is 4:1. The early larvae of *P. exigua* are similar to the late brachiolaria of *Patiriella* species that have planktonic development: all have one long central brachium and two short lateral brachia (Table II). The relative sizes of the brachia of unhatched *P. exigua* are particularly similar to the central and lateral arms of the lecithotrophic brachiolariae of *P. calcar* and *P. gunnii* (Table II).

The hatching process begins on the fourth day of development (Fig. 1e). This takes several days and involves softening of the fertilization envelope, which presumably results from hatching enzyme activity. During hatching the envelope is stretched and torn by movement of the arms. Differential growth of the lateral brachia results in the formation of three arms equal in length. When removed from their fertilization envelope, the larvae adhere weakly to the substratum or swim away into the overlying water.

Hatching occurs 5–6 days after fertilization and, by this time, the brachia are noticeably muscular and extend through breaks in the envelope to attach to the substratum. Hatched brachiolariae ($\bar{X} = 566$ μm, length; SE = 12.1; $n = 9$) have a well-developed brachiolar complex composed of three brachia equal in length ($\bar{X} = 243$ μm; SE = 6.4; $n = 9$) and a large central adhesive disk (Figs. 1e; 2d). The body-to-arm-length ratio of these larvae is

Table I

Chronology of development of Patiriella exigua *at 19–21°C*

Time	Stage
0	Fertilization
10 h	Blastula
15 h	Wrinkled blastula
24 h	Gastrula with large blastopore and spacious archenteron
2 days	Gastrula elongates along archenteric axis to form future preoral lobe; blastopore almost closed; anterior coelom present
3 days	Early brachiolaria, with 1 long central arm and 2 short lateral arms; each arm is occupied by a branch of the anterior coelom; adhesive disk forms; gut rudiment closes off from coelom; left and right posterior coeloms present
4 days	Hatching process begins with softening of fertilization envelope; brachiolaria have 3 arms equal in length; left and right posterior coeloms separate from anterior coelom and meet below gut; posterior coeloms are partially confluent; gut closed off; left and right hydrocoels present
5–6 days	Hatched brachiolaria: arms and adhesive disk well-developed; arms muscular and starting to become translucent; hydrocoel lobes form; hydropore opens; right hydrocoel pinches off and becomes filled with cells; ventral horn fuses with anterior coelom; skeletal spicules present; the larvae become pentamerous as adult arm rudiments become visible externally
6–7 days	Late brachiolaria: arms translucent; left posterior coelom spacious and right posterior coelom elongate; terminal and interradial ossicles present
8 days	Metamorphosis begins with flexure of the larval body and initiation of resorption of the larval arms and anterior coelom; hydrocoel lobes evident on oral surface
9–10 days	Larvae are stellate, first tube feet present; the anterior coelom closes; fused posterior coeloms on aboral side of gut; ventral horn on oral side of gut
11–12 days	Brachia reduced to stumps around adhesive disk; disk resorption initiated; two pairs of tube feet present in each radius; all primary skeletal plates present
13–14 days	Disk reduced to a plug in mouth region; eye spots present on terminal tube feet
15–18 days	Mouth opens

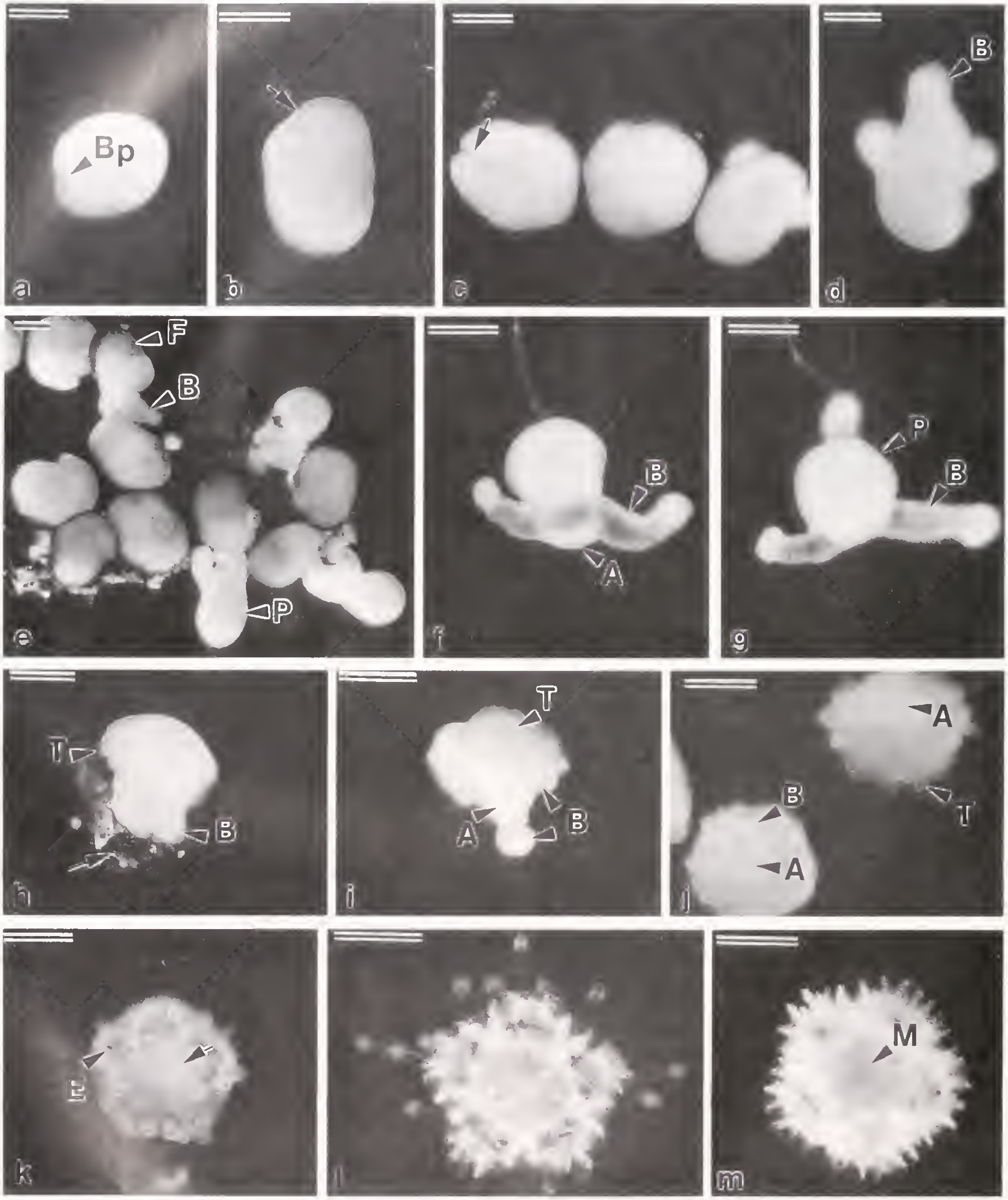

Figure 1. Light microscopy of development of live specimens. Scale bars = 200 μm. (a) Twenty-four hours: slightly elongate gastrula, dissected from the fertilization envelope, swimming in the culture dish. Bp, blastopore. (b) Thirty hours: left side of an elongate gastrula, dissected from the fertilization envelope, with a protrusion (arrow) at its anterior end marking formation of the preoral lobe. (c) Fifty-five hours: early

2.3:1. The brachiolariae resemble tripods, with the three muscular arms supporting the spherical posterior region. Growth of the brachia continues after hatching. They become more muscular and are translucent along their length, with bulbous tips (Figs. 1f, g; 2d, f). With these features, the larval arms bear a striking resemblance to adult tube feet. The adhesive disk is a large flat structure ($\bar{X}$ = 123 μm; diameter, SE = 3.1, n = 4) occupying most of the width of the preoral lobe (Figs. 1f, g; 2f). The entire preoral portion (243 μm, length; SE = 6.4, n = 9) of the larvae consists of the hypertrophied brachiolar complex with which they adhere tenaciously to the substratum (Fig. 1g). Raised nodules of epithelial cells covering the tips of the arms and the disk may be composed of adhesive-secretory cells (Fig. 2e, f). Fragments of the fertilization envelope remain attached to the larvae for a variable amount of time after hatching (Fig. 1h). Before or during hatching, the hydropore opens as a shallow invagination on the left side of the plane of bilateral symmetry (Fig. 2d). The posterior region of the body starts to become pentamerous as the adult arm rudiments become visible externally (Fig. 1g).

After hatching, the larvae usually remain in one place, but often rock back and forth on their arms. They occasionally move by attaching and detaching their arms. Occasionally, the larvae attach the adhesive disk to the substratum. In response to a strong current the brachia stretch in the direction of flow, and only concentrated flow from a pipette will dislodge the larvae. Late brachiolaria, 7 to 8 days old, have a mean length of 690 μm (SE = 14.6, n = 7) with three arms each 310 μm in length (SE = 10.3, n = 7). The ratio of body to brachium is 2.2:1, similar to that for the central brachia of *P. calcar* and *P. gunnii* (Table II). Compared with unhatched *P. exigua*, the lateral brachia of the late larvae have about doubled in length (Table II).

On about the 8th day of development, metamorphosis starts with flexure of the larval body to the left side and flattening of the body to mark the future oral and aboral surfaces (Figs. 1h, 2g). The larvae have a distinct angular, pentamerous shape. Four lobes of the hydrocoel appear at the base of the preoral lobe on the future oral surface. A gap between lobes one and four is occupied by the preoral portion of the larva. If the larvae are placed on their aboral surface, they remain in this position and creep across the substratum, propelled by their cilia (Fig. 2h). Resorption of the brachiolar complex also starts on day 8 and is a gradual process that occurs concomitant with development of the tube feet (Figs. 1i–k; 2g, i). Nine-day-old metamorphosing larvae look like yolky stars and have the first pairs of tube feet present in four ambulacra (Figs. 1i, 2i). These tube feet move across the surface while the larvae remain attached to the substratum by the adhesive disk. By days 10 or 11, the brachia are reduced to small stumps around the base of the disk (Figs. 1j, 2k). The ciliary cover of the aboral surface is also reduced (*cf.* Fig. 2h, j). As the arms are resorbed, the adhesive disk plays a major role in attachment and the fifth hydrocoel lobe appears on the oral surface. When the tube feet associated with the fifth hydrocoel lobe develop, the positions of the five adult ambulacra are apparent (Figs. 1k; 2k, l). By day 12, resorption of the adhesive disk is under way as the tube feet take over the role of benthic attachment (Figs. 1k; 2l–n). In most larvae all traces of the larval arms are gone. By the time the disk is reduced to a plug in the mouth region of 13-day-old larvae, eye spots are present on the terminal tube feet (Figs. 1k; 2l–n). The tube feet now function in benthic attachment and, when placed on their aboral surface, the young stars are able to right themselves. The disk remains as a plug in the mouth region for several days until the mouth opens 15 to 18 days after fertilization (Fig. 1m). Metamorphosis is now complete and the juveniles extrude their stomach to feed. Yolk reserves present in the gut give the young stars a yellow color for several weeks. When these reserves are exhausted, the juveniles are virtually transparent and the gastric lobes and anal openings are evident.

Juvenile *P. exigua* were maintained in the laboratory for several months. They exhibited negative geotaxis, climbing the walls; upon reaching the air-water interface, they attached their tube feet to the surface of the water

Figure 1. (*Continued*) brachiolaria with folds at anterior end (arrow) that mark the formation of the larval arms. (d) Dorsal view of a swimming early brachiolaria dissected from envelope. B, brachium. (e) Five-day-old hatching brachiolariae. B, brachium; F, fertilization envelope; P, posterior region. (f) Six-day-old hatched brachiolaria. A, adhesive disk; B, brachium. (g) Seven-day-old late brachiolaria resemble tripods supported by tube-foot-like arms (B). The posterior region (P) is beginning to become pentamerous. (h) Side view of a 10-day-old metamorphosing larva. The brachia (B) are being resorbed and the larval body has flexed. The first tube feet (T) have formed. Arrow, remnant of fertilization envelope. (i) Ten-day-old metamorphosing larva viewed from the future oral surface of the juvenile. The adhesive disk (A) attaches the larva to the substratum as the tube feet (T) form. B, resorbing brachia. (j) Oral surface of two metamorphosing larvae—one (bottom) with resorbing brachia (B) and adhesive disk (A), and one (top) with the disk reduced to a plug in the mouth region. T, tube foot. (k) Fourteen days: the disk has been resorbed (arrow) and eye spots (E) are present on the terminal tube feet. (l) Seventeen days: aboral surface of juvenile. (m) Seventeen days: oral surface of juvenile with mouth (M) open.

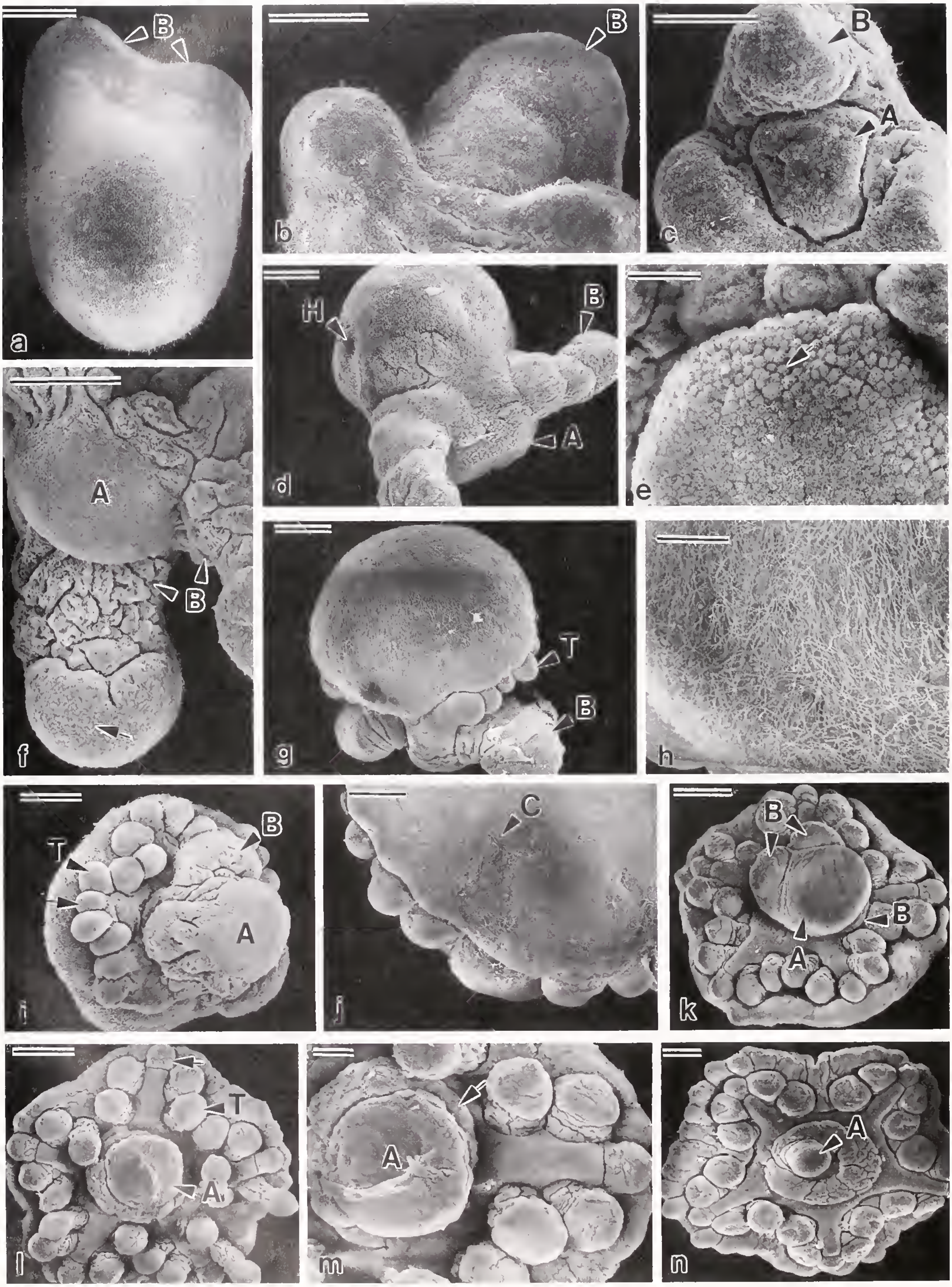
B
a
B
b
B
A
c
H
B
A
d
e
A
B
B
f
T
B
g
h
B
T
A
i
C
j
B
B
A
k
T
A
l
A
m
A
n

and floated attached by surface tension for periods from hours to days.

Internal morphogenesis

The chronology of internal morphogenesis of *P. exigua* is outlined in Table I. Gastrulae (24 h) have a spacious archenteron and the blastocoel is a narrow space in which mesenchyme cells are evident (Fig. 3a). A single coelom forms at the anterior end of the archenteron of 2-day-old elongate gastrulae and grows to occupy most of the anterior preoral region (Fig. 3b). This coelom subsequently forms the lumen of the central brachium. By the time the three brachial rudiments are evident externally in 3-day-old larvae, the anterior coelom has branched into the two lateral arms. The right and left posterior coeloms are also present in 3-day-old larvae as elongate extensions of the anterior coelom on either side of the gut (Fig. 3e). The gut wall has thickened and starts to close off from the coelom (Fig. 3c). During days 3 and 4, the right and left coeloms extend posteriorly and meet below the gut (Fig. 3c). These two coeloms become partially confluent and, depending on the plane of section, appear either as a single coelomic space or as two spaces separated by a mesentery. During the fourth day of development, the left and right posterior coeloms separate from the anterior coelom (Fig. 3d). On the left side the anterior coelom gives rise to the hydrocoel (Fig. 3d–f). The equivalent structure on the right side (Fig. 3d, e) corresponds to what MacBride (1896) termed the right hydrocoel in *Asterina gibbosa.* As in *A. gibbosa,* this structure subsequently buds off and the lumen becomes occluded by cells (Fig. 3f). Skeletal spicules appear as birefringent rods late on the fourth day or during the fifth day of development (Fig. 4a).

By the time the hatching process is near completion, on day 5, all five hydrocoel lobes have formed and the hydropore opens *via* the ciliated hydroporic canal (Fig. 3e). On days 5–6, the left posterior coelom gives rise to the ventral horn, which grows anteriorly to meet and fuse with the right anterior coelom (Fig. 3g, h). Prior to fusion, a mesentery separates the ventral horn and the anterior coelom (Fig. 3g). In 7-day-old larvae, the left posterior coelom is spacious and the right posterior coelom is a narrow coelomic space along the gut (Fig. 3i). A minute coelomic vessel appears between the left posterior coelom and the gut (Fig. 3i) and may represent the oral coelom described in *A. gibbosa* (MacBride, 1896), in which it forms the adult peripharyngeal coelom. The origin and fate of this structure in the ontogeny of *P. exigua* could not be determined. By the sixth day of development, terminal and interradial ossicles can be identified. The terminals are small fenestrated plates positioned in the adult arm rudiments (Fig. 4b).

In 8-day-old metmorphosing larvae, the anterior coelom becomes closed off and is resorbed along with the brachiolar complex. Most of the primary skeletal elements viewed through the aboral surface have grown to form fenestrated plates, and additional spicules—including the terminal spines—have formed (Fig. 4c). The posterior region of 9-day-old larvae takes on the stellate appearance of the juvenile with formation of the tube feet and identifiable oral and aboral regions (Fig. 3k). The right posterior coelom lies along the aboral side of the gut, and the left posterior coelom/ventral horn lies along the oral side of the gut (Fig. 3j, k). On the aboral side of 11-day-old larvae, five terminal plates, five interradial plates, and one central plate are identifiable. On the oral side, five pairs of elongate oral plates are present, one on each side of the radial canal, and five pairs of triradiate ambulacral spicules are present at the base of the tube feet. The marginal plates are also present. The next ossicles to appear on the aboral side, on about day 12 of development, are the radials (Fig. 4d).

Figure 2. Scanning electron microscopy of external development. Scale bars: Fig. 2a–d, f, g, i, k, l = 80 μm; Fig. 2e, h = 25 μm; Fig. 2j, l, m = 50 μm. (a) Right side of an early brachiolaria showing development of the preoral lobe and arm rudiments (B). (b) Ventral view of the preoral region and arm rudiments (B) of an early brachiolaria. (c) Ventral view of the preoral region showing the developing adhesive disk (A) positioned between the three brachia (B). (d) Left side of a hatched brachiolaria with well-developed arms (B) and adhesive disk (A). H, hydropore. (e) Detail of adhesive disk showing the raised knobs of epithelial cells (arrow). (f) Detail of the brachiolar complex one day after hatching, showing the contracted tube-foot-like appearance of the brachia. The tips of the brachia (B) are covered by raised knobs of epithelial cells (arrow). A, adhesive disk. (g) Metamorphosing larva with body flexed. B, brachium; T, tube foot. (h) Ciliary cover of the future aboral surface of the juvenile. (i) Oral surface of a metamorphosing larva, tube feet (T) are present in four radii. The brachia are being resorbed while the disk (A) maintains benthic attachment. Arrow, terminal tube foot. (j) As metamorphosis continues, the ciliary (C) cover of the future aboral surface of the juvenile is reduced. (k) A metamorphosing larva viewed from the future oral surface. The larval arms (B) are reduced to small protrusions around the disk (A). Two pairs of tube feet are present in each radius. (l) Advanced metamorphosis: the disk (A) is reduced to a plug in the mouth region. T, tube foot; arrow, terminal tube foot. (m) Detail of resorbing disk (A) and one arm. The rim (arrow) surrounding the disk is the developing mouth. (n) Resorption of the disk (A) is nearly complete.

Table II

Body and arm dimensions of the brachiolaria larvae of Patiriella *species (SE, n)*

Species	Larva	Mean length larval body (μm)	Length central brachium (μm)	Length lateral brachia (μm)	Ratio L:CB	Ratio L:LB
Patiriella regularis	Planktotrophic brachiolaria	1204 (250, 7)	331 (61, 7)	100 (32, 7)	3.6:1	12:1
Patiriella calcar	Planktonic lecithotrophic brachiolaria	590 (14.5, 8)	293 (18.7, 8)	141 (3.5, 8)	2.0:1	4.2:1
Patiriella gunnii	Planktonic lecithotrophic brachiolaria	490 (23.4, 12)	236 (14.3, 12)	120 (4.9, 12)	2.1:1	4.1:1
Patiriella exigua (Unhatched, 3 day)	Benthic lecithotrophic brachiolaria	500 (4.9, 6)	175 (7.2, 6)	124 (4.6, 6)	2.9:1	4.0:1
Patiriella exigua (Hatched, 8 day)	Benthic lecithotrophic brachiolaria	690 (14.6, 7)	310 (10.3, 7)	310 (10.3, 7)	2.2:1	2.2:1

CB, central brachium; L, total larval length; LB, lateral brachium.

By the time the mouth opens (15–18 days), rudiments of the pyloric caeca are present. The timing of completion of the digestive tract with formation of the anal opening is variable and is delayed until most of the yolk reserves are exhausted. The oral plates form a frame around the mouth region, and the terminals are prominent rectangular plates over the terminal tube feet (Fig. 4e). The skeleton grows by adding branches that anastomose, with eventual intercalation of the plates (Fig. 4f).

Discussion

The ontogeny of *Patiriella exigua* exhibits many modifications that appear to be associated with the evolution of benthic and lecithotrophic development. The major changes associated with the evolution of benthic development are (1) the adhesive properties of the jelly coat that serve to keep the embryos attached to the substratum; (2) the hardening of the fertilization envelope to form a tough protective case around the embryos; (3) the delay in hatching until the brachiolaria stage, at which time the larval arms are sufficiently developed to take over the role of attachment; and (4) the hypertrophied growth of the brachiolar complex, which serves as a tenacious attachment device for the larvae throughout their development. In contrast to *P. exigua*, *Patiriella* species with planktonic development hatch as gastrulae (Byrne, 1991). As in other asteroids with lecithotrophic development (Chia, 1968; Strathmann, 1978, 1988; Chia and Walker, 1991), in *P. exigua* the acquisition of a large egg and the independence of an exogenous food source are considered to be derived features (Byrne, 1991). Compared with the planktotrophic development of *P. regularis* (Byrne and Barker, 1991), the major modifications associated with the shift to lecithotrophy by *P. exigua* are (1) the absence of the bipinnaria larva and ciliated bands; (2) the early closure of the blastopore; and (3) the failure of the archenteron to connect with a stomodeum. The larval gut becomes a closed structure that serves as the rudiment for the adult gut. The transient appearance of a larval stomodeum and anus, described for *Asterina gibbosa* (MacBride, 1896; Marthy, 1980), was not observed in *P. exigua*.

Larvae similar to the brachiolaria of *P. exigua* are also characteristic of several other species in the family Asterinidae. These include species that attach their eggs to the substratum and species that brood their young externally (MacBride, 1896; Komatsu *et al.*, 1979; Marthy, 1980). All of these asterinids hatch as brachiolaria (MacBride, 1896; Komatsu *et al.*, 1979; Marthy, 1980). Like *P. exigua*, *Asterina minor* and *A. gibbosa* abandon their deposited eggs and develop through modified benthic brachiolaria (MacBride, 1896; Komatsu *et al.*, 1979; Marthy, 1980). The diminutive sea star *A. phylactica* also deposits its eggs and has a modified benthic brachiolaria, but in this species the adult remains with the developing progeny (Marthy, 1980; Crump and Emson, 1983). *A. minor* has a tripod larva virtually identical to that of *P. exigua*, whereas *A. gibbosa* and *A. phylactica* have brachiolariae with an asymmetrical attachment complex. The bilobed brachiolar complex of these species, with one lobe larger than the other, appears to be unique in the Asteroidea (MacBride, 1896; Marthy, 1980). Examination of the detailed work of MacBride (1896) suggests that the large lobe of the brachiolaria of *A. gibbosa* corresponds to the central brachium of the early brachiolaria of *P. exigua*, while the smaller lobe may have resulted from fusion of the two lateral arms. This speculation requires verification through detailed comparison of the development of the anterior coeloms of *A. gibbosa* and *P. exigua*.

Benthic development is also characteristic of the arctic genus *Leptasterias* of the order Forcipulatida. *Leptasterias* includes species that deposit their egg masses and species that release their eggs into an external brood space under the arms or into an internal brood space in the gut (Kubo, 1951; Chia, 1968; Hendler and Franz, 1982; Himmelman *et al.*, 1982; Strathmann, 1987). Adults of *L. ochotensis similispinis* remain with the eggs, which are attached to the substratum, and the embryos develop through a tripod brachiolaria similar to the larva of *P. exigua* (Kubo, 1951). Other *Leptasterias* species that keep their young within a brood spaces also have tripod brachiolaria (Chia, 1968; Hendler and Franz, 1982; Himmelman *at al.*, 1982; Strathmann, 1987). Like *P. exigua,* these *Leptasterias* species produce young that hatch at the brachiolaria stage (Kubo, 1951; Chia, 1968).

Before they hatch, the larvae of *Patiriella exigua* are similar to the brachiolaria of *Patiriella* species with planktonic development because they have one long central brachium and two short lateral brachia (Table II). They are virtually identical to the early larvae of *P. calcar* and *P. gunnii* in the relative size of the brachia (Table II) and in their overall appearance and behavior. When dissected from their fertilization envelope, the larvae of *P. exigua* swim in the overlying water and, like the larvae of *P. calcar* and *P. gunnii,* have a uniform cover of cilia (Byrne, 1991; Byrne and Barker, 1991). Development of *P. exigua* through an early larval stage similar to the planktonic lecithotrophic brachiolariae of *P. calcar* and *P. gunnii* suggests that the tripod larval form results from differential growth of the lateral brachia. It appears that the evolution of benthic development by *P. exigua* involved modification of a lecithotrophic planktonic larva (Fig. 5). The delay in hatching from the early gastrula to the late brachiolaria stage would have been a parallel change for benthic life and presumably involves a delay in expression of the hatching enzyme. The robust brachia of *P. exigua* are more muscular than those of planktonic brachiolaria and are strikingly similar in structure and function to adult tube feet. The central adhesive disk also appears to be larger. This hypertrophic development of the brachiolar complex in *P. exigua* is undoubtedly an adaptation for permanent benthic attachment, as suggested for the benthic larvae of *Asterina minor* (Komatsu *et al.*, 1979).

Despite the taxonomic distance between *Leptasterias* and the Asterinidae, the similarity of their modified brachiolariae is striking (Chia, 1968; Komatsu *et al.*, 1979). In both *P. exigua* and *Leptasterias hexactis,* the early brachiolaria have one long and two short lateral brachia, while the late brachiolaria have arms that are equal in length (Chia, 1968). This suggests the possibility of convergence in the sequence of developmental changes associated with the evolution of benthic development in these two lineages. Considering that planktotrophic larvae are generally accepted as being ancestral in the Asteroidea (Strathmann, 1978), both groups probably had an ancestor with a planktonic lecithotrophic brachiolaria.

The possession of similar developmental patterns in asteroids that abandon their deposited eggs and asteroids that brood their young suggests that egg laying was an integral step in the sequence of reproductive and developmental changes that led to the evolution of brooding in the Asteroidea. Egg laying appears to be a preadaptive feature that made the shift to external brooding a relatively simple matter of the adult remaining with the egg mass, as seen in *Asterina phylactica* and several *Leptasterias* species (Chia, 1968; Hendler and Franz, 1982; Himmelman *at al.*, 1982; Crump and Emson, 1983; Strathmann, 1987). The converse could also occur, with loss of the brooding habit resulting in unattended egg masses.

In addition to the internal changes that result in the loss of larval feeding structures in *P. exigua,* there are also changes in coelomogenesis. The larvae of *P. exigua* form a single large anterior enterocoel instead of the paired anterior enterocoels and the single posterior enterocoel seen in *P. regularis* (Byrne and Barker, 1991). The changes in coelomogenesis are similar to those seen in other asteroids with lecithotrophic brachiolaria (MacBride, 1896; Chia, 1968), including *P. calcar* and *P. gunnii* (Byrne, unpub). A small posterior enterocoel on the left side of the larval gut of *P. regularis* is a characteristic feature of the bipinnaria of asterinids, and recent work with *Asterina pectinifera* indicates that this enterocoel is the site of origin of the germ cells (Newman, 1925; Byrne and Barker, 1991; Inoue *et al.*, 1992). Although the presence of this posterior coelom in several planktotrophic asteroid larvae is suggested to result from heterotopy, similar to that described for the 'mesogen' of *Pteraster tesselatus* (Janies and McEdward, 1993), the original hypothesis—that it is a rudiment of a posterior coelom present in a common enteropneust-echinoderm ancestor—remains an alternative view (Gemmill, 1914; Byrne and Barker, 1991).

The timing of skeleton formation has also apparently been altered in the development of *P. exigua:* the first spicules appear early in the larvae, well before the start of metamorphosis. In contrast, the skeleton of *P. regularis* forms later in development, just before, and during, metamorphosis (Byrne and Barker, 1991).

Unlike the brachiolaria of *P. regularis,* in which the attachment complex takes up a relatively small portion of the preoral lobe (Byrne and Barker, 1991), the brachiolar complex of *P. exigua* is large and occupies most of the preoral portion of the larva. As a result, resorption of this substantial structure during metamorphosis is gradual, taking 6 to 7 days. The transformation from the larval to the juvenile form in *P. exigua* takes about half the duration of larval life. In contrast, *P. regularis* and the other species with planktonic development have a discrete settlement stage, and their metamorphic period oc-

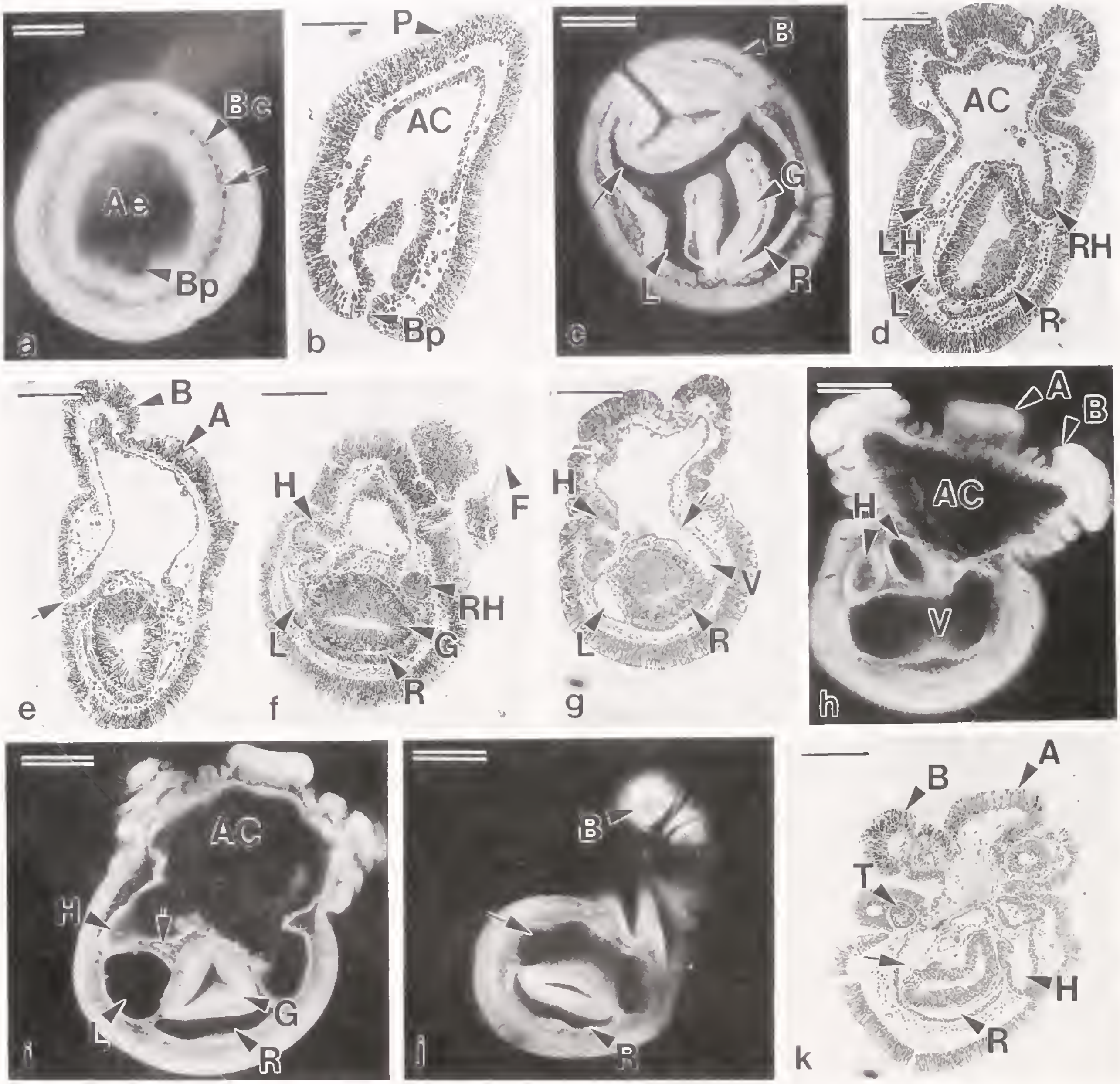

Figure 3. Confocal microscopy (Fig. 3a, c, h–j) and light microscopy (Fig. 3b, d–g, k) of internal development. Larvae are orientated to facilitate presentation of right and left structures. Scale bars = 100 μm. (a) Thirty hours: early gastrula with large archenteron (Ae) and narrow blastocoel (Bc) containing mesenchyme cells (arrow). Bp, blastopore. (b) Fifty hours: sagittal section of an elongate gastrula/early brachiolaria dissected from its fertilization envelope, with the anterior coelom (AC) occupying the preoral lobe (P). Bp, blastopore. (c) Frontal section of a three-day-old early brachiolaria in fertilization envelope. The large ectodermal cleft at anterior end of larva arises as the brachia (B) are formed. Internally, the anterior coelom branches (arrow) into the three brachia. The left (L) and right (R) coeloms meet below the gut (G). Adjacent optical sections in the series show that the coelom is starting to separate from the gut. (d) Frontal section of a five-day-old brachiolaria. The left (L) and right (R) posterior coeloms have separated from the anterior coelom (AC). The blind extensions of the anterior coelom form the left (LH) and right (RH) hydrocoels. (e) Sagittal section of a five-day-old brachiolaria showing hydroporic canal opening (arrow) on dorsal surface. A, adhesive disk; B, brachium. (f) Frontal section of a hatching six-day-old brachiolaria with hydrocoel lobes (H), left (L) and right (R) posterior coeloms, and the detached right hydrocoel (RH) occluded by cells. F, fertilization envelope; G, gut. (g) Frontal section of a six-day-old brachiolaria showing ventral horn (V) fusing with anterior coelom. The two spaces are separated by a mesentery (arrow). H, hydrocoel lobe; L, left coelom; R, right coelom. (h) Frontal section of a seven-day-old brachiolaria showing the ventral horn (V) crossing the larva to connect with the anterior coelom (AC). Adjacent optical sections show that these two spaces have become confluent. A, adhesive disk; B, brachium; H, hydrocoel lobes. (i) Frontal section of a seven-day-old brachiolaria showing

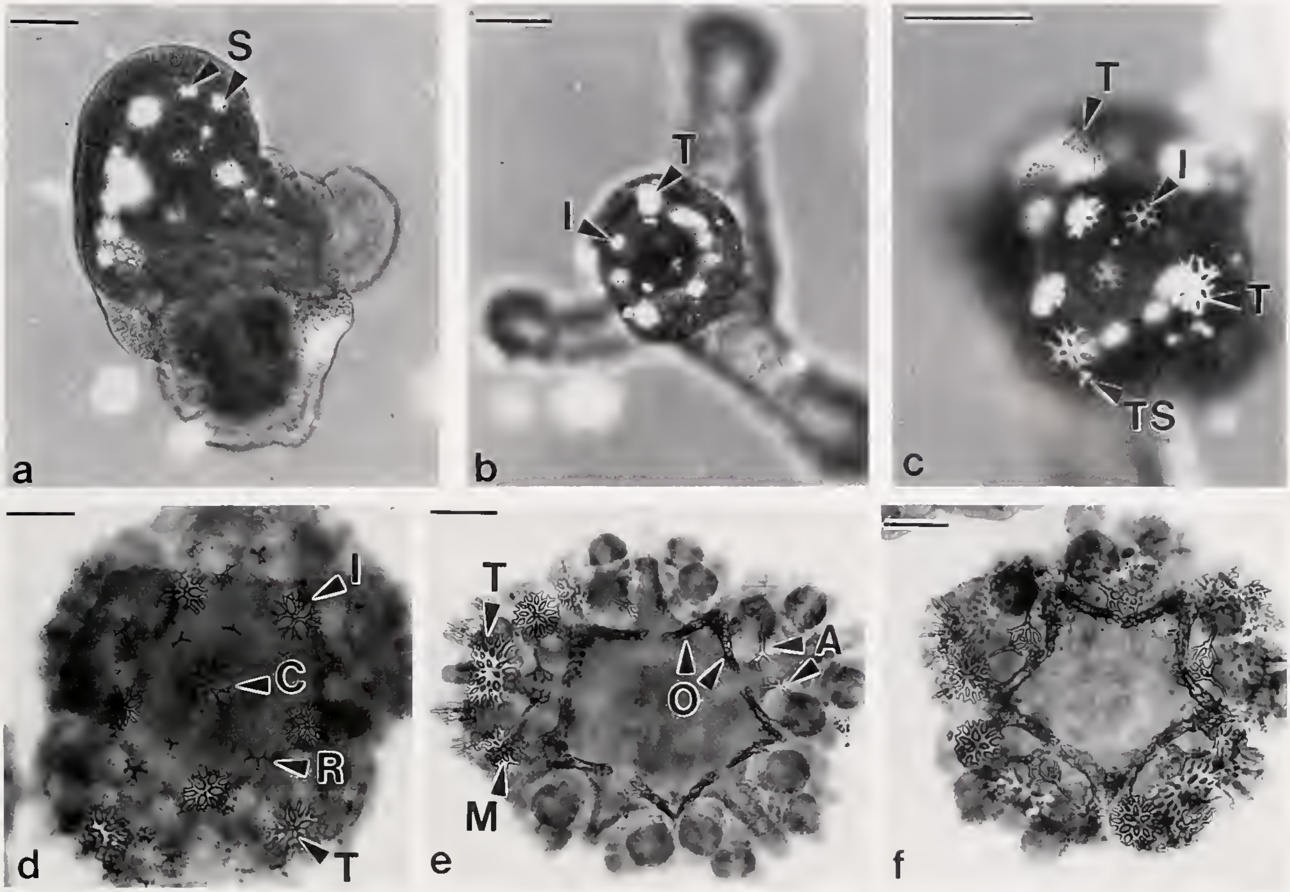

Figure 4. Development of the skeleton: a–c viewed with polarized light; d–f viewed with bright-field illumination. Scale bars = 100 μm. (a) The first spicules (S) appear in four-day-old brachiolaria. (b) Seven-day-old brachiolaria, the terminal (T) and interradial (I) ossicles are present. (c) Eight-day-old larva, the terminals (T) and interradials (I) are fenestrated plates. TS, terminal spine. (d) Aboral surface of a 12-day-old metamorphosing larva showing the central (C), interradial (I) and terminal (T) plates and small radial (R) ossicles. (e) Oral surface of a 15-day-old metamorphosed larva. The orals (O) frame the mouth. A, ambulacral ossicle; M, marginal plate, T, terminal plate. (f) Intercalation of skeletal plates in juvenile.

cupies much less of their development time. Development of *P. regularis* takes 7–9 weeks, and the larval body is reduced to a wispy stalk within 2 days of the onset of metamorphosis (Byrne and Barker, 1991). Despite the difference in the size of the attachment complexes of *P. regularis* and *P. exigua*, the appearance of the adhesive surfaces is similar (Byrne and Barker, 1991). The adhesive disk and larval arms of *P. exigua* are covered by raised epithelial knobs which, in sectioned material, appear to be batteries of secretory cells, similar to those reported for the brachiolaria of *Stichaster australis* and *Coscinasterias calamaria* (Barker, 1978; Byrne, pers. obs.). Resorption of the adhesive disk typically occurs after the brachia in asteroid metamorphosis, emphasizing the importance of disk adhesion prior to the formation of functional tube feet (Birkeland *et al.*, 1971; Barker, 1978).

The negative geotaxis and floating behavior of juvenile *P. exigua* are also reported for *P. pseudoexigua* and *Asterina minor* and are suggested to be a means of dispersal (Soliman and Nojima, 1984; Chen and Chen, 1992). In

---

Figure 3. (*Continued*) the spacious left coelom (L) and elongate right coelom (R). A small coelomic vesicle (arrow) is present between the gut (G) and anterior coelom (AC). (j) Radial section of a metamorphosing nine-day-old brachiolaria with flexed larval body. The right posterior coelom (R) lies on the aboral side of the gut and the left posterior coelom/ventral horn (arrow) lies on the oral side of the gut. (k) Radial section of a metamorphosing nine-day-old brachiolaria resorbing the brachia (B). A, adhesive disk; H, hydroporic canal; R, right posterior coelom; T, tube foot; arrow, left posterior coelom/ventral horn.

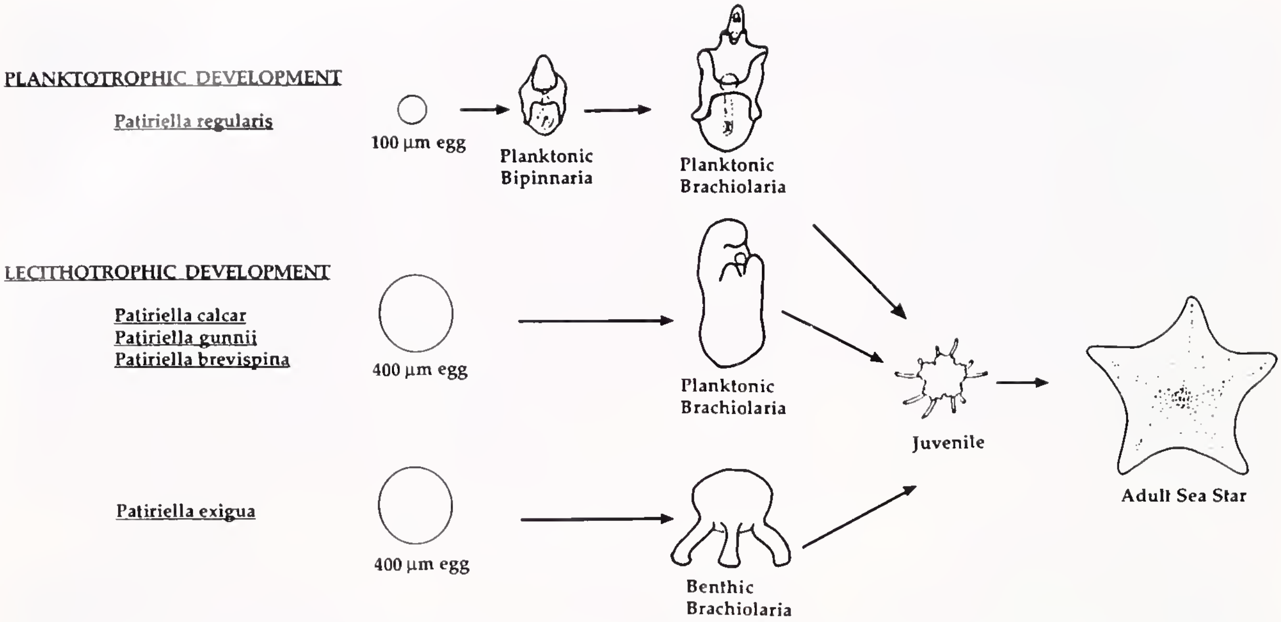

Figure 5. Diagram illustrating the developmental patterns of *Patiriella* species with the development of *P. regularis* (top) presumed to represent the ancestral state. The similarity of the early larva of *P. exigua* to the brachiolariae of *P. calcar* and *P. gunnii* (Table II) suggests that the tripod larval form and benthic development in *P. exigua* arose *via* an intermediate ancestor with pelagic lecithotrophy. The evolutionary changes in developmental pattern are suggested to be from planktotrophy to pelagic lecithotrophy to benthic lecithotrophy.

contrast, newly metamorphosed *P. calcar* and *P. gunnii* do not exhibit this floating behavior (Byrne, pers. obs.). *P. exigua* occupies shallow tide pools, and at low tide the adults are often covered by only a few millimeters of water with occasional emersion (Byrne, 1992). If juveniles in the field exhibit the same floating behavior observed in the laboratory, their attachment to the water surface during low tide may disperse them from the hatching area. *P. exigua* is widely distributed in southeastern Australia and is also found in South Africa, where its presence has been attributed to adult rafting and west-wind drift (Fell, 1962). The behavior of juvenile *P. exigua* indicates that transport of newly metamorphosed individuals may also be a means of dispersal. *P. exigua* lacks a planktonic larva, hence juvenile rafting may be an important mechanism for enhancing gene flow in this species. On the basis of field evidence, Highsmith (1985) suggested that juvenile rafting may account for the widespread distribution of species that lack a planktonic phase.

Comparison of the developmental chronologies of *P. exigua* and *P. regularis* reveals the embryological landmarks and structures that have been modified in the evolution of lecithotrophic development by *P. exigua*. Due to the presence of large yolk reserves, *P. exigua* has lost a feeding bipinnaria, a deletion that undoubtedly influences the duration of development in this species. In comparison with *P. regularis*, whose development is dominated by the bipinnaria stage and takes 7–9 weeks, *P. exigua* has a dominant brachiolaria stage and development takes about 15 days. This difference is independent of temperature (Byrne and Barker, 1991). The similarity of the unhatched larvae of *P. exigua* to the brachiolariae of *P. calcar* and *P. gunnii* suggests that the shift to benthic development involved modification of a planktonic brachiolaria through the hypertrophy of the attachment structures. The evolution of benthic lecithotrophy by *P. exigua* also involved heterochronic changes such as the delay in hatching from the gastrula to the brachiolaria stage and the acceleration in the development of the juvenile form and the adult skeleton, the latter being similar to that described for echinoids with lecithotrophic development (Wray and Raff, 1990).

Acknowledgments

Thanks to Ms. A. Cerra and Ms. P. Laedgsgaard for technical assistance and to Dr. O. Heogh-Guldberg for reading the manuscript. Ms. H. Sowden and Mr. R. Kelly provided assistance in the field. Mr. R. Smith and the staff of the Electron Microscope Unit (EMU) of the University of Sydney also provided technical assistance. Thanks especially to Mr. T. Romeo of the EMU. Two anonymous reviewers are acknowledged for their constructive comments on the manuscript. This work was supported by a grant from the Australian Research Council.

Literature Cited

Barker, M. F. 1978. Structure of the organs of attachment of the brachiolaria larvae of *Stichaster australis* (Verrill) and *Coscinasterias calamaria* (Gray) (Echinodermata: Asteroidea). *J. Exp. Mar. Biol. Ecol.* **33:** 1–36.

Birkeland, C., F.-S. Chia, and R. R. Strathmann. 1971. Development, substratum selection, delay of metamorphosis and growth in the sea star *Mediaster aequalis* (Stimpson). *Biol. Bull.* **141:** 99–108.

Byrne, M. 1991. Developmental diversity in the starfish genus *Patiriella.* Pp. 499–508 in *Biology of the Echinodermata.* T. Yanagisawa, I. Yasumasu, C. Oguro, N. Suzuki, and T. Motokawa, eds. A. A. Balkema, Rotterdam.

Byrne, M. 1992. Reproduction of sympatric populations of *Patiriella calcar, P. exigua* and *P. gunnii,* asterinid sea stars with abbreviated development. *Mar. Biol.* **114:** 297–316.

Byrne, M., and M. F. Barker. 1991. Embryogenesis and larval development of the asteroid *Patiriella regularis* viewed by light and scanning electron microscopy. *Biol. Bull.* **180:** 332–345.

Byrne, M., and M. J. Anderson. 1994. Hybridization of sympatric *Patiriella* species (Echinodermata: Asteroidea) in New South Wales. *Evolution* **48:** 564–576.

Cerra, A., and M. Byrne. 1995a. Cellular events of wrinkled blastula formation and the influence of the fertilization envelope on wrinkling in the sea star *Patiriella exigua. Acta. Zool.* **76:** 155–165.

Cerra, A., and M. Byrne. 1995b. The structure of the extraembryonic matrices around the embryos and larvae of *Patiriella exigua* (Asteroidea) and their role in benthic development, a comparison with the planktonic larvae of *P. regularis. J. Morphol.* **225:** 1–13.

Chen, B.-Y., and C. P. Chen. 1992. Reproductive cycle, larval development, juvenile growth and population dynamics of biology of *Patiriella pseudoexigua* (Echinodermata: Asteroidea) in Taiwan. *Mar. Biol.* **113:** 271–280.

Chia, F. S. 1968. The embryology of a brooding starfish, *Leptasterias hexactis* (Stimpson). *Acta. Zool.* **49:** 321–364.

Chia, F. S., and C. W. Walker. 1991. Echinodermata: Asteroidea. Pp. 301–353 in *Reproduction of Marine Invertebrates Vol. VI, Echinoderms and Lophophorates.* A. C. Giese, J. S. Pearse, and V. B. Pearse, eds. Boxwood Press, Pacific Grove, CA.

Crump, R. G., and R. H. Emson. 1983. The natural history, life history and ecology of the two British species of *Asterina. Field Studies* **5:** 867–882.

Dartnall, A. J. 1971. Australian sea stars of the genus *Patiriella* (Asteroidea, Asterinidae). *Proc. Linn. Soc. N. S. W.* **96:** 39–51.

Fell, H. B. 1962. West-wind drift dispersal of echinoderms in the southern hemisphere. *Nature* **193:** 759–761.

Gemmill, J. F. 1914. The development and certain points in the adult structure of the starfish *Asterias rubens,* L. *Phil. Trans. Roy. Soc. London Ser. B* **205:** 213–294.

Hendler, G., and D. R. Franz. 1982. The biology of a brooding sea star, *Leptasterias tenera,* in Block Island Sound. *Biol. Bull.* **162:** 273–289.

Highsmith, R. C. 1985. Floating and algal rafting as potential dispersal mechanisms in brooding invertebrates. *Mar. Ecol. Prog. Ser.* **25:** 169–179.

Himmelman, J. H., Y. Lavergne, A. Cardinal, G. Martel, and P. Jalbert. 1982. Brooding behavior of the northern sea star, *Leptasterias polaris. Mar. Biol.* **68:** 235–240.

Inoue, C., M. Kiyomoto, and H. Shirai. 1992. Germ cell differentiation in starfish: the posterior enterocoel as the origin of germ cells in *Asterina pectinifera. Develop. Growth Differ.* **34:** 413–418.

Janies, D. A., and L. R. McEdward. 1993. Highly derived coelomic and water-vascular morphogenesis in a starfish with pelagic direct development. *Biol. Bull.* **185:** 56–76.

Kanatani, H. 1969. Induction of spawning and oocyte maturation by 1-methyladenine in starfishes. *Exp. Cell Res.* **57:** 333–337.

Keough, M. J., and A. J. Dartnall. 1978. A new species of viviparous asterinid asteroid from Eyre Peninsula, South Australia. *Rec. S. Aust. Mus.* **17:** 407–416.

Komatsu, M., Y. T. Kano, H. Yoshizawa, S. Akabane, and C. Oguro. 1979. Reproduction and development of the hermaphroditic sea-star, *Asterina minor* Hayashi. *Biol. Bull.* **157:** 258–274.

Kubo, K. 1951. Some observations of the development of the sea-star *Leptasterias ochotensis similispinus* (Clark). *J. Fac. Sci., Hokkaido Univ. Ser. 6 Zool.* **10:** 97–105.

Lawson-Kerr, C., and D. T. Anderson. 1978. Reproduction, spawning and development of the starfish *Patiriella exigua* (Lamarck) (Asteroidea, Asterinidae) and some comparisons with *P. calcar* (Lamarck). *Aust. J. Mar. Freshwater Res.* **29:** 45–53.

MacBride, E. W. 1896. Development of *Asterina gibbosa. Quart. J. Microsc. Sci.* **38:** 221–293.

Marthy, H. J. 1980. Etude descriptive du developpement de l'oeuf d'*Asterina* (Echinoderme, Asteride) son interet en embryologie experimentale. *Vie Milieu* **30:** 75–80.

Newman, H. H. 1925. An experimental analysis of asymmetry in the starfish, *Patiria miniata. Biol. Bull.* **49:** 111–138.

Soliman, E. S., and S. Nojima. 1984. Some observations on dispersal behavior of the early juvenile of the sea-star, *Asterina minor. Publ. Amakusa Mar. Biol. Lab.* **7:** 81–93.

Strathmann, M. F. 1987. *Reproduction and Development of Marine Invertebrates of the Northern Pacific Coast.* University of Washington Press, Seattle. Pp. 535–555.

Strathmann, R. R. 1978. The evolution and loss of feeding larval stages of marine invertebrates. *Evolution* **32:** 894–906.

Strathmann, R. R. 1988. Functional requirements and the evolution of developmental patterns. Pp. 55–61 in *Echinoderm Biology,* R. D. Burke, P. V. Mladenov, P. Lambert, and R. L. Parsley, eds. A. A. Balkema, Rotterdam.

Wray, G. A., and R. R. Raff. 1990. Pattern and process heterochronies in the early development of sea urchins. *Semin. Develop. Biol.* **1:** 245–251.

Reference: *Biol Bull* **188:** 306–312. (June, 1995)

Reproductive Biology, Taxonomy, and Aspects of Chemical Ecology of Latrunculiidae (Porifera)

MICHA ILAN

Department of Zoology, Tel Aviv University, Tel Aviv 69978, Israel

Abstract. Sexual reproduction has been observed for the first time within the widely distributed sponge family, the Latrunculiidae. *Latrunculia magnifica* Keller 1889 was studied mainly in the northern Red Sea in the Gulf of Eilat and the Gulf of Suez. The sponge is hermaphroditic and viviparous. The embryo develops to a large (mean 868 ± 144 μm, max. 1200 μm) parenchymella larva. The period of reproduction lasts for several months, ceasing only during the winter. Like oocytes, sperm appear to develop from archeocytes, which is uncommon among sponges. The presence of brooded larvae in *L. magnifica* supports the position of Latrunculiidae within the order Poecilosclerida, subclass Ceractinomorpha, rather than within the Tetractinomorpha. The absence of a periflagellar sleeve from around the base of the choanocyte's flagellum lends further support to this idea. Nuclear magnetic resonance (NMR) analysis of secondary metabolites within the sponge and its nudibranch predator (*Chromodoris quadricolor*) confirms that both species contain the same latrunculin homologue (either A or B). The latter finding indicates the presence of a compound derived from the diet (*i.e.*, sponge) within the nudibranch.

Introduction

Sponge species belonging to the family Latrunculiidae are distributed from the polar region (*e.g.*, *Latrunculia apicalis*) to the tropics (*e.g.*, *L. corticata*) and from shallow to deep (2460 m) water (Hartman, 1982). Despite the wide distribution of this family, the biology of its members has rarely been studied, and their mode of sexual reproduction is virtually unknown. The sole evidence about latrunculiid development is that on some occasions young sponges were observed developing directly within the parental body without first going through a free larval stage (Bergquist, 1978).

The Latrunculiidae is characterized by small spicules (microscleres) of the discorhabd type, which are usually densely packed in the dermal crust (Fig. 5). The large spicules (macroscleres) are monoactinal, diactinal, or both, and are arranged either radially at the surface with an additional axial orientation or in a confused disposition at the inner parts of massive forms (Bergquist, 1978; Hartman, 1982; Soest, 1984). Latrunculiidae is one of three sponge families that do not possess chelae microscleres, but which Lévi (1973) (following Topsent, 1928) assigned to the order Poecilosclerida (subclass Ceractinomorpha). His arguments are based on the family's affinities with two other well-established Poecilosclerid families (Mycalidae and Esperiopsidae). The taxonomic position of the Latrunculiidae is, however, still not clear. In fact, some researchers believe this family should be assigned to the order Hadromerida, subclass Tetractinomorpha (Dendy, 1922; Burton, 1930; Bergquist, 1978; Hartman, 1982). Their association of the Latrunculiidae to this order relies on the type of the megascleres, their arrangement within the sponge, and the surface position of the microscleres. Soest (1984) states that the arguments are weak for either choice of association of Latrunculiidae with any of these orders.

A representative species within this family, *Latrunculia magnifica* Keller 1889, is a bright red branching sponge, prominent in the coral reefs of the Red Sea. Its geographical distribution stretches from Djibouti (Gulf of Aden, Indian Ocean) to Eilat (Northern Red Sea) (Keller, 1889; Row, 1911; and Ilan, unpub.).

The major aim of the present study was to determine the mode of reproduction of this species. But in addition to the ecological implications of revealing the previously unknown mode of reproduction in the Latrunculiidae, such an investigation would also help clarify the taxo-

Received 8 June 1994; accepted 16 March 1995.

nomic position of the Latrunculiidae. This is because the mode of embryonic development is a major criterion for distinguishing between the two subclasses Tetractinomorpha and Ceractinomorpha. An additional criterion distinguishing Hadromerida from other sponge orders is the presence of a periflagellar sleeve around the base of the choanocytes' flagella (Vos *et al.*, 1991). Therefore, a study of the choanocyte chambers was also carried out.

Chemical studies have established that *L. magnifica* contains macrolides, termed latrunculins, that are ichthyotoxic. These compounds interfere with actin rather than tubulin organization and thus alter cell shape and disrupt microfilament organization (Neeman *et al.*, 1975; Spector *et al.*, 1983, 1989; Schatten *et al.*, 1986). Several closely related macrolides were isolated from *L. magnifica*, with the two homologues latrunculin A and B constituting the major components (Groweiss *et al.*, 1983). Of 20 different animal collections, all those collected from the Gulf of Eilat contained latrunculin B, the two from the Gulf of Suez contained latrunculin A, and those from the Tiran straits contained a mixture of both macrolides (Groweiss *et al.*, 1983). The chemical content of different sponge populations from throughout the range of the species distribution has not yet been carefully examined. So the validity and significance of this geographical trend as well as the possibility that it extends to larger regions remain open.

The nudibranch *Chromodris quadricolor* preys upon *L. magnifica*. Mebs (1985) raised the possibility that latrunculin derived from the sponge might protect its nudibranch predator from predation by fish. He demonstrated that spots of extracts made from *L. magnifica, C. quadricolor*, and nudibranch mucus appear in thin layer chromatography (TLC) to have the same retention time (Rf) as latrunculin B (although with TLC one cannot differentiate latrunculin A from B). More conclusive evidence has not yet been provided. Other studies have also exhibited the presence of the same secondary metabolites in various sponge species and their nudibranch predators (*e.g.*, Faulkner and Ghiselin, 1983; Rogers and Paul, 1991; Gavagnin *et al.*, 1992). Because *L. magnifica* contains both latrunculin A and B, we may ask: (1) Are these compounds distributed among sponges in geographically distinct populations, and can the compounds be used as chemotaxonomical markers to distinguish between populations? (2) What kind of compounds are unambiguously present within the nudibranchs, and do they follow the geographical distribution pattern exhibited by the sponges?

Materials and Methods

Sponge collection

The study area was in the northern Red Sea. Most of the samples were collected in the vicinity of the Interuniversity Institute, Marine Biological Laboratory, Eilat, located at the northern end of the Gulf of Eilat. Additional samples were collected along the Sinai Peninsula: along the Gulf of Eilat, in the vicinity of the Tiran straits, and at several locations in the Gulf of Suez. One collection is from the Central Red Sea (27°44′N, 34°07′E), one from the South Red Sea (Dahlak Island), and one from the Gulf of Aden—Indian Ocean (Djibouti).

On average three sponges were collected each month in the northern Red Sea, but occasionally (once or twice a year) oocytes and embryos were sought in cuts made in tens to hundreds of sponges during their collection for chemical studies in other locations in the Red Sea.

Anatomical studies

Samples of tissue were fixed each month either in preparation for electron (EM) or light (LM) microscopy. The fixative was 2.5% glutaraldehyde for EM and 4% formalin for LM. Both solutions were buffered in seawater. Preparation for transmission EM and LM included dissolving the siliceous spicules by treatment with hydrofluoric acid for 4–6 h. For scanning EM the procedure included washing, dehydration, critical-point-drying in liquid CO_2 and coating with gold palladium. A JEOL JSM-840A SEM was used. For transmission EM the samples were postfixed with 1% OsO_4, dehydrated, embedded, sectioned and stained with acetate and lead citrate. A JEOL 1200-EX TEM was used. Samples for LM were rinsed in 70% ethanol, dehydrated, embedded, sectioned, and stained with hematoxylin and eosin.

Every sponge was examined for reproductive elements. If present, these were measured and the developmental stages determined. The aim was to establish the timing and duration of the reproductive season, whether the species is gonochoric (separate sexes) or a simultaneous hermaphrodite, whether it broods its embryos or sheds gametes to the water, what kind of embryos develop in this species, and what type of cells give rise to the gametes.

Chemical analysis

For this study, sponges were collected from different sites in the North Red Sea (Eilat, Tiran straits, Gulf of Suez), the South Red Sea (Dahalak Archipelago), and the Indian Ocean (Djibouti). Nudibranchs were collected only in Eilat and the Gulf of Suez. The content of latrunculin within the sponges (*L. magnifica*) and nudibranchs (*C. quadricolor*) was evaluated as follows. Sponges and nudibranchs were freeze-dried and then extracted three times in a mixture of CH_2Cl_2-MeOH (9:1, v:v). The solvent was then removed under vacuum, and the residue of each extract was separated into three fractions by vacuum chromatography through a short silica gel column, with CH_2Cl_2, 2% MeOH-CH_2Cl_2, and 10% MeOH-CH_2Cl_2, as

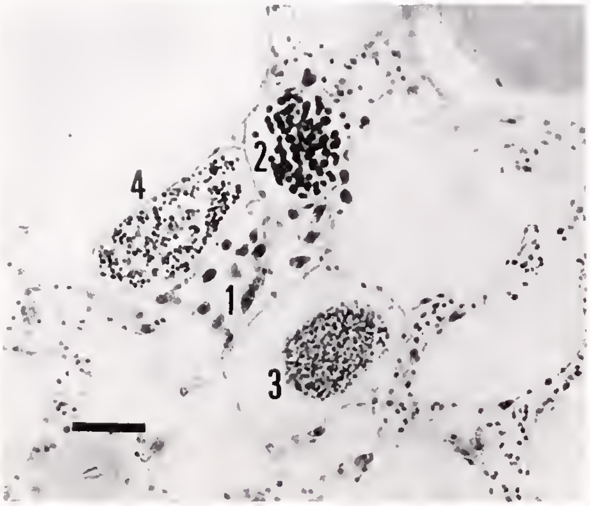

Figure 1. *Latrunculia magnifica* spermatogenesis. Four developmental stages of spermatozoa (1–4), demonstrating an increase in number coinciding with decrease in size of the spermatids in each spermatic cyst. The development appears to start with a few large archeocytes (1) which diminish in size and proliferate to become many small sperm (4). Scale bar size = 25 μm.

eluant. The solvent was removed from each fraction under vacuum. The fractions obtained from nudibranch extracts were compared by TLC and ^{1}H and ^{13}C NMR (Nuclear Magnetic Resonance) with authentic samples of latrunculins and with extracts of the sponge.

Results

Latrunculia magnifica was usually found in water deeper than 3 m, but also in shallower water near the Tiran straits or in other locations with strong water currents. In shallow water, the encrusting form was more common, while among deeper sponge populations the usual branching form was dominant (data not shown). The sponge prefers walls with a steep to negative slope, or protruding bodies (*sensu* Abelson *et al.*, 1994). Frequently the sponge harbored epi- and endosymbionts, such as brittle stars, barnacles, starfishes, amphipods, polychaetes, and the associated nudibranch *Chromodoris quadricolor*.

L. magnifica individuals contained reproductive products during most months of the year. The small number of sponges collected during some months hampered quantitative determination of the proportion of sponges within the population that were reproducing. Individuals were devoid of reproductive elements only during winter (November to January). Primary oocytes were noticed (in some, but not all sponges) starting from February until September. Incubated larvae were detected between June and October.

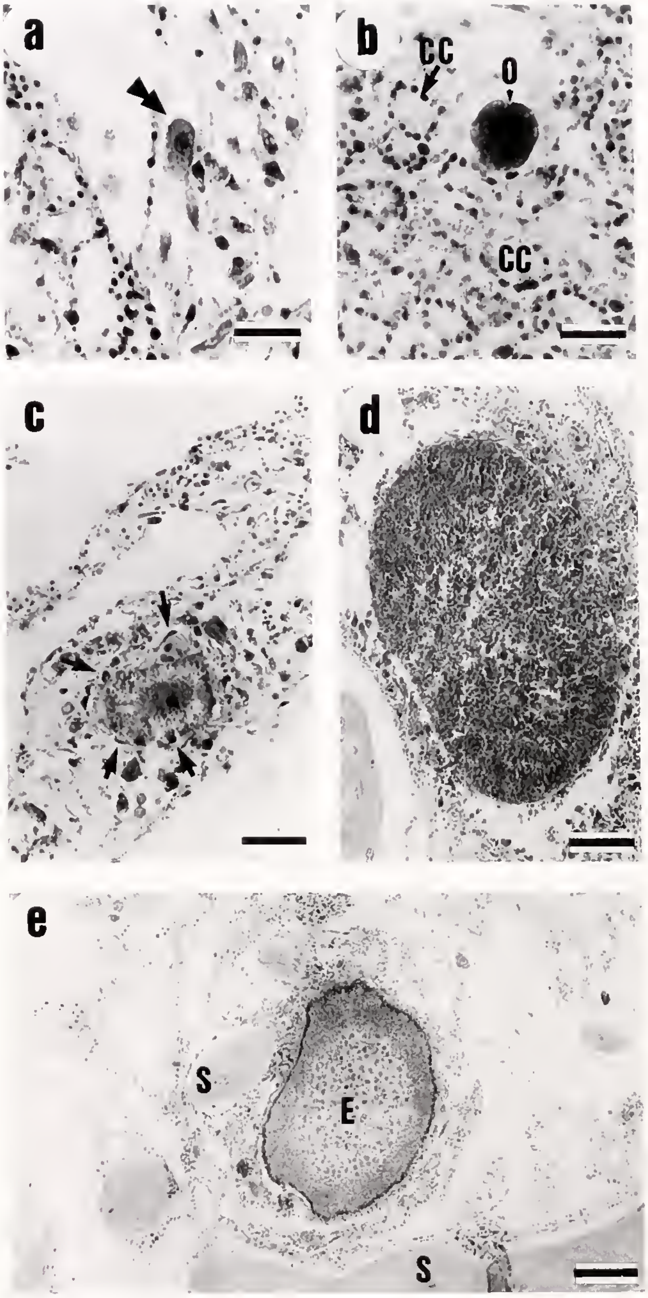

Figure 2. *Latrunculia magnifica* oocyte and embryonic development. (a) Primary oocytes (arrowhead) are slightly larger than nearby amebocytes. Scale bar = 25 μm. (b) Primary oocytes (o) larger than in 2a. For comparison see choanocyte chamber (cc) adjacent to the developing oocyte. Scale bar = 25 μm. (c) The growing oocyte, still with a prominent nucleus and nucleolus, is surrounded by nurse cells (arrows). Scale bar- 50 μm. (d) A mature oocyte that has reached 570 μm. The nucleus is no longer evident. Scale bar = 100 μm. (e) A developing embryo (E) contains several types of cells. Those that will differentiate into ciliated cells are at the periphery of the embryo. Spongin fibers (s) can also be seen. Scale bar = 100 μm.

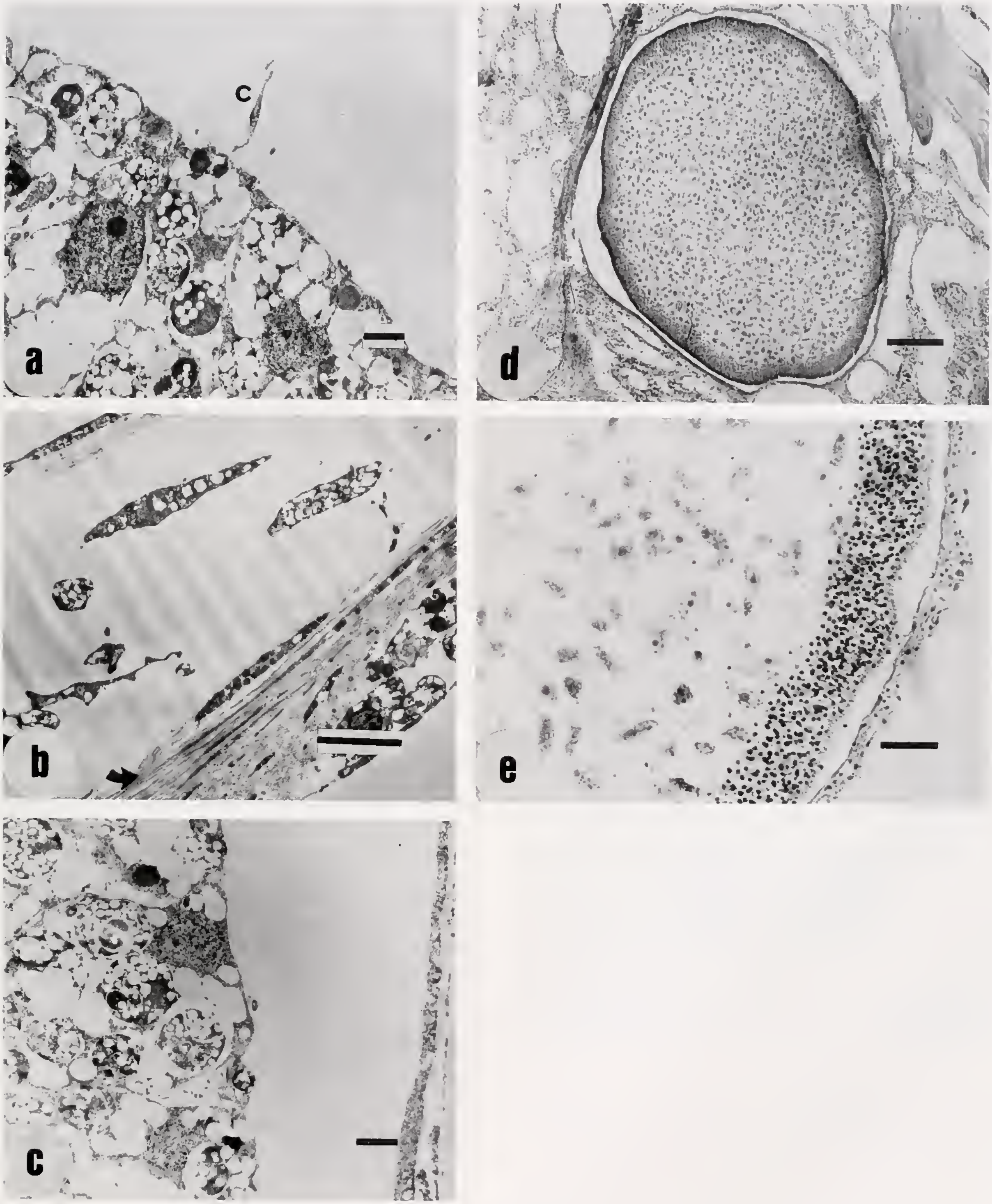

Figure 3. *Latrunculia magnifica* larval development. (a) Surface of the embryo. Elongated cells, with only a few having a cilium (c). Scale bar = 2 μm (TEM). (b) The area surrounding the developing embryo. Collagen deposition (arrow). Scale bar = 5 μm (TEM) (c) Embryo (left) and its cyst envelope (right). Scale bar = 2 μm (TEM). (d) Cross section through an incubating larva. Several cell types are evident, and some collagenous deposition inside the larva occurs. Scale bar = 100 μm (LM). (e) The surface of a developing larva is densely beset with ciliated cells. Inside the larva various cell types are evident. Scale bar = 25 μm (LM).

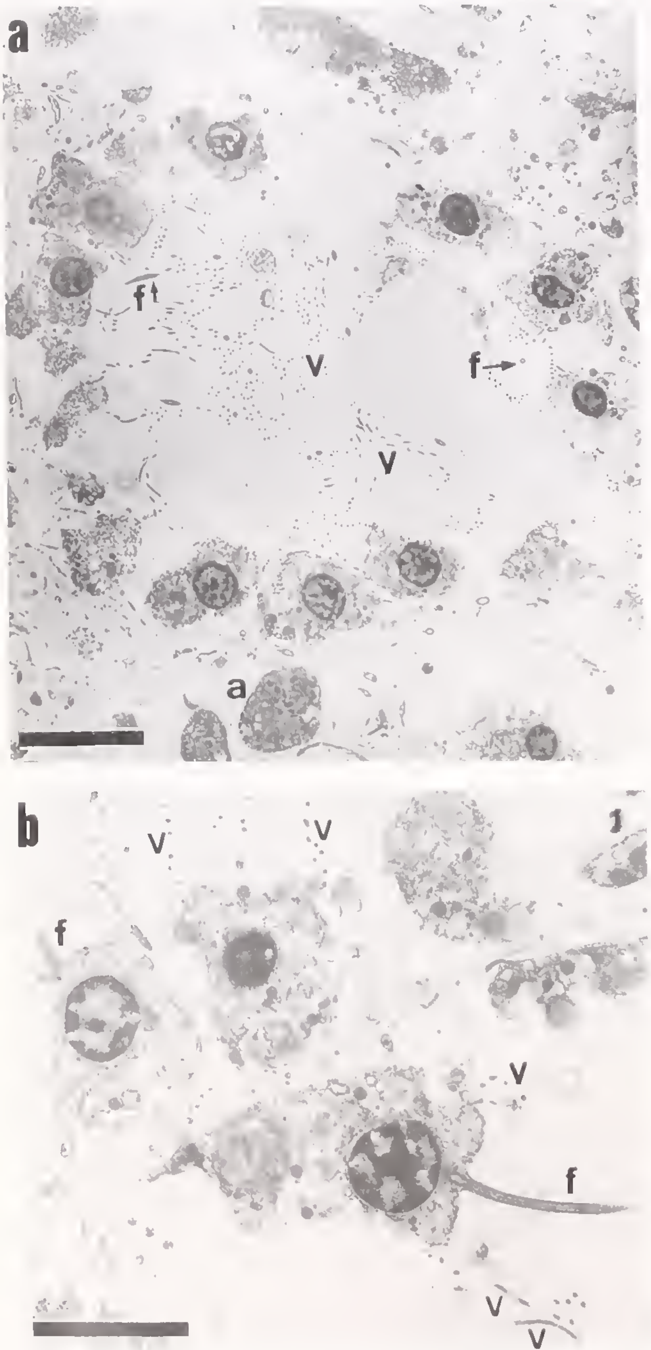

Figure 4. *Latrunculia magnifica* choanocyte chamber. (a) Choanocyte chamber. Note the flagellum (f), microvilli (v), and the amebocyte (a) that destroys the captured particles. Scale bar = 5 μm (TEM). (b) Two enlarged choanocytes. Cell body, microvilli (v), and flagellum (f). Scale bar = 2.5 μm (TEM). No periflagellar sleeve is present in either picture.

L. magnifica proved to be a simultaneously hermaphroditic species and the gametes of both genders were present in some of the reproducing sponges. The spermatozoa appear to develop from archeocytes (Fig. 1). The spermatic cysts are encircled by surrounding cells, and the sperm grow in number while decreasing in size (Fig. 1). The diameter of the cyst is 47 ± 13 μm, and they are present in different developmental stages (Fig. 1). Oocytes develop in size by engulfing surrounding nurse cells (Fig. 2). Large oocytes (393 ± 91 μm) are fertilized internally and are incubated until they develop into mature parenchymella larvae (Fig. 3d). The embryos are bright orange to red in color. They are distributed throughout the mesohyl (never in the cortex) and are very distinct against the pale red color of the inner parts of *L. magnifica*. The developing embryos are encircled with a layer of cells, some of which secrete a collageneous coat of fibrils around the embryo (Fig. 3b). The inner cells of the embryo are of several types (Fig. 3a–e). The fully ciliated larva is large and reaches up to 1200 μm (mean 868 ± 144 μm). No free-swimming larva was observed during this study.

Figure 4 depicts a choanocyte chamber. It is apparent that no periflagellar sleeve is present around the base of the choanocyte's flagellum. The chamber has a diameter of about 25 μm and is constructed of 3-μm-wide choanocytes.

The discorhabd microscleres, which are typical of the Latrunculiidae, are found mostly at the dermal crust of the sponge (Fig. 5). In addition, the sponge contains some spongin fibers. The gross morphology of *L. magnifica* is highly variable, and specimens collected in the different localities were within the variation found in any of the given localities, and thus indistinguishable. The chemical analysis, however, confirmed the existence of different geographical distributions of latrunculins within sponge and nudibranch populations and thus provided a means of distinguishing between sponge populations (as well as those of their nudibranch predator).

The latrunculin content of *L. magnifica* amounts to 1–2% of the sponge dry weight (except for sponges from Djibouti, in which it is only 1%). NMR analysis established that the nudibranch *C. quadricolor* from the Gulf of Eilat contains latrunculin B, the same as its prey *L. magnifica* collected at the same locality. Samples taken from sponges and nudibranchs found in the Gulf of Suez contain latrunculin A. In the Tiran straits, however, the sponges possess either latrunculin A or latrunculin B (but not both within the same individual). Sponges from the South Red Sea (Dahlak Island) contain only latrunculin A. Specimens of *L. magnifica* collected from a sponge population in Djibouti contained both homologs (A & B). No nudibranchs were collected at the two latter collection sites.

Discussion

The presence of spermatic cysts in different stages suggests that more than one short sperm release event occurs during a reproductive season. The presence of larvae dur-

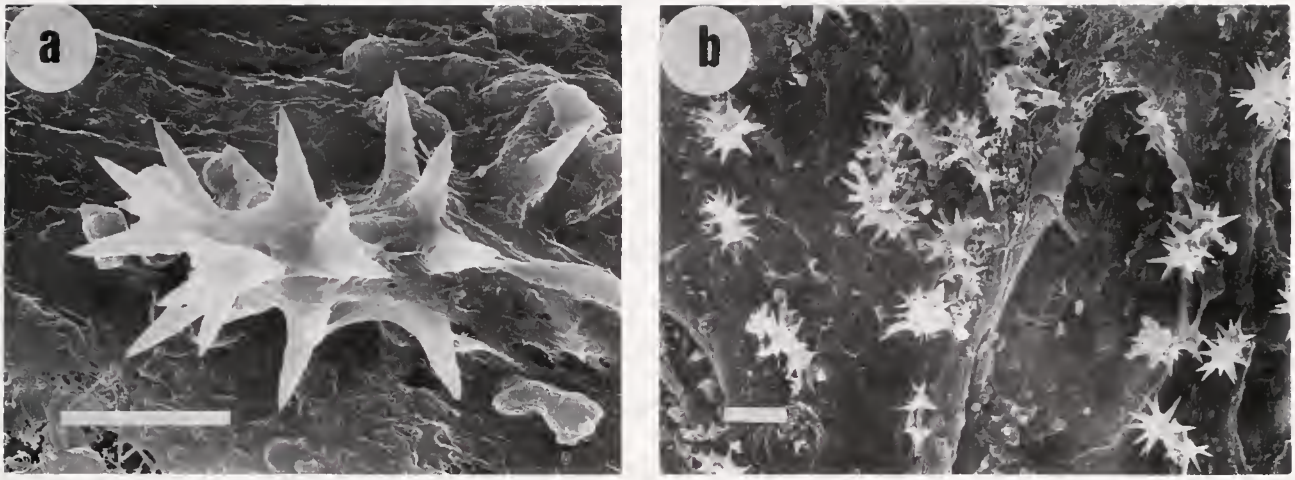

Figure 5. *Latrunculia magnifica* typical discorhabd microscleres. (a) A spicule embedded in spongin. Scale bar = 10 μm (SEM). (b) A layer of discorhabds near the sponge's surface. Scale bar-20 μm (SEM).

ing many months of the year serves to confirm this conclusion. An extended reproductive season has been found among other brooding sponges in the Red Sea (Ilan and Loya, 1988, 1990; Ilan and Vacelet, 1993). This strategy could be a means of ensuring settlement on vacant spots as they become available on the reef. Like *Niphates* sp. (Ilan and Loya, 1988), *L. magnifica* also does not release larvae during winter, possibly avoiding the cover of post larvae by the seasonal algal bloom. As in the present study, the development of sperm from archeocytes has been documented among other sponges as well, although spermatozoids are generally thought to develop from choanocytes (Reiswig, 1983). The *L. magnifica* spermatic cyst is within the regular size found for sponges (Bergquist, 1978; Reiswig, 1983; Simpson, 1984), although the larva is larger than the average parenchymella (Bergquist, 1978; Fell, 1983; Simpson, 1984).

The large size of the larva may provide an advantage for rapid settlement and possession of a relatively large size compared with other invertebrate larvae. This initial large size is considered to elevate post-larval survivorship (*e.g.*, Hughes and Connell, 1987). The apparent difference in the size of oocytes and larvae can be attributed to the gain of nutrients by the embryo from the parental sponge, or, as Fell (1983) indicated, the mature oocyte is probably the size of the larvae, but what seems to be an initial stage of embryogenesis is actually a developing oocyte with nonhomogeneous cytoplasm that eventually reaches the size of a larva.

This study is the first to document the brooding embryonic mode of development within the Latrunculiidae. The finding that *L. magnifica* is a viviparous species is of taxonomic importance because it supports the view that the Latrunculiidae should be placed within the order Poecilosclerida, subclass Ceractinomorpha (Topsent, 1928; Lévi, 1973; Soest, 1984). An additional species from the same family (*Negombata* sp.) studied at the same locations was also found to brood embryos (Ilan, unpub. data), which further supports this idea. In addition, the absence of a periflagellar sleeve from around the base of the choanocyte's flagellum, which is typical of hadromerid sponges (Vos *et al.*, 1991), also strengthens this view. It should be noted that the presence of spongin fibers in this species (as well as in the *Negombata* species mentioned before), which gives the species elastic properties, also supports the non-Hadromerid positioning of the Latrunculiidae, since this order is characterized by the absence of spongin fibers and therefore is firm but non-elastic (Bergquist, 1978; Hartman, 1982). This example demonstrates that when skeletal morphology is not sufficient to distinguish between two taxa, other characters, including anatomical and developmental ones, may be used.

The chemical composition of sponges has been used to assist in their classification (*e.g.*, Bergquist *et al.*, 1984). But latrunculins occur within other sponge species such as *Spongia mycofijiensis* (Crews *et al.*, 1988; Quinoa *et al.*, 1988). Thus they cannot be used as chemotaxonomical characters to distinguish between species. Within *L. magnifica* the type of latrunculin homologs is, however, a solid character with which to distinguish between different populations. In addition, *L. magnifica* and the nudibranch *C. quadricolor*, when collected at the same location, have the same latrunculin homolog. In the Gulf of Eilat, this is latrunculin B, while south to the Tiran straits and in the Gulf of Suez, the sponges and nudibranchs contain latrunculin A. The identical geographic appearance of the latrunculin homologs in the sponge and the nudibranch populations provides strong circumstantial evidence to support the idea of dietary origin of the compounds found within the nudibranch tissues.

Some questions remain. Why does latrunculin, a potent disrupter of actin microfilament organization (Spector *et al.*, 1989), not affect *C. quadricolor?* Do the larvae of the nudibranchs use the different latrunculin homologs as chemical inducers for specific settlement on their prey? The occurrence of both homologs in Djibouti is not well understood. One explanation is that the cells producing the latrunculin within the sponge are symbiotic bacteria. If so, such bacteria could also be found in several other species—like the taxonomically unrelated *Spongia mycofijiensis*—and within different populations of the same species.

Acknowledgments

I thank Prof. Y Kashman and the members of his group for the chemical work on the sponge and nudibranch tissues. The constructive remarks of two reviewers improved the manuscript and are acknowledged.

Literature Cited

Abelson, A., D. Weihs, and Y. Loya. 1994. Hydrodynamic impediments to settlement of marine propagules, and adhesive-filament solutions. *Limnol Oceanogr.* **39:** 164–169.

Bergquist, P. R. 1978. *Sponges.* University of California Press, Los Angeles.

Bergquist, P. R., M. P. Lawson, A. Lavis, and R. C. Cambie. 1984. Fatty acid composition of Porifera. *Biochem Sys Ecol.* **12:** 63–84.

Burton, M. 1930. Norwegian sponges from the Norman collection. *Proc. Soc. Zool. Lond* **22:** 487–546.

Crews, P., Y. Kakou, and E. Quinoa. 1988. Mycothizole, a polyketide heterocycle from a marine sponge. *J Am Chem. Soc.* **110:** 4365.

Dendy, A. 1922. Report on the Sigmatotetraxonida collected by H.M.S. "Sea Lark" in the Indian Ocean. *Trans. Linn. Soc. Lond Zool.* **18:** 1–164.

Faulkner, D. J., and M. T. Ghiselin. 1983. Chemical defense and evolutionary ecology of dorid nudibranchs and some other opistobranch gastropods. *Mar. Ecol. Prog. Ser.* **13:** 295–301.

Fell, P. E. 1983. Porifera. Pp. 1–29 in *Reproductive Biology of Invertebrates. Vol I, Oogenesis, Oviposition, and Oosorption,* K. G. Adiyodi and R. G. Adiyodi, eds. Wiley & Sons, New York.

Gavagnin, M., R. R. Vardaro, C. Avila, G. Cimino, and J. Ortea. 1992. Ichthyotoxic diterpenoids from Cantabrian nudibranch *Chromodoris luteorosea J Nat. Prod* **55:** 368–371.

Groweiss, A., U. Shmueli, and Y. Kashman. 1983. Marine toxins of *Latrunculia magnifica J. Org. Chem.* **48:** 3512–3516.

Hartman, W. H. 1982. Porifera. Pp. 640–666 in *Synopsis and Classification of Living Organisms,* S. P. Parker, ed. McGraw-Hill. New York.

Hughes, T. P., and J. H. Connell. 1987. Population dynamics based on size or age? A reef-coral analysis. *Am Nat* **129:** 818–829.

Ilan, M., and Y. Loya. 1988. Reproduction and settlement of the coral reef sponge *Niphates* sp. (Red Sea). Proc. Coral Reef Symp. Australia **2:** 745–749.

Ilan, M., and Y. Loya. 1990. Sexual reproduction and settlement of the coral reef sponge *Chalinula* sp. from the Red Sea. *Mar Biol.* **105:** 25–31.

Ilan, M., and J. Vacelet. 1993. *Kebira uteoides* (Porifera, Calcarea), a recent "Pharetronid" sponge from coral reefs. *Ophelia* **38:** 107–116.

Keller, C. 1889. Die spongienfauna des Rothen *Meeres. Z. Wiss. Zool.* **48:** 311–405.

Lévi, C. 1973. Systematique de la class de Demospongiaria (Demosponges). Pp. 577–631 in *Traite de la Zoologie 3,* P. P. Grass, ed Masson.

Mebs, D. 1985. Chemical defense of a dorid nudibranch, *Glossodoris quadricolor,* from the Red Sea. *J. Chem. Ecol.* **11:** 713–716.

Neeman, I., L. Fishelson, and Y. Kashman. 1975. Isolation of a new toxin from the sponge *Latrunculia magnifica* in the gulf of Aqaba (Red Sea). *Mar Biol.* **30:** 293–296.

Quinoa, E., Y. Kakou, and P. Crews. 1988. Fijianolides, polyketide hetrocycles from a marine sponge. *J Org. Chem.* **53:** 3642.

Reiswig, H. M. 1983. Porifera. Pp. 1–21 in *Reproductive Biology of Invertebrates Vol. II Spermatogenesis and Sperm Function,* K. G. Adiyodi and R. G. Adiyodi, eds. Wiley & Sons, New York.

Rogers, S. D., and V. J. Paul. 1991. Chemical defenses of three *Glossodoris* nudibranchs and their dietary *Hyrtios* sponges. *Mar. Ecol. Prog Ser* **77:** 221–232.

Row, R. W. H. 1911. Report on the sponges collected by Mr. Cyril Crossland in 1904–05. Part II, Non Calcarea. *J Linn. Soc. Lond.* **31:** 287–400.

Schatten, G., H. Schatten, I. Spector, C. Cline, N. Paweletz, C. Simerly, and C. Petzelt. 1986. Latrunculin inhibits the microfilament-mediated processes during fertilization, cleavage and early development in sea urchins and mice. *Exp. Cell Res.* **166:** 191.

Simpson, T. L. 1984. *The Cell Biology of Sponges.* Springer Verlag, New York.

vanSoest, R. W. M. 1984. Marine sponges from Curacao and other Caribbean localities. Part III Poecilosclerida. *Stud Fauna Curacao Caribb Islands* **199:** 1–187.

Spector, I., N. R. Shochet, Y. Kashman, and A. Groweiss. 1983. Latrunculin: novel marine toxins that disrupt microfilament organization in cultured cells. *Science* **219:** 493–495.

Spector, I., N. R. Shochet, D. Blasberger, and Y. Kashman. 1989. Latrunculins—novel marine macrolides that disrupt microfilament organization and affect cell growth: I. Comparison with cytochalsin D. *Cell Motil. Cytoskl.* **13:** 127.

Topsent, E. 1928. Spongiaires de l'Atlantique et de la Mediterranee provenant des criosieres du Prince Albert I^{er} de Monaco. *Result. Camp Scient. Prince Albert I Monaco* **74:** 1–376.

Vos, L. de, K. Rützler, N. Boury-Esnault, C. Donadey, and J. Vacelet. 1991. Atlas of sponge morphology. Smithsonian Institution Press, Washington, DC.

Reference: *Biol. Bull.* **188:** 313–328. (June, 1995)

Experimental and Histological Studies of Four Life-History Stages of the Eastern Oyster, *Crassostrea virginica,* Exposed to a Cultured Strain of the Dinoflagellate *Prorocentrum minimum*

GARY H. WIKFORS[1] AND ROXANNA M. SMOLOWITZ[2]

[1]*National Oceanic and Atmospheric Administration, National Marine Fisheries Service, Northeast Fisheries Science Center, Milford, Connecticut 06460; and* [2]*Laboratory for Marine Animal Health, University of Pennsylvania, Marine Biological Laboratory, Woods Hole, Massachusetts 02543*

Abstract. Effects of the dinoflagellate *Prorocentrum minimum* (strain EXUV) upon four life-history stages of the eastern oyster—embryos, feeding larvae, newly set spat, and juveniles—were investigated in laboratory exposure studies. Embryonic development was not affected significantly by living, heat-killed, or sonicated cells, or by growth-medium extracts from *P. minimum* cultures. Feeding larvae, however, showed poor growth and poor development of the digestive system when fed *P. minimum,* as compared with larvae fed *Isochrysis* sp. (strain T-ISO). Growth of larvae fed mixed *P. minimum* + *Isochrysis* diets was intermediate. Larvae and newly set spat that had been fed a diet of ⅓ *P. minimum* + ⅔ *Isochrysis* exhibited distinctive changes in digestive-system anatomy. Spat showed an abnormal accumulation of lipid in the stomach epithelium. Absorptive cells in the digestive glands of both larvae and spat contained accumulation bodies, often with a laminated, fibrous appearance in preparations for transmission electron microscopy. These accumulation bodies were PAS (periodic acid-Schiff) positive and may correspond to autolysosomal bodies within *P. minimum* cells. Juvenile oysters developed the ability to digest *P. minimum,* but only after a refractory period of about 2 weeks, during which most *P. minimum* was filtered but rejected as pseudofeces. The linking of accumulation bodies within absorptive cells of oyster digestive diverticula with dinoflagellate autolysosomal bodies suggests a mechanism by which some dinoflagellates interfere with feeding in phytoplankton grazers.

Received 1 September 1994; accepted 21 February 1995.

Introduction

Harmful algal blooms are viewed as an increasing threat to utilization of living marine resources (Hallegraeff, 1993). Studies of interactions between dinoflagellates and molluscan shellfish have focused mainly on the accumulation of mammalian neurotoxins by molluscs feeding on toxic dinoflagellates (Sakamoto *et al.,* 1987). More recently, the detrimental effects of toxic dinoflagellates, as well as the effects of some algae that produce no known mammalian toxins, upon the shellfish themselves have been identified (Shumway, 1990). Responses ranging from reduced filtering to increased metabolic rates, paralysis, and mortality have been noted for molluscs feeding upon natural populations of dinoflagellates or cultured strains (Gainey and Shumway, 1988). It has, in fact, been suggested that detrimental effects upon shellfish by a number of phytoplankton taxa may be undetected rather than uncommon (Parry *et al.,* 1989).

Among dinoflagellate taxa implicated in toxic effects are members of the genus *Prorocentrum.* Two benthic *Prorocentrum* species, *P. lima* and *P. mexicanum,* produce ciguatoxin, which accumulates in tropical finfish food chains and renders apex predators unfit for human consumption (Steidinger, 1983). There are historical accounts of *P. minimum*—and its taxonomic equivalents *P. mariae-lebouriae, Exuviaella mariae-Lebouriae,* and *P. triangulatum* (Dodge, 1982)—causing toxic effects in both shellfish and human consumers of shellfish harvested from *P. minimum* bloom water (Shumway, 1990). One strain of *P. minimum* that is cultured in a number of laboratories, clone EXUV (CCMP1329), yielded negative results in previous (Schmidt and Loeblich, 1979) mouse bioassays for water-soluble mammalian toxins (PSP) and in assays carried out during the present study (S. E. Shumway, pers. comm.). Despite the negative finding for mammalian toxin in this strain, we demonstrated previously that EXUV cultured in our laboratory did not support the growth of juvenile northern quahogs, *Mercenaria mercenaria*, and was acutely toxic to juvenile bay scallops, *Argopecten irradians* (Wikfors and Smolowitz, 1993). Complete mortality of scallops exposed to the EXUV strain occurred within 1–4 weeks of first exposure. Affected scallops had severe attenuation of epithelial cells associated with absorptive-cell necrosis and sloughing of cells into central lumens. Large melanized hemocyte clots were present throughout the open vascular system; these histologic observations are strong evidence for the presence of a molluscan enterotoxin in EXUV.

Because *P. minimum* is a normal component of the summertime flora in the coastal waters of the northeastern United States (Marshall, 1980; Sellner *et al.*, 1993; Wikfors, in prep.), it seemed possible that native oysters, which spawn during summer, could be exposed to this dinoflagellate at any stage of their life history. Timing, density, and geographic extent of *Prorocentrum* populations could play some role in the recruitment success of oysters if there are detrimental effects at particular life-history stages. Therefore, the present study was undertaken to expose oysters at four life-history stages—prefeeding embryos, feeding larvae, newly set spat, and juveniles—to cultured *P. minimum*, both alone and in combination with a known "good-food" alga, *Isochrysis* sp. (strain T-ISO). Survival, development, growth, and histologic condition were evaluated and compared with those of starved oysters and oysters fed T-ISO alone—an algal diet known to support normal growth and development (Wikfors, unpub.).

Materials and Methods

Phytoplankton culture

The EXUV strain of *P. minimum* (CCMP1329) was obtained from the Provasoli-Guillard Center for the Culture of Marine Phytoplankton; *Isochrysis* sp. strain T-ISO was in the Milford Microalgal Culture Collection. Both axenic algal strains were cultured in enriched natural seawater medium, E formulation (Ukeles, 1973), in 16-l carboy assemblies housed in a temperature-controlled (20°C) room with constant illumination of 500–600 μE m^{-2} s^{-1} from cool-white fluorescent lamps. Cultures were managed semi-continuously, with daily harvests of sufficient volumes to satisfy experimental regimes and weekly replacement of harvested volumes with sterilized medium. Culture densities were determined as packed-cell volumes by centrifugation in specially modified Hopkins tubes (Ukeles, 1973), and daily feeding regimes were specified according to packed-cell volume (specified for larvae or postset below). Cell counts were made in an Improved Neubauer hemocytometer.

Oyster rearing

Broodstock oysters from the Milford Laboratory were spawned by warm-water stimulation (Loosanoff and Davis, 1963); 5 females and 8 males contributed gametes to the cohort used in experiments. All oyster rearing was in Milford Harbor seawater (27–28‰ salinity) that was temperature-adjusted to 25°C, filtered to 0.5 μm, and passed through a flow-through ultraviolet sterilizer and an activated-carbon organic-removal cartridge. For the experiment with embryos, fertilized eggs were distributed into 1-l polypropylene beakers at a concentration of 20 ml^{-1}. Embryos were exposed to experimental treatments (see below) within 2 h of fertilization. Remaining embryos were incubated in seawater treated as above for 48 h before experiments were begun with feeding larvae. Subsamples of 48-h larvae were collected on a 36-μm-mesh monofilament nylon screen and distributed into 1-l beakers at a concentration of 20 ml^{-1}. Larvae not used in feeding experiments were reared on a diet of T-ISO and *Pavlova lutheri* (Milford strain MONO) through metamorphosis and then grown on natural phytoplankton amended with cultured algae (mostly *Tetraselmis maculata* strain TTM and *Pavlova gyrans* strain 93, with small amounts of diatoms and other flagellates). Four days before use in juvenile feeding studies, oysters were placed in filtered seawater to empty the digestive systems.

Experimental design

Oyster embryos were exposed to a variety of live and killed cells and extracts from *P. minimum* and the control alga, T-ISO, shortly after fertilization of eggs. Live algal cultures were added, along with the culture medium in which they were grown, as aliquots providing the number of cells given as a first feeding according to the regime of Rhodes and Landers (1973); *i.e.*, 0.005 ml packed cells l^{-1} larval culture containing 20 larvae ml^{-1}; for T-ISO, this was 60×10^6 cells l^{-1}, and for EXUV, 3.9×10^6 cells l^{-1}. Equal amounts of both algal strains were subjected to the following treatments before being added to embryo suspensions: (1) removal of cells by filtration to 0.22 μm, (2) sonication for 5 min at 250 W with 50/50 timed pulse, or (3) heating to 80°C for 30 min. In addition to the above treatments, live and sonicated EXUV culture, and medium from EXUV culture, were added at 5 times standard volume. Seawater-only and sterile algal medium controls were included as well. All treatments were in triplicate. Embryos were incubated on a temperature-controlled water table (25°C) for 48 h, and then evaluated microscopically for effects upon survival and development.

Counts of live-normal, live-abnormal, dead-normal, and dead-abnormal larvae were made for all treatments.

Larval oysters, which had been permitted to develop for 48 h in filtered seawater, were distributed into 1-l beakers for larval feeding experiments, also incubated on the 25°C water table. Larval populations in triplicate beakers were given the following daily feeding regimes: (1) EXUV, (2) ⅓ EXUV + ⅔ T-ISO, (3) ⅔ EXUV + ⅓ T-ISO, (4) T-ISO, and (5) unfed. Daily rations were adjusted according to packed-cell volume, following the progressively increasing schedule of Rhodes and Landers (1973). Concentrations (cells per liter) of T-ISO and EXUV alone on the first day of feeding are given in the previous paragraph; cells in mixed diets and in increasing rations can be calculated from these. Three days each week, larvae were collected on a 75-μm monofilament nylon screen, washed with a pressurized flow of seawater, and resuspended in newly filtered seawater. At this time, subsamples of larvae were counted on a Sedgewick-Rafter slide under a dissecting microscope and measured (shell length) on a compound video-microscope using image-analysis PC-computer software. *In vivo* fluorescence, pH, and salinity of spent larval-culture water were measured every 3 days as well; water for these samples was poured gently through a 36-mesh nylon screen to minimize the effect of fecal material upon the fluorescence measurements. Subsamples of larvae were taken periodically and fixed for histological examination; results for samples taken 8 days after spawning are reported. Larvae fed T-ISO, EXUV, and the ⅓ EXUV + ⅔ T-ISO diet were observed live, 60 min after feeding on day 14, under epifluorescence microscopy (Babinchak and Ukeles, 1979) to determine if larvae were ingesting and digesting algal cells.

In cultures that produced pedi-veligers, whole oyster shells were provided as setting substrate, and setting success was determined by counting spat on shell surfaces. Newly set spat continued to receive the diet provided to them as larvae. Spat were sampled for histological examination 5 days after setting.

The subpopulation of oysters from the same cohort, which was reared separately to a mean size of 8.3 mm shell length, was divided into groups of between 15 and 25 and placed in molluscan rearing chambers designed for conducting nutritional studies with young shellfish (Ukeles and Wikfors, 1982). Seawater supplying the chambers was filtered to 0.5 μm, passed through an ultraviolet sterilizer, and temperature-adjusted to 25°C in a head tank. Seawater then was distributed to chambers at a flow rate of 600 ml min^{-1} through a flow-adjustable manifold. The same unialgal and mixed diets were fed to juvenile oysters as were fed to larvae. Daily rations were 0.006 ml packed cells $\text{oyster}^{-1}\ \text{d}^{-1}$, and percentage mixes were made by packed-cell volume, not cell number. A full ration of T-ISO consisted of 143×10^6 cells per oyster, and a full ration of EXUV was 9.27×10^6 cells per oyster; cell numbers in percentage diets can be calculated from these values. Seawater flow through the chambers was continuous, except for the 4 h after feeding, during which flow was stopped. Fluorometer measurements showed that all algal food suspensions were cleared within 2 h of feeding. Each week, for 6 weeks, oysters were removed from chambers and cleaned with a pressurized spray of seawater; with the aid of image-analysis software on an IBM-compatible microcomputer, shell lengths were measured from video images.

Histology

Subsamples of 48-h larvae, feeding larvae, and newly set spat were processed in plastic (Embed 812, Electron Microscopic Sciences). Briefly, samples fixed in 1% glutaraldehyde/4% formalin in 28‰ NaCl (1G4F) (Howard and Smith, 1983) were rinsed with phosphate buffer, secondarily fixed in 1% osmium, and hydrated to unbuffered water. Oysters were decalcified in 2% ascorbic acid in 0.9% sodium chloride at pH 2.3 for 15–20 h, followed by a rinse of unbuffered water. Samples were concentrated before removal of each solution by centrifuging at $1300 \times g$ for 3 min, followed by removal of the supernatant. Oysters then were embedded in 3% agarose (aqueous). Enbloc staining was done in 2% uranyl acetate (aqueous) overnight. Staining was followed by infiltration, embedment in Embed 812, and polymerization by standard methods. Thick sections cut from the plastic-embedded samples were stained with 1% methylene blue in 1% borax (sodium borate) and 1% azure II. Ultrathin sections were stained with 2% uranyl acetate and counter-stained with Reynolds lead-citrate. Thick sections were examined and photographed using an Olympus BH-2 photomicroscope. Thin sections were examined on a Zeiss 10 transmission electron microscope.

Juvenile oysters were fixed *in situ* by placing the oyster shells with attached juveniles into large bottles containing 1G4F. After a minimum of 1 week, fixed juveniles were carefully pried from the large shell on which they had settled and were decalcified in formic acid. After decalcification and rinsing, animals were processed in paraffin by standard methods (Humanson, 1979).

P. minimum cultures were diluted with 1G4F fixative (10 ml/100 ml culture) and concentrated by settling in an Imhoff cone. Supernatant was poured off, and concentrated cells were resuspended in 10 ml 1G4F for observation with transmission electron microscopy (TEM). These cultures were processed in paraffin with the agarose embedding methods described above.

Periodic acid-Schiff (PAS) staining of plastic-embedded sections was accomplished as follows: plastic was removed from thick sections of plastic-embedded larvae by incu-

Table I

Development of oyster embryos exposed for 48 h to cultured phytoplankton and culture extracts (means of three replicates, SD in parentheses)

Added	% Live normal	% Dead normal	% Live abnormal	% Dead abnormal
Seawater	91.3	0.4	5.9	2.4
	(1.5)	(0.4)	(0.9)	(0.6)
Medium	88.3	0.8	9.5	1.4
	(3.4)	(0.4)	(2.6)	(0.7)
Live T-ISO	89.5	1.0	8.4	1.2
	(2.8)	(0.8)	(2.5)	(0.2)
Live EXUV	84.1	1.7	9.3	4.9
	(4.0)	(0.8)	(1.3)	(2.2)
T-ISO Medium	88.9	0.7	9.3	1.1
	(1.3)	(0.4)	(1.0)	(1.0)
EXUV Medium	84.6	1.6	11.2	2.6
	(2.8)	(0.6)	(1.0)	(1.4)
Sonicated T-ISO	88.6	0.9	7.9	2.6
	(3.4)	(0.3)	(2.5)	(0.6)
Sonicated EXUV	80.2	1.5	15.2	3.1
	(1.0)	(0.8)	(2.4)	(2.2)
Heated T-ISO	74.2	1.0	24.1	0.7
	(25.7)	(0.4)	(25.2)	(0.1)
Heated EXUV	88.3	1.0	8.5	2.2
	(3.3)	(0.9)	(3.0)	(0.6)
Sonic. EXUV 5 ×	72.0	2.0	19.0	6.0
EXUV Medium 5×	87.0	2.0	10.0	1.0
Live EXUV 5×	88.0	1.0	9.0	1.0

bating slides with thick sections in a solution of 66% NaOH/33% ethanol for 15 min, followed by rehydration (Erlandsen *et al.*, 1979). Rehydrated sections were stained with Harris' hematoxylin counterstain (Sorvall, 1981) as previously described.

Results

Embryos

Counts of embryos developing to the straight-hinge larval stage after 48 h exposure to experimental treatments are shown in Table I. Development to straight-hinge stage was more than 80% in all treatments except for embryos exposed to heat-killed T-ISO and 5× sonicated EXUV; however, differences between these treatments and all others were not statistically significant (ANOVA, $p = 0.05$). Percentages of larvae in the other three categories were not statistically different either. Thus, none of the treatments interfered significantly with survival, development, or gross morphology as observed with the dissecting microscope.

Histologic observation by light and electron microscopy revealed only subtle differences between some treatments. Only samples of oysters exposed to seawater only, sonicated T-ISO, or 5× sonicated EXUV were examined. Although animals exposed to seawater only or to sonicated T-ISO had well-developed organ systems, oysters exposed to 5× sonicated EXUV showed mildly decreased numbers and sizes of lipid droplets in the mantle, velar cells, and absorptive cells of the digestive gland.

Feeding larvae

The salinity in all experimental cultures remained between 27‰ and 28‰ throughout the experiment, but differences in pH and *in vivo* fluorescence between treatments revealed differences in ingestion of the algal foods added and in the resultant water chemistry. Percentage of the diet consumed, averaged over the entire experiment, for each diet is listed in Table II. Larvae fed diets including EXUV filtered less of the diet from suspension. It was not, however, clear from fluorescence measurements alone if depressed filtration was a result of physical inability of the larvae to ingest *P. minimum* or to detrimental effects of the *P. minimum* cells that were ingested. The observation of *P. minimum* cells within digestive systems of larvae by epifluorescence microscopy and the histologic observations detailed below provided evidence that *P. minimum* cells were ingested. No significant differences in pH between diets were noted (Table II).

Differences in survival and growth of larvae on experimental diets were found, with *P. minimum* having consistent, detrimental effects. Numbers of larvae decreased for all feeding regimes, partly as a result of losses in sampling and handling. However, larvae fed only EXUV or the ⅔ EXUV + ⅓ T-ISO diet decreased in number more rapidly than larvae in the other treatments between days 13 and 17 (ANOVA, $p < 0.01$). Unfed larvae all starved within 27 days (Fig. 1). Growth of larvae on experimental diets was related directly to the amount of T-ISO in the diet (Fig. 2). Growth rates ranged from 1.10 to 6.52 $\mu m\ d^{-1}$, and differences between diets were significant (ANOVA, $p < 0.01$) (Table III).

Table II

Percentages of food filtered, as measured by in vivo *fluorescence decrease, and pH of larval culture water after 48-h incubation with larvae (means of 154 measurements, SE in parentheses)*

Feeding regime	% Fluorescence decrease	pH
T-ISO	36.1 (6.7)^{1}	7.96 (0.02)^{1}
⅓ EXUV + ⅔ T-ISO	32.4 (3.0)^{1,2}	7.87 (0.05)^{1}
⅔ EXUF + ⅓ T-ISO	14.9 (5.4)^{2}	8.01 (0.01)^{1}
EXUV	14.1 (8.6)^{2}	7.94 (0.01)^{1}
Unfed	−0.3 (0.3)^{3}	7.89 (0.02)^{1}

Different superscript numbers denote statistically different means by Duncan's multiple range test.

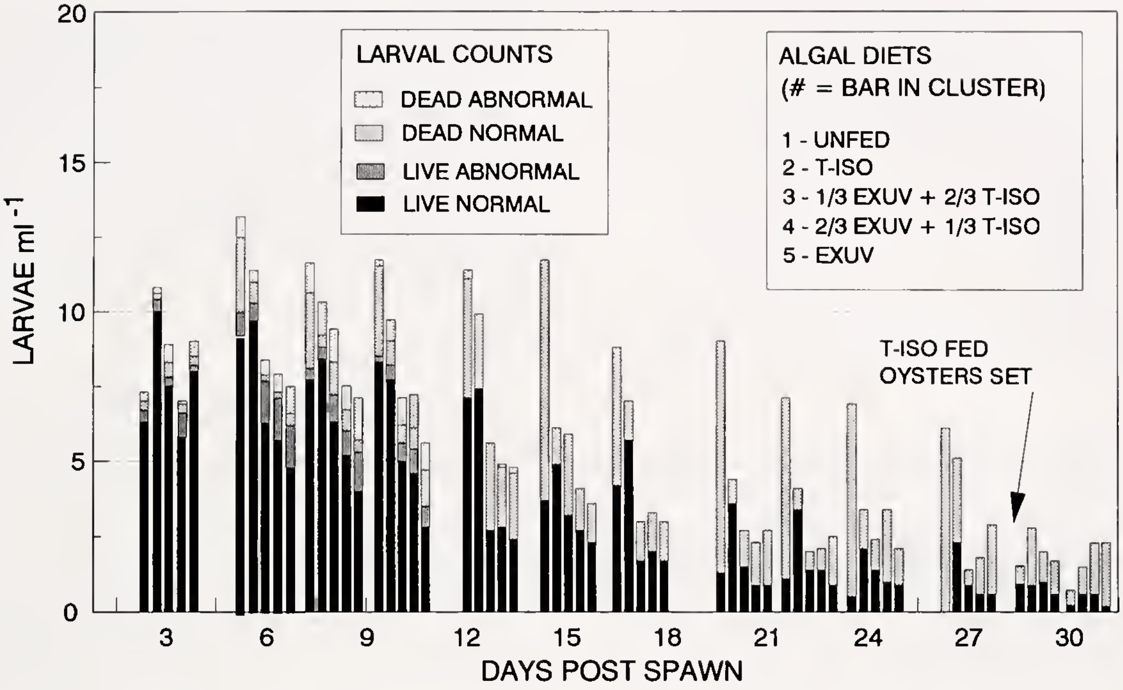

Figure 1. Counts of oyster larvae (means of three replicates) from experimental feeding regimes.

Histologic observation of larvae from day 8 revealed clear differences between EXUV-fed, T-ISO-fed, mixed-diet, and unfed treatments (Figs. 3, 4). Animals fed on T-ISO were in the prodissiconch II stage of development (Elston, 1980) and demonstrated excellent cellularity of developing organs (Fig. 3A). Stomach and intestinal epi-

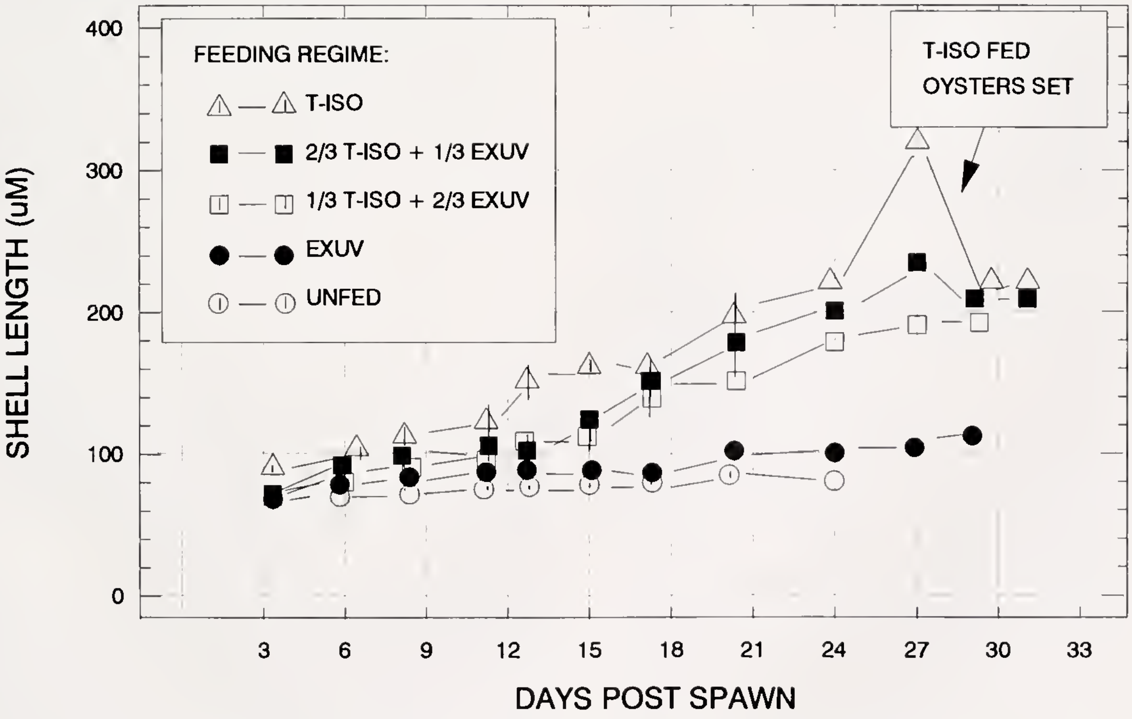

Figure 2. Shell-length measurements of larvae from experimental feeding regimes.

Table III

Growth rates, in micrometers per day (±SE), of larval oysters fed algal diets

Algal diet	Growth rate
Unfed	0.744 (.103)^{a}
EXUV	1.10 (.447)^{a}
⅔ EXUV	3.49 (.940)^{ab}
⅓ EXUV	5.63 (1.33)^{bc}
T-ISO	6.52 (1.54)^{c}

Superscript letters indicate homogeneous subsets, according to Least Square Difference Multiple Range Test.

thelium was high-cuboidal in outline, and the intestinal epithelium contained many prominent lipid droplets. The digestive gland contained numerous tall-columnar absorptive cells. Examination with TEM showed that phagolysosomes within absorptive cell cytoplasm contained moderately electron-dense flocculent substances (Fig. 4A). Rare phagolysosomes present at the basal side of some cells contained dense, irregular inclusions.

Starved animals were still in the prodissiconch I stage of development (Elston, 1980). All organ development was poor, and organs demonstrated low cellularity (Fig. 3B). Stomach epithelium was low-cuboidal to squamous, and intestinal profiles were rare. Lipid droplets were not present in these animals. The digestive glands were small, with poor cellularity, as demonstrated by the greatly reduced numbers of low-columnar to cuboidal absorptive cells. Examination with TEM showed that rare phagolysosomes within the absorptive cell cytoplasm contained mildly flocculent contents.

All EXUV-fed larvae were in the late prodissiconch I stage of development. Organ development and cellularity was greater than in starved oysters, but was only about one-third that of T-ISO-fed animals (Fig. 3C). Stomach and intestinal epithelium was cuboidal to sometimes squamous. Lipid droplets were not seen in any cell type. Absorptive cells of the digestive glands were about one-third larger than in starved oysters. Interestingly, many dense inclusions were present throughout the cytoplasm of these cells (Fig. 3D). Examination with TEM showed these inclusions to be a continuum of phagolysosome profiles (which we have termed accumulation bodies)—from phagolysosomes containing possible autolysosome and other dinoflagellate debris, to those filled with densely flocculent material, to residual bodies containing haphazardly arranged, laminated, dense bundles of fibers with both loose and condensed appearances (Fig. 4B and 4C).

Eight-day-old oysters fed a diet containing ⅔ EXUV + ⅓ T-ISO were in the early prodissiconch II stage of development. Organ development and cellularity was slightly greater than in animals fed entirely on EXUV. Stomach and intestinal epithelia were cuboidal. Lipid droplets were rare in the stomach epithelium and very rare in the intestinal epithelium. Digestive glands appeared to be slightly more cellular than in animals fed EXUV only, as demonstrated by increased numbers of absorptive cells within any section of the glands. Phagolysosomes, as seen in control animals, and the distinctive accumulation bodies were noted under both light and transmission electron microscopy.

Newly set spat

Only larvae fed T-ISO alone or ⅓ EXUV + ⅔ T-ISO developed into pedi-veligers and set, and only about 100 spat were obtained with the latter diet including EXUV, as compared with more than 2000, from three initial populations of 2000, for the unialgal T-ISO diet. Spat from these treatments were maintained on their respective larval diets for 5 days after setting. Histologically, animals fed T-ISO alone exhibited well-developed organs with excellent cellularity (Fig. 5A). The stomach epithelium was cuboidal, with rare, small lipid granules in the cytoplasm. There were two to four profiles of intestine per section, and intestinal epithelial cells were cuboidal to columnar in outline. Lipid droplets were abundant and prominent in the intestinal epithelium. Phagocytes within the perivisceral cavity contained clear to lightly foamy cytoplasm. Absorptive cells of the digestive gland were of the tall-columnar type, with foamy, vacuolated cytoplasm. Examination with TEM demonstrated abundant phagolysosomes containing flocculent, irregular, granular material of various densities, as noted in pre-set larvae fed T-ISO.

Newly set spat fed the mixed diet showed distinctive and striking differences from the T-ISO controls (Fig. 5A). Animals contained moderately to poorly developed organ systems with reduced cellularity (Fig. 5B). Stomach epithelium was low-cuboidal to squamous and contained moderate to heavy accumulations of large lipid droplets. Only one to two cross-sections of intestine could be seen in some sections. Intestinal cells were cuboidal with variable (moderate to small) amounts of lipid droplets in the cytoplasm. Absorptive cells of the digestive gland were cuboidal to low-columnar in outline. Both light and electron microscopic examination showed that the absorptive cells contained abundant accumulation bodies, as described above (Fig. 5C). Examination of the intestinal epithelium with TEM showed that it also contained moderate numbers of accumulation bodies.

Distinctive effects of EXUV in the diet were seen in the perivisceral space of newly set oysters with both light and transmission electron microscopy. Phagocytes within the space were plump and although some contained only clear vacuoles, most phagocytes contained various numbers of large, dense, irregular particles, 3–

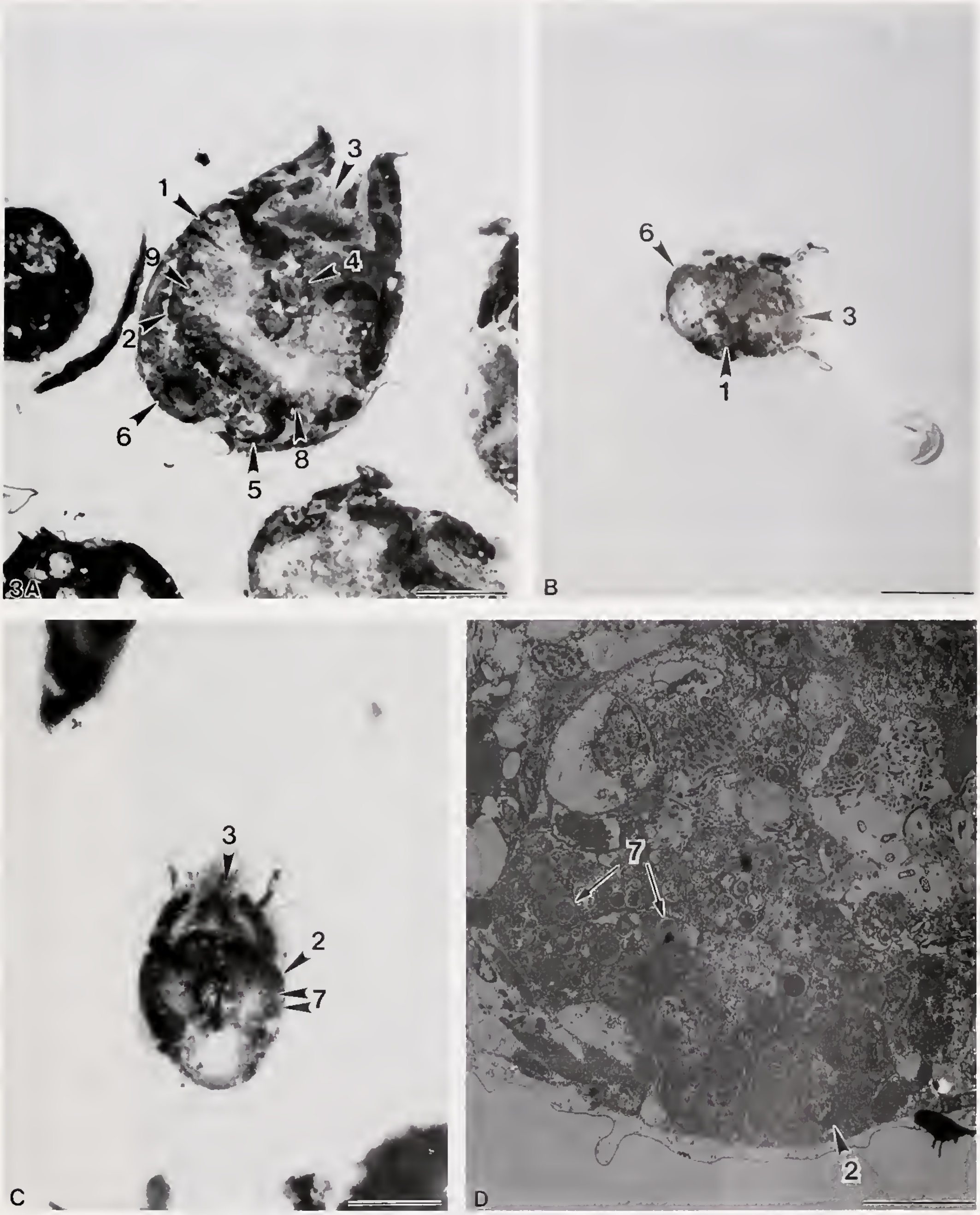

Figure 3. Feeding larvae. Photomicrographs A, B, and C are all at the same magnification. Animals are embedded in plastic, thick-sectioned, and stained with methylene blue (1, digestive gland absorptive cells; 2, digestive gland enzymatic cell; 3, velum; 4, esophagus; 5, intestine; 6, style sac; 7, accumulation bodies in absorptive cells; 8, lipid globules; 9, phagolysosomes). (A) Control animals (T-ISO-fed) show well-developed organs. (B) Starved larvae show poor development of all organs. (C and D) Animals fed 100% EXUV show poorly to moderately developed organs with distinctive accumulation bodies in the absorptive cells. (A to C, bar = 20 μm; D, bar = 12.5 μm.)

10 μm in diameter. Other phagocytes surrounded and appeared to be in the process of engulfing similar large, irregular, dense particles (Fig. 6A). Rarely, less degenerate particles showed profiles consistent with the dinoflagellate. Examination with TEM showed partially degraded dinoflagellates that contained small, round bodies (possible autolysosomes) (Fig. 6B). Focal, multicellular necrosis within organs was not evident in

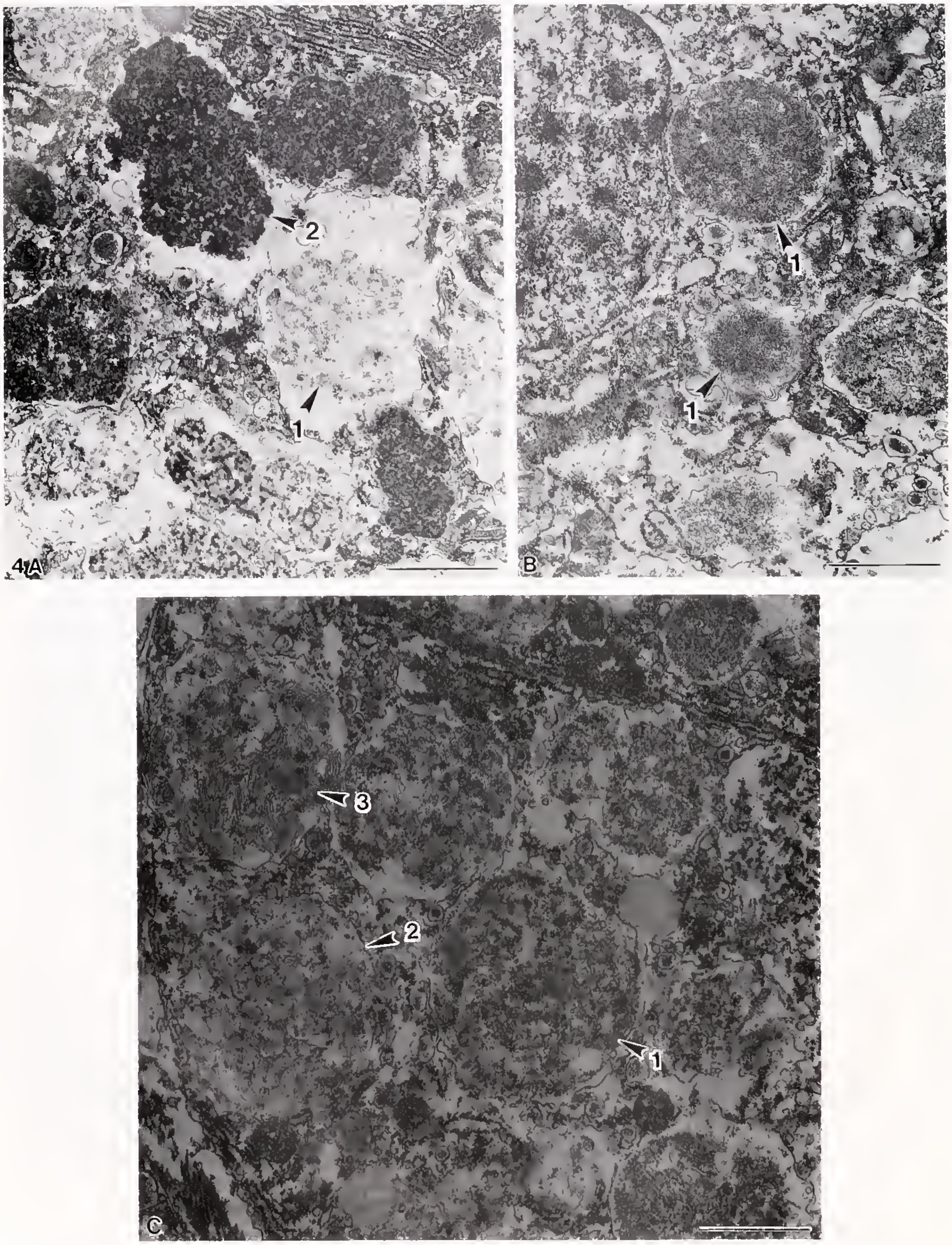

Figure 4. Feeding larvae (transmission electron micrographs). (A) T-ISO-fed animals show moderately electron-dense, flocculent substances (1) and dense, irregular inclusions (2) in phagolysosomes. (Bar = 2 μm.) (B and C) Distinctive accumulation bodies (oyster phagolysosomes containing dinoflagellate autolysosomes and other debris) are present in absorptive cells of EXUV-fed animals and show a progression from phagolysosomes containing debris and round bodies similar to autolysosomes (1), to phagolysosomes containing distinctive flocculent material (2), to residual bodies containing dense bundles of fibers (3). (B, bar = 2 μm; C, bar = 2 μm.)

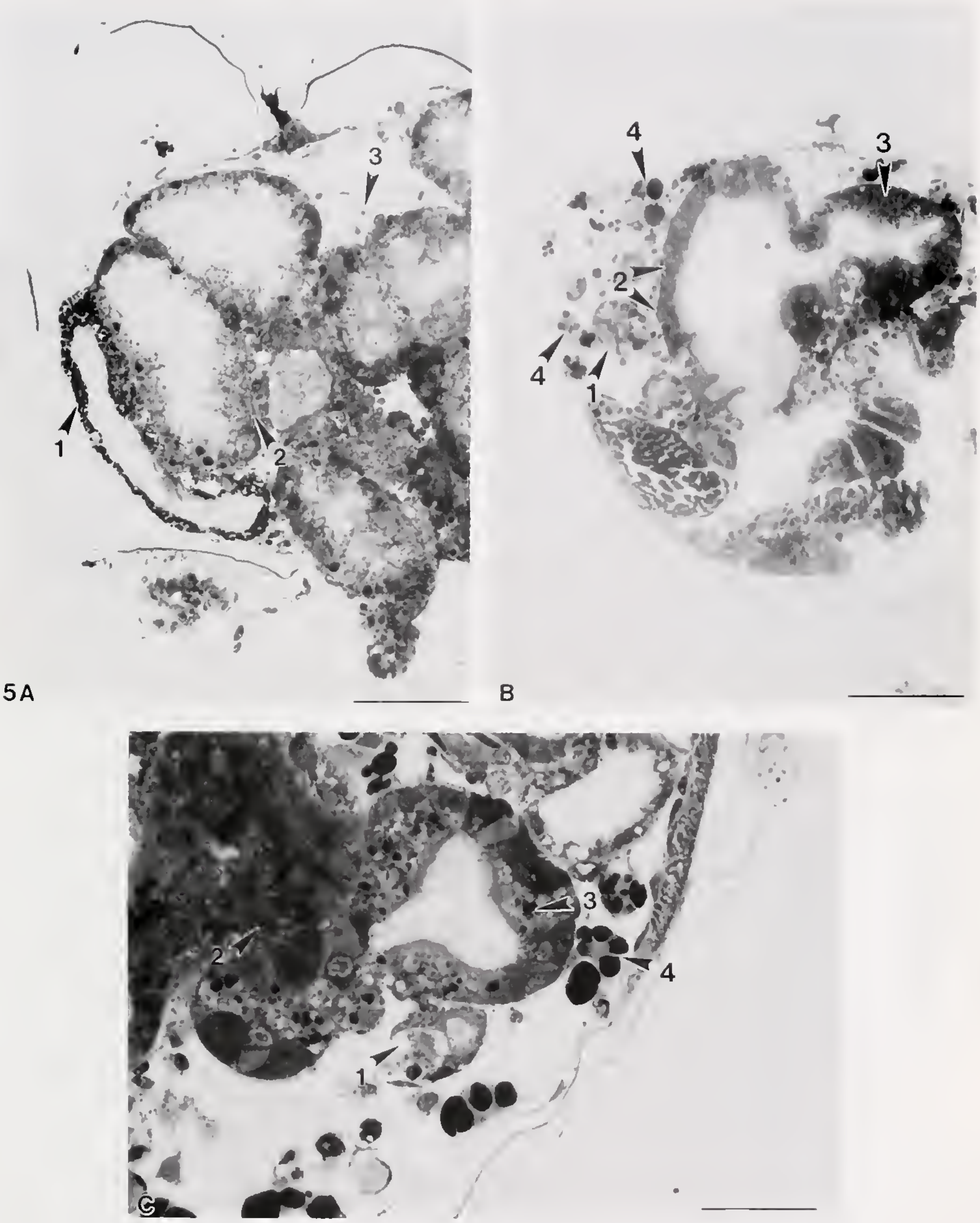

Figure 5. Newly set spat. Animals are embedded in plastic, thick-sectioned, and stained with methylene blue. (A) A T-ISO-fed control animal shows good development of organs with abundant lipid droplets in the intestinal epithelium (1), columnar absorptive cells in the digestive glands (2), and rare phagocytes in the perivisceral space (3). (Bar = 40 μm.) (B and C) An EXUV-fed animal shows poor development of intestine epithelium with vacuolation and lack of lipid droplets (1), abundant lipid droplets in the style-sac epithelium (2), and distinctive accumulation bodies in the absorptive cells of the digestive gland (3). Dinoflagellates in various stages of degeneration are present within phagocytes or are being engulfed by phagocytes in the perivisceral space (4). (B, bar = 40 μm; C, bar = 11.4 μm.)

EXUV-fed oysters; however, individual cell necrosis of the intestinal, digestive-gland, and stomach epithelium appeared to be present.

Histological examination of plastic-embedded larvae stained with PAS showed positive staining of accumulation bodies within the cytoplasm of absorptive cells of EXUV-fed (7A) but not T-ISO-fed oysters (Fig. 7B). The partially degraded dinoflagellates within the perivisceral space of newly set spat fed the mixed diet were positively stained with PAS.

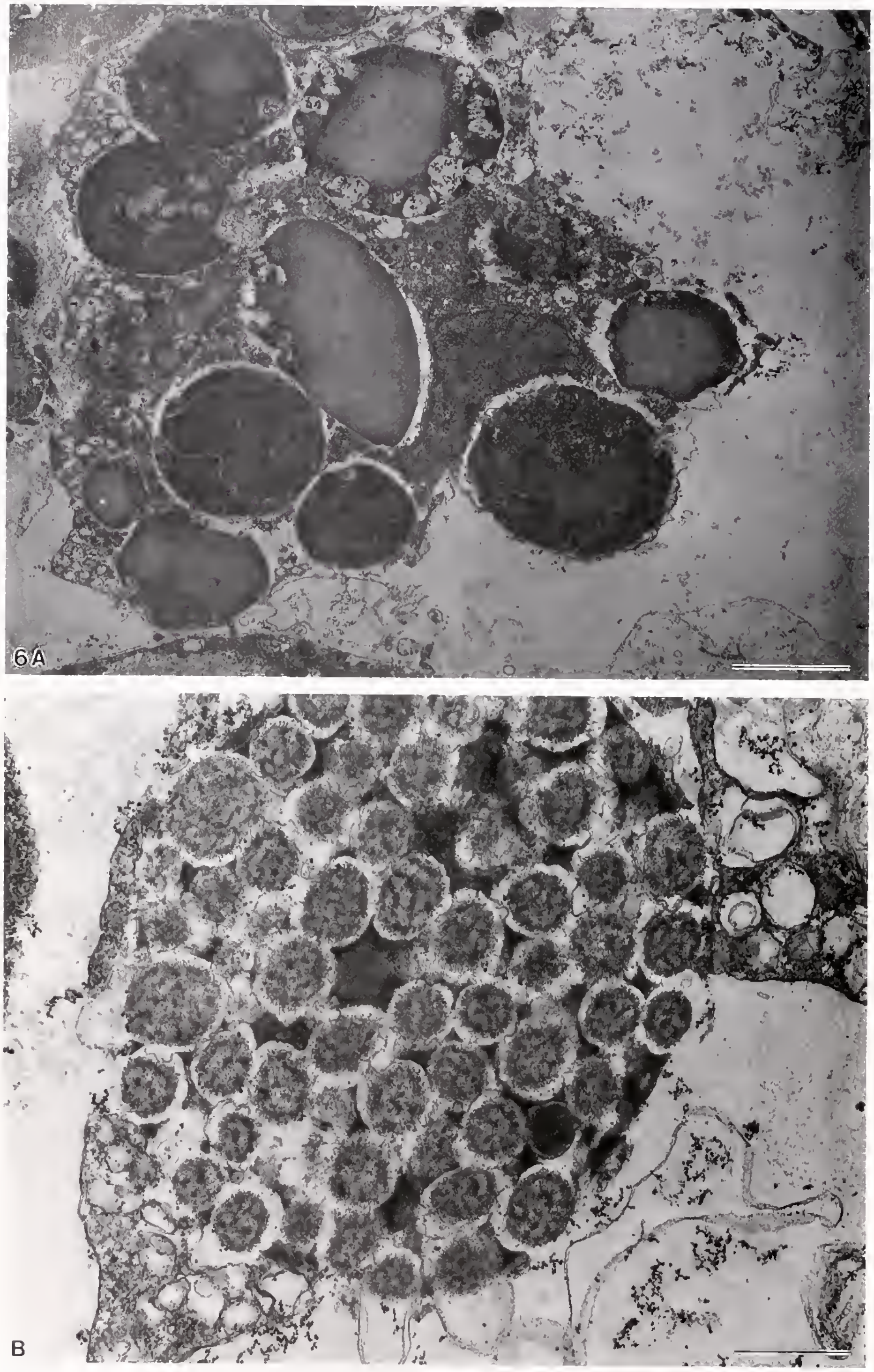

Figure 6. Newly set spat (transmission electron micrographs). (A) A perivisceral phagocyte of a mixed-diet-fed animal shows engulfment and digestion of the dinoflagellates. (Bar = 5 μm.) (B) A dinoflagellate within the perivisceral space has numerous autolysosomes. (Bar = 1.25 μm.)

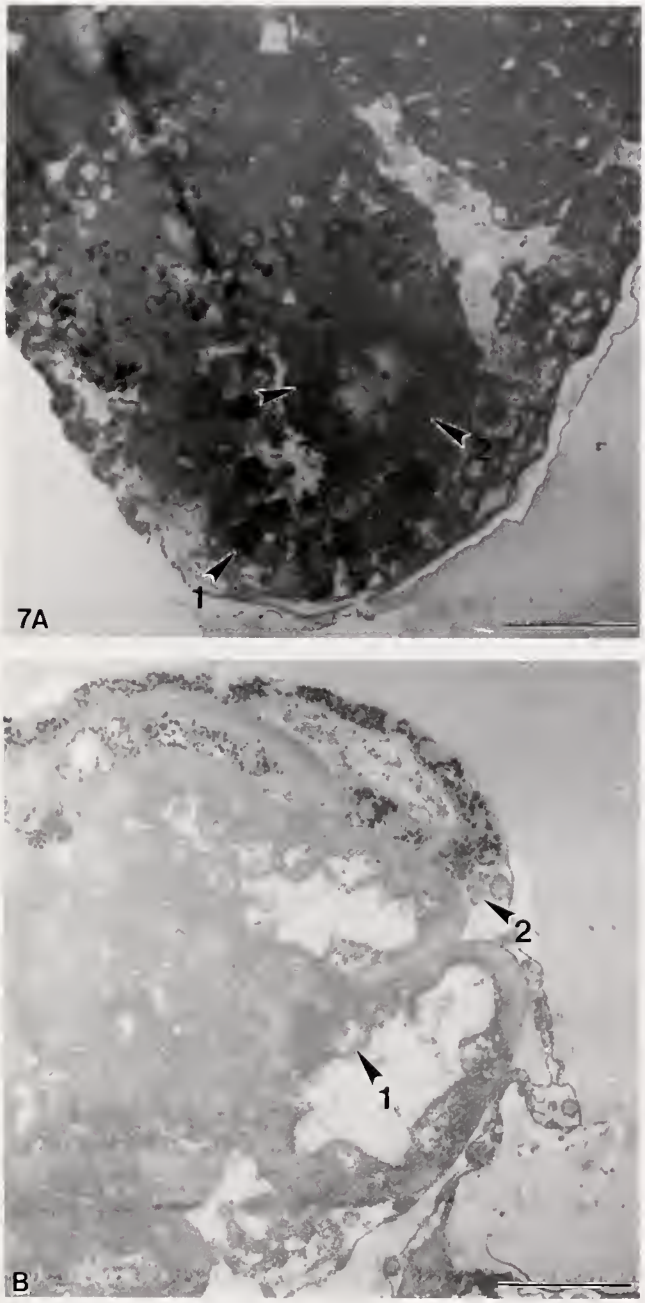

Figure 7. Newly set spat. PAS staining of plastic-embedded, thick-sectioned spat. (A) A mixed-diet-fed animal shows positive PAS staining of dinoflagellates in the perivisceral space (1) and accumulation bodies in the absorptive cells (2). (B) A T-ISO-fed animal shows no PAS staining in the perivisceral space (1) or in the absorptive cells of the digestive gland (2). Lipid granules are numerous in the intestine (3), and many absorptive cell nuclei are dense (4). (Bar = 40 μm.)

Juveniles

Juvenile oysters that had been feeding on natural Milford Harbor phytoplankton amended with cultured algae showed two different responses when subsequently exposed to experimental diets. Oysters fed T-ISO alone, or the ⅓ EXUV + ⅔ T-ISO diet, filtered the entire ration rapidly, produced normal fecal strands, and began growing immediately upon experimental feeding (Fig. 8). In contrast, oysters fed EXUV alone or the ⅔ EXUV + ⅓ T-ISO diet filtered the ration, but produced pseudofeces and grew poorly for the first week or two of experimental feeding. Thereafter, most oysters produced normal fecal strands and grew at rates the same as or higher than those on other diets (Table IV).

Histologic observations of oysters from each feeding regime sampled at the end of the experiment revealed that although the appearance of the absorptive cells in the digestive diverticula varied with diet, all were generally healthy except the negative controls (starved). Animals fed T-ISO showed absorptive cells with moderately columnar outlines and consistent foamy, vacuolated cytoplasm (Fig. 9A). In addition to generally poorly developed organ systems, starved oysters showed digestive diverticula cells that were cuboidal to low-columnar in outline with vacuolated/fine granular cytoplasm (Fig. 9B). In general, animals fed partially or wholly on EXUV had abundant columnar epithelia with taller absorptive-cell outlines than those seen in T-ISO-fed animals. The cytoplasmic contents of EXUV-fed animals were similar to those of the positive (T-ISO-fed) controls in vacuolation, but were more coarsely granular (Fig. 9C); additionally, reserve cells appeared to be more common in these diverticula. Interestingly, a subset of several oysters from the EXUV unialgal feeding regime exhibited varying degrees of development of absorptive cells. In the most severely affected oysters from this subset, the digestive gland epithelial cells were cuboidal to low-columnar, with relatively homogeneous eosinophilic cytoplasm intermingled with many brown granules about 2 μm in size (Fig. 9D).

Discussion

Our previous experience with feeding the EXUV strain of *P. minimum* to other molluscs led us to expect that oysters could experience detrimental effects that might include mortality, as with scallops, or growth inhibition, as with clams (Wikfors and Smolowitz, 1993). Exposures of prefeeding oyster embryos to spent algal growth media and live, killed, and extracted cells were intended to determine if a soluble toxin would affect embryonic development; if so, larval bioassay might be a useful method for quantification of toxin content in *P. minimum.* This clearly is not the case. No experimental treatments yielded statistically significant differences in development, and any possible histological effects were subtle and fell within the limits of normal variation. Lack of detrimental effects upon prefeeding larvae could, however, have been attributed to insufficient dosage in the experimental protocol, although even the higher, 5× EXUV exposures were not

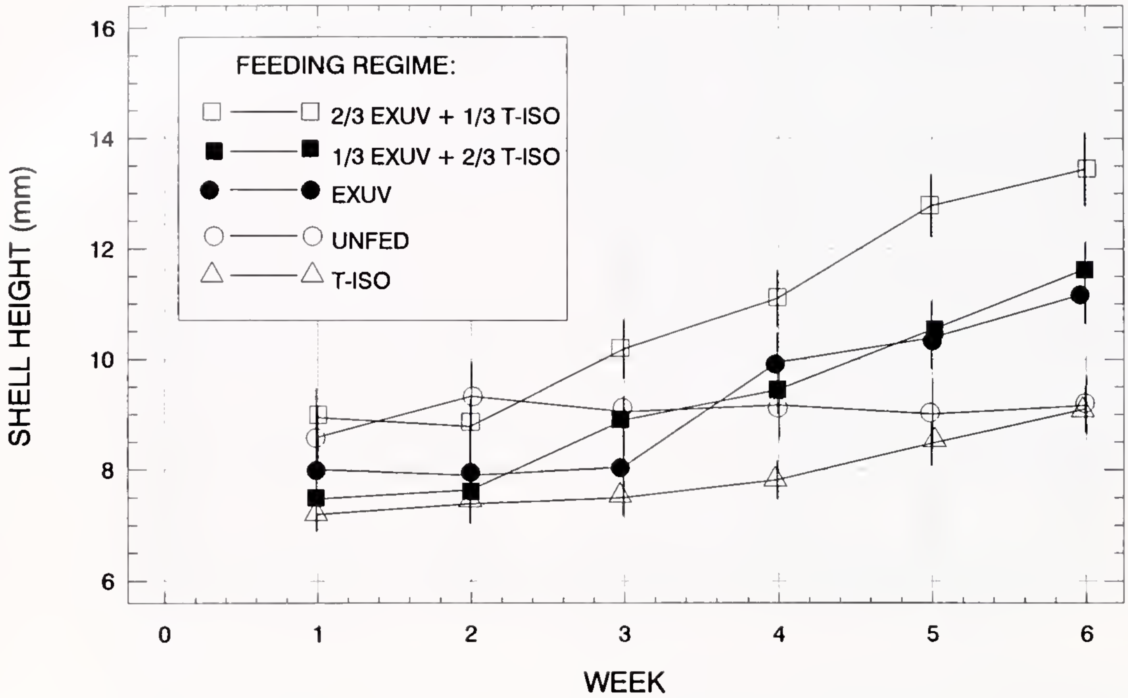

Figure 8. Shell-length measurements of juvenile oysters from experimental feeding regimes.

harmful (Table I). Because our experimental exposures were greater than exposures expected in natural waters, except possibly under extreme bloom conditions, we conclude that harm to oyster embryos from *P. minimum* exudates is unlikely in nature. Furthermore, it appears unlikely that the putative molluscan enterotoxin in this dinoflagellate is released into solution in a form harmful to shellfish. Davis and Chanley (1956) reported that a dinoflagellate bloom in Milford Harbor (most likely a species of *Prorocentrum*) interfered with development of oyster and clam embryos in filtered seawater; however, the effectiveness of the filtration in removing the dinoflagellate cells was not evaluated. The "bag-filtering" process employed at Milford at that time probably would not remove *P. minimum* effectively.

Feeding *P. minimum* to oyster larvae yielded clear detrimental effects, but it was not apparent from experimental results alone if reduced survival and growth resulted from toxic effects or from starvation. EXUV, with a size of about 9 × 6 μm, is near the maximum size of particles that molluscan larvae can ingest (Riisgard *et al.*, 1980). Observations of fed larvae by epifluorescence microscopy, and monitoring of larval-culture fluorescence after feeding, indicated that larval consumption was lower with EXUV than with T-ISO (Table II). Epifluorescence microscopy and histologic evidence do, however, support the contention that larvae can ingest EXUV cells. Accumulation bodies originating from intracellular digestion of EXUV cells were seen in larvae fed EXUV, but not in larvae starved or fed T-ISO alone. Thus, pathologic

Table IV

Growth rates, in millimeters per week, of juvenile oysters fed algal diets

	Diet				
Week interval	Unfed	EXUV	⅔ EXUV	⅓ EXUV	T-ISO
1–2	0.74 (.067)^{a}	−0.10 (.010)^{c}	−0.16 (.023)^{c}	0.16 (.027)^{b}	0.19 (.047)^{b}
2–3	−0.28 (.056)^{c}	0.15 (.015)^{b}	1.4 (.036)^{a}	1.3 (.039)^{a}	0.11 (.019)^{b}
3–4	0.12 (.056)^{e}	1.9 (.039)^{a}	0.91 (.022)^{b}	0.55 (.017)^{c}	0.32 (.018)^{d}
4–5	−0.16 (.012)^{d}	0.44 (.025)^{c}	1.7 (.056)^{a}	1.2 (.077)^{b}	0.66 (.047)^{c}
5–6	0.15 (.011)^{c}	0.80 (.021)^{b}	0.66 (.093)^{b}	0.98 (.043)^{a}	0.62 (.020)^{b}

Superscript letters indicate homogeneous subsets, according to Least Square Difference Multiple Range Test.

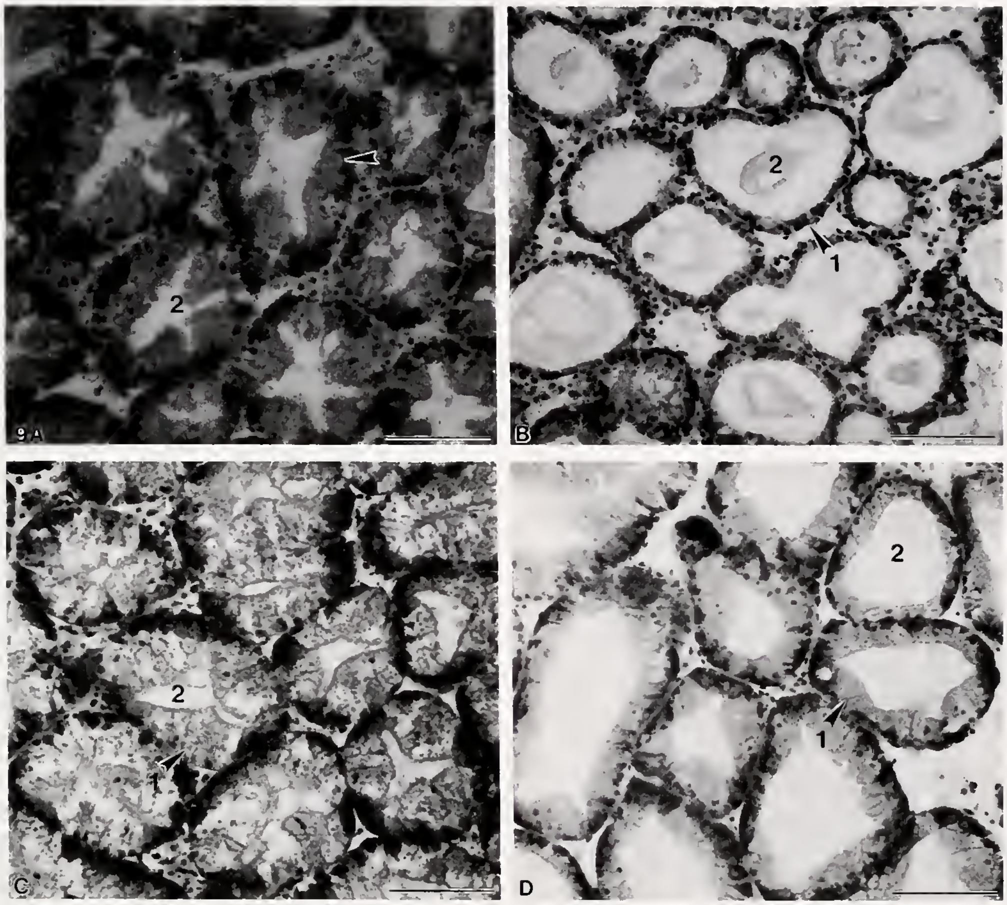

Figure 9. Juvenile oysters. Sections of paraffin-embedded animals are stained with hematoxylin and eosin. (Bar = 40 μm.) (A) A positive control animal (fed 100% T-ISO) shows moderate columnar absorptive cells (1) and star-shaped lumens (2). (B) Starved juveniles show cuboidal epithelium (1) with dilated, rounded lumens (2). (C) Most EXUV-fed animals showed high-columnar epithelium with foamy cytoplasm (1) and small lumens (2). (D) Some EXUV-fed animals showed low-columnar epithelium (1) and dilated lumens (2).

changes associated specifically with *P. minimum* feeding were identified; the chief feature was the presence of accumulation bodies within absorptive cells of the digestive diverticula. Metamorphosis and setting of very few larvae fed ⅓ EXUV + ⅔ T-ISO (less than 100, as compared with more than 2000 in larvae reared on T-ISO alone) provided further evidence that limited growth and development in the mixed algal diet was not simply a result of quantitative malnutrition.

The presence of accumulation bodies within absorptive cells of digestive diverticula in larvae fed 100% EXUV suggests that some specific component of the *P. minimum* cell interfered with cellular digestive processes. Similar accumulation bodies were found in recently set spat that we continued to feed the larval diet of ⅓ EXUV + ⅔ T-ISO. These spat also had large amounts of lipid in the stomach, but modest to very low amounts of lipid in the moderately to poorly developed intestinal epithelium. In contrast, oysters fed T-ISO alone had large amounts of lipid in the moderately to well-developed intestine and only rare lipid droplets in the stomach. Clearly, digestive processes in larvae and young spat were disrupted by the presence of *P. minimum* in the diet.

The occurrence of large numbers of partially digested dinoflagellates within phagocytes of the perivisceral cavity again demonstrated the reduced ability of the oysters' cells to degrade these organisms even though they did elicit a phagocytic response. Only rarely, however, was a relatively intact dinoflagellate seen in the perivisceral space, and even those were in the process of being, or had just been, phagocytized. We do not know how these organisms, either whole or partially degraded, entered the perivisceral space, but they could have passed through breaks in the epithelial integrity of the digestive gland or intestine during setting. Certainly their occurrence within the perivisceral space would significantly stress the animals.

In light of results with younger animals, findings with juvenile oysters were somewhat surprising. A previous study on filtration of EXUV by adult *C. virginica* revealed that cultured EXUV was filtered from suspension but not digested very effectively in short-term exposures (Shumway *et al.*, 1985). Further experiments by Luckenbach *et al.* (1993) demonstrated complete mortality in 14 days of juvenile oysters fed a high density of *P. minimum* (a Chesapeake Bay isolate). Oysters fed a lower density of this same culture showed 43% mortality in the first 22 days of exposure, after which survival stabilized; 5% *P. minimum* added to a mixed algal diet improved growth of oysters in these latter experiments (Luckenbach *et al.*, 1993). Thus, in the present study the initial depression in growth rates of oysters fed EXUV alone—or as a mixed diet of ⅔ EXUV and ⅓ T-ISO—was expected. The sudden acceleration in growth on these diets after 2 weeks was different from results obtained by Luckenbach *et al.* (1993), but it was not wholly inconsistent with their findings. The survival of all oysters still alive after 22 days of exposure to the lower *P. minimum* concentration in the Luckenbach *et al.* (1993) study suggests that some oysters are more resistant than others, or that some recovery is possible. Our feeding regime resulted in feeding densities within the "bloom" (high) range of Luckenbach *et al.* (1993); hence, differences in mortality of oysters in the two studies may result from differences in the algal strains or in the initial nutritional condition of the oysters. In our experiment, before oysters were used in exposure trials they were fed a diet known to support rapid growth; they may have had sufficient nutrient stores to survive initial stress.

Growth data from the present study show widening variance as mean sizes increased, suggesting that some oysters were growing more rapidly than others. A number of oysters were selected, therefore, for histological examination. Individuals that were from the EXUV-fed group and had well-developed absorptive cells were most likely growing rapidly. In contrast, some oysters from the same group were in poor condition, judging by digestive-system appearance, and resembled younger oysters fed *P. minimum* in their histologic characteristics, including low-columnar epithelium and comparatively large, granular cytoplasmic inclusions. The intragroup variance in the appearance of the digestive diverticula cells is interesting. We speculate that spat needed specific enzymes to digest or eliminate *P. minimum* material that might otherwise accumulate in epithelial cells of the digestive diverticula. Whether such enzymes are induced by the presence of the dinoflagellate or occur as part of the normal developmental sequence of the digestive gland is unknown. In the feeding larvae and newly set spat, we believe that the contents of accumulation bodies, when present in large amounts within the absorptive cells, may have interfered with digestion.

The nature of the material contained within accumulation bodies in absorptive cells was investigated through PAS staining of oyster tissues. We were fortunate to obtain sections through *P. minimum* cells inside the digestive lumen of the oyster. These sections revealed structures within the dinoflagellate cells that appeared in TEM preparations to correspond with dinoflagellate autolysosomes (Schmitter, 1971; Schmitter and Jurkiewicz, 1981). About 20 of these organelles were seen within each dinoflagellate. A recent report has demonstrated that autolysosomes in *Prorocentrum* cells are strongly PAS positive (Zhou and Fritz, 1994a); individual *Prorocentrum* cells contained more than 20 autolysosomes, corresponding well with our observations. PAS reaction offered a possible method for investigating whether accumulation bodies in oyster absorptive cells contained material from *P. minimum* autolysosomes. PAS-positive staining of accumulation bodies in absorptive cells of oysters fed *P. minimum*, but not in oysters fed T-ISO, is strong evidence that dinoflagellate autolysosomes are involved in the detrimental effects that some dinoflagellates have upon shellfish. The evidence is not definitive: some substance produced by the oyster lysosome could be responsible for the PAS staining seen in newly set spat. We have, however, no evidence that this is the case. Widdows *et al.* (1979) noted a similar increase in PAS-positive phagolysosomes of pathologically affected absorptive cells in *Mytilus edulis* fed *Gyrodinium aureolum*.

Comparing results of this study with our previous laboratory exposures of northern quahogs and bay scallops to *P. minimum* (Wikfors and Smolowitz, 1993) suggests a possible scenario linking dinoflagellate autolysosomes with effects upon shellfish. Quahogs did not grow during six weeks of feeding on diets containing EXUV, but no mortalities occurred; apparently these bivalves were unable to digest EXUV. Unfortunately, we did not examine these clams histologically to determine if poor digestion resulted from damage to digestive diverticula or from inability of enzymes in the digestive lumen to lyse dinoflagellate cells. In bay scallops fed a diet containing EXUV, mortality was rapid. No accumulation bodies were seen in scallop absorptive cells; instead, these cells appeared to be rapidly sloughed into the lumen. If digestive enzymes in the scallops' diverticular lumen were able to lyse *P. minimum* cells and autolysosomes, thereby releasing dinoflagellate autolysosomal enzymes into the lumen, and if these dinoflagellate enzymes were damaging to scallop absorptive cells, then the enterotoxic effects we observed could have resulted. Bay scallops are thought to accomplish essentially all digestion extracellularly within the digestive-gland lumen (Reid, 1982); oysters, on the other hand, are considered to be phagotrophs (Galtsoff, 1964).

In oysters, dinoflagellate autolysosomes may be taken whole by phagocytosis into absorptive cells, where partial degradation and subsequent accumulation as persistent phagolysosome (residual bodies) occurs. We have termed these characteristic phagolysosomes and residual bodies "accumulation bodies." Older, juvenile oysters appear to develop digestive enzymes, either released into the lumen or within absorptive cells, that completely digest the dinoflagellates—including any dinoflagellate-derived autolysosomes. It is interesting to note that feeding algal cells contaminated with cadmium to juvenile oysters causes degradation of the diverticular epithelium that is similar to the effects of *P. minimum* upon bay scallops (Wikfors, in prep.). Apparently *P. minimum* does not release a chemical toxin into the diverticular lumen of the oyster, though it appears to do so in the scallop. A recent study has shown that okadaic acid (DSP toxin) is localized in organelles, including autolysosomes, in *P. lima* and *P. maculosum* (Zhou and Fritz, 1994b); thus, digestive degradation of the organelles seems to be necessary for release of the toxin. Differences in symptoms in different bivalves seem to offer clues as to how the molluscs respond to *P. minimum*, in terms of digestive sequences and sites, and to highlight the diversity of digestive methods and enzymes among various types of bivalves. Further research is needed to elucidate fully the possible relationships between dinoflagellate autolysosomes, molluscan digestive processes, and susceptibility of bivalve molluscs to harmful algal blooms.

Acknowledgments

This study was supported by the NOAA Oyster Disease Initiative, administered through the Northeast Region of NOAA's National Marine Fisheries Service.

Technical assistance of B. C. Smith, L. Garvey, T. Godfrey, and Michelle McCafferty is gratefully acknowledged. We thank S. E. Shumway for providing bioassay results of cultured *P. minimum*. Constructive comments were provided by E. N. Wikfors, R. A. Robohm, and A. Calabrese.

Literature Cited

Babinchak, J., and R. Ukeles. 1979. Epifluorescence microscopy, a technique for the study of feeding in *Crassostrea virginica* veliger larvae. *Mar. Biol.* **51:** 69–76.

Davis, H. C., and P. E. Chanley. 1956. Effects of some dissolved substances on bivalve larvae. *Proc. Natl. Shellfish. Assoc.* **47:** 59–74.

Dodge, J. D. 1982. *Marine Dinoflagellates of the British Isles.* Her Majesty's Stationery Office, London.

Elston, R. 1980. *The Larval American Oyster,* Crassostrea virginica. *Its Functional Anatomy, Histology and Ultrastructure and Response to Challenge with the Bacterium, Vibrio spp.* Cornell University, Ph.D. Thesis.

Erlandsen, S. L., J. A. Parsons, and C. B. Rodning. 1979. Technical parameters of immunostaining of osmicated tissue in epoxy sections. *J. Histochem. Biochem.* **27:** 1286–1289.

Gainey, L. F., and S. E. Shumway. 1988. A compendium of the responses of bivalve mollusks to toxic dinoflagellates. *J. Shellfish Res.* **7:** 623–628.

Galtsoff, P. S. 1964. The American oyster. *Fishery Bull.* **64:** 1–480.

Hallegraeff, G. M. 1993. A review of harmful algal blooms and their apparent global increase. *Phycologia* **32:** 79–99.

Howard, D. W., and C. S. Smith. 1983. *Histological Techniques for Marine Bivalve Mollusks.* NOAA Technical Memorandum NMFS-F/NEC-25. U.S. Dept. of Commerce.

Humanson, G. L. 1979. Pp. 210–212 in *Animal Tissue Techniques.* W. H. Freeman and Co., San Francisco.

Loosanoff, V. L., and H. C. Davis. 1963. Rearing of bivalve mollusks. *Adv. Mar. Biol.* **1:** 1–136.

Luckenbach, M. W., K. G. Sellner, S. E. Shumway, and K. Greene. 1993. Effects of two bloom-forming dinoflagellates, *Prorocentrum minimum* and *Gyrodinium uncatenum,* on the growth and survival of the eastern oyster, *Crassostrea virginica* (GMELIN 1791). *J. Shellfish Res.* **12:** 411–415.

Marshall, H. G. 1980. Seasonal phytoplankton composition in the lower Chesapeake Bay and Old Plantation Creek, Cape Charles, Virginia. *Estuaries* **3:** 207–216.

Parry, G. D., J. S. Langdon, and J. M. Huisman. 1989. Toxic effects of a bloom of the diatom *Rhizosolenia chunii* on shellfish in Port Phillip Bay, Southeastern Australia. *Mar. Biol.* **102:** 25–41.

Reid, R. G. B. 1982. Aspects of bivalve feeding and digestion relevant to aquaculture nutrition. Pp. 231–251 in *Proceedings of the Second International Conference on Aquaculture Nutrition: Biochemical and Physiological Approaches to Shellfish Nutrition.* G. D. Pruder, C. J. Langdon, and D. E. Conklin, eds. Louisiana State University, Baton Rouge.

Rhodes, E. W., and W. S. Landers. 1973. Growth of oyster larvae, *Crassostrea virginica,* of various sizes in different concentrations of the chrysophyte, *Isochrysis galbana. Proc. Natl. Shellfish. Assoc.* **63:** 53–59.

Riisgard, H. U., A. Randlov, and P. S. Kristensen. 1980. Rates of water processing, oxygen consumption and efficiency of particle retention in veligers and young post-metamorphic *Mytilus edulis. Ophelia* **19:** 37–47.

Sakamoto, Y., R. F. Lockey, and J. J. Krzanowski, Jr. 1987. Shellfish and fish poisoning related to the toxic dinoflagellates. *Southern Med. J.* **80:** 866–872.

Schmidt, R. J., and A. R. Loeblich, III. 1979. Distribution of paralytic shellfish poison among Pyrrophyta. *J. Mar. Biol. Assoc. U. K.* **59:** 479–487.

Schmitter, R. E. 1971. The fine structure of *Gonyaulax polyedra,* a bioluminescent marine dinoflagellate. *J. Cell Sci.* **9:** 147–173.

Schmitter, R. E., and A. J. Jurkiewicz. 1981. Acid phosphatase localization in PAS bodies of *Gonyaulax. J. Cell Sci.* **51:** 15–23.

Sellner, K. G., F. Sawangwong, R. Dawson, W. R. Boynton, W. M. Kemp, and J. H. Garber. 1993. Fate of dinoflagellates in Chesapeake Bay: Is sedimentation likely? Pp. 825–830 in *Toxic Phytoplankton Blooms in the Sea.* T. J. Smayda and Y. Shimizu, eds. Elsevier, Amsterdam.

Shumway, S. 1990. A review of the effects of algal blooms on shellfish and aquaculture. *J. World Aquacult. Soc.* **21:** 65–104.

Shumway, S. E., T. L. Cucci, R. C. Newell, and C. M. Yentsch. 1985. Particle selection, ingestion, and absorption in filter-feeding bivalves. *J. Exp. Mar. Biol. Ecol.* **91:** 77–92.

Sorvall Instruction Manual. 1981. *Staining Procedures for Plastic Embedded Tissue.* DuPont Company, Instrument Products, Biomedical Division, Newtown, Connecticut.

Steidinger, K. A. 1983. A re-evaluation of toxic dinoflagellate biology and ecology. Pp. 148–188 in *Progress in Phycological Research.* F. E. Round and D. J. Chapman, eds. Elsevier, New York.

Ukeles, R. 1973. Continuous culture—a method for the production of unicellular foods. Pp. 233–254 in *Handbook of Phycological*

Methods—Culture Methods and Growth Measurements. J. R. Stein, ed. Cambridge University Press, London.

Ukeles, R., and G. H. Wikfors. 1982. Design, construction, and operation of a rearing chamber for spat of *Crassostrea virginica* (Gmelin). *J. Shellfish Res.* **2:** 35–39.

Wikfors, G. H., and R. M. Smolowitz. 1993. Detrimental effects of a *Prorocentrum* isolate upon hard clams and bay scallops in laboratory feeding studies. Pp. 447–452 in *Toxic Phytoplankton Blooms in the Sea.* T. J. Smayda and Y. Shimizu, eds. Elsevier, Amsterdam.

Widdows, J., M. N. Moore, D. M. Lowe, and P. N. Salkeld. 1979. Some effects of a dinoflagellate bloom (*Gyrodinium aureolum*) on the mussel, *Mytilus edulis. J. Mar. Biol. Assoc. U. K.* **59:** 522–524.

Zhou, J., and L. Fritz. 1994a. PAS/accumulation bodies in *Prorocentrum lima* and *Prorocentrum maculosum* (Dinophyceae) are dinoflagellate autolysosomes. *J. Phycol.* **30:** 39–44.

Zhou, J., and L. Fritz. 1994b. (abstract). DSP toxin localizes to plastids in producer *Prorocentrum* cells. ASLO & PSA 1994 Joint Meeting Conference Program and Book of Abstracts, p. a-85.

Reference: *Biol. Bull.* **188:** 329–337. (June, 1995)

Life-History Variation Among Three Temperate Hermit Crabs: The Importance of Size in Reproductive Strategies

DAVID B. CARLON[1,2] AND JOHN P. EBERSOLE

Department of Biology, University of Massachusetts at Boston, Boston, Massachusetts 02125

Abstract. The supply and quality of empty gastropod shells may play important roles in the ecology and evolution of hermit crabs. We compare the life histories of three subtidal hermit crabs in Nantucket Harbor, Massachusetts: *Pagurus annulipes, P. longicarpus,* and *P. pollicaris.* Specifically, we examine seasonal patterns of reproduction in females, male and female size structure, reproductive effort, and temporal patterns of larval abundance. We also compare shell size among the three species. Life-history features vary with size among the three species. The smallest species (*P. annulipes*) reproduce soon after metamorphosis and have a high reproductive effort. The two larger species (*P. longicarpus* and *P. pollicaris*) delayed reproduction to an intermediate size, and have lower reproductive efforts than *P. annulipes.* There is no effect of body size on reproduction in *P. annulipes,* but there is a strong positive effect in *P. longicarpus* and *P. pollicaris.* Seasonal patterns of early stage larvae correlated with seasonal patterns of ovigery in all three species, with highest larval densities sampled in *P. annulipes* and *P. longicarpus.* Size differences among species were related to patterns of shell usage. Male and female *P. annulipes* were always found in large shells relative to body size. In comparison, male and female *P. longicarpus* and *P. pollicaris* were found in small shells compared to body size. We suggest that early maturity and high reproductive effort have evolved in response to a high risk of mortality associated with small shells. Delayed maturity and low reproductive effort are favored in species that reach a size refuge from shell-crushing predators. Effects of shell limitation are more likely to be common in large species and may also be an important selective in shaping hermit crab life histories.

Introduction

Studies on the ecology and evolution of hermit crabs (Decapoda, Anomura) have often focused on the consequences of limited shell resources. Hermit crabs are dependent on an external shelter to protect them from physical stress and predation (Reese, 1969). Typically, empty gastropod shells are used as mobile shelters, but a few species may also live within sponges and other animals. Because hermit crabs cannot manufacture their own shells, they are entirely dependent on the processes that make suitable shells available for their use, including snail mortality and intra- and inter-specific shell exchanges (Hazlett, 1981). Three observations are commonly used to support the hypothesis that shells are in short supply: (1) empty shells are often rare in habitats that support hermit crab populations (Hazlett, 1970; Childress, 1972; Kellogg, 1976; Abrams, 1978, 1980; Bertness, 1980), (2) natural populations of hermit crabs are often in smaller shells than preferred in laboratory experiments (Vance, 1972; Bach *et al.*, 1976; Abrams, 1978; Scully, 1979; Bertness, 1980), and (3) hermit crabs often have ritualized shell-exchange behavior (reviewed by Hazlett, 1981) that may be beneficial when shell resources are scarce.

Field experiments have shown effects of limited shell supply at the population and community level. Vance (1972) added shells to an experimental reef on the coast of Washington State during a one-year period, increasing the density of *Pagurus hirsutiusculus* compared to a control reef where no shells were added. In the tropics, Bach *et al.* (1976) and Bertness (1981a) found that competitive subordinates occupied smaller shells when competitive

---

Received 2 November 1994; accepted 13 February 1995.

[1] To whom all correspondence should be addressed.

[2] Present address: Department of Zoology, University of New Hampshire, Durham, NH 03824.

dominants were present, compared to when competitive dominants were absent. In the Bay of Panama (Bertness, 1981a), experimental addition of shells to tide pools containing three potential competitors increased rates of shell acquisition by competitive dominant species compared to subordinate species. Thus, interactions within species and among co-existing species may both be affected by shell supply.

Variation in the supply and quality of shell resources may affect hermit crab life histories. In the tropics, Bertness (1981b) found clutch size and size at maturity to respond to shell supply. Experimental treatments in which shells were added increased the size at maturity and reduced clutch size in several tropical species. In this example, a phenotypically plastic reproductive strategy was hypothesized as a way in which hermit crabs could maximize fitness when confronted with changing resource levels. Shell quality and supply may also vary with shell size. For example, small shells are generally less effective deterrents to shell-crushing predators than larger shells (Bertness and Cunningham, 1981; Borjesson and Szelistowski, 1989; Buckley and Ebersole, 1994). In addition, small shells are typically more abundant than large shells (Hazlett, 1981; D. B. Carlon, pers. obs.). The negative effects of shell limitation may therefore be more common in hermit crabs that use large shells compared to small shells. These size-specific selective pressures associated with shell resources may have important consequences for hermit crab life histories.

In this paper, we compare and contrast size distributions, effects of size on reproduction, individual reproductive allocation, and seasonal patterns of reproductive activity among three *Pagurus* hermit crabs in a temperate New England harbor. We then show how shell size varies among species. We suggest that hermit crab life histories have evolved in response to size-specific mortality patterns. Early maturity and high reproductive effort are favored when the risk of adult mortality is high. In contrast, delayed reproduction and low reproductive effort are optimal when the risk of adult mortality is low and shells are rare.

Materials and Methods

Study location and species

Nantucket Harbor is a temperate, semi-enclosed coastal lagoon located on Nantucket Island, Massachusetts. The shallow harbor (max. depth <10 m) has a sandy bottom with deeper areas covered with the shell remnants of gastropods (especially *Crepidula* spp.) and bay scallops (*Aequipecten irradians*). Eelgrass (*Zostera marina*) forms dense stands in shallow regions (<3 m). Surface temperature may range from 0°C in the winter to 25.5°C in late summer, and complete freeze-over occurs in some, but not all, winters (W. Tiffney, pers. obs.).

Three hermit crab species commonly occur in Nantucket Harbor: *Pagurus annulipes* (Stimpson), *Pagurus longicarpus* (Say), and *Pagurus pollicaris* (Say). *P. longicarpus* occurs in both littoral and subtidal zones, often near or within patches of eelgrass. *P. annulipes* is only found subtidally, typically at depths >4 m. This species appears to prefer coarse sediments that occur in tidal channels within the harbor. The third species, *P. pollicaris,* is found in littoral and subtidal habitats. The shell species most commonly used vary among the three species. *P. annulipes* is almost always found in two *Anachis* spp.: *A. avara* and *A. translirata.* In comparison, *P. longicarpus* uses several species, most commonly: *Littorina littorea, Nassarius trivittatus,* and *Polinices duplicatus. P. pollicaris* is also found in several species: *Lunatia heros, Polinices duplicatus,* and *Busycon canaliculatum.*

Adult features

To determine male and female size distributions and temporal patterns of reproductive activity, benthic populations were sampled weekly from March to October of 1990. This period was chosen because previous work in Nantucket Harbor and the Cape Cod region indicated that the reproductive season for these three *Pagurus* species begins in early spring and ends in late summer (Nyblade, 1970; Johnson and Ebersole, 1989, unpub. data). Hermit crabs were sampled at two sites separated by 3 km within the harbor. The first site, First Bend, is in a tidal channel near the harbor entrance. The second site, Quaise, is located on the eastern shore of the harbor, close to the University of Massachusetts Field Station. In March and April, crabs were sampled by boat-towed scallop dredge. Though scallop dredges employed in Nantucket Harbor have a large mesh size (2.5 cm), hermits as small as 2.0 mm carapace length were captured due to clogging of the net with shells, eelgrass, and macroalgae. From May through October, crabs were sampled by divers using scuba, and a sample consisted of every crab found during a 45-min dive. There were no significant differences between the sizes of crabs collected by these two different methods. In the laboratory, each crab was removed from its shell by drilling a small hole in the shell apex with an electric drill and then tickling the abdomen with a thin piece of monofilament line. Hermit size was determined by measuring the distance from the rostrum to the edge of the calcified portion of the carapace with vernier calipers [equivalent to the whole carapace measurement of Markham (1968)]. Sex was determined by the position of the gonopores and pleopod morphology (McLaughlin, 1980). Female reproductive condition was scored as ovigerous if an extruded egg mass was attached to the pleopods. To determine temporal patterns in female reproductive activity (proportion of the sample ovigerous), weekly samples were pooled for each month. At least two benthic samples were taken per month, and typically four were taken from April to September. One sample was collected during the last week of March and the first week of October.

The relationship between female size and reproduction was determined by constructing species-specific size categories (Table I). Size categories were chosen so that similar numbers of individuals were distributed among three categories. The association between size and reproduction was tested for each species with a two-way contingency table defined by size (three categories) and reproductive condition (ovigerous or non-ovigerous). The log-likelihood statistic (G^2) was used for all tests of significance. Tests of significance were robust to the choice of size classes for size comparisons.

To compare reproductive allocation among the three species, females were collected during August 1990 and May 1991. Estimates of reproductive allocation in *P. pollicaris* sampled in August 1990 could not be determined because no ovigerous females were sampled on this date. Female *P. pollicaris* were collected near the First Bend site and female *P. annulipes* and *P. longicarpus* were collected at the Quaise site. Each crab was removed from its shell and fixed in a 5% formalin-seawater solution. Eggs of all individuals were in a similar developmental condition: the eggs were a rich purple and no differentiation was visible. Eggs were carefully removed from the pleopods with forceps and placed in a preweighed petri dish. Eggs and somatic tissue were weighed to the nearest 0.001 g after drying at 100°C for 48 h. Pilot studies showed that water content stabilizes after two days. Reproductive allocation was estimated as the dry weight of eggs divided by the dry weight of somatic tissue. A two-way analysis of variance (ANOVA) was used to compare reproductive allocation between species and sampling dates. In this analysis there were two levels of the factor "species": *P. annulipes* and *P. longicarpus;* and two levels of the factor "date": August 1990 and May 1991. Both factors were considered fixed in the analysis. A single factor ANOVA was used to compare reproductive allocation among the three species during May of 1991. Individual means were compared with the Tukey HSD method. Reproductive allocation data remained heteroscedastic [determined by Cochran's test (Winer *et al.*, 1991)] after a number of transformations. Following the recommendations of Underwood (1981) and Winer *et al.* (1991), untransformed data were used in both ANOVAs, and significance tests were interpreted conservatively. All statistical tests were performed with Systat software (Systat, Inc., Evanston, IL).

Table I

Size of three hermit crab species (carapace length) in three size categories used in the analysis of the relationship between body size and reproduction

Species	Size category (mm)		
	Small	Medium	Large
Pagurus anullipes	1.9–3.1	3.2–3.5	3.6–4.6
P. longicarpus	2.2–5.0	5.1–7.0	7.1–12.0
P. pollicaris	5.4–14.6	14.7–22.0	22.1–34.7

Temporal patterns of larval availability

To determine the seasonal pattern of larval abundance, plankton tows were made weekly from March to October 1991. On each date, two surface tows were made at five stations located at 1.5-km intervals along the principal axis of the harbor (SW–NE). All tows were taken between 1000 hours and noon. Volume of water sampled was determined with a mechanical flow-meter (General Oceanics #2030). After collection, each sample was halved with a plankton splitter and preserved in 5% buffered formalin. In the laboratory, samples were sorted with a dissecting microscope to species and stage of development using the keys of Nyblade (1970), Roberts (1970), and Sadler (1984). Mean abundances were calculated on each date by pooling the two replicate samples from five sites ($n = 10$). There was no difference among species in patterns of spatial abundance within the harbor: larval abundances were high at stations near the harbor entrance and decreased with distance from the entrance. Because very few megalops stage larvae were sampled ($n = 3$), they were combined with stage zoea 4 larvae for analysis.

Patterns of shell size among species

To determine if shell size relative to crab size varied among species, each crab collected during 1990 was assigned to a shell size/crab size category. Categories were determined by tapping the claws of a crab to encourage retraction, viewing the aperture, and noting how far the claws and walking legs extended beyond the aperture. Four categories were defined: Category 1 = no part of crab visible; Category 2 = tips of claws visible; Category 3 = first segment of major claw visible; Category 4 = second segment of major claw visible. The four categories ranged from a high shell size/crab size ratio (Category 1 = large shell, small crab) to a low shell size/crab size ratio (Category 4 = small shell, large crab). Heterogeneity of shell fit among species was tested with a two-way contingency table defined by three levels of species (*P. annulipes, P. longicarpus,* and *P. pollicaris*) and the four shell-fit categories. Independence among species was tested with the log-likelihood statistic.

Results

Reproductive features

Female *P. longicarpus* (mean carapace length = 5.9 mm) were almost twice as large as *P. annulipes* (mean carapace length = 3.3 mm) and much smaller than *P. pollicaris* (mean carapace length = 19.1 mm) (Fig. 1). Mean size of females correlated with size at maturity: the smallest *P. annulipes* found with eggs was 2.2 mm, whereas the smallest ovigerous *P. longicarpus* was 3.8 mm. The species with the largest females, *P. pollicaris*, matured at the largest size; the smallest ovigerous female was 13.4 mm carapace length. Males of *P. annulipes* and *P. longicarpus* were significantly larger than conspecific females (Student's t-test for paired comparisons, $t = -6.945$, df = 380, $P < 0.001$; and $t = -4.008$, df = 1012, $P < 0.001$, respectively), but there was no difference in size between sexes in *P. pollicaris* (Fig. 1; $t = 0.341$, df = 171, $P = 0.734$).

The probability of reproduction does not increase with size in the smallest species, *P. annulipes*, but does increase with size in the two larger species: *P. longicarpus* and *P. pollicaris* (Fig. 2). In *P. annulipes* there was no difference in the percentage of ovigerous females in the small, medium, and large size categories ($G^2 = 5.29$, df = 2, $P = 0.071$). When all three categories are combined, 68.9% of the *P. annulipes* females were ovigerous during 1990. In contrast, there was a strong effect of size on the probability of reproduction in *P. longicarpus* ($G^2 = 32.72$, df = 2, $P < 0.001$) and *P. pollicaris* ($G^2 = 13.15$, df = 2, $P = 0.001$); the probability of reproduction increased with increasing size in both species. The proportion of ovigerous *P. longicarpus* and *P. pollicaris* was less than *P. annulipes* during 1990, with 33% of female *P. longicarpus* ovigerous and 36.9% of female *P. pollicaris* ovigerous.

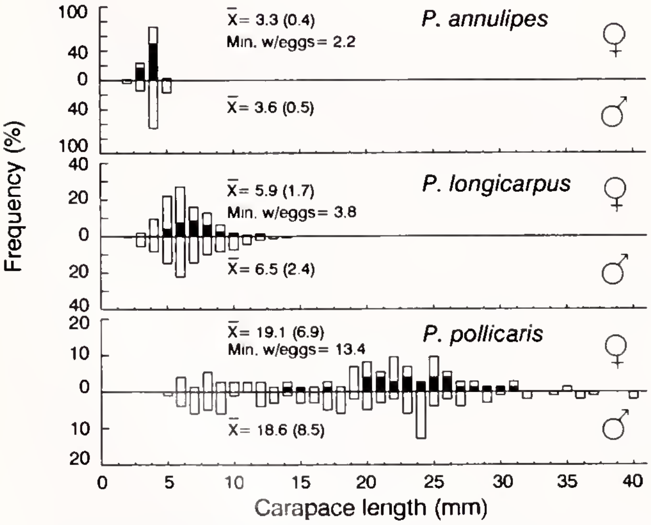

Figure 1. Size distribution of three *Pagurus* hermit crabs. Dark bars are ovigerous females. Standard deviations are given in parentheses. Total sample sizes are 382 for *P. annulipes*, 1022 for *P. longicarpus*, and 174 for *P. pollicaris*.

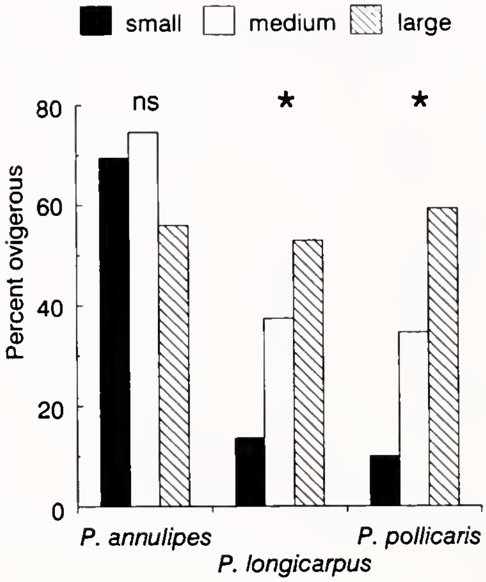

Figure 2. The distribution of ovigerous females in three size categories for three hermit crab species. Stars indicate a statistically significant effect of size on probability of ovigery at the 0.05 level of significance. See Table I for definition of the size categories for each species. Sample sizes = 238 for *P. annulipes*, 303 for *P. longicarpus*, and 73 for *P. pollicaris*.

Reproductive allocation was highest in the smallest species, *P. annulipes*, and lower in the two larger species, *P. longicarpus* and *P. pollicaris* (Fig. 3). In August 1990 *P. annulipes* females allocated 49.5% dry body weight to reproduction. The following spring (May 1991) allocation in *P. annulipes* decreased to 32.6% but was still greater than *P. longicarpus* on either sampling date or that of *P. pollicaris* (sampled only in May 1991). The reproductive allocation of *P. longicarpus* was similar on the two sampling dates: 25.1% in August 1990 and 25.8% in May 1991. *P. pollicaris* sampled in the spring of 1991 had the lowest allocation of any of the three species at 20% dry body weight. Considering the reproductive allocation of *P. longicarpus* and *P. annulipes* on the two sampling dates, a two-way ANOVA indicated a significant interaction between species and date ($F_{1,109} = 8.07$, $P < 0.005$, Table II), confirming the decline in *P. annulipes* reproductive allocation from the late summer 1990 to the spring 1991. The effect of species remained highly significant ($F_{1,109} = 25.02$, $P < 0.001$) in this analysis, much more so than the effect of date ($F_{1,109} = 6.78$, $P = 0.01$). Considering the effect of species on reproductive allocation during 1991,

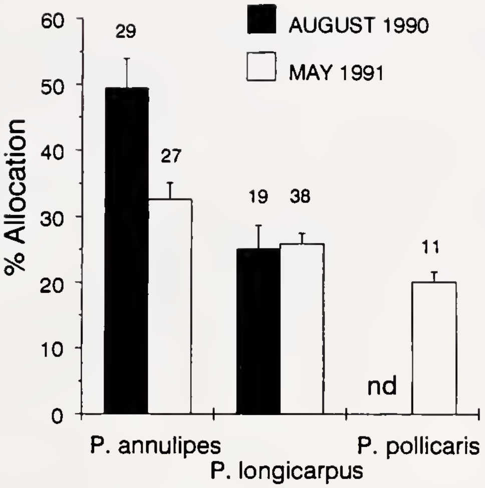

Figure 3. Reproductive allocation among three hermit crabs on two dates. Reproductive allocation = total dry weight of brood/(total dry crab weight–dry weight of brood). Vertical bars are standard errors and sample sizes are given above error bars. See text for statistical interpretation. No data (nd) were collected for *P. pollicaris* during August 1990 due to a lack of reproductive activity at this time.

a one-way ANOVA revealed a significant effect of species ($F_{2,73} = 6.20$, $P = 0.003$), and *post hoc* comparison of the means using the Tukey HSD procedure revealed a significant difference between *P. annulipes* and both *P. longicarpus* ($P = 0.039$) and *P. pollicaris* ($P = 0.004$) but no significant difference between *P. longicarpus* and *P. pollicaris* ($P = 0.205$).

There were striking differences in seasonal patterns of reproductive activity among the three species (Fig. 4). A single ovigerous *P. annulipes* was collected on 28 April; however, both males and females were extremely scarce at this time. By 15 May, individual *P. annulipes* had emerged from the sediments and were easily collected. The proportion of ovigerous females increased from 38% in May to 82% in June and remained high (>60%) until September, when a mean of 39.8% of the population was ovigerous. The reproductive season appeared to be over by 6 October, when 29 females were collected and none was ovigerous. In contrast to *P. annulipes*, active *P. longicarpus* and *P. pollicaris* were collected at the earliest sampling date of 31 March. No ovigerous specimens of *P. longicarpus* were observed on this date ($n = 3$), but reproductive activity was high during the following month of April, with a mean of 85.7% ovigerous. Reproduction declined during May and June to 0% in July but increased to 19.3% in August and 8.3% in September. None of 15 *P. longicarpus* females collected on 6 October was ovigerous. Five of the eight female *P. pollicaris* collected on 31 March were ovigerous. Reproductive activity was high in April with a mean of 81.3% ovigerous, and declined during May and June to 0% during the months of July, August, and September. No *P. pollicaris* females were collected on the last sampling date of 6 October. From these data, it is apparent that *P. annulipes* has high reproductive activity from late spring through the summer; *P. longicarpus* reproduces mainly in the spring, with a second smaller peak in August; *P. pollicaris* has the shortest reproductive period, with all reproduction occurring in the spring.

All three species are capable of producing multiple broods. Unfertilized eggs were often observed in the abdominal ovaries of ovigerous females in all three species, particularly as the extruded, fertilized eggs approached the last stage of development (eye spots clearly visible through egg cuticle).

Temporal patterns of larval availability

Temporal patterns in the availability of first stage larvae (zoea 1) generally reflected temporal patterns of reproductive activity in the three species (Figs. 4, 5). *P. annulipes* larvae were sampled in highest density on 14 June (2.06 larvae m^{-3}) and were collected in low densities (0.012–0.536 larvae m^{-3}) from June to September (Fig. 5a). *P. longicarpus* zoea 1 larvae were found earlier in the season compared to *P. annulipes* larvae: a mean density of 6.16 larvae m^{-3} was sampled on 18 May. *P. longicarpus* zoea 1 larvae occurred at low densities (<1 larvae m^{-3}) from June to September (Fig. 5b). The first zoeal stage of *P. pollicaris* was sampled at greatest densities on 29 May and 30 June, with mean densities of 0.16 and 0.075 larvae m^{-3} collected respectively (Fig. 5c). While availability of zoea 1 larvae generally reflected temporal patterns of reproductive activity of benthic adults, there were two dates when larvae were found in the water column but adult reproductive activity was not detected in Nantucket Harbor. No ovigerous *P. longicarpus* were sampled during the month of July (Fig. 4), yet low densities of zoea 1 larvae (<0.334 larvae m^{-3}) were collected on three dates during this month. Similarly, *P. pollicaris* zoea 1 larvae were sampled in low abundance (<0.034 larvae m^{-3}) at three times during September, even when no reproductive activity in adults was detected after June (Fig. 4). These

Table II

*ANOVA table evaluating effects of two dates (August 1990 and May 1991) and two species (*Pagurus longicarpus *and* Pagurus pollicaris*) on reproductive allocation*

Source	df	MS	*F*	*P*
Date	1	0.175	6.783	0.010
Species	1	0.644	25.024	<0.001
Date × Species	1	0.208	8.067	0.005
Error	109	0.026		

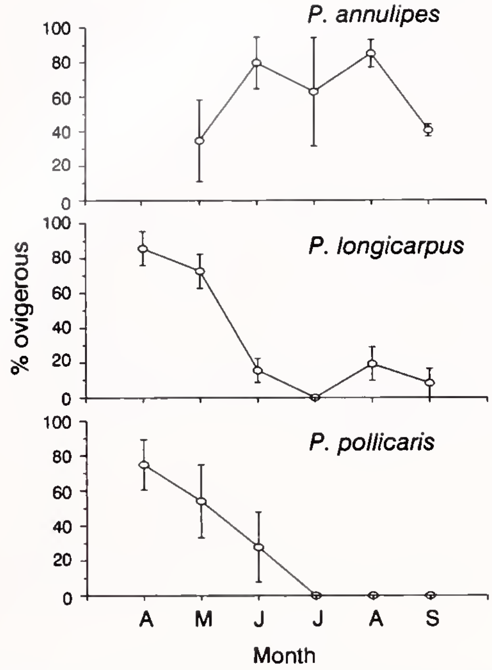

Figure 4. The percentage of ovigerous females collected in benthic samples for three *Pagurus* hermit crabs during the spring, summer, and fall of 1990. Means and standard errors (vertical bars) were calculated from samples collected weekly during each month. Single samples collected in April for *P. annulipes* and in October for all three species are not included because a mean could not be calculated.

results are most likely due to an influx of larvae produced at other locations, where the timing of adult reproduction may differ from Nantucket Harbor (Williams, 1984).

Fewer larvae were found for *P. pollicaris* than for *P. annulipes* and *P. longicarpus*. This was especially apparent in the later larval stages (no zoea 4 and megalops *P. pollicaris* larvae were found in 1990 harbor samples). Abundances of later stage larvae (zoea 2, 3, 4, and megalops) were comparable for *P. annulipes* and *P. longicarpus*. The maximum mean density of *P. annulipes* and *P. longicarpus* zoea 3 sampled was the same at 0.209 larvae m^{-3} (Fig. 5a, b). Larval availability was also similar for the last larval stages (zoea 4 and megalops). In these two species, two peaks in mean density of larvae ($>0.01\ m^{-3}$) were recorded during the summer months (Fig. 5a, b).

Patterns of shell size among species

P. annulipes inhabited larger shells compared to body size than either *P. longicarpus* or *P. pollicaris* (Fig. 6). Greater than 80% of *P. annulipes* were found in shell size/crab size category 1 and <3% were found in categories 3 and 4. By comparison, *P. longicarpus* and *P. pollicaris* were more likely to have lower shell size/crab size ratios. Only 45.2% of *P. longicarpus* and 53.8% of *P. pollicaris* were found in category 1, and the percentages of these two species in shell fit categories 2, 3, and 4 were much higher than for *P. annulipes*. A two-way contingency table defined by hermit crab species and shell size/crab size category indicated that the distribution of individuals in the four categories varied among species ($G^2 = 192.53$, df = 6, $P < 0.001$). Comparisons of shell size/crab size categories between species indicated that there was no difference in the distribution of categories between *P. longicarpus* and *P. pollicaris* ($G^2 = 6.96$, df = 3, $P = 0.073$). However, the distribution of categories was significantly different between both *P. annulipes* and *P. longicarpus* ($G^2 = 188.75$, df = 3, $P < 0.001$) and between *P. annulipes* and *P. pollicaris* ($G^2 = 63.42$, df = 3, $P < 0.001$).

Discussion

Seasonal reproductive effort is evidently higher in smaller hermit crab species. The reproductive strategy of *P. annulipes*, the smallest species, includes the traits of early maturity after metamorphosis, high reproductive allocation per brood, and high reproductive activity throughout the spring and summer. In contrast, *P. pollicaris*, the largest species, uses a very different strategy, delaying reproduction until achieving large body size, allocating a low proportion of energy per brood, and becoming reproductively active only in the spring. The reproductive strategy of *P. longicarpus* appears to lie somewhere between *P. annulipes* and *P. pollicaris*. Reproductive effort per brood is lower than in *P. annulipes* but not statistically different from that of *P. pollicaris*. On the other hand, *P. longicarpus* females reach maturity at relatively small body size, are reproductive over a longer period than *P. pollicaris*, and are reproductively active in the spring and summer months, like *P. annulipes*.

The relationship between size and life-history traits described here was also found in the hermit crab fauna of the Pacific coast of Washington State. Nyblade (1974) compared reproductive traits among 16 intertidal and subtidal hermit crab species that spanned a broad size range. His data show a strong positive relationship between average body size and minimum size at ovigery ($R^2 = 0.511$, $F_{1,14} = 14.622$, $P = 0.002$; data from table 4.10). There is also a negative relationship between body size and annual reproductive effort (larval production female body weight^{-1} year^{-1}; $R^2 = 0.325$, $F_{1,14} = 7.918$, $P = 0.021$; data from tables 4.7a and 4.10). In Nyblade's study, small intertidal species typically matured at a small body size and had large annual reproductive efforts. In comparison, large subtidal species delayed reproduction and had low annual reproductive efforts. The relationship between size and life history traits seen in *Pagurus* hermit crabs of Nantucket Harbor may be a general phenomenon among other hermit crab assemblages.

An explanation for the reproductive strategies documented here and elsewhere lies in the risk of mortality

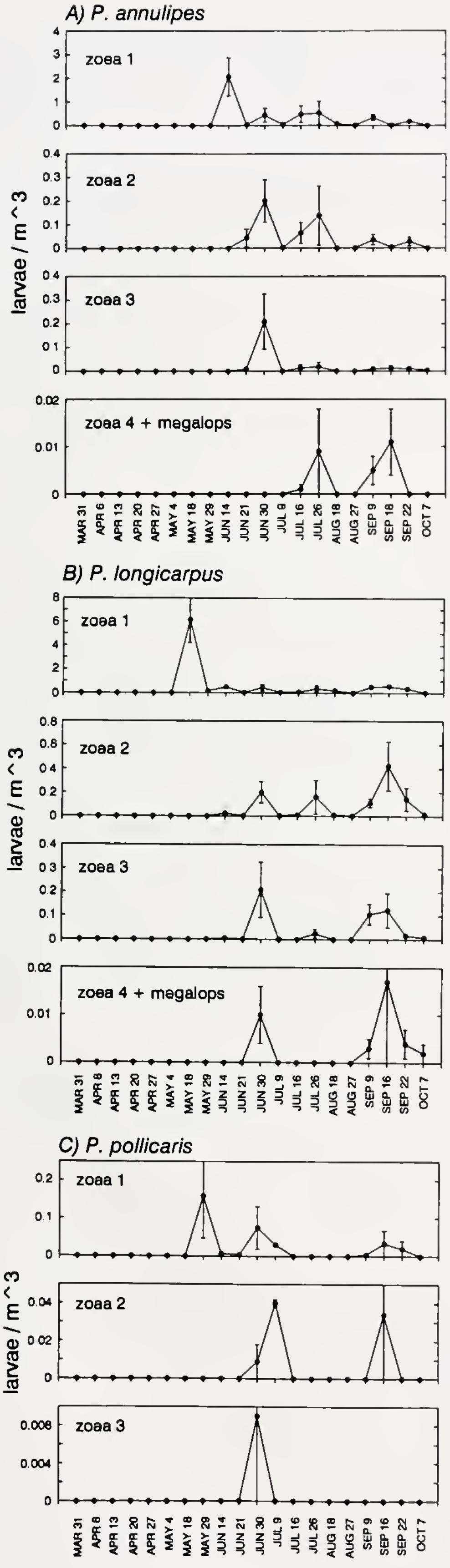

associated with using different sized shells. Small shells are more easily damaged or destroyed by shell-crushing predators than are larger shells (Bertness and Cunningham, 1981; Borjesson and Szelistowski, 1989; Buckley and Ebersole, 1994). It follows that the risk of mortality should be greater for species or size classes inhabiting small shells compared to large shells. Hermit crabs that use small shells as adults (*e.g., P. annulipes*) will have high adult mortality due to their susceptibility to shell-crushing predators. The juveniles of large species will also have high mortality rates; however, adults can potentially escape in size by using shells that are immune to shell-crushing predators (*e.g., P. longicarpus* and *P. pollicaris*). Several life-history models predict early maturity and high reproductive effort when adult mortality is high, and delayed maturity and low reproductive effort when juvenile mortality is greater than adult mortality (Gadgil and Bossert, 1970; Schaffer, 1974; Law, 1979; Michod, 1979; Charlesworth, 1980). Age-specific mortality is therefore a potential selective mechanism that explains the life-history variation observed in the hermit crabs of Nantucket Harbor as well as on the coast of Washington.

As Reznick and Endler (1982) have pointed out, size-specific predation can mediate intraspecific competition. When predators eat small juveniles, the larger adults tend to accumulate in populations. Increased intraspecific competition among adults is predicted to select for delayed maturity and a decrease in reproductive investment (MacArthur and Wilson, 1967). Large hermit crab species may experience the negative effects of intraspecific competition more commonly than smaller species due to their immunity to shell-crushing predators, and the general scarcity of suitable shells. The high shell size/crab size ratios observed in the small *P. annulipes* and the low shell size/crab size ratios in the larger *P. longicarpus* and *P. pollicaris* are consistent with the hypothesis that the effects of intraspecific competition (*e.g.,* reduced shell availability) are more common in large species. However, this interpretation of shell size/crab size ratios assumes that all three *Pagurus* species prefer large to small shells. Because no selection experiments were conducted in Nantucket Harbor, variation in shell size preference among species can also explain the observed pattern. Nevertheless, increased intraspecific competition among adults is predicted in populations where adult mortality is low. If size-selective predation is important in hermit crabs in general, then selective pressures associated with intraspecific competition may also contribute to life-history variation.

Figure 5. Temporal abundance of four stages of larvae from three hermit crab species (A, B, and C) during 1990. Means and standard errors (vertical bars) calculated from 10 plankton tows on each date. No zoea 4 or megalops larvae were collected for *Pagurus pollicaris* during 1990.

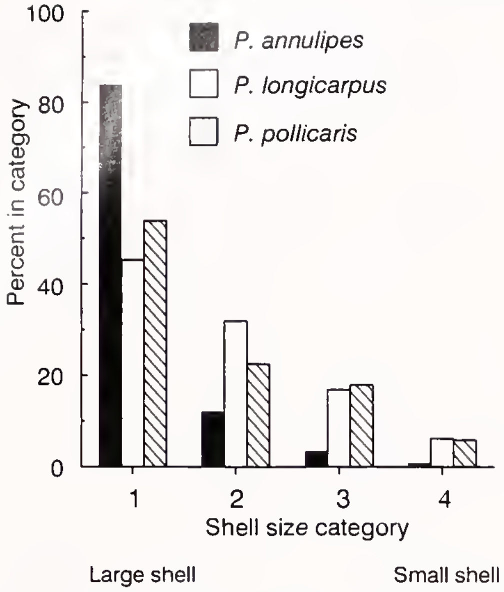

Figure 6. The distribution of three hermit crab species in four categories of shell size. See text for definition of shell size categories. Sample size for each species is the same as in Figure 2.

Reproductive allocation in *P. annulipes* was >15% higher in August 1990 than in May 1991. One explanation for this pattern is that female size varied between samples. However, this was not the case: there was no significant difference in female size between samples (*t*-test for paired comparisons, $t = -0.373$, df = 54, $P = 0.711$). A more likely explanation for this pattern is related to strong seasonal changes in water temperature in Nantucket Harbor. Water temperature in Nantucket Harbor may vary by as much as 10°C between May and August (Carlon, 1991). If growth and reproduction are temperature-dependent in *P. annulipes*, then colder spring temperatures may result in reduced reproductive allocation compared to the late summer when water temperature reaches its maximum.

Within a species, the importance of body size on reproductive decisions varied among the three species. It appears that body size does not play an important role in reproductive decisions of *P. annulipes*, with reproduction by females of every size. In comparison, there was a strong positive effect of body size on reproduction in the two larger species (*P. longicarpus* and *P. pollicaris*). This pattern supports the idea that *P. annulipes* has a high reproductive effort throughout its lifetime: females reach maturity quickly and reproduce regardless of body size. Size plays a more important role in the reproductive decisions of *P. longicarpus* and *P. pollicaris*. Two mechanisms may explain this pattern. The first is that maturity is typically delayed until a large body size is reached. This would increase the likelihood of sampling large ovigerous females. The second mechanism involves inter-sexual mate selection. Active choice of larger females over smaller females by males would result in higher fertilization rates of large females. Interestingly, Harvey (1991) found that male *Clibanarius digueti* does not select a female mate on the basis of body size in the Gulf of California. He also found no relationship between body size and the probability of being ovigerous in this species. *Clibanarius digueti* is similar in size (males 4.69 mm, females 3.38 mm) to *P. annulipes* in this study. Thus, it is possible that strong sexual selection for female body size is unimportant in small species but may play a more important role in larger species such as *P. longicarpus* and *P. pollicaris*.

Patterns of larval abundance in Nantucket Harbor were consistent with the higher seasonal reproductive efforts of *P. annulipes* and *P. longicarpus*. Early stage larvae of *P. annulipes* were 20 times more abundant and larvae of *P. longicarpus* 80 times more abundant than *P. pollicaris* larvae at the peak of reproduction. These differences are even more apparent in the later stages, with only a single zoea 3 larva of *P. pollicaris* sampled during 1990, and no zoea 4 or megalops sampled at all. Previous sampling of Nantucket Harbor gave the same result (Carlon, 1991): only two zoea 3 larvae and one zoea 4 larva of *P. pollicaris* were collected during 1989 with a similar sampling effort. The ranking of larval abundances among species was the same in 1989 and 1991 (*P. longicarpus* > *P. annulipes* ≫ *P. pollicaris*). On the Washington Coast, Nyblade (1974) measured hermit crab recruitment rates with settlement traps and found that species with high seasonal larval outputs also had high recruitment. The large number of larvae produced by *P. longicarpus* and *P. annulipes* throughout the summer may increase the probability of successful settlement and metamorphosis compared to *P. pollicaris*.

Acknowledgments

This research was completed as partial fulfillment of the requirements for the degree of Master of Science at the University of Massachusetts, Boston. Discussions with E. Gallagher, M. Rex, and R. Stevenson were always fruitful. D. Beattie, C. Hoffman, M. Lowenstein, and E. Weissberger provided assistance in the field, and Eric led many rousing renditions of "Foggy Mountain Breakdown" on his banjo. W. Tiffney directed the use of the University of Massachusetts Field Station on Nantucket. The comments of C. Chester, T. Dolan, W. Hammy, E. Weissberger, and three anonymous reviewers greatly improved the manuscript.

This research was supported by the Herb Lipke Endowment Fund and the Biology Department of the University of Massachusetts. A Grant in Aid of Research from the Lerner Gray Fund of the American Museum of Natural History is also gratefully acknowledged.

Literature Cited

Abrams, P. 1978. Shell selection and utilization in a terrestrial hermit crab, *Coenobita compressus* (M. Milne Edwards). *Oecologia* **34:** 239–253.

Abrams, P. 1980. Resource partitioning and interspecific competition in a tropical hermit crab community. *Oecologia* **46:** 365–379.

Bach, C., B. A. Hazlett, and D. Rittschof. 1976. Effects of interspecific competition on the fitness of the hermit crab *Clibanarius tricolor. Ecology* **57:** 579–586.

Bertness, M. D. 1980. Shell preference and utilization patterns in littoral hermit crabs of the Bay of Panama. *J. Exp. Mar. Biol. Ecol.* **48:** 1–16.

Bertness, M. D. 1981a. Competitive dynamics of a tropical hermit crab assemblage. *Ecology* **62:** 751–761.

Bertness, M. D. 1981b. Pattern and plasticity in a tropical hermit crab assemblage. *Am. Nat.* **117:** 754–773.

Bertness, M. D., and C. Cunningham. 1981. Crab shell-crushing predation and gastropod architecture defense. *J. Exp. Mar. Biol. Ecol.* **50:** 213–230.

Buckley, W. J., and J. P. Ebersole. 1994. Symbiotic organisms increase the vulnerability of a hermit crab to predation. *J. Exp. Mar. Biol. Ecol.* **182:** 49–64.

Borjesson, D. L., and W. A. Szelistowski. 1989. Shell selection, utilization and predation in the hermit crab *Clibanarius panamensis* Stimpson in a tropical mangrove estuary. *J. Exp. Mar. Biol. Ecol.* **133:** 213–228.

Carlon, D. B. 1991. *Reproductive Features and Life-history Patterns of Three* Pagurus *Hermit Crabs in a Temperate Harbor (Nantucket, Massachusetts).* M.Sc. Thesis. University of Massachusetts at Boston, Boston, Massachusetts. 93 pp.

Charlesworth, B. 1980. *Evolution in Age Structured Populations.* Cambridge University Press, New York. 300 pp.

Childress, J. R. 1972. Behavioral ecology and fitness theory in a tropical hermit crab. *Ecology* **53:** 960–964.

Gadgil, M., and W. Bossert. 1970. Life historical consequences of natural selection. *Am. Nat.* **104:** 1–24.

Harvey, A. W. 1991. Sexual differences in contemporary selection acting on size in the hermit crab *Clibinarius digueti. Am. Nat* **136:** 292–304.

Hazlett, B. A. 1970. Interspecific shell fighting in three sympatric species of hermit crabs in Hawaii. *Pac. Sci.* **24:** 472–482.

Hazlett, B. A. 1981. The behavioral ecology of hermit crabs. *Ann. Rev. Ecol. Syst.* **12:** 1–22.

Johnson, R. W., and J. P. Ebersole. 1989. Seasonality in the reproduction of the hermit crab *Pagurus longicarpus* Say, 1817 (Decapoda, Paguridea). *Crustaceana* **57:** 311–312.

Kellogg, C. W. 1976. Gastropod shells: a potential limiting resource for hermit crabs. *J. Exp. Mar. Biol. Ecol.* **22:** 101–111.

Law, R. 1979. Optimal life histories under age-specific predation. *Am. Nat.* **114:** 399–417.

MacArthur, R., and E. O. Wilson. 1967. *The Theory of Island Biogeography.* Princeton University Press, Princeton. 203 pp.

Markham, J. C. 1968. Notes on growth-patterns and shell-utilization of the hermit crab *Pagurus bernhardus* (L.). *Ophelia* **5:** 189–205.

McLaughlin, P. A. 1980. *Comparative Morphology of Recent Crustacea.* W. H. Freeman and Company, San Francisco. 177 pp.

Michod, R. E. 1979. Evolution of life histories in responses to age-specific mortality factors. *Am. Nat.* **113:** 531–550.

Nyblade, C. F. 1970. Larval development of *Pagurus annulipes* (Stimpson 1862) and *Pagurus pollicaris* (Say 1817) reared in the laboratory. *Biol. Bull.* **139:** 557–573.

Nyblade, C. F. 1974. *Coexistence in Sympatric Hermit Crabs.* Ph.D. Thesis. University of Washington, Seattle, Washington. 241 pp.

Reese, E. S. 1969. Behavioral adaptations of intertidal hermit crabs. *Am. Zool.* **9:** 343–355.

Reznick, D. N., and J. A. Endler. 1982. The impact of predation on life history evolution in Trinidadian guppies (Poecilia reticulata). *Evolution* **36:** 160–177.

Roberts, M. H. 1970. Larval development of *Pagurus longicarpus* Say reared in the laboratory. I. Description of the larval instars. *Biol. Bull.* **139:** 188–202.

Sadler, P. W. 1984. *The Spatial and Temporal Distribution of the Larvae of Sympatric Pagurid Hermity Crabs (Decapoda, Anomura) in Virginian Estuarine and Coastal Waters.* Masters Thesis, Old Dominion University, Norfolk, Virginia.

Schaffer, W. M. 1974. Selection for optimal life histories: the effects of age structure. *Ecology* **55:** 291–303.

Scully, E. P. 1979. The effects of gastropod shell availability and habitat characteristics on shell utilization by the intertidal hermit crab *Pagurus longicarpus* Say. *J. Exp. Mar. Biol. Ecol.* **37:** 139–152.

Underwood, A. J. 1981. Techniques of analysis of variance in experimental marine biology and ecology. *Oceanogr. Mar. Biol. Rev.* **19:** 513–605.

Vance, R. R. 1972. Competition and mechanisms of coexistence in three sympatric species of intertidal hermit crabs. *Ecology* **53:** 1062–1074.

Williams, A. B. 1984. *Shrimps, Lobsters, and Crabs of the Atlantic Coast of the Eastern United States, Maine to Florida* Smithsonian Institution Press, Washington, DC. 550 pp.

Winer, B. J., D. R. Brown, and K. M. Michels. 1991. *Statistical Principles in Experimental Design, Third Edition.* McGraw-Hill, Inc. New York. 1055 pp.

INDEX

A

Abdomen, 157
Abraham, V. C., A. L. Miller, and R. A. Fluck, Microtubule arrays during ooplasmic segregation in the medaka fish egg (*Oryzias latipes*), 136
Actin, 1
Adhesion, 255
Age-specific mortality, 329
Aggregation, 32, 255
Aggression, 83
Akiyama, Tadashi, see Masayuki Saigusa, 166
Alfredsson, Karin, see Mats Carlberg, 78
Alviniconcha hessleri, 5
Ammonium metabolism in the green hydra symbiosis, 210
Amphioxus, 231
Anderson, Peter A. V., see Mats Carlberg, 78
Apoptosis, 23
Aragonite, 8
Articular capsule, 120
Ascidian, 16, 23
Asteroid, 293
Atomic force microscope, 8
Axial organ, 98

B

Bates, William R., Direct development in the ascidian *Molgula retortiformis* (Verrill, 1871), 16
Bayne, Christopher J., see Jiun-Hong Chen, 255
Behavior, 89, 231
Behavioral rhythm, 166
Benthic development, 293
Biomechanics, 197
Biomineralization, 8, 281
Bivalve mollusc hemocyte behaviors: characterization of hemocyte aggregation and adhesion and their inhibition in the California mussel (*Mytilus californianus*), 255
Bivalve shell, 57
Black, Nancy A., Richard Voellmy, and Alina M. Szmant, Heat shock protein induction in *Montastraea faveolata* and *Aiptasia pallida* exposed to elevated temperatures, 234
Botryllus schlosseri, 23
Bryozoa, 281
Byrne, M., Changes in larval morphology in the evolution of benthic development by *Patiriella exigua* (Asteroidea), a comparison with the larvae of *Patiriella* species with planktonic development, 293

C

Caffeine, 255
Calcite, 281
Calcitic nacreous ultrastructures in bryozoans: implications for comparative biomineralization of lophorphorates and molluscs, 281
Calcium, 1
  cage, 1
Callinectes sapidus, 111
Cardiac regulation, 179
Carlberg, Mats, Karin Alfredsson, Sven-Olle Nielsen, and Peter A. V. Anderson, Taurine-like immunoreactivity in the motor nerve net of the jellyfish *Cyanea capillata*, 78
Carlon, David B., and John P. Ebersole, Life-history variation among three temperate hermit crabs: the importance of size in reproductive strategies, 329
Cassidy, Paul M., see Francesca Gherardi, 68
Catch in the primary spines of the sea urchin *Eucidaris tribuloides:* a brief review and a new interpretation, 120
Cerrato, Robert M., see Kurt Thorn, 57
Chang, Wen-Teh, and Robert J. Lauzon, Isolation of biologically functional RNA during programmed death of a colonial ascidian, 23
Changes in larval morphology in the evolution of benthic development by *Patiriella exigua* (Asteroidea), a comparison with the larvae of *Patiriella* species with planktonic development, 293
Chemical ecology, 306
Chemoreception, 111
Chen, Jiun-Hong, and Christopher J. Bayne, Bivalve mollusc hemocyte behaviors: characterization of hemocyte aggregation and adhesion and their inhibition in the California mussel (*Mytilus californianus*), 255
Chlorella, 210
Choanocyte, 306
Cilia, 231
Ciliary hovering in larval lancelets (=amphioxus), 231
Circulation, 186
Clark, Eugenie, see Sidney K. Pierce, 219
Cnidaria, 234
Coelenterate, 78
Collagen, 120, 219
Coral, 234
Crab, 111, 186
Crinoid, 89
Csányi, Vilmos, see Ádám Miklósi, 83
Cyclostomata, 281
Cytochalasin D, 146
Cytological analysis of the urn cell complex of *Sipunculus nudus* before and after serum-induced secretion, 267
Cytoskeletal architecture and organelle transport in giant syncytia by fusion of hexactinellid sponge tissues, 241
Cytoskeleton, 241

D

del Castillo, José, David S. Smith, Ada M. Vidal, and César Sierra, Catch in the primary spines of the sea urchin *Eucidaris tribuloides:* a brief review and a new interpretation, 120
Demecolcine, 146
Denny, Mark W., see Kristina S. Mead, 46
Development, 32, 46
Dinoflagellate effects on shellfish, 313
Direct development in the ascidian *Molgula retortiformis* (Verrill, 1871), 16

E

Ebersole, John P., see David B. Carlon, 329
Echinoderm, 32, 89, 98, 197

Echinoidea, 120
Elemental distributions in marine bivalve shells as measured by synchrotron x-ray fluorescence, 57
Emergence, 166
Emson, Roland H., see Craig M. Young, 89
Engrailed, 157
Estuary, 111
Eucidaris tribuloides, 120
Evidence for selection against heterozygotes: post-settlement excess of allozyme homozygosity in a cohort of the Chilean oyster, *Ostrea chilensis* Philippi, 1845, 117
Evolution, 157
Experimental and histological studies of four life-history stages of the eastern oyster, *Crassostrea virginica*, exposed to a cultured strain of the dinoflagellate *Prorocentrum minimum*, 313
Expression of the *engrailed* gene reveals nine putative segment-anlagen in the embryonic pleon of the freshwater crayfish *Cherax destructor* (Crustacea, Malacostraca, Decapoda), 157

F

Ferguson, John C., The structure and mode of function of the water vascular system of a brittlestar, *Ophioderma apressum*, 98
Fertilization, 46
  ecology, 46
Finelli, Christopher M., see Richard K. Zimmer-Faust, 111
Fish development, 1, 136, 146
Fluck, Richard A., Responses of the medaka fish egg (*Oryzias latipes*) to the photolysis of microinjected nitrophenyl-EGTA, a photolabile calcium chelator, 1
Fluck, Richard A., see V. C. Abraham, 136; Tamika A. Webb, 146
FMRFamide-related peptides, 186
Fusion, 241

G

Gherardi, Francesca, and Paul M. Cassidy, Life history patterns of *Discorsopagurus schmitti*, a hermit crab inhabiting polychaete tubes, 68
Giant octopus, 219
Giles, R., S. Manne, S. Mann, D. E. Morse, G. D. Stucky, and P. K. Hansma, Inorganic overgrowth of aragonite on molluscan nacre examined by atomic force microscopy, 8
Green hydra, 210
Guirguis, M. S., and J. L. Wilkens, The role of cardioregulatory nerves in mediating heart rate responses to locomotion, reduced stroke volume, and neurohormones in *Homarus americanus*, 179

H

Haller, József, see Ádám Miklósi, 83
Halonen, S. K., see Earl Weidner, 128
Hamel, Jean-François, and Annie Mercier, Prespawning behavior, spawning, and development of the brooding starfish *Leptasterias polaris*, 32
Hansma, P. K., see R. Giles, 8
Harmful algal blooms, 313
Hatching, 68
Heart rate, 179
Heat shock protein induction in *Montastraea faveolata* and *Aiptasia pallida* exposed to elevated temperatures, 234
Hemocyte, 255
Hemoglobin in the symbiont-harboring gill of the marine gastropod *Alvinichoncha hessleri*, 5
Hermit crab, 68, 329
Heterozygote deficiency, 117
Hexactinellid, 241
Holland, N. D., see M. D. Stokes, 231
Homarus, 179
Hovering, 231
Hydrodynamics, 111
Hydrostatic skeleton, 197

I

Ilan, Micha, Reproductive biology, taxonomy, and aspects of chemical ecology of Latrunculiidae (Porifera), 306
Inorganic overgrowth of aragonite on molluscan nacre examined by atomic force microscopy, 8
Intertidal midge, 166
Isolation of biologically functional RNA during programmed death of a colonial ascidian, 23

J

Jellyfish, 78

K

Kier, William M., see Skyler R. McCurley, 197
Kowalski, Wendy J., see Tamika A. Webb, 146

L

Lancelet, 231
Larvae, 231
Lauzon, Robert J., see Wen-Teh Chang, 23
Leptasterias, 32
Leys, Sally P., Cytoskeletal architecture and organelle transport in giant syncytia by fusion of hexactinellid sponge tissues, 241
Life history patterns of *Discorsopagurus schmitti*, a hermit crab inhabiting polychaete tubes, 68
Life-history variation among three temperate hermit crabs: the importance of size in reproductive strategies, 329
Ligament, 120
Locomotion, 231
Lophophorate, 281
Lynn, J. W., see Earl Weidner, 128
Lysosome, 313

M

Madreporite, 98
Manale, S. B., see Earl Weidner, 128
Mann, S., see R. Giles, 8
Manne, S., see R. Giles, 8
Maugel, Timothy K., see Sidney K. Pierce, 219
McAuley, P. J., Ammonium metabolism in the green hydra symbiosis, 210
McCurley, R. Skyler, and William M. Kier, The functional morphology of starfish tube feet: the role of a crossed-fiber helical array in movement, 197
McGaw, I. J., and B. R. McMahon, The FMRFamide-related peptides F1 and F2 alter hemolymph distribution and cardiac output in the crab *Cancer magister*, 186
McMahon, B. R., see I. J. McGaw, 186
Mead, Kristina S., and Mark W. Denny, The effects of hydrodynamic shear stress on fertilization and early development of the purple sea urchin *Strongylocentrotus purpuratus*, 46
Medaka, 1, 136, 146
Memory, 83
Mercenaria mercenaria, 57, 111
Mercier, Annie, see Jean-François Hamel, 32
Microsporidian invasion tubes, 128
Microtubule arrays during ooplasmic segregation in the medaka fish egg (*Oryzias latipes*), 136
Microtubule-based movements during ooplasmic segregation in the medaka fish egg (*Oryzias latipes*), 146
Miklósi, Ádám, József Haller, and Vilmos Csányi, The influence of opponent-related and outcome-related memory on repeated ag-

gressive encounters in the paradise fish (*Macropodus opercularis*), 83
Miller, A. L., see V. C. Abraham, 136
Molgula retortiformis, 16
Mollusc, 5, 281
Morse, D. E., see R. Giles, 8
Mussel, 255
Mya arenaria, 57

N

Nacre, 8, 280
Navigation, 111
Nerves, 78
Neurogenesis, 157
Neurohormones, 186
Nicosia, Santo V., and Janice M. Sowinski, Cytological analysis of the urn cell complex of *Sipunculus nudus* before and after serum-induced secretion, 267
Nielsen, Sven-Olle, see Mats Carlberg, 78

O

Octopus giganteus, 219
Odor plumes and animal navigation in turbulent water flow: a field study, 111
On the giant octopus (*Octopus giganteus*) and the Bermuda Blob: homage to A. E. Verrill, 219
Ooplasmic segregation, 136, 146
Ophiuroidea, 98
Organelle transport, 241
Orientation, 111
Oryzias latipes, 1
Ostrea chilensis, 117
Oyster larvae and spat, 313

P

Paleothermometry, 57
Paradise fish, 83
Paramyosin muscle, 120
Parasitism, 68
Patiriella, 293
Pentcheff, N. Dean, see Richard K. Zimmer-Faust, 111
Peptides, 186
Pierce, Sidney K., Gerald N. Smith, Jr., Timothy K. Maugel, and Eugenie Clark, On the giant octopus (*Octopus giganteus*) and the Bermuda Blob: homage to A. E. Verrill, 219
Polychaete tube, 68
Population ecology, 329
Predation, 111
Prespawning behavior, spawning, and development of the brooding starfish *Leptasterias polaris*, 32
Prey, 111
Primary spines, 120
Programmed cell death, 23
Protein, heat shock, 234
Protein-membrane interaction is essential to normal assembly of the microsporidian spore invasion tube, 128

R

Rapid arm movements in stalked crinoids, 89
Recapitulation, 157
Red tide, 313
Reproduction, 306
Reproductive biology, taxonomy, and aspects of chemical ecology of Latrunculiidae (Porifera), 306
Responses of the medaka fish egg (*Oryzias latipes*) to the photolysis of microinjected nitrophenyl-EGTA, a photolabile calcium chelator, 1
Rhizocephalan, 68
Rivers, Mark L., see Kurt Thorn, 57

S

Saigusa, Masayuki, and Tadashi Akiyama, The tidal rhythm of emergence, and the seasonal variation of this synchrony, in an intertidal midge, 166
Scholtz, Gerhard, Expression of the *engrailed* gene reveals nine putative segment-anlagen in the embryonic pleon of the freshwater crayfish *Cherax destructor* (Crustacea, Malacostraca, Decapoda), 157
Sea anemone, 234
Sea urchin, 46
Secretion, 267
Segment formation, 157
Shear stress, 46
Sierra, César, see José del Castillo, 120
Sipunculus nudus, 267
Skeleton, 281
Smith, David S., see José del Castillo, 120
Smith, Gerald N., Jr., see Sidney K. Pierce, 219
Smolowitz, Roxanna M., see Gary H. Wikfors, 313
Sowinski, Janice M., see Santo V. Nicosia, 267
Spawning, 32
Spine-test articulation, 120
Sponge, 241, 306
Starfish, 32
Stein, Jeffrey L., see Jonathan Wittenberg, 5
Stokes, M. D., and N. D. Holland, Ciliary hovering in larval lancelets (=amphioxus), 231
Strongylocentrotus purpuratus, 46
Stucky, G. D., see R. Giles, 8
Symbiosis, 5, 210
Synchrotron x-ray fluorescence, 57
Synctium, 241
Szmant, Alina M., see Nancy A. Black, 234

T

Taurine-like immunoreactivity in the motor nerve net of the jellyfish *Cyanea capillata*, 78
Taxonomy, 306
Taylor, Paul D., see Michael J. Weedon, 281
The effects of hydrodynamic shear stress on fertilization and early development of the purple sea urchin *Strongylocentrotus purpuratus*, 46
The FMRFamide-related peptides F1 and F2 alter hemolymph distribution and cardiac output in the crab *Cancer magister*, 186
The functional morphology of starfish tube feet: the role of a crossed-fiber helical array in movement, 197
The influence of opponent-related and outcome-related memory on repeated aggressive encounters in the paradise fish (*Macropodus opercula*), 83
The role of cardioregulatory nerves in mediating heart rate responses to locomotion, reduced stroke volume, and neurohormones in *Homarus americanus*, 179
The structure and mode of function of the water vascular system of a brittlestar, *Ophioderma apressum*, 98
The tidal rhythm of emergence, and the seasonal variation of this synchrony, in an intertidal midge, 166
Thorn, Kurt, Robert M. Cerrato, and Mark L. Rivers, Elemental distributions in marine bivalve shells as measured by synchrotron x-ray fluorescence, 57
Tidal and semilunar cycles, 166
Toro, J. E., and A. M. Vergara, Evidence for selection against heterozygotes: post-settlement excess of allozyme homozygosity in a cohort of the Chilean oyster, *Ostrea chilensis* Philippi, 1845, 117
Trace element, 57
Tube feet, 98, 197
Tunicate, 23
Turbulence, 46

U

Ultrastructure, 281
Ultraviolet light, 1, 146
Urn cell complex, 267

V

Vergara, A. M., see J. E. Toro, 117
Verrill, A. E., 219
Vidal, Ada M., see José del Castillo, 120
Voellmy, Richard, see Nancy A. Black, 234

W

Water vascular system, 197
Webb, Tamika A., Wendy J. Kowalski, and Richard A. Fluck, Microtubule-based movements during ooplasmic segregation in the medaka fish egg (*Oryzias latipes*), 146
Weedon, Michael J., and Paul D. Taylor, Calcitic nacreous ultrastructures in bryozoans: implications for comparative biomineralization of lophorphorates and molluscs, 281
Weidner, Earl, S. B. Manale, S. K. Halonen, and J. W. Lynn, Protein-membrane interaction is essential to normal assembly of the microsporidian spore invasion tube, 128
Wethey, David S., see Richard K. Zimmer-Faust, 111
Whale blubber, 219
Wikfors, Gary H., and Roxanna M. Smolowitz, Experimental and histological studies of four life-history stages of the eastern oyster, *Crassostrea virginica,* exposed to a cultured strain of the dinoflagellate *Prorocentrum minimum,* 313
Wilkens, J. L., see M. S. Guirguis, 179
Wittenberg, Jonathan B., and Jeffrey L. Stein. Hemoglobin in the symbiont-harboring gill of the marine gastropod *Alvinichoncha hessleri,* 5

Y

Young, Craig M., and Roland H. Emson, Rapid arm movements in stalked crinoids, 89

Z

Zimmer-Faust, Richard K., Christopher M. Finelli, N. Dean Pentcheff, and David S. Wethey, Odor plumes and animal navigation in turbulent water flow: a field study, 111

CONTENTS

RESEARCH NOTE

Stokes, M. D., and N. D. Holland
Ciliary hovering in larval lancelets (=amphioxus) 231

PHYSIOLOGY

Black, Nancy A., Richard Voellmy, and Alina M. Szmant
Heat shock protein induction in *Montastraea faveolata* and *Aiptasia pallida* exposed to elevated temperatures 234

CELL BIOLOGY

Leys, Sally P.
Cytoskeletal architecture and organelle transport in giant syncytia formed by fusion of hexactinellid sponge tissues 241

Chen, Jiun-Hong, and Christopher J. Bayne
Bivalve mollusc hemocyte behaviors: characterization of hemocyte aggregation and adhesion and their inhibition in the California mussel (*Mytilus californianus*) 255

Nicosia, Santo V., and Janice M. Sowinski
Cytological analysis of the urn cell complex of *Sipunculus nudus* before and after serum-induced secretion 267

ECOLOGY AND EVOLUTION

Weedon, Michael J., and Paul D. Taylor
Calcitic nacreous ultrastructures in bryozoans: implications for comparative biomineralization of lophophorates and molluscs 281

Byrne, M.
Changes in larval morphology in the evolution of benthic development by *Patiriella exigua* (Asteroidea: Asterinidae), a comparison with the larvae of *Patiriella* species with planktonic development 293

Ilan, Micha
Reproductive biology, taxonomy, and aspects of chemical ecology of Latrunculiidae (Porifera) . . . 306

Wikfors, Gary H., and Roxanna M. Smolowitz
Experimental and histological studies of four life-history stages of the eastern oyster, *Crassostrea virginica,* exposed to a cultured strain of the dinoflagellate *Prorocentrum minimum* 313

Carlon, David B., and John P. Ebersole
Life-history variation among three temperate hermit crabs: the importance of size in reproductive strategies 329

Index to Volume 188 338

MBL/WHOI LIBRARY
WH 1B2S 5